Advances in Intelligent Systems and Computing 325

L Padma Suresh
Subhransu Sekhar Dash
Bijaya Ketan Panigrahi *Editors*

Artificial Intelligence and Evolutionary Algorithms in Engineering Systems

Proceedings of ICAEES 2014, Volume 2

Springer

Advances in Intelligent Systems and Computing

Volume 325

Series editor

Janusz Kacprzyk, Polish Academy of Sciences, Warsaw, Poland
e-mail: kacprzyk@ibspan.waw.pl

About this Series

The series "Advances in Intelligent Systems and Computing" contains publications on theory, applications, and design methods of Intelligent Systems and Intelligent Computing. Virtually all disciplines such as engineering, natural sciences, computer and information science, ICT, economics, business, e-commerce, environment, healthcare, life science are covered. The list of topics spans all the areas of modern intelligent systems and computing.

The publications within "Advances in Intelligent Systems and Computing" are primarily textbooks and proceedings of important conferences, symposia and congresses. They cover significant recent developments in the field, both of a foundational and applicable character. An important characteristic feature of the series is the short publication time and world-wide distribution. This permits a rapid and broad dissemination of research results.

Advisory Board

Chairman

Nikhil R. Pal, Indian Statistical Institute, Kolkata, India
e-mail: nikhil@isical.ac.in

Members

Rafael Bello, Universidad Central "Marta Abreu" de Las Villas, Santa Clara, Cuba
e-mail: rbellop@uclv.edu.cu

Emilio S. Corchado, University of Salamanca, Salamanca, Spain
e-mail: escorchado@usal.es

Hani Hagras, University of Essex, Colchester, UK
e-mail: hani@essex.ac.uk

László T. Kóczy, Széchenyi István University, Győr, Hungary
e-mail: koczy@sze.hu

Vladik Kreinovich, University of Texas at El Paso, El Paso, USA
e-mail: vladik@utep.edu

Chin-Teng Lin, National Chiao Tung University, Hsinchu, Taiwan
e-mail: ctlin@mail.nctu.edu.tw

Jie Lu, University of Technology, Sydney, Australia
e-mail: Jie.Lu@uts.edu.au

Patricia Melin, Tijuana Institute of Technology, Tijuana, Mexico
e-mail: epmelin@hafsamx.org

Nadia Nedjah, State University of Rio de Janeiro, Rio de Janeiro, Brazil
e-mail: nadia@eng.uerj.br

Ngoc Thanh Nguyen, Wroclaw University of Technology, Wroclaw, Poland
e-mail: Ngoc-Thanh.Nguyen@pwr.edu.pl

Jun Wang, The Chinese University of Hong Kong, Shatin, Hong Kong
e-mail: jwang@mae.cuhk.edu.hk

More information about this series at http://www.springer.com/series/11156

L Padma Suresh · Subhransu Sekhar Dash
Bijaya Ketan Panigrahi
Editors

Artificial Intelligence and Evolutionary Algorithms in Engineering Systems

Proceedings of ICAEES 2014, Volume 2

Springer

Editors
L Padma Suresh
Electrical and Electronics Engineering
Noorul Islam Centre for Higher Education
Kumaracoil
Tamil Nadu
India

Bijaya Ketan Panigrahi
Electrical Engineering
IIT Delhi
New Delhi
Delhi
India

Subhransu Sekhar Dash
Electrical and Electronics Engineering
SRM Engineering College
Kattankulathur
Tamil Nadu
India

ISSN 2194-5357
ISBN 978-81-322-2134-0
DOI 10.1007/978-81-322-2135-7

ISSN 2194-5365 (electronic)
ISBN 978-81-322-2135-7 (eBook)

Library of Congress Control Number: 2014950644

Springer New Delhi Heidelberg New York Dordrecht London

© Springer India 2015
This work is subject to copyright. All rights are reserved by the Publisher, whether the whole or part of the material is concerned, specifically the rights of translation, reprinting, reuse of illustrations, recitation, broadcasting, reproduction on microfilms or in any other physical way, and transmission or information storage and retrieval, electronic adaptation, computer software, or by similar or dissimilar methodology now known or hereafter developed. Exempted from this legal reservation are brief excerpts in connection with reviews or scholarly analysis or material supplied specifically for the purpose of being entered and executed on a computer system, for exclusive use by the purchaser of the work. Duplication of this publication or parts thereof is permitted only under the provisions of the Copyright Law of the Publisher's location, in its current version, and permission for use must always be obtained from Springer. Permissions for use may be obtained through RightsLink at the Copyright Clearance Center. Violations are liable to prosecution under the respective Copyright Law.
The use of general descriptive names, registered names, trademarks, service marks, etc. in this publication does not imply, even in the absence of a specific statement, that such names are exempt from the relevant protective laws and regulations and therefore free for general use.
While the advice and information in this book are believed to be true and accurate at the date of publication, neither the authors nor the editors nor the publisher can accept any legal responsibility for any errors or omissions that may be made. The publisher makes no warranty, express or implied, with respect to the material contained herein.

Printed on acid-free paper

Springer is part of Springer Science+Business Media (www.springer.com)

Preface

This AISC volume contains the papers presented at the *International Conference on Artificial Intelligence and Evolutionary Algorithms in Engineering Systems* (ICAEES) held on 22 and 23 April, 2014 at Noorul Islam Centre for Higher Education, Noorul Islam University, Kumaracoil. ICAEES 2014 received 526 paper submissions from various countries across the globe. After a rigorous peer-review process, 235 full length articles were accepted for oral presentation at the conference. This corresponds to an acceptance rate of 45 % and is intended for maintaining the high standards of the conference proceedings. The papers included in this LNAICS volume cover a wide range of topics on Genetic Algorithms, Evolutionary Programming, and Evolution Strategies such as AIS, DE, PSO, ACO, BFA, HS, SFLA, Artificial Bees and Fireflies Algorithm, Parallel Computation, Membrane, Grid, Cloud, DNA, Mobile Computing, Computer Networks and Security, Data Structures and Algorithms, Data Compression, Data Encryption, Data Mining, Digital Signal Processing, Digital Image Processing, Watermarking, Security and Cryptography, AI methods in Telemedicine and eHealth, Document Classification and Information Retrieval, Optimization Techniques, and their applications for solving problems in these areas.

In the conference, separate sessions were arranged for delivering the keynote address by eminent members from various academic institutions and industries. Eight keynote lectures were given in two different venues as parallel sessions on 22 and 23 April, 2014. In the first session, Dr. Shivashankar B. Nair, Professor and Head, Department of Computer Science and Engineering, Indian Institute of Technology, Guwahati gave a talk on "Emulating Bio-Inspired Mechanisms Using Mobile Agents" in Venue 1 and Dr. D. Deva Raj, Professor, Department of Electrical and Electronics Engineering, Kalasalingam University gave his lecture on "Multi Objective Evolutionary Algorithms" and covered various evolutionary algorithms and its applications to Power Systems in Venue 2. In the second session, Dr. Rusli Haji Abdullah, Software Engineering and Information System Department Faculty of Computer Science and Information Technology, Universiti Putra Malaysia gave his talk on "Artificial Intelligent in Knowledge Engineering: A Case of Knowledge Management System with Agent Technology Environment"

at Venue 1 and Dr. S.S. Dash, Professor, SRM University, Chennai gave his lecture on "Intelligence Computing Toward Renewable Energy Applications" and clarified the queries raised by the participants at Venue 2. He has explained the importance of soft computing in solar plant, wind mills, etc. Similarly on the second day in the first session, Dr. Ramachandran Kaimal, Professor and Chairperson, Department of Computer Science and Engineering, Amirta School of Engineering delivered his keynote address on "High Dimensional Data Analysis" at Venue 1 and the lecture by Prof. B.K. Panigrahi of IIT Delhi, India, on "Recent Advances in Bio Inspired Computing" gave an overall idea about the need for bio-inspired computing applications to the society at Venue 2. Dr. P. Karuppanan, Associate Professor, from National Institute of Technology, Allahabad gave a talk on "Artificial Intelligence Applications in Embedded Systems" at Venue 1 and Dr. Swagatam Das, from Indian Statistical Institute, Kolkata gave his lecture on "Computational Swarm Intelligence in Engineering Systems" and discussed the applications of Intelligent Systems in real-life problems at Venue 2. All these lectures generated great interest among the participants of ICAEES 2014 in paying more attention to these important topics in their research work.

We take this opportunity to thank the authors of all the submitted papers for their hard work, adherence to the deadlines, and suitably incorporating the changes suggested by the reviewers. The quality of a refereed volume depends mainly on the expertise and dedication of the reviewers. We are indebted to the Program Committee members for their guidance and coordination in organizing the review process.

We would also like to thank our sponsors for providing all the support and financial assistance. We are indebted to the Chairman, Vice-Chancellor, Advisors, Pro-Vice-Chancellor, Registrar, Faculty members, and Administrative Personnel of Noorul Islam Centre for Higher Education, Noorul Islam University, Kumaracoil for supporting our cause and encouraging us to organize the conference on a grand scale. We would also like to thank all the participants for their interest and enthusiastic involvement. Finally, we would like to thank all the volunteers whose tireless efforts in meeting the deadlines and arranging every detail meticulously made sure that the conference could run smoothly. We hope the readers of these proceedings find the papers useful, inspiring, and enjoyable.

April 2014

L Padma Suresh
Subhransu Sekhar Dash
Bijaya Ketan Panigrahi

Contents

Web Information Extraction on Multiple Ontologies Based on Concept Relationships upon Training the User Profiles 1
S. Vigneshwari and M. Aramudhan

A Study on Competent Crawling Algorithm (CCA) for Web Search to Enhance Efficiency of Information Retrieval 9
S. Saranya, B.S.E. Zoraida and P. Victor Paul

High Payload Reversible Watermarking for Securing Medical Images in a Cloud Environment 17
R. Sukanesh and N. Karthikeyan

Enhanced Security Framework for Data Integrity Using Third-party Auditing in the Cloud System 25
Balamurugan Balusamy, P. Venkatakrishna, Abinaya Vaidhyanathan, Meenakshi Ravikumar and Nirmala Devi Munisamy

An Intelligent Cloud Security System for Critical Applications 33
Balamurugan Balusamy, P. Venkatakrishna, Gomathi Palani and Umamageshwari Ravikumar

An Efficient Framework for Health System Based on Hybrid Cloud with ABE-Outsourced Decryption 41
B. Balamurugan, P. Venkata Krishna, N. Saravana Kumar and G.V. Rajyalakshmi

A Knowledgeable Feature Selection Based on Set Theory for Web Intrusion Detection System 51
Nalini Priya Ganapathi and Vivek Duraivelu

FLC-Based Adaptive Neuro-Fuzzy Inference System for Enhancing the Traveling Comfort 61
K.K. Sneha, Lakshmi Ponnusamy and R. Kalaivani

State Variable Filter Design Using Improvised Particle Swarm Optimization Algorithm 71
Aakash Indoria, Varatharajan Varrun, Akshay, Murali Krishna Reddy, Tejaswi Sathyasai, Baskaran Anand and Nirmala M. Devi

A Novel Algorithm on IP Traceback to Find the Real Source of Spoofed IP Packets 79
M. Vijayalakshmi, N. Nithya and S. Mercy Shalinie

A Queueing Model for e-Learning System 89
T. Senthil Kumar and K.I. Ohhm Prakash

Development of Common Parallel Programming Platform for MPI and PVM 95
Veerabasavantha Swamy, S. Sampath, B.R. Nanjesh and Bharat Bhushan Sagar

Association Rule Mining and Refinement Using Shared Memory Multiprocessor Environment 105
P. Asha and T. Jebarajan

Design of Low-Power Multiplier Using UCSLA Technique 119
S. Ravi, Anand Patel, Md Shabaz, Piyush M. Chaniyara and Harish M. Kittur

Hyperspectral Image Compression Algorithms—A Review 127
K. Subhash Babu, V. Ramachandran, K.K. Thyagharajan and Geeta Santhosh

Reliable Virtual Cluster-Based Opportunistic Routing Protocol for Mobile Ad hoc Networks 139
E. Sahaya Rose Vigita, E. Golden Julie and S. Tamil Selvi

Weighted Euclidean Distance Based Sign Language Recognition Using Shape Features 149
S. Nagarajan and T.S. Subashini

Event Monitoring for Adaptive Multi-priority Streaming Time Sensitive-Based EDF Scheduling 157
P. Leela, S. Sathees babu and K. Balasubadra

How Does Consciousness Overcome Combinatorial Complexity? 167
Reji Kumar

Website Re-organization for Effective Latency Reduction Through Splay Trees and Concept-Based Clustering 173
M.B. Thulase and G.T. Raju

Algorithms for Zumkeller Labeling of Full Binary Trees and Square Grids 183
B.J. Balamurugan, K. Thirusangu and D.G. Thomas

Memetic Framework Application—Analysis of Corporate Customer Attitude in Telecom Sector 193
V. Balakumar and C. Swarnalatha

Contourlet-Based Multiband Image Fusion for Improving Classification Accuracy in IRS LISS III Images 201
K. Venkateswaran, N. Kasthuri, K. Balakrishnan and K. Prakash

Computer-Aided Diagnosis of Breast Elastography and B-Mode Ultrasound 213
Shirley Selvan, S. Shenbagadevi and S. Suresh

A Convivial Energy Based Clustering (CEBC) Solution for Lifetime Enhancement of Wireless Sensor Networks 225
Betty Madhurya Vallapuram, Gokul P. Nair and Kaliraja Thangamani

Wind Power in India—An Overview 235
T.V. Gowtham, G.R. Venkatakrishnan and R. Rengaraj

Series Resonant Converter-based Unified Power Quality Conditioner Using Fuzzy Controller 243
R. Anand and P. Melba Mary

MRI Brain Image Classification Using Haar Wavelet and Artificial Neural Network 253
J.C. Smitha and S. Suresh Babu

Adaptive Modified Hysteresis Current Control for Switching Loss Reduction in Photovoltaic-Fed Dual-Function Grid-Connected Inverters 263
Preethi Thekkath and S.U. Prabha

Low-complexity Power Spectral Density Estimation 273
N. Balasaraswathy and R. Rajavel

Intensified Scheduling Algorithm for Virtual Machine Tasks in Cloud Computing 283
K.A. Saranu and Suresh Jaganathan

Design of Neural Network Model for Emotional Speech Recognition 291
H.K. Palo, Mihir Narayana Mohanty and Mahesh Chandra

Intelligent Decision Making with Improved Energy Detection for Precise Spectrum Sensing in Cognitive Radios 301
K. Muthumeenakshi, S. Radha, R. Sudharsana and R. Tharini

Human Action Recognition by Employing DWT and Texture 309
V. Thanikachalam and K.K. Thyagharajan

Modeling and Performance Evaluation of Switched Reluctance Motor Drives in MATLAB/Simulink Atmosphere with Estimation of SRM Parameters Using Finite Element Analysis 317
P. Magdelin Jennifer Princy, S. Ram Prasath and P. Ramesh Babu

Classification of Right Bundle Branch Block and Left Bundle Branch Block Cardiac Arrhythmias Based on ECG Analysis 331
Sukanta Bhattacharyya and U. Snekhalatha

Content-based Algorithm for Color Image Enhancement Using Fuzzy Technique 343
C. Reshmalakshmi and M. Sasikumar

Frequent Itemset Mining with Elimination of Null Transactions Over Data Streams 353
B. Subbulakshmi, A. Periya Nayaki and C. Deisy

Protograph-Based Design of Non-Binary LDPC Codes 363
I. Divya and M. Anbuselvi

Extraction of Binary Sequences in a Frequency Shift Keying-Modulated Signal by Empirical Mode Decomposition Algorithm Against Ambient Noises in Underwater Acoustic Channel 371
L. Suvasini, S. Prethivika, S. Sakthivel Murugan and V. Natarajan

A Model for the Effective Steganalysis of VoIP 379
N. Jayasree and P.P. Amritha

Automatic Genre Classification from Videos 389
S. Karthick, S. Abirami, S. Murugappan, M. Sivarathinabala and R. Baskaran

Computer-aided Diagnosis of Breast Cancer by Hybrid Fusion of Ultrasound and Mammogram Features 403
R. Lavanya, N. Nagarajan and M. Nirmala Devi

A Machine Learning Approach to Cluster the Users of Stack Overflow Forum 411
J. Anusha, V. Smrithi Rekha and P. Bagavathi Sivakumar

Data Storage Optimization in Cloud Environment 419
M. Deivamani, Rashmi Vikraman, S. Abirami and R. Baskaran

Study on Fingerprint Images Using Delaunay Patterns to Identify Hereditary Relations Among Family Members of Three Generations 431
C. Karthikeyini and V. Rajamani

Evaluation of Worst-Case Execution Time of Tasks on Multi-core Processor 441
R. Suraj, P. Chitra and S. Madumidha

Back-Emf-Based Sensorless Field-Oriented Control of PMSM Using Neural-Network-Based Controller with a Start-Up Strategy 449
V.S. Nagarajan, M. Balaji and V. Kamaraj

FPGA-based Intelligent Control of AC Motors 459
Valantina Stephen and L Padma Suresh

Secretly Shared QR Code and Its Applications 473
G.S. Devisree and K. Praveen

Phish Indicator: An Indication for Phishing Sites 481
S. Aparna and Kandasamy Muniasamy

Using Signature for Hidden Communication Prevention in IP Telephony 489
Ajvad Rahman and P.P. Amritha

Classification Using Fractal Features of Well-Defined Mammographic Masses Using Power Spectral Analysis and Differential Box Counting Approaches 495
P.S. Menon Dhanalekshmi and A.C. Phadke

Efficient Silhouette-based Input Methods for Reliable Human Action Recognition from Videos 503
G. Glorindal Selvam and D. Gnanadurai

Vertical Handoff Scheme in Integrated WiMAX and WLAN Networks 513
A. Anitha and J. JayaKumari

An Analysis of Various Edge Detection Techniques on Illuminant Variant Images 521
S.H. Krishna Veni and L Padma Suresh

CBAODV: An Enhanced Reactive Routing Algorithm to Reduce Connection Breakage in VANET 533
N. Arulkumar and E. George Dharma Prakash Raj

An Enhanced Associative Ant Colony Optimization Technique-based Intrusion Detection System 541
Chetan Gupta, Amit Sinhal and Rachana Kamble

Fuzzy-Based Sign Language Interpreter 555
P. Anitha and S. Vijayakumar

Optimized Distributed Text Document Clustering Algorithm 565
J.E. Judith and J. Jayakumari

A Study on Medical Data Hiding Using Wireless Capsule Endoscopy 575
R. Suji Pramila and A. Shajin Nargunam

Video Data Mining Information Retrieval Using BIRCH Clustering Technique 583
D. Saravanan and S. Srinivasan

Handwritten Tamil Character Recognition Using Zernike Moments and Legendre Polynomial 595
Amitabh Wahi, S. Sundaramurthy and P. Poovizhi

Encrusted CRF in Intrusion Detection System 605
S. Vinila Jinny and J. Jaya Kumari

Effective Pattern Discovery and Dimensionality Reduction for Text Under Text Mining 615
T. Vijayakumar, R. Priya and C. Palanisamy

A Cross-Layer Analysis for Providing Mobility in Wireless Body Area Networks 625
R. Venkateswari, S. SubhaRani, V. Sudharshan and R. Umadharshini

Multiview Clustering in Heterogeneous Environment 633
A. Bharathi and S. Anitha

Implementation of Isolated Two Inductor Boost Converter for Induction Motor Drive Applications 643
S. Lavanya and T. Annamalai

A Generic Bio-inspired Framework for Detecting Humans Based on Saliency Detection 655
R. Aarthi, J. Amudha and Usha Priya

Efficient Approach to Detect and Localize Text in Natural Scene Images 665
S.R. Surem Samuel and C. Seldev Christopher

Enhanced Certificate-Based Authentication for Distributed Environment 675
A. Jesudoss and N.P. Subramaniam

Diagnosis and Segmentation of Brain Tumor from MR Image 687
S.V. Srinivasan, K. Narasimhan, R. Balasubramaniyam and S. Rishi Bharadwaj

Improving the Accuracy of Latent Fingerprint Matching Using Texture Descriptors 695
V. Dhanusha and T.R. Swapna

Control Strategy for PQ Improvement in an Autonomous Microgrid Using Bacterial Foraging Optimization Algorithm 705
N. Chitra, A. Senthil Kumar, P. Priyadharshini and K.M. Shobana

Maximum Intensity Block Code for Action Recognition in Video Using Tree-based Classifiers 715
J. Arunnehru and M. Kalaiselvi Geetha

An Efficient Coding Method for Indexing Hand-based Biometric Databases 723
Ilaiah Kavati, Munaga V.N.K. Prasad and Chakravarthy Bhagvati

Optic Disk and Optic Cup Segmentation for Glaucoma Screening 733
G. Veerasenthilkumar, S. Vasuki and R. Rajkumar

Deadline-based Priority Management in Cloud 745
E. Iniya Nehru, Saswati Mukherjee and Abhishek Kumar

Countering Flood Attacks and Routing Misbehavior in DTN 753
J. Karunya Priyadarshini, P. Jesu Jayarin and J. Visumathi

Static ATC Estimation Using Fully Complex-Valued Radial Basis Function Neural Network 763
M. Karuppasamypandiyan, R. Narmatha Banu and P.M. Manobalaa

Big Data and Cloud: A Survey 773
K.S. Sangeetha and P. Prakash

An E-mail Application on Named Data Networking 779
Sandhya Giri, Anupama Josyula and V. Vetriselvi

Hierarchical Character Grouping and Recognition of Character Using Character Intensity Code 789
V.C. Bharathi and M. Kalaiselvi Geetha

Multi-view Face Expression Recognition—A Hybrid Method 799
Prakash Natarajan and Vijayalakshmi Muthuswamy

A Scheme to Create Secured Random Password Using Markov Chain 809
S. Vaithyasubramanian and A. Christy

Analysis of Shortest Route for Heterogeneous Node in Wireless Sensor Network 815
L. Lakshmanan and T.C. Tomar

Design of a Triple Band Slit-loaded Patch Antenna with DGS for Bandwidth Enhancement 823
Pristin K. Mathew and Sneha Mohan

Segmentation of Nuclei from Breast Histopathology Images Using PSO-based Otsu's Multilevel Thresholding 835
J. Angel Arul Jothi and V. Mary Anita Rajam

Wavelet Transform-Based Land Cover Classification of Satellite Images 845
D. Menaka, L Padma Suresh and S. Selvin Premkumar

Tamil Speech Recognizer Using Hidden Markov Model for Question Answering System of Railways 855
G. Vignesh and S. Sankar Ganesh

Constrained Optimal Bidding Strategy in Deregulated Electricity Market 863
D. Palit and N. Chakraborty

About the Editors

Dr. L Padma Suresh obtained his doctorate from MS University and Dr. M.G.R. University, respectively. He is presently working as a Professor and Head in Department of Electrical and Electronics Engineering, Noorul Islam University, Kumaracoil, India. Dr. Suresh is well known for his contributions to the field in both research and education contributing over 50 research articles in journals and conferences. He is the editorial member of International Journal of Advanced Electrical and Computer Engineering and also served as reviewer for various reputed journals. He has been a life member of the Indian Society for Technical Education. He also served in many committees as Convener, Chair, and Advisory member for various external agencies. His research is currently focused on Artificial Intelligence, Power Electronics, Evolutionary Algorithms, Image Processing, and Control Systems.

Dr. Subhransu Sekhar Dash is presently working as a Professor in the Department of Electrical and Electronics Engineering, SRM Engineering College, SRM University, Chennai, India. He received his Ph.D. degree from College of Engineering, Guindy, Anna University. He has more than 17 years of research and teaching experience. His research areas are Power Electronics and Drives, Modeling of FACTS Controller, Power Quality, Power System Stability, and Smart Grid. He is a Visiting Professor at Francois Rabelais University, POLYTECH, France. He is the chief editor of International Journal of Advanced Electrical and Computer Engineering.

Dr. Bijaya Ketan Panigrahi is an Associate Professor in Electrical and Electronics Engineering Department in Indian Institute of Technology Delhi, India. He received his Ph.D. degree from Sambalpur University. He is serving as a chief editor to the International Journal of Power and Energy Conversion. His interests include Power Quality, FACTS Devices, Power System Protection, and AI Application to Power System.

Web Information Extraction on Multiple Ontologies Based on Concept Relationships upon Training the User Profiles

S. Vigneshwari and M. Aramudhan

Abstract There is a need of personalized Web information extraction. Mining vast information across the Web is not an easy task. We need to undergo various reduction techniques to remove unwanted data and to grab the useful information from the Web resources. Ontology is the best way for representing the useful information. In this paper, we have planned to develop a model based on multiple ontologies. From the constructed ontologies based on the mutual information among the concepts the taxonomy is constructed, then the relationship among the concepts is calculated. Thereby, the useful information is extracted. An algorithm is proposed for the same. The results show that the computation time for data extraction is reduced as the size of the database increases. This shows a healthy improvement for quick access of useful data from a huge information resource like the Internet.

Keywords Information extraction · Ontologies · User profiles · Concept similarity · Ontological relationship · Training the ontology

1 Introduction

Current Web information gathering systems attempt to satisfy user requirements by capturing their information needs. To simulate user concept models, ontologies (knowledge description and formalization models) are utilized in personalized

S. Vigneshwari (✉)
Department of Computer Science and Engineering, Sathyabama University, Chennai, India
e-mail: jayam3@rediffmail.com

M. Aramudhan
Perunthalaivar Kamarajar Institute of Engineering and Technology, Karaikal
Tamil Nadu, India
e-mail: aramudhan1973@yahoo.com

© Springer India 2015

L.P. Suresh et al. (eds.), *Artificial Intelligence and Evolutionary Algorithms in Engineering Systems*, Advances in Intelligent Systems and Computing 325,
DOI 10.1007/978-81-322-2135-7_1

Web information gathering. Such ontologies are called ontological user profiles or personalized ontologies [1]. Ontology is an explicit, formal specification of a shared conceptualization of a domain of interest, where formal implies that the ontology should be machine-readable and shared that it is accepted by a group or community. The process of ontology merging takes as input two (or more) source ontologies and returns a merged ontology based on the given source ontologies. Manual ontology merging using conventional editing tools without support is difficult, labor intensive, and error prone. Therefore, several systems and frameworks for supporting the knowledge engineer in the ontology merging task have recently been proposed [2]. In this work, we have planned to extend the existing work with effective ontologies and ontology mining algorithm.

2 Review of Related Works

Tao et al. [3] proposed a model for knowledge description and formalization. Ontologies are widely used to represent user profiles in personalized Web information gathering. And, their proposal is based on two ontologies, which are the local ontology, constructed from the Local Instance Repository and the global ontology constructed from the World Knowledge base, which is nothing but the knowledge from the web.

Clearwater [4] suggested a set of ontologies from which public scientific data can be shared in the semantic Web. Jayasri and Manimegalai [5] proposed an efficient cross-ontology-based similarity measure for retrieving biological documents. Here, the authors utilized WordNet ontology and MESH (a medical ontology), for extracting medical terms.

Rodriguez and Egenhofer [6] identified various semantic similarity measures that exist on the entity classes, from a variety of ontologies. Stemme and Maedche [2] identified the importance of merging federated ontologies which are specific to autonomous Web-based systems.

Bagheri Hariri et al. [7] proposed a new methodology for creating compound metrics based on neural networks. This supervised learning approach is specifically used for aligning multiple ontologies.

3 Proposed Web Information Extraction Method

The proposed approach concentrates on the Web-information-extraction-based user profile, i.e., based on the user's needs, regarding a particular knowledge. A rich relation mining algorithm is used for the above-said process. Let us discuss the proposed method in detail.

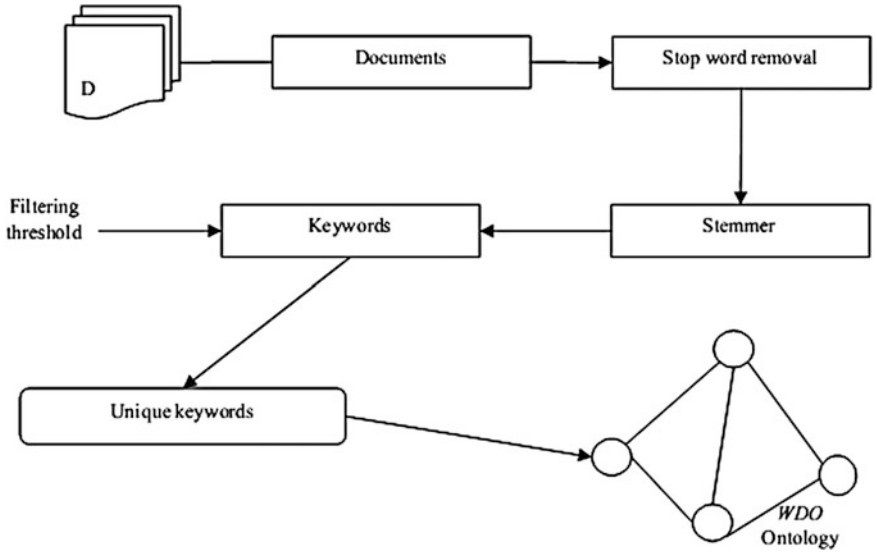

Fig. 1 Web ontology construction

3.1 Web-based Ontology

The Web ontology is considered to be the main ontology for the proposed Web information gathering model. The particular ontology is constructed from the data extracted from different Web sites

$$D = [d_1, d_2, \ldots, d_n] \tag{1}$$

where $d_1, d_2, \ldots, d_n$, are the different concept extracted from the whole extracted Web documents. Each and every Web document contains the key words concerning them. The key words are then filtered by avoiding duplication and redundancy. Now different relations are selected for embedding with the concepts.

Figure 1 represents the block diagram for the construction of Web ontology. So according to the above procedure, Web ontology for the topic "database" is constructed.

3.2 User Profiling Ontology

The user profiling-based ontology is the second major ontology for the proposed Web information-gathering model. In this ontology, the user-given tags for the Web retrieval are extracted, and the ontology is constructed based on the tags.

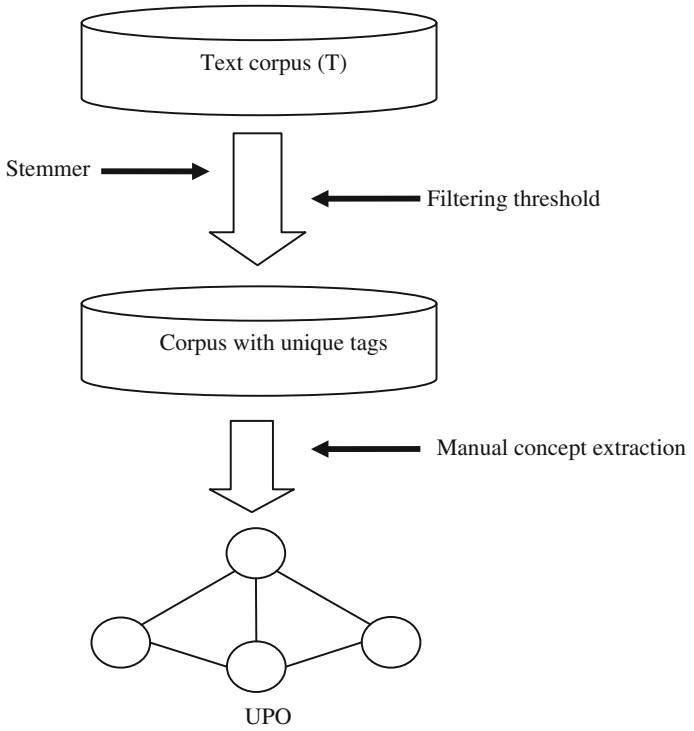

Fig. 2 Construction of UPO

$$T = [d_1^t, d_2^t, \ldots, d_n^t] \tag{2}$$

In Eq. (2), $d_1^t, d_2^t, \ldots . d_n^t$ are the set of tags contained in each of the Web documents. These tags are processed with their frequency. The most frequent tags are selected in the next step. And then, redundant and duplicates are omitted from the text corpus T. Figure 2 shows the detailed steps for constructing the user profiling ontology.

Consider the following example on Fig. 3, which is based on the topic database. Here, T represents the topic and R represents the relation.

$$T = [data, database, administrator, developer]$$
$$R = [is_a, has, part_of, union_of]$$

Fig. 3 A sample of UPO

3.3 Cross-Ontology Mining Algorithm for Web Information Extraction

The proposed mining algorithm possess three steps:

- Similarity calculation
- Relation count
- Information extraction
- Training the UPO

Similarity calculation The similarity calculation is the initial step of the proposed method, which is characterized by calculating the similarity between the concepts of different ontologies. In the following equations, c_i, c_j refers to concepts and $P()$ represents the probability function.

$$\text{Mutual similarity} = \log \frac{P(c_i) + P(c_j)}{P(c_i), P(c_j)} \tag{3}$$

$$p(C_i) = \frac{w_c}{w} \tag{4}$$

$P(c_i, c_j)$ is the joint probability for both of the keywords to be present in the text window, and the $P(c_i)$ is the probability that a keyword k_i to be appeared in the text window. A text window indicates the text frame, considered in the Web document for finding the presence and relevance of the keywords.

Relation Count The relation count is the second major step in the mining process. The relation count process starts by selecting the concepts with top similarity values. A particular concept from the UPO extracts n concepts from the Web ontology and from the set of concepts extracted, those with top similarity are selected.

$$R = \text{priority}(\text{is_a:1},\ \text{part_of:2}, \text{has_a:3}, \text{union_of:4}] \tag{5}$$

Information Extraction The final step in the proposed mining method is the information extraction based on the top-ranked concepts. In this step, we associate the concepts from UPO with the concepts from Web ontology.

$$C_{\text{UPO}} = [c^1_{(wo)}, c^2_{(wo)}, \ldots c^n_{(wo,)}] \tag{6}$$

Training the UPO Train the UPO by validating the root-mean-square (RMS) deviation of the query with that of the document searched.

$$E = \frac{\sqrt{wq_i^2 + wd_i^2}}{\text{mean weight}} \tag{7}$$

Here, wq_i is the query weight and wd_i is the document weight. The weight is based on the mutual similarity rank and the relationship rank.

$$\text{WX} = \text{MSM} + \frac{\text{Threshold}}{\text{priority value}} \tag{8}$$

WX stands for weight of a query or a document. Apriori algorithm [8] is applied for training the documents based on RMS.

Algorithm information mining

Input: web ontology, User profiling ontology
Output: extracted information

Step1. Select web ontology
Step2. Select user profiling ontology
Step3. Subject concept similarity method
Step4. Apply mutual _similarity measure
Step5. Apply threshold t_r
Step6. Select the concepts, where
$mutual_similarity_measure > t_r$
Step8. Apply relation count
Step9. Select top ranked concepts
Step10. Extract web information
Step 11. Train the UPO and repeat step 2 until all the concepts are matched with the input query
Step12. End

4 Experimental Setup and Dataset Description

The experimentation is conducted on system with core i5 processor with RAM of 4 GB and hard disk space of 250 GB. All the programs were written in java with JDK 1.7.0. The dataset used for the experimentation is the data extracted from the Web documents, which are downloaded from the Internet by giving the search parameter as database. The two ontologies are constructed semi-automatically by referring a set 50 Web documents.

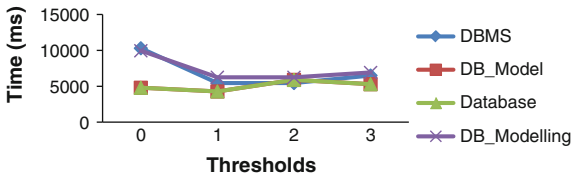

Fig. 4 Computation time

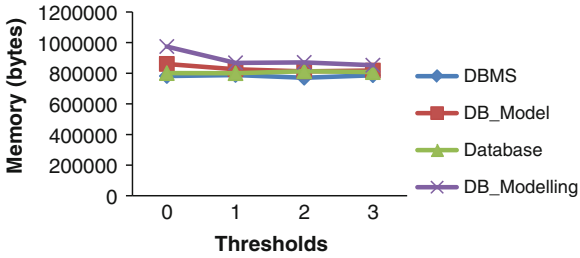

Fig. 5 Memory usage

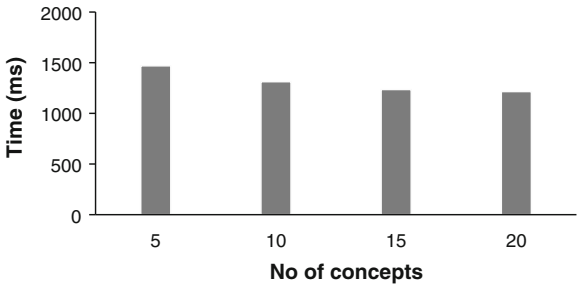

Fig. 6 Computation time

4.1 Performance Analysis

The evaluation of the results is plotted in the graphs according to the responses of the dataset to the proposed algorithm. The evaluation results are plotted in the following section, based on different criteria such as time and memory utilized.

Figures 4 and 5 represent time for execution and the memory usage required for extracting the information by the proposed approach. The varying parameters used for the analysis are manually set as threshold values. The analysis from the figures shows that the time for execution has much variation when compared to the memory usage, as the threshold varies. The time for execution varies as the threshold value increases but in irregular manner. But for the memory usage, it shows a balanced behavior.

In the Fig. 6, we plot the execution time for the proposed approach to extract information from different number concepts. The ontology with different number of concepts is given for particular evaluation. The response of the proposed algorithm

is remarkable for the particular evaluation. As the number of concepts increases, the time for execution comes to an optimum level, as the number of concepts increases. The highest time marked by the proposed approach is 1,469 ms, and the optimum time noted is 1,215 ms.

5 Conclusion

In this paper, we have presented an efficient approach for effective information extraction from Web-based ontologies. We have used two different ontologies based on a single topic in our proposed method. The two different ontologies used are Web ontology and the user profiling-based ontology. The aim of the proposed method is to extract information from the Web documents, based the on two different ontologies. An improved cross-ontology mining method is used for the above-mentioned Web information extraction. Then, ontology-based mining procedure will be devised in future, with the consideration of all the properties and relation included in it. The effectiveness of information mined from those ontologies will be analyzed. The experimental evaluation has shown that the highest time marked by the mining method is 1,469 ms and the optimum time noted is 1,215 ms. Accordingly, we have planned to include the more relations such as "is_a", "has_a", "union_of", "disjoint_of" "part_of" "syn_set" in the ontology, so that the generated ontology will be more effective.

References

1. C.A. Wu, W.-Y. Lin, C.C. Wu, An active multidimensional association mining framework with user preference ontology. Int. J. Fuzzy Syst. **12**(2), 125–135 (2010)
2. G. Stumme, A. Maedche, Ontology merging for federated ontologies on the semantic web, in *Institute for Applied Computer Science and Formal Description Methods (AIFB)*, vol. 3(12) (2005) pp. 1–9
3. X. Tao, Y. Li, N. Zhong, A personalized ontology model for web information gathering. IEEE Trans. Knowl. Data Eng. **23**(4), 496–511 (2011)
4. A. Clearwater, The new ontologies: the effect of copyright protection on public scientific data sharing using semantic web ontologies. **10**, 182–205 (2010)
5. D. Jayasri, D. Manimegalai, An efficient cross ontology based similarity measure for bio-document retrieval system. J. Theor. Appl. Inf. Technol. **54**(2), 245–254 (2013)
6. M.A. Rodriguez, M.J. Egenhofer, Determining semantic similarity among entity classes from different ontologies. IEEE Trans. Knowl. Data Eng. **15**, 442–456 (2000)
7. B. Bagheri Hariri, H. Sayyadi, H. Abolhassani, A neural-networks-based approach for ontology alignment, in *Joint 3rd International Conference on Soft Computing and Intelligent Systems and 7th International Symposium on Advanced Intelligent Systems* (2006)
8. L.M. de Campos, J.M. Fernandez, J.F. Huete, Query expansion in information retrieval systems using a Bayesian network-based thesaurus, in *Proceedings of the Fourteenth Conference on Uncertainty in Artificial Intelligence* (1998)

A Study on Competent Crawling Algorithm (CCA) for Web Search to Enhance Efficiency of Information Retrieval

S. Saranya, B.S.E. Zoraida and P. Victor Paul

Abstract Today's Web is very huge and evolving continually in dynamic nature. Search engines are the interface to retrieve information from huge repository of the World Wide Web. Due to the difficulty in accessing the information from massive storage of Web, search engines depend on the crawlers for locating and retrieving relevant Web pages. A Web crawler is a software system, which systematically finds and retrieves Web pages from the Web documents. Crawlers use many Web search algorithms for retrieving Web pages. This paper proposes a competent Web search crawling algorithm, which is derived from page rank and BFS Web search algorithm to enhance the efficiency of the relevant information search. In this paper, an attempt has been made to study and examine the work nature of crawlers and crawling algorithms in search engines for efficient information retrieval.

Keywords Web search crawling algorithm · BFS Web search algorithm · Web crawler · URL address · CCA

1 Introduction

Search engines are the software tools widely used by people to retrieve information from Internet [1]. Web crawling algorithm is the process by which a search engine gathers pages from the Web crawler to index them and support a search engine.

S. Saranya (✉) · B.S.E. Zoraida
Department of Computer Science and Engineering, Bharathidasan University, Trichy 620023, India
e-mail: saran.aamec@gmail.com

B.S.E. Zoraida
e-mail: chayav88@gmail.com

P. Victor Paul
Teknuance Info Solutions, Chennai 600099, India
e-mail: victorpaul.ind@gamil.com

© Springer India 2015

L.P. Suresh et al. (eds.), *Artificial Intelligence and Evolutionary Algorithms in Engineering Systems*, Advances in Intelligent Systems and Computing 325,
DOI 10.1007/978-81-322-2135-7_2

The search engines use Web crawlers to provide up-to-date data. The crawler is an important component of a Web search engine [2]. The quality of a Web crawler may directly affect the information searching quality. A Web crawler [3] algorithm is used to traverse a web page by extracting inlinks and outlinks. Extracted links are seeded in URL list for future use. The Web documents are linked by multiple hypertext links which connect diverse resources. Web crawler implements various Web search algorithms for retrieving and locating Web documents, such as page rank algorithm, best first, breadth first, shark search, and hypertext-induced topic selection (HITS). The implementation of different Web search crawling algorithms provides different search efficiencies. By analyzing various Web search algorithms, this paper proposes a competent crawling algorithm (CCA), which is derived from best crawling algorithms.

2 Crawler

A Web crawler [3, 4] is a relatively simple automated program or script that methodically scans or "crawls" through Internet pages to retrieve information from Web data. Alternative names for a Web crawler include Web spider, Web robot, bot, crawler, and automatic indexer. The documents in Web contain graph structure, i.e., connected through hyperlinks (Fig. 1).

Crawl manager starts [2] crawling from a given set of URLs, progressively fetches and scans them for new URLs (*out-links*), and then fetches these pages in turn, in an endless cycle. The newly founded URLs are taken for next cycle process to extract *in-links* and *out-links* of the respective Web pages. The traversed or visited pages are stored in buffer for future use, and the *out-links* of Web pages are stored to visit list in frontier. These URLs are classified using ontology editing tools

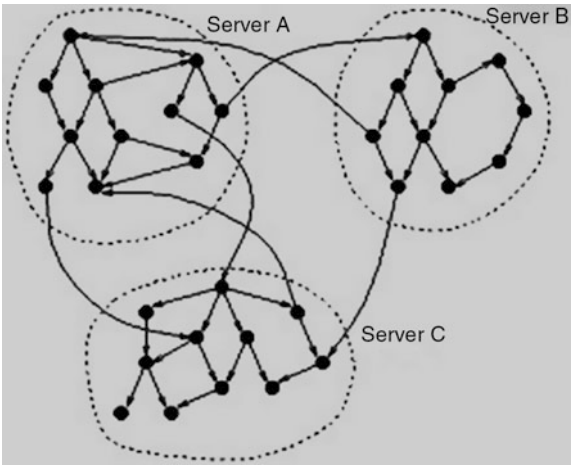

Fig. 1 Hyperlinked graph structure of Web documents

and indexed by indexer mechanism to enhance the Web search efficiency. The Web page (HTML/XML) contents are parsed using parser mechanisms, and the interpreted data are used for constructing inverted matrix system. The inverted matrix index contains the number of occurrences of words and location of the text in particular document. The indexer constructs keyword/search key from the inverted index using ontology classification to enhance the information retrieval.

2.1 Web Crawler Architecture

The architectural design of crawler (Fig. 2) describes the sequential flow of URL extraction and parsing of Web documents for efficient information retrieval. The in-links and out-links present in traversed Web pages are extracted and listed in frontier to visit.

To avoid duplication in URL extraction, the URL manager implements exclusion function, so that already extracted URLs will automatically get deleted from the frontier list. The extracted URLs are stored in hash table based on URL ranking

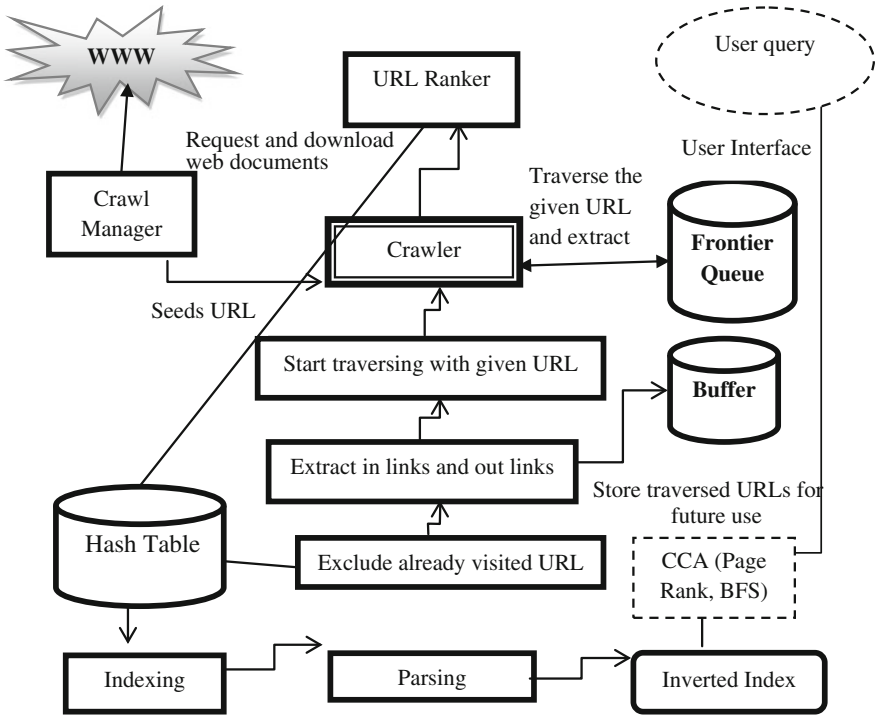

Fig. 2 Architecture of Web crawler

without any duplication. The indexer generates index from hash table. The parser interprets the data from Web pages and classifies the data based on ontology mechanisms to construct inverted index. The page ranker prioritizes the URLs and displays the result to user interface based on the user queries.

2.2 Work Flow of Crawlers

In this section, the work flow of crawlers illustrated using a Win Web Crawler tool [5].

Step 1: The crawler gets URL as an input (Fig. 3).

In step 1, URL www.csbdu.in is given as input to the Win Web Crawler. From the input, URL crawler starts the process by extracting the in-links and out-links.

Step 2: Retrieve and download the Web page. In step 2, the URLs associated with www.csbdu.in are extracted and processed by Win Web Crawler (Fig. 4).

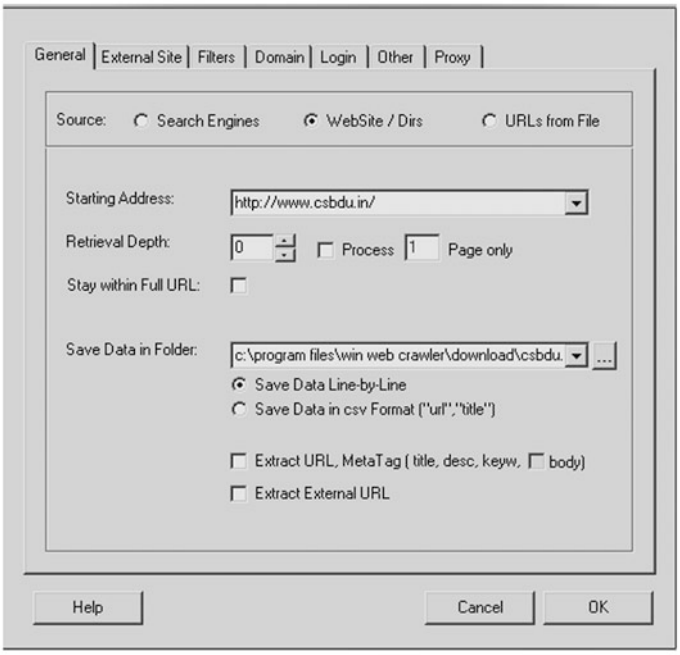

Fig. 3 Cycle 1—input

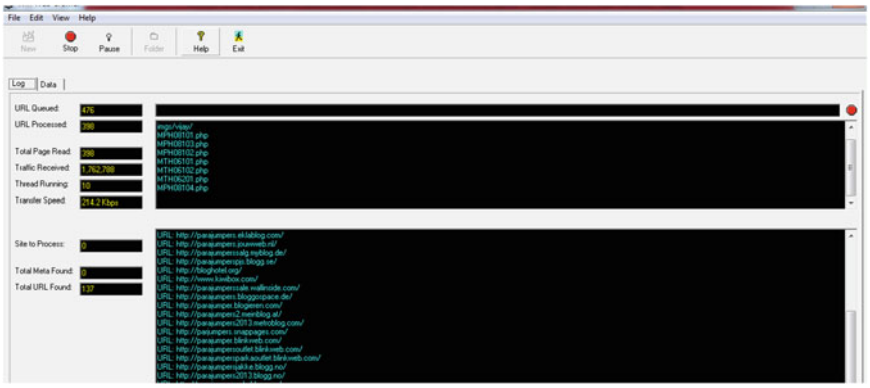

Fig. 4 Extract URLs

The process provides the count of processed URLs, queued URLs, total page read, traffic received, and total URLs found in the particular URL.

Step 3: Parse and extract the in-links and out-links from the retrieved Web pages to traverse (Fig. 5).

After the completion of step 3, the crawler produced the count 1,758 of total URLs found in www.csbdu.in. The extracted 1,758 URLs are stored in frontier to visit it. The crawler will traverse 1,758 URLs to extract and download the in-links and out-links of these URLs. The cycles will get repeated, until it reaches the first URL.

Step 4: The process is repeated, until it reaches the starting node.

Fig. 5 Completion of first cycle

2.3 Crawling Algorithm's Performance Comparisons

Generally, five different crawling algorithms are used for Web search. They are breadth first, best first, fish search, shark search, and page rank. In this section, the efficiency of different crawling algorithms is examined to find out the best one. The efficiency of the crawling algorithms is measured by the following important factors: precision, recall and F-score values [6].

$$\text{Precision}(P) = \text{No. of Relevant Pages Retrieved}/\text{Total Number of Retrieved Pages}$$
$$\text{Recall}(R) = \text{No. of Relevant Pages Retrieved}/\text{Total number of Relevant Pages}$$
$$\text{F-Score} = 2(P * R)/(P + R)$$

By considering the above factors, the efficiency of crawling algorithms is analyzed and stated below. The widely used popular crawling Web search algorithm is page rank algorithm. It was proposed by Tripathy and Patra [2] as a possible algorithm for monitoring and analyzing the user behaviors. The page rank algorithm works on the basis of number of in-links and out-links to a Web page. Initially, the page rank is set to 1 for all [7]. A page's score is calculated recursively upon the scores of the pages that point to it, called *in-links*. A Web page will get more score and priority, if it has more number of in-links. Best-first crawlers have been studied by Cho et al. [2] and Hersovici et al. [2]. The phenomenon of the best-first search is based on the factors such as precision, recall, accuracy, and F-score. The URL is selected for crawling, using the frontier as a priority queue based on maximum visit or by its popularity. In this algorithm, the URL selection process is guided by the lexical similarity between the topic's keywords and the source page of the URL [8] (Fig. 6).

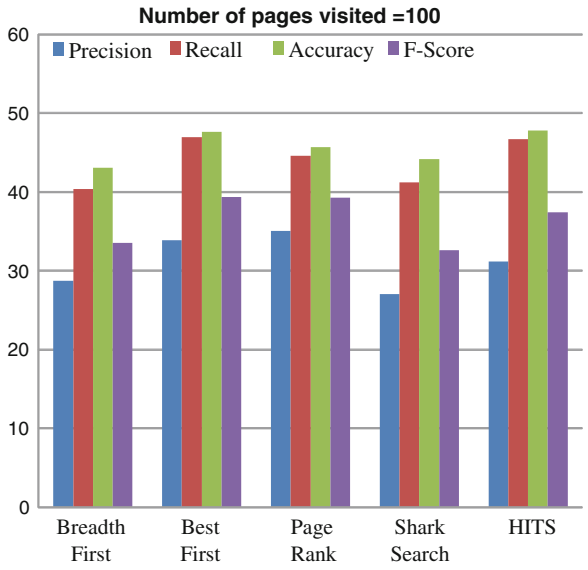

Fig. 6 Graphical view of crawling algorithms: performance measures

Table 1 Performance measures

Algorithms	Precision	Recall	Accuracy	F-score
Breadth first	28.8	40.4	43.12	33.61
Best first	33.93	47	47.7	39.41
Page rank	35.09	44.63	45.78	39.29
Shark search	27.05	41.23	44.25	32.66
HITS	31.23	46.77	47.85	37.45

Breadth-first algorithm [7] is the simplest and easy technique to traverse in the order of first in first out. BFS algorithm uses the frontier URL list of traversing the Web pages. Frontier is used as FIFO queue and crawls the links in the order in which they are encountered. The HITS algorithm works on the basis of relevant topic search. The algorithm classifies Web pages into two types in order to calculate page scores. If a page provides trustworthy information for a given topic, then it is classified as authority pages. The Web pages that give links to authority pages are called hub. Weights are assigned to every hub, and authority pages and page score will be calculated accordingly.

The experimental dataset for comparing these Web search algorithms is taken from [7]. Experiments are conducted using the Lund dataset containing 100 attributes. The precision, recall, accuracy, and F-score factor are examined using breadth-first, best-first, fish search, shark search, and page rank algorithms. The results and finding of the experiment are shown in Table 1.

Based on the dataset experiments [2, 7] with the following performance measures such as precision, recall, accuracy, and F-score, which are taken into account for their assessment, it is observed that page rank algorithm outperforms other algorithms by various performance measures.

2.3.1 Competent Crawling Algorithm

To enhance the performance of the crawler, in this paper, competent crawling algorithm (CCA) is proposed from the existing Web search crawling algorithms, to increase the efficiency of information retrieved. From the conclusion of the last section, page rank algorithm performs better than other algorithms. The proposed algorithm CCA combines the functionality of both page rank and BFS algorithms to enhance the efficiency of Web search. Compared to existing crawling algorithms, CCA has several advantages to increase the time efficiency by dequeuing the visited URLs from buffer before the crawler encounters it. The major advantages of the CCA are scalability and robustness. In CCA, dynamic hash tables are used for scalability and the system is reliable to crawler crashes. The complexity of the searching problem will overcome by CCA.

Pseudo code **:**

```
CCA (Starting Url){ For ( P=0; p <=Starting Url; p++){ Enqueue (Frontier, url,max_trip_sc) RetrivedUrl=Dequeue (Fortier);Do{RetrivedPage=Fetch(RetrivedUrl);If ( multiples(trip)){ Max_trip_sc;}     Trip+=1;
          }While(visited<maxPages);ENQUEUE(BufferedPages ,max_trip_sc,Frontier) If(max_trip_sc>VisitedPages){
          DEQUEUE (max_trip_sc);
}If(Frontier>max_buffer){     DEQUEUE (Frontier);}Merge(Frontier,max_trip,BufferedPages);}
```

3 Conclusion

In this paper, the best features of page rank algorithm and best-first algorithm are combined together to provide the best output. The functions of Web crawler components are described using the architectural design. Win Web Crawler tool clearly examines the working process of a crawler using an example. The comparative study on various crawling algorithms gives clear idea for better information retrieval. An attempt has been made to implement CCA, which provides the efficiency, scalability, and robustness. The newly proposed algorithm is time-efficient by dequeuing the repeated pages. Implementation of CCA in C# has taken as future work of this paper.

References

1. K.S. Shetty, S. Bhat, S. Singh, Symbolic verification of web crawler functionality and its properties, in *International Conference on Computer Communication and Informatics* (*ICCCI*, 2012)
2. A. Tripathy, P.K. Patra, A web mining architectural model of distributed crawler for internet searches using PageRank algorithm, in *IEEE Asia-Pacific Services Computing Conference* (2008)
3. A. Guerriero, F. Ragni, C. Martines, A dynamic URL assignment method for parallel web crawler. IEEE
4. A. Vadivel, S.G. Shaila, R.D. Mahalakshmi, J. Karthika, Component based effective web crawler and indexer using web services, in *IEEE-International Conference on Advances in Engineering, Science and Management* (*ICAESM*, 2012)
5. R.R. Trujillo, Simulation tool to study focused web crawling strategies (2006)
6. Accuracy, Precision, Recall and F-Score. Wikipedia, the free encyclopedia
7. S. Jaiganesh, P. Babu, K. Nimmati Satheesh, Comparative study of various web search algorithms for the improvement of web crawler. Int. J. Eng. Res. Technol. (IJERT) **2**(4) (2013)
8. Y. Yang, Y. Du, Y. Hai, Z. Gao, A topic-specific web crawler with web page hierarchy based on HTML Dom-Tree, in *Asia-Pacific Conference on Information Processing* (2009)

High Payload Reversible Watermarking for Securing Medical Images in a Cloud Environment

R. Sukanesh and N. Karthikeyan

Abstract This paper proposes a high payload reversible data hiding technique in integer lifting transform domain, with a special application to medical images stored in a cloud-based medical enterprise archive. Owing to the nature of these image statistics, the neighbor pixel values are similar mostly, and hence, their differences are observed to be close or equal to zero. A histogram constructed out of this difference factor is exploited for reversible data embedding. Further, data are embedded at multiple levels, and hence, the proposed scheme facilitates higher payload capacity than the conventional single-level histogram-based techniques. The distortion introduced due to secret payload embedding is alleviated to the minimum, and hence, the perceptual quality of the stego images is exceptional, since the embedding is done in the integer lifting wavelet transform domain. The experimental results with medical images demonstrate that the proposed scheme provides a better security with larger payload and a better image quality than some advanced prior schemes.

Keywords Difference-expansion-based schemes · Histogram-shifting-based schemes · Prediction-based schemes · Interpolation-based schemes · Robustness-based schemes · HVS-based schemes

1 Introduction

The healthcare industry demands the organizations to store, analyze, and reference historical medical imaging data for a long period of time. Most of the healthcare disciplines such as endoscopy and pathology preserve their complete personal clin-

R. Sukanesh (✉)
Department of ECE, Thiagarajar College of Engineering, Madurai, India
e-mail: drsukanesh@gmail.com

N. Karthikeyan
Department of CSE, Syed Ammal Engineering College, Ramanathapuram, India
e-mail: nkarthikkeyan@syedengg.ac.in

© Springer India 2015

L.P. Suresh et al. (eds.), *Artificial Intelligence and Evolutionary Algorithms in Engineering Systems*, Advances in Intelligent Systems and Computing 325,
DOI 10.1007/978-81-322-2135-7_3

ical systems in some local data repositories which comprises of a storage area network, direct-attached storage, or network-attached storage. Despite of the recent flattening of growth in medical imaging procedure volumes in the USA, the rate of growth of image data volumes keeps on accelerating. In reality, the pressing data store needs for the ever incrementing and cumulating storage and archiving of the primary and secondary image copies are resulting in a "Big Data" explosion in imaging.

While it is exciting to have convenient medical imaging archive which is completely interoperable across disciplines, there are some crucial security and privacy risks which could impede its wide adoption. The main concern is about the integrity control and the privacy preservation of the medical images while those images are stored and shared over the network, especially when they are stored on a third-party server which people may not fully trust. This situation leads to an open issue—on the one hand, in spite of the strict healthcare regulations such as HIPAA to incorporate business associates, cloud providers are not usually covered. On the other hand, due to the high value of the sensitive medical images, the third-party storage servers frequently become the targets of various malicious behaviors which may lead to exposure/alteration of the image content. To ensure integrity control and privacy protection of the medical images, it is essential to have some effective security mechanisms that operate with semi-trusted servers.

A feasible and promising approach would be to add some additional header information for indicating tamperproof and integrity control, but this is constrained by the image file format. A bad truth is that these header files are prone to alteration, and loss of information may occur during file format conversion process. For instance, digital imaging and communications in medicine (DICOM) image header information might be lost when it is converted to the Joint Photographic Experts Group (JPEG) format.

In this paper, we endeavor to investigate the secure archiving of medical images stored on semi-trusted servers and focus on addressing the complicated and challenging integrity control and privacy preservation issues. In order to protect the medical images stored on a semi-trusted server, a novel reversible data hiding scheme is proposed as the main security primitive.

2 Literature Survey

The existing reversible data hiding schemes can be categorized into six streams based on their key concerns and method adapted. They are (1) difference-expansion (DE)-based schemes; (2) histogram-shifting-based schemes; (3) prediction-based schemes; (4) interpolation-based schemes; (5) robustness-based schemes; and (6) HVS-based schemes.

The DE method is one among the earliest reversible data hiding schemes [1]. The scheme adapts the idea followed in wavelet transforms, which converts the luminance values in the spatial domain into frequency components. The secret data are embedded into the frequency coefficients, with reversible feature. In the same

manner, every two neighboring pixels are grouped together as a pair and are converted into frequency components. The secret message is hidden into the difference between the pixels in each pair that did not cause overflow/underflow problems. The authors demonstrated that the payload size and the picture quality of the stego images were superior among the existing works at that time. The scheme attained a payload of 0.5 bpp in a single pass embedding process. An improvement over this scheme was proposed in [2], where the author applied the DE logic on vectors instead of pixel pairs. They demonstrated their algorithm in color as well as grayscale images and reported a better payload capacity than [1]. Another variant of DE was proposed by Hsiao et al. in [3], where data bits are hidden in two categories: user data and side/auxiliary information. The image pixels are classified as belonging to any one of the three regions, namely smooth region, normal region and complex region. Smooth and normal regions contained secret messages. The complex regions are ignored since they are incapable of withstanding any alterations and did not hold any stego bit. A disjoint, agreed upon area in the image for holding the side/auxiliary information contained the overhead bits, i.e., location map. This was used for perfect recovery of payload as well as the host image. Tseng and Hsieh [4] came out with an algorithm for lossless data hiding which used the invariability of the sum of pixel pairs and pair-wise difference adjustment (PDA). The scheme reported commendable picture quality since the pixel pairs were subjected to smaller modifications. Another advantage of the scheme is that the overhead information size was reduced. A high-capacity data hiding scheme was proposed by Hu et al. [5] which employed compressed location map. The authors demonstrated the high capacity of their scheme over diverse image types. Yang and Tsai [6] proposed a scheme that exploited the coefficient bias for data hiding. Both spatial domain and frequency domain were employed for secret embedding. Hence, the scheme exhibited good robustness property.

The majority of the above methods [8] addressed only a few of the desired characteristics, namely lossless/reversible, imperceptible, high payload capacity, robustness, and minimal side information involved and not all. This paper proposes a reversible data hiding technique based on the multilevel histogram shifting applied on lifting integer transform domain on medical images. The method is aimed at realizing all the desired characteristics to an optimal level.

3 Proposed System

3.1 Data Embedding Algorithm

The proposed scheme introduces a preliminary layer of security by a small preprocessing step. The image pixels are scanned in the inverse "*S*" pattern (Fig. 1).

INPUT Clean/Host image *C* with M-rows and N-columns, Secret payload '*w*' in bits, Scan Pattern—stego_Key_1, Embedding Level EL—stego_Key_2

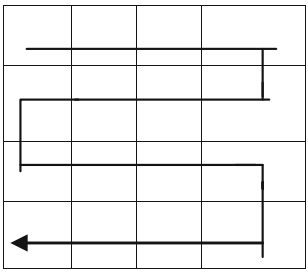

Fig. 1 Inverse "*S*" scan pattern this sample caption

OUTPUT Stego image $\hat{C}$

Procedure

Step 1 Clean image C undergoes single-level integer lifting wavelet transform which results in 4 sub-bands (*LL*, *LH*, *HL*, *HH*) of size $M/2 \times N/2$ each. *For each sub-band, do Step 2 to Step 11.*

Step 2 Scan the sub-band according to the inverse "*S*" *scan* ($1 \le i \le M/2 \times N/2$) and obtain the four-, single-dimensional pixel sequence $p_1, p_2, \ldots, p_{(M/2)\times(N/2)}$.

Step 3 Find the pixel difference over the pixel sequence obtained in Step 2 by the formula

$$\text{pixdiff}(i) = \begin{cases} p_1 & \text{if} \quad i = 1 \\ p_{i-1} - p_i & \text{if} \quad 2 \le i \le \frac{M}{2} \end{cases} \tag{1}$$

Construct a histogram for the pixdiff values.

Step 4 Select embedding level (*EL*) which is the stego_Key_2. *EL* should be less than 9 to avoid distortion. If $EL = 0$, implement the steps 5, 6, 7, and 8, else implement from Step 6, 7, and 8, skipping Step 5.

Step 5 Data embedding for $EL = 0$.

Step 5.1 Shift the right bins of $b(0)$ rightward one level as:

$$\text{pixdiff}'_i = \begin{cases} p_1 & \text{if } i = 1 \\ \text{pixdiff}_i & \text{if pixdiff}_i \le 0,\ 2 \le i \le \frac{M}{2} \times \frac{N}{2} \\ \text{pixdiff}_i + 1 & \text{if pixdiff}_i > 0,\ 2 \le i \le \frac{M}{2} \times \frac{N}{2} \end{cases} \tag{2}$$

Step 5.2 Examine $\text{pixdiff}_i = 0$ $\left(2 \le i \le \frac{M}{2} \times \frac{N}{2}\right)$ one by one. Each difference equaling 0 can be used to hide one secret bit. If the current processing secret bit $w = 0$, it is not changed. If $w = 1$, it is added by 1. The operation is as follows:

$$\text{pixdiff}_i'' = \begin{cases} p_1 & \text{if } i = 1 \\ \text{pixdiff}_i' + w & \text{if pixdiff}_i' = 0,\ 2 \le i \le \frac{M}{2} \times \frac{N}{2} \\ \text{pixdiff}_i' & \text{if pixdiff}_i' \ne 0,\ 2 \le i \le \frac{M}{2} \times \frac{N}{2} \end{cases} \tag{3}$$

Step 6 Data embedding for $EL > 0$.

Step 6.1 Shift the right bins of $b(EL)$ rightward $EL + 1$ levels and shift the left bins of $b(-EL)$ leftward EL levels as:

$$\text{pixdiff}_i' = \begin{cases} p_1 & \text{if } i = 1 \\ \text{pixdiff}_i & \text{if } -EL \le \text{pixdiff}_i \le EL,\ 2 \le i \le \frac{M}{2} \times \frac{N}{2} \\ \text{pixdiff}_i + EL + 1 & \text{if pixdiff}_i > EL,\ 2 \le i \le \frac{M}{2} \times \frac{N}{2} \\ \text{pixdiff}_i - EL & \text{if pixdiff}_i < -EL,\ 2 \le i \le \frac{M}{2} \times \frac{N}{2} \end{cases} \tag{4}$$

Step 6.2 Examine $\text{pixdiff}_i' = 0\ \left(2 \le i \le \frac{M}{2} \times \frac{N}{2}\right)$ in the range of $[-EL, EL]$ one by one. The multilevel data embedding strategy is described as follows.

Step 6.2.1 Embed the secret data as:

$$\text{pixdiff}_i'' = \begin{cases} p_1 & \text{if } i = 1 \\ \text{pixdiff}_i' & \text{if } -EL < \text{pixdiff}_i' < EL,\ 2 \le i \le \frac{M}{2} \times \frac{N}{2} \\ 2 \times EL + w & \text{if pixdiff}_i' = EL,\ 2 \le i \le \frac{M}{2} \times \frac{N}{2} \\ -2 \times EL - w + 1 & \text{if pixdiff}_i' = -EL,\ 2 \le i \le \frac{M}{2} \times \frac{N}{2} \end{cases} \tag{5}$$

Step 6.2.2 EL is decreased by 1.

Step 6.2.3 If $EL \ne 0$, execute Step 5.2.1 and Step 5.2.2 repeatedly. If $EL = 0$, execute Eq. (6) and then go to Step 6:

$$\text{pixdiff}_i'' = \begin{cases} p_1 & \text{if } i = 1 \\ \text{pixdiff}_i' + w & \text{if pixdiff}_i' = 0,\ 2 \le i \le \frac{M}{2} \times \frac{N}{2} \\ \text{pixdiff}_i' & \text{if pixdiff}_i' \ne 0,\ 2 \le i \le \frac{M}{2} \times \frac{N}{2} \end{cases} \tag{6}$$

Step 7 Generate the marked pixels sequence $p_1', p_2', \ldots p_{\frac{M}{2} \times \frac{N}{2}}'$ as:

$$p_i' = \begin{cases} p_1 & \text{if } i = 1 \\ p_{i-1} - \text{pixdiff}_i'' & \text{if } 2 \le i \le \frac{M}{2} \times \frac{N}{2} \end{cases} \tag{7}$$

Step 8 Rearrange the pixels $p'_1, p'_2, \ldots p'_{\frac{M}{2}\times\frac{N}{2}}$ in the reverse order of the scan pattern decided by stego_Key_1. Apply inverse integer lifting wavelet transform with the four sub-bands as input and construct the output image $\hat{C}$ with M-rows and N-columns (Stego version of C).

3.2 Data Extraction Algorithm

The reverse process is executed to extract the cover image and the secret payload separately.

4 Results and Discussions

The proposed algorithm has been implemented in a MATLAB environment on a Pentium IV PC. Four grayscale medical images, image sizes of 399 × 405, 424 × 508, 360 × 480, and 417 × 450, respectively, were used in the experiments. They are shown in Fig. 2a–f. Ultrasound has been recognized as the most often used imaging tool in clinical environments. The applications of X-ray imaging in orthopaedic surgery are pervasive, both pre-operatively and intra-operatively. Cepaholgrams are clinically useful image data for diagnosis and treatment in orthodontics. In the medical enterprise archives, the database comprises of a variety of medical images. To show the general applicability of the proposed method, we have shown the use of 4 commonly used types of images. To implement security, authentication information such as image digest can be embedded into the medical images. Also, the encrypted electronic patient record (EPR) data can be hidden, which might require more space in the cover image. The proposed method is found to be suitable for embedding the EPR information into the medical image.

As a preliminary test, we evaluated the proposed algorithm on these 4 images. The performance is measured in PSNR, which is given by (Table 1)

$$\text{PSNR} = 10 \times \log_{10} \frac{255^2}{\text{MSE}} (\text{dB}) \tag{8}$$

$$\text{MSE} = \frac{1}{M.N} \times \sum_{i=1}^{M} \sum_{j=1}^{N} (C(i,j) - \hat{C}(i,j))^2 \tag{9}$$

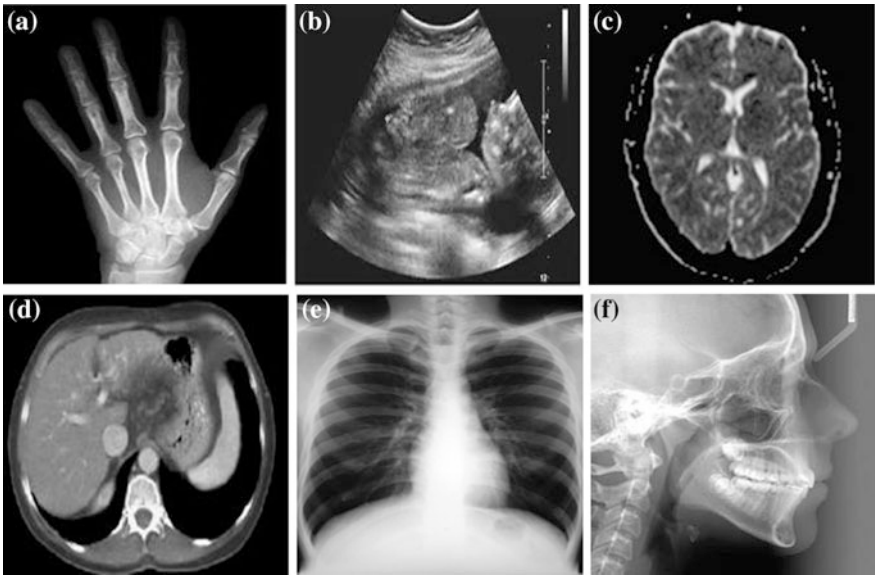

Fig. 2 Sample medical images. **a** Palm X-ray image. **b** Ultra scan fetus image. **c** Brain MRI scan image. **d** Brain CT scan image. **e** Thorax X-ray image. **f** Cephalogram dental image

Table 1 Performance comparison of the proposed system versus Ni et al. [7]

Images	Ni et al. [7]		Proposed method	
	Payload capacity	PSNR	Payload capacity	PSNR
Medical image 1	4,792	47.91	874,44	49.97
Medical image 2	19,287	49.06	137,955	48.71
Medical image 3	7,871	48.50	152,483	49.93
Medical image 4	16,591	48.23	164,787	50.39
Medical image 5	48,608	48608	70,681	70,681
Medical image 6	29,398	29398	52,442	52,442

References

1. J. Tian, Reversible data embedding using a difference expansion. IEEE Trans. Circ. Syst. Video Technol. **13**(8), 890–896 (2003)
2. A.M. Alattar, Reversible watermark using the difference expansion of a generalized integer transform. IEEE Trans. Image Process. **13**(8), 1147–1156 (2004)
3. J.Y. Hsiao, K.F. Chan, J.M. Chang, Block-based reversible data embedding. Sig. Process. **89** (4), 556–569 (2009)
4. H. Tseng, C.P. Hsieh, Prediction-based reversible data hiding. Inf. Sci. **179**(14), 2460–2469 (2009)

5. Y. Hu, H.K. Lee, J. Li, DE-based reversible data hiding with improved overflow location map. IEEE Trans. Circ. Syst. Video Technol. **19**(2), 250–260 (2009)
6. C.H. Yang, M.H. Tsai, Improving histogram-based reversible data hiding by interleaving predictions. IET Image Proc. **4**(4), 223–234 (2010)
7. Z. Ni, Y.Q. Shi, N. Ansari, W. Su, Reversible data hiding. IEEE Trans. Circ. Syst. Video Technol. **16**(3), 354–361 (2006)
8. Q. Pei, X. Wang, Y. Li, H. Li, Adaptive reversible watermarking with improved embedding capacity. J. Syst. Softw. **86**(11), 2841–2848 (2013)

Enhanced Security Framework for Data Integrity Using Third-party Auditing in the Cloud System

Balamurugan Balusamy, P. Venkatakrishna, Abinaya Vaidhyanathan, Meenakshi Ravikumar and Nirmala Devi Munisamy

Abstract Cloud computing is an evolving paradigm that has been resulted as an adoption of available technologies. Although cloud technology allows users to take more benefits from available infrastructures, and virtualization, which is an enabling technology provided by the cloud allows users to manage and use the resources in an efficient and easiest manner, it does not guarantee data integrity and security over the resources stored in the cloud. Though many security frameworks have been developed for the cloud, still there may be loss of data or loss of control over data uploaded into the cloud. And also, many solutions for data integrity by third-party auditor are available but they are semi-trustable, if third-party auditors (TPA) compromise unauthorized access over the resource in the cloud. Hence, our proposed scheme focuses on extended framework that guarantees data integrity by involving data owner to perform auditing on the outsourced data in the cloud. And so, our proposed scheme achieves data integrity and guarantees security to the data owners for their resource in the cloud to major extent. Therefore, this type of TPA approach creates awareness to the data owner of their resource and thereby guarantees data integrity for every resources stored in the cloud.

Keywords Cloud service provider · Data integrity · Third-party auditor

B. Balusamy (✉) · P. Venkatakrishna · A. Vaidhyanathan · M. Ravikumar
N. Devi Munisamy
VIT University, Vellore, India
e-mail: balamuruganb@vit.ac.in

P. Venkatakrishna
e-mail: pvenkakrishna@vit.ac.in

A. Vaidhyanathan
e-mail: abinaya.v2010@vit.ac.in

M. Ravikumar
e-mail: meenakshi.r2010@vit.ac.in

N. Devi Munisamy
e-mail: nirmaladevi.m2010@vit.ac.in

© Springer India 2015

L.P. Suresh et al. (eds.), *Artificial Intelligence and Evolutionary Algorithms in Engineering Systems*, Advances in Intelligent Systems and Computing 325,
DOI 10.1007/978-81-322-2135-7_4

1 Introduction

Cloud computing is a technology that is growing tremendously in our competitive world. Cloud computing generally provides easy way in tracking the data's of users whenever and wherever possible. Mostly people think the security of the cloud is not as secure as possible because of this reason [1]. Therefore, auditing of the data's stored in the cloud is done by the third-party auditors (TPA) [2] who are assigned confidentially by the cloud service providers (CSPs). Many insecure actions or incidents make cloud users to think more in auditing the cloud data storage [3]. The TPA may turn out to be a malicious user and can hack the cloud data or some critical applications stored in the cloud at the time of auditing.

The TPA are the persons who are extravagant in all process and have the skill of auditing process. These people generally checks out each and every process the user does and maintains a log that represents date, time and name of the files, the user accessed, and mode of the file that has been provided to the users. The TPA make many levels of auditing that ensures the current progress of the users of the cloud and the data owner of the files are in correct stage. Not only other malicious users but also the TPA [4] who are actually tied up with the CSP may also be induced by some malicious thoughts that make them to do unwanted auditing process and produce always good results. These reasons are made as the stepping stone for introducing the verification technique of the auditing process done by TPA. The verification technique is implemented by notifying the data owners about the file access information and makes sure the correctness of the auditing log. Hence, the need for the involvement of the data owners is inevitable (Table 1).

If the user does not opens his/her account frequently, then the files uploaded by them may be insecure. The auditing process [5] will be carried out generally, and the notifications are sent. In case if the notification is not appropriate to the user's expectation, then he/she does not accept the auditing process done by the TPA and verifies the auditing process. He/she may verify the whole process or the part of the process that needs verification. User can ask them to redo the auditing process (rare occasions). If the data owner needs to know the progress or present status of his account suddenly when they are in need, then he/she can request for an audit. The network problem is another issue that makes the user feel uncomfortable and insecure in using the cloud.

Table 1 Verification technique

Period of time (time interval)	T
Files	F
Medium of data storage	M
Log	L

2 Related Works

In Marshal [6], "Secure Audit Service By Using TPA for Data Integrity in Cloud System," they explained their proposed scheme through four major modules such as audit service system. This explains about security that is designed with cryptographic method and also proves the soundness property and zero knowledge property. Second module is about data storage [7] service system, and they considered four entities to store the data. Third module is an audit-outsourcing service system uses the secret key to process the file. And the last module is about secure and performance analysis which verifies the correctness of cloud data on demand hence in such a way they are allocating the security requirements to the file [8]. This scheme involves minimum overhead with correctness of the system. In Vinaya and Sumathi [9], "Implementation of Effective Third Party Auditing for Data Security in Cloud," they proposed a scheme that is an enhancement of data integrity concept [10]. Here, integrity is guaranteed by measuring correctness of the system. This work verifies correctness of the data on the cloud without retrieving complete copy of the file, and it is proven with the help of service-level agreement (SLA). In this paper, integrity is verified by developing hash code by the server and sends back the file name and a signature from the hash code. TPA in return takes an old signature back from TPA database and checks the equality between the two signatures. And this is again assured by SLA. In Xu [11], "Auditing the Auditor: Secure Delegation of auditing operation over cloud storage," they defined about the audit protocol that explains with three phases such as release plan, execute plan, and review plan. And, in release plan data owner selects an audit plan. In the execute plan, TPA sends the request to CSP and reply to the request in the specified time interval. Review plan verifies whether the request has been executed in particular time interval. And other module known as time secured that involves two processes are backward-timed secure and forward-timed secure. In backward process, TPA performs audit within a time interval; if exists, it will reject in the review plan. In forward process, TPA performs audit process and checks the request after the time interval; this will take place in review plan. This whole work goes in such a way that all above plan will be performed sequentially. First phase is a set up in which it produces the secret key pair of (pk,sk) which is used to divide the files into block and encrypt the file. Next phase is the release plan phase that chooses the time for audit plan. And, in the execute plan phase, message is decrypted using the secret key. Review plan phase finally retrieves the message from receiver (Fig. 1).

3 Proposed Work

Usage of TPA scheme guarantees the data integrity, which allows data owner to audit the resource in the cloud. Framework includes auditing by data owner/client, notifications for the resource access, and validating time complexity for resource.

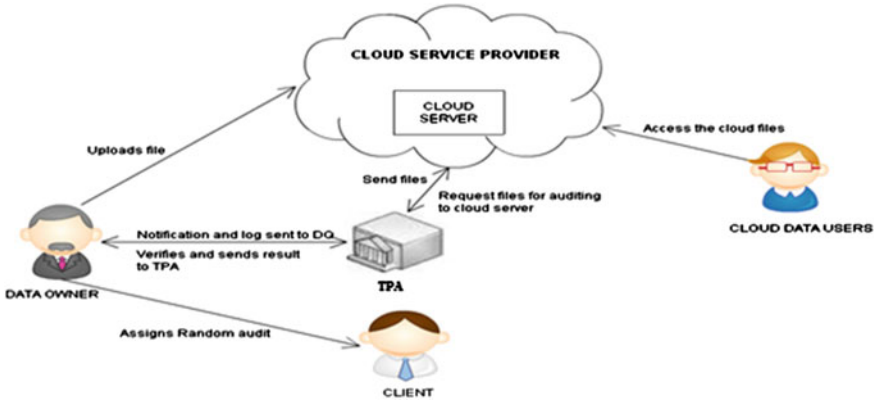

Fig. 1 Architecture of third-party auditing

3.1 Auditing by Data Owner/Client

Data integrity has been achieved by the usage of TPA scheme, in which allowing TPA to audit the outsourced data in the cloud. Auditing process is done on the resource by TPA using resource information provided by the CSP. Data owners are provided with notifications that when his/her resource has been accessed by users, and hence, data owners are aware of the resource and thus provides resource integrity. Thereby, data owners validate the notifications and log report generated by the normal auditing process with the resource list available with the data owners, and hence, data integrity is achieved. If data owner found that the notifications have some error with his/her resource status database, then "surprise auditing" is performed by the data owner or client employed by the data owner to audit the resource in the cloud. Hence, data owner can able to track an unauthorized access to the resource by notification provided with him.

3.2 Notifications for the Resource Access

Notification scheme involves issuing notifications to the data owner when his/her resource has been accessed by cloud users. This methodology is used to create awareness to the data owner with the status of his/her resource. Hence, this technique is used to inform data owner with resource status information that helps him to verify integrity of that particular resource in the cloud. This helps data owner to track an unauthorized access over the resource with the user details and system information (Fig. 2).

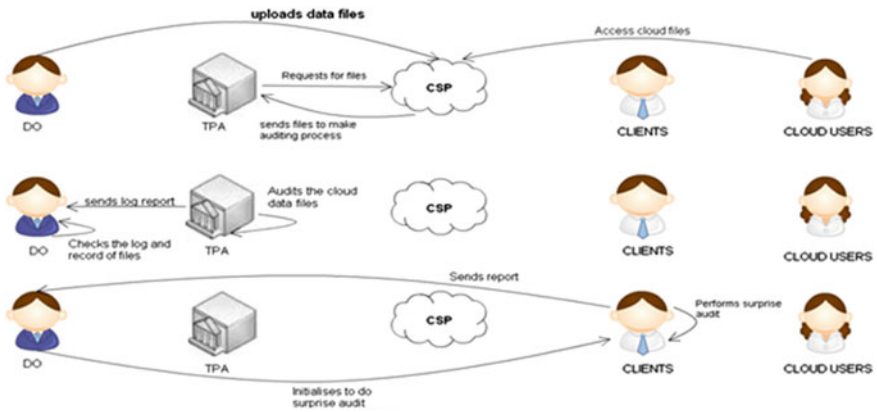

Fig. 2 Overall system architecture

3.3 Validating Time Complexity for Resource

For every critical resources in the cloud, "threshold value" is assumed or calculated by the data owner based on the random time generation technique and every critical resource has been validated by verifying response time with the time lesser than threshold value assigned to the resource. If response time to the data owner exceeds, then threshold value helps data owner to perform surprise auditing over the resource in the cloud. Hence, integrity has been achieved by validating the time complexity and medium of storage complexity [12] over that resource. Since response time to the users depends upon the storage medium by which the resource has been stored in the CSP, thereby, data owners are able to find the storage medium of his/her critical resources in the cloud.

4 Validation

Validating audit process models include the following steps:

Step 1: **Request initialization and response verification**

This step is to ensure that TPA sends request to CSP to get an essential information needed to perform auditing by appropriate period. And to ensure that the response given by CSP matches with the resource details available with the data owner.

Step 2: **Report examination**

To inspect an audit report or audit log generated by CSP and compare with the notifications provided with data owner to validate the exact status of the resource.

Step 3: **Resource scheduling**

To check the response time and storage medium of any critical resource by finalizing time and resource scheduling with an employed client or data owner.

Step 4: **Follow-up**

Employing third-party cloud users for managing and verifying closure audit verification.

Audit process is validated by,

$$\text{Val_Flag} = \sum_{(i=1)}^{n} \left(\left(\text{TPA}_{\log_{\text{report}}} \right) \right) . (\text{DO}_{\text{notifications}}) . \left(\text{surprise}_{\text{audit}_{\text{report}}} \right)$$

where

n number of resources of data owner.
i 'i'th number of resource that goes for auditing
DO data owner.

Case 1 *Val_Flag is true, if*

(i) Log report generated by TPA matches with the resource status database of data owner (DO).
(ii) Notifications provided to data owner matches with the list of resource access list.
(iii) Surprise audit report generated by client or data owner matches with the available resource database contents.

Case 2 *Val_Flag is false, if*

(i) Log report generated by TPA does not match with the resource status database of data owner (DO).
(ii) Notifications provided to data owner does not match with the list of resource access list.
(iii) Surprise audit report generated by client or data owner does not match with the available resource database contents.

5 Conclusion and Future Work

This paper focuses on auditing process of the resource in the cloud. Our proposed scheme also involves data owner/client to audit the resource. This helps to reduce the problem that occurs in the auditing process. This technique also helps us to make data owner to feel secured about their resources. Thus, security is achieved through this activity. Also, this process promises data owner that their resources are

stored in safer place. Thus, reduces misplace of file that are stored in a particular location. Finally, our work has some extravagant properties like proving the security, reduces the overhead through the client, and also achieves the integrity.

References

1. G. Roopa, S. Manjunath, Secure way of storing data in cloud using third party auditor. IOSR J. Comput. Eng. (IOSR-JCE) **12**(4), 69–74 (2013)
2. L. Li, L. Xu, J. Li, C. Zhang, Study on the third-party audit in cloud storage service, in *International Conference on Cloud and Service Computing* (2011)
3. C. Wang, S.S.M. Chow, Q. Wang, K. Ren, W. Lou, Privacy-preserving public auditing for secure cloud storage. IEEE Trans. Comput. **62**(2), 362–375 (2013)
4. G. Delong, Use of Third Party Audit to Verify Sources from Farm to Supplier
5. U. Vijayaraghavan, R.M. Arieth, K. Geethanjali, Proof of retrievability: a third party auditor using cloud computing. Int. J. Emerg. Technol. Adv. Eng. ISO 9001:2008 Certified J. **3**(7) (2013)
6. S.V. Marshal, Secure audit service by using TPA for data integrity in cloud system. Int. J. Innovative Technol. Exploring Eng. (IJITEE) **3**(4) (2013)
7. S. Han, J. Xing, Ensuring data storage security through a novel third party auditor scheme in cloud computing, in *Proceedings of IEEE CCIS* (2011)
8. M. Hussain, H. Abdulsalam, SECaaS: security as a service for cloud-based applications
9. V. Vinaya, P. Sumathi, Implementation of effective third party auditing for data security in cloud. Int. J. Adv. Res. Comput. Sci. Softw. Eng. **3**(5) (2013)
10. T.J. Salma, A flexible distributed storage integrity auditing mechanism in cloud computing
11. J. Xu, *Auditing the Auditor: Secure Delegation of Auditing Operation Over Cloud Storage* (National University of Singapore, Singapore)
12. L.D. Dhinesh Babu, P. Venkata Krishna, Versatile time-cost algorithm (VTCA) for scheduling non-preemptive tasks of time critical workflows in cloud computing systems. Int. J. Commun. Netw. Distrib. Syst. **11**(4), 390–411 (2013)

An Intelligent Cloud Security System for Critical Applications

Balamurugan Balusamy, P. Venkatakrishna, Gomathi Palani and Umamageshwari Ravikumar

Abstract Cloud has proven to a cost-effective technology for computing and storage for IT industry. Cloud security has often referred as app security and used to solve the communication issues between the cloud user and the cloud. Cloud security technology will be more attentive. While transforming critical application into a cloud, there is a need for a privacy and security. Cloud technology has not yet compromised with the security especially malicious insider. This paper introduces a novel idea, an intelligent agent system, which is used for an automated security. Whenever there is an alert of hackers/snoopers, the secret intelligent agent will be automatically generated to secure the data from malicious insider attacks. This paper has validated using weighted undirected mathematical model.

Keywords Cloud system · Intelligent system · Malicious insider

1 Introduction

Cloud computing is a huge lay which acts as a storage resource pool. It is an empowering technique to use the resources and IT services. It has been widely used in business and social network where the resources can be accessed through the network. Normally, organization information can be stored in any storage place. But it becomes a difficult work to carry based on security and costs. So cloud

B. Balusamy (✉) · P. Venkatakrishna · G. Palani · U. Ravikumar
VIT University, Vellore, India
e-mail: balamuruganb@vit.ac.in

P. Venkatakrishna
e-mail: pvenkakrishna@vit.ac.in

G. Palani
e-mail: gomathipalani16@gmail.com

U. Ravikumar
e-mail: umamageshwari.r2011@vit.ac.in

© Springer India 2015

L.P. Suresh et al. (eds.), *Artificial Intelligence and Evolutionary Algorithms in Engineering Systems*, Advances in Intelligent Systems and Computing 325,
DOI 10.1007/978-81-322-2135-7_5

computing become more attentive toward storage resources and computing technology. Many organizations are storing their backup data and some important details in the cloud. Many researches are going for storing the apps in the cloud. Cloud computing has to afford security to the computer, network, and information. Still, cloud computing security has many controls for safety and security to reduce the attacks from snoopers or hackers. The controls are deterrent, preventative, corrective, and detective.

Though the cloud has been supporting the apps, still there is a need for a security to store the application securely and to recover the data when there is any issue. [1] defines and compares the traditional marketing and cloud marketing with some suggestions. According to the 2011 survey, 80 % of IT people believe in cloud, which was taken by the Apptio and worldwide executive council. Currently 60 % of small-to-medium enterprises are using the cloud services and 72 % of them are vitalizing the significant portion of them. The available cloud service providers are VMware, Windows Azure, BlueLock, Citrix, Joyent, Verizon/terremark, Salesforce.com, CenturyLink/Savvis, Rackspace, Amazon. Amazon cloud has 69 % of business-critical application. 75 % of VMware customers realized that there exists at least one business-critical app in their invention atmosphere. The real-time critical applications like Icertis, Webzen, Telenor, Toyota, Milliman, GM/Digital Air Strike, Avanade, BMW Latin America have been already moved into the Windows Azure cloud [2]. And many cloud-based products such as ABBYY reached close to 400,000 users, online game company agate studio has become very quickly grown company, Baycloud System adds 60 more new customers to it throughout Europe.

Many researchers are involved in the cloud security issues to solve the problems. In [3], they proposed denial of access based on IP spoofing for enhancing the network security. In same manner, another enhanced work has been developed as a digital signature technique to make the network security to be more secured [4]. Likewise, many algorithms are proposed, but still, the critical application in the cloud is not compromised with the security. This paper proposals an intelligence agent system for cloud to enhance the security by making use of the intelligent system.

2 Related Works

In paper [5], they proposed a mechanism which focuses to develop a realistic data security and solutions regarding security issues. They also focused on products for the application and cloud computing services. They also found out the experimental results that determine the enactment for intrusion detection. The critical issues involve information security problems which includes user authentication and secure communication channel. They have provided assertion to rectify the data confidentiality, non-repudiation and integrity. Cloud application and security help us to recognize the cloud-authorized users and hackers/snoopers. In paper [6], they proposed an assessment about insider attacks in cloud computing and also they had given existing insider threat explanations, classifications, and its applications.

They have given examples of insider attacks that are exact to cloud environments. Insider attacks will be exceedingly hard to detect in the cloud ecosystem for a selection of reasons, namely the modus operandi of cloud computing. They have shown a difference to identify outsiders and insiders in the cloud network to focus on real threats. In paper [7], they proposed a mechanism about the threats of using business apps in the cloud system. Threats like losing control to manage the system, data can be stolen by insiders, problem with suppliers and customers, etc. This can be managed by being a smart customer/consumer and involve the authorized person to make cloud decisions. Most importantly monitoring the actions of supplier will help to make cloud service more flexible with economical cost. In paper [8], they proposed an approach for securing information in the cloud using offensive decoy technology. They have monitored and detected the information accessed in the cloud and the access of irregular data. When they have detected unauthorized access, they launch a large amount of decoy data to the insider. This approach results data security in cloud networks. Monitoring user performance in accessing the system can help to detect the malicious insider in cloud systems.

3 Proposed Work

A critical application in cloud system is mostly referred to the private cloud system [9]. Basically, cloud system is used for utilizing the IT infrastructures and resources. So the app to be put into the public cloud and make use of the resource sharing completely and storage resources too. The cloud computing work flows for sustainable enterprise management can be fairly scheduled [10]. Provably, 72 % of the low-to-middle-level business are transferred into the cloud. After migrating the business-critical application into the cloud system there exist several attacks like SQL injection, unauthorized person resource access, remote file inclusion, spam, OWASP, Malicious Insider, and DDos [11]. Attackers always target for the bandwidth, processing power, and storage capacity.

The reference architectures [12–15] shows the connectivity among the inter cloud system, cloud with cloud service providers and the cloudwith end users. Figure 1 represents the cloud user architecture. Malicious insider is a type of user in the cloud services [16]. Explains about the communication services between the cloud system. It is mostly unavoidable to prevent the malicious insider. But we can save our information from them. The following section explains about this.

3.1 Malicious Insider

Malicious Insider is a collection of computers which is handled by some insiders without the knowledge of owner. Snoopers/hackers are gathering the information without the concern of the people who own that. So there is a need for a system to

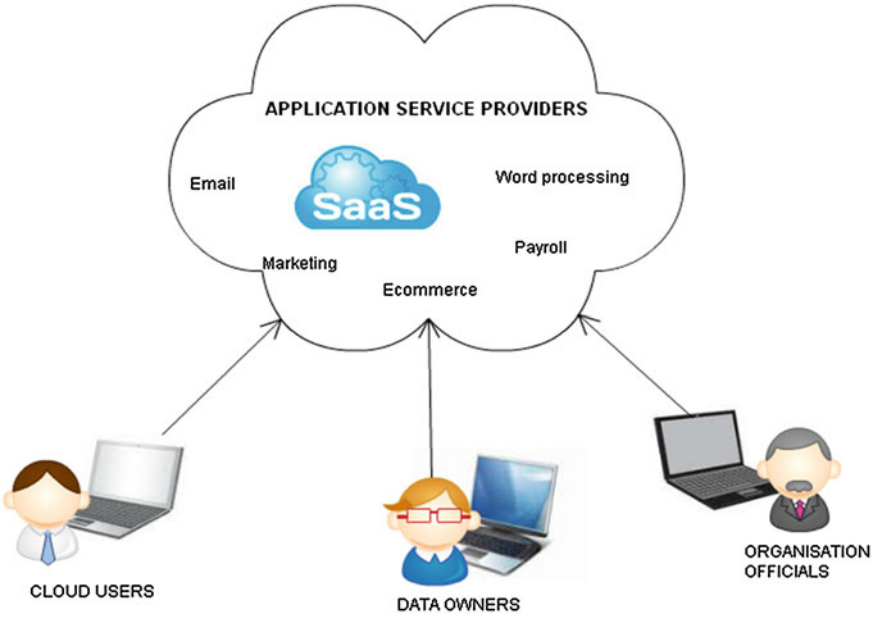

Fig. 1 Cloud user architecture

hide the information from them. In [8], they proposed a fog computing system for insider attack by monitoring the data access. [17] describes about the monitoring and managing cloud computing security using denial-of-service bandwidth allowance for an insiders. Paper [6] surveys about the insider attacks in cloud computing. Many researchers have done research on malicious insider attack to secure the data by access control method [3, 18]. Here, we can make use of the intelligent system to make our system effectively and efficiently. Generally, the intelligent system will be useful for automatic and security purpose. Secret agent is used to make the system information hidden from the malicious insiders. But this paper proposal will prevent the attack before it happens by monitoring the process. If the monitoring system finds any illegal authorization, immediately the secret agent will be generated without the knowledge of the insiders and makes a warning message to the cloud user. So, we can operate the secret agent based on our control and the system also completely will be under user control. The malicious insider issues cannot be avoided by the cloud service providers.

Figure 2 explains about the intelligent cloud security system. Each and every tenant's information will be a cluster by the administration and stored in the cloud. The system will move under normal services, and it will be under monitoring security. If the system gets any unauthorized alert means, then immediately the secret agent will be generated and it makes the service unavailable to the malicious insiders.

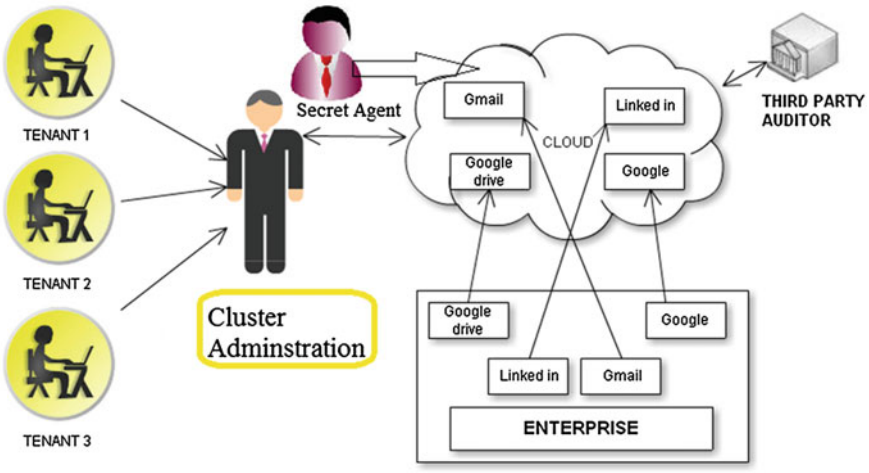

Fig. 2 Intelligent cloud security system

3.2 Application Algorithm

This application algorithm explains the sequence of steps which will be carried for the security over the cloud computing. This frame work is described in the following steps:

- After migrating the critical application into the cloud, the cloud user will start their services through cloud for their community.
- Then, the cloud user access the critical application in read and write mode.
- Obviously, there is need for a security for storing the critical application. This framework acts like a security agent for cloud on the user side.
- Normally organization flow will be monitored by cloud service providers and cloud user.
- If any unauthorized access is detected, then automatically the agent will be generated without the knowledge of insiders.
- The agent is a secret agent, so it will control the process by providing an alert message to the cloud user.
- And it marks the insiders to hide the information by making the service unavailable.
- Each and every activity will be monitored by the agent from the unauthorized access. So it will be easy to trace the insiders completely.
- This makes system to act safe and secure from the client side.

The above steps explain the process of secret agent in the cloud security system, and it explains the features of the intelligent system with the cloud computing. It will be an enhanced framework for an available cloud security system.

4 Validation

This paper has validated by the mathematical notations in passing weighted undirected graph and application algorithm.

$$\text{CS_A} = \left(\text{SF}_{ij},\ \text{OF}_{ij}\right)$$

where
CS_A Secret agent (an intelligent agent)
SF_{ij} Storage flow in bidirectional (cloud user to cloud/cloud to cloud user)
OF_{ij} Organizer flow in both cases

Organizer Flow:

Case 1: The cloud user can access the information from cloud; the secret agent must identify the exact person who is accessing the cloud and to monitor that (only for an enterprise people).

Case 2: If any users try to access the cloud, other than the authorised cloud users, the application activates the automated security system, which thereby triggers the function of intelligent agent for monitoring the activities of the unknown users.

Validation Model:

1. $\left(\text{SF}_{ij},\ \text{OF}_{ij}\right) \leq \text{CS_A}$

$\text{SF}i$ CS_A monitor cloud_user surface (while storing)
SF_j CS_A monitor the cloud surface (while retrieving)

2. $\left(\text{SF}_{ij},\ \text{OF}_{ij}\right) \leq \text{CS_A}$

OF_i CS_A monitor cloud_user surface (while accessing)
OF_j CS_A monitor other than clients (while insiders/hackers/snoopers accessing)

Finally, we can validate according to the following:

Case 1: $\text{SF}_{ij} \leq \text{CS_A}$.

The storage of data to the cloud and retrieval of data are in control.

Case 2: $\text{SF}_{ij} \geq \text{CS_A}$.

The application has been affected by threats, so the storage and retrieval of data has lost the control. In this time, the secret agent will be generated automatically to secure the data and to identify the hackers by monitoring them.

Case 3: $OF_{ij} \leq CS_A$.

If the organizer flow is under control, no threats will enter.

Case 4: $OF_{ij} \geq CS_A$.

If the organiser flow are not in control, then the secret agent will be automatically generated to block the service which will make an service unavailable to the threatens.

Above cases explain the activities that can be done to the cloud when using the critical application in cloud environment. Each and every activity will be taken by the secret agent to work automatically. And it makes the application security under the control of cloud user and flow of services to be normal.

5 Conclusion

This paper presents an intelligent agent system to support critical application in the cloud environment. This paper overcomes the drawbacks of threats like malicious insider, and it has been validated using the mathematical model, weighted undirected graph. This paper also speaks about the secret intelligent agent, generated for a security over the cloud and to make 100 % privacy in public cloud. Future work can also be extended by using an intelligent agent in a proper way to secure the information in the cloud. This framework ended with a hopeful for the enterprise cloud user to move their storage toward cloud.

References

1. G. Boss, P. Malladi, D. Quan, L. Legregni, H. Hall, Cloud computing (2007), www.ibm.com/developerworks/websphere/zones/hipods/
2. http://www.azure.microsoft.com
3. R. Piplode, U.K. Singh, An overview and study of security Issues and challenges in cloud computing. Int. J. Adv. Res. Comput. Sci. Softw. Eng. **2**, 115–120 (2012)
4. D. Chen, H. Zhao, Data security and privacy protection issues in cloud computing, in *2012 International Conference on Computer Science and Electronics Engineering (ICCSEE),* 2012, pp. 647, 651
5. C.-L. Tsai, U.-C. Lin, A.Y. Chang, C.-J. Chen, Information security issue of enterprises adopting the application of cloud computing, in *2010 Sixth International Conference on Networked Computing and Advanced Information Management (NCM)*, 2010, pp. 645, 649
6. A.J. Duncan, S. Creese, M. Goldsmith, Insider attacks in cloud computing, in *2012 IEEE 11th International Conference on Trust, Security and Privacy in Computing and Communications (TrustCom)*, 2012, pp. 857, 862
7. S. Shrum, P. Murray, *Common Risks of Using Business Apps in the Cloud*. Carnegie Mellon University, Produced for US-CERT, a government organization (2012)

8. S.J. Stolfo, M.B. Salem, A.D. Keromytis, Fog computing: mitigating insider data theft attacks in the cloud. *Security and Privacy Workshops (SPW) 2012 IEEE Symposium on*, 24–25 May 2012 (Angel Diaz, Chris Ferris, IBM's open cloud architecture, 2013), pp. 125, 128
9. Easy Deployment of Mission Critical Application to the Cloud—GigaSpace Cloudifies
10. L.D.D. Babu, A. Gunasekaran, P.V. Krishna, A decision based pre-emptive fair scheduling strategy to process cloud computing work-flows for sustainable enterprise management. Int. J. Bus. Inf. Syst. **16**, 409–430 (Inderscience Publishers) (2013)
11. D. Catteddu, G. Hogben, *Benefits, Risks and Recommendations for Information Security* (2009)
12. Cloud Reference Architecture. An Oracle White Paper November (2012)
13. S. Horrow, S. Gupta, A. Sardana, A. Abraham, Secure private cloud architecture for mobile infrastructure as a service, in *2012 IEEE Eighth World Congress on Services (SERVICES),* 2012, pp. 149, 154
14. Y. Demchenko, M.X. Makkes, R. Strijkers, C. Ngo, *Intercloud Architecture for Interoperability and Integration*. System and Network Engineering Group UvA (2012)
15. Architecture for Managing Clouds. A White Paper from the Open Cloud Standards Incubator
16. J.M. Suri, B.K. Nath, *Communication Services in Cloud Computing Environment*. Telecommunication Servicing Centre (2011)
17. B. Panja et al., Monitoring and managing cloud computing security using denial of service bandwidth allowance. Recent Patents Comput. Sci. **6**, 73–81 (2013)
18. E.E. Schultz, A framework for understanding and predicting insider attacks. Comput. Secur. **21**, 526–531 (2002)

An Efficient Framework for Health System Based on Hybrid Cloud with ABE-Outsourced Decryption

B. Balamurugan, P. Venkata Krishna, N. Saravana Kumar and G.V. Rajyalakshmi

Abstract Cloud computing is the emerging paradigm that allows the user to access the data using Internet [1]. Growing medical records and difficult data management intends to health department to move toward cloud. The security and privacy are major issues in cloud. The mission-critical applications are limited in cloud though it has numerous small- and medium-sized business applications. We proposed the hybrid cloud-based framework for overall healthcare system with attribute-based encryption with verifiable outsourced decryption for efficient data access and integration of hospitals using community cloud. Secure data transfer and integration of hospital are made possible using hybrid cloud. Our framework overcomes security flaws by achieving data integrity and data confidentiality with secure authentication and authorization. Thus, cloud provides scalable, efficient data access with cost-effective approach.

Keywords Cloud computing · Hybrid cloud · Framework cloud health · ABE · Security privacy

1 Introduction

Cloud computing is a type of computing that relies upon sharing of resources rather than having personal devices [2]. With the advent of cloud computing, most of the applications in every field are currently transformed into cloud-based applications

B. Balamurugan (✉) · P. Venkata Krishna · N.S. Kumar · G.V. Rajyalakshmi
VIT University, India, Vellore
e-mail: balamuruganb@vit.ac.in

P. Venkata Krishna
e-mail: pvenkatakrishna@vit.ac.in

N.S. Kumar
e-mail: saravanakumar.n2011@vit.ac.in

G.V. Rajyalakshmi
e-mail: raji.desire@gmail.com

© Springer India 2015

L.P. Suresh et al. (eds.), *Artificial Intelligence and Evolutionary Algorithms in Engineering Systems*, Advances in Intelligent Systems and Computing 325,
DOI 10.1007/978-81-322-2135-7_6

as it has numerous advantages compared to traditional computing [3]. The first and foremost advantage of cloud is cost-effectiveness [3]. The other benefit of cloud includes availability, performance, and scalability [4]. Though cloud has large number of applications in terms of health care, it is limited. The reasons were it involves high-level data security because medical records are highly confidential in nature. The security, privacy, and integrity are the major concerns of cloud computing [2]. These factors inhibit the growth of cloud computing to the critical application like health care. For critical applications in cloud such as health care, it should have high-level security, privacy, and data integrity. In this paper, we proposed the framework for overall cloud healthcare applications with security and access mechanism.

The healthcare systems had undergone major changes since the advent of computing. The medical health records of the patient are being stored electronically in the hospital system as it will be helpful for future reference. The management of data is more systematic with high-level security and authentication. However, nearly 30 % of the costs were spent for data management [5]. A number of data in electronic health system are gradually increasing in all countries, especially in developing countries like India. As a result, the application of cloud in electronic health system is highly appealing. The benefit of cloud-based electronic health includes cost-effective data management, availability, scalability, platform independence, and performance [6].

2 Cloud Deployment Models

The cloud computing is commonly known as Internet computing as the services are being offered online. The cloud computing has three deployment models: public, private, and hybrid.

In public cloud, the data can be accessed anywhere across the globe [7]. As the data in public cloud are being publicly accessed, it will prone to get attacks and lead to security flaws. Thus, public cloud is less secure and storing medical record in public is highly critical [8]. Thus, it needs high-level security features with access control mechanism.

Replacing single large server into multiple internal servers with data management either by the organization or by the third party to attain the benefit of cloud is known as private cloud. However, the benefits of private cloud are limited. Organization needs to own the data center. The private cloud is secured than public cloud as its access is limited to the organization [9]. The highly critical data such as electronic healthcare data and banking data can be stored and accessed as it was secure within the organization.

Hybrid cloud is the combination of both public and private clouds. The data are stored locally in multiple internal servers such as private cloud. Separate application is being run in public cloud environment for data access outside the organization. Thus, drawback of private cloud is overcome by hybrid cloud [10]. The proposed

framework is based on hybrid cloud with access mechanism and security features. Hybrid cloud provides the solution to overcome the security issues. The critical personal health record (PHR) of the patient is stored in data centers with many internal servers in the organization. The patient Health Record (PHR) of the patient can be shared with a cluster of hospitals. Thus, the sharing of PHR takes place among the partner organizations. The management of data is done by the third party. EHR of the patient might contain the numerous EMRs such as cardiology, ENT, and neurology. For client access, the cloud provides central public application for sharing of PHR with relatives and friends. The public cloud contains only the overview of PHR. The unique client-based public cloud application centrally stores the EHR of various hospitals of the client. For example, the application contains only the client profile and date of consulting the doctor with remarks. Thus, it does not contain the whole EMR of patient. This central client-based public cloud application is enough for insurance companies.

3 Motivation and Background

The medical health data were gradually increasing across the globe. Data storage is limited in traditional servers. Hence, the hospitals need to buy another server if the data limits exceed. The hospitals need to spend huge amount of money for data storage. It is difficult to manage the huge amount of medical record without the aid of IT professionals. Unlike other applications, in healthcare data, access is considered to be highly critical. Loss of data leads to even death of an individual. Thus, medical data are highly sensitive. It is improper to blame the cloud service provider as it was not managed by the single party. This fears the health sector to move to the cloud. Thus, cloud has very less number of applications related to health department. With high-level security, privacy and integrity for critical data with suitable access control would make health sector to move toward cloud. Thus, cloud is suitable for health care.

Mission-critical applications are available in cloud, but they are limited to software as a service. For example, Microsoft HealthVault cloud application and Google Health enable the user to store personal health record. These applications were client centric and used to share the personal health data to others.

4 Related Works

Many research papers dealt with electronic health, but none of them clearly have explained the data storage and access mechanism for overall health care with security features. The research paper by He et al. [11] provides a solution to cloud-based healthcare systems. The limitation includes data access and data security. Since the proposed concept is based on private cloud, the data access is limited

within particular locality. Once again, the research paper by Dimitrova [7] explains framework without security features. Scalable and secure sharing of personal health records using attribute-based encryption by Li et al. [12] is promising, it suffers from serious disadvantage of expensive decryption. The accessibility of outsourced health data in public cloud is critical as the patient depends on it for survival and storing the data in hybrid cloud will increase the availability factor. Cloud-based trusted accountability framework with automatic logging by Vidhyalakshmi and Prassanna [13] provides the secure electronic infrastructure for health care. The paper by Chen and Hoang [14] provides data security with fine-grained access using role-based access control. The RBAC is well suited for small- and medium-sized enterprises, but it fails for critical applications as it involves huge amount of data. As a result, performance of the application is reduced.

The research paper provides the information regarding the three-tier architecture for efficient data access with security and privacy in cloud. The three-factor authentication is necessary as the data were prone to be critical in nature. The research paper explains general framework for critical applications. Limitation includes lack of security features in it. The cloud auditing confirms the presence of data in cloud. The paper explains the algebraic way to audit the cloud data [15]. As data checking process was done in a random manner, there is chance of missing any data.

5 Proposed Work

Electronic Medical Record (EMR): The EMR is generally the medical records of the patient of particular department. Single patient might be having multiple EMRs [16]

Electronic Health Record (EHR): The collection of multiple EMRs of the known patient is EHR. However, the EHR of the patient is limited to a particular hospital.

Personal Health Record (PHR): The PHR is a client-oriented application. The PHR is a collection of EHR of various hospitals.

5.1 Detailed Framework

Figure 1 explains that the proposed framework is based on hybrid cloud with efficient access using attribute-based encryption with outsourcing decryption. The attribute-based encryption is a public key asymmetric encryption. The advantage of attribute-based encryption was it handles the huge amount of data [12]. By outsourcing the decryption, it provides a cost-effective approach with high performance

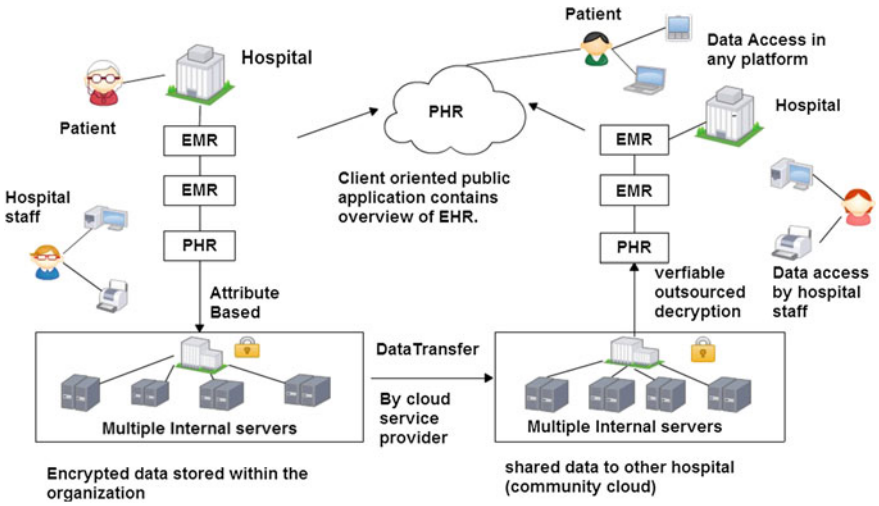

Fig. 1 Framework based on hybrid cloud

and data confidentiality. The patient medical records were stored by the medical staff of the hospital. By means of data collector, the multiple EMRs are collected as EHR. Then, EHR is being encrypted and stored in the data center. With the help of multiple internal servers and access control, secure data access is possible within the hospitals. The main objective of cloud is to efficiently share data with other hospitals. The secure share of PHR is possible to community of hospitals. As the data are encrypted, it was only shared with its community cloud. Thus, secure data transfer is possible to the pool of hospitals. However, cloud service provider transfers only encrypted PHR. By means of outsourcing the decryption to third party, the data confidentiality is achieved. Moreover, performance is high as data encryption in ABE is much smaller in size compared to other models. The public cloud application contains the overview of PHR-like patient profile including blood group and health problems of patient and doctor visit with date. The client-centric application does not contain full medical record of the patient rather overview. Thus, patient can freely share the PHR with relatives and friends without bothering about security issues. Secondly, it benefits the insurance companies to know the health status of clients.

5.2 Scenario-Based Explanation with Data Flow in Hybrid Cloud

Integration of hospital provides efficient transfer of EHR of the patient for treatment. For example, consider the patient has some health cardiac problems. The patient underwent several tests such as electrocardiogram, treadmill test, and angiogram. The EMRs of patient are stored in hospital's data center. Certain

advanced treatment for patient might be unavailable. The PHRs of the patient are transferred to the partner hospital for future treatment. Thus, it reduces the data storage overheads. Thus, integration of hospital is possible with hybrid cloud. Majority of the hospitals never accept the test results taken by other hospitals. As a result, there is no need for patient to undergo another same test in another hospital. In case of emergency situation like accidents, patient profile can be easily viewed for immediate treatment with the help of data available in the public cloud. This depicts the importance of integration of hospitals and the value of cloud computing.

Figure 2 portrays that hospitals were the cloud data owner (CDW). The physicians upload EHR of the patients using biometric three-factor authentication scheme like biometric, username, and password. The data were stored in data center with respective patient PHR. There will be a secure private line for data transfer. Once getting the request, the third-party cloud personals send PHR. Before transmitting the data, the proxy server will re-encrypt the encrypted PHR for secure transmission. The partner company will sent the acknowledgment for proof of data retrieval. And frequent data auditing has done by both third party and data owner.

Figure 3 describes that the client-oriented cloud applications are limited to abstract of PHR of patients for benefits such as sharing of PHR with friends and

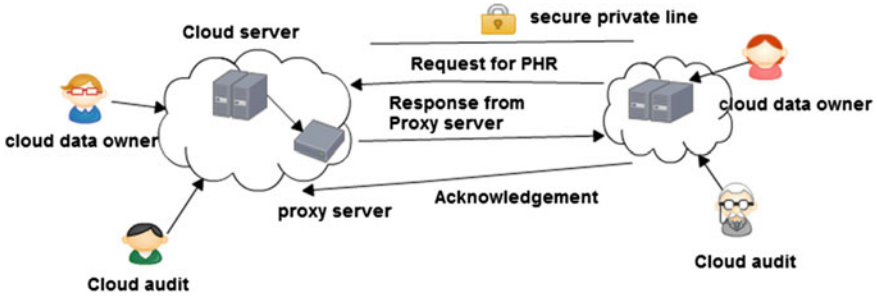

Fig. 2 Data flow for community of hospitals

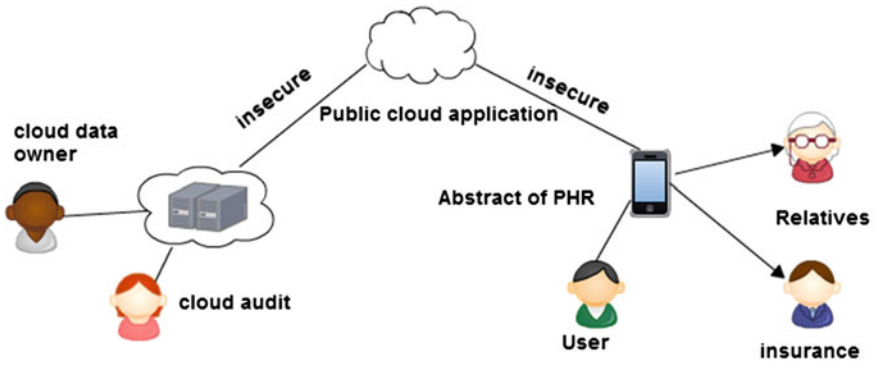

Fig. 3 Data flow for client-oriented applications

insurance companies. The client-centric application does not contain the EMR of the patient rather it contains the data such as patient problem and doctor visit by the patient. The client-centric cloud application is considered to be insecure as the data travel through public network.

6 Issues in Cloud

There are four major issues to be overcome for secure access of data. The issues are data security, data confidentiality, data integrity, secure authentication, and authorization [16]. The security of the PHR is based on two types. One is based on storage and other on access. The data will be secured when stored within the organization. However, PHR data are being shared with community of hospital in public. Various attacks such as denial-of-service attacks are major threats to availability. The healthcare systems should follow the ISO standards to overcome the cloud-based attacks. International Standard Organization ISO-2799 2008 provides guidelines for security to overall healthcare information systems [9]. ISO also stated that the security is not only based on data security but also involved physical, IT services, and software security. The ultimate objective is to protect the PHR without any compromise. As data are stored internally and data access is limited only to its community cloud, the architecture is secure. Moreover, by using attribute-based encryption, it overcomes the security issues.

The SQL injection is the threat to authentication. SQL injections were ranked first by online Web application project (OWASP 2013) [17]. The high-level authentication is required in public cloud. Smart cards with one-time password are provided for physicians in community cloud. The high-level security is not necessary for client-oriented public cloud as it contains only overview of PHR. The data confidentiality is achieved by encrypting the data [12]. The data are stored in private cloud; however, the data are managed by the third party. Therefore, the data are being encrypted by means of ABE and stored in data center. By outsourcing, decryption of data is cost-effective with high-level data confidentiality. The third party does not know the exact information in the data center as the data were encrypted. The cloud service provider shares the encrypted PHR with the members of community cloud. The data transferred were decrypted by another third party. Thus, data confidentiality is achieved. According to ISO- 7498-2:1989, confidentiality is defined "as property that information is not made available or disclosed to unauthorized individuals, entities, or processes" [9].

The ISO 7498-2:1989 defines the data integrity as "property that data has not been altered or destroyed in an unauthorized manner" [18]. As EHR data are sensitive in nature, any changes to the medical record subsequently affect the treatment. Considering the scenario, where a radiologist uploads an EMR of a patient enabling the physician to download and use it for diagnosis. This avoids the need of IT professional in the hospital as it was done by the radiologist itself. Thus, secure authentication overcomes the data integrity issues.

7 Conclusion and Future Work

Thus, we have proposed the new framework for overall health system using hybrid cloud with ABE with outsourced decryption. Though hybrid cloud is not cost-effective compared to public cloud, it ensures the security of the data as the data are huge and critical. The data sharing is limited to the pool of hospitals using hybrid cloud architecture. The ABE with outsourcing decryption might be an overhead in terms of performance, but it provides the security of data from threats and attacks. By means of client-oriented public health cloud application, the patient easily shares data with others. As public cloud application contains only the overview of EHR, the security is no longer a serious issue. Proposed framework overcomes major issues of critical cloud applications. Using hybrid cloud, the data management cost was cut down nearly by 40 % though it requires infrastructural investment. Framework had been proposed but will be implemented in future. Thus, cloud is ready for mission-critical applications such as electronic health system.

References

1. S. Sundareswaran, A.C. Squicciarini, D. Lin, Ensuring distributed accountability for data sharing in the cloud. IEEE Trans. Dependable Secure Comput. **9**(4), 556, 568 (2012)
2. C. Modi, D. Patel, B. Borisaniya, A. Patel, M. Rajarajan, A survey on security issues and solutions at different layers of cloud computing. J. Supercomput. **63**(2), 561–592 (2013)
3. M.A. Alzain, E. Pardede, B. Soh, J.A. Thom, Cloud computing security. From single to multi-clouds. HICSS, 5490–5499 (2012)
4. G. Kulkarni, J. Gambhir, T. Patil, A. Dongare, A security aspects in cloud computing, in *2012 IEEE 3rd International Conference on Software Engineering and Service Science (ICSESS)*, 2012, pp. 547, 550
5. X. Huang, Y. Xiang, A. Chonka, J. Zhou, R.H. Deng, A generic framework for three-factor authentication. Preserving security and privacy in distributed systems. IEEE Trans. Parallel Distrib. Syst. **22**(8), 1390, 1397 (2011)
6. K. Kalaiselvan, P. Venkata Krishna, Performance based QoS for cloud's infrastructure as a service. Int. J. Cloud Comput. **2**(4), 325–339 (2013)
7. M. Dimitrova, S. Lozanova, L. Lahtchev, C. Roumenin, A framework for design of cloud compatible medical interfaces. CompSysTech 195–200 (2012)
8. X. Liu, X. Qiu, X. Xie, B. Chen, K. Huang, Implement of a light-weight integrated virtualized environment manager for private cloud computing, in *2012 International Conference on Computer Science and Service System (CSSS)*, 2012, pp. 523, 526
9. http://www.redcardsecurity.com/pages/resources_files/ISO27799-2008.pdf
10. L. Freitas, P. Watson, Formalising workflows partitioning over federated clouds: multi-level security and costs, in *2012 IEEE Eighth World Congress on Services (SERVICES)*, 2012, pp. 219, 226
11. C. He, X. Fan, Y. Li, Toward ubiquitous healthcare services with a novel efficient cloud platform. IEEE Trans. Biomed. Eng. **60**(1), 230, 234 (2013)
12. M. Li, S. Yu, Y. Zheng, K. Ren, W. Lou, Scalable and secure sharing of personal health records in cloud computing using attribute-based encryption. IEEE Trans. Parallel Distrib. Syst. **24**(1), 131,143 (2013)

13. J. Vidhyalakshmi, J. Prassanna, Providing a trustable healthcare cloud using an enhanced accountability framework, in *Proceedings of the International Conference on Computer Science and Information Technology* (2013)
14. L. Chen, D.B. Hoang, Novel data protection model in healthcare cloud, in *2011 IEEE 13th International Conference on High Performance Computing and Communications (HPCC)*, 2011, pp. 550, 555
15. L.Chen, Using algebraic signatures to check data possession in cloud storage. Future Gener. Comp. Syst. **29**(7) (2013)
16. R. Zhang, L. Liu, Security models and requirements for healthcare application clouds, in *2010 IEEE 3rd International Conference on Cloud Computing (CLOUD)*, 2010, pp. 268, 275
17. https://www.owasp.org/index.php/Top_10_2013-Top_10
18. http://www.ecma-international.org/activities/Communications/TG11/s020269e.pdf

A Knowledgeable Feature Selection Based on Set Theory for Web Intrusion Detection System

Nalini Priya Ganapathi and Vivek Duraivelu

Abstract Web intrusion detection systems are security programs to decide whether events and activities occurring in a Web application or network are legitimate. The objective of Web IDS is to identify intrusions with high false alarms and low detection rate while consuming minor properties. Similarly, intelligent Web IDS have snags of concert efficiency, false positive, and false negative, while today's advance Web page creation approaches are also facing training/learning in the clouds, great false alarms, and truncated detection rate. In this paper, an efficient feature selection approach is proposed by selecting an optimum subset of features. Hybrid feature selection relevance algorithm is used for optimum subset feature selection that decouples relevance and redundancy analysis. Empirical results show that the new proposed system gives better and robust representation of an ideal intrusion detection system while having the reduced total number of features, truncated false alarms, great detection rate, and least computation cost.

Keywords IDS · Feature selection · Hybrid approach · Web IDS

1 Introduction

A Web application is a solicitation that is accessed by users over a network such as the Internet. The period also means a computer software application that is coded in a browser reinforced programming language and trusting on common Web browser

N.P. Ganapathi (✉)
Department of Information Science and Technology, Anna University, Chennai, Tamil Nadu, India
e-mail: nalini.anbu@gmail.com

V. Duraivelu
Department of Software Engineering, Saveetha Engineering College, Anna University, Chennai, Tamil Nadu, India
e-mail: vivekprasanth87@gmail.com

© Springer India 2015

L.P. Suresh et al. (eds.), *Artificial Intelligence and Evolutionary Algorithms in Engineering Systems*, Advances in Intelligent Systems and Computing 325,
DOI 10.1007/978-81-322-2135-7_7

to render the application executable [1]. The Web pages convoluted in drive-by-download attacks typically include malicious JavaScript code. This code is usually confused, and it fingerprints the visitor's browser, identifies vulnerabilities in the browser itself, or the plugs in that the browser uses and finally take-offs one or more exploits. These attacks target memory sleaze vulnerabilities or insecure APIs that, if successfully exploited, enable the attackers to execute arbitrary code of their choice [1]. However, Web IDS approach is used to detect the Web attacks such as URL interpretation attack, input validation attack, session hijacking, SQL injection attack, buffer overflow, XSS attack, and directory traversal attack. The IDS approach is used to reduce the analysis time and increases the adeptness of the system.

It is a challenge to obtain a feature set that is inclusive enough to separate normal data from anomaly as well as keep the size of this set to a minimum. In general, the more features, the more difficult the problem is to solve and in the case of machine-learning algorithms, increasing the number of types significantly increases the training time required to learn the intrusion task.

2 Related Works

Denial of service attacks are large-scale cooperative attacks on the networking structure. It disables servers/victims from providing services to its clients. These attacks adversely affect the network badly. Therefore, they must be detected on time [2]. Introducing a classification technique plays a significant role in detecting such intrusions, but it takes significant classification time due to large number of features. It reduces its efficiency. So in order to improve efficiency or to reduce classification time, researcher provides relevant set of features for detection of DOS attacks. For this purpose, researcher is using NSL KDD dataset and analysis is performed on orange canvas V2.6.1 data mining tool.

In another paper, a concise analysis of classification of 10 % of KDD cup'99 datasets based on intrusion detection was introduced [3]. Analysis of data is performed using different techniques, i.e., k-mean, which is based on clustering, and k-nearest neighbor, support vector machine are classification techniques. Firstly, the flat results are analyzed then preprocessed data are used. For preprocessing, statistical normalization has been used. For analysis, only two groups are considered that are normal and abnormal, and no further division of abnormal category has been done. MATLAB is used as a tool. As a result classification, technique proves good in classifying data, abnormal data separately and normal and abnormal data collectively, for classification potentiality.

An efficient intrusion detection system is proposed by Ahmed and his colleagues [4] using features subset selection based on MLP. They used principal component analysis (PCA) and GA for preprocessing and MLP for feature classification using

KDD cup dataset. LDA outperforms PCA, and PCA is not suitable for large dataset [5], hence their work is limited for small-size datasets and results are not more realistic to actual network traffic as there are approved deficiencies in KDD cup dataset. An ensemble approach for features reduction is adopted by [2]. As PCA is not suitable for nonlinear dataset as well as for large dataset, in their work, authors preferred generalized discriminant analysis (GDA) over PCA for features selection. Besides reduction in number of input features, GDA reduces classifiers training time by selection of most discriminant features. It also increases classification accuracy. In GDA approach, every network connection is distorted into input data vector to reduce high-dimensional data vectors. Each feature vector is labeled as normal or an attack.

3 Existing Feature Selection

From the existing system, different types of feature selection algorithm have been analyzed, the way in which they have some of the merits and demerits as follows.

mRMR The mutual information of two random variables is a quantity that measures the mutual dependence of the two variables. The mRMR method uses the mutual information between a feature and a class as relevance of the feature for the class [6]. The mRMR measure has the following form to optimize D and R simultaneously:

$$\max \Phi(D\,R), \quad \Phi = D - R, \tag{1}$$

In this equation, D and R mean relevance and redundancy of each feature.

RELIEF is a well-known feature-weighting (ranking) approach that was first introduced by Kira and Rendell [4]. The basic idea is to measure the relevance of features in the neighborhoods around target samples. For each target sample, RELIEF finds the nearest sample in feature space of the same category, called the 'hit' sample, then measures the distance between the target and hit samples [7].

4 KDD CUP 99 Dataset

The KDD training dataset consist of 10 % of original dataset that is approximately 494,020 single connection vectors each of which contains 41 features and is labeled with exact one-specific attack type, i.e., either normal or an attack. Each vector is labeled as either normal or an attack, with exactly one-specific attack type. Deviations from 'normal behavior,' everything that is not 'normal,' are considered attacks [18]. Attacks labeled as normal are records with normal behavior. The simulated attack falls in one of the following four categories [8]:

1. Denial of Service (DOS) Attack: In this category, the attacker makes some computing or memory resources too busy or too full to handle legitimate request, or deny legitimate users access to machine. DOS contains the attacks: 'neptune,' 'back,' 'smurf,' 'pod,' 'land,' and 'teardrop.'
2. Users to Root (U2R) Attack: In this category, the attacker starts out with access to a normal user account on the system and is able to exploit some vulnerability to obtain root access to the system. U2R contains the attacks: 'buffer_overflow,' 'load module,' 'root kit,' and 'perl.'
3. Remote to Local (R2L) Attack: In this category, the attacker sends packets to machine over a network but who does not have an account on that machine exploits some vulnerability to gain local access as a user of that machine. R2L contains the attacks: 'warezclient,' 'multihop,' 'ftp_write,' 'imap,' 'guess_passwd,' 'warezmaster,' 'spy,' and 'phf.'
4. Probing (PROBE) Attack: In this category, the attacker attempts to gather information about network of computers for the apparent purpose of circumventing its security. PROBE contains the attacks: 'portsweep,' 'satan,' 'nmap,' and 'ipsweep.'

The major objectives performed by detecting network intrusion are stated as recognizing rare attack types such as U2R and R2L, increasing the accuracy detection rate for suspicious activity, and improving the efficiency of real-time intrusion detection models. This detects that the training dataset consisted of 494,019 records, among which 97,277 (19.69 %) were 'normal,' 391,458 (79.24 %) DOS, 4,107 (0.83 %) Probe, 1,126 (0.23 %) R2L, and 52 (0.01 %) U2R attacks. Each record has 41 attributes describing different features and a label assigned to each either as an 'attack' type or as 'normal' (Fig. 1).

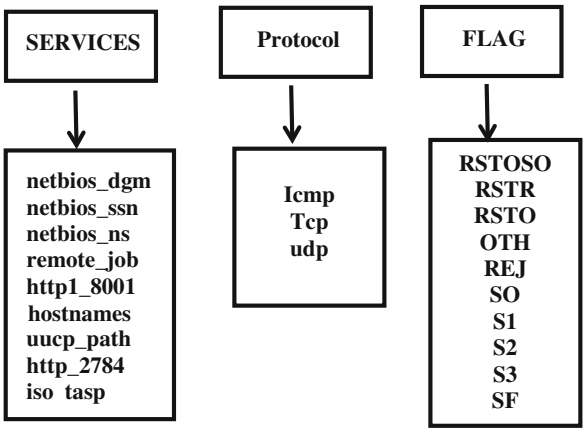

Fig. 1 Types of threats based on services, protocol, and flag

Fig. 2 Intelligent hybrid relevant feature algorithm

Input: KDD cup dataset, N/w trace dataset, HTTP dataset

Output: Reduced ranked dataset

Step 1: max⍉(D,R)

Step 2: Rank the feature set (R)

Step 3: select feature subset (S) = [1…….d]

Step 4: repeat until all features are ranked

Step 5: compute the weight vector

Step 6: compute the ranking scores for features in set S: c(i) = $(w(i))^2$

Step 7: find the feature with smallest ranking score: e=arg min(c(i))

Step 8: S=S-[e]

5 Proposed Work

The proposed feature selection algorithm is the hybrid algorithm, where two algorithms are combined to form a relevant feature set to get a relevant detection. KDD cup dataset, which as 41 attributes, based on basic, content, and traffic features. These 41 features are based on the network intruders, which traces the data and gives the output as normal or abnormal. HTTP datasets are the data, which analyzes the Web intruders. However, the detection of the attacks is made by the protocols in the renowned sets. The threats are based on the services that have 72 attributes and 3 protocols and 10 flag attributes. The main aim of the detection is based on the protocol type, which is analyzed by the featured relevance algorithm. The algorithm is used to maintain the rank for the attributes and analyze the priority for the attacks; this makes the easier detection of attacks by scanning in Web application (Fig. 2).

In this proposed algorithm, the hybrid algorithm has been introduced for getting the reduced ranked datasets. KDD cup datasets are the input data with 41 attributes and HTTP datasets with 13 attributes, which is taken from the Web application. The 10 % of KDD 99 training dataset has three distinct protocols namely TCP, UDP, and ICMP. Study reveals that these protocols are interrelated to any of the network attacks. We have designed a mathematical set of Eqs. (2), (3), and (4), which state the number of attacks in protocol type ‘TCP,’ ‘UDP,’ and ‘ICMP,’ respectively.

$$A = \{x|x \in \text{attack_name} \ \forall \ \text{TCP} \in \text{protocol_type}\} \quad (2)$$

$$B = \{y|y \in \text{attack_name} \ \forall \ \text{UDP} \in \text{protocol_type}\} \quad (3)$$

$$C = \{z|z \in \text{attack_name} \ \forall \ \text{ICMP} \in \text{protocol_type}\} \quad (4)$$

The following results were obtained:

Equation (2)—'TCP' protocol got affected by 20 different attack types
Equation (3)—'UDP' protocol got affected by five different attack types
Equation (4)—'ICMP' protocol got affected by seven different attack types

From the above 3 equations, we obtain Eq. (5) which shows the intersection of Eqs. (1), (2), and (3) applied to the training dataset, wherein the three attacks, normal, satan, and nmap are found to be common in all the three protocols, namely, TCP, UDP, and ICMP.

$$A \cap B \cap C = \{a|a \in A \ \text{and} \ a \in B \ \text{and} \ a \in C\} \quad (5)$$

In the 10 % KDD cup training dataset, the attribute attack_name contains a value either normal or an attack out of the above-mentioned 22 attacks. All of the records in the dataset are divided into 2 classes: normal or attack (anomaly).

6 Implementation

This work has been implemented by .net for the classification accuracy of datasets with full features first using the learning algorithms by 10-fold CV and LOOCV. Then, we reorganized the datasets using selected (reduced) features by each method and evaluated each method by the same process.

The scanner tool is introduced for the dynamic feature selection process. The main aim of the feature selection is to select the relevant attributes from the Web application which we developed from the .net application. The framework of the scanner tool estimates the error occurred in the LOC of the code in the Web application. The main error occurred in the Web is SQL injection, which affects the database of the Web site. Once the database is injected by the SQL attack, automatically the entire Web application will get collapsed while using that Web site. For example, the Web applications are developed with an attacker code, and different attacks are identified in various lines of code. At first, the Web application that was created is scanned and uploaded in the scanner tool, and the scanner tool is constructed with the IHRF algorithm techniques.

The proposed algorithm is compared with the existing algorithm to show the accuracy of the hybrid algorithm. Using a redundancy and relevance algorithm separately, the major properties of Web application will have only less detection rate and high false alarm rate while construction of decision table. Comparatively,

Table 1 Hybrid feature relevance decision class between $\{a_1, a_2, \ldots\}$ versus $\{c_1, c_2, \ldots\}$

a/c	C_1	C_2	C_3	C_4	Dc
A_1	100	009	013	019	1
A_2	007	264	011	215	1
A_3	009	064	241	321	0
A_4	100	016	158	009	0
A_5	009	261	005	016	1
A_6	007	154	461	012	0
A_7	154	009	154	237	1

the hybrid feature relevance algorithm that decouples the attributes have better accuracy on detecting the faults based on all three protocols namely TCP, UDP, and ICMP, which is shown in Table 1. The results of the decision table show that the hybrid algorithm comparatively has higher detection rate and lesser false alarm rate.

The comparison of the previous and proposed work is given by graphical representation to differentiate the accuracy of the system. The result shown in Table 1 and its statistical view in Fig. 3 obtained after 1,000 clusters indicate that 50 % of the total clusters have attacks with high count of centroid value. In TCP protocol, all the four attack categories DoS, R2L, U2R, and PROBE are active as shown in Fig. 3 (Fig. 4).

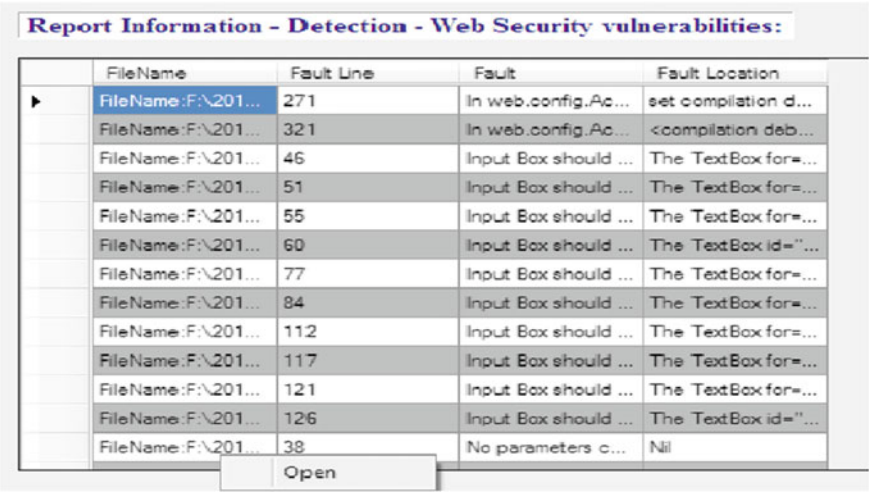

Fig. 3 Featured data report

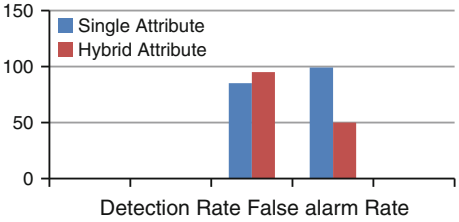

Fig. 4 Comparison of single attribute and hybrid algorithm

7 Conclusions

The feature selection methods that were newly proposed and tested with public data have shown improved performance in terms of the feature size and the classification accuracy. In particular, the result of IHRF method demonstrated the most powerful and stable performance over all the other methods considered. Meanwhile, some methods such as I-RELIEF were unstable, dependent on the data or the learning algorithm. Future work is to fine-tune the settings of our experiment and include comparison of execution time of each method. This is because each method needs to be compared with its results obtained by the best parameter setting, as well as with its actual running time for a fair comparison. Finally, a novel feature subset selection method based on this experimental study can also be developed.

References

1. A. Jain, D. Zongker, Feature selection: evaluation, application, and small sample performance. IEEE Trans. Pattern Anal. Mach. Intell. **19**(2), 153–158 (1997)
2. P. Bhoria, K. Garg, Determining feature set of DOS attacks. Int. J. Adv. Res. Comput. Sci. Softw. Eng. **3**(5) (2013)
3. R. Lath, M. Shrivastava, Analytical study of different classification technique for KDD Cup Data'99. Int. J. Appl. Inf. Syst. **3**(6) (2012)
4. K. Kira, L.A. Rendell, A practical approach to feature selection, in *Proceedings of the 9th International Workshop*
5. Z. Zhao, H. Liu, Searching for interacting features, in *Proceedings of International Joint Conference on Artificial Intelligence* (2007), pp. 1156–1161
6. H. Peng, F. Long, C. Ding, Feature selection based on mutual information: criteria of max-dependency, max-relevance, and min-redundancy. IEEE Trans. Pattern Anal. Mach. Intell. **27** (8), 1226–1238 (2005)
7. Y. Sun, J. Li, Iterative RELIEF for feature weighting, in *Proceedings of the 23rd International Conference on Machine Learning* (2006), pp. 913–920
8. S. Dudoit, J. Fridlyand, T.P. Speed, Comparison of discrimination methods for the classification of tumors using gene expression data. J. Am. Stat. Assoc. **97**(457), 77–87 (2002)
9. A.L. Blum, D.P. Langley, Selection of relevant features and examples in machine learning. Artif. Intell. **97**(1–2), 245–271 (1997)

10. H. Liu, L. Yu, Toward integrating feature selection algorithms for classification and clustering. IEEE Trans. Knowl. Data Eng. **17**(4), 491–502 (2005)
11. F. Fleuret, Fast binary feature selection with conditional mutual information. J. Mach. Learn. Res. **5**, 1531–1555 (2004)
12. I. Guyon, A. Elisseeff, An introduction to variable and feature selection. J. Mach. Learn. Res. **3**, 1157–1182 (2003)
13. M.J. Martin-Bautista, M.-A. Vila, A survey of genetic feature selection in mining issues. Proc. Congr. Evol. Comput. **2**, 1314–1321 (1999)
14. I. Guyon, J. Weston, S. Barnhill, V. Vapnik, Gene selection for cancer classification using support vector machines. Mach. Learn. **46**(1–3), 389–422 (2002)
15. R. Tibshirani, T. Hastie, B. Narasimhan, G. Chu, Diagnosis of multiple cancer types by shrunken centroids of gene expression. Proc. Natl. Acad. Sci. USA. **99**(10), 6567–6572 (2002)
16. S. Beniwal, J. Aror, Classification and feature selection techniques in data mining. Int. J. Eng. Res. Technol. **1**(6) (2012)

FLC-Based Adaptive Neuro-Fuzzy Inference System for Enhancing the Traveling Comfort

K.K. Sneha, Lakshmi Ponnusamy and R. Kalaivani

Abstract In this paper, pioneering adaptive neuro-fuzzy inference system (ANFIS) which is trained with the data obtained from well-known intelligent control technique fuzzy logic controller (FLC) for half-car (HC) model is proposed to improve the traveling comfort. In automobile industries, the traveling performance of the vehicle is tested at the design stage by simulating the vehicle response to various road excitations under different loading conditions. In this work, the disturbance from the road is assumed to be a dual bump. Initially, a FLC is designed to give better performance. Secondly, a flexible machine learning approach artificial neural network (ANN) that is trained with the FLC data by considering the performance measure as mean square error (MSE) is designed and used. At last, an ANFIS with the adaptive and generalizing features of ANN and intelligence of FLC is used for control purpose. In the modeling of system, simulation with and without controllers is carried out in MATLAB/Simulink environment. A comparison is made among the responses of the system with these controllers, and it shows that the system with FLC-based ANFIS gives significant reduction of the body acceleration (BA) and thus improves the traveling comfort.

Keywords Adaptive neuro-fuzzy inference system · Fuzzy logic controller · Artificial neural network · Mean square error · Body acceleration

K.K. Sneha (✉) · L. Ponnusamy · R. Kalaivani
Department of EEE, College of Engineering Guindy, Chennai, India
e-mail: snehakk1990@gmail.com

L. Ponnusamy
e-mail: lakshmi_p_2000@yahoo.com

R. Kalaivani
e-mail: kalaivanisudhagar@gmail.com

© Springer India 2015

L.P. Suresh et al. (eds.), *Artificial Intelligence and Evolutionary Algorithms in Engineering Systems*, Advances in Intelligent Systems and Computing 325,
DOI 10.1007/978-81-322-2135-7_8

1 Introduction

It is a challenging task for the automobile industries to reduce the vertical vibrations transmitted to the passengers. Multi-objective control for half-car (HC) suspension systems using linear matrix inequalities is detailed in [1]. The suspension systems support the vehicle body, decrease the road surface-induced vehicle vibrations, and help to improve ride comfort and road holding [2]. When designing vehicle suspensions, main goal is to play down the vertical forces transmitted to the passengers to improve the comfortness [3]. Numerous papers about the theoretical and experimental investigation on the dynamic behavior [4] of passive system which has fixed system parameters, semi active system [5] which has the variable magneto rheological (MR) or electro rheological or fluid damper and active suspension system which has the additional actuator to provide the control force, have been published in the past.

In [6], the control of quarter-car (QC) and HC model with optimum damping coefficients with fixed other system parameters has been explained by state space approach of the system. A valuable road-adaptive nonlinear control [7] which continuously monitors suspension travel and adjusts online the shape of the filter nonlinearity in response to different road profiles has been described and compared with back-stepping control and optimal control for active suspension HC model. Adaptive neuro-fuzzy inference system (ANFIS) which has the advantages of expert knowledge of the fuzzy inference system (FIS) and the learning capability of NN proved to be better than ordinary FLC when applied to a QC model [8].

For the QC model, the performance of fuzzy logic controller (FLC) controlled active suspension, linear quadratic regulator (LQR) controlled active suspension, and passive suspensions are compared in [9]. The ANFIS for suspension system of vehicle is explained in [10]. In [11–13], FLC for vehicle suspension is discussed. [14] clarified some issues related to system controllability and extended previous analytical results to HC models with unsprung mass, wheel-hop dynamics. Enhancement of traveling comfort using sliding mode neural network inference FLC is discussed in [15]. In [16] is designed and implemented the BP neural network predictive controller for active suspension system. In [17], author deals with finite element method (FEM)-based neural network approach. Based on fishhook maneuver method [18], the comparison of various rollover critical factors and the relationships among vehicle lateral and anti-rollover stability have been investigated.

Conventional PID control [19] approaches with various structures which are the basics of many of the intelligent control approaches are effective for control action. ANFIS which has the advantages of expert knowledge of the FIS and the learning capability of NN proved to be better than ordinary FLC when applied to a quarter-car model [20]. A decentralized neuro-fuzzy controller [21] has been created in order to improve the ride comfort and to increase the stability of semi-active HC suspension system.

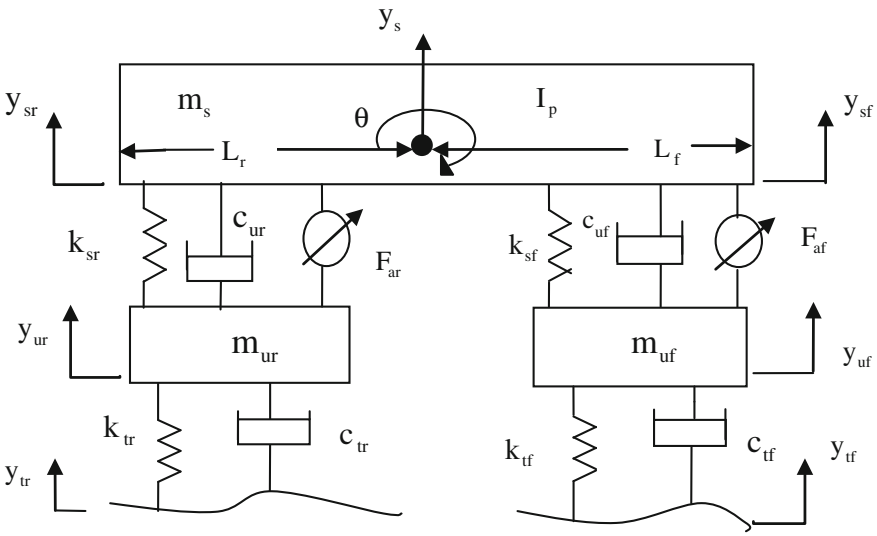

Fig. 1 Half-car model

2 Half-Car Model

HC model (Fig. 1) considered in this study [1] is commonly used because of its simplicity and ability to hold many important features of full-car model. It consists of the chassis (sprung mass) and two-wheel (front and rear) axle parts (unsprung mass). An actuator assembly is present at the front and rear suspensions of HC. The passive spring damper system is connected with actuator in parallel to achieve better ride comfort and to improve the ride quality. It is assumed that the HC model is linear, and always the tires having contact with the road and the forces due to moment and backlash in various joints, linkages, and gear are negligible.

3 Controllers

The proposed control structure is as shown in Fig. 2. In this control structure, suspension deflection of front (SD_f) and sprung mass velocity of front (SV_f) are fed back as input to the controller (C_f) in the front. Similarly, the suspension deflection of rear (SD_r) and sprung mass velocity of rear (SV_r) are fed back as input to the controller (C_r) at the rear. The output of C_f and C_r is used to provide the control force at the front (Fa_f) and rear (Fa_r). The actuator is assumed to be ideal. The different control techniques to provide the control actions used in this work are explained in the following subsections.

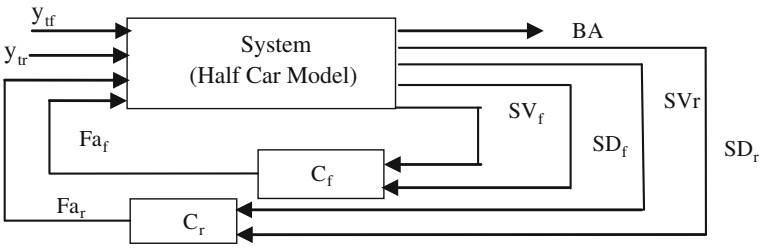

Fig. 2 Proposed control structure

3.1 Fuzzy Logic Controller

FIS structure [21] basically consists of a knowledge base—rule base and a database and reasoning mechanism—a decision-making unit, fuzzification inference, and defuzzification inference which derives the output depending on the input. The fuzzification stage converts real number (crisp) input values into fuzzy values, while the fuzzy inference machine processes the input data and computes the controller outputs to cope with the rule base and database. These outputs, which are fuzzy values, are converted into real numbers by the defuzzification stage.

The controllers C_f and C_r in Fig. 2 are FLCs. The triangular membership function (Fig. 3) is chosen, and using the linguistic variables negative (N), zero (Z), and positive (P), a set of (3 × 3) fuzzy rule base [9] with suspension deflection (SD) and sprung mass velocity (SV) are shown in Table 1. Fuzzy rules are in the form of

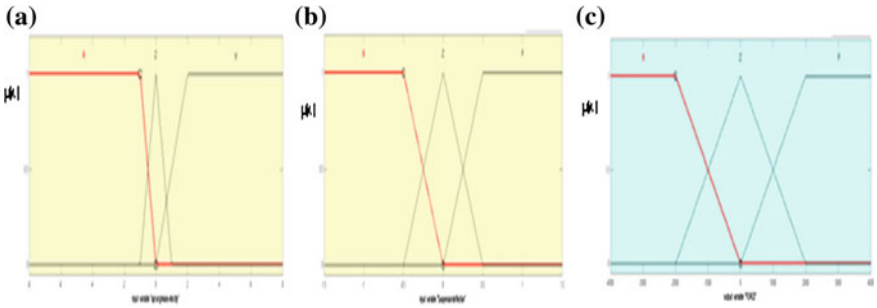

Fig. 3 Membership functions of **a** sprung mass velocity, **b** suspension deflection, and **c** force

Table 1 Rule base

SV \ SD	N	Z	P
N	P	P	Z
Z	P	Z	N
P	Z	N	N

linguistic variables using fuzzy conditional statements. The center of gravity method is used to defuzzify the inferred output.

3.2 Artificial Neural Network Controller

ANN [17] has the ability to adapt with complicated system or system with imprecise data. It consists of at least two physical components, namely neurons and connection links between the neurons. The weight parameters are associated with each link. The neurons are interconnected to form a network which mimics the biological nervous system information processing method. In this paper, ANN is created, trained, simulated, and generated using FLC input–output data. The FLC_f input–output data set is used for ANN_f training process, and FLC_r input–output data set is used for ANN_r training process. After the generation of ANN, the FLC_f and FLC_r are replaced with ANN_f and ANN_r.

The parameters of ANN are given by network type: feed-forward back-propagation, training function: Levenberg–Marquardt (trainlm), adaption learning function: Learngdm, number of layer: 2, number of neurons: 25, transfer function: tansig, number of epochs: 1000, training algorithm: random data division.

3.3 Adaptive Neuro-Fuzzy Inference System

ANFIS [19] a class of adaptive networks that are functionally equivalent to FISs consists of membership functions and rules with adjustable parameters that are determined by ANN. Using the FLC_f and FLC_r inputs, output data sets $ANFIS_f$ and $ANFIS_r$ are trained for front and rear. Figure 4 shows the general structure of the ANFIS. FLC-based ANFIS loading and training data are mapped in Fig. 5.

ANFIS information used in this work is given by number of nodes: 35, number of linear parameters: 27, total number of parameters: 45, number of training data pairs: 50001, number of fuzzy rules: 9, membership functions tuning method: hybrid, number of epochs: 100.

4 Simulation Results and Discussion

The system described in Sect. 2 with different controllers discussed in further sections is simulated in MATLAB environment with front road input y_{tf} which is a dual bump of 0.06 m, 0.03 m height, and a 0.84-s time-delayed rear road input y_{tr} (Fig. 6). The simulation results are shown in Fig. 7a–g.

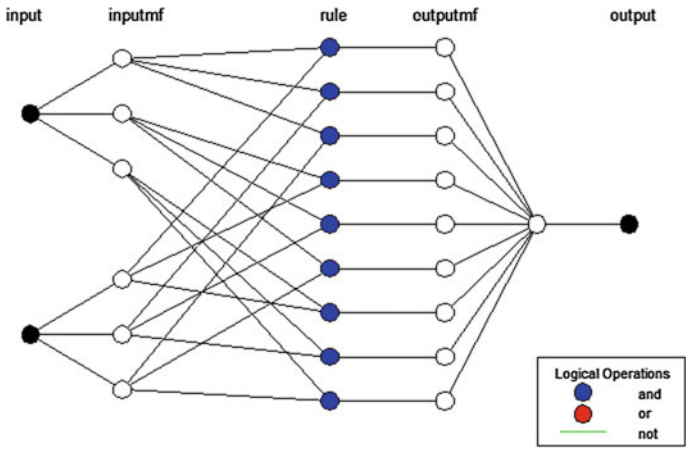

Fig. 4 ANFIS structure

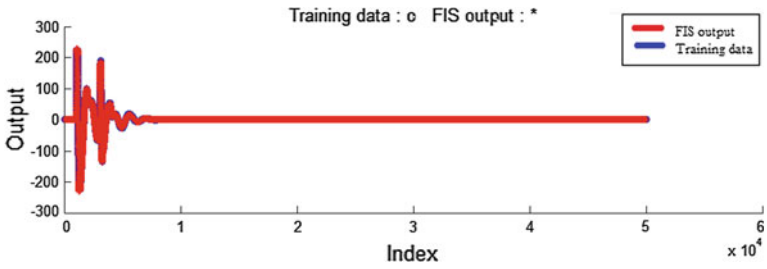

Fig. 5 ANFIS loading and training data

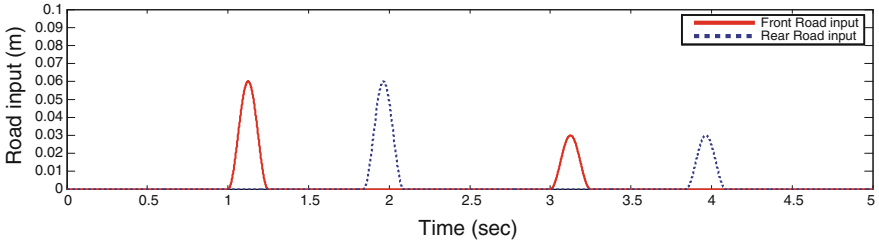

Fig. 6 Road input

Figure 7a shows the comparison of the total body acceleration (BA) for FLC, ANN that is trained with FLC, and FLC-based ANFIS. Similarly, the comparison of BA of front wheel and rear wheel is shown in Fig. 7b, c, respectively. It is clear from Fig. 7a–c how effectively FLC-based ANFIS-based active suspension system reduces the total BA; BA of front and rear is compared to other controller-based

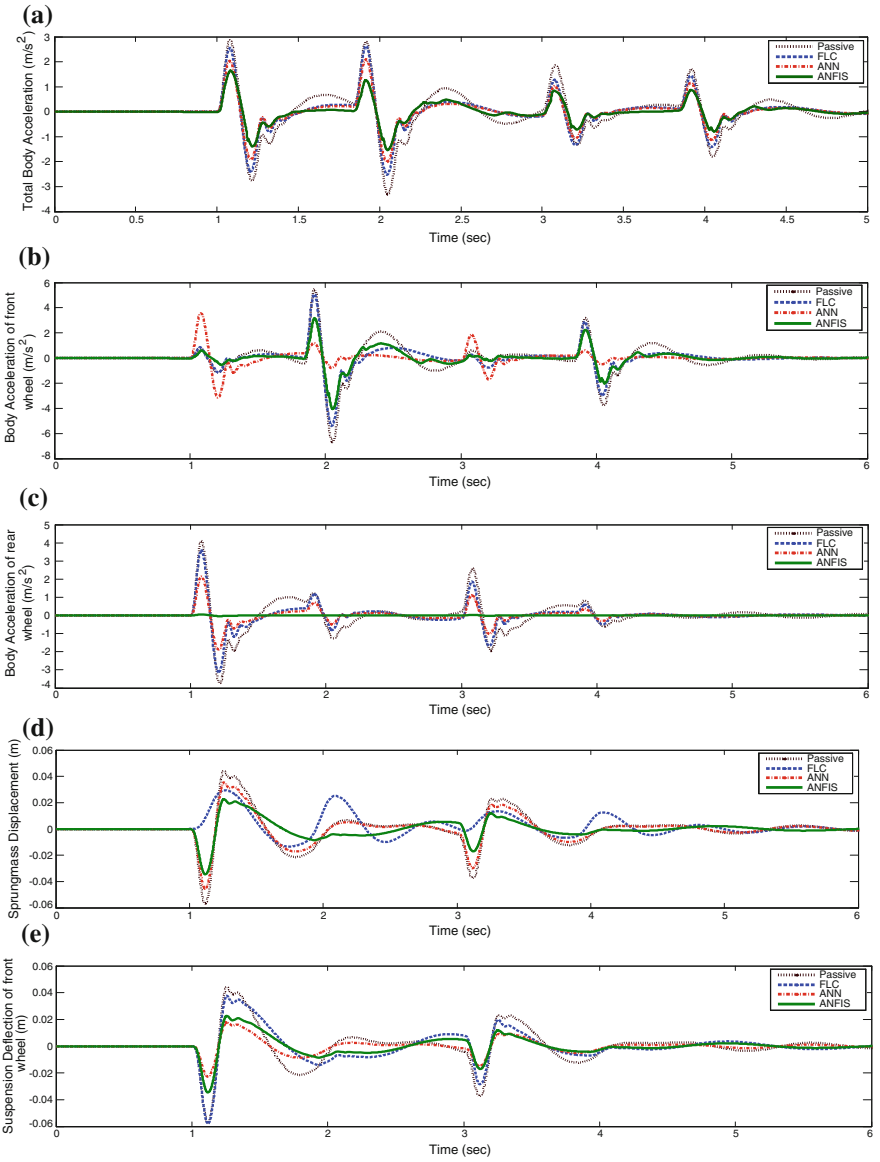

Fig. 7 **a–g** Responses of half-car with various controllers. **a** Body acceleration. **b** Body acceleration of front. **c** Body acceleration of rear. **d** Sprung mass displacement. **e** Suspension deflection for front wheel. **f** Suspension deflection of rear wheel. **g** Power spectral density of body acceleration

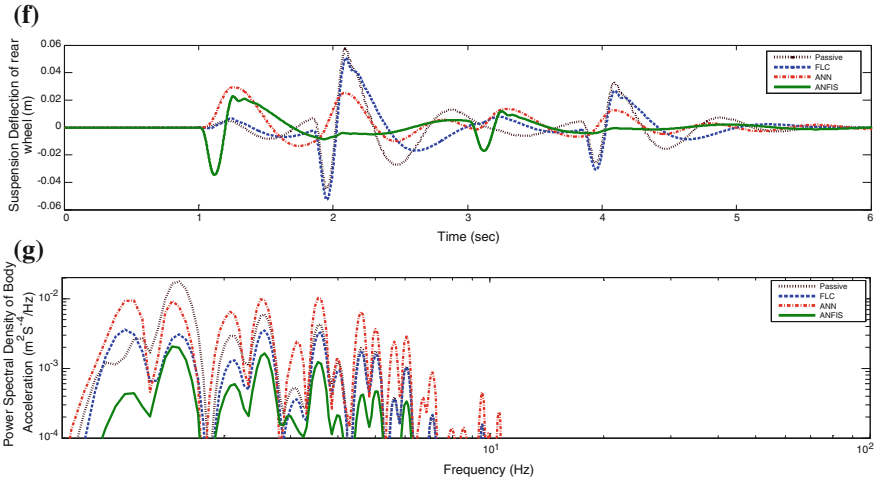

Fig. 7 continued

Table 2 RMS values

Controllers	BA	BA_f	BA_r	SMD	SD_f	SD_r
FLC	0.4667	0.6118	0.7198	0.0067	0.0089	0.0094
ANN	0.4762	0.4582	0.6607	0.0079	0.0040	0.0067
ANFIS	0.2837	0.0060	0.5296	0.0053	0.0053	0.0053

active suspension system. The sprung mass displacement (SMD) is much reduced by FLC-based ANFIS compared to FLC-based ANN and FLC. Figure 7d shows the SMD response comparison of the system. From Fig. 7e, f, it is clear that the SD_f and SD_r are within the static deflection (±8 cm). The variation of power spectral density (PSD) with the road dual bump for total BA is given by Fig. 7g, and that proves the efficacy of the FLC-based ANFIS. The comparison of RMS value of total BA, BA of front (BA_f), BA of rear (BA_r), SMD, SD_f, and SD_r for the system with various controllers is given in Table 2, which shows the effectiveness of FLC-based ANFIS. Thus, FLC-based ANFIS controller guarantees better ride comfort.

5 Conclusion

In this paper, the design procedures of controllers have been discussed for a half-car model with an ideal actuator. The designing of the FLC-based ANFIS controller guarantees better performance compared to passive system, intelligent FLC, and FLC-based ANN controller for active suspension systems. Also it intelligently

reduces the BA and sprung mass displacement and ensures traveling comfort to passengers when subjected to dual bump input. In future, optimization-based controllers can be designed to give better results.

References

1. C.-S. Ting, T.-H.S. LI, F.C. Kung, Design of fuzzy controller for active suspension system. J. Mechatron. **5**(4), 365–383 (1995)
2. S.I. Ihsana, M. Ahmadianb, W.F. Farisa, E.D. Blancardb, Ride performance analysis of half-car model for semi-active system using RMS as performance criteria. Shock Vibr. **16**, 593–605 (2009)
3. S. Turkay, H. Akcay, Influence of tire damping on mixed H_2/H_∞ synthesis of half-car active suspensions. J. Sound Vib. **322**, 15–28 (2009)
4. R.A. Irani, R.J. Bauer, A. Warkentin, A dynamic terramechanic model for small lightweight vehicles with rigid wheels and grousers operating in sandy soil. J. Terrramech. **48**, 307–318 (2011)
5. J. Cao, H. Liu, P. Li, D.J. Brown, State of the art in vehicle active suspension adaptive control systems based on intelligent methodologies. IEEE Trans. Intell. Transp. Syst. **9**(3), 392–405 (2008)
6. A. Faheem, F. Alam, V. Thomas, The suspension dynamic analysis for a quarter car model and half car model, in *3rd BSME-ASME International Conference on Thermal Engineering*, Dhaka (2006), pp. 20–22
7. C.-J. Huang, J.-S. Lin, C.-C. Chen, Road-adaptive algorithm design of half-car active suspension system. Expert Syst. Appl. **37** (2010)
8. C.Y. Tang, G. Zhao, H. LI, S.W. Zhou, Research on suspension system based on genetic algorithm and neural network control, in *2009 Second International Conference on Intelligent Computation Technology and Automation* (2009), pp. 468–471
9. K. Rajeswari, P. Lakshmi, Control of active suspension using fuzzy logic, in *International Conference on Modeling and Simulation*, Coimbatore, 27–29 Aug 2007
10. K. Rajeswari, P. Lakshmi, Adaptive neuro-fuzzy controller for vehicle suspension systems, in *International Conference on System Dynamics and Control—ICSDC* (2010), pp. 134–140
11. N. Yagiz, L.E. Sakman, R. Guclu, Different control applications on a vehicle using fuzzy logic control. Sadhana **33**, 15–25 (2008)
12. J. Campos, F.L. Lewis, L. Davis, S. Ikenaga, Backstepping based fuzzy logic control of active vehicle system, in *Proceedings of the American Control Conference Chicago*, Illinois, June (2000)
13. N.E. Nawa, T. Furuhashi, T. Hashiyama, Y. Uchikawa, A study on the discovery of relevant fuzzy rules using pseudobacterial genetic algorithm. IEEE Trans. Ind. Electron. **46**(6) (1999)
14. R. Krtolic, H. Chan, U. Orguner, H. Hrovat, A two-time-scale analysis of active suspension control of a 2D/4DOF half-car model, in *Proceedings of American Control Conference Seattle,* Washington (1995), pp. 1162–1168
15. N. Al-Holou, T. Lahdhiri, D.S. Joo, J. Weaver, F. Al-Abbas, Sliding mode neural network inference fuzzy logic control for active suspension systems. IEEE Trans. Fuzzy Syst. **10**(2) (2002)
16. J. Xu, J. Fei, Neural network predictive control of vehicle suspension, in *2010 IEEE Conference* (2010) 978-1-4244-7618-3/10
17. J. Kalkkuhl, K.J. Hunt, H. Fritz, FEM-based neural-network approach to nonlinear modeling with application to longitudinal vehicle dynamics control. IEEE Trans. Neural Netw. **10**(4) (1999)

18. Y. Li, W. Sun, J. Huang, L. Zheng, Y. Wang, Effect of vertical and lateral coupling between tyre and road on vehicle rollover vehicle system dynamics. Int. J. Veh. Mech. Mobility 1–26 (2013)
19. P. Solatian, S.H. Abbasi, F. Shabaninia, Simulation study of flow control based on PID ANFIS controller for non-linear process plants. Am. J. Intell. Syst. **2**(5), 104–110 (2012)
20. M.A. Eltantawie, Decentralized neuro-fuzzy control for half car with semi-active suspension system. Int. J. Autom. Technol. **13**(3), 423–431 (2012)
21. M.V.C. Rao, V. Prahlad, A tunable fuzzy logic controller for vehicle suspension systems. Fuzzy Sets Syst. **85**, 11–21 (1997)

State Variable Filter Design Using Improvised Particle Swarm Optimization Algorithm

Aakash Indoria, Varatharajan Varrun, Akshay, Murali Krishna Reddy, Tejaswi Sathyasai, Baskaran Anand and Nirmala M. Devi

Abstract State variable filter design using particle swarm optimization algorithm proves to be better when compared to the conventional design method. It gives several solutions to the component values which are useful in designing the state variable filter. The automatic termination technique gives the best possible solution in lesser time. This technique has several advantages in terms of a quicker convergence rate and efficient computation toward the suitable output, where an added advantage gives the user a control over the output's precision. The performance parameter here can be defined as the trade-off between the convergence time and accuracy of the resulting solution, which is determined by the precision value. The results also indicate that the solution with a predefined precision level can be obtained with the minimum number of iterations in minimum time.

Keywords Particle swarm optimization algorithm · Real-world optimization problems · Complex optimization problems · PSO algorithm

1 Introduction

Particle swarm optimization (PSO) algorithm which was introduced by Kennedy and Eberhart in 1995 [1] is one of the most important swarm theories which find several analogies with nature in day-to-day life. Faster convergence of the swarm is an important parameter which defines the efficiency of the system, where every other particle tends to seek a global best solution. Lesser implementation complexities

A. Indoria (✉) · V. Varrun · Akshay · M.K. Reddy · T. Sathyasai · B. Anand · N.M. Devi
Department of Electronics and Communication Engineering, Amrita School of Engineering, Amrita Vishwa Vidyapeetham, Coimbatore, India
e-mail: aakashindoria2@gmail.com

V. Varrun
e-mail: varun.theofficial@gmail.com

© Springer India 2015

L.P. Suresh et al. (eds.), *Artificial Intelligence and Evolutionary Algorithms in Engineering Systems*, Advances in Intelligent Systems and Computing 325,
DOI 10.1007/978-81-322-2135-7_9

associated with particle swarm has led to its ever-increasing usage in the past decade. Being an iterative algorithm, which produces outcomes based on population, it is extremely capable of solving real-world optimization problems [2–6].

Complex optimization problems which generally involve multimodal equations possess the greatest threat to a conventional PSO algorithm, where the particles get trapped in local optima [7]. Various methodologies have been devised in the recent past to overcome this problem. Increasing the convergence efficiency and speed has always been the greatest priority of a PSO research. However, it has so far been difficult to achieve both the objectives in tandem.

The technique introduced in this paper allows the trade-off between precision and time taken for computation, which is in contrast to the methodologies devised in other techniques [8]. Performance parameter is defined by the control over precision. The other great advantage of this PSO algorithm is that it could easily solve the N-dimensional problem without much increase in complexity. In this paper, state variable filter design problem is chosen, where the optimal value for 6 resistors and 2 capacitors has to be found. This algorithm effectively computes this 8-dimensional problem and gives out the efficient values for the components such that the error is very low.

2 PSO

Several modifications have been proposed to improve the performance of the conventional PSO. A particle in a swarm of PSO indicates a potential solution, where the former is associated with a velocity and position vectors. Any variations to these vectors are governed by Eqs. 1 and 2

$$V_i^D = \omega V_I^D + c_1 * \text{rand_}1_i^d * \left(p\text{best}_i^d - x_i^d\right) + c_2 * \text{rand_}2_i^d * \left(g\text{best}^d - x_i^d\right) \quad (1)$$

$$x_i^d = x_i^d + v_i^d \quad (2)$$

where ω is the inertia weight, c_1 is the cognitive coefficient and c_2 is the social coefficient, and rand_1 and rand_2 are two random numbers within [0, 1] that are independently generated for the dth dimension [1]. Equation 1 is used to compute the velocity of each particle within the search space. The velocity thus computed is used to update the position of the particle. When these two equations are iterated for N number of individual particles in the search space, the particles converge to a certain point where the global best solution exists.

3 Proposed Improvements to Conventional PSO

3.1 Inertia Weight Variation

When compared to the different approaches [9, 10], the scheme proposed in [11] is proved to be better. This scheme allows linear variation of ω with respect to iteration number, as shown in Eq. 3

$$\omega_i = \left(1 - \frac{i}{i_{\max}}\right) * 0.99 \tag{3}$$

where the symbols i and $i_{\max}$ denote the iteration number and the maximum number of iterations, respectively.

3.2 Self-Termination

Traditionally, the specified number of iterations is chosen as the stopping criteria for the algorithm. Some systems might require higher number of iterations, whereas some systems require less; hence, the specific number of iterations required is unknown. The modified algorithm proposed in [11] overcomes this problem (Fig. 1).

The method proposed in this paper is a modified version of that in [11] wherein all the particles are constrained to a certain region in each dimension, and if some particles inadvertently move outside the specified region, their position is updated with the position of the global best particle. The mean fitness of all the particles is computed and equated to that of the global best particle only when the number of particles moving outside the bounded region is less than half of the total number of particles. If the mean fitness value is computed and equated to the global best particle after every iteration, then it may lead to the premature convergence since when most of particles which move out of the bounded region are updated with global best position, the average fitness becomes equal to the global best value at that point of time which leads to termination.

Since this technique requires only two additional simple tasks, which are computation of average value of all the particles and comparison of average value with the global best value, it will be fairly simple to implement it in hardware.

3.3 Validation on Benchmark Functions

In order to test the proposed improved approaches, four benchmark problems from [10] are employed to test the approaches proposed in [11]. For these functions, the problem tends to be only in two dimension and the precision of the converged value

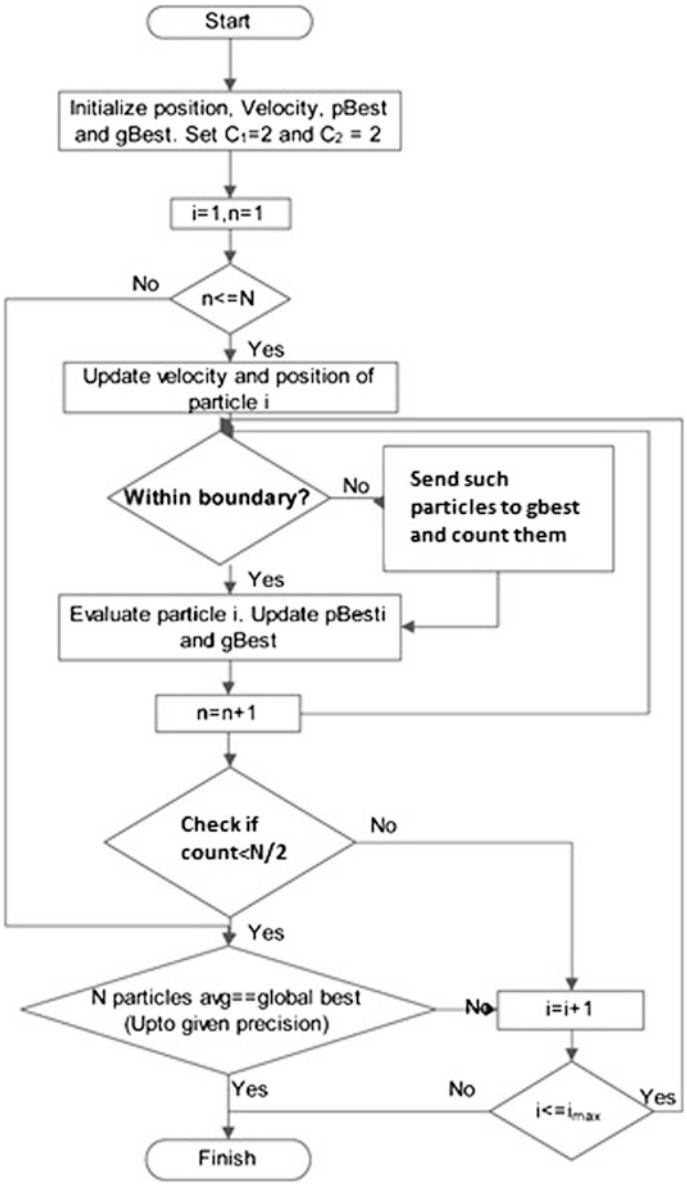

Fig. 1 Flowchart of improvised PSO algorithm

was set to four decimal points; that is, the computation stops when all the particles have the same g_{best} value up to four decimal points. The algorithm is implemented in MATLAB on the machine having Intel i5 first-generation processor with 2 GB of RAM memory. It is observed that the iteration required and the time taken is much less than the conventional PSO algorithm.

Table 1 Optimum solution obtained for benchmark functions and its computation time

Functions	Obtained value, f_{min}	Estimated value	Convergence time (ms)	Iterations required
Sphere	7.6695e−012	0	287	166
Michalewicz	−1.801	−1.8013	323	167
Shubert	−186.7309	−186.7309	589	296
Rastrigin	−40	−40	366	198

f_{min} is the minimum fitness value of the function

Table 1 shows the theoretically estimated values and the computed values with proposed algorithm. It also shows the time taken for convergence and number of iterations required. The graphs for average fitness value of all particles versus iterations for the various benchmark functions in Table 1 are shown in Fig. 2.

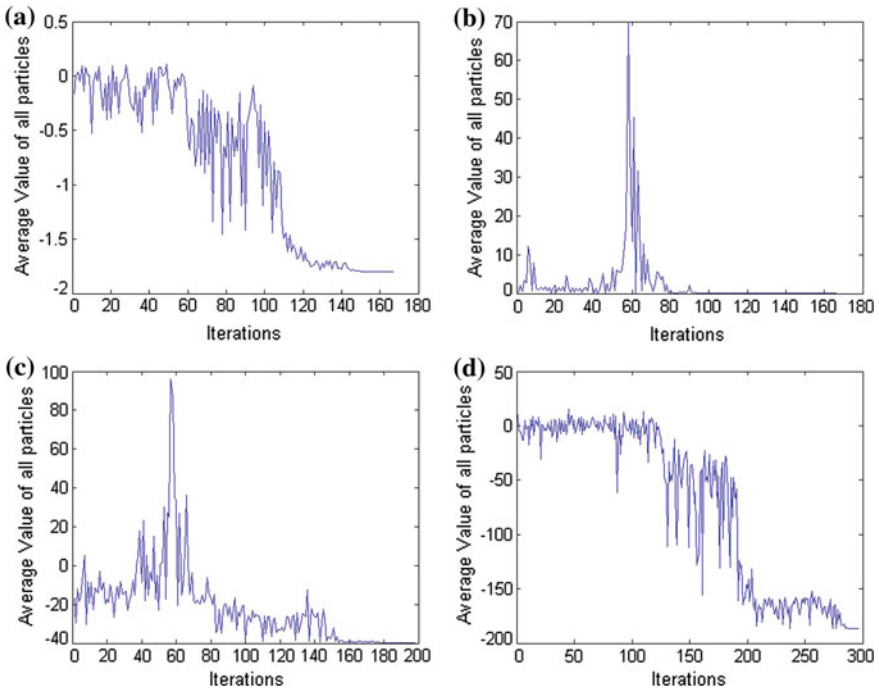

Fig. 2 Average fitness value of all particles for **a** Michalewicz function; **b** Sphere function; **c** Rastrigin function; and **d** Shubert function

4 State Variable Active Filters

Active filters are an important part of communication systems. They are mostly used to selectively allow certain frequencies to pass through and filter out the unwanted frequencies. In the conventional method, values of all resistors are chosen to be equal, except resistor R_2, and the values of both the capacitors are chosen to be the same. But, however, this convention of fixing all the seven component values and varying a single component reduces the versatility of this filter. When an effective filter is needed for critical communication application, we cannot tolerate even a small error. The design of filter with desired cutoff frequency, pass-band gain, and selectivity factor is a great challenge, because solving this is equivalent to solving a N-dimensional problem looking for the least value in the $N + 1$th dimension [12]. The improvised PSO algorithm effectively computes all the dimensions and converges to the value which results in least possible error (Fig. 3).

Even though the desired factors are fixed, it is not easy to devise the resistor and capacitor values. And due to this, the error in the filter gets added up. The total error of the state variable filter is given by Eq. 4

$$\text{Error}_{\text{total}} = 0.5\frac{\left|\sqrt{\frac{R_4}{R_3}\left(\frac{1}{C_1C_2R_5R_6}\right)} - \omega_0\right|}{\omega_0} + 0.5\frac{\left|\frac{R_3(R_1+R_2)}{R_1(R_3+R_4)}\sqrt{\frac{C_1R_4R_5}{C_2R_3R_6}} - Q\right|}{Q} \tag{4}$$

where ω_0 is the cutoff frequency and Q is the selectivity factor. The value of cutoff frequency and selectivity factor was selected as 10,000 rad/s and 0.707, respectively. The error function is optimized using the improvised PSO algorithm to achieve very low error values. The boundary condition of the resistors is given to be between 10 Ω and 100×10^4 Ω and that of capacitors to be between 10 pF and 100×10^4 pF.

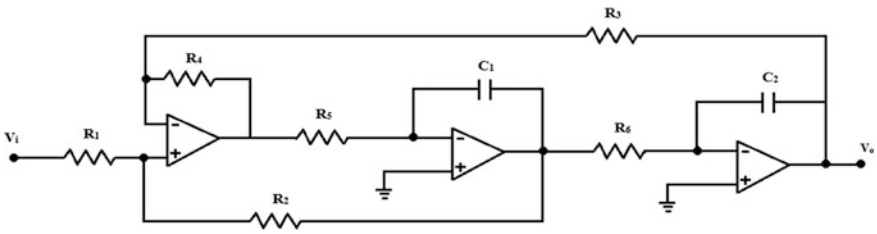

Fig. 3 State variable low-pass filter

Table 2 Values obtained for the components of state variable filter

	Conventional method	Component values using improvised PSO			
		Algorithm (first run)	NP	Algorithm (second run)	NP
R_1 (Ω)	4,000	2,571	2,580	499.36	499
R_2 (Ω)	1,656	3,738	3,740	3,519.41	3,520
R_3 (Ω)	4,000	570	569	3,643.88	3,650
R_4 (Ω)	4,000	1,991	2,000	1,214.51	1,210
R_5 (Ω)	4,000	305	305	2,763.74	2,770
R_6 (Ω)	4,000	362	361	890.97	887
C_1 (μF)	0.025	0.424	0.470	0.00423	0.0047
C_2 (μF)	0.025	0.745	0.680	0.3193	0.330
Error function	0	6.1459e−10	0.05	9.4281e−11	0.0531

5 Results and Analysis

The algorithm has been implemented with the desired boundary conditions. The algorithm gives out various combinations of the component value for every time it runs. This gives a choice for the designer on the selection of the component values. And for any chosen combination, the error occurred will be significantly zero. Table 2 represents the traditional values used in the filter, and it also projects the algorithm's value and the nearest possible (NP) values available in the market.

The average time taken by the function to converge for 30 runs was found to be 1,612 ms, and the average number of iterations that the algorithm took for convergence was found to be 444. This clearly shows that the time taken for the convergence and the iterations required for computing this 8-dimensional problem is very less when compared to the conventional way of solving (Fig. 4).

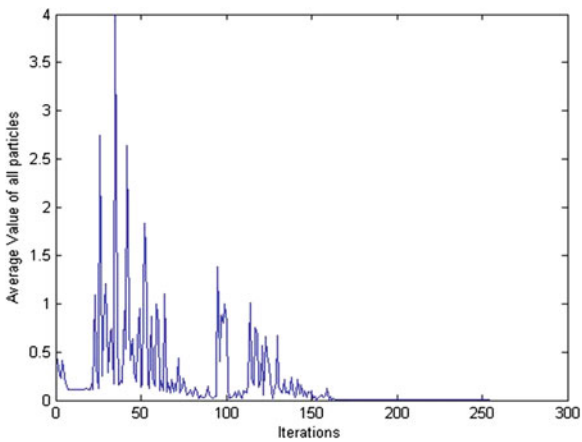

Fig. 4 Average value of all particles versus iterations for Eq. 4

6 Conclusion

The linear variation of inertia with respect to the iteration number proved to be better for unimodal functions. The automatic termination technique in which the solution is obtained when the average fitness of the swarm becomes equal to the global best value proved to be useful in terminating the process with least number of iterations, which in turn reduces computation time. This method is useful for systems where time is a major constraint. For the design of state variable filter, this technique proved to be efficient in both time and accuracy. However, the range of exploration has to be constrained in order to achieve the best solution in the specified region.

References

1. J. Kennedy, R.C. Eberhart, Particle swarm optimization, in *IEEE International Conference on Neural Network*, Perth, Australia, vol. 4 (1995), pp. 1942–1948
2. J. Kennedy, R.C. Eberhart, Y.H. Shi, *Swarm Intelligence* (Morgan Kaufmann, San Mateo, 2001)
3. X.D. Li, A.P. Engelbrecht, Particle swarm optimization: an introduction and its recent developments, in *Proceedings of Genetic Evolutionary Computation Conference* (2007), pp. 3391–3414
4. R.A. Krohling, L. dos Santos Coelho, Coevolutionary particle swarm optimization using Gaussian distribution for solving constrained optimization problems. IEEE Trans. Syst. Man Cybern. B Cybern. **36**(6), 1407–1416 (2006)
5. S.-Y. Ho, H.-S. Lin, W.-H. Liauh, S.-J. Ho, OPSO-orthogonal particle swarm optimization and its application to task assignment problems. IEEE Trans. Syst. Man Cybern. A Syst. Hum. **38**(2), 288–298 (2008)
6. B. Liu, L. Wang, Y.H. Jin, An effective PSO-based memetic algorithm for flow shop scheduling. IEEE Trans. Syst. Man Cybern. B Cybern. **37**(1), 18–27 (2007)
7. J.J. Liang, A.K. Qin, P.N. Suganthan, S. Baskar, Comprehensive learning particle swarm optimizer for global optimization of multimodal functions. IEEE Trans. Evol. Comput. **10**(3), 281–295 (2006)
8. Y. Shi, R.C. Eberhart, A modified particle swarm optimizer, in *Proceedings of IEEE World Congress on Computational Intelligence* (1998), pp. 69–73
9. Z.-H. Zhan, J. Zhang, Adaptive particle swarm optimization, in IEEE Trans. Syst. Man Cybern. Part B Cybern. **39**(6) (2009)
10. T.-Y. Chen, T.-M. Chi, On the improvements of the particle swarm optimization algorithm. Adv. Eng. Softw. **41**, 229–239 (2010)
11. I. Aakash, V. Varrun, Akshay, M.K. Reddy, T. Sathyasai, B. Anand, N.M. Devi, Improvisation of particle swarm optimization algorithm, in *International Conference on Signal Processing and Integrated Networks* (2014)
12. R.A. Vural, T. Yildirim T, State variable filter design using particle swarm optimization. in *Symbolic and Numerical Methods, Modeling and Applications to Circuit Design (SM2ACD)* (2010), pp. 1–4

A Novel Algorithm on IP Traceback to Find the Real Source of Spoofed IP Packets

M. Vijayalakshmi, N. Nithya and S. Mercy Shalinie

Abstract With the availability of Internet at the doorsteps in recent years, there has been a wide range of invasions from strangers such as distributed denial of service (DDoS) attacks. DDoS can be launched from any location, draining resources of the victim machine or network. The original IP address of the attacker is more often spoofed; hence, an IP traceback scheme is needed to trace the source of a packet. In this paper, we propose a novel marking algorithm which provides a single packet traceback directly at the victim's location. The marking algorithm is simple to use with negligible computation and no storage overhead, compared to existing system. Further, the traceback is in convenience to the victim as the entire network traversal or out of band message to identify the attack source is not needed.

Keywords Network security · DDoS attacks · IP traceback · Packet marking

1 Introduction

Distributed denial of service (DDoS) attack is one of the wide spread attacks in the Internet. Popular e-commerce Web sites such as Amazon and eBay have been the victim of DDoS attack. DDoS attack has grown up with lot of sophistication as the Internet is widely available on all devices. Mobile applications and ubiquitous environments have also become the target for DDoS attack. A recent survey [1] reveals that DDoS attacks have amplified intensely in past few years. Different

M. Vijayalakshmi (✉) · N. Nithya · S. Mercy Shalinie
Department of Computer Science and Engineering, Thiagarajar College of Engineering, Madurai 600015, Tamil Nadu, India
e-mail: mviji@tce.edu

N. Nithya
e-mail: nithyaarun@tce.edu

S. Mercy Shalinie
e-mail: shalinie@tce.edu

© Springer India 2015

L.P. Suresh et al. (eds.), *Artificial Intelligence and Evolutionary Algorithms in Engineering Systems*, Advances in Intelligent Systems and Computing 325,
DOI 10.1007/978-81-322-2135-7_10

solutions with various approaches have been proposed over years on advent of this attack. A detailed survey on the nature of the attack, including the meticulous changes that the attack has undergone, and countermeasures put forth for DDoS attack variations is presented in [2]. With these many techniques in hand, the detection and protection against DDoS stand to be a persistent issue. Detecting DDoS attack is a challenging issue due to the difficulty in distinguishing the normal packets from DDoS attack packets, and identification of the attacking source is tedious due to the anonymous nature of the Internet where the source IP address is most often spoofed. Based on [2], IP traceback is one of the reactive techniques used to identify the source of DDoS attack. Traceback up to the level of zombie is claimed to be a successful IP traceback to prevent the source from attacking further. The source of attack may be any compromised host, a reflector or a zombie, etc. With the emergence of DDoS attack, different kinds of traceback schemes are proposed such as link testing, packet marking [broadly classified as deterministic packet marking (DPM) and probabilistic packet marking (PPM)], packet logging, ICMP traceback, hybrid schemes (comprising packet marking and logging), schemes using evolutionary and machine learning algorithm, and information metrics. The proposed technique is a packet marking technique which provides a single packet traceback at the victim's location, without traversing the network.

2 Related Work

A number of IP traceback schemes are proposed to identify the attacker. Following is the condensed presentation of various IP traceback mechanisms. Link testing [3] comprises of two variations—input debugging and controlled flooding. In input debugging [4], the pattern of attack has to be identified at the victim, and the network operator has to install a filter to eliminate the detected attack pattern. The filter identifies the upstream router from which the packet arrives. This process of installation of the filter and the identification of the upstream router continues until the origin of attack is found. Practical difficulty lies in the coordination of the network operator. Control flooding [5] iteratively floods each link to see the effect on the incoming traffic, but flooding in itself is a denial of service attack. Packet marking scheme consists of two types—PPM and DPM. PPM was proposed by Savage et al. [6]. Each router marks the incoming packet with some probability say p where $p = 1/1{,}000$ means one packet is marked for every 1,000 received packets. Several variations to the PPM scheme are proposed in [7–10] enhancing the scheme by minimizing the number of bits for marking, number of packets required for traceback, reducing the false-positive rate in determining the attacker, etc. DPM was first suggested in [11], with an insight of overcoming the difficulties of PPM which suffers from spoofed marking by the attacker, computational load in requiring large number of packets for traceback, etc. In this scheme, every packet is marked, minimizing the number of packets required for traceback. Some schemes require few numbers of packets for traceback [12, 13]. Paper [14] recommends

DPM with single packet IP traceback. Flexible deterministic packet marking (FDPM) is proposed in [15, 16], where the length of marking field is flexible and the marking rate can be changed adaptively. In ICMP traceback (iTrace) [17], each router samples the incoming packets with a low probability (e.g. 1/20,000) and sends a special ICMP message which has the details of neighboring routers along with the original packet. The updated version of iTrace, enhancing the number of useful iTrace packets, is proposed in [18–21]. Packet logging [22–25] provides single packet IP traceback. The drawbacks of this scheme are additional storage requirement and computation at each router. As the storage is so huge, it may lead to false-positive (default in Bloom filter) or false-negative errors (happens when the table is refreshed). Hybrid scheme combines packet marking and logging to overcome the drawbacks of marking and logging schemes when used independently. Several hybrid schemes are suggested in [26–30]. IP traceback with header compression is suggested in [31], which facilitates the increase in space for marking by compression.

3 Proposed Scheme

The proposed scheme provides enhanced the packet marking algorithm minimizing the computations involved in [31]. Aljifri et al. [31] follows RFC 2507 to accommodate its marking data. RFC 2507 proposes header compression which provides 144 bits after compression. RFC 2507 is supported by CISCO which occupies 85 % of global router market [32]. This scheme utilizes a maximum of 96 bits. This scheme offers single packet traceback algorithm directly at the victim.

3.1 Assumptions

The assumptions of the proposed scheme are as follows:

- Each router creates a degree table of its neighbors in advance.
- Each router has a marking code table shown in Table 1 which consists of the OUT node degree (node that forwards the packet), IN node degree (node that receives the packet), and the corresponding marking code. Marking code is a three bit code, which is appended in the marking field of the packet forwarded.
- A router can distinguish the packet coming from a router and an external network.
- This marking and traceback scheme is implemented on all routers.
- The routers with degree less than or equal to four are named (treated) as individual category, and those with degree greater than four are considered as a single category and are not considered for marking and traceback. Figure 1 illustrates the above-discussed router categories based on their degree.

Table 1 Marking code table

Out node (based on degree)	In node (based on degree)	Marking code
B	B	000
B	C	001
B	D	010
C	B	001
C	C	011
C	D	100
D	B	010
D	C	100
D	D	101

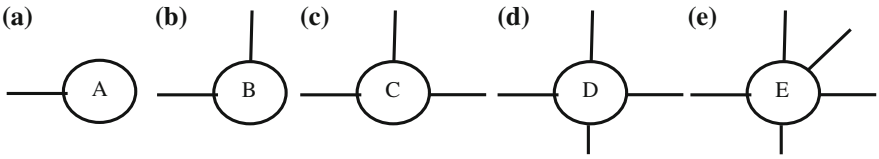

Fig. 1 Router categories. **a** Router/Host with degree 1 as Node A; **b** Router/Host with degree 2 as Node B; **c** Router/Host with degree 3 as Node C; **d** Router/Host with degree 4 as Node D; **e** Router/Host with degree greater than 4 as Node E

3.2 Marking Scheme

Every packet is marked at every router using the algorithm shown in Fig. 2. It is illustrated with the sample network given in Fig. 3. In the sample network, node B is the border router receiving the packet; hence, the packet is marked with '0' initially. Node D receives the packet from node B; therefore, the marking code from B to D (010) is appended to the packet's marking field and the value of field will be 0010. When the packet reaches node C, the marking field value will be 0010100. If the destination is B, the marking field value will be 0010100001. If the destination is node A (node of degree 1), then the marking field value will be 001010001.

3.3 Traceback Scheme

To implement path reconstruction, traceback algorithm shown in Fig. 4 is called at the victim with the mark field value of the received packet. In Fig. 3, when the destination is B, the marking field value is 0010100001. Degree of B is 2 (>1); therefore, the last 3 bits are considered in 0010100**001**; the trace back path is BC.

```
If border router (Router which receives packets from an external network)
   Mark '0' into the packet's marking field
End If
If core router (Router which receives packets from any other router)
   Get the degree of the receiving node from the degree table
   If degree > 1 and degree < 5
      Get the marking code value from the marking code table corresponding to the
sending and receiving routers.
       Append the marking code in the packet's marking field.
   End If
   If degree ==1
      Append 00 or 01 or 10 to the packet's marking field corresponding to the routers
with degree 2 or 3 or 4.
    End If
End If
Forward the packet to the next router until destination is reached.
```

Fig. 2 Marking algorithm

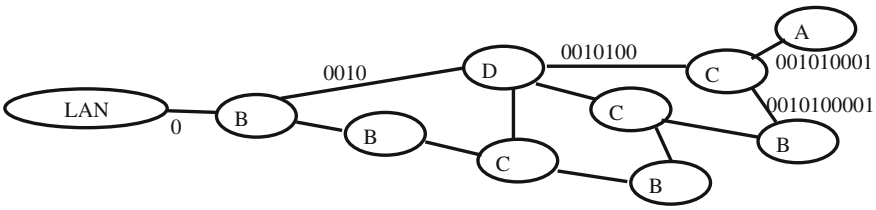

Fig. 3 Marking scheme illustration

```
Get the degree of the node.
  If degree > 1 and degree < 5
      Get the sender node information from the marking code table with the last 3 bits of
the packet's marking field.
      Replace the marking field value with the sender node
   End If
    If degree ==1
      Appended value 00 or 01 or 10 to the packet's marking field corresponding to the
routers is replaced by the sender
   End If
Repeat until '0' is remaining. The router is the closest border router to the attacker.
```

Fig. 4 Traceback algorithm

With C as the receiver, the next 3 bits are considered in 0010**100**, and the trace back path is BCD. Again with D as the receiving node, the next 3 bits are considered in 0**010**, and the trace back path is BCDB. '0' is alone remaining, and therefore, the node B is closer to the attacker. Consider the path with destination A, the marking field value is 001010001. Degree of A is 1, so the last 2 bits are checked 001010**01** to see the upstream router, and the traceback path is AC. From C, the traceback is same as the previous one.

4 Implementation and Result Analysis

The test environment consists of AMD dual-core processor C70 1.333 GHz, 4 GB DDR3 Memory, 500 GB HDD, Ubuntu Linux 12.04. BRITE topology generator is used for topology generation. The generated topology is integrated with NS2.

4.1 Precision

Figure 5 shows the topology generated on BRITE for 20 nodes. Consider the path, 1—16—0—12—17—13—3—15—4 (path).The degree of the nodes is, 5—3—4—4—2—3—6—2—7 (degree).

Here, 1 is the attacker and 4 is the victim. Based on marking algorithm, the marking code generated is 0100101010000100. At times, this path reconstruction

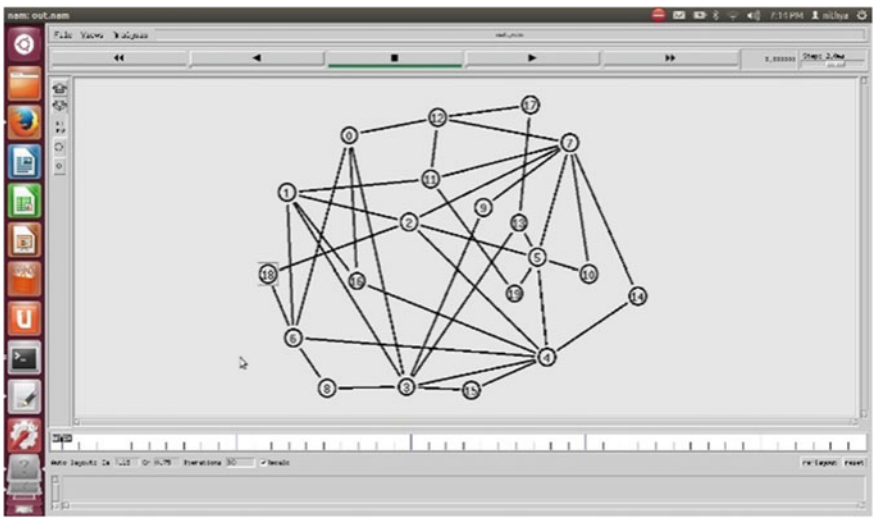

Fig. 5 BRITE topology for 20 nodes

also returns false-positive paths. Consider the path in the same 20 node topology, 7—11—12—0—3—15—4 where node 7 is the source and 4 is the victim, the paths generated during traceback are as follows:

(a) 4—15—3—0—12—11—Original Path
(b) 4—14—7—11—12—0—False Path

The number of false paths generated against the attackers for a minimum number of hops is shown in the graph Fig. 7, for BRITE topology of 50 nodes shown in Fig. 6.

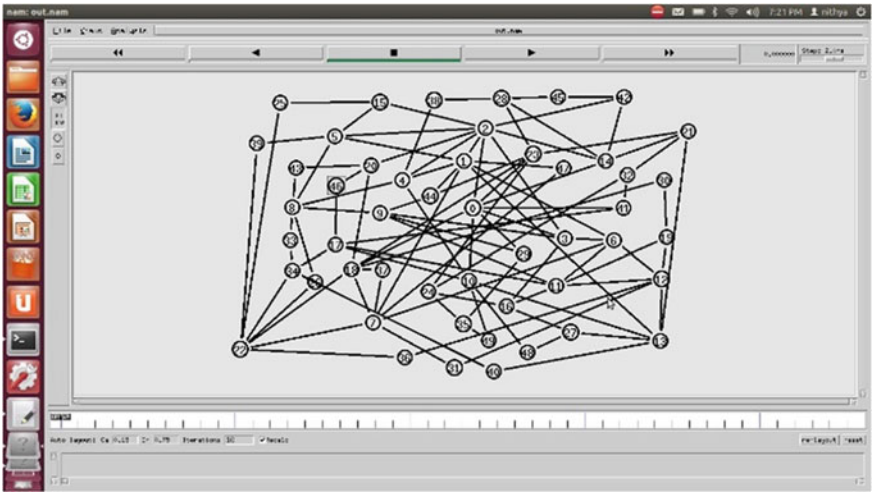

Fig. 6 BRITE topology for 50 nodes

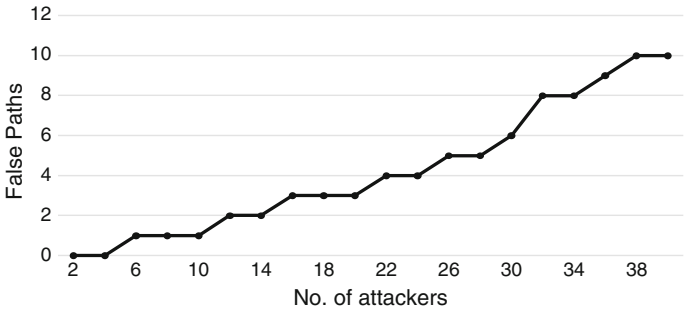

Fig. 7 Analysis on False path generation

4.2 Marking Bit Length

This scheme uses a maximum of 3 bit code for each link, and therefore, the maximum total bits used will be 3H, where 'H' is the hop count. According to CAIDA dataset [33], the maximum and average hops taken by a packet in Internet are 32 and 16, respectively. Therefore, maximum and average number of bits used by this scheme will be 96 and 48 bits, respectively.

4.3 Storage

This scheme requires no logging and no storage of packets at the routers.

5 Conclusion and Future Work

The work presented in this paper implements a novel marking and traceback scheme achieving single packet traceback at the victim's site with negligible computation and no storage overhead. The future work will focus on developing an overlay network on the existing scheme to reduce the occurrence of false paths, and comparison with the header compression scheme will be presented.

References

1. Arbor, IP Flow-Based Technology (2011), http://www.arbornetworks.com
2. H. Beitollahi, G. Deconinck, Analyzing well-known countermeasures against distributed denial of service attacks. Comput. Comm. **35**, 1312–1332 (2012)
3. S. Savage, D. Wetherall, A.R. Karlin, T.E. Anderson, Network support for IP traceback. IEEE/ACM Trans. Networking **9**(3), 226–237 (2001)
4. R. Stone, Centertrack: an IP overlay network for tracking DoS floods, in *Proceedings of the 9th conference on USENIX Security Symposium*, Berkeley, USA (2000), pp. 199–212
5. H. Burch, B. Cheswick, Tracing anonymous packets to their approximate source, in *Proceedings of the 14th USENIX conference on System administration* (2000), pp. 319–328
6. S. Savage, D. Wetherall, A.R. Karlin, T. Anderson, Practical network support for IP traceback, in *Proceedings of ACM SIGCOMM* (2000), pp. 295–306
7. D. Song, A. Perrig, Advanced and authenticated marking schemes for IP traceback, in *Proceedings of IEEE INFOCOM* (2001), pp. 878–886
8. T.K.T. Law, D.K.Y. Yau, J.C.S. Lui, You can run, but you can't hide: an effective statistical methodology to trace back DDoS attackers. IEEE Trans. Parallel Distrib. Syst. **16**(9), 799–813 (2005)
9. A. Yaar, A. Perrig, D. Song, FIT: fast internet traceback, in *Proceedings IEEE INFOCOM* (2005), pp. 1395–1406

10. M.T. Goodrich, Probablistic packet marking for large scale IP traceback. IEEE/ACM Trans. Networking **16**(1), 15–24 (2008)
11. A. Belenky, N. Ansari, IP traceback with deterministic packet marking. IEEE Comm. Lett. **7** (4), 162–164 (2003)
12. A. Belenky, N. Ansari, Tracing multiple attackers with deterministic packet marking (DPM), in *Proceedings of IEEE PACRIM'03*, Victoria, BC, Canada (2003), pp. 49–52
13. A. Belenky, N. Ansari, On deterministic packet marking. Comput. Netw. **51**(10), 2677–2700 (2007)
14. G. Jin, J. Yang, Deterministic packet marking based on redundant decomposition for IP traceback. IEEE Comm. Lett. **10**(3), 204–206 (2006)
15. Y. Xiang, W. Zhou, J. Rough, Trace IP packets by flexible deterministic packet marking (FDPM), in *Proceedings of IEEE International Workshop IP Operations and Management (IPOM '04)* (2004), pp. 246–252
16. Y. Xiang, W. Zhou, M. Guo, Flexible deterministic packet marking: an IP traceback system to find the real source of attacks. IEEE Trans. Parallel Distrib. Syst. **20**(4), 567–580 (2009)
17. S.M. Bellovin, M.D. Leech, T. Taylor, ICMP traceback messages, Internet Draft: Draft-Ietf-Itrace-04.Txt (2003)
18. H.C.J. Lee, V.L.L. Thing, Y. Xu, M. Ma, ICMP traceback with cumulative path, an efficient solution for IP traceback, in *International Conference on Information and Communications Security*. Springer Lecture Notes in Computer Science, vol. 2836 (2003), pp. 124–135
19. V.L.L. Thing, H.C.J. Lee, M. Sloman, J. Zhou, Enhanced ICMP traceback with Cumulative Path, in *61st IEEE Vehicular Technology Conference* (2005)
20. W. Felix, On design and evaluation of intention-driven ICMP traceback, in *Proceedings of IEEE International Conference on Computer Communications and Networks* (IEEE CS Press, 2001), pp. 159–165
21. A. Izaddoost, M. Othman, M.F.A. Rasid, Accurate ICMP traceback model under DoS/DDoS attack, in *Proceedings of the 15th International Conference on Advanced Computing and Communications* (2007)
22. A.C. Snoeren et al., Single-packet IP traceback. IEEE/ACM Trans. Networking **10**(6), 721–734 (2002)
23. T. Baba, S. Matsuda, Tracing network attacks to their sources. IEEE Internet Comput. **6**(3), 20–26 (2002)
24. J. Li et al., Large-scale IP traceback in high-speed internet: practical techniques and theoretical foundation, in *Proceedings of IEEE Symposium Security and Privacy* (S&P '04) (2004), pp. 115–129
25. M.S. Siddiqui, S.O. Amin, C.S. Hong, Hop by hop traceback in wireless sensor networks. IEEE Comm. Lett. **16**(2), 242–245 (2012)
26. B. Al-Duwariand, M. Govindarasu, Novel hybrid schemes employing packet marking and logging for IP traceback. IEEE Trans. Parallel Distrib. Syst. **17**(5), 403–418 (2006)
27. C. Gong, K. Sarac, A more practical approach for single-packet IP traceback using packet logging and marking. IEEE Trans. Parallel Distrib. Syst. **19**(10), 1310–1324 (2008)
28. K.H. Choi, H.K. Dai, A marking scheme using Huffman codes for IP traceback, in *Proceedings of 7th Int. Symposium Parallel Architectures, Algorithms Networks (SPAN'04)*, Hong Kong, China (2004), pp. 421–428
29. S. Malliga, A. Tamilarasi, A hybrid scheme using packet marking and logging for IP traceback. Int. J. Internet Protocol Technol. **5**(1/2), 81–91 (2010)
30. M.H. Yang, M.C. Yang, RIHT: a novel hybrid IP traceback scheme. IEEE Trans. Inf. Forensics Secur. **7**(2), 789–797 (2012)
31. H. Aljifri, M. Smets, A. Pons, IP Traceback using header compression. Comput. Secur. **22**(2), 136–151 (2003)
32. Reuters ltd, *Cisco gaining share in routers, switches*. (The mercury news, London, 2002)
33. CAIDA's Skitter Project CAIDA, 2010 [Online]. http://www.caida.org/tools/skitter/

A Queueing Model for e-Learning System

T. Senthil Kumar and K.I. Ohhm Prakash

Abstract There has been much written about e-Learning practice; however, little attention has been given to come out with a mathematical model for e-Learning. As the lack of a proper mathematical model will hinder providing better service to the customers, we have come up with an attempt to make a study on which of the existing mathematical models could fit e-Learning. We argue with statistical data that (M/M/C): (∞/FIFO) is one of the models which best fit e-Learning. This paper aims to provide inputs that the suggested queuing model can be used for e-Learning system in real conditions.

Keywords Queue · Model · Service · Hypertext · Parameters

1 Introduction

1.1 Introduction to Queuing Theory

A queue represents the number of units waiting for service. A queue forms when demand exceeds the capacity. In other words, when the arrival rate is more than the service rate, a queue is formed. A queuing system consists of one or more servers that provide service of some sort to arriving customers [1]. A queuing system is characterized by three components:

T. Senthil Kumar (✉) · K.I. Ohhm Prakash
Department of Computer Science and Engineering,
Amrita School of Engineering, Amrita Vishwa Vidyapeetham,
Coimbatore 641105, India
e-mail: drtsk111@gmail.com

K.I. Ohhm Prakash
e-mail: ohhm_prakash@yahoo.com

© Springer India 2015

L.P. Suresh et al. (eds.), *Artificial Intelligence and Evolutionary Algorithms in Engineering Systems*, Advances in Intelligent Systems and Computing 325,
DOI 10.1007/978-81-322-2135-7_11

- Arrival process,
- Service mechanism,
- Queue discipline.

Notation for Queues Since all queues are characterized by arrival, service, and queue and its discipline, the queue system is usually described in shorten form by using these characteristics [2]. The general notation is as follows:

$$[a/b/c] : [d \ / \ e]$$

where

a Probability distribution of the arrivals,
b Probability distribution of the departures,
c Number of servers,
d The capacity of the queue(s),
e Queue discipline.

Modeling the queuing theory to real-time applications is of vital challenge and interesting. It provides insights for real-time problems catering to business solutions [3].

1.2 Introduction to e-Learning

e-Learning is a new form of learning introduced in this century. e-Learning decreases the educational costs, and it is more effective learning the traditional learning. Globally, it allows the fast dissemination of new techniques and processes, canceling geographic challenges. In addition, time efficiency plays a role, as travel is reduced. Users can conveniently access training materials from home via the Internet.

2 Problem

Identify the network traffic as a queuing problem and identify the difficulties expected during any Internet program for specific purpose. This leads to place our study materials and sequencing of lesson plans and get into a model of the hyper text, which is our e-Learning object.

3 Introduction to Hypertext

Hypertext refers to interlinked pieces or text or other objects stored electronically. Each unit of information is called a node, module, or topic, and is associated with other modules or external texts or objects by links. Modules or nodes are connected with links. Links can be made to external as well as internal ideas [4]. These links, which readers are free to navigate at will, can make connections between texts, graphics, audio, or video. This nonlinear form of writing emulates the way we think through an association of ideas [3].

Characteristics of hypertext

- Association of ideas through links.
- A choice of paths for readers and not all readers follow the same path.
- Immediate access to reference documents.
- Movement through hypertext by browsing or navigating.
- Focus of thought is always shifting in a hypertext environment.

4 Application of Queuing Model in Computer Network

Queuing model has a variety of applications from basic reservation system to multilane system processing. The request needs to be processed from users and handled in an efficient manner. Queuing model offers a better solution so that the service is provided to users in a right time in a right manner without starvation [5]. The request has a capacity that differs from application to application based on the constraints in the domain. Today's environment provides a lot of challenges as the communication among users happens through wired and wireless manner. The underlying infrastructure also provides a challenge to the queuing model designers [6]. The flow mechanism can be understood considering a stochastic environment [7]. A two-station network is a typical example for real-time scenario [8, 9].

5 Problem Specification

To give a queuing model for e-Learning when the study materials are placed in different locations of any course work. The model considers assumptions of both static and dynamic conditions, assuming that the traffic flow is constant. The transactional information that is maintained during user access becomes the basis for the queuing model in this work [10].

6 Data Statistics

6.1 Data Collection

The portals of IEEE, Science Direct, and Google Scholar were taken for our consideration. The time taken for the Web page to load was taken as the arrival time, and the time taken to search a particular document, view it and logout and reach the home page was taken as the service time.

6.2 Markov Distribution

We take (M/M/C): (∞/FIFO) model for consideration. In this model, the arrivals follow Poisson's distribution, service time is exponentially distributed, and there are C servers with infinite capacity. The queue discipline is FIFO. This model is found to be one among the models that could fit e-Learning module.

6.3 Calculations and Computations

In our experiment, the arrival rate and service rate were found to be $\lambda = 5.33$ and $\mu = 2.57$, respectively. We now calculate the various probabilities and expected values for the model taken for consideration.

The list of parameters is as follows:

$$\begin{aligned} \lambda &= 5.33 \\ \mu &= 2.57 \\ C &= 3 \\ \rho &= \lambda/\mu \\ &= 2.07 \\ \rho_0 &= \lambda/(\mathrm{C}\mu) \\ &= 0.67 \end{aligned}$$

6.3.1 Probability that the System Is Idle

The probability that the system is idle is given by *P0*.

$$\text{We know that } \frac{1}{P_0} = \left[\sum_{n=0}^{C-1} \frac{\rho^n}{n!} + \frac{\rho^C}{C!}\frac{1}{(1-\rho_0)}\right]$$

$$= 23.14$$

$$\mathrm{P}_0 = 0.04$$

6.3.2 Expected Number of Customers in the Queue

The expected number of customers in the queue is given by *Lq*.

$$\text{We know that } L_q = P_0 \frac{\rho^C}{C!} \frac{\rho_0}{(1-\rho_0)^2}$$
$$= 0.36$$

6.3.3 Expected Number of Customers in the System

The expected number of customers in the system is given by *Ls*.

$$\text{We know that } L_s = L_q + \rho_0$$
$$= 1.03$$

6.3.4 Expected Waiting Time in the Queue

The expected waiting time in the queue is given by *Wq*.

$$\text{We know that } W_q = \frac{1}{\lambda} L_q$$
$$= 0.07 \text{ s}$$

6.3.5 Expected Waiting Time in the System

The expected waiting time in the system is given by *Ws*.

$$\text{We know that } W_s = W_q + \frac{1}{\mu}.$$
$$= 0.46 \text{ s}$$

7 Conclusion

From the values we have obtained, we conclude that (M/M/C): (∞/FIFO) model is one among the models that could fit e-Learning module. This could also be applied with approximation mechanisms [11]. It leads to a new direction of research in this field. The advantage of finding a queuing model that would fit e-Learning is that it enables to provide better service to the customers, by calculating the service time, waiting time, etc., mathematically and improving service by taking necessary action like increasing the number of servers to reduce the waiting time, because in this competitive world, a customer waiting too long in queue is potentially a lost customer. The approach can be further extended for many users in a wireless

environment with more types of request handled from the users. The approach can be compared against actions in users in a fast-food restaurant as the traffic becomes infinite [4]. The queuing in real time for a complex system like vehicle ad hoc networks is also of prime importance [12]. Learning approaches could also be applied for improving the strength and learning capabilities of the queuing model [13]. Brownian models can also be applied for investigating the proposed results [14].

References

1. P. Sherman, Queuing theory and practice: a source of competitive advantage. http://www.isixsigma.com/industries/retail/queuing-theory-and-practice-source-competitive-advantage/
2. J.D.C. Little, A Proof for the Queuing Formula: L = λW". Oper. Res. **9**(3), 383–387 (1961)
3. M. Laguna, J. Marklund, *Business Process Modeling, Simulation and Design* (Pearson Prentice Hall, NJ, 2005). ISBN 0-13-091519-X
4. S.A. Curin, J.S. Vosko, E.W. Chan, O. Tsimhoni, Reducing service time at a busy fast food restaurant on campus, in *Proceedings of the 2005 Winter Simulation Conference*, IEEE Press (2005)
5. M. Zukerman, Introduction to queuing theory and stochastic teletraffic models. http://www.ee.cityu.edu.hk/~zukerman/classnotes.pdf
6. S. Aljawarneh, Z. Muhsin, A. Nsour, F. Alkhateeb, E. AlMaghayreh, e-Learning Tools and Technologies in Education, *A Perspective. LINC Proceedings* (2010)
7. J.M. Harrison, *Brownian Motion and Stochastic Flow Systems* (Wiley, New York, 1985)
8. J.M. Harrison, L.J. Wein, Scheduling networks of queues: heavy traffic analysis of a two-station closed network. Oper. Res. **38**, 1052–1064 (1990)
9. L.J. Wein, Scheduling networks of queues: heavy traffic analysis of a two-station network with controllable inputs. Oper. Res. **38**, 1065–1078 (1990)
10. R. Larson, The queue inference engine: deducing queue statistics from transactional data. Manage. Sci. **36**, 586–601 (1990)
11. D.Y. Burman, An analytic approach to diffusion approximation in queueing. Ph.D. Dissertation, Department of Mathematics, New York University, 1979
12. R. Jain, J.M. Smith, Modelling vehicular traffic flow using M/G/C/C state dependent queueing models. Transp. Sci. **31**, 324–336 (1997)
13. J.G. Dai, On positive Harris recurrence of multiclass queueing networks. A unified approach via fluid limit models. Ann. App. Prob. **5**, 49–77 (1995)
14. J.M. Harrison, V. Nguyen, Brownian models of multiclass queueing networks: Current status and open problems. Queueing Syst. Th. Appl. **13**, 5–40 (1993)
15. J.M. Harrison, Brownian models of queueing networks with heterogeneous customer populations, in *PTOCI. MA Workshop on Stoc. Diff. Sys.* Springer. (1988), pp. 147–186

Development of Common Parallel Programming Platform for MPI and PVM

Veerabasavantha Swamy, S. Sampath, B.R. Nanjesh and Bharat Bhushan Sagar

Abstract Parallel virtual machine (PVM) and message-passing interface (MPI) are the most successful message-passing libraries to map parallel algorithm onto parallel computing platform. Configuration of MPI and PVM in the nodes present in parallel computing environment (desktop PC's interconnected using ethernet LAN) is the time-consuming task for a user. This configuration procedure requires lot of knowledge about the steps to be followed to make them work properly. Configuration becomes the difficult task when there are more number of nodes in the parallel computing environment. Our work aims on developing a common parallel programming platform, which allows a user to get MPI and PVM in the nodes without any time-consuming configuration steps. This is done by integrating the recent version of PVM: PVM3.4.6 into the MPI's MPICH2 packages in order to simplify the time-consuming task of configuring them separately.

Keywords Parallel virtual machine · Parallel computing environment · LINUX platform

V. Swamy (✉)
Department of CS and E, Prodha Devaraya Institute of Technology, Hospet, Karnataka, India
e-mail: veera.basava@gmail.com

S. Sampath
Department of CS and E, Shri Venkateshwara University, Gajraula, Uttarpradesh, India
e-mail: 23.sampath@gmail.com

B.R. Nanjesh
Department of IS and E, Adichunchanagiri Institute of Technology, Chikmagalur, Karnataka, India
e-mail: nanjeshbr@gmail.com

B.B. Sagar
Department of IS and E, Birla Institute of Technology, Noida, Uttarpradesh, India
e-mail: drbbsagar@gmail.com

© Springer India 2015

L.P. Suresh et al. (eds.), *Artificial Intelligence and Evolutionary Algorithms in Engineering Systems*, Advances in Intelligent Systems and Computing 325,
DOI 10.1007/978-81-322-2135-7_12

1 Introduction

Many numbers of parallel computing tools are developed to create parallel programming environment such as parallel virtual machine (PVM), message-passing interface (MPI), OpenMP, RPC, etc. In our work, we are considering MPI and PVM. MPI is specification for message-passing libraries that can be used for writing portable parallel programs. In MPI programming, a fixed set of processes is created at program initialization. Each process knows its personal number. Each process knows number of all processes, and they can communicate with other processes. Process cannot create new processes, and the group of processes is static. PVM is a software package that allows a collection of nodes (host pool) to function as a single high-performance parallel virtual machine. The PVM system consists of the daemon (or pvmd), the console process, and the interface library routines. MPI and PVM have many versions, among which we are considering their recent versions, namely PVM3.4.6 and MPICH2.

1.1 MPICH2

MPICH2 is a freely downloadable source code via MPI organization Web site: http://www.mpich.org.

An all-new implementation of MPI is designed to support both MPI-1 and MPI-2 and to enable further research into MPI implementation technology [1]. To achieve high performance and scalability and to encourage experimentation, the design of MPICH2 is strongly modular. In MPICH2, the collective routines are significantly faster, and it has very low communication overhead than the classic MPI and MPICH versions [5].

1.2 PVM3.4.6

PVM3.4.6 is freely downloadable source code via PVM organization Web site: http://www.netlib.org/pvm3/pvm3.4.6.tgz.

PVM3.4.6 [6] is the recent version of PVM. It includes both Windows and UNIX versions and improved use on Beowulf clusters. It also includes the latest patches for working with the latest versions of Linux (like fedora 14), Sun, and SGI systems. New features in PVM 3.4.x include communication contexts, message handlers, and persistent messages.

2 Literature Survey

Ismail et al. [2] performed the concurrent matrix multiplication on multicore processors. This study is a part of an ongoing research for designing a new parallel programming model SPC3 PM for multicore architectures. Mancini et al. [3] presented off-line performance prediction of message-passing applications on cluster systems. They described a simulation-based technique for the performance prediction of message-passing applications on cluster systems. Jin et al. [4] discussed the incentive for using clusters as well as the technologies available for building clusters and also discussed a number of Linux-based tools such as MPI, PVM, etc., and utilities for building clusters. Eclipse PTP project provides an integrated development environment to support the development of parallel applications written in C, C++, and Fortran. It Supports the MPI, OpenMP and UPC programming models, as well as OpenSHMEM and OpenACC. Our work provides an integrated version of MPI and PVM to support development of parallel applications using MPI and PVM separately in a common platform.

3 Development of Common Parallel Programming Platform

Development of common platform for MPI and PVM programming involves three phases:

1. Configuration of MPICH2.
2. Configuration of PVM3.4.6
3. Integration of PVM3.4.6 into MPICH2 packages. Initially, configuration of MPI and PVM is done over the LINUX platform separately.

3.1 Configuration of MPICH2

Download the mpich-2 package and type the following commands in the terminal to install [5].
Unpack the tar file and go to the top-level directory:
tarxzf mpich2-1.3.2.tar.gz cd mpich2-1.3.2
Configure MPICH2 specifying the installation directory:
./configure–prefix=/home/<USERNAME>/mpich2-install
|& tee c.txt
Build MPICH2:make 2>&1 | tee m.txt
Install the MPICH2 commands: Make install 2>&1 | tee mi.txt
Add the bin subdirectory of the installation directory to your path in your startup script (.bashrc for bash,.cshrc for csh):
PATH=/home/<USERNAME>/mpich2-
Install/bin:$PATH; export PATH.

3.2 Configuration of PVM3.4.6

Download the software package [7]
from http://www.netlib.org/pvg3
Unpacking: Command:
$tar zxvf pvm3.4.6.tgz
Open the .bhrc file through terminal using vi editor and set the following lines in the file and close the file. The .bhrc is a hidden file of course and can be done as follows:
$home
$ls –a
$vi .bhrc
Going to the insert mode add the following lines as follows:
PVM_ROOT=$HOME/pvm3
PVM_DPATH=PVM_ROOT/lib/pvmd
Export PVM_ROOT PVM_DPATH
Going to pvm3 directory ($cd pvm3) type make ($make). This would make pvm (the PVm console), pvmd3 (the pvm daemon), libpvm3.a (PVM C/C++ library), libfpvm3.a
(PVM Fortran library) and libgpvm3.a (PVM group library). All these files would be placed in the
$/pvm3/lib/LINUX and pvmgs (PVM group server) would be placed in $/pvm3/bin/LINUX.
Open .rhosts file in the home directory ($vi .rhosts) and add the name of the node (computer) in the cluster of computers. Set the following environment variables in .bashrc file as follows:
exportPVM_ARCH='$PVM_ROOT/lib/pvmgetarch'
export PVM_ROOT=$HOME/pvm3/xpvm export PATH=$PATH:
$PVM_ROOT/lib
exportPATH==$PATH:$PVM_ROOT/lib/$PVM_ARCH.

3.3 Integration of PVM3.4.6 into MPICH2 Packages

After configuration of MPI and PVM, we need to do the following procedure:

Copy the architecture-named directory present in pvm3.4.6 directory into mpich2 1.3.2p1.

Merge the files present in conf, lib directory of pvm3.4.6 to conf, lib directory respectively of mpich2-1.3.2p1.

Copy the libfpvm, include, xdr, pvmgs, tracer, shmd, src directory to (new features of pvm3.4.6) to mpich2-1.3.2p1. Merge the makefile and makefile.aimk, makefile.in.

In mpich2-install directory, add (few are copied or few are merged) the lib, bin, and include files of pvm3.4.6 to the respectively named directories. The above steps give us the directories **mpich2-1.3.2p1** and **mpich2-install** containing the packages of both MPICH2 and PVM3.4.6. These two are now portable and can be used in any node where PVM and MPI programming environment needs to be established.

3.4 User Guidelines

A user must do the following steps to make the new programming model to work properly:

Step1 Paste the two integrated files mpich2-1.3.2p1 and mpich2-install in the node. We use two supporting files along with the above two integrated directories, namely supporting_file1 and supporting_file2 shown in Figs. 1 and 2, respectively.

Step2 vi $HOME/.bashrc

Remove all contents of this file and paste the contents of supporting file1 to it and save. Instead of specifying PVM_RSH, PVM_ROOT, and PVM_ARCH, user should specify only his/her user name of the LINUX platform in the first line of the contents shown in supporting file1.

Step3 vi $HOME/.bash_profile

Remove all contents of this file and paste the contents of supporting file2 to it and save. User must specify the his/her user name of the LINUX platform and architecture of the LINUX-based node in the fourth and sixth line of the contents shown in supporting file2.

Fig. 1 Contents of supporting_file1

```
PVM_ROOT=$HOME/pvm3
export PVM_ROOT
PVM_RSH=/usr/bin/ssh
export PVM_RSH
if [ -f /etc/bashrc ]; then
      . /etc/bashrc
fi
if [ -z $PVM_ROOT ]; then
   if [ -d ~/pvm3 ]; then
      export PVM_ROOT=~/pvm3
   else
      echo "Warning - PVM_ROOT not defined"
   fi
fi
if [ -n $PVM_ROOT ]; then
   export PVM_ARCH=`$PVM_ROOT/lib/pvmgetarch`
   export
PATH=$PATH:$PVM_ROOT/lib/$PVM_ARCH
   export
PATH=$PATH:$PVM_ROOT/bin/$PVM_ARCH
fi
```

```
PVM_RSH=/usr/bin/ssh
export PVM_RSH
PVM_ROOT=/home/username/mpich2-1.3.2p1
export PVM_ROOT
PVM_ARCH=architecture_name
#(example:LINUX64)
export PVM_ARCH
if [ -f ~/.bashrc ]; then
. ~/.bashrc
 fi
PATH=$PATH:$HOME/bin
export PATH
```

Fig. 2 Contents of supporting_file2

```
Paste program files into the directory mpich2-
1.3.2p1→examples
Type the following:
1)  cd /home/username/mpich2/1.3.2p1/examples
2) PATH=/home/username/mpich2-install/bin:$PATH; export
PATH
3) mpicc –c programname.c –o programname.o mpiexec-f
machine –n x /home/username/mpich2-
1.3.2p1/examples/programname
4) mpicc programname.o –o programname
mpiexec –f machine –n x /home/username/mpich2-
1.3.2p1/examples/programname

/* in the above lines x is the number of slaves needed for computation
and machine is machine file containing list of hosts (in the form
host1:2 host2:2 and so on), this file is created in cd
/home/username/mpich2-1.3.2p1/examples).
```

Fig. 3 MPI program compilation and execution

3.5 Program Compilation and Execution

Program compilation and execution in newly developed programming model is same as we do in the single programming environment. User can compile and execute parallel code using MPI or PVM depending on his/her need. It is shown in Figs. 3 and 4 for MPI and PVM, respectively.

4 Testing

Testing is very much needed to check the programming model for its proper working. Testing is made under two cases as testing over single node (Table 1) and testing over multiple nodes (Table 2). In both the cases, we are using parallel matrix

```
Paste master and slave program files into the directory mpich2-
1.3.2p1→examples: Type the following:
1) cd /home/username/mpich2-1.3.2p1/examples
2) gcc –g –ggdb –I/home/username/mpich2-install/include –
L/home/username/mpich2-
   3.2p1/lib /home/username/mpich2-
1.3.2.p1/examples/masterprogramname.c –o
   /home/mpich2-1.3.2p1/examples/masterprogramname
/home/username/mpich2-
   1.3.2p1/lib/architecturename/libpvm3.a /home/username/mpich2-
   1.3.2p1/lib/architecturename/libgpvm3.a
3) gcc –g –ggdb –I/home/username/mpich2-install/include –
L/home/username/mpich2-
   3.2p1/lib /home/username/mpich2-
1.3.2.p1/examples/slaveprogramname.c –o
   /home/mpich2-1.3.2p1/examples/slaveprogramname
/home/username/mpich2-
   1.3.2p1/lib/architecturename/libpvm3.a /home/username/mpich2-
   1.3.2p1/lib/architecturename/libgpvm3.a
4) cp masterprog $PVM_ROOT/bin/architecturename
5) cp slaveprog $PVM_ROOT/bin/architecturename
   /* in our work architecture name is LINUX64 */
```

Fig. 4 PVM program compilation and execution

Table 1 Testing over single node

Testing type	Type of parallel programming	Size of the matrix	Remarks
Testing over single node	MPI	1,000 × 1,000	Obtained correct results in both the case MPI and PVM
		1,500 × 1,500	
		2,000 × 2,000	
	PVM	1,000 × 1,000	
		1,500 × 1,500	
		2,000 × 2,000	

multiplication program which is designed using MPI and PVM separately. This program is made to run over single and multiple nodes for the different sizes of the matrices and checked for correctness. For the execution over the multiple nodes, all the nodes are configured with ssh for password-less login from one node to the other during the computation.

5 Configuration Time Comparison

An approximate comparison of time required for the configuration of MPI and PVM separately and time required for installing MPI and PVM using our programming model can be done as below:

Table 2 Testing over multiple nodes

Testing type	Number of nodes	Type of parallel programming	Size of the matrix	Remarks
Testing over multiple nodes	Two nodes	MPI	1,000 × 1,000	Obtained correct results in both the case MPI and PVM
			1,500 × 1,500	
			2,000 × 2,000	
		PVM	1,000 × 1,000	
			1,500 × 1,500	
			2,000 × 2,000	
		MPI	650 × 650	Obtained correct results in both the case MPI and PVM
			2,500 × 2,500	
			3,000 × 3,000	
		PVM	650 × 650	
			2,500 × 2,500	
			3,000 × 3,000	

- Time required for configuring MPI and PVM separately in a LINUX-based node with dual-core processors and 2-GB RAM (old method):
  For MPI 20 min per node + For PVM10 min per node = Total around 30 min.
- Time required for getting MPI and PVM in a LINUX-based node with dual-core processors and 2-GB RAM using proposed integrated programming model: For MPI and PVM together max 5 min per node.

6 Conclusion

The parallel programming model developed by integrating PVM into MPI has the following advantages:

- Provides a common platform for both MPI and PVM programming.
- Easy configuration: No separate configuration is needed for MPI and PVM.
- Highly portable as software (zipped into one file containing two supporting files and two integrated directories)
- Much less time needed for getting MPI and PVM installed in the nodes.

7 Future Works

Since the packages are integrated, the functions provided by both MPI and PVM must be checked for proper working. The proposed model allows the user to use either MPI or PVM in a common platform but not both in a single program. MPI and PVM both are having their own advantages and disadvantages; further, this model can be modified such that MPI advantages overcome the PVM disadvantages and vice versa; this is possible if both of them are made to work together programmatically.

References

1. MPICH2.:A new start for MPI implementations, in *Recent Advances in Parallel Virtual Machine and Message Passing Interface*. Lecture Notes in Computer Science, vol. 2474 (2002), pp. 7–15
2. M.A. Ismail, S.H. Mirza, T. Altaf, Concurrent matrix multiplication on multi-core processors. Int. J. Comput. Sci. Secur. **5**(2), 208–220 (2011)
3. E. Mancini, M. Rak, R. Torella, U. Villano, Off-line performance prediction of message-passing applications on cluster systems, in *Euro PVM/MPI* (2003), pp. 45–54
4. H. Jin, R. Buyya, M. Baker, Cluster computing tools, applications, and Australian initiatives for low cost supercomputing. MONITOR Mag. (The Institution of Engineers Australia) **25**(4) (2001)

Association Rule Mining and Refinement Using Shared Memory Multiprocessor Environment

P. Asha and T. Jebarajan

Abstract Rules that represent an association between the values of certain attributes and those of others are called association rules. The process of extracting such rules from a given dataset is called association rule mining (ARM). The work aims at effective utilization of all the cores present in the system with less time wastage and also balance the workload among them. Full fledged use of system resources and load balance can be achieved by perfect scheduling and providing efficient parallel algorithms. This paper discusses such a parallel ARM algorithm and rule generation based on the frequent combinations obtained. As the rules generated are also more in number as well as redundant, insignificant, and unproductive, it is compulsory to filter and refine the rules.

Keywords Data mining · Candidate generation · Rule filtration · Interestingness measures · Parallelism

1 Introduction

Data mining is used to transform data into useful pattern. Handling and mining huge amount of records seems to be difficult with traditional data mining techniques. The process of mining data into useful patterns took longer duration [1]. So many algorithms were proposed to mine data from large databases, but every algorithm has its own limitations such as multiple data scans, tree generation, updation and maintenance, and vast and redundant rule generation. Literature survey of few algorithms and techniques is discussed below.

P. Asha (✉)
Computer Science and Engineering Department, Sathyabama University, Chennai, India
e-mail: ashapandian225@gmail.com

T. Jebarajan
Computer Science and Engineering, Rajalakshmi Engineering College, Chennai, India
e-mail: drtjebarajan@gmail.com

© Springer India 2015

L.P. Suresh et al. (eds.), *Artificial Intelligence and Evolutionary Algorithms in Engineering Systems*, Advances in Intelligent Systems and Computing 325,
DOI 10.1007/978-81-322-2135-7_13

Zaki M. and Hsiao C. discussed the redundancy of traditional frequent itemset-based association rule generation framework and introduced the concept of closed frequent itemsets and corresponding mining algorithms. A framework based on closed frequent itemsets could cut redundancy caused by traditional means dramatically and without loss of information (whereas maximal frequent itemsets would). This presents the case where attributes are treated as categorical only, i.e., with two-level hierarchies [2].

Michihiro Kuramochi and George Karypis implemented an alternate way of modeling the objects in such a way that the data sets were represented using the graph structures. One way of formulating the frequent pattern discovery problem is to discover subgraphs that occur frequently over the entire set of graphs. The results showed that despite the underlying complexity associated with frequent subgraph discovery, it is also effective in finding all frequently occurring subgraphs in datasets [3].

Agarwal. R and Srikanth. R have given a database of sequences, in which each sequence is just a list of transactions, that is, the itemsets, ordered based on transaction time. The problem is actually to discover every sequential pattern with a user-specified minimum support count, in which the support count of the pattern is the number of data sequences that contain the pattern. The paper presents GSP, a new algorithm that discovers these generalized sequential patterns. The empirical evaluation using real-life and synthetic data indicates that GSP is much faster than the Apriori. GSP scales linearly with the number of data sequences and has very good scale-up properties with respect to the average data sequence size [4].

San. R and Fu. Y made the transactional database domain to incorporate the concept of hierarchy/taxonomy into association rule mining (ARM). It detailed a progressive deepening rule mining algorithm and variants based on frequent itemsets and Apriori strategies, which aimed at finding multiple-level rules [5] at same levels. The paper also had discussions on considering mixed hierarchies and learning rules involving concepts of different levels in a hierarchy [6].

Gunopulos. D, Mannila. H, and Saluja. S introduce an approach to find all maximal frequent itemsets, which were frequent itemsets of maximal size, i.e., extending them into any supersets would result in non-frequent itemsets. Given a complete set of maximal frequent itemsets, data miners could generate all other frequent itemsets by taking non-empty subsets of them. As compared with traditional approaches to find all frequent items, finding maximal frequent itemsets was proved to be computationally much cheaper [7].

Tsur et al. [8] proposed a system that was written from the database management perspective and presented a notation "query flock," which consisted of a parameterized query and a filter that selects values for the parameters by applying a condition to the query results. Apriori technique was generalized to apply to such query flocks.

Existing system implements Apriori algorithm that involves finding of frequent itemsets with minimum support threshold and generating association rule among them with minimum confidence threshold. The task of discovering all frequent itemsets from large dataset requires a lot of computations which can be minimized by exploiting parallelism to the sequential algorithms. In this system, we provide

the preliminaries of basic concepts about ARM and different sequential ARM algorithms on different hardware platforms and also focus on the challenges in exploiting parallelism to these algorithms [9, 10, 11].

2 Phases in Proposed ARM

To recover the problem of the existing system, we propose a new method for mining a frequent itemset. One of the currently best-ever and most fashionable algorithms for frequent itemset mining is the Apriori algorithm. Apriori is a classic algorithm for frequent itemset mining and association rule learning over transactional databases. It proceeds by means of identifying the frequent individual itemset from the database and extending them to larger and larger itemsets as long as those itemsets appear sufficiently and terminate when no further combinations can be made. The frequent itemsets determined by Apriori can be used to determine association rules which highlight general trends in the database.

2.1 Frequent Pattern Generation

The work is to identify the closely associated patterns. Given the occurrence of one item, find out the closely associated item and the one which occurs frequently. This is done with the parallel Apriori ARM algorithm. Find the frequent patterns using the algorithm and then generate the rules based on it. Next fine-tune the rules as redundant, unproductive, and insignificant rules may exist. The entire procedure is executed in parallel in all the cores available so as to reduce the total execution time. Effective and efficient computing with multicore environment is much required as we are in the era of supercomputing. The processes are distributed among various resources (processors) of better configuration for better efficiency (Fig. 1).

2.2 Parallel Association Rule Mining Algorithm

Our proposed parallel shared memory algorithm is built on top of the sequential Apriori association mining algorithm proposed by Agarwal.

$F1$ = frequent 1-itemsets g;
For ($k = 2$; $L_{k-1} \neq \emptyset$; k++) Ck = set of new candidates;
For all transactions t to D check if(supp($Ck >$ minsupp) then push to set Ln
Repeat and find the best Ln from Fn. Set of all frequent itemsets = Ln.

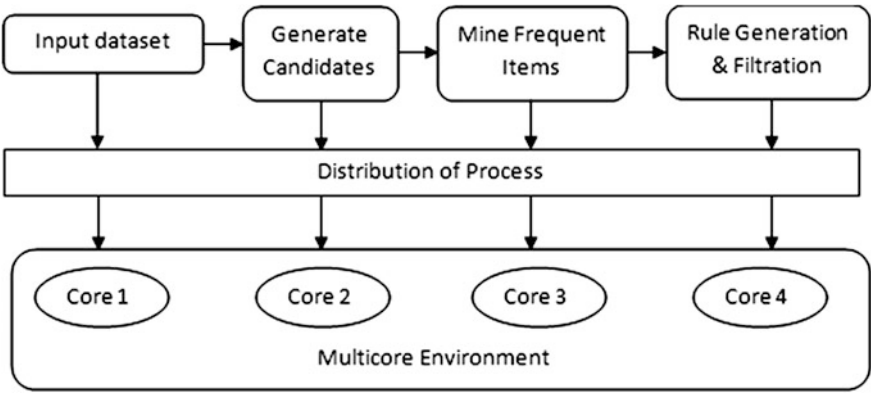

Fig. 1 Architecture diagram

First, the 1-frequent itemsets (k) are framed. Then, the database is scanned and the support for each candidate is found. Only, the frequent k-itemsets are retained for the future iterations, which are used for generation of the candidate set for the next iteration. This iterative process is repeated for $k = 1$; 2, and 3, until there are no more frequent k-itemsets to be found. There are two main steps in the algorithm: candidate generation and support counting [12, 13].

Sample OpenMP code of Parallelization (portion of producing item combinations):

```
#pragma omp parallel for
for(comb_tracker=0;comb_tracker<no_items+1;comb_tracker++)
{  k=0;  if(comb_tracker!=0){
 #pragma omp parallel for
 for(j=1;j<no_items;j++){
  #pragma omp parallel for
  for (i=2;item_combn[i]!=0;i++){
if((int)(item_combn[i]/(pow(10,comb_tracker-1)))>j)
{   backup_combn[++k]=(item_combn[i]+(j*pow(10,comb_tracker)));
    printf("\n%lu,%lu,%lu ,",backup_combn[k],comb_tracker,j);   }}}}
```

Rule Generation algorithm:

For all large k-itemsets l_k , k>=2 do begin
H_1={rule consequents from l_k with single item in the consequent}
Call ap-genrules(l_k, H_1);
end
Procedure ap-genrules(l_k : large k-itemset,H_m :set of m-item consequents)
If(k>m+1) then begin H_{m+1} = apriori-gen(H_m);
For all $h_{m+1} \in H_{m+1}$ do begin Conf=support(l_k / support(l_k - h_{m+1});
If(conf>=minconf) then
Output the rule (l_k - h_{m+1}) => h_{m+1} with confidence=conf and support = support(l_k);
Else Delete h_{m+1} from H_{m+1} ; end ; Call ag-genrules(l_k ,H_{m+1});
end

The merits of the proposed system include decrease in process waiting time, producing output faster than that of multimodal function, and whenever there exist an increased number of resources, the processing time gets decreased.

3 Interestingness Measures

3.1 Rule Refinement

Filter out the rules generated by providing threshold via various rule filtering properties [14, 15] such as confidence, support, lift, completeness, conviction, Laplace, and P–S measure.

3.1.1 Lift

Lift ($L \rightarrow R$) = count (L U R)/count (L) * support(R)

Lift of a rule, $L \rightarrow R$, measures how many more times the items in L and R occur together in transactions than would be expected if the itemsets L and R were statistically independent. Support(R) is the proportion of transactions matched by R.

3.1.2 Confidence

It is given by P (L U R)/P (L), that is, the proportion of right-hand sides predicted by the rule that are correctly predicted.

3.1.3 Support

It is given by P (L U R)/N_{total}, where N_{total} represents the total number of instances, that is, the proportion of training set correctly predicted by the rule.

3.1.4 Completeness

It is given by P (L U R)/P(R), that is, the proportion of matching right-hand sides that are correctly predicted by the rule.

3.1.5 Conviction

Conviction ($L \rightarrow R$) = Conviction (L, R) = P (L) * P ($\neg R$)/P ($LU\neg R$)

3.1.6 Laplace Measure

$\text{Lapl}(L \rightarrow R) = \text{Lapl}\ (L, R) = ((P(LUR) + 1)/(P(L) + 2)$

3.1.7 P–S Measure

Gregory Piatetsky–Shapiro (P–S) proposed the rule interestingness measure RI, where RI is defined as follows: $\text{RI} = P\ (L\ U\ R) - (P\ (L) * P\ (R))/N_{\text{total}}$. **RI** measures the difference between the actual number of matches and the expected number if the left- and right-hand sides of the rule were independent. Usually, RI value is positive. If RI = 0, then the rule is no better than chance. If RI = negative, then the rule is less successful than chance.

4 Experimental Results and Discussion

We have installed Mosix cluster and made virtual machines (VM). The parallelization of Apriori algorithm based association mining has been done in shared memory environment using virtual machines. The shared memory programming is done with the help of Openmp programming paradigm.

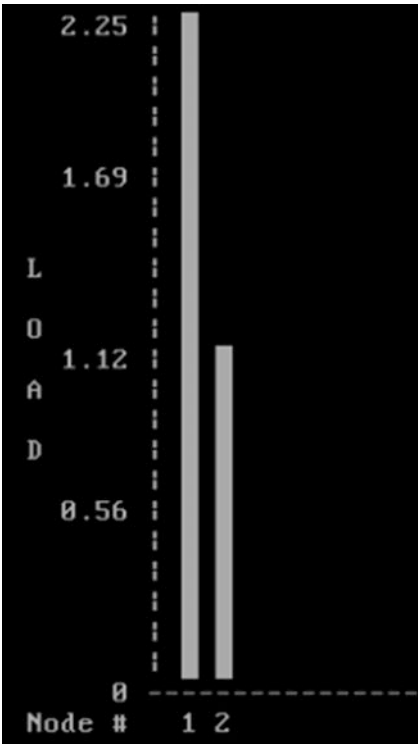

Fig. 2 Load of node 1 > node 2

By means of effectively parallelizing the code, we try to balance the load in all the cores available, that is, all the VM available. For simplicity, consider only two nodes. Before parallelizing the ARM task, the workload of every node is not uniform. One node has a higher workload than the other. As in case of super-computing, we have a single large computer with very high capacity and would possess multicore architectures within them. If we are able to balance all those cores present and make every individual core to function parallel and with equal load, then compulsorily the system performance would improve. Instead of the system functioning as a solo performer, if all the cores of the single system can function parallel, their total task execution time would be so less. Consider Fig. 2, as the task is not parallelized, the node on one node seems to be higher than the other node. Here, node 1 has a greater load than node 2.

In Fig. 3, node 2 has a greater load than node 1. So we try to parallelize the ARM task, and if load on some node increases, then it is better to migrate few tasks from the heavily loaded node to the lightly loaded node. After effective parallelization, it is observed that both the nodes share equal load as in Fig. 4.

The set of filtered association rules generated by the algorithm are shown in Fig. 5.

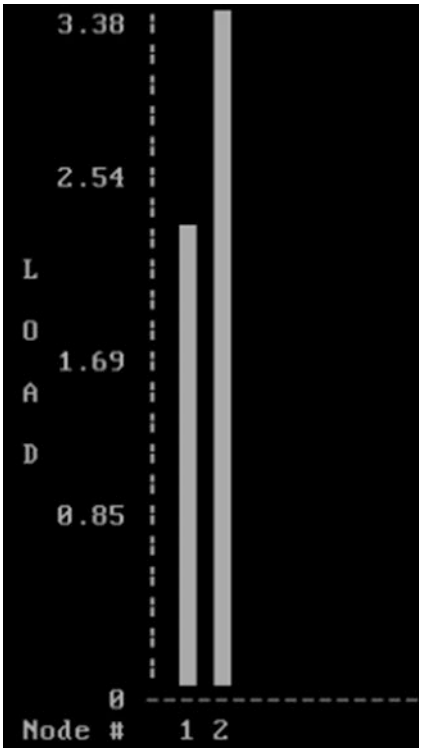

Fig. 3 Load of node 2 > node 1

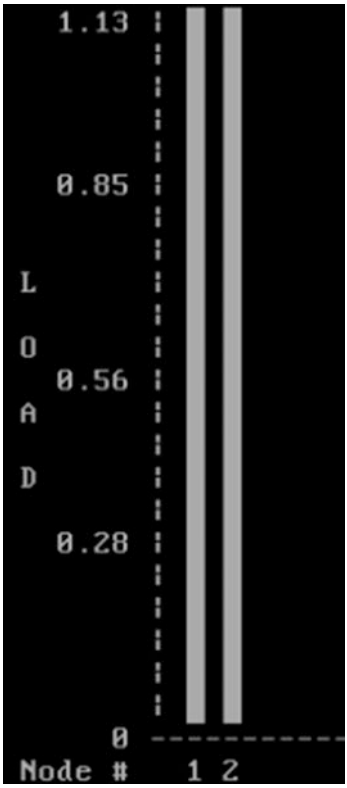

Fig. 4 Equal load on both nodes

```
Association Rules
[Outlook = overcast] --> [Temperature] (confidence: 0.800)
[Humidity] --> [Temperature] (confidence: 0.800)
[Outlook = sunny] --> [Wind] (confidence: 0.800)
```

Fig. 5 Resultant rules

Premises	Conclusion	Supp...	Confi...	LaPl...	Gain	p-s	Lift	Convict
Outlook = overc	Temperature	0.286	0.800	0.947	-0.429	0.107	1.600	2.500
Humidity	Temperature	0.286	0.800	0.947	-0.429	0.107	1.600	2.500
Outlook = sunr	Wind	0.286	0.800	0.947	-0.429	0.133	1.867	2.857

Fig. 6 Rules with measurements

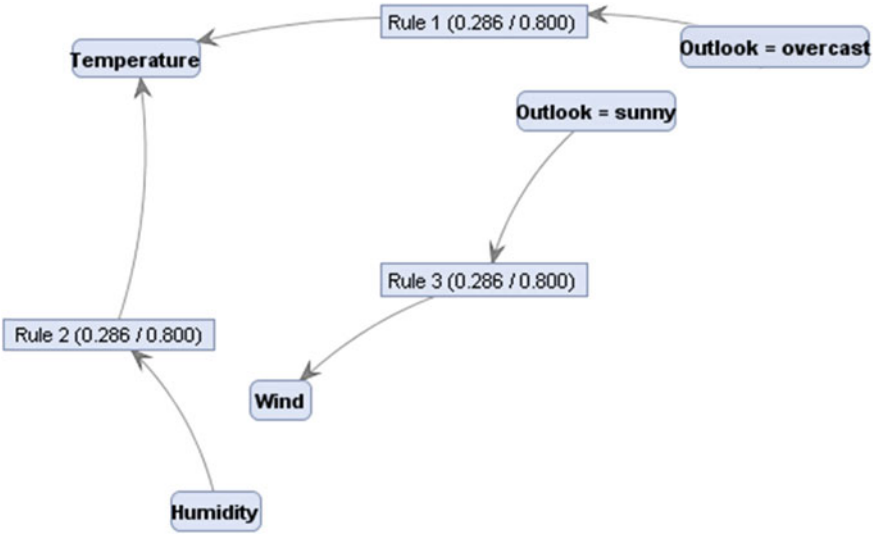

Fig. 7 Best rules based on confidence

Figure 6 narrates the set of rules that have satisfied all the rule interestingness measures considered for this work. Out of 42 rules generated by the algorithm, only 3 rules have satisfied every constraint imposed to the proposed work.

The minimal constraints taken for this work are support threshold = 20 %, confidence threshold = 80 %, P–S = +ve, Laplace > 0.5, gain > −0.001, lift > 1.0, and conviction > 2.

These are the rules generated based on only the confidence measure. From Fig. 7, it is understood that only Rule 1, Rule 2, and Rule 3 contain a confidence value ≥ minimum confidence threshold. The minimum confidence threshold chosen for the problem is 80 %.

These are the rules generated based on the gain measure. From Fig. 8, it is understood that only Rule 1 and Rule 2 satisfy the minimum gain threshold. Rules 1 and 2 were generated by the attributes temperature, humidity, and outlook. From Fig. 9, it is understood that only Rule 3 has satisfied the Laplace threshold considered.

Considering an employee dataset for the algorithm, the following are the set of filtered rules obtained. From Fig. 10, we can observe that the conviction values can even range to ∞, but still it can be considered as a best rule as the criterion specified for conviction is >5.00.

As shown in Fig. 11, Rules 2, 3, 4, and 5 were the one that were based on conviction constraint.

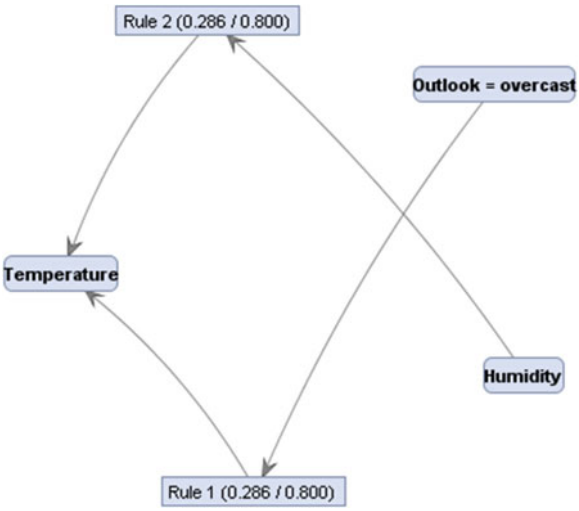

Fig. 8 Best rules based on gain factor

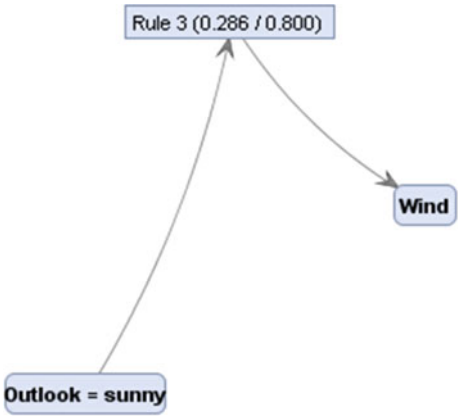

Fig. 9 Best rules based on Laplace

4.1 Performance Parameters

Figure 12 shows the total execution time (ms) taken by the sequential and parallel Apriori algorithm. The time of the parallel algorithm has been reduced a lot when compared to sequential one. It displays the speedup and efficiencies of a parallel Apriori with support count = 4 and cores = 4. Speedup is the ratio of sequential execution time to parallel execution time.

$$\text{Speedup} = \text{SET}/\text{PET}$$

Premises	Conclusion	Supp...	Confi...	LaPl...	Gain	p-s	Lift	Convic
wage-inc-2nd	wage-inc-1st	0.225	0.900	0.980	-0.275	0.112	2	5.500
bereavement-	wage-inc-3rd	0.225	0.900	0.980	-0.275	0.150	3	7
duration	wage-inc-3rd	0.300	0.923	0.981	-0.350	0.202	3.077	9.100
wage-inc-3rd	duration	0.300	1	1	-0.300	0.202	3.077	∞
bereavement-	duration	0.225	1	1	-0.225	0.152	3.077	∞

Fig. 10 Rules with measurements

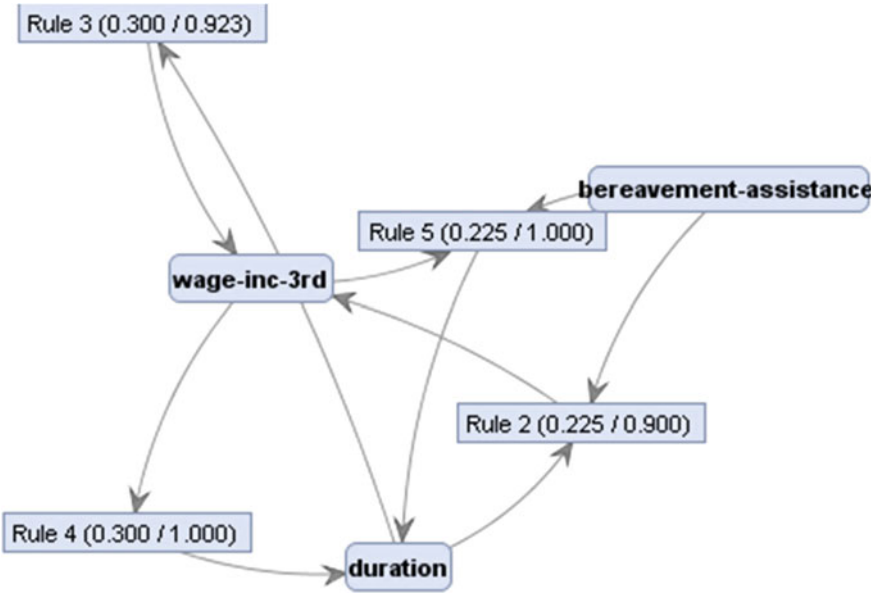

Fig. 11 Conviction-based best rules

Sequential	Parallel	Speed Up	Efficiency
113.5137	0.024	4.729	1.182

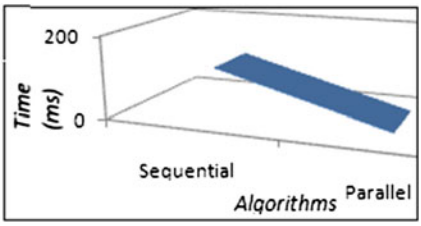

Fig. 12 Comparison between sequential and parallel algorithm

Efficiency of a parallel program is a measure of processor utilization. It is defined as the ratio of speedup to number of processors used.

$$\text{Efficiency} = \text{Speedup}/\text{Processor Used}$$

5 Conclusion

Hence, the association rules were generated which calculate the percentage of each item as a single as well as combination of other items. This tells the probability in which an item is purchasable. Rule refinement based on various interestingness measures has been done, which shows that only the best rules are listed. From the experimental discussions, it is clear that the computation time of the proposed parallel mining algorithm has reduced a lot and we have also supported the system with balanced workload on all the nodes.

References

1. Q Wan, A An, Discovering transitional patterns and their significant milestones in transaction databases. IEEE Trans. Knowl. Data Eng. **21**(12), 1692–1707 (2009)
2. M. Zaki, C. Hsiao, An efficient algorithm for closed itemset mining. 2nd international conference on data mining, Arlington (2010), pp. 16–25
3. M. Kuramochi, G. Karypis, An efficient algorithm for discovering frequent sub graphs. IEEE Trans. Knowl. Data Eng. **16**(9), 22–26 (2009)
4. R. Agarwal, R. Srikanth, Mining sequential patterns. 29th international conference on data engineering, Taiwan (2009), pp. 62–65
5. M.M. Mazid, A.B.M.S. Ali, K.S. Tickle, A comparison between rule based and association rule mining algorithms. Third international conference on network and system security (2009), pp. 452–455
6. R. San, Y. Fu, Discovery of multiple-level association rules from large databases. In the proceedings of the 21st international conference on very large databases, Zurich, Switzerland (2008), pp. 22–36
7. D. Gunopulos, H. Mannila, S. Saluja, Discovering all the most specific itemsets by randomized algorithms. In the international conference on database theory (2008), pp. 23–26
8. D. Tsur, J.D. Ullman, S. Abitboul, C. Clifton, R. Motwani, S. Nestorov, A generalization of association-rule mining. In the proceedings of ACM- SIGMOD (2007), pp. 1–12
9. R. Agrawal, J.C. Shafer, Parallel mining of association rules. Distributed systems online (2004)
10. R. Garf, P.K. Mishra, Exploiting parallelism in association rule mining algorithms. Int. J. Adv. Technol. **2**(2), 10–13 (2011)
11. J. Li, Y. Liu, A. Choudhary, *Parallel Data Mining Algorithms for Association Rules and Clustering*, ed. by S. Rajasekaran, J. Reif. Handbook of Parallel Computing: Models, Algorithms and Applications (CRC Press, Boca Raton, 2011)
12. P. Asha, T. Jebarajan, Analyzing the sequential and parallel ARM algorithms and its impact in grid computing environments. Int. J. Adv. Comput. **36**(1), 1109–1114 (2013)

13. J. Ronga, H.Q. Vua, R. Lawb, G. Lia, A behavioral analysis of web sharers and browsers in Hong Kong using targeted association rule mining. Tourism Manage. **33**, 731–740 (2012)
14. P. Asha, T. Jebarajan, Mining interesting association rules with a heterogeneous environment. In the international joint conferences on CNC and CSEE 2013. Conference proceedings published by the Springer (2013), pp. 222–228
15. P. Kongchai, N. Kerdprasop, K. Kerdprasop, Dissimilar rule mining and ranking technique for associative classification. In proceedings of the international multi conference of engineers and computer scientists (2013), p. 1

Design of Low-Power Multiplier Using UCSLA Technique

S. Ravi, Anand Patel, Md Shabaz, Piyush M. Chaniyara and Harish M. Kittur

Abstract Multiplication is one of the major fundamental operations and key hardware blocks in any digital system. This paper presents the comparison of the VLSI design of uniform carry select adder (UCSLA)-based multiplier technique with the variable carry select adder (VCSLA)-based multiplier technique. The analysis is carried out on the different bit sized values of unsigned inputs, and output results show that the area, power, and delay are reduced in the UCSLA-based multiplier technique compared to VCSLA-based technique. The timing delay in 64-bit VCSLA-based multiplier technique is 95.25 ns for performing the multiplication, which is reduced by 11.11 % in the UCSLA-based multiplier technique. In the same manner, area is reduced by 39.42 % and power also reduced by 19.28 % in UCSLA-based multiplier technique. The simulation works of multipliers are carried out in Verilog-HDL (Modelsim). After the simulation, the results are obtained using cadence tool.

Keywords UCSLA · VCSLA · CSKA · BEC-1 · Low power

1 Introduction

To design area-, power-, and time-efficient logical process is the most significant role in any research of VLSI design. The four basic elementary arithmetic operations of any digital systems are addition, subtraction, multiplication, and division.

S. Ravi (✉) · A. Patel · M. Shabaz · P.M. Chaniyara · H.M. Kittur
SENSE, VIT University, Vellore, Tamil Nadu, India
e-mail: msravi@vit.ac.in

A. Patel
e-mail: patelanand91@yahoo.com

M. Shabaz
e-mail: md.shabaz2013@vit.ac.in

H.M. Kittur
e-mail: kittur@vit.ac.in

© Springer India 2015

L.P. Suresh et al. (eds.), *Artificial Intelligence and Evolutionary Algorithms in Engineering Systems*, Advances in Intelligent Systems and Computing 325,
DOI 10.1007/978-81-322-2135-7_14

In this paper, we are dealing with the method of addition of partial products to implement the operation of multiplication.

Multiplication is the most fundamental operation in many digital systems such as digital signal processors (DSPs), FIR filters, arithmetic logic unit (ALU) subsystems, microprocessors, and microcontrollers. In multiplier, addition is the main building block and there are various methods to do the addition. The key process of any VLSI designer is to reduce the area, power, and delay [1, 2]. Our proposed solution to perform the addition of partial products is to use uniform carry select adder (UCSLA). This paper presents the VLSI design of area- and power-efficient multiplier using UCSLA technique.

Basically, there are two types of carry select adder (CSLA): One is variable carry select adder (VCSLA) and the other is UCSLA. In the VCSLA, it uses the different variable-sized groups which contains the different size of ripple carry adder (RCA) block with carry in as an input in the upper part of the group and different size of binary to excess 1 (BEC-1) converter in the lower part of the group [3], whereas in the case of UCSLA, it uses the uniform-sized groups which contain the carry skip adder (CSKA) with carry input equal to zero in the upper part of the group and BEC-1 converter in the lower part of the group. The working details of VCSLA and UCSLA are explained in Sects. 2 and 3. Section 4 deals with the multiplication algorithm and the process of using the UCSLA and VCSLA blocks in the multiplication process. The simulation results and performance analysis are presented in Sect. 5. Finally, the objective of the research is concluded in Sect. 6.

2 Variable Carry Select Adder (VCSLA)

The VCSLA architecture for 128 bits is shown in Fig. 1 in which there are different sizes of CSLA used. In VCSLA method of addition, the RCA is used in the upper part of the adder and BEC-1 converter is used in the lower part of addition. The group 1 contains only 2 bits of RCA block with carry in signal. The carry out C1 which is generated is used as the control signal in the multiplexer for the next block. The group 2 contains two set of blocks, in which upper block is 2-bit RCA with Cin = 0, instead of Cin = 1, and lower block contains 3-bit BEC-1. The input of 2 bits is given to the upper part of the adder, and output of the upper part is given to the lower part, which is BEC-1, as well as to the multiplexer. The multiplexer will

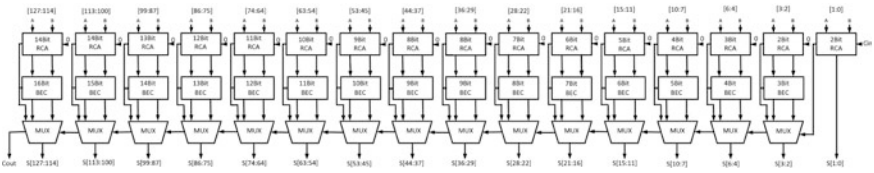

Fig. 1 128-bit VCSLA architecture

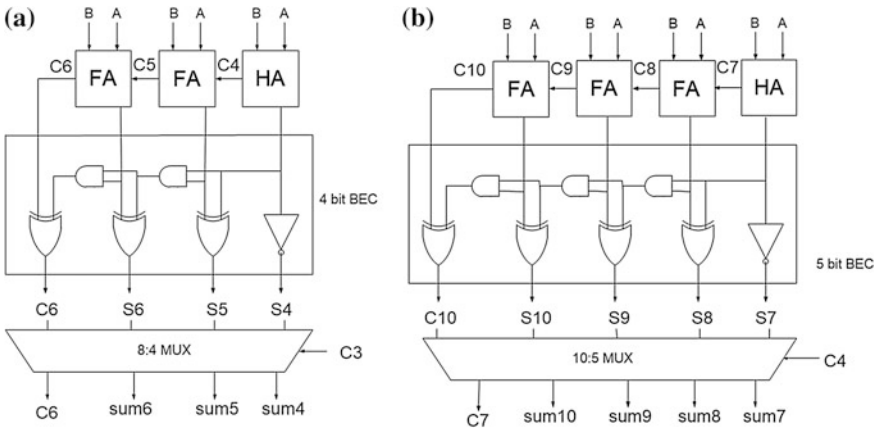

Fig. 2 **a** Group 3 VCSLA architecture. **b** Group 4 VCSLA architecture

select the output of the upper adder block or lower adder block according to the input of the multiplexer which is the C1 generated by the group 1 block. Now, the sum [3:2] and carry out C3 will be generated.

$$\{\text{C2, Sum } [3:2]\} = \{\text{C1 + Multiplexer}\}$$

The operations of the other variable-sized blocks are also similar to the above block, and in same manner, the sum and carry are evaluated.

$$\{\text{C6}, \text{sum}[6:4]\} = \text{C3} + \text{multiplexer}$$
$$\{\text{C10}, \text{sum}[10:7]\} = \text{C6} + \text{multiplexer}$$
$$\{\text{C15}, \text{sum}[15:11]\} = \text{C10} + \text{multiplexer}$$
$$\{\text{C21}, \text{sum}[21:16]\} = \text{C15} + \text{multiplexer}$$
$$.$$
$$\{\text{Cout}, \text{sum}[127:114]\} = \text{C113} + \text{multiplexer}$$

The block diagram of 128-bit VCSLA is shown in Fig. 1, and internal architecture of some groups is shown in Fig. 2a, b.

3 Uniform Carry Select Adder (UCSLA)

In the design of UCSLA, the upper part has the CSKA block with Cin = 0, instead of the RCA with Cin = 1 and the lower part has the BEC-1 block [4]. The UCSLA architecture for 128 bits is shown in Fig. 3. In the group 1 of UCSLA, it has only one set of four-bit CSKA block with carry in signal and the carry out of this group is used as the control signal for multiplexer in the next group.

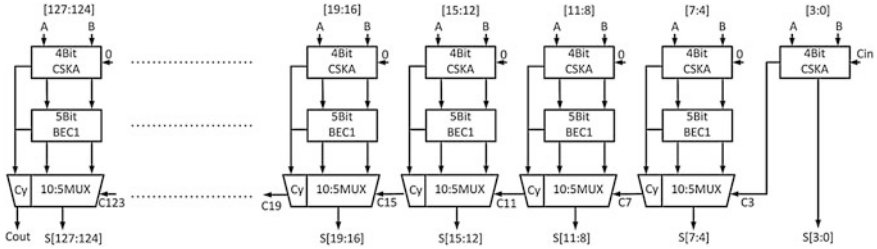

Fig. 3 128-bit UCSLA architecture

In the group 2 of UCSLA, it has 2 parts in which the upper part consists of 1 set of four-bit adder and the output of the upper part is given to the lower part of the group which is 5 bits BEC-1 converter. The output of both upper part and lower part is fed to the input of the multiplexer, and the multiplexer will then generate the output sum and carry bits according to the input of the multiplexer, which is the carry out of the previous block. The working function of the other blocks can also be evaluated in the same manner, and the sum and carry out are evaluated.

$$\{C7, \text{sum}[7:4]\} = C3 + \text{multiplexer}$$
$$\{C11, \text{sum}[11:8]\} = C7 + \text{multiplexer}$$
$$\{C15, \text{sum}[15:12]\} = C11 + \text{multiplexer}$$
$$.$$
$$\{\text{Cout}, \text{sum}[127:124]\} = C123 + \text{multiplexer}$$

The block diagram of 128-bit UCSLA is shown in Fig. 3, and the internal architecture of first group and second group is shown in Fig. 4a, b.

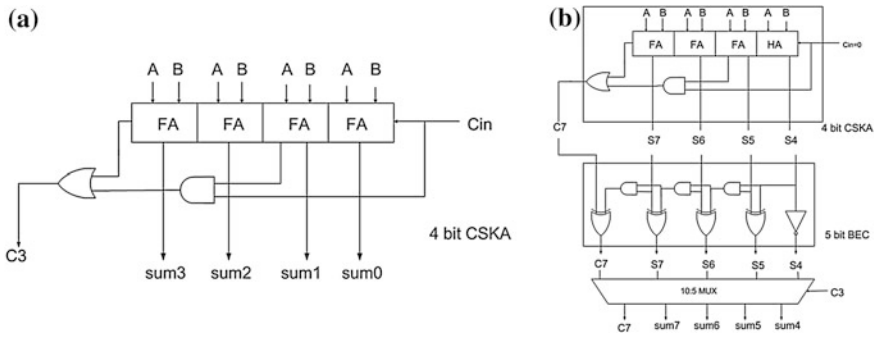

Fig. 4 **a** Group 1 UCSLA architecture. **b** Group 2 UCSLA architecture

4 Multiplication Algorithm

The process of multiplication involves the formation of partial products by performing logical AND operation of each bit of multiplicand with multiplier. The addition of these partial products leads to the formation of final product. The multiplication of two 64-bit unsigned numbers results in a final product of maximum of 128-bit number. Therefore, the partial products are stored in 128-bit registers. After the formation of partial products, the multiplication process is carried out using 128-bit UCSLA or VCSLA adder by repeating following steps:

1. The second partial product is logical left shifted (LLS) by one bit and added with first partial product, and the resulted value is stored in a register out1.
2. The third partial product is LLS by two bits and added with out1, and the resulted value is stored in a register out2.
3. The same procedure is carried out 63 times, the 64th partial product is LLS by 63 bits and added with out62, and the resulted value is final product.

The generation of partial products can be done in the following way

$$\begin{aligned} &\text{pp1} = \{64\{\text{X}[0]\}\}\&\text{Y}[63:0] \\ &\text{pp2} = \{64\{\text{X}[1]\}\}\&\text{Y}[63:0] \\ &\text{pp3} = \{64\{\text{X}[2]\}\}\&\text{Y}[63:0] \\ &\text{pp4} = \{64\{\text{X}[3]\}\}\&\text{Y}[63:0] \\ &. \\ &\text{pp64} = \{64\{\text{X}[63]\}\}\&\text{Y}[63:0] \end{aligned}$$

5 Verilog Simulation and Result Analysis

The design work has been simulated using Verilog-HDL (Modelsim) and synthesized utilizing Cadence RTL compiler with TSMC 45 nm technology slow library. The multiplier of sizes 8, 16, 32, and 64 bits are designed in Verilog-HDL and simulated using Modelsim. After the simulation, all the Verilog files of UCSLA- and VCSLA-based multiplier are imported to the Cadence tool for synthesizing and the corresponding values of timing delay, area, and power are noted [5, 6]. The synthesis report contains the details of area, power, and timing analysis for different size of UCSLA- and VCSLA-based multiplier design.

Table 1 shows the details about timing delay, area, leakage power, dynamic power, total power, power–delay product, and area–delay product for different bit sizes of multiplier design using UCSLA method and those are compared with the design of multiplier using VCSLA method [3].

From the obtained results, it is observed that the timing delay for the 64-bit multiplier using VCSLA technique is 95.257 ns, which is reduced to 84.678 ns in the UCSLA-based multiplier technique [7]. So the percentage reduction in the

Table 1 Comparison of UCSLA- and VCSLA-based multiplier for different bit size

Word size (bits)	Multiplier	Delay (ns)	Area (μm^2)	Power (μW)			Power–delay prod (10^{-15})	Area–delay prod (10^{-21})
				Leakage power	Dynamic power	Total power		
8	UCSLA	8.045	688	0.03	51.78	51.8	416.8	5,534.96
	VCSLA	8.290	814	0.04	56.06	56.1	465.0	6,748.06
16	UCSLA	16.244	3,645	0.17	442.14	442.3	7,184.9	59,209.38
	VCSLA	16.785	4,493	0.22	498.70	498.9	8,374.3	75,415.00
32	UCSLA	41.403	12,715	0.58	2,819.19	2,819.7	116,746.8	526,439.14
	VCSLA	43.799	19,036	1.02	3,342.98	3,344.0	146,463.9	833,757.76
64	UCSLA	84.678	50,712	2.29	17,801.9	17,804	1,507,624.3	4,294,190.7
	VCSLA	95.257	83,719	2.41	220,542	22,056	2,101,055.2	7,974,820.7

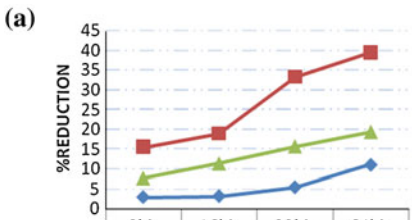

	8bit	16bit	32bit	64bit
delay	2.96	3.22	5.47	11.11
area	15.48	18.87	33.21	39.42
power	7.72	11.35	15.67	19.28

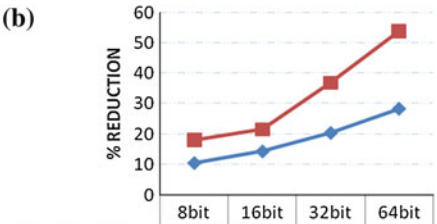

	8bit	16bit	32bit	64bit
power-delay product	10.37	14.2	20.29	28.24
area-delay product	17.97	21.49	36.86	53.84

Fig. 5 **a** Percentage reduction in timing. **b** Percentage reduction in product value delay, area, and power of area–delay and power–delay

timing delay obtained in the UCSLA-based multiplier is 11.11 %. In the same way, the area obtained from the results is 50,712 μm^2 for the 64-bit multiplier using UCSLA-based method and 83,719 μm^2 for the 64-bit multiplier using VCSLA-based method. So the percentage reduction in the area obtained in the UCSLA-based multiplier is 39.42 %. Similarly, the total power for 64-bit VCSLA- and UCSLA-based multipliers is 22.0567 and 17.8042 mW simultaneously. So the percentage reduction in the power in the UCSLA-based multiplier obtained is 19.28 %, which is shown in Fig. 5. In UCSLA-based multiplier, all the three parameters are reduced in comparison with the VCSLA-based multiplier.

6 Conclusion

In this paper, a multiplier is designed by using UCSLA and VCSLA methods. By analyzing the results, a simple approach to reduce the area, power, and delay is to design multiplier with UCSLA technique, in which UCSLA is designed by using a combination of uniform-sized CSKA with more number of half adders compared to VCSLA which uses more full adders as bit size is varied. The results show that the power–delay product is reduced by 28.24 % and area–delay product is reduced by 53.84 % in the 64-bit UCSLA-based multiplier. Therefore, a multiplier UCSLA designed with CSKA blocks is compact, power efficient, and fast for VLSI-based applications.

References

1. J.M. Rabaey, *Digital Integrated Circuit-A Design Perspective* (Prentice-Hall, Upper Saddle River, NJ, 2001)
2. T.Y. Ceiang, M.J. Hsiao, Carry-select adder using single ripple carry adder. Electron. Lett. **34** (22), 2101–2103 (1998)

3. B. Ramkumar, H.M. Kittur, Low-power and area-efficient carry select adder. IEEE Trans. Very Large Scale Integr. (VLSI) Syst. 20(2), 371–375 (2012)
4. A. Tyagi, A reduced area scheme for carry-select adders. Computer design: VLSI computers and processors. IEEE international conference (1990), pp. 255–258
5. R. Hemima, C. Chrisjin Gnana Suji, Design of 4 bit low power carry select adder. International conference on signal processing, communication, computing and networking technologies (ICSCCN). IEEE Conference Publications (2011), pp. 685–688
6. K. Allipeers, S. Ahmed Basha, An efficient 64-bit carry select adder with less delay and reduced area application. Int. J. Eng. Res. Appl. **2**(5), 550–554 (2012)
7. D.O. Reddy, P. Ramesh Yadav, Carry select adder with low power and area efficiency. IJERD **3** (3), 29–35 (2012)

Hyperspectral Image Compression Algorithms—A Review

K. Subhash Babu, V. Ramachandran, K.K. Thyagharajan and Geeta Santhosh

Abstract Satellite-based remote sensing applications require collection of high volumes of image data of which hyperspectral images are a particular type. Hyperspectral images are collected by high-resolution instruments over a very large number of wavelengths on board a satellite/airborne vehicle and then sent onwards to a ground station for further processing. Compression of hyperspectral images is undertaken to reduce the on-board memory requirement, communication channel capacity, and the download time. Compression algorithms can be either lossless or lossy. The purpose of this paper is to review a number of compression techniques employed for onsite processing of hyperspectral image data, to reduce the transmission overhead. A review of the theory of hyperspectral images and the compression techniques employed therein with emphasis on recent research developments is presented. Recent research on video compression techniques for hyperspectral imaging (HSI) is also discussed.

Keywords Hyperspectral imaging · Compression · Lossless · Lossy

K.S. Babu (✉)
CSE Department, Jawaharlal Nehru Technological University-Kakinada, Kakinada, Andhra Pradesh, India
e-mail: subashbabuk@ssn.edu.in

V. Ramachandran
RMD Engineering College, Kavaraipettai, Tamil Nadu, India
e-mail: kkthyagharajan@yahoo.com

K.K. Thyagharajan
NIT, Dimapur 797103, Nagaland, India
e-mail: rama5864@gmail.com

G. Santhosh
MCA Department, SSN College of Engineering Kalavakkam, Chennai 603110 Tamil Nadu, India
e-mail: geetas@ssn.edu.in

© Springer India 2015

L.P. Suresh et al. (eds.), *Artificial Intelligence and Evolutionary Algorithms in Engineering Systems*, Advances in Intelligent Systems and Computing 325,
DOI 10.1007/978-81-322-2135-7_15

1 Introduction

Spectral imaging is a study of partial or complete spectral information collected at every location in an image plane. This spectral information can be based on the range and resolution of the spectrum, number, width, and adjacency of bands. Based on these various distinctions, we have different terms namely multilayer imaging, multispectral imaging, super spectral imaging, and hyperspectral imaging (HSI). Spectral images are often represented as an image cube, a type of data cube. Spectral imaging enlarges the size of a pixel until it includes an area for which a spectral response can be obtained for the surface cover to be discriminated. The pixels need not be placed immediately adjacent to each other in order to facilitate identification of the pixel contents, as the identification of a pixel's contents could be based on the spectral response of that pixel only. This helps in bringing down to a large extent the number of pixels needed to represent a given area. A hyperspectral image can be regarded as a stack of individual images of the same spatial scene. Each such image represents the scene viewed in a narrow portion of the electromagnetic spectrum [1] as depicted in Fig. 1. These individual images are referred to as spectral bands. Hyperspectral images typically consist of more than 200 spectral bands; the voluminous amounts of data comprising hyperspectral images make them good candidates for data compression. In HSI, each pixel records the intensity at different wavelengths of the light reflected by a specified area, which is divided into a number of consecutive bands. The hyperspectral images are represented as a two dimensional matrix or image cube [2] as shown in Fig. 2, where each pixel is a vector

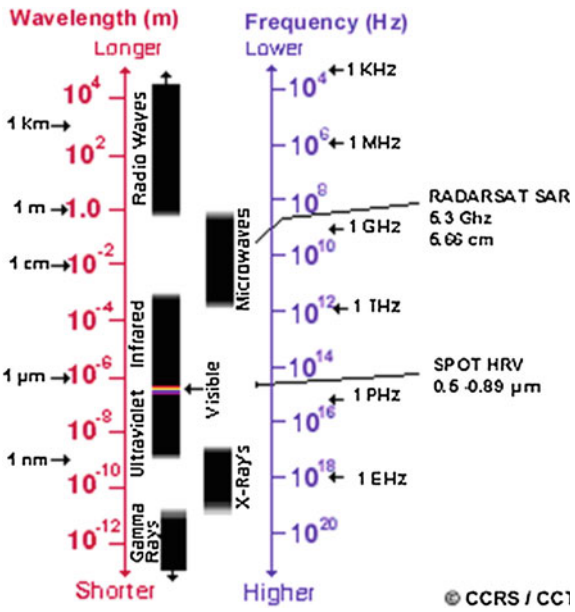

Fig. 1 Electromagnetic spectrum depicted as a spectrum

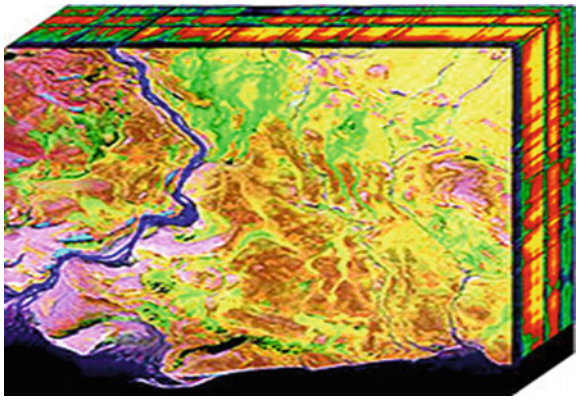

Fig. 2 Two dimensional projection of a hyperspectral cube

having one component for each spectral band. Hyperspectral images that provide high resolution spectral information are useful for many remote sensing applications. They generate massively large image data sets. Hence, capture and onward transport of large hyperspectral image data sets entail efficient processing, storage, and transmission capabilities. One way to address this problem is through image compression.

2 Conventional Compression Algorithms

Compression algorithms take digital image files as input. This input can also be a text or sound file. It then constructs an efficient encoded representation using as few bits as possible so that it can be transmitted with minimum usage of bandwidth and reconstructed at the destination with minimum loss of bits. Depending on the quality of reconstruction desired, compression algorithms can be classified as lossless or lossy. In lossless compression schemes, the image formed at the end of the compression process should be an exact replica of the original image. Lossless algorithms strive to transmit the image data without any loss of information. Due to this constraint, only a modest amount of compression is possible. In general, lossless compression is employed for character data, numerical data, icons, and executable components. On the other hand, lossy algorithms are based on the presumption that it is not necessary to transmit the image file in its entirety as not all parts of the image are significant. The extraneous or insignificant image parts could be removed without affecting the visual impact of the image. In addition, the redundant information need not be transmitted hence can be completely discarded. Therefore, the lossy compression algorithms provide a higher degree of compression, albeit with some loss of information and degradation in the image quality. Therefore, lossy compression has been extensively employed for the compression of multimedia files and has been the trigger for the immense popularity of multimedia. This has been possible due to the fact that the human visual and hearing

system is insensitive to certain kinds and levels of distortion. Thus, selective loss of information can be used to significantly enhance the compression performance of the lossy algorithms.

3 Classification of Compression Algorithms

Some of the important classifications [3] of compression algorithms are as follows:

A. *Statistical (SI)*
The idea of statistical coding or the statistical approach is to use statistical information to replace a fixed-size code of symbols/patterns by a, hopefully, shorter variable-sized code. Generally, most common patterns are replaced with shorter patterns and least common ones with longer patterns.

B. *Dictionary (DI)*
DI approaches build a list of frequently occurring words and phrases and associate an index with them. While compressing, it replaces the words/phrases with the respective indices.

C. *Pattern finding (PF)*
PF approaches seek to find and extract regular patterns from the file and perform compression based on these patterns. Most common PF approach namely run length coding takes the consecutive symbols or patterns (runs) that occur recurrently in the source file and replaces them with an 8-bit ASCII code pair. This code pair can be either the symbol that is being repeated and the number of times it occurs or a sequence of symbols that are non-repetitive.

D. *Approximation (AP)*
Approximate solutions approach employs quantization. For a given set of data, certain computations are applied and approximations are arrived at and a simpler form of the data is generated.

E. *Programmable solutions (PR)*
Programming solutions entail creation of an entirely new programming language for encoding the data and thereby reducing the file size.

F. *Wavelet solutions (WA)*
A wavelet-based compression solution creates AP for the data by adding together a number of basic patterns known as wavelets that are weighted by different coefficients. These coefficients replace the original patterns and make the input file compact. Cosine function is the most prevalent wavelet in use.

G. *Adaptive solutions (AD)*
AD try to adapt to local conditions in an input file. Certain patterns may be found only in the beginning, certain in the middle, and certain only in the end. AD may adapt accordingly while performing compression.

In general, DI-based compression algorithms are better suited for text data. Statistical methods are better suited for image data. Some statistical-based algorithms such as Huffman coding or Arithmetic coding are used for text compression too. But, whenever a file has fairly long words or phrases, DI-based algorithms score above Huffman coding and arithmetic coding. DI schemes, however, would fare worse in situations where there are no long repeated words and phrases. Adaptive techniques are generally used when the amount of overhead in a file has to be reduced. Statistical methods will usually ship some table summarizing the statistical information at the beginning of a file. Adaptive methods can reduce this amount, in some cases, because they often do not ship any additional data. Most statistical approaches can be changed, or adapted through one simple idea. Instead of building a statistical model for all of the characters or tags in a file, the model is constructed for a small group and updated frequently. Programming approach entails compressing data with executable files mostly in situations where the data are well structured. It is not suited for audio files.

4 Compression Techniques for Hyperspectral Images

A typical compression algorithm utilizes statistical structure in the image data set. In hyperspectral images, two types of correlation are possible. One is spatial correlation that exists between adjacent pixels in the same band, and the other is spectral correlation that exists between pixels in adjacent bands. We have considered only spectral correlation-based studies for our review.

4.1 Lossless Compression Techniques for Hyperspectral Imaging

In HSI, considerable research has been done using lossless compression techniques. In the following section, we describe various techniques employed and the results obtained. Keyan Wang et al. employ adaptive edge-based prediction in [4]. This is done by concentrating on increased affinity between the pixels present in the edge of the images to put forth a new high performance compression algorithm. The algorithm uses three different types of predictors for different modes of prediction. Intraband prediction is done using an improved median predictor (IMP) that can detect the diagonal edge. An adaptive edge-based predictor (AEP) is used for interband prediction that takes into account the redundancy in the spectrum. In case of the band that does not have any prediction mode, the pixels are entropy coded.

This algorithm shows an improvement in the lossless compression ratio for both standard airborne visible/infrared imaging spectrometer (AVIRIS) 1997 hyperspectral images and the newer consultative committee for space data systems (CCSDS) test images. Quang Zhang et al. discuss a new double-random projection method in [5] that uses randomized dimensionality reduction techniques for efficiently capturing global correlation structures and residual encoding. This new method extended from the randomized matrix decomposition methods for achieving rapid lossless compression and reconstruction of HSI data ensures effective lossless compression of HSI data. It shows empirically that the entropy of the residual image decreases significantly for HSI data. It expects that the conventional entropy-based methods for integer coding will perform well on these low-entropy residuals. The paper concludes that the integration of advanced residual coding algorithms with the randomized algorithm can be an important research topic for the future study. A transform-based lossless compression for hyperspectral images is presented by Kai-jen Cheng et al in [6]. which is inspired by Shapiro's (1993) embedded zerotree wavelet (EZW) algorithm. The method that is proposed for compression employs a hybrid transform which is a combination of an integer Karhunen–Loève transform (KLT) and integer discrete wavelet transform (DWT). The proposed method was applied to AVIRIS images and compared to other state-of-the-art image compression techniques. It is shown that the lossless compression algorithm proposed has higher efficiency and compression ratio than other similar algorithms. Nor Rizuan Mat Noor et al. propose an algorithm in [7] that performs lossless hyperspectral image compression by employing the Integer KLT, an integer AP of the KLT. This paper explores the effect of single-bit errors on the performance of the integer KLT. This algorithm is of a low complexity and is capable of detecting and correcting a single-bit error. Changguo Li et al. discuss in [8] how their algorithm can exploit both interband and intraband statistical correlations, and in turn give superior compression performance as compared to existing classical algorithms. In this paper, linear prediction is combined with a gradient adjusted prediction and an interband version of gradient-adjusted prediction (GAP) is proposed. Jinwei Song et al. in [9] propose a lossless compression algorithm that is based on a recursive least squares (RLS) filter. They show that this algorithm generates state-of-the-art performance with relatively low complexity. It looks at lots of conventional lossless compression algorithms for red–green–blue images, such as JPEG-lossless (LS), Diff.JPEG and clustered-differential pulse code modulation. Jarno Mielikainen in [10] makes use of lookup tables to propose an algorithm for hyperspectral image compression. By using interband correlation as a means of prediction, this low-complexity algorithm achieves good compression ratio and makes it highly suitable for onboard image compression. Lin BAI et al. present in [11] context prediction-based lossless compression algorithm for hyperspectral images. The algorithm performs sequentially linear prediction,

followed by 3D context prediction followed by arithmetic coding and exhibits low complexity and a compression ratio of 3.01 which is better than many state-of-art algorithms. Aaron B. Kiely et al. compare [12] the compression performance of standard AVIRIS hyperspectral raw images that do not contain appreciable calibration-induced artifacts and the images containing calibrated artifacts and concludes that raw images achieve a worse compression performance than processed images.

4.2 Lossy Compression Techniques for Hyperspectral Imaging

Lucana Santos et al. in [13] address the urgent need for defining new hardware architectures for the implementation of algorithms for hyperspectral image compression onboard satellites. Their algorithms demonstrate the use of graphics processing units (GPUs) for enhancing greatly the computation speeds for parallel tasks and data. The algorithm also specifies the parallelization strategy used and discusses solutions to the probable problems that are encountered during attempts at acceleration of hyperspectral compression algorithms. It also throws light on the effects of various configuration parameters on the compression algorithms. An architecture is proposed by Lucana Santos et al. in [14] that enables hastening of the compression task by employing a parallel algorithm for onboard lossy hyperspectral image compression by implementing it on the GPU. The algorithm uses block-based operation and provides an optimized GPU implementation incurring a negligible overhead in comparison with the original single-threaded version. Barbara Penna et al. in [15] propose a lossy algorithm for pixel anomaly detection which uses a hybrid of spectral KLT + spatial JPEG2000 and achieves better distortion rate. It can be employed for both coding and decoding of images.

4.3 Lossless and Lossy Compression Techniques for Hyperspectral Imaging

Yongjian Nian et al. talk about distributed source coding (DSC) compression algorithms in [16] for both lossy and lossless compressions. The complexity of the algorithm is found to be very low. It uses regression model to improve the compression performance of distributed lossless compression algorithm, and optimal scalar quantization for distributed lossy compression. The proposed algorithm is on par with other similar algorithms on competitive compression performance. This encoder has low complexity, and hence, it is most suitable for onboard compression (Table 1).

Table 1 Comparison of hyperspectral compression algorithms

Hyperspectral compression algorithm	Parameters for comparison		
	Classification used	Analysis criteria	Results
Adaptive edge-based prediction (lossless)	Statistical based (least squares optimization and entropy encoding)	Compression ratio	The algorithm makes good use of the high correlation among the pixels based on the edges to formulate a new lossless compression algorithm for hyperspectral images namely adaptive edge-based prediction algorithm. The results show an improvement in the lossless compression ratio for AVIRIS 1997 hyperspectral images
Double-random projection method (combination of random method and residual coding algorithm) (lossless)	Approximation-based low rank approximation	Use of randomized dimensionality reduction techniques for efficiently capturing global correlation structures and residual encoding	Algorithm employs randomized dimensionality reduction techniques for efficiently capturing global correlation structures, residual encoding and provides lossless compression. Entropy of the residual decreases significantly for HSI data
3D binary EZW algorithm (lossless)	Wavelet solutions-based	Compression ratio	Has combined merits of EZW and SPIHT algorithms. Is computationally simpler and efficient. It also has higher compression ratio than other algorithms
Hybrid transform [integer Karhunen-Loève transform (KLT) + integer discrete wavelet transform (DWT)] (lossless)	Hybrid of wavelet solution and statistical based	Compression ratio	Low complexity and is capable of detecting and correcting a single-bit error Experimental results on the compression performance, latency and power consumption are reported
Linear + gradient adjusted prediction (GAP) an interband version of GAP is proposed (lossless)	Statistical based	Bit rate compression	Achieves better compression performance compared with those existing classical algorithms as the encoder complexity is found to be low

(continued)

Table 1 (continued)

Hyperspectral compression algorithm	Parameters for comparison		
	Classification used	Analysis criteria	Results
Recursive least squares (RLS) filter (lossless)	Statistical based	Complexity	The algorithm gives state-of-art performance with low complexity. It attempts to eliminate both spatial and spectral correlation in hyperspectral images. Highly suitable for on-board compression in real time
Graphics processing units (GPUs) (lossy)	Statistical (use of Golomb entropy code)	Throughput	New hardware architecture supporting parallelization shows enhanced performance. It is done by comparing the performance of the GPU implementation with a single-threaded CPU implementation
Block-based operation and optimized GPU implementation (lossy)	Wavelet solutions (discrete cosine transforms)	Rate distortion optimization	Gives a competitive compression performance and low encoder complexity. The results make a good study for usage of space qualified GPUs
Hyperspectral image compression in band-interleaved-by-line (BIL) format using lookup tables (lossless)	Prediction based on the interband correlation	Compression ratio	The algorithm achieves a low algorithmic complexity and high compression ratios compared to other standard algorithms. It simplifies both compression and decompression process
Spectral Karhunen–Loève transform followed by spatial JPEG 2000 (lossy)	Wavelet based	Rate distortion optimization	Anamoly detection performance is better than state-of-art algorithms
Hybrid algorithm for context prediction based (lossless)	Prediction based on the spectral correlation	Compression ratio	Low complexity achieves a compression ratio of 3.01
Calibration-induced algorithm (lossless)	Statistical based	Compression ratio	Calibrated images give better performance

Table 2 Video compression algorithms for hyperspectral image data

Video compression algorithms	Analysis criteria	Observations
MPEG and JPEG	Compression fidelity	Lossless coding. Achieves reasonable compression ratio
Generic algorithm for multiterminal video coding	Slepian-Wolf coded quantization	Witsenhausen–Wyner video coding, layered Wyner-Ziv video coding, and multiterminal video coding have been compared with the standard JMVM joint encoding scheme
H.264/AVC video coding standard	Compression ratio, accuracy of unmixing, and computation time	Reduction in complexities of potential low-power/real-time hyperspectral encoders

5 Comparative Study of Hyperspectral Compression Algorithms

6 Video Compression Algorithms

Video compression algorithms have gained widespread popularity on account of their simplicity, cost, and interoperability. Efforts have been made in order to explore the feasibility of employing these algorithms for the compression of hyperspectral images. Table 2 summarizes some of these algorithms. Timothy S. Wikinson et al. have compared in [17] various compression techniques that can be applied for HSI. Zixiang Xiong discusses the compression of video images based on DSC principles in [18]. Lucana Santos et al. in [19] evaluate the performance of H.264/AVC video coding standard for lossy compression of hyperspectral images and conclude that it can reduce the future design complexities of such encoders.

7 Conclusion

Although a wide variety of compression algorithms are available, there is no single algorithmic solution that is universally applicable. Non-adaptive algorithms do not modify their operations based on the characteristic of input, whereas the perceptive algorithms take into consideration the special characteristics of the data and modify their operations accordingly. Symmetric algorithms use the same algorithm for both compression and decompression but in reverse order of each other and non-

symmetric ones use different algorithms for compression and decompression. The researchers mostly combine a number of the algorithms mentioned in Sect. 3 to arrive at a hybrid algorithm that is most suited to their imaging application. Commercially available software packages also do the same. Most of the papers considered for this study have employed statistical or wavelet-based compression algorithms or a combination of both. In addition, the algorithm proposed in most of the studies is lossless and focuses on encoding schemes only. Further, video compression algorithms can reduce the design complexities present in the hyperspectral image data compression algorithms.

References

1. Canada Centre for Remote Sensing, *Fundamentals of Remote Sensing*. Remote Sensing Tutorial (2013)
2. http://commons.wikimedia.org/wiki/File:HyperspectralCube.jpg
3. P. Wayner, *Data Compression for Real Programmers* (Morgan Kaufman Inc., Los Altos, 1999)
4. K. Wang, L. Wang, H. Liao, J. Song, Y. Li, Lossless compression of hyperspectral images using adaptive edge-based prediction. Proceedings of SPIE 8871, satellite data compression, communications, and processing IX, 887105 (2013). doi:10.1117/12.2022426
5. Q. Zhang, V.P. Pauca, R. Plemmons, Randomized methods in lossless compression of hyperspectral data. J. Appl. Remote Sens. **7**(1), 074599–1 (2013)
6. K.-J. Cheng, J. Dill, Hyperspectral images lossless compression using the 3D binary EZW algorithm. in *Proceedings of SPIE 8655, Image Processing: algorithms and Systems XI*, vol. 8655, ed. by K.O. Egiazarian, S.S. Agaian, A.P. Gotchev (Burlingame, California, 2013), p. 8655. doi:10.1117/12.2002820
7. N. Rizuan, M. Noor, T. Vladimirova, Parallelised fault-tolerant integer KLT implementation for lossless hyperspectral image compression on board satellites. 2013 NASA/ESA conference on adaptive hardware and systems (AHS 2013)
8. C. Li, K. Guo, Lossless compression of hyperspectral images using interband gradient adjusted prediction. 4th IEEE international conference on software engineering and service science (ICSESS 2013), 23–25 May 2013. ISBN:978-1-4673-5000-6/13. doi:10.1109/ICSESS 2013.6615408
9. J. Song, Z. Zhang, X. Chen, Lossless compression of hyperspectral imagery via RLS filter. Electron. Lett. **49**(16) (2013)
10. J. Mielikainen, Lossless compression of hyperspectral images using lookup tables. IEEE Signal Process Lett. **13**(3), 157–160 (2006)
11. L. Bai, M. He, Y. Dai, Lossless compression of hyperspectral images based on 3D context prediction. 3rd IEEE conference on industrial electronics and applications (2008), pp. 1845–1848. ISBN:978-1-4244-1717-9
12. A.B. Kiely, M.A. Klimesh, Exploiting calibration-induced artifacts in lossless compression of hyperspectral imagery. IEEE Geosci. Remote Sens. Lett. **47**(8), 2672–2678 (2009)
13. L. Santos, E. Magli, R. Vitulli, A. Núñez, J.F. López, R. Sarmiento, Lossy hyperspectral image compression on a graphics processing unit: parallelization strategy and performance evaluation. J. Appl. Remote Sens. doi:10.1117/1.JRS.7.074599
14. L. Santos, E. Magli, R. Vitulli, J.F. López, R. Sarmiento, Highly-parallel GPU architecture for lossy hyperspectral image compression. IEEE J. Sel. Top. Appl. Earth Obs. Remote Sen. 6(2), 670–681 (2013)

15. B. Penna, T. Tillo, E. Magli, G. Olmo, Hyperspectral image compression employing a model of anomalous pixels. IEEE Geosci. Remote Sens. Lett. **4**(4), 664 (2007)
16. Y. Nian, M. He, J. Wan, Low-complexity compression algorithm for hyperspectral images based on distributed source coding. Math. Probl. Eng., Article ID 825673 (2013)
17. T.S. Wilkinson, V.D. Vaughn, Application of video based coding to hyperspectral imagery. Proceedings of SPIE 2821, hyperspectral remote sensing and applications, vol. 44 (1996). doi:10.1117/12.257183
18. Z. Xiong, Video compression based on distributed source coding principles. Conference record of the forty-third Asilomar conference on signals, systems and computers (2009)
19. L. Santos, G.M. Callicó, J.F. Lopez, R. Sarmiento, Performance evaluation of the H.264/AVC video coding standard for lossy hyperspectral image compression. IEEE J. Sel. Top. Appl. Earth Obs. Remote Sens. **5**(2), 451–461 (2012). doi:10.1109/JSTARS.2011.2173906

Reliable Virtual Cluster-Based Opportunistic Routing Protocol for Mobile Ad hoc Networks

E. Sahaya Rose Vigita, E. Golden Julie and S. Tamil Selvi

Abstract Geographic opportunistic routing protocols overcome the failure of traditional routing protocols which fail due to the dynamic nature of mobile ad hoc networks. When link stability is considered for forwarder selection, the hop count and delay become unpredictable. Hence, a new protocol, delay-aware cluster-based opportunistic Routing (DACOR) protocol, has been proposed. In DACOR, nodes with high transmission range form loose clusters with surrounding nodes. When such high-power nodes are not available, nodes with lower transmission range enable the routing process by opportunistically selecting the best forwarder based on link stability. When no neighbors are found, a routing hole handling mechanism is also proposed. Simulation results show that the presence of high transmission nodes reduces the hop count, thus ensuring low delay, and opportunistic routing guarantees reliable data delivery.

Keywords Mobile ad hoc networks · Loose virtual clustering · Opportunistic routing · Reliability · Low delay · Mobility · Link stability

1 Introduction

Opportunistic routing [1] prioritizes the neighboring nodes according to some metrics to choose the next forwarder at each hop. To prevent the routing information from becoming stale, geographic routing [2] was proposed. It helps to reach

E. Sahaya Rose Vigita (✉) · E. Golden Julie
Department of Computer Science and Engineering, Anna University, Chennai, India
e-mail: sahaya.r.vigita@gmail.com

E. Golden Julie
e-mail: juliegolden18@gmail.com

S. Tamil Selvi
Department of ECE, National Engineering College, Tirunelveli, India
e-mail: tamilgopal2004@yahoo.co.in

© Springer India 2015

L.P. Suresh et al. (eds.), *Artificial Intelligence and Evolutionary Algorithms in Engineering Systems*, Advances in Intelligent Systems and Computing 325,
DOI 10.1007/978-81-322-2135-7_16

the destination in a hop-by-hop fashion. No energy is spent on route discovery [3]. Memory overheads due to routing table maintenance are reduced. Traffic caused by route queries and replies is reduced. When stability of a link is taken as the metric for forwarder selection, the number of hops may not be minimum, resulting in unpredictable delays. Hence, the problem is how to improve the reliability of a routing protocol as well as ensure lower end-to-end delay with minimal hops. The advantages of clustering are exploited to achieve this [4].

The rest of the paper is organized as follows. In Sect. 2, we review the related literature. In Sect. 3, the routing algorithms of the protocol are detailed. In Sect. 4, the simulation results of the protocol are presented. Finally, we conclude the paper in Sect. 5.

2 Review of Literature

Numerous routing protocols with cluster formation have been proposed earlier for MANETs. In [5], nodal residual energy is considered to establish a route to conserve energy. However, a packet has to wait for a proper transmission period resulting in longer delay. In [6], nodes in a virtual backbone become forwarders. Mapping of the virtual backbone to the physical topology becomes difficult under high node mobility. MC routing [7] ensures better reliability, larger throughput, and reduced number of hops. However, the assumption that the routing area is fixed and that the nodes move around in a fixed territory does not support high mobility of nodes. RCM [8] achieves high throughput, whereas the number of vehicles in each region unit is limited to reduce the contention period.

3 Proposed Protocol

3.1 Architecture

A loose virtual clustering-based routing protocol for MANETs is proposed. As shown in Fig. 1, the nodes are classified into two types, backend nodes (B-nodes) which are high transmission nodes with higher priority for routing and general nodes (G-nodes) with lower transmission range [9]. B-nodes with larger coverage tend to minimize the hop counts. When a B-node is found, it becomes the virtual cluster head and **backend routing** is done. If no B-node is found, **general routing** is done by G-nodes. When no potential forwarders are found, a routing hole handling mechanism is adopted.

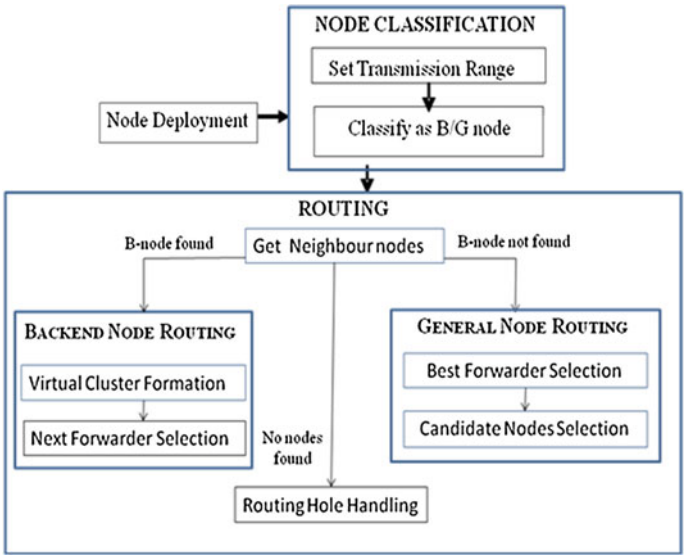

Fig. 1 Architecture diagram

3.2 Backend Routing Mechanism

Backend routing shown in Fig. 2 involves a B-node which acts as the forwarder. A B-node has the highest priority in forwarding a packet. Neighbor list is checked for the presence of B-nodes. If a B-node is found, then a loose virtual cluster is formed by that B-node. If several B-nodes are found, the one nearest to the destination is selected to form the virtual cluster. The B-node now acts as a cluster

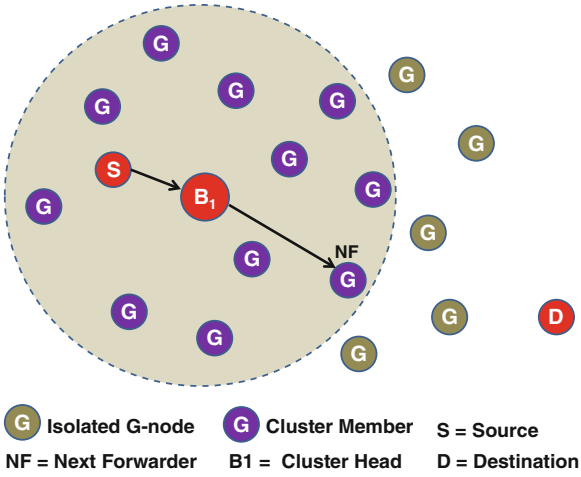

Fig. 2 Backend routing

head. It selects the node nearest to destination as the next forwarder. Backend routing consists of three phases, namely Phase-I discovers neighbors, Phase-II deals with virtual cluster formation, and Phase-III selects the next forwarder.

Algorithm 1: Backend Routing
Phase I: Neighbor Discovery

1. *Node broadcasts Neighbour Discovery (ND) packets with its ID and type.*
2. *Node waits for time T_{BND} to collect ND packets.*
3. *Using IDs received, node constructs Neighbour Table (NT).*
4. *Exit.*

Phase II: Loose Virtual Cluster Formation

1. *Node selects the B-node nearest to Destination as Cluster Head.*
2. *Sends Cluster Head Selection (CHS) packet to that B-node.*
3. *B-node broadcasts Cluster Head Declare (CHD) packet.*
4. *Surrounding nodes send Cluster Member Register (CMR) packet to that B-node.*
5 *B-node adds nodes that sent CMR to Cluster Member list (CML).*
6. *B-node sends Cluster Head Confirmation (CHC) packet to nodes in CML.*
7. *Exit.*

Phase III: Next Forwarder Selection

1. *Select neighbours that make positive progress towards destination.*
2. *Sort them according to their distance from the destination.*
3. *Select the node nearest to destination as the next forwarder.*
4. *Exit.*

3.3 General Routing

When a B-node is not available for routing, general routing is done. Neighbors are prioritized based on their link stability and distance toward the destination. The node with power of reception greater than a threshold is chosen as best forwarder. Candidate nodes [10] are also selected to take over the forwarding function in case the best forwarder fails. In Fig. 3, node S has chosen node B as next best forwarder and nodes A, H, and F as candidate nodes.

Distance calculation between any two nodes, say node a and node b, is based on Euclidean distance given by Eq. 1.

$$d = \sqrt{(x_1 - x_2)^2 + (y_1 - y_2)^2} \tag{1}$$

where x_1 and x_2 are the x-coordinates of nodes a and b, respectively, and y_1 and y_2 are the y-coordinates of nodes a and b, respectively.

Power of reception is calculated using Eq. 2 [11, 12].

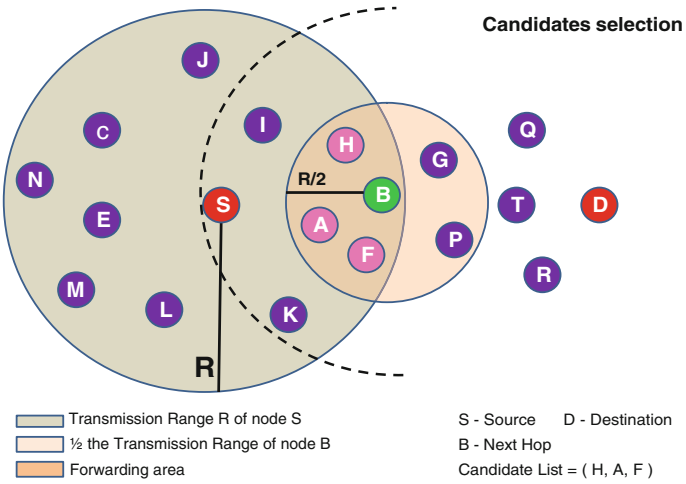

Fig. 3 Candidate selection

$$P_r(d) = P_t G_t G_r \frac{h_t^2 h_r^2}{d^4 L} \tag{2}$$

where P_t = Power transmitted by the transmitter

G_t = Antenna gain of transmitter
G_r = Antenna gain of receiver
h_r = Height of receiver antenna
h_t = Height of transmitter antenna
L = System loss
d = Euclidean distance between sender and receiver

Algorithm 2: General Routing—Best Forwarder Selection

1. *Find if Destination node is found among the neighbours.*
2. *If found, set the next hop as Destination node and Exit. Else continue.*
3. *For each G-node among the neighbours, do the following:*
   Check for positive progress towards destination.
4 *Check if its distance from the Destination node is greater than or equal to the distance between the current forwarder and Destination node. If yes, break. Else, add node to an array.*
5 *Sort the nodes in the array based on their distance to destination.*
6 *Calculate the reception power for array nodes using* Eq. 2, *starting from the first node.*
7. *If the node has reception power greater than the threshold value, choose that node as the Best Forwarder. Else consider the next node in array.*
8. *Exit.*

Algorithm 3: General Routing—Candidates Selection

1. *For each node in the array obtained in Algorithm 2, other than the Best forwarder, do the following:*
   - 1.a. *Check if it is within half the radius of the Best Forwarder's transmission range.*
   - 1.b. *If yes, check if its distance to the destination is lesser than the distance of the source node to the destination and the node's distance to destination is greater than distance of the Best Forwarder to the destination.*
   - 1.c. *If yes, add the node to Candidate list.*
2. *Exit.*

3.4 Routing Hole Handling Mechanism

Communication holes may exist due to non-uniform distribution of nodes. When the best forwarder finds no potential forwarders, a communication void is said to be encountered. The protocol then switches to a routing hole handling mechanism as shown in Fig. 4. Node B encounters a void and triggers node A to route around the void.

Algorithm 4: Routing Hole Handling

1. *If the Best forwarder finds no neighbors, then do the following:*
   - 1.a. *Send void warning signal to previous forwarder.*
   - 1.b. *Set the Best Forwarder as Void node.*
   - 1.c. *Set the previous forwarder as Trigger node.*
2. *Ignoring the void node, find the Best Forwarder for the Trigger node.*

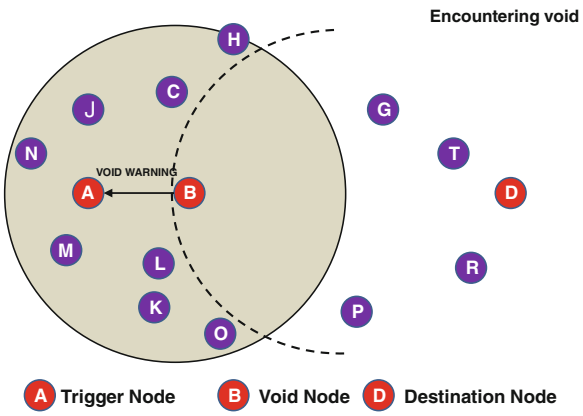

Fig. 4 Routing hole handling

3. *If the next hop node is the Destination node, send acknowledgement to the Trigger node. Exit.*
4. *If no forwarders are found, send Disrupt message to the Trigger node. Exit.*
5. *If a forwarder is found, switch to normal routing.*
6. *Exit.*

4 Performance Evaluation

The performance of DACOR is evaluated through a simulation study using NS-2.34. The protocol chosen for comparison is link- and position-based opportunistic routing (LPOR) protocol. LPOR selects the next forwarder with maximum reception power opportunistically at each hop. LPOR is proposed for nodes with the same transmission range without any cluster formation. Hence, all the nodes in LPOR are G-nodes. Simulation results are shown in the graphs below.

B-nodes with high transmission power enhance the delivery ratio as seen in Fig. 5, whereas the absence of such nodes in L-POR results in lesser delivery ratio. The presence of B-nodes minimizes the hop counts in DACOR, thereby reducing the end-to-end delay as seen in Fig. 6. LPOR does not guarantee minimal hop count since forwarder selection is based on link stability and not on distance metric.

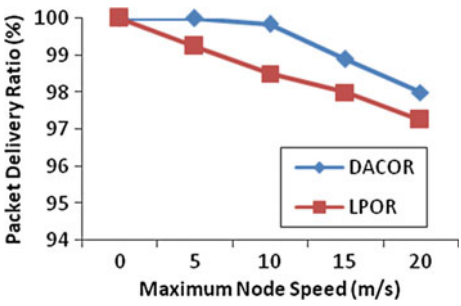

Fig. 5 Comparison of PDR

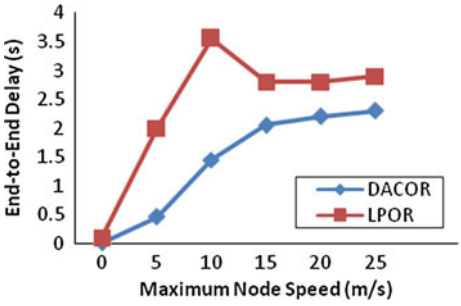

Fig. 6 Comparison of delay

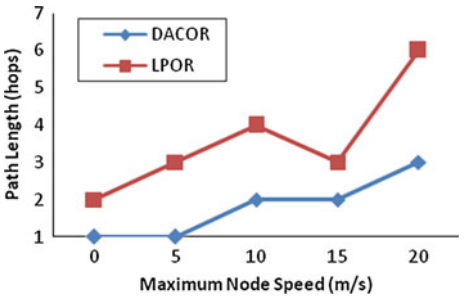

Fig. 7 Comparison of hops

The presence of B-nodes with high transmission range leads to a larger coverage area in DACOR resulting in minimal hop count as seen in Fig. 7. In DACOR, the number of B-nodes is always less than the number of G-nodes ensuring lesser interference resulting in higher throughput as shown in Fig. 8. The comparison graph for the FTH of the two protocols is shown in Fig. 9. Packet forwarding times per hop [FTH] is calculated using Eq. 3.

$$\mathrm{FTH} = \frac{N_s + N_f}{\sum_{i=1}^{N_r} N_{\mathrm{hi}}} \tag{3}$$

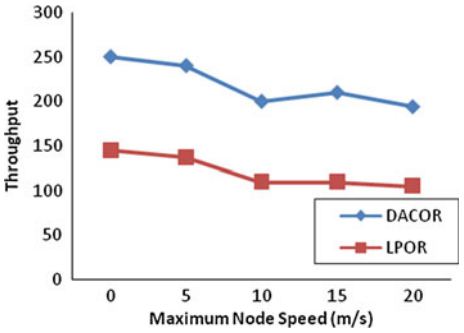

Fig. 8 Comparison of throughput

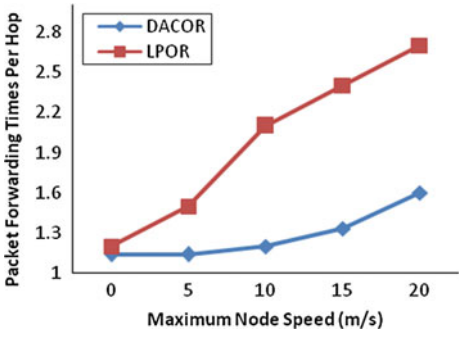

Fig. 9 Comparison of FTH

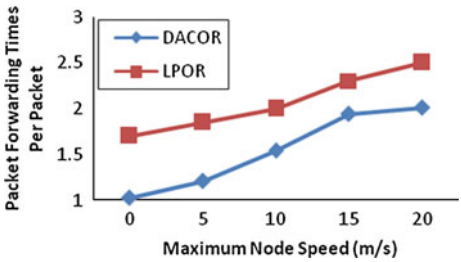

Fig. 10 Comparison of FTP

where, N_s, N_f, and N_r are the number of packets sent at the source, forwarded at intermediate nodes, and received at the destination, respectively. N_{hi} is the number of hops for the *i*th packet that is successfully delivered. The presence of high-power B-nodes reduces retransmissions leading to a lesser FTH compared to LPOR as seen in Fig. 10. The forwarding times per packet are calculated using Eq. 4. The comparison graph for the FTP of the two protocols is shown in Fig. 10. The presence of B-nodes can be accounted for the decrease in FTP compared to LPOR.

$$\text{FTP} = \frac{N_s + N_f}{N_r} \tag{4}$$

5 Conclusion and Future Work

A delay-aware routing protocol that takes advantage of different communication ranges of nodes in mobile ad hoc networks has been proposed. DACOR protocol utilizes the more powerful nodes as backend nodes (B-nodes) to form loose virtual clusters with the surrounding nodes. General nodes (G-nodes) have lesser transmission range. Since B-nodes have a larger transmission range and hence larger coverage, the number of hops is considerably decreased. Opportunistic routing ensures reliable packet delivery. Simulation tests demonstrate that DACOR performs much better than LPOR in terms of reliability, packet delay, throughput, and hop count.

Congestion control algorithms and proper scheduling methods can be incorporated into DACOR as future work.

References

1. A. Trivino-Cabrera, S. Canadas-Hurtado, Survey on opportunistic routing in multihop wireless networks. Int. J. Commun. Netw. Inf. Secur. (IJCNIS). **3**(2), 1–329 (2011)
2. D. Chen, P.K. Varshney, A survey of void handling techniques for geographic routing in wireless networks. IEEE Commun. Surv. **9**(1), 50–67 (2007)

3. A.M. Popescu, I.G. Peng, A.H. Kemp, Surveying position based routing protocols for wireless sensor and ad-hoc networks. Int. J. Commun. Netw. Inf. Secur. (IJCNIS) **4**(1), 325–349 (2012)
4. Y. Jane, Y. Peter, H.J. Chong, A Survey of clustering schemes for mobile adhoc networks. IEEE Commun. Surv. **7**(1), 32–48 (2005)
5. W. Liu, C. Zhang, G. Yao, F. Yuguang, Delar, A device energy-load aware relaying framework for heterogeneous mobile adhoc networks. IEEE J. Sel. Areas Commun. **29**(8), 1572–1584 (2011)
6. J. Wu, F. Dai, Virtual backbone construction in MANETs using adjustable transmission ranges. IEEE Trans. Mob. Comput. **5**(9), 1188–1200 (2006)
7. X. Du, D. Wu, W. Liu, Y. Fang, Multiclass routing and medium access control for heterogeneous mobile adhoc networks. IEEE Trans. Veh. Technol. **55**(1), 270–277 (2006)
8. Y.-C. Lai, P. Lin, W. Liao, C.-M. Chen, A Region-based Clustering mechanism for channel access in Vehicular adhoc networks. IEEE J. Sel. Areas Commun. **29**(1), 83–93 (2011)
9. P. Zhao, X. Yang, W. Yu, X. Fu, A Loose Virtual Clustering based Routing for Heterogeneous MANETs. IEEE Trans. Veh. Technol. **99**, 2290–2302 (2013)
10. S. Yang, C.K. Yeo, B.S. Lee, Towards reliable data delivery for highly dynamic mobile adhoc networks. IEEE Trans. Mob. Comp. **11**(1), 111–124 (2012)
11. Stepanov, D. Herrscher, K. Rothermel, On the impact of radio propagation models on MANET simulation results. *Proceedings of 7th International Conference on Mobile and Wireless Communications Networks.* (2005)
12. J. Schiller, *Mobile Communications* (Pearson, New Jersey, 2009), pp. 36–41

Weighted Euclidean Distance Based Sign Language Recognition Using Shape Features

S. Nagarajan and T.S. Subashini

Abstract This paper proposes a real-time static hand gesture recognition system for American Sign Language alphabets. The input hand gestures from a simple background are captured by a camera and an image database is created. The proposed system consists of four stages namely preprocessing, segmentation, feature extraction, and classification. In the training phase, the hand region is detected and segmented from the gesture database images and various shape-based features such as area, perimeter, and roundness are extracted. The extracted features form a unique feature vector for a particular gesture. In the testing phase, the feature vector of an input test image is compared with each of the feature vectors of database images using weighted Euclidean distance. The gesture is correctly recognized if the distance is the least. This system is tested using a dataset of twenty-four ASL alphabets with three different signers. The experimental results show that the proposed system offers the recognition rate of 91.6 %.

Keywords Euclidean distance · Feature extraction · Hand gesture recognition · Human–computer interaction · Shape features · Sign language recognition

1 Introduction

Hand gesture recognition is a technique by which the gestures made by the user are recognized by a receiving person. Gestures are used as the mode of communication by the community of hearing impaired. The gestures are involving the movements of the fingers, head, face, arms, or body with a main intention of conveying

S. Nagarajan (✉) · T.S. Subashini
Department of Computer Science and Engineering, Faculty of Engineering and Technology, Annamalai University, Annamalainagar, Chidambaram 608002, India
e-mail: ernagain@yahoo.co.in

T.S. Subashini
e-mail: rtramsuba@gmail.com

© Springer India 2015

L.P. Suresh et al. (eds.), *Artificial Intelligence and Evolutionary Algorithms in Engineering Systems*, Advances in Intelligent Systems and Computing 325,
DOI 10.1007/978-81-322-2135-7_17

information and for human–computer interaction [1]. Hand gesture recognition system is implemented by either color gloves-based or vision-based approaches. The sensors attached with color data gloves convert the hand trajectories into electrical signals. Vision-based techniques perceive information about the surroundings, and the information is processed by a computer. Gesture recognition has a variety of applications which include sign language recognition, development of the aids for the hearing impaired, helping very young children to interact with computers, navigation of medical images during surgery, creation of a visual interface for controlling appliances/devices, video games control through hand gestures, tele-teaching assistance, and communication in video conferencing.

This work is based on vision-based hand gesture recognition which involves two phases, namely training and testing. In the training phase, the signer shows one or more hand gestures that represent American Sign Language alphabets in front of a camera. All these gesture images are captured and stored in a database. In the testing phase, the recognition system compares the feature vector of input test image given at run time with the feature vector of each of the stored database images using weighted Euclidean distance measure. Based on the least distance, the gesture is classified and interpreted in the form of text.

2 Related Work

There are many earlier techniques to recognize the hand gestures in real time. But it is inevitable to create a vision-based system for recognition of language-specific gestures. The data gloves-based recognition approaches give accurate result, but they are more expensive as they need sophisticated hardware and wired connections. Skin color-based techniques offer poor results as they employ segmentation of hand from the complex background. A neural network-based hand gesture recognition system is discussed in [2]. A novel technique for recognition of Tamil sign alphabets is proposed in [3]. A feature matching technique [4] is used to recognize the ASL alphabets using neural networks. References [5, 6] used skin filtering techniques for hand gesture recognition. These techniques separated the skin-colored pixels from the non-skin-colored pixels to extract the hand from the background. Reference [7] presents a simple and efficient approach to recognize the hand gestures representing numbers from zero to nine. Nasser. H presented a novel method to control the video games via hand gestures using bag of features in [8].

3 Proposed Method

In the proposed method, the RGB images representing ASL alphabets in a simple, plain, and uniform background are first captured by a camera with a resolution of 320×240 pixels and an image database is created. The system does not require the

signer to wear any color gloves or sophisticated equipments. In the preprocessing stage, the captured RGB images are converted into grayscale images. Thresholding technique is used to convert the grayscale images into binary images. Then various image morphological operations such as dilation, erosion, and median filtering are performed on the segmented binary images to eliminate the unwanted noises. All the connected components in the binary image are labeled using bounding box. Only the biggest connected component, i.e., hand, is retained by removing the smaller connected components. Then, the unwanted wrist portion is cropped by a wrist cropping technique. Canny edge detection is applied on the ROI-extracted binary image to find the edges. The flow diagram of the proposed system is shown in Fig. 1.

In the feature extraction stage, the following shape-based features are extracted using the region props in MATLAB.

Centroid: The centroid of a hand (*Xc*, *Yc*) is calculated as follows:

$$Xc = \frac{\sum_{i=1}^{k} xi}{k}, \quad Yc = \frac{\sum_{i=1}^{k} yi}{k} \tag{1}$$

where *Xc* and *Yc* represent the centroid of the hand, *xi* and *yi* are the *x* and *y* coordinates of the *i*th pixel in the binary hand region. '*k*' denotes the total number of pixels representing only the hand portion.

Area: The area measures the size of the foreground object in an image. Hence, the area is given as the total number of 'on' pixels in the hand image.

Perimeter: The perimeter is measured as the sum of all the distances between each adjoining pair of pixels in the boundary of the labeled binary image.

Roundness: The roundness of a foreground hand object is measured as

$$\text{Roundness} = (4 * \text{Area} * \pi) \tag{2}$$

where $\pi = 3.14$.

Orientation: It is defined as the inclination angle between the *x*-axis and the major axis of the ellipse which has the same second moments as that of the hand region. Normally, orientation ranges from −90° to 90°. It is given by

$$\text{Orientation} = \frac{(4 * \text{Area} * \pi)}{(\text{perimeter})2} \tag{3}$$

Convex Area: It is a scalar specifying the number of pixels in the convex image.

Equivdiameter: It is a scalar value specifying the diameter of a circle with the same area as the hand region. It is given by

$$\text{Equivdiameter} = \sqrt{(4 * \text{Area})/\pi} \tag{4}$$

Once the feature extraction is completed for all the training images, these features are saved in a.mat file as row vectors. The resultant feature vector x obtained

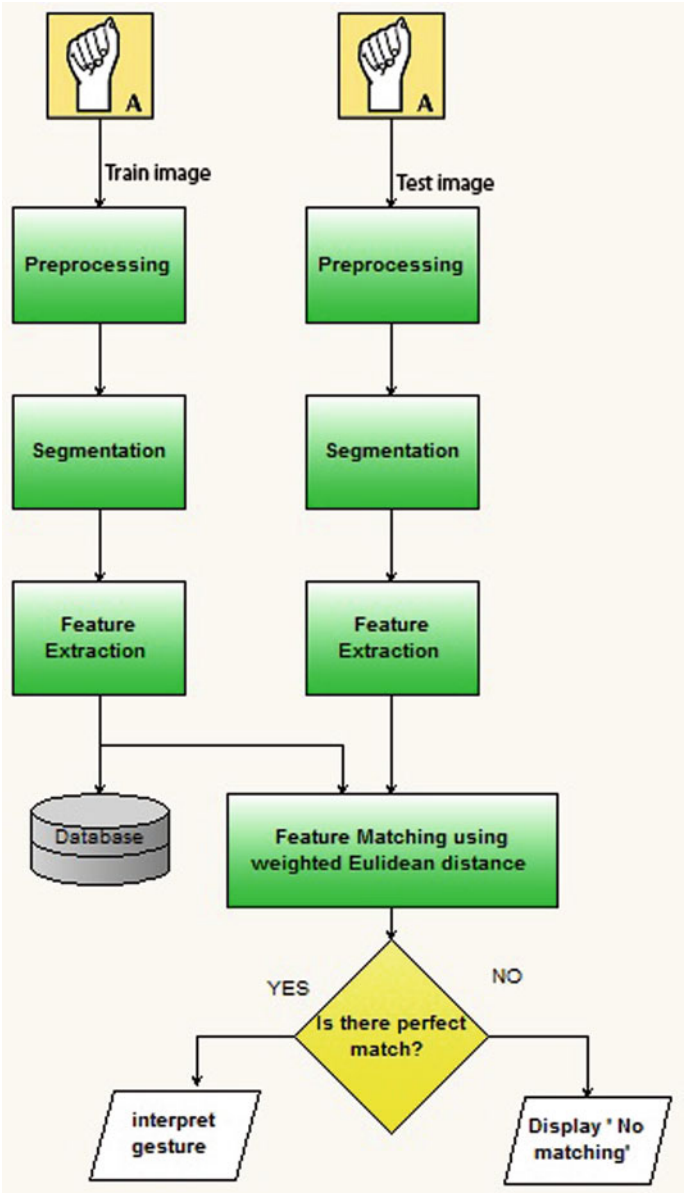

Fig. 1 Flow diagram of the proposed system

for each input image is written as $x = [F1\ F2\ F3\ F4\ F5\ F6\ F7\ F8]$, where $F1 = x$ coordinate of centroid, $F2 = y$ coordinate of centroid, $F3$ = area, $F4$ = perimeter, $F5$ = orientation, $F6$ = roundness, $F7$ = convex area, and $F8$ = equivdiameter. In the testing phase, the feature matching is performed using

weighted Euclidean distance. The Euclidean distance between the feature vector of input test image at run time and the feature vector of each training image is first calculated using the formula

$$\text{E.D} = \sqrt{(x2 - x1)^2 + (y2 - y1)^2} \tag{5}$$

where, $x1$, $y1$ and $x2$, $y2$ are the two feature elements in a vector. Then, the rowwise weighted Euclidean distance is calculated as the cumulative sum of all the Euclidean distances measured using Eq. (5). If both the test and train images match with each other, the weighted Euclidean distance would be the least and the corresponding gesture is interpreted.

4 Experimental Results and Discussion

The static hand gesture recognition system proposed in this paper was implemented in MATLAB 2013a. With three different signers, each showing 10 samples per gesture, totally 720 images were captured and saved in the database. Out of these 720 images, 480 images were used for training and 240 images for testing. In this paper, only 24 signs are considered for recognition except the alphabets J and Z because they are dynamic signs [9] having finger movements. The following assumptions are made in this work:

- A simple, plain background is to be used for image acquisition.
- The system recognizes only static gestures.
- The real-time gestures are to be captured in vertical orientation, without rotating the hand. Because no orientation detection mechanism is incorporated in this work.
- One feet distance is to be maintained between the signer and camera.
- Proper lighting should be given for capturing a clear gesture image.

The experimental results for feature extraction and classification of gestures are shown in Table 1. The overall gesture recognition rate is given as

$$\text{Recognition Rate} = \frac{\text{No. of correctly recognized gestures}}{\text{Total number of input gestures}} \times 100\,\% \tag{6}$$

Number of test images used for each alphabet = 10. Hence, a total of 240 images were used for testing. Among these, 220 gesture images were correctly recognized. Using Eq. (6), the overall recognition rate is calculated as 91.6 %.

From Table 1, it is observed that the gesture B is correctly recognized, since its weighted Euclidean distance has the least value. Table 2 gives the performance comparison between the proposed work and the earlier works which have been already implemented in the related field.

Table 1 Experimental results for feature extraction and gesture classification

Gesture	Shape-based feature vector								Weighted Euclidean distance ($\times 10^4$)
	*F*1	*F*2	*F*3	*F*4	*F*5	*F*6	*F*7	*F*8	
A	86	102	23,933	687	0.63	50.0	25,625	19.7	0.2924
B	72	111	21,063	707	0.49	−80.3	22,791	23.0	**0.0451**[a]
C	104	89	16,500	754	0.36	−46.2	21,997	34.4	0.8426
D	97	118	15,986	672	0.43	−43.7	20,377	29.0	1.0441
E	68	96	20,131	614	0.70	88.0	25,670	17.7	0.2727
F	107	109	18,914	910	0.28	−66.4	25,151	43.8	0.6814
G	110	87	19,163	738	0.47	−51.3	23,137	26.3	0.4222
H	106	100	17,919	680	0.51	−46.9	21,026	24.1	0.6943
I	76	110	19,012	713	0.45	65.0	22,882	27.3	0.3224
K	124	103	20,472	696	0.57	−61.8	24,679	25.5	0.2786
L	81	118	18,043	855	0.39	−76.9	23,577	40.5	0.5424
M	74	123	13,514	753	0.29	66.2	20,822	36.1	1.2501
N	90	98	28,409	711	0.70	52.8	29,653	17.8	0.8678
O	86	100	26,869	790	0.56	68.8	30,309	22.1	0.2094
P	80	87	14,677	596	0.63	−40.7	17,301	19.6	0.0808
Q	111	70	16,256	762	0.35	−29.2	23,936	35.7	0.7544
R	97	79	21,990	867	0.40	20.3	27,822	34.2	0.4485
S	87	120	19,761	728	0.50	−75.9	23,100	26.8	0.1998
T	81	92	25,474	673	0.71	85.4	26,834	17.8	0.7365
U	102	103	27,187	740	0.62	64.7	29,113	20.1	0.0492
V	96	105	21,634	767	0.46	52.5	25,523	27.2	0.2378
W	86	111	20,991	862	0.35	−86.7	30,197	35.4	0.6589
X	74	100	15,426	706	0.41	−79.2	20,079	30.5	0.5516
Y	110	98	13,051	636	0.44	−48.1	15,476	28.4	1.8330

[a] Least weighted Euclidean distance

In the HSV skin color-based method [10], the feature vector with highest score is evaluated first, and then, the system selects the hypothesis of those features leading to higher computational time. Reference [11] is used to recognize only few signs, and hence, its accuracy is 100 %. The misclassification rate is high in [12, 13] due to variations in scaling, rotation, and transformation in the database samples. Reference [14] is used the Gabor filters for extracting desirable features of hand and PCA for feature reduction. Due to the complexity of this algorithm, the computation time is high. In [15], K-L transform is applied to extract hand features. But this method is not able to recognize few signs correctly due to misclassification.

Table 2 Performance comparison between our work and other existing techniques

Name of the technique used	Type of features	Classifier	Rate of recognition (%)
HSV skin color based [10]	Numerical features	Learning vector quantization (LVQ)	98
Laboratory color space based [11]	Number of peaks and valleys	SVM	100
Segmentation based [12]	Invariant moments, K-curvature geometric, shape descriptors	Multilayer perceptron	91
Neural network based [13]	Haar wavelet features	Multilayer perceptron	94.06
PCA, Gabor filter based [14]	Geometrical features	SVM	95.2
K-L transform based [15]	Edge features	Euclidean distance	96
Proposed method	Shape features	Weighted Euclidean distance measure	91.6

By overcoming these difficulties, our work is able to recognize 24 different static gestures from the bare single hand and it does not require the user to wear any data gloves or sophisticated hardware. By taking shape-based features, it is proved that the proposed method offers good recognition accuracy with less computational time than the other existing approaches.

5 Conclusion

A static hand gesture recognition system for ASL alphabets using weighted Euclidean distance with MATLAB tools is discussed in this paper. The proposed system is capable of recognizing static gestures after training. The experimental results reveal that the proposed system allows fast training and learning of new gestures and the overall recognition accuracy of 91.6 % is achieved. Using more gesture samples with different orientation, lighting conditions, and scaling for training, the classifier may improve the performance of the system in future. The only limitation of this system is that, it works only for simple, uniform background. The future work will include developing a background-independent hand gesture recognition system dealing with video signs of isolated sign language words or phrases. Further, the classification accuracy may be still improved by incorporating hand orientation detection mechanism.

References

1. M. Panwar, P.S. Mehra, Hand gesture recognition for human computer interaction, in *International Conference on Image Information Processing* (2011)
2. T. Ahmed, A neural network based real time hand gesture recognition system. Int. J Comput Appl **59**(4) (2012)
3. P.S. Rajam, G. Balakrishnan, Recognition of Tamil sign language alphabet using image processing to aid deaf-dumb people. Proceedia Eng. **30**, pp. 861–868 (2011). (SciVerse ScienceDirect, Elsevier)
4. Md. Atiqur Rahman, Ahsan-Ul-Ambia, Md. Aktaruzzaman, Recognition of Static Hand Gestures of Alphabet in ASL. IJCIT **2**(1) (2011)
5. C. Yu, X. Wang, H. Huang, J. Shen, K. Wu, Vision based hand gesture recognition using combinational features, in *IEEE Sixth International Conference on Intelligent Information Hiding and Multimedia Signal Processing* (2010) pp. 543–546
6. I.G. Incertis, J.G.G. Bermejo, E.Z., Casanova: hand gesture recognition for deaf people interfacing, in *The 18th International Conference on Pattern Recognition* (2006)
7. A. Pradhan, M.K. Ghouse, M. Pradhan, A hand gesture recognition using feature extraction. Int. J. Curr. Eng. Technol. **2**(4) (2012)
8. N.H. Dardas, N.D. Georganas, Real time hand gesture detection and recognition using bag-of-features and support vector machine. IEEE Trans. Instrum. Meas. **60**(11) (2011)
9. ASL dataset, http://www.lifeprint.com/ASL101/fingerspelling/index.htm
10. L. Lamberti, F. Camastra, Real time hand gesture recognition using a color glove, in *Springer 16th International Conference on Image Analysis and Processing* (2011), pp. 365–373
11. R. Mapari, G. Kharat, Hand gesture recognition using neural network. Int. J. Comput. Sci. Netw. **1**(6) (2012)
12. M.M. Hasan, P.K. Mishra, HSV brightness factor matching for gesture recognition system. Int. J. Image Process. **4**(5), pp. 456–467 (2011)
13. A. Karami, B. Zanj, A.K. Sarkaleh, Persian sign language (PSL) recognition using wavelet transform and neural networks. Expert Syst. Appl. **38**, 2661–2667 (2011)
14. D.Y. Huang, W.C. Hu, S.H. Chang, Vision based hand gesture recognition using PCA+ Gabor filters and SVM, in *IEEE Fifth International Conference on Intelligent Information Hiding and Multimedia Signal Processing* (2009), pp. 1–4
15. J. Singha, K. Das, Hand gesture recognition based on Karhunen-Loeve transform, in *Mobile and Embedded Technology International Conference (MECON)* (2013), pp. 365–371

Event Monitoring for Adaptive Multi-priority Streaming Time Sensitive-Based EDF Scheduling

P. Leela, S. Sathees babu and K. Balasubadra

Abstract Real-time systems are bounded with strict time constraints. To accomplish this, task scheduling is needed. Earlier approaches are restricted to fixed priority scheduling policies, which follows static priority algorithm. It assigns a priority statically and schedules dynamically. It does not support dynamic priority requests. To overcome this, preemptive earliest deadline first (EDF) scheduling is used, which is a dynamic priority scheduling algorithm. It ensures that higher priority requests are executed first and they experience lower mean waiting time, without leading lower priority requests to overstarvation. But preemptive EDF leads to increase in runtime overhead. Hence, proposed method uses limited preemption EDF scheduling, which assigns an approximate deadline for each request, and the requests are serviced with limited preemption. It splits the request into multiple jobs and assigns fixed preemption points (FPP) to each sub job. Only at FPP position, preemption is allowed. Hence, it is proved experimentally that the mean waiting time for higher and lower priority tasks are the minimum with less runtime overhead.

Keywords Earliest deadline first · Fixed preemption points · Fixed priority scheduling · Limited preemption

P. Leela (✉)
P.S.N.A College of Engineering and Technology, Anna University, Dindigul, India
e-mail: tanuleela@gmail.com

S. Sathees babu
Department of Computer Science and Engineering, P.S.N.A College of Engineering and Technology, Dindigul, India
e-mail: ssbabu@psna.edu.in

K. Balasubadra
Department of Information and Technology, RMD College of Engineering and Technology, Chennai, India
e-mail: balasubadra@yahoo.com

© Springer India 2015

L.P. Suresh et al. (eds.), *Artificial Intelligence and Evolutionary Algorithms in Engineering Systems*, Advances in Intelligent Systems and Computing 325,
DOI 10.1007/978-81-322-2135-7_18

1 Introduction

A real-time system is one that must process information and produce a response within a specified time, else risk severe problems, including failure. If we consider the ATM network as an example of real-time system, when the system becomes overloaded due to improper scheduling, some transaction fails. To avoid such failures, proper scheduling algorithm should be used. Each task needs resources such as processor, memory, I/O devices, etc. for execution. Scheduling algorithms are used in assigning these resources to task and to execute the tasks in possible order with less average waiting time. Previously, fixed priority scheduling algorithms such as first come first serve (FCFS), shortest job first (SJF), and round robin (RR) are used. But these algorithms are static priority algorithms, they schedule process that are already in queue and not work on process arriving dynamically. Hence, they are not suitable for real-time systems. In dynamic priority algorithms, the priority assigned to task can change during its execution. In soft real-time systems, it is not necessary that every time constraint be met. Some deadline miss is tolerated. But in hard real-time systems, every resource management system must work in the correct order to meet time constraints. No deadline miss is allowed. The most important dynamic priority algorithm is earliest deadline first (EDF) scheduling. It is a dynamic scheduling algorithm that assigns deadline to every process based on its burst time and arrival time. Priority of job (process) is inversely proportional to its deadline. In other words, the highest priority job is the one with the minimum deadline and executed first. Each request stream are queued and serviced in the order of their increasing deadlines [1]. If two tasks have the same absolute deadlines, chose one of the two at random (ties can be broken arbitrarily). Here, the terms job and task are used synonymously to refer a request that needs to be serviced and the term class and stream to refer a request stream. The loss ratio under the EDF scheduling policy is found to be smaller than that of FCFS [2]. EDF scheduling algorithm balance between priority classes and minimizes mean waiting time of higher priority tasks. Hence, EDF is found to be optimal in performing tasks without missing deadlines compared to that of rate monotonic (RM) policy [3]. Existing work is scheduling job in RTOS based on preemptive EDF scheduling algorithm. It achieves best (minimum) waiting time for higher priority tasks. But, in a fully preemptive system, the running task can be interrupted by another task with higher priority at any time and be resumed to continue when all higher priority tasks have completed. Thus, the preemption method increases runtime overhead. Since preemptive method requires specific concurrency control protocols for accessing shared resources [4], it introduces additional overhead and complexity. And in preemptive technique, delay and jitter are maximized. In using non-preemptive method, these drawbacks can be minimized. Hence, it is viable alternative between the two extreme cases of fully preemptive and non-preemptive scheduling. Hence, we proposed limited preemption method.

2 Related Work

Many previously used deadline-based scheduling to differentiate service processing is discussed in Sect. 1. The most relevant work is discussed within this section.

In existing work, the occurrence of runtime overload is the main problem. To overcome this problem of overload in real-time distributed system, combining both static and dynamic algorithm together is used. In regular load, system will use EDF scheduling and when load in the system reached certain level, system uses RM to make system back to safe state [5]. But resource utilization is not possible here in this technique. Precedence-based round robin with dynamic time quantum (PRRDTQ) gives preference to all processes according to their priority and burst time. And then, it applies the RR algorithm on it. But it is a fixed priority scheduling, which is not suitable for dynamic scheduling. In [6], EDF is found to be better in improving schedulability on multiprocessor platforms. And under fixed priority scheduling, for task with higher priority fixed preemption point (FPP), concept is optimal than fully preemptive method [7]. When all resources are available for running tasks, then EDF is found to be optimal than RM [8]. Least laxity first (LLF) is also method of scheduling, which uses deadline of the process. Also it uses time of execution, and remaining time of process yet to be executed. The only drawback of this scheduling is, it is not possible during overloaded condition. The combination of LLF with DM scheduling is used to overcome this problem but with high complexity [9]. In [10], FCFS scheduler and EDF scheduler are compared on the basis of QOS requirements such as miss ratio and delay. And EDF is proved to be better than FCFS. The method assigning preemption threshold for each process based on previous priorities is worked out to improve schedulability [11]. In [12, 13] performance is carried out with exponentially distributed service times. But here we consider only number of switches and runtime overhead.

3 Proposed Model

This section presents the performance of limited preemption concept with EDF scheduling. According to this approach, a task implicitly executes in non-preemptive mode and preemption is allowed only at predefined locations inside the task code called preemption points. In this way, a task is divided into number of sub jobs and considers its boundaries as FPP. Between two preemption points, it is considered as non-preemptive regions. If a task with higher priority arrives between two preemption points of the running task, preemption is deferred until the next preemption point. Since higher priority tasks are favored at preemption points and resumed back to running task, both the higher priority task and running lower priority task are favored. It reduces runtime overhead. And since preemption points are fixed in task code itself, number of preemptions is less, and the location of the preemption is also known. It is found that when number of tasks increases, the

average number of preemptions decreases. This is because larger set of tasks allowed by CPU will have only smaller computational times, which have less chance to be preempted. As preemptive EDF scheduling reduces mean waiting time of higher priority requests and non-preemptive EDF scheduling reduces mean waiting time of lower priority requests, we propose limited preemption EDF scheduling. It uses merits of both preemptive and non-preemptive method. Thus, the proposed model found to be optimal in reducing runtime overhead and minimizing number of preemptions.

4 Experimental Evaluation

The main metric measured here is mean waiting time, deadline, and average number of preemptions. Compared to other scheduling algorithms, EDF scheduling provides less waiting time. And in using FPP, average number of preemptions is reduced with increase in number of tasks. Here, we use Intel Pentium-IV 2.4 GHz to process the request from ready queue using limited preemptive EDF scheduling. This uses 1 GB DDR-2 RAM to load and store requirements needed for the process execution.

Limited preemption EDF prioritizes jobs during runtime using deadlines assigned by system. When a job J_0 with deadline D_0 is first selected for execution at t_0 time, it executes normally. Suppose a job J_1 with deadline $<D_0$ arrives dynamically and job J_0 has e_0 units of execution remaining, job J_0 does not allow preemption immediately. Till job J_0 attains preemption point P1, higher priority task J_1 is not allowed to execute. At preemption point position, job J_1 is allowed to preempt.

Here, deadline assignment is based on burst time and arrival time of jobs. If burst time is measured as b_0 and arrival time as A_0, then deadline D_0 is calculated as follows,

$$D_0 = (2 * b_0) + A_0. \tag{1}$$

And preemption points are allotted based on burst time b_0. If job J_0 arrives with burst time of 6 ms, then 3 sub jobs are created by assigning 2 ms per job. The boundary region of sub jobs is called as preemption points. Hence, there will be 2 preemption points in job J_0. Though job J_2 has minimum deadline compared to that of J_1, it is not allowed to preempt. At first preemption point P_1 in job J_1, J_2 is allowed to execute. At the preemption point P_1 in job J_2, again the job J_1 is allowed to execute. Here, the running task is also considered and the dynamically arrived higher priority tasks are also favored. Figure 1 shows that increase in number of tasks, decreases number of preemptions.

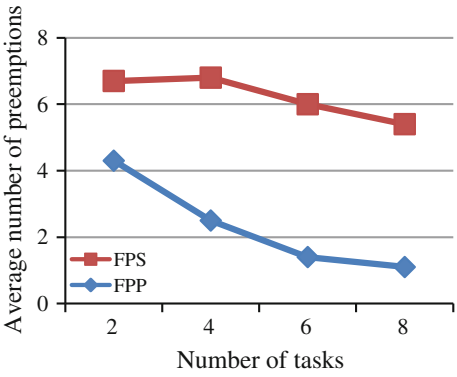

Fig. 1 Average number of preemptions versus number of tasks

Algorithm 1: Assigning Deadline for process

```
Input: Pi – process, BT – burst time,
       AT – arrival time, Dᵢ – deadline.
Output: Assignment of deadline to process.
   1. Process ()
   2.  for each Pi in ready queue do
   3.   BT (Pi) ← burst time (Pi);
   4.   AT (Pi)←arrival time (Pi);
   5.  for each entry of Pi do
   6. Use admission control algorithm;
   7.  If CPU satisfy non-functional requirements then
   8.      Dᵢ ← ((BTᵢ *2) + ATᵢ));
   9.  return Deadline
```

Limited preemption EDF scheduling reduces runtime overhead by making one execution at a time and not allowing all higher priority requests to preempt anywhere.

Algorithm 2: Assigning Preemption points for process

```
Input: Pi – process, BT – burst time,
      nPP – number of FPP, FPP – fixed preemption point.
Output: Assignment of Preemption points to process.
   1. Process ()
   2.  for each Pi in ready queue do
   3.    BT (Pi) ←burst time (Pi);
   4.  for each entry of Pi do
   5.  If BT (Pi) > 10 then
   6.    nPP = BT (Pi) % 20;
   7.  Else nPP = BT (Pi) % 2;
   8. Process is divided by nPP and boundaries as FPP
   9.  return process with preemption points as sub jobs
```

Since preemption points are assigned to every job, maximum number of times a particular task can preempt is not possible. Hence, limited preemption using preemption points is found to be optimal with EDF scheduling. As mentioned earlier in EDF scheduling, system assigns deadline for each process dynamically based on its computational time. And based on these deadlines, priority is assigned to requests.

Process with fewer deadlines is considered to be higher priority request and allow for execution. And requests in ready queue are allowed to execute in the order of increasing deadlines. Algorithm 1 shows assignment of deadlines for process. Limited preemption method is combining both non-preemptive and preemptive. It divides request into multiple jobs based on computational time of request. Normally, requests schedule as non-preemptive and when request with higher priority arrives dynamically, scheduler uses preemption method that too only at preemption point. Algorithm 2 shows assignment of preemption points for process in ready queue.

For example, from Table 1, at time 0 ms, P1, P2, and P3 come with burst time of 6, 4, and 2 ms, respectively. Here, deadline for each process is calculated as 12, 8, and 4 ms for the process P1, P2, and P3, respectively using Algorithm 1. According to preemptive EDF scheduling, the process with fewer deadlines is allowed to execute first. Hence, process P3 is executed first and in the increasing order of deadlines, requests are executed. But at time 3 ms process, P4 arrives dynamically with burst time of 1 ms, and so, its deadline is 5 ms. So process P4 is considered as higher priority compared to that of process P2. And when process P5 arrives with higher priority at time 5 ms, then process P2 still suspended until the completion of P5. Since in preemptive EDF, higher priority request preempts lower priority request at any time, the waiting time of running process which is considered to be lower priority is more. It is shown in Fig. 2 that when 4 processes participate, the waiting time of process P2 is 3 ms, and after the arrival of P5, the waiting time of P2 becomes 4 ms. But in limited preemption EDF scheduling, the process is divided into sub jobs using Algorithm 2. By division process, P1 has 2 preemption points at 2 and 4 ms, and similarly, P2 has 1 preemption point at 2 ms. Though P4 arrives dynamically only at preemption point of P2, it is allowed to preempt and till that it acts as non-preemptive EDF scheduling. And hence in limited preemption concept, only at time 7 ms, P5 is allowed to preempt. In using limited preemption method, the waiting time of P2 after the arrival of P4 is 3 ms. And the waiting time of P2

Table 1 Process in ready queue

Arrival time	Process	Burst time	Deadline
0	P1	6	12
0	P2	4	8
0	P3	2	4
3	P4	1	5

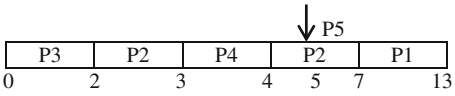

Fig. 2 Gantt chart of preemptive EDF scheduling for Table 1

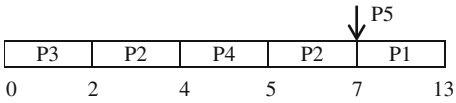

Fig. 3 Gantt chart of limited preemptive EDF scheduling for Table 1

after the arrival of P5 is also 3 ms. Hence, it favors both higher priority request that arrives and lower priority requests that is running. It is shown in Fig. 3 that when normally proposed concept schedules as EDF scheduling and when higher priority request arrives dynamically, it acts as RR scheduling. In RR, it uses fixed time quantum but here in limited preemption, it uses preemption points as time quantum.

Though SJF scheduling provides minimum average waiting time, RR is considered to be optimal in providing response to every request. And thus, this method favors running task more than the higher priority request that arrives dynamically and provides fulfillment for every requests in ready queue. Let us consider an example task set, {T1, T2, T3, T4} = {(0, 4), (1, 1), (2, 1), (3, 1)}, where the first value represents arrival time and the second its deadline to prove that the limited preemption reduces switching overhead.

Figure 4 represents the non-preemptive method in EDF scheduling. Here, task T1 allows task with higher priority only after its execution. Only after 4 ms, T2 is allowed to execute. This concept does not have any switching overhead, but it increases waiting time of all other tasks.

Figure 5 represents EDF scheduling with fully preemptive method. This method of scheduling prefers higher priority tasks and so reduces waiting time of those tasks. And since this concept preempts the running task whenever higher priority tasks arrive, it leads to switching time and runtime overhead. Hence, the proposed method of EDF scheduling with limited preemption is used to reduce this switching time overhead. Figure 6 represents EDF scheduling with limited preemption. Here, running tasks are not preempted whenever higher priority tasks arrive. In Fig. 6, task T1 allows task T2 only at the preemption point of T1, which is calculated using Algorithm 2. And hence, limited preemption method found to be better than existing preemptive method. Figure 7 shows how limited preemption method is better than fully preemptive in reducing switching overhead. In non-preemptive method, occurrence of switching is not possible but in fully preemptive method, number of

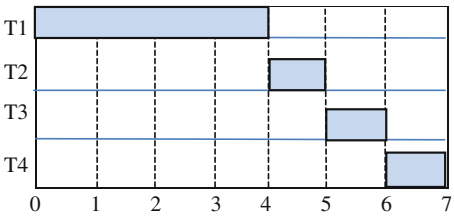

Fig. 4 EDF scheduling with non-preemptive case

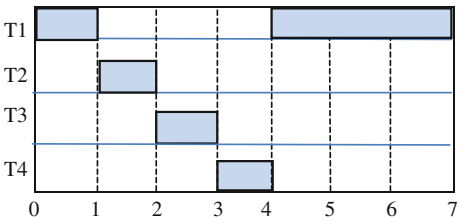

Fig. 5 EDF scheduling with fully preemptive case

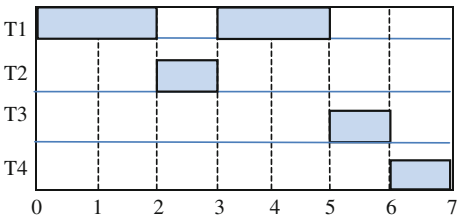

Fig. 6 EDF scheduling with limited preemptive case

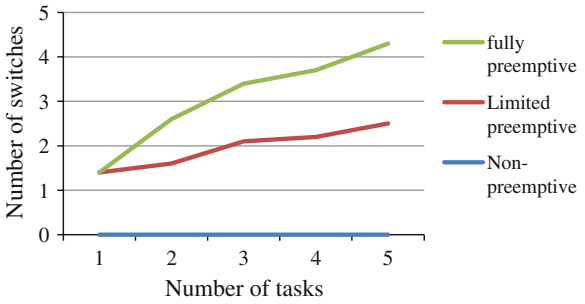

Fig. 7 Number of tasks versus number of switches

switches increases with increase in number of tasks. Limited preemption method allows only minimum number of preemptions for each task. Hence, the number of switches is not as high as fully preemptive with increase in number of tasks.

5 Conclusion

Under fixed priority scheduling, number of scheduling algorithms are used and it dominates in terms of preemption cost both in case of fully preemptive and non-preemptive methods. Using FPP method in limited preemption, number of

preemption and their positions are fixed and it produces less preemptions which is one of the significant advantages of this method as well as increase in resource utilization also. This suggested work presented the performance of limited preemptive method in EDF scheduling algorithm, as method reducing runtime and switching overhead, which provides efficiency of real-time systems. Since limited preemption method used EDF scheduling algorithm, higher priority requests are favored and they experience lower mean waiting times, without leading lower priority requests to overstarvation. Still achieving portability of legacy code is challenge for future works.

Acknowledgments We like thank all those who gave us their support to complete this paper.

References

1. V. Gamini, T Zahir, P. Zeephongsekul, A.Y. Zomaya, Performance analysis of EDF scheduling in a multi priority preemptive M/G/1 Queue. IEEE Trans. (2013)
2. S. Das, L. Jenkins, D. Sengupta, *Comparison of Loss Ratios of Different Scheduling Algorithms.* Cornell University (2011)
3. G.C. Buttazzo, *Rate Monotonic vs. EDF: Judgment Day*. Springer Science, The Netherlands (2005)
4. G.C. Buttazzo, M. Bertogna, G. Yao, Limited preemptive scheduling for real time systems. IEEE Trans. Ind. Inf. **9**(1) (2013)
5. A.F.M.S. Akhter, M.R. Khan, M.D.S. Islam, Overload avoidance algorithm for real-time distributed system. Int. J. Comput. Sci. Netw. Secur. **12**(9) (2012)
6. M. Bertogna, M. Cirinei, G. Lipari, Improved schedulability analysis of EDF on multiprocessor platforms. ECRTS (2005)
7. G. Yao, G. Buttazzo, M. Bertogna, Feasibility analysis under fixed priority scheduling with fixed preemption points, in *International Workshop on Real-Time Computing Systems and Applications* (2010)
8. T.P. Baker, Stack-based scheduling for real-time processes. Real-Time Syst. **3**(1), 67–99 (1991)
9. V. Prajapati, A. Shah, P. Balani, Design of new scheduling algorithm LLF_DM and its comparison with existing EDF, LLF, and DM algorithms for periodic tasks, in *ISSP Conference* (2013)
10. M. Saleh, L. Dong, Comparing FCFS & EDF scheduling algorithms for real-time packet switching networks, in *ICNSC Conference* (2010)
11. Y. Wang, M. Saksena, Scheduling fixed-priority tasks with preemption threshold, in *IEEE Conference* (1999)
12. M. Kargahi, A. Movaghar, A method for performance analysis of earliest-deadline-first scheduling policy. J. Supercomputing **37**(2), 197–222 (2006)
13. J. Lehoczky, Real-time queueing theory, in *Real-Time Systems Symposium*. IEEE (1996)

How Does Consciousness Overcome Combinatorial Complexity?

Reji Kumar

Abstract Mind is a complex information-processing mechanism which causes consciousness—the processed information content of mind. Models are the basic units of information processed in the mind. Comparison is one of the operations that causes consciousness. When we compare two models, the problem of combinatorial complexity (C.C.) arises. In this paper, we describe the way our mind overcomes the difficulty of C.C. and its consequences.

Keywords Mind · Consciousness · Comparison · Combinatorial complexity · Models · Mathematical models

1 Introduction

Perlovsky, in his comprehensive review article [1], describes the current status of the research, which aims to understand and explain the intriguing phenomenon of human consciousness. He has given a brief historical account of the research activities in this field, giving emphasis to contributions of many great philosophers. It contains the strengths of the current research as well as its weakness. In his own language, *Simple object perception involves signal from sensory organs and internal minds representations (memories) of objects. During perception, the mind associates subsets of signals corresponding to objects with representations of object. This produces object recognition; it activates brain signals leading to mental behavioral responses, parts of understanding. Developing mathematical description of the very first recognition step in the simple association—recognition—understanding process has not been easy, a number of difficulties have been encountered during the past fifty years.* A major limitation that the current research has encountered is combinatorial complexity (C.C.) of comparison, verification, etc. This problem was

R. Kumar (✉)
Department of Mathematics, N. S. S. College, Nilamel 689501, Kerala, India
e-mail: rkkmaths@yahoo.co.in

© Springer India 2015

L.P. Suresh et al. (eds.), *Artificial Intelligence and Evolutionary Algorithms in Engineering Systems*, Advances in Intelligent Systems and Computing 325,
DOI 10.1007/978-81-322-2135-7_19

first identified in 1960s in pattern recognition and classification research and was named *the curse of dimensionality.* When mind identifies an object or a phenomenon, it compares the incoming signals with the representation of the object or phenomenon. If there are n component parts to compare, the number of comparisons is n^n, a very big number when n is large. C.C. refers to multiple combinations of various elements in a complex system. For example, recognition of a scene often requires concurrent recognition of its multiple elements. If there are 100 elements, the total number of combinations of the elements is 100^{100}. This number exceeds all elementary particle events in the life of the universe.

There are many similar situations resulting into C.C. Rule-based systems proposed in 1970s to solve the problem of learning complexity faced the problem of C. C. of rules. In the early years of 1980s, model-based systems were proposed, which depended on adaptive parameters. Knowledge was represented by models, and the unknown aspects of a particular situation were to be learned by fitting parameters of models. But this method too faced C.C. Combinatorial complexity refers to all these difficulties associated with the multiple combinations of the component elements (see [2]).

Information coming from the outer world (the physical world) and that generated in the inner world (our mind) are equally being processed in the mind. There are many unanswered questions regarding creation and processing of knowledge in our mind. How knowledge is formed in our mind? What is the meaning of knowledge? What is the meaning of truth? How could we verify whether a piece of knowledge is true or false? To what extent is such verification reliable? Is knowledge different from information? In case if the answer is affirmative, how could we explain the difference in an objective way? Is it possible to describe the processing of knowledge in the mind and the formation of knowledge at higher levels using knowledge at relatively lower levels? All these questions can be answered successfully to a great extent, if we adopt a new approach to the problem of consciousness, which is discussed in [3–6]. The central idea in this approach is a set of axioms and a related mathematical model. Axioms are those verifiable statements in a theory, which are accepted as true without any proof. Its function is to provide a simple and clear beginning to a theory. The following are the model axioms.

1. Model is the basic unit of the information being processed in the mind.
2. Mind compares, classifies, characterizes, and differentiates various models and establishes relations among them. Such relations are new models.
3. Existing models can be expressed in terms of new models.
4. Mind associates some value or preference with each model.

Any representation of information, knowledge, or a part of the reality in our mind is a model. Models used in this study are not a physical object. Models are generated by the complex processes in our brain. It is amenable to continuous modification. In this paper, we address the specific issue of C.C. of comparison and verification, which we face continuously throughout our life.

2 The Problem of Truth Faces Combinatorial Complexity

Models in our discussion include all linguistic entities such us alphabets, words, sentences, and groups of sentences which generate knowledge. But the scope of models is much wider because it includes all sorts of information, both structured or unstructured, which are received by our mind. Models are classified into three groups. The first group contains α-models, which are direct representation of information received from the outer world. They are the main source of subjectivity due to the variations in the representation caused by personal differences. Also, α-models are created unconsciously in our mind and have no external manifestations, other than some responses. These models create firsthand experience in the mind. It can independently exist without any conscious interference of man. So these models can be called *pre-linguistic models* or *natural models*.

The other two types of models (β-models and γ-models) originate from the needs of man as a member of our society. It is hypothesized that the β-models and the γ-models are developed in our consciousness due to the continuous interactions with other consciousness. A representation of sound, gesture, a mental state, or an external reality is a β-model. Further, β-models represent a reality through a one-to-one connection. The third type of model is related to languages. Our ability in a language can be improved by increasing quantity and quality of the models. In essence, any idea that we develop using languages is composed of external representations of γ-models.

The problem of truth is very live in philosophy, which discusses the questions such as "What is the meaning of truth?" "What is the nature of truth?" "Which linguistic entities (sentences) are true?" There are many theories, which try to find answer to the above questions. Scope of those theories is limited in the sense that they define truth within the limits of languages. Every linguistic entity in a language has some meaning. When we test whether a sentence is true, we simply check whether this meaning is in conformity with the external reality. If the sentence is about an internal state of mind, it is possible to verify, but only within the limitations of subjectivity. A sentence is true if and only if its meaning perfectly matches with the reality, which is represented by it. Models generalize languages, knowledge, and information. As such, the notion of truth is extendable to handle models effectively. Thus, the problem of truth can be extended to the generalized theory of modeling. A γ-model is *true* if and only if each of its sub-models represents the reality well. On the other hand, whether an α-model or a β-model is true is decided in an abstract way. These models have got a meaning associated with it through its repeated use. If there is a deviation from the acquired meaning, then the consciousness concludes that the model is false. Otherwise, it is true. Verification that whether a model is true or false becomes more and more difficult as we go from lower to higher level in the hierarchy. It requires a one-to-one correspondence from each sub-model of a γ-model to various aspects of the reality, which in turn results into C.C. If this task is done by a machine, then it cannot complete the verification within a reasonable time. But interestingly enough, human consciousness easily overcomes this difficulty. The details are discussed in the following section.

3 How Does Consciousness Overcome C.C.?

Consciousness normally accepts an advanced model without any comparison or verification, presuming that it perfectly matches with the reality. This state of mind is *belief*. There is a broad class of models which are accepted without making any modifications, throughout our life. Such models belong to α and β category, which play a crucial role in the development of languages.

In this study, we concentrate only on the truth values of γ-models. Let $\boldsymbol{M} = [M_1, M_2, M_3, \ldots]$ denote a collection of models which make the model $\boldsymbol{M}$. We use different symbols to denote a model $\boldsymbol{M}$ and the collection of all sub-models, which define the model $\boldsymbol{M}$ (i.e., $\boldsymbol{M}$). If $\boldsymbol{M}_1$ is a sub-model of $\boldsymbol{M}$, then we write $M_1 \in \boldsymbol{M}$. The dots in the notation indicate that the number of sub-models is not limited. This is justified by the fact that the relation between any two models, say, $M_1 \boldsymbol{R} M_2$ is also a sub-model of $\boldsymbol{M}$. According to modeling theory, we say that a model $\boldsymbol{M}$ *represents a reality* (or its truth value is *TRUE*) if and only if each sub-model in $\boldsymbol{M}$ represents the corresponding part of the reality. Two models $\boldsymbol{M}_1$ and $\boldsymbol{M}_2$ are equal if and only if for all $M \in \boldsymbol{M}_1$, $M \in \boldsymbol{M}_2$, and vice versa.

We denote the consciousness of an individual by $\boldsymbol{C}$. Consider two individual consciousness $\boldsymbol{C}_1$ and $\boldsymbol{C}_2$. There is no guaranty that the models in $\boldsymbol{C}_1$ and $\boldsymbol{C}_2$, which represent the same reality, are same. It is due to the reason that selection of sub-models and formation of relations among them considerably vary in two consciousness. This variation causes individual differences, to a great extent.

If we want to verify whether a model $\boldsymbol{M}$ is true or valid, we must consider all sub-models of the model. It is impossible according to theory. But in practice, we easily overcome this difficulty. Consciousness initially assumes that a model $\boldsymbol{M}$ completely represents its reality. This initial state is belief. But if the mind is inquisitive, it comes down to the sub-models and performs validity checkup in each case. If a difference is noticed, then the model is declared invalid. The number of differences is a measure of validity of the model. Models remain true or valid until a disagreement is noticed. Mind, in normal circumstances, withdraws from the validity checkup, after performing a number of comparisons. The number of comparison varies depending on consciousness. Thus, it is possible that a model is true for $\boldsymbol{C}_1$, but only partially true or completely false for $\boldsymbol{C}_2$. Yet another reason for individual difference is the difference in the degree of verification done by consciousness, while checking for validity and truth values of models.

Let $M_1 \in \boldsymbol{C}_1$ and $M_2 \in \boldsymbol{C}_2$ represent the same reality. We can verify whether these models are equal. We require a one-to-one correspondence between the sub-models in $\boldsymbol{M}_1$ and $\boldsymbol{M}_2$, which verifies the equality of the sub-models. If the correspondence is onto, then we say that the models are equal. This definition works only if there is a collection of models which act as fundamental units. α and β models become important in this context. When we compare two complex γ-models for equality checkup, the number of verification increases exponentially. Hence, verification for equality of models too faces the problem of C.C.

If $\boldsymbol{M} \in \boldsymbol{C}$ and $\boldsymbol{C}$ is a perfect believer of the model $\boldsymbol{M}$, then we denote $\boldsymbol{M} = [M_1, M_2, \ldots M_n]$. This notation differs from the earlier notation of the model $\boldsymbol{M}$ by the number of sub-models. The latter contains only a finite number of sub-models.

A developing mind acquires a large number of complex γ-models. There are new models, modified models, and completely revised models among them. The observation that no model could completely represent the reality is worth to mention. Consequently, we could revise the model continuously so that in every step a new model is developed, which represents the reality more accurately than the previous one.

We conclude this short discussion explaining the possible way our consciousness tests whether a γ-model is true or false and its consequence. A model is true, if the internal signals generated by all the sub-models of a model match with the signals received from the reality, through the sense organs. Consciousness initially assumes that the model completely represents the reality. It compares the sub-models with the reality by counting its matches. When it finds a disagreement, it concludes that the model is false. The number of comparisons that consciousness makes depends on the nature of the consciousness. In general, consciousness stops comparison within few steps, while there are some consciousness which continue the procedure indefinitely. The first case results into belief, and the latter case makes the consciousness progressive and the thinking scientific. As the number of sub-models of a representation would be infinite or even if it is finite, the number of comparisons would be beyond the capacity of any machine, and the procedure for verification of truth faces the problem of C.C. But consciousness easily overcomes this difficulty by limiting the number of comparison. This is the reason for variations in consciousness.

We can give reasons for objectivity of mind and a partial cause of subjectivity of human experience, in terms of models and the discussions above. If a model is indefinitely subjected to verification and the mind is ready to reject it any time, when it finds that there is some disagreement, then the mind is objective about the model. On the other hand, if it stops the comparison and accepts the model forever, the chance of bias toward the model increases. This is a subjective position.

4 Conclusion and Future Research

In this paper, we have seen an explanation of subjectivity and objectivity of our experiences and the possible way our consciousness overcomes difficulties caused by C.C. This study also partially gives the reason for difference in the consciousness of two different individuals and opens new ways for possible research in many directions. We could develop a method to differentiate various consciousness using the procedure given above, and thus, we can classify different personalities. It also

suggests a quantitative approach, which will enable us to measure the strength of personalities. Furthermore, it is possible to study the social aspects of human consciousness. We conclude with the following remark. Taylor, in his survey paper entitled "Mind and consciousness: towards a final answer" [7], envisages a final theory of consciousness. But it is interesting to note that if a theory is accepted as final, it would cause subjectivity and in turn would undermine the basic requirement of science, i.e., objectivity.

Acknowledgments A part of the work presented here was financially supported by DRDO, India. I express my sincere thanks to DRDO for supporting my research through the Project No: ERIP/ER/0704385/M/01/1023.

References

1. L.I. Perlovsky, Towards physics of the mind, concepts, emotions, consciousness and symbols. Phys. Life Rev. **5**, 23–55 (2006)
2. L.I. Perlovsky, Conundrum of combinatorial complexity. IEEE Trans. PAMI **20**(6), 666–670 (1998)
3. K. Rejikumar, Modeling of consciousness: mathematics, science and other forms of knowledge, manuscript (2009)
4. K. Rejikumar, Mathematical modeling of consciousness (2010)
5. K. Rejikumar, Modeling of consciousness: classification of models. Adv. Stud. Biol. **2**(3), 141–146 (2010)
6. K. Rejikumar, Modeling of consciousness: a model based approach. Far East J. Appl. Math. **57** (1), 1–14 (2011)
7. J.G. Taylor, Mind and consciousness: towards a final answer. Phys. Life Rev. **2**(3), 1–45 (2005)

Website Re-organization for Effective Latency Reduction Through Splay Trees and Concept-Based Clustering

M.B. Thulase and G.T. Raju

Abstract Interest in the analysis of user behavior on the Web has been increasing rapidly. This increase stems from the realization that added value for visitor of the Website is not gained merely through larger quantities of data on a site, but through easier access to the required information at the right time and in the most suitable form. Hence, understanding users' navigation on the Web is important toward improving the quality of information and the speed of accessing large-scale Web data sources. As the interests of the user change over the time, a static Website will soon become outdated. Hence, the usage of the Website needs to be monitored and structure of the Website has to be modified to suit the user requirements periodically. In this paper, we propose a novel splay tree-based approach that reduces the latency in accessing the Web page by reorganizing the Website for group of user's interest rather than single user, such that the most recently and frequently accessed pages by the user group that belongs to some concept/category are placed nearer to the root. Experimental results show that splaying along with the concept-based clustering gives better performance for seasonal Websites that need a change periodically.

Keywords Network congestion · Low bandwidth · Propagation delay · User-perceived latency · Splay tree

M.B. Thulase (✉)
R & D Centre, Department of Computer Science and Engineering,
RNS Institute of Technology, Bangalore 560098, India
e-mail: mbthulase@yahoo.com

G.T. Raju
Department of Computer Science and Engineering, RNS Institute of Technology,
Bangalore 560098, India
e-mail: gtraju1990@yahoo.com

© Springer India 2015

L.P. Suresh et al. (eds.), *Artificial Intelligence and Evolutionary Algorithms in Engineering Systems*, Advances in Intelligent Systems and Computing 325,
DOI 10.1007/978-81-322-2135-7_20

1 Introduction

In recent years, Web has become the primary means for information dissemination. It is being used for commercial, entertainment, or educational purposes, and thus, its popularity resulted in heavy traffic in the Internet. Since the amount of network traffic has rapidly increased with the WWW expansion, users have experienced a long latency when retrieving the Web pages. Potential sources of latency are the Web servers' heavy load, network congestion, low bandwidth, bandwidth under-utilization, and propagation delay. Design of a Website centers around organizing the information on each page and the hypertext links between the pages in a way that seems most natural to the site users in order to facilitate their browsing. Monitoring and analyzing the behavior of visitors in the past may lead to valuable insights into their information needs and help in continually adapting the design of the site. Knowledge about navigation patterns occurring in or dominating the usage of a Website can greatly help the owner or administrator of the Website in improving its quality.

Accessing the variety of information stored on various servers of the World Wide Web (WWW) will experience the various latencies. The rapid growth of the WWW has inspired numerous techniques to reduce user-perceived latency (UPL) which is defined as UPL = TResponse − TRequest. Reducing the UPL is one of the major research issues. One of the techniques to reduce the Web latency is reorganizing the Website periodically to suit the user's interest. For the ease of the users, many Websites have grouped their Web pages into clusters based on concepts. Hence, the Website can be visualized as a collection of pages clustered under some concepts. Websites will have categories/concepts and also categories may have the subcategories. In this paper, we tried to make use of statistics collected at regular intervals: weekly, fortnightly, monthly, and quarterly about the recently and frequently visited Web pages from the Web usage data (WUD) and reorganize the Website using splay tree approach along with the concept-based clustering.

1.1 Splay Tree

A splay tree is a self-adjusting binary search tree (BST) with the additional property that recently accessed elements are quick to access again. It performs basic operations such as insertion, lookup, and removal in $O(\log n)$ amortized time. A randomly built BST is often a good choice for an application that requires fast lookup of items. However, if the item distribution is heavily skewed, the lookup time increases. Hence, a splay tree might be a better choice as it organizes the tree for faster lookup. In heavily skewed distributions, there is a small set of items that are accessed very frequently, forming a "working set." Sleator and Tarjan [1] have proved that splay tree access times to the items in a working set are fast. This is true

even if the working set changes over time. This feature of the splay tree is desirable in our approach because the exact access distribution is unknown a priori, and the set of frequently accessed items changes over time.

Splaying the tree for a certain element rearranges the tree so that the element is placed at the root of the tree. This can be done in two ways, viz. top-down approach and bottom-up approach. In bottom-up approach, first perform a standard binary tree search for the element in question and then use tree rotations on the access path to bring the element to the top. Alternatively, in top-down approach, the search and the tree reorganization are combined into a single phase. The three patterns of rotations used in reorganizing the splay tree are named as zig, zig-zag, and zig-zig [1].

2 Related Work

Web usage mining (WUM) that is defined as discovery of useful information from the WUD has been proposed by many researchers to analyze the usage of Web. Web server logs provide an insight into the trends and patterns in user access. Several studies have been conducted in WUM. Some focuses on mining of association rules and navigation patterns in the user access paths, and others build data cubes from server logs for OLAP and data mining. In this research, it is required to preprocess the server log and extract the features such as PgId, UId, and TimeSpent that are essential for reorganizing the Website.

Recently, researches into adaptive Websites have been proposed by some researchers. Perkiwitz and Etzioni [2–4] have presented the initial definition for adaptive Websites in 1997. Srikant and Yang [5] propose an algorithm to automatically discover pages in a Website whose location is different from where visitors expect to find them, in improving the Website organization. Christopoulou et al. [6] define techniques and mechanisms to reorganize Websites based on structural information and probability model to compute a suitable refining factor. Christopoulou et al. [7] suggest a combined XML and object-oriented hypermedia framework that will enhance and automate the instantiation of any site reorganization and page classification proposals. Makris et al. [8] present twofold algorithmic framework for the adaption of Web content to the users' choices. Sakkopoulos et al. [9] in their work have used the burst of visits in personalizing the Website using splay and heap data structures.

In this paper, an attempt is made to improve the performance of the Web retrieval process presented in [10] by performing the splaying operations on the concept-based clusters instead of the Web pages. The page access information of the users is coupled with the characteristics of splay tree in reorganizing the Website.

3 Problem Formulation

Consider a Website with n number of pages denoted as $p_1, p_2, \ldots, p_n$ and s number of clusters denoted as $c_1, c_2, \ldots, c_s$, where each page p_i belongs to one of the clusters.

Let $\boldsymbol{L}$: $\boldsymbol{l_1, l_2, l_3, \ldots, l_m}$ be the preprocessed log file of the Website, where each $\boldsymbol{l_i}$ consists of the fields ***PgId, UId, and TimeSpent***.

Let the time spent on each page be $\boldsymbol{\tau_{p1}, \tau_{p2}, \tau_{p3}, \ldots, \tau_{pn}}$.

Let $\boldsymbol{M\tau_p}$ be the ***minimum time threshold***.

Then, the *average frequency of access* of each cluster is $\mathrm{A}\boldsymbol{f_{c1}}$, $\mathrm{A}\boldsymbol{f_{c2}}$ …, $\mathrm{A}\boldsymbol{f_{cs}}$,…, $\mathrm{A}\boldsymbol{f_{ci}}$ which is computed by considering the number of times the page request belonging to the particular cluster appears in the log file that has time spent value $\boldsymbol{\tau_{pi} \geq M\tau_p}$. We define the *most frequently accessed cluster* as the cluster with $\mathrm{A}\boldsymbol{f_{ci} \geq Mf_c}$ (**minimum frequency threshold**).

The list of interesting clusters **c[]** contains the clusters with $\mathrm{A}\boldsymbol{f_{ci} \geq Mf_c}$ with $\boldsymbol{\tau_{pi.} \geq M\tau_p}$ in the given time interval $\boldsymbol{\tau}$ (***daily***, ***weekly***, ***fortnightly***, ***monthly***, ***quarterly***, ***yearly***…).

The problem is formulated as "*Given the PgId, and Timespent details from the preprocessed WUD, the objective is to:*

- *Cluster the pages based on the* ***frequency of access*** *(*$\boldsymbol{f_p}$*).*
- *Compute and tabulate the* ***Average frequency of access*** *(*$\mathrm{A}\boldsymbol{f_{ci}}$*) for each cluster,*
- *Reorganize the website with the knowledge obtained through Splay tree constructed based on the cluster frequency statistics.*"

4 Splaying with Concept-Based Clustering Approach (SCCA)

As the *splay tree approach* demands BST, the initial BST *T* for the Website is constructed with CId's as nodes, based on the designer's preferences for the clusters, as the initial structure of the Website. In this work, frequency of access is used as the concept for clustering.

After observing the usage of the Web pages for the required time interval (***daily***, ***weekly***, ***fortnightly***, ***monthly***, ***quarterly***, ***yearly***…), the clusters are formed based on the access frequency of the Web pages. We compute the average frequency of access for each cluster and apply the proposed SCCA algorithm for reorganizing the Website structure. The proposed SCCA algorithm is given below.

SCCA Algorithm.

1. [Compute the Average frequency of access for each cluster using the preprocessed log file $\mathbf{L}$ *and rebuild the clusters]*
For *(each log entry* $\mathbf{l_i}$ *)*
If $(\tau pi >= M\tau_p)$
Increment $\mathbf{fa_{ci}}$ *Where page* $\mathbf{p_i} \in \mathbf{c_i}$
$\mathbf{Af_{ci}} = \sum \mathbf{fa_{ci}} / |ci|$
2. Create the initial BST with cluster centers ($\mathcal{A}f_{ci}$*) as the nodes*
3. [consider the clusters that have atleast mininmum frequency threshold]
Create a list of clusters $\mathbf{C[]}$ *with* $\mathbf{Af_{ci}} >= \mathbf{Mf_c}$ *and arrange* $\mathbf{C[]}$ *in ascending order of the "time of access" of the clusters.*
4. [Consider the initial tree T and restructure the tree by splaying such that the most recently accessed cluster is at the root.]
For (each cluster C_i *in* $\mathbf{C[]}$ *)*
Splay on c_i *to create* $\mathbf{T_{splay}}$
5. Rearrange the website using $\mathbf{T_{splay}}$

Based on the average access frequency and recency of the pages in the clusters, the initial BST T is splayed to reorganize the Website structure. The improvement in the access time can be observed by plotting the access delay before reorganization of the Website and after reorganization of the Website.

The clusters that have frequently and recently accessed pages are considered to be very interesting. A cluster that is more frequently accessed but is not recently accessed is not an interesting cluster, but it may be nearer to the root in the initial tree. But, in case of splay tree approach, since splaying is based on interesting clusters, it can be seen that the Website is well reorganized with interesting clusters nearer to the root. The number of splay operations performed is minimum as it is based on the interesting clusters only.

Splay technique is suggestive to seasonal Websites. Seasonal Websites are those Websites that need to be reorganized periodically based on the season, for example, Websites for e-shopping and educational institutions. As the user tends to access the pages that are relevant to that particular season, it is suggestive to reorganize the Website using splay technique, at the beginning of the season, based on the recent Web access log, such that the interested clusters, thereby the recently accessed pages, are nearer to the root.

5 Experimental Results

For experimental purpose, a log for the time interval of a quarter is considered. K-means cluster algorithm with k values as 3, 8, and 10 has been used. Initial tree, T, is constructed based on the initial preferences of the clusters in the Website. The reorganized tree T_{splay} is constructed according to the algorithm proposed above. The comparative study of cluster access delay before reorganization and after

reorganization of the Website using splay tree approach with the varied value of *K* (3, 8, 10) is shown in Figs. 1, 2, and 3. The splay order of the cluster Id and the corresponding average frequencies for $k = 8$ are shown in Table 1. The splay order is created based on the recency of the cluster usage. Cluster that is recently accessed, i.e., cluster 7, is splayed at the end in order to make it the root. Even though the most frequently accessed cluster is 8, it is not recently accessed; hence, it is not nearer to the root compared to cluster 7.

It is observed from the experiments that the clusters with interesting Web pages, i.e., the clusters that are frequently and recently accessed, are nearer to the root. Reorganization requires less time as the splaying operation is performed on frequently and recently accessed clusters only.

On the similar lines, experiments are conducted using the log collected at different time intervals like *daily*, *fortnightly*, *and quarterly* and with varied number of

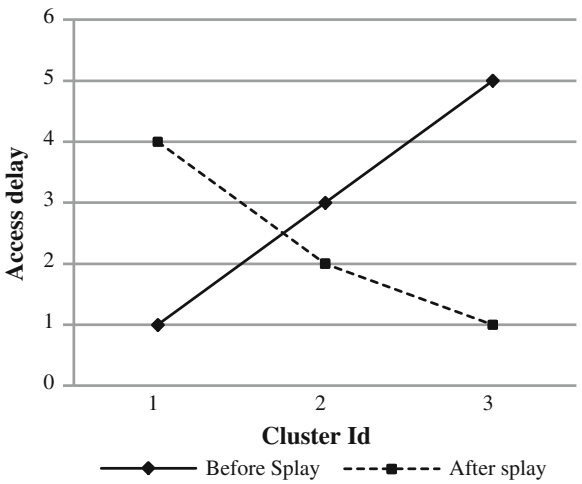

Fig. 1 Access delay with $k = 3$

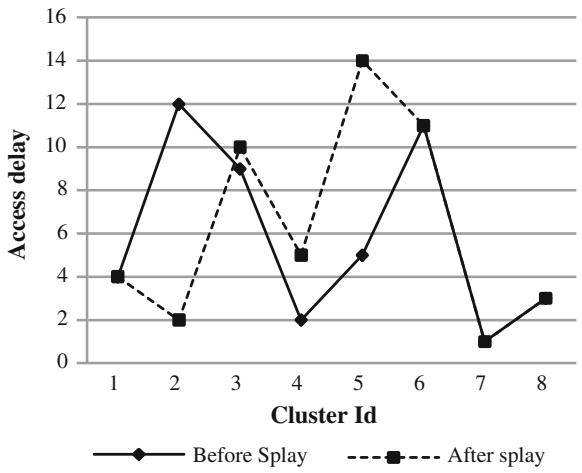

Fig. 2 Access delay with $k = 8$

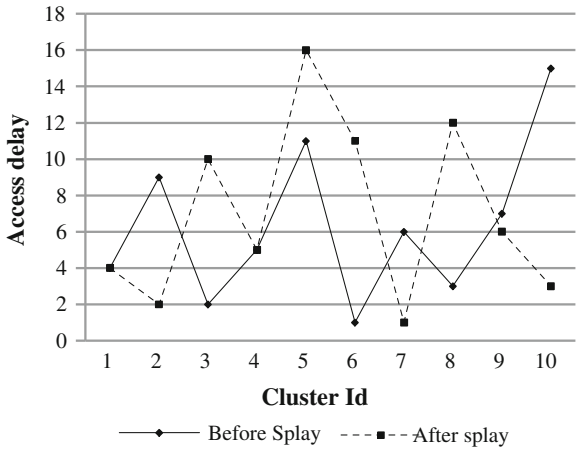

Fig. 3 Access delay with $k = 10$

Table 1 Splay order for $k = 8$

Cluster Id.	Average frequency
4	17
8	30
6	22
5	19
2	11
3	14
1	8
7	27

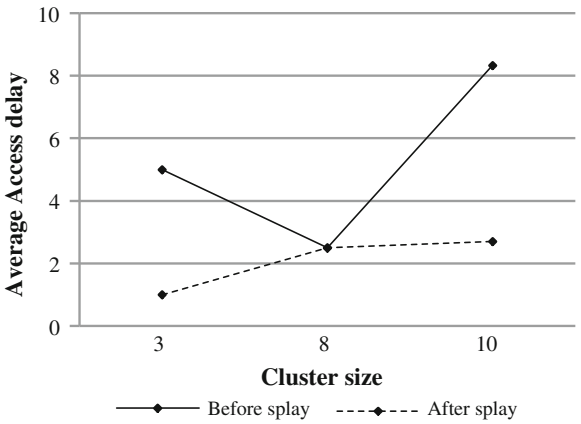

Fig. 4 Average access delay for 30 % recency

clusters. The experimental results show that the pages are not uniformly distributed among the clusters if the time interval is too short like a day, a week, a fortnight, or a month. Hence, better results are obtained only when the time interval is long enough,

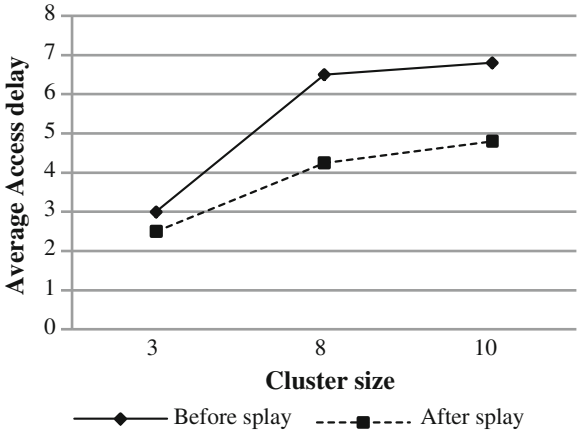

Fig. 5 Average access delay for 40 % recency

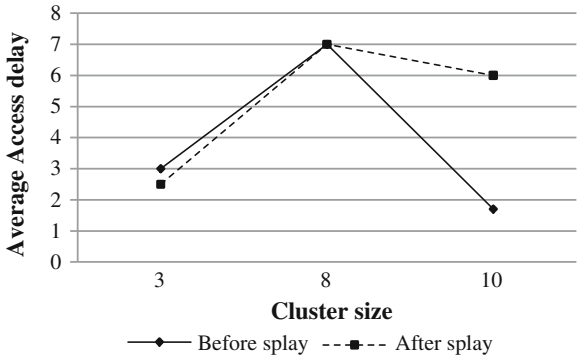

Fig. 6 Average access delay for 70 % recency

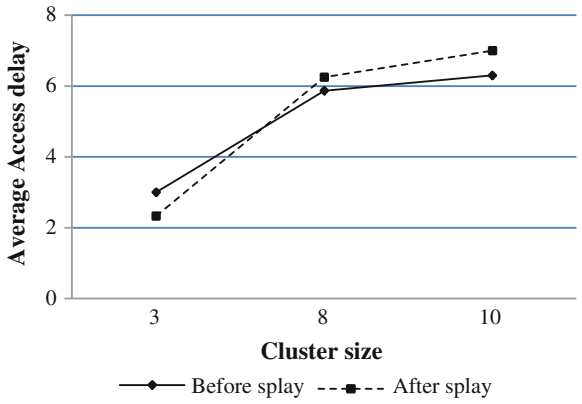

Fig. 7 Average access delay for 100 % recency

Cluster size	Percentage of latency reduction
3	16.7
8	34.6
10	29.4
Average	26.9

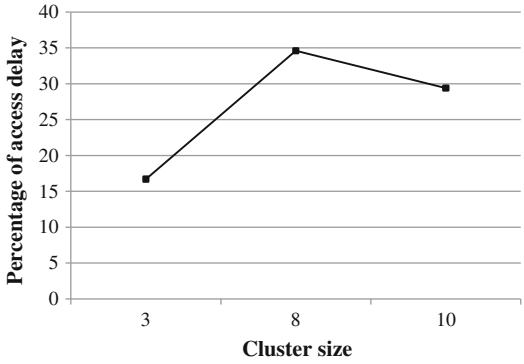

Fig. 8 Analysis of reduction in access delay

depending on the Website usage. Hence, the time period for reorganization depends on the usage of the Website. Very frequently, reorganizing the Website becomes an overhead for the Website designers and is confusing for the users.

Figures 4, 5, 6, and 7 show comparative analysis of the average access delay for frequently accessed clusters considering varied size of *recency*—only some percentage of recently accessed clusters are considered.

6 Conclusions

Recommendation and personalization algorithms suggest Web pages to users based on their current visit and past user's navigational patterns. In this paper, a novel approach for Website reorganization through splay tree with concept-based clustering and performance analysis for varied number of clusters has been presented.

It is observed from the experimental results that splay technique is applicable for seasonal Websites and performs well, when reorganized after a suitable period of time. As shown in Fig.8, this approach contributes up to an average of 26.9 % of effective reduction in UPL, and the user of the Website is facilitated with the pages that are accessed recently and frequently, at higher levels in the Website structure.

References

1. D.D. Sleator, R.E. Tarjan, Self-adjusting binary trees. J. ACM. **32**(3), 652–686 (1985)
2. M. Perkiwitz, O. Etzioni, Adaptive Websites: an AI challenge, in *International Joint Conference on Artificial Intelligence (IJCAI)* (1997), pp. 16–23
3. M. Perkiwitz, O. Etzioni, Adaptive Websites: automatically synthesizing web pages, in *Proceedings of the Fifteenth National Conference on Intelligence (AAAI)* (1998)

4. M. Perkiwitz, O. Etzioni, Towards adaptive Websites: conceptual framework and case study, in *Proceedings of the Eighth International World Wide Web Conference* (1999)
5. R. Srikant, Y. Yang, Mining web logs to improve website organization, in *WWW'01 Proceedings of the 10th international conference on World Wide Web*, (ACM New york, NY, USA 2001), pp. 430–437
6. E. Christopoulou, J. Gorofalakis, C. Makris, Y. Panagis, E. Sakkopoulos, A. Tsakalidis, Techniques and metrics for improving website structure. J. Web Eng. **2**(1–2), 090–104 (2003)
7. E. Christopoulou, J. Gorofalakis, C. Makris, Y. Panagis, E. Sakkopoulos, A. Tsakalidis, Automating restructuring of web applications (2002), pp. 11–15
8. C. Makris, Y. Panagas, E. Sakkopoulos, A. Tsakalidis, An algorithmic framework for adaptive web content, in *Proceedings of Adaptive and Personalized Semantic Web* (2006), pp. 1–10
9. E. Sakkopoulos, D. Antoniou, P. Adamopoulou, N. Tsirakis, A. Tsakalidis, A web personalizing technique using adaptive data structures : the case of bursts in web visit. J. Syst. Softw. **83**, 2200–2210 (2010)
10. M.B. Thulase, G.T. Raju, Website re-organization for effective latency reduction through splay and heap tree structures. Int. J. Comput. Eng. Technol. **3**(2), 487–498 (2012)

Algorithms for Zumkeller Labeling of Full Binary Trees and Square Grids

B.J. Balamurugan, K. Thirusangu and D.G. Thomas

Abstract Let $G = (V, E)$ be a graph. An injective function f: $V \rightarrow N$ is said to be a Zumkeller labeling of the graph G, if the induced function f^*: $E \rightarrow N$ defined as $f^*(xy) = f(x)\, f(y)$ is a Zumkeller number for all $xy \in E$, $x, y \in V$. A graph $G = (V, E)$ which admits a Zumkeller labeling is called a Zumkeller graph. In this paper, we provide algorithms for Zumkeller labeling of full binary trees and grid graphs.

Keywords Zumkeller labeling · Number theory · Code-making · Breaking

1 Introduction

The study of graph labeling has focused on finding classes of graphs which admits a particular type of labeling. Many practical problems in real-life situations have motivated the study of labelings of the graph $G = (V, E)$ subject to certain conditions. A systematic presentation of diversion applications of graph labelings is presented in [2]. The problems arising from the effort to study various labeling schemes of the elements of a graph is a potential area of challenge. Most of the labeling techniques found their origin with graceful labeling introduced by Rosa (1967) [8]. There is an enormous literature dealing with several kinds of labelings of graphs over the past three decades and for a survey of various graph labeling

B.J. Balamurugan (✉)
Department of Mathematics, Agni College of Technology Thalambur,
Chennai 600130, India
e-mail: balamuruganbj@yahoo.com

K. Thirusangu
Department of Mathematics, SIVET College Gowrivakkam,
Chennai 600073, India
e-mail: kthirusangu@gmail.com

D.G. Thomas
Department of Mathematics, Madras Christian College Tambaram,
Chennai 600059, India
e-mail: dgthomasmcc@yahoo.com

© Springer India 2015

L.P. Suresh et al. (eds.), *Artificial Intelligence and Evolutionary Algorithms in Engineering Systems*, Advances in Intelligent Systems and Computing 325,
DOI 10.1007/978-81-322-2135-7_21

problems, we refer to Gallian [4]. For all notations and terminology in graph theory, we follow Harary [5].

Graph labeling is a strong communication between number theory and structure of graphs. The study of Zumkeller numbers [7] forms part of the branch of mathematics called number theory. Some parts of number theory have found a use in code-making and breaking. Labeled graphs are becoming an increasingly useful family of mathematical models for a broad range of applications. Since Zumkeller numbers are recent developments of number theory and graph labeling have often been motivated by practical problems, we are interested in Zumkeller labeling of graphs. The concept of strongly multiplicative Zumkeller labeling of graphs has been introduced and investigated in the literature [1]. It is proved that some well-known graphs, namely path, cycle, wheel, star, bipartite graphs, are strongly multiplicative Zumkeller graphs.

In this paper, we provide algorithms to obtain Zumkeller labeling for full binary trees [6] and grid graphs $P_n \times P_n$. We refer a programming language slightly adapted to *C*, given by Frank Buss [3] to identify the Zumkeller numbers and Zumkeller partitions.

2 Zumkeller Numbers and Their Properties

In this section, we recall the notion of Zumkeller numbers and few properties of Zumkeller numbers [7]. A positive integer n is called a perfect number [9] if n equals the sum of its proper positive factors. Generalizing this concept in 2003, Zumkeller [7] published in Sloane's sequences of integers A083207 a sequence of integers n with the property that the positive factors of n can be partitioned into two disjoint parts so that the sums of the two parts are equal.

Definition 1 A positive integer n is said to be a Zumkeller number if all the positive factors of n can be partitioned into two disjoint parts so that the sum of the two parts is equal.

We shall call such partition as Zumkeller partition.

Example 1 6, 12, and 20 are Zumkeller numbers.
For 12, the factors of 12 are 1, 2, 3, 4, 6, and 12.
We can partition these factors into 2 disjoint sets, such as
$A = \{2, 12\}$ and $B = \{1, 3, 4, 6\}$.
The sum of the elements of A is $2 + 12 = 14$.
The sum of the elements of B is $1 + 3 + 4 + 6 = 14$.
Therefore, 12 is a Zumkeller number.

2.1 Properties of Zumkeller Numbers

1. Let the prime factorization of an even Zumkeller number n be $2^k p_1^{k_1} p_2^{k_2} \ldots p_m^{k_m}$. Then, at least one of k_i must be an odd number.

2. If n is a Zumkeller number and p is a prime with $(n, p) = 1$, then np^{ℓ} is a Zumkeller number for any positive integer ℓ.
3. Let n be a Zumkeller number and $p_1^{k_1}p_2^{k_2}\ldots p_m^{k_m}$ be the prime factorization of n. Then for any positive integers $\ell_1, \ell_2,\ldots, \ell_m$, $p_1^{k_1+\ell_1(k_1+1)}p_2^{k_2+\ell_2(k_2+1)}\ldots p_m^{k_m+\ell_m(k_m+1)}$ is a Zumkeller number.
4. For any prime $p \neq 2$ and a positive integer k with $p \leq 2^{k+1} - 1$, $2^k p$ is a Zumkeller number.

3 Main Results

In this section, we introduce a new labeling of graphs using Zumkeller numbers and we prove that full binary trees and grid graphs admit Zumkeller labeling. We also provide algorithms for Zumkeller labeling of full binary trees and grid graphs.

Definition 2 Let $G = (V, E)$ be a graph. An injective function f: $V \rightarrow N$ is said to be a Zumkeller labeling of the graph G, if the induced function f^*: $E \rightarrow N$ defined as $f^*(xy) = f(x)\, f(y)$ is a Zumkeller number for all $xy \in E$, $x, y \in V$.

Definition 3 A graph $G = (V, E)$ which admits a Zumkeller labeling is called a Zumkeller graph.

For example, a Zumkeller labeling of a graph is given in Fig. 1.

Proposition 1 *A non-totally disconnected subgraph of a Zumkeller graph is a Zumkeller graph.*

Proof Let $G = (V, E)$ be a Zumkeller graph. Let $G' = (V', E')$ be a subgraph of G obtained by removing some vertices or some edges or both such that G' is not a totally disconnected. Since the Zumkeller numbers on the edges of G' are obtained by multiplying the labels of the end vertices of the edges in G, obviously, the non-totally disconnected subgraph G' is a Zumkeller graph. □

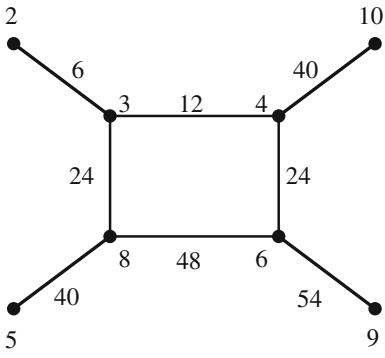

Fig. 1 A Zumkeller graph

Definition 4 A binary tree is a rooted tree in which each vertex has either no children or one child or two children.

Definition 5 A full binary tree is a binary tree in which each vertex has either two children or no children [6].

Example 2 A third-level full binary tree T is given in Fig. 2.

Remark 1 A full binary tree is a tree where each internal vertex has degree 3, each leaf has degree 1 and the root has degree 2.

Remark 2 Every full binary tree has odd number of vertices and even number of edges.

Now we present an algorithm for the Zumkeller labeling of a full binary tree.

Algorithm 1 (*Zumkeller Labeling of a Full Binary Tree*) This algorithm labels the edges of a full binary tree with Zumkeller numbers.

Input : A full binary tree T with m levels having $2^{m+1}-1$ vertices and $2^{m+1}-2$ edges.
Output : Zumkeller full binary tree.
Procedure : Zum_lab_full binary tree(T).
Let v_0 be the root of the full binary tree T.
$f(v_0) = 1$ // f is a function defined on the vertex set of T.
for i := 1 **to** 2 **do**
  begin
    $f(v_{1i}) = 3(2^i)$
    $f^*(v_0\, v_{1i}) = f(v_0)\, f(v_{1i})$ // f^* is an induced function defined on the edge set of T.
  end
for j := 1 **to** 2^2 **do**
  begin
    $f(v_{2j}) = 2^j$
    for i := 1 **to** 2 **do**
      begin
        for j := 2i−1 **to** 2i **do**
          $f^*(v_{1i}\, v_{2j}) = f(v_{1i})\, f(v_{2j})$
      end
  end
for r := 3 **to** m **do**
  begin
    for i := 1 **to** 2^r **do**
      begin
        if r is odd **then**
          $f(v_{ri}) = 3(2)^{i+2^{r-2}}$
        else
          $f(v_{ri}) = 2^{i+2^{r-2}}$
      end
  end
for r := 2 **to** m−1 **do**
  begin
    for i := 1 **to** 2^r **do**
      begin
        for j := 2i−1 **to** 2i **do**
          $f^*(v_{ri} v_{r+1j}) = f(v_{ri})\, f(v_{r+1j})$
      end
  end
return(T)
end Zum_lab_full binary tree

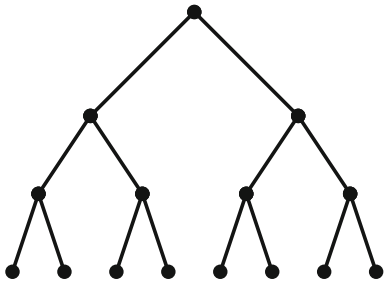

Fig. 2 A third-level full binary tree T

The time complexity of this algorithm is tightly bounded, and the time complexity is $\theta(m\ 2^m)$.

Theorem 1 *Every full binary tree admits a Zumkeller labeling.*

Proof Let T be a full binary tree with m levels. Let $V = \{v_0,\ v_{ri} \mid 1 \le r \le m,\ 1 \le i \le 2^r\}$ be the vertex set where v_0 is the root of the tree, which is a zero-level vertex and v_{ri} are the vertices on the rth level of the tree T, from left to right and $E = \{v_0\ v_{1i} \mid 1 \le i \le 2\} \cup \{v_{ri}\ v_{r+1j} \mid 1 \le r \le m-1,\ 1 \le i \le 2^r,\ 2i-1 \le j \le 2i\}$ be the edge set of the full binary tree T. □

Clearly, the rth level of the tree has 2^r vertices. Since T has m levels, the number of vertices of T is $2^{m+1} - 1$ and the number of edges is $2^{m+1} - 2$. We initiate the labeling from left to right at each level of the tree T.

Define an injective function f: $V \to N$ as follows

$f(v_0) = 1$
$f(v_{1i}) = 3(2)^i$, $1 \le i \le 2$ where v_{1i} are the first-level vertices of T.
$f(v_{2i}) = 2^i$, $1 \le i \le 2^2$ where v_{2i} are the second-level vertices of T.
$f(v_{3i}) = 3(2)^{i+2^1}$, $1 \le i \le 2^3$, where $v_{3\mathrm{i}}$ are the third-level vertices of T.
$f(v_{4i}) = 2^{i+2^2}$, $1 \le i \le 2^4$, where v_{4i} are the fourth-level vertices of T.
$f(v_{5i}) = 3(2)^{i+2^3}$, $1 \le i \le 2^5$, where v_{5i} are the fifth-level vertices of T.

In general,

$$f(v_{mi}) = \begin{cases} 2^{i+2^{m-2}} & \text{if } m \text{ is an even number} \\ 3(2)^{i+2^{m-2}} & \text{if } m \text{ is an odd number} \end{cases}$$

where $1 \le i \le 2^m$, $m \ge 3$ and an induced function f^*: $E \to N$ is defined as follows.

$f^{*}(v_0v_{1i}) = f(v_0)\, f(v_{1i})$, $1 \le i \le 2$
$f^{*}(v_{ri}v_{r+1j}) = f(v_{ri})\, f(v_{r+1j})$ where $1 \le r \le m-1$ and $1 \le i \le 2^r$, $2i-1 \le j \le 2i$.

Now, we claim that the numbers on the edges are Zumkeller numbers.

Case (i): $f^{*}(v_0v_{1i}) = f(v_0)\, i(v_{1i}) = (1)3(2)^i$, $1 \le i \le 2$ is a Zumkeller number
Case (ii): $f^{*}(v_{1i}v_{2j}) = f(v_{1i})\, f(v_{2j}) = 3(2)^i\,(2)^j = 3\,(2)^{i+j}$ is a Zumkeller number
Case (iii): $f^{*}(v_{2i}v_{3j}) = f(v_{2i})\, f(v_{3j}) = (2^i)\,(3)\,(2)^{j+2} = 3\,(2)^{i+j+2}$ is also a Zumkeller number
Case (iv): $r \equiv 1 \pmod 2$, $r \ge 3$, $f^{*}\left(v_{ri}v_{r+1j}\right) = f(v_{ri})f\left(v_{r+1j}\right) = 3(2)^{i+2^{r-2}}2^{j+2^{r+1-2}}$ $= 3(2)^{i+j+2^{r-2}+2^{r-1}}$ is a Zumkeller number
Case (v): $r \equiv 0 \pmod 2$, $r \ge 4$, $f^{*}\left(v_{ri}v_{r+1j}\right) = f(v_{ri})f\left(v_{r+1j}\right) = 2^{i+2^{r-2}}3(2)^{j+2^{r+1-2}} =$ $3(2)^{i+j+2^{r-2}+2^{r-1}}$ is a Zumkeller number.

In all cases, the labels on the edges of the full binary tree are Zumkeller numbers. Hence, the full binary tree T admits a Zumkeller labeling.

Corollary 1 Every binary tree admits a Zumkeller labeling.

Example 3 The Zumkeller full binary tree T with 3 levels is given in Fig. 3.

Now we give an algorithm to label the grid graph $P_n \times P_n$ with Zumkeller numbers.

Algorithm 2 (*Zumkeller Labeling of the Grid Graph* $P_n \times P_n$) This algorithm processes the integers to the vertices of the $n \times n$ square grid to label the edges of the square grid with Zumkeller numbers.

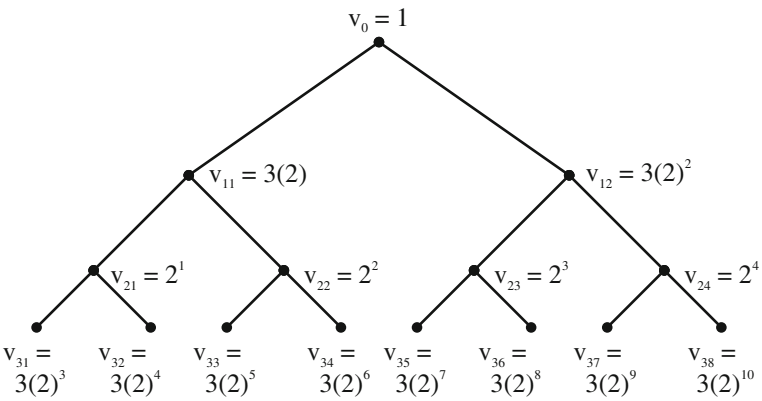

Fig. 3 Zumkeller labeling of the binary tree T

Input : An $n \times n$ square grid.
Output : Zumkeller square grid of order n.
$f(v_{ij})$ = positive integer // f is a function defined on the vertex set of G.
SubProcedure
begin

$$f(v_{ij}) = 2^{n\left(\frac{i-1}{2}\right)+\left(\frac{j+1}{2}\right)}$$

$$f(v_{ij+1}) = 3\left\lfloor 2^{n\left(\frac{i-1}{2}\right)+\left(\frac{j-1}{2}\right)} \right\rfloor$$

$$f(v_{i+1j}) = 3\left\lfloor 2^{n\left(\frac{i+1}{2}\right)+\left(\frac{j+1}{2}\right)} \right\rfloor$$

$$f(v_{i+1j+1}) = 2^{n\left(\frac{i+1}{2}\right)+\left(\frac{j-1}{2}\right)}$$

for $1 \le i \le n$ **do**
begin
for $1 \le j \le n$ **do**
begin
$f^*(v_{ij}\ v_{ij+1}) = f(v_{ij})\ f(v_{ij+1})$
$f^*(v_{ij}\ v_{i+1j}) = f(v_{ij})\ f(v_{i+1j})$
$f^*(v_{i+1j}\ v_{i+1j+1}) = f(v_{i+1j})\ f(v_{i+1j+1})$
$f^*(v_{ij+1}\ v_{i+1j+1}) = f(v_{ij+1})\ f(v_{i+1j+1})$
end
end
end
end Subprocedure
Procedure : Zum_lab_square grid of order n(G).
if n is even **then**
begin
for i = 1, 3, 5, ..., n−1 **do**
begin
for j = 1, 3, 5, ..., n−1 **do**
begin

$$f(v_{ij}) = 2^{n\left(\frac{i-1}{2}\right)+\left(\frac{j+1}{2}\right)}$$

$$f(v_{ij+1}) = 3\left\lfloor 2^{n\left(\frac{i-1}{2}\right)+\left(\frac{j-1}{2}\right)} \right\rfloor$$

$$f(v_{i+1j}) = 3\left\lfloor 2^{n\left(\frac{i+1}{2}\right)+\left(\frac{j+1}{2}\right)} \right\rfloor$$

$$f(v_{i+1j+1}) = 2^{n\left(\frac{i+1}{2}\right)+\left(\frac{j-1}{2}\right)}$$

```
                    for 1 ≤ i ≤ n–1 do
                        begin
                            for 1 ≤ j ≤ n–1 do
                                begin
                                    f*(v_ij v_ij+1) = f(v_ij) f(v_ij+1)
                                    f*(v_ij v_i+1j) = f(v_ij) f(v_i+1j)
                                    f*(v_i+1j v_i+1j+1) = f(v_i+1j) f(v_i+1j+1)
                                    f*(v_ij+1 v_i+1j+1) = f(v_ij+1) f(v_i+1j+1)
                                end
                        end
                end
        end
    else
        for i = 1, 3, 5, ..., n do
            begin
                for j = 1, 3, 5, ..., n do
                    call Subprocedure
            end
    return (G)
    end Zum_lab_square grid of order n(G).
```

The time complexity of this algorithm is tightly bounded, and the time complexity is $\theta(n^2)$.

Theorem 2 *A grid graph $P_n \times P_n$ admits a Zumkeller labeling.*

Proof Let G be a grid graph of order $n \times n$. □

Let $V = \{v_{ij} \mid 1 \le i \le n,\ 1 \le j \le n\}$ be the vertex set of the square grid.

Let $E = \{v_{ij}\ v_{ij+1},\ v_{ij}\ v_{i+1j},\ v_{i+1j}\ v_{i+1j+1},\ v_{ij+1}\ v_{i+1j+1} \mid 1 \le i \le n,\ 1 \le j \le n\}$ be the edge set of the square grid.

Define an injective function f: $V \to N$ such that

$$f(v_{ij}) = 2^{n\left(\frac{i-1}{2}\right)+\left(\frac{i+1}{2}\right)}$$

$$f(v_{ij+1}) = 3\left[2^{n\left(\frac{i-1}{2}\right)+\left(\frac{j-1}{2}\right)}\right]$$

$$f(v_{i+1j}) = 3\left[2^{n\left(\frac{i+1}{2}\right)-\left(\frac{j+1}{2}\right)}\right]$$

$$f(v_{i+1j+1}) = 2^{n\left(\frac{i+1}{2}\right)-\left(\frac{j-1}{2}\right)}$$

where $i = 1, 3, 5, \ldots, j = 1, 3, 5, \ldots$ and an induced function f^*: $E \to N$ is defined as

(i) $f^*(v_{ij}\ v_{ij+1}) = f(v_{ij})\ f(v_{ij+1})$
(ii) $f^*(v_{ij}\ v_{i+1j}) = f(v_{ij})\ f(v_{i+1j})$
(iii) $f^*(v_{i+1j}\ v_{i+1j+1}) = f(v_{i+1j})\ f(v_{i+1j+1})$
(iv) $f^*(v_{ij+1}\ v_{i+1j+1}) = f(v_{ij+1})\ f(v_{i+1j+1})$

for $1 \le i \le n$ and $1 \le j \le n$.

Now we can prove that the labels on the edges of the grid graph are Zumkeller numbers through the following cases.

(i) $f^*(v_{ij}v_{ij+1}) = f(v_{ij})f(v_{ij+1}) = 2^{n\left(\frac{i-1}{2}\right)+\left(\frac{i+1}{2}\right)}3\left[2^{n\left(\frac{i-1}{2}\right)+\left(\frac{j-1}{2}\right)}\right] = 3\left[2^{n(i-1)+j}\right]$ is a Zumkeller number.

(ii) $f^*(v_{ij}v_{i+1j}) = f(v_{ij})f(v_{i+1j}) = 2^{n\left(\frac{i-1}{2}\right)+\left(\frac{i+1}{2}\right)}3\left[2^{n\left(\frac{i+1}{2}\right)-\left(\frac{j+1}{2}\right)}\right] = 3[2^{ni}]$ is a Zumkeller number.

(iii) $f^*(v_{i+1j}\,v_{i+1j+1}) = f(v_{i+1j})f(v_{i+1j+1}) = 3\left[2^{n\left(\frac{i+1}{2}\right)-\left(\frac{j+1}{2}\right)}\right]\left[2^{n\left(\frac{i+1}{2}\right)-\left(\frac{j-1}{2}\right)}\right]$ $= 3\left[2^{n(i+1)-j}\right]$ is also a Zumkeller number.

(iv) $f^*(v_{ij+1}v_{i+1j+1}) = f(v_{ij+1})f(v_{i+1j+1}) = 3\left[2^{n\left(\frac{i-1}{2}\right)+\left(\frac{j-1}{2}\right)}\right]\left[2^{n\left(\frac{i+1}{2}\right)-\left(\frac{j-1}{2}\right)}\right] = 3[2^{ni}]$ is a Zumkeller number.

In all cases, the integers on the edges of the grid graph are Zumkeller numbers. Therefore, the grid graph of order $n \times n$ admits a Zumkeller labeling.

Corollary 2 A lattice grid $P_m \times P_n$ admits a Zumkeller labeling.

Example 4 Zumkeller labeling of a 5 × 5 grid graph is given in Fig. 4.

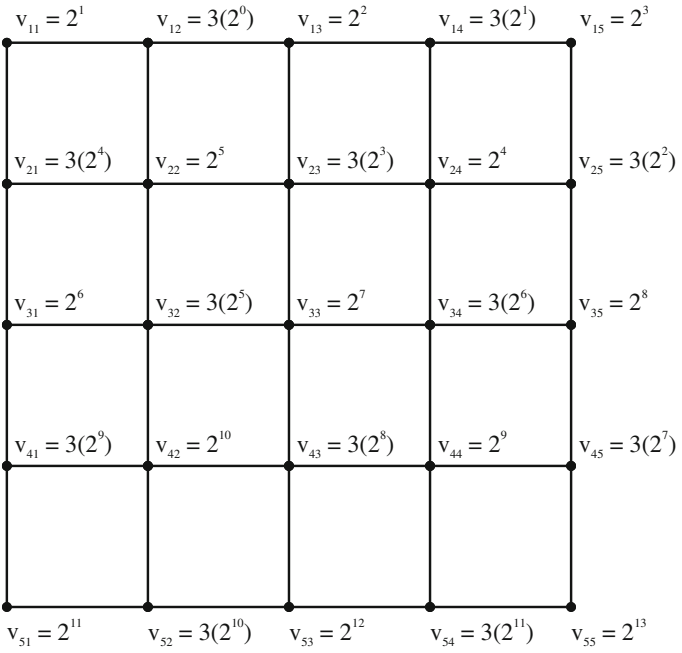

Fig. 4 Zumkeller labeling of a 5 × 5 grid graph

4 Conclusion

In this paper, we have proved the existence of Zumkeller labeling for full binary trees and grid graphs by presenting algorithms.

References

1. B.J. Balamurugan, K. Thirusangu, D.G. Thomas, Strongly multiplicative Zumkeller labeling of graphs. Int. Conf. Inf. Math. Sci. 349–354 (2013)
2. G.S. Bloom, S.W. Golomb, Applications of numbered undirected graphs. IEEE **165**(4), 526–570 (1977)
3. F. Buss, Zumkeller numbers and partitions. http://groups.google.de/group/de.sci.mathematik/msg/e3fc5afcec2ae540
4. J.A. Gallian, A dynamic survey of graph labeling. Electron. J. Comb. **16** (2013)
5. F. Harary, *Graph theory* (Addison-Wesley, Reading Mass, 1972)
6. R. Johnsonbaugh, *Discrete mathematics* (Pearson Education, Asia, 2001)
7. Y. Peng, K.P.S. Bhaskara Rao, On zumkeller numbers. J. Number Theory **133**(4), 1135–1155 (2013)
8. A. Rosa, On certain valuations of the vertices of a graph, in *Theory of Graphs. International Symposium* (1966), pp. 349–359
9. A.K. Srinivasan, Practical numbers. Curr. Sci. **17**, 179–180 (1948)

Memetic Framework Application—Analysis of Corporate Customer Attitude in Telecom Sector

V. Balakumar and C. Swarnalatha

Abstract Natural and cultural evolutionary processes shall be well implemented in the real-time applications by using memetic computing process. Popular researches based on the evolutionary processes have been dealing with the universal criteria. So the need for location-dependent population searches lead to the research based on the cultural traits of the individual, i.e., memetic computational applications. In the telecom sector, the decision-making process of the corporate customers is taken for study with the applications based on the memetic computation. This paper presents an innovative approach to analyze the customer attitude with objective, subjective, and inter-subjective criteria in the multi-attribute deterministic environment. The two metrics, viz. value of business (VOB) and number of services (NOS), are taken as reference using the memetic attributes. Experimental analysis shows that with respect to the telecom sector, memetic framework has improvised the corporate customer attitude toward the services in the betterment of customer relation management.

Keywords Memetic computational applications · Value of business · Intelligence-based genetic algorithms · Deterministic environment · Data mining portals

V. Balakumar (✉)
Research Scholar, (JTO – CRM, Enterprise Business Cell, BSNL),
Anna University Madurai Regional Centre,
Madurai 625002, Tamil Nadu, India
e-mail: vinbalakumar@gmail.com

C. Swarnalatha
Department of Management Studies, Anna University Madurai Regional Centre,
Madurai 625002, Tamil Nadu, India
e-mail: swarna@autmdu.ac.in

© Springer India 2015

L.P. Suresh et al. (eds.), *Artificial Intelligence and Evolutionary Algorithms in Engineering Systems*, Advances in Intelligent Systems and Computing 325,
DOI 10.1007/978-81-322-2135-7_22

1 Introduction

For the period of over past 30 years, various population-based search optimization techniques are used to handle sample based on landscape parameters [1–4]. Intermediary states involved in the decision-making process of an individual largely depend on the inspiration from the user. For such processes, evolutionary and swarm intelligence-based genetic algorithms [5] are used for optimization techniques. The set of population is nothing but a group of individuals. These individuals are governed by the processes functioning on them.

Nowadays, nature inspired process is used as source of optimization in various environments, specifically in population-based genetics. For the development of defined hypothesis for a human mind, memetic science has been serving as the motivational tool. Memetic computing defines the pattern for real-world model with domain-specific knowledge for effective problem solving. "Meme" is known to be basic building block for the transmittable and receivable cultural traits [6, 7]. This term has led to the development of new domain namely memetic science, which deals the mind-universe spreading across various fields. One of the major breakthroughs in the memetic computation is the problem solving for location-dependent population searches.

Versatility is one concept that is attracting various researches in finding the solution for their frameworks. Landscape parameters are vital ingredients in selection of a particular solution for a specified community or group of population. Based on geographical- or location-based characteristics, the need for the tailor-made solutions varies vastly from group to group. The multimodal complexity and the optimization problems shall be addressed using memetic computing approaches and their usage in the real-time applications. Rather than going for the universally applicable frameworks, researchers are interested in giving optimal solutions that are customized and tailor-made for specific problems of the specified group and place [8]. Analysis of the problems based on the decision space and the fitness to specific boundary is addressed by memetic computational algorithms. Various evolutionary algorithms have been used so far with respect to the landscape problems and the relevant solutions [9]. During different evolutionary time periods, different fitness parameters are calculated for the same problem. These uncertainties in the evolutionary algorithms have been broadly classified into two categories: (1) deterministic environment and (2) non-deterministic environment [10].

Deterministic environment is one where the shape of the fitness landscape is variable and the fitness parameters changes dynamically during the run time. The real-time applications where such environments can be visualized are telecommunication sectors, data mining portals, and industrial control engineering segments. Non-deterministic environments involve noisy fitness functions. In these environments, fitness parameters hold the approximation within themselves.

Though considerable numbers of research works are yet to be done based on the dynamically changing memetic computing applications, an important work by Wee Tat Koo and others [10] proposes a predictive strategy based on evolutionary

algorithms in dynamically changing environments. In the approach, only the most suitable and most promising approaches are stored in the evolutionary process by using the prediction logics. This approach reduces the overhead of the environment considerably. Another vital contribution based on differential evolutionary processes is done by Ernesto Mininno [10]. In this work, the evolutionary framework is modeled as the hybrid of local search process and optimization of scale factor. Non-deterministic framework is analyzed in his work. Peak problems in the memetic computation have been studied by Irene Moser [10] using the dynamic optimization in the hybrid environment. All these three approaches vary in terms of local search process. Dynamic genetic operators are therefore required to optimize the local search process [11].

2 Cultural Evolution—Selection of Memes

Various cultural evolutionary processes have been proposed with meme as agent. In these simulation models, agents simply copy the knowledge shown by the filtering parameters in the run time. But in the real-time scenario, there will not be any previous reference to ascertain the fitter, interacted or the receiver. Later models proposed agents as simple neural network in which it will not be mere copying but will be an active reinterpretation of the message.

For a sociocultural model with evolutionary process, the entity classes can be classified based on the dependent information, viz. referring object, assimilating subject, and inter-subjective communication process. These categories have inter-dependent deterministic relations (Fig. 1).

Based on the three criteria tabulated in the above chart, the meme agents have various parameters. These parameters will hold the key values in the evolutionary process in the population-based landscape models.

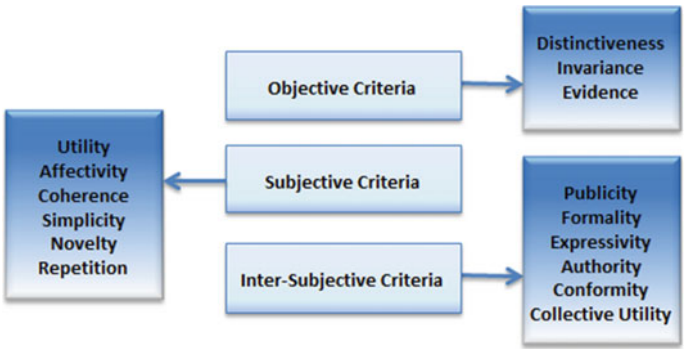

Fig. 1 Sociocultural model with evolutionary process

3 Memetic Framework in Telecom Marketing

Our telecom marketing process involves various strategies and plans to attract the customer to avail telecom services. With the help of the evolutionary schemas, nomination of different genetic parameters and properties and the optimized solution based on the genetic operators shall be fixed based on the chart shown in Fig. 2.

3.1 Representing Potential Problem Solution

While approaching the corporate customer in the telecommunication market for the provision of new services, the following points need to be studied carefully

- Loyalty for the brand
- Actual requirement of the customer in terms of service or products
- Modality of billing and payments
- Fault reporting mechanism and post-purchase service

The customer with cultural traits will have strong affinity toward region or geographical or national representing products and services. Also, the customer may expect personal rapport with the service personal while approaching for fault reporting and post-purchase service. These potential parameters have to be analyzed while choosing a memetic-based customized application for the customer.

3.2 Exploiting Genetic Operators for Evolution

Various cultural and social activities shall be marked as the operator for the evolutionary process. Some auspicious occasions, festive seasons, and holy days are observed among the business community for availing new services. These genetic operators shall be considered for the evolutionary process.

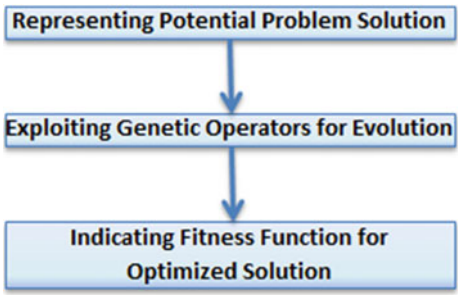

Fig. 2 Memetic framework in telecom marketing

3.3 Indicating Fitness Function for Optimized Solution

For optimal solution in the business realization, fitness parameters among the chosen genetic operators need to be selected based on the local knowledge about the customer and the specific occurrence. The evolution of the fitness function yields repeated iteration process and the subsequent selection of the more appropriate solution.

4 Configuring Meme Agents for Telecom Services

For choosing the specific telecom services and customize the tariff and plan structure based on memetic computing framework, the three categories viz. objective, subjective, and inter-subjective criteria, the configuration based on the sub-criteria is tabulated in the below chart (Table 1).

The chart-tabulated above clearly indicates the selection criteria are taken for choosing the meme agents in the telecom services. This will facilitate the customers with evolutionary process and provide them the multi-criterion options to choose the telecom services. The two metrics, viz. value of business (VOB) and number of services (NOS), are taken as reference using the memetic agents.

Table 1 Meme agents for telecom services

Criteria	Sub-criteria	Configured values for telecom services
Objective	Distinctiveness	Brand value
	Invariance	Tariff pattern
	Evidence	Network coverage
Subjective	Utility	Database repository
	Affectivity	Emotional bond
	Coherence	Knowledge database
	Simplicity	Customized service
	Novelty	Advertisement
	Repetition	Brand registration
Inter-subjective	Publicity	Personalized service
	Formality	Grievance mechanism
	Expressivity	Mouth talk
	Authority	Trust
	Conformity	Terms and conditions
	Collective utility	Linguistic approaches

5 Exploring Memetic Framework: Experimental Analysis

A novel methodology is adopted in this paper for analyzing the attitude among the corporate telecom customers toward availing of the telecom services. The standard tariff card mentioning the traditional services with their base plan, tariff, and modality of payment and terms and conditions is prepared as one set, and the customized tariff card with turn-key solutions, tailor-made service plans, flexibility in billing patterns, inclusion of value-added services, and personal fault reporting mechanism using memetic computing framework is prepared as another set.

Our experimental analysis was conducted among 20 number of enterprise customers from the telecom sector. The experimental analysis was taken over a period of three from September 2013 to November 2013. The customers belonged to small- and medium-enterprise segments. The entire customer group was divided into two subgroups with 10 members in each group. The first group termed as "A" was given with various telecom service plans with standard pattern of services. The second group "B" was provided with the telecom service plans with tailor-made solutions after analyzing their specific requirements. The standard pattern of service was the one which was already available in the market without any customization, whereas tailor-made solution was designed based on the memetic application. All the group members were provided options to choose among the telecom services listed under various categories based on their requirements. The experiment was conducted based on two parameters as the reference, viz. volume of business (VOB) generated from the customer and the NOS chosen by the customer. The customer attitude toward availing of the telecom services based on these two parameters was calculated using the five-point scale.

The following figure illustrates the attitude of the customers from both the subgroups. It is well understood that the group "B" provided with memetic application-based telecom solutions has better value in terms of both VOB and NOS. The implication clearly shows that memetic implementation improvises the

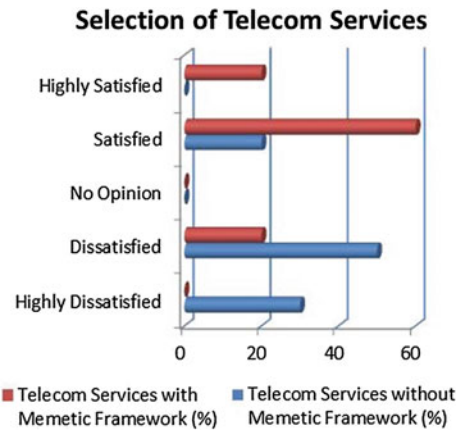

Fig. 3 Memetic framework —selection of telecom services

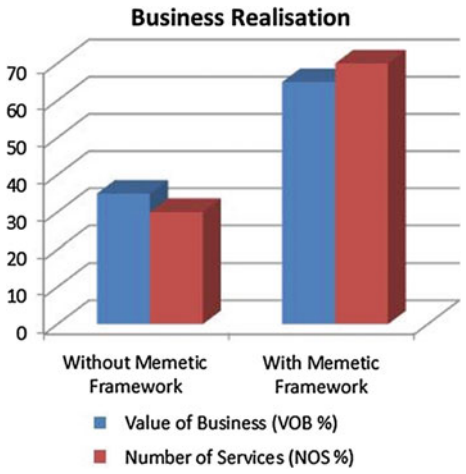

Fig. 4 Memetic framework —business realization

customer relation management process and orients the customers' attitude toward availing of telecom services for higher VOB and more number of allied value addition to the services (Figs. 3 and 4).

6 Conclusion

Using the integrated approach based on distribution and tailor-made approach using memetic computing, the proposal suggested in this paper produces good results. The flexibility that was available in choosing different plans and tariff structure among the telecom services significantly enhanced the business opportunities. The personalization of the billing patterns and the flexibility of usage pattern with the customized system representable formats attract the customer toward availing of the telecom services. Thus, implementation of memetic computing applications in the telecom sector has improvised the corporate customer attitude toward the services in the betterment of customer relation management. Memetic framework can be well suited and feasible in the Indian environment, considering the long-term overlook for the telecommunication sector. Lot of cultural traits are there in practice which have direct or indirect impact in the selection of the particular service by the corporate customers. So including memetic framework-based solutions will enrich the long-term customer relation management in the Indian telecommunication sector.

References

1. K.C. Tan, E.F. Khor, T.H. Lee, *Multiobjective Evolutionary Algorithms and Applications. Advanced Information and Knowledge Processing* (Springer, Berlin 2005)
2. X.S. Yang, *Nature-Inspired Metaheuristic Algorithms* (Luniver press, 2008)
3. Y. Jin, J. Branke, Evolutionary optimization in uncertain environments: a survey. IEEE Trans. Evol. Comput. **9**(3), 303–317 (2005)
4. K. Miettinen, *Evolutionary Algorithms in Engineering and Computer Science Recent Advances in Genetic Algorithms Evolution Strategies, Evolutionary Programming* (Wiley, Hoboken, 1999)
5. M. Mitchell, An introduction to genetic algorithms (complex adaptive systems). Bradford Book, Third Printing Edn. **55**, 02146–1493 (1998)
6. R. Aunger, in *Memes*, ed. by A. Kuper and J. Kuper. The Social Science Encyclopedia, 3rd edn. (London, Routledge, 2004)
7. F. Heylighen, K. Chielens. Cultural evolution and memetics. Encycl. Complex. Syst. Sci.
8. D. Liu, K.C. Tan, C.K. Goh, W.K. Ho, A multiobjective memetic algorithm based on particle swarm optimization. IEEE Trans. Syst. Man Cybern. Part B Cybern. **37**(1), 42–50 (2007)
9. H. Ishibuchi, N. Tsukamoto, Y. Nojima, Diversity improvement by non-geometric binary crossover in evolutionary multiobjective optimization. IEEE Trans. Evol. Comput. **14**(6), 985–998 (2010)
10. F. Neri, S. Yang, Guest editorial: memetic computing in the presence of uncertainties. Memetic Comput. **2**, 85–86 (2010)
11. K. Morikawa, S. Ozawa, S. Abe, Tuning membership functions of kernel fuzzy classifiers by maximizing margins. Memetic Comput. J. **1**(3), 221–228 (2009)

Contourlet-Based Multiband Image Fusion for Improving Classification Accuracy in IRS LISS III Images

K. Venkateswaran, N. Kasthuri, K. Balakrishnan and K. Prakash

Abstract Unsupervised classification plays a vital role in overseeing the transformations on the earth surface. Unsupervised classification has an indispensable role in an immense range of applications such as remote sensing, motion detection, environmental monitoring, medical diagnosis, damage assessment, agricultural surveys, and surveillance. In this paper, a novel method for unsupervised classification in multitemporal optical images based on image fusion and Gaussian RBF kernel K-means clustering is proposed. Here, the image is generated by performing contourlet-based multiband image fusion on the red, green, and near-IR images. On the finest image generated by collecting the information from three bands, Gaussian RBF kernel K-means clustering is performed. In Gaussian RBF kernel K-means, nonlinear clustering is performed, as a result the false alarm rate is reduced and accuracy of the clustering process is enhanced. The aggregation of image fusion and RBF kernel K-means clustering is seen to be more effective in detecting the changes than its preexistences.

Keywords Contourlet · K-means · LISS III image and fusion

K. Venkateswaran (✉) · N. Kasthuri · K. Balakrishnan · K. Prakash
Department of ECE, Kongu Engineering College, Erode, India
e-mail: vvenkates05@gmail.com

N. Kasthuri
e-mail: kasthuri@kongu.ac.in

K. Balakrishnan
e-mail: kbala2289@gmail.com

K. Prakash
e-mail: prakashskp@gmail.com

© Springer India 2015

L.P. Suresh et al. (eds.), *Artificial Intelligence and Evolutionary Algorithms in Engineering Systems*, Advances in Intelligent Systems and Computing 325,
DOI 10.1007/978-81-322-2135-7_23

1 Introduction

In the classification process, images are taken and processed to identify the changes that may have taken place. The output is the accurate classified image, indicating the different features. Two types of classification, namely supervised and unsupervised. In supervised classification, a training set is required for the learning process of the classifiers. This training set is obtained from the ground truth data [1]. The latter technique performs classification by different algorithms, namely K-means, C-means, and Fuzzy C-means [2]. The process of clustering is of widespread interest since it is having a wide variety of applications in diverse domains such as remote sensing [3], motion detection [4], video surveillance [5], damage assessment [6], agricultural surveys [7], environmental monitoring [8], analysis of urban changes [9], and medical diagnosis [10].

Due to the massive growth of the geographic database, it is more practical to focus on the unsupervised approach than the supervised one. Currently, many unsupervised classification techniques have been proposed. Some of these are hard clustering, soft clustering, and hierarchical clustering with the advancement in the remote sensing technology, and unsupervised classification in remote sensing images is becoming vital.

In [11], wavelet-based image fusion techniques are applied to improve the change detection classification accuracy in synthetic aperture radar images. This paper aims to improve only the classification accuracy in optical images. In order to improve the classification accuracy, contourlet-based multiband image fusion technique is used. On the finest fused image, different types of kernel K-means, linear, polynomial, Gaussian, and logarithmic, are used to convert into the higher dimensional feature space, and the performance is analyzed using silhouette value, PSNR, and accuracy assessment using ground truth data.

2 Materials

The multitemporal multiband satellite sensor images used in this study of Madurai city in Tamil Nadu are shown [12] in Fig. 1a. The three bands, red, near-IR, and green, are taken for fusion as shown in Fig. 1b–d. Madurai is the second largest city in Tamil Nadu and is one of the oldest cities in India. It is one of the 12 heritage cities in India, and it is situated between longitudes. The topography of Madurai is above 101 m above the sea level. The land cover features are used in these study regions, urban, wasteland, vegetation, water body, and hilly region. The scene details of the area are given in Table 1.

The Linear Imaging Self Scanner III (LISS III) has spatial resolution of 23.5 m, multispectral channels in the visible and near-infrared wavelength. Observation spectral characteristics of LISS III are as follows:

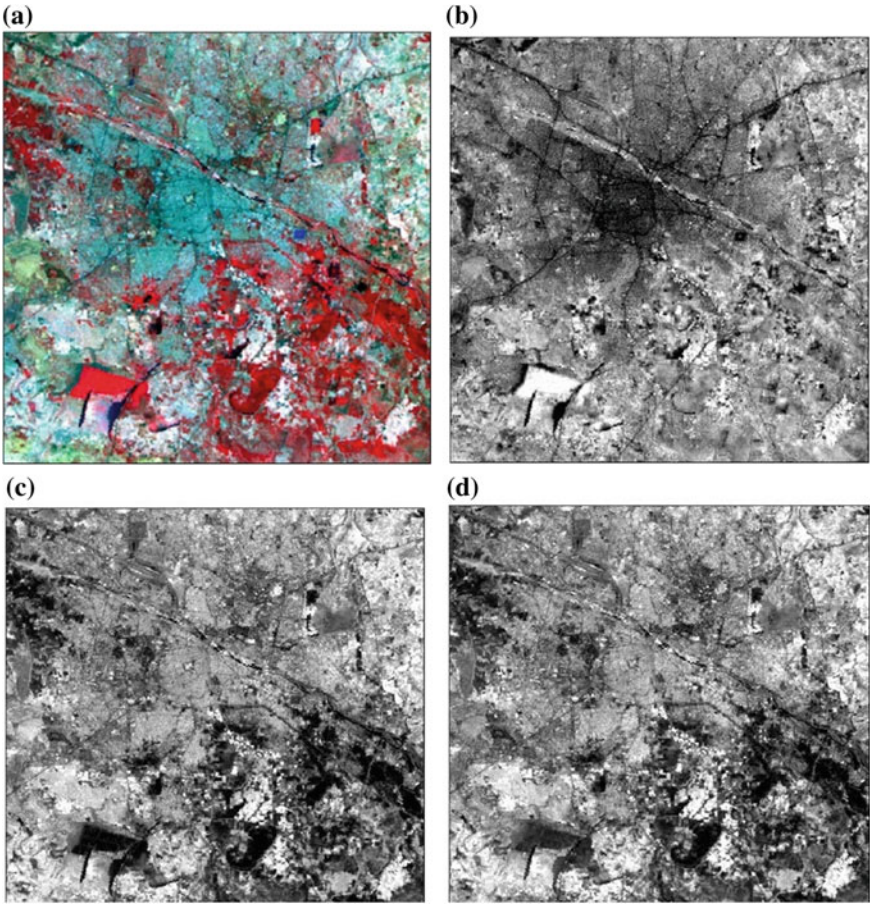

Fig. 1 Input image along with its different band images **a** input image, **b** red band, **c** green band, and **d** NIR band

Table 1 Details of the image taken for processing

	Date of acquisition	Satellite/Sensor	Resolution
Image 1	March 19, 2004	IRS P6/LISS III	23.50 m

- Band 2 0.52–0.59 μm
- Band 3 0.62–0.68 μm
- Band 4 0.77–0.86 μm
- Band 5 1.55–1.70 μm

3 Methodology

3.1 Contourlet-Based Fusion

Contourlets form a multiresolution directional tight frame designed to efficiently approximate images made of smooth regions separated by smooth boundaries. The contourlet transform has a fast implementation based on a Laplacian pyramid decomposition followed by directional filter banks applied on each bandpass subband [13] as shown in Fig. 2a. A filter bank structure can deal effectively with piecewise smooth images with smooth contours. The resulting image expansion is a directional multiresolution analysis framework composed of contour segments. This will overcome the challenges of wavelet and curvelet transform.

- Captures smooth contours and edges at any orientation
- Filters noise
- Derived directly from discrete domain instead of extending from continuous domain
- Can be implemented using filter banks

The transform decouples the multiscale and the directional decompositions

- The multiscale decomposition is handled by a Laplacian pyramid.
- The directional decomposition is handled by a directional filter bank.

The decomposed image after applying the contourlet transform is shown in Fig. 2b.

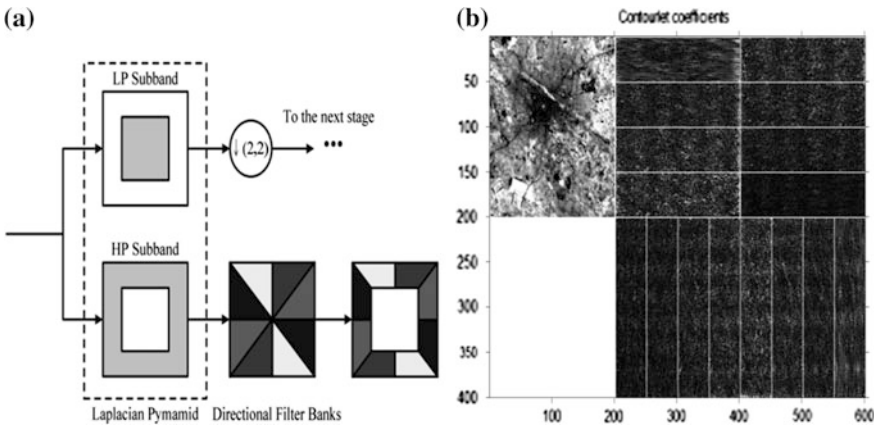

Fig. 2 Contourlet transform processing and output of decomposed red band image after applying contourlet transform **a** process of contourlet and **b** decomposed red band image

Step 1: The contourlet transform for both the red, green, and near-IR image is taken. Due to very low visibility, blue band is discarded. Here, one level of decomposition is done on both the images.

Step 2: Equations (1) and (2) show the fusion rule [14] to be applied on the approximate low-frequency (pyramidal filter bank) and high-frequency (directional filter bank). The fusion rule is defined below:

$$F_{LL} = \frac{L_{LL} + M_{LL} + H_{LL}}{2} \tag{1}$$

$$F_{\rho}(i,j) = \begin{Bmatrix} M_{\rho}(i,j), & \text{if, } E^{M}(i,j) < E^{L}(i,j) < H^{L}(i,j) \\ L_{\rho}(i,j), & \text{if, } E^{M}(i,j) < E^{L}(i,j) < H^{L}(i,j) \end{Bmatrix} \tag{2}$$

where M_{LL}, F_{LL}, and L_{LL} represent the approximate coefficients (low frequency band) of the red, green, and the near-IR band and the fused image, respectively. Then, F_{ρ} represents the high-frequency bands (directional filter banks). E^{M} and E^{L} represent the energy coefficients of the red, green, and the near-IR images.

Step 3: Perform inverse contourlet transform to get the fused image which is the reconstructed image shown in Fig. 4a.

For the low-pass coefficients, an averaging fusion rule is used. For the directional high-frequency coefficients, the higher value of edge information measurement is used to select the better coefficients for fusion.

3.2 Kernel K-means Clustering

The purpose to process the finest image is to discriminate the classification accurately. The finest image obtained by image fusion is sorted out into classification using kernel K-means clustering algorithm. Different kernel functions [15] such as linear kernel (Eq. 3), polynomial kernel (Eq. 4), logarithmic kernel (Eq. 5), and Gaussian RBF kernel (Eq. 6) can be used to generate the higher dimensional feature space.

$$k(x) = x_1^T x_2 + c. \tag{3}$$

$$k(x) = \left(\alpha x_1^T x_2 + c\right)^d. \tag{4}$$

where alpha is slope, the constant term c and the polynomial degree d

$$k(x) = -\log\left(\| x_2 - x_1 \|^d + 1\right). \tag{5}$$

$$k(x) = \exp\left(\frac{\| x_2 - x_1 \|^2}{2\sigma^2}\right). \tag{6}$$

The kernel techniques allow linear evaluation of data in higher dimensional feature space, which results in nonlinear clustering of data samples present in the input space. The higher dimensional feature space is generated by a mapping function $\phi(\cdot)$ applied on the image obtained by fusing the NIR and red and green image. The common cost function used to perform K-means clustering is Euclidean distance. The feature mapped image obtained by applying kernel on the coordinates of finest image is clustered into five features. The classification is generated by considering minimum angle criteria which is given by Eq. (7),

$$\frac{\langle m_i, m_j \rangle}{\sqrt{m_i m_j}\sqrt{m_i m_j}} = \cos \angle (m_i, m_j) \tag{7}$$

where the m_i and m_j in Eqs. (8) and (9) are the mean vectors of feature space data clusters corresponding to the data points associated with the finest image.

$$\text{where} \quad m_i = \frac{1}{N_i} \sum_{x_n \in D_i} \phi(x_n). \tag{8}$$

$$m_j = \frac{1}{N_j} \sum_{x_m \in D_j} \phi(x_m). \tag{9}$$

Euclidean distance is replaced by minimum angle criteria. The kernel technique is used instead of dot product; it returns the inner product of the fused image directly in higher dimensional feature space. The flow diagram given below depicts the steps involved in performing clustering on fused image shown in Fig. 3.

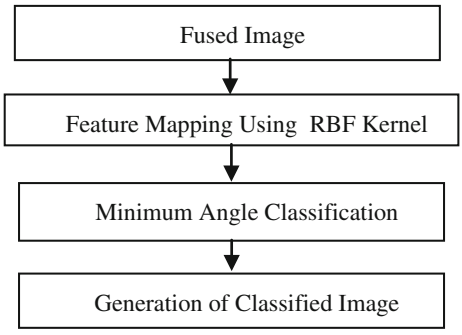

Fig. 3 The steps involved in clustering on fused image

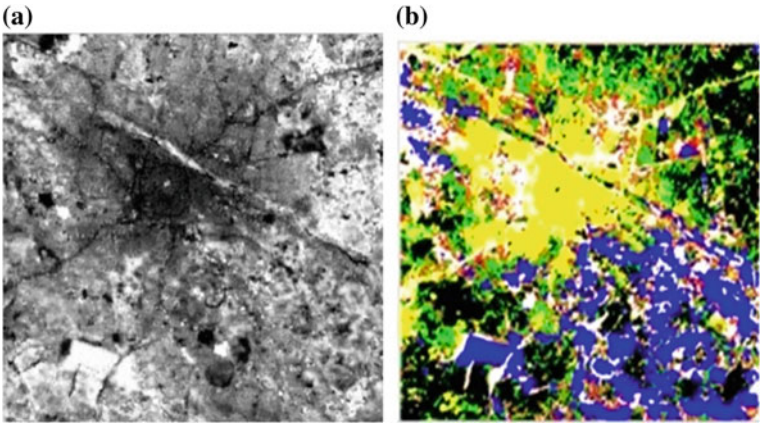

Fig. 4 Fused image after reconstruction and clustered image after of fused image obtained from classification **a** reconstructed image after fusion and **b** clustered image

The image after applying the fusion rule was reconstructed shown in Fig. 4a, and clustered image shown in Fig. 4b is obtained after applying RBF kernel to the fused image.

4 Results and Discussion

4.1 Accuracy Assessment

Various accuracy indices such as overall accuracy, producer accuracy, and user accuracy have been discussed in determining the accuracy of classification. Commonly, most of the researchers recommended the use of the kappa coefficient of agreement as the standard measure for accuracy. Using the field visit data, the classification rate can be computed and performance of classification algorithm can be analyzed. Field visit plays an imperative role in determining land cover features in real world. Thousand ground truth data obtained from the visits were compared with the satellite image to know the accuracy of classification. The field visits will ensure the accuracy and the success of the project.

4.2 Performance Analysis

Classification error matrix is one of the most common means of expressing classification accuracy is the preparation of a classification error matrix [16] also called as a confusion matrix. Error matrices compare, on a category by category basis, the

Table 2 Performance of the contourlet +RBF kernel K-means

	Urban	Vegetation	Waste land	Hilly	Water
Urban	216	79	124	25	56
Vegetation	34	143	80	22	21
Waste land	30	8	52	6	4
Hilly	12	0	18	12	8
Water	30	0	12	0	8
User accuracy: 36.57 Producer accuracy: 34.82			Overall accuracy: 55.92 Kappa coefficient: 0.6906		

relationship between known reference data (ground truth) and the corresponding results of an automated classification. Table 2 shows the calculation of accuracy and kappa coefficient from the matrix for RBF kernel K-means.

Using the ground truth data, the classification results and performance analysis of different kernel functions obtained using kernel K-means clustering on the difference images are tabulated in Table 3. In Fig. 5a, performance comparison of K-means using minimum angle and minimum distance is shown.

The performance of the different kernel functions is compared using ground truth data. Among all the above-mentioned kernel functions, Gaussian RBF kernel is most suitable for change detection process because the accuracy is high for Gaussian RBF kernel than its counterparts. The RBF kernel helps us to pick hyper spheres, whereas linear kernels pick hyper planes, only Gaussian RBF kernel K-means clustering algorithm is applied on the data samples of the fused image in order to perform nonlinear clustering. Since the input images are subjected to various noises during acquisition, it is necessary to evaluate the robustness [17] of the fusion algorithm to noise as shown in Fig. 5a. It can be done by plotting the values of PSNR Eq. (10) and tau Eq. (11) which can be determined as follows:

$$\text{PSNR} = 10 \quad \log_{10}\left(\frac{255}{\sum_{i=1}^{M}\sum_{j=1}^{N}\left(x(i,j)-\hat{x}(i,j)\right)^2}\right) \tag{10}$$

Table 3 Performance of the contourlet + various kernel K-means

Techniques used	K-means	
	Overall accuracy (%)	Kappa coefficient
Linear kernel	43.10	0.6120
Polynomial kernel	53.15	0.6519
Logarithmic kernel	55.02	0.6735
RBF kernel	55.92	0.6906

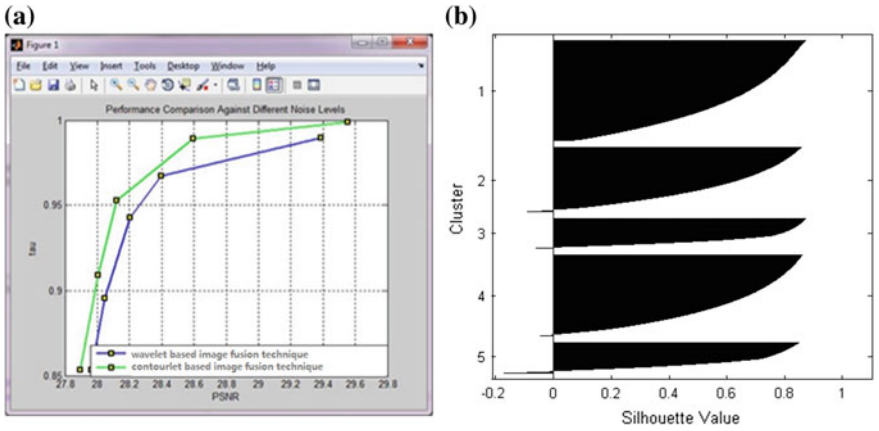

Fig. 5 Comparison of robustness of image fusion algorithms and the cluster validation using silhouette plot for kernel K-means algorithm **a** performance comparison and **b** silhouette plot

$$\tau = 1 - \frac{\sum_{i=1}^{M}\sum_{j=1}^{N}|c_1(i,j) - c_2(i,j)|}{MN} \tag{11}$$

where M and N in Eq. (12) are number of rows and number of columns of the input image, $x(i,j)$ is the input image in the absence of noise, and $\hat{x}(i,j)$ is the noisy version of the input image. Where $C_1(i,j)$ the fused image is generated from the input images in the absence of noise and $C_2(i,j)$ is fused image generated using the noisy version of the input images. The robustness of fusion algorithms was represented in the Fig. 5a.

Silhouette is a measure of interpretation and validation of clusters of data [18]. It is a measure of how similar that point is to the other points in the own cluster compared with points in other clusters. Its value range from +1 indicating points that are distant from neighboring clusters, through 0 indicating points that are not distinct to any given cluster, −1 indicates that are assigned to wrong cluster. The smaller the silhouette value, better the matching. The silhouette value is represented in Eqs. (12) and (13)

$$s(i) = \frac{b(i) - a(i)}{\max\{a(i), b(i)\}}. \tag{12}$$

$$s(i) = \begin{cases} 1 - \frac{a(i)}{b(i)}, & \text{if } a(i) < b(i) \\ 0, & \text{if } a(i) = b(i) \\ \frac{b(i)}{a(i)} - 1, & \text{if } a(i) > b(i) \end{cases}. \tag{13}$$

where $a(i)$ and $b(i)$ are the two clusters.

Silhouette plot for kernel K-means using minimum angle classification is shown in Fig. 5b.

5 Conclusion

An innovative method for unsupervised classification in optical images which is based on image fusion and kernel K-means clustering has been implemented in this paper. Here, full advantage of the contourlet transform has been utilized to form the fusion rule and hence to get a finest image containing complementary information from the multiband images. On the fused image, RBF kernel K-means clustering has been performed. Since kernel K-means clustering takes into consideration nonlinearity, it is suited well for the clustering process in optical images. Consequently, this approach for classification accuracy yields better results than its preexistences.

References

1. G.M. Food, Status of land cover classification accuracy assessment. Remote Sens. Environ. **80**, 185–201 (2001)
2. M.B.R. Jipkate, M.V.V. Gohokar, A comparative analysis of fuzzy C-means clustering and K-means clustering algorithms. Int. J. Comput. Eng. Res. **2**(3), 737–739 (2012)
3. L. Bruzzone, D.F. Prieto, An adaptive semiparametric and context-based approach to unsupervised change detection in multitemporal remote-sensing images. IEEE Trans. Image Proces. **11**(4), 66–77 (1996)
4. C. Dumontier, F. Luthon, J.-P. Charras, Real-time DSP implementation for MRF-based video motion detection. IEEE Trans. Image Process. **8**(10), 1341–1347 (1999)
5. R. Collins, A. Lipton, T. Kanade, Introduction to special section on video surveillance. IEEE Trans. Pattern Anal. Mach. Intell. **22**(8), 745–746 (2000)
6. K. Grover, S. Quegan, C. da Costa Freitas, Quantitative estimation of tropical forest cover by SAR. IEEE Trans. Geosci. Remote Sens. **37**(1), 479–490 (1999)
7. P.S. Chavez Jr, D.J. MacKinnon, Automatic detection of vegetation changes in the south western united states using remotely sensed images. Photogramm. Eng. Remote Sens. **60**(5), 1285–1294 (1994)
8. K.R. Merril, L. Jiajun, A comparison of four algorithms for change detection in an urban environment. Remote Sens. Environ. **63**(2), 95–100 (1998)
9. N. Abu-Zeid, R, Kashif, O.M. Badawy, Immune based clustering for medical diagnosyic systems, in *IEEE Xplore, Advanced Computer Science Applications and Technologies* (2012)
10. M. Sezgin, B. Sankur, A survey over image thresholding techniques and quantitative performance evaluation. J. Electron. Image **13**(1), 146–165 (2004)
11. M. Gong, J. Zhou, Z. Ma, Change detection in SAR images based on image fusion and improved fuzzy clustering. IEEETrans. Image Process. **21**(4), 2141–2151 (2012)
12. R.A. Alaguraja, V. Anand, S. Maidani, Wavelet frame based feature extraction technique for improving classification accuracy. J Indian Soc. Remote Sens. **37**, 423–471 (2009)
13. M.N. Do, M. Vetterli, The contourlet transform: an efficient directional multiresolution image representation. IEEE Trans. Image Process. **14**(12), 2091–2106 (2005)

14. Y. Zheng, C. Zhu, J. Song, X. Zhao, Fusion of multiband SAR images based on contourlet transform, in *IEEE International Conference on Information Acquisition* (2006), pp. 420–424
15. K. Venkateswaran, N. Kasthuri, C. Arathy, V. Haran, D.D. Jeni, A survey on unsupervised change detection algorithms, in *IEEE International Conference on ICCPCT* (2013), pp. 897–903
16. R.A. Alaguraja, V. Anand, S. Maidani, Wavelet based post classification change detection technique for urban growth monitoring. J Indian Soc. Remote Sens. **41**(1), 35–43 (2013)
17. S.S. Al-amri, N.V. Kalyankar, S.D. Khamitkar, A comparative study of removal noise from remote sensing image. IJSCI. **7**(1), (2010)
18. M.S. Shifa, M.S. Naweed, M. Omar, M.Z. Jhandir, T. Ahmed, Classification of cotton and sugarcane plants on the basis of their spectral behavior (2011), pp. 2119–2125

Computer-Aided Diagnosis of Breast Elastography and B-Mode Ultrasound

Shirley Selvan, S. Shenbagadevi and S. Suresh

Abstract Ultrasound (US) elastography, a new technique that images the elasticity of tissues, is now into the course of breast cancer diagnosis. The purpose of this study was to assess the diagnostic performance of a neural network using a combination of US elastography technique and US B-mode. A back-propagation neural network (BPN) is used to classify the breast masses as benign cyst, benign solid mass, or malignant solid mass using texture, strain, and morphological features computed from the segmented lesions. Sixty-two breast lesions in US elastography and US B-scan images that are biopsy proved are examined. A classification accuracy using a combination of US elastography and B-scan images is 87.09 %, sensitivity 89.29 %, specificity 85.29 %, positive predictive value 83.33 %, and the negative predictive value is 90.63 %. With statistically significant features, the classification accuracy using a combination of US elastography and B-scan images is reported to be 82.25 % with sensitivity 92.86 %, specificity 73.53 %, positive predictive value 74.29 %, and negative predictive value 92.59 %. The classification results indicate that US elastography in combination with US B-mode improves both sensitivity and specificity.

Keywords Ultrasound elastography · Elastic properties of tissues · Hardness and softness of lesions · Level set segmentation · Jacquard coefficient · Neural network

S. Selvan (✉) · S. Shenbagadevi
Centre for Medical Electronics, College of Engineering, Anna University, Chennai 600025, India
e-mail: shirleycharlethenry@gmail.com

S. Shenbagadevi
e-mail: s_s_devi@annauniv.edu

S. Suresh
Department of Fetal Medicine, Mediscan Systems, Chennai 600014, India
e-mail: mediscan@gmail.com

© Springer India 2015

L.P. Suresh et al. (eds.), *Artificial Intelligence and Evolutionary Algorithms in Engineering Systems*, Advances in Intelligent Systems and Computing 325,
DOI 10.1007/978-81-322-2135-7_24

1 Introduction

Mechanical measurements have shown that pathological tissue can be up to 30 times harder than normal tissue [1]. US elastography described by Ophir et al. [2–4] is a method for measuring the stiffness/elastic properties of tissues [5–7]. The basic operating principle of US elastography involves the comparison of the spatial arrangement of tissue before and after compression. This scanning modality, which can provide information about stiffness of the lesion, is currently used for detecting and identifying lesion in the breast. Paired images are obtained, consisting of the standard B-mode image on the left and a pure strain image on the right [8].

Benign lesions usually appear smaller or of the same size on sonograms as well as on elastograms. In case of malignant lesions, the size appears larger on the elastogram [9]. Unlike benign lesions that have smoother borders and are more loosely bound to the adjacent perilesional tissue, thereby being more mobile, malignant tumors are known to form stellate boundaries that become firmly bound to the surrounding tissue through infiltration. During an applied compression, benign lesions tend to undergo motion in an opposite direction to that of the compression. On the other hand, malignant lesions move in the direction of compression while pulling the perilesional tissue in the same direction, thereby causing the perilesional tissue also to appear harder on the elastogram as well [10]. Because of the ease with which compression can be applied to the breast, it is an ideal organ on which to perform elastography. Due to the relative stiffness of breast cancer tissue, as compared to benign fibroadenomas and cysts, a method such as elastography, which estimates tissue stiffness, may be an attractive tool for distinguishing benign from malignant lesions [5]. Computer-aided diagnosis using artificial neural network, genetic algorithm, and fuzzy logic have the potential to be a valuable decision-making tool for radiologists.

In this work, lesion areas in preprocessed ultrasound images of the breast, namely the B-scan and elastographic images, are segmented. Three sets of features, namely texture, strain, and shape features, are computed from the segmented lesions of both image types. A fully automated neural network classifier based on a combination of US B-scan and US elastography images is used for the classification of biopsy-proved benign solid mass, malignant solid mass, and benign cyst.

2 Methodology

2.1 Image Acquisition

This study is a retrospective analysis of stored images and has no impact on the clinical management of the patients, as all the patients have already been treated or were undergoing treatment. The stored images used for the study were anonymous. The US B-scan and US elastography images of 62 biopsy-proven lesions were taken from the database.

2.2 Segmenting the Lesion

The principal approach used in segmentation is to partition an image into two regions that are similar according to a set of predefined criteria [11]. Our automatic lesion segmentation algorithm involves the following steps: (1) preprocessing of US elastography and US B-scan images by speckle reducing anisotropic filter [12] to reduce noise and speckle, (2) an automatic threshold determination method proposed by Otsu [13] is used to convert the grayscale image into a binary image, (3) selecting a binary mask from the image, and (4) applying level set algorithm to segment the area of lesion. This algorithm is applied to both US B-scan and US elastography images. Figures 1, 2, and 3 show segmentation results of US B-scan images and elastograms of a malignant solid mass, benign solid mass, and benign cyst.

As seen in Figs. 1, 2, and 3, malignant masses are harder and therefore deform less than benign masses, besides they appear darker and larger than benign masses on an elastogram. A benign tumor would be of comparable size in both sonogram

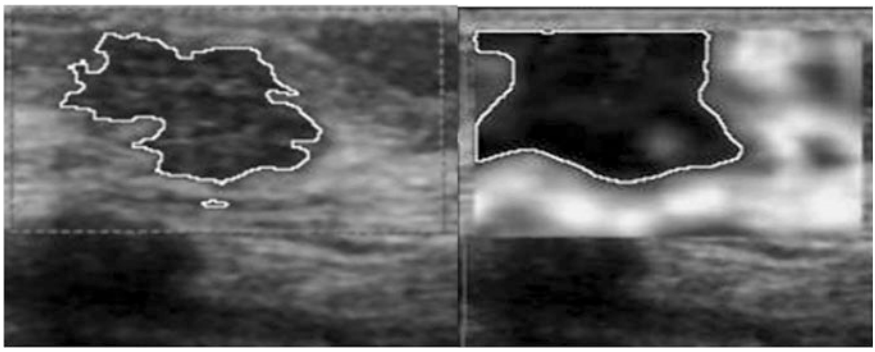

Fig. 1 Computer-delineated margin of malignant solid mass in ultrasound image and elastogram

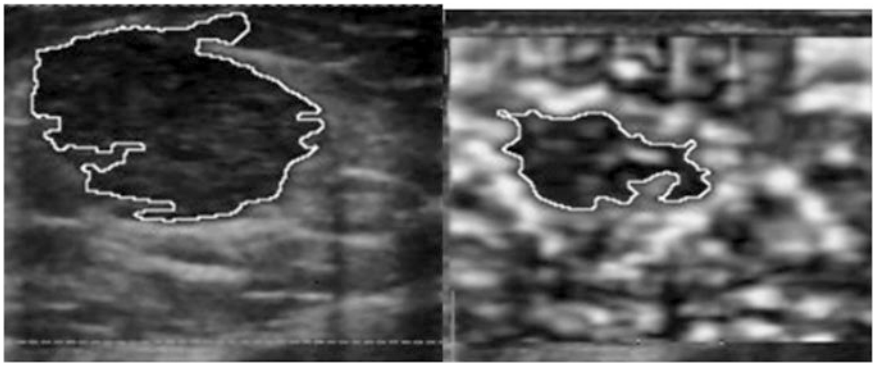

Fig. 2 Computer-delineated margin of benign solid mass in ultrasound image and elastogram

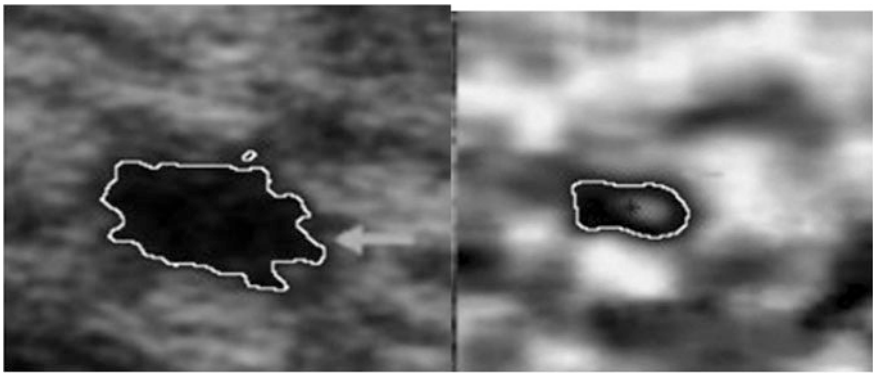

Fig. 3 Computer-delineated margin of benign cyst in ultrasound image and elastogram

and elastogram. A cyst is characterized by its inner echogenic substance and thin echogenic outer wall nature. As seen in Fig. 3, certain cysts are depicted as nidus (bull's eye appearance) in an elastogram [10]. The following section deals with the method of feature extraction used in our work.

2.3 Feature Extraction

The automatic feature extraction methodology from breast US B-scan and US elastography images used in this work has been described in our previous works [14, 15]. Based on the difference in size and shape of malignant solid mass, benign solid mass and benign cysts of elasticity images, and B-scan ultrasound images [4, 9], five features are extracted for each computer-determined lesion contour. They are area difference, perimeter difference, contour difference, solidity ratio, and width-to-height ratio [16]. Based on the fact that texture features represent changes of gray-level intensity, six second-order statistical features are computed for each computer-determined lesion contour from the gray-level co-occurrence matrix [17], namely standard deviation, energy, entropy, dissimilarity, homogeneity, and contrast. Four gray run length features, namely short-run emphasis (SRE), long-run emphasis (LRE), run length non-uniformity (RLN), and gray-level non-uniformity (GLN), are computed from GLRM [18]. Shape features, namely lesion area, eccentricity, solidity, form factor, height-to-width ratio of lesion, orientation, and perimeter, are computed. Based on pixel intensities, the features, mean gray value of lesion, softness of lesion, and hardness of lesion, are calculated. The posterior acoustic behavior is described using the feature minimum side difference [19]. The total number of features extracted is 45. The classification stage of the system which uses these features is described in the following subsection.

2.4 Classifier

In this work, a three-layer feed-forward back-propagation neural network (input layer, hidden layer, and output layer) is used to classify the type of lesion given strain, shape, and textural features indicative of malignant solid mass, benign solid mass, and benign cyst, as inputs. Sigmoid function is used as the activation function for the hidden layer and pure linear activation function for the output layer. The network has 'n' input nodes which would accept the 'n' input features and two output nodes to represent the three categories of breast masses. The input vector is of size $n \times 1$, and output vector is of size 2×1. A hidden layer consisting of seven neurons and an output layer consisting of two neurons are used. The number of nodes in the hidden layer, learning rate (0.01), and momentum constant are chosen based on the performance goal (mean square error = 0.0001), minimum execution time, and average number of epochs needed to converge. These parameters are chosen by trial and error.

In the present work, three neural networks are formed. One network is trained with only US B-scan features as inputs, another with only US elastography features, and the third with both US B-mode and US elastography features. A jackknife procedure is used to train the neural network. The neural network is trained with 61 samples, and the network is tested with the remaining one sample. The training procedure is repeated 62 times. The performances of the three networks in classifying the three groups are compared.

3 Results and Discussion

The above algorithm has been tested on 62 pairs of US B-scan and US elastography biopsy-proven images wherein 10 are benign cyst, 24 are benign solid mass, and the remaining 28 are malignant solid mass. The gold standard here is that all the images are biopsy proven.

3.1 Segmentation and Objective Measure of Segmentation Quality

The segmentation results are shown in Figs. 1, 2, and 3. For the purpose of evaluation of level set method of segmentation in US B-scan and US elastography images of breast, the sixty-two breast lesions in US B-scan and US elastography images were also segmented using k-means clustering. A radiologist verified the segmentation results. Tanimotto coefficient [20] which is also known as the Jacquard coefficient is used to provide some quantitative segmentation evaluation by measuring the region coincidence between the results of human segmentation and

Table 1 Performance analysis of segmentation methods

Method of segmentation	Tanimotto coefficient
Level set	0.816373
K-means clustering	0.3412

automatic segmentation. The Tanimotto coefficient is a measure of overlap between user-segmented lesion and algorithm-segmented lesion. The similarity metric, namely Tanimotto coefficient, is calculated for both methods. Tanimotto coefficient has a range from 0 to 1, where 0 indicates that the segmentations have no pixels in common and 1 indicates that the segmentations are identical. For a good overlap, the value of Tanimotto coefficient equals one. Tanimotto coefficient is defined using Eq. (1). In Eq. (1), n_a is number of pixels inside user-segmented lesion, n_b is number pixels inside algorithm-segmented lesion, and n_{ab} is the number of pixels common to both user-segmented lesion and algorithm-segmented lesion.

$$\text{Tanimotto coefficient} = \frac{n_{ab}}{(n_a + n_b - n_{ab})} \tag{1}$$

Table 1 shows that level set method is superior to *k*-means clustering in segmentation of ultrasound B-mode and elastography images

3.2 Feature Extraction

LRE is highly dependent on the occurrence of long runs and is large for coarse structural textures. It is greater for homogeneous masses compared to non-homogeneous masses. A benign mass tends to appear uniform and has more number of long runs. A malignant mass is heterogeneous, appears to be non-uniform, and has less number of long runs. LRE is high for benign mass and low for malignant mass. SRE is low for benign mass and high for malignant mass. RLN measures similarity of length of runs throughout the image. It is less if run lengths are alike throughout. RLN is less for homogeneous masses and greater in non-homogeneous masses. In an elastogram, soft tissues are displayed as lighter shades of gray and harder tissues are displayed as darker shades of gray. Cancers are much harder than any of the other breast tissues and benign masses. They appear uniformly and much darker (firmer) than the surrounding tissue and many other benign lesions. Cysts also appear as a uniformly dark area or as an area with both bright and dark regions [21]. The feature, mean gray value is the average of pixel intensities inside the mass. It is high for benign cysts and benign solid masses and is low for malignant solid masses. The grayscale intensities in an ultrasound image vary from 0 to 255. A breast elastogram is a grayscale image whose grayscale intensities correspond to strain incurred in the breast tissues following a slight compression. Hard tissues undergo less strain on compression and are displayed as darker shades of gray in an elastogram.

In the present work, with the above idea, pixels with intensities 255 down to 128 are considered to be soft pixels and pixels with intensities 0–128 are noted as hard pixels. This is followed by calculation of hardness of a mass as the average of hard pixels (pixel intensities less than 128). Hardness is more for malignant solid mass and less for benign solid mass and cyst. Soft tissues are displayed as lighter shades of gray. Softness of a mass is the average of soft pixels (pixel intensities greater than 128). Softness is less for malignant solid mass and large for benign solid mass and cyst. The posterior acoustic behavior feature is minimum side difference (MSD) defined as

$$\mathrm{MSD} = \min\left(A_{\mathrm{posterior}} - A_{\mathrm{left}},\, A_{\mathrm{posterior}} - A_{\mathrm{right}}\right) \tag{2}$$

In Eq. (2), $A_{\mathrm{posterior}}$, A_{left}, and A_{right} are average gray-level values over the appropriate ROI. It is more negative for malignant solid masses [19].

Solidity representing the regularity of a lesion is greater for benign solid mass and benign cyst having smooth shapes. Form factor, a shape feature equals one, when the mass appears as a perfect circle and equals zero for a wavy and twisty mass. It is low for malignant and high for benign masses. Eccentricity, a shape feature is less than one when the mass appears elliptical and equals zero when the mass appears as a perfect circle. Perimeter refers to number of pixels in the boundary of a lesion. It is length of the nuclear envelope calculated as the length of a polygonal approximation of the boundary (B), where p is perimeter of lesion.

$$p = \sum_{x \in B} l \longrightarrow \tag{3}$$

Area of malignant mass is larger in an elastogram. Hence, perimeter is larger for malignant mass compared to the other masses. A statistical analysis of US B-mode, US elastography, and strain features is done using SPSS version 17. A one-way ANOVA is run to determine whether there were significant differences in features between the three groups, malignant solid mass, benign solid mass, and benign cyst. One-way ANOVA test revealed that there is a statistically significant difference in US B-mode features among the three groups in terms of height to width of lesion (p value = 0.032), SRE (p value = 0.029), and RLN (p value = 0.020). However, the results of one-way ANOVA tests indicate that there is no significant difference between the three groups as far as the other features extracted from ultrasound B-mode images are concerned. There is no statistically significant difference among the three groups in terms of strain features. There is a statistically significant difference among the three groups in terms of elastographic entropy (p value = 0.016). Differences between the three groups were statistically very significant for values of elastographic homogeneity (p = 0.016), lesion area (p = 0.020), mean gray value (p = 0.011), hardness of the lesion (p = 0.029), and softness of the lesion (p = 0.034). Hence, it is appropriate to combine the information obtained from both US elastography and US B-scan images for better diagnosis.

Receiver operating characteristic (ROC) analysis is used to evaluate the performance of individual computer-extracted features in the task of distinguishing the three groups. Figure 4a shows ROC curves of statistically significant ultrasound features for benign solid masses and their A_z values. Figure 4b shows ROC curves of statistically significant ultrasound features for malignant solid masses and their A_z values. Figure 4c shows ROC curves of statistically significant ultrasound features for benign cysts and their A_z values. Figure 5a shows ROC curves of statistically significant US elastography features for benign solid masses and their A_z values. Figure 5b shows ROC curves of statistically significant US elastography features for malignant solid masses and their A_z values. Figure 5c shows ROC curves of statistically significant US elastography features for benign cysts and their A_z values.

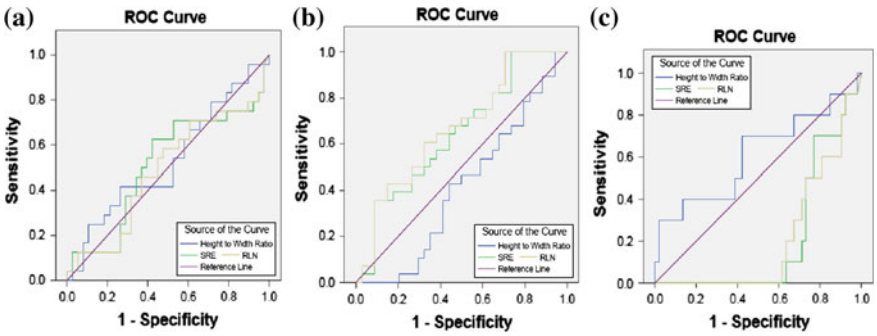

Fig. 4 ROC curve for significant ultrasound features of **a** benign solid masses, **b** malignant solid masses, and **c** benign cysts

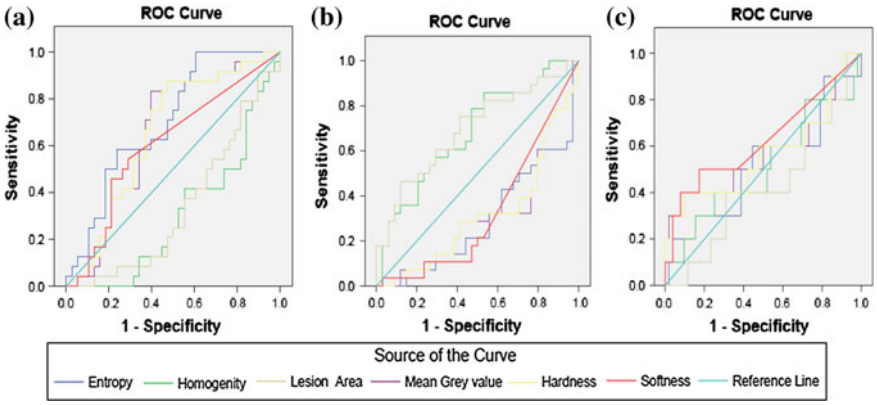

Fig. 5 ROC curve for significant elastography features of **a** benign solid masses, **b** malignant solid masses, and **c** benign cysts

Table 2 Performance analysis of the network trained with US B-scan, US elasto, and strain features

Modality	Features	Sensitivity (%)	Specificity (%)	Positive predictive value	Negative predictive value	Accuracy (%)
US B-scan	MSD, SRE, RLN, GLN	96.43	67.65	71.05	95.83	80.64
US elastography	Energy, contrast, eccentricity, mean gray value, hardness, softness, perimeter	85.71	70.59	70.59	85.71	77.42
Strain, US B-scan and US elastography	MSD, SRE, RLN, GLN, energy, contrast, eccentricity, mean gray value, hardness, softness, perimeter, solidity ratio, perimeter difference	89.3	85.31	83.33	90.63	87.1

3.3 Classification

Sixty-two pairs of ultrasound B-mode and US elastography biopsy-proven images are used for testing, of which 10 are benign cysts, 24 are benign solid masses, and the remaining 28 are malignant solid masses. The gold standard here is that all the images are biopsy proven. The performance analysis of networks trained with ultrasound B-mode features, US elastography features, and combination of both ultrasound and elastographic features are shown in Table 2.

Table 3 shows the performance analysis of networks trained with statistically significant ultrasound B-mode features, US elastography features, and combination of ultrasound B-mode and ultrasound elastographic features.

Ultrasound B-mode features provide more sensitivity, and elastography features provide more specificity. Therefore, a combination of both ultrasound B-mode and elastography features improves the accuracy rate.

Table 3 Performance analysis of the network trained with significant one-way ANOVA US B-scan and US elastography features

Modality	Features	Sensitivity	Specificity	Positive predictive value	Negative predictive value	Accuracy
US B-scan	Height to width, SRE, RLN	96.43	47	60	94.11	69.35
US elastography	Entropy, homogeneity, lesion area, mean gray value, hardness, softness	85.71	61.76	64.86	84.00	72.58
US B-scan and US elastography	Height to width, SRE, RLN, entropy, homogeneity, lesion area, mean gray value, hardness, softness	92.86	73.53	74.29	92.59	82.25

4 Conclusion

Our study results suggest that the use of B-mode sonography with high sensitivity, in combination with US elastography with high specificity, may increase diagnostic performance when differentiating between benign and malignant breast masses. In summary, we have developed a CAD method based on strain, shape, and texture features for the classification of breast masses. The study is performed on a database of 62 image pairs. The classifier showed encouraging results in case of sensitivity for different combinations of features. From experimental results, we can conclude that more number of samples have to be used both for training and testing to obtain better results. Neural network can provide better results, if care is taken in design of network architecture. In the forthcoming work, the performance of classifiers trained with only GLCM texture features, only GRLM run length features, only strain features, only shape features, and finally a combination of all the above features is to be compared. The computerized level set segmentation in the present study is semiautomatic. Seed point selection and contour initialization can be automated in both US B-scan and US elastography images to make segmentation of breast lesions computationally easier, more accurate, and fast.

References

1. D.M. Parkin, F. Bray, J. Ferlay, P. Pisani, Global cancer statistics. CA Cancer J. Clin. **55**, 74–108 (2005)
2. J. Ophir, I. Cespedes, H. Ponnekanti, Y. Yazdi, X. Li, Elastography: a quantitative method for imaging the elasticity of biological tissues. Ultrasound Imag. **13**, 111–134 (1991)

3. J. Ophir, I. Cespedes, B. Garra, H. Ponnekanti, Y. Huang, N. Maklad, Elastography: ultrasonic imaging of tissue strain and elastic modulus in vivo. Eur. J. Ultrasound **3**, 49–70 (1996)
4. J. Ophir, S.K. Alam, B. Garra, F. Kallel, E. Konofagou, T. Krouskop, C.R.B. Merritt, R. Righetti, R. Souchon, S. Srinivasan, T. Varghese, Elastography: imaging of the elastic properties of soft tissues with ultrasound. J. Med. Ultrason. **29**, 155–171 (2002)
5. J. Ophir, S.K. Alam, B. Garra, F. Kallel, E. Konofagou, T. Krouskop, T. Varghese, Elastography: ultrasonic estimation and imaging of the elastic properties of tissues. Proc. Instn. Mech. Engrs. **213**, 203–233 (1999)
6. T. Rago, F. Santini, M. Scutari, A. Pinchera, P. Vitti, Elastography: new developments in ultrasound for predicting malignancy in thyroid nodules. J. Clin. Endocrinol. Metab. **92**, 2917–2922 (2007)
7. T. Wilson, Q. Chen, J.A. Zagzebski, T. Varghese, L. Van Minddlesworth, Initial clinical experience imaging scatterer size and strain in thyroid nodules. J. Ultrasound Med. **25**, 1021–1029 (2006)
8. T.J. Hall, Y. Zhu, C.S. Spalding, In vivo real-time freehand palpation imaging. Ultrasound Med. Biol. **29**, 427–435 (2003)
9. E.E. Konofagou, T. Harrigan, J. Ophir, Shear strain estimation and lesion mobility assessment in elastography. Ultrason. **38**, 400–404 (2000)
10. R.G. Bar, A.E. Lackey, The utility of the "bull's-eye" artifact on breast elasticity imaging in reducing breast lesion biopsy rate. Ultrasound Q. **27**(3), 151–155 (2011)
11. C. Li, C. Xu, C. Gui, M.D. Fox, Level set evolution without re-initialization: a new variational formulation, in *Proceedings of the IEEE Conference on Computer Vision and Pattern Recognition*, (2005) pp. 430–436
12. Y. Yu, S.T. Acton, Speckle reducing anisotropic diffusion. IEEE Trans. Image Process. **11**, 1260–1270 (2002)
13. N. Otsu, A threshold selection method from gray-level histograms. IEEE Trans. Syst. Man Cybern. **9**(1), 62–66 (1979)
14. S. Selvan, M. Kavitha, S. Shenbagadevi, S. Suresh, Feature extraction for characterization of breast lesions in ultrasound echography and elastography. J. Comput. Sci. **6**(1), 67–74 (2010)
15. S. Selvan, M. Kavitha, S.S. Devi, S. Suresh, Fuzzy based classification of breast lesions using ultrasound echography and elastography. Ultrasound Q. **28**(3), 159–167 (2012)
16. S. Selvan, M. Kavitha, S. Shenbagadevi, S. Suresh, Automatic segmentation and feature extraction of breast lesions. Int. J. Comput. Intell. Healthc. Inform. **3**(2) 65–69 (2010)
17. R. Haralick, K. Shanmugam, I. Dinstein, Texture features for image classification. IEEE Trans. Syst. Man Cybern. **3**, 610–621 (1973)
18. M.R. Chandraratne, S. Samarasinghe, D. Kulasiri, R. Bickerstaffe, Prediction of lamb tenderness using image surface texture features. J. Food Eng. **77**(3), 492–499 (2006)
19. K. Horsch, M.L. Giger, Computerized diagnosis of breast lesions on ultrasound. Med. Phys. **29**(2), 157–164 (2002)
20. R.O. Duda, P.E. Hart, *Pattern classification and scene analysis* (John Wiley & Sons, Menlo Park, California, 1973), p. 216
21. T.A. Krouskop, T.M. Wheeler, F. Kallel, B.S. Garra, T. Hall, Elastic moduli of breast and prostate tissues under Compression. Ultrason. Imaging **20**, 260–274 (1998)

A Convivial Energy Based Clustering (CEBC) Solution for Lifetime Enhancement of Wireless Sensor Networks

Betty Madhurya Vallapuram, Gokul P. Nair and Kaliraja Thangamani

Abstract Wireless sensor network requires robust and energy efficient communication protocols to minimize the energy consumption as much as possible. Numerous energy-based cluster head election algorithms have been proposed and implemented. However, the capacities and workloads of the neighbors of cluster heads have not been considered in large wireless sensor networks. A convivial energy-based cluster (CEBC) head selection scheme where cluster heads are elected based on the energy value of a node and the energy values of its neighbors is proposed in this paper. This is to ensure that the neighbor nodes within the one hop range of a cluster head do not drain off their energy while forwarding the data to the other member nodes, especially in large networks. Simulations in network simulator have proved that CEBC cluster head selection scheme has improved the lifetime of the network compared to the LEACH protocol.

Keywords CEBC · LEACH protocol · Wireless sensor network · Multi-hop communication · HEED

B.M. Vallapuram (✉)
Vee Eee Technologies Solutions Pvt. Ltd, Chennai, Tamil Nadu, India
e-mail: valpabetty@yahoo.com

G.P. Nair
ENZEN Global Solutions Pvt Ltd, Madiwala, Bangalore, Karnataka, India
e-mail: gokulpnair@outlook.com

K. Thangamani
Electronics and Communication Engineering, SKR Engineering College, Agarmel, Chennai, Tamil Nadu, India
e-mail: kali_thangamani@yahoo.com

© Springer India 2015

L.P. Suresh et al. (eds.), *Artificial Intelligence and Evolutionary Algorithms in Engineering Systems*, Advances in Intelligent Systems and Computing 325,
DOI 10.1007/978-81-322-2135-7_25

1 Introduction

Wireless sensor network (WSN) requires robust and energy efficient communication protocols to minimize the energy consumption as much as possible. All sensor nodes continuously sense the information that they are meant to and the sensed information will be delivered to one or more sinks, generally via multi-hop communication.

The sensor nodes are often deployed to not easily accessible or hostile environment, sometimes in large quantities, and are typically expected to operate with batteries only. It can be difficult or impossible to replace the batteries of the sensor nodes. Conversely, the base station (sink) is typically rich in energy as it requires continuously receiving the sensed information transmitted by the various sensor nodes and updating its corresponding database. The efficient utilization of the energy to prolong the network lifetime has been the focus of much of the research on the WSN. Since multi-hop routing is generally needed for distant sensor nodes from the sinks to save energy, the nodes near a sink can be burdened with relaying a large amount of traffic from other nodes.

1.1 Characteristics and Challenges of Wireless Sensor Networks

The main characteristics and challenges of a WSN include: power consumption limitations for nodes using batteries or energy harvesting; ability to cope with node failures that are likely to occur; heterogeneity of nodes; scalability to large-scale deployment; communication failures that occur unpredictably; and potential to withstand harsh environmental conditions.

Out of all the above issues, power consumption is one of the major and significant concerns during the design of a WSN. The ways and methods to preserve best energy during the network operations aim at distribution of tasks to all the wireless sensor nodes for extending the lifetime of the WSN. Sensing operation in wireless sensor networks consumes lesser energy than the energy consumed by a node to perform cluster head operation. Hence, there is a need for a rotation of the cluster heads at every interval of time. Energy consumption in wireless systems is directly proportional to the square of the distance, and single-hop communication is expensive in terms of energy consumption [1]. During such a rotation process, this paper proposes a solution to perform efficient cluster head election called convivial energy-based clustering scheme. The simulation and analysis of the proposed scheme is performed by means of network simulator explained in the sections that follow.

2 Literature Review

As consequence of a lot of research being done in this area, a good number of methods have emerged to extend the lifetime of the wireless sensor network. In LEACH, each cluster head cluster heads (CH) directly communicates with the base station (BS) which will consume a lot of its energy if the distance is far. On the other hand, multi-hop LEACH protocol by Xiangning [2] selects optimal path concerned between the CH and the BS through other CHs and use these CHs as relay stations to transmit data over through them. Multi-hop communication is initially adopted among CH's. According to the selected optimal path, these CHs transmit data to a CH, which is nearest to BS that ultimately sends the information to the BS. M-LEACH protocol only makes communication mode from single-hop to multi-hop between CHs and BS.

The hybrid energy efficient distributed clustering protocol (HEED), proposed by Younis and Fahmy [3], picks up the cluster head from a group of nodes on the basis of a residual energy and other parameters like the node degree or proximity of the nodes to the sink node. The protocol was found to be providing an extended lifetime to the network compared to the LEACH network. This model employs dynamic hierarchical clustering in which the cluster head changes after particular intervals of time on the basis of the residual energy and duty cycle of the nodes. The efficiency is enhanced when hierarchical clustering is implemented by considering the traffic in the network.

The idea of considering energy remaining in a node as a selection factor for a node a cluster head during the clustering operation remains as a strong motivation for the proposal of the convivial energy-based cluster (CEBC) clustering algorithm.

3 Proposed Algorithm

Clustering-based algorithms are believed to be the most efficient routing algorithm for the WSNs. The steps involved in the CEBC clustering algorithm are as follows: data collection by the base station, energy-based clustering, and cluster head selection based on node degrees.

3.1 Data Collection

During the data collection process, the base station collects the data from all the nodes. Mostly, the data collected by the base station could be the node id's, locations, etc. In this algorithm, the data collection of the energy values of each node is a necessary criterion.

Figure 1 shows the architecture of the CEBC clustering algorithm. In the above figure, the nodes 1, 2, 3, 4, and 5 form the neighbor list of the node 0 considered for

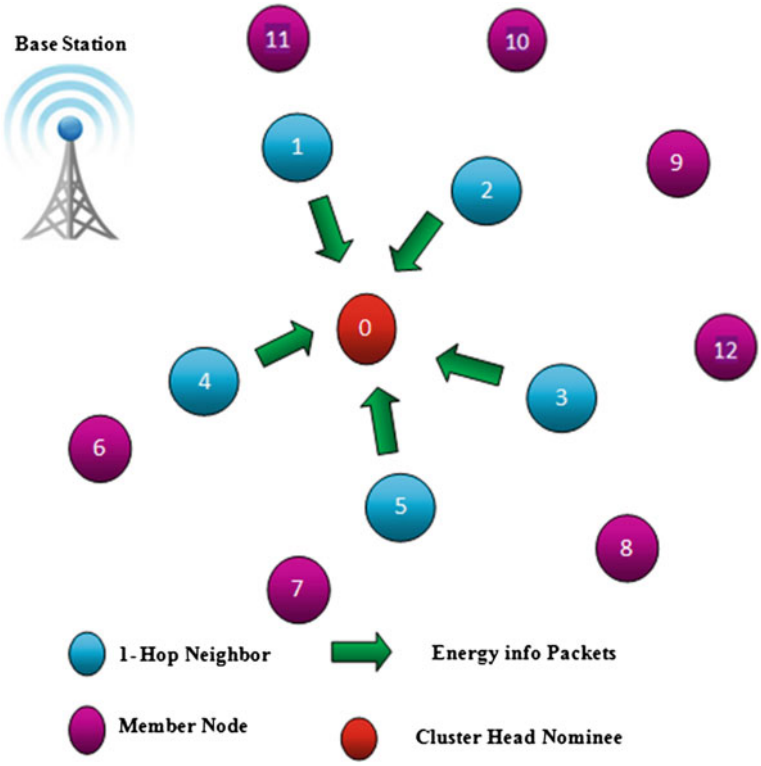

Fig. 1 Architecture of CEBC illustrating the significance of neighbor nodes

the cluster head selection (called as the cluster head nominee). The energy values of the nodes in the neighbor list are considered to make efficient cluster head selection process in this architecture. All these nodes should be within one hop distance of the cluster head nominee. Only energy information from these nodes is considered, and the CEBC algorithm uses this information to decide whether to promote the cluster head nominee to the cluster head or to find another nominee.

3.2 Cluster Head Selection Using CEBC

The cluster heads are special nodes with higher energy than normal node depending on the algorithm and application. Cluster head selection process is one of the main key processes in clustering, and it has a lot of significance in the lifetime of a wireless sensor network. The cluster head selection process should not be too complicated that is consumes a lot of time, energy, and other resources, yet it has to be able to select the appropriate cluster head.

Determine the maximum energy node The first step in the cluster section process is to find the node that has the maximum energy. When the data collection process is completed, the energy values of the nodes $e(n)$ are analyzed. The node with the maximum energy value is considered for the next step of this process. The working flow of this process is illustrated in Fig. 2.

Calculate Convivial Energy Value The convivial energy value is a parameter that is designed for the calculation of the energy value of a node to be a cluster head in relation to the energy value of the neighbors. This is calculated by using the AvgE (j) value and the $e(n)$ value as in the following Eq. (1).

$$\mathrm{Ce}(n) = W1{*}\mathrm{AvgE}(j) + W2\ e(n) \tag{1}$$

Fig. 2 Working of CEBC

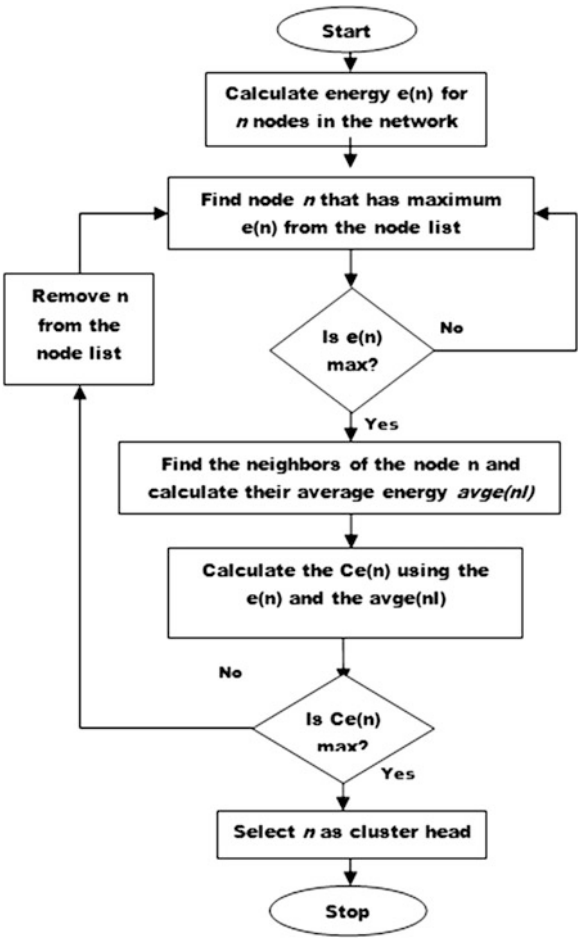

where $W1$ and $W2$ are the weights of AvgE(n) and $e(n)$, usually, $W2 > W1$ because the energy of the CH has more significance than the energy of the neighbors to the CH. Based on this equation, the node with the highest Ce(n) value will be the cluster head. If two nodes have equal $e(n)$ or Ce(n) values, then the node closest to the base station is preferred to be the CH.

3.3 Cluster Head Selection Using CEBC

The CH performs computational functions such as data aggregation and data compression in order to reduce the number of transmissions to the base station (or sink) thereby saving energy. The sensed information is processed after the collection of the same from the various cluster members by the CH. Inter-cluster communication and intra-cluster communication can be implemented from the conventional methods (e.g., HEED [4]). The weights can be calculated by [5] or [6].

4 Simulation Results

The simulator that is used to analyze the system performance is the network simulator (NS2). The NS2 is a discrete event time-driven simulator that is used to analyze the performance of a network. In this simulation, the nodes are distributed in the simulation area 1,420 × 500 and the ad hoc on-demand distance vector (AODV) routing protocol. The parameters used in the CEBC simulation are described in Table 1.

4.1 Packet Delivery Rate

The packet delivery ratio is one of the quality of service (QoS) metrics to evaluate the performance of network. Low PDR depletes the network performance. In Fig. 3, the packet delivery rates of the conventional energy-based clustering for the WSN

Table 1 Simulation parameters for the simulation of CEBC scheme

Parameter	Value
Channel type	Wireless channel
Network interface type	Wireless Phy
Number of nodes	25
Radio propagation model	Two ray ground
Antenna type	Omni antenna
Simulation time	60 ms
Routing protocol	AODV
Traffic model	Constant bit rate

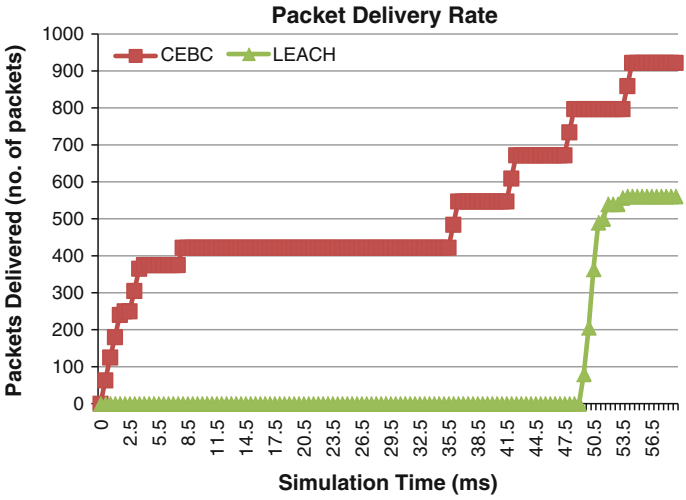

Fig. 3 Packet delivery ratio of CEBC and LEACH

considered (LEACH) and the CEBC clustering algorithm are shown in the form of a graph against time. The CEBC clustering scheme has high packet delivery ratio than LEACH in the network.

4.2 Packet Loss Rate

The packet loss ratio is the maximum number of packets possible to be dropped by a node. Figure 4 shows the graph plotted between the number of packets dropped and the time period. The green color curve shows the performance of LEACH, and the red color curve denotes the performance of the CEBC clustering. For the proposed scheme, packet loss ratio for CEBC clustering is lower than LEACH.

4.3 Residual Energy

The residual energy is energy remaining in a node. Figure 5 shows the residual energy of CEBC clustering is considerably higher than LEACH. Residual energy analysis shows the actual energy difference. The green color curve shows the energy performance of LEACH, and the red color curve denotes the energy performance of the CEBC clustering.

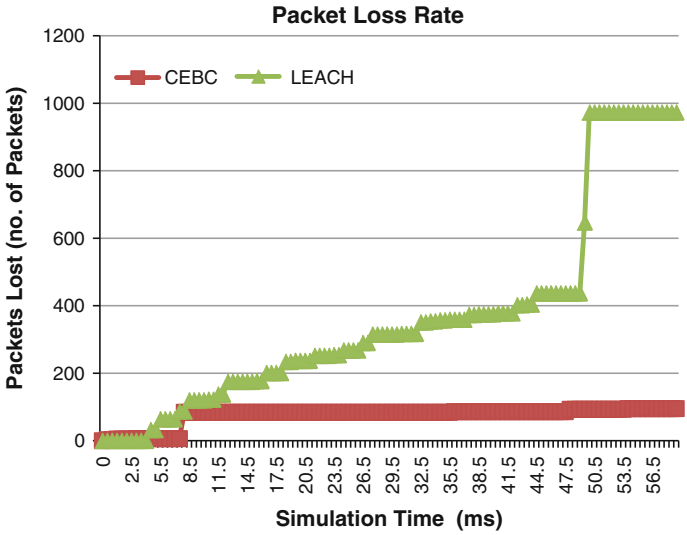

Fig. 4 Packet loss ratio of CEBC and LEACH

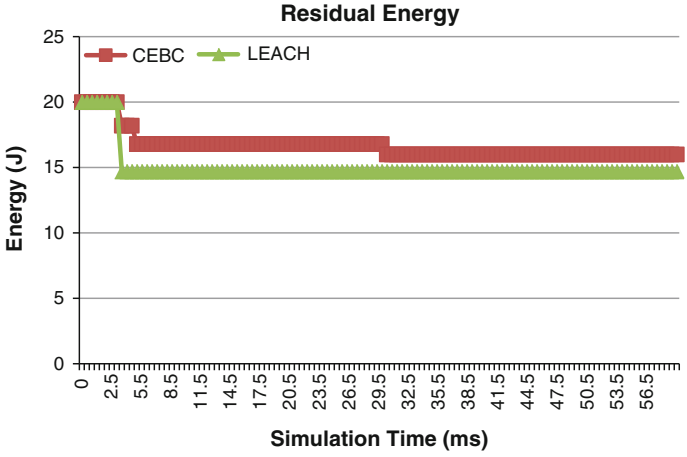

Fig. 5 Residual energy of CEBC and LEACH

4.4 Delay

The delay occurred during data transmission in LEACH and CEBC is shown in Fig. 6. The neighbor energy computation does not take much time, and hence, the dynamic computation shows lesser delay in CEBC.

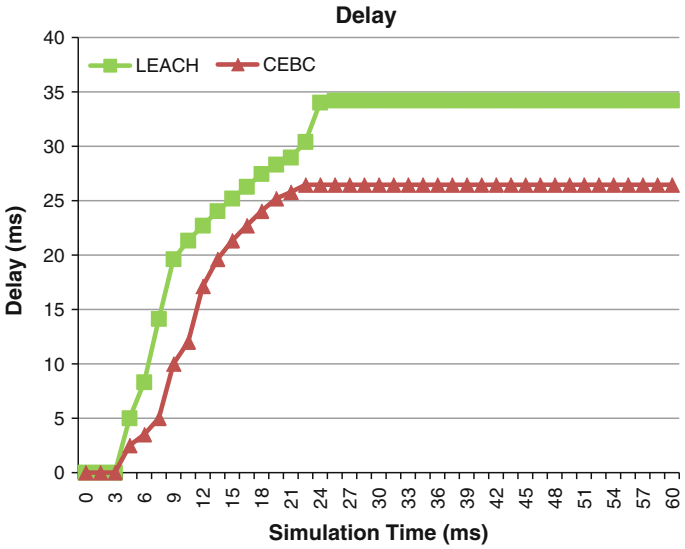

Fig. 6 Delay of CEBC and LEACH

5 Conclusion

A CEBC head selection scheme, where cluster heads are evaluated based on the energy values of the node and the energy values of its neighbors, was proposed in this work. This is to ensure that the neighbor nodes within the one hop range of a cluster head do not drain off their energy while forwarding the data to the other member nodes. Simulations in network simulator have proved that CEBC scheme has improved the lifetime of the network compared to the cluster head selection based on energy of the cluster head alone.

Real-time implementations of this CEBC protocol can be implemented in a test bed scenario in the future research. Further research can be done on how this CEBC clustering algorithm can be further simplified and yet can stand alone as an efficient clustering protocol satisfying the needs of a day-to-day operation of WSNs at large.

Acknowledgments I express my gratitude to my lecturers Mr. James Malcolm, Ms. Hannan Xiau, and Dr. Najah Khadim, University of Hertfordshire, UK, for teaching me the wireless networking concepts and simulation methods using network simulator.

References

1. A.K. Thomas, R. Devanathan, Variable duty-cycle based efficient network discovery in WSN. Eur. J. Sci. Res. **93**(2), 266–278 (2012)
2. F. Xiangning, S. Yulin, Improvement on LEACH protocol of wireless sensor network, in *International Conference on Sensor Technologies and Applications* (*SensorComm '07*), (*IEEE, October 2007*), pp. 260–264
3. O. Younis, S. Fahmy, HEED: a hybrid, energy-efficient, distributed clustering approach for ad hoc sensor networks. IEEE Trans. Mob. Comput. **3**(4), 366–379 (2004)
4. A. Abbasi, M. Younis, A survey on clustering algorithms for wireless sensor networks. Comput. Commun. 2826–2841 (2007)
5. R. Tandon, B. Dey, S. Nandi, Weight based clustering in wireless sensor networks, in *Proceedings of the IEEE National Conference on Communications* (*NCC*) (2013)
6. S.H.N. Choi, K.O. Lee, K.W. Rim, A weight-based unequal clustering routing protocol in wireless sensor network, in *Proceedings of IEEE International Conference on Information and Communication Technology* (*ICT4M*) (2010)
7. L.H.M. Mercy, K. Balamurugan, M. Vijayaraj, Maximization of lifetime and reducing power consumption in wireless sensor network using protocol. Int. J. Soft Comput. Eng. (IJSCE) **29**(6) (2013)
8. D.G. Reina, S.L. Toral, P. Jonhson, F. Barrero, Hybrid flooding scheme for mobile ad hoc networks. IEEE Commun. Lett. **17**(3) (2013)

Wind Power in India—An Overview

T.V. Gowtham, G.R. Venkatakrishnan and R. Rengaraj

Abstract The present scenario in the world including India experiences increase in electrical power demand due to the recent advancement in the technologies. Fossil fuels are predominantly used to meet the increase in demand, leading to the depletion. Henceforth, it is necessary that an alternative source of energy must be utilized along with the fossil fuels to meet the demands. Renewable energy sources, an eco-friendly source of energy, could be effectively used in meeting the crises faced by the world in terms of power demand, emission of greenhouse gases, and so on. Wind energy, a type of renewable energy sources, could be used in an effective manner, compared to other renewable energy sources, to meet the crisis. The problem faced in dispatching and integrating wind energy with the grid is the randomness of the wind, which makes the wind prediction, a necessary factor to determine. This paper explores the difficulties and challenges faced in integrating and dispatching wind power generation with the existing grid in India.

Keywords Renewable energy sources · Solar energy · Wind energy · Hydropower · Conventional energy

1 Introduction

In general, the electrical power can be generated in two ways: (1) using conventional energy sources and (2) using renewable energy sources. The present electrical grid in general performs three main operations namely generation, transmission,

T.V. Gowtham (✉) · G.R. Venkatakrishnan · R. Rengaraj
Department of Electrical and Electronics Engineering, SSN College of Engineering, Kalavakkam, Chennai 603110, India
e-mail: gautham-eee2008@gmail.com

G.R. Venkatakrishnan
e-mail: grvk89@gmail.com

R. Rengaraj
e-mail: rengaraj81@gmail.com

© Springer India 2015

L.P. Suresh et al. (eds.), *Artificial Intelligence and Evolutionary Algorithms in Engineering Systems*, Advances in Intelligent Systems and Computing 325,
DOI 10.1007/978-81-322-2135-7_26

and distribution along with interconnection of network. In present electricity grid, the demand in the distribution network has been accomplished by using conventional energy sources.

Conventional power generation sources such as coal, fossil fuel, and so on lead to environmental issues such as greenhouse effect which causes global warming, depletion of ozone layer, carbon emissions, and so on. Due to the disadvantages of the conventional energy sources, the world would be in a situation, where conventional power generation will become impossible and causing to a destruction of our green planet by global warming. The renewable energy sources when combined with conventional energy sources for energy production reduces the effect of conventional energy sources to the planet.

The different renewable energy sources that are used across the globe are solar, wind, biomass, hydrothermal and geothermal. Solar energy, a good source of energy, with zero emission does not work during night time and winter season. Wind energy, a form of solar energy which does not contribute to global warming, is unpredictable. Biomass, a better source involving burning of gas, causes global warming. Hydro power, which does not contribute to global warming, is almost constant throughout the year but place to construct a dam must be considered.

Conventional power generation around the world is about 78.3 % and in India is about 68 % by the end of 2012, and the renewable energy generation around the world is 21.7 % and in India is 32 %. Wind energy contributes 6 % of the total renewable energy in the world and 70.4 % in India. Section 2 discusses the drawback of conventional and importance of renewable energy. The importance of wind energy and general process of wind energy, its potential sites, and techniques adapted around the world are discussed in Sect. 3. The economic growth and availability of high wind potential in India, problems faced in integrating wind energy, and obtaining optimal solutions for effectively utilizing wind power with policies developed by the government are discussed in Sect. 4.

2 Importance of Renewable Energy

The increase in consumption of power across the world is due to increase in population. Due to this increasing factor, there exists an increase in generation of power from conventional sources, which results in depletion of natural resources and also the earth crust becomes unstable due to mining which causes earthquake and pollution to the earth.

The total power generated through conventional sources is nearly 80 %. The carbon dioxide and carbon monoxide developed cause greenhouse effect producing so much of pollution throughout the year and depletes the fossil fuel rapidly and also ozone layer. Mining of fossil fuels from earth's crust also disturbs the earth's surface and leaving the layer of the earth unstable.

As a remedy, and to avoid maximum use of conventional resources, renewable resources can be utilized, which are eco-friendly. World is focussing on renewable resources to meet the demand, without affecting the environment.

Hydropower, delivering 19 % of the world's electrical energy, requires very high investments, but extremely reliable and has low maintenance cost in playing its lead role for more than a century [1]. Peak electricity demand can be managed by natural and pumped storage dams. Hydropower is cheap compared to conventional energy.

Although it has advantages, land and eco-systems are lost, also altering the drainage and sedimentation. Through siltation, about 0.5–1 % of capacity is lost. Apart from the effect of climatic changes, recent type dams have failure rate of 0.5 %. Awareness of political risks, social, and ecological risks are greater than before. Dams with less than 10 MW generations can be considered to be less precautious.

Wind energy contributes nearly 7 % of renewable energy generation in the world. Worldwide, there are great sites found in coastal areas for wind power, which is considered as indirect solar energy, as wind depends on heat, creating low and high pressures. The contained energy in the wind increases with cube of the wind speed, causing big change in output, even in small wind speed variation, which is limited to [1]. Wind sites in most countries have not been assessed. Energy extracted from the wind is limited to 59 % (BETZ limit), making necessary for good potential wind site.

For potential wind sites, offshore wind energy is preferred. About 20–25 % of rated power output is got from land and about 30 % from offshore, annually. Due to lack of calibration or environmental issues, the weather station statistics are undependable. Wind mills have average service life of 20 years and operating wind speeds of 3–25 m/s. The land used for wind energy production is much less than hydropower plant and can be used for agricultural purpose. The noise from the wind production plant has been largely minimized in recent years.

Dissimilar to wind, solar a direct solar energy is considered as being virtually limitless. It contributes nearly 0.5 % of total renewable energy production. Its nature is distributed, which is an advantage of this energy [1]. This power could be extracted only during day time. Climatic condition also affects the power generation from this energy source.

Biomass, contributes 1.3 % of renewable among the world is produced using biogas, corresponds to nearly 30 % of sugarcane, by sugarcane crushing. This is used for cogeneration in sugar mill in 300 million tonnes of sugarcane; 90 million tonnes of biogas are produced [1].

Among the various energy resources, wind energy is one of the fast developing resources around the world and in India. Wind energy affects power quality and creates fluctuations; as random nature power cannot be generated constantly, it can be generated only when wind is available and on connecting such source to grid it creates problem, which will be discussed in the next section.

3 Wind Energy

Wind is being used as a source of power for many years. Due to environmental issues and depleting conventional resources, generation of electricity from wind plays a key role [2]. The operational characteristics are very much unlike the others and face a challenge to integrate in facilitating wind in achieving its maximum energy [3].

Wind power is being utilized for many years. Because of depleting conventional energy resources, wind energy has gained advantage and has become a safe and competitive means of electric power generation [2]. Therefore, developing wind energy has become main objective among all countries [4].

Wind turbines consist of wind energy conversion system, converting wind power into mechanical power and then into electrical power by means of generator. These turbines are placed in the potential sites of wind power energy [5]. The energy thus produced is free from pollution and environmental effects. Wind energy used is limited, due to restriction on the climatic and environmental aspects as in [5].

To utilize the wind energy to possible extent, pre-assessment of wind energy is particularly important, which is done by meteorological office [5].

The paper [6], for wind energy system, discusses about an accurate procedure for choosing the best site and suitable wind turbine depending on minimum cost for kWh.

4 Wind Energy in India

India is rich in natural resources and sources of energy, and these resources are unevenly dispersed throughout the country. India along with China is being predicted that it is one of the countries to consume 28 % of energy among the total world's energy consumption [4, 7], and therefore, India's demand on electricity continued to raise bringing electricity shortages and 40 % of the population have no access to modern energy services. The energy available can be used optimally to make available reliable supply of power to every house in the country [8]. India is one of the fastest wind energy growing countries in the world [9]. The key-driving features for such a development are the favorable revenue policies by Indian government and supportive regulatory policies. Geographical location and wind potential are the main advantage for such a growth and are blessed with 7,516 km of coastline [10]. India's territorial waters extend into the sea to a distance of 22.2 km [11], so that offshore wind energy potential is more increasing offshore wind turbines.

Electricity is the main factor for economic growth, industrialization, improvement of quality of life in society, and urbanization [12]. The paper [13] discusses about the necessity of wind power, potentials, and barriers in implementing wind energy and also solutions for financial viability, approvals for renewable energy

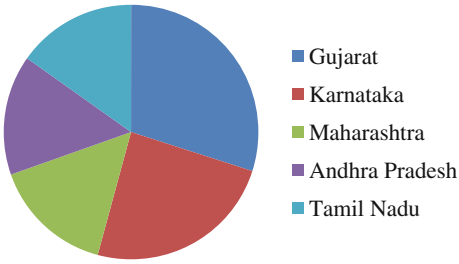

Fig. 1 Top five states in India producing wind energy

projects, and infrastructure setup is also discussed. Almost all states of India face energy scarcity, which ranges from 3 to 21 % with national average energy scarcity of 10.3 %, and scarcity in high demand is 15.4 % [14]. India being keen to develop renewable energy sources has developed 24,914 MW, as on March 31, 2012 [15]. In that, wind energy plays the major part in producing renewable energy. According to [8], wind energy that developed as on January 31, 2013 is 19,564.95 MW and top five wind energy producing areas states are, Tamil Nadu (7,154 MW), Gujarat (3,093 MW), Maharashtra (2,976 MW), Rajasthan (2,355 MW), Karnataka (2,113 MW) and other states (862.4 MW), shown in Fig. 1.

In 12th five year plan, Indian Government has fixed a reference target of 15,000 MW in installing new capacities and materialistic target of 25,000 MW, since India has always met an extended target set under both 10th and 11th plan in wind energy [4]. Government of India has set a target to achieve 38,500 MW from wind by 2022 [8]. In world power market, wind turbine production continues to rapidly grow, and wind turbine prices will continue to fall [16]. It is also a fact that exists many challenges and issues to overcome in integrating wind power to the grid, it has been necessary to find possible solutions for these issues. Although certain issues persist, possible solutions are discussed in [15].

Wind power is fluctuating, uncertain, and intermittent. Therefore, predicting wind energy is very much necessary for harvesting the wind energy potential [17]. The potential of energy taken through the wind, solar, and biomass is analyzed, and a model is developed and optimized for best output energy as discussed in [18]. The average wind speed and wind power density is calculated using shape and scale factor of Weibull function [19], and these factors will be more helpful to ensure optimum selection of wind turbine for a potential site. Integrating significant wind power into power system is a major challenge. Impacts of grid integration of wind turbine are discussed in [20]. In lead time, system operator is required to commit appropriate wind energy. Hence, a conditional probability approach is discussed in [21]. A model depicting the future prospects of Indian power sector and recommend change of power from thermal to renewable energy gradually is discussed in [12].

The various issues and challenges affecting power quality are discussed in [22, 23]. In [24], it is discussed how reliable is wind energy and how it can assist the power system in periods of low frequency. Wind energy is applied as a backup for

Table 1 Top 10 states with high wind potential in India

States with high potential	Potential at 50 m level (MW)
Gujarat	10,609
Karnataka	8,591
Maharashtra	5,439
Andhra Pradesh	5,394
Tamil Nadu	5,374
Jammu and Kashmir[a]	5,311
Rajasthan	5,005
Madhya Pradesh	920
Orissa	910
Kerala	790

[a] Wind potential still to be validated with measurements

cellular mobile telephony base station with solar hybrid energy system. It is discussed in [25], which takes hourly wind speed data and solar radiation from central India and studies the mobile base stations load consumption patterns and finds the system as more environment-friendly and cost-effective. A system, which can breakthrough the development bottlenecks of wind power, utilizing maximum rate of wind power and can save large number of equipment for wind power grid connection is discussed in [26]. Because of irrigation load, power supply gets interrupted for domestics, commercial, and industrial loads. An optimal solution for managing the load of irrigation pump is discussed in [27]. The top 10 potential sites of India are shown in the Table 1. Wind power is meager in northeast part of India. Possible utilization of wind energy with hybrid system is discussed in [28]. Feasibility study assessing the wind energy output is discussed in [29]. The Ministry of New and Renewable Energy is the common ministry for developing wind energy and for other renewable energy sources. Few promotional and financial incentives given by central government of India are stated in [30]. The Indian Wind Energy Association (InWEA) also offers advisory services to any stakeholder interested in wind sector. A mini wind mill is modeled in [31] to use it for household, as each family consumes 1.5 KW a day, which reduces the energy demand.

The power generated from the wind can be optimized and increased by reducing the pressure behind the wind turbine, making the turbine to draw more air, increasing the flow of air at improved velocity through the rotor, by using a diffuser [32]. A prototype of such turbine having potential for domestic application is discussed in [31]. Wind energy system has also been brought out in comparison with classical back to back converter DFIG system for stand-alone power supplies [33].

5 Conclusion

The necessity for an alternative source of energy is discussed by analyzing the disadvantages of conventional energy sources. Importance of renewable energy sources, an eco-friendly source of energy helps in facing the world in terms of power demand, emission of greenhouse gases, is discussed. Among the available renewable energy sources, wind energy that could be used in an effective manner is discussed. The usage of wind energy in India has been analyzed. As a future work, the power generation by conventional energy sources can be reduced whenever there exists a surplus of wind power thereby meeting the renewable energy production targets and environmental goals. Thus, India's role in wind energy development is discussed.

References

1. D. Holm, D. Arch, Renewable energy future for the developing world. Int. Sol. Energ. Soc. White Pap.
2. T. Shanker, R.K. Singh, Wind energy conversion system: a review, in *Student Conference on Engineering and Systems* (2012), pp. 1–6
3. I.F. MacGill, Impacts and best practices of large-scale wind power integration into electricity markets-some Australian perspectives, in *IEEE Power Energy Society General Meeting* (2012), pp. 1–6
4. D. Ting, S. Bin, S. Sheng-wen, Study on the wind energy resources assessment in wind power generation, in *2nd International Conference on Artificial Intelligence*, *Management Science and Electronic Commerce* (2011), pp. 6804–6807
5. A.M. Eltamaly, Design and simulation of wind energy system in Saudi Arabia, in *4th International Conference on Intelligent Systems Modeling & Simulation* (2013), pp. 376–383
6. U. Anitha, U. Vanitha, U. Nivedha, S. Usha Rani, Renewable energy technology in India: Panacea for sustainable development, in *International Conference on Advances in Engineering, Science and Management* (2012), pp. 137–141
7. S. Ghosh, P.P. Sengupta, Energy management in the perspective of global environment crisis: an evidence from India, in *International Conference on Management and Service Science* (2011), pp. 1–5
8. A. Raj Kumar, K.R.S. Ram Jeyanth, Outburst of renewable energy in India is it towards the target, in *International Conference on Advances in Engineering*, *Science and Management* (2012), pp. 36–41
9. B. Singh, S.N. Singh, L. Wang, Technical and economical practices for alternative energy in India, in *IEEE Power and Energy Society General Meeting* (2012), pp. 1–8
10. A.S. Anees, Grid integration of renewable energy sources: challenges, issues and possible solutions, in *IEEE 5th India International Conference on Power Electronics* (2012), pp 1–6
11. A. Ashwin Kumar, A study on renewable energy resources in India, in *International Conference on Environmental Engineering and Applications* (2010), pp. 49–53
12. M. Rizwan, S. Saini, U. Singh, Prediction of wind energy using intelligent approach, in *IEEE 5th International Conference on Power Electronics* (2012), pp 1–5
13. K.M. Rafi, M. Jamil, A. Mubeen, Energy potential & generation through IRES in city of Faridabad-India, in *IEEE Global Humanitarian Technology Conference* (2011), pp. 238–241

14. B.G. Kumaraswamy, B.K. Keshavan, Y.T. Ravikiran, Analysis of seasonal wind speed and wind power density distribution in Aimangala wind form at Chitradurga Karnataka using two parameter Weibull distribution function, in *IEEE Power and Energy Society General Meeting* (2011), pp. 1–4
15. N.M. Chowdhury, M.E. Haque, M. Aktarujjaman, M. Negnnevitsky, A. Gargoom, Grid integration impacts and energy storage systems for wind energy applications-a review, in *IEEE Power and Energy Society General Meeting* (2011), pp. 1–8
16. S. Thapa, R. Karki, R. Billinton, Evaluation of wind power commitment risk in system operation, in *IEEE Electrical Power and Energy Conference* (2011), pp. 284–289
17. A. Abrantes, Overview of power quality aspects in wind generation, in *North American Power Symposium* (2012), pp. 1–6
18. S. Shi, K.L. Lo, Reliability assessment of power system considering the impact of wind energy, in *47th International Universities Power Engineering Conference* (2012), pp. 1–6
19. A. Shah, S. Pillai, N.S.M. Rao, Integration of wind energy into grid in India- perceptions and realities, in *IEEE PES Transmission and Distribution Conference and Exposition* (2010), pp. 1–8
20. P. Nema, S. Rangnekar, R.K. Nema, Pre-feasibility study of PV-solar/wind hybrid energy for GSM type mobile telephony base station in central India, in *The 2nd International Conference on Computer and Automation Engineering* (2010), pp. 152–156
21. B.S. Saravana, K. Srinivasan, R.B. Jeyapradha, Future prospects of non-grid-connected wind power in India, in *Annual IEEE India Conference* (2011), pp. 1–4
22. C. Gupta, S. Singh, Energy management scheme for irrigation pump load, in *International Conference on Computer and Communication Engineering* (2012), pp. 779–782
23. S. Bhattacharjee, S. Acharya, Exploring wind energy for hybrid power generation in a low wind regime, in *1st International Conference on Power and Energy in NERIST* (2012), pp. 1–5
24. P. Kondapani, S.G. Sakri, Preliminary study to assess the wind energy potential in Gulbarga, Karnataka state, in *IEEE Region 10 Conference TENCON* (2008), pp. 1–4
25. www.inwea.org
26. P.D. Haridas, A.A. Sagade, N.N. Shinde, S. Aher, Experimental performance evaluation of 500 W mini wind mill, in *International Conference on Energy Efficient Technologies for Sustainability* (2013), pp. 312–319
27. S.A. Kale, Y.R. Gunjal, S.P. Jadhav, A.N. Tanksale, CFD analysis for optimization of diffuser for a micro wind turbine, in *International Conference on Energy Efficient Technologies for Sustainability* (2013), pp. 257–260
28. K. Vijayakumar, N. Kumaresan, N.G.A. Gounden, Operation of inverter-assisted wind-driven slip-ring induction generator for stand-alone power supplies. IET Electr. Power Appl. **7**(4), 256–269 (2013)

Series Resonant Converter-based Unified Power Quality Conditioner Using Fuzzy Controller

R. Anand and P. Melba Mary

Abstract The improvisation of power quality at grid is widely done by one of the custom power device, i.e., unified power quality conditioner (UPQC). This paper presents a three-phase unified power quality conditioner based on fuzzy controlled resonant converters, which has the capability to obtain a good transient current response and voltage response. The fuzzy logic controller is used to control the resonant converter. The simulation results based on MATLAB/Simulink are given to illustrate the effectiveness of the proposed UPQC based on resonant converter. The obtained result has been compared to other topologies which were proposed earlier.

Keywords Unified power quality conditioner · Fuzzy logic controller · Feedback linearization technique · Transform decomposition algorithm · Total harmonic distortion

1 Introduction

It is essential to contain some genus of compensation in power system to convince the power quality, because of the raise in harmonic current injecting loads in the modern world [1]. Sreenivasachar et al. [2] deal with dynamic stability of multi-machine multi-UPFC with the different control structures. They evaluated the system stability using the parameters such as DC link capacitor. Preceding this, Won et al. [3] analyzed the dynamic response of UPFC switching level model. In

R. Anand (✉)
Department of Electrical and Electronics Engineering, National College of Engineering, Maruthakulam, Tirunelveli, Tamilnadu, India
e-mail: anandrb.pk@gmail.com

P. Melba Mary
VV College of Engineering, Tisaiyanvilai, Tamilnadu, India
e-mail: principal@vvcoe.org

© Springer India 2015

L.P. Suresh et al. (eds.), *Artificial Intelligence and Evolutionary Algorithms in Engineering Systems*, Advances in Intelligent Systems and Computing 325,
DOI 10.1007/978-81-322-2135-7_27

power system, the importance given to dynamic stability has to be retained to transient stability also. To obtain transient stability, numerous controlling methods had been proposed such as transient energy function analysis based on time domain [4], voltage and current mode control [5], and direct feedback linearization technique [6]. Even though, by the use of the above-mentioned controls, it gives reasonable results, it leads to some limitations such as bulk system and high initial cost. Sannino et al. [7] gave the solutions of power quality problems based on power electronic switches. Asymmetrical inverter legs [8], series, and shunt active filter [9] are the earlier proposed operating methods with active filters used to mitigate the voltage unbalance. Kwan et al. [10] used a Kalman filter to regulate the output of UPQC, but the harmonic level was not so reduced. Forghani et al. [11] introduced wavelet transform decomposition algorithm to reduce the voltage and current harmonics. Here, even though the total harmonic distortion (THD) of current harmonics reduced, the transient harmonics of voltage was not reduced to the extent. Like this, feedback controller using PSO had also been proposed in [12]. But still the problems with harmonics were retained. In order to reduce THD level, fuzzy controller had been introduced in [13], but the harmonic distortion was not reduced. Babaei et al. [14] gave a new topology of UPFC with asymmetrical cascaded multilevel inverter for voltage unbalanced problems. But the THD level of that scheme was high. In continuation of that, some of the new topologies had been introduced in UPQC such as removal of DC link capacitor [15], four leg voltage source inverter [16], and more than one series VSCs [17], and current source topology [18]. Still the problem in reduction of distortion was not sorted out.

In this paper, a novel configuration of a UPQC named resonant converter-based UPQC is presented. The proposed topology can be used for concurrent compensation of voltage and current imperfections in UPQC output. While using this topology, the limitations mentioned in the above have been overcome to a considerable level. Section 2 gives the explanation of resonant converter-based UPQC, and Sect. 3 describes the significance of fuzzy logic controller used in proposed topology. In Sect. 4, simulation results are discussed. Finally, Sect. 5 concludes.

2 Resonant Converter-based UPQC

The execution of power converters can be enhanced by the usage of soft switching. The detailed connection diagram of resonant converter which is used in the proposed scheme of resonant converter-based UPQC (Fig. 1) is shown in Fig. 2. The proposed topology has an ability to reduce the total harmonic distortion of the injecting current in the UPQC.

The inductive reactance X_{Leq} and capacitive reactance X_{ceq} values are expressed as [19]

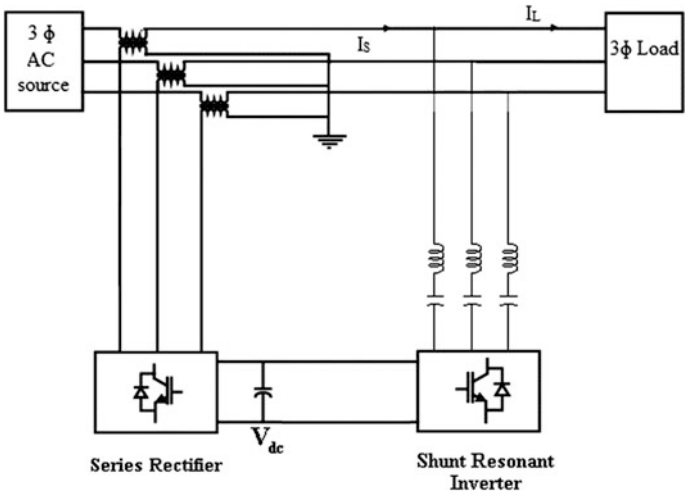

Fig. 1 Common block diagram of resonant converter-based UPQC

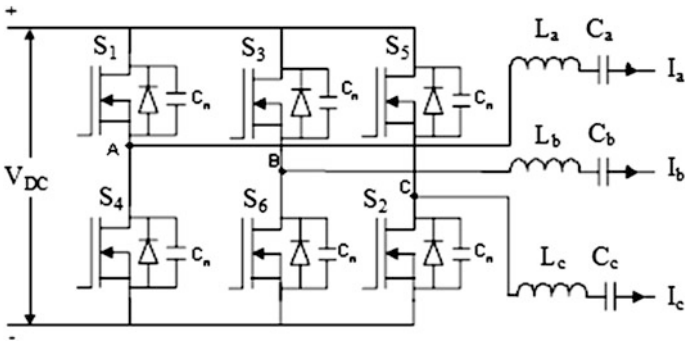

Fig. 2 Resonant converter used in UPQC

$$X_{\mathrm{Leq}} = Qf \tag{1}$$

$$X_{\mathrm{ceq}} = \frac{Q}{f} \tag{2}$$

where

$$Q = \frac{w_{\mathrm{rs}} L_{\mathrm{eq}}}{Z_L} \tag{3}$$

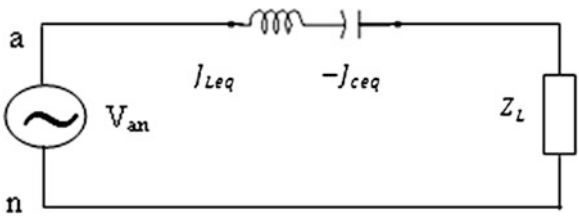

Fig. 3 Per phase (line-to-neutral) phasor equivalent circuit of resonant converter

Here,

$$w_{\mathrm{rs}} = \frac{w_s}{f} \tag{4}$$

where f_s is the switching frequency and f_{rs} is the series resonance frequency.

The inverter line-to-line voltages can be expressed in terms of supply voltage V_S as [19] (Fig. 3).

$$V_{\mathrm{ab}} = \frac{2\sqrt{3}}{\pi} V_S \sin\left(w_{\mathrm{st}} + \frac{\pi}{6}\right) \tag{5}$$

$$V_{\mathrm{bc}} = \frac{2\sqrt{3}}{\pi} V_S \sin\left(w_{\mathrm{st}} + \frac{\pi}{2}\right) \tag{6}$$

$$V_{\mathrm{ca}} = \frac{2\sqrt{3}}{\pi} V_S \sin\left(w_{\mathrm{st}} + \frac{7\pi}{6}\right) \tag{7}$$

The peak current through laboratory can be expressed as

$$i = \frac{V_{\mathrm{an}}}{\left(jX_{\mathrm{Leq}} - jX_{\mathrm{ceq}}\right) + Z_L} \tag{8}$$

The THD of injected voltage can be expressed as [18]

$$\mathrm{THD}_{V_{\mathrm{an}}} = \frac{1}{V_{\mathrm{an_1}}} \sqrt{\sum_{h=2}^{\infty} \left(V_{\mathrm{an},h}\right)^2} \tag{9}$$

where V_{an} be the fundamental components and $V_{\mathrm{an,h}}$ corresponds to the h harmonic of the voltage.

The parameters of the resonant tools are given in Table 1.

Table 1 Resonant tools value

Resonant Inductor	Resonant Capacitor
17.52 µH	0.02 µF

3 Fuzzy Logic Controller

In this paper, fuzzy logic controller is used to control the output voltage of the resonant inverter. Fuzzy logic control is one of the fresh counts to control premise. Its design attitude deviates from all the preceding methods by obliging expert knowledge in controller design. FLC is one of the most thriving applications of fuzzy set theory. Fuzzy control rules are acquired from the scrutiny of the system behavior. Fuzzy logic controller can improve the resonant inverter performances in terms of transient response and heftiness to a great extent. The control rule that associates the fuzzy output to the fuzzy inputs is derived from general knowledge of the system activities. The fuzzy control system includes error calculation, fuzzification, decision making, and defuzzification [20].

The membership functions and rules used to control the output voltage of the resonant converter are given below (Fig. 4).

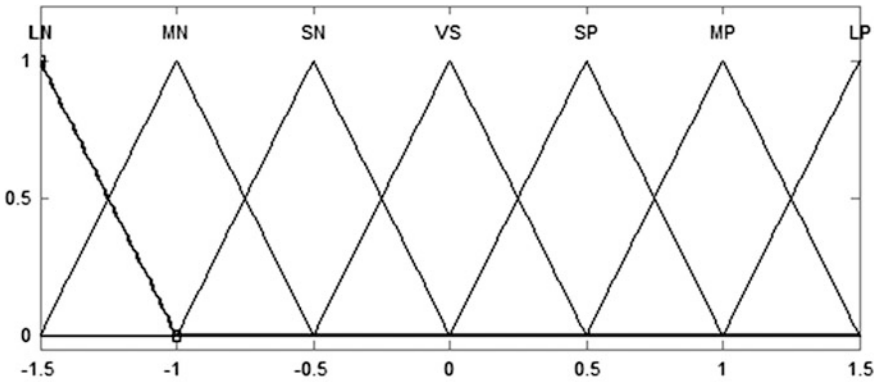

δe \ e	LN	MN	SN	VS	SP	MP	LP
LN	NB	NB	NB	NM	NM	NS	Z
MN	NB	NB	NM	NM	NS	Z	PS
SN	NB	NM	NM	NS	Z	PS	PM
VS	NM	NM	NS	Z	PS	PM	PM
SP	NM	NS	Z	PS	PM	PM	PB
MP	NS	Z	PS	PM	PM	PB	PB
LP	Z	PS	PS	PM	PB	PB	PB

Fig. 4 Membership functions and rules

4 Simulation Results and Analysis

The SIMULINK toolbox in the MATLAB software is used in order to model and test the proposed scheme under steady-state and transient conditions using fuzzy logic controller. The system parameters are input voltage (V_{in}) = 22 kV, resonant inductor (La = Lb = Lc) = 17.52 micro-Henry, and resonant capacitor (Ca = Cb = Cc) = 0.02 micro-Farad. Shunt inverter is controlled by fuzzy logic controller. The THD of the 'b' phase voltage of the existing UPQC system is assumed to be 5.11 %. While considering the sensitive load, the resonant converter-based UPQC injects the necessary compensating voltages, making the load voltage free from distortion. The resulting load voltage of 'b' (Fig. 5a) has THD of 0.09 % which is shown in Fig. 5b. The THD values of voltages of phase 'a' and 'c' are, respectively, 0.07 % and 0.13 %.

Simultaneously, the resonant converter-based UPQC injects the compensating currents to attain the balanced source current without distortion. The 'b' phase current (Fig. 6a) has THD of 0.07 % which is shown in Fig. 6b. The THD values of currents of phase 'a' and 'c' are, respectively, 0.10 and 0.11 %. When considering the nonlinear load, the THD value of 'b' phase current is 3.25 % which is within the

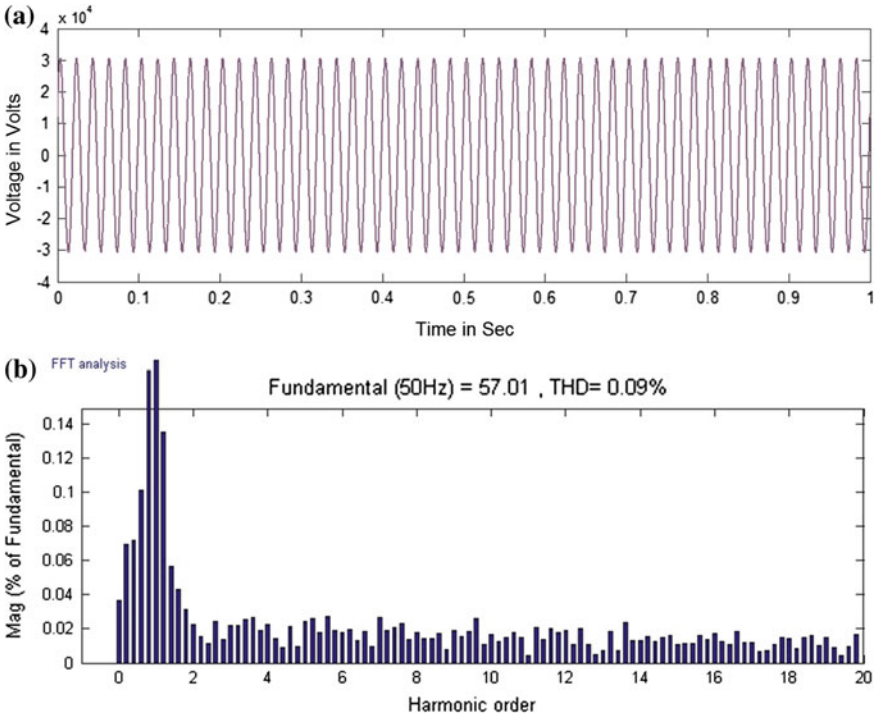

Fig. 5 **a** Load voltage of 'b' phase. **b** FFT analysis of 'b' phase voltage

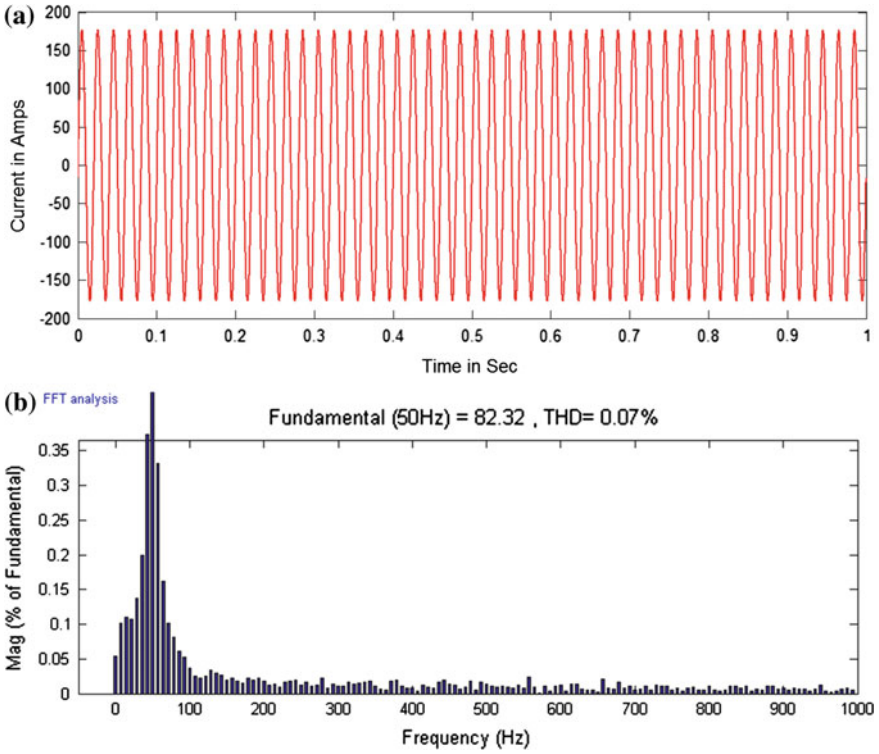

Fig. 6 **a** Current of 'b' phase. **b** FFT analysis of 'b' phase current

Table 2 Comparison of other UPQC topologies with resonant converter-based UPQC

THD in Percentage		
UPQC topology	Voltage	Current
MLI UPFC [17]	1.47	0.54
LQR-based UPFC [16]	1.1	2.1
PSO-based UPFC [16]	1.5	0.6
3-phase 4-wire UPFC [13]	1.5	2.3
Resonant converter-based UPQC	0.09	0.07

IEEE 519 allowable limits which is 5 %. Table 2 shows the comparison between resonant converter-based UPQC and other UPQC topologies. This clearly shows that the THD level of resonant converter-based UPQC which is controlled by fuzzy logic controller has been considerably improved than other topologies.

5 Conclusion

In this paper, a new configuration named resonant converter-based unified power quality conditioner for concurrent compensation of voltage and current has been proposed. The new configuration is compared to existing UPQC topologies; the proposed topology is competent of fully protecting critical and sensitive loads against distortions and sags/swell. The MATLAB-/Simulink-based simulation results confirm that the distorted load voltages and currents seen from the utility side act as absolutely balanced source currents and are free from distortion.

References

1. D. Graovac, V. Katic, A. Rufe, Power quality compensation using universal power quality conditioning system. IEEE Power Eng. Rev. 58–60 (2000)
2. K. Sreenivasachar, S. Jayaram, M.M.A. Salama, Dynamic stability improvement of multi-machine power system with UPFC. Electr. Power Syst. Res. **55**, 27–37 (2000)
3. D.-J. Won, Y. Chung, S. Moon, Determination of equivalent impedances of UPFC voltage-source model from the dynamic responses of UPFC switching-level model. Electr. Power Energ. Syst. **25**, 463–470 (2003)
4. I.S. Jacobs, C.P. Bean, Fine particles, thin films and exchange anisotropy. Magn. III 271–350 (1963)
5. A. Ghosh, G. Ledwich, A unified power quality conditioner (UPQC) for simultaneous voltage and current compensation. Electr. Power Syst. Res. **59**, 55–63 (2001)
6. H. Chen, Y. Wang, R. Zhou, Transient stability enhancement via coordinated excitation and UPFC control. Electr. Power Energ. Syst. **24**, 19–29 (2002)
7. A. Sannino, J. Svensson, T. Larsson, Power-electronic solutions to power quality problems. Electr. Power Syst. Res. **66**, 71–82 (2003)
8. B.-R. Lin, T.-Y. Yang, Implementation of active power filter with asymmetrical inverter legs for harmonic and reactive power compensation. Electr. Power Syst. Res. **73**, 227–237 (2005)
9. A. Jindal, A. Ghosh, A. Joshi, The protection of sensitive loads from inter harmonic currents using shunt/series active filters. Electr. Power Syst. Res. **73**, 187–196 (2005)
10. K.H. Kwan, M.P.L. So, Y.C. Chu, An output regulation-based unified power quality conditioner with kalman filters. IEEE Trans. Ind. Electron. **59**(11) (2012)
11. M. Forghani, S. Afsharnia, Online wavelet transform-based control strategy for UPQC control system. IEEE Trans. Power Deliv. **22**(1) (2007)
12. E. Babaeia, S.H. Hosseini, G.B. Gharehpetian, M. Tarafdar Haquea, M. Sabahi, Reduction of dc voltage sources and switches in asymmetrical multilevel converters using a novel topology. Electr. Power Syst. Res. **77**, 1073–1085 (2007)
13. V. Khadkikar, A. Chandra, A novel structure for three-phase four-wire distribution system utilizing unified power quality conditioner (UPQC). IEEE Trans. Ind. Appl. **45**(5), 1897–1902 (2009)
14. B. Geethalakshmi, P. Dananjayan, Investigation of performance of UPFC without DC link capacitor. Electr. Power Syst. Res. **78**, 736–746 (2008)
15. H.R. Mohammadi, A.Y. Varjani, H. Mokhtari, Multiconverter unified power-quality conditioning system: MC-UPQC. IEEE Trans. Power Deliv. **24**(3), 1679–1686 (2009)
16. S.B. Karanki, M.K. Mishra, B.K. Kumar, Particle swarm optimization-based feedback controller for unified power-quality conditioner. IEEE Trans. Power Deliv. **25**(4), 2814–2823 (2010)

17. M.E. Elgamal, A. Lotfy, G.E.M. Ali, Voltage profile enhancement by fuzzy controlled MLI UPFC. Electr. Power Energ. Syst. **34**, 10–18 (2012)
18. P.E. Melín, J.R. Espinoza, L.A. Morán, J.R. Rodriguez, V.M. Cardenas, C.R. Baier, J.A. Muñoz, Analysis, design and control of a unified power-quality conditioner based on a current-source topology. IEEE Trans. Power Deliv. **27**(4) (2012)
19. M.S. Almardy, A.K.S. Bhat, Three-phase (LC)(L)-type series-resonant converter with capacitive output filter. IEEE Trans. Power Electron. **26**(4), 1172–1183 (2011)
20. L. Saribulut, M. Tumay, I. Eker, Performance analysis of fuzzy logic based unified power flow controller. Int. J. Electr. Electron. Eng. **3**(12), 717–722 (2009)

MRI Brain Image Classification Using Haar Wavelet and Artificial Neural Network

J.C. Smitha and S. Suresh Babu

Abstract A combined approach with MRI brain image denoising and abnormality detection process is proposed in this paper. The proposed technique is comprised of three stages, namely (i) image preprocessing, (ii) feature extraction, and (iii) image classification. Initially, in the preprocessing stage, denoising is performed on the input brain MRI image. The denoising process on the input image increases the accuracy of feature extraction stage. In feature extraction phase, the image features such as mean, variance, and multilevel 2D Haar wavelet decomposition are extracted for classifying the images in the database into normal and abnormal. By using these extracted features, the MRI brain images are classified by the well-known classification technique such as feed forward back propagation neural networks (FFBNN). The implementation of the proposed method shows improvements in classification of MRI images.

Keywords Image preprocessing · Feature extraction · Image classification · Feed forward back propagation neural networks

1 Introduction

Brain is the most essential part of a living thing, which regularizes and controls all other organs. If a patient is not in normal condition, then the brain might have been affected through diseases [1]. Hence, it necessitates analyzing the condition of the

J.C. Smitha (✉)
Department of Computer Science and Engineering, Lourdes Matha College of Science and Technology, Thiruvananthapuram 695574, Kerala, India
e-mail: smithajc@gmail.com

S.S. Babu
Department of Electronics and Communication, TKM College of Engineering, Kollam 691005, Kerala, India
e-mail: drssbtkm@gmail.com

© Springer India 2015

L.P. Suresh et al. (eds.), *Artificial Intelligence and Evolutionary Algorithms in Engineering Systems*, Advances in Intelligent Systems and Computing 325,
DOI 10.1007/978-81-322-2135-7_28

brain. Many research works were done in the area of brain MRI image abnormality segmentation. But, the performance of such works lacks in the image pre-analysis. During pre-analysis through MRI for detecting the abnormality, it is important to correctly analyze the patient's image thoroughly. If the analysis of the image is giving a wrong result, the treatment given to the patient will also be wrong and that will affect the patient. Hence, there is a need to improve the abnormality detection accuracy by incorporating the vital pre-analysis of the MRI image.

Brain MRI images have a number of features. First, they are statistically simple and are theoretically piecewise constant with a small number of classes. Secondly, they have relatively high contrast between different tissues [2]. Till date, an optimally accurate and efficient method for characterizing brain structure from medical images remains elusive, and current methods remain imperfect. This paper proposes an efficient MRI image classification technique using feed forward back propagation neural networks (FFBNN), which effectively classifies MRI brain images into normal and abnormal classes.

2 Proposed MRI Brain Image Classification Technique

The proposed MRI brain image classification technique classifies the images into normal and abnormal images. The proposed technique mainly is comprised of three stages: (i) image preprocessing, (ii) feature extraction, and (iii) image classification.

Considered $D^r = \{I_1, I_2, \ldots, I_n\}$ and $D^e = \{I_1, I_2, \ldots, I_m\}$ be the training and testing MRI brain image database, and n, m denotes the total number images in the database with size $n \times m$. The MRI images from both databases D^e and D^r are given to the preprocessing and feature extraction phases. Before the feature extraction, the given images in the databases are converted into gray-scale images. The gray-scale images from both databases are represented as I_n', I_m'. After the conversion, the feature extraction process is performed by using the three features.

2.1 Preprocessing

The denoising process is performed by computing the new pixel values for the input images from the MRI image database. The noises in the input gray-scale MRI images are removed by changing the pixel values with new pixel values. The process of noise pixel removal and the new pixels computation is described by the algorithm, which is given below.

Input: Images $I_n^{a'}, I_m^{a'}$.
Output: Noise-free image $I_n^{a''}, I_m^{a''}$

Step 1: Initially, we create a random mask P with the size of $M \times N \times 2$

$$P = \begin{bmatrix} \begin{bmatrix} (1,1) & (1,2) & \ldots & (1,N) \\ (2,1) & (2,2) & \ldots & (2,N) \\ \vdots & \vdots & \vdots & \vdots \\ (M,1) & (M,2) & \vdots & (M,N) \end{bmatrix} \\ \begin{bmatrix} (1,1) & (1,2) & \ldots & (1,N) \\ (2,1) & (2,2) & \ldots & (2,N) \\ \vdots & \vdots & \vdots & \vdots \\ (M,1) & (M,2) & \vdots & (M,N) \end{bmatrix} \end{bmatrix} \tag{1}$$

Step 2: Take the images $I_n^{a'}, I_m^{a'}$ and find the difference matrix by,
For i = 1, 2, …, M

For j = 1, 2, …, N

$$x(I_n^{a'}) = \text{new}(p(i+1), p(j)) = p(1,\ 1) - (p(i+1), p(j)) \tag{2}$$

End

End
For i = 1, 2, …, M

For j = 1, 2, …, N

$$\begin{aligned} X(x(I_n'')) &= \text{new}(p(i), p(j+1)) \\ &= (p(i), p(j+1)) + p(1,1) - (p(i), p(j+1)) \end{aligned} \tag{3}$$

End

End

The result matrix from the difference process is X. This same process is followed for the image $I_m^{a'}$ and gets the matrix result Y.
Step 3: Compute new matrixes X′ and Y′ by,

$$X' = \begin{cases} X(r(i)) = P(r(i));\ \ i = 1 \\ X(r(M)) = P(r(M)) \\ X(c(j)) = P(c(j));\ j = 1 \\ X(c(N)) = P(c(N)) \end{cases} \tag{4}$$

$$Y' = \begin{cases} Y(r(i)) = P(r(i)); \ i = 1 \\ Y(r(M)) = P(r(M)) \\ Y(c(j)) = P(c(j)); \ j = 1 \\ Y(c(N)) = P(c(N)) \end{cases} \tag{5}$$

Step 4: Update the images $I_n^{a'}, I_m^{a'}$ by,

$$I_n^{a''} = u_{I_n^{a'}} = I_n^{a'} - \theta X' \tag{6}$$

$$I_m^{a''} = u_{I_m^{a'}} = I_m^{a'} - \theta Y' \tag{7}$$

Step 5: Compute forward derivative by extracting the column and row values $u_{I_n^{a'}} c(j+1), u_{I_n^{a'}} r(i+1)$ (where j = 1–N and i = 1–M) and put into the new mask $\mathrm{d}u^2 I_n^{a'}$ and $\mathrm{d}u^1 I_n^{a'}$. For image $u_{I_m^{a'}}$ also we compute the forward derivative matrices $\mathrm{d}u^2 I_m^{a'}$ and $\mathrm{d}u^1 I_m^{a'}$.

$$u_{I_n^a} = \begin{bmatrix} (1,1) & (1,2) & (1,3) & \cdots & (1,N) \\ (2,1) & (2,2) & (2,3) & \cdots & (2,N) \\ \vdots & \vdots & \vdots & \vdots & \vdots \\ (M,1) & (M,2) & (M,3) & \cdots & (M,N) \end{bmatrix} = \begin{bmatrix} 1 & 2 & 3 & N-1 & N \\ (1,2) & (1,3) & \cdots & (1,N) & (1,N) \\ (2,2) & (2,3) & \cdots & (2,N) & (2,N) \\ \vdots & \vdots & \vdots & \vdots & \vdots \\ (M,1) & (M,2) & \cdots & (M,N) & (M,N) \end{bmatrix} = du_{I_n^a} \tag{8}$$

Step 6: Compute distinction value

$$D\left(I_n^{a'}\right) = D^1 I_n^{a'} = D^2 I_n^{a'} = \left(1 + ((t/\theta)/g). * \left|\sqrt{(\mathrm{d}u^1 I_n^{a'})^2 + (\mathrm{d}u^2 I_n^{a'})^2}\right|\right) \tag{9}$$

$$D(I_m^{a'}) = D^1 I_m^{a'} = D^2 I_m^{a'} = \left(1 + ((t/\theta)/g). * \left|\sqrt{(\mathrm{d}u^1 I_m^{a'})^2} + (\mathrm{d}u^2 I_m^{a'})^2\right|\right) \tag{10}$$

Step 7: Modify the mask P values by,

$$P' = (P - (t/\theta). * \left(\mathrm{d}u^2 I_n^{a'} * \mathrm{d}u^1 I_n^{a'}\right)./D(I_n^{a'}) \tag{11}$$

Step 8: The process is repeated until the maximum number of iterations S is reached.

Step 9: Finally, we get the noise-free images $I_n^{a'}$ and $I_m^{a''}$.

Thus, the resultant denoised images $I_n^{a''}$ and $I_m^{a''}$ are given to the average filtering to further enhance the images for the classification process.

3 Feature Extraction

In feature extraction, phase five features such as mean, variance, and multilevel 2D Haar wavelet decomposition [3] features such as horizontal, vertical, and diagonal bands of wavelet transform features are extracted from both training and testing database images for image classification. The process of feature extraction for image classification is explained below.

The features are extracted from the database images I_n' and I_m' and that image pixel values are represented as P. The features mean and variance are directly computed from the input images, and the wavelet features are extracted by applying wavelet transform. In this work, a two-level Haar wavelet transform is applied on the input images and three features are extracted from the resulting image. The extracted five features are stated as,

$$M(I_n\prime) = \frac{1}{M \times N} \sum_{a=1}^{M} \sum_{b=1}^{N} p_{ab} \tag{12}$$

$$E(I_n\prime) = \left(\frac{1}{M \times N} \left(\sum_{a=1}^{M} \sum_{b=1}^{N} (p_{ab} - M(I_n\prime))^2 \right) \right) \tag{13}$$

$$H(I_n\prime) = \frac{1}{c} \sum_{c=1}^{C} h_c \tag{14}$$

$$V(I_n\prime) = \frac{1}{c} \sum_{c=1}^{C} v_c \tag{15}$$

$$D(I_n\prime) = \frac{1}{c} \sum_{c=1}^{C} d_c \tag{16}$$

In Eq. (12), p_{mn} is the pixel value of the image and in Eqs. (14), (15), and (16), h_c, v_c, and d_c are the horizontal, vertical, and diagonal wavelet coefficients of the image I_n'. Similarly, these features are calculated for the I_m' images. These extracted features are given to the FFBNN for image classification process described in the following section.

4 Image Classification

In image classification, we classify training and testing database images into normal and abnormal. For the image classification, the extracted features $M(I_n\prime)$, $E(I_n\prime)$, $H(I_n\prime)$, $V(I_n^{'})$, and $D(I_n\prime)$ are given to the FFBNN.

Network training and testing process are performed by using the extracted features. The basic structure of FFBNN network is shown in Fig. 1. In the training phase, the MRI images are taken out from the given database. The extracted features are given to FFBNN network. The FFBNN network is well trained by these extracted features. The network is created with five input units, H_a hidden units and one output unit.

The following steps describe the function of the neural network:

Step 1: Initialize the weights to every neuron except the input neurons in the network.

Step 2: The neural network is designed with five neurons in the input layers, H_a hidden layers and one output layer. The weights are then added to the neural network, and it is biased.

Step 3: The planned bias function and activation function for the neural network is described below.

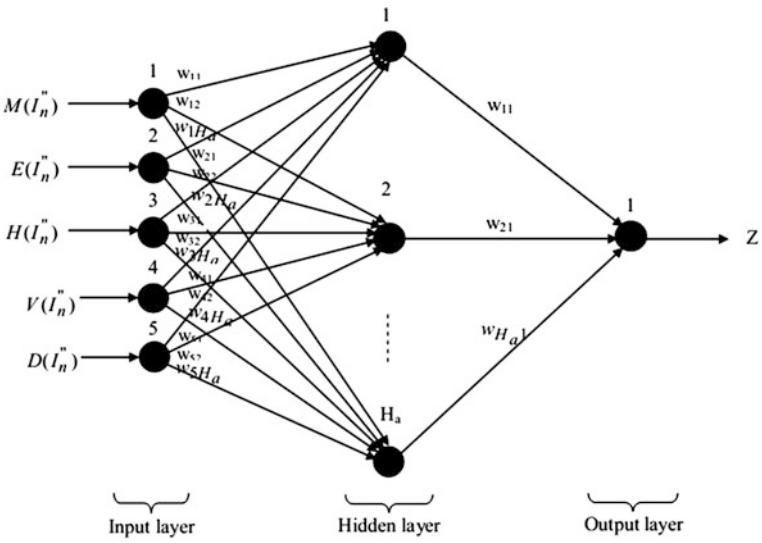

Fig. 1 Basic structure of the FFBNN

$$B_{(I_n\prime)} = \beta + \sum_{h=1}^{H_a} (w_{(h)} M(I_n\prime)(h) + w_{(h)} E(I_n\prime)(h) + w_{(h)} H(I_n\prime)(h) + w_{(h)} V(I_n\prime)(h) + w_{(h)} D(I_n\prime)(h)) \tag{17}$$

$$A\left(B_{(I_n\prime)}\right) = \frac{1}{1 + e^{-B_{(I_n\prime)}}} \tag{18}$$

The input layer bias function is given in Eq. (17). In Eq. (17) $M(I_n\prime)$, $E(I_n\prime)$, $H(I_n\prime)$, $V(I_n\prime)$, and $D(I_n\prime)$ are the extracted features from the image $I_n\prime$. The activation function for the output layer is given in Eq. (18).

Step 4: Compute the learning error for the neural network.

$$L^{(e)} = \frac{1}{H_a} \sum_{h=0}^{H_a} D_h - Z_h \tag{19}$$

In Eq. (19), $L^{(e)}$ is the learning error rate of FFBNN network, D_h and Z_h are the desired and actual outputs, respectively.

4.1 Minimization of Error by Back Propagation Algorithm

The steps involved in the training of BP algorithm-based NN are given below:

(i) Weights are allocated to the hidden layer and output layer neurons by randomly chosen weights. The input layer neurons have a constant weight.

(ii) Determine the bias function by Eq. (18). The activation function is computed by Eq. (19).

(iii) Calculate BP error for each node and update the weights as follows

$$w_{(h)} = w_{(h)} + \Delta w_{(h)} \tag{20}$$

(iv) Using Eq. (20), the weight $\Delta w_{(h)}$ is changed, it can be determined as,

$$\Delta w_{(h)} = \delta \cdot X_{(B_{(I_n\prime)}h)} \cdot E^{(Bp)} \tag{21}$$

where δ is the learning rate, which normally ranges from 0.2 to 0.5, and $E^{(Bp)}$ is the *BP* error.

(v) Then, repeat the steps (2) and (3) until the BP error gets minimized. The process is repeated until it satisfies $E^{(Bp)} < 0.1$.

(vi) The error gets minimized to a minimum value, and the FFBNN is well trained for performing the testing phase.

The result of this FFBNN network is represented as Z, and this value Z is compared with threshold value t_1.

$$\text{result} = \begin{cases} \text{Abnormal;} & Z \geq t_1 \\ \text{Normal;} & Z < t_1 \end{cases} \tag{22}$$

In this way, the brain MRI images are classified into normal and abnormal classes.

5 Experimental Results and Discussion

The brain MRI images are taken from the database and that images are given to the preprocessing process. After getting the noise-free images, the feature extraction process is carried out and features are extracted and given to the FFBNN for the image classification process. The classification result is given in Fig. 2 and Table 1.

In this paper, we have considered 18 MRI brain images in which 5 are normal and 13 are abnormal images. The abnormal image database consisted of tumor images, stroke images, and trauma images. By using the extracted features such as mean, median, variance, and wavelet features, our proposed FFBNN classifies four images as normal and 14 as abnormal. Hence, our proposed image classification process by FFBNN has attained 94 % classification accuracy.

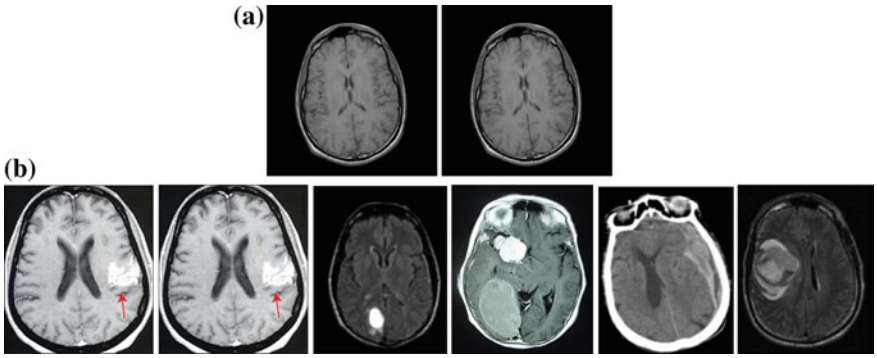

Fig. 2 Classified image results **a** normal and **b** abnormal

Table 1 Image classification result

No. of images	Correctly classified images	Wrongly classified images
18	17	1

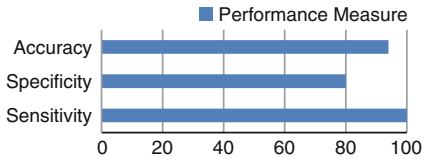

Fig. 3 Classification performance in terms of accuracy, sensitivity, and specificity

To do the statistical measures calculation of the classification process true positive (TP), true negative (TN), false positive (FP), and false negative (FN) values are utilized. In the performance measure, each image has been tested 10 times on all dataset and the computed performance measures are given below (Fig. 3):

Sensitivity = TP/(TP + FP) * 100 % = 130/(130 + 0) = 100 %
Specificity = TN/(TN + FP) * 100 % = 40/(40 + 10) = 80 %
Accuracy = (TP + TN)/(TP + TN + FP + FN) * 100 % = 130 + 40/(130 + 40 + 10 + 0) = 94 %

6 Conclusion

In this paper, we proposed an efficient MRI brain image classification technique that effectively classifies the MRI images into normal and abnormal classes. Initially, the MRI image noises were removed and classified based on the extracted features. The performance of the proposed technique is evaluated by more number of MRI images. The implementation result shows that the proposed MRI brain image classification technique efficiently classifies the MRI images into normal and abnormal classes than the existing classifier.

References

1. J.C. Smitha, S.S. Babu, A Broad review of noteworthy researches on brain abnormality detection with the aid of medical images. Eur. J. Sci. Res. **85**(2), 279–304 (2012)
2. Y. Zhang, M. Brady, S. Smith, Segmentation of brain MR images through a hidden Markov random field model and the expectation-maximization algorithm. IEEE Trans. Med. Imaging **20** (1), 45–57 (2001)
3. S. Radomir, R.S. Stankovic, B.J. Falkowski, The Haar wavelet transform: its status and achievements. Comput. Electr. Eng. **29**, 25–44 (2003)

Adaptive Modified Hysteresis Current Control for Switching Loss Reduction in Photovoltaic-Fed Dual-Function Grid-Connected Inverters

Preethi Thekkath and S.U. Prabha

Abstract Current control logic plays a very important role in the overall performance of grid-connected inverters. Adaptive modified hysteresis current control is used in this work for switching loss reduction, optimization of inverter switching frequency, and reduction in total harmonic distortion of supply current. Photovoltaic-fed grid-connected inverter injects real power from photovoltaic array into the grid, controls real power flow in the grid, and functions as a shunt active filter. Good DC bus stabilization, reactive power compensation, satisfactory performance under unbalanced source and load conditions, and good dynamic response is also achieved.

1 Introduction

Proliferation of power electronic loads has posed a real threat to power quality. Distributed generation (DG) has increased the severity of power quality problems. Search for pollution-free energy source has led to the development of renewable energy systems. Among the renewable energy sources, solar energy is abundant and inexhaustible. DC power from photovoltaic (PV) arrays is boosted using DC–DC converters and further converted to AC using inverters before connecting to the grid [1, 2]. Maximum power point tracking [3–5], proper control of power injected into the grid, low harmonic distortion of currents injected into the grid, and high power factor are some of the requirements of grid-connected inverters. In the present scenario of energy crisis, many studies are being done on feasibility of using grid-connected inverters fed from photovoltaic arrays, fuel cells, etc., with active filter functions [6, 7].

P. Thekkath (✉)
Department of EEE, Toc H Institute of Science and Technology, Kochi, India
e-mail: preethi.tkt@gmail.com

S.U. Prabha
Department of EEE, Bannari Amman Institute of Technology, Erode, India
e-mail: prabhasu@bitsathy.ac.in

© Springer India 2015

L.P. Suresh et al. (eds.), *Artificial Intelligence and Evolutionary Algorithms in Engineering Systems*, Advances in Intelligent Systems and Computing 325,
DOI 10.1007/978-81-322-2135-7_29

Quality of photovoltaic power depends on output current of the inverter which necessitates efficient current control of grid-connected inverters.

Hysteresis control [8], sliding mode control [9], adaptive control [10], modified hysteresis control [11], etc., are some of the current control techniques.

Conventional hysteresis current control method suffers from variable switching frequency and high switching losses owing to control of all the six switches of the inverter. Modified hysteresis controller [11] in which only two switches are controlled reduces switching losses to one-third of that of the conventional one but is insufficient to maintain current THD within the specified limits. To overcome this, pulses to the modified hysteresis controller is generated employing adaptive control by modifying pulses from the conventional hysteresis controller. Problem of variable switching frequency with modified hysteresis controller is also sought out with adaptive control.

In the present work reference, current generation is done using modified Icosϕ algorithm [7] and current control is achieved through adaptive modified hysteresis current control. Photovoltaic-fed grid-connected inverter functions as a dual-function grid-connected inverter. Instantaneous switching frequency is optimized, reduced, and maintained nearly constant, and THD is brought within the limits specified by the standards using adaptive control. Better DC bus voltage stabilization is also achieved.

2 Configuration of Three-Phase Photovoltaic-Fed Grid-Connected Inverter

Configuration of photovoltaic-fed grid-connected inverter is shown in Fig. 1. The maximum power point tracking is obtained through perturb and observe (P&O) algorithm. DC–DC converter boosts the output voltage of PV array to 300 V which

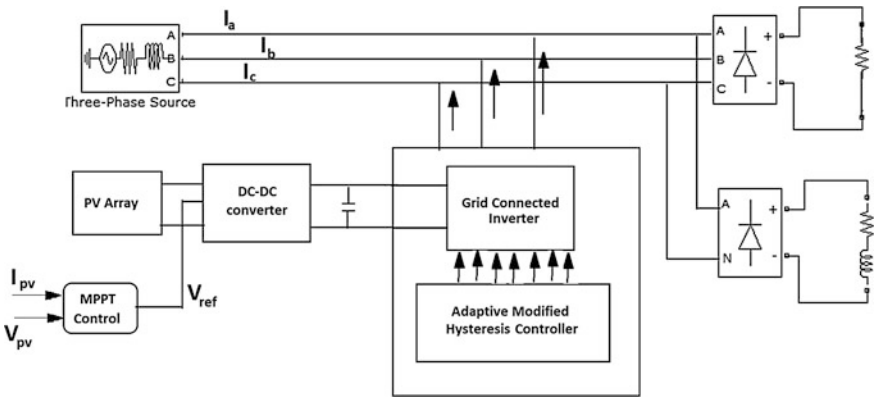

Fig. 1 Configuration of photovoltaic-fed grid-connected inverter

charges the capacitor of the grid-connected inverter. Compensation process also involves PLL synchronization and a PI controller for DC bus voltage regulation. The photovoltaic-fed grid-connected inverter injects real power from photovoltaic array into the grid, controls real power flow in the grid, and functions as a shunt active power filter.

3 Reference Current Generation Using Modified Icosϕ Algorithm

Modified Icosϕ algorithm provides real power support from the renewable energy source along with harmonic, reactive power and unbalances compensation in three-phase system, under balanced and unbalanced source and load conditions [7].

Magnitude of real component of fundamental load current in each phase is given by

$$\begin{aligned} |\mathrm{Re}(i_{\mathrm{La1}})| &= |i_{\mathrm{La}}| \cos \phi_a \\ |\mathrm{Re}(i_{\mathrm{Lb1}})| &= |i_{\mathrm{Lb}}| \cos \phi_b \\ |\mathrm{Re}(i_{\mathrm{Lc1}})| &= |i_{\mathrm{Lc}}| \cos \phi_c \end{aligned} \tag{1}$$

where i_{La1}, i_{Lb1}, and i_{Lc1} are three-phase fundamental current amplitudes, i_{La}, i_{Lb}, and i_{Lc} are the unbalanced harmonic-rich source currents, and ϕ_a, ϕ_b, and ϕ_c are the phase angles of fundamental currents. To ensure balanced sinusoidal currents at unity power factor to be drawn from the source, the magnitude of desired source current can be expressed as average of magnitudes of real components of fundamental load currents in the three phases.

$$I_{s(\mathrm{ref})} = [|\mathrm{Re}(i_{\mathrm{La1}})| + |\mathrm{Re}(i_{\mathrm{Lb1}})| + |\mathrm{Re}(i_{\mathrm{Lc1}})|]/3 \tag{2}$$

Using modified Icosϕ algorithm, desired source currents in three phases are expressed as

$$\begin{aligned} I_{\mathrm{sa(ref)}} &= K\left|I_{S(\mathrm{ref})}\right| * U_a = K\left|I_{s(\mathrm{ref})}\right| * \sin(\omega t) \\ I_{\mathrm{sb(ref)}} &= K\left|I_{S(\mathrm{ref})}\right| * U_b = K\left|I_{s(\mathrm{ref})}\right| * \sin(\omega t - 120^\circ) \\ I_{\mathrm{sc(ref)}} &= K\left|I_{S(\mathrm{ref})}\right| * U_c = K\left|I_{s(\mathrm{ref})}\right| * \sin(\omega t + 120^\circ) \end{aligned} \tag{3}$$

Here U_a, U_b, and U_c are unit amplitude templates of phase to ground voltages in three phases, respectively. Real power supplied by the grid is determined by the load factor K. Reference compensation currents for shunt active filter are deduced as difference between actual load currents and desired source current in each phase.

$$
\begin{aligned}
I_a(\text{comp}) &= i_{\text{La}} - I_{\text{sa(ref)}} \\
I_b(\text{comp}) &= i_{\text{Lb}} - I_{\text{sb(ref)}} \\
I_c(\text{comp}) &= i_{\text{Lc}} - I_{\text{sc(ref)}}
\end{aligned} \tag{4}
$$

4 Modified Hysteresis Controller with Adaptive Band

In three-wire system, it is sufficient to control current in only two phases. For compensating harmonic current at source side, harmonic current has to be injected into the grid from the inverter. To inject harmonic current, a generalized switching algorithm is developed based on grid voltage and injected current polarities [11]. Phases having same polarity of voltage are selected for control which results in low rate of change of inductor current and easier control. From the selected phases, controlling switches are selected based on the current polarity. Table 1 shows controlled and uncontrolled phases corresponding to different grid voltage regions. Table 2 shows controlled and uncontrolled switches corresponding to 60°–120° grid voltage region. Pulses to the modified hysteresis controller are generated using adaptive control by modifying pulses from the conventional hysteresis controller and are used to activate the power switches of the inverter. If IL < (IL_{ref} − HB), the upper switch is off and lower switch is on, for a particular leg. If IL > (IL_{ref} + HB), the upper switch is on and lower switch is off, for the same leg. IL_{ref} is the line reference current, and IL is the actual filter current of the respective leg. Variable hysteresis band is given by

Table 1 Selection of controlled phases

Voltage sector	U_a	U_b	U_c	Controlled	Uncontrolled
0°–60°	+ve	−ve	+ve	A, C	B
60°–120°	+ve	−ve	−ve	B, C	A
120°–180°	+ve	+ve	−ve	A, B	C
180°–240°	−ve	+ve	−ve	A, C	B
240°–300°	−ve	+ve	+ve	B, C	A
300°–360°	−ve	−ve	+ve	A, B	C

Table 2 Selection of controlled switches (60°–120°) region (t_2)

I_a	I_b	I_c	S_{ap}	S_{bp}	S_{cp}	S_{an}	S_{bn}	S_{cn}
+ve	−ve	−ve	On				C	C
+ve	−ve	+ve	On		C		C	
+ve	+ve	−ve	On	C				C
−ve	+ve	+ve	Off	C	C			
−ve	−ve	+ve	Off		C		C	
−ve	+ve	−ve	Off	C				C

$$\mathrm{HB} = \left\{ \frac{0.125 U_{\mathrm{DC}}}{f_c L} \left[1 - \frac{4L^2}{U_{\mathrm{DC}}^2} \left(\frac{U_s}{L} + m \right) \right]^2 \right\} \tag{6}$$

where f_c is modulation frequency, $m = \mathrm{d}I_c^{\mathrm{ref}}/\mathrm{d}t$ is the slope of reference current wave, U_{DC} is capacitor voltage of voltage source inverter, L is the interface inductance, and U_s is the voltage of respective phase. Adaptive hysteresis band current controller changes the hysteresis bandwidth according to slope of reference current to optimize switching frequency of inverter and THD of supply current.

4.1 Switching Algorithm

Let t_1, t_2, t_3, t_4 t_5, and t_6 represent the regions 0°–60°, 60°–120°, 120°–180°, 180°–240°, 240°–300°, and 300°–360° of the voltage sector, respectively [11]. Switches of the grid-connected inverter are S_{ap}, S_{an}, S_{bp}, S_{bn}, S_{cp}, and S_{cn}. Let symbols X_a, X_b, and X_c represent the polarity of reference currents I_a^{ref}, I_b^{ref}, and I_c^{ref}, respectively. Boolean expressions formulated for enabling signals to switch S_{cp} in terms of t_1, t_2, t_3, t_4, t_5, t_6 and X_a, X_b, X_c are given below. C_p is the pulse from conventional hysteresis controller. Similar expressions can be obtained for S_{ap}, S_{an}, S_{bp}, S_{bn}, and S_{cn}.

$$S_{\mathrm{cp}}(c) = (t_1 + t_2 + t_4 + t_5) \cdot X_c \tag{7}$$

$$S_{\mathrm{cp}}(\mathrm{on}) = t_6 \cdot X_c \tag{8}$$

$$S_{\mathrm{cp}} = S_{\mathrm{cp}}(c) \cdot C_p + S_{\mathrm{cp}}(\mathrm{on}) \tag{9}$$

5 Materials and Methods

Simulation was carried out in MATLAB/Simulink to demonstrate the effectiveness of adaptive modified hysteresis current controlled photovoltaic-fed grid-connected inverter in power quality enhancement. Simulation parameters are shown in Table 3.

Hardware setup for REALTIME implementation was done using REALTIME WINDOWS TARGET. Advantech PCI-1711 was used for real-time data acquisition. Efficient computer performs the operation of control circuitry. Signals were captured and graphed in SIMULINK scope blocks by using SIMULINK's external mode which enables us to observe the behavior of the real-time system.

Table 3 Design parameters used in simulation

Source voltage	180 V *L–L*
System frequency	50 Hz
DC link voltage	300 V
DC bus capacitance	5,000 μF
Interfacing inductance	1.5 mH
AC-side resistance	1 Ω
Nonlinear load	Three-phase diode rectifier feeding R = 2 kW
Unbalanced load	Single-phase diode rectifier feeding R = 50 Ω, L = 1 mH

6 Simulation and Experimental Results

THD of uncompensated source current which is 18.35 % is shown in Fig. 2. Total harmonic distortion of compensated source current was found to be 1.81 % as shown in Fig. 3. Figure 4 shows the optimized inverter frequency which is nearly 8KhZ. Figure 5 shows that DC bus voltage is nearly 300 V. Dynamic response of adaptive grid-connected inverter with modified hysteresis controller is shown in Fig. 6. A comparison of grid-connected inverter with conventional hysteresis

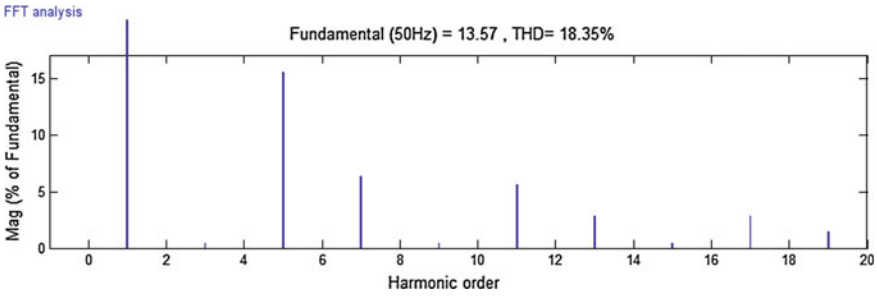

Fig. 2 THD of uncompensated source current

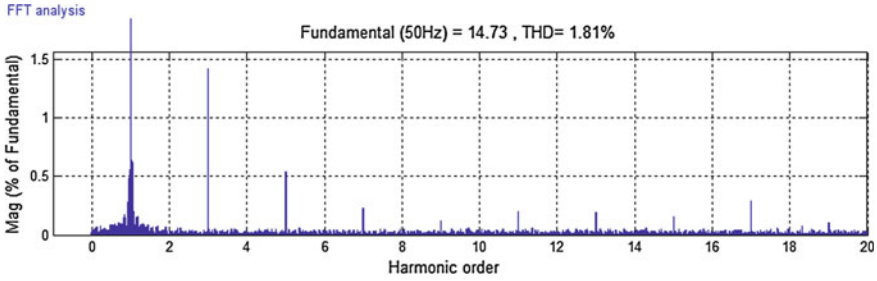

Fig. 3 THD of compensated source current

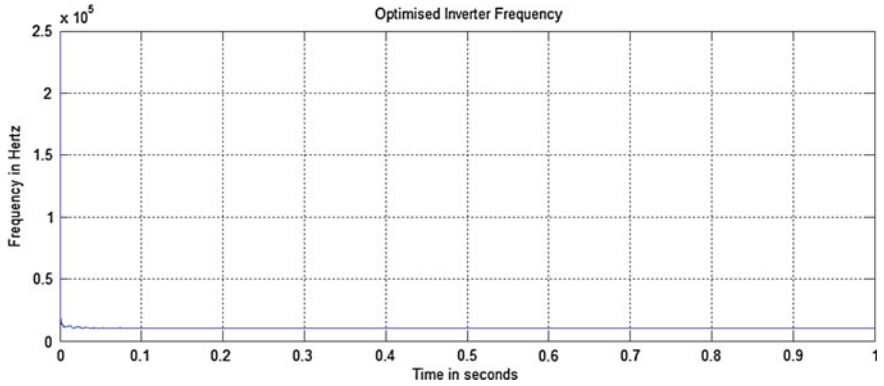

Fig. 4 Optimized inverter frequency

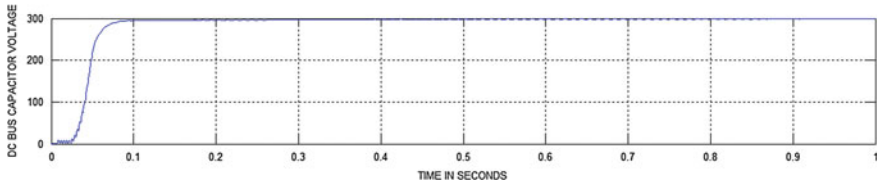

Fig. 5 DC bus capacitor voltage

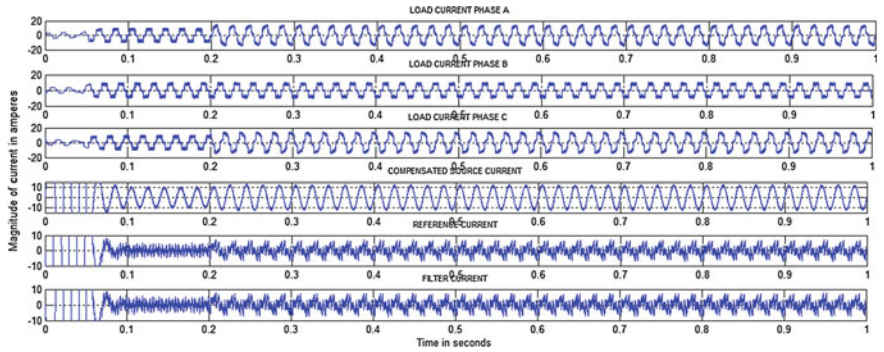

Fig. 6 Dynamic response to unbalanced load conditions

controller and modified hysteresis controller with and without adaptive control is shown in Table 4. Figure 7 depicts the power sharing between the grid and PV system.

Capacitor voltage stabilizes in almost 0.1 s. Till 0.1 s active power delivered by the filter (PV) is minimum and that delivered by the grid (source) is maximum. A

Table 4 Comparison of conventional and modified hysteresis controller

Current controller used	THD of supply current (%)	Switching frequency	Switching losses
Conventional hysteresis controller	4.17	Variable	Increased switching losses since all the six switches of the three-phase inverter are controlled at high frequency
Modified hysteresis controller	7.82	Variable	Switching losses reduced to one-third since only two switches are controlled at a time
Conventional hysteresis controller with adaptive control	2.67	Nearly constant	Increased switching losses since all the six switches of the three-phase inverter are controlled at high frequency
Modified hysteresis controller with adaptive control	1.81	Nearly constant	Switching losses reduced to one-third since only two switches are controlled at a time

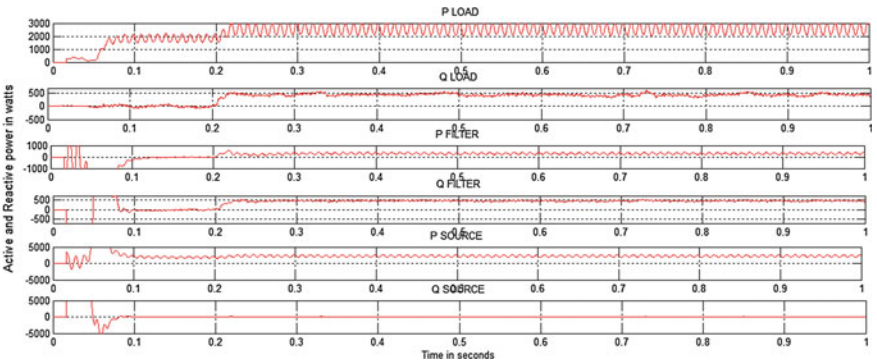

Fig. 7 Power sharing between grid and PV system

change in load current, reference current, and filter current occurs at 0.2 s when unbalanced load is turned on. Active power consumed by the load is the sum of active power supplied by the grid and active power supplied from the PV array (filter power). Reactive power requirement of the load is met by the shunt active power filter, maintaining that supplied by the source nearly zero.

7 Conclusion

Adaptive modified hysteresis current control can be successfully employed in photovoltaic-fed grid-connected inverters which help in reducing the switching losses to one-third of that of the conventional controller. Inverter switching

frequency is reduced and optimized with reduction in total harmonic distortion of supply current. Photovoltaic-fed grid-connected inverter functions as a dual-function grid-connected inverter. Good DC bus stabilization, reactive power compensation, satisfactory performance under unbalanced source and load conditions, and good dynamic response are also achieved.

References

1. R. Belaidi, A. Haddouche, H. Guendouz, Fuzzy logic controller based three-phase shunt active power filter for compensating harmonics and reactive power under unbalanced mains voltages. Energy Procedia. **18**, pp. 560–570 (2012)
2. M.N. Hossain, T.K. Routh, A.H. Bin Yousuf, M.M. Asasduzzaman, M.I. Hossain, U. Husnaeen, Design and development of a grid tied solar inverter. Int. Conf. Infonnatics Electron. Vis. pp. 1054–1058 (2012). doi: 10.1109/ICIEV.2012.6317344
3. N. Hamrouni, M. Jraidi, A. Cherif, New control strategy for 2-stage grid-connected photovoltaic power system. Renew. Energy **33**, pp. 212–2221 (2008)
4. K.M. Tsang, W.L. Chan, Three-level grid-connected photovoltaic inverter with maximum power point tracking. Energy Convers. Manag. **65**, pp. 221–227 (2013)
5. N.A. Ahmed, A.K. Al-Othman, M.R. Alrashidi, Development of an efficient utility interactive combined wind /photovoltaic/fuelcell power system with MPPT and DC bus voltage regulation. Electr. Power Syst. Res. **81**, pp. 1096–1106 (2011)
6. R. Noroozia, G.B. Gharehpetian, An investigation on combined operation of active power filter with photovoltaic arrays. Electr. Power Energy Syst. **46**, pp. 392–399 (2013)
7. K. Ilango, P.V. Manitha, M.G. Nair, Modified IcosΦ controller for shunt active filter interfacing renewable energy source and grid. AASRI Procedia. **2**, pp. 62–68 (2012)
8. N. Zaveri, A. Chudasama, Control strategies for harmonic mitigation and power factor correction using shunt active filter under various source voltage conditions. Electr. Power Energy Syst. **42**, pp. 661–671 (2012)
9. S.G. Tesfahunegn, A. Hajizadeh, T.M. Undeland, O. Ulleberg, P.J.S. Vie, Modelling and control of grid-connected PV/fuel cell/battery hybrid power system. Int. Rev. Model. Simul. **2**, pp. 381–388 (2009)
10. M. Kale, Engin Ozdemir.: An adaptive hysteresis band current controller for Shunt active power filter. Electr. Power Syst. Res. **73**, pp. 113–119 (2005)
11. M. Nanda Kumar, K. Vasudevan, A novel hysteresis switching strategy for harmonic compensation. Int. J. Energy Technol. Policy **4**, pp. 379–393 (2006)

Low-complexity Power Spectral Density Estimation

N. Balasaraswathy and R. Rajavel

Abstract This paper presents a method of feature extraction to detect seizure in epileptic patients. Epileptic seizures are characterized by high amplitude and synchronized electrocephalogram (EEG) waveforms. Power spectral density (PSD) of the EEG signal plays an important role in diagnosis of epilepsy. Many automated diagnostic systems for epileptic seizure detection have emerged in recent years. This paper proposes a method of extracting PSD of EEG sub-bands using low-complex PSD estimation method which would reduce the automatic diagnostic system complexity and also enhances the speed. Low-complexity PSD estimation method was implemented in digital signal processor (TMS320C6713), and the result was very much similar to traditional Welch PSD estimation method with 30 % reduction in computation time.

Keywords Electrocephalogram · Power spectral density · Digital signal processor · SONAR · RADAR

1 Introduction

One of the most important application areas of digital signal processing (DSP) is the power spectral estimation of periodic and random signals. Power spectrum estimation is used in SONAR and RADAR systems, to track signals of interest and in bio-medical systems to extract relevant information.

N. Balasaraswathy (✉) · R. Rajavel
ECE Department, SSN College of Engineering,
Kalavakkam, Chennai, India
e-mail: nbalasaraswathy@gmail.com

R. Rajavel
e-mail: rajavelr@ssn.edu.in

© Springer India 2015

L.P. Suresh et al. (eds.), *Artificial Intelligence and Evolutionary Algorithms in Engineering Systems*, Advances in Intelligent Systems and Computing 325,
DOI 10.1007/978-81-322-2135-7_30

Power spectrum describes the frequency content of the signal. Wiener–Khintchine theorem proves that power spectral density (PSD) $S(\omega)$ is the autocorrelation $R_{xx}(\tau)$ of the signal as given in Eq. (1)

$$S(\omega) = \int_{-\infty}^{\infty} R_{xx}(\tau) e^{j\omega t} d\tau \tag{1}$$

However, the above equation is not useful in computing the PSD in practice. Different estimation methods developed to compute PSD can be divided into two groups, parametric and nonparametric. Parametric methods are based on parametric models of a time series. The nonparametric methods do not need any parametric models, and they could calculate PSD directly from the signal. Two examples of nonparametric methods include periodogram-based methods and multiple-window method. Due to the availability of computationally efficient FFT algorithms, the periodogram method is often preferred to the parametric methods.

The Welch method [1] is a popular method to estimate PSD and is a nonparametric method based on the periodogram. Modifications to Welch method had been found in literature [2, 3], to reduce its computational complexity and its variance. But, these advantages come with some penalty, i.e., reduction in accuracy.

Automatic Seizure prediction system is one of the bio-medical signal processing systems which uses features of electrocephalogram (EEG) sub-bands from patients to detect epilepsy. A past research [4–6] reveals that PSD features are the most robust and reliable features to detect epilepsy in EEG. The PSD features of EEG sub-bands can be computed using Welch method or modified Welch method. However, the modified Welch method can drastically reduce computational complexity for PSD estimation. This paper presents a method to find computationally efficient PSD features from the EEG sub-bands to detect epilepsy.

This paper is organized as follows. Section 2 gives a brief overview of the low-complexity PSD computation. In Sect. 3, the proposed feature extraction scheme to detect seizure is described, and performance analysis is presented in Sect. 4. The conclusion and future direction is given in Sect. 5.

2 Low-complexity PSD Computation

2.1 Welch PSD

Welch suggests an effective method for measuring power spectra [1]. The algorithm is described as follows.

1. Divide the data sequence $x(n)$ into $L \leq N/M$ segments
2. Multiply a segment by an appropriate window
3. Take the Fourier transform of the product

4. Multiply procedure 3 by its conjugate and divide it by length of the segment to obtain modified periodogram of the segment as given in Eq. (2).

$$S_W^{\mathrm{l}}(f) = \frac{1}{\mathrm{PM}} |X_{M\mathrm{l}}|^2 \tag{2}$$

where P is the power of window function, and $X_{M\mathrm{l}}$ is the FFT of windowed segment $x_{\mathrm{l}}(n)$.

5. Averaging these periodograms would give the Welch PSD estimate.

The normalizing factor P is required so that the spectral estimate will be unbiased. With an overlap of 50 %, half the samples over two consecutive segments will be the same. If two consecutive $N/2$-point FFTs can be combined into one N-point FFT, then the number of computations can be reduced to $(L + 1)$ $N/2$-point FFTs, instead of LN FFT as in Welch method. A modified Welch algorithm based on this observation to reduce the number of computations required has been proposed [2].

2.2 Modified Welch Method

The main idea of modified Welch Method proposed in [2] is to compute the FFT of the individual non-overlapped parts (i.e., half of the original segments) and obtain the FFT of the overlapped segments by combining those of the non-overlapped segments. The window function for these non-overlapped parts will be different over two consecutive segments. Therefore, the windowing operation has to be performed in the frequency domain.

The modifications include two new steps in the algorithm:

(i) Perform the windowing operation in the frequency domain
(ii) Merge two $(N/2)$-point FFTs into an N-point FFT.

2.2.1 Windowing in Frequency Domain

The window function will be applied in the frequency domain instead of the time domain to take advantage of the overlapped segments. Mathematically, the multiplication operation in the time domain will be transformed into convolution in the frequency domain. However, the window functions used in the PSD computation typically represent raised cosine functions and these can be represented by three or five nonzero coefficients in the frequency domain. Figure 1 shows a 256-point hamming window and its frequency-domain counterpart.

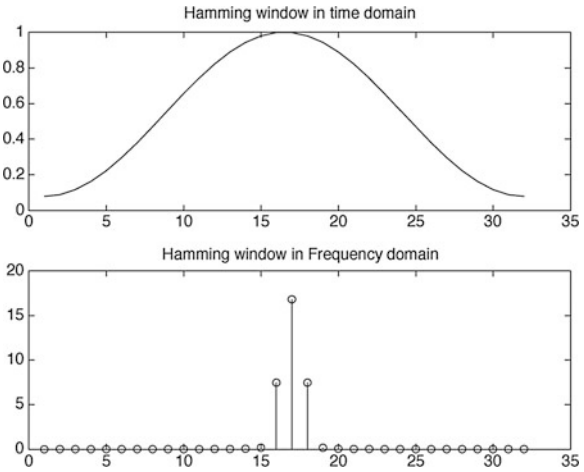

Fig. 1 Hamming window

2.2.2 Merging of Two N/2 FFTs

Due to the frequency-domain windowing, half of the samples are same in the two consecutive windows. The computational complexity can be reduced if the *N*-point FFT is obtained by combining two *N*/2-point FFTs. Using this approach, $(L + 1)$ *N*/2-point FFTs need to be computed instead of LN-point FFTs for every frame of the signal. Figure 2 illustrates the idea of merging two FFTs into one FFT to form an overlapped segment [2]. The mathematical derivation to merge the FFTs is presented below.

Consider a signal, $x(n)$, $n = 0, 1, \ldots, N - 1$ of length N. The FFT is given by

$$X(k) = \sum_{n=0}^{N-1} x(n) \mathrm{e}^{-j2\Pi nk} \tag{3}$$

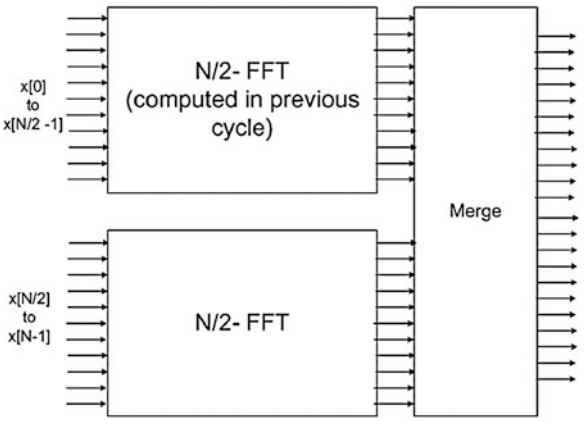

Fig. 2 Merging of two FFTs

Substituting $k = s + 2u$ and $n = 1 + mM$ in Eq. (3), where $M = N/2$, $s = \{0, 1\}$, $u = 0, \ldots, M - 1$, $m = \{0, 1\}$ and $1 = 0, 1, \ldots, M - 1$.

$$X(s+2u) = \sum_{m=0}^{1} \sum_{l=0}^{M-1} x(1+mM) e^{-j\frac{2\Pi}{N}ls} e^{-j\frac{2\Pi}{N}lu} e^{-j\Pi ms} \tag{4}$$

Define $X_1(k)$, $X_2(k)$, $X_3(k)$, $X_4(k)$ as

$$\begin{aligned} X_1(k) &= \sum_{n=0}^{M-1} x(n) e^{-j(2\Pi/M)nk} & X_2(k) &= \sum_{n=0}^{M-1} x(n+M) e^{-j(2\Pi/M)nk} \\ X_3(k) &= \sum_{n=0}^{M-1} x(n) e^{-j2\Pi nk} e^{-j\Pi n/M} & X_4(k) &= \sum_{n=0}^{M-1} x(n+M) e^{-j2\Pi nk} e^{-j\Pi n/M} \end{aligned} \tag{5}$$

All DFTs in (5) are of length $N/2$. From Eqs. (4), (5) and substituting, $s = 0$ and $s = 1$, Eqs. (6a) and (6b) are obtained, respectively [2]

$$X(2u) = X_1(k) + X_2(k) \tag{6a}$$

$$X(2u+1) = X_3(k) - X_4(k) \tag{6b}$$

Even samples can be computed exactly based on two $N/2$ FFTs $X_1(k)$ and $X_2(k)$. The exact computation of odd samples requires another set of two i/2-point FFTs, which does not lead to any reduction in the computational complexity. Equation (6a) can be rewritten as [2],

$$X(2u+1) = X_1(u+1/2) + X_2(u+1/2) \tag{7}$$

Two $N/2$-point FFTs can be merged into one N-FFT using Eqs. (6a) and (7).The even samples are computed exactly, but the odd samples can only be approximated due to fractional-delay (FD) shift. Figure 3 shows the direct implementation of Eq. (7) [2]. The circuit requires a positive shift by 0.5 which is non-causal. This can be converted into a causal system by adding the required number of pipeline stages [2], as shown in Fig. 4. Half-sample delay filter can be used to estimate the odd samples.

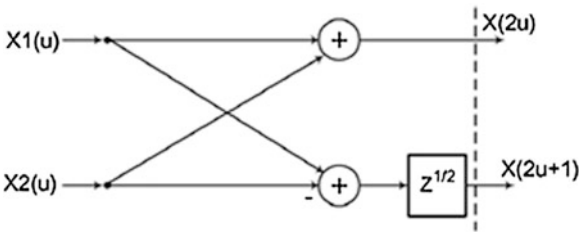

Fig. 3 Implementation of Eq. (7) in hardware

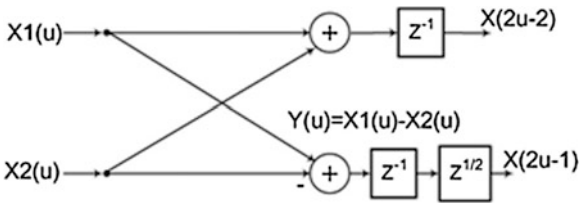

Fig. 4 Merging of FFTs by FD filter

Several design methods exist for both finite impulse response (FIR) and infinite impulse response (IIR) FD filters [7, 8]. FD filters are widely utilized in DSP such as speech coding and synthesis, arbitrary sampling-rate conversion, and timing adjustment in digital modems. Consider a delay element whose purpose is to delay the incoming discrete time signal by D samples, where D is a non-integer. The output signal can be expressed as $y[n] = x[n - D]$. The ideal impulse response for this system would be a sinc function. Different approaches have been published in the literature [7]. The least-squared integral error design approach is considered in this work. The impulse response $h[n]$ of an Nth-order least-square FD FIR filter can be expressed as

$$h_{id}(n) = \begin{cases} \sin c(n - D - N/2 + 1), & 0 < n \leq N - 1 \\ 0, & \text{otherwise} \end{cases} \tag{8}$$

Figure 4 shows the implementation of Eq. (7) based on least-square FD filter design. A delay is added to make it a causal system. The filter will estimate the output $X(2u - 1)$ based on the current sample $Y(u)$ and previous samples $Y(u - 1)$.

2.3 DSP Processor Implementation

The 32-bit floating point processor TMS320C6713 from Texas Instruments is very powerful for real-time speech, audio, and bio-medical signal processing algorithm implementations. This DSP processor is based on the VLIW technology and its operating speed is 225 MHz. TMS320C6713 is used to implement Welch and Modified Welch methods to estimate PSD.

An EEG signal with 2 min duration and sampling rate of 256 Hz is shown in Fig. 5. The Welch and Modified Welch methods are used to estimate the PSD of this EEG signal as shown in Fig. 6. As is shown in Fig. 6, the low-complexity PSD estimate follows the envelope of Welch PSD estimate, with little amount of distortion. However, experimental results showed that Welch method takes 400 ms to compute PSD, whereas Modified Welch method took only 280 ms to compute the same. This clearly indicates the reduction of computational complexity by 30 %.

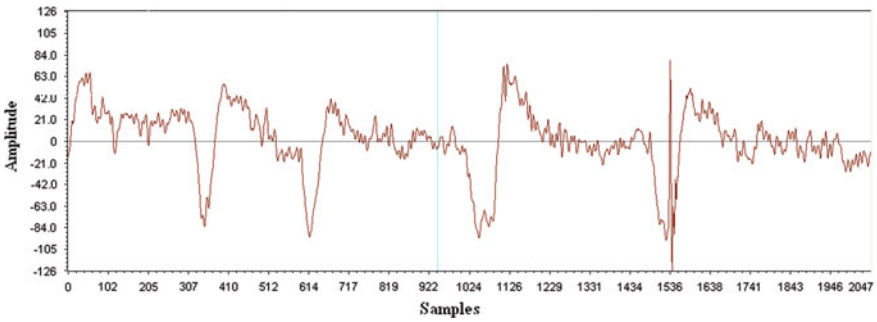

Fig. 5 EEG signal

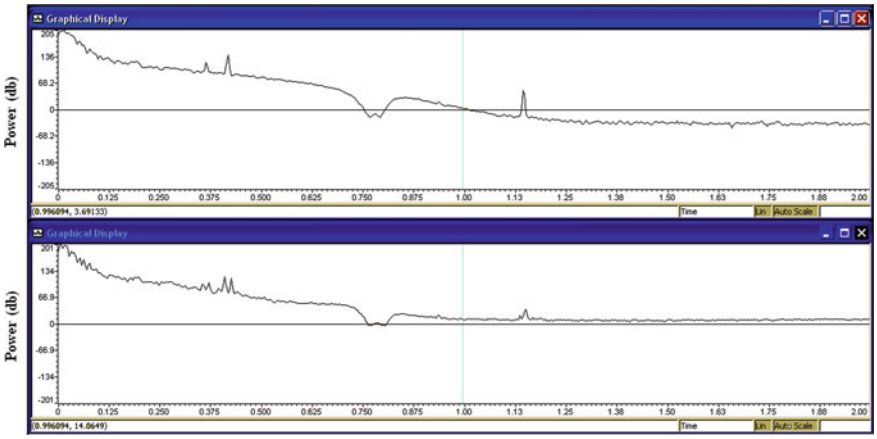

Fig. 6 PSD of EEG signal *Top panel* Welch, *Bottom panel*–modified welch (Implemented in DSP processor)

3 Feature Extraction to Detect Epilepsy

Epilepsy is one of the most common neurological disorders characterized by a sudden and recurrent malfunction of the brain, a "seizure." During seizures, the scalp EEG of patients with epilepsy is characterized by high-amplitude synchronized EEG waveforms. The PSD of EEG signal sub-bands has been used as a good measure to detect seizures in epileptic patients [9]. Applying low-complexity PSD estimate method in any seizure prediction system can reduce its computational complexity greatly.

Several methods have been proposed to automatically detect epilepsy by analyzing EEG data. The entire procedure of methodologies adopted by the researchers can be divided into following steps: Signal acquisition, feature selection and classification. PSD has been used as a useful feature to analyze EEG signals [4–6], since it is a good indicator of signal information, simple and quick to calculate and very robust.

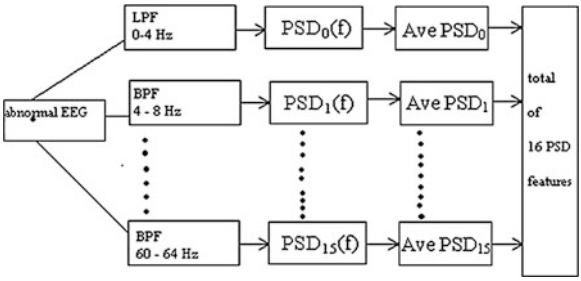

Fig. 7 PSD extraction from EEG signal

3.1 Dataset

EEG dataset maintained by Department of Epileptology, University of Bonn which is publicly available has been utilized in this work [10]. This dataset has been used widely in many reports [9, 11]. The complete dataset consists of five sets (denoted A–E), each containing 100 single-channel EEG signals of 23.6 s and sampling frequency 173.6 Hz. Sets *A* and *B* have been recorded extra cranially, from healthy volunteers, whereas sets *C*, *D*, and E have been recorded intra-cranially from epileptic patients. Set *D* contains data of epileptic patients during seizure-free intervals and Set *E* gives data of epileptic patients during seizures. For this work, only datasets *D* and *E* have been utilized.

3.2 Spectra of EEG Sub-bands

The 0–64 Hz frequency range of EEG signal was decomposed into 16 sub-bands with 4 Hz bandwidth. The averaged EEG log-power spectrum (using Modified Welch method) from each sub-band is shown in Fig. 7 considered as a spectral feature for classifiers.

The spectral feature of each sub-band i ($0 \le i \le 15$) is computed by Eq. (9).

$$\mathrm{PSD}_i = \mathrm{Mean}\,\mathrm{PSD}(f), \quad 4i < f \le 4(i+1) \tag{9}$$

where PSD(f) is the log power of frequency f.

4 Experimental Result

Sets *D* and *E* are taken and their PSD features are extracted to differentiate between seizure and non-seizure EEGs in epileptic patients. Figure 8 shows the result for average PSD of EEG sub-bands for 17th sample from Set D and 41st sample from Set E. It can be seen that both Welch and Modified Welch Methods give the same

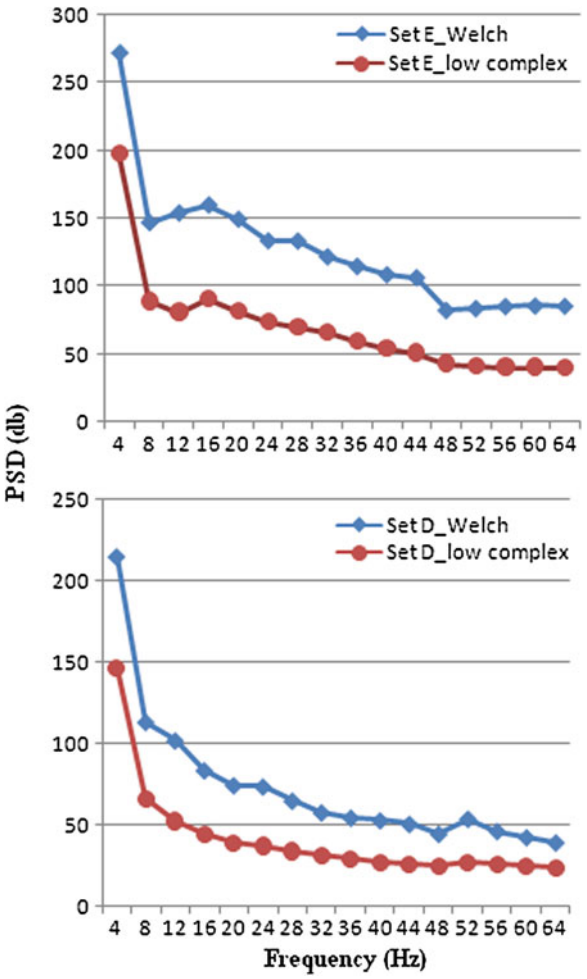

Fig. 8 PSD of EEG from dataset *D* and *E*

result as expected, i.e., Set *E* (EEG signal during seizure) has greater amplitude than Set *D* (EEG signal at seizure-free intervals of epileptic patients). But modified Welch method has computed these features at a faster rate. To compute PSD of each sub-band, Welch method took 79 ms, while it is only 57.5 ms in modified Welch method.

5 Conclusion and Future Work

This work proposed a method for PSD computation to be used in automatic seizure prediction by bio-medical systems. The PSD was computed based on Welch and Modified Welch method using TMS320C6713 DSP processor. The experimental

results show that the PSD computed using Modified Welch method differentiates seizure and non-seizure EEG waveforms with approximately 30 % reduction in computation time.

The future work would be to train Mahalanobis distance-based classifier [12] to automatically detect seizures from the extracted PSD features and estimate classification accuracy.

References

1. P.D. Welch, The use of fast fourier transform for the estimation of power spectra: A method based on time averaging over short, modified periodograms. IEEE Trans. Audio Electroacoust. 70–73 (1967)
2. K.K. Parhi, M. Ayinala, Low-complexity welch power spectral density computation. IEEE Trans. Circuit Syst. (2013)
3. K. Barbé, R. Pintelon, J. Schoukens, Welch method revisited: Nonparametric power spectrum estimation via circular overlap. IEEE Trans. Sig. Process. **58**(2), 553–556 (2010)
4. S.-F. Liang, H.-C. Wang, W.-L. Chang, Combination of EEG complexity and spectral analysis for epilepsy diagnosis and seizure detection. EURASIP J. Adv. Signal Process (2010)
5. S.R. Mousavi, M. Niknazar, B.V. Vahdat, in *Epileptic Seizure Detection Using AR Model on EEG Signals*. Proceedings of Cario International Biomedical Engineering Conference (CIBEC '08), 1–4 Dec 2008
6. B.C. Kuo, D.A. Landgrbe, Nonparametric weighted feature extraction for classification. IEEE Trans. Geosci. Remote Sens. **42**, 1096–1105 (2004)
7. T.I. Laakso, V. Valimaki, M. Karjalainen, U.K. Laine, Splitting the unit delay [FIR/all pass filters design]. IEEE Signal Process. Mag. **13**(1), 30–60 (1996)
8. E. Hermanowicz, Explicit formulas for weighing coefficients of maximally flat tunable FIR delayers. Electron. Letters. **28**(20), 1936–1937 (1992)
9. G. Garg, S. Behl, V. Singh, Assessment of non-parametric and parametric PSD estimation methods for automated epileptic seizure detection. J. Comput. **3**(5), 160–163 (2011)
10. http://epileptologie-bonn.de/cms/front_content.php?idcat=193
11. R.G. Andrzejak, K. Lehnertz, C. Rieke, Indications of non linear deterministic and finite dimensional structures in time series of brain electrical activity dependence on recording region and brain state. Phys.Rev.E. 64 (2001)
12. http://pub.ist.ac.at/~schloegl/publications/MDBC_classifier.pdf

Intensified Scheduling Algorithm for Virtual Machine Tasks in Cloud Computing

K.A. Saranu and Suresh Jaganathan

Abstract Scheduling of jobs is essential with distribution of load on processors and dynamic allocation of resources in order to get maximum benefit in terms of make-span. In scheduling the mapping of tasks are done based on its characteristics and user requirements. Many task parameters such as cost, load and required resources for the task completion are to be considered while scheduling. In cloud, the resources should be utilized efficiently and hence scheduling should consider the resource utilization to reduce the execution time and thereby increasing the throughput of the system. In this paper, we proposed a new scheduling algorithm supporting load balancing in cloud with respect to various types of quality services based on resources. To evaluate the scheduling algorithm, the performance metrics such as execution time, average execution time of each resource and number of tasks assigned to each resource are taken into consideration.

Keywords Scheduling · Cloud computing · Virtual machine · CloudSim

1 Introduction

The Cloud Computing is a pay-per-use on-demand model that can share resources through Internet. With the ownership of Internet connection, the users can make use of platform, hardware, software, storage and applications that are distributed over the network. The Cloud is a type of distributed and parallel system, where there is a collection of virtualized and interconnected computer resources. Virtual machines are created for providing and supporting heterogeneous platform by the Cloud

K.A. Saranu (✉) · S. Jaganathan
Department of Computer Science and Engineering, SSN College of Engineering, Anna University, Chennai, Tamil nadu, India
e-mail: saranu.ka@gmail.com

S. Jaganathan
e-mail: whosuresh@gmail.com

© Springer India 2015

L.P. Suresh et al. (eds.), *Artificial Intelligence and Evolutionary Algorithms in Engineering Systems*, Advances in Intelligent Systems and Computing 325,
DOI 10.1007/978-81-322-2135-7_31

Computing environment. Based on the Service Level Agreements negotiated between the providers and users, the resources are dynamically provisioned as unified computing resources. To assist the users, the cloud computing environment provides the job scheduling [1] in order to accomplish the user's tasks with reasonable time. There are different types of scheduling algorithms [2, 3] available to assign the jobs to the resources to get their tasks executed efficiently.

1.1 Scheduling in Cloud Computing

Task scheduling [4, 5] plays an important role in cloud computing, which maps the users tasks to resources to be executed efficiently in order to benefit both the service providers and customers. There are two main categories of Task Scheduling in Cloud Computing [6] namely Online Mode Heuristic Algorithms and Batch Mode Heuristic Algorithms. In online mode, the tasks are scheduled as soon as they arrive in the system. The best example for online mode algorithm is Most Fit Task Scheduling algorithm. In batch mode, the arriving tasks are queued and collected into a set. After a fixed period of time, the scheduling of tasks to resources is done. First Come First Serve, Round Robin, Max–Min and Min–Min algorithms are based on batch mode. The remaining part of this paper is organized as Sect. 2 describes the various scheduling algorithms in cloud. Then in Sect. 3, the flow diagram and pseudo code of the proposed algorithm are illustrated. Section 4 specifies the implementation details of the proposed algorithm. In Sect. 5, the Min–Min, Max–Min and proposed ISA scheduling algorithms are compared and results of comparison are analyzed. Finally, Sect. 6 concludes the paper.

2 Related Work

First Come First Serve (FCFS) algorithm is the default scheduling algorithm which is very simple to implement. It is a straight forward approach where the tasks are assigned to the first available resource which executes it. As the first available resources are assigned with tasks, the efficient utilization of resources and load balancing is not achieved in FCFS. Round Robin (RR) is another task scheduling algorithm which focuses mainly of load balancing. The RR scheduling algorithm allocates task to resource in cyclic manner and switching happens with specified time quantum between the tasks assigned to the resource. In RR, for selecting the time quantum, the current load has to be considered each time which is complex process. Min–Min algorithm works based on the expected completion time which is calculated based on the users task and available resource specifications. Min–Min algorithm performs its execution in two steps. In the first step it finds the task-machine correspondence that is done by selecting a task first and selecting machine with minimum completion time of that task among all existing machines. In the

second step, select and assign the task to machine which has minimum completion time among the task-machine correspondence. By doing so, the shorter jobs are executed faster. Max–Min [7] algorithm, first finds the task-machine correspondence that is done by selecting a task first and selecting machine with minimum completion time of that task among all existing machines. In the second step, select and assign the task to machine which has maximum completion time among the task-machine correspondence. By doing so, the longer jobs are executed faster.

3 Proposed Work

The Intensified Scheduling Algorithm for Virtual machine Tasks (ISA) works on batch mode of scheduling where the tasks are queued upon their arrival and are assigned with resources for execution based on the expected completion time of each task on the resources. Figure 1 specifies the flow diagram of the Intensified Scheduling Algorithm.

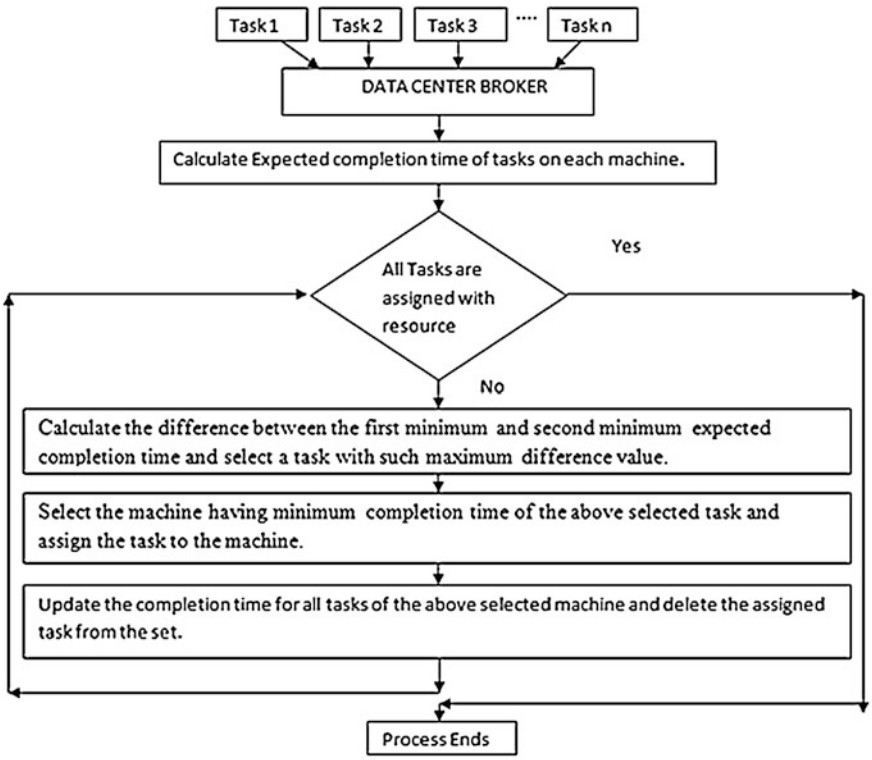

Fig. 1 Proposed work-flow diagram

The expected completion time is calculated based on certain parameters of task and machine. For tasks, the parameters such as file length and the Random Access Memory (RAM) size required for the task to be executed are taken into consideration. For virtual machines (VM), the parameters such as Million Instructions per Second (MIPS) rate and RAM size are taken into consideration. For each task, the difference between the first minimum and second minimum expected completion time is calculated and a task with such maximum difference value is selected. For the selected task, find the VM which executes it faster. That is, the VM having minimum completion time of the selected task is taken and the task is assigned to the VM. After submitting the task to a VM, update the completion time for all other tasks of the above selected VM and delete the assigned task from the set. The process is continued until all the tasks are assigned with resources. Algorithm 1 specifies the pseudo code for Intensified Scheduling Algorithm for virtual machine tasks.

Algorithm 1 (*Pseudo code for ISA*)

Input: User submission of Jobs
Output: Job completion

1. For all tasks t_i submitted to Cloud
2. For all available machines (resources) VM_j
3. Compute Completion time for each task i on machine j (CT_{ij})
   [End step 2 loop]
   [End step 1 loop]
4. Repeat step 5 to 9 until all tasks are mapped to machines
5. For each task t_i in meta-task
   Find the First minimum completion time (First_Min)
   Find the Second minimum completion time (Second_Min)
   Difference Value=ABS (Second_Min - First_Min)
   [End step 5 loop]
6. Select the task (t_p) having maximum difference value as per Step 5.
7. Allocate task to machine (VM_p) that will complete t_p in minimum time.
8. Update completion time of all unmapped tasks on machine VM_p
9. Delete task t_p
   [End step 4 loop]
10. Compute execution time of each machine, count number of tasks assigned for each machine and average execution time.

4 Implementation

The Proposed algorithm is tested by varying the number of resources i.e. 4, 3, 4, 6 on number of tasks i.e. 10, 20, 40, 40 respectively. The algorithm is compared with the existing algorithms such as Min–Min and Max–Min. The parameters such as number of tasks executed on each machine and average execution time of each

Table 1 Specifications of tasks

Parameter	Tasks									
	*T*1	*T*2	*T*3	*T*4	*T*5	*T*6	*T*7	*T*8	*T*9	*T*10
Task length	251	609	174	215	738	244	221	234	863	268
RAM (GB)	2	4	8	8	4	2	4	8	2	4

Table 2 Specifications of VM

Parameter	VM		
	*M*1	*M*2	*M*3
MIPS rate	1000	1000	500
RAM (GB)	2	4	8

machine are considered and the results are taken in comparison with all the three algorithms. CloudSim toolkit is useful for testing scheduling algorithms repeatedly with varying specifications of tasks and resources. By varying the Processing Elements (PE) specifications and number of tasks, the Min–Min, Max–Min and proposed algorithm are tested. It has been observed that the average execution time of proposed algorithm is less when compared to Min–Min and Max–Min in all the cases. For expected completion time calculation, here we have taken three VM available in the cloud and ten tasks are submitted to the cloud. The task parameters such as task length and RAM size are represented in Tables 1 and 2, the VM parameters such as MIPS Rate and RAM are listed. Based on the values of Tables 1 and 2 the expected completion time is calculated as follows. The ratio of the task length required for task to the MIPS rate of VM is added to the ratio of RAM size required for the task to the RAM size of VM. The obtained value is then multiplied with constant value of 100 to get the expected completion time of each task to each VM and is denoted in Table 3.

Table 3 Expected completion time of 10 tasks on 3 VM (milliseconds)

Machine	Tasks									
	*T*1	*T*2	*T*3	*T*4	*T*5	*T*6	*T*7	*T*8	*T*9	*T*10
*M*1	26.1	62.9	21.4	25.5	75.8	47.6	24.1	27.4	87.3	28.2
*M*2	25.6	61.9	19.4	23.5	74.8	47.1	23.1	25.4	86.8	27.8
*M*3	50.5	122.4	35.9	44.0	148.1	93.4	44.8	47.8	172.9	54.1

5 Result and Analysis

The Min–Min, Max–Min and ISA algorithms are implemented and the results are analyzed.

5.1 Results of 3 Virtual Machines and 20 Tasks

Figure 2a shows the overall execution time of each virtual machine with respect to each algorithm. By Min–Min, the tasks are executed at equal or slightly faster than ISA. When compared to Max–Min, tasks are executed almost faster in ISA, for example in Fig. 2a for virtual machine 3 there is a drastic increase in execution time of Max–Min when compared to ISA. Figure 2b clearly specifies the number of tasks assigned to each virtual machine with respect to all the three algorithms. For virtual machine 3, even though eight tasks are assigned by ISA its execution time less when compared to Min–Min and Max–Min as mentioned in Fig. 2a.

5.2 Results of 6 Virtual Machines and 40 Tasks

Figure 3a shows the overall execution time of each virtual machine with respect to each algorithm. When compared to Max–Min, the tasks are executed on an average of less time in ISA. In ISA, tasks are executed faster than Min–Min except for fewer cases, for example in the Fig. 3a for virtual machine 1 and 4 only there is an increase in execution time of ISA whereas it yields better results on all virtual

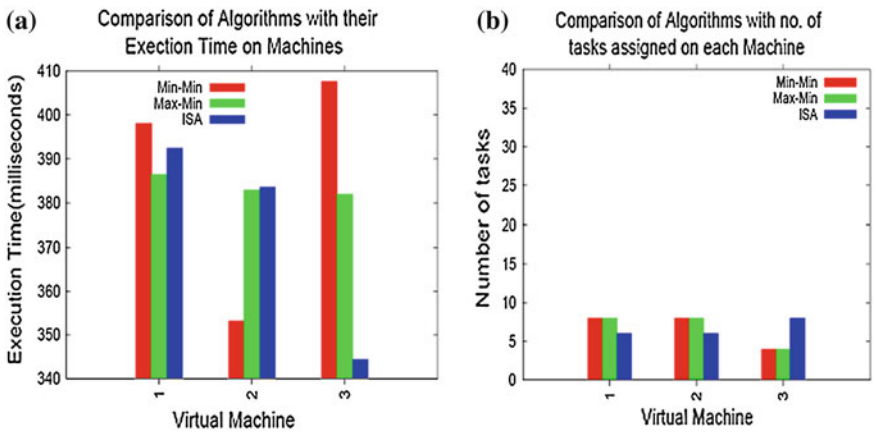

Fig. 2 **a** VM versus execution time (3 × 20) **b** VM versus no. of tasks (3 × 20)

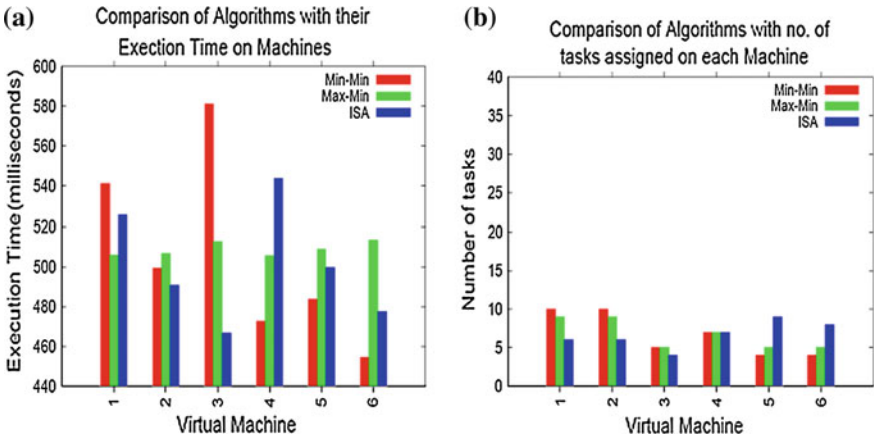

Fig. 3 **a** VM versus execution time (6 × 40) **b** VM versus no. of tasks (6 × 40)

machines. Figure 3b clearly specifies the number of tasks assigned to each virtual machine with respect to all the three algorithms. For virtual machine 5, even though nine tasks are assigned by ISA its execution time is less when compared to Min–Min as mentioned in Fig. 3a which ensures load balancing.

5.3 Comparison Algorithms with Their Average Execution Time

Table 4 gives the average completion time of all the algorithms with varying the number of VM and number of tasks. Figure 4 shows the average execution time of machines with respect to each algorithm with reference to values of Table 4. When compared to Min–Min and Max–Min, ISA has the execution time average value as minimum in all the four cases.

Table 4 Comparison of algorithms with their average execution time (milliseconds)

VM × Tasks	Algorithm		
	Min–Min	Max–Min	ISA
4 × 10	148.66	149.63	146.83
3 × 20	386.17	383.64	373.37
4 × 40	662.75	665.89	652.25
6 × 40	505.33	508.64	500.64

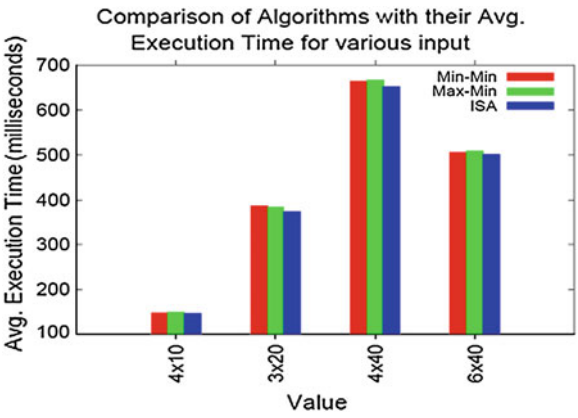

Fig. 4 Machine × tasks versus avg. execution time

6 Conclusion

In Cloud Computing, the task scheduling plays a major role where the efficient utilization of resources for both service providers and customers is taken into consideration. Here we have proposed batch mode scheduling algorithm. The average execution time of ISA in all cases is less when compared to Min–Min and Max–Min which ensures the efficient resource utilization. Also the parameter, number of tasks executed on each machine is taken into account which ensures load balancing.

References

1. S. Supreeth, S. Biradar, Scheduling virtual machines for load balancing in cloud computing platform. Int. J Sci Res. **2**(6), 2319–7064 (2013)
2. S. Sindhu, S. Mukherjee, Efficient task scheduling algorithms for cloud computing environment, in *High Performance Architecture and Grid Computing* (Springer, Berlin, 2011). pp. 79–83
3. Y. Chawla, M.A. Bhonsle, Study on scheduling methods in cloud computing. Int. J. Emerg. Trends Technol. Comput. Sci. **1**(3), 12–17 (2012)
4. S. Selvarani, G.S. Sadhasivam, Improved cost-based algorithm for task scheduling in cloud computing, in *Computational Intelligence and Computing Research, IEEE International Conference* (2010), pp. 1–5
5. Y. Fang, F. Wang, J. Ge, A task scheduling algorithm based on load balancing in cloud computing, in *Web Information Systems and Mining* (Springer, Berlin, 2010), pp. 271–277
6. I.A. Mohialdeen, Comparative study of scheduling algorithms in cloud computing environment. J. Comput. Sci. **9**(2), 252–263 (2013)
7. E.S.T. El-kenawy, A.I. El-Desoky, M.F. Al-rahamawy, Extended max-min scheduling using petri net and load balancing. Int. J. Soft Comput. **2**(4), 2231–2307 (2012)

Design of Neural Network Model for Emotional Speech Recognition

H.K. Palo, Mihir Narayana Mohanty and Mahesh Chandra

Abstract Human–computer interaction (HCI) needs to be improved for the field of recognition and detection. Exclusively, the emotion recognition has major impact on social, engineering, and medical science applications. This paper presents an approach for emotion recognition of emotional speech based on neural network. Linear predictive coefficients and radial basis function network are used as features and classification techniques, respectively, for emotion recognition. Results reveal that the approach is effective in recognition of human speech emotions. Speech utterances are directly extracted from audio channel including background noise. Totally, 75 utterances from 05 speakers were collected based on five emotion categories. Fifteen utterances have been considered for training and rest are for test. The proposed approach has been tested and verified for newly developed dataset.

Keywords Emotion recognition · LPCC · RBFN · Autocorrelation function · Radial basis function · Artificial neural networks

1 Introduction

In case of human-to-human communication, emotion recognition plays a major role. Over last decades, many researchers have worked on human emotions. But, the human–machine interaction is a major challenge and the focus point of current research. Recognition systems based on emotional speech [1–3] have various

H.K. Palo (✉) · M.N. Mohanty
Siksha 'O' Anusandhan University, Ranchi, India
e-mail: hemantapalo@soauniversity.ac.in

M.N. Mohanty
e-mail: mihirmohanty@soauniversity.ac.in

M. Chandra
Birla Institute of Technology, Ranchi, India
e-mail: shrotriya69@rediffmail.com

© Springer India 2015

L.P. Suresh et al. (eds.), *Artificial Intelligence and Evolutionary Algorithms in Engineering Systems*, Advances in Intelligent Systems and Computing 325,
DOI 10.1007/978-81-322-2135-7_32

applications in medical field, psychological test, security, robotic control, mobile communication, etc. Emotion is a multimodal concept, and its detection is a difficult task. Automatic emotion recognition [4–6] from speech signal has become a major research area for human–computer interaction (HCI) in recent times due to variety of applications. The acoustic properties of speech signal are the main focus for emotion recognition in this paper.

The most commonly used acoustic features in literature are LPC features and prosody features such as pitch, intensity, and speaking rate [2, 7]. Although it seems easy for a human to detect the emotional classes of an audio signal, but researches have shown average score of identifying different emotional classes such as neutral, surprise, happiness, sadness, and anger. Emotion recognition is one of the fundamental aspects to build man–machine environment that provide theoretical and experimental basis of the right choice of emotional signal for understanding and expression of emotion.

The variability of expression can be represented as amplitude, frequency, and other parameters. Nonverbal information (e.g., the emotional state) is important in communication between humans. Sometimes, the verbal information is more important than the emotional states. The communication between humans and computers is spreading day by day for various applications.

2 Related Literature

The work done on emotion recognition from speech signal by various researchers is presented in this section. In [1], authors have attempted to detect with domain-specific emotions using language and discourse information in conjunction with acoustic correlates of emotion in speech signals. Also, authors suggested a combination of three sources of information—acoustic, lexical, and discourse for emotion recognition. Optimization of the acoustic correlates of emotion with respect to classification error was accomplished by investigating different feature sets obtained from feature selection, followed by principal component analysis. They claimed that the method improves emotion classification by 40.7 % for males and 36.4 % for females. In [2], authors took attempt for emotional speech recognition with the most frequent acoustic features such as the pitch, the formants, the vocal tract cross-sectional areas, the mel-frequency cepstral coefficients, the Teager energy operator-based features, the intensity of the speech signal, and the speech rate. They classify speech into emotional states with techniques based on hidden Markov models, artificial neural networks, linear discriminant analysis, k-nearest neighbors, and support vector machines [3, 4].

Many authors attempted with neural network such as multi-layer perception (MLP), back propagation algorithm, and recurrent neural network as the recognizing model. Some of them applied the same for real-time applications. For many applications of emotion recognition, such as virtual agents, the system must select

responses while the user is speaking. However, some emotion recognition systems are based on turn-wise processing [8–10].

Most of the models have been proposed based on Linear Discriminant Classifier (LDC), Maximum Likelihood Bay's (MLB) Classifier. In the recent years, Gaussian mixture models (GMM), neural networks (NN), multilayer perception (MLP), k-nearest neighbor (KNN), hidden Markov model (HMM), and support vector machine (SVM) were used to recognize speech emotion [11–15].

3 Proposed Method for Recognition

Emotional speech recognition systems are combined process of feature extraction and classification.

3.1 Feature Extraction

Extracting suitable features is a challenging task in the emotion recognition system. Linear prediction coefficients (LPC) are one of the popular and important features used in speech signal processing. Initially, LPC features were used for speech recognition [11, 13, 16] tasks, but later on, they have given excellent performance for emotion recognition tasks as well. The Linear predictive cepstral coefficients (LPCC) feature extraction technique has further improved the recognition performance.

The algorithm for LPCC features is explained as follows:

Digital Filtering (*Pre-emphasis*): The digitized speech signal, $s(n)$, is put through a low-order digital system, to spectrally flatten the signal and to make it less susceptible to finite precision effects later in the signal processing.
Frame Blocking: The output of pre-emphasis is blocked into frames of N samples, with adjacent frames being separated by M samples.
Windowing: Next, it is required to window each individual frame so as to minimize the signal discontinuities at the beginning and end of each frame. Generally, the Hamming window is considered in this case.
Autocorrelation Analysis: It has to be performed for each frame of windowed signal so as to give the autocorrelation coefficients.
LPC Analysis: In this analysis, the Durbin's method is used to convert each frame of $p + 1$ autocorrelations into LPC parameter sets.
LPC Parameter Conversion to Cepstral Coefficients: To find the cepstral coefficients, it is derived directly from the LPC using the following relation:

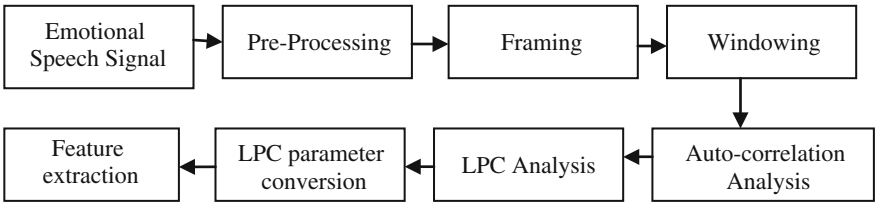

Fig. 1 Block diagram of LPCC feature

$$\text{LPCC} = \text{LPC}_i + \sum_{k=1}^{i-1} \left(\frac{k-i}{i}\right) \text{LPCC}_{i-k} \text{LPC}_k \tag{1}$$

The block diagram for feature extraction is shown in Fig. 1.

3.2 Emotion Recognition

Speaker and speech recognition systems have been developed by many authors [7, 11, 12] as described in literature. Radial basis function network (RBFN) is one of the most effective models for classification. In this work, the neural network model has been used for emotion recognition with RBF network.

3.2.1 Radial Basis Function Network

A radial basis function neural network has an input, hidden layer, and output layer. The input layer is composed of an input vector as shown in Fig. 2. The hidden layer consists of RBF activation function as networks neuron. The net input to the RBF activation function is the vector distance between its weight (w) and the input vector (i), multiplied by the bias b. Each neuron in the network includes an activation function (f). Radial functions are a special class of functions whose value increases

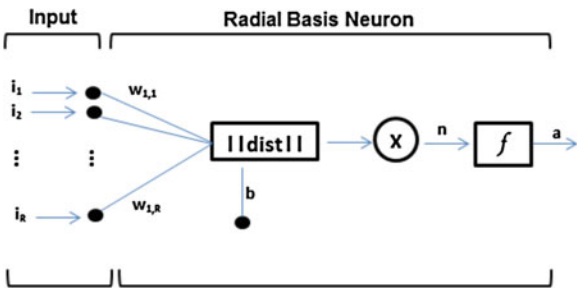

Fig. 2 Radial basis network with R inputs

or decreases in relation to the distance from a central point. The RBF network is shown in Fig. 2.

The RBF model for emotion recognition selects responses when the user is speaking. A novel approach is presented for online emotion recognition using RBF neural networks and LPC features. Emotion is recognized using frame-wise speech signal. In contrast to current state-of-the-art approaches, recognition is performed on signal frames, similar to those used for speech recognition. The Gaussian function is preferred in pattern classification applications although various functions have been tested as activation function for RBF networks [15, 16]. The RBF networks with Gaussian activation function is given by

$$\varphi_j(X) = \exp\left[-(X-\mu_j)^T \sum_j^{-1} (X-\mu_j)\right] \tag{2}$$

For $j = 1\ldots, L$, where X is the input feature vector, L is the number of hidden units.

Geometrically, a radial basis function is represented in a multi-dimensional space. Its mean vector represents the location, while shape of the activation function is modelled by the covariance matrix. The output layer implements a weighted sum of hidden-unit outputs:

$$\psi_k(X) = \left[\sum_{j=1}^{L} \lambda_{jk}\varphi_k(X)\right] \tag{3}$$

For $k = 1\ldots, M$, where λ_{jk} are the output weights, each corresponding to the connection between a hidden unit and an output unit and M represent the number of output units. The weights λ_{jk} show the contribution of hidden unit to the respective output unit.

3.2.2 Training Algorithms

The neural network models the underlying function of a certain mapping through training. In supervised application, a set of data samples called training set is provided for which the corresponding network outputs are known. In this case, the network parameters are calculated in such a way so that they minimize a cost function.

$$\min \sum_{i=1}^{Q} [Y_k(X_i) - F_k(X_i)]^T [Y_k(X_i) - F_k] \tag{4}$$

where Q is the total number of vectors from the training set, denotes the RBF output vector, and represents the output vector associated with the a data sample from the training set. A large variety of training algorithms has been tested for training RBF networks. In initial stage, each data sample was assigned a basis function. In RBF,

centers are uniformly distributed in the data space. The function to be modeled is obtained by interpolation. To train the RBF model a variety of training algorithms has been tested for different data. A least squares solution minimizes the interpolation error is proposed and is expressed as,

$$\left\|X_i - \widehat{\mu}_j\right\| = \min_{k=1}^{L} \left\|X_i - \widehat{\mu}_j\right\| \tag{5}$$

where, $\left\|X_i - \widehat{\mu}_j\right\|$ is represented as the Euclidean norm. The Euclidean distance can be replaced with the Mahalanobis distance [14]. In order to avoid the singularity of the covariance matrix computation, sufficient large number of data samples must be considered for the covariance matrix calculation used in the Mahalanobis distance for which it has not been considered. A set of generator functions is proposed for hidden unit activation function selection.

4 Result and Discussion

The database has been prepared for five emotions for a group of five students. The emotions include anger, happiness, boredom, sadness, and surprise. Database of five students, including two men and three women, was recorded in English for 1.5–4 s duration. Speech was recorded at 8 kHz sampling rate with 8 bits.

The feature vector we used to represent the emotional speech in our approach aims to preserve the information needed to determine the emotional content of such a signal. First, each speech utterance was segmented into 30 ms frames with a 15 ms overlap with next frame.

From the Fig. 3, it was observed that the surprise emotion has highest peaks among all the four emotions followed by angry emotion. Sad, boredom, and happy

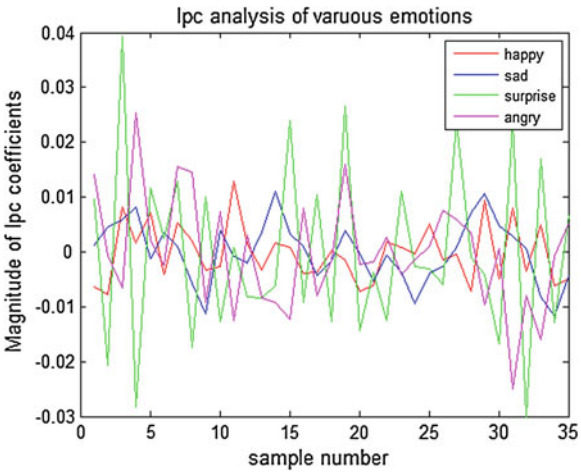

Fig. 3 LPC analysis of emotions happy, sad, surprise, and angry

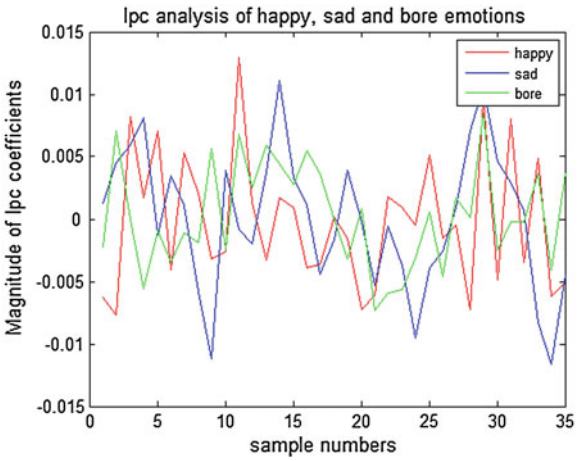

Fig. 4 LPC analysis of emotions happy, sad, and bore

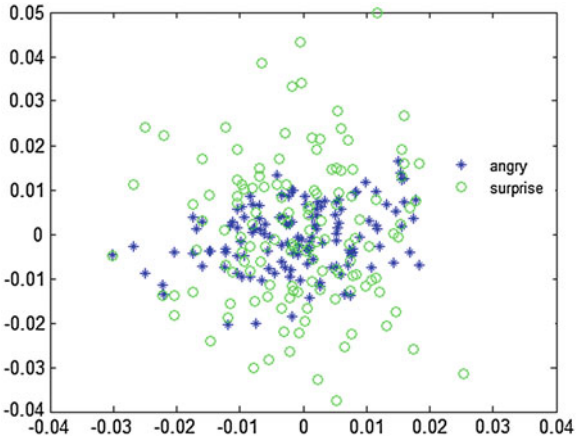

Fig. 5 Spatial representation of the angry and surprise emotion

emotions mostly have similar peaks as observed from Fig. 4. It is observed that spatial spread of surprise emotion is more than angry emotion from Fig. 5. Similarly, the results have been shown in Figs. 6, 7, and 8 for various emotions.

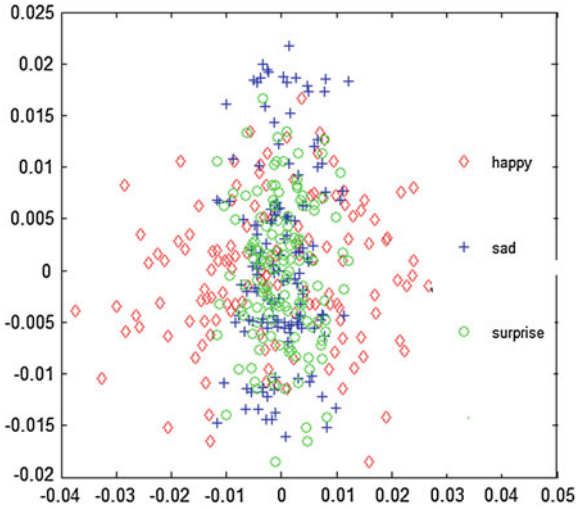

Fig. 6 Spatial representation of the happy, sad, and surprise emotion

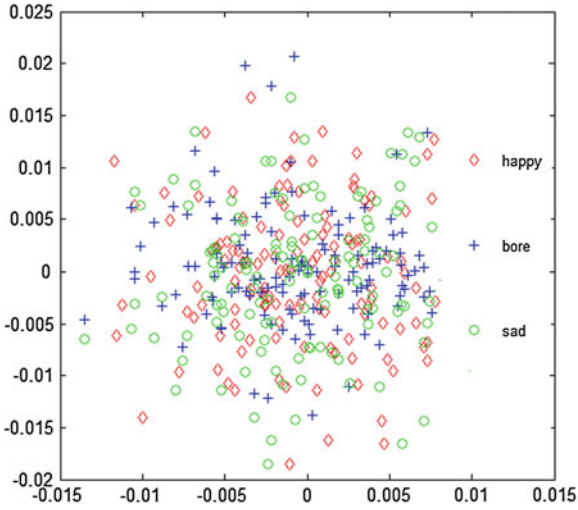

Fig. 7 Spatial representation of the happy, bore, and sad emotion

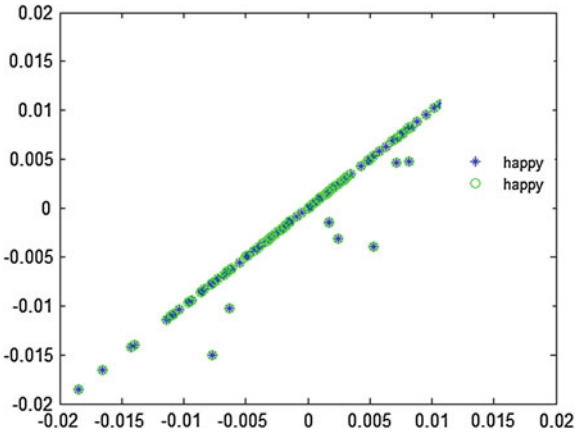

Fig. 8 Spatial representation of the happy emotion

5 Conclusion

It was observed from Fig. 3 that surprise and angry emotion are higher class emotions having higher peaks among all other emotions. Surprise emotions have highest peaks followed by the angry emotions. Sad emotions have lowest peak out of all emotions. It was also observed from Fig. 4 that among lower class emotions, happy emotions have the highest peak followed by sad emotions. Bore emotions have the lowest peaks among all. It was observed from Fig. 6 that higher class emotions, surprise and angry, are more spatially spread than sad emotions. Further, we observed from Fig. 7 that all the three sad, bore, and happy emotions are having lower peaks, and they are evenly clustered with respect to each other.

References

1. C.M. Lee, S.S. Narayanan, Toward detecting emotions in spoken dialogs. IEEE Trans. Speech Audio Process. **13**(2), 293–303 (2005)
2. D. Ververidis, C. Kotropoulos, Emotional speech recognition: resources, features, and methods. Speech Commun. **48**, 1162–1181 (2006)
3. N. Fragopanagos, G. Taylor, Emotional speech recognition: resources, features, and methods. Neural Networks **18**, 389–405 (2005)
4. F. Eyben et al., On-line emotion recognition in a 3-D activation-valence-time continuum using acoustic and linguistic cues. J. Multimodal User Interfaces **3**, 7–19 (2010)
5. T. Polzehl, A. Schmitt, F. Metze, M. Wagner, Anger recognition in speech using acoustic and linguistic cues. Speech Commun. **53**(9–10), 1198–1209 (2011)
6. F. Dellaert, T. Polzin, A. Waibel, Recognizing emotion in speech, in *ICSLP* (1996), pp. 1970–1973
7. B.S. Atal, Automatic recognition of speakers from their voices. IEEE **64**(4), 460–476 (1976)
8. M.M. Javidi, F. Roshan, Speech emotion recognition by using combinations of C5.0, neural network (NN), and support vector machines (SVM) classification methods. J. Math. Comput. Sci. **6**, 191–200 (2013)

9. M.N. Mohanty, B. Jena, Analysis of stressed human speech. Int. J. Comput. Vision Robot. **2** (2), 180–187 (2011)
10. M.N. Mohanty, A. Routray, P. Kabisatpathy, Voice detection using statistical method. Int. J. Eng. Techsci. **2**(1), 120–124 (2010)
11. J. Makhoul, Linear prediction: a tutorial review. Proc. IEEE **63**, 561–580 (1975)
12. B.S. Atal, S.L. Hanauer, Speech analysis and synthesis by linear prediction of the speech wave. J. Acoust. Soc. Am. **50**(2), 637–655 (1971)
13. T.F. Quatieri, *Discrete-Time Speech Signal Processing*, 3rd edn. (Prentice-Hall, Upper Saddle River, 1996)
14. A. Samal, D. Parida, M.R. Satpathy, M.N. Mohanty, On the use of MFCC feature vectors clustering for efficient text dependent speaker recognition, in *Proceedings of the International Conference on Frontiers of Intelligent Computing: Theory and Application (FICTA)-2013*, vol. 247 (2013), pp. 305–312
15. S. Haykins, *Neural Networks* (Prentice-Hall, Upper Saddle River, 1999)
16. J.H.L. Hansen, B.D. Womack, Feature analysis and neural network based classification of speech under stress. IEEE Trans. Speech Audio Process. **4**, 307–313 (1996)

Intelligent Decision Making with Improved Energy Detection for Precise Spectrum Sensing in Cognitive Radios

K. Muthumeenakshi, S. Radha, R. Sudharsana and R. Tharini

Abstract Energy detection is best suited for the spectrum sensing when prior knowledge about the licensed user is unavailable. The performance of this technique is primarily influenced by the available test statistic, number of samples used to compute the test statistic and the decision threshold and described in terms of probability of detection and false alarm. This paper focuses on an intelligent sensing scheme with improved energy detection algorithm in which the test statistic is computed using an arbitrary positive power instead of squaring operation. The detection performance is found to be considerably improved compared to the traditional energy detection algorithm. Simulations are performed, and the results confirm the accuracy of the analysis.

Keywords Energy detection · Wireless communication · Cognitive radio · Signal-to-noise ratio

1 Introduction

Recent studies on wireless spectrum demonstrate that the wireless communication systems suffer from spectrum scarcity and inefficient spectrum usage, which leads to the reformation in the static spectrum assignment policies by the FCC [1]. The new policy schemes would allow the vacant portions of the licensed spectrum bands to be used by the unlicensed users (called secondary users) without causing interference to the licensed users (called primary users). Cognitive radio (CR), identified as a novel paradigm, is anticipated to make this policy reformation successful.

CRs are devices that can alter its transmission/reception parameters based on the changes monitored in the environment and identify opportunities to transmit data

K. Muthumeenakshi (✉) · S. Radha · R. Sudharsana · R. Tharini
Department of ECE, SSN College of Engineering, Chennai, India
e-mail: muthumeenakshik@ssn.edu.in

© Springer India 2015

L.P. Suresh et al. (eds.), *Artificial Intelligence and Evolutionary Algorithms in Engineering Systems*, Advances in Intelligent Systems and Computing 325,
DOI 10.1007/978-81-322-2135-7_33

when the incumbent is not using [2]. To achieve this intelligent functionality, CRs employ a key enabling technology called spectrum sensing. Spectrum sensing techniques enable the CR to find the best available spectrum bands. Energy detection, matched filter detection, and cyclostationary feature detection [3] are popular among them. Among these methods, energy detection is a simple and non-coherent technique, which compares the energy of the received signal with a pre-evaluated threshold. The performance of the existing techniques provide different trade-offs between detection accuracy, sensing time, and computational complexity. The original energy detector was proposed in [4] for an unknown deterministic signal assuming a flat band-limited Gaussian channel. Recently, the energy detector proposed in [4] is being used extensively for CR spectrum sensing owing to its simplicity and lesser computational requirements. An improved energy detector is proposed for spectrum sensing in [5], where the performance is analyzed both theoretically and using experimentation observations. Another improved version of energy detector is proposed in [6], in which the test statistic of the energy detector is computed with an arbitrary positive power instead of squaring. In [7], the use of optimized positive power to compute the test statistic which outperforms under low signal-to-noise ratio (SNR) conditions is discussed. In this paper, we propose an improved energy detection scheme with arbitrary positive power used for the computation of test statistic. The performance of the proposed scheme is analyzed in terms of the receiver operating characteristic (ROC) and compared with the existing schemes. The sensing error is analyzed for varying signal-to-noise ratio (SNR) is investigated.

2 Spectrum Sensing Preliminaries

The CR spectrum sensing is a binary hypothesis testing problem and can be formulated as follows.

$$y(n) = \begin{cases} w(n) & ;H_0 \\ s(n) + w(n) & ;H_1 \end{cases} \quad n = 1, 2, \ldots .N, \tag{1}$$

where hypothesis H_0 denotes the absence of the primary user, and hypothesis H_1 denotes the presence of the primary user. $y(n)$ is the signal received at the CR, $w(n)$ is the AWGN of variance σ_w^2, and $s(n)$ is the primary user signal assumed to be real Gaussian with variance σ_s^2. The conventional energy detector that uses squaring operation to compute the test statistic is given by

$$Y = \frac{1}{N} \sum_{n=1}^{N} \left| \frac{y(n)}{\sigma_w} \right|^2, \tag{2}$$

where Y is the test statistic, and N is the number of samples used for computation. The test statistic Y is compared with a pre-evaluated threshold λ. If $Y \geq \lambda$, the decision is hypothesis H_1, otherwise hypothesis H_0. Practically, errors arising from spectrum sensing algorithms are classified as missed detections and false alarms. A missed detection occurs when the outcome of the spectrum sensing is H_0 and the primary signal is actually present. Alternatively, a false alarm occurs when the sensing outcome is H_1, and the primary spectrum is idle. These errors are often denoted by the following probabilities. The probability of missed detection, $P_{md} = P(H_0/H_1)$, and the probability of false alarm, $P_f = P(H_1/H_0)$. The complementary probability of missed detection is denoted as $P_d = P(H_1/H_1) = 1 - P_d$. It is required to have large P_d and low P_f for any spectrum sensing algorithm. However, there exists a trade-off between the two values.

3 The Proposed Intelligent Sensing Scheme

In this section, we discuss the proposed intelligent sensing scheme that employs improved energy detection algorithm. The enhanced energy detector [5] makes use of an arbitrary positive power p to compute the test statistic instead of squaring operation. The modified test statistic of the improved energy detector Y_m with pth power summer is given by,

$$Y_m = \frac{1}{N}\sum_{n=1}^{N}\left|\frac{y(n)}{\sigma_w}\right|^p \underset{H_0}{\overset{H_1}{\gtrless}} \lambda_m \tag{3}$$

where λ_m is the modified decision threshold. Using [7], the mean and variance of $|y(n)/\sigma_w|^p$ is given by,

Under H_0:

$$\mu_0 = \frac{2^{p/2}}{\sqrt{\pi}}\Gamma\left(\frac{p+1}{2}\right) \quad \text{and} \quad \sigma_0^2 = \frac{2^p}{\sqrt{\pi}}\left[\Gamma\left(\frac{2p+1}{2}\right) - \frac{1}{\sqrt{\pi}}\Gamma^2\left(\frac{p+1}{2}\right)\right]$$

Under H_1:

$$\mu_1 = \frac{2^{p/2}(1+\alpha)^{p/2}}{\sqrt{\pi}}\Gamma\left(\frac{p+1}{2}\right) \quad \text{and}$$
$$\sigma_1^2 = \frac{2^p(1+\alpha)^p}{\sqrt{\pi}}\left[\Gamma\left(\frac{2p+1}{2}\right) - \frac{1}{\sqrt{\pi}}\Gamma^2\left(\frac{p+1}{2}\right)\right]$$

The P_d and P_f of the IED are given by $P_f = Q\left(\frac{\lambda-\mu_0}{\sigma_0/\sqrt{N}}\right)$ and $P_f = Q\left(\frac{\lambda-\mu_0}{\sigma_0/\sqrt{N}}\right)$

The proposed intelligent sensing scheme with improved energy detection algorithm is explained as follows:

1. At every *i*th sensing instant, the signal energy value is calculated using *N* samples and compared with the modified decision threshold.
2. If the signal energy falls below the threshold, the signal energy value of its pervious instant $(i - 1)$ and the average signal energy values of the past *M* sensing instants are compared with the modified decision threshold. This step is performed to avoid any misdetection or false alarm due to instantaneous signal energy variations.
3. If the signal energy is greater than these values, then the detection outcome is H_1, else H_0.
4. The detection probability is analyzed for varying *p,* and the optimal value of *p* with the best detection performance is chosen. For practical spectrum sensing, the optimal *p* can be found for various *N*, Pf, and SNR values and can be stored in a lookup table. Based on the requirement, the optimal parameters can be quickly obtained from the table.

The algorithm is analytically as follows. The mean and variance of the average signal energy of the past *L* sensing instants are given by [5],

$$\mu_{\text{avg}} = \frac{M}{L}\mu_1 + \frac{L-M}{L}\mu_0 \text{ and } \sigma^2_{\text{avg}} = \frac{M}{L^2}\sigma^2_1 + \frac{L-M}{L^2}\sigma^2_0,$$

where *M* denotes the number of times the licensed user is detected out of *L* sensing instants. The probability of detection of the proposed intelligent sensing algorithm P_d^i is given by,

$$P_d^i = P_d + (1 - P_d)P_d\left\{Q\left(\frac{\lambda - \mu_{\text{avg}}}{\sigma_{\text{avg}}}\right)\right\} \tag{4}$$

The corresponding false alarm probability P_f^i is given by,

$$P_f^i = P_f + (1 - P_f)P_f\left\{Q\left(\frac{\lambda - \mu_{\text{avg}}}{\sigma_{\text{avg}}}\right)\right\} \tag{5}$$

The probabilities of detection and false alarm are bounded by $P_d \le P_d^i \le 2P_d - P_d^2$ and $P_f \le P_f^i \le 2P_f - P_f^2$ as the value of *Q* function lies between 0 and 1. Also, these probabilities depend on the value of *p*, which further improves the performance of the sensing algorithm. It is possible to find an optimum choice of *p* for which the detection performance is the best.

4 Simulation Results and Discussions

To verify the accuracy of the proposed algorithm, the ROC curves, SNR performance, and the sample complexity analysis are performed and compared with the existing algorithms. We refer to the traditional energy detection with $p = 2$ as CED,

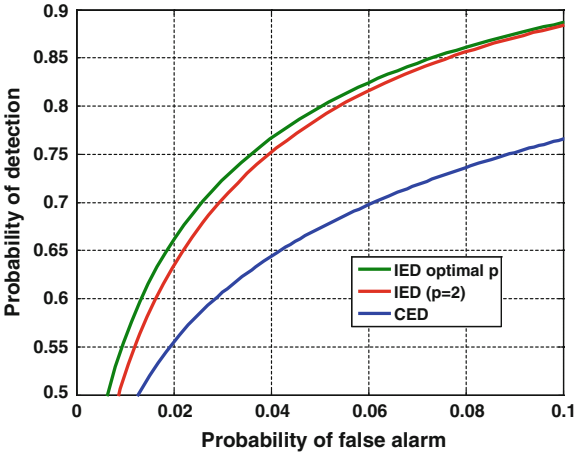

Fig. 1 ROC performance for $M = 10$, SNR = −5 dB

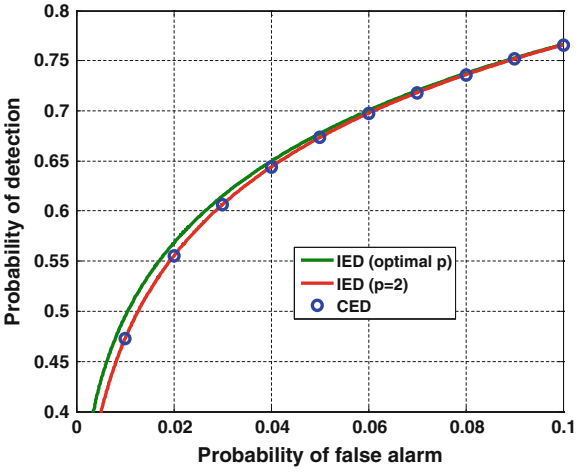

Fig. 2 ROC performance for $M = 0$, $N = 100$ and $N = 100$, and SNR = −5 dB

improved energy detection algorithm with $p = 2$ as IED and the proposed improved energy detection algorithm with optimal p as the IED with optimal p.

Figures 1 and 2 shows the ROC performance of the intelligent sensing with improved energy detection algorithm for $M = 0$ and $M = 10$, respectively. We have compared the ROC performance of the traditional energy detector ($p = 2$), improved energy detector ($p = 2$), and the proposed detector with optimal p. As depicted, for the IED with optimal p, the performance improvement is guaranteed for values of p other than 2 and shows that the traditional detector is not the optimal detector. The ROC performance is analyzed for lower values of P_f in the range of 0–0.1. In this range, the improvement is P_d for the proposed optimal detector is substantial. Even for the lower end, i.e., when $M = 0$, the performance improvement can be noticed.

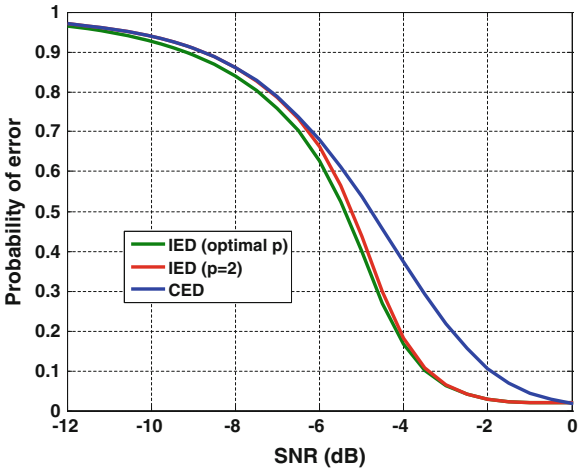

Fig. 3 Probability of error against SNR $M = 10$, $P_f = 0.01$, and $N = 100$

Next, the total probability of error ($P_f + P_{md}$) is computed and plotted against SNR in Figs. 3 and 4. It shows that the total error probability declines as SNR increases. In the low SNR regime, the IED algorithm has a probability of error similar to that CED algorithm. This is because of the degradation experienced in the false alarm probability. However, the degradation of the false alarm probability is not as large in our proposed algorithm with optimal p. Hence, it gives a low error probability over the wide range of SNR. Both under $M = 0$ and $M = 10$, the error probability is found to be less for the proposed algorithm compared to CED and IED.

Finally, in Fig. 5, the number of samples required to achieve a target P_d and P_f is analyzed and found to be less for the proposed algorithm than others.

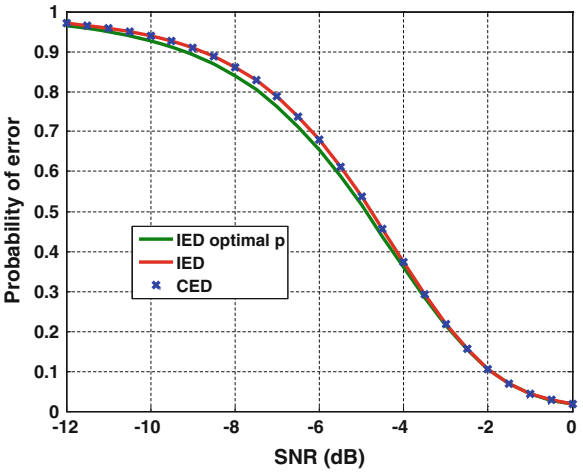

Fig. 4 Probability of error against SNR $M = 0$, $P_f = 0.01$, and $N = 100$

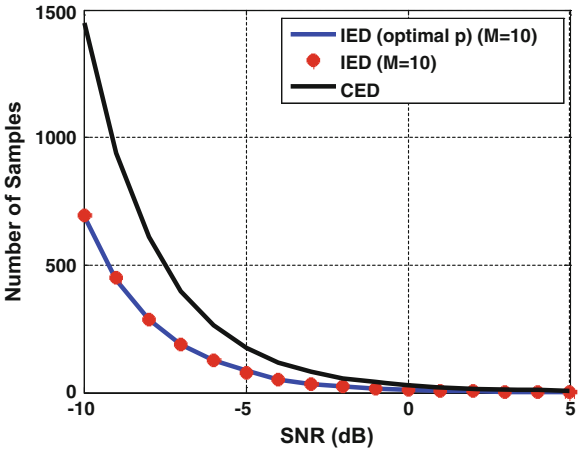

Fig. 5 Sample complexity ($P_d = 0.9$ and $P_f = 0.1$)

5 Conclusion

Energy detection has gained much popularity owing to its simplicity and low computational complexity. In this paper, we proposed an intelligent decision making for spectrum sensing with improved energy detection algorithm to enhance the performance of sensing accuracy. First, the probability of detection and false alarm for the proposed algorithm is derived. It is observed that the detection performance varies with p and considerable performance improvement is achieved for values of p other than 2. Then, the sensing error is measured in terms of the total probability of error and found to be low compared to the existing algorithms. Finally, the number of samples required for a target performance is computed and found to be less compared to the existing algorithms. Simulation results validate the efficacy of the proposed algorithm and found to be superior over the existing schemes.

References

1. F. Akyildiz, W.Y. Lee, S. Mohanty, Next generation/dynamic spectrum access/cognitive radio wireless networks: a survey. Comput. Netw. J. (Elsevier) **50**, 2127–2159 (2006)
2. T. Arslan, A survey of spectrum sensing algorithms for cognitive radio applications. Commun. Surv. Tutor. IEEE. **11**(1), 116–130 (First Quarter 2009)
3. H. Urkowitz, Energy detection of unknown deterministic signals. Proc. IEEE. **55**, 523–531 (1967)
4. M. López-Benítez, F. Casadevall, Improved energy detection spectrum sensing for cognitive radio. Commun. IET **6**(8), 785–796 (2012)
5. Y. Chen, Improved energy detector for random signals in Gaussian noise. IEEE Trans. Wirel. Commun. **9**(2), 558–563
6. J. Song, Z. Feng, P. Zhang, Z. Liu, Spectrum sensing in cognitive radios based on enhanced energy detector. Commun. IET **6**(8), 805–809 (2012)
7. Federal Communications Commission, Spectrum policy task force report (2002)

Human Action Recognition by Employing DWT and Texture

V. Thanikachalam and K.K. Thyagharajan

Abstract Human action recognition is a very challenging task due to the great variability with which different people may perform the same action. It involves in the development of applications such as automatic monitoring, surveillance, and intelligent human–computer interfaces. We propose an action recognition scheme to classify human actions based on positive portion using template-based approach from a video. We first define the accumulated motion image (AMI) using frame differences to represent the spatiotemporal features of occurring actions. Then, the direction of motion is found out by computing motion history image (MHI). Texture and spatial information are extracted from AMI and MHI using (LBP) local binary pattern and (DWT) discrete wavelet transform, respectively. The detection of object and extraction of moving objects are done by feature extraction over LBP and DWT. The feature vectors are computed by employing the seven Hu moments. The system is trained using nearest neighbor classifier, and the actions are classified and labeled accordingly. The experiments are conducted on Weizmann dataset.

Keywords Accumulated motion image · Discrete wavelet transform · Human action recognition · Local binary pattern · Motion history image · Nearest neighbor algorithm

1 Introduction

Due to the popularization of surveillance cameras and personal video devices, video-based human motion analysis and recognition have become a highly active area in computer vision. Human action recognition is difficult for many reasons,

V. Thanikachalam (✉)
SSN College of Engineering, Chennai, India
e-mail: thanikachalamv@ssn.edu.in

K.K. Thyagharajan
RMD Engineering College, Chennai, India
e-mail: kkthyagharajan@yahoo.com

© Springer India 2015

L.P. Suresh et al. (eds.), *Artificial Intelligence and Evolutionary Algorithms in Engineering Systems*, Advances in Intelligent Systems and Computing 325,
DOI 10.1007/978-81-322-2135-7_34

such as high dimension of video data, intra-class variability caused by scale, viewpoint and illumination changes, low resolution, and video quality. Human action recognition is the process of identifying human actions that occur in the video sequences. Its application is involved in surveillance footage, user interfaces, robotics, automatic video organization, patient monitoring systems, athletic performance analysis, etc. Even though this topic has been studied for several years, it has some problem in classifying the actions performed by human accurately.

2 Review of Related Work

Various surveys have been done in this area on recognition methodologies and approach-based and general overview-based taxonomies [1, 2]. Tracking motion of human and action recognition from the sequence of images is analyzed [3]. The extension of [3] in the development of motion analysis has been surveyed by Wang et al. [4]. This paper is organized in hierarchical manner which describes issues caused during detection, tracking, and behavior understanding within human motion analysis system. Kim et al. [5] proposed the scheme over an ordinal measure of accumulated motion in a single query action video without considering whole silhouette of human body as in the earlier [6].

A set of activities is described using motion template system in [7]. Various methods which employ MHI have been proposed in [8] and provide variants and its applications of this method. The combined prompt of MHI and MEI is proposed in [9] for representation of motion based on optical flow-based directional history and energy image templates. To extract the judicial information from given video sequences, Shao et al. [10] proposed a system using wavelet transform-based descriptors for representation and recognition of human action. A multiscale representation has been proposed in [11] by comparing the efficiency with Gabor filter and discrete wavelet transform (DWT) which applied prior to dimensionality reduction. It results Gabor has the highest efficiency in recognition.

The local binary pattern (LBP) has been used from past 10 years, and it is widely used for texture classification proposed in [12–14].

3 Proposed Work

The proposed method consists of the following stages: accumulated motion image (AMI), motion history image (MHI), DWT, LBP, feature extraction, training, and classification. The overall procedure is shown in the flow diagram Fig. 1.

Fig. 1 Flow diagram

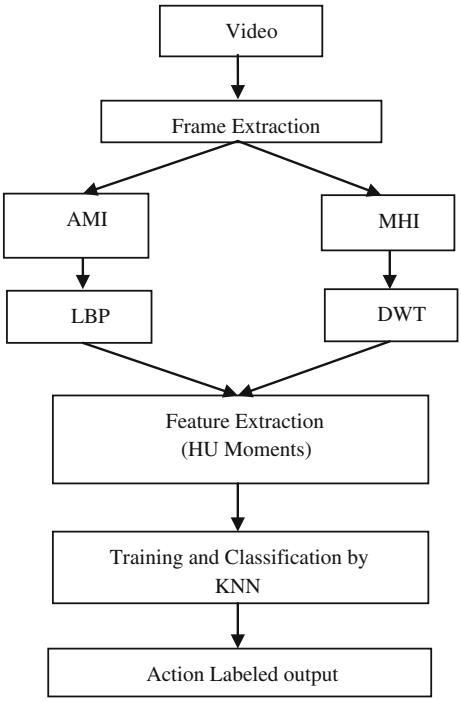

3.1 Accumulated Motion Image (AMI)

In the proposed system to represent the spatiotemporal features of human actions, we define AMI and it is computed by using frame differences. AMI is computed using frame differences as in Eq. 1

$$\mathrm{AMI} = \frac{1}{T}\sum_{t=1}^{T} |D(x, y, t)| \tag{1}$$

where $D(x, y, t) = I(x, y, t) - I(x, y, t-1)$ and T denotes the total number of frames present in a single action video.

Figure 2 shows the AMI computed for a jacking video and one-hand wave action.

3.2 Motion History Image (MHI)

MHI is extensively used in action recognition research areas. It provides motion shape information of a video to recognize actions.

Fig. 2 AMI for jack and one-hand wave action

To represent how the motion occurs in a video, form a motion history image (MHI) is computed by using a simple replacement and decay operator as in Eq. 2

$$H_\tau(x,y,t) = \begin{cases} \tau & \text{if } D(x,y,t) = 1 \\ \max(0, H_\tau(x,y,t-1) - 1) & \text{otherwise} \end{cases} \quad (2)$$

where τ is the current time stamp and D is the absolute value of silhouette difference between frames t and $t - 1$. The result will be the scalar-valued image where brighter pixel shows the most recently occurred action.

Figure 3 shows the MHI computed for a jacking action and one-hand wave action video

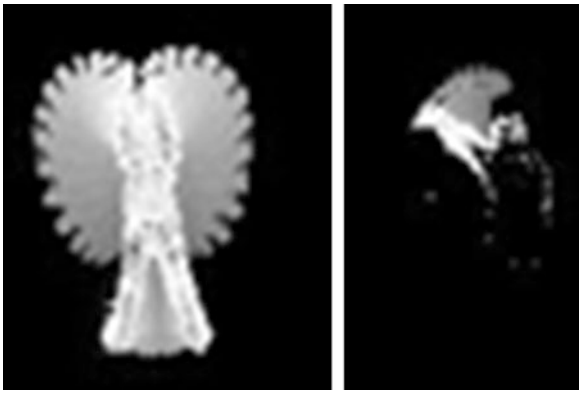

Fig. 3 MHI for jacking and one-hand wave action

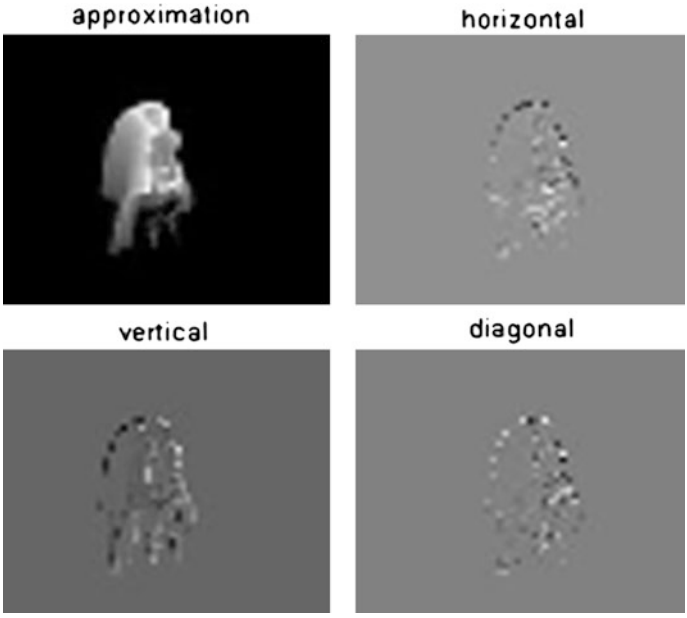

Fig. 4 DWT of MHI in different directions

3.3 Discrete Wavelet Transform (DWT)

DWT is used to extract the spatial features and for dimensionality reduction. In the proposed system, we use Haar wavelet filter for decomposition of the MHI image.

Figure 4 shows the output of the DWT.

3.4 Local Binary Pattern (LBP)

LBP is applied over AMI to extract the edge information. In texture analysis, the sampling is done on equally spaced sampling points P on a circular neighborhood with radius R. The value of the LBP code of the pixel is given in P-bit binary number as in Eq. 3

$$\mathrm{LBP}_{P,R} = \sum_{P=0}^{P} S(g_p - g_c)2^p \quad s(x) = \begin{cases} 1, & \text{if } x \geq 0 \\ 0, & \text{otherwise} \end{cases} \tag{3}$$

where

g_c gray value of center pixel (x_c, y_c, t_c)

g_p gray value at p_{plane} sampling points

Figure 5 shows the output of the LBP.

Fig. 5 LBP of AMI

3.5 Feature Extraction

In the present work, the moment invariants are evaluated using central moments of the image function $I(x, y)$ up to third order. Regular moments are defined as in Eq. 4

$$M_{pq} = \sum_{x} \sum_{y} x^p y^q \tag{4}$$

where for $p, q = 0, 1, 2, \ldots$ and is M_{pq} the order moment $(p + q)$th of the continuous image function $I(x, y)$. The central moments of order up to 3 are calculated using Eq. 4 which is invariant under translation.

3.6 Training and Classification

The system has to be trained with some classification algorithm which helps and finds the exact match of test actions. In the proposed system, K-nearest neighbor (KNN) classification method is applied. KNN algorithm is a part of supervised learning that has been used in many applications in the field of data mining, statistical pattern recognition, and many others.

KNN is a method for classifying objects based on closest training examples in the feature vector. An object is classified by a majority vote of its neighbors. K is always a positive integer. If $K = 1$, it is then called as nearest neighbor (NN). The neighbors are taken from a set of objects for which the correct classification is known.

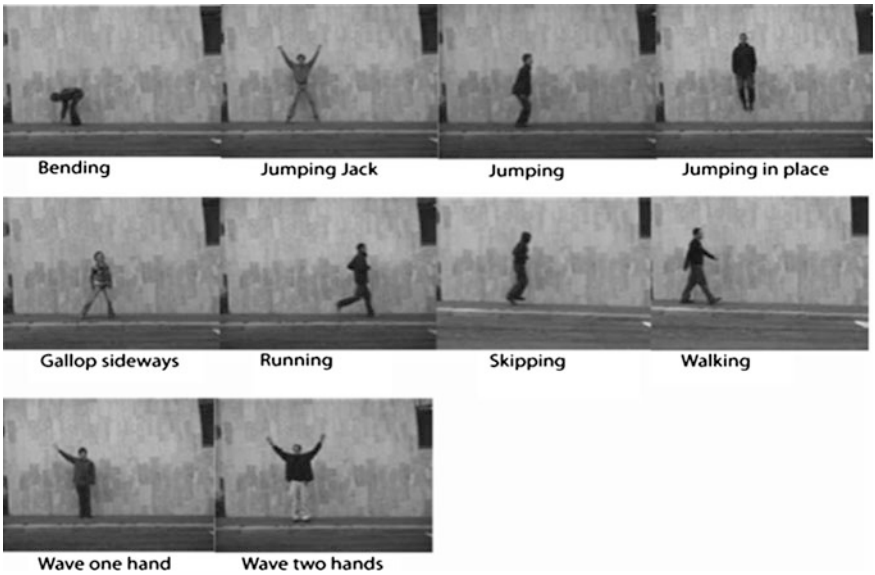

Fig. 6 Some sample of 10 action classes in Weizmann dataset

3.7 Weizmann Dataset

The Weizmann dataset has been used in the proposed system which consists of large number of subjects and actions. It includes 81 low-resolution videos from nine different people, each performing 10 natural actions. A sample is shown in Fig. 6.

4 Results and Discussion

The proposed system is worked out with Weizmann dataset consists of 8 actions of different persons. The actions including bend, jumping jack, jumping, walk, run, skip, gallop side, and wave.

Number of actions taken for testing = N

The total classification rate of the proposed system is calculated as follows

$$C = \frac{(N - \text{Actions wrongly recognized})}{N}$$

The percentage of video giving correct output is 90 %, and the percentage of video giving wrong output is 10 %. The accuracy given above is obtained by using

both accumulated motion image and MHI with LBP and DWT, respectively. It gives better result when both the techniques are concatenated rather than applied separately. This proposed method is able to recognize 9 out of 10 actions.

5 Conclusions

AMI evaluation helps us in handling the variations of appearance and clearly shows the moving pixels. MHI is defined, and its determination gives direction of motion. LBP gives shape and texture information of AMI and also helped to improve recognition accuracy. DWT aids in extracting spatial features of MHI. Then, the feature vectors of LBP and DWT obtained by Hu seven moments and distance metric calculated using KNN classifier and the actions are labeled accordingly. The proposed system gives the high performance when compared with previous proposals which uses KNN. The computation is simpler and less time consuming.

References

1. J.K. Aggarwal, M.S. Ryoo, Human activity analysis: a review. ACM Comput. Surv. **43**(3), 16 (2011)
2. T. Moeslund, E. Granum, A survey of computer vision based human motion capture. Comput. Vision Image Understand. **81**, 231–268 (2001)
3. J.K. Aggarwal, Q. Cai, Human motion analysis: a review. Comput. Vision Image Understand. **7**(3), 428–440 (1999)
4. L. Wang, W. Hu, T. Tan, Recent developments in human motion analysis. Pattern Recognit. **36**, 585–601 (2003)
5. W. Kim, J. Lee, M. Kim, D. Oh, C. Kim, Human action recognition using ordinal measure of accumulated motion. EURASIP J. Adv. Signal Process. **2010**, 1–12 (2010)
6. V.H. Chandrashekhar, K.S. Venkatesh, Action energy images for reliable human action recognition, in *Proceedings of the Asian Symposium on Information Display* (*ASID '06*), pp 484–487 (2006)
7. J. Davis, A. Bobick, in *The representation and recognition of action using temporal templates*. IEEE Conference on Computer Vision and Pattern Recognition (1997)
8. M.A.R. Ahad, J.K. Tan, H. Kim, S. Ishikawa, in *Human Activity Analysis: Concentrating on Motion History Image and Its Variants*. ICROS-SICE International Joint Conference (2009)
9. M.A.R. Ahad, J.K. Tan, H. Kim, S. Ishikawa, Action recognition by employing combined directional motion history and energy images. Image Vision Comput. 73–78 (2010)
10. L. Shao, R. Gao, Y. Liu, H. Zhang, Transform based spatiotemporal descriptors for human action recognition. Neurocomputing **74**, 962–973 (2010)
11. R. Shrivastava, A. Pratap Singh, Analysis and performance of three methods of human action recognition. Int. J. Adv. Res. Electr. Commun. Eng. (IJARECE). **19**(3), 72 (2012)
12. T. Ahonen, A. Hadid, M. Pietikainen, Face description with local binary patterns: application to face recognition. IEEE Trans. Pattern Anal. Mach. Intell. **28**(12), 2037–2041 (2006)
13. T. Ojala, M. Pietikainen, T. Maenpaa, Multiresolution gray-scale and rotation invariant texture classification with local binary patterns. IEEE Trans. Pattern Anal. Mach. Intell. **24**(7), 971–984 (2002)
14. P. Guo, Z. Miao, Motion description with local binary pattern and motion history image: application to human motion recognition, in *IEEE International Workshop on Haptic Audio Visual Environments and their Applications,* pp 18–19(2008)

Modeling and Performance Evaluation of Switched Reluctance Motor Drives in MATLAB/Simulink Atmosphere with Estimation of SRM Parameters Using Finite Element Analysis

P. Magdelin Jennifer Princy, S. Ram Prasath and P. Ramesh Babu

Abstract This manuscript deals with modeling and performance analysis of switched reluctance motor drive using MATLAB. The per phase equivalent circuit of switched reluctance motor (SRM) which includes voltage, current, torque, and electro-mechanical equations is used to build the mathematical model of SRM drives. Finite element analysis (FEA-Version 4.2) is used to predict the torque produced at various currents and rotor positions as well as to calculate the phase inductances. With the aid of the developed model, characteristics of speed and torque in addition to voltages and currents of SRM can be efficiently examined and evaluated. This proposed model can be projected to trouble-free design tool for the development of SRM drives.

1 Introduction

Switched reluctance motor is an old member of electrical machines family. Nowadays, its simple structure, ruggedness, high-speed capability, and low manufacturing cost make them more attractive for industrial applications. Switched reluctance motor is a doubly salient and singly excited motor. This means that both stator and rotor have salient poles, but stator alone has winding for excitation. SRM works on variable reluctance principle. Motion is produced as a result of the variable reluctance in the air gap between the rotor and the stator. When a stator winding is energized, producing a single magnetic field, reluctance torque is produced by the tendency of the rotor to move to its minimum reluctance position. In switched

P.M. Jennifer Princy (✉) · S. Ram Prasath · P. Ramesh Babu
Department of EEE, Saranathan College of Engineering, Tiruchirappalli, Tamil Nadu, India
e-mail: magdelin.vijay@gmail.com

S. Ram Prasath
e-mail: ramprasath-eee@saranathan.ac.in

P. Ramesh Babu
e-mail: rameshbabu-eee@saranathan.ac.in

© Springer India 2015

L.P. Suresh et al. (eds.), *Artificial Intelligence and Evolutionary Algorithms in Engineering Systems*, Advances in Intelligent Systems and Computing 325,
DOI 10.1007/978-81-322-2135-7_35

reluctance motor, switching of supply from one stator to the next causes minimum reluctance position of the rotor to change continuously thus producing rotation [1]. By controlling the switching strategy and the current flowing through the stator coils, we can control the speed and the torque of the motor. Because of their simple mechanical construction, switched reluctance motors are of low cost. This has motivated a large amount of research on these motors in the last decade. The model developed in this manuscript will be effective for monitoring and analyzing the performance of SRM motor drive system in MATLAB/Simulink environment.

2 Mathematical Model of Switched Reluctance Motor

2.1 Voltage and Electromechanical Equation

Figure 1 represents the per phase equivalent circuit of switched reluctance motor [1]. From the equivalent circuit, voltage equation is given by,

$$V = R_s i + \frac{\mathrm{d}\lambda(\theta, i)}{\mathrm{d}t} \tag{1}$$

$$\lambda(\theta, i) = L(\theta, i) i \tag{2}$$

The phase voltage equation, then, is

$$V = R_s i + \frac{\mathrm{d}\{L(\theta, i) i\}}{\mathrm{d}t} \tag{3}$$

$$V = R_s i + L(\theta, i)\frac{\mathrm{d}i}{\mathrm{d}t} + \frac{\mathrm{d}L(\theta, i)}{\mathrm{d}t}\omega_m i \tag{4}$$

The Eq. (4) is similar to the series excited DC motor voltage equation.

The induced emf, e, is obtained as

$$e = \frac{dL(\theta, i)}{dt}\omega_m i = K_b \omega_m i \tag{5}$$

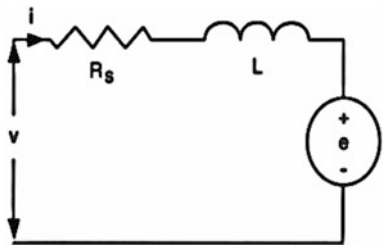

Fig. 1 Single-phase equivalent circuit of SRM

Torque equation [1] is given by,

$$T = \frac{1}{2} i^2 \frac{\mathrm{d}L(\theta, i)}{\mathrm{d}\theta} \tag{6}$$

Electromechanical equation is given by,

$$T - T_L = J\frac{\mathrm{d}\omega}{\mathrm{d}t} + B\omega \tag{7}$$

$$\omega = \int \frac{(T - T_L - B\omega)}{J} \mathrm{d}t \tag{8}$$

2.2 Change in Inductance with Respect to Rotor Position

Assumption made is that rotor pole arc is greater than stator pole arc ($\beta r > \beta s$). Here, θ is the angle between stator and rotor pole axis. βr and βs are rotor and stator pole arc, respectively (Figs. 2, 3, 4, 5, 6, 7, 8, and 9).

From Eq. (2),the flux linkage is a product of inductance and current. Since flux linkage is a function of current and rotor position, inductance also will be a function of current and rotor position. It is necessary to calculate inductance for various position.

Fig. 2 At $\theta = 0$ and $L = L_a$

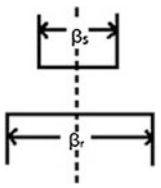

Fig. 3 At $\theta = \frac{\beta_r - \beta_s}{2}$ and $L = L_a$

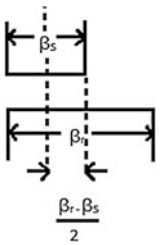

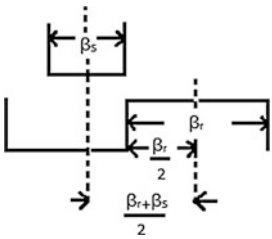

Fig. 4 At $\theta = \frac{\beta_r+\beta_s}{2}$ and $L = L_u$

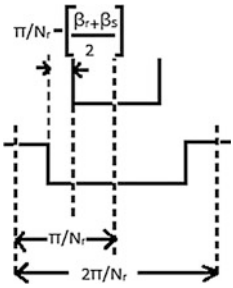

Fig. 5 At $\theta = \frac{\pi}{N_r}$ and $L = L_u$

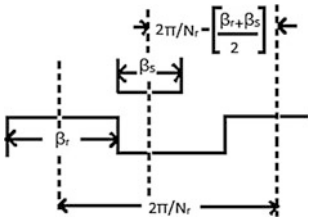

Fig. 6 At $\theta = \frac{\beta_r+\beta_s}{2}$ after $\frac{\pi}{N_r}$ and $L = L_u$

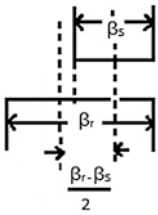

Fig. 7 At $\theta = \frac{\beta_r-\beta_s}{2}$ after $\frac{\pi}{N_r}$ and $L = L_a$

Fig. 8 At $\theta = \frac{2\pi}{N_r}$ and $L = L_a$

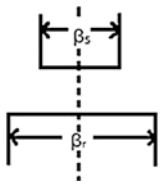

Fig. 9 Variation of inductance

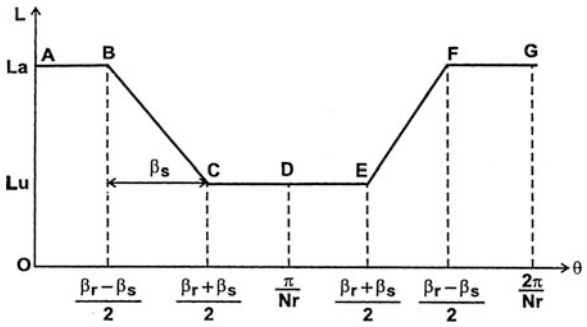

3 Finite Element Analysis on SRM Parameters

Finite element analysis (FEA) discussed in [2, 3] is used to predict the torque produced at various currents and rotor positions as well as to calculate the phase inductance. Software used in this paper is FEMM 4.2.

3.1 Estimation of Inductance

Switched reluctance motor was constructed in FEMM 4.2 software using the parameter from [4]. The finite element mesh is constructed with 17,234 nodes and 34,136 elements for aligned position and 17,331 nodes and 34,332 elements for unaligned position. The finite element model of SRM is constructed and simulated for every 5° interval from unaligned position to aligned position. The plot of inductance versus position for different currents from 0 A to above-rated current and the plot of torque versus position for different currents from 0 A to above-rated current can be obtained (Figs. 10, 11, 12, and 13).

Aligned inductance and unaligned inductance for rated current of 5A is

$$L_a = 0.00700368 \text{ H}; \; L_u = 0.00177542 \text{ H}$$

Similarly for various rotor positions, flux linkage and torque can be obtained from 0 to 5 A (rated current).

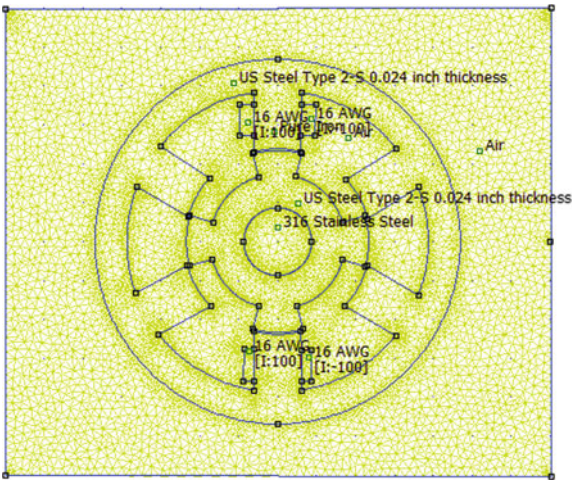

Fig. 10 Aligned position

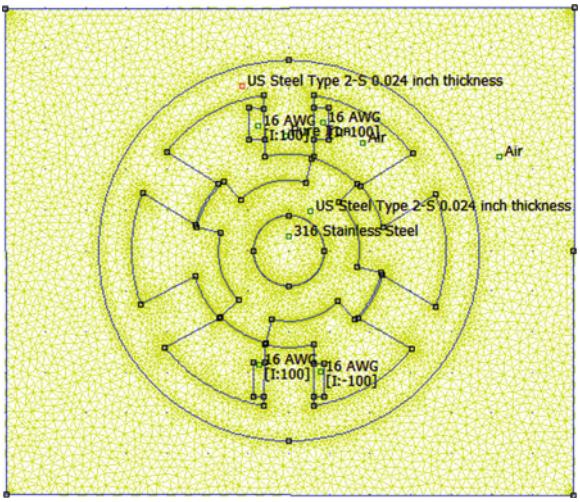

Fig. 11 Unaligned position

4 Simulink Model of Switched Reluctance Motor

6/4 switched reluctance motor is simulated with the data from [4]. The simulated block is explained as follows (Fig. 14).

The electrical and electromechanical equations discussed in Sect. 2 were simulated in the overall model of SRM. In order to excite the motor winding, we need to sense the rotor position (θ). Theta value is got by first converting rated speed of the motor in rpm to rad/s by a conversion ratio (π/30), and then, speed in rad/s is integrated to get theta (Figs. 15 and 16).

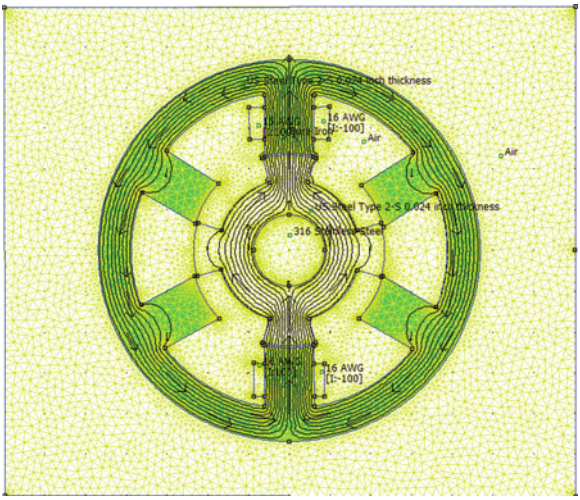

Fig. 12 Flux path at aligned position

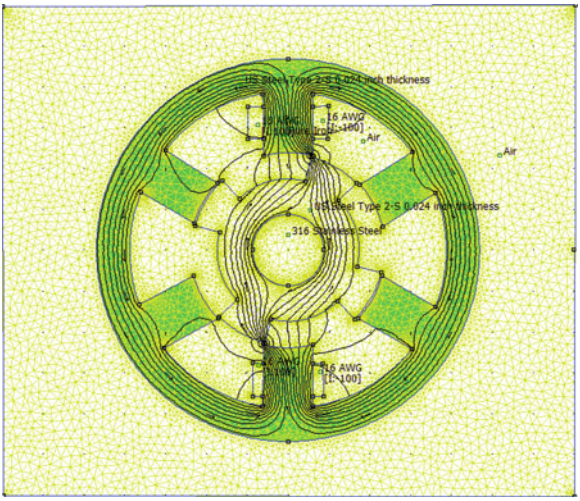

Fig. 13 Flux path at unaligned position

Simulink model of phase 'A' current has two MATLAB function block, Sa (switching function for phase a), La (for creating inductance profile for phase a), two lookup table block (flux linkage–theta–current and torque–theta–current), and modulo pi/2 block (Fig. 17).

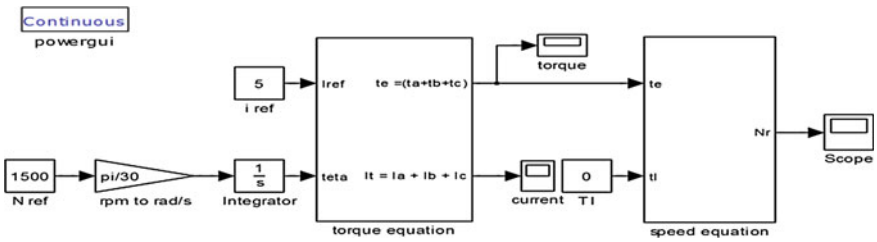

Fig. 14 Simulink block diagram of SRM

Fig. 15 Simulink model of phase current and torque

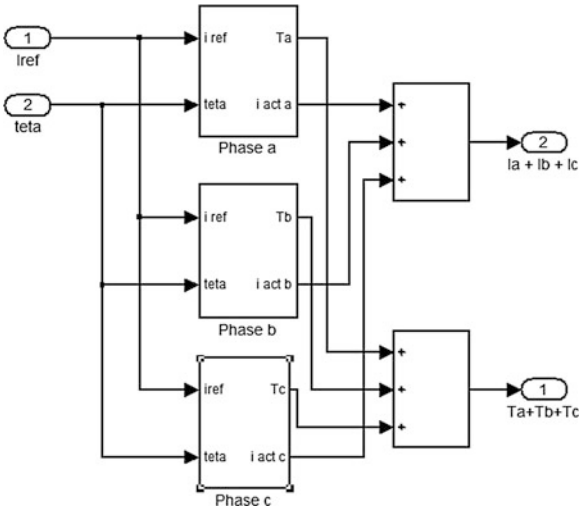

Fig. 16 Subsystem of electromechanical equation

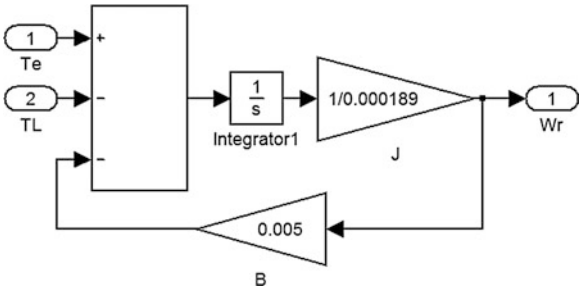

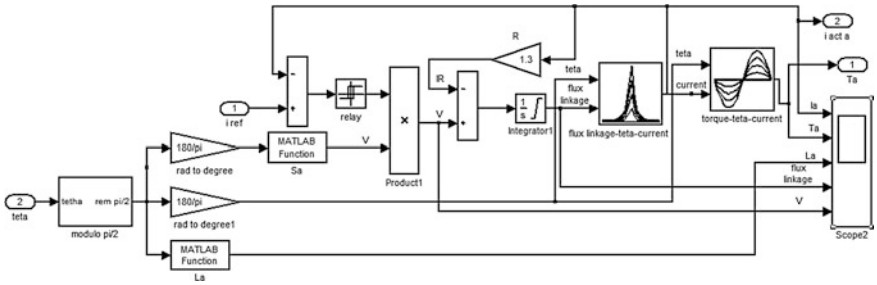

Fig. 17 Simulink model of phase 'A' current

4.1 Inductance Profile

Each phase has the periodicity of $2\pi/N_r$ (90° in case of 6/4 SRM), and program was written appropriately,

(1) For first 30° interval, inductance value will be La—(slope * angle)
(2) For second 30° interval, inductance value will be Lu
(3) For third 30° interval, inductance value will be Lu—(slope*(angle—60))

Similarly, phase *b* and *c* are also programmed, and the simulated results of 3 phases are given (Figs. 18 and 19).

4.2 Switching Function

Switching functions permit to assure the power converter commutation at θ_{on} and θ_{off}. Based on the periodicity and the concept about θ_{on} (advance angle) and θ_{off} (commutation angle) [5], switching program was written.

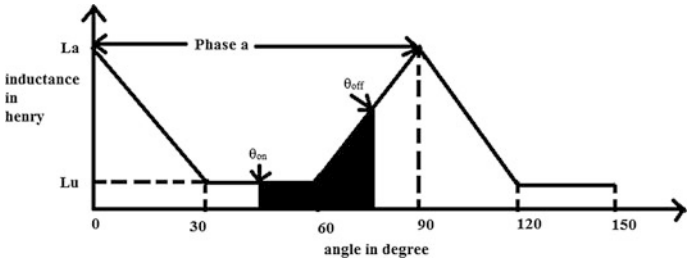

Fig. 18 Inductance profile for phase 'A'

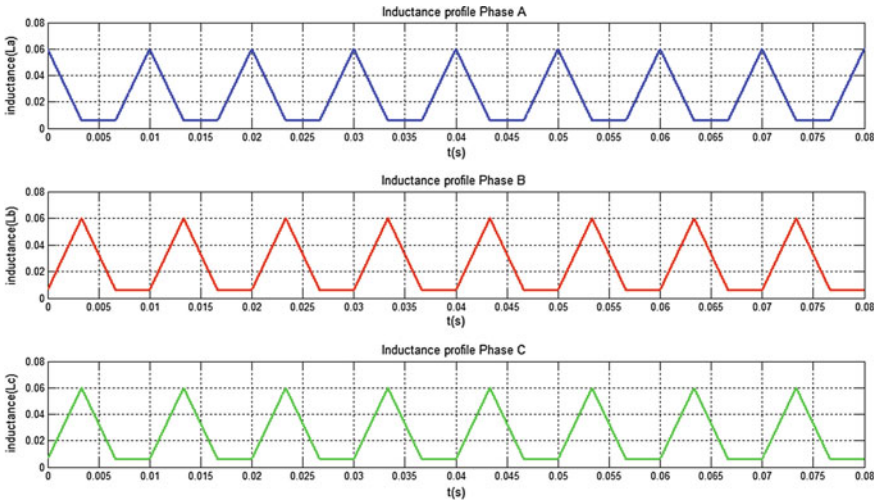

Fig. 19 Simulated inductance profile of all 3 phases

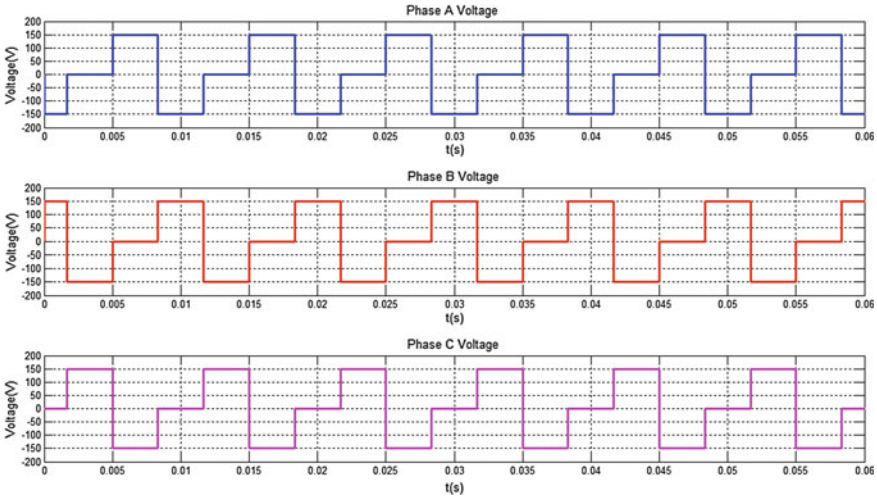

Fig. 20 Simulated voltage profile of all 3 phases

For phase *a,*

(1) 45°–75° switch is turned on by giving voltage of +150 V
(2) At 75°, switch is turned off by giving voltage of −150 V (from 75 to 105) and zero voltage from 105° to 135° (Fig. 20).

5 2D Lookup Table Block

2D lookup Table is formed using FEM software. The 3D plot of flux linkage versus theta versus current and torque versus theta versus current obtained from MATLAB is shown in Figs. 21, 22, 23, 24, 25, and 26.

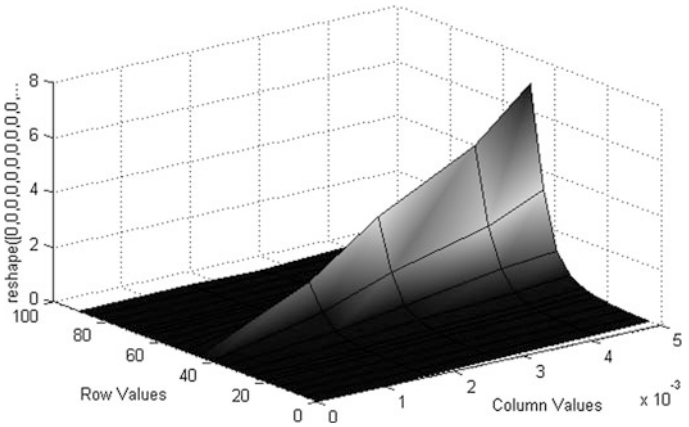

Fig. 21 Flux linkage versus theta versus current

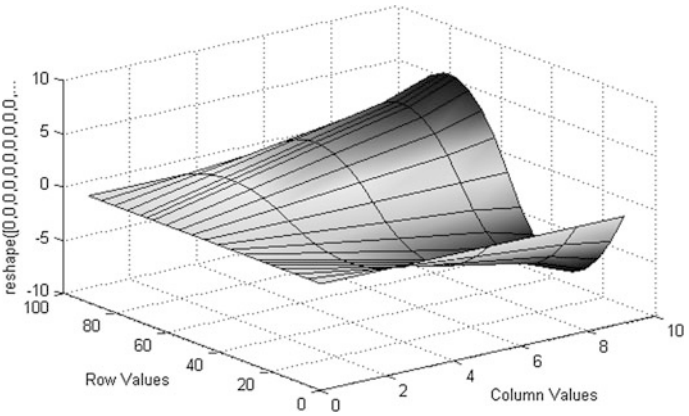

Fig. 22 Torque versus theta versus current

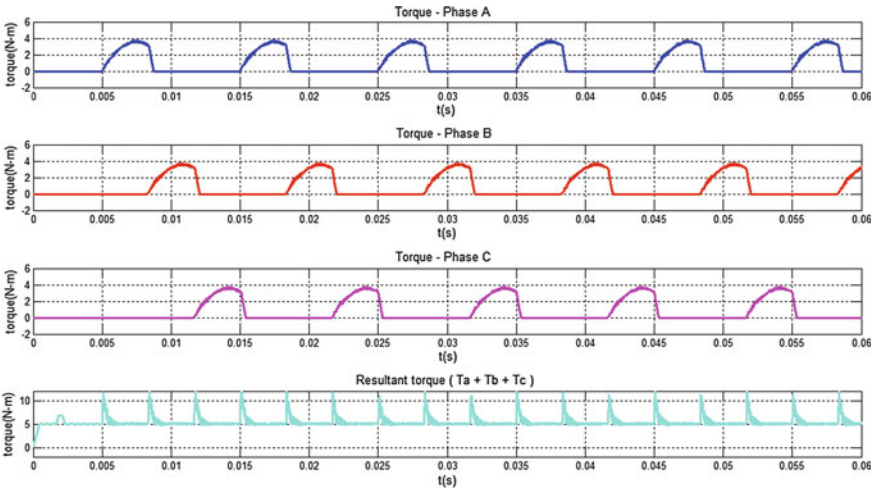

Fig. 23 Simulated torque profile of all 3 phases

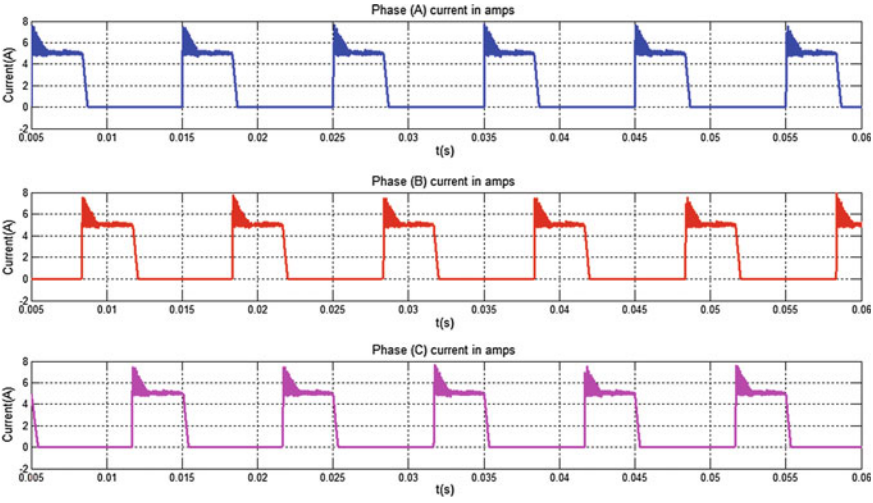

Fig. 24 Simulated current profile of all 3 phases

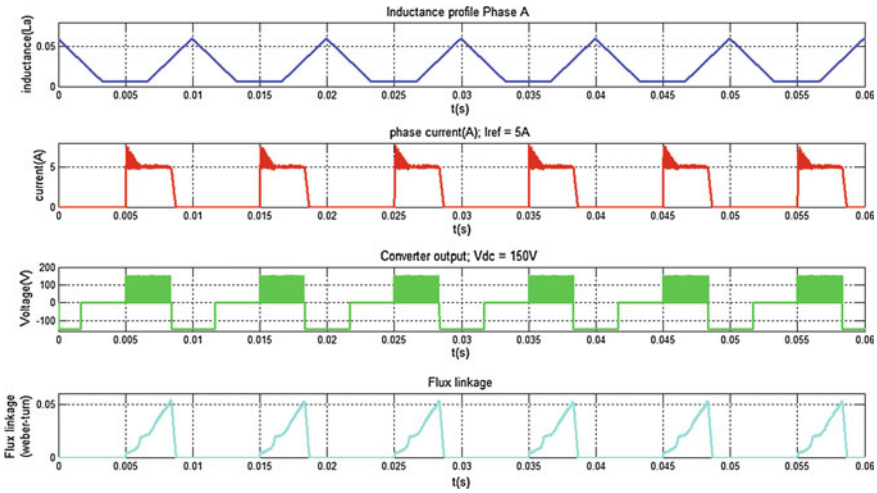

Fig. 25 Variation in current and converter voltage for the corresponding inductance profile

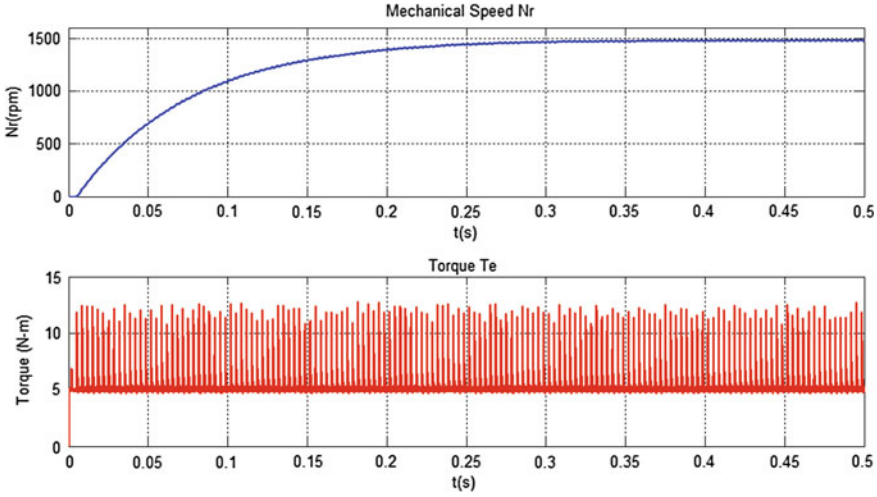

Fig. 26 Simulated speed and torque profile of 6/4 SRM

6 Conclusion

In this manuscript, modeling and performance analysis of switched reluctance motor has been verified with the help of MATLAB/Simulink and FEM 4.2. The characteristics are efficiently and more precisely analyzed. The proposed model is split into many functional simulation blocks, so that it can be very well applied with

a minor modification to other special machine applications which incorporates the permanent magnet AC motor, BLDC motor, the synchronous reluctance motor and the like.

References

1. R. Krishnan, *Switched Reluctance Motor Drive, Modeling, Simulation, Analysis, Design and Application* (CRC Press, New York, 2001)
2. A. Guettaf, F. Chabane, A. Arif, S. Benramache, Dynamic modeling in a switched reluctance motor SRM using finite elements. J. Power Technol. **93**(3), 149–153 (2013)
3. J. Faiz, S. Pakdelian, Finite-element analysis of a switched reluctance motor under static eccentricity fault. IEEE Trans. Magn. **42**(8), 2004 (2006)
4. F. Kentli, H. Calik, Matlab-Simulink modelling of 6/4 SRM with static data produced using finite element method. **8**(6) (2011)
5. H.E. Akhter, V.K. Sharma, K.A. Haddad, Determination of optimum switching angle for speed control of switched reluctance motor drive system. Ind. J. Eng. Mater. Sci. **11**, 151–168 (2004)

Classification of Right Bundle Branch Block and Left Bundle Branch Block Cardiac Arrhythmias Based on ECG Analysis

Sukanta Bhattacharyya and U. Snekhalatha

Abstract Heart is a vital organ of the human body which plays an important role in the circulation of the blood throughout the body and also serves as the power source of the electrical impulses that generate the rhythmicity of the heart, thus resulting in the successful circulation of the blood. Now, any disturbance in the proper functioning of the heart results in some type of diseases termed as cardiovascular diseases or arrhythmias. These diseases can be diagnosed and consequently treated. The diagnosis is done by an efficient technique known as electrocardiogram (ECG). This paper focuses on the area of biomedical signal analysis, where a method for detection of two types of cardiac arrhythmias, namely right bundle branch block (RBBB) and left bundle branch block (LBBB), is discussed. The signal processing and analysis have been carried out on the data collected from MITBIH (Berbari in Principles of Electrocardiography, pp 2–11, 2000, [1]) database. Implementation is done on the MATLAB platform. Signal analysis is done through a number of steps like preprocessing, feature extraction, and classification, and the results are generated in the form of waveforms, thus classifying the cardiac arrhythmias RBBB and LBBB.

Keywords Arrhythmia · MITBIH · Savitzky–Golay filter · LBBB · RBBB

1 Introduction

The heart is a powerful muscle that pumps blood throughout the body by means of a coordinated contraction. The contraction is generated by an electrical activation, which is spread by a wave of bioelectricity that propagates in a coordinated manner

S. Bhattacharyya (✉) · U. Snekhalatha
Department of Biomedical Engineering, SRM University,
Kattanankulathur, Chennai, India
e-mail: sukantabhattacharyya99@gmail.com

U. Snekhalatha
e-mail: sneha_samuma@yahoo.co.in

© Springer India 2015

L.P. Suresh et al. (eds.), *Artificial Intelligence and Evolutionary Algorithms in Engineering Systems*, Advances in Intelligent Systems and Computing 325,
DOI 10.1007/978-81-322-2135-7_36

throughout the heart. Under normal conditions, the sinoatrial node initiates an electrical impulse that propagates through the atria to the atrioventricular node, where a delay permits ventricular filling before the electrical impulse proceeds through the specialized His-Purkinje conduction system that spreads the electrical signal at speeds of meters per second throughout the ventricles. This electrical impulse propagates diffusively through the heart and elevates the voltage at each cell, producing an action potential, during which a surge in intracellular calcium initiates the mechanical contraction. The normal rhythm is altered when one or more spiral (reentrant) waves of electrical activity appear.

Any disturbance in the heart's normal rhythmic contraction is called cardiac arrhythmia [2] or simply arrhythmia. There are a number of cardiac arrhythmias like atrial fibrillation, bradycardia, tachycardia, left bundle branch block, right bundle branch block, and many more. The underlying cause of many arrhythmias is the development of a reentrant circuit of electrical activity that repetitively stimulates the heart and produces contractions at a rapid rate. Cardiovascular diseases are defined as diseases and injuries of the cardiovascular system: the heart, the blood vessels of the heart, and the system of blood vessels (veins and arteries) throughout the body and within the brain. Stroke is the result of a blood flow problem in the brain. It is considered a form of cardiovascular disease.

Since 1952, the cardiovascular death rate in Canada has declined by more than 75 % and nearly 40 % in the last decade—largely due to research advances in surgical procedures, drug therapies, and prevention efforts [3].

Heart disease and stroke are two of the three leading causes of death in Canada. Every 7 min in Canada, someone dies from heart disease or stroke. In 2008, cardiovascular disease accounted for 29 % of all deaths in Canada (69,703 deaths or more than 69,500), 28 % of all male deaths, and 29.7 % of all female deaths. In 2008, of all cardiovascular deaths, 54 % were due to ischemic heart disease, 20 % to stroke, and 23 % to heart attack. Nine in 10 Canadians (90 %) have at least one risk factor for heart disease or stroke (smoking, alcohol, physical inactivity, obesity, high blood pressure, high blood cholesterol, diabetes)

The electrocardiogram [4] (ECG) is the electrical manifestation of the contractile activity of the heart. The ECG is characterized by a recurrent wave sequence of P, QRS, T, and U wave associated with each beat. The QRS complex is the most striking waveform, caused by ventricular depolarization of the human heart. It provides information about the heart rate, rhythm, and morphology. The importance of the electrocardiography is remarkable since heart diseases constitute one of the major causes of mortality in the world. ECG varies from person to person due to the difference in position, size, anatomy of the heart, age, relatively body weight, chest configuration, and various other factors. In this paper, ECG analysis is done for the classification of arrhythmias RBBB and LBBB [5].

Right bundle branch carries nerve impulses that cause contraction of the right ventricle. The two bundles start together at a junction called the bundle of His. Nerve impulses come through the sinus node of the heart to the bundle of His and then move into the bundle branches. During the RBBB, a right ventricle is not directly activated by impulses traveling through the right bundle branch.

Left bundle branch carries nerve impulses that cause contraction of the left ventricle; the two bundles start together at a junction called the bundle of His. Nerve impulses come through the sinus node of the heart to the bundle of His and then move into the bundle branches. During the left bundle branch block, left ventricles are not directly activated by impulses traveling through the left bundle branch.

Constant research works are carried out for the classification and detection of cardiac arrhythmias that implemented a number of techniques ranging from quantized threshold method for QRS detection [6], correlation coefficient [7] method for detection of cardiac arrhythmia in the ECG waveform, to the construction of mathematical models for determining the shape and form of QRS complexes for classification purposes. But all these above-mentioned methods have some constrains like complexities of the techniques and less computation of statistical parameters.

In this paper an attempt is made for classifying the two types of arrhythmias namely RBBB and LBBB following a thorough of methods and techniques like preprocessing, filtering and feature extraction steps followed by a classification stage.

2 Methodology

A flow of different methods is implemented for the analysis process. The different steps involved are depicted in the block diagram (Fig. 1).

The raw data is collected from MITBIH database. The analysis is done here on an experimental basis taking into account 12 lead systems. For both the cases, we have used the 12 lead datasets. While going through the database, it is found that the LBBB and RBBB features are prominently noted in leads *I*, *V*1, and *V*6. The algorithm and the further processes are carried out taking into account these three mentioned leads. After the collection of data, we go for the preprocessing stage. In this stage, the original signals containing the noisy and baseline wandering noises are filtered out implementing fast Fourier transform over the signals with sampling frequency of 360 Hz. After this stage, further filtering and smoothing is carried to remove the high-frequency components by Savitzky–Golay (S-Golay filter) with polynomial order of 6 and frame length of 21.

Next stage is the feature extraction stage. This is the most complex and lengthiest stage. When the input data to an algorithm is too large to be processed and is suspected to be notoriously redundant, the input data will be transformed into the set of features called as feature extraction. In this stage, each filtered and

Fig. 1 Block diagram for the ECG signal analysis

smoothened signal is analyzed for the feature extraction process. Here, we try to detect all the peaks such as *P*, *Q*, *R*, *S,* and *T*. The individual peaks are detected by applying some threshold parameters for each peak range, and the respective peaks so obtained are plotted. Next, we try to analyze the shape of complexes such as QRS, RsR', W shape, and M shape patterns. Also we noted down the direction of T wave with respect to the QRS complex. Better results are seen in leads *V*1 and *V*6 for both the cases. Following this stage is the computation stage where we calculated the parameters such as duration of QRS complex, *R* peak time, and the RR interval.

Finally, we come to the final stage, the classification stage. Currently, we are working on this stage. We have planned to use the multilayer perceptron (MLP) classifier where a large dataset is to be implemented for the classification process and to obtain the desired results with good sensitivity and specificity measures.

2.1 System Design

The following section describes the necessary perquisites for carrying out the project. The perquisites include both hardware and software components which are listed down

Hardware Requirements

- 1-GB random access memory (RAM)
- Intel dual-core processor
- 320-GB hard disk for storage

Software Requirements

- Operating system : Windows XP, WIN 7
- Software : MATLAB (version 7.10.0.499 (R2010a))
- Data collected form MITBIH database

2.2 Algorithm

The algorithm steps are listed below

Step 1 Raw ECG signals from MITBIH ECG database are taken

Step 2 Filtering and smoothing of the signals are done by using Savitzky–Golay (S-Golay filter) filtering technique of polynomial order of 6 and frame length of 21

Step 3 Carry out the feature extraction stage taking into account all the 12 lead data

Step 4 Feature extraction is done for detecting the individual peaks, analyzing over the shapes of different complexes such as QRS, RsR', *M,* and *W* shape patterns

Step 5 Computation of some parameters such as QRS duration, *R* peak time, and RR interval

Step 6 If the amplitude and interval is similar to the standard normal ECG, our method will categorize it as normal. If there is deviation in the amplitude and durations, etc., from the standard ECG, then that particular ECG is treated as diseases ECG

Step 7 Then, classify the type of diseases as LBBB and RBBB using an MLP classifier

2.3 RBBB and LBBB Characteristics

Figure 2 depicts the waveform of RBBB arrhythmia which is characterized with duration of QRS complex is equal or more than 120 ms, dominant *R* wave in leads *V*1, *I* and slurred wave in *V*6, (RSR') *M*-shaped complex in lead *V*1 and *W* shaped in *V*6, Slurred *S* wave in lead *V*6, *T* wave is in the direction of QRS complex in *V*6 and inverted in leads *V*1 and *I*.

Figure 3 depicts the waveform of LBBB arrhythmia which is characterized by QRS equal to or greater than 120 ms (adults), dominant *R* wave in lead *V*6, and dominant *S* wave in *V*1; *T* wave is in the opposite direction of QRS complex in *V*1 and same in *V*6, (RsR') *M*-shaped complex in *V*6, and *W* shaped in *V*1.

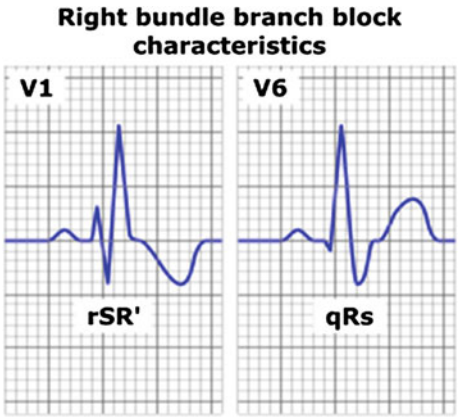

Fig. 2 RBBB characteristics

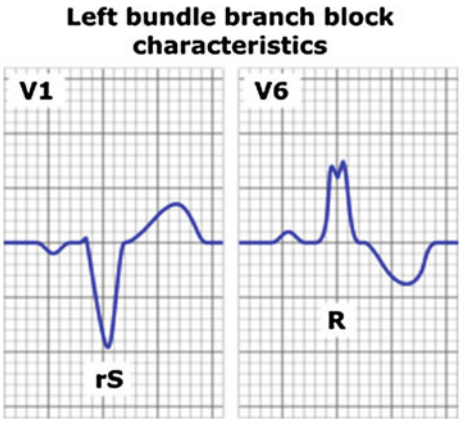

Fig. 3 LBBB characteristics [9]

3 Results and Discussions

The 12 lead raw data are collected from the database and plotted as shown in Figs. 4 and 5. Similarly, we plot the 12 lead data for the RBBB as shown in Figs. 6 and 7.

After plotting the original signals for all the leads, we apply our algorithm for each data lead data. However, we find the desired LBBB features in leads *V*1 and *V*6. The Figs. 8 and 9 show the filtering, smoothing, and feature extraction stages for leads *V*6 and *V*1.

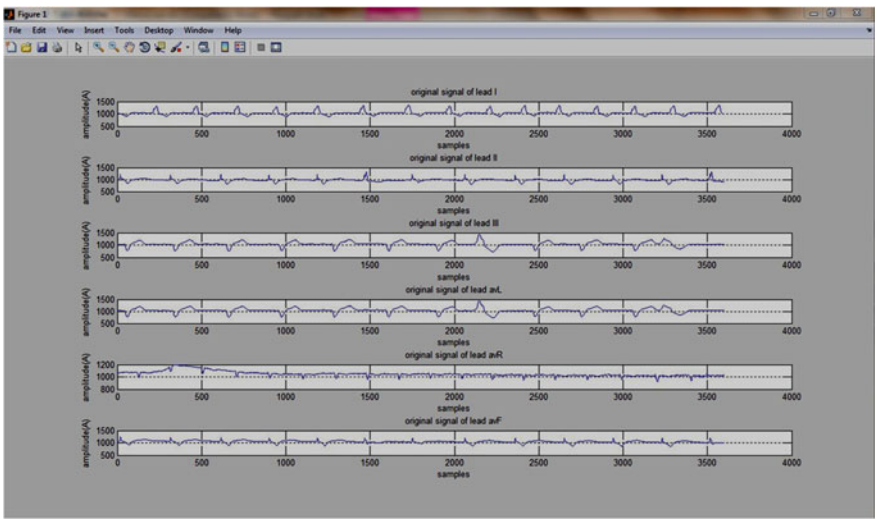

Fig. 4 First 6 lead data of LBBB from MITBIH

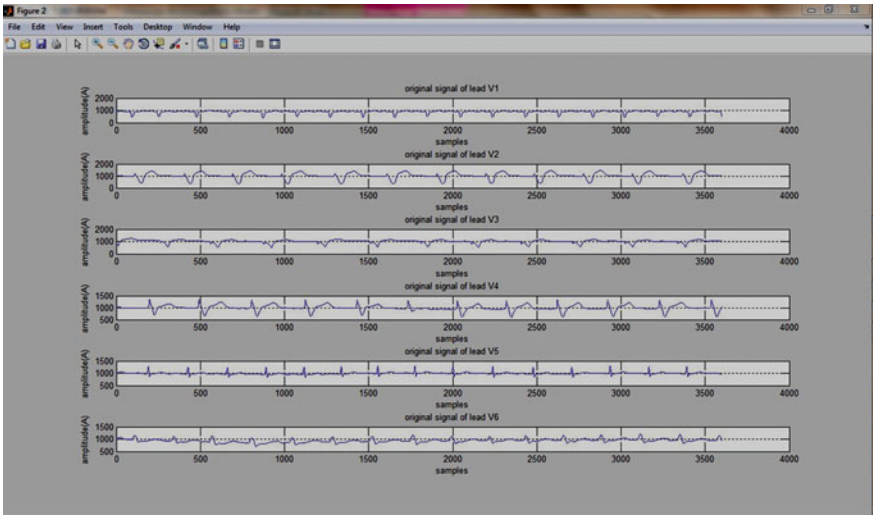

Fig. 5 Second 6 lead data of LBBB form MITBIH

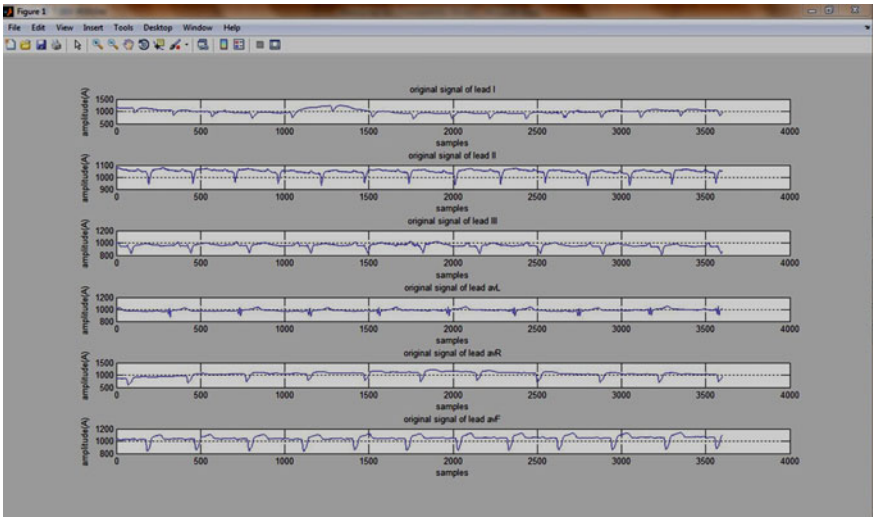

Fig. 6 First 6 lead data of RBBB from MITBIH

After the feature extraction stage, we note the following features like dominant *R* waves and absence of *q* waves. The direction of *T* wave is in the same direction of QRS complex. An M-shaped RsR' complex is seen. These features match the characteristics of LBBB (Figs. 10 and 11).

After the feature extraction stage, we note the following features like dominant *S* waves and prominent rS pattern. Also the direction of *T* wave is opposite to qRS

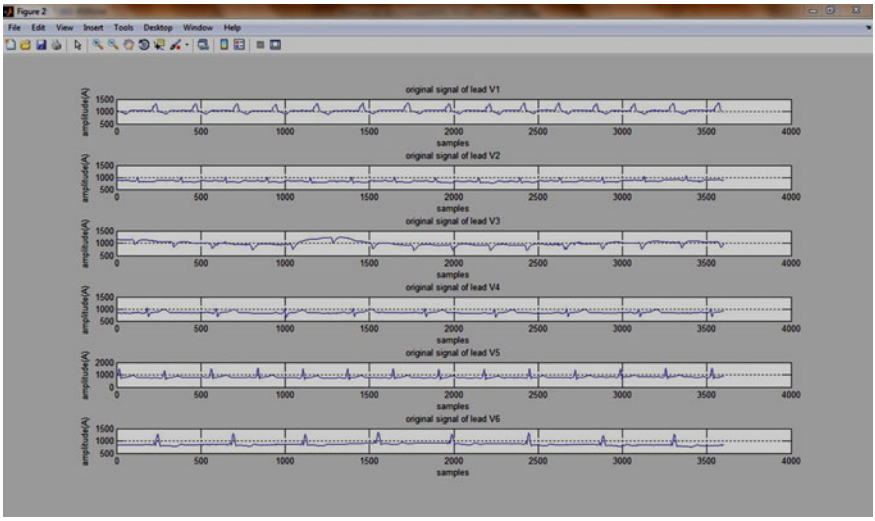

Fig. 7 Second 6 lead data of RBBB form MITBIH

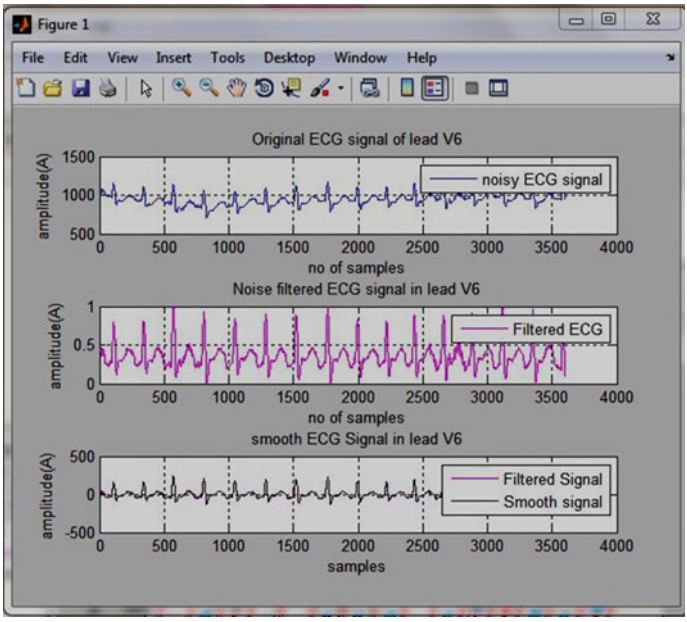

Fig. 8 Filtered and smoothened *V*6 lead data for LBBB

wave/inverted qRS complex. A *W*-shaped RsR' complex is observed. These features also denote the LBBB characteristics. Similar approach is applied to the leads *V*6 and *V*1 for RBBB which are shown in the Figs. 12 and 13.

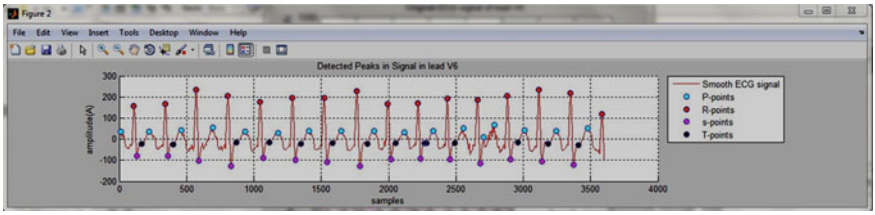

Fig. 9 Feature extraction process of lead *V*6 for LBBB

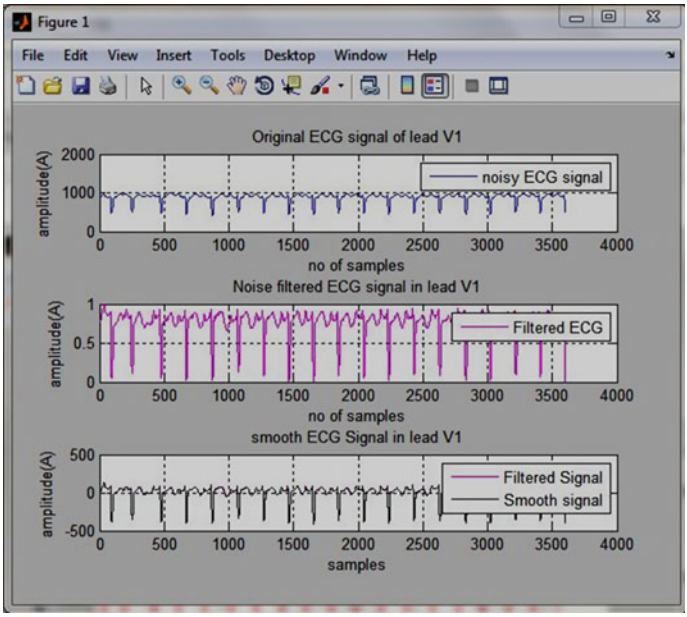

Fig. 10 Filtered and smoothened *V*1 lead data for LBBB

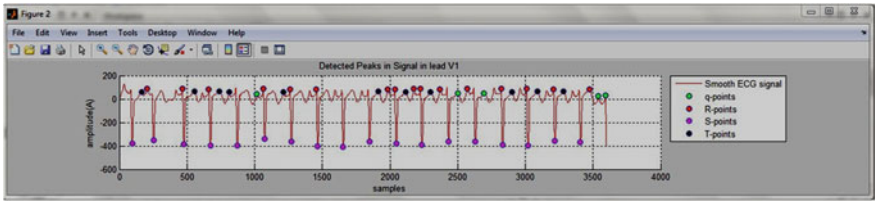

Fig. 11 Feature extraction process of lead *V*1 for LBBB

After the feature extraction stage, we note the following features like qRs pattern; T wave is in the direction of QRS complex, wide *S* wave. A *W*-shaped RsR' pattern is seen. These features resemble the RBBB characteristics.

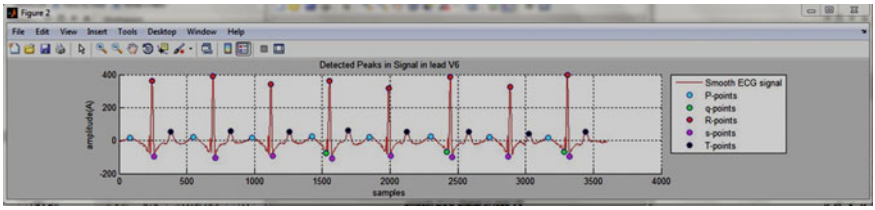

Fig. 12 Feature extraction process of lead *V6* for RBBB

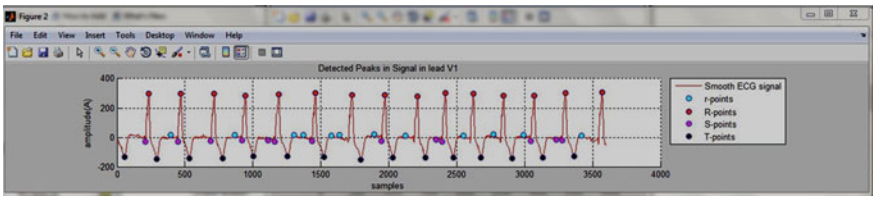

Fig. 13 Feature extraction process of lead *V1* for RBBB

After the feature extraction stage, we note the following features like dominant *R* waves, tiny r wave denoted in blue color dots, is seen forming the pattern rSR. The *T* wave is in the direction opposite to QRS complex. An *M*-shaped RsR' complex is seen. So from the so far feature extraction process, we have done the analysis for determining the shape of the complexes such as M- and W-shaped patterned complexes which are noted as prominent features of LBBB and RBBB.

The dominance of the individual wavelets such as *R*, *S* also helped in arriving at a better approach in classifying the arrhythmias. We further calculated some statistical parameters such as QRS complex duration and peak time for the *R* wave in order to increase the accuracy of the obtained results. Calculating the QRS complex duration, we get a value of 130 ms which is quite close to 120 ms.

Currently, we are working on the classification stage. This is the last stage of our proposed work. Here, we will be implementing the neural network-based MLP classifier which will classify the diseases into three types, namely normal, LBBB, and RBBB. The constrain to this process is that it requires the training of a large number of datasets, but the method is undoubtedly a good one expecting a better sensitivity and specificity measures.

4 Conclusion and Future Enhancement

The ECG signal analysis is done on the data collected from MITBIH database through a number of processing stages like preprocessing and feature extraction. The results are discussed in Sect. 3. The leads *V1* and *V6* are mostly considered for

the feature extraction process where individual peaks are found by thresholding technique and their direction of propagations, and also some pattern shapes such as *M* and *W* are obtained. These are followed by the computation stage where we computed the QRS duration and *R* peak time. The classification stage is in progress which will be implemented by NN-based MLP technique that is supposed to yield good accuracy and sensitivity measures.

The implementation of the work is carried out on an efficient tool platform called MATLAB (version 7.10.0.499 (R2010a)). The algorithm discussed in Sect. 2.2 is followed, and so far, results obtained are shown. The project is aimed at giving a better idea to the doctors and non-doctors about the classification of different types of cardiac arrhythmias.

References

1. G.B. Moody, R.G. Mark, The impact of the MIT-BIH Arrhythmia Database. IEEE Eng in Med and Biol **20**(3), 45–50 (May-June 2001). (PMID: 11446209)
2. T. Nag, A. Ghosh, Cardiovascular disease risk factors in Asian Indian population: a systematic review. J. Cardiovasc. Dis. Res. **4**, 222–228 (2013)
3. S. Reddy, A. Bahl, K.K. Talwar, Congestive heart failure in Indians: how do we improve diagnosis & management? Indian J. Med. Res. **132**, 549–560 (2010)
4. E.J. Berbari, Principles of electrocardiography. in *The Biomedical Engineering Handbook*, 2nd edn., ed. by J.D. Bronzino (2000)
5. B. Aarathi, S. Fathima, ECG analysis for the detection of RBBB and LBBB. World J Sci Technol **2**(10), 198–203 (2012)
6. W.H. Chang, K.P. Lin, S.Y. Tseng, ECG analysis based on Hilbert transform descriptor, in *IEEE Engineering in Medicine and Biology Society 10th Annual International Conference.* (1988)
7. C.-C. Chiu, T.-H. Lin, B.-Y. N. Nikolaev, A. Gotchev, Using correlation coefficient in ECG waveform for arrhythmia Detection. Biomed. Eng. Appl. Basis Comm. **17**, 147–152 (2005)

Content-based Algorithm for Color Image Enhancement Using Fuzzy Technique

Research centre: LBS Institute for Science and Technology

C. Reshmalakshmi and M. Sasikumar

Abstract Fuzzy technique offers interesting and challenging frame for developing new methods in the field of image processing. Nowadays, enhancing color images is considered as one of such demanding work in image processing. This paper introduces the nonlinear and knowledge-based behavior of fuzzy technique to enhance color images referred as 'content-based algorithm.' The resulting image not only exposes the fine details but also enhances the images by processing the approximate components of the image in human visual system with content-based algorithm in fuzzy domain. The knowledge-based characteristics of both 'fuzzy technique' and 'color' coincide effectively to get better experimental results in this field. Also, the subjective and objective evaluations listed over here show that this algorithm performs better than any other existing fuzzy and non-fuzzy approach.

Keywords Content-based algorithm · Pattern recognition · Histogram equalization · Fuzzification · Transformation · Defuzzification

1 Introduction

Fuzzy technique has proven its ability to solve many control system issues in the engineering field. But in the last few decades, fuzzy systems extend its popularity to image processing too. The nonlinearity and knowledge-based behavior made fuzzy technique suitable for image processing. Images may be of low quality or noisy due

C. Reshmalakshmi (✉) · M. Sasikumar
Department of Electronics and Communication, Marian Engineering College, Trivandrum, Kerala, India
e-mail: reshmasujeer@gmail.com

M. Sasikumar
e-mail: drmsasikumar@yahoo.com

© Springer India 2015

L.P. Suresh et al. (eds.), *Artificial Intelligence and Evolutionary Algorithms in Engineering Systems*, Advances in Intelligent Systems and Computing 325,
DOI 10.1007/978-81-322-2135-7_37

to the effect of image transmission and image acquisition system. But an image should be good enough not only for human perception but also for some applications such as feature extraction or pattern recognition. So it is necessary to represent and resolve uncertainty encountered with image effectively to improve the quality of image. Since fuzzy system is a mathematical tool for representing vagueness, it is possible to describe the low quality of image as uncertainty/vagueness in an image. If the 'low quality' of image can be represented in terms of verbal language, it will be very easy to solve problems of images using fuzzy techniques.

To improve the quality of image, suitable for applications, the pixel values of image should be manipulated. Since color image is a combination of three different primary colors, it is difficult to enhance the color image compared to gray-level image. Many research works are still going on in this area to make improvements in the existing techniques [4]. Some other studies have explored different types of functions and [3] introduced trigonometric functions for image enhancement. Color is human experience, and several algorithms have been proposed to enhance color image. One of the simplest and widely used methods is histogram equalization (HE) [2–5]. But this approach fails to enhance the smooth region and degrades the sharp region of the image. Also, HE produces the washout effect when the original histogram fails to occupy the entire dynamic range. In general, existing enhancement algorithms produce artifacts and require significant computational time because of their complex approach. In addition, these methods produce the color-shifting problem. To overcome these problems, some modifications have been proposed [4]. In which the idea of content-aware algorithm tries to improve the quality of dark image. The goal of enhancement is to enhance the dark areas so that even fine details are visible for perception. But unfortunately, this is a challenging task to treat every region independently. Also, number of regions depends on the image too. Thus, splitting an image directly into regions will definitely produce undesirable effects. The content-based algorithm analyzes the pixel characteristics and groups them into regions by simulation in human visual domain. Consequently, this paper proposes modified content-based algorithm in which approximate components of images are grouped to form regions in fuzzy domain by analyzing the characteristics of each pixel and by simulating the image in human visual system. Since each region (also called as fuzzy sets) has independent characteristics, it requires separate attention. Hence, different fuzzy transformation functions are used to modify these pixels. Then, the final result is obtained by aggregating transformation functions with weight function. Then, the enhanced image is obtained in the defuzzified plane.

This paper is organized as follows. Section 2 describes briefly about the frame work of fuzzy image processing. Proposed algorithm and different types of fuzzification, transformation, and defuzzification functions along with wavelet and human visual systems are described in Sect. 3. Section 4 shows the evaluation parameter and results. Section 5 describes the concluding remarks of the paper.

2 Fuzzy Image Processing Frame Work

In the last few decades, fuzzy technique has obtained enormous popularity in image processing. Fuzzy sets are capable of solving imperfect data caused by vagueness and ambiguity rather than randomness [6]. The main steps of fuzzy image processing are fuzzification Φ, a suitable operator Γ to modify the membership values and, if needed, defuzzification Ψ. An image X of size $M \times N$ with L gray levels $g = 0, 1, 2\ldots L-1$ can be defined as an array of fuzzy singletons as shown (1) (singleton is a fuzzy set with single supporting element). This singleton represents membership values of each pixels based on their properties such as brightness, smoothness, and edginess.

$$X = \bigcup_{m=1}^{M} \bigcup_{n=1}^{N} \frac{\mu_{mn}}{g_{mn}} \quad \text{with } \mu_{mn} \in [0, 1] \tag{1}$$

where μ_{mn}/g_{mn} denotes fuzzy set at mn-th pixel with membership function μ_{mn}, as the degree of belongingness of each pixel to its original pixel. The output Y of the system for input X is given by

$$Y = \Psi(\Gamma(\Phi(X))) \tag{2}$$

Compared to other methodologies, fuzzy technique processes the input image X in membership plane where one can apply abundance features of fuzzy technique rather than in pixel plane. So in the membership plane, image is decomposed into different fuzzy sets depending on the image intensity property. Existing membership functions for fuzzifying an image are Guassian, triangular, trapezoidal, exponential, etc. Modifications of fuzzified gray-level values are done in the inference engine to get the desired enhancement. If necessary, images from membership plane are mapped back to pixel plane with the technique called defuzzification. The modified gray-level values are obtained in the pixel plane where enhanced image can be compared with the input image.

3 Proposed Enhancement Technique

This paper is focused to produce a better color image enhancement algorithm without artifacts and color-shifting problem. Initially, image pixels are grouped into regions based on their intensity variation and hence, pixels with similar intensities are grouped into one region. If some pixels share similar characteristic (such as dark or gray and gray or bright), they are grouped into both the regions, but with varying degree of membership grade, no matter if neighboring pixels have extreme (dark or bright) intensities. These regions are then modified by different transformation functions which are designed according to their properties to form *content*. These *contents* are the building blocks of this algorithm and help to reduce the amount of

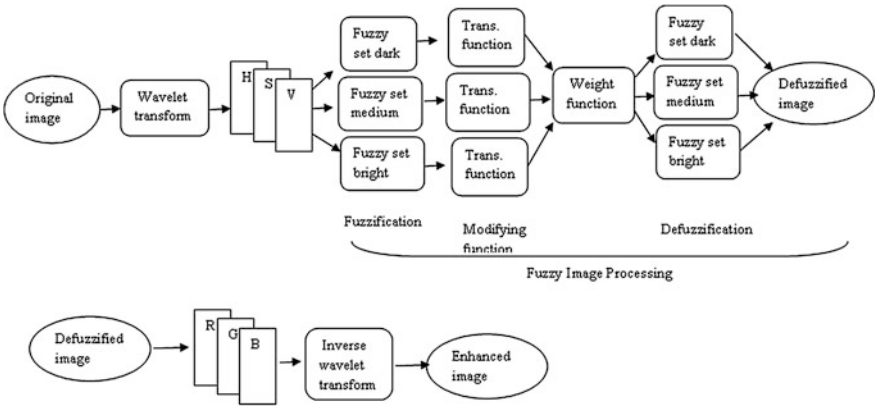

Fig. 1 Proposed content-based algorithm

artifacts and color-shifting problem in the enhancement process. Enhanced image in the pixel plane is obtained by aggregating these *contents* using 'content-based algorithm.' Figure 1 summarizes the entire algorithm.

To implement of proposed algorithm, start with wavelet transform which performs the first level of enhancement and decomposition of image. The approximate component contains most of the information and is used for further enhancement of the image. Since image enhancement gives human subjective preference, proposed algorithm is processed in human visual system. Due to the absorption characteristics of human eye, colors can be viewed as variable combination of primary colors (*RGB)* and it can be encapsulated in terms of hue–saturation–value (HSV). In order to preserve true color of the image, compared to existing technique, this algorithm focussed on the image intensity (V component) of the image without changing the other components (hue and saturation). After the pixel manipulation in fuzzy space, hue (H) and saturation (S) components of the original image are merged to the manipulated image intensity. Finally, enhanced image is obtained by the inverse process as shown below.

Above-stated algorithm improves the brightness while preserving the actual color (hue and saturation) of the image in the fuzzy domain by decomposing image intensity as *dark*, *gray,* and *bright* based on their pixel intensities. Formation of number of regions is user defined and improves the quality of image with definite number of groups. So after these steps (wavelet transformation, HSV conversion and normalization of image) in the pixel domain, the image is taken into fuzzy domain for further enhancement procedures.

3.1 Fuzzification Plane

As discussed, in the membership plane, decomposed image regions are considered as fuzzy sets and each fuzzy set is formed with relevant membership function. The

membership function maps elements of pixels in the decomposed region into its membership plane with values ranging from 0 to 1. And hence, separate attention is given to each region in the decomposed image. This paper makes use of the versatile mapping function called Gaussian to map the image regions from pixel plane to fuzzy plane. The normalizing function selected in this paper is a logarithmic function which is not only a well-defined mathematical function but also a characteristic of human brightness perception.

So decomposed regions of the original image are $X\text{dec} = \{X\text{dark}, X\text{gray}, X\text{bright}\}$ with pixel ranges from $0 \leq X\text{dark} \leq 150$, $50 \leq X\text{gray} \leq 200$, and $127 \leq X\text{bright} \leq 255$ which means Xdec is Xdark for the pixel value ranges from 0 to 150. The normalization function $N(m, n)$ for decomposed region with pixel (*m, n*) with Xdecmin, Xdecmax as minimum and maximum value of each region (for Xdark, the minimum value is 0 and maximum value is 150 and so on) is defined as

$$N(m,n) = \log_2\left[1 + \frac{X\text{dec}(m,n) - X\text{decmin}}{X\text{decmax} - X\text{decmin}}\right] \tag{3}$$

After applying normalization function, fuzzy sets are formed by the membership function defined over the pixel region. The shape of membership function (which shows the degree of belongingness of pixel to its pixel region) depends on the pixel belongingness. The Gaussian function maps it effectively. If Xdec is the set of various fuzzy set, the Gaussian function is defined with two parameters called *sigma* (σ) and *center* where *sigma* defines the width and *center* defines the center or maximum value of the function. It is mathematically represented by using symbol Φ as

$$\Phi(X\text{dec}) = e\frac{-(X\text{dec} - \text{centre})^2}{2\sigma^2} \tag{4}$$

So fuzzy sets are computed using (4) in which *Xdec* is replaced by *Xdark*, *Xgray* and *Xbright* with varying values of *sigma* and *center*. So these fuzzy sets are defined over entire range of image as discussed above.

3.2 Enhancement Plan

Those fuzzy sets which are generated during the fuzzification process are now taken to transformation plane for further enhancement. Since trigonometric functions perform a vital role in the modification of pixel values (5), different modifications functions are used to enhance the fuzzy sets. That is to enhance dark portion of the image (Xdark), a cosine function is used because of its brightening capability. The sine and tangential terms help to modify the flat (Xgray) and sharp (Xbright) regions of the image.

$$\Gamma(\Phi(X\text{dark})) = \cos[(\Pi(\Phi(X\text{dark}) - Xc) + 1)/4] \tag{5}$$

$$\Gamma(\Phi(X\text{gray})) = \sin[(\Pi(\Phi(X\text{gray}) - Xc) + 1)/4] \tag{6}$$

$$\Gamma(\Phi(X\text{bright})) = \tan[(\Pi(\Phi(X\text{bright}) - Xc) + 1)/4] \tag{7}$$

A final modification in the transformation plane is done by modified contrast intensification operator (8) defined over crossover point *Xc* (*Xc* is the point at which fuzzy set has its maximum fuzziness) of the fuzzy set. And hence, *content* $\Psi(\Gamma(\Phi(X\text{dec})))$ are obtained in the enhancement plane.

$$\begin{aligned}\Psi(\Gamma(\Phi(X\text{dec}))) &= \Gamma(\Phi(X\text{dec})) + X\text{dec}^2;\ \text{if } X\text{dec} \le 0.5 \\ &= \Gamma(\Phi(X\text{dec})) - (1 - X\text{dec})^2 + Xc; \quad \text{if } X\text{dec} \ge 0.5\end{aligned} \tag{8}$$

3.3 Defuzzification Plane

Defuzzification plane is used to get back the image in the pixel plane. Here, defuzzification is done by scaling the input image with the mean of *content* as shown in the equations below.

$$Y = wt * X \tag{9}$$

$$\begin{aligned}mean &= \sum_{\substack{Xdec=Xdark,\\ Xgray,Xbright}} mean(\Gamma(\Phi(Xdec))) \\ wt &= \sum_{\substack{Xdec=Xdark,\\ Xgray\\ Xbright}} (\Gamma(\Phi(Xdec))) + (Xc * mean) + 1\end{aligned} \tag{10}$$

The weight (*wt*) function is obtained by adding *content* with mean as a function of crossover point. These modified *content* replaces value component of HSV and without altering hue and saturation, the image is enhanced. Next step is to apply inverse wavelet transform as an inverse process.

4 Evaluation Parameters and Results

It is a fact that the viewer is the ultimate judge for evaluating the performance of any image enhancement method. However, image enhancement algorithms can be evaluated by the quantitative or qualitative approach. Some of the objective

measures are entropy, luminance index, and error metrics MSD and PEOIR. Measure of entropy (*ME*) defines the statistical measure of randomness in an image and is used to characterize the texture of an image. The metric is defined as:

$$ME = -\sum_{m}\sum_{n} p(m,n)\log_2 p(m,n) \tag{11}$$

where P is the probability of occurrence of histogram count of particular pixels. This value is high for good quality image. To measure the structural similarity of the image, following parameters can be used. The measure of luminance index (*MLI*) is a measure of intensity metric defined as the ratio of mean (*MI*) of enhanced image X_e to the mean of original image X.

$$MI(X) = \frac{1}{m,n}\sum_{m,n} X(m,n) \tag{12}$$

$$MI(X_e) = \frac{1}{m,n}\sum_{m,n} X_e(m,n) \tag{13}$$

$$\mathrm{MLI}(X_e, X) = \frac{MI(X_e)}{MI(X)} \tag{14}$$

There could be huge difference between each and every pixel of the two images for good enhancement. Hence, we need an evaluation parameter which describes the pixel-by-pixel change of an image as whole. Those two metrics are mean squared difference (MSD) and peak enhanced to original image ratio (*PEOIR*) which helps to find the difference as well as similarity between the images and the contrast of image in decibels. So for a better quality image, large MSD and low PEOIR values are preferable.

$$\mathrm{MSD} = \frac{1}{mn}\sum_{m,n}(X_e - X)^2 \tag{18}$$

$$\mathrm{PEOIR} = 10\log_{10}\left(\frac{255^2}{\mathrm{MSD}}\right) \tag{19}$$

To observe the subjective performance of the algorithm, four test images (‘peppers,’ ‘baboon,’ ‘art,’ and ‘flower’) of different characteristics are chosen as shown in Fig. 2. Objective measures are evaluated using test images ‘building,’ ‘mountain,’ and ‘peppers’ and are tabulated in Table 1. To emphasize the performance of proposed algorithm, it is compared with histogram equalization (HE) and one of the non-fuzzy approaches implemented in spatial domain [1].

From all the above findings, it is clear that proposed algorithm works effectively with all type of images. While examining the above result shown in Fig. 3, it is

Fig. 2 Subjective evaluation of proposed algorithm: original image (*up*) and corresponding enhanced image (*down*)

Table 1 Objective measures

Sl. no.	Images	Method	ME	MLI	MSD	PEOIR
1	Building	Original	6.78	1	0	Inf
		HE	5.24	1.68	2,011.2	22.13
		Non-fuzzy	6.99	1.24	2,162.1	15.62
		Proposed	7.63	2.56	3,210.5	10.85
2	Mountain	Original	6.89	1	0	Inf
		HE	5.90	0.89	37.797	19.11
		Non-fuzzy	6.54	0.99	253.62	14.3
		Proposed	7.96	1.98	3,128.1	11.42
3	Peppers	Original	6.68	1	0	Inf
		HE	5.92	0.68	89.878	17.65
		Non-fuzzy	6.98	1.56	2,621.3	13.88
		Proposed	7.73	2.03	3,421.6	11.01

obvious that even if HE scores high, it has color-shifting problem (in 'peppers' the background changes to blue color). The proposed method is considered to be better than non-fuzzy approach. In addition, it gives better enhancement for both edges and smooth regions of the image even if the image is washed out (in proposed method, the wires of the electric lines in 'mountain' are clear in proposed method). So the proposed method was able to enhance a wide range of images.

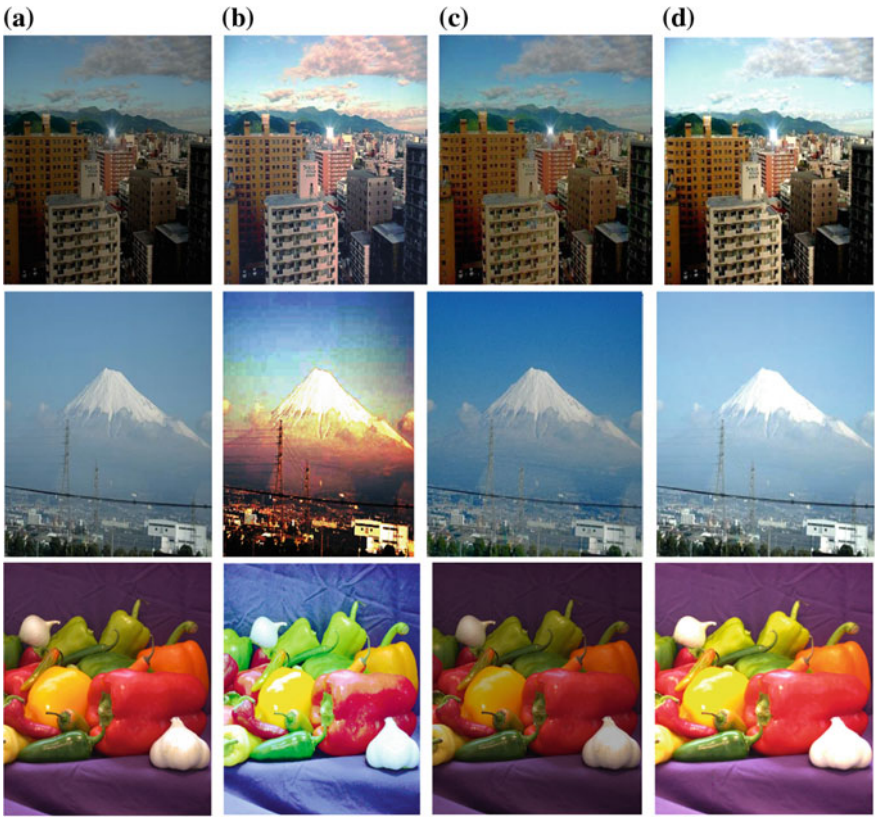

Fig. 3 **a** Original image. **b** HE result. **c** Non-fuzzy approach. **d** Proposed

5 Conclusion

This paper proposed a content-based color image enhancement algorithm in fuzzy domain which can improve a large variety of images along with dark images of different characteristics. In this algorithm, the original image is scaled by a weight function defined by the transformation function derived from the fuzzy set. The scaling process follows the usual defuzzification method under fuzzy image processing. Enhancing color images using human visual system along with wavelet transform in fuzzy domain for better human perception and feature extraction added a new chapter in the field of fuzzy image processing. Robustness of this work is the correct degree of enhancement with no color-shifting problem.

References

1. X. Ding, O. Jun, Contrast enhancement of color images based on wavelet transform and human visual system, in *Proceedings of IASTED International Conference* (2007), pp. 562–804
2. R.C. Gonzalez, R.E. Woods, *Digital Image Processing.* (Prentice hall Upper Saddle River, New Jersey, 2006)
3. C. Reshmalakshmi, M. Sasikumar, Image Contrast Enhancement using Fuzzy Technique. *IEEE Conference ICCPCT* (2013), pp. 861–865
4. A.R. Rivera, B. Ryu, O. Chae, Content-aware dark image enhancement through channel division. IEEE Trans. Image Process. **21**(9), 3967–3980 (2012)
5. P. Vijayalakshmi, S. Rajasekharan, *Neural Networks, Fuzzy Logic, and Genetic Algorithms Synthesis and applications.* (PHI Learning Pvt Ltd., Delhi, 2003)
6. Z. Zhou, Cognition and removal of impulse noise with uncertainty. IEEE Trans. Image Process. **21**(7), 3157–3167 (2012)

Frequent Itemset Mining with Elimination of Null Transactions Over Data Streams

B. Subbulakshmi, A. Periya Nayaki and C. Deisy

Abstract A data stream is an input massive data that arrives at high speed and it is unbounded. The sliding window model is used to extract the recent frequent patterns by adjusting the window size containing only the recent transactions and eliminating the old transactions. Another acute challenge in frequent pattern mining is the presence of null transactions. Null transaction is a transaction which contains only a single item and its presence does not contribute toward frequent pattern discovery. Most of the existing streaming algorithms did not consider the overhead of null transactions, and hence, they fails to discover the frequent patterns faster during mining process. To overcome these issues, a new algorithm called frequent itemset mining using variable size sliding window with elimination of null transactions (FIM-VSSW-ENT) is used for extracting recent frequent patterns from data streams. Experimental results using synthetic and real datasets show that our proposed algorithm gives better result in terms of processing time and memory storage.

Keywords Sliding window model · Data streams · Concept change

1 Introduction

Frequent pattern mining plays an important role in the field of data mining community today. The problem of frequent pattern mining is to extract all the itemsets which are greater than or equal to the user defined minimum support threshold. Recently, the large amount of data has been generated from various heterogeneous

B. Subbulakshmi (✉) · A. Periya Nayaki · C. Deisy
Department of Computer Science and Engineering, Thiagarajar College of Engineering, Madurai, India
e-mail: bscse@tce.edu

A. Periya Nayaki
e-mail: kalakeerthi97@gmail.com

C. Deisy
e-mail: cdcse@tce.edu

© Springer India 2015

L.P. Suresh et al. (eds.), *Artificial Intelligence and Evolutionary Algorithms in Engineering Systems*, Advances in Intelligent Systems and Computing 325,
DOI 10.1007/978-81-322-2135-7_38

sources. Hence, mining data stream is a challenging research area in the field of data mining community. There are three data processing models in the data stream process [1]: landmark model, time fading model or time decay model, and sliding window model. The landmark model extracts the data over the entire history of data streams. The time fading model mines the data based on the weight assigned for each transaction. In sliding window model, the stream data is processed using sliding windows which focus on only the recent transactions and gives the recent frequent patterns alone. Examples of sliding window model include stock market analysis, web click streams etc. The difficulty in using sliding window model is the determination of window size. It can be handled by having a variable size sliding window wherein the size of window is identified based on the amount of changes in the set of frequent patterns across continuous windows.

In addition to that, the presence of a single item (Null Transaction) in dataset could not give any patterns for frequent pattern mining, and hence, it can be removed from the dataset so that the time required to mine frequent patterns could be reduced. In our study, we proposed a new algorithm called frequent itemset mining using variable size sliding window with elimination of null transactions (FIIM-VSSW-ENT) to determine an optimal window size automatically based on the amount of changes (concept change) occurred in the set of frequent patterns. Based on the concept change, the stale transactions are diminished from the window and size of the window is adjusted automatically. The frequent patterns extracted from the sliding window are stored in frequent itemset tree (FIS-tree), and the tree is updated incrementally.

2 Related Works

In 2002, Jian and Gruenwald [2] proposed an algorithm for frequent items mining and extending their work for stream itemset mining. All frequent itemsets are outputted with an error bound, and there are no false negatives in their result. In 2004, Gianella et al. [3] proposed an algorithm for identifying the complete set of frequent pattern with an approximate error bound. In 2004, Manku and Motwani [4] proposed an algorithm based on landmark model to mine over the entire history of data streams. In 2006, Li et al. [5] proposed an algorithm called DSTree, a prefix tree-based data structure for mining complete set of recent frequent patterns using the sliding window model. Tanbeer et al. [1] proposed an algorithm namely compact prefix tree-based structure (CPS) which was used to extract the exact and complete set of recent frequent itemsets. In 2012, Deypir et al. [6] proposed LDS method to extract the frequent itemsets based on list conversion strategy in the current window. The number of list conversion affects the processing time during data stream processing.

From all these reviews, it is observed that the old information was deleted without estimating the notable changes in the set of frequent patterns. But some of

the infrequent patterns may become frequent patterns due to upcoming transactions. Hence, the stale information cannot be deleted directly without detecting the concept change or concept shift, or concept drift. The concept change [7] refers to the change that occurs in the set of frequent patterns. In addition, most of the streaming algorithms collect frequent patterns covering all the transactions, including null transactions. In our proposed work, the aim is to identify the concept change to reasonably delete the oldest information and determining the window size automatically with the elimination of null transactions from the dataset. This saves a lot of computation time and memory usage.

3 Proposed Work

The algorithm FIM-VSSW-ENT has the following steps: (i) removal of null transactions, (ii) window initialization and frequent pattern mining, (iii) pane insertion and window sliding phase, and (iv) construction of FIS-tree.

3.1 Removal of Null Transactions

Null transaction [8] is a transaction that does not contain any itemset being examined. In real-life applications, most of the transactions contain only a single item and such transactions may not be helpful in identifying useful correlation between items. And they also contribute more in terms of memory space and processing time. So this step eliminates those null transactions, thereby reduce the processing time for finding the frequent itemsets.

3.2 Window Initialization and Frequent Pattern Mining

The sliding window model is used to extract the recent frequent patterns from the transactional data stream. The window size is used to restrict the amount of transactions to be processed at a time in the data stream. For this purpose, the user wants to give the initial window size, pane size (increment window size) of the sliding window. The window initialization phase is activated to find the starting and ending transaction of a window in a stream of data. Once the window is initialized, the ECLAT algorithm [9] is applied to the window to find the frequent patterns. This algorithm is a depth first method operating on the vertical layout of the database for the fast computation of itemsets.

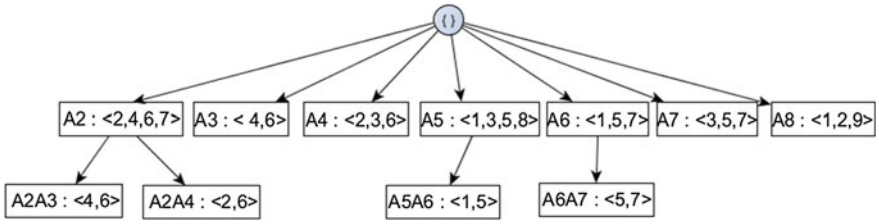

Fig. 1 Construction of FIS-tree (initial window)

3.3 Pane Insertion and Window Sliding Phase

As the new transactions are inserted (comprising a pane of transactions) into the current sliding window, the frequent pattern mining algorithm (ECLAT) is applied to the pane. A new measure called FChange [7] is used to calculate amount of change in the set of frequent patterns between initial window and the pane of transactions. Based on this FChange value, the algorithm takes the decision that whether to delete or maintain the old information. To determine the acceptable amount of change, user has to give the minimum change threshold value that is change threshold. The measure FChange can be calculated by,

$$\text{FChange} = \frac{|F^+| + |F^-|}{|F| + |F^+|} \tag{1}$$

where
F^+ newly emerged frequent itemsets
F^- newly disappeared frequent itemsets

To implement the FChange measure, a checkpoint is specified by the algorithm to diagnose the changes in the set of frequent patterns. This checkpoint is not fixed during the data stream processing and moves forward if the concept change is detected after inserting pane of transactions. Initially, a checkpoint is placed at the last transaction id of the initial window. After inserting the pane of transactions to the window, the set of newly emerged frequent patterns is mined and results are updated in the monitoring FIS-tree. At this point, the change ratio has to be computed. If the significant change (greater than the minimum change threshold) has occurred on the set of frequent patterns, the information before the checkpoint has to be deleted. Furthermore, the effects of these transactions are also deleted from the monitoring FIS-tree. If there is no significant change, then the window, checkpoint, monitoring FIS-tree is not changed and data stream processing continues.

3.4 Construction of FIS-tree

The frequent itemset tree (FIS-tree) data structure has been proposed to store the set of frequent patterns mined using ECLAT algorithm on the initial window and at every pane insertion. The FIS-tree has two fields: itemset (X) and transaction ids that contain the itemset (X). The sample FIS-tree is constructed with minimum support threshold σ = 20 % for initial window, and it is shown in Fig. 2. The support of an itemset is calculated with respect to number of TID's that contains the itemset and current window size.

The root node of this tree is null {} or [∅]. The Level 1 of the tree contains frequent 1-itemset. The frequent k-itemsets (where k ≥ 2) are stored in the successive levels, and they also share the prefixes in their upper levels. Each node of the tree contains frequent item and its transaction identifiers.

Initial Window

Item	TID's
A1	1
A2	2,4,6,7
A3	4,6
A4	2,3,6
A5	1,3,5,8
A6	1,5,7
A7	3,5,7
A8	1,2,9
A9	7

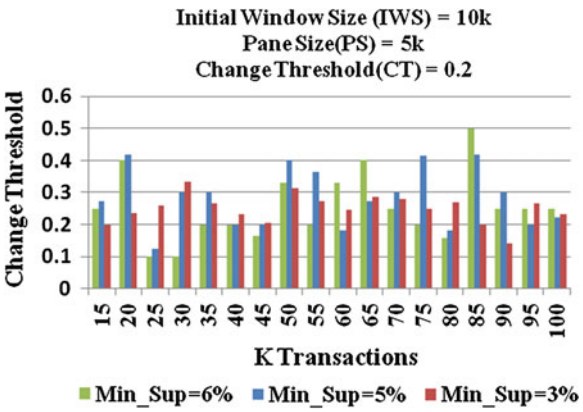

Fig. 2 Window resizing behavior using T40I10D100K

As pane of transactions are inserted into the window, the tree is either updated with the set of frequent patterns when the window gets expanded or new set of frequent patterns are stored when the window shrinks. The expansion or the shrinkage of window happens based the amount of concept change measured using the FChange measure. So, the FIS-tree maintains only the frequent patterns.

4 Experimental Results

In this section, we present the performance results of the proposed algorithm using real and synthetic datasets. All programs were written in Java NetBeans IDE 7.3 environment and executed using a system with windows 7, core i5, and 4 GB memory. The experimental datasets were downloaded from FIMI repository [10]. Table 1 shows the statistical information about the datasets used for our analysis. We considered two real-life datasets BMS WebView-1 and BMS WebView-2 from a small dot com company named as Gazelle.com. These datasets contains several months of click stream data. In these datasets, each transaction is considered as the Web session and consists of product detail Web pages viewed in that session. Each product view in a transaction is considered as an item. These datasets were considered as stream data because clicking behaviors of the customers were changed over a time.

The real datasets were used to compare the run time, memory storage, and length of frequent patterns generated by the proposed algorithm and the existing algorithm. We use synthetic dataset to verify the window resizing behavior based on the amount of changes occurred in the set of frequent patterns during data stream processing.

Figure 2 shows the amount of changes occurred after each pane insertion with respect to different minimum support threshold values. The first checkpoint is placed at the end of initial window (i.e., 10 k). This checkpoint is then moved to the place where the concept change is detected. Concept change is monitored using the change threshold measure, which is given as input by the user. The window shrinks, if the detected concept change is above the change threshold value and the checkpoint is adjusted. Otherwise, window expands and data stream processing continues. As shown in Fig. 3, whenever the detected change is above the threshold value, the old transactions are deleted from the window based on the checkpoint and frequent patterns are updated in the FIS tree accordingly.

Table 1 Dataset characteristics

Dataset	No. of transactions	No. of unique items	Average transaction length
BMS WebView-1	59,602	497	2.5
BMS WebView-2	77,512	3,340	5.0
T40I10D100K	1,00,000	942	39.6

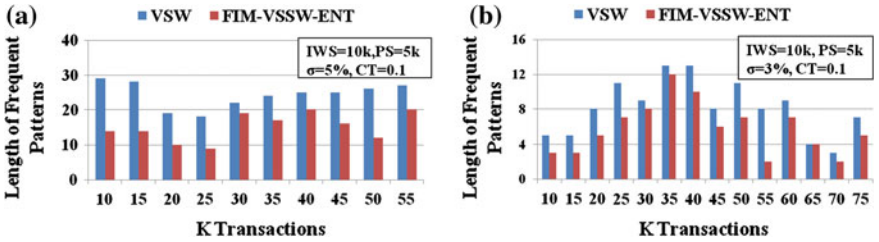

Fig. 3 Number of frequent patterns (IWS = initial window size, PS = pane size, σ = minimum support, CT = change threshold). **a** BMS webview-1, **b** BMS webview-2

Figure 3 shows the number of frequent patterns generated by frequent itemset mining using variable size sliding window with elimination of null transactions (FIM-VSSW-ENT) and variable size sliding window (VSW) algorithms using BMS WebView-1 and BMS WebView-2 datasets. Since these two real datasets contain lots of null transactions which are no longer used to generate frequent patterns, they were eliminated using the proposed approach. From this, we can be observed that the performance of FIM-VSSW-ENT algorithm increases due to reduction in number of frequent patterns.

The experimental results shown in Fig. 4 are about the memory usage (Kilobytes). Since the proposed algorithm stores the set of frequent pattern in a FIS tree, the size of the tree is taken as an important performance metric to evaluate the algorithm. From Fig. 3, it is known that the number of patterns generated by the proposed algorithm is minimal compared to the existing algorithm. When the patterns are stored as tree, they will occupy only a limited memory compared to the existing scenario. Hence, it can be seen from Fig. 4 that the memory size of FIM-VSSW-ENT algorithm is significantly lower than the VSW algorithm.

Figure 5 shows the running time (in seconds) of algorithms for BMS WebView-1 and BMS WebView-2 datasets. The run time includes the time to find the frequent patterns and the time involved in the construction and maintenance of FIS tree. Since the null transactions are eliminated from the original inputs, the proposed algorithm gives reduced running time compared to the existing algorithm.

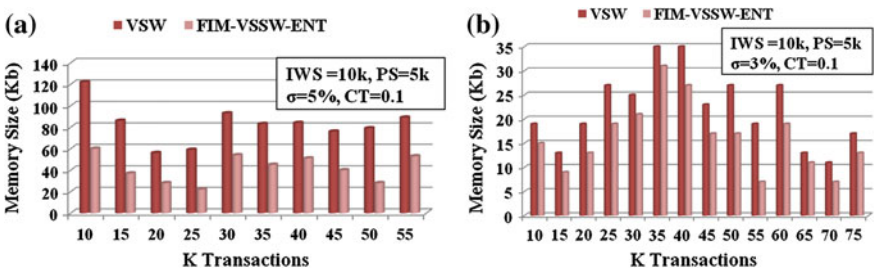

Fig. 4 Memory usage. **a** BMS webview-1, **b** BMS webview-2

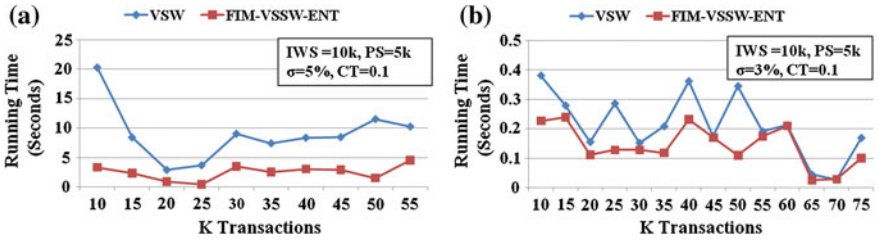

Fig. 5 Comparison of running time. **a** BMS webview-1, **b** BMS webview-2

Input: Data Stream S, Initial Window Size (IWS), Pane Size (PS), Minimum Support (σ), Change Threshold (CT)

Output: FIS-Tree contains Recent Frequent Itemsets

Step 1: Scan and Remove "Null Transactions" from the dataset.

Step 2: Window Initialization ()

2.1: W = Window Initialization (IWS);

2.2: Checkpoint Cp: =Last-Tid (W);

2.3: FP = Eclat (W [IWS], σ);

2.4: Insert (FIS, FP);

Step 3: Pane Insertion ()

3.1: W: =W U{ Pane Size (PS)};

3.2: New FP: =Eclat (W [PS], σ);

3.3: If $(F^{+} + F^{-}) / (F + F^{+}) > CT$

3.3(a): Delete (CP, FP, FIS)

3.3(b): Update (FIS, NewFP);

3.4: else

3.4(a): Update (FIS, NewFP);

End If

Fig. 6 FIM-VSSW-ENT algorithm

5 Conclusion

The proposed algorithm FIM-VSSW-ENT (Fig. 6) uses flexible window size to detect the concept changes over data streams. The window size is dynamically adjusted based on the amount of concept change within the data stream. Comparative results also show that FIM-VSSW-ENT algorithm is more sensitive toward recent changes than the time decay model and landmark models. The reason is that the proposed algorithm uses a change threshold to measure the changes and finds frequent patterns from the most recent information. Moreover, elimination of null transactions from the dataset increases the performance of the algorithm as the number of frequent patterns, memory storage, and running time is decreased.

As a future work, we intend to perform weighted frequent pattern mining over data streams by considering the weight of each item (i.e., worth/importance of an

item) is more appropriate than the frequency of item. The concept of flexible window size and screening of null transactions can be applied for weighted frequent pattern mining.

References

1. S.K. Tanbeer, C.F. Ahmed, B.S. Jeong, Y.-K. Lee, Sliding window-based frequent pattern mining over data streams. Elsevier, Inf. Sci. **179**, 3843–3865 (2009)
2. N. Jiang, L. Gruenwald, Research issues in data stream association rule mining. ACM SIGMOD Rec. **35**(1), 14–19 (2006)
3. C. Gianella, J. Han, J. Pei, X. Yan, P.S. Yu, Mining frequent patterns in data streams at multiple time granularities, in *Proceedings of Data Mining: next generation challenges and future directions* (2004) pp. 191–212
4. G.S. Manku, R. Motwani, Approximate frequency counts over data streams, in *Proceedings of the 28th international conference on very large databases* (2002), pp. 346–357
5. H.F. Li, S.Y. Lee, M.K. Shan, An efficient algorithm for mining frequent itemsets over the entire history of data streams, in *Proceedings of the First International Workshop on Knowledge Discovery in Data Streams Conjunction With ECML and PKDD* (2004)
6. M. Deypir, M.H. Sadreddini, A dynamic layout of sliding window for frequent itemset mining over data streams. Elsevier, J. Syst. Sofware. **85**, 746–759 (2012)
7. M. Deypir, M.H. Sadreddini, S. Hashemi, Towards a variable size sliding window model for frequent itemset mining over data streams. Elsevier, Comput. Ind. Eng. **63**, 161–172 (2012)
8. B. Nair, A.K. Tripathy, Accelerating Closed Frequent Itemset Mining by Elimination of Null Transactions. J. Emerg. Trends Comput. Inf. Sci. **2**(7), 317–324 (2011)
9. B. Goethals, *Frequent Set Mining. Data Mining and Knowledge Discovery Handbook*. (Springer, New York, 2005), pp. 377–397
10. C.K.S. Leung, Q.I. Khan, DSTree-a tree structure for the mining of frequent sets from data streams, in *Proceedings ICDM* (2006), pp. 928–932

Protograph-Based Design of Non-Binary LDPC Codes

I. Divya and M. Anbuselvi

Abstract This paper presents construction of non-binary LDPC codes using protograph method. A new class of LDPC codes is constructed from a template called a protograph. The protograph serves as a blueprint for constructing LDPC codes of arbitrary size in which the performance can be predicted by analyzing the protograph. The significance of this approach is the reduction of number of nodes of computation in the decoding process. Furthermore, they also benefit for low memory requirements, simple design procedure, as well as hardware-friendly implementation. ARA-based code is a kind of linear class codes having self-correcting capabilities. It is used to transmit messages over noisy transmission channel. Due to this, the information loss can be made as small as possible. These codes constitute a subclass of LDPC codes with very fast encoder structure. They also have a projected graph or protograph representation that allows for high-speed decoder implementation. Because of the unique feature the, ARA code is mainly used in supporting remote sensing, digital video broadcasting, and data delay applications. The decoding performance of the ARA-based LDPC codes with varied punctured patterns and repetition rates is analyzed. Computation of weighted enumerators for the design of non-binary LDPC codes is done. The simulation results of protograph-based LDPC codes are calculated by bit error rate (BER) performance.

1 Introduction

Low-density parity check codes (LDPC) are a kind of linear block codes. It was proposed by Gallager in 1962. These LDPC codes are used for error-correcting capabilities. They are the best error correction codes in existence at present [1].

I. Divya (✉) · M. Anbuselvi
ECE Department, SSN College of Engineering, Kalvakkam, Chennai, India
e-mail: inbarajdivya@gmail.com

M. Anbuselvi
e-mail: anbuselvi@ssn.edu.in

© Springer India 2015

L.P. Suresh et al. (eds.), *Artificial Intelligence and Evolutionary Algorithms in Engineering Systems*, Advances in Intelligent Systems and Computing 325,
DOI 10.1007/978-81-322-2135-7_39

These codes are used to transmit the message over noisy channel efficiently. The important feature of LDPC codes is that the data transmission rate approaches Shannon limit, which is the theoretical maximum data transfer rate of the channel for particular noise level [2]. It is mainly used in bandwidth-limited communication link where designers seek to achieve maximal information transfer, in the presence of data-corrupting noise. A new class of LDPC codes is constructed from a template called a protograph. The protograph serves as a blueprint for constructing LDPC codes of arbitrary size whose performance can be predicted by analyzing the protograph. Hence, the decoding algorithms are simple and relatively easier to implement. However, the encoder complexity is high. Thus, we go for accumulate repeat accumulate (ARA) codes which have fast encoder structure [3].

2 Protograph-Based LDPC Codes

Protograph is a graphical representation of LDPC code, also known as a projected graph. A protograph G = (V, C, E) consists of a set of variable nodes V, a set of constraint nodes C, and a set of edges E. Protograph-based codes aim at minimizing the number of nodes [2]. Copy-and-permute operations can be applied to obtain larger derived graphs of various sizes. The accumulate repeat accumulate (ARA) codes are a subclass of protograph-based LDPC codes. They have a protograph or projected graph representation, which paves the way for high-speed iterative decoding. Also, the number of iterations required for decoding is less. They have fast encoder structure; hence, the encoder complexity is reduced [4].

2.1 Accumulate Repeat Accumulate

ARA codes are a subclass of LDPC codes. These are characterized by a protograph or projected graph representation which allows for high-speed iterative decoding. Figure 1 shows the block diagram of ARA encoder. The message length is represented by the term N, and then, the input of the message is accumulated by using EX-OR operation. The repetition repeats the accumulated message, then it is permuted, and then the permuted message is accumulated once again [5]. Finally, the

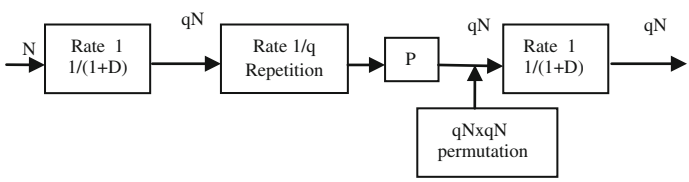

Fig. 1 Block diagram of ARA encoder

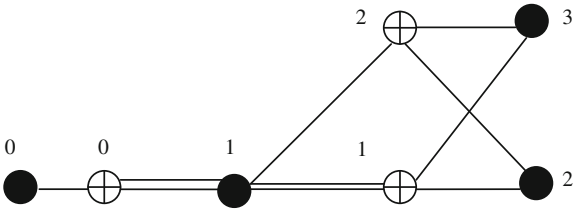

Fig. 2 Protograph of ARA encoder

output of the encoded message is represented by the term qN. Figure 2 shows the diagram of protograph of ARA encoder in which the input message is given to the accumulator, and then, the accumulator performs the accumulation for the input messages. The accumulated message is repeated three times, and once again, the accumulation is done. Finally, the output of the encoded message is received. Puncturing is the process of removing some of the parity bits after encoding with an error correction code [4]. Thus, puncturing considerably increases the flexibility of the system without significantly increasing its complexity. The different puncturing patterns xx0, 0x, 000x, and 0xxx0x were used where 0's indicates the puncturing positions. The repetition rates of 2, 3, and 4 were used for the ARA codes.

Figure 3 shows the punctured ARA pattern encoder. The x0x pattern that has been used for the repetition rate of 3 is shown. The input of the message is repeated three times, and then, the message is permuted. The permuted message is accumulated, and then, the accumulated message is punctured by using the pattern x0x. Finally, the output of the encoded message is received.

Figure 4 shows the protograph of punctured ARA code. This protograph consists of 4 variable nodes and 4 check nodes, connected by 12 edges. Three variable nodes are connected to the channel (transmitted nodes) and are shown as dark filled circles. One of the variable node is connected to the channel (i.e., it is punctured) and is depicted by a blank circle. Figure 5 shows the decoding performance of the non-binary ARA code with four different puncture patterns 000x, 000x0x, xx0, and 0x, respectively. The signal-to-noise ratio at the range of 4 dB the bit error rate obtained for the puncture pattern 000x is 0.16 and for the puncture pattern 0xxx0x bit error rate is 0.15. It is inferred that the BER decreases with the increased puncturing rate.

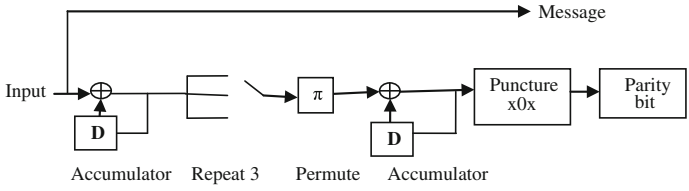

Fig. 3 Punctured ARA encoder

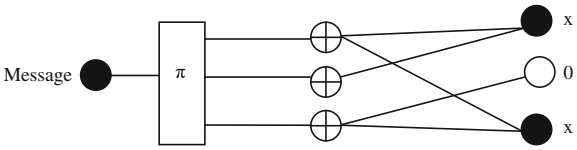

Fig. 4 Protograph of punctured ARA encoder

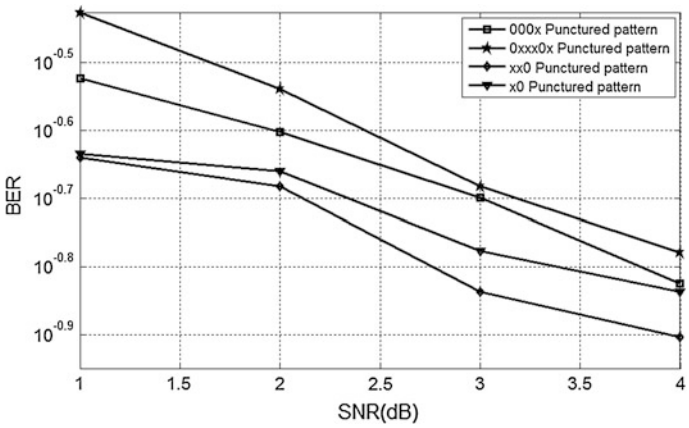

Fig. 5 Punctured patterns of 000x, 0xxx0x, xx0, and 0x of non-binary ARA

3 Weight Enumerator of Protograph

A protograph G = (*V*, *C*, *E*) is a relatively small bipartite graph, containing a set $V = \{v_1, v_2, v_3..\}$ of variable nodes (*VN*s), a set $C = \{c_1, c_2, c_3..\}$ of constraint nodes (*CN*s), and a set $E = \{E_1, E_2, E_3 \ldots E|E|\}$ of edges from which a larger graph can be obtained by the following copy-and-permute procedure [6, 7]. The protograph is copied N times, and the edge copies are reconnected between *VN* and *CN* copies to obtain an expanded graph, as follows. The N copies of protograph VN v_i will be said to be of type *vi*, the N copies of protograph CN c_j will be said to be of type c_j, and the N copies of a protograph edge E_k connecting v_i to c_j will be said to be of distinct type (v_i, c_j, k) or simply of type k. The weight enumerator of the non-binary protograph ensemble is given by

$$A(d) = \sum_{\{w_{m,u}\}} \frac{\prod_{j=1}^{n_v} A^{v_i}(w_i)}{\prod_{s=1}^{n_v} \prod_{r=1}^{q_{vs}} \binom{N}{w_{s,r}}} \frac{\prod_{j=1}^{n_c} A^{c}(z_j)}{} = \frac{\prod_{j=1}^{n_{cj}} A^{c_j}(d_j)}{\prod_{i=1}^{n_v} \binom{N}{d_i}^{q_{v_i}-1}} \tag{1}$$

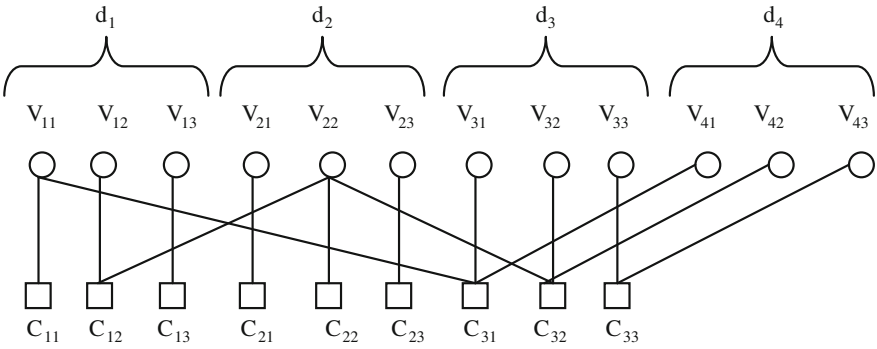

Fig. 6 Vectorized protograph

$A^{C_j N}(d_j)$ is the weight vector enumerator of the code C_j^N induced by the N copies of the check node c_j. Here, the elements of d_j comprise a subset of the elements of $d = [d_1, d_2, \ldots, d_{n_v}]$, and this subset is obtained from the edge connections in the mother protograph G in Fig. 6.

$$A^C(w) = \sum C(N, n_1, n_2, n_3 \ldots, n_k) \tag{2}$$

where $C\ (N, n_1, n_2, \ldots, n_k)$ is the multinomial coefficient.

$$\sum C(N, n_1, n_2, \ldots, n_k = \frac{N!}{n_1! n_2! \ldots n_k} \tag{3}$$

and $\{n\}$ is the set of integer vector solutions to $w = n \cdot M^C$ with $n_1, n_2, \ldots. n_k \geq 0$.

4 Performance Analysis

The ARA code decoding performance for the code length k = 24 is performed using the FFT-SPA and min-sum decoding algorithms for the repetition rates 3 and 4. Performance curves for bit error rate (BER) for a range of signal-to-noise ratio (SNR) are plotted.

Figure 7 shows that the decoding performance is analyzed with the help of measures such as bit error rate (BER) for typical values of signal-to-noise ratio in dB (SNR) values that are plotted for the code length 24. The signal-to-noise ratio at the range of 3 dB the bit error rate obtained for min-sum algorithm for the repetition 3 the bit error rate is 0.20 and for the FFT–SPA the bit error rate is 0.18.

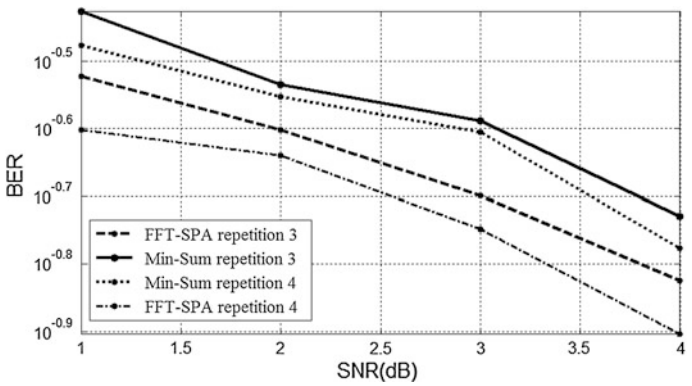

Fig. 7 Non-binary ARA decoding performance for min-sum and FFT-SPA decoding algorithms for repetition 3 and 4

5 Conclusion and Future Work

This paper is aimed at designing and analyzing the non-binary ARA code for different punctured patterns and repetition rates. As a result, it is found that when the punctured pattern increases, the bit error rate gets increased, and when the repetition rate is increased, the BER gets decreased. The decoding performance is analyzed using FFT-SPA and min-sum decoding algorithms. It is inferred that the FFT-SPA algorithm performs better compared to min-sum decoding algorithm. In future, the optimized hardware realization of the decoder architecture of ARA-based non-binary LDPC codes is to be done. The performance analysis of the designed architecture is to be evaluated and validated.

References

1. R.G. Gallager, Low density parity check codes. IRE Trans. Inf. Theor. (1962)
2. J. Thorpe, *Low-Density Parity-Check Codes Constructed from Protographs* (IPN Progress Report, JPL, USA, 2003), pp. 42–154
3. A. Abbasafar, D. Divsalar, K. Yao, A comparison of MC/DC, MUMCUT and several other coverage criteria for logical decisions. J. Syst. Softw. (2007)
4. A. Abbasafar, Accumulate repeat accumulate codes. IEEE Trans. commun. **55**, 692–702 (2007)
5. D. Divsalar, C. Jones, S. Dolinar, J. Thorpe, Protograph based LDPC codes with minimum distance linearly growing with block size, in *IEEE Globecom* (2005)
6. D. Divsalar, Ensemble weight enumerators for protograph LDPC codes, in *Proceedings of IEEE International Symposium on Information Theory*. (Seattle, WA, 2006), pp. 1554–1558
7. D. Divsalar, W. Ryan, Enumerators for protograph- based ensembles of LDPC and generalized LDPC codes. IEEE Trans. Theor. **57**(2) (2011)
8. D. Divsalar, Low-rate LDPC codes with simple protograph structure. in *IEEE ISIT* (2005), pp. 4–9

9. D. Divsalar, Short protograph- based LDPC codes. IEEE Trans. Commun. (2010)
10. L. Costantini, Non-binary protograph low-density parity-check codes for space communications. Int. J. Satellite Commun. Netw. **30**, 43–51 (2012)
11. D. Divsalar, L. Dolecek, *Graph cover ensembles of non-binary protograph LDPC Code* (IEEE ISIT, Boston, 2012)
12. D. Declercq, M. Fossorier, Decoding algorithms for nonbinary LDPC codes over GF(q). IEEE Trans. commun. **55**(4) (2007)

Extraction of Binary Sequences in a Frequency Shift Keying-Modulated Signal by Empirical Mode Decomposition Algorithm Against Ambient Noises in Underwater Acoustic Channel

L. Suvasini, S. Prethivika, S. Sakthivel Murugan and V. Natarajan

Abstract Frequency shift keyed acoustic signals transmitted in underwater sensor networks are affected by numerous factors such as ambient noise, ocean interference, and other random sources which make them nonlinear and non-stationary in nature. In recent years, the use of empirical mode decomposition (EMD) technique to analyze modulated acoustic signals has gained importance. In this paper, an EMD-based approach is proposed to extract frequency shift keying (FSK)-modulated acoustic stationary signals in the underwater channel that are affected by above-mentioned factors in shallow water over a range of 100 Hz to 10 kHz. EMD is an experimental technique which decomposes a signal into a set of oscillatory modes known as intrinsic mode functions (IMF). The proposed algorithm makes use of FFT for the identification and extraction of oscillatory signal. To validate the proposed algorithm, computer simulation is carried out by exploiting the real-time data perturbed by ambient noises. It is observed from the simulation results that the proposed EMD approach identifies and extracts two FSK stationary signals against various ambient noises present in the channels of the underwater sensor network.

Keywords Frequency shift keyed acoustic signals · Empirical mode decomposition · Intrinsic mode functions · Wavelet decomposition · Fast Fourier transform

L. Suvasini (✉) · S. Prethivika · S. Sakthivel Murugan
Department of ECE, SSN College of Engineering, Chennai, India
e-mail: suva92@gmail.com

S. Prethivika
e-mail: prethivi1993@gmail.com

S. Sakthivel Murugan
e-mail: sakthivels@ssn.edu.in

V. Natarajan
Instrumentation Department, MIT Campus, Anna University, Chennai, India

© Springer India 2015

L.P. Suresh et al. (eds.), *Artificial Intelligence and Evolutionary Algorithms in Engineering Systems*, Advances in Intelligent Systems and Computing 325,
DOI 10.1007/978-81-322-2135-7_40

1 Introduction

When an acoustic signal is transmitted using water as a channel, apart from various types of losses such as reverberation, attenuation, absorption, and scattering, the acoustic signal also undergoes distortion due to ambient noises. Ambient noises in underwater acoustics are the background noises in the ocean. The sources for ambient noises can be either natural (due to rain, wind, seismic, mammals, etc.,) or man-made (due to ships, boat, harbor activities, aircraft just above the sea, etc.,).

The underwater acoustic channel is a time-varying, frequency-selective, spatially uncorrelated channel with additive Gaussian noise. Due to this wide variety of interferences, any acoustic signal transmitted through underwater channel will undergo severe noise disturbances and hence, it should be recovered properly.

Researchers have proposed a fast empirical mode decomposition (EMD) algorithm and identified that any signal can be decomposed into various stationary signals using EMD algorithm [1]. Lidar signals such as acoustic underwater signals are typically non-steady and non-stationary. Therefore, they are difficult to be dealt by traditional filtering methods. Combination of EMD with Savitzky-Golay filter is proposed for denoising lidar echo signals that removes the noise besides retaining useful signal effectively [2].

A nonlinear time series analysis of a signal using EMD and wavelet decomposition (WD) has been presented in [3], and it has been inferred that EMD determines the instantaneous balance position by acquiring the intrinsic mode functions (IMFs) compared with WD. They have also identified that WD is better for the analysis of linear signals, whereas EMD is better for both linear and nonlinear analysis. The authors of [4] investigate how EMD behaves for a composite two-tone signal, and the analysis is also extended for nonlinear model. The concept of applying Hilbert transform to the IMF is analyzed, thereby deriving the instantaneous frequency evolving with time [5]. The authors of [6] discuss the use of EMD for biomedical applications and focus on the extraction of ECG signal corrupted with white Gaussian noise. The authors of [7] have analyzed the environmental effect and signal processing approaches for 4 kHz frequency shift keying (FSK) reference signal for underwater acoustic communication by conventional signal processing method.

2 Proposed System Model

In this section, we address the proposed algorithm which uses EMD method to extract the frequency components of the modulated signal. In contrast to [1], here, we consider the problem of signal extraction by using the dominant signal extraction approach from FSK-modulated signal affected by various ambient noises. Figure 1 shows the proposed model for signal extraction.

In order to describe the signal extraction with the block diagram, let us consider the reference signals $r_1(t)$ and $r_2(t)$ that correspond to binary bits 1 and 0, respectively. After line encoding, the line encoded data denoted by $r(t)$ be FSK

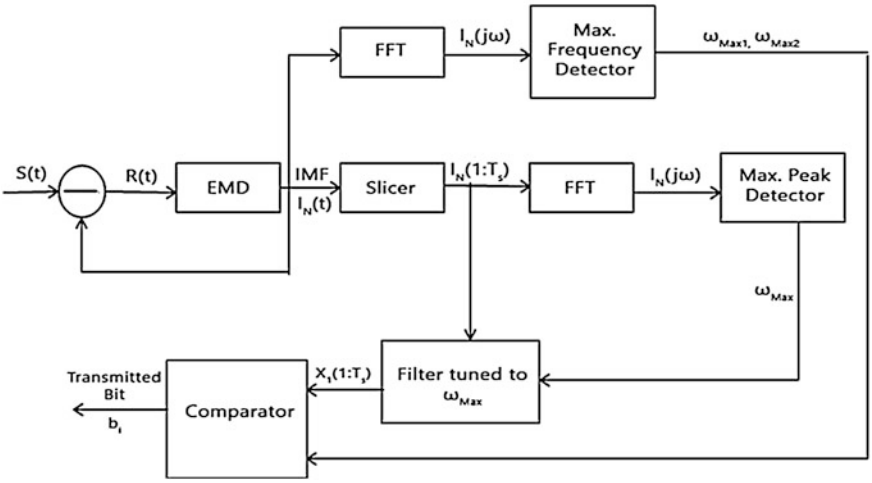

Fig. 1 Proposed model for extraction of stationary FSK signal using EMD

modulated and transmitted with the non-stationary ambient noise signal $n(t)$ which can be expressed as

$$\text{Noisy signal, } S(t) = r(t) + n(t) \tag{1}$$

When EMD is applied to received noisy signal S (t), it calculates the extrema points of the noisy signal as Max and Min as follows in Eqs. (2) and (3).

$$\text{Max} = \text{Maxima}\,[S(t)] \tag{2}$$

$$\text{Min} = \text{Minima}\,[S(t)] \tag{3}$$

The interpolation of Max and Min results in deriving the upper envelop $E_{\text{UE}}(t)$ and lower envelop $E_{\text{LE}}(t)$ of the signal $S(t)$, as represented in Eqs. (4) and (5).

$$E_{\text{UE}}(t) = \text{Interpolation}\,[\text{Max}] \tag{4}$$

$$E_{\text{LE}}(t) = \text{Interpolation}\,[\text{Min}] \tag{5}$$

where

$E_{\text{UE}}(t)$ is the upper envelope of the signal

$S(t)E_{\text{LE}}(t)$ is the lower envelope of the signal $S(t)$

The mean of received signal $m(t)$ is calculated by averaging the upper and lower envelop

$$m(t) = [E_{\text{UE}}(t) + E_{\text{LE}}(t)]/2 \tag{6}$$

Sifting process is then carried out by eliminating the non-stationary components by subtracting the mean signal $m(t)$ which results in the formation of detail signal $h_{K+1}(t)$

$$h_{K+1}(t) = h_K(t) - m_K(t) \tag{7}$$

where

The detail signal in the first stage, $h_1(t) = S_1(t)$

$h_K(t)$ is the kth stage detail in the sifting process.

$m_K(t)$ is the kth stage mean in the sifting process.

$h_{K+1}(t)$ is the $k + 1$th stage detail in the sifting process.

The detail signal is iterated till the mean $m(t)$ becomes zero. The final-stage detail results in the formation of IMF signal $I(t)$. The $I(t)$ is subtracted from the received signal $S(t)$ which yields the residue signal $R(t)$. Applying EMD on $R(t)$ over several iterations leads to the extraction of all available stationary signals.

In contrast to applying Hilbert transform [2], our approach invokes FFT on the IMF output for identifying the dominant frequency. Applying FFT to the Nth IMF output results in

$$I_N(j\omega) = F[I_N(t)] \tag{8}$$

where

$I_N(j\omega)$ is the frequency domain signal of Nth stage IMF.

The two maximum frequencies in the IMF corresponding to the two carrier frequencies are computed with the aid of FFT as given by

$$\text{imf}(\omega_{\max 1}) = \max[I_N(j\omega)] \tag{9}$$

$$\text{imf}(\omega_{\max 2}) = \max[I_N(j\omega) - \text{imf}(\omega_{\max 1})] \tag{10}$$

To assist the modulated signal extraction, the output of EMD is divided into number of subsignals depending upon the number of bits transmitted using slicer. To be specific, the EMD output is divided according to the bit intervals $I_N(1 : Ts)$ where Ts is the bit interval of the transmitted bit sequence. The proposed algorithm is applied to the signal in each bit interval separately, and the dominant signal in that particular bit interval is identified.

Applying FFT to each subinterval results in

$$I_{1N}(\omega) = F[\text{imf}(1 : Ts)] \tag{11}$$

The dominant signal in each subinterval is found as follows

$$I_{1N}(\omega_{\max}) = \max[I_{1N}(\omega)] \tag{12}$$

The final extracted signal from the IMF is computed as follows

$$F(\omega) = I_{1N}(\omega_{\max}) \cdot H(\omega) \tag{13}$$

where

$F(\omega)$ is the frequency domain representation of the extracted acoustic signal. If this signal corresponds to $f\omega_{\max}()$, then the transmitted bit is '1' otherwise '0'.

The filtering operation is repeated for all subsignals of IMF in order to obtain the complete bit sequence transmitted. This proposed approach results in complete extraction of the FSK-modulated acoustic signal by eliminating all the ambient noises from $S(t)$.

3 Algorithm

1. FSK signal $F_1(t)$ with two carrier signals $r_1(t)$ and $r_2(t)$.
2. Noisy signal $S_1(t) = F_1(t) + n_1(t)$ where $n_1(t)$ is a real-time ambient noise.
3. FSK signal $F_2(t)$ with carrier signals $r_3(t)$ and $r_4(t)$.
4. Noisy signal $S_2(t) = F_2(t) + n_2(t)$ where $n_2(t)$ is a real-time ambient noise.
5. $ST(t) = S_1(t) + S_2(t)$.
6. Identify all extrema points of $ST(t)$.
7. Compute $E_{\mathrm{UE}}(t)$ and $E_{\mathrm{LE}}(t)$ by interpolating the Max and Min, respectively.
8. Calculate mean $m(t) = [E_{\mathrm{UE}}(t) + E_{\mathrm{LE}}(t)]/2$.
9. Extract the detail by $h_{K+1}(t) = h_K(t) - m_K(t)$
10. Iterate till $m(t)$ becomes zero.
11. Applying FFT, $I_N(j\omega) = F[I_N(t)]$
12. Compute $\omega_{\max1}, \omega_{\max2}$ using $\mathrm{imf}(\omega_{\max1}) = \max[I_N(j\omega)], \mathrm{imf}(\omega_{\max2}) = \max[I_N(j\omega) - \mathrm{imf}(\omega_{\max1})]$
13. Slice the output of EMD as $I_N(1:Ts)$ and apply FFT by $I_{1N}(\omega) = F[\mathrm{imf}(1:Ts)]$
14. Compute the dominant signal $I_{1N}(\omega_{\max}) = \max[I_{1N}(\omega)]$
15. Extract dominant frequency by filter tuned to $\omega_{\max}$.
16. If $\omega_{\max} = \omega_{\max1}$, bit transmitted is 1 and if $\omega_{\max} = \omega_{\max2}$, bit transmitted is 0 else unknown noise signal.
17. Repeat till both the sequences are detected.

4 Results and Discussion

In this section, we provide the performance results to quantify the performance of our proposed algorithm. The data for carrying out the analysis have been collected using a self-designed fixture at depths of 5, 10 m using Reson 4,032 type of hydrophones at Bay of Bengal, Chennai, for various wind speeds ranging from 2 to 6 m/s

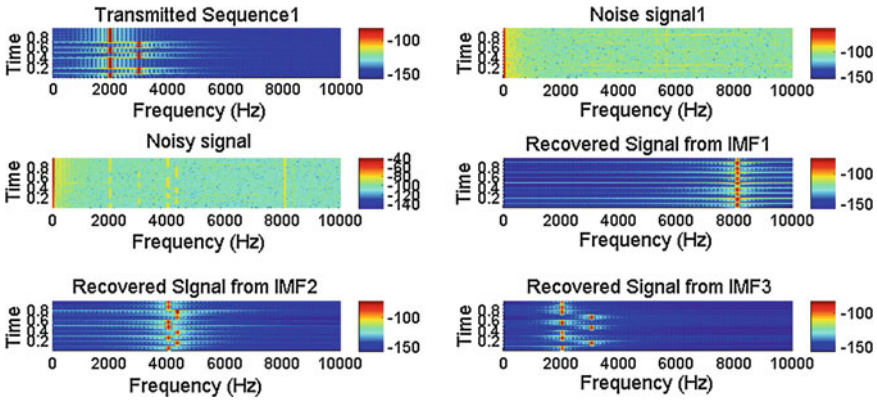

Fig. 2 Spectrogram for the detection of FSK signal $F1(t)$

with a sampling frequency of 50 kHz. The collected data comprise of ambient noises in the range of 100 Hz to 10 kHz.

In practical real-time scenario, modulated signals are transmitted underwater. Hence, two FSK-modulated source signals from different sources are combined additively and transmitted through a channel. These signals are then demodulated at the receiver. When transmitted in an underwater wireless sensor network, the two source signals are subjected to various ambient noises. The spectrogram for the extraction of sequence 1 is shown in Fig. 2. The spectrogram for the extraction of sequence 2 is shown in Fig. 3.

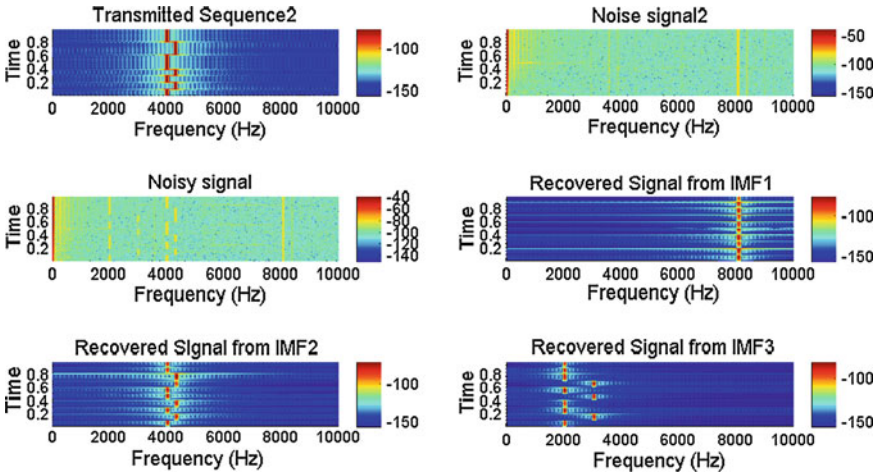

Fig. 3 Spectrogram for the detection of FSK signal $F2(t)$

Table 1 SNR comparison of Hilbert transform, Hilbert Huang transform, and fast Fourier transform

Input SNR (db)	Output SNR		
	Hilbert transform (dB)	HHT (dB)	FFT (dB)
−30	35.4232	35.4856	51.7059
−20	35.7976	35.9208	49.0360
−10	39.1053	39.5524	48.7213
0	41.1226	41.2958	47.3699
10	41.2234	41.6034	49.0718
20	42.3839	41.7192	52.1512
30	46.8626	42.3329	53.5268

Table 1 shows the performance analysis of Hilbert transform, Hilbert Huang transform (HHT) and fast Fourier transform (FFT) in terms of signal to noise ratio (SNR). It is seen that FFT has better SNR than Hilbert transform and HHT.

5 Conclusion

In this paper, an EMD-based FSK signal identification and extraction algorithm have been proposed for acoustic signals affected by ambient noise in shallow water. EMD is an effective decomposition technique to denoise the underwater acoustic signals affected by ambient noise. The advantage of this technique is it does not require any prior information about the transmitted source signal compared to adaptive filtering techniques. The performance of the proposed algorithm is evaluated for real-time acoustic data. Simulation results obtained indicate that the proposed method is effective for denoising ambient noise in shallow water. Further, this method can also be applied to any real-time underwater wireless sensor network.

References

1. C.D. Blakely, *A fast empirical mode decomposition technique for nonstationary nonlinear time series*. Center for Scientific Computation and Mathematical Modeling, University of Maryland, College Park, USA (2005)
2. Y.K. Zhang, X.C. Ma, D.X. Hua, Y.A. Cui, L.S. Sui, An EMD-based denoising method for lidar signal 2010, in *3rd International Congress on Image and Signal Processing (CISP2010)* (2010)
3. X. Wang, G. Feng, A. Feng, *On performance difference of EMD and WD in the nonlinear time series analysis*, in 2011 Eighth International Conference on Fuzzy Systems and Knowledge Discovery (FSKD) (2011)

4. G. Rilling, P. Flandrin, One or two frequencies? The empirical mode decomposition answers. IEEE Trans. Signal Process. **56**(1), 85–95 (2008)
5. D. Kim, H.-S. Oh, EMD: a package for empirical mode decomposition and hilbert spectrum. R J. **1/1**, 40–46 (2009) (Contributed Research Article)
6. A. Karagiannis, P. Constantinou, Noise-assisted data processing with empirical mode decomposition in biomedical signals. IEEE Trans. Inf. Technol. Biomed. **15**(1), 11–18 (2011)
7. W.-B. Yang, P.C. Yang, High frequency HF FSK underwater acoustic communication: the environmental effects and signal processing, in *AIP conference proceedings*, vol. 728, pp. 106–113 (2004)

A Model for the Effective Steganalysis of VoIP

N. Jayasree and P.P. Amritha

Abstract The latest studies and applications in steganography are based on Internet, particularly voice over IP (VoIP). VoIP has proved itself to be a perfect carrier for hidden data. Most of the approaches for VoIP steganalysis focus on detecting hidden data in the payload of the packets, by extending audio steganalysis methods. Here, we propose an effective steganalysis method which considers the speech behavior as well as network protocol structure to detect hidden communication. The common statistical features, like mean, covariance, etc., are also considered for effective classification.

Keywords LSB embedding · VoIP · Steganalysis · MFCC · Statistical · SVM · GMM

1 Introduction

Currently, voice over IP (VoIP) technology is being used as a new infrastructure of the public phone network which has resulted in rapid increase in the number of users. VoIP uses many techniques to reduce bandwidth requirements and latencies in order to improve speech quality and scalability. Encoding/decoding schemes compress the voice stream and reduce the bandwidth requirements as long as communicating parties support the same encoder/decoder (codec). The huge volume of traffic generated by VoIP applications can be used for surreptitious communication with good or bad motives [1].

N. Jayasree (✉) · P.P. Amritha
Tifac Core in Cyber Security, Amrita Vishwa Vidyapeetham,
Coimbatore 641112, India
e-mail: jayasree.narain@gmail.com

P.P. Amritha
e-mail: ammuviju@gmail.com

© Springer India 2015

L.P. Suresh et al. (eds.), *Artificial Intelligence and Evolutionary Algorithms in Engineering Systems*, Advances in Intelligent Systems and Computing 325,
DOI 10.1007/978-81-322-2135-7_41

Steganography encompasses various information hiding techniques, whose aim is to embed a secret message (steganogram) into a carrier. Network steganography is to perform hidden communication and utilizes network protocols and/or relationships between them as the carrier for steganograms. Because of its popularity, IP telephony is becoming a natural target for network steganography. Steganographic methods aim at hiding the very existence of the communication, and therefore, any third-party observers should remain unaware of the presence of the steganographic exchange.

Recently, different steganography methods [2] have drawn the attention of researchers which focus on the speech that is exchanged or the codec of the speech. But the present steganalysis methods are also not universal, and many are not efficient enough to be practically deployed in the telecommunication network to perform real-time detection.

In this paper, we propose a steganalysis technique which can be implemented in real time. We try to extract appropriate features from the captured RTP packets to effectively classify the VoIP traffic as malicious or benign. We use standard data mining and classification technique to classify the feature set into the two classes. We are using SVM for classification of data. We have also used GMM to model the speech data. Section 2 describes the proposed system. Section 3 explains the feature space used for classification of captured RTP packets. Section 4 deals with the implementation of system for VoIP Steganalysis and its evaluation. Section 5 concludes the work and outlines the future direction for steganalysis.

2 Proposed System

To better define the problem, we assume that the warden will not be able to physically listen to the speech carried in RTP packets because of the privacy issues related with this matter. Also the warden can monitor/inspect the traffic only in a single location (at the RTP packet receiver end). We are not considering any packet losses or traffic congestions. Encryption of the packets or compression using any codec other than G.711 is not taken into account.

In this proposed system, we are trying to classify the VoIP traffic as suspicious or benign. At the outset, the VoIP packets are captured using any network-monitoring tool. The features required for the analysis of the packet headers are extracted from the captured packets. These features are explained further in the next section. The payload is extracted from the packet and saved in a .wav file format for further analysis. The signal is then divided into smaller frames, and features are calculated for each frame. A reference signal is generated by performing some denoising functions on the data. The calculated features for each frame along with the features of the packet headers and the difference between reference signal and data form the combined feature vector (Fig. 1).

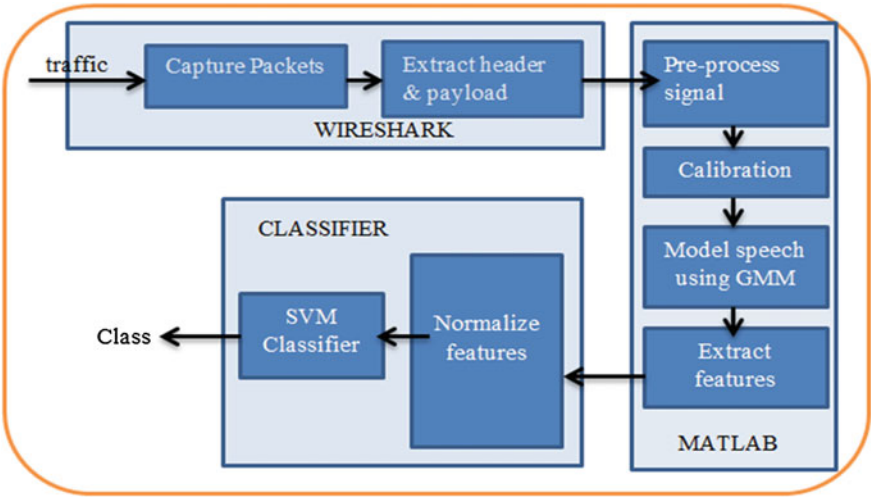

Fig. 1 Architecture

2.1 Data Acquisition

Packets are captured using a network-monitoring tool. The payload of the RTP stream is extracted and saved in a .wav format.

2.2 Feature Extraction

The header of the packet is taken, and the features are extracted as per the RTP and the UDP fields which are not empty. The speech signal divided into frames of 20-m shamming windows. Each frame is taken and features are extracted from frames with voice activity.

2.3 Analysis

A reference signal is generated by applying a denoising function on the captured signal. The difference between the reference signal and the captured signal is calculated and used as another feature. The subsequent analysis as the final step in the steganalysis process is done using a support vector machine (SVM) for classification of the signals [3]. The SVM technique is based on Vapniks statistical learning theory and was used as a classification device in different steganalysis-related publications [4].

3 Feature Set

3.1 MFCC Coefficients

Basically, a cepstrum is the result of taking the Fourier transforms (FT) or short-time Fourier analysis of the decibel spectrum as if it were a signal. The cepstrum can be interpreted as information about the rate of power change in different spectrum bands. Generally, a cepstrum S can be computed from the input signal S (usually a time-domain signal) as

$$\check{S} = \mathrm{FT}(\log(\mathrm{FT}(S))) \tag{1}$$

A modified cepstrum called mel-cepstrum can be used in speaker identification and the general description of the human auditory system (HAS). The mel-cepstrum is considered as an excellent feature vector for representing the human voice and musical signals. For all applications which are computing the cepstrum of acoustical signals, the spectrum is usually first transformed using the mel frequency bands. The result of this transformation is called the mel spectrum and is used as the input of the second FT computing the mel-cepstrum represented by the mel frequency cepstral coefficients (MFCCs). The complete transformation for the input signal S is described in equation below:

$$\mathrm{MelCepstrum} = \mathrm{FT}\left(\mathrm{MelScaleTransformation}\left(\mathrm{FT}(\check{S})\right)\right) \tag{2}$$

MFCC features provide a compactre presentation of speech signals [5]. A good property of MFCC is that its feature dimensions are weakly correlated; hence, we can use diagonal covariance matrix for the Gaussian models to greatly reduce system complexity and the amount of data required to robustly estimate the model parameters. In addition, MFCC features are also found to be very sensitive to channel distortions.

3.2 Statistical Features

Based on the initial idea of a universal blind steganalysis tool for multimedia steganalysis, a set of statistical features used in image steganalysis was transferred to the audio domain [6]. Originally, the set of statistical features (SF) computed for windows of the signal (intra-window) consisted of empirical variance, covariance, entropy, LSB ratio, LSB flipping rate, mean of samples in time domain, and median of samples in time domain.

3.2.1 Mean

The mean of a random process is the average of all realizations of that process

$$m_x(t) = -\int_{\infty}^{\infty} xf(x)\ \mathrm{d}x, \tag{3}$$

3.2.2 Empirical Variance

An unbiased estimate of variance would be as follows, often called the sample variance

$$\text{Variance } = \sum_{\mathrm{i}} (\mathrm{x_i} - \text{mean})^2/(\mathrm{n} - 1), \tag{4}$$

3.2.3 Median

The median is the numerical value separating the higher half of a data sample, from the lower half.

3.2.4 Covariance

Covariance is a measure of how much the deviations of two or more variables or processes match. Mathematically, covariance is defined as

$$\mathrm{cov}(X, Y) = E[(X - X')(Y - Y')] \tag{5}$$

3.2.5 Entropy

An important property of a signal is its entropy or information content. In information theory, entropy is a measure of the uncertainty in a random variable. The entropy H of a discrete random variable X with possible values $\{x1 \ldots x\mathrm{n}\}$ and probability mass function $P(X)$ is

$$H(X) = -\sum_{i} P(X_i)\ \log_b P(x_i) \tag{6}$$

3.2.6 LSB Ratio

This is the ratio of zeroes and ones in the least significant bits of the signal.

3.2.7 LSB Flip Ratio

This measures the count of least significant bits that flipped after a masking function is performed.

3.2.8 Weighted Value for Packet Header Fields

The packet header is extracted and analyzed. Each vulnerable field is given a weight. The packet will thus have a weighted sum corresponding to all the vulnerable fields. This will represent the probability of protocol embedding: greater the value, greater is the risk.

3.2.9 KL Divergence from Reference Signal

The Kullback–Leibler (KL) divergence, $D(f\|g)$, between two distributions $f(x)$ and $g(x)$ is also known as the "relative entropy" of f relative to g. It is defined as

$$< \log f(x) - \log g(x) > \tag{7}$$

$$< y(x) > \; = \int f(x) y(x) \mathrm{d}x \tag{8}$$

The KL divergence equals 0 if and only if $f(x) = g(x)$ almost everywhere.

4 Experimental Results

4.1 Capturing RTP Packets and Payload

A VoIP call was set up using the micro-SIP soft phone. The codec to be used was set to G.711A [7]. After setting up the call, the packets were captured using wires hark. The payload was extracted from the RTP stream and saved in .au format. Using an audio converter, the .au file was converted to a 16-bit PCM .wav file. Further, feature extraction was performed on these .wav files.

4.2 Embedding Schemes

In this experiment, simple LSB embedding on the A-Law encoded PCM .wav files was used. Protocol embedding was simulated by changing the values on the captured packets and using it for further training and classification.

4.3 Extracting Features

The embedded .wav files were segmented into 20-ms windows, and the features explained in Sect. 4 were extracted from each of the window.

4.4 Training and Classification

Before classification, all cover–stego pairs were divided into 80 % for training and 20 % testing.

4.4.1 Reference Signal and GMM

A reference signal was generated by performing some denoising functions on the embedded file. This reference signal was used to model a "normal" behavior. The embedded signal is then used to model the abnormal behavior [8]. These models are then used to classify the rest of the data as malicious or benign. This is done by calculating the KL divergence between the two probability distributions. The figure below shows the result of modeling using GMM in MATLAB.

4.4.2 SVM

The software LIBSVM [9] was used to classify the packets to malicious and normal. The results obtained after implementation are presented in Table 1 (Fig. 2).

4.5 Performance Evaluation

Only MFCC coefficients were used for modeling using GMM. All the features discussed are tested with SVM, and the results are tabulated below.

From the above table, we can infer that the features discussed help in detecting the LSB steganographic algorithm effectively.

Table 1 Performance evaluation of SVM classification

Steganographic algorithm	Relative payload	Length of sample (s)	Accuracy
LSB Embedding	0.1	1	0.55
	0.15	2	0.72
	0.2	3	0.73

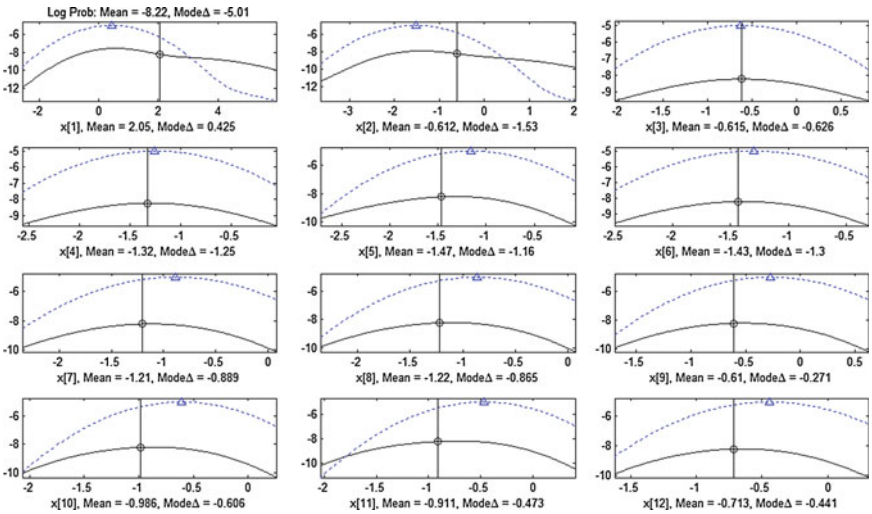

Fig. 2 Two classes modeled using GMM

5 Conclusion

The experiments were evaluated by calculating the recognition accuracy as the percentage of correct detections of normal and abnormal transmissions against all recognition trials. The results show that in some cases the accuracy grows steadily as the length of speech data increases, and becomes saturated at 5–6 s. Simple LSB-based embedding on VoIP calls could be detected effectively by using the proposed system.

But if the overt channel contained no speech, but a piece of music, noise or just silence, the detectability would be seriously affected. If SRTP is utilized, there is no efficient method to detect hidden communications. There are no effective techniques to detect steganographic methods such as LACK.

Future work includes finding a solution to the above-stated problems. Further study also should be done to understand different embedding techniques other than LSB. Analysis should be performed on the effect of embedding in other codecs [10], e.g., speex, G.723.

References

1. T. Takahashi, W. Lee, An assessment of VoIP covert channel threats, in *Security and Privacy in Communications Networks and the Workshops. Third International Conference on IEEE* (2007), pp. 371–380
2. W. Mazurczyk, VoIP steganography and its detection—a survey. ACM Comput. Surv. (CSUR) **46**(2), 20 (2013)
3. C.J. Burges, A tutorial on support vector machines for pattern recognition. Data Min. Knowl. Disc. **2**(2), 121–167 (1998)

4. F.G. Mohammadi, M.S. Abadeh, A survey of data mining techniques for steganalysis, in *Recent Advances in Steganography* (2012), pp. 1–25
5. C. Kraetzer, J. Dittmann, Mel-cepstrum-based steganalysis for VoIP steganography, in *Electronic Imaging* (2007), p. 650505
6. A. Janicki, W. Mazurczyk, K. Szczypiorski, Steganalysis of transcoding steganography, in *Annals of telecommunications* (2012), pp. 1–12
7. W. Mazurczyk, P. Szaga, K. Szczypiorski, Using transcoding for hidden communication in IP telephony, in *Multimedia Tools Applications* (2012), pp. 1–27
8. XXX
9. C.C. Chang, C.J. Lin, LIBSVM: a library for support vector machines. ACM Trans. Intell. Syst. Technol. (TIST). **2**(3), 27 (2011)
10. Y. Huang, S. Tang, C. Bao, Y.J. Yip, Steganalysis of compressed speech to detect covert voice over Internet protocol channels. Inf. Secur. IET. **5**(1), 26–32 (2011)
11. W. Mazurczyk, K. Szczypiorski, Steganography of VoIP streams, in *On the Move to Meaningful Internet Systems: OTM*, ed. by R. Meersman, Z. Tari (Springer, Berlin, 2008), pp. 1001–1018
12. J. Dittmann, D. Hesse, R. Hillert, Steganography and steganalysis in voice-over IP scenarios: operational aspects and first experiences with a new steganalysis tool set, in *Electronic Imaging* (2005), pp. 607–618

Automatic Genre Classification from Videos

S. Karthick, S. Abirami, S. Murugappan, M. Sivarathinabala and R. Baskaran

Abstract In recent decades, there has been a huge growth in the amount of multimedia content stored in networked repositories. Many video hosting websites exists in today's scenario such as youtube, metacafe and google video etc., where people are uploading and downloading their videos. At present, indexing and categorization of these videos is a tiresome job. Either the system asks the user to suggest tags for the videos which they upload or people are employed to tag the video manually. Manual tagging has been done based on the views of users, search terms, etc. In order to eliminate this problem, this paper proposes a model that automatically categorizes the videos based on their genres. The main aim of this work was to categorize the videos broadly on major domains such as sports, music and news using temporal, textural, motion, and color features. In sports, the videos have been classified further into cricket and football. The hierarchical SVM has been used for automatic training and selection of the genre of the video. A total of 350 videos from various Web sites have been used for training the classification system. This system achieves an overall average detection ratio up to 98 % while maintaining very low false detection rate of 2 %.

Keywords Video genre classification · Video categorization · Image processing

S. Abirami (✉) · M. Sivarathinabala
Department of Information Science and Technology, College of Engineering, Anna University, Chennai, India
e-mail: abirami_mr@yahoo.com

R. Baskaran
Department of Computer Science and Engineering, College of Engineering, Anna University, Chennai, India

S. Murugappan
Department of Computer Science and Engineering, Tamilnadu open University, Chennai, India

S. Karthick
Department of Information Science and Technology, Anna University, Chennai, India

© Springer India 2015

L.P. Suresh et al. (eds.), *Artificial Intelligence and Evolutionary Algorithms in Engineering Systems*, Advances in Intelligent Systems and Computing 325,
DOI 10.1007/978-81-322-2135-7_42

1 Introduction

Rapid increase in the amount of multimedia content stored in Internet in today's world has lead to many researches such as storage optimization, faster video content transmission, and multimedia content retrieval especially videos. Among these popular researches, video content retrieval requires many tagging for categorization of videos. Because of the massive amount of video contents, automatic classification is an essential area which needs to be actively researched. In literatures, three automated methods have been demonstrated by the existence of the TRECVid video retrieval benchmarking evaluation campaign. TRECVid provides data sets and common tasks that allow researchers to compare their methodologies under similar conditions. While much of the TRECVid has been devoted to video information retrieval, video classification tasks exist by limiting it by identifying clips containing faces or on-screen text, distinguishing between clips representing outdoor or indoor scenes, or identifying clips with speech or instrumental sound. Therefore, existence of fully automated video classifier on this genre becomes mandatory. In order to address these shortcomings, this research concentrates on the development of an automatic genre classification system.

2 Previous Works

Large number of approaches has been attempted in the literature for performing automatic classification of videos. These approaches could be broadly divided into four groups: Text-based approaches, audio-based approaches, visual-based approaches, and hybrid features approaches. These approaches draw features from three different modalities such as texts, audio, and visual. Text-only approaches are uncommon method. Here, viewable text could be text on objects that are filmed (scene text), such as an athlete's name on a jersey or the address on a building, or it could be text placed on-screen (graphic text), such as the score for a sports event or subtitles [1]. Text features are produced from this viewable text by identifying text objects followed by the use of optical character recognition (OCR) [2] to convert these objects to usable text. Zhu et al. [3] classified news stories using features obtained from closed captions. Audio-only approaches are found slightly more often than text-only approaches. Roach and Mason [4] used audio, in particular MFCC, from videos for genre classification. Moncrieff et al. [5] classified the videos into commercial, basketball game, football game, news report, and weather forecast based on their audio features. Roach et al. [6] used audio-based cinematic principles to distinguish between horror and non-horror movies. In visual-based approaches, frame differencing and optical flow techniques have been used in the classification of videos. Fakheri et al. [7] investigated found that the frame differencing [1, 8] method has lower computational requirements than optical flow method in classification of video. Wei et al. [9] classify four types of TV programs:

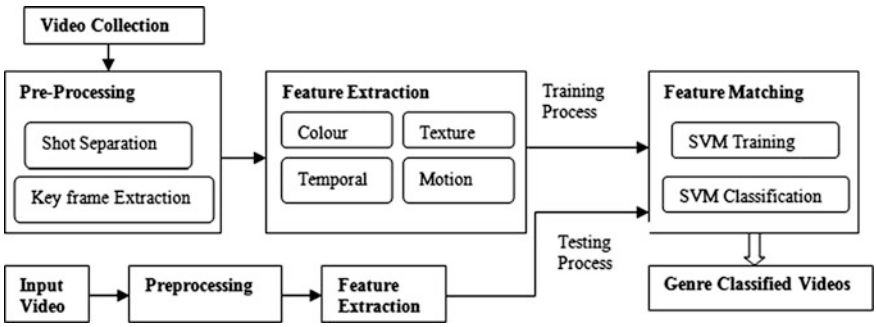

Fig. 1 Automatic video genre classification system

news, commercials, sitcoms, and soap operas. Roach et al. classified the video as either cartoon or non-cartoon. Yuan et al. [10] proposed two new classification methodologies using a series of support vector machine classifiers arranged in a hierarchy. This paper attempts to classify the different genres of videos using a hybrid approach of visual, temporal, and motion features.

3 Video Genre Classification System

In this paper, a novel method has been attempted to automatically classify the videos. News, cartoon, music, cricket, and football are the major genres taken and classified using this system. The overall genre classification system is shown in Fig. 1. The input video has been preprocessed. Next to it, the features are extracted from the key frames extracted. Color, texture, temporal, and motion features are extracted. Once the features are extracted, SVM classifier is used to classify the video.

3.1 Preprocessing

Initial step in video analysis is to preprocess the input video. In preprocessing, the video has been split into several shots/frames for further processing. Shot separation needs to be done after preprocessing.

3.1.1 Shot Separation

A video shot is a small image sequence captured continuously by a single camera. There are two major approaches available for shot separation such as pixel-difference method and histogram-based method. Both the methods involve a threshold to

be fixed in advance. Fixing a single threshold for all the videos are a poor technique and leads to erroneous results. The different threshold values are required for different categories of video. Hence, we attempted a saturation-based approach in this paper to separate shots.

Saturation-based Approach

Saturation-based approach finds the frames when there is an abrupt change in the frame, by calculating the saturation value for each frame. The saturation values change gradually either in an increasing or decreasing nature, when the scenes did not have much of changes. The saturation value changes abruptly when there is a huge change in the scene. This is used to obtain the shots from the video. In this system, we make use of the saturation-based shot separation approach to determine the shots.

3.1.2 Key Frame Extraction

Processing all the frames resulting shot separation is very expensive and time consuming made use in further processing. We make use of the entropy difference method which is used in [11] to identify the key frames from each shot. More similar frames and duplicate key frames have been removed by similarity match. Sample key frames extracted for a shot length of 180 frames have been shown in Fig. 2.

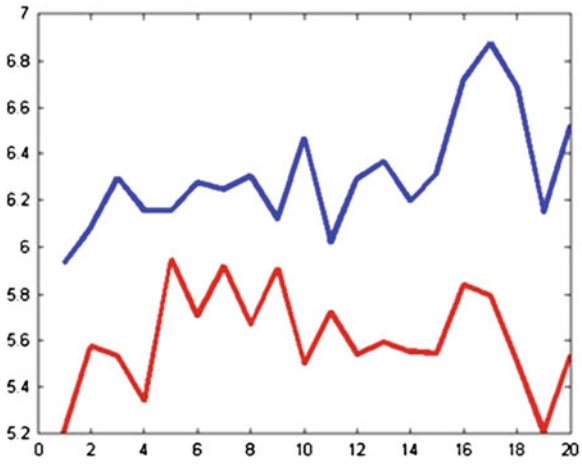

Fig. 2 Entropy comparisons for football and cricket

3.2 Feature Extraction

There are several features [12], which can be extracted from the key frames. In this system, four major features are concentrated as they help in providing improved results and easier categorization of genres in videos. The four major features extracted are: Temporal features, motion features, texture features, and color features.

3.2.1 Temporal Features

Temporal features of class populations define some time-dependent constraints that the population must satisfy. Hence, temporal feature can be considered as an important descriptor in genre classification [+1]. It is clearly seen that there will be larger number of shots when there is a frequent scene change. News genres do not have many changes as the news reader is stationary and there is not much of motion. It has observed that the number of shots obtained for news videos will be comparably lesser than the other genres. Comparably, music videos have frequent shot changes. As a result, it has been proposed here to calculate the shot rate, key frame rate, and average length from the input videos as the features for texture measurement. The number of shots per 1,000 frames is calculated and has been given in Eqs. (1) and (2):

$$\text{Shot rate} = (\text{No. of Shots found}/\text{Total no. of frames}) \times 100 \tag{1}$$

The average number of frames in a shot is defined as the shot size. Number of key frames per 100 shots gives the key-frame rate and it is calculated as follows:

$$\text{Key-frame rate} = \text{Average key-frames per shot} \times 100 \tag{2}$$

3.2.2 Motion Features

The effective use of motion information is essential for content-based video retrieval. In this system, foreground motion activity is extracted using the pixel-difference method [13]. The rate of change in the successive key frames presents the foreground motion activity. The percentage of the pixels whose values have been changed will be high in case of frames involving motion activity than the frames which have low movements. This factor has been used to estimate the amount of motion activity in videos.

3.2.3 Texture Features

Texture features give information about the spatial arrangement of color or intensities in an image or selected region of an image. A statistical method of examining texture that considers the spatial relationship of pixels is the gray-level co-occurrence matrix (GLCM), also known as the gray-level spatial dependence matrix. The texture of an image has been characterized by the GLCM functions. The GLCM functions have been calculated how often pairs of pixel with specific values and in a specified spatial relationship occur in an image. From the GLCM function, statistical measures have been extracted from this matrix. The GLCM is created by calculating how often a pixel with the intensity (gray-level) value '*i*' occurs in a specific spatial relationship to a pixel with the value '*j*.' By default, the spatial relationship is defined as the pixel of interest and the pixel to its horizontally adjacent. Other spatial relationships can also be represented between two pixels. Each element $p(i, j)$ in the resultant GLCM is simply the sum of the number of times that the pixel with value i occurred in the specified spatial relationship to a pixel with value j in the input image. Energy, entropy, and homogeneity features are extracted from GLCM which could better represent the textural values. The energy also known as the angular second moment is the sum of the square values of all the elements in the calculated gray-level co-occurrence matrix. The nature of the gray-level co-occurrence matrix shows that the energy for the uniform image would be maximum and would reduce as the uniformity in the image decreases. It is calculated using the formula given in Eq. (3) as:

$$\text{Energy} = \sum_{i,j} p(i,j)\text{^}2 \tag{3}$$

Entropy is a statistical measure of randomness that can be used to characterize the texture of the input image. Entropy has been calculated as in Eq. (4) follows:

$$\text{Entropy} = -\text{sum}(\text{p}. * \log 2\ (\text{p})) \tag{4}$$

Homogeneity measures the closeness of the distribution of elements in the GLCM to the GLCM diagonal. An image which is uniform has its values concentrated over the diagonal of the gray-level co-occurrence matrix. The homogeneity is calculated using the formula given in Eq. (5) as:

$$\text{Homogeneity} = \sum_{i,j} p(i,j)/(1 + |i - j|) \tag{5}$$

Brightness of the each key frame has been calculated and averaged over the entire video. The average brightness for a key frame is calculated using Eq. (6) as follows:

$$B = \mu_i \times \sigma_i^2 \tag{6}$$

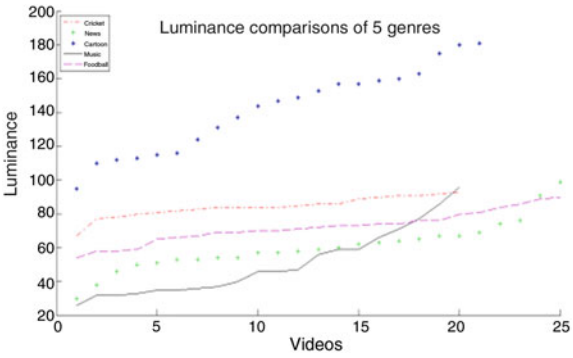

Fig. 3 Luminance comparisons for various genres

where B is average brightness of the frame, μ_i is the mean of the pixels above a threshold, and σ_i^2 is variance of the pixels above a threshold. Here, energy, entropy, brightness, and homogeneity have been calculated for all videos. It has been observed that the brightness is comparatively low in cricket and football. Energy is greater in football than in cricket because football videos possess greater uniformity in their frames resulting in concentration of values in GLCM. Similarly, entropy is lesser in football than in cricket because cricket videos have high camera motion and less uniformity. The randomness of the pixel values is greater in cricket than football videos. Entropy comparison of cricket and football genres has been shown in Fig. 2. Here, cricket has been represented in blue and football in red color. The comparison of luminance values for videos of different genres is shown in Fig. 3.

3.2.4 Color Features

Color feature is another important feature used in video categorization. Most of the early systems [14, 15] have color as its main or at least a component of their feature set. This shows the importance of color features. In this system, three major color features have been extracted, namely luminance, pitch factor, and grass factor. Among the color descriptors, we retain color histogram which captures global color distribution in an image. Here, the color space selected is RGB space, since it is the most commonly used color space. Luminance of a pixel is calculated and represented as in the following Eq. (7):

$$Y = 0.3\,R + 0.59\,G + 0.11\,B \tag{7}$$

The video frames of different genre have been processed and the maximum and the minimum bin values of the frames are obtained. It has been found that the cartoon videos have a higher luminance when compared to the videos from other genres. The reason behind this is that the cartoon videos are luminant. The major steps involved in cartooning an image are luminance quantization and edge blurring [16]. Thus, this effect is taken into account in this system. The grass factor

calculates the amount of predominant green pixels contained in the image. Foot ball and cricket are kind of sports that are played in lush green grounds. So, the key frames extracted would contain a huge amount of green pixels. This can be extracted to separate these two genres from the rest of the genres. The green pixel can be identified in a RGB model by the dominance carried by the '*g*'-value of the pixel which is more than both '*r*' and '*b*' pixels. The pitch factor finds the presence of the cricket pitch in the key-frame. The pitch is characterized by the dominant '*r*'-value in the RGB representation of the image surrounded by the dominant *g*-values of the grass. This identification of the pitch helps in separating the football videos from the cricket videos, since no pitches exist in a foot ball field. The algorithm for detecting the pitch is as follows:

```
Input : Videos
Output : Keyframes to detect pitch
Algorithm:
function detect_pitch(frame)
Step 1: Identify the red dominant pixels in the frame.
Step 2 : Compute the centroid of the regions found.
Step 3 : if( any region's centroid is in the center of the ground)
          check if the area of the region is greater than threshold
                    May be a pitch frame.
          else
                    Not a pitch frame.
Step 4 : End
Step 5 : Identify green dominant pixels in the frame using detect_grass()
          if there is a layer of grass below the pitch
                    Not a pitch frame
          else
Step 6 : if(green_count>45 % && pitch_count/green_count>20%)
          Pitch detected.
          else
                    Grass value too low to distinguish Pitch.
Step 7 : End
```

A sample set of key frames with high grass content from the entire key frames is shown in Fig. 4 and the sample set of key frames with pitch from the entire key frames is shown in Fig. 5.

3.3 SVM Training and Classification

Once the features have been extracted, they are fed as input to the SVM classifier for genre classification. The model chosen here for training and classification of videos is the support vector machine (SVM). The local optimal SVM tree approach is used for training and classification of the videos. The news seems to be the most easily separable genre from the rest. Initially, we check for news video versus the rest. The feature set used for training SVM in step 1 are foreground motion, shot rate, shot size,

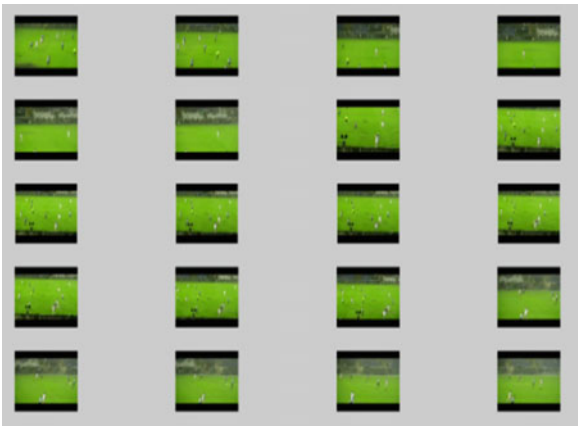

Fig. 4 Key frames to detect grass

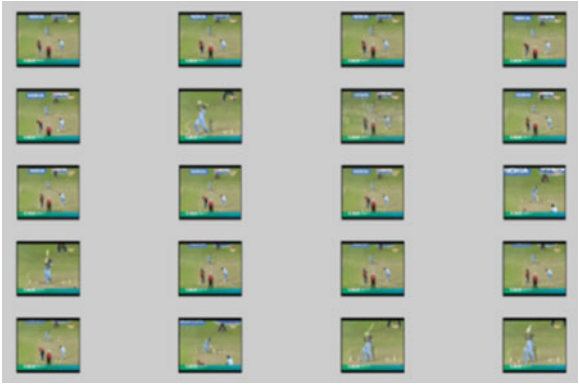

Fig. 5 Key frames to detect pitch

key frame rate, and homogeneity. The cartoon is the next genre to be classified from the rest of genres. This is made by making use of the luminance factor. In the step 3, we aim to separate music genre from the rest. Shot rate, shot size, key frame rate, brightness, and grass factor are used for training. Let the cricket genre is separated from others using the features pitch factor, energy, and entropy. Next to this, the football is compared with the others to separate football genre from the remaining genres and out of boundary conditions. The energy and entropy features are made use of in this step. The SVM-trained objects are stored and used for classification. During the testing phase, the preprocessing is done on the input video and all the eleven features are extracted from the key frames. The feature vector is given as input to the trained SVM in a five step processes are as follows:

1. Foreground motion, shot rate, shot size, key frame rate, and homogeneity features are given as input to the SVM. The SVM feature is lying to the training object of layer 1 for classification. If the classification output is positive, then news genre is confirmed, else step 2 is proceeded.

2. Luminance feature of input video is given as input to the SVM and classified against the SVM training object in layer 2. If positive classification is achieved, then cartoon genre is separated, else proceed to step 3.
3. Input video's shot rate, shot size, key frame rate, brightness, and grass factor features have been given as input to the SVM against SVM training object of layer 3. In case of positive classification, music genre is confirmed, else go to step 4.
4. Pitch factor, energy, and entropy features of input video are considered as input to the SVM against the SVM training object in layer 4. Cricket genre is confirmed if positive, else proceed to step 5.
5. The input videos energy and entropy features have been given as input to the SVM to check against the SVM training object in level 5. If positive, then football genre is confirmed else the input video may be probably out of boundary.

4 Results and Performance Analysis

The videos have been collected from various sources such as YouTube and Video. fy. A total of 350 videos have been processed. Among them 65 videos considered from news, 65 videos from cartoon, 70 videos from music, 85 videos from cricket, 65 videos from football, and 150 videos have been chosen randomly from all genres and used for training SVM. The Table 1 below shows the basis of confusion matrix. The basic metrics used for analyzing the performance are listed in Table 1: Apart from that, fall metrics have also used.

$$\text{Specificity} = \frac{\text{TN}}{(\text{TN} + \text{FP})} \tag{8}$$

$$\text{Sensitivity} = \frac{\text{TP}}{(\text{TP} + \text{FN})} \tag{9}$$

$$\text{Accuracy} = \frac{(\text{TP} + \text{TN})}{(\text{TP} + \text{FP} + \text{TN} + \text{FN})} \tag{10}$$

$$\text{Hit Rate} = \frac{\text{No. of videos classified}}{\text{Total no. of videos to be classified}} \tag{11}$$

Table 1 Confusion matrix

	Predicted class		
Actual prediction		Yes	No
	Yes	True positive (TP)	False negative (FN)
	No	False positive (FP)	True negative (TN)

Table 2 Hit rate and miss rate

Genres	Hit rate (%)	Miss rate (%)
News	100	0
Cartoon	97	3
Music	97.5	2.5
Cricket	98	2
Football	99	1

Table 3 Specificity, sensitivity, and accuracy

Times	P	N	TP	FP	TN	FN	Specificity (%)	Sensitivity (%)	Accuracy (%)
News	30	50	30	0	50	0	100	100	100
Cartoon	30	60	29	3	57	1	95	96.67	95.56
Music	100	75	92	5	70	8	93.33	92	92.57
Cricket	65	50	63	3	47	2	94	96.92	95.65
Football	30	50	29	4	46	1	92	96.67	94.35

$$\text{Miss Rate} = \frac{\text{No. of videos not classified correctly}}{\text{Total no. of videos to be classified}} \tag{12}$$

The hit rate defines the number of correct predictions and miss rate defines the number of wrong predictions. The hit rate and miss rate for the five genres have been shown in Table 2.

The specificity, sensitivity, and accuracy for the five genres tested have been given in Table 3. The news videos are most efficiently classified, while football suffered significantly in classification.

Shots comparison for various methods such as the saturation-based method, the histogram-based, and pixel difference-based methods with respect to the hit rate/miss rate of shot detection are shown in the Table 4.

Table 4 Miss rate and hit rate of the video shots

Genre	Hit rate of video shots			Miss rate of video shots		
	Saturation based (%)	Histogram based (%)	Pixel difference based (%)	Saturation based (%)	Histogram based (%)	Pixel difference based (%)
News	99.79	98.07	98.46	0.03	0.05	0.10
Cartoon	99.74	98.14	97.55	0.3	0.5	0.54
Music	98.69	96.30	94.06	0.5	1.78	2.8
Cricket	99.32	97.04	98.43	0.47	0.68	0.56
Football	98.40	98.37	97.72	0.29	0.34	0.31

5 Conclusion and Future Work

In this work, the videos have been categorized into five genres namely, news, cartoon, music, cricket, and football. A total of 350 videos have been trained and 150 videos are tested properly. The videos have been collected from various sources such as YouTube. The videos have been first preprocessed and shots have been separated. From the key frames extracted, four major categories of features namely, temporal, motion, texture, and color features have been extracted. The eleven dimensional feature vectors have been given as input to the SVM with linear kernel for training and classification of genres from videos. The combination of the chosen feature vector improves the specificity, accuracy. and sensitivity of this system compared to the existing system [14]. This system achieved overall average correct detection ratio up to 98 % while maintaining very low false detection rate, namely 2 %. In future, this system could be extended to more number of genres and spatial-related values.

References

1. D. Gowsikhaa, A.S. Manjunath, Suspicious human activity detection from surveillance videos, Int. J. Internet Distrib. Comput. Syst. **2**(2), 141–149 (2012)
2. A. Hauptmann, R. Yan, Y. Qi, R. Jin, M. Christel, M. Derthick, M.-Y. Chen, R. Baron, W.-H. Lin, T.D. Ng, Video classification and retrieval with the informedia digital video library system, in *Text Retrieval Conference (TREC02)* (2002)
3. W. Zhu, C. Toklu, S.-P. Liou, Automatic news video segmentation and categorization based on closed-captioned text, in *IEEE International Conference on Multimedia and Expo (ICME 2001)* (IEEE, 2001), pp. 829–832
4. M. Roach, J. Mason, Classification of video genre using audio. Eurospeech **4**, 2693–2696 (2001)
5. S. Moncrieff, S. Venkatesh, C. Dorai, Horror film genre typing and scene labeling via audio analysis (2003)
6. M.J. Roach, J.S. Mason, M. Pawlewski, Motion-based classification of cartoons, in *Proceedings of the International Symposium on Intelligent Multimedia* (2001), pp. 146–149
7. M. Fakheri, M.C. Amirani, T. Sedghi, Gabor wavelets and GVF functions for feature extraction in efficient content based colour and texture images retrieval. (IEEE, 2011), pp. 1–5
8. D. Gowsikhaa, S. Abirami, R. Baskaran, Automated human behavior analysis from surveillance videos, in *Artificial Intelligence Review* (2012), pp. 1–19
9. G. Wei, L. Agnihotri, N. Dimitrova, TV program classification based on face and text processing, in *IEEE International Conference on Multimedia and Expo*, vol. 3 (IEEE, 2000), pp. 1345–1348
10. X. Yuan, W. Lai, T. Mei, X.-S. Hua, X.-Q. Wu, S. Li, Automatic video genre categorization using hierarchical SVM, in *IEEE International Conference on Image Processing (ICIP)* (IEEE, 2006), pp. 2905–2908
11. M. Mentzelopoulos, A. Psarrou, Key frame extraction algorithm using entropy difference, in *MIR'04* (2004)
12. D. Gowsikhaa, S. Abirami, R. Baskaran, Construction of image ontology using low level features for image retrieval, in *Proceedings of the International Conference on Computer Communication and Informatics (ICCCI 2012)* (2012), pp. 1–7

13. M.J. Roach, J.S. Mason, M. Pawlewski, Video genre classification using dynamics, in *the proceedings of IEEE International Conference on Acoustics, Speech, and Signal Processing, (ICASSP '01)* (2001)
14. B. Ionescu, C. Rasche, L. Florea, C. Vertan, P. Lambert, Classifying documentary, music, news and animated genres with temporal, color and contour information (IEEE, 2011), pp. 1–4
15. M. Guironnet, et al., Video classification based on low-level feature fusion model. Author manuscript, published in *European Signal Processing Conference (EUSIPCO'2005)* (2005)
16. M.-H. Han, H.N. Song, K.-H. Yoon, Cartooning using reference images, in *Proceedings of 2010 IEEE 3rd International Conference on Human-Centric Computing* (2010), pp. 1–5

Computer-aided Diagnosis of Breast Cancer by Hybrid Fusion of Ultrasound and Mammogram Features

R. Lavanya, N. Nagarajan and M. Nirmala Devi

Abstract Ultrasound images are increasingly being used as an important adjunct to X-ray mammograms for diagnosis of breast cancer. In this paper, a computer-aided diagnosis system that utilizes a hybrid fusion strategy based on canonical correlation analysis (CCA) is proposed for discriminating benign and malignant masses. The system combines information from three different sources, i.e., ultrasound and two views of mammogram, namely, mediolateral oblique (MLO) and craniocaudal (CC) views. CCA is employed on ultrasound-MLO and ultrasound-CC feature pairs to explore the hidden correlations between ultrasound and mammographic view. The two pairs of canonical variates are fused at the feature level and given as input to support vector machine (SVM) classifiers. Finally, decisions of the two classifiers are fused. Results show that the proposed system outperforms unimodal systems and state-of-the-art fusion strategies.

Keywords Breast cancer · Canonical correlation analysis · Computer-aided diagnosis · Hybrid fusion · Mammogram · Ultrasound

1 Introduction

Accurate classification of breast lesions is essential to reduce the number of unnecessary biopsies or even more serious implications like loss of life [1]. Some research studies have reported that the diagnostic performance of radiologists is higher when both ultrasound images and mammograms are used in combination [2].

R. Lavanya (✉) · M.N. Devi
Department of Electronics and Communication Engineering, Amrita School of Engineering, Amrita Vishwa Vidyapeetham University, Amritanagar, Coimbatore 641112, India
e-mail: r_lavanya@cb.amrita.edu

N. Nagarajan
Department of Computer Science and Engineering, Coimbatore Institute of Engineering and Technology, Narasipuram, Coimbatore 641109, India

© Springer India 2015

L.P. Suresh et al. (eds.), *Artificial Intelligence and Evolutionary Algorithms in Engineering Systems*, Advances in Intelligent Systems and Computing 325,
DOI 10.1007/978-81-322-2135-7_43

In this work, a new multimodal computer-aided diagnostic system (CADx) system has been proposed for classification of breast masses by combining information from ultrasound and mammogram modalities.

Karla Horsch et al. [3] have demonstrated an improvement in the radiologist's performance in classifying lesions, when they are aided by two independent CADx systems based on mammogram and ultrasound images. Jesneck et al. [4] have combined ultrasound and mammogram features using feature fusion based on concatenation resulting in high classification accuracy. Jesneck et al., [5] also explored the use of decision fusion using product rule to combine the two modalities. The system has been shown to outperform the CADx system based on feature fusion in [4]. The current techniques for combining ultrasound and mammogram information involve either feature or decision fusion. Feature fusion and decision fusion are advantageous when sources to be combined are correlated and independent, respectively. However, a better strategy for fusion is the hybrid fusion technique that combines feature fusion and decision fusion to exploit the advantages of both [6]. In this paper, a hybrid fusion technique based on canonical correlation analysis (CCA) has been proposed for combining information from ultrasound and two views of mammogram, i.e., mediolateral oblique (MLO) and craniocaudal (CC) views for classification of masses. Proposed by Hotelling [7], CCA solves the maximization problem in Eq. (1) to determine optimal directions W_X and W_Y, respectively, in which two datasets S_X and S_Y are maximally correlated.

$$\max_{W_X,W_Y}\{\mathrm{corr}[U_X,U_Y]\} = \max_{W_X,W_Y}\frac{W_Y^T R_{YX} W_X}{\sqrt{W_X^T R_{XX} W_X}\sqrt{W_Y^T R_{YY} W_Y}} \tag{1}$$

where U_X and U_Y are the transformed canonical variates, R_{XX} and R_{YY} are the autocorrelation matrices of S_X and S_Y, respectively, and R_{YX} is the cross correlation matrix of (S_X, S_Y).

2 Proposed Methodology

The schematic of the proposed system is shown in Fig. 1. The ultrasound and mammogram (both MLO and CC) images are cropped to regions of interest (ROIs) containing mass regions marked by the radiologists. Median filtering followed by contrast-limited adaptive histogram equalization (CLAHE) is employed for preprocessing. A multiresolution analysis-based adaptive thresholding [8] is employed to segment the mammographic masses. Morphological features (area and perimeter of the mass, statistical measures of the mass radius, circularity, roughness, zero crossing, long axis-to-short axis ratio, depth-to-width ratio, average length of subsequences of freeman chain code, Hu's moments) and texture features (entropy of segmented mass, Haralick's features) are extracted from the segmented masses

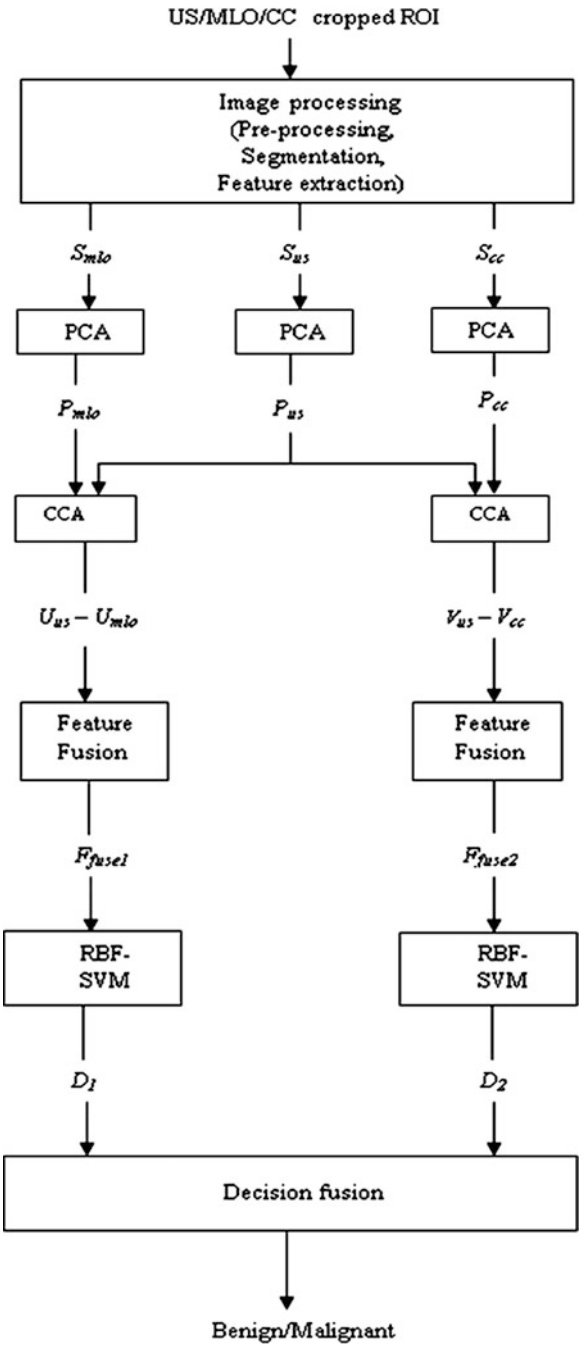

Fig. 1 Schematic of the proposed system

[9]. The ultrasound ROIs are subjected to preprocessing steps which include median filtering and unsharp masking. An active contour model [10] is used for segmenting the masses. The same morphological and textural features extracted from mammogram images and three acoustic features specific to ultrasound images (average gray intensity, internal echo pattern, and posterior acoustic feature) are extracted [11].

Let S_{us}, S_{mlo}, and S_{cc} represent ultrasound, MLO, and CC features, respectively. Principal component analysis (PCA) is applied on each of the datasets resulting in P_{us}, P_{mlo}, and P_{cc}, respectively, wherein the criterion adopted for dimensionality reduction is maximization of area under curve (AUC) of the system.

CCA is employed on the ultrasound-MLO (P_{us}, P_{mlo}) and ultrasound-CC (($P_{\text{us}}, P_{\text{cc}}$)) feature pairs, resulting in two-paired canonical variates $(U_{\text{us}}, U_{\text{mlo}})$ and $(V_{\text{us}}, V_{\text{cc}})$. As the canonical variates are highly correlated, feature fusion is appropriate for fusing them. Performing CCA prior to feature fusion maximizes the benefits of feature fusion by maximizing the correlation between the datasets to be fused. Thus, each paired canonical feature set is fused by concatenation yielding F_{fuse1} and F_{fuse2}.

$$F_{\text{fuse1}} = [U_{\text{us}} U_{\text{mlo}}] \tag{2}$$

$$F_{\text{fuse2}} = [V_{\text{us}} V_{\text{cc}}] \tag{3}$$

To exploit the statistically independent information provided by the sources as well, a decision fusion is employed in the final stage. To accomplish this, each canonical variate pair that is fused at the feature level is given as input to individual support vector machine (SVM) classifiers with radial basis function (RBF) as the kernel. The posterior probability outputs of the two classifiers are combined using product rule to yield the final decision D_{prod}.

$$D_{\text{prod}} = \arg\max_{j} \left(\prod_{i=1}^{2} \left(P\left(C_j | F_{\text{fusei}}\right)\right)\right)^{\frac{1}{2}}, \quad j = 1, 2 \tag{4}$$

Here, the posterior probability outputs of the ith classifier for which F_{fusei} is the input are $P(C_1|F_{\text{fusei}})$ and $(P(C_2|F_{\text{fusei}}))$, where C_1 and C_2 represent the malignant and benign classes, respectively. A two-level tenfold cross validation is used for model selection and performance estimation of the system.

3 Results and Discussion

The dataset used for validating the proposed system was collected from a private hospital. The images in the dataset consists of ultrasound and corresponding MLO and CC mammograms of 53 cases, where 36 cases are benign and 17 are malignant. The ground truth related to the mass contours and the diagnostic findings of the

Table 1 Comparison of AUC and EER

System		AUC	EER
Ultrasound		0.9390	0.1081
MLO		0.7755	0.2432
CC		0.7487	0.3514
Feature fusion (concatenation)	Ultrasound-MLO	0.8567	0.1892
	Ultrasound-CC	0.9253	0.1081
	Ultrasound-MLO-CC	0.8825	0.1892
Decision fusion (product rule)	Ultrasound-MLO	0.9165	0.1622
	Ultrasound-CC	0.9307	0.1081
	Ultrasound-MLO–CC	0.9139	0.1351
CCA-based hybrid fusion (proposed)		0.9852	0.0027

masses are provided by expert radiologists. The proposed system is compared with single modality systems and also with bimodal systems, wherein ultrasound is combined with MLO view or CC view, using feature fusion (concatenation) and decision fusion (product rule). Comparison is also performed with systems that combine information from all three sources using the above-said fusion techniques.

Table 1 compares the AUC and equal error rate (EER) obtained from the receiver-operating characteristics (ROC) of all the systems. The performance of state-of-the-art fusion techniques is observed to be the best for ultrasound-CC (bimodal) combination. However, it is inferior when compared to the proposed system and even the ultrasound (unimodal) system. It can be observed from Table 1 that the proposed fusion technique combining all the three information sources has the highest AUC and least EER when compared to all the other systems, which demonstrates its effectiveness.

Achieving a high sensitivity is of utmost importance in a clinical decision-making system. However, an increased sensitivity generally reduces the specificity and positive prediction value (PPV), due to the trade-off between these metrics. For further validation of the proposed system, the high-sensitivity portion of the ROC is analyzed in Table 2 for unimodal systems, state-of-the-art fusion techniques (ultrasound-CC combination), and the proposed system. It can be observed from

Table 2 Comparison of specificity and PPV for high-sensitivity region of ROC

System	Sensitivity = 88 %		Sensitivity = 94 %		Sensitivity = 100 %	
	Specificity	PPV	Specificity	PPV	Specificity	PPV
US	95	87	86	75	70	59
MLO	59	48	14	32	8	32
CC	49	42	43	42	8	32
Feature fusion	89	78	89	79	51	47
Decision fusion	89	78	89	79	84	73
Proposed	97	93	97	94	97	94

Table 2 that the improvement in specificity for the proposed system when compared to other systems is at least 2, 8, and 13 % at sensitivities of 88, 94, and 100 %, respectively. Also, the improvement achieved by the proposed system in PPV is at least 6, 15, and 21 % at sensitivities of 88, 94, and 100 %.

4 Conclusion

A hybrid fusion strategy that utilizes both correlated and statistically independent information for combining three modalities, i.e., ultrasound and two standard mammographic views is proposed for breast mass classification. The proposed system uses a combination of feature fusion and decision fusion, wherein the feature fusion scheme is made more effective by applying CCA to maximize the correlation of the information to be fused. The CCA-based feature fusion is applied on the ultrasound-MLO and ultrasound-CC combinations, thereby exploiting the correlation between these paired modalities. The independent decisions from these experts are then combined to arrive at one single decision regarding the nature of the mass, i.e., whether it is malignant or benign. From the ROC analysis, it can be observed that the proposed system outperforms the current fusion techniques. In particular, the specificity and PPV of the proposed system at 100 % sensitivity are reasonably high and equal to 97 and 94 %, respectively. This suggests the usefulness of the proposed system in achieving a low rate of misclassifying benign masses as malignant, while not missing out any cancerous case.

References

1. N.H. Eltonsy, G.D. Tourassi, A.S. Elmaghraby, A concentric morphology model for the detection of masses in mammography. IEEE Trans. Med. Imag. **2**, 880–889 (2007)
2. S. Malur, S. Wurdinger, A. Moritz, W. Michels, A. Schneider, Comparison of written reports of mammography, sonography and magnetic resonance mammography for preoperative evaluation of breast lesions, with special emphasis on magnetic resonance mammography. Breast Cancer Res. **3**, 55–60 (2001)
3. K. Horsch, M.L. Giger, C.J. Vyborny, L. Lan, E.B. Mendelson, R.E. Hendrick, Classification of breast lesions with multimodality computer-aided diagnosis. observer study results on an independent clinical data set. Radiology **240**, 357–368 (2006)
4. J.L. Jesneck, J.Y. Lo, J.A. Baker, Breast mass lesions: computer-aided diagnosis models with mammographic and sonographic descriptors. Radiology **244**, 390–398 (2007)
5. J.L. Jesneck, L.W. Nolte, J.A. Baker, C.E. Floyd, J.Y. Lo, Optimized approach to decision fusion of heterogeneous data for breast cancer diagnosis, Med. Phys. **33**, 2945–2954 (2006) http://www.ncbi.nlm.nih.gov/pubmed/16964873
6. P.K. Atrey, M.A. Hossain, A. El-Saddik, M.S. Kankanhalli, Multimodal fusion for multimedia analysis: a survey. Multimedia Syst. **1**, 345–379 (2010)
7. H. Hotelling, Relations between two sets of variates. Biometrika **28**, 321–377 (1936)

8. K. Hu, X. Gao, F. Li, Detection of suspicious lesions by adaptive thresholding based on multiresolution analysis in mammograms. IEEE Trans. Instrum. Meas. **60**, 462–472 (2011) http://www.informatik.uni-trier.de/~ley/db/indices/a-tree/l/Li:Fei.html
9. A. Mencattini, M. Salmeri, Metrological characterization of a CADx system for the classification of breast masses in mammograms. IEEE Trans. Instrum. Meas. **59**, 2792–2799 (2010)
10. T.F. Chan, L.A. Vese, Active contours without edges. IEEE Trans. Image Process. **10**, 266–277 (2001)
11. W.C. Shen, R.F. Chang, W.K. Moon, Y.H. Chou, C.S. Huang, Breast ultrasound computer-aided diagnosis using bi-rads features. Acad. Radiol. **14**, 928–939 (2007)

A Machine Learning Approach to Cluster the Users of Stack Overflow Forum

J. Anusha, V. Smrithi Rekha and P. Bagavathi Sivakumar

Abstract Online question and answer (Q&A) forums are emerging as excellent learning platforms for learners with varied interests. In this paper, we present our results on the clustering of Stack Overflow users into four clusters, namely naive users, surpassing users, experts, and outshiners. This clustering is based on various metrics available on the forum. We use the X-means and expectation maximization clustering algorithms and compare the results. The results have been validated using internal, external, and relative validation techniques. The objective of this clustering is to be able to trace and predict the activity of a user on this forum. According to our results, majority of users (71 % of 40,000 users under consideration) fall in the 'experts' category. This indicates that the users in Stack Overflow are of high quality thereby making the forum an excellent platform for users to learn about computer programming.

Keywords Clustering · Naive users · Surpassing users · Bayesian information criterion

J. Anusha (✉) · P.B. Sivakumar
Department of Computer Science and Engineering, Coimbatore Campus,
Amrita Vishwa Vidyapeetham, Coimbatore, India
e-mail: anunrs@gmail.com

P.B. Sivakumar
e-mail: pbsk@cb.amrita.edu

V.S. Rekha
Center for Research in Advanced Technologies for Education, Amritapuri Campus,
Amrita Vishwa Vidyapeetham, Kochi, Kerala, India
e-mail: smrithirekha@gmail.com

© Springer India 2015

L.P. Suresh et al. (eds.), *Artificial Intelligence and Evolutionary Algorithms in Engineering Systems*, Advances in Intelligent Systems and Computing 325,
DOI 10.1007/978-81-322-2135-7_44

1 Introduction

In recent times, online question and answer forums such as Quora and Stack Overflow are being used as learning platforms for users across the globe and of different age groups. While Quora is a generic forum, Stack Overflow deals exclusively with computer programming. This paper aims at clustering the users of Stack Overflow based on their usage and performance on the forum. We use a number of parameters to cluster the users. The main objective of clustering the users is to understand what types of users dominate the forum and how their expertise levels impact their reputation on the forum.

2 Background and Related Work

SO has nearly a million registered users and provides a fertile platform for analytics research. Each user on SO is given a number of badges and carries a reputation score depending on his/her performance on the forum. The reputation score increases as the contribution of the user increases in the forum [1].The current categorization of users in SO does not give enough scope for predicting the effectiveness of the forum. SO data have been analyzed from different perspectives. A correlation between reputation and age has been identified by [2]. The questions posted on SO have been analyzed by authors of [3–5], and specifically, 'closed' questions have been analyzed by [6]. Our approach differs from these works in that we analyze SO users to understand its effectiveness while the works mentioned here analyze SO posts. The metrics based on which we cluster the users are number of posts owned by each user (NOP), number of badges won by each user (NOB), cumulative score of all the posts owned by a user (SC), lifetime: number of days between the user's creation date and last accessed date (LT), up-votes (UV), down-votes (DV), number of answers which were marked 'accepted' by others (NOA), and number of posts the user has edited to make them more readable and understandable (NOE). We are clustering users of SO into four types, and the characteristics of users in each group are tabulated in Table 1.

Table 1 Users and their characteristics on the forum

Users	Characteristics
Naive users	Users who post very less number or no queries or answers have a low lifetime in SO and own very few or no badges
Surpassing users	Users who post very less number of queries or answers stay with SO for more number of days than naive users and own a few badges
Experts	Users who post good number of queries and answers with many UV stay with SO for a long time and own a variety of large NOB
Outshiners	Users who post maximum number of queries and answers with most UV stay with SO for a really long time and own a variety of maximum NOB

We use X-means clustering algorithm [7] to cluster the users based on the observed metrics. X-means clustering algorithm is an extension of K-means algorithm (which performs better and efficient for large data sets as discussed in [8–14]) with an additional feature of efficient estimation of the optimal K value for the given data set using Bayesian information criterion. The results produced by X-means algorithm are validated by three validation techniques, namely (a) internal validation, (b) external validation, and (c) relative validation.

3 Implementation

The methodology adopted undergoes a series of steps as shown in Fig. 1. Relevant data about users, posts, and badges are collected from Data Explorer of Stack Exchange. The data under consideration are about the set of users who registered

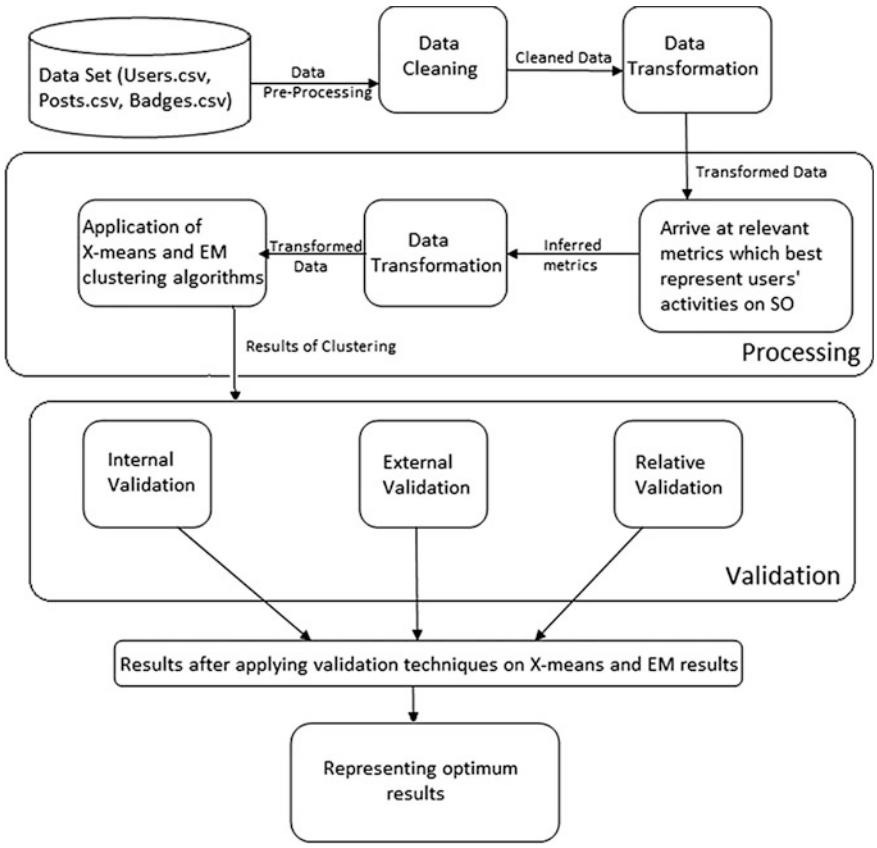

Fig. 1 Flow diagram showing the sequence of steps undergone to cluster the users and validate the results

themselves to Stack Overflow in the year 2008 and 2009 (50,000 users).The data are cleaned and transformed, after which the metrics described in Sect. 2 are derived from the data.

Regression is performed to find out the significance of the metrics over the user's standard reputation (given by SO administrator). X-means clustering algorithm is applied to arrive at different groups of the users based on the value the users posses with respect to different metrics. X-means clustering algorithm results in four different clusters. The output of X-means clustering algorithm is validated using three validation techniques as discussed below:

- **Internal Validation**: The mean value of all parameters values per user in each cluster is calculated using the formula [10],

$$\left(\frac{1}{N}\right)\sum_{i=1}^{N}\frac{1}{n}\sum_{j=1}^{n}x_j \tag{1}$$

  N Number of instances per cluster,
  n Number of parameters per instance,
  x_i Each parameter's value per instance (NOP, NOB, SC, LT, UV, DV, NOA, and NOE per user).

  The results are tabulated in Table 2.
  From the results of internal validation, we can infer that users of cluster 3 have the best performance, and users of cluster 4 come next, followed by cluster 1 and then cluster 2. Here, by cluster i, we mean the users who were put to ith cluster by the X-means clustering algorithm, where i ranges from 1 to 4.
- **External Validation**: The results of clustering are compared with the standard reputation value given by the administrator of SO to its users based on their performance on the forum. The average reputation of users belonging to same cluster (by cluster, we mean the results produced by X-means clustering algorithm) is tabulated in Table 3.
- **Relative Validation**: Another clustering algorithm, expectation maximization algorithm, is applied on the data, and the results are compared against the results of X-means clustering algorithm. To verify the correctness of EM algorithm, we apply internal validation to the results of EM clustering algorithm. The internal validation results of EM clustering algorithm are tabulated in Table 4. This

Table 2 Internal validation results

Cluster number	Mean performance
Cluster 1	17.6498
Cluster 2	15.3287
Cluster 3	94.7790
Cluster 4	73.0177

Table 3 External validation results

Cluster number	Average reputation
Cluster 1	669
Cluster 2	86
Cluster 3	3,880
Cluster 4	2,086

Table 4 Internal validation of EM algorithm

Cluster number	Mean performance
Cluster 1	106.567362505
Cluster 2	42.6407734198
Cluster 3	289.354604691
Cluster 4	168.83544838
Cluster 5	127.014831185
Cluster 6	77.5645175588
Cluster 7	111.136258025
Cluster 8	51.7669452854
Cluster 9	91.0248281517

Table 5 Combining similar clusters

Performance range	Clusters (merged)
0–80	Clusters 2, 6, and 8
80–130	Clusters 1, 5, 7, and 9
130–170	Cluster 4
Greater than 170	Cluster 3

shows that EM clustering algorithm does not converge definitely at minimum number of clusters. If we fix a performance range, we find that users who have similar performance range are put into different clusters by EM clustering algorithm as tabulated in Table 5.

- **Sum-Of-Squared error**: The sum-of-squared error is calculated for the two algorithms using the following formula.

$$\sum_{j=1}^{k} \sum_{i=1}^{n} x_i - m_j \tag{2}$$

k Number of clusters; n: number of instances per cluster
x_i Each instance's mean; m_j: each cluster's mean (Table 6).

Table 6 Sum-of-squared error

Algorithm	Sum-of-squared error
X-means	27,797,863.2797
EM	33,146,858.4724

4 Results

From the results of validation, we find that the results of X-means clustering best suit our context and give better results than EM clustering algorithm for our data set. From internal and external validation, we find that, performance wise, cluster 3 stands first and cluster 4 stands next followed by cluster 1 and then cluster 2. This is shown in Fig. 3a. The average reputation value with respect to users belonging to each cluster (results of external validation) also shows that the performance of clusters is ranked in the same way as done by internal validation (cluster 3, 4, 1, 2 in the decreasing order of excellence). This is shown in Fig. 3b. A graph depicting the performance of the best set of users (outshiners) is plotted in Fig. 2a, and the reputation of users belonging to outshiners' category is plotted in Fig. 2b. These graphs show that the users labeled 'outshiners' by our algorithm do perform very well in real time too. We name the users belonging to each cluster, fix a performance range, and explain the nature of users belonging to each cluster as tabulated in Table 7. From Table 7, we find that there are maximum number of users in the 'experts' category which is the second best performing group. Minimum number of users belongs to 'surpassing users,' and almost 2 % of users (905 users) belong to the best set of users. So, we conclude saying that a user who is new to the forum and wants help technically can first refer to the discussions which involve these 905 people since these 905 users possess technical excellence among the 40,000

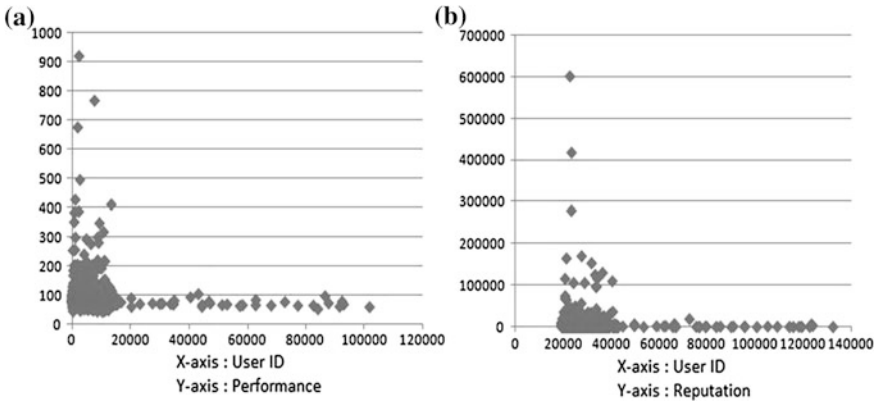

Fig. 2 Outshiners profile in real time. **a** Performance *(Y-axis)* of users belonging to outshiners category on SO. **b** Reputation *(Y-axis)* of users belonging to outshiners category on SO

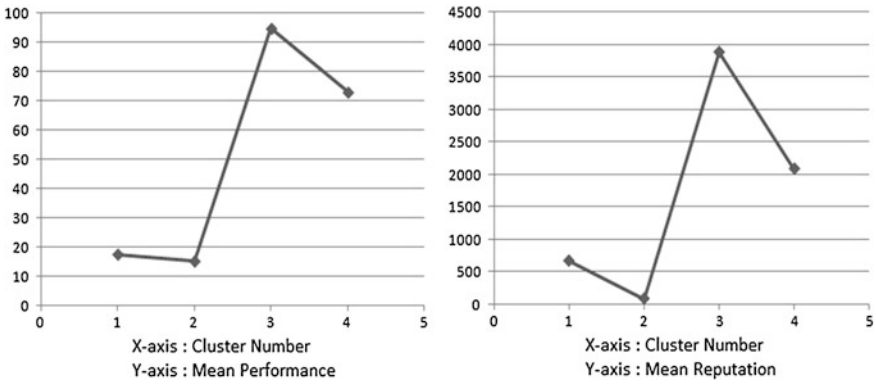

Fig. 3 Graphical view of internal and external validation results. (*i*) Mean performance *(Y-axis)* of users belonging to four different clusters denoted by the cluster numbers 1, 2, 3, and 4 in *X-axis*. (*ii*) Mean reputation *(Y-axis)* of users belonging to four different clusters (*X-axis*)

Table 7 Defining clusters

Category	Cluster	Performance range	Number of users	Nature of users
Outshiners	3	90–100	905	Possess excellent score, large number of Q and A largest NOB
Experts	4	70–90	28,384	Possess good score, good number of Q and A and good NOB
Surpassing users	1	16–70	131	Possess fair score, lesser number of Q and A, owns few badges
Naïve users	2	0–16	10,580	Possess low score, rarely posts Q and A, owns very few or no badges

(10,000 training set and 40,000 testing set) users under consideration. Also, each user can find where he stands with respect to his technical knowledge and the bonding with the forum which helps the user to asses himself in relation to others on the forum. Performance evaluation is performed in two ways:

- Performance of X-means algorithm is evaluated by (i) comparing the results against the results produced by EM clustering algorithm (relative validation) and (ii) comparing the results of X-means algorithm against the real-world ranking of the user (external validation). For instance, we verify whether a user who falls under 'Outshiners' category in our results really has a high 'reputation' value on SO or not.
- Performance of users belonging to each cluster is calculated by the formula (1) which is the simple mean value of all the metrics under consideration with respect to each user. That is, (NOP + NOB + SC + LT + UV + DV + NOA + NOE)/8 is the performance of the corresponding user with respect to our metrics under consideration.

5 Conclusions and Future Work

In this paper, we have made a preliminary effort to cluster the users of SO forum into four categories. We find that while most people belong to 'expert category,' only 2 % of the users perform beyond that. This indicates that SO is definitely an excellent learning platform, but at the same time, more active interactions may be required to push more people into higher categories. Future work could be done to arrive at a prediction technique to predict what will the rate of growth (improving from a lower cluster to a higher one) of such a user be with respect to his bond with the forum. Such a prediction scheme would serve as a motivating factor for people who belong to low categories to improve themselves faster.

References

1. http://www.stackoverflow.com
2. P. Morrison, E. Murphy-Hill, *Is programming knowledge related to age? an exploration of stack overflow* (MSR, San Francisco, CA, USA 2013)
3. M. Allamanis, C. Sutton, *Why, when, and what: analyzing stack overflow questions by topic, type, and code* (MSR, San Francisco, CA, USA 2013)
4. M. Asaduzzaman, A.S. Mashiyaty, C.K. Roy, K.A. Schneider, Answering Questions about Unanswered Questions of Stack Overflow (2013)
5. C. Treude, O. Barzilay, M.-A. Storey, How do programmers ask and answer questions on the web? (NIER Track). ICSE 11. (2011)
6. D. Correa, A. Sureka, *Fit or unfit: analysis and prediction of closed questions on stack overflow* (2013)
7. D. Pelleg, A. Moore, X-Means: extending k-means with efficient estimation of the number of clusters, ICML '00 in *Proceedings of the Seventeenth International Conference on Machine Learning*, pp. 727–734 (2000)
8. B. Chaudhari, M. Parikh, A comparative study of clustering algorithms using weka tools. Int. J. Appl. Innovation Eng Manage (IJAIEM). **1**(2) (2012)
9. O.A. Abbas, Comparisons Between Data Clustering Algorithms. Int Arab J Info Technol. **5**(3) (2008)
10. O.J. Oyelade, O.O. Oladipupo, I.C Obagbuwa, Application of k-means clustering algorithm for prediction of students academic performance. Int. J. Comput. Sci. Inf. Secur. **7**(1) (2010)
11. R. Mauro, M. De Luca, G. DellAcqua, Using a K-means clustering algorithm to examine patterns of vehicle crashes in before-after analysis. Modern Appl. Sci. **79**(10) (2013)
12. D. Morrison, I. McLoughlin, A. Hogan, C. Hayes, Evolutionary clustering and analysis of user behavior in online forums. *Proceedings of the Sixth International AAAI Conference on Weblogs and Social Media*. (2012)
13. J.-. Wen, J.-Y. Nie, H.-J. Zhang, Query clustering using user logs. ACM Trans. Inf. Syst. **20**(1) (2002)
14. S. Padmavathi, C. Rajalaxmi, K.P. Soman, Texel identification using K-Means clustering method, Adv. Compu. Sci.Eng. Appl. AISC Springer-Verlag Berlin Heidelberg. **167,** 285–294 (2012)

Data Storage Optimization in Cloud Environment

M. Deivamani, Rashmi Vikraman, S. Abirami and R. Baskaran

Abstract Data de-duplication is a process which stores a single copy of the data in the storage by eliminating the redundant copies of the data and provides a reference to the existing unique data. On the other hand, cloud storage is growing day by day due to the large volumes of data generated every day. The users make use of cloud to store the large amount of data available with them. Many Internet services such as blogs and social networks which produces huge amount of data may contain a lot of redundancies between them. To efficiently store and manage such kind of data, de-duplication comes into existence. This paper intends to apply data de-duplication framework in the cloud environment and to assess their performance of compressed storage area with respect to two de-duplication strategies such as file level and chunk level. The combination of performing de-duplication along with compression has also improved the compression rate of the storage device. This research achieves efficiency in terms of storage in large. Also it is obvious from the experiments that the performance of the chunk level is better than the file-level data de-duplication.

Keywords Data de-duplication · Cloud storage

1 Introduction

Modern society is a digital universe. Almost no information or industry applications can survive without this digital universe. The most critical issue is that nearly half of the data cannot be stored properly. This is due to lot of reasons such as non-

M. Deivamani · R. Vikraman (✉) · S. Abirami · R. Baskaran
Department of Information Science and Technology, College of Engineering, Anna University, Chennai, India
e-mail: vikramanrashmi@gmail.com

S. Abirami
e-mail: abirami_mr@yahoo.com

© Springer India 2015

L.P. Suresh et al. (eds.), *Artificial Intelligence and Evolutionary Algorithms in Engineering Systems*, Advances in Intelligent Systems and Computing 325,
DOI 10.1007/978-81-322-2135-7_45

availability of such a large container for storage, inefficiency to maintain the big data, and the cost related to managing such data. Fortunately, with the rocket-like development of cloud computing, the cloud storage provides a major advantage and the concept of cloud storage has become vastly accepted by the community. Cloud backup service has become a cost-effective choice for data protection of personal computing devices. In recent years, similar to cloud computing, cloud storage has received increasing attention from industry and academia as it offers virtually infinite storage resources that are available on demand and charged according to usage. Since traditional backup services require data to be backed up to dedicated external drives, which can be inconvenient or costly to the users, data backup for personal computing has emerged to be a particularly attractive application for outsourcing to the cloud storage providers because users can manage data much more easily without having to worry about maintaining the backup infrastructure. This is possible because the centralized cloud management has created efficiency and cost inflection point and offers simple offsite storage, always a critical concern for data backup. To manage the storage issues of cloud, data de-duplication comes into rescue. Data de-duplication, an effective data compression, partitions large data objects into smaller parts, called chunks, and represents and replaces these chunks by their fingerprints (i.e., generally a cryptographic hash of the chunk data) for the purpose of communication or storage efficiency. At present, mainly the file level, block level, and byte level deletion strategies are there to optimize the storage capacity. File-level de-duplication is often referred to as single instance storage (SIS). It checks the index backup or archive files for the attributes stored in the file with the comparison. If not the same file, it will store and update the index; otherwise, only a reference pointer is added to the existing file, in the index. Chunk-level de-duplication takes the data stream and divide it into chunks/blocks, check the data chunk, and determine whether the chunk content is similar to one that of already existed. If not the same chunk, it will store and update the index; otherwise, only a reference pointer is added to the existing chunk, in the index. In byte level de-duplication, the new data stream is checked against already stored bytes of data stream one by one, to achieve higher accuracy.

2 Related Work

There are various ways of classifying the data de-duplication such as based on technologies of how it is done, based on the process, and based on where it happens like source side or target side [7, 8]. Various existing works based on various technologies of data de-duplication have been discussed below.

Upadhyay et al. proposed De-duplication and Compression Techniques in Cloud Design [1] which aims at reduction in storage space in large backups. Multiple metadata structures have been used for a better duplicate detection.

Harnik et al. [2] proposed the estimation of de-duplication ratios in large data sets. This paper focuses on finding the de-duplication ratio efficiently. It involves

two phases, i.e., sampling phase where chunking and hashing is done and scanning phase where the duplicate detection and estimation of the de-dupe ratio is made. Hi et al. [3] had given a brief study on various data de-duplication techniques. This work deals with the various de-duplication strategies that have been used. The various strategies involve file level, byte level, and block level. The algorithm for hashing is mostly SHA or MD5.

Zhang et al. explored Data de-duplication Techniques [4] in which various data de-duplication technologies which are used to optimize the storage system which can greatly reduce the large amount of data and hence reducing the storage space and heat emission are discussed.

Zhu et al. proposed An Intelligent Data De-duplication Based Backup System [2]. Backup de-dupe includes four de-duplication strategies, that is, SIS, FSP, CDC, and SW. It supports the online source-side de-duplication and is capable of selecting different de-duplication algorithms according to the corresponding data types. Meanwhile, it offers the data reliability and security in the backup process.

Zeng et al. presented Research on Cloud Storage Architecture and Key Technologies [5] which proposes layered architecture of cloud storage also discusses the deployment, virtualization and availability, data organization, data migration and load balance, redundant data deletion, storage capacity, etc.

Rashid et al. proposed A Secure Data De-duplication Framework for Cloud Environments [6] which focuses on data privacy and security issues. This framework uses an efficient de-duplication algorithm where the file is segmented and hashed and the hash values stored in the index tree for faster retrieval. The index tree is encrypted with an asymmetric hashing algorithm.

3 Architecture

The overview on how this data de-duplication system has been implemented is given in Fig. 1. The client produces the data which undergoes either SIS or FSP for de-duplication. For SIS, the whole file is taken as such for the de-duplication. Here, the whole file hashing is taken under consideration for duplicate detection. For FSP, the file is split into number of small segments called chunks. The hash values for the chunks are taken into consideration for duplicate detection. The metadata of the file is extracted for every file and chunk.

The metadata of the file is placed in the File Metadata DB and is sent to the storage server. The metadata of the file will consist of information such as the file name, file length, address of the file and in case of FSP, the chunk name as well as chunk offset is included as well. The metadata of the file is important for the reconstruction of the file once requested. The storage server makes the comparisons and decides on whether to store the data in the storage system or not. Storage server not only stores the de-dupe data transmitted by de-dupe client but also sends the data requested by de-dupe client. It maintains a Hash Table to map hash to data chunk position, containing address to read and write data. The hash table adopts

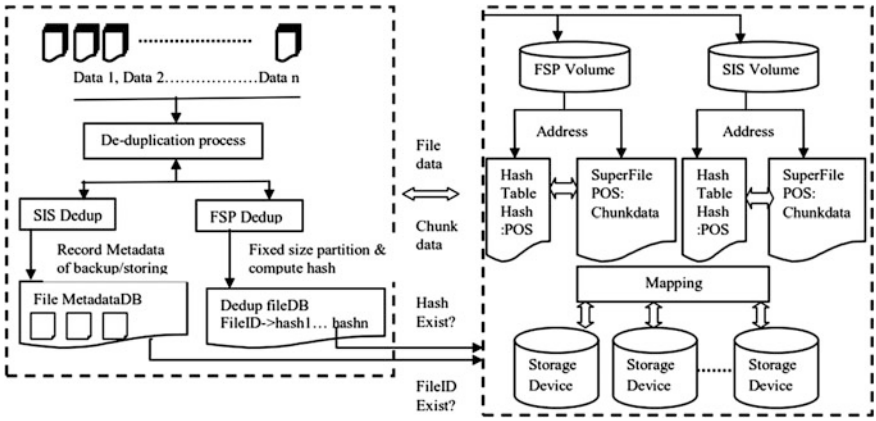

Fig. 1 Data storage architecture

two-stage index mechanism. It establishes the level-1 index according to the second byte of the hash value and locates the chunk position on the basis of the 8–11 bytes of the hash value and employs double hashing policy to solve potential conflicts.

3.1 De-dupe Client

De-dupe client generates data to be de-duped and upload the file to the server to trigger de-duplication task. First, client user creates de-dupe task by uploading the file, forming a de-dupe task set. Once de-dupe has been done by the server, client can also initiate reconstruction of files as and when they require.

3.2 Server Module

Server involves performing the de-duplication strategies. Both the strategies, SIS (File level) and FSP (Chunk level), have been discussed below:

File-level De-duplication (SIS). De-duplication at the file level compares any two files as a whole for redundancies. If the whole file is found duplicate, then the file has to be de-duplicated. Figure 2 shows file-level de-duplication. For each file uploaded by the client, a copy of input file is temporarily stored in the server for preprocessing (finally, recycled after every process). It generates unique hash code for each file using MD5 algorithm. Then, it compares the generated hash value with the list of hash values already stored in the index in the storage server. If the hash value matches with any one of the existing hash values, then the file is identified to be a duplicate/replicated file. Instead of storing the file again, a reference to the existing file is added in the index for future retrieval.

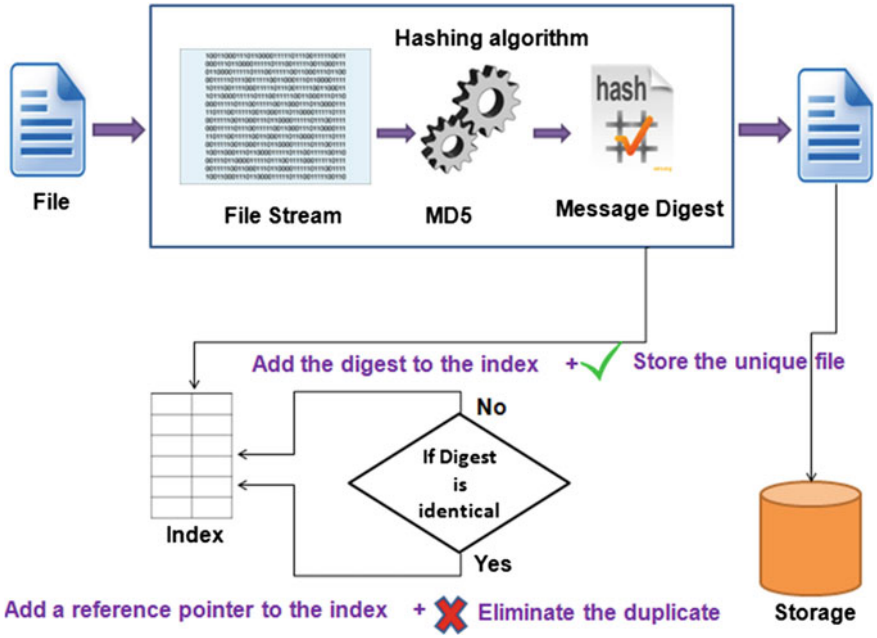

Fig. 2 File-level de-duplication

Chunk-level De-duplication/Partition-level De-duplication. Chunk-level or partition-level data de-duplication takes the data stream, divide it into blocks/chunks, check the data chunk, and determine whether it met the same data of the already stored chunks (usually by implementing the hash algorithm for each data chunk to form a digital signature or unique identifier).

If the chunk is unique, then it will be written to disk; its identifier is also stored in the index; Otherwise a reference pointer will be assigned for the same data chunk's existing location. Figure 3 shows chunk-level/block-level/partition-level de-duplication.

3.3 Compression and Decompression Techniques

The compression technique reduces the file size and saves the storage space more. The files uploaded to the server gets compressed after the de-duplication process and then stored permanently in the cloud storage. In this phase, gzip compression algorithm has been used to compress files. The decompression technique decompresses the file from the storage space when the user requests for that particular file. The files are retrieved from storage which is in compressed form and reconstructed to form the original file. This is done using gzip decompression algorithm.

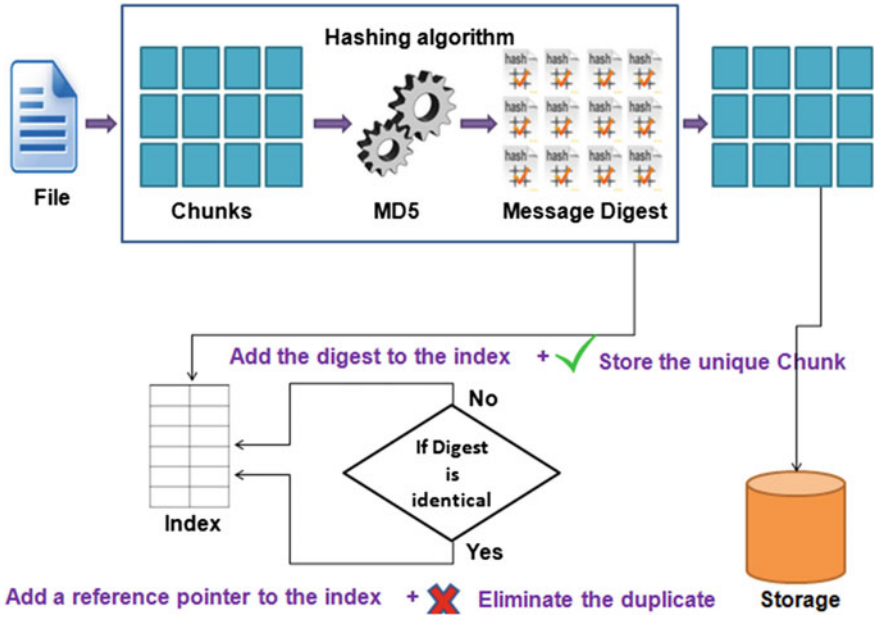

Fig. 3 Chunk-/partition-level de-duplication

3.4 File Retrieval

This takes care of transmitting files over the network on user's request. When a user requests for a particular file, the corresponding compressed file gets decompressed and checked as a whole with the reference of index. If the file is de-duplicated, then original contents are composed by referring location of the already existing ones, and files have been produced to send back to the client. After successful restoration of the particular file, the file is made available at the client side to download.

4 Experimental Setup and Deployment

4.1 Cloud Setup

This paper implements OpenNebula, one of the open source tools available for cloud setup and works under LINUX platform. OpenNebula is an open source virtual infrastructure engine that enables the dynamic deployment and replacement of virtualized services (groups of interconnected virtual machines) within and across sites. The system requirements for KVM hypervisor hosts are Ubuntu Server −12.04, Libvirt −0.9.4 or higher, qemu/kvm −1.0 or higher, 500 GB disk capacity. In addition, within a single cluster, the hosts must be of the same distribution

Table 1 Test data sets

Data Set	S1	S2	S3	S4	S5	S6
DAT	0.99 MB, 5	1.01 MB, 3	1.58 MB, 5	1.64 MB, 3	1.69 MB, 3	1.79 MB, 5
TXT	3.99 MB, 3	4.68 MB, 3	5.20 MB, 7	9.01 MB, 2	9.90 MB, 3	11.8 MB, 2
DOC	2.18 MB, 5	3.22 MB, 5	3.13 MB, 6	4.09 MB, 7	4.25 MB, 3	5.91 MB, 4
WEB	5.91 MB, 2	7.17 MB, 2	9.81 MB, 6	10.6 MB, 3	11.3 MB, 3	13.7 MB, 4

version, i.e., all hosts within a cluster must be homogeneous. The CPUs must be of same type, count, and feature flags. It must support HVM, Intel-VT or AMD-V-enabled 64-bit × 86 CPU (more core results in better performance), 4 GB of memory, and at least 1 NIC. When deploying cloud stack, the hypervisor host must not have any VMs already in running state.

5 Performance Evaluation

5.1 Data Sets

Different data sets such as Web source files (.html, .xml, .css) and editing files (.txt, .doc) have been selected for testing the de-duplication performance. Table 1 represents the files in the form of grids s1, s2, s3, s4, s5, and s6. Each grid s1 to s6 represents the various backup sets collected over a week. The files over the week may be added, updated, or deleted. Within each grid, the first element stands for the size of the file set and the second for the total number of files included in each set.

5.2 Experimental Results and Evaluation

The performance factor used here to identify the de-duplication efficiency is de-duplication ratio. Equation 1 shows the formula for calculating the de-duplication ratio.

$$\text{De}-\text{duplication ratio} = \frac{\text{Size of the original data}}{\text{Size of the dedup data}} \tag{1}$$

The de-dupe size of the each file is found after performing the file-level or chunk-level de-duplication. The results have been shown in Figs. 4, 5, 6, 7, 8, and 9. In those figures, the *X* axis represents the test data file set which have been used

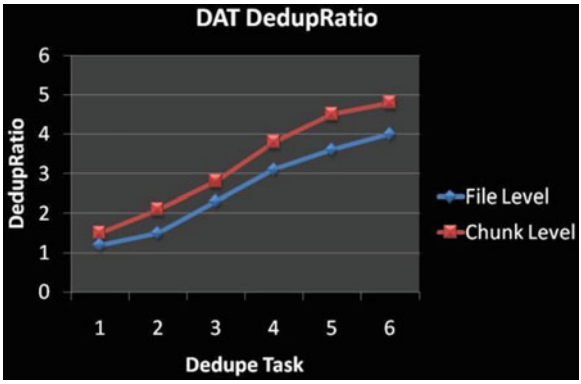

Fig. 4 Dat file de-duplication

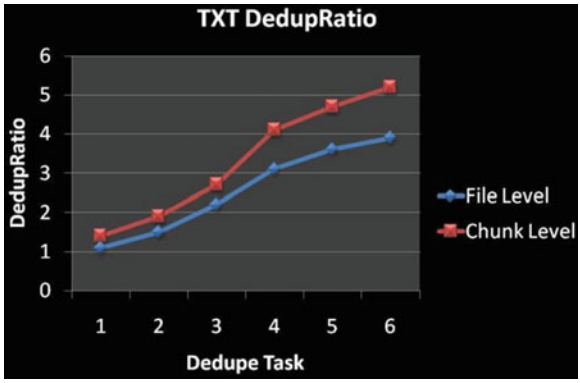

Fig. 5 Text file de-duplication

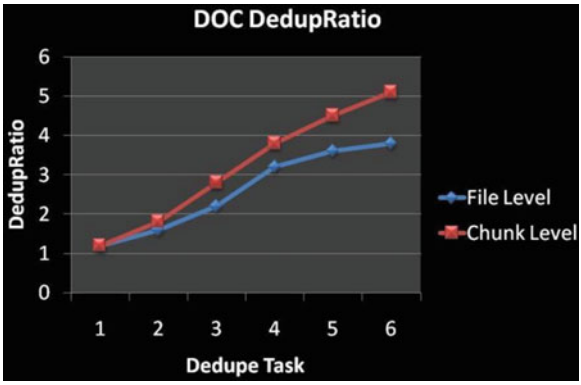

Fig. 6 Doc file de-duplication

for performance evaluation and *Y* axis stands for the de-duplication ratio to represent how much storage efficiency have been achieved in the proposed system across different types of files.

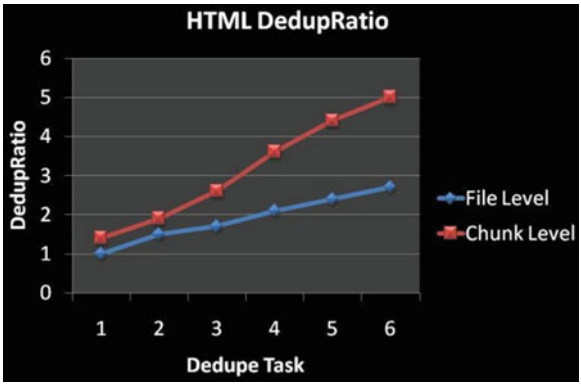

Fig. 7 HTML file de-duplication

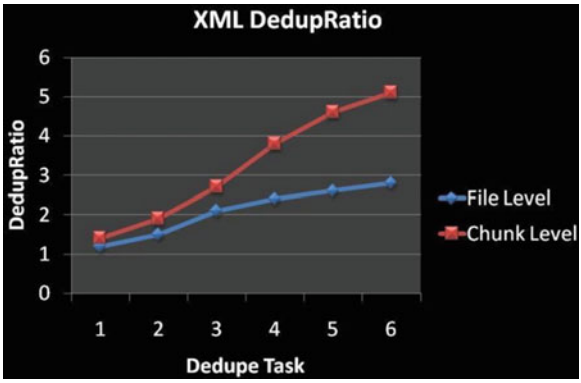

Fig. 8 XML file de-duplication

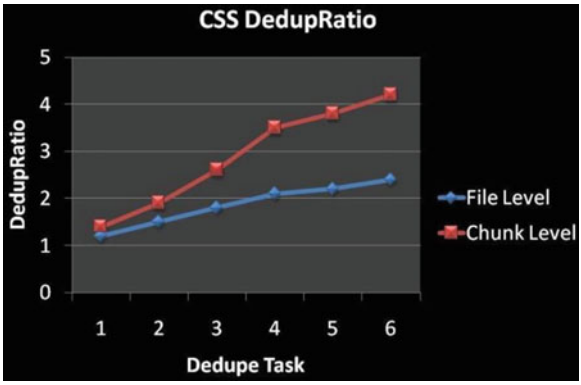

Fig. 9 CSS file de-duplication

5.3 Inference

For the same file type of same data sets, different de-dupe ratios have been obtained for different de-duplication strategies. Therefore, by considering the testing results as well as the system performance, it is obvious that the chunk-level de-duplication gives a better result than the file-level de-duplication. The reason for chunk-level de-duplication being better than file-level de-duplication is due to the fact that the file-level de-duplication involves the whole file as such and we get only a single whole file hash for making comparisons, whereas in chunk-level de-duplication every chunk inside the file produces hash values that are used across and within the files for comparisons and hence giving better results on duplicate detection. Here, the grid s6 provides better results than others because over the period of a week, more files are added, updated, and deleted due to which more duplicates would have been occurred in s6 and s5. Simulation results also shows that as the number of files increases duplicated count also increases based on the nature of the backup dataset. Hence, in the grid s3, s4, and s6, the number of files and duplicates is more.

6 Conclusion and Future Enhancement

In this research, the data de-duplication has been simulated in the cloud environment where a lot of redundancies in the data exist. By applying the de-duplication in the cloud, the storage space reductions have been achieved to a large extent. Testing and the results obtained delineate the efficiency in storage space. De-duplication benefits in saving the storage space. The user can upload any file to the cloud and retrieve any file data dynamically whenever they need. Thus, the de-duplication process is achieved on the storage space of the cloud server node. The future work may be done by providing security services to the cloud VM to avoid attacks and loss of file during the transfer of files between two systems. The performance analysis can also be improved by using better algorithms for chunking.

References

1. A. Upadhyay, P.R Balihalli, S. Ivaturi, S. Rao, De-duplication and compression techniques in cloud design. *Proceedings of the IEEE International Systems Conference*. (2012), pp. 1–6
2. H. Qinlu, L. Zhanhuai, Z. Xiao, Data de-duplication techniques. *Proceedings of the International Conference on Future Information Technology and Management Engineering*. **1**, 430–433 (2010)
3. G. Zhu, X. Zhang, L. Wang, Y, Zhu, X. Dong, An intelligent data de-duplication based backup system. *Proceedings of the 15th IEEE International Conference on Network-Based Information Systems*. (2012), pp. 771–776

4. W. Zeng Y. Zhao K. Ou W. Song, Research on cloud storage architecture and key technologies. *Proceedings of the 2nd ACM International Conference on Interaction Sciences: Information Technology, Culture and Human*. (2009), pp. 1044–1048
5. S. Patidar, D, Rane, P. Jain, A survey paper on cloud computing. *Proceedings of the 2nd IEEE International Conference on Advanced Computing and Communication Technologies*. (2012), pp. 394–398
6. F. Rashid, A. Miri, I. Woungang, A secure data de-duplication framework for cloud environments. *Proceedings of the 10th IEEE International Conference on Privacy, Security and Trus*. (2012), pp. 81–87
7. D.D. Harnik, D. Naor, D. Sotnikov, G. Vernik, O. Margali, Estimation of de duplication ratios in large data sets. *Proceedings of the 28th IEEE Symposium on Mass Storage Systems and Technologies.* (2012) pp. 1–11
8. Y. Fu, H. Jiang, N. Xiao, L. Tian, F. AA-dedupe, An application aware source de-duplication approach for cloud backup services in the personal computing environment. *Proceedings of the IEEE International Conference on Cluster Computing*. (2011), pp. 112–120

Study on Fingerprint Images Using Delaunay Patterns to Identify Hereditary Relations Among Family Members of Three Generations

C. Karthikeyini and V. Rajamani

Abstract In this work, an effort is taken to identify hereditary relation among intraclass family members using fingerprint minutiae features. These minutiae features include endings and bifurcations. The fingerprint images are collected from 324 subjects of 54 different families, of three generations, comprising three members in each family. As the quality of the fingerprint images needs to be improved for minutiae feature extraction from thinned ridge image, a series of preprocessing and postprocessing steps are sequentially applied. Using structural elements, thinned ridge pattern was obtained from the preprocessed image. Then, morphological operations are performed over the thinned ridge pattern to remove spurious elements such as spurs, bridges, breaks, and dots. After removing the spurious elements, valid minutiae points (endings and bifurcations) are obtained using morphological operators. The minutiae points are analyzed to study the hereditary relation with the help of Delaunay patterns which is formed with the help of the coordinate points of the minutiae features. The result shows that the intra-family members are having the similar type of Delaunay patterns and it proves the presence of hereditary relation among intrafamily members.

Keywords Directional field estimate · Finger code · Minutiae triplets · Fingerprint image acquisition · Image preprocessing · Morphological operation

C. Karthikeyini (✉)
Centre for Research and Development, Department of Electronics and Communication Engineering, PSNA College of Engineering and Technology, Dindigul 624622, Tamil Nadu, India
e-mail: ckarthiraja@gmail.com

V. Rajamani
Department of Electronics and Communication Engineering,
Veltech Multi Tech Dr. Rangarajan Dr. Sakunthala Engineering College,
Avadi, Chennai 600062, Tamil Nadu, India
e-mail: rajavmani@gmail.com

© Springer India 2015

L.P. Suresh et al. (eds.), *Artificial Intelligence and Evolutionary Algorithms in Engineering Systems*, Advances in Intelligent Systems and Computing 325,
DOI 10.1007/978-81-322-2135-7_46

1 Introduction

Fingerprints have been most widely used over a century for personal identification. Galton [1] stated that fingerprints are the unique patterns and are persistent and immutable. The personal characteristics exist in minute particulars. Fingerprints are composed of many ridges and furrows. Their formations depend on the initial conditions of the embryonic mesoderm from which they develop [2]. Consequently, fingerprints are a unique marker for a person, even for identical twins [3]. Since fingerprints are said to be unique, a variety of automatic fingerprint identification and recognition systems were developed using minutiae matching techniques. Researchers followed different methods to extract minutiae points for their system. Afsar et al., Zhao and Tang, and Sudiro and Yuvono [4–6, 21, 22] proposed fingerprint identification and classification system which is based upon fingerprint minutiae details that are extracted using crossing number algorithm. Using the extracted minutiae point, the system that was developed by Eckert et al. [7, 8] for fingerprint matching was invariant to translation, rotation, distortion effects, and side-channel attacks. Minutiae points are extracted from skeletonized image as well as grayscale image and binary image. Maio and Maltoni [9] developed an algorithm for identification model using minutiae that are extracted directly from the grayscale image. Indexing fingerprint databases were developed by de Boer [10] based on multiple features such as directional field estimate, finger code, and minutiae triplets. Minutiae extraction was done from the thinned fingerprint image. Bansal et al. [11] used hit-or-miss transform of mathematical morphology to obtain thinned ridge image for effective extraction of true fingerprint minutiae, and this method results in effective minutiae detection and saves a lot of efforts in postprocessing stage. Alessandro Farina presented a novel set of algorithm for the extraction of fingerprint minutiae from skeletonized binary images. This work extracts 40–60 minutiae of a fingerprint image from 2,000 to 3,000 that are contained in typical skeletonized and binarized images [12]. A different approach was defined by Yoon et al. [13] for investigating the impact of fingerprint alteration and developing a technique to automatically detect altered fingerprints based on analyzing orientation filed and minutia distribution. Literature shows that fingerprint is not only used for personal identification but also used in the areas like sex determination. Gungadin [14] analyzed fingerprints in which he proved the hypothesis that women tend to have a statistically significant greater ridge density than men. As mentioned previously, the fingerprints were formed depending on the initial conditions of the embryonic mesoderm from which they develop, and this process is genetically controlled. Based on this scientific truth, some of the authors used fingerprint images for gender classification [15]. The results attained proved that fingerprint images are genetically related and they give valuable discrimination between male and female categories. The work on gender classification provides evidence about the presence of genetic information in the fingerprints. Many researchers used crossing number algorithm to extract minutiae points, which requires postprocessing algorithm to remove spurious points. In the present work, to overcome the

problem of postprocessing, a more number of structural elements are used, followed by morphological operators. The effort is taken to identify the existence of hereditary information in fingerprints by studying the similarities between minutiae points in terms of its coordinate location in 2D space, number of minutiae points, and Delaunay triangulation pattern between intrafamily members.

2 Image Acquisition and Preprocessing

The fingerprints are captured using the optical scanner. In the present work, images with the resolution of 500 dpi were collected from 54 different families of three different generations, comprising of 324 images. A family tree is formed with three generations, which includes grandfather, grandmother, son, daughter, grandson, and granddaughter. The family members of the same tree are considered to be intraclass family members, and members in different families are interclass members. The blood group of each intraclass member is ensured to be the same because, to a certain extent, it justifies the genetic mapping of fingerprint. The age of first generation varies between 65 and 75 years, the age of second generation is within 40–55 years, and the age of third generation lies in between 15 and 25 years.

3 Implementation Methodology

The implementation part of the work, as given in Fig. 1, consists of five steps such as 1. fingerprint image acquisition, 2. image preprocessing and enhancement, 3. ridge thinning using structural elements, 4. morphological operation, 5. minutia extraction, and 6. analyzing minutiae points. The images are preprocessed and enhanced using suitable algorithms to improve the quality of the image.

Thinned ridge pattern is obtained using more number of structural operators. Then, morphological operators are used to remove the spurious elements which affect the valid minutiae points and make the feature extraction easy and superior. Finally, the extracted minutiae points are analyzed to study the existence of hereditary relation in fingerprints of intraclass family members. The preprocessing steps are as follows:

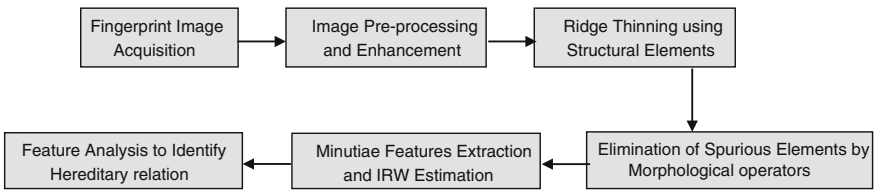

Fig. 1 Implementation methodology—steps involved in identifying hereditary relation using fingerprints

Removal of nonuniform illumination: Morphological opening used here smoothens the contour of an object, breaks, and eliminates thin protrusions. Then, the raw fingerprint image is subtracted from the opened image results in enhanced image called top-hat-transformed image (f_{top}).

Contrast enhancement: Contrast enhancement is a method to stretch the dynamic range of gray-level intensity values in the fingerprint image for further processing. The intensity transformation maps the values in f_{top} to a new value, which results in contrast-enhanced image f_c. The mapping is done by setting (r_1, s_1) = ($r_{\min}$, 0) and (r_2, s_2) = ($r_{\max}$, $L - 1$) where $r_{\min}$ and $r_{\max}$ denote the minimum and maximum intensity values in the fingerprint image, respectively.

Binarization by thresholding: Image binarization converts 256 gray-level images to a binary image by thresholding. Since the fingerprint image does not have the same contrast characteristics, single threshold cannot be used. So a locally adaptive thresholding is used to overcome the multilevel contrast changes [16] using Eq. (1). Here, n_1 and n_2 are local pixels under window of size 16 × 16.

Median filtering: Median filtering was done to avoid the black-and-white noise (salt and pepper) in the thresholded image, since noise becomes more prominent after threshold operates on the image.

$$f_T(n_1, n_2) = \begin{cases} 1 & \text{if } f_c(n_1, n_2) \geq \text{LocalMean} \\ 0 & \text{otherwise} \end{cases} \tag{1}$$

This is the best-known order statistic filter which uses a 3 × 3 neighborhood to compute the median and pads the border of the input image with 0's. Median filtering with default settings reduces the variance of the intensity values in the image, and it changes the image intensity mean value if the spatial noise distribution in the image is not symmetrical within the window [17]. Histogram equalized FFT enhancement: To improve the representation of ridges and furrows of the median-filtered image, in most of the fingerprint recognition and identification systems, Fourier transform technique is used [18]. The median-filtered binary image obtained earlier is divided into small processing blocks of 32 × 32 pixels, and Fourier transform is applied on each block based on the following equation:

$$F(u, v) = \sum_{x=0}^{M-1} \sum_{y=0}^{N-1} f(x, y) \times \exp\left\{-j2\pi\left[\frac{ux}{M} + \frac{vy}{N}\right]\right\} \tag{2}$$
$$\text{for } u = 0, 1, 2, 3, \ldots, 31 \text{ and } v = 0, 1, 2, 3, \ldots, 31$$

To enhance a specific block by its dominant frequencies, the FFT of the block is multiplied by its magnitude a set of times. The enhanced block is obtained by

$$g(x, y) = F^{-1}\left\{F(u, v) \times |F(u, v)|^k\right\} \tag{3}$$

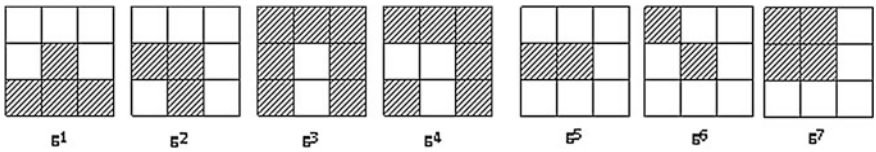

Fig. 2 Structural elements used for ridge thinning

'K' in the above equation is FFT factor chosen as 0.45 to calculate $g(x, y)$. Having higher 'K' improves the appearance of the ridges. But high K values fill up small holes in termination, and they might become bifurcation [18]. The FFT-enhanced image, as shown in the figure, has greater improvement to connect some falsely broken points on ridges. Histogram equalization is applied, followed by FFT transformation. It is used to expand the pixel distribution of the image so as to increase the perceptional information.

Ridge Thinning: The final image processing operation prior to interpreting the ridge pattern is ridge thinning. It is the process of reducing the thickness of each line of patterns to just single-pixel width [19, 20]. To satisfy the requirements of thinning algorithm, structural elements (g_{nm}) and morphological operators were used. Morphological thinning operator is the subtraction of the input image from the subgenerating operator with the structural element (Fig. 2) defined as follows:

$$f_T \otimes g_{nm} = f_T - (f_T * g_{nm}) = f_T \cap (f_T * g_{nm}) \tag{4}$$

$$g_{nm} = (g_{11}, g_{12}, g_{13}, g_{14}, g_{21}, g_{22}, g_{23}, g_{24}, g_{31}, g_{32}, g_{33}, g_{34}, g_{41}, g_{42}, g_{43}, g_{44}, g_{51}, g_{52}, g_{53}, g_{54}, g_{61}, g_{62}, g_{63}, g_{64}, g_{71}, g_{72}, g_{73}, g_{74}) \tag{5}$$

where f_T is the thresholded image and g_{nm} is the structural element and $1 \leq n \leq 7$ and $1 \leq m \leq 4$. The number and combination of structural element patterns selected decide the quality of ridge patterns to remove spurious elements such as spurs, breaks, dots, bridges, bifurcations, and endings which are considered here. In the present work, 28 structural elements have been used for ridge thinning which increases the efficiency of thinning operation. Here, g_1 includes g_{11}, g_{12}, g_{13}, g_{14}; g_2 includes g_{21}, g_{22}, g_{23}, $g_{24;}$ g_3 includes g_{31}, g_{32}, g_{33}, g_{34}; g_4 includes g_{41}, g_{42}, g_{43}, g_{44}; g_5 includes g_{51}, g_{52}, g_{53}, g_{54}; g_6 includes g_{61}, g_{62}, g_{63}, $g_{64;}$ g_7 includes g_{71}, g_{72}, g_{73}, g_{74}. All the 28 structural elements are obtained by rotating each (gn) in the clockwise direction by 90°.

Elimination of spurious elements: After obtaining the thinned ridge pattern, it can be seen that there is a presence of isolated regions and misconnections, which leads to unwanted spurious elements such as spurs, bridges, breaks, and isolated points as shown in Fig. 3. The presence of spurious elements does not affect the interpretation of ridge patterns, but it has an erroneous comprehension in minutiae formation.

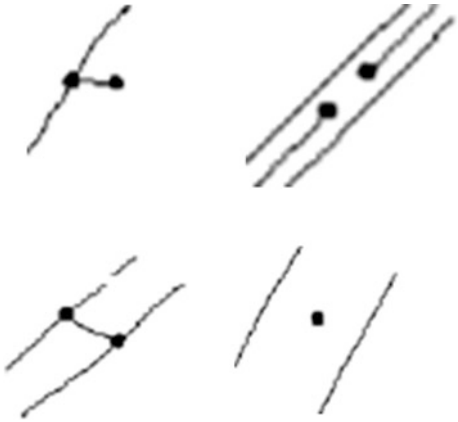

Fig. 3 Spurious elements in fingerprint images: **a** spurs, **b** bridges, **c** breaks, and **d** isolated points

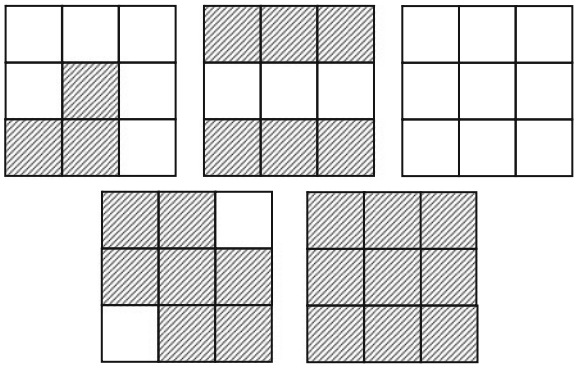

Fig. 4 Operators to remove spurious elements. **a** Spur removal, **b** bridge removal, **c** isolated point removal, and **d**, **e** break removal

These spurious elements are identified as true minutiae, and hence, they are removed using appropriate morphological operators. The operators used are spur removal operators, bridge removal operators, break removal operators, and dot removal operators as in Fig. 4. Using these operators, the spurious elements are removed from the fingerprint image. Thereby, using this minutiae extraction process, the true minutiae points can be obtained.

Minutia Extraction: Minutiae extraction becomes relatively easy after fingerprint ridge thinning using structural elements, followed by removing spurious elements using morphological operators. Many methods are available for minutiae detection. Mostly used methods are the crossing number (CN) concept [21, 22] and 3 × 3 mask method. These methods are extensively used because of its computational efficiency and inherent simplicity. In our work, the mask is used in which minutia is extracted by scanning the local neighborhood of each ridge pixel in the image using a 3 × 3 window. The windows used to extract true endings and bifurcations are as shown in Fig. 5, since all other spurious elements are removed by morphological operators. Applying these mask endings and bifurcations is marked on the thinned ridge map as shown in Fig. 6.

(a)

0	1	0
0	1	0
1	0	1

(b)

0	0	0
0	1	0
0	0	1

Fig. 5 Minutiae extraction operators: **a** ridge bifurcation operator and **b** ridge ending operator

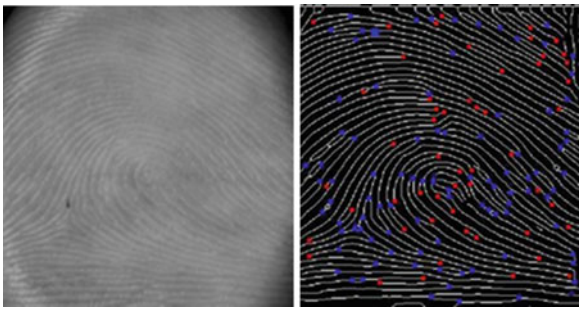

Fig. 6 Original image and image with minutiae points (endings and bifurcations)

4 Results and Discussion

The fingerprint images of 324 members from 54 families of three generations having the same blood group within intrafamily members are acquired using the optical scanner. The fingerprint images with the resolution of 500 dpi are collected and used for analysis. The preprocessing and enhancement techniques are applied on the fingerprint images. Then, using ridge orientation methods, ridge orientation map is obtained. The pattern types of fingerprint images are noted from the visual interpretation of ridge orientation map. Then, ridge thinning using structural elements followed by removing spurious elements using morphological operators is performed over the ridge orientation map. Level 2 minutiae points are extracted from the thinned image using 3 × 3 window operators. The minutiae points constitute endings and bifurcations. From the results obtained, the statistical data such as ridge pattern types, number of minutia points, and their location in 2D space are noted from the ridge pattern types obtained and it is observed that among 54 families, 46 families are having the same ridge patterns, whereas the other 8 families are having dissimilar ridge patterns. This shows that 85.19 % of intrafamily members are having similar ridge pattern types and 14.81 % of the members are having dissimilar ridge pattern types. Further, it is observed that the total number of minutiae points including endings and bifurcations for all 324 members varies between a minimum of 43 and a maximum of 84. The number of minutiae points for the members having similar ridge patterns is more or less equal. For example, in family #2, the number of minutiae points is 62, 63, and 67 for first-, second- and third-generation members, respectively. The family for which the pattern types are

dissimilar, the number of minutiae points get differs between first-, second-, and third-generation members. For example, family #4 has dissimilar ridge pattern, and the minutiae points are 84, 68, and 53, respectively, for three generation members. Here, the variation in minutiae point values is high compared to family #1.

Further, to analyze the hereditary relation using minutiae points observed, a pattern is generated. Usually, particular pattern cannot be generated using minutiae points since the locations are random in nature. Therefore, for the analysis, Delaunay triangulation pattern is chosen which forms a Delaunay triangulation for a set of P points in a plane such that no point in P is inside the circumcircle of any triangulation. For the analysis, the families #6, #23, and #44 are considered here that are having similar ridge patterns and the number of minutiae points is as shown in Table 1. With the help of the minutiae points obtained and its corresponding coordinate locations, Delaunay triangulation patterns were drawn. Figure 7 shows the patterns obtained for family #23. From the patterns obtained, it is observed that within intrafamily members, the patterns are similar, which shows that there is the presence of some hereditary relation within intrafamily members.

Table 1 Number of minutiae points

Family	Number of minutiae points (endings and bifurcations)		
	Gen. 1	Gen. 2	Gen. 3
#6	70	74	67
#23	79	77	75
#44	51	54	52

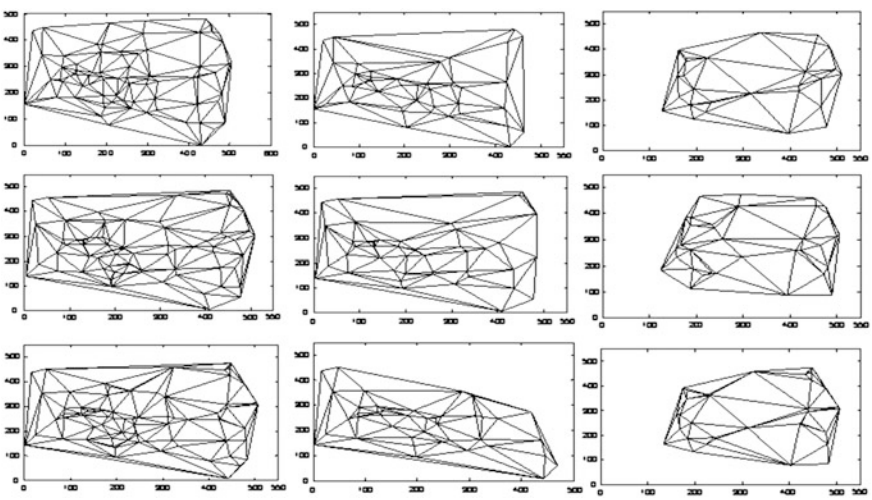

Fig. 7 Delaunay triangulation patterns for family #23 (all, bifurcations, and endings)

5 Conclusion

In this work, an effort has been taken to extract minutiae points from the fingerprint images to study the presence of hereditary relation in intra- and inter-class family members. The fingerprints are acquired from family comprising of three generations. The fingerprint images are processed to obtain the thinned ridge pattern using various enhancement methods and structural elements. The morphological operators are used to remove spurious elements in the thinned ridge pattern which reduces the complication in terms of false minutiae while extracting level 2. The proposed method ultimately yields expected ridge pattern with true bifurcations and endings' number that matches with existing methods used in available database. It is also observed that the most of the family members have similar minutiae values within a family that give appreciable evidence about the presence of hereditary relation in fingerprints. The study using Delaunay triangulation patterns is also providing some evident proof for hereditary relation.

References

1. F. Galton, Personal identification and description. Nature **38**, pp. 201–202 (1888)
2. A.K. Jain, Y. Chen, M. Demirkus, Pores and ridges: fingerprint matching using level 3 features. IEEE Trans. Pattern Anal. Mach. Intell. **29**(1), 15–26 (2007)
3. D.R. Ashbaugh, *Quantitative and Qualitative Friction Ridge Analysis. An Introduction to Basic and Advanced Ridgeology* (1999)
4. F.A. Afsar, M. Arif, M. Hussain, Fingerprint identification and verification system using minutiae matching, in *National Conference on Emerging Technologies* (2004)
5. Feng Zhao, X. Tang, Preprocessing and Postprocessing for skeleton—based fingerprint minutiae extraction. Pattern Recogn. **40**, 1270–1281 (2007)
6. S.A. Sudiro, R.T. Yuwono, Adaptable fingerprint minutiae extraction algorithm based on crossing number method for hardware implementation using FPGA device. Int. J. Comput. Sci. Eng. Inf. Technol. **2**(3) (2012)
7. G. Eckert, S. Muller, T. Wiebesiek, Efficient minutiae based fingerprint matching. *IAPR Conference on Machine Vision and Applications* (2005), pp. 554–557
8. S. Ynag, I.M. Verbauwhede, Secure fingerprint matching technique. WBMA'03 (2003)
9. D. Maio, D. Maltoni, Direct gray –scale minutiae detection in fingerprint. IEEE Trans. Pattern Anal. Mach. Intell. **19**(1), 27–40 (1997)
10. J. de Boer, A.M. Bazen, S.H. Gerez, Indexing fingerprint databases based on multiple features, in *Proceedings of RISC Workshop on Circuits, Systems and Signal Processing* (2001)
11. R. Bansal, P. Sehgal, P. Bedi, Effective morphological extraction of true fingerprint minutiae based on the hit and miss transform. Int. J. Biometrics Bioinf. **4**(2), 71–85 (2010)
12. A. Farina, Z.M. Kovacs-Vajna, A. Leone, Fingerprint minutiae Extraction from Skeletonized binary images. J. Pattern Recogn. Soc. **32**, 877–889 (1999)
13. S. Yoon, J. Feng, A.K. Jain, Altered fingerprint: analysis and detection. IEEE Trans. Pattern Anal. Mach. Intell. **34** (2012)
14. S. Gungadin, Sex determination from fingerprint ridge density. Internet J. Med. Update **2**, 4–7 (2007)
15. O.L. Gorman, Overview of fingerprint verification technologies. Inf. Secur. Tech. Rep. **3**(1), 21–32 (1998)

16. A.K. Jain, Fundamentals of Digital Image Processing. Pearson Education Inc. (1988)
17. A.J. Wills, M. Myers, A cost effective fingerprint recognition system for use with low quality prints and damaged fingertips. Pattern Recogn. **34**(2), 255–271 (2001)
18. L. Lam, S.W. Lee, C.Y. Suen, Thinning methodologies: a comprehensive survey. IEEE Trans. Pattern Anal. Mach. Intell. **14**(9), 869–885 (1992)
19. J. Cheng, J. Tian, Fingerprint enhancement with dyadic scale-space. Pattern Recogn. Lett. **25** (11), 1273–1284 (2004)
20. D. Maltoni, D. Maio, A.K. Jain, S. Prabhakar, *Handbook of Fingerprint Recognition* (Springer Verlag, Berlin, 2003)
21. D. Rutovitz, Pattern Recogn. **129**, 504–530 (1966)
22. L. Lam, S.-W. Lee, C.Y. Suen, Thinning methodologies—a comprehensive survey. IEEE Trans. Pattern Anal. Mach. Intell. **14**(9), 869–885 (1992)

Evaluation of Worst-Case Execution Time of Tasks on Multi-core Processor

R. Suraj, P. Chitra and S. Madumidha

Abstract In hard real-time systems, it is required to compute the worst-case execution time (WCET) of each task that has become a difficult problem. The increasing complexity of modern processor architectures makes achieving this objective more and more challenging. To measure the WCET of a task, it is necessary to develop a framework on multi-core platform considering the nature of a program and shared resources. Path analysis, one of the static-based approaches is used. It is important to take into account the analysis of paths as it calculates the execution time of each basic block with respect to the cache behavior. The WCET estimates of this analysis are performed using SimpleScalar simulator.

Keywords WCET · Static-based approach · SimpleScalar · Cache analysis · Loop analysis

1 Introduction

Real-time systems such as avionics controllers have been widely used in our society. In order to safely run these systems, time predictability plays a major role. Missing deadlines in those applications may result in catastrophic consequences or the quality may get decreased. Consequently, it is important to know the worst-case execution time (WCET) of each task, which provides the basics for hard real-time systems and safety-critical systems.

R. Suraj (✉) · P. Chitra · S. Madumidha
Department of Computer Science and Engineering, Thiagarajar College of Engineering, Madurai 625015, Tamil Nadu, India
e-mail: suraj@tce.edu

P. Chitra
e-mail: pccse@tce.edu

S. Madumidha
e-mail: madumidha20@yahoo.com

© Springer India 2015

L.P. Suresh et al. (eds.), *Artificial Intelligence and Evolutionary Algorithms in Engineering Systems*, Advances in Intelligent Systems and Computing 325,
DOI 10.1007/978-81-322-2135-7_47

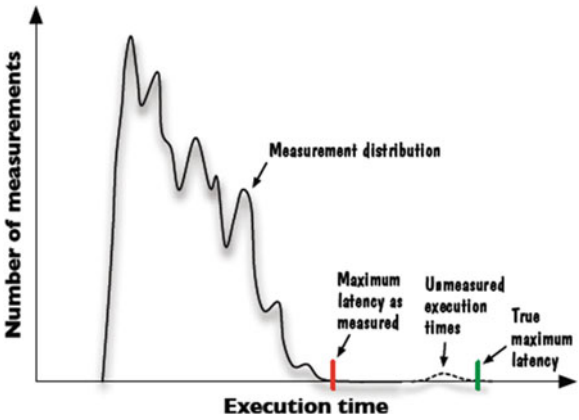

Fig. 1 Execution time for real-time tasks

WCET estimate based on manual measurement alone is generally not feasible as it does not give safe and tight upper bound of the execution time for real-time applications. For applications with complex control flow measurements, it leads to misprediction. As a result, a static analysis technique (i.e., WCET analysis) becomes a challenging approach to find the tight upper bound. Given hardware components with a fixed latency, the WCET of each task could be computed from the partial WCET of each basic block of the task. The control flow graphs (CFGs) generated are used for visualization purpose.

Figure 1 shows the measurements that relate to the possible program execution and timings. The darker curve shows the probability distribution of the execution time. Its minimum and maximum are the best-case execution time (BCET) and WCET, respectively. The gray curve shows the set of actually observed and measured times.

The process of estimating WCET from a program can be divided into cache analysis [1] and loop analysis. The task of the cache analysis is to determine the possible hits and misses in basic blocks. The basic blocks are sequence of instructions that are executed. For each basic block, cache behavior is analyzed. In loop analysis, how many times loop iterates is considered, which is analyzed for calculating the WCET estimates. Finally, in the calculation phase, the WCET estimate is calculated.

This paper is focused on the estimation of the WCET using cache and loop analysis. Such analysis is becoming increasingly a difficult problem due to new features in processors, such as caches and pipelines. Estimating the timing behavior has been the way for approaching this problem, but this may become difficult since the increasing number of processors is a critical problem, as every new processor requires its own timing model.

The main contribution of this paper is that the number of loops in a given task and its hits and misses are analyzed for relatively simple architectures. The proposed method derives the execution time of program by statically analyzing the execution time of the whole program.

2 Related Work

Static analysis methods [2] might produce glorified results if conformist decisions due to the lack of information during the analysis have to be taken. It is avoided in this paper, as the correct configurations are provided at the beginning of the analysis and also depends on the abstract hardware models.

In [3] measurement-based approach, measuring the WCET of programs is presented on the actual hardware and tackles the problem of too many paths by splitting the programs into blocks. But this is a tedious process as it does not know about hardware internal parts. Compared to our work, this method does not produce safe values.

Finding WCET of programs using dynamic method is covered by many groups. Approaches using different algorithms became the most successful ones [4]. But there was no guarantee regarding the safety of the results.

In [5], minimum propagation algorithm that can obtain a safe parametric estimate of the WCET of a task is proposed. But this algorithm is not cost-effective. Compared to our work, it is cost-effective

3 Method Outline

The overall design of the system for estimating the WCET is simplified and shown in Fig. 2. Given the task, i.e., program, it is complied to get an assembly code and executable code. The executable code is disassembled using disassembler program to form an intermediate code. This intermediate code is used for representation of basic blocks. To view the process of the system, CFGs are generated. Finally, to calculate the WCET, the parameters used are basic blocks, loops, hits, and misses. It should be noted that the whole process depends on the basic blocks which is represented using intermediate codes.

In essence, the method works in nine steps:

1. The task is given as an input. The input is in the form of C program.
2. The given C program is converted to an assembly code, object code, and an executable code. These conversions are done by the SimpleScalar GCC compiler.
3. The executable code is converted to an intermediate code by using disassembler program.
4. Combining intermediate code and assembly code forms the basic blocks of a given tasks.
5. When the conversions made from the executable code to an intermediate code, a TCFG is generated.
6. Trace control flow graph (TCFG) generated gives the information about the connection between the nodes.
7. With the help of TCFG, CFGs can be formed.

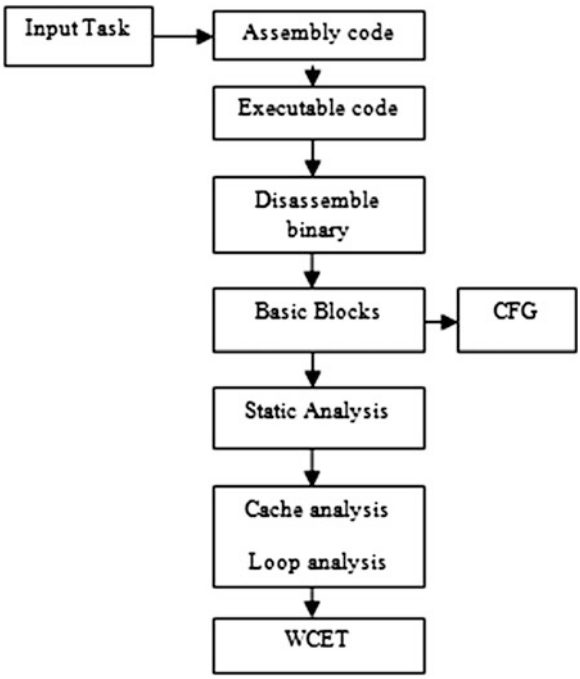

Fig. 2 The overall design of the system

8. The basic blocks obtained are analyzed using static-based approach.
9. The execution times of the each basic block are calculated using MIPS instructions.

3.1 Limitations of the Approach

It should be noted that these functions can be applied only to the "for loop" statements. This is true for the majority of instructions and for most simple architectures. Furthermore, the method is not applicable to systems with buses. Here, only caches are considered for the estimation of WCET.

4 Path Analysis

The task of the analysis is to determine the WCET of individual basic blocks. It is based on defining the execution time of a basic block as the difference between the time instant when the first instructions of the basic block are fetched, and the time instant when the first instruction of any of the successors of the basic blocks is fetched.

4.1 Loop Analysis

In loop analysis, for the given task, the numbers of iterations are found while executing the program. The conditions used here are for loop statements. The iterations are counted and used for the further procedures.

4.2 Cache Analysis

Abstract interpretation approach as described is used for analyzing the caches. Instructions are opened as all-hit (AH), all-miss (AM), persistence (PS), or not-classified (NC).

In cache analysis, with respect to hardware components, the number of hits and misses is obtained through the SimpleScalar. It builds modeling application that simulate real programs running on processors. With the help of SimpleScalar simulator, cache analysis and loop analysis are performed to calculate WCET of a given task.

4.3 Control Flow Graph

In a CFG, each node in the graph represents a basic block, i.e., a straight-line piece of code without any jumps or jump targets; jump targets start a block, and jumps end a block [6]. To visually represent how the work flow and process works, this CFG is represented.

5 Experimental Setup

5.1 Measuring Execution Times

There are several approaches to measure execution time; each has its own advantages and disadvantages. The two widely known approaches are using clock cycle counters and using timers.

A clock cycle counter counts clock cycles from the CPU cores. The advantages are that this approach is exact; time can be measured with the help of fine granularity. It does not disturb the execution of software in any way.

Timers are implemented in different ways: fully dependent in hardware or combination of software. In this paper, clock cycle counters are used.

5.2 Measuring Basic Blocks

To measure the total time taken for the execution of basic blocks, first it is necessary to find the cost of each basic block using Eq. 1. The costs of basic blocks are found using cycles. The cycles are calculated using MIPS instructions [7].

$$\mathrm{BT}_i = n\mathrm{hit}_i + n\mathrm{miss}_i + (\text{Total number of iterations in loop} * \mathrm{BC}_i) \quad (1)$$

where i = 1, 2, …n, number of basic blocks
BT_i total time taken for each block to execute
BC_i block cost
$n\mathrm{hit}_i$ number of hits occurred on ith basic block
$n$miss number of misses occurred on ith basic block.

5.3 Calculating WCET

To estimate WCET, sum of execution times of all the basic blocks (BT) is computed. To calculate the WCET, the formula used is given in Eq. 2.

$$\mathrm{WCET} = \sum_{i=1}^{n} \mathrm{BT}_i \quad (2)$$

6 Results and Discussions

To illustrate the path analysis, an example is shown in Fig. 3.

For the above program, basic blocks are generated. The basic blocks are generated along with cost and loop iterations and shown in Fig. 4.

```
int j=5;
    for (i=0;i<5;i++)
     {
     j+=j;
     }
printf("j=%i", j);
```

Fig. 3 Simple "for loop" program

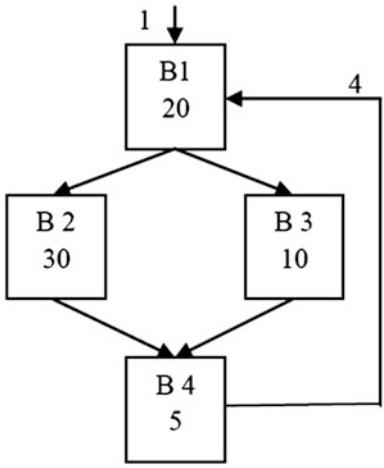

Fig. 4 Basic block for the example code

Here, *B*1, *B*2, *B*3, and *B*4 are the basic block. The above diagram shows the loop that has five iterations. 20, 30, 10, and 5 are the cost of each block, respectively. Therefore, to calculate WCET, the above values are substituted in the Eq. 1.

BT1 = *n*hit1 + *n*miss1 + 100;
BT2 = *n*hit2 + *n*miss2 + 150;
BT3 = *n*hit3 + *n*miss3 + 50;
BT4 = *n*hit4 + *n*miss4 + 25;

The calculated values are listed:

BT1	105
BT2	155
BT3	55
*n*hit1	5
*n*miss1	0
*n*hit2	0
*n*miss2	5
*n*hit3	0
*n*miss3	5
*n*hit4	5
*n*miss4	0

Therefore, to calculate WCET, substitute all the above values in Eq. 2,

$$\begin{aligned} \text{WCET} &= 105 + 155 + 55 + 25 \\ &= 340 \end{aligned}$$

The measurements are measured in microseconds. So to calculate the above program, its takes 340 µs to estimate the WCET.

Table 1 Worst-case execution time of each input program

Benchmark function	CFG size		WCET estimate (μs)
	Nodes	Edges	
binary_search	13	16	37
bsort10	11	15	438
insert_sort	8	11	38

Table 1 shows the WCET of each input program calculated by using the proposed approach. The analysis made is with respect to the basic block and CFG. The timing analysis is done by calculating the instruction cycles in each basic block.

7 Conclusion

To estimate the WCET of a task, static-based approach is used. This approach helps to analyze the behavior of cache and path. SimpleScalar simulator is used to evaluate the precision of the analysis. Experimental results indicate that the path analysis can be used to obtain the worst-case execution of a task, and thus, it is preferable for real-time applications. The main limitation of the approach is that only "for loop" conditions are used for analyzing the WCET of a task. As a future work, it is proposed to validate the analysis using "measurement-based approach."

References

1. J. Segarra, L.C. Aparicio, Improving the WCET computation in the presence of a lockable instruction cache in multitasking real-time systems. Proc. ACM Trans. J. Syst. **57**(7), 695–706 (2011)
2. Y. Ding, W. Zhang, Loop-based instruction prefetching to reduce the worst-case execution time. Proc. IEEE Trans. Comput. **59**(6), 855–864 (2010)
3. P. Radojkovic, S. Girbal, A. Grasset, On the evaluation of the impact of shared resources in multithreaded COTS processors in time-critical environments. Proc. ACM Trans. Archit. Code Optim. **8**(4), 34 (2012)
4. S. Bygde, A. Ermedahl, B. Lisper, An efficient algorithm for parametric WCET calculation. Proc. ACM Trans. J. Syst. Archit. **57**(6), 614–624 (2011)
5. Y. LI et al., Timing analysis of concurrent programs running on shared cache multicores, in *Proceedings of IEEE on Real-time Systems Symposium* (2009)
6. R. Sen, Y.N. Srikant, WCET estimation for executables in the presence of data caches, in *Proceedings of 7th ACM and IEEE International Conference and Embedded Software* (1998), pp. 203–212
7. X. Li, Y. Liang, T. Mitra, A. Roychoudhury, Chronos: a timing analyzer for embedded software. Sci. Comput. Program. **69**, 1–3 (2007)

Back-Emf-Based Sensorless Field-Oriented Control of PMSM Using Neural-Network-Based Controller with a Start-Up Strategy

V.S. Nagarajan, M. Balaji and V. Kamaraj

Abstract This paper describes back-emf-based sensorless field-oriented control (FOC) of permanent magnet synchronous motor (PMSM) of surface-mounted type, employing neural-network-based controller for current and speed control. The dynamic response is improved. Further, rotor position is estimated by back-emf method. To overcome the shortcoming of back-emf-based control in zero and low speed, a start-up strategy is proposed, to predict the initial rotor position. The PMSM drive model is simulated in MATLAB/Simulink environment, and the results show improved dynamic response with a start-up strategy.

Keywords Neural network · Back emf · Rotor position · Startup

1 Introduction

Permanent magnet synchronous motor (PMSM) drives, having numerous advantages over the conventional DC drives and induction drives, is widely being used in the industries for various applications. The importance of PMSM lies in the fact that it has high efficiency, with high torque to inertia ratio and high power density [1].

For the past few years, in order to achieve high-performance control for nonlinear drive system, researchers have explored in depth, the application of soft computing [2] based controller design employing artificial neural network (ANN), fuzzy logic, and ANFIS. Neural networks using parallel and distributed processing units can achieve the functions of system modeling and control for nonlinear systems.

V.S. Nagarajan (✉) · M. Balaji · V. Kamaraj
Department of EEE, SSNCE, Chennai, India
e-mail: snsnaga@gmail.com

M. Balaji
e-mail: balajim@ssn.edu.in

V. Kamaraj
e-mail: kamarajv@ssn.edu.in

© Springer India 2015

L.P. Suresh et al. (eds.), *Artificial Intelligence and Evolutionary Algorithms in Engineering Systems*, Advances in Intelligent Systems and Computing 325,
DOI 10.1007/978-81-322-2135-7_48

There are several unique features, which make them suitable for high-performance drive applications, making the drive system robust, accurate, and insensitive to parameter variations [3]. The unknown nonlinear dynamics of the motor and the load are captured by the ANN [4]. For an instance, a nonlinear mapping between input and output of an electric drive system can be established using ANN without the need of predetermined model [5]. A neural-network-based speed and current controller is proposed for PMSM drive.

In PMSM, the stator excitation needs to be synchronized with the rotor position which necessitates a rotor position sensor or a position estimation algorithm. Sensorless control of PMSM has been explored in detail over the last few decades, because it reduces the cost and complexity, improvising the reliability of the drive system [1]. From the various available literatures employing sensorless control, back-emf-based sensorless control of PMSM is preferred and chosen, since it is employed in many industrial applications due to its control simplicity, robustness, and high machine efficiency. The major drawback in this estimation method is its application in zero- and low-speed regions. To overcome the above drawback, a start-up strategy is proposed and the performance of the drive is analyzed under loaded conditions.

The paper is organized as follows. Section 2 describes about the modeling of PMSM. Section 3 describes about the field-oriented control (FOC) of PMSM using neural-network-based controller. Section 4 describes about the rotor position estimation by back-emf method. Section 5 describes about the start-up strategy for sensorless FOC.

2 Modeling of PMSM

The modeling of PMSM is done using *d–q* transformation [6] as it is advantageous by viewing the machine parameters such as the voltages and currents as DC equivalents from the rotor side, even though an AC supply is provided at the stator side.

The model equations obtained using *d–q* transformations are as follows.

$$D\text{-axis current equation: } \frac{\mathrm{d}}{\mathrm{d}t} i_d = \frac{1}{L_d} v_d - \frac{R}{L_d} i_d + \frac{L_q}{L_d} p\omega_r i_q \tag{1}$$

$$Q\text{-axis current equation: } \frac{\mathrm{d}}{\mathrm{d}t} i_q = \frac{1}{L_q} v_q - \frac{R}{L_q} i_q + \frac{L_d}{L_q} p\omega_r i_d - \frac{\lambda p\omega_r}{L_q} \tag{2}$$

$$\text{Torque equation: } T_e = 1.5\, p[\lambda i_q + (L_d - L_q) i_d i_q] \tag{3}$$

Equation relating torque, inertia, input torque, output torque, and speed:

$$\frac{\mathrm{d}}{\mathrm{d}t}\omega_r = \frac{1}{J}(T_e - F\omega_r - T_m) \tag{4}$$

$$\text{Speed equation: } \frac{\mathrm{d}\theta}{\mathrm{d}t} = \omega_r \tag{5}$$

The inputs to the model are v_d, v_q, and T_m, which are the d- and q-axes voltages and the mechanical torque, respectively. The outputs from the model are i_d , i_q, ω_r, T_e and θ, which are d- and q-axes currents, angular velocity of rotor, electromagnetic torque, and rotor angle, respectively.

3 Field-oriented Control of PMSM Using Neural-network-based Controller

A schematic of the FOC of PMSM, using neural-network-based controller, is shown in Fig. 1. The intention of the speed and current controllers of the PMSM drive is to translate the speed and current errors into a driving voltage signal, to the input of the PMSM. This objective must be met for all load conditions and for any type of disturbances.

An ANN controller is designed to achieve the above prerequisite of the control problem. The structure of the neural-network-based controller consists of an input layer with 5-neurons, a hidden layer with 2-neurons, and an output layer with a single neuron. The tan-sigmoid activation function is used for the input and hidden layers and purelin is used for the output layer [7]. The training data for the neural network are obtained from the fundamental simulation model. The input variables to the ANN are scaled to be within (±1) [8]. The back-propagation algorithm is used by which weights and biases are updated at each sampling instant.

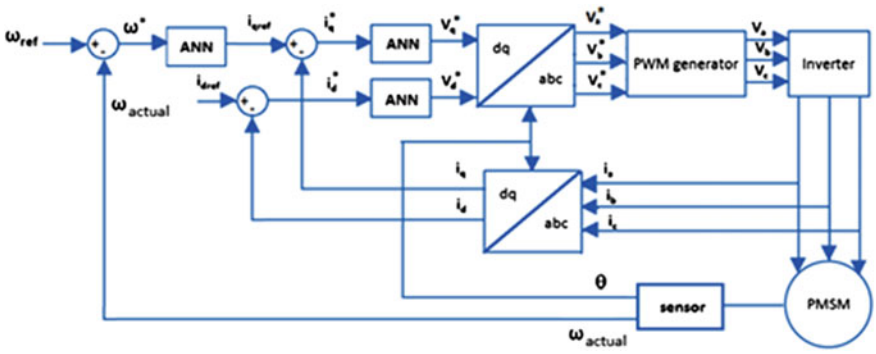

Fig. 1 Field-oriented control of PMSM using neural-network-based controller

Table 1 Machine parameters

Parameter	Value
Number of poles, p	4
Amplitude of flux induced by permanent magnets of rotor in stator phases, λ	0.175 Wb
Resistance of stator windings, R	2.875 Ω
D- and q-axes inductances, L_d and L_q	8.5 mH
Inertia, J	0.0008 kg/m^2
Friction coefficient, F	0.001 Nms

Under the FOC scheme, decoupling of torque- and flux-producing components of the stator current is done, so that control of torque and flux separately, is feasible as in the case of DC motors [9]. Usually, the d-axis current reference is made zero in order to approximately eradicate the couplings between angular velocity and currents. With properly designed current controllers, the output satisfies $i_d^* = i_d$. Then, the d-axis flux linkage is unchanging and the developed torque is then proportional to q-axis current, which is determined by closed-loop control.

The machine parameters chosen for the simulation is shown in Table 1.

The speed response of PMSM is shown in Fig. 2 for a reference speed of N = 2,000 rpm. It is seen that the speed of the PMSM settles at 2,000 rpm at 0.02 s.

From the speed response, the transient response parameters obtained are peak overshoot which is 4.94 %, settling time which is 0.02 s and speed ripple which is 0.05 %. Therefore, the dynamic response is improvised by the neural-network-based controller.

The torque response of PMSM is shown in Fig. 3. The load applied to the PMSM is a step load with a magnitude of 0 Nm from t = 0 to 0.02 s and a magnitude of 1 Nm from t = 0.02 s. It is seen that a torque output of 1 Nm is obtained from t = 0.02 s.

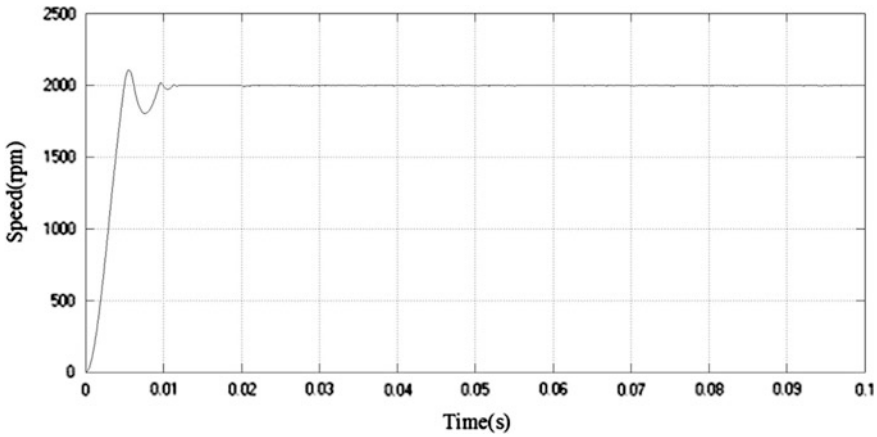

Fig. 2 Speed response

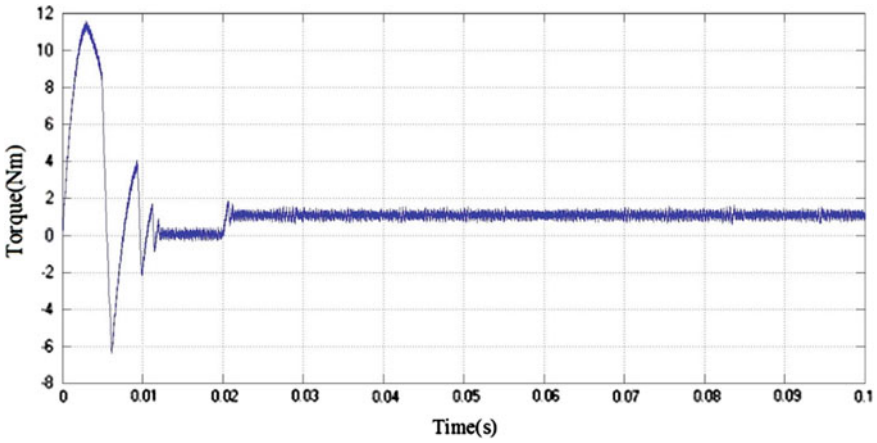

Fig. 3 Torque response

4 Rotor Position Estimation by Back-emf Method

The choice of angular-position and speed sensors and the consequent choice of the related signal conditioning circuit are not much influenced by the electrical-drive rated power. Then, the influence of the aforementioned sensor's cost grows up in percentage with respect to the electrical-drive comprehensive cost, when the rated power of an electrical machine is small or fractional [10]. A type of sensorless speed control of PMSM is based on the strategy of estimating the rotor position by analyzing the motor-induced back-electromotive force (emf) voltage, using a mathematical motor model [11]. By this back-emf method, the signals to be sensed are the currents i_α and i_β and voltages u_α and u_β. It eliminates the high cost incurred by the usage of a speed sensor with high precision and noise immunity. It therefore becomes a cost-effective and simple method that can be easily implemented.

The back emf can be estimated [12] as follows:

$$\text{Back emf equations: } \hat{e}_{s\alpha} = -u_\alpha + Ri_\alpha + L_d i_\alpha \tag{6}$$

$$\hat{e}_{s\beta} = u_\beta - Ri_\beta - L_q i_\beta \tag{7}$$

$$\text{Rotor position estimation equation: } \theta_r = \tan^{-1}\left(\frac{\hat{e}_{s\alpha}}{\hat{e}_{s\beta}}\right) \tag{8}$$

$$\text{Speed estimation equation: } \omega_r = \frac{\mathrm{d}\theta_r}{\mathrm{d}t} \tag{9}$$

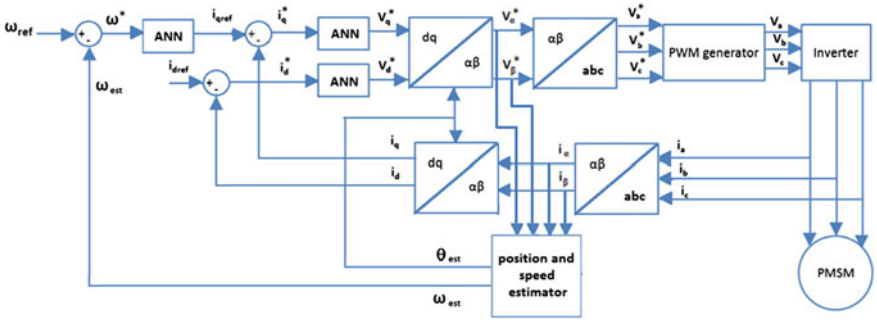

Fig. 4 Sensorless field-oriented control of PMSM using neural-network-based controller with rotor position estimation by back-emf method

The functional block diagram representing the sensorless FOC of PMSM using neural-network-based controller with rotor position estimation by back-emf method is shown in Fig. 4.

The estimated rotor position and actual rotor position for N = 2,000 rpm is shown in Fig. 5. It is seen that from t = 0 to 0.02 s, the rotor position estimation is not appropriately done due to the absence of back emf at the starting conditions. From t = 0.021 s, the rotor position is estimated correctly by the back-emf equations.

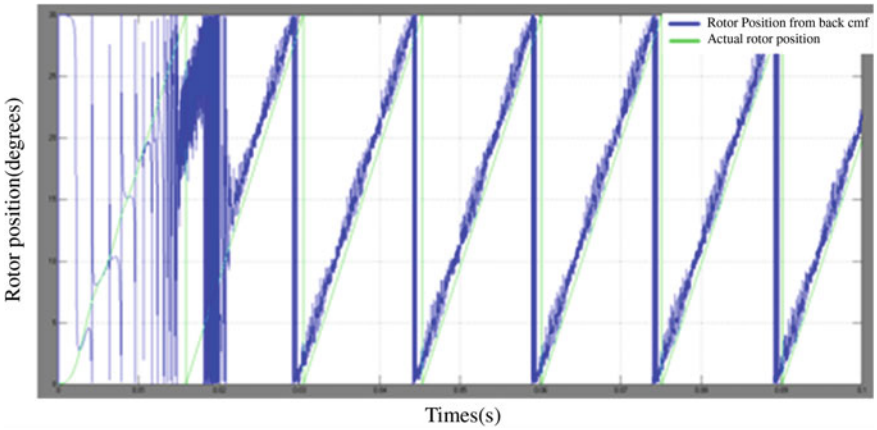

Fig. 5 Estimated rotor position versus actual rotor position

5 Start-up Strategy for Sensorless Field-oriented Control

This back-emf-based position estimation algorithm has good performance in the medium-to-high-speed range [13]. In zero- and low-speed regions, the back emf is nearly zero and hence cannot be accurately detected. Though there are various methods such as extended Kalman filter [14], high-frequency signal-injection method [15] and evaluation using drive stiffness have been discussed in the literature, the implementation of methods involves complex processing and analysis of signals and the cost involved in the implementation is high. A simple start-up is sufficient, wherein the rotor position can be predicted by integrating the reference-speed input when the back-emf algorithm fails in detection of rotor position. Suitable transition can be made by switching operations. This method is applicable only during initial conditions, when the rotor position detection is unable to be

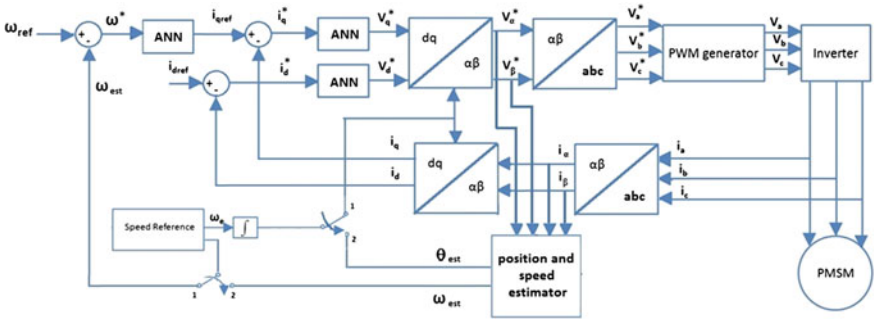

Fig. 6 Sensorless field-oriented control of PMSM using neural-network-based controller with rotor position estimation by back-emf method with start-up strategy

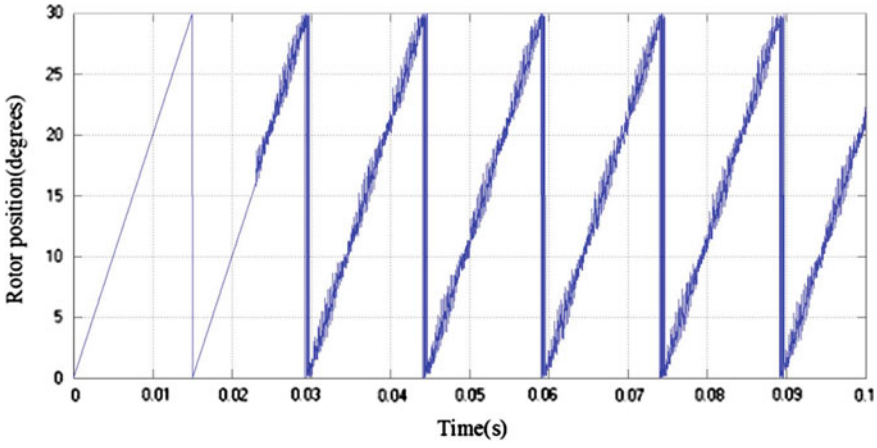

Fig. 7 Rotor position from start-up strategy switched to rotor position estimated from back emf

detected correctly (i.e., at start-up). The functional block diagram representing the sensorless FOC of PMSM using neural-network-based controller with rotor position estimation by back-emf method with start-up strategy is shown in Fig. 6.

The estimated rotor position for N = 2,000 rpm with the start-up strategy is shown in Fig. 7. It is seen that from $t = 0$ to = 0.023 s, the rotor position is estimated by the start-up strategy and from $t = 0.024$ s, the rotor position is estimated by the back-emf equations.

6 Conclusion

In this paper, neural-network-based controller is employed for FOC of PMSM. The controller is robust to load variations, having less peak overshoot, faster settling time and minimal steady-state error. Back-emf method was employed to estimate the rotor position, which is proved to be effective after a certain period of starting of PMSM drive. To overcome the difficulty posed by the back-emf method, a start-up strategy is employed which is used to predict the initial rotor position during starting condition until a particular time after which back-emf method takes over. Thus, the method of rotor position estimation has been proved to advantageous. Further studies can be carried out to reduce the ripple in speed and torque output. The effect of start-up method on various other parameters can be further analyzed. Hybrid control structures can be introduced in the control system in order to improvise the transient and steady-state conditions.

References

1. R. Krishnan, *Electric Motor Drives: Modeling, Analysis, and Control* (Prentice Hall, Englewood Cliffs, 2001)
2. S. Rajasekaran, G.A. Vijayalakshmi Pai, *Neural Networks, Fuzzy logic and Genetic algorithms: Synthesis and Applications* (2003)
3. M.A. Rahman, M.A. Hoque, On-line adaptive artificial neural network based vector control of PMSM. IEEE Trans. Energy Convers. **13**(4), 311–318 (1998)
4. R. kumar, R.A. Gupta, A.K. Bansal, Identification and control of PMSM using artificial neural network, in *IEEE International Symposium on Industrial Electronics, ISIE* (2007), pp. 30–35
5. D.H. Nguyen, B. Widrow, Neural network for self learning control systems. IEEE Control Syst. Mag. **10**(3), 31–35 (1990)
6. P. Pillay, R. Krishnan, Modeling of permanent magnet motor drives. Ind. Electron. IEEE Trans. Ind. Electron. **35**, 537–541 (1988)
7. Kh.I. Saleh, M.A. Badr, A.S. Elwer, S. Wahsh, Analysis of controlled permanent magnet synchronous motor using artificial neural network. Fifth Int. Conf. Electr. Mach. Syst. ICEMS **2**, 791–795 (2001)
8. C. Busca, *Open Loop Low Speed Control for PMSM in High Dynamic Applications* (2012)
9. F.G. Rosario, C. Rando, G.R. Galluzzo, Back EMF sensorless-control algorithm for high-dynamic performance PMSM. IEEE Trans. Ind. Electron. **57**(6), 2092–2100 (2010)

10. P. Hutterer, H. Grabner, S. Silber, W. Amrhein, W. Schaefer, A study on systematic errors concerning rotor position estimation of PMSM based on back EMF voltage observation, in *Electric Machines and Drives Conference, 2009. IEMDC '09. IEEE International* (2009), pp. 1393–1400
11. H. Zhou, M. Kuang, J. Wu, A rotor position and speed estimation method for sensorless control of permanent magnetic synchronous motor, in 3rd *IEEE International Symposium on Power Electronics for Distributed Generation Systems PEDG* (2012), pp. 211–215
12. Zihui Wang, K. Lu, F. Blaabjerg, A Simple startup strategy based on current regulation for back-EMF-based sensorless control of PMSM. IEEE Trans. Power Electron. **27**(8), 3817–3825 (2012)
13. Z. Zheng, Y. Li, M. Fadel, Sensorless control of PMSM based on extended kalman filter, in *Proceedings of the European Conference on Power Electronics and Applications* (2007)
14. O. Wallmark, L. Harnefors, Sensorless control of salient PMSM drives in the transition region. IEEE Trans. Ind. Electron. **53**(4), 1179–1187 (2006)
15. R.W. Hejny, R.D. Lorentz, Evaluating the practical low-speed limits for back-EMF tracking-based sensorless speed control using drive stiffness as a key metric. IEEE Trans. Ind. Electron. **47**(3), 1337–1343 (2011)

FPGA-based Intelligent Control of AC Motors

Valantina Stephen and L Padma Suresh

Abstract The most commonly used controller in the industry field is the proportional-plus-integral (PI) controller, which requires a mathematical model of the system. Fuzzy logic controller (FLC) provides an alternative to conventional PI controller, especially when the available system models are inexact or unavailable. Also, rapid advances in digital technologies have given designers the option of implementing controllers using field programmable gate array (FPGA) which depends on parallel programming. This method has many advantages over classical microprocessors. In this research work, a FLC, which is fabricated on modern FPGA card (Spartan-3A, Xilinx Company), is proposed to implement a prototype of a speed controller for three-phase induction motor (squirrel cage type). The FLC and the PWM inverter strategies which have been built in FPGA appeared fast speed response and good stability in controlling the three-phase induction motor. For comparison purpose, a conventional PI controller has been implemented in the same FPGA card to examine the performance of the FLC. These controllers have been tested using MATLAB/Simulink program under various reference speeds. The designed FPGA-based closed-loop FLC's performance is weighed against with that of a conventional PI controller. The system has been simulated in MATLAB/Simulink, and the results have been attached. The simulation and experimental results obtained using a FPGA-based conventional PI controller and the FPGA-based FLC have been compared in terms of settling time, and it has been found out that the proposed FPGA-based FLC shows a better performance than the conventional PI controller.

V. Stephen (✉)
Department of Electronics and Communication Engineering,
Loyola Institute of Technology and Science, Thovalai, Kanyakumari District,
Tamilnadu, India
e-mail: valantina2000@yahoo.com

L Padma Suresh
Electrical and Electronics Engineering, Noorul Islam Centre for Higher Education,
Kumaracoil, Tamilnadu, India

© Springer India 2015

L.P. Suresh et al. (eds.), *Artificial Intelligence and Evolutionary Algorithms in Engineering Systems*, Advances in Intelligent Systems and Computing 325,
DOI 10.1007/978-81-322-2135-7_49

Keywords Field programmable gate array (FPGA) · Sinusoidal PWM (SPWM) · 60 degrees PWM · Random frequency PWM (RFPWM) · Third harmonic injection (THI) PWM · Inverter · Total harmonic distortion (THD) · Harmonic spread factor (HSF) · VHSIC hardware description language (VHDL)

1 Introduction

Solid state power devices have reached a state where PWM inverter-fed induction motor drives have become more popular in many industrial applications [1]. In solid state power devices, many technologies are being improved including the pulse width modulation since it is important for the drive performance. Several pulse width modulation techniques share a common aim to reduce the amount of harmonics in general or to eliminate some of them [2]. The significant feature of a random PWM inverter is that the acoustic noise can be reduced since the output harmonic spectra are dispersed and continuously distributed. Out of the existing random PWM schemes, in random PWM switching, the triangular wave is replaced by random PWM signal in SPWM, but the performance will greatly degrade when the modulation index is low (Kim et al. 2009).

Each of the above-mentioned PWM methods possesses different patterns of pulse width modulation and harmonic components [3, 4]. Although sinusoidal pulse width modulation has many advantages, its foremost disadvantage is the limitation of fundamental magnitude which can be overcome through over modulation by increasing duty cycle [5]. But when this method is operated beyond a particular modulator voltage, it introduces lower order harmonics. In order to minimize unwanted harmonic content, i.e., a THD, a number of PWM techniques have been developed to reduce THD, HSF, and switching losses [6].

For real-time control of power inverters, very large-scale integrated circuits (VLSI) are used because of its extensive availability. Field programmable gate array (FPGA) offers the most preferred way of designing PWM signals for power inverter applications. When a design is implemented in FPGA, they are designed in such a way that they can be easily modified if any need arises in future. We have to just change the interconnection between the logic blocks in FPGA. This feature of reprogramming capability is an added advantage of FPGA. Also, using FPGA, we can implement design within a short time. Thus, FPGA is the best way of designing digital PWM generators. Also, implementation of FPGA-based digital control schemes proves to be less costly, and hence, they are economically suitable for small designs [19]. In recent years, fuzzy logic control has been suggested as an alternative approach to conventional process control techniques. Since the first paper on fuzzy sets was published, fuzzy logic control has attracted great attention from both the academic and industrial communities. Much progress has been made in successfully applying FLC in industrial control systems. FLC techniques represent means of both collecting human knowledge and expertise and dealing with

uncertainties in the process of control. They have a number of advantages. Although fuzzy logic control is not the solution for all problems, it can play an important role in making automated processes more intelligent.

Hardware implementation of the controller can be achieved in a number of ways to create new products. The most popular method of implementing fuzzy controller is using a general purpose microprocessor or microcontroller. Generally, an 8-bit microprocessor can handle most of the necessary computations. Microprocessor-based controllers are more economical, but often face difficulties in dealing with control systems that require high processing and input/output handling speeds. Rapid advances in digital technologies have given designers the option of implementing a controller on a variety of programmable logic device (PLD), FPGA, etc. Both open-loop and closed-loop control of the speed of an AC induction motor can be implemented based on the constant V/Hz principle. Open-loop speed control is used when accuracy in speed response is not a concern such as in heating, ventilation and air conditioning (HVAC), fan and blower applications. In this case, the supply frequency is determined based on the desired speed and on the assumption that the motor will roughly follow its synchronous speed. The error in speed resulted from the slip of the motor is considered acceptable.

2 Materials and Methods

2.1 Generation of Pulses Using FPGA

2.1.1 Sine Wave Generation

The first and foremost aspect in generating sine PWM is to generate voltage-controlled oscillations. The regular sampling has certain advantages when implemented using digital techniques [16]. Let the clock frequency be 50 MHz which is the set frequency that the sine wave generator receives. It is quite a common thing to generate sine wave of set frequency using the governing equation given by, $V(t) = Vm \sin 2\pi ft$.

But in digital logic, the problem arises in describing the limits for t, the time for which the wave has to be generated and the period of oscillations. Hence, the methodology we have adopted for creating the lookup table is that the instantaneous values of sinusoidal oscillations are fragmented to 200 values at equal intervals. These values are stored as an integer array named as memory. Further, instead of the factor $2\pi ft$, it is multiplied with an offset value and an integer which would in turn point to the value stored in the sine wave array.

The sine array is incremented in steps of one so that to represent a half cycle of the oscillation corresponding to 360°, it is essential to make 199 increments of the counter. Since we are in need of three-phase sine wave, we need to have three sine wave generators, whose outputs are displaced by 120° each. That means, the output of the second generator must start from the initial value of zero when the first

generator has swept an angle of 120°. Similarly, the third and second generators should follow the same fashion.

This is achieved by correlating the relation between the angular displacement and the sine array. Initially, the output of first sine wave generator alone is activated, and the remaining two are maintained at zero output condition. We have 360° of the sine wave corresponds to 199 increments of the counter. Hence, 120° of the wave would correspond to

$$\frac{199}{360}(120) = 66 \tag{1}$$

Therefore, at the 66th increment of the sine array of first generator, the output of second generator is activated. Similarly, at the 66th increment of the sine counter of the second generator, the output of third one is activated. Once they are activated in this manner, then throughout the process, they are all displaced by 120° or 66 counts.

2.1.2 Ramp Wave Generation

The high-frequency carrier chosen for comparison is of ramp in nature. This is also digitally generated. The frequency of the ramp is chosen as a high value of 5 kHz or any value greater than this can be chosen. Unlike the sine wave, the frequency of the ramp is maintained constant. This carrier frequency would be the deciding factor of the output frequency.

2.1.3 Generation of PWM

Pulse width modulation is achieved by comparing the triangular wave and the sine wave. The instantaneous value of the sine wave is compared with the corresponding triangular wave in a comparator. The comparator provides active high output whenever the magnitude of the sine wave is greater than that of the ramp; otherwise, it is low.

This pulse width modulation technique is described by VHDL and simulated using modelsim environment. Since this method is flexible, an important advantage of VHDL is that it is technology independent [17]. The pulses that are obtained as output are fed to the three-phase bridge inverter using HDL co-simulation block. Here, a three-phase inverter is controlled by SPWM, RFPWM, THI-PWM, and Hybrid RF-THIPWM. Powergui block in the circuit measures the fundamental voltage, THD, and HSF for various values of modulation index ranging from 0.2 to 1.2.

The experimental setup is based on the 0.75 kW three-phase induction motor drive and is shown in the Fig. 1. In order to produce the inverter PWM pulses using SPWM, 60 degrees PWM, RFPWM and 60 degrees PWM, a Spartan FPGA

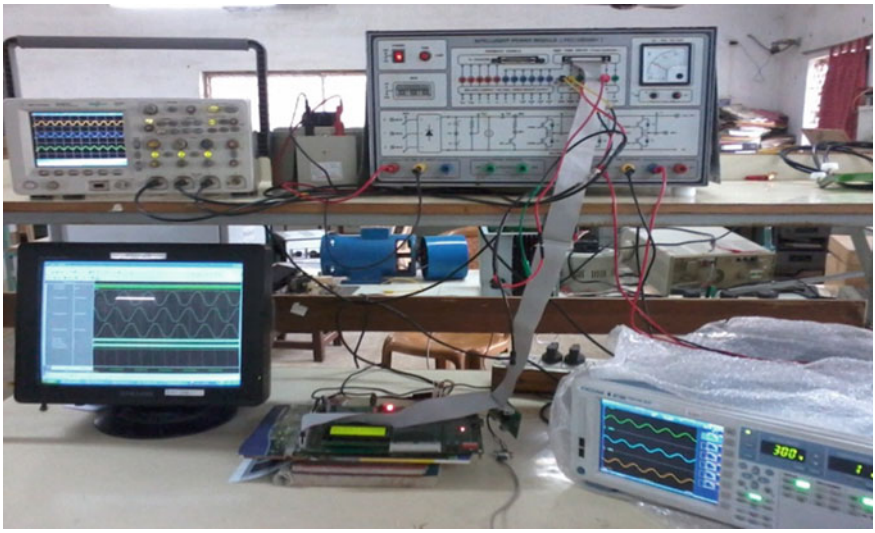

Fig. 1 Diagram of the experimental assembly

Table 1 Experimental parameters

Fundamental frequency	f = 50 Hz
Motor	Three-phase squirrel cage induction motor (0.75 kW)
Rated current	1.8 A
Rated speed	1,440 rpm

processor is used. Table 1 summarizes the experimental parameters. The inverter is fed by a voltage of 300 V with the help of an autotransformer and is connected to the induction motor with the help of a three-phase inverter.

Speed control of induction motor is done by both fuzzy logic and PI controller using a Hybrid RF-THIPWM inverter, and the settling time is compared in both the cases. An increase in the number of applications requiring variable speed drives instigated the need for stable and versatile electrical machine and control scheme. Figure 2 illustrates the general principle of the speed PI/fuzzy control loop.

The actual rotor speed is compared with its reference value, Omega_Required, and the error is processed through a controller, a PI and fuzzy logic, and a limiter to obtain the slip speed command, ω_{s1}^{*}. The limiter ensures that the slip speed command is within the maximum allowable slip speed of the induction motor. The slip speed command is added to electrical rotor speed to obtain the stator frequency command. Thereafter, the stator frequency command is processed as in an open-loop drive. Kdc is the constant of proportionality between the DC load voltage and the stator frequency.

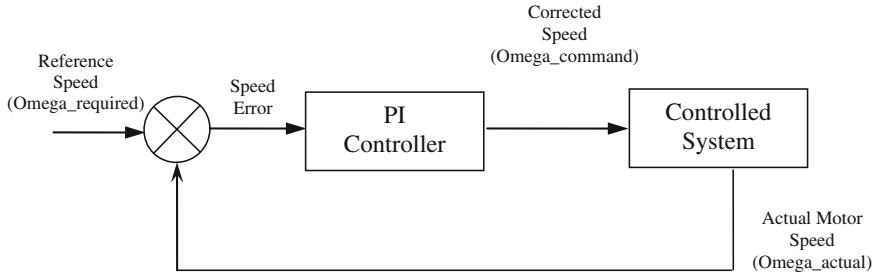

Fig. 2 Control system using closed-loop operation

In the closed-loop induction motor drive, the limits on the slip speed, offset voltage, and reference speed are externally adjustable variables. This external adjustment allows the tuning and matching of the induction motor to the inverter and the tailoring of its characteristics to match the load requirements.

3 Results and Discussion

For the purpose of testing the advantages of the random PWM, it will be compared with the most commonly used PWM techniques such as SPWM, 60 degrees PWM and THIPWM. To compare different PWM techniques, a set of parameters must be defined to measure them. The parameters adopted are as follows:

3.1 Analysis of Fundamental Voltage and Total Harmonic Distortion

The fundamental voltage is varied as a function of modulation index ranging from 0.2 to 1.2 for all the different types of PWM strategies. When compared to SPWM, 60 degrees PWM, RFPWM and THI-PWM, the fundamental component value is higher in Hybrid RF-THIPWM for the entire range of modulation index. The impact is much more significant in the higher values of modulation index. The important sources of distortion in power electronic systems are as follows: the type of modulation technique employed and the nonlinearities in the output voltage. Total harmonic distortion (THD) is a standard measure used to characterize the distortion in the output. Waveform of practical inverter is non-sinusoidal and contains certain harmonics. For low- and medium-power application, square wave or quasi square waveform voltage may be acceptable, but for high-power application, sinusoidal waveform with low distortion is required. Harmonic content present in the output of a DC–AC inverter can be eliminated either by a filter circuit or by employing pulse width modulation (PWM) techniques. Use of filter has the

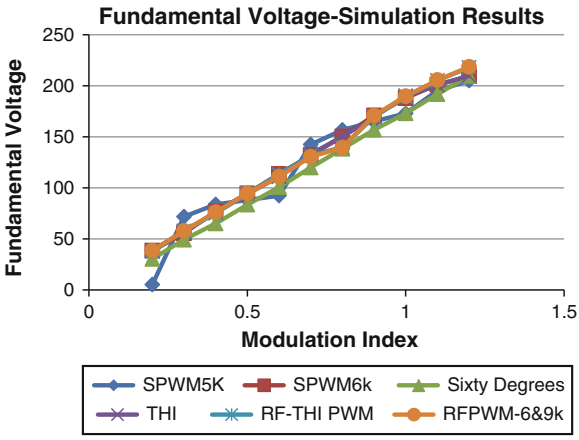

Fig. 3 Comparison of simulated output of different control strategies

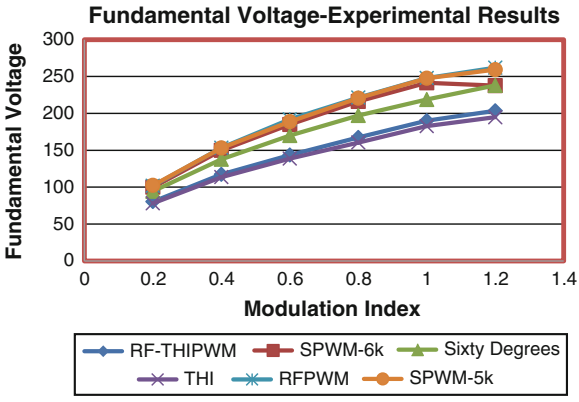

Fig. 4 Variation of fundamental voltage for different control strategies

disadvantage of large size and cost, whereas use of PWM techniques reduces the filter requirement to a minimum or to zero depending on the type of application. Along with this, linearity is retained between the fundamental voltage and modulation index as shown in Figs. 3 and 4. Figures 5 and 6 illustrate typical simulated and experimental results with their respective harmonic spectra for the PWM strategies considered in previous sections. It is found that when the THD is lower, the more the signal approximates a more perfect sine wave since the contribution from harmonics will be very weak. The experimental results are obtained using a Xilinx Spartan 3A Spartan Trainer kit for the PWM signal generation.

The fundamental voltage and total harmonic distortion for all the PWM strategies for a modulation index ranging from 0.2 to 1.2 as well as the line to line voltage, line to neutral voltage, line to line current, and harmonic graph are obtained by a precision power analyzer. Finally, it has been found out that the Hybrid RF-THIPWM method produces a very significant increase in the fundamental term

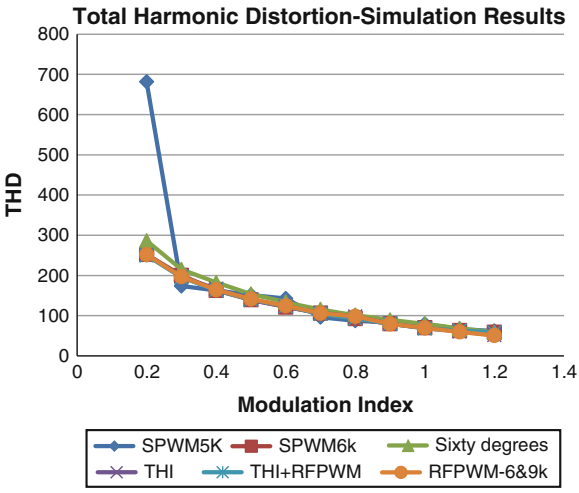

Fig. 5 Variation of THD for different control strategies simulation

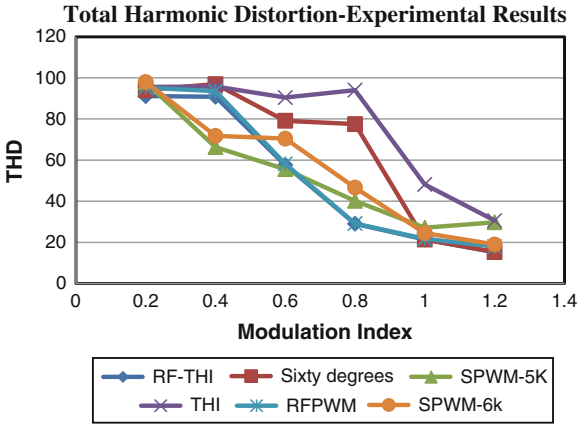

Fig. 6 Variation of THD for different control strategies

of the output voltage as well as a substantial decrease in harmonics thereby reducing the heat of the motor which is connected to the inverter.

All the five methods are applied to a FPGA-based 0.75 kW three-phase induction motor drive under the condition of fundamental frequency f = 50 Hz and with a minimum carrier frequency of either 6 kHz and maximum carrier frequency of 9 kHz. The simulation and experimental results reveal that the Hybrid RF-THIPWM reduces the harmonic spectra significantly.

3.2 Harmonic Spread Factor

For evaluating the PWM techniques, a simple indicator of the quality of the voltage spectra would be useful. Harmonic spread factor is one of the deciding factors to

indicate noise generation in the motor. The harmonic spread factor can be calculated for evaluating the quality of voltage spectra of inverters using the formula,

$$\mathrm{HSF} = \sqrt{\frac{1}{N}\sum_{j=2}^{N}\left(H_j - H_0\right)^2} \tag{2}$$

where

N Total number of frequency components considered
H_j Amplitude of the jth component
H_0 Average value of all components given by

$$H_0 = \frac{1}{N}\sum_{j=2}^{N} H_j \tag{3}$$

The harmonic spread factor quantifies the spread spectra effect of the Hybrid RF-THIPWM scheme and it should be small. For ideally flat spectra of white noise, the harmonic spread factor would be zero. The HSF of the Hybrid RF-THIPWM reaches 1.032 during experimentation and 3.598 during simulation which is lower than those of the other methods. While comparing these results, we can observe that harmonic spectra are reduced significantly when using Hybrid RF-THIPWM technique. So it is clear that the Hybrid RF-THIPWM strategy results in a significant improvement in acoustic noise reduction relative to other strategies.

The results show that Hybrid RF-THIPWM possesses an excellent harmonic spectrum spreading capability (HSF) as shown in Figs. 7 and 8, an improved fundamental voltage and total harmonic distortion when compared with the other PWM schemes. This thesis presents a methodology for implementation of a

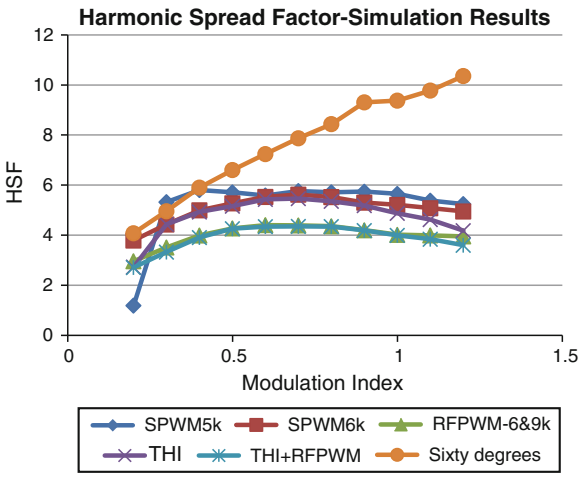

Fig. 7 Variation of HSF for different control strategies

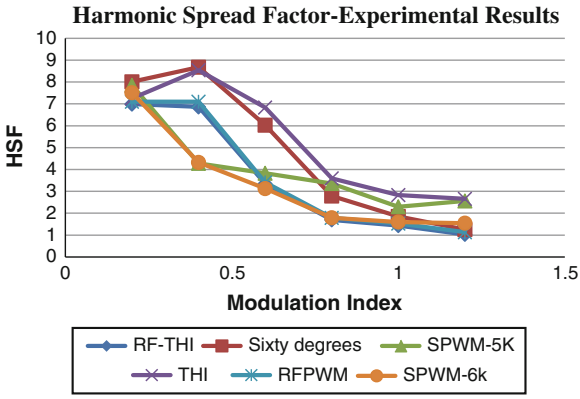

Fig. 8 Variation of HSF for different control strategies

rule-based fuzzy logic controller (FLC) and a conventional controller applied to a closed-loop Volts/Hz induction motor speed control using Hybrid RF-THIPWM.

3.3 Closed-loop PI and Fuzzy Controller

A comparison of different types of PWM strategies has been presented in the form of fundamental voltage, THD, and HSF characteristics. Finally, Hybrid RF-THIPWM produces significantly reduced THDs and HSFs and higher fundamental voltage. The Hybrid RF-THIPWM fed inverter is designed for an input voltage of 300 V in order to supply a 0.75 kW induction motor. After confirming the correctness of the proposed Hybrid RF-THIPWM controller's VHDL codes by simulation, the codes are directly applied to the FGPA-based induction motor drive system. Employing FPGA to realize PWM strategies provides advantages such as simple hardware and software design and high switching frequency. The main focus is to develop a FPGA-based FLC so as to achieve precision in control. The controller attempts to attain a certain level of human intelligence by utilizing the linguistic variables instead of numerical ones. Its main advantage is that it completely avoids the mathematical computations, which relieves the designer from using cumbersome techniques. All FLC needs is a set of if-then rules and a knowledge base, which can be easily provided by the programmer. Hence, it becomes simpler to implement fuzzy logic for the design of controller in electric drive systems. In order to evaluate the merits of the fuzzy logic techniques compared to a classical approach, the induction motor was implemented first using PI controller and then using fuzzy logic.

The frequency voltage and supply voltage of the induction motor are varied such that it operates at steady state at the desired speed. In the scalar control method, both the input and output commands are speed, unlike the vector control mode where it is torque/flux and reference current. Even though vector control drives provide excellent performance in terms of dynamic speed regulation, implementation of the

same is tedious owing to online coordinate transformations that convert line currents into two axis representation and vice versa. Hence, the use of scalar control method is used in this case. The use of speed as reference signal is justified as the output of the system is speed, and our aim is to control the speed of the induction motor. A quadrature position encoder attached to the shaft of the induction motor provides the current speed of the motor which is compared with the reference speed, thus providing us with the speed error.

A feedback mechanism is used to provide the quality of automation to the control system. The information about the instantaneous state of the output is fed back to the input which in turn is used to revise fuzzification and also to achieve a desired output. Change of error, that is, the derivative of speed error is computed and both error and change of error is fed to the fuzzifier for fuzzification. The inference system then processes these two fuzzy inputs using the fuzzy control rules and the database which is defined by the programmer based on the chosen membership function and fuzzy rule table to give an output fuzzy variable. The fuzzy output thus obtained is defuzzified by the defuzzifier to give a crisp value, i.e., change of control. This in turn forms the input for the two-level three-phase inverter. The performance of the fuzzy controller and conventional PI controller in terms of settling time is shown for variation in reference speed, which demonstrates the improved regulation with smaller value of settling time as shown in Tables 2 and 3 show the settling time for different values of reference speed. The induction motor using Xilinx Spartsing a dq axis theory. The designed FLC's performance is weighed against with that of a PI controller using FPGA.

Table 2 Performance indicators for pi and fuzzy logic controllers

Controller			Metrics settling time	
			Simulation (s)	Experimental (s)
Proportional integral	K_p	K_i		
	0.1	0.01	4.4	8.35
	1	0.1	0.5	1.69
	1	0.5	0.72	1.2
	1	1	0.45	3.76
Fuzzy logic controller			0.15	1.13

Table 3 Performance indicators for change in reference speed

Reference speed (RPM)	Metrics settling time			
	PI controller		Fuzzy logic	
	Simulation (s)	Experiment (s)	Simulation (s)	Experiment (s)
1,500	0.45	3.76	0.15	1.13
1,000	3.5	5.6	1.45	3.26
500	6	8.67	2.5	4.95

4 Conclusions

- A comparative study on PWM techniques such as SPWM, 60 degrees PWM, third harmonic injection PWM, random PWM, and hybrid RF-THIPWM for a three-phase inverter was done using FPGA aiming at the improvement in fundamental voltage, total harmonic distortion, and harmonic spread factor. The methods were applied to a 1 hp three-phase induction motor drive, and it has been shown that the Hybrid RF-THIPWM strategy produces a very significant increase in the fundamental term of the output voltage as well as a substantial decrease in total harmonic distortion and harmonic spread factor for varying modulation index.
- Using Hybrid RF-THIPWM-based inverter, a FLC has been developed for volts/hertz control of induction motor for a practical 0.75 kW three-phase induction motor using Xilinx Spartan 3A FPGA processor. The performance of the fuzzy controller and conventional PI controller in terms of settling time is shown for various reference speeds, which demonstrates the improved regulation with lesser value of settling time. Both the simulation and experimental results confirmed that the fuzzy logic approach is feasible and can be an interesting alternative to conventional control.

References

1. S. Mekhilef, N.A. Rahim, Xilinx FPGA three phase PWM inverter and its application for utility connected PV system, in *IEEE Proceedings* (2002), pp. 2079–2082
2. M.J. Meco-Gutiérrez, A. Ruiz Gonzalez, F. Vargas Merino, J.R. Heredia-Larrubia, Reduction in induction motor heating fed by a new PWM technique, IEEE Trans. Ind. Electron **57**(1), 228–236
3. M.A. Boost, P.D. Ziogas, State-of-art-carrier PWM techniques: A critical evaluation. IEEE Trans. Ind. Appl. **24**, 271–280 (1988)
4. J. Holtz, Pulse Width Modulation-A survey. IEEE Trans. Ind. Electron. **39**, 410–420 (1992)
5. R.J. Kerkman, D. Leggate, B.J. Seibel, T.M. Rowan, Operation of PWM voltage source-inverters in the over modulation region. IEEE Trans. Ind. Electron. **43**, 132–141 (1996)
6. S. Jeevananthan, P. Dananjayan, S. Venkatesan, A novel modified carrier PWM switching strategy for single-phase full-bridge inverter. Iran. J. Electr. Comp. Eng. **4**, 101–108 (2005)
7. N.D. Patel, U.K. Madiwala, A bit-stream-based PWM technique for sine-wave generation, IEEE Trans. Ind. Electron. **56**, 2530–2539 (2009)
8. L.C.Y. Huang, Y.Y. Tzou, Design and Implementation of an FPGA-Based Control IC for the Single-Phase PWM Inverter Used in UPS (1997), pp 344–349
9. P.N. Enjeti, P.D. Ziogas, J.F. Lindsay, Programmed PWM techniques to eliminate harmonics, IEEE Trans. Ind. Electron. **26,** 302–316 (1990)
10. Y.M. Chen, Y.M. Cheng, Modified PWM control for the DC-AC inverter with a non-constant voltage source vol. 2 (1999), pp. 938–941
11. A. Kawamura, T. Haneyoshi, R.G. Hoft, Deadbeat controlled PWM inverter with parameter estimation using only voltage sensor. IEEE Trans. Power Electron. **3**, 576–583 (1988)
12. H.Hussin, A. Saparon, M. Muhamad, M.D. Risin, Sinusoidal pulse width modulation (SPWM) design and implementation by focussing on reducing harmonic content, vol. 125 (2010), pp. 620–623

13. B. Farid, O. Amar, A Study of controlled PWM inverters. Eur. J. Sci. Res. **32**(1), 77–87 (2009)
14. J. Deepthi, S.N. Saxena, Study of variation of THD in a diode clamped multilevel inverter with respect to modulation index and control strategy, in *2nd International Conference and workshop on Emerging Trends in Technology. International Journal of Computer Applications* (2011), pp. 37–42
15. B. Huo, A.M. Trzynadlowski, Random pulse width PWM modulator for inverter-fed induction motor based on the TMS320F240 DSP controller (2006)
16. T.C. Green, M. Mirkazemi, J.K. Good Fellow, Programmable gate-arrays and semi-custom designs for sinusoidal and current regulated PWM, in *ASIC Technology for power electronics equipment. IET Conference Publications* (1992)
17. Faa-Jeng Lin, Jonq-chin Hwang, Po-Huan Chou, Ying-Chih Hung, FPGA-based intelligent-complementary sliding-mode control for pmlsm servo-drive system. IEEE Trans. Power Electron. **25**, 2573–2587 (2010)
18. A. Olivia, H. Chiacchiarin, A. Aymonino, P. Mandolesi, Reduction of total harmonic distortion in power inverters. Lat. Amer Appl. Res. **35**, 89–93 (2005)
19. E. Koutroulis, A. Dollas, K. Kalaitzakis, High frequency pulse width modulation implementation using FPGA and CPLD ICs, J. Syst. Architecture **52**, 332–344 (2006)

Secretly Shared QR Code and Its Applications

G.S. Devisree and K. Praveen

Abstract Quick response codes (QR codes) are widely being used for various applications such as user authentication and advertisements. The data in QR codes can easily be read with the help of a QR code reader application installed in a smartphone with camera. Here, we cannot neglect the possibility of an attacker tampering the QR code data. For example, in authentication, the attacker can forge the text password. In order to avoid such attacks as well as hide this data from the public, we propose a secret sharing scheme with reversing. This scheme not only splits the QR code into different shares, but also allows us to perfectly reconstruct back the original QR code.

Keywords Quick response codes · Visual cryptography · Stenographic technique · Secret sharing scheme

1 Introduction

As security is a main concern nowadays, the urge to find practical solutions prevails. The confidentiality of a word or a phrase is more important as these can be used as a password, security code, coupon code, etc. If we are able to conceal these words in a proper way, we can assure the security to an extent [1]. The idea is to encode the word, phrase, or message in a quick response (QR) [2] code which is basically an image. QR code is a two-dimensional bar code in which large amount of data is stored vertically and horizontally. Due to the advantages such as large data capacity, small print out size, and damage resistance, QR codes have rapidly

G.S. Devisree (✉) · K. Praveen
TIFAC CORE in Cyber Security, Amrita Vishwa Vidyapeetham,
Coimbatore, Tamil Nadu, India
e-mail: devi.45229@gmail.com

K. Praveen
e-mail: praveen.cys@gmail.com

© Springer India 2015

L.P. Suresh et al. (eds.), *Artificial Intelligence and Evolutionary Algorithms in Engineering Systems*, Advances in Intelligent Systems and Computing 325,
DOI 10.1007/978-81-322-2135-7_50

gained popularity in many countries. Another high light is that with the help of a smartphone, it can be easily decoded by a QR code reader application. Even though color QR codes are available in market, our application requires the basic black and white QR code.

Visual cryptography-based secret sharing scheme is used to split the QR code into several shares. These shares are constructed based on the algorithm in ideal contrast visual cryptography schemes with revering. The advantage of using this technique is that we are able to perfectly reconstruct back the original QR code. Another proposal that this paper aims is to find an access matrix with an essential participant with enough distribution of black-and-white pixels in the access matrix. Also the share of the essential participant should not be guessable by a third party. This essential participant and one of the other participants combined can perfectly reconstruct back the secret message or in this case the QR code. The motivation behind this proposal is that it can be efficiently used for joint accounts in banking applications as well as in e-coupons to hide the e-coupon codes from the customers.

2 Related Work

In order to make the data encoded in the QR code secure, a combined effort of visual cryptographic technique and stenographic technique is used [3]. At the encoder side, the QR code is made into several shares with the help of secret sharing technique. Then, the each share image is embedded in a cover image using stenographic technique. For the decoding, the share image is extracted from the cover image and then combined according to the secret sharing technique to get back the original QR code. Steganography is used to ensure more security to the QR code but in turn increases the computational module.

Visual cryptography has been introduced by Naor and Shamir in 1994 [4], which divides each black or white pixel into two sub-pixels or four sub-pixels. These sub-pixels are the shares of the secret message (Fig. 1).

The different visual cryptographic schemes proposed by Naor and Shamir [4] are as follows:

- (n, n) visual secret sharing scheme—The secret is divided into n shares, and all the n shares are stacked to get back the secret message.
- (k, n) visual secret sharing scheme—The secret is divided into n shares, and any k or more of these shares can be stacked together to get back the secret message.

The general techniques to construct visual cryptography schemes for any access structure have been proposed Atenises, Blundo, and Stinson [5], which is an extension of the Naor and Samir schemes. A visual cryptographic scheme to perfectly reconstruct the black pixels has been proposed in [1] where all the sub-pixels associated to a black pixel are black. It is evident from the above schemes that the probability of getting back the white pixel is only 50 %. This means that the perfect reconstruction of white pixel is not possible by the stacking of shares.

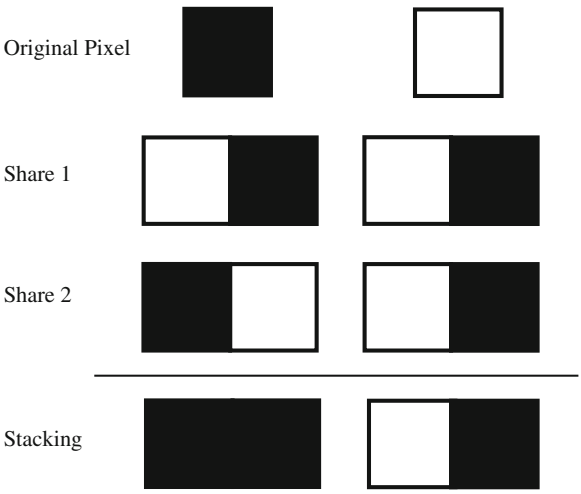

Fig. 1 Visual cryptographic scheme (inferred from Naor and Shamir [4])

Lio and Lee [6] proposed a scheme where the number is shared using conventional secret sharing schemes and the shares are embedded in a QR Code. But the disadvantage is the use of secret sharing scheme increases the computational module. Also Sharma and Rao [7] have proposed an alternative security on ID cards with the help of 2D data matrix codes and visual cryptography.

The perfect reconstruction of both black-and-white pixels has been proposed in [8] with the technique of visual cryptography with reversing. This scheme has a certain pixel expansion of m pixels, and it requires each participant to store m transparencies. Each of the transparency will be having the same number of pixels as of the original image.

A (2, n) visual cryptographic technique for banking applications have been proposed by Pal et al. [9] where any two participants can recover the secret message or password. But if any two participants can recover the password and one of them needs not be the share of the bank, then this scheme may fail at such cases. For example, in the case of a joint account, we may have two participants and the third participant will be the bank.

3 Proposed Framework

The word or secret message is primarily encoded into a QR code with the help of a QR code generator. Then, the QR code is subdivided into n number of shares with the technique of perfect reconstruction of black-and-white pixels [8]. Each of the participants will be getting the n number of shares out of which only $k<n$ or more than k participants can recover the secret message. Any number less than k participants cannot recover the secret message (Fig. 2). At the decoder side (Fig. 3), the technique proposed in [8] has been implemented on the shares to perfectly reconstruct back the QR code.

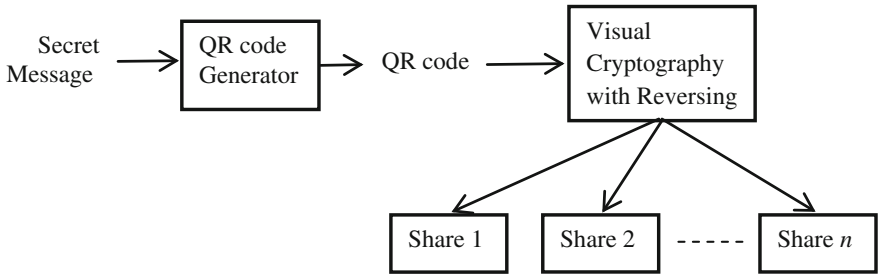

Fig. 2 Architecture of encoder

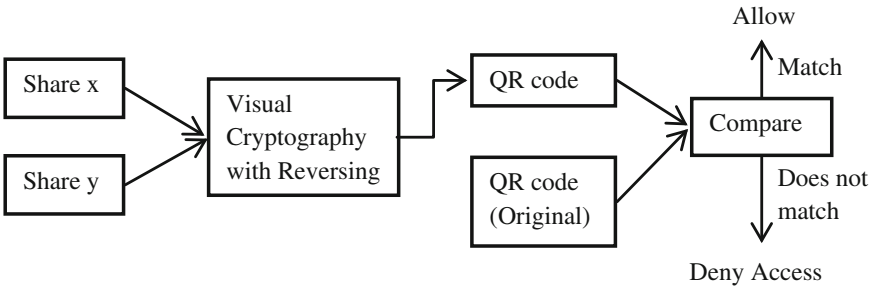

Fig. 3 Architecture of decoder

As an example, let $P = \{P_1, P_2, P_3\}$ be the set of participants. Suppose the secret matrix is given as I. The minimal qualified set is given by Γ_0={{1,2},{2,3},{1,3}}. The basis matrices for the (2, 3)-VCS which perfectly reconstructs black-and-white pixels are given by $S^0 = \begin{bmatrix} 0 & 1 & 1 \\ 0 & 1 & 1 \\ 0 & 1 & 1 \end{bmatrix}$ and $S^1 = \begin{bmatrix} 1 & 0 & 1 \\ 1 & 1 & 0 \\ 0 & 1 & 1 \end{bmatrix}$. Then, according to the construction proposed in paper [8], the secret matrix I can be reconstructed ideally.

3.1 Illustrative Example

Consider the secret message "NET209". This is encoded in a QR code with the help of a QR code generator [10] (Fig. 4).

The above QR code will be a consisting of only 1's and 0's. Now, consider 4 participants such as $P = \{1, 2, 3, 4\}$ and $\Gamma_0 = \{\{1, 2\}, \{2, 3\}, \{3, 4\}\}$. The basis matrices S^0 and S^1 in a visual cryptography scheme realizing the access structure Γ_{Qual} whose basis is Γ_0 are $S^0 = \begin{bmatrix} 0 & 1 & 1 & 0 \\ 0 & 1 & 1 & 1 \\ 0 & 1 & 1 & 1 \\ 0 & 1 & 0 & 1 \end{bmatrix}$, and $S^1 = \begin{bmatrix} 1 & 0 & 0 & 1 \\ 1 & 1 & 1 & 0 \\ 1 & 1 & 0 & 1 \\ 1 & 0 & 1 & 0 \end{bmatrix}$.

Fig. 4 QR code encoded with the message "NET209"

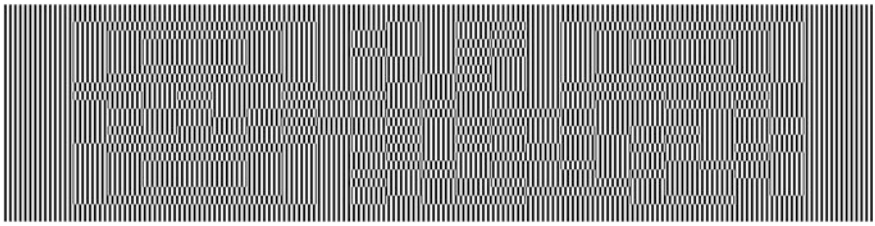

Fig. 5 Share of participant 1

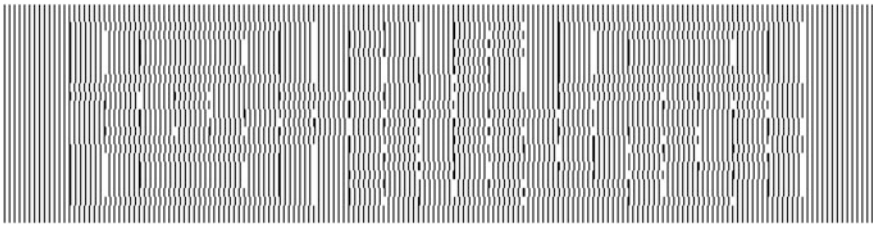

Fig. 6 Share of participant 2

According to the construction method prescribed, we generate the following shares (Figs. 5, 6, 7, and 8).

Each of the 4 participants will be having each share. Because of the construction, only participants 1 and 2 or participants 2 and 3 or participants 3 and 4 can recover back the QR code. Any other combination of shares would not produce the QR code, thus ensuring security.

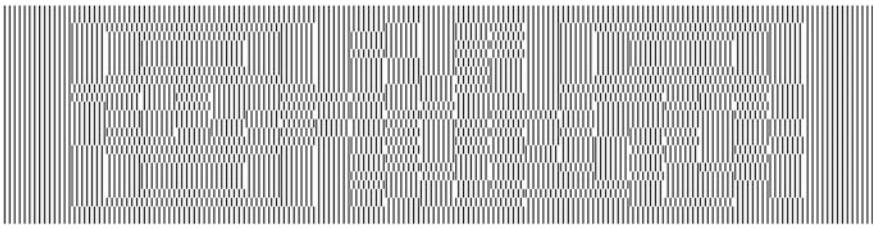

Fig. 7 Share of participant 3

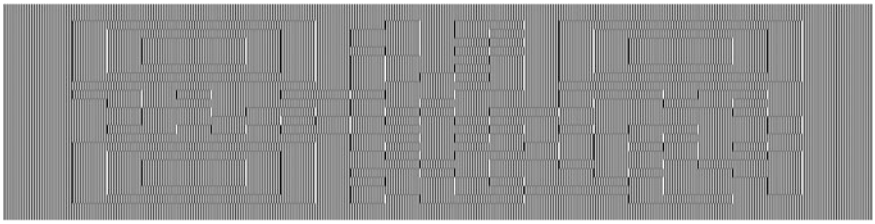

Fig. 8 Share of participant 4

3.2 Applications

E-coupons and Banking applications. In the case of e-coupons or banking applications, we will have to go for an essential participant. The access matrices constructed should be in consideration of the essential participant. This means that the essential participant should be one of the two participants to perfectly reveal the secret message. No other two participants should be able to recover the secret message, in this case the QR code.

Let us consider the example of e-coupons in which an online shopping store provides e-coupons to its customers. Their customers will be in many parts of the country, and they may provide e-coupons to customers based on their locations or based on a specific customer. Nowadays e-coupons have been misused by many customers where they would randomly try out e-coupon codes. If they are lucky, the offer code is accepted by the server, and the unintended customer gets the offer price. We suggest encoding these e-coupon codes inside the QR code and then dividing them into shares. The essential share will be retained by the online shopping store, and rest of the shares is given only to the intended customers. Since the customers are not viewing the codes directly, a layman cannot do a brute force attack on e-coupon codes. The added advantage is that to get the QR code, we will have to get the share of the online shopping store. No other combination of the fellow customer's shares will be able to get back the QR code. Also inside the QR code is our e-coupon code, which is securely stored.

For banking application (2, 2) secret sharing scheme is secure if the participants are only the bank and the customer. But in the case of a joint account, it will only consume the storage space of the bank if we are using (2, 2) secret sharing scheme for each customer. Instead if we are able to provide one share to the bank which is the essential share, then it will save the storage space. Therefore, the essential share of the bank combined with any one of the joint account holder's shares will retrieve the password in the form of QR code. Since the password is encoded in the QR code, it gives another level of security.

4 Future Research

One of the future scopes of this proposal is to construct an access matrix in which essential participant is present. But the problem there will be that the shares won't have equal distribution in many cases of access matrix construction. Or else the share of essential participant can be guessed by other participant. In other cases, the essential participant share will be same as that of one of the other participants. So this makes it difficult for the construction of an access matrix where there is enough distribution of black-and-white pixels and is unique.

5 Conclusion

In this paper, a secret sharing scheme with reversing to perfectly reconstruct QR code has been proposed. This can be efficiently used on applications such as e-coupons and banking applications. There is a need to find an access matrix with essential participant, which can support the applications mentioned here. By the construction of such a system, we are able to solve the problem of saving lot of shares in the server.

References

1. C. Blundo, A. De Santis, Visual cryptography schemes with perfect reconstruction of black pixels. J. Comp. Graphics **22**(4), 449–455 (1998)
2. P. Kieseberg, M. Leithner, M. Mulazzani, L. Munroe, S. Schrittwieser, M. Sinha, E. Weippl, QR code security, in *Proceedings of 8th International conference on Advances in Mobile Computing* (2010)
3. Omprasad Deshmukh, Shefali Sonavane, Multi-share crypt-stego authentication system. IJCSMC **2**(2), 80–90 (2013)
4. M. Naor, A. Shamir, *Visual cryptography, advances in cryptology: eurpocrypt'94* (Springer, Berlin, 1994), pp. 1–12
5. G. Ateniese, C. Blundo, A. De Santis, D.R. Stinson, Visual cryptography for general access structures. Inf. Comput. **129**(2), 86–106 (1996)

6. K.C. Liao, W.H. Lee, A novel user authentication scheme based on QR-Code. J. Netw. **5**, 937–941 (2010)
7. M.A. Sharma, M.C. Rao, Visual cryptography authentication for data matrix code. Int. J. Comp. Sci. Telecommun. **2**(8), 58–62 (2011)
8. S. Cimato, A. De Santis, A.L. Ferrara, B. Masucci, ideal contrast visual cryptography schemes with reversing. Inf. Process. Lett. **93**, 199–206 (2005)
9. Jayanta Kumar Pal, J.K. Mandal, Kousik Dasgupta, A (2, N) visual cryptographic technique for banking applications. Int. J. Netw. Secur. Appl. (IJNSA) **2**(4), 118–127 (2010)
10. Chuang Jun-Chou, Hu Yu-Chen, Ko Hsien-Ju, A novel secret sharing technique using QR code. Int. J. Image Process.(IJIP) **4**(5), 468–475 (2010)

Phish Indicator: An Indication for Phishing Sites

S. Aparna and Kandasamy Muniasamy

Abstract Phishing is a simple social engineering technique that functions by creating a fake Web site, often imitating a legitimate site. Despite many anti-phishing tools are developed, the phishing attacks are still a drift of trust in Internet security. In this paper, the indicator acts as an enhancement toward the usability of the cyber trust mechanisms. Here, the phish indicator is developed as a browser extension, which will detect and classify the URL as phishing or genuine site. The classification of the URL visited by the user is done using Levenshtein algorithm and some heuristic criterions. It will alert the user with a message of whether the URL visited is a phishing site or a genuine site. Thus, the indication will help whenever the user attempts to give away his information to a Web site that is considered untrusted.

Keywords Phishing · Trust indicators · Whitelist · Browser extension

1 Introduction

Phishing is currently the most widespread financial threat on the Internet. Phishing is an example of a semantic attack. By making an incorrect decision, the user can give away the personal information to Web site that is considered untrusted. Most of the security vulnerabilities are due to human factor. The applications build to protect will get attacked or destroyed when the users apply them improperly. While a variety of security software and security features exist, security software is rarely used to facilitate a primary task. Security software usually runs in the background and only communicates risks via trust indicators. Computer security software cannot detect all threats and automatically act on the user's behalf. As a result,

S. Aparna (✉) · K. Muniasamy
TIFAC CORE in Cyber Security, Amrita Vishwa Vidyapeetham, Coimbatore, India
e-mail: aparnasreelatha04@gmail.com

K. Muniasamy
e-mail: kandamuniasamy@yahoo.com

© Springer India 2015

L.P. Suresh et al. (eds.), *Artificial Intelligence and Evolutionary Algorithms in Engineering Systems*, Advances in Intelligent Systems and Computing 325,
DOI 10.1007/978-81-322-2135-7_51

we are required to make security decisions. It is easier for attackers to exploit these decisions than a technical vulnerability.

The purpose of these browser warnings [1] is to serve as the last line of defense against divulging his or her sensitive information to an untrusted party. Phishers are improving their techniques for making the targeted Web sites look more realistic and to convince the users that they are visiting the legitimate site. The indicators should be made to capture the attention of the user from entering into an illegitimate site. It should be able to clearly state the risk and consequences and should make the user feel that he or she should not trust the Web site. The indicators have a great role in making the users to take the right decisions. In this paper, the indication of a phishing site is done based on the URL [2] of the Web site. Our approach is to calculate the distance between the URL in the browser and the whitelisted URL using the Levenshtein algorithm and also uses some heuristics criterion to distinguish the legitimate and the phishing site. In this, purely an URL-based analysis is occurring. Hence, the components of the URL are extracted, and we apply these heuristics and the matching algorithm, and the comparison is made with whitelist.

2 Related Works

In spite of better and efficient tools on phishing detection, the problem is not mitigated as we are witnessing the growing number of victims of the phishing attack. Most of them are not able to detect and give the user the proper indication, regarding the site which may give rise to false positives. According to a study by CyLab, Carnegie Mellon University, heuristics and blacklist are the most popularly used methods against phishing [3]. There are different parameters, which are used for the indication of phishing site, that include Web link-based identity, encryption and security-based, source code and client side verification-based, page layout and content-based, Web address bar-based, and social human factor-based.

Anti-phishing refers to detection and prevention of phishing attack and thereby giving users timely notifications regarding the possibilities of the attack. Most of the detection of the phishing sites is done on the features, which include textual features, linguistic features, and structural features. Machine learning algorithms are also used for the detection and classification of the legitimate and phishing site. The most common algorithms used are Naïve Bayesian classifier, decision trees, and support vector machines. The different anti-phishing techniques are as follows: attribute-based anti-phishing, an identity-based anti-phishing, character-based anti-phishing approach, content-based anti-phishing, etc. All these have their own advantages and disadvantages.

Some anti-phishing tools, which uses blacklist of phishing URLs to identify the phishing sites, include Google Safe Browsing, Netcraft tool bar [4], etc. The blacklist contains only the reported malicious URL. PhishNet [5], which is an anti-phishing tool, comprises of five heuristics combinations to discover new phishing URLs and a matching algorithm that divides an URL into multiple components, and

they are verified against the entries in the blacklist. These two ideas are to improve efficiency of blacklists. The disadvantage of using the blacklist is that non-blacklisted phishing sites are not recognized.

PhishTester [6], another add-on on the Mozilla Firefox, is based on a behavior model. It considers the Web site as a Web application and test the application based on the model. The model is described using the notion of FSM that captures submission of forms with fake inputs and corresponding responses. Several heuristic criterions are used to detect inconsistencies that led to the conclusion that a Web site is phishing or real.

A novel browser extension [7], which aims to protect the user from spoofed Web sites, uses an automated whitelist that will be updated and maintained automatically for the user. They use the machine learning algorithm Naïve Bayesian algorithm for the classification and maintenance of the list. In this paper, when the user enters data into form field, it checks whether the information entered by user is in the list. If yes, then verifies the corresponding domain and classifies it as trusted and untrusted Web site.

3 Proposed System

In this paper, an indicator in the browser client is developed which will detect phish sites and alert the user with a message whenever the user attempts to give away his information to a Web site that is considered untrusted. In this paper, the indication or the classification of a phishing or a genuine site is done purely based on the URL of the site visited by the user.

Framework In this, the phish indicator is designed on the goal of giving active notifications to warn or give an indication for the users on the legitimacy of the Web site. The phish indicator is developed as an add-on for the Google Chrome. Currently, there are several products available that is used to detect or prevent the user from giving away the sensitive information to a site that is unsafe. Here, the phish indicator uses the Levenshtein algorithm [8] that compares the URL and the IP address from the whitelist with the URL of the requested site. The domain name of the site to be visited may be hidden from the user, and instead of the name, the URL contains an IP address that redirects the user to a phishing site. To avoid this type of replacing domain name attack, we compare the IP address and give an indication to the user.

The Levenshtein distance is a measure of the similarity between two strings, which we will refer to as the source string (s) and the target string (t). The distance is the number of deletions, insertions, or substitutions required to transform s into t. The greater the Levenshtein distance, the more different the strings are.

The Algorithm

Step 1 Set n to be the length of s
Set m to be the length of t
Construct a matrix containing $0 \ldots m$ rows and $0 \ldots n$ columns

Step 2 Initialize the first row to 0…n
Initialize the first column to 0…m
Step 3 Examine each character of s (i from 1 to n)
Examine each character of t (j from 1 to m)
Step 4 If s[i] equals t[j], the cost is 0
If s[i] does not equal t[j], the cost is 1
Step 5 Set cell d[i, j] of the matrix equal to minimum of:

(a) The cell immediately above plus 1: d[$i-1$, j] + 1
(b) The cell immediately to the left plus 1: d[i, $j-1$] + 1
(c) The cell diagonally above and to the left plus the cost: d[$i-1$, $j-1$] + cost

Step 6 After the iteration steps (3, 4, 5) are complete, the distance is found in cell d[n,m]
Step 7 The minimum distance calculated is then compared with the threshold value

(a) If the minimum edit distance value is greater than the threshold value, then it is not a legitimate site
(b) If the value is less, then go for the IP check.

As early mentioned, most of the phishing site uses the host name, which would be very near to the legitimate site, in order to make the user difficult to distinguish the legitimate and the phishing site. By doing so, the edit distance value may be lower than the minimum threshold [9]. Hence, if the value is less than the threshold value, then the IP address as well as the TLDs of the entered site is compared with the IP addresses of the site in the black list. An example of the Levenshtein distance is shown in the Fig. 1. Here, the distance between two strings is calculated. The

Fig. 1 Example of Levenshtein distance matrix

		O	N	L	I	N	E	S	B	I
	0	1	2	3	4	5	6	7	8	9
O	1	0	1	2	3	4	5	6	7	8
N	2	1	0	1	2	3	4	5	6	7
L	3	2	1	0	1	2	3	4	5	6
I	4	3	2	1	0	1	2	3	4	5
N	5	4	3	2	1	0	1	2	3	4
E	6	5	4	3	2	1	0	1	2	3
S	7	6	5	4	3	2	1	0	1	2
B	8	7	6	5	4	3	2	1	0	1
L	9	8	7	6	5	4	3	2	1	1

edit distance

source string or the domain name is "ONLINESBI," and the target string or the replaced string is "ONLINESBL." Here, "ONLINESBI" is transformed into "ONLINESBL" by substituting "L" instead of "I." This corresponds to our intuitive realization that the source string can be transformed into target string either by substituting or adding letters.

The main goal of this paper is to give the user the indication or warning regarding the site he or she is visiting and to protect the user and detect the untrusted site; some features of URL are also taken into consideration. Hence, as to improve the efficiency of the phish indicator or as a second approach, we also use some heuristics [10] to identify the phishing sites. Based on the analysis of the URL, some of the features such as number of dots (.), number of at-signs (@), number of double slash (//), and the port number in the URL are considered. While in the count of dots in the URL, if the number of dots is greater than 3, then a warning will be given to the user to recheck the site he or she is going to visit. Similarly, the count of each feature taken into consideration will be verified and gives warning to the users accordingly. The study made by McGrath et al. [11] identified by analyzing the phishing URLs and domains that most of the phishing sites may not be hosted from the country they claimed in their TLD. Hence, we will also verify the country code top-level domains in the URL. Also while in the analysis of the response page of the visiting site, if they request for the login with passwords and IDs, then it will check whether the site is secure with the https protocol.

Some of the heuristics used to distinguish the phishing and legitimate Web sites can be summarized as follows:

1. Number of dots (.) in the URL
2. Number of at-signs (@) in the URL
3. Number of double slash (//) in the URL
4. Existence of an IP address in the URL
5. Port number in the URL
6. TLD evaluation in the domain name
7. Country code and TLD comparison
8. HTTPS

When any one of these features is detected by the phish indicator, it will give an alert or warning to the user accordingly. The features, which are extracted from the URL, are then verified such that when the number of counts of the corresponding exceeds the limit or the threshold which is set, it shows a sign of untrusted entry. Since @, //, etc., may lead to yet another page or destination as needed by the attacker, their unusual count in the URL would be considered and the user will be alerted. Then, the user will be notified of this unsafe condition and will be getting altered. Figure 2 describes the architecture of the proposed system of the phish indicator.

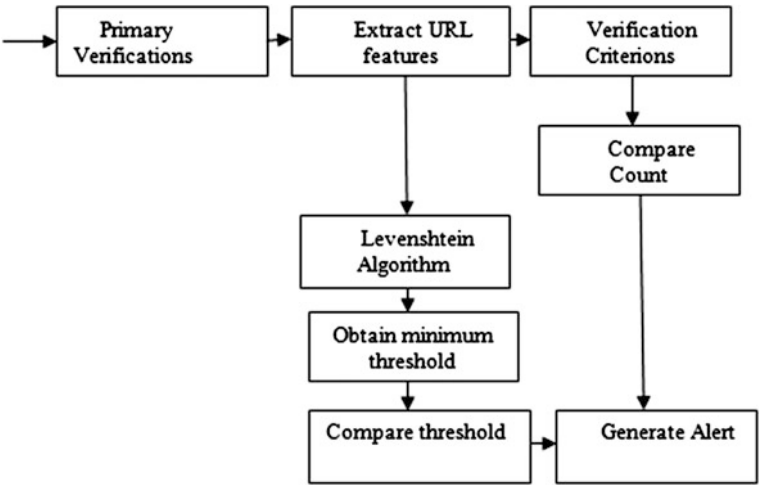

Fig. 2 Architecture of proposed system

4 Experiments and Results

In this section, some experiments are carried out to verify the efficiency of the detection system. Phish indicator was developed as an add-on for Google Chrome. When compared to other browsers, using Chrome would be more securable and not inherent to most of the browser vulnerabilities. It has been developed using the Java in Eclipse IDE and Java Scripts. The plug-in was installed in the Chrome browser and tested with different URLs.

Experiments with different sites, both from the whitelisted and blacklisted URLs, were taken to test the phish indicator. The URL of the site is the input to the system, and then, the system classifies the URL as genuine or phishing. Most of the URLs, which indicate as phishing, were due to the changes in the domain name rather than the counts in the special characters. Since the detection system mainly focuses on the domain of the URL, the false positiveness of the system was small and obtained satisfactory results. Indication results of the ONLINESBI and ONLINESBL are shown in Figs. 3 and 4.

Fig. 3 Example of genuine site indication

Fig. 4 Example of phishing site indication

5 Conclusions and Future Work

A browser extension in chrome that is capable of detecting and alerting the user about a phishing site. Most of the phishing sites have very short lifetime of 2–3 days. Since we are using the whitelist, some of the disadvantages in using the blacklist like, checking of URLs or IPs with only the blacklisted ones, can be avoided. And thereby using the whitelisted information, we can detect the URL-based zero attack, which is an advantage of this indicator. Hence, most of the URL-based attack can be avoided and also the user gets a warning with the help of this phish indicator.

Future works include adding some more heuristic characteristics of both the URL and the content or characteristics of Webpage and can also evaluate of the lifetime and history of the site.

References

1. H.-J. Hof, Towards enhanced usability of it security mechanisms-how to design usable it security mechanisms using the example of email encryption, Int. J. Adv. Secur **6**(1&2), 78–87 (2013)
2. M. Abramson, D.W. Aha, What's in a URL?Genre Classification from URLs, in *Association for the Advancement of Artificial Intelligence* (2012)
3. L. Cranor, S. Egelman, J. Hong, Y. Zhang, Phinding Phish: An evaluation of anti-Phishing toolbars (2009)
4. A. Jain, V. Richariya, Implementing a web browser with phishing detection techniques. World Comp. Sci. Inf. Technol. J. (WCSIT) ISSN: 2221-0741 **1**(7), 289–291 (2011)
5. H. Shahriar, M. Zulkernine, *Phish tester: automatic of testing phishing attacks in secure software integration and reliability improvement (SSIRI)* (IEEE CS Press, Singapore, 2010), pp. 198–207
6. P. Prakash, M. Kumar, R.R. Kompella, M. Gupta, PhishNet: Predictive blacklisting to detect phishing attacks (2009) INFOCOM, in *Proceedings IEEE*, 14–19 March 2010, pp. 1–5
7. Y. Cao, W. Han, Y. Le, Anti-phishing based on automated individual white-list (2008)
8. V.P. Reddy, V. Radha, M. Jindal, Client side protection from phishing attack, Int. J. Adv. Eng. Sci. Technol.(IJAEST) **3**, 39–45 (2011)
9. A. Barth, A.P. Felt, P. Saxena, A. Boodman, Protecting Browsers from Extension 208 Vulnerabilities (2010)
10. S. Gastellier-Prevost, G.G. Granadillo, M. Laurent, Decisive heuristics to differentiate legitimate from phishing sites (2010)
11. D.K. McGrath, M. Gupta, Behind phishing: an examination of phisher modi operandi, in *Proceedings of the 1st Usenix Workshop on Large-Scale Exploits and Emergent Threats* (2008), p. 4

Using Signature for Hidden Communication Prevention in IP Telephony

Ajvad Rahman and P.P. Amritha

Abstract This paper prevents the steganographic method for IP telephony called transcoding steganography (TranSteg). Typically, in TranSteg, it is the overt data that is to compress to make space for steganogram. TranSteg finds appropriate codec that will result in the voice quality similar to the original. In signature-based system, the signature of the voice payload is appended to the packet to provide integrity. The signature of the data becomes invalid when there is some change in voice data. This method detects the hidden communication between a VoIP call. The signature-based scheme concept is described in this paper.

Keywords Voice over IP · Network steganography · Hidden communication · Data hiding

1 Introduction

Voice over IP or IP telephony is a real-time service, which allows users to make voice call over data channel. IP telephony is the service that is changing the entire telecommunication network. VoIP has two phases: signaling phase and conversation phase.

- **Signaling phase**: In this phase-signaling protocol, messages are exchanges between calling parties. Example for signaling protocol is session initiation protocol (SIP). These messages are intended to setup and negotiate calling parameters.
- **Conversation phase**: After completion of the signaling phase, conversation phase starts. Two bidirectional audio streams are set up for conversation.

A. Rahman (✉) · P.P. Amritha
TIFAC Core in Cyber Security, Amritha Vishwa Vidyapeetham, Coimbatore, India
e-mail: ajvadrahman@gmail.com

P.P. Amritha
e-mail: amuuviju@gmail.com

© Springer India 2015

L.P. Suresh et al. (eds.), *Artificial Intelligence and Evolutionary Algorithms in Engineering Systems*, Advances in Intelligent Systems and Computing 325,
DOI 10.1007/978-81-322-2135-7_52

Steganography is a method to hide data inside a carrier in such a way that the presence of the hidden message is undetectable. Voice over IP can be utilized for steganographic communication. Voice over IP is a popular service, thus its usage will not be suspicious. Also high steganographic bandwidth can be achieved. In a G.711 conversation, each RTP packet contains 20 ms voice in a rate of 50 packets per second. By hiding 1 bit in a packet gives a bandwidth of 50 bits/s. These two reasons make voice over IP attractive to the steganographic research community.

The purpose of communication can be varied; it may be either legal or illicit. The network steganography can be used for improving resistance to VoIP packet loss [2], or it can be used for key distribution. Every VoIP steganographic technique can be classified into three groups.

- **Modifying PDU**: Steganographic method to modify headers or payload field. Example modifying RTP, UDP, or IP redundant header fields.
- **Modifying PDU Time relation**: Modifying protocol data unit's inter-packet delay or by affecting the PDU's sequence order.
- **Hybrid**: In this, method modifies both PDU and its time relation.

Information-hiding techniques proposed for a particular codec or audio file format can also be used for VoIP. Most of the current research is based on the first method (modifying PDU). Transcoding steganography (TranSteg) is a new steganographic method proposed by Mazurczyk et al. [1]. In TranSteg, overt data are compressed to make space for steganogram. This is done by transcoding voice data from higher bit rate to lower bit rate using a lossy compression technique. This makes original large payload reduced to small size, but the payload type and size fields in the header are not modified. The remaining space created by transcoding is filled with hidden data.

TranSteg communication scenario can be of four different types (Fig. 2). The first three scenarios at least one of the calling parties are involved in the secret communication. In the fourth scenario, both calling parties are unaware of the hidden data transfer between two intermediate network nodes. In this paper, we are introducing a new technique to provide integrity of data to both calling parties to avoid the third-party involvement. Digital signature for the voice payload is appended to the packet so that tampering of the digital voice can be prohibited. Extended voice payload field can be use for saving the digital signature (Fig. 1).

2 Related Work

Voice over IP as a hidden data carrier for steganography is a recent discovery. Steganographic methods are of mainly two types. Firstly from well established image and audio steganography targeted the digital representation of voice carrier. Second based on covert channel, which targets VoIP protocol field [3]. Dittmann et al. proposed digital voice signal as a hidden data carrier in 2005 [4]. This work is further extended and published in 2006 in [5]. Wand and Wu [6] suggested using

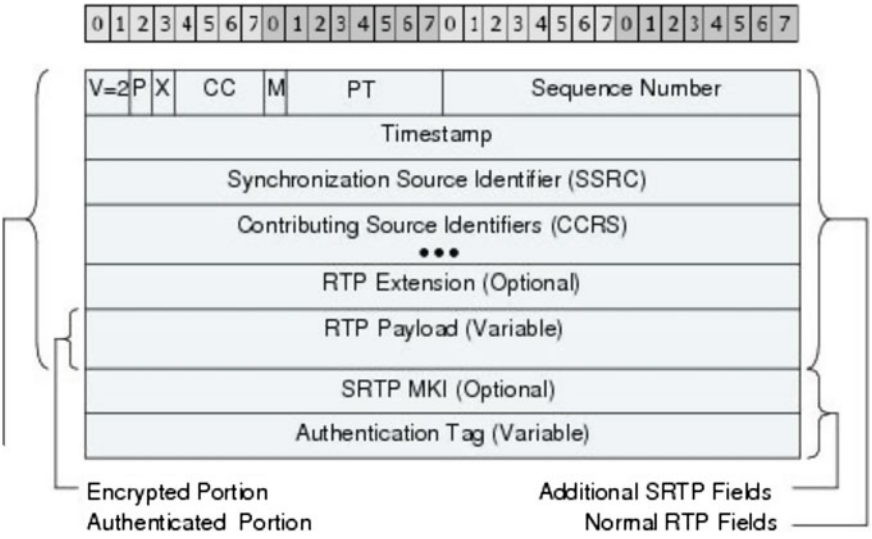

Fig. 1 RTP packet header

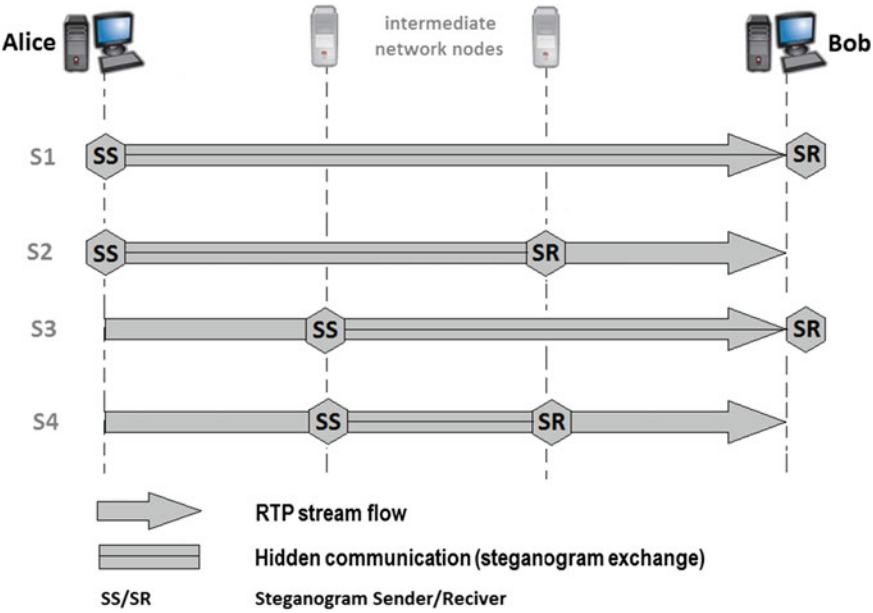

Fig. 2 Communication scenario

the least significant bits of voice samples to carry secret communication. In [7], Takahashi and Lee proposed a similar approach and presented its proof of concept implementation, which can establish a hidden conversation by embedding compressed voice data into the regular PCM-based voice traffic. Aoki in [8] proposed a steganographic method based on the characteristics of pulse code modulation.

Utilization of the VoIP-specific protocols as a steganogram carrier was first proposed by Mazurczyk and Kotulski in 2006 [9]. In [10], a novel method called lost audio packets steganography (LACK) was introduced. Bai et al. proposed a covert channel based on the jitter field of the RTCP header [11]. This is performed in two stages: firstly, statistics of the value of the jitter field in the current network are calculated. Next, the secret message is modulated into the jitter field according to the previously calculated parameters. In 2010, Andreas Plies et al. [12] proposed a signature-based method to give authentication to calling parties. Mazurczyk et al. [1] proposed TranSteg on voice over IP in 2011. In this paper, the voice payload codec is transcoding to another lossy codec to make a room for the hidden message.

3 Framework

Voice over IP is a perfect carrier for steganography. In [1], Wojciech Mazurczyk et al. saying about the four different scenarios for the VoIP communication (Fig. 2). In the fourth scenario, intermediate person sending a secret message to another person using a VoIP call between Alice and Bob. To avoid this scenario, we introduce a signature-based scheme to provide integrity (Fig. 3).

We create a signature for the voice data payload and save the signature in the extended payload in the RTP packet, see Fig. [1]. The digital signature saved in the extended payload provides the integrity to the voice call. If the intermediate node in between the Alice and Bob conversation tries to hide the data inside the RTP voice

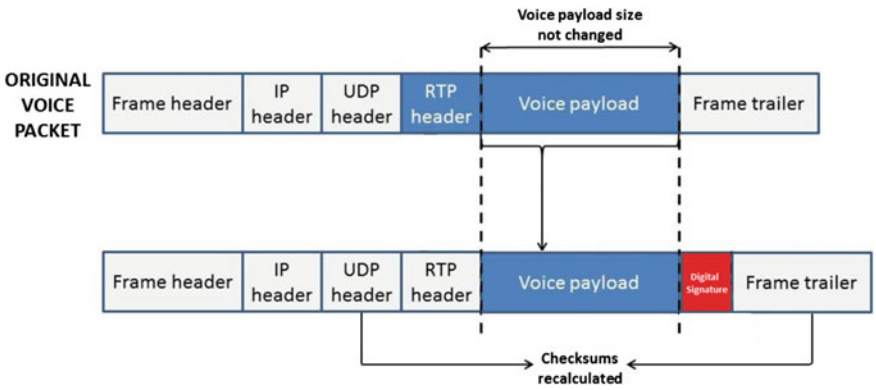

Fig. 3 Framework

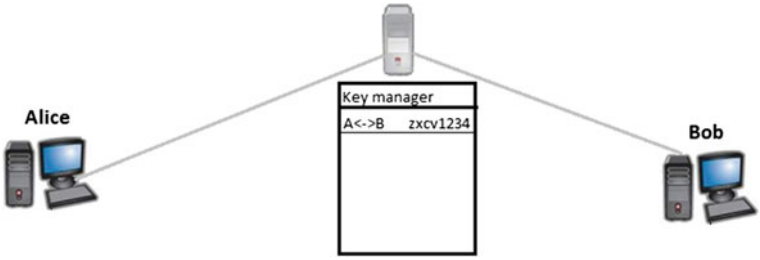

Fig. 4 Alice and Bob follow the server-based VoIP system

data payload, the signature in the extended field becomes invalid. There may be different scenarios possible to exchange the key for the signature.

Scenario 1: **Alice and Bob follow the server-based VoIP system**: Alice and bob connected to a centralized server to make VoIP calls. In this scenario, both the calling parties can exchange key in the initial phase with the help of the server (Fig. 4).
Scenario 2: **Alice and Bob using end-to-end topology**: In this scenario, the key management is a major task. To make the signature-based scheme efficient, there should be fixed number of people. So that the secret session key for a particular user can be saved in a database (Fig. 5) and this key can be used to make an authenticated signature for the corresponding voice payload. This scenario might be suitable for an organization.

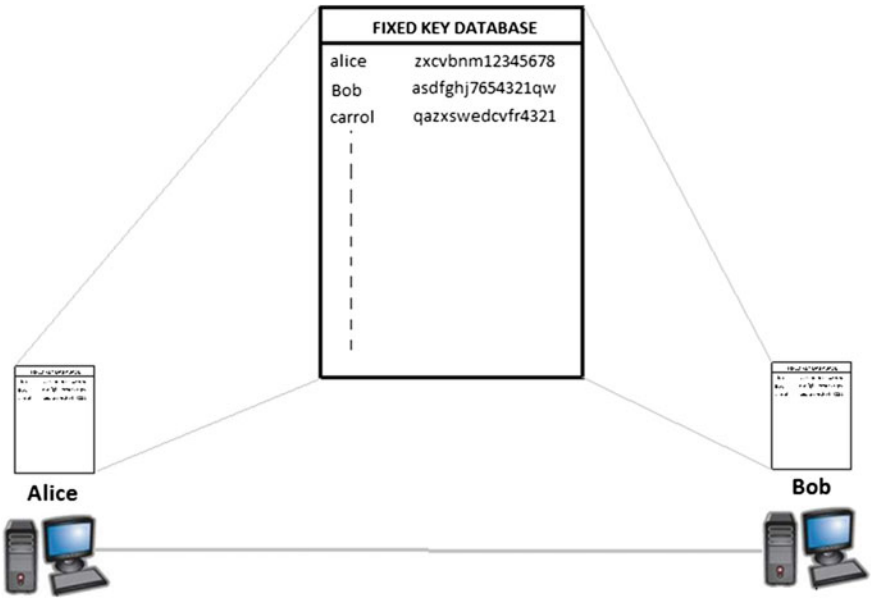

Fig. 5 Alice and bob using end-to-end topology

4 Conclusion

This paper is a new method to give integrity to the voice data. The hidden communication scenarios (Fig. 2) are avoided using this method. It was shown that the steganogram sender and receiver in this scenario cannot break the signature-based scheme. Future work involves the depth analysis of signature scheme.

References

1. W. Mazurczyk, P. Szaga, K. Szczypiorski, Using transcoding for hidden communication in IP telephony. Multimedia Tools Appl. 1–27 (2011)
2. A. Naofumi, VoIP packet loss concealment based on two-side pitch waveform replication technique using steganography, in *2004 IEEE Region 10 Conference TENCON 2004*, vol. 100 (2004)
3. K. Ahsan, D. Kundur, Practical data hiding in TCP/IP, in *Proceedings of Workshop on Multimedia Security at ACM Multimedia 2002* (2002)
4. J. Dittmann, D. Hesse, R. Hillert, Steganography and steganalysis in voice-over IP scenarios: operational aspects and first experiences with a new steganalysis tool set, in *Proceedings of SPIE Security, Steganography, and Watermarking of Multimedia Contents VII*, vol 5681 (2005), pp. 607–618
5. C. Krätzer, J. Dittmann, T. Vogel, R. Hillert, Design and evaluation of steganography for voice-over-IP, in *Proceedings of IEEE International Symposium on Circuits and Systems*, (*ISCAS*) (2006)
6. C. Wang, W. Wu, Information hiding in real-time VoIP streams, in *Ninth IEEE International Symposium on Multimedia* (*ISM 2007*) (2007) pp. 255–262
7. T. Takahashi, W. Lee, An assessment of VoIP covert channel threats, in *Proceedings of 3rd International Conference on Security and Privacy in Communication Networks* (2007)
8. N. Aoki, A technique of lossless steganography for G.711 telephony speech, in *International Conference on Intelligent Information Hiding and Multimedia Signal Processing* (*IIHMSP 2008*) (2008) pp. 608–611
9. K.W. Mazurczy, Z. Kotulski, New security and control protocol for VoIP based on steganography and digital watermarking, in *Proceedings of 5th International Conference on Computer Science—Research and Applications* (*IBIZA 2006*) (2006)
10. K. Mazurczy, S. Szczypiorski, Steganography of VoIP streams, in *Proceedings of on the Move Federated Conferences and Workshops. The 3rd International Symposium on Information Security* (IS'08) (2008), pp. 1001–1018
11. L.Y. Bai, Y. Huang, G. Hou, B. Xiao, Covert channels based on jitter field of the RTCP header, *International Conference on Intelligent Information Hiding and Multimedia Signal Processing* (2008)
12. A. Plies, M. Massoth, R. Marx, Approach to identity card-based voice-over-IP authentication. *2010 Second International Conferences on Advances in Multimedia* (*MMEDIA*). IEEE (2010)

Classification Using Fractal Features of Well-Defined Mammographic Masses Using Power Spectral Analysis and Differential Box Counting Approaches

P.S. Menon Dhanalekshmi and A.C. Phadke

Abstract Computer-aided diagnosis (CAD) of mammograms assists the radiologists to detect the mammographic mass presence. Since the variability of shapes of such breast masses occurs very frequently, it is more difficult to classify them into benign and malignant stages. One efficient approach to classify them is the fractal analysis by deriving their shape features. Various methods have been proposed for the fractal dimension (FD) computation of region of interest (ROI) in biomedical images. Among those, two methods, namely power spectral analysis (PSA) and differential box counting method (DBCM), are used here for the FD computation of breast contour margins. Fractal analysis by PSA method is a frequency-domain approach which is applied to the one-dimensional (1D) signatures of the two-dimensional (2D) breast mass contours. However, the DBCM model assigns the smallest number of boxes that cover the whole image surface. Finally, a comparative analysis is performed between the above-said two methods which show the PSA method yields better accuracy than the DBCM.

Keywords Breast masses · Differential box counting · Fractal dimension · Power spectral analysis · Signatures

1 Introduction

Breast cancer is one of the most important health problems and is the most common type of cancer among the women in the world. Worldwide, the breast cancer comprises 22.9 % of all cancers [1] and in urban areas of India, it accounts for about

P.S. Menon Dhanalekshmi (✉) · A.C. Phadke
Department of Electronics and Telecommunication, Maharashtra Institute of Technology, Pune 411038, India
e-mail: dhanamenon@yahoo.com

A.C. Phadke
e-mail: anuradha.phadke@mitpune.edu.in

© Springer India 2015

L.P. Suresh et al. (eds.), *Artificial Intelligence and Evolutionary Algorithms in Engineering Systems*, Advances in Intelligent Systems and Computing 325,
DOI 10.1007/978-81-322-2135-7_53

22–33 % of all cancers in women [2]. The early detection of this cancer is very important because the breast cancer cell can travel through the blood and lymphatic system when the tumor is still small. So far, the most efficient and economical breast imaging modality for the early detection is the X-ray mammography due to its simplicity and cost-effectiveness [3].

Breast pathologies indicated by a mammogram can be microcalcifications, masses, and architectural distortions. Appearance of masses occurs in dense regions possessing different sizes. They may appear as circular, oval, lobular, or irregular as shown in Fig. 1. The similarity in intensities with the normal tissue and morphology with normal breast textures makes the detection of breast masses more difficult compared with other calcifications [4]. Generally, benign masses have well-defined boundary, whereas malignant ones are associated with irregular or spiculated appearance. Analysis of mammographic images is a complex and cumbersome task which requires highly specialized radiologists.

The performance of the observer can be degraded by human factors such as varying decision criteria, distraction by other image features, and simple oversight. To increase the diagnostic efficiency, computer-assisted schemes are developed which can give a "second opinion" to the radiologists during diagnosis.

Fractal geometry acts as a mathematical model to describe many complex patterns in nature [5]. However, researchers have found the usefulness of this concept in biomedical images as well [6], because of their ability to describe the irregular shape features which can be characterized by non-integer dimension where traditional Euclidean geometry fails to analyze. Non-differentiation is one of the key features of fractals that can be quantified by fractal dimensionality (FD). Thus, the FD has been applied in texture analysis to extract the region of interest (ROI).

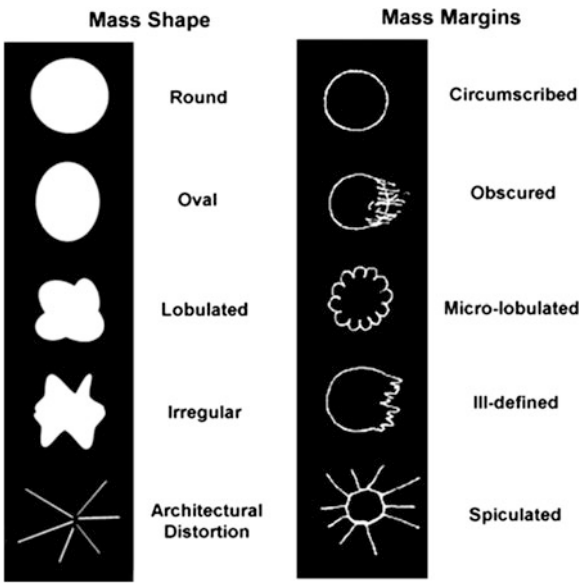

Fig. 1 Different mass shapes and its associated margins

Don S. used box counting (BC) and ruler methods to compute the FD of two-dimensional (2D) contours as well as their one-dimensional (1D) signatures [7]. The FD of breast mass contours was computed using the ruler and BC methods by Rangayyan [8] as well. In addition, circular and lobulated masses were successfully classified by power spectral analysis (PSA) using contour signatures in [9].

The paper is organized according to the following sections: Section 2 highlights a brief introduction on fractals and its applications in image analysis, Section 3 discusses the application of PSA using shape analysis of contours in mammographic well-defined masses, whereas Sect. 4 describes briefly DBCM. In Sect. 5, experimental results and discussions are explained. Finally, Sect. 6 concentrates on conclusion and possible future scope of improvement of this paper.

2 Fractal Analysis

2.1 Basics of Fractals

French mathematician Benoit Mandelbrot introduced the concept of fractals as "a form composed by copies transformed of it." In addition, as one looks more deeply or more closely at a fractal, its inner parts have a similar design to that of the whole object. An example to illustrate this concept is the measurement of length of a coastline (B. Mandelbrot, 1967). While flying and looking at the coast, it looks exactly straight from one end to the other from such a great distance. But as one approaches nearer to the coast, it can be understood that the coast is not exactly straight. However, as one gets closer and closer, the presence of thousands of details can be realized.

While the Euclidean geometry works with objects which exist with integer dimensions, fractal geometry deals with objects in non-integer dimensions. While a straight line has a dimension of exactly one, a fractal curve will have a dimension which exceeds one. Taking this into consideration, biomedical images, especially mammographic images, can be described better with dimension being part of the way between two whole numbers.

2.2 Fractal Properties

As with the example of the coast line examined above, when parts of some objects are similar to the entire object, it is said to be self-similar. This is one of the most important properties of fractals. However, it is not always necessary to have the shapes to be a perfectly similar. Such objects are referred as approximately self-similar. Reiteration is another property which plays a vital role in fractals. In reiteration, the answer to the formula recycles into the original formula to generate the next solution. Each round is an iteration of the formula. The third property

exhibited by fractals is the infinite within the finite. With this, fractals facilitate the phenomenon of infinite surface area within a finite space. Fractals diverge with decreasing scales which highlights the irregularity at all scales and FD. Divergent means to go to infinity. With this reference, the final property of the fractal can be named as scale divergence.

2.3 Fractals in Mammographic Image Analysis

The concept of fractals can be effectively applied for the study of tumors which produces prominent results. The application and relevance of the fractal analysis in mammographic images can be justified by a fractal property called self-similarity. The images especially mammograms exhibit appropriate similarities associated with it at various different spatial scales. This fact justifies the fact that fractal analysis describes the complex patterns by using simple texture features, since texture provides minute details of images at various different scales and orientations.

2.4 Fractal Dimension and Computation Methods

Fractal dimensions can be explained by defining a fractal set as given in Eq. 1.

$$N(a) = \frac{Z}{rD} \tag{1}$$

where $N(a)$ is the number of fragments with the linear dimension defined as r. Z is constant, and D defines the FD. If the above Eq. 1 is rearranged, it yields the result given in Eq. 2 as

$$D = \frac{\ln N(a) + \frac{1}{N(a)}}{\ln\left(\frac{r}{r+1}\right)} \tag{2}$$

If given a unit length line, it can be divided into varying ways and thus compute the D for the fragmented pieces of the line. A formula which will work with all the shapes of the figures when divided and zoomed in number of times is given in Eq. 3 as

$$FD = \frac{\ln(N)}{\ln(l)} \tag{3}$$

where N is the number of divisions and l is the magnification factor.

There are various numbers of methods adopted for the fractal analysis like BC, differential box counting (DBC), Higuchi, sand box, PSA, triangular prism (TP), and variogram. Among those, DBC and PSA methods are used for the FD computation in this paper.

3 Power Spectral Analysis Using Shape Analysis

Here, before applying the PSA to the extracted breast mass contours, those are undergone with shape analysis to know the exact behavior of contour margins.

3.1 Shape Analysis Using Signatures

The computation of the contour signature plays a prominent role to analyze the contour behavior such as smooth or irregular one. In this method of shape analysis, 2D contour margins are converted into 1D signature. The signatures are estimated by first computing the centroid of the breast contour under consideration. It is followed by the calculation of the Euclidean distance from the calculated contour centroid to all the points in the contour.

3.2 Power Spectral Analysis (PSA)

In the case of self-affine fractals, PSA is the most effective method for the computation of the FD. In this approach, each image line is applied with Hanning window and the result is Fourier transformed to calculate their power spectrums. Finally, linear regression is applied to the computed spectrum in log–log plot. FD is calculated as the slope of the averaged power spectra. According to the $(1/f)$ model given in Eq. 4, the relationship between the spectrum and their radial frequency is established.

$$P(f) = \left(\frac{1}{f}\right)^{\beta} \tag{4}$$

where β is the slope of the spectral component. Here, the fractal analysis via PSA is applied to the signature of the contour.

4 Differential Box Counting Method (DBCM)

The DBCM is the extension of the conventional BC method. In BC, the whole image is divided into number of boxes having equal box size. The basic formula to calculate the FD using BC is given in Eq. 5.

$$D = \left(\frac{\ln N_r}{\ln\left(\frac{1}{r}\right)} \right) \tag{5}$$

where N_r is the total count of the number of boxes covering the image and r is the scaling ratio.

In DBCM, assume the image as a three-dimensional space having (x, y) as the image plane and (z) as the gray level. The (x, y) is divided into number of grids of size $a \times a$. Each grid consists of a column of boxes of $a \times a \times a'$. If the gray level of the image is represented by G, then a' is calculated by $\frac{G}{a'} = \frac{S}{a}$. Assume that the minimum and maximum image gray levels in (i,j)th grid fall in respective box numbers $z_{\min}$ and $z_{\max}$. Thus, the N_r of all the boxes present in the image is computed by using the Eq. 6 as

$$N_r = \sum_{i,j} n_r(i,j) \tag{6}$$

where N_r is the less number of copies in the bounded set with a scale of$r$ and $n_r(i,j) = z_{\max} - z_{\min} + 1$. Here, if an image of size $S \times S$ is scaled down to a size of $a \times a$, where $S/2 \geq a > 1$, then a ratio of $r = \frac{a}{S}$ occurs. FD is computed as the linear fit of the least squares of Eq. 5.

5 Experimentation Results and Discussions

Experimentation results are analyzed for the images from Mammographic Image Analysis Society (MIAS) database. As this paper particularly focuses only on the well-defined mass classification, 22 total numbers of images possessing such characteristics are analyzed on 322 mammographic images.

Table 1 gives an overview of the range of the computed FD values using PSA via shape analysis and DBC methods. For the PSA using contour signatures, the benign stages have the FD values ranging between the interval [0.70–1.10] and the malignancy stage occurs between [1.12–1.6] intervals. However, in DBCM, the range of classifying the stages as benign and malignancy are [1.8–1.89] and [1.90–1.93], respectively.

On 22 images, PSA via shape analysis classified 18 images correctly, and thus, this method yielded an accuracy of 82 %. While the DBCM yielded a success rate of 72.72 % only due to the presence of gaps between any two adjacent boxes

Table 1 Comparison between PSA via shape analysis and DBCM for FD computation

Image No.	Methods for FD computation	
	PSA via shape analysis	DBCM
005	0.70	1.827
141	1.5914	1.91
142	1.1	1.88
270	1.121	1.899

spatially and the presence of artifacts in the images, as well as the number of box calculation. In addition, in the below table, the results for only four mammographic images possessing well-defined mass characteristic are considered as an illustrative example for FD values in this paper.

6 Conclusion and Future Scope

Fractal analysis serves as a very prominent and as a good feature extracting technique for the discrimination between the benign and the malignant mass stages. However, it was observed from the experimentation results that the performance of the 2D contour representation with the PSA method resulted in the highest classification accuracy than the DBCM.

As a future scope, the improvement in the classification accuracy can be obtained by using some other shape analysis methods. In addition, other fractal analysis techniques such as Higuchi or Sand box methods can also be implemented for better classification rates.

References

1. G. Danaei, S. Vander Hoorn, A.D. Lopez, M. Ezzati, E.M. Murray, Causes of cancer in the world: comparative risk assessment of nine behavioral and environmental risk factors. J. Nat. Center Biotechnol. Inf. (NCBI) **366**(9499), 1784–1793 (2005)
2. B.B. Mandelbrot, The Fractal Geometry of Nature (1982)
3. J. Keller, R. Crownover, S. Chen, Texture description and segmentation through fractal Geometry. Comput. Vision Graph. Image Process. **45**, 150–166 (1989)
4. S. Don, D. Chung, K. Revathy, E. Choi, D. Min, A new approach for mammogram image classification using fractal properties. Cybern. Inf. Technol. **12**(2) (2012)
5. R.M. Rangayyan, T.M. Nguyen, Fractal analysis of contours of breast masses in mammograms. J. Digital Imaging **20**(3), 223–237 (2007)
6. P.S.M. Dhanalekshmi, A.C. Phadke, Classification of circular and lobuted masses in mammograms using fractal analysis, in *IEEE International Conference on Circuit, Power and Computing Technologies* (*ICCPCT-2013*) (2013)

Efficient Silhouette-based Input Methods for Reliable Human Action Recognition from Videos

G. Glorindal Selvam and D. Gnanadurai

Abstract In this paper, we deal the problem of classification of activities in videos by learning in a different way of modifying the usual input features to enrich the efficiency by reducing the space and time consumption. For efficient action recognition, representing important information is important for reliability. The motivation here is to extract binary silhouette (shape) information from real or raw videos. Most of the researchers are using sequence matching scheme consists of a set of successive silhouette frame that consumes much time and space for learning the system. Here, we adopted recently proposed subspace learning method: spectral regression discriminant analysis (SRDA) for dimensionality reduction. Median Hausdorff distance was used for similarity measures to match the embedded action trajectories. Then, action classification is achieved in a nearest neighbor framework. For efficient learning using SRDA, we use (i) raw silhouette, (ii) images obtained after doing distance transform (DT) in the raw silhouette, (iii) images obtained after extracting edges from the raw silhouettes—edge representation (iv) silhouette history image (SHI), and (v) silhouette energy image (SEI) that gives shape and motion information as an input feature. Using these different input methods, we achieved 100 % correct recognition rate (CRR) for each cases. From the result, it is evident that SHI and SEI is found effective input method than other methods in terms of time and space consumption.

Keywords Action recognition · Silhouette energy image · Silhouette history image · Spectral regression discriminant analysis (SRDA) · Edge representation · Distance transform

G. Glorindal Selvam (✉)
MS University, Tirunelveli, Tamil Nadu, India
e-mail: glorygj@yahoo.com

D. Gnanadurai
J.P. College of Engineering, Aykudi, Tenkasi, Tamil Nadu, India

© Springer India 2015

L.P. Suresh et al. (eds.), *Artificial Intelligence and Evolutionary Algorithms in Engineering Systems*, Advances in Intelligent Systems and Computing 325,
DOI 10.1007/978-81-322-2135-7_54

1 Introduction

The human action recognition technology can be applied widely on a range of fields, such as video surveillance for, content-based video search and analysis of sports events, etc. Recognition will require the fusion of different modalities such as head/face detection action recognition, action categorization, gait recognition, 2D/3D tracking, etc. Human action and activity analysis can be categorized on the basis of: geometrical models of human body parts, appearance-based representation, shape or form features-based representation, interest point-based representation, and motion/optical flow-based representation. However, foreground segmentation is not the focus of this paper, and we assume that reliable silhouettes of the human body are available. Most of the literatures from recent past adopted various dimensionality reduction techniques to project the original data that are usually in a very high-dimensional space to a low-dimensional one. The popular linear dimensionality reduction methods are principal component analysis (PCA) [1], linear discriminant analysis (LDA) [2], and locality preserving projections (LPP) [3]. Most of the real-world problem is nonlinear in nature, nonlinear methods such as isometric feature mapping (Isomap) [4], locally linear embedding (LLE) [5], Laplacian eigenmaps (LE) [6], and diffusion maps [7] are proposed. In addition, there are kernel-based methods [8–11]. In all the above-mentioned methods, there exists a common problem, i.e., the large amount of computation caused by the eigen-decomposition of dense matrices. It is expensive in both time and memory. In order to overcome this difficulty, Cai et al. [12, 13] proposed a new subspace learning algorithm, spectral regression discriminant analysis (SRDA). SRDA simply casts projective function learning into a regression framework, which results in linear-time complexity, compared with cubic-time complexity in the other subspace learning algorithms. SRDA has shown to be a promising approach in several applications, such as face recognition [13], speech letter recognition [14], text clustering and categorization [12], and handwritten digital classification [14]. In this paper, we aim to investigate SRDA for dimensionality reduction in silhouette-based human action recognition and compare its performance with one of the linear subspace learning method LPP.

In this work, we use (i) raw silhouettes, (ii) silhouette images obtained after doing distance transform (DT) from the raw silhouette, (iii) silhouette images obtained after extracting edges from the raw silhouettes—Edge representation (iv) silhouette history image (SHI), and (v) silhouette energy image (SEI), which are given as a input for subspace learning during training and testing. SRDA is used as subspace learning for dimensionality reduction, and then, the action classification is achieved in NN framework.

2 Framework of the Proposed Methodology

This section explains various methods of representation visual inputs, activity classification and preprocessing. The experimentation is then carried out to demonstrate the proposed methodology.

2.1 Various Methods of Representing Visual Inputs

Raw Silhouette: For obtaining the raw silhouette, extract the moving silhouette from the original video (see Fig. 1). That extracted moving silhouette is taken as foreground images, which are then centered and normalized on the basis of keeping the aspect ratio property so that they contain as much foreground as possible and are all of equal dimensions. The resulting normalized images are named as raw silhouette representations.

Edge Representation: The resulted normalized image that is the raw silhouettes are processed to represent the edge clearly using Sobel operator [15]. The Sobel operator is used as edge detection algorithms. The Sobel operator is based on convolving the image with a small, separable, and integer-valued filter in horizontal and vertical direction and is therefore relatively inexpensive in terms of computations.

Distance Transform: An input DT is obtained from the raw silhouettes by representing each shape instance as an implicit function by using the DT technique [16]. The result of the transformation is a gray scale. For each pixel in the binary image I, the DT assigns a number that is the distance between that pixel and the nearest nonzero pixel of I and it is used as input.

Silhouette Energy Image (SEI): SEI [17] is defined as the image where the time variation of an action is represented by the overall body shape information. Let us assume $x_t(x, y) = f(x, y, t)$ is the silhouette image in a sequence at time t, which includes an action under duration or a period as shown in Fig. 1. Therefore, SEI (SEI = S(x, y)) is defined by (1). Moreover, (2) and (3) give the standard deviation image as well as motion variation expressions.

$$S(x,y) = \frac{1}{t_e - t_s} \int_{t_s}^{t_e} x_t \mathrm{d}t = \frac{1}{F} \sum_{t=1}^{F} x_t(x,y) \tag{1}$$

$$\sigma(x,y) = \sqrt{\frac{\int_{t=t_e}^{t_e} x_t^2 \mathrm{d}t}{t_e - t_s} - \left(\frac{1}{t_e - t_s} \int_{t=t_s}^{t_e} x_t \mathrm{d}t \right)^2} \tag{2}$$

$$c_v(x,y) = \frac{\sigma(x,y)}{S(x,y)} \tag{3}$$

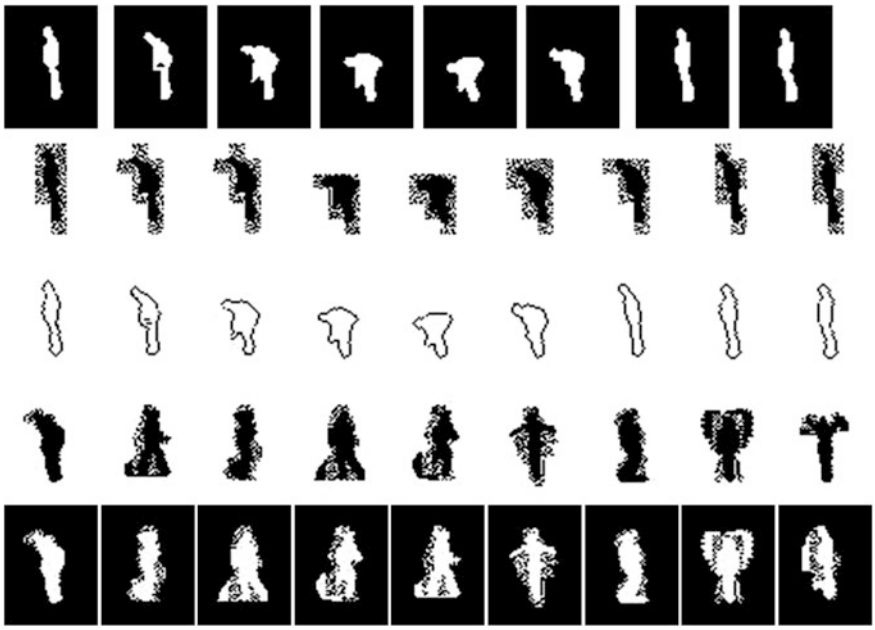

Fig. 1 Visual input representation from top to bottom raw silhouette, DT, edge representation, SEI, and SHI

Here, t_s and t_e are the starting and ending states of an action. Alternately, we can represent total number of frame by F, and hence, the period is F. Therefore, the period or duration becomes $F = t_e - t_s$. Since the average 2D stores the information of global motion distribution and orientation of the silhouette images, it designates this as a SEI. The number of frames in the action depends on the person, time, and type of action performed.

Silhouette History Image (SHI): SHI [16] refers to the shape variation of the image sequence in time. SHI represents how the silhouette of an image sequence is moving. SHI represents the clear information about both body shape and global motion change. The brighter region symbolizes the regency of the global human body shape. The current human body pose is related to the previous one, so here the method of MHI [7] is used. We use silhouette images instead of motion images for making an SHI given by (4).

$$H_t(x, y, t) = \begin{cases} \tau, & \text{if } x_t(x, y) > 1 \\ \max(0, H_t(x, y, t-1)), & \text{otherwise} \end{cases} \tag{4}$$

where τ is the duration of temporal extension to previous silhouette image, and x_t (x, y) is a silhouette image representing the region of human at time t.

The above-mentioned input methods are used as input methods to learn the system using SRDA separately.

2.2 Activity Classification

Action recognition can be achieved through measuring motion similarities between the reference motion patterns and test samples in the low-dimensional embedding space. For finding motion similarity, median Hausdorff distance is used. It measures the resemblance of one point set to another, by examining the fraction of points in one set that lie near points in the other set (and vice versa). We use a variant of the Hausdorff metric, i.e., the median value of the minimum

$$s(\mathrm{A}_1, \mathrm{A}_2) = \mathrm{median}_{\mathrm{i}}\left(\mathrm{min}_{\mathrm{j}}(||\mathrm{A}_1(\mathrm{i}) - \mathrm{A}_2(\mathrm{j})||)\right) \tag{5}$$

Since the Hausdorff distance is oriented, to ensure symmetry, modification of the final distance measure is

$$d = s(\mathrm{A}_1, \mathrm{A}_2) + s(\mathrm{A}_2, \mathrm{A}_1) \tag{6}$$

The smaller the distance measure is the best match. Action classification is performed by means of nearest neighbor framework. Let TA represent a test action sequence and R_i represent the ith reference action sequence for classification. We will classify this test as the class that can minimize the similarity distance between the test sequence and all reference patterns.

$$c = \arg_{\mathrm{i}}\mathrm{mind}(\mathrm{TA}, R_i) \tag{7}$$

where d is the similarity mentioned above. It is efficient to evaluate the discriminatory powers of the used features.

2.3 Preprocessing and Representations of Visual Inputs

A good feature representation is important in pattern recognition. We can obtain sequence of regions of interest (ROI) (i.e., the silhouettes of a moving human) from the original video (see Fig. 1). When there is a static background, a simple but efficient way to find the silhouettes in a sequence is background subtraction, which is out of the scope of this paper. Therefore, we make use of the off-the-shelf silhouette masks in [18] directly. In this paper, we compare and analyze the training time taken by the various forms of necessary mass input information and also the usage of memory for quick recognition. For that, we employ and compare the sequential silhouette methods (raw silhouette, DT, Edge representation) and compressed silhouette (SEI, SHI) obtained from the original video to describe the dynamic shapes of human actions. Figure 1 shows the raw silhouettes of a bending sequence. These foreground images are then centered and normalized to make it of an equal dimensions. The resulting normalized images are named as raw silhouette representations. From the raw silhouettes, other input repetitions used in this paper can be easily computed.

The activity classification framework is explained in Fig. 2.

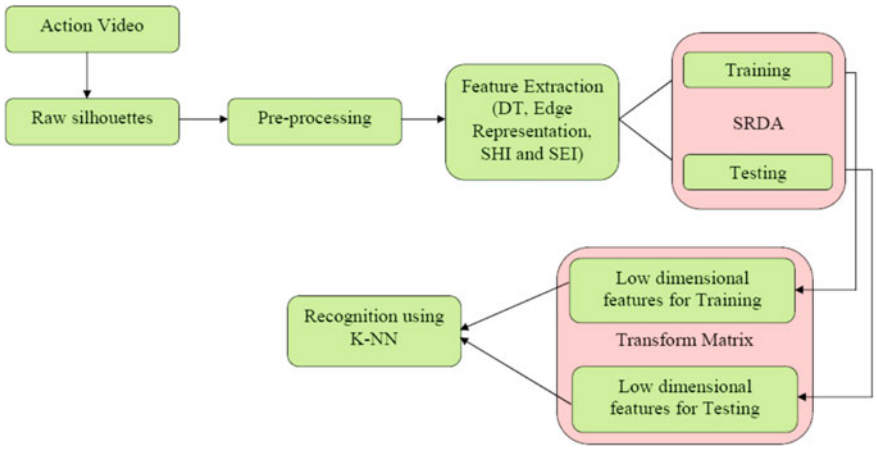

Fig. 2 Block diagram of the proposed framework

3 Experimental Results

To evaluate the performance of the proposed algorithm, a widely used Weizmann action database reported in [19] is used. It includes 90 low-resolution videos (180 × 144; 25 fps) of nine different subjects, each performing 10 natural actions (bending, jumping, jumping-forward-on-two-legs, running, jumping-in place-on-two-legs, walking, galloping-sideways, waving one-hand, skipping, and waving two-hands). Also, each action in this dataset is performed by different people with different physical characteristics and motion styles, thus providing more realistic data for testing the versatility of the proposed method.

3.1 Results and Discussions

We compare and analyze with the input methods such as (i) raw silhouettes (ii) DT (iii) edge representation, (iv) SHI, and (v) SEI refer from different methods by using the Weizmann database and SRDA. For defining the rate of recognition, correct recognition rate (CRR) is used.

$$\mathrm{CRR} = \frac{N_C}{N_a} \times 100 \tag{8}$$

where N_C is the total number of correct recognition sequences, while N_a is the number of total action sequences. Here, we adopt leave-one-out scheme for computing all recognition rates. That is, use eight out of the nine persons in the dataset to train the classifier, and the ninth person is utilized in the test phase. Repeat this

	bend	jack	jump	pjump	run	side	skip	walk	wave1	wave2
bend	1.0	0.00	0.00	0.00	0.00	0.00	0.00	0.00	0.00	0.00
jack	0.00	1.0	0.00	0.00	0.00	0.00	0.00	0.00	0.00	0.00
jump	0.00	0.00	1.0	0.00	0.00	0.00	0.00	0.00	0.00	0.00
pjump	0.00	0.00	0.00	1.0	0.00	0.00	0.00	0.00	0.00	0.00
run	0.00	0.00	0.00	0.00	1.0	0.00	0.00	0.00	0.00	0.00
side	0.00	0.00	0.00	0.00	0.00	1.0	0.00	0.00	0.00	0.00
skip	0.00	0.00	0.00	0.00	0.00	0.00	1.0	0.00	0.00	0.00
walk	0.00	0.00	0.00	0.00	0.00	0.00	0.00	1.0	0.00	0.00
wave1	0.00	0.00	0.00	0.00	0.00	0.00	0.00	0.00	1.0	0.00
wave2	0.00	0.00	0.00	0.00	0.00	0.00	0.00	0.00	0.00	1.0

Fig. 3 Confusion matrix of SRDA

procedure for all nine persons and the resulting correct recognition rates are then averaged. For the classification purpose, we use k-nearest neighbors ($K = 1$) with median Haudsroff distance used for similarity measure. Figure 3 shows the confusion matrices of the SRDA subspace learning technique. The cross-line values in the tables are the correctly classified rates, while the nonzero values indicate the probabilities of the actions that are mis-classified.

From Fig. 3 we can infer that SRDA have not mis-classified any of the actions given in the dataset. An overall comparison of CRR is shown in Table 1.

We also compare our result of training time taken and memory usage for all selected inputs of raw silhouettes, DT, edge representation, SHI, and SEI in Table 2. These methods are tested on the same dataset of Weizmann [19]. As expected, by the method with selected input features of SHI and SEI is quiet good because it compressed the frames of all essential silhouette image sequences occurred in the each action videos into single frame. That in turn reduces the consumption time and memory to learn the system than when it compared with the

Table 1 Comparison with other techniques

Literature	Method	CRR (%)
Kellokumpu et al. (2008) [20]	LBP	97.8
Jia et al. (2008) [21]	ASTDE	90.9
Wang and Suter (2010) [17]	LPP	97.8
Zhen et al. (2010) [22]	SSDM	98.8
Shao and Chen (2010) [23]	SRDA (BoW-histogram of body poses)	100
	SRDA (raw silhouettes)	100
Proposed methods	SRDA (DT)	100
	SRDA (edge representation)	100
	SRDA (SHI)	100
	SRDA (SEI)	100

Table 2 Training details for different input features

Input method for learning using SRDA	Training time taken (ms)	Memory usage (mb)
Raw silhouettes	1,695.86	36
DT	46,820.7	36
Edge DT	1,773.87	36
SHI	29.44	30
SEI	24.99	31

input of using raw silhouettes, DT, and edge representation. The adopted dimensionality reduction technique SRDA for our proposed work also yields the 100 % CRR for all the cases taken for study.

4 Conclusion and Scope for Future Research

In this research, work for human action recognition problem and SRDA-based methodology is proposed and discussed. *K*-NN is used for action classification. To test the performance of SRDA-based proposed methodology, five input methods were proposed such as raw silhouettes, DT, edge representation, SHI, and SEI. We achieved 100 % CRR for all the cases. In addition to that, following conclusions are drawn.

- By adapting the method of using compressed image as single input feature, for each action of SHI and SEI with SRDA as subspace learning method on silhouette-based human action recognition for dimensionality reduction gives comparably better result than using other input methods (raw silhouettes, DT, and edge representation) having large sequence of frames as input.
- Our effective analysis avoids the complexity for learning the system as well as the large computation in sequence matching-based methods (refer Table 2).

In future, we would like to extend our approach to detect multiple activities in the same video to provide a more complete understanding of the complete scene in both space and computation time for recognition of actions.

References

1. M. Turk, A. Pentland, Eigenfaces for recognition. J. Cogn. Neurosci. **3**(1), 71–86 (1991)
2. R.O. Duda, P.E. Hart, D.G. Stork, Pattern Classification (2000)
3. X. He, S. Yan, Y. Hu, P. Niyogi, H. Zhang, Face recognition using laplacian faces. IEEE Trans. Pattern Anal. Mach. Intell. **27**(3), 328–340 (2005)
4. J.B. Tenenbaum, V. de Silva, J.C. Langford, A global geometric framework for non linear dimensionality reduction. Science **290**, 2319–2323 (2000)

5. S.T. Roweis, L.K. Saul, Nonlinear dimensionality reduction by locally linear embedding. Science **290**, 2323–2326 (2000)
6. M. Belkin, P. Niyogi, Laplacian eigenmaps for dimensionality reduction and data representation. Neural Comput. **15**, 1373–1396 (2003)
7. R.R. Coifman, S. Lafon, A.B. Lee, M. Maggioni, B. Nadler, F. Warner, S. Zucker, Geometric diffusions as a tool for harmonics analysis and structure definition of data. Proc. Natl. Acad. Sci. **102**(21), 7426–7431 (2005)
8. B. Schlkopf, A.J. Smola, Learning with Kernels (2002)
9. L. Wang, D. Suter, Recognizing human activities from silhouettes: motion subspace and factorial discriminative graphical model, in *Computer Vision and Pattern Recognition* (2007), pp. 1–8
10. S. Mika, G. Ratsch, J. Weston, B. Scholkopf, K.-R. Muller, Fisher discriminant analysis with kernels, in *Proceedings of IEEE Neural Networks for Signal Processing Workshop* (*NNSP*) (1999)
11. G. Baudat, F. Anouar, Generalized discriminant analysis using a kernel approach. Neural Comput. **12**, 2385–2404 (2000)
12. D. Cai, X. He, J. Han, Regularized locality preserving indexing via spectral regression, in *ACM International Conference on Information and Knowledge Management* (2007)
13. D. Cai, X. He, J. Han, Spectral regression for efficient regularized subspace learning, in *IEEE International Conference on Computer Vision* (*ICCV*) (2007)
14. D. Cai, X. He, J. Han, SRDA: an efficient algorithm for large scale discriminant analysis. IEEE Trans. Knowl. Data Eng. **20**(1), 1–12 (2008)
15. H. Scharr, Optimal second order derivative filter families for transparent motion estimation, in *15th European Signal Processing Conference* (*EUSIPCO 2007*) (2007)
16. M. Ahmad, I. Parvin, S.-W. Lee, Silhouette history and energy image information for human movement recognition. J. Multimedia **5**(1), 12–21 (2010)
17. L. Wang, D. Suter, Learning and matching of dynamic shape manifolds for human action recognition. IEEE Trans. Image Process. **16**(6), 1646–1661 (2007)
18. M. Blank, L. Gorelick, E. Shechtman, M. Irani, R. Basri, Actions as space-time shapes. IEEE Int. Conf. Comput. Vision **2**, 1395–1402 (2005)
19. M. Blank, L. Gorelick, E. Shechtman, M. Irani, R. Basri, Actions as space-time shapes. IEEE Int. Conf. Comput. Vision **2**, 1395–1402 (2005)
20. V. Kellokumpu, G. Zhao, M. Pietikainen, Texture based description of movements for activity analysis, in *Proceedings of 3rd International Conference on Computer Vision Theory and Applications* (2008)
21. K. Jia, D. Yeung, Human action recognition using Local Spatio-Temporal Discriminant Embedding, in *IEEE Conference on Computer Vision and Pattern Recognition* (2008)
22. F. Zheng, L. Shao, Z. Song, Eigen-space Learning Using Semi-supervised Diffusion Maps for Human Action Recognition, in *ACM International Conference on Image and Video Retrieval (CIVR)* (2010)
23. L. Shao, X. Chen, Histogram of body poses and spectral regression discriminant analysisfor human action categorization, in *Proceedings of the British Machine Vision Conference*(2010)

Vertical Handoff Scheme in Integrated WiMAX and WLAN Networks

A. Anitha and J. JayaKumari

Abstract This paper deals with a proactive vertical handoff method to provide the QoS in the integration of WLAN and WiMAX networks. The handoff process is controlled by the vertical handoff management scheme. For every neighboring node in the destination network, the QoS metrics such as bandwidth and delay is measured. Based on the QoS metrics measured, the handoff process is initiated. This work is simulated in NS-2.34 network simulator. The simulation result shows a high performance increase in the increase in speed. This work also analyzed the performance of the integration of networks from WLAN–WiMAX and WiMAX–WLAN. From the analysis, the minimum delay is achieved in WLAN–WiMAX and high bandwidth in WiMAX–WLAN networks.

Keywords WLAN · WiMAX · Handoff · Bandwidth · Delay

1 Introduction

Wireless networking is the technology which enables communication between two or more computers using standard network protocols without any wires. The wireless networking revolution made communication changes to data networks and telecommunication and made the integrated networks a reality. The wireless networks transmit large number of applications and data such as video and real-time voice applications [1]. For the successful transmission of these data and applications, the network must provide a secure and guaranteed service. To achieve this, the network resources should be managed properly. The network resources in the network can be managed by a technique known as quality of service (QoS).

A. Anitha (✉)
CSE Department, Noorul Islam Centre for Higher Education, Kumaracoil, India
e-mail: anidathi@yahoo.co.in

J. JayaKumari
ECE Department, Noorul Islam Centre for Higher Education, Kumaracoil, India
e-mail: jkumaribharat@yahoo.com

© Springer India 2015

L.P. Suresh et al. (eds.), *Artificial Intelligence and Evolutionary Algorithms in Engineering Systems*, Advances in Intelligent Systems and Computing 325,
DOI 10.1007/978-81-322-2135-7_55

The metrics to achieve QoS are delay, bandwidth, jitter, and packet drop should be properly managed. This work mainly focuses on the integration of worldwide interoperability for microwave access (WiMAX) and wireless local area network (WLAN). WLAN is the wireless method for connecting two or more devices using access point (AP). WiMAX is a standard technology that enables high-speed wireless Internet. To integrate both the networks, a handoff method is used. The handoff method maintains the active connection of the nodes even it switches to another network. Based on the number of connections, the handoff is classified as soft and hard handoff. Hard handoff occurs when the mobile terminal associated with only one point of attachment at a time. In this case, the mobile terminal sets a new connection at the target point of attachment after the old connection. The soft handoff occurs when the mobile terminal communicates with more than one point of attachment. The mobile terminal's connection is also created at the target point of attachment before the old connection is released [2].

Vertical and horizontal [3, 4] are the two network types of handoff. Horizontal handoff (intrasystem handoff) is a handoff between two base stations of the same network. The vertical handoff (intersystem handoff) is a handoff between two base stations of the different networks. This work focuses on the integration between two different networks. So the vertical handoff method is used. The vertical handoff is of two types: upward handoff and downward handoff. The upward vertical handoff is a handoff with a larger cell size and lower bandwidth. The downward handoff is a handoff with a smaller cell size and higher bandwidth.

The vertical handoff scheme provides best QoS. The mobile movement of the nodes from one network to other is supported by the handoff process by changing the type of the network connection. If there is more than one network, then the vertical handoff process considers more metrics. QoS and user preference are the two metrics considered by the vertical handoff process. The QoS metrics: If a node in the connected network does not satisfy the QoS requirements, then the node from that network moves to another network to improve the performance. User preferences are power, cost, and speed. In this work, we have considered the QoS metrics in the vertical handoff process. The QoS metrics are evaluated for the neighbor nodes in the destination network. If the network satisfies the QoS metrics such as bandwidth and delay, then the handoff process is initiated, i.e., best quality network is selected.

The rest of the paper is organized as follows. Section 2 surveys the previous works related to our method. Section 3 explains the proposed work. Section 4 explains the evaluation of our proposed, work and the paper is concluded in Sect. 5.

2 Related Work

Guo et al. [5] proposed a movement-aware vertical handoff algorithm to reduce the unnecessary handover. This MAV handover algorithm exploited the movement pattern to avoid the unnecessary handovers in the integrated WLAN and Mobile WiMAX networks. It adjusted the dwell time according to MS mobility. When the

ping-pong effect was detected, dwell time reduced the vertical handover process. The two desirable features such as seamlessness and proactiveness were considered in the vertical handoff scheme in [6]. This paper proposed a vertical handoff management scheme that controls the handoff process. The proactive handoff performed the handoff process such as handoff initiation, handoff decision, and handoff execution. The available bandwidth and delay of the network are estimated. This method finds the best node of the target network, and then, the handoff process is performed. So, it does not maintain the QoS of the whole network. The QoS metrics are considered in [7, 8] for handoff decision.

The handover scheme is proposed in [7], to meet the QoS parameters such as minimum data rate, maximum data block delay, and the maximum bit error rate. The intersystem handover scheme to the IEEE 802.11b network was performed only if the QoS requirements satisfied the IEEE 802.11b network. Two components such as connection manager and virtual connectivity proposed in [8] for roaming across heterogeneous wireless networks such as WWAN and WLAN pose considerable challenges; it is difficult to maintain the existing connections and guarantee the necessary QoS. Moreover, an application layer subscription/notification service was introduced to support mobility.

The bandwidth recycling scheme was proposed to recycle the unused bandwidth in [9]. Three scheduling algorithms such as priority-based scheduling algorithm, rejected bandwidth algorithm, and hybrid scheduling algorithm are used to improve the throughput. And also the authors claimed that it reduces the delay with negligible overhead and without degrading the QoS requirements. Such complexity introduced large overhead and thus subsequently degraded the QoS guarantees. The CSMA/CA was proposed in the IEEE 802.11 MAC protocol for wireless networks. The queuing characteristics of WLAN are analyzed in [10] and also evaluated the accuracy for the MAC layer service time. It concluded that the service time distributions are approximated by the exponential distribution.

3 Proposed Method

Handoff [11] is the process that the mobile node keeps its connection active when it moves from one network to another. The vertical handoff process is divided into three phases such as handoff initiation, handoff decision, and handoff execution. In the handoff initiation phase, the vertical handoff management scheme measures the performance of the applications. The handoff decision phase is the ability to decide when to perform the vertical handoff process and determines the best network. The handoff execution phase transfers the connections [6].

In the proposed approach, before handover to the new network, QoS value is estimated for all the available neighbor nodes depicted in Fig. 1. The QoS verification module verifies the parameter of the node when the node moves along the boundary. The QoS value of the node can be estimated in terms of bandwidth and delay. From that, the neighbor network which provides the best QoS value is

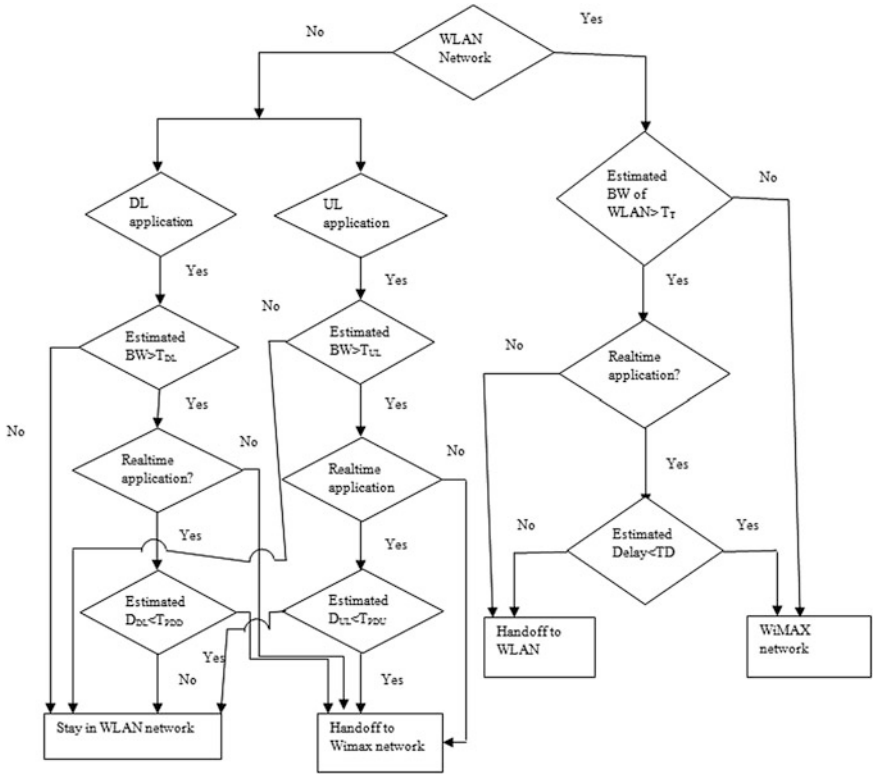

Fig. 1 Proposed decision algorithm

selected, and then, the handoff process is initiated. If the source network is the WLAN network, the handoff decision is done as follows. First, check whether the bandwidth [12] of WLAN is greater than the threshold of WLAN. If so, it is the real-time application; then, the handoff process is done. If not, the handoff process is not done. If the application is real time, then the packet delay of WLAN is checked with the threshold value. If the packet delay is less than the threshold value, then the handoff process is done to WLAN. Else, the network stays in WiMAX.

If the source network is the WiMAX network, the handoff decision is done as follows. First, the application is checked to find whether it is the UL/DL application. UL is the communication from ground to satellite, and DL is the communication from satellite to the ground. If the application is DL, then check whether the bandwidth of DL WiMAX is greater than the threshold of DL WiMAX. If not, stay in WLAN network. Then, check for real-time and non-real-time application. If it is a real-time application, then check whether the average packet delay of DL WiMAX is less than the threshold value. If yes, then the handoff process is done to WiMAX. Else, stay in WLAN network. If the application is UL, then check

Table 1 Parameters used in decision algorithm

Parameters	Meaning
UL	UpLink
DL	DownLink
T_T	Bandwidth threshold of WLAN
TD	Average packet delay threshold of WLAN
T_{DL}	Bandwidth threshold of DL WiMAX
T_{UL}	Bandwidth threshold of UL WiMAX
T_{PDD}	Average packet delay threshold of DL WiMAX
T_{PDU}	Average packet delay threshold of UL WiMAX

whether the bandwidth of UL WiMAX is greater than the threshold of UL WiMAX. If not, stay in WLAN network. Else, check for real-time and non-real-time application. If it is a real-time application, then check whether the average packet delay of UL WiMAX is less than the threshold value; then, the handoff process is done to WiMAX. Else, stay in WLAN network. The vertical handoff management scheme performs the handoff mechanisms. Table 1 gives the parameters used in the proposed decision algorithm.

4 Evaluation of the Proposed Work

The WiMAX and WLAN networks [13] are created using NS-2.34 simulator in Red Hat Linux Environment. The first topology WiMAX is created using MAC, and the second topology WLAN too is created using MAC. The nodes are created in a configurable fashion, and the required NAM is created to view the simulation. In this approach, the QoS parameter of a particular node is measured when it roams along the boundary. The QoS parameters are bandwidth and delay. Bandwidth refers to the data rate supported by the network. Delay is the end-to-end transfer time between two communicating mobile stations. The QoS of the source and destination node will be verified as per the proposed concept before the handoff process is initiated.

After verifying the QoS parameters such as bandwidth and delay of both the networks, initiate the handoff process. So to initiate the handoff process, select the best node of the neighbor nodes of the available destination network. And then, the handoff process takes place to that particular node of the destination network.

First, the source network considered is the WLAN network; the handoff decision is done as follows. First, the bandwidth of WLAN is checked with the threshold value 1.4 MB. The value is greater and is the real-time application. So the handoff process is done. Then, the packet delay of WLAN is checked with the threshold value 1.4 MB and is less than the threshold value; then, the handoff process is done to WLAN. Next, the source network is considered as WiMAX network and the

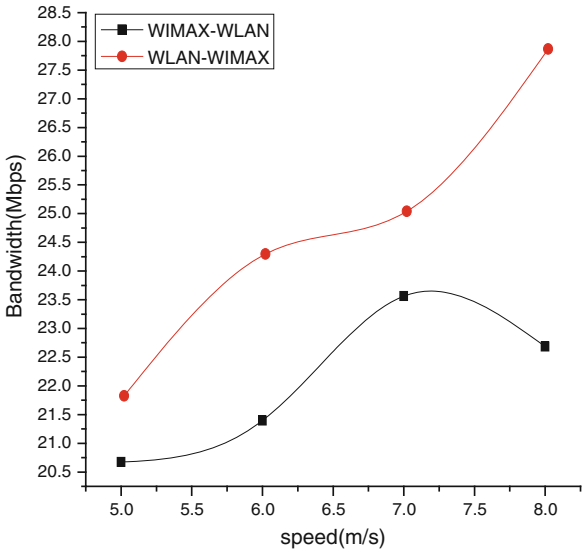

Fig. 2 Bandwidth under different speeds for WIMAX–WLAN and WLAN–WIMAX

application is the DL application. The bandwidth of DL WiMAX is greater than the threshold of DL WiMAX (1.4 MB), and average packet delay of DL WiMAX is less than the threshold value; then, the handoff process is done to WiMAX. In the UL application, the bandwidth of UL WiMAX is greater than the threshold of UL WiMAX (1.4 MB) and the average packet delay of UL WiMAX is less than the threshold value; then, the handoff process is done to WiMAX.

Figure 2 shows the values of bandwidth under different speeds of both WiMAX–WLAN networks and WLAN–WiMAX networks. From the figure, at 5 s speed, the bandwidth of WiMAX–WLAN is higher. But when the speed is incremented, the bandwidth of WLAN–WiMAX is higher than the previous. Under different speeds, the bandwidth varies with a small change on both the networks.

Figure 3 shows the delay of both the networks under various speeds. It shows that at speed 5, speed 6, speed 7, and speed 8, the delay increases in WiMAX–-WLAN networks compared to WLAN–WiMAX networks. We estimated the QoS parameters such as bandwidth and delay under different speeds of both WiMAX–WLAN and WLAN–WiMAX networks. After performing the handoff process, the throughput of both the networks is measured. Figure 4 shows the throughput of WLAN–WiMAX and WiMAX–WLAN networks. The result shows that when the speed is increased, both the networks gave high throughput. Based on the handoff decision process, the effectiveness of the proposed scheme is proved.

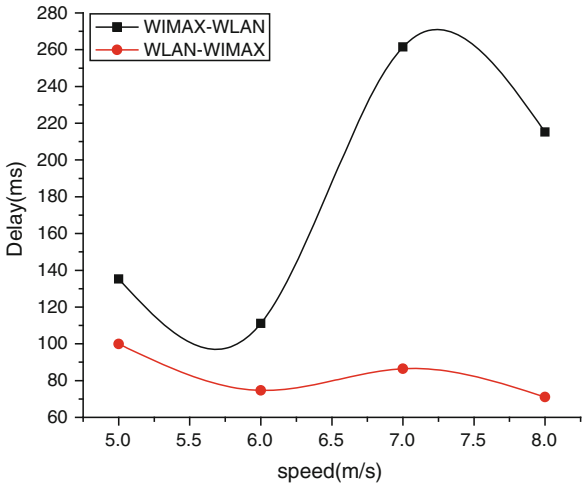

Fig. 3 Delay of WIMAX–WLAN and WLAN–WIMAX under different speeds

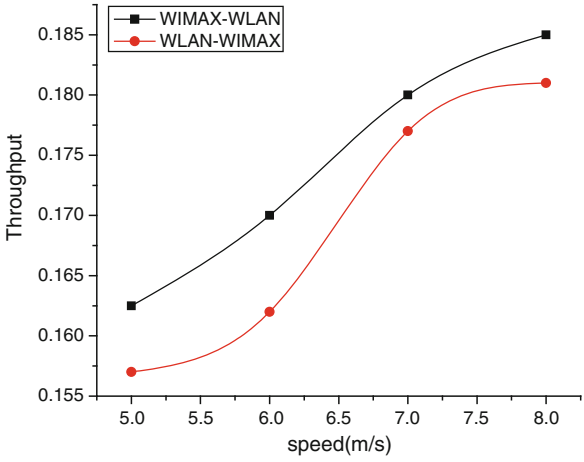

Fig. 4 Throughput of WIMAX–WLAN and WLAN–WIMAX networks under different speed

5 Conclusion

In this work, the vertical handoff scheme is performed between the WiMAX and WLAN networks. The vertical handoff management scheme controls the handoff operations such as handoff initiation, handoff decision, and handoff execution. To maintain the QoS of the whole network, we selected the best QoS value of the neighbor network, and then, the handoff process is performed. This work is simulated in Ns-2.34 network simulator in the Red Hat Linux operating system. The simulation results achieved better performance while integrating the WiMAX and WLAN networks.

References

1. H. Zhai, Y. Kwon, Y.G. Fang, Performance analysis of IEEE 802.11 MAC protocols in wireless LANs. Wirel. Commun. Mob. Comput. **4**(8), 917–931 (2004)
2. W. Lee, E. Kim, J. Kim, I. Lee, C. Lee, Movement-aware vertical handoff of WLAN and mobile WiMAX for seamless ubiquitous access. IEEE Trans. Consum. Electron. **53**(4), 1268–1275 (2007)
3. C.W. Lee, L.M. Chen, M.C. Chen, Y.S. Sun, A framework of handoffs in wireless overlay networks based on mobile IPv6. IEEE J. Sel. Areas Commun. **23**(11), 2118–2128 (2005)
4. N. Nasser, A. Hasswa, H. Hassanein, Handoffs in fourth generation heterogeneous networks. IEEE Commun. Mag. **44**(10), 96–103 (2006)
5. C. Guo, Z. Guo, Q. Zhang, W. Zhu, A seamless and proactive end-to-end mobility scheme for roaming across heterogeneous wireless networks. IEEE J. Sel. Areas Commun. **22**(5), 834–848 (2004)
6. D. Chuck, J. Chang, Bandwidth recycling in IEEE 802.16 networks. IEEE Trans. Mob. Comput. **9**(10), 1451–1464 (2010)
7. D. Ma, M. Ma, A QoS oriented vertical handoff scheme for WiMAX/WLAN overlay networks. IEEE Trans. Parallel Distrib. Syst. **23**(4), 598–606 (2012)
8. A.V. Garmonov et al., QoS-oriented intersystem handover between IEEE 802.11b and overlay networks. IEEE Trans. Veh. Technol. **57**(2), 1142–1154 (2008)
9. R. Rathiya, A. Anitha, J. JayaKumari, Efficient QoS oriented vertical handoff scheme in the integration of WIMAX/WLAN networks, in *Proceedings of IEEE Conference on Information and Communication Technologies (ICT 2013)* (2013), pp. 378–381
10. N. Nasser, A. Hasswa, H. Hassanein, Handoffs in fourth generation heterogeneous networks. IEEE Commun. Mag. **44**(10), 96–103 (2006)
11. S.F. Yang, J.S. Wu, Handoff management schemes across hybrid WiMAX and Wi-Fi networks, in *Proceedings of IEEE TENCON* (2007), pp. 680–683
12. R. Prasad, C. Dovrolis, M. Murray, K. Claffy, Bandwidth estimation: metrics measurement techniques and tools. IEEE Network **17**(6), 27–35 (2003)
13. W. Yang, Y. Wang, Y. Tseng, B.P. Lin, Energy-efficient network selection with mobility pattern awareness in an integrated WiMAX and WiFi network. Int. J. Commun. Syst. **23**(2), 213–230 (2010)

An Analysis of Various Edge Detection Techniques on Illuminant Variant Images

S.H. Krishna Veni and L Padma Suresh

Abstract One of the key challenges of face recognition is varying illumination. Many feature-based methods were developed in the recent years to detect the illuminant invariant facial features. This paper mainly focuses on the effect of various edge detection algorithms on illuminant variant images. The conventional sobel and adaboost are applied. Along with that, the proposed NSCT integrated ant colony optimization (ACO) approach is also used. The proposed method comprises a normal shrink filter in NSCT domain which produces illuminant invariant for the given image. Then, to capture the important geometrical structures and to reduce the feature dimensionality, ACO algorithm is performed. This combined approach fairly detects the edges with improved quality. Finally, for recognition, a graph matching algorithm is employed. This algorithm utilizes a group of feature points to explore their geometrical relationship in a graph arrangement. While applying the three methods to the YaleB database, experimental results show that the proposed work yields the better recognition.

Keywords Illuminant invariant · Non-subsampled contourlet · Feature subset · Ant colony optimization · Weighted graph matching

1 Introduction

The most challenging aspects of face recognition are variations in head pose, expression, and illumination. Among these factors, head pose and illumination changes become a great issue. Various approaches have been proposed in the last decades to eradicate the illumination problems.

S.H. Krishna Veni (✉)
Noorul Islam Centre for Higher Education, Kumaracoil, Kanyakumari, India
e-mail: veni_shk@ymail.com

L Padma Suresh
Electrical and Electronics Engineering, Noorul Islam Centre for Higher Education, Kumaracoil, Tamil Nadu, India
e-mail: suresh_lps@yahoo.co.in

© Springer India 2015

L.P. Suresh et al. (eds.), *Artificial Intelligence and Evolutionary Algorithms in Engineering Systems*, Advances in Intelligent Systems and Computing 325,
DOI 10.1007/978-81-322-2135-7_56

In earlier developments, techniques such as logarithm transform and histogram equalization [1] were used. They work well for low illumination variant images but difficult to deal with complicated illumination variations. Liu et al. proposed a method for illumination changes using a ratio image [2] between the face image and a reference face image, both of which are blurred by a Gaussian filter. Fixed illumination condition is possible here. Still complex illumination problems cannot be rectified completely. Park et al. use retinex theory [3] for illumination estimation and normalization using several low-pass filters with different cutoff frequencies. LCE [4] efficiently improves visibility of the fine textures, but it may result in problems of visible gradient reversal or generate undesired halos. A comparative study of illumination preprocessing methods [5] were proposed by Han et al. shows that holistic illumination preprocessing approaches, e.g., HE, GIC, LTV, and TT, improve the performance. Also, the face reflectance field estimation-based methods only decompose a face image into two bands. Two-band decomposition is still insufficient for analyzing the importance of individual feature bands in face recognition.

In recent years, the development was focused on multiband decomposition of face images. Under this, multi-resolution concepts were spread rapidly. Wavelet [6] transforms emerge which has better edge preserving ability in low-frequency illumination fields and better useful information saving ability in high-frequency fields. But it fails to preserve the important feature extraction properties such as directionality and anisotropy. Also, it can only detect the edges in horizontal, vertical, and 45° orientations. Later, a new image representation was proposed, namely the contourlet transform which is a new two-dimensional extension of the wavelet transform using multiscale and directional filter banks. But, oversampling becomes an issue. Hence, recent developments focus on non-subsampled contourlet transforms.

The proposed work adopts a normal shrink filter in NSCT domain [7] to extract illumination invariant. Compared with the existing methods, the proposed method can better preserve edges due to the non-subsampled contourlet transform with multiscale, multi-direction analysis and shift invariance. The peculiar feature of the proposed work is integrating ant colony optimization (ACO) algorithm to the extracted illuminant invariant image [8, 9]. Experimental results on the YaleB database show that the proposed method is robust and effective for face recognition with varying illumination conditions.

2 Methodology

The methodology of implementation is organized as follows: Sect. 2.1 explains about preprocessing method. Section 2.2 describes the NSCT-based method for illumination invariant extraction. In Sect. 2.3, ACO algorithm is explained, and in Sect. 2.4, graph matching algorithm is discussed. Experimental results are discussed

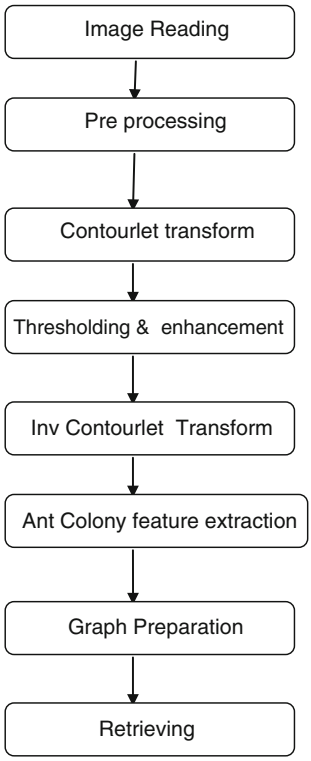

Fig. 1 Data flow diagram

in Sect. 3. Finally, Sect. 4 deals with conclusions and future work. The data flow diagram for the proposed method is given in Fig. 1.

2.1 Preprocessing

A gray scale face image F under illumination conditions is represented by,

$$F(x, y) = I(x, y) \cdot R(x, y) \tag{1}$$

where $I(x, y)$ and $R(x, y)$ are the illumination and the reflectance at a point (x, y). The value of R cannot be obtained directly; hence, a normal shrink-based denoising model is applied to extract R. To apply denoising model, logarithmic transform is computed. Thus, Eq. (1) can be rewritten as

$$F' = I' + R' \tag{2}$$

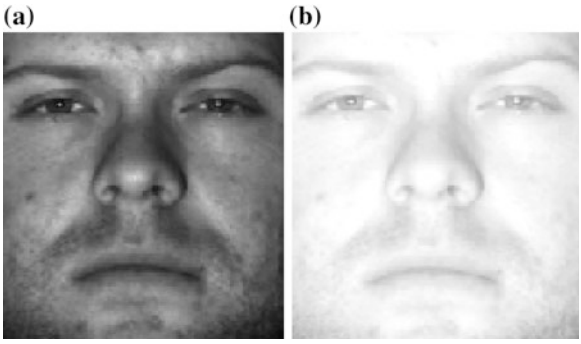

Fig. 2 **a** Original image. **b** Preprocessed logarithmic image

The transformation of this type expands the values of dark pixels in an image while compressing the higher level values. As a result, logarithm transform can partially reduce the effect of various illumination conditions. Figure 2a and b shows the original and logarithm image of low illuminant variant image.

2.2 NSCT-Based Denoising Model for Illumination Invariant Extraction

The stages to generate the NSCT are (1) 2-directional wavelet transform to generate *LL*, *Hh,* and *Hv,* (2) finer directional decomposition of *Hh* and *Hv, and* (3) iterate the one-level NSCT on *LL*. All the NSCT sub-bands are given as the following:

$$\begin{aligned}\left\{Ci_0, C_{ij}\right\}, i, \quad & i_0 = 1, 2, \ldots, n;\ i \le i_0; \\ & j = 2, 4, 8 \ldots, m;\ n \in N,\ m \in 2^N,\end{aligned} \tag{3}$$

where i is the scale of decomposition, j is the direction of decomposition, Ci_0 is the low-frequency coefficient, and $C_{i,j}$ is the high-frequency coefficient at the jth directional sub-band of the ith scale. In this model, $i_0 = 3$ and $j = \{2, 4, 8\}$.

The next step is to select a threshold for image denoising.

$$t_{ij} = \frac{\beta \sigma_{ij}^2}{\sigma_{ij}^x} \tag{4}$$

$$\beta = \sqrt{\log\left(\frac{L_{ij}}{S}\right)} \tag{5}$$

$$\sigma_{ij} = \frac{\text{Median}\left|C_{ij}\right|}{\lambda} \tag{6}$$

Fig. 3 Illuminant invariant

$$\sigma_{ij}^{x} = \frac{1}{m \cdot n} \sum_{k=1}^{m} \sum_{l=1}^{n} \left(C_{ij}(k,l) - \overline{C_{ij}} \right)^2 \tag{7}$$

where λ is a parameter, whose general value is 0.6745, m and n are the height and width of an image, L_{ij} is the length of the jth directional sub-band of the ith scale, S is the maximal scale of NSCT, and C_{ij} is the average of coefficients at the jth directional sub-band of the ith scale.

$$c_{ij}^{\text{thr}} = \begin{cases} 0 & |c_{ij}| < t_{ij} \\ c_{ij} - wt_{ij} & c_{ij} \geq t_{ij} \\ c_{ij} + wt_{ij} & c_{ij} \leq t_{ij} \end{cases} \tag{8}$$

$$w = \frac{t_{ij}}{|c_{ij}(k,l)| \exp\left(|c_{ij}(k,l)| - t_{ij} \right)} \tag{9}$$

The algorithm for extracting the illuminant variant features is given below.

1. Take the logarithm operation for the original face image F, $F' \approx = \log(F)$.
2. Perform multiscale decomposition of the logarithm facial image F' using NSCT.
3. Compute threshold t_{ij} at each directional sub-band of each scale using Eqs. (4)–(7).
4. Apply soft thresholding to each directional sub-band of each scale using Eqs. (8) and (9).
5. Reconstruct illumination I' from the modified NSCT coefficients by inverse NSCT. The sample of illuminant invariant is shown in Fig. 3.

2.3 ACO Feature Selection

In an artificial ant colony system developed by imitating the real ant's behavior, ant chooses its next step depending upon the transition probability matrix which is a function of the amount of pheromone on the path and the heuristic factor, e.g., the

Fig. 4 Optimal feature extracted image

distance between the points. We now assume that there are M ants constituting an ant colony. Initially, at $t = 0$, let the value of the pheromone present on each edge be $\tau_{ij}(0)$. In K iterations, each ant moves through a distance making a route. The pheromone deposited on every route is computed from:

$$\tau_{ij}(k+1) = \rho\tau_{ij}(k) + \Delta\tau_{ij}(k+1) \tag{10}$$

$$\tau_{ij}(k+1) = \begin{cases} \frac{Q}{\mathrm{Lm}} & \text{if ant uses edges } ij \text{ in its route} \\ 0 \end{cases} \tag{11}$$

where $0 < \rho < 1$ is a coefficient that represents the attenuation of trail. Q is a positive constant. Lm is the length of the route which an ant has traversed in its tour. The transition probability matrix, $P_{ij}(t)$, is given by:

$$P_{ij} = \left\{ \frac{\left(\left[\tau_{ij}(t)\right]^{\alpha}\right)\left(\left[\eta_{ij}\right]^{\beta}\right)}{\sum ij\varepsilon\,\mathrm{allowed}_{ij}\left(\left(\left[\tau_{ij}(t)\right]^{\alpha}\right)\left(\left[\eta_{ij}\right]^{\beta}\right)\right)} \right\} \tag{12}$$

When η_{ij} is the heuristic factor, $\mathrm{allowed}_{ij}$ is the set of points available, and α and β are two application-dependent parameters that control the relative importance of the two main factors τ_{ij} $(t)j$ and η_i. Transition probability matrix is obtained for every ant, and those ants whose matrix remains null are not moved. When all ants have stopped moving, it means that we have reached the minima. The corresponding output is shown in Fig. 4.

2.4 Graph Transformation Matching

In this algorithm, the relationship between adjacent features relies on the angular distances between neighboring features. Also, the matching between corresponding features in two images will proceed only if the angles between each feature and its neighboring features provide sufficient support to that matching. The angular

distance is also less sensitive to the noise originating from lens distortion. Following steps describe the proposed algorithm.

1. Assume there are two sets of N-feature points with an initial one-to-one relationship ($P = \{pi\}$ and $P' = \{pi'\}$). Two median $K - NN$ graphs $G_P = (V_P, E_P)$ (with adjacency matrix A_P) and $G_{P'} = (V_{P'}, E_{P'})$ (with adjacency matrix $A_{P'}$) are generated for the sets P and P', respectively. A vertex v_i for each match correspondence pi, such that $VP = \{v1,\ldots, vN\}$. A directed edge (i, j) exists when pj is one of the closest neighbors of pi and also $\| pi - pj \| \leq \eta$. Here, η is defined by

$$\eta = (l, m \in) \overset{\text{median}}{V_p \times V_p} \|p_l - p_m\| \tag{13}$$

2. Find all vertices of GP with at most one edge (connection) with other vertices ($\{v_i \,|\sum_{\forall\ j,(i,\ j)\in Ep} A_{P(i,\ j)} \leq 1\}$) and remove them and their correspondences from G_P and $G_{P'}$. Recompute both G_P and $G_{P'}$. Repeat this step until all vertices of G_P have minimum of two edges.
3. A weight matrix W is generated for each point p_i using graph G_P. For the edge that connects vertex v_i to $v_{m,}$ compute a weight value using the following equation:

$$w_{(i\cdot m)} = \left| A\cos\left(\frac{(p_m - p_i).\left(\left(p'_{m-} p'_i\right)\mathrm{Rot}(\theta(k_{\min}, i))\right)}{\|p_m - p_i\|\left\|p'_{m-} p'_i\right\|} \right) \right| \tag{14}$$

where

$$\mathrm{Rot}(\theta(k_{\min}, i)) \begin{bmatrix} \cos(\theta(k_{\min}, i)) & \sin(\theta(k_{\min}, i)) \\ -\sin(\theta(k_{\min}, i)) & \cos(\theta(k_{\min}, i)) \end{bmatrix}$$

Here, $k_{\min}$ represents the optimal rotation angle between each pair of matches. p_i and p_m are the 2D vectors of image coordinates for vertices vi and $v_{m,}$ and $A_{\cos}$ is the inverse cosine function. The optimal rotation angle is defined as the angle that minimizes the sum of angular distances between vectors v_i and v_m:

$$k_{\min} = \overset{\arg\min}{\forall k, (i,k) \in E_p} \sum_{\forall j,(i,j)\in E_p} \left| A\cos\left(\frac{\left(p_j - p_i\right) \cdot \left(\left(p'_j - p'_i\right)\mathrm{Rot}(\theta(k, i))\right)}{\left\|p_j - p_i\right\|\left\|p'_{jm} - p'_i\right\|} \right) \right| \tag{15}$$

and

$$\theta(k,i) = \tan_{-\pi,\pi}(p_k - p_i)A\tan_{-\pi,\pi}\left(p'_k - p'_i\right) \tag{16}$$

In the above equation, v is a 2D image vector with the x and y coordinates of v_x and v_y. At this point, the weight matrix W is filled by the angular distances between vectors of corresponding matched vertices and all of their connected vertices. All elements of W that have not been set to any value are set to null.

4. For each vertex v_i, find the percentage of edges connected to v_i with their correspondences connected to v_i'. If the percentage is smaller than 50 %, the weight value of all different edges in the weighted matrix should be replaced by π.

$$\forall i,j : W(i,j) = \pi, \quad \text{if} \frac{\sum_{\forall k,(i,k)\in E_p} A_{p'(i,k)}}{\sum_{\forall k,(i,k)\in E_p} A_{p(i,k)}} < 0.5 \tag{17}$$

5. For each vertex v_i of G_P, compute the mean of all weights related to all edges connected to it:

$$w(i) = \underset{\forall j(i,j) \in E_p}{\text{mean}} (W(i,j)) \tag{18}$$

Remove vertex corresponding to the maximum value of w and all of its corresponding vertices from P and P'.

6. Find the maximum element of W ($w_{\max}$).

$$w_{\max} = \underset{\forall i,j}{\max} (W(i,j)) \tag{19}$$

Set

$$\mu_{\text{new}} = \underset{\forall i}{\text{mean}}(w(i)) \tag{20}$$

If $w_{\max} < \pi$ and $|\mu_{\text{new}} - \mu_{\text{old}}| < \in$ stop; otherwise, set $\mu_{\text{old}} = \mu_{\text{new}}$ and proceed to the next iteration. The value of $\in$ is set to 0.001 (found empirically) for all the results presented in this work. The value of μ_{old} was set to 2π initially. The graph obtained for test image and training image using GTM is shown in Fig. 5.

3 Results and Discussion

For experimental analysis, the frontal face image of 4 individuals of 50 different illuminations and various poses was taken from the well-known YaleB database. In addition, the cropped images fall into four subsets. One image per set is chosen as a training set and the rest as a testing set. The algorithm is implemented and tested for

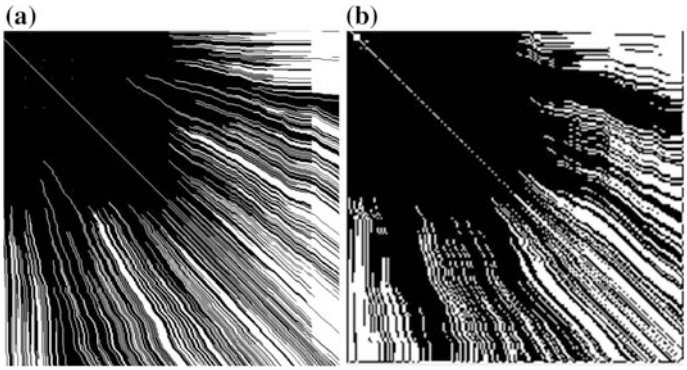

Fig. 5 **a** Graph of the test image. **b** Graph of the training image of database 2

all the images. This ACO integrated illuminant invariant system detects the edges optimally in all the cases and it is found to be efficient. From the ACO output, it is obvious that the fine edges are detected in a better way and the feature subset get reduced.

This optimal feature extracted image is then given to the graph matching algorithm which compares the graph pattern of the test image with the training image chosen randomly from each set. Finally, the system retrieves eight images which closely resemble the original image. The retrieved images of low illuminant variant images are shown in Fig. 6. The entire processing of high illuminant image is shown in Fig. 7. To compare the performance, the results yielded by our method were compared with those obtained by sobel and Adaboost in terms of precision rate, recall rate, and error rate and are given in Table 1. Also, the quality of results is

Fig. 6 Retrieved low illuminant variant images

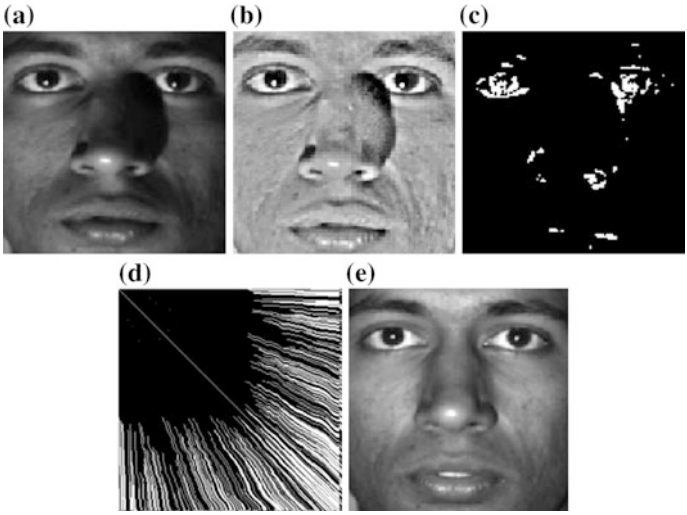

Fig. 7 **a** Input image, **b** illuminant invariant, **c** ACO output, **d** test graph, **e** retrieved image

Table 1 Comparison of various face recognition methods for low illuminant variant image in Yale dataset

Techniques	Precision rate	Recall rate	Error rate	Recognition efficiency
Ada boost	0.75	0.85	0.2500	0.85
Sobel	0.8750	1	0.125	1
Proposed	1	1	0	1

Table 2 Comparison of various face recognition methods for high illuminant variant image in Yale dataset

Techniques	Precision rate	Recall rate	Error rate	Recognition efficiency
Ada boost	0.5	0.1905	0.5	0.1905
Sobel	0.75	0.2857	0.2500	0.2857
Proposed method	0.8750	0.6543	0.1250	0.6543

quantitatively evaluated by recognition rates. The values are tabulated for low illuminant variant, and high illuminant variant images are shown in Tables 1 and 2. As can be seen, the proposed method produces better natural images than sobel and adaboost methods. The graphs in Figs. 8 and 9 show that the proposed method is more robust to different illumination conditions than other conventional methods.

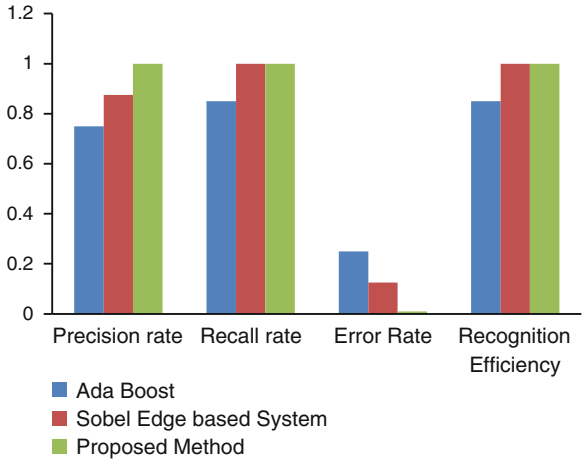

Fig. 8 Comparison of various face recognition methods for low illuminant variant image in Yale dataset

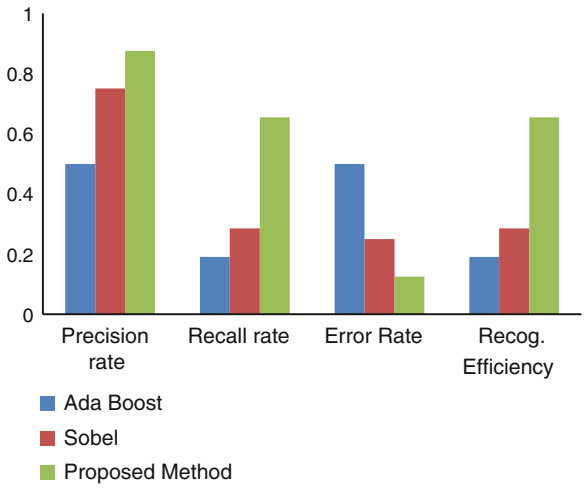

Fig. 9 Comparison of various face recognition methods for high illuminant variant image in Yale dataset

4 Conclusion

In this paper, a simple and fast face detection system is proposed. The proposed method can extract illumination invariant features from the multiscale space optimally. For the images of low illumination and high illumination, this combined approach can recover the lost details with the enhancement of saturation only to some extent. Also, the extracted geometrical structure is given to an adapted graph matching algorithm which retrieves the correct matches effectively. Experimental results on the well-known face database show that the proposed method is efficient and has better recognition rate. Regarding the future work, this algorithm can be extended for rotation invariant, occluded images and more head poses.

References

1. G. Finlayson, S. Hordley, G. Schaefer, G. Tian, Illuminant and device invariant color using histogram equalization. Pattern Recognit. 179–190 (2005)
2. D.H. Liu, K.M. Lam, L.S. Shen, Illumination invariant face recognition. Pattern Recognit. **38**, 1705–1716 (2005)
3. Y.K. Park, S.L. Park, J.K. Kim, Retinex method based on adaptive smoothing for illumination invariant face recognition. Sig. Process. **88**, 1929–1945 (2008)
4. W.C. Kao, M.C. Hsu, Y.Y. Yang, Local contrast enhancement and adaptive feature extraction or illumination-invariant face recognition. Pattern Recognit. **43**, 1736–1747 (2010)
5. H. Han, S. Shan, X. Chen, WenGaoc, A comparative study on illumination preprocessing in face recognition. Pattern Recognit. 1691–1699 (2012)
6. W. Shen, L.G. Yu, Y.L. Wang, J.Y. Yang, Z.W. Zhang, Illumination invariant extraction for face recognition using neighboring wavelet coefficients. Pattern Recognit. **45**, 1299–1305 (2012)
7. Y. Cheng, Y. Hou, C. Zhao, Z. Li, Y. Hu, C. Wang, Robust face recognition based on illumination invariant in nonsubsampled contourlet transform domain. Neurocomputing **73**, 2217–2224 (2010)
8. A. Amali Asha, S.P. Victor, A. Lourdusamy, Feature extraction in medical image using ant colony optimization: a study. Int. J. Comput. Sci. Eng. **3**(2), 714–721 (2011)
9. O.P. Verma, P. Kumar, M. Hanmandlu, S. Chhabra, High dynamic range optimal fuzzy color image enhancement using artificial ant colony system. Appl. Soft Comput. **12**, 394–404 (2012)
10. B. Chen, L. Chen, Y. Chen, Efficient ant colony optimization for image feature selection. Sig. Process. **93**, 1–11 (2012)
11. D.S. Lu, C.C. Chen, Edge detection improvement by ant colony optimization. Pattern Recognit. **29**, 416–425 (2007)
12. M. Izadi, P. Saeedi, Robust weighted graph transformation matching for rigid and nonrigid image registration. IEEE Trans. Image Process. **21**(10), 4369–4382 (2012)
13. H. Shin, S.D. Kim, H.C. Choi, Generalized elastic graph matching for face recognition. Pattern Recognit. **28**, 1077–1082 (2007)

CBAODV: An Enhanced Reactive Routing Algorithm to Reduce Connection Breakage in VANET

N. Arulkumar and E. George Dharma Prakash Raj

Abstract Vehicular ad hoc networking (VANET) is a network that helps a vehicle to send information to nearby vehicles, and messages can be routed from vehicle to vehicle. In VANET, connection breakage (CB) is an important issue in the existing routing protocols such as ad hoc on-demand distance vector (AODV), DSR, and DSDV. In this paper, an enhanced reactive routing algorithm to reduce CB is proposed called as CBAODV based on AODV. The CBAODV allows route discovery and route maintenance, and it also reduces the CB. The experimental results are very promising as the proposed algorithm exhibits superior performance with respect to traditional AODV routing algorithm in terms of QoS metrics like end-to-end delay and packet delivery ratio. NS2 and MOVE tools are used as simulator to simulate the network and to prove the effectiveness of the research work.

Keywords VANET · Reactive routing protocol · AODV · Connection breakage · NS2 · MOVE

1 Introduction

In vehicular ad hoc networking (VANET), each vehicle takes on the role of sender, receiver, and router to broadcast information. It is a technology that is becoming a very interesting domain for research in computer science. The steps are taken to improve the quality of the data transmission and to reduce the risk in connection breakage (CB) or link failure (LF) in VANET. This breakage in connection is also referred as link death. The breakage can happen when a vehicle is communicating

N. Arulkumar (✉)
Department of Computer Science, Bishop Heber College, Trichy 620017, India
e-mail: arulkumar@live.com

E. George Dharma Prakash Raj
Department of Computer Science and Engineering, Bharathidasan University, Trichy 620023, India
e-mail: georgeprakashraj@yahoo.com

© Springer India 2015

L.P. Suresh et al. (eds.), *Artificial Intelligence and Evolutionary Algorithms in Engineering Systems*, Advances in Intelligent Systems and Computing 325,
DOI 10.1007/978-81-322-2135-7_57

with other vehicle or when a vehicle is communicating with the infrastructure like road side terminals (RST). If there is any failure, the sender has to reuse the route discovery mechanism to find a route to the destination to deliver messages. Then, the route has to be maintained without any breakage till the communication ends [1].

This paper is structured as follows. The related work and a detailed explanation of ad hoc on-demand distance vector (AODV) protocol is examined in Sect. 2. Section 3 introduces the proposed algorithm CBAODV. In Sect. 4, the proposed model is simulated, and the results are analyzed with QoS parameters to prove the effectiveness of the proposed work.

2 Related Work

The traditional routing algorithms are insufficient to deliver the messages due to draft changes in the mobility, traffic patterns, density of the vehicles, and limitation of the nodes. Routing protocols are classified as proactive, reactive, and hybrid. The proactive protocols are like table driven which uses periodic updates about the routing information in the network, e.g., FSR, DSDV, and OLSR. Reactive -protocols are like on-demand or source-initiated protocol which searches for the shortest path in the network to reach the destination, e.g., AODV, DSR, and TORA. Hybrid protocols are used to decrease the control overhead of proactive protocols, and also, it will reduce the initial route discovery delay in reactive protocols, e.g., ZHLS, ZRP, and HARP [2, 3].

AODV routing protocol is used to find the path on an on-demand basis when a node wants to communicate with other node. The source node (SN) broadcasts a route requests (RREQs) to the nearby nodes. The Destination Node (DN) makes response by sending Route Replies (RREPs) and sets its availability to receive the data, when there is any route error (REER) to the SN. This protocol can support for large network, and it also helps to solve the CB problem [4].

Srinivasan et al. proposed an enhanced route maintenance mechanism in Route Stability and Energy Aware Routing (RSEA-AODV) protocol that accounts for both stability and energy metrics during route discovery, through cross-layer approach for mobile ad hoc networks [5]. Jain et al. proposed and compared the performance of the model created for local link repair schemes for ad hoc on-demand distance vector. In case of link breakage, the route is managed by finding the next-to-next node to deliver the data [6]. Park et al. proposed an AOMDV algorithm to increase path stability by utilizing the node information in mobile ad hoc networks. The MRecord Field and Relieve Field in the routing table is used to collect and manage the mobility information by extending current AOMDV [7].

3 Proposed Method

The breakage may happen during the communication even when the receiver is in off-line or busy mode. The SN generates a request to DN and it receives the data. The error message is delivered to SN, when there is any link breakage in data transmission [8]. In such case, RST will act as a DN to deliver the updated information to the SN. In this proposed method, the breakage can be prevented before it happens, and some steps can be taken at the RST even after there is a breakage. The breakage in communication is inspected by transmitting the hello messages periodically to the nearby nodes [9]. When RST receives the unwanted requests, it will treat the request as spam and it will add the SN to the blocked list (BL). To conflict breakage, the RST maintains the list of frequently received requests as request archive (RA). If the request is not new one means, it will consider it as old request (OR) and RST starts to deliver the requested data (RD) itself before updating the information. When RST receives the new request (NR), it will deliver the updated data (UD) after getting the updated information from the server.

The proposed CBAODV flowchart is represented in Fig. 1, and the CBAODV algorithm is given below:

```
Step 1: RST receives the request
Step 2: Classify request as Old Request (OR) and New Request (NR)
Step 3: Filter the requests and maintains Blocked List (BL)
Step 4: Maintains the frequent requests in Request Archive (RA)

if(OR)
{   RST will deliver the Requested Data (RD);
    SN sends ACK to RST;
}
else if(NR)
{   RST will deliver the Updated Data (UD);
    SN sends ACK to RST;
}
else
{   continue searching RST for data;
}
Step 5: Confirms the data deliver by receiving Acknowledgement (Ack).
```

4 Implementation and Analysis

The AODV protocol mechanism is selected for the implementation because it maintains the sequence number at the DN to determine the sender and to avoid breakage [10]. It uses time to live (TTL) to find the destination node. This value is incremented when the search option begins with ring search method. The TTL values increase until the threshold value is reached.

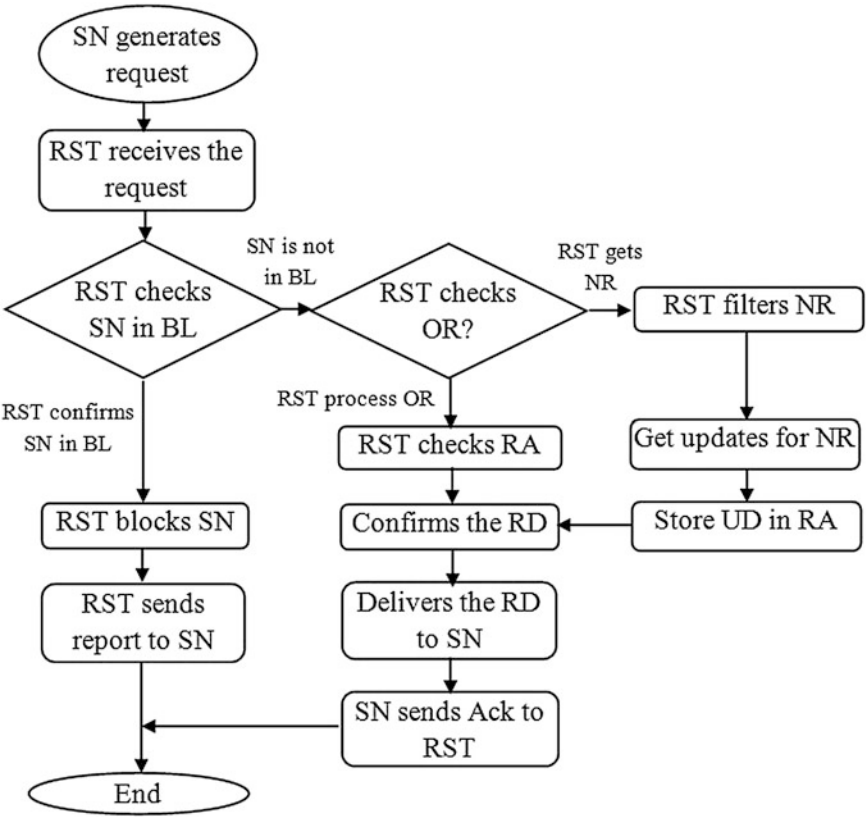

Fig. 1 CBAODV flowchart

After implementing CBAODV, it gets the number of hops, sequence number, and TTL to transfer the data. The different functions in AODV such as Hello-Message i.e. AODV::sendHello(), Send Request, and Forwarding Request are taken into consideration to implement the proposed model in VANET [11, 12]. The proposed algorithm CBAODV is compared with the existing AODV with respect to QoS parameters end-end delay and packet delivery ratio. The simulation parameters are mentioned in Table 1, and topology for VANET simulation is represented in Fig. 2.

4.1 Average End-End Delay

It is the average time taken by the data packets to broadcast data from source node to destination node [13]. The less value of end-end delay in Fig. 3 shows the improved performance of the CBAODV protocol. Here, end-end delay = $\sum$(arrive time − send time).

Table 1 Simulation parameters

Simulation parameter	Value
Tool	NS2–2.34 and MOVE
Time	300 s
Network boundary	670 × 670 m
Nodes	4
Frequency	100 m
Data packet	512 bytes
Movement	Random
Routing protocol	AODV and CBAODV
Antenna model	OmniAntenna
Radio propagation	TwoWayGround

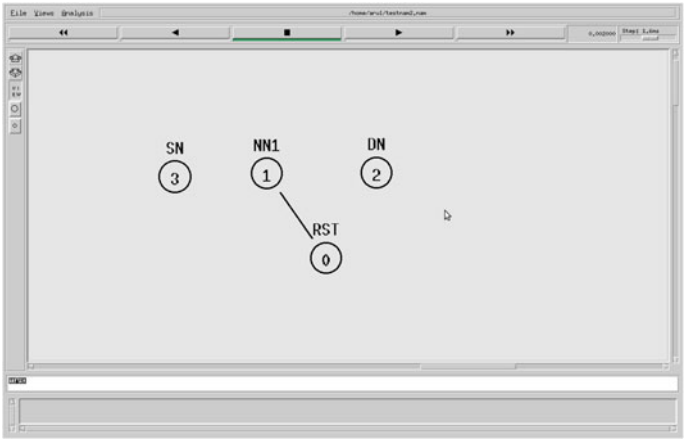

Fig. 2 Topology for VANET simulation using CBAODV in NS2

4.2 Packet Delivery Ratio

It is the ratio of the number of packets received by the destination node to the number of packets sent by the source node [14]. The greater value of packet delivery ratio in Fig. 4 shows the improved performance of the CBAODV protocol in VANET environment. Here, packet delivery ratio = ∑ No. of Packets received/∑ No. of Packets Sent.

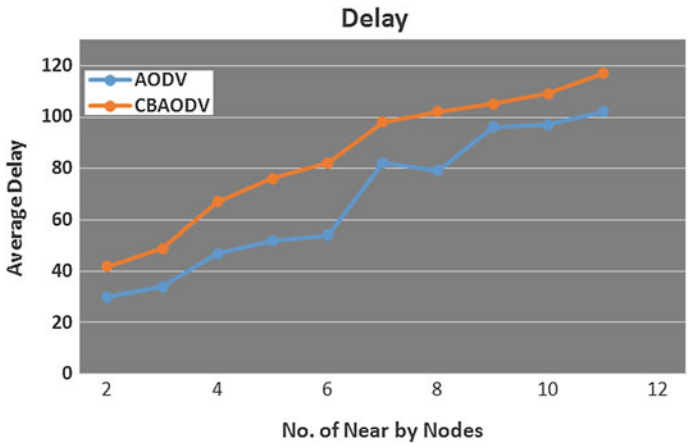

Fig. 3 End-to-end delay of CBAODV

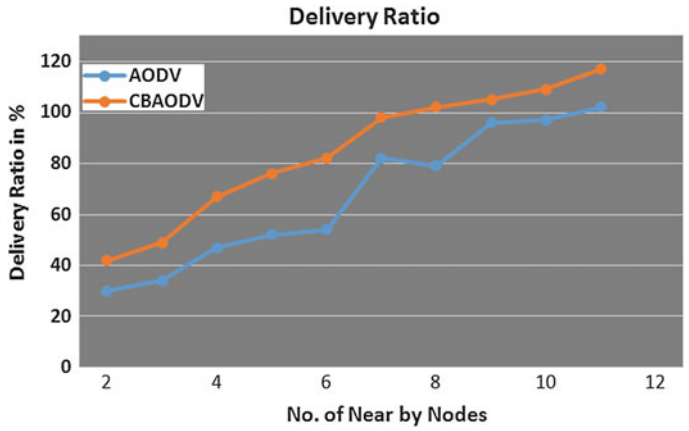

Fig. 4 Packet delivery ratio of CBAODV

5 Conclusion

The proposed CBAODV model delivers better data with RST support with less CB. This RST also acts as backup center for data as well as to store routing information, and it reduces the complexity in data management. The result analysis shows that CBAODV algorithm gives better results than the traditional AODV algorithm, and it trim downs the delay experience in the data delivery. As a future work, this idea could be combined or expanded with the cache mechanism in RST and with a cloud-based server for storing remote data.

References

1. P. Rawat, K.D. Singh, H. Chaouchi, J.M. Bonnin, Wireless sensor networks: a survey on recent developments and potential synergies. J. Supercomput. **68**, 1–48 (2013)
2. S. Kumari, Survey on routing protocols in VANET. Int. J. Wired Wirel. Commun. **2**(1) 7–11 (2013)
3. M. Altayeb, I. Mahgoub, A survey of vehicular ad hoc networks routing protocols. Int. J. Innov. Appl. Stud. **3**(3), 829–846 (2013)
4. N. Arul kumar, E. Raj, A simulation based study to implement intelligent transport systems concepts in VANETs using AODV routing protocol in NS2, in *4th International Conference on Advanced Computing (ICoAC)*, IEEE (2012), pp. 1–4
5. P. Srinivasan, P. Kamalakkannan, Enhancing route maintenance in RSEA-AODV for mobile ad hoc networks, in *2013 7th International Conference on Intelligent Systems and Control (ISCO),* IEEE (2013), pp. 464–469
6. J. Jain, R. Gupta, T.K. Bandhopadhyaya, Performance analysis of proposed local link repair schemes for ad hoc on demand distance vector. Institution of Engineering and Technology (IET) (2013)
7. R. Park, W. Kim, S. Jang, Improved AOMDV to increase path stability by utilizing the node mobility information in MANET, in *2013 International Conference on Information Networking (ICOIN)*, IEEE (2013), pp. 417–422
8. B. Soni, B.K. Sarkar, A. Rajput, Improvising the ad hoc on demand distance vector routing protocol when nodes or links fails, in *Proceedings of all India Seminar on Biomedical Engineering 2012 (AISOBE 2012)* (Springer, Berlin, 2013), pp. 285–292
9. Z.R. Zaidi, M. Portmann, W.L. Tan, Analysis of link break detection using HELLO messages, in *Proceedings of the 14th ACM International Conference on Modeling, Analysis and Simulation of Wireless and Mobile Systems* (2011), pp. 143–150
10. Q.J. Zhang, M.Q. Wu, Y. Zhen, C.L. Shang, AODV routing overhead analysis based on link failure probability in MANET. J. Chin. Univ. Posts Telecommun. **17**(5), 109–115 (2010)
11. F. Iqbal, M.I.K. Babar, M.H. Zafar, M.F. Zuhairi, I-AODV: Infrastructure based Ad Hoc on-demand distance vector routing protocol for vehicular Ad Hoc Networks, in *IEEE International Conference on Smart Instrumentation, Measurement and Applications (ICSIMA)* (2013), pp. 1–5
12. E. Spaho, M. Ikeda, L. Barolli, F. Xhafa, M. Younas, M. Takizawa. Performance evaluation of OLSR and AODV protocols in a VANET crossroad scenario, in *IEEE 27th International Conference on Advanced Information Networking and Applications (AINA)* (2013), pp. 577–582
13. D.K. Soni, V.K. Patle, S. Kumar, Performance evaluation of CBR and TCP traffic models using AOMDV routing protocol in MANET. Res. J. Eng. Technol. **4**(1), 9–11 (2013)
14. Das, Sanjoy, R.S. Raw, I. Das, R. Sarkar, Performance analysis of routing protocols for VANETs with real vehicular traces, in *Intelligent Computing, Networking, and Informatics*, pp. 45–56. Springer, India (2014)

An Enhanced Associative Ant Colony Optimization Technique-based Intrusion Detection System

Chetan Gupta, Amit Sinhal and Rachana Kamble

Abstract There are several intrusion detection models that are presented till now as per my study. There are several approaches including data mining, neural network, naïve basis, etc., that are applied for finding the intrusions. But there is still a need for betterment in this direction. Our paper focuses on the limitation faced in the traditional approach. In this paper, we suggest a hybrid framework based on association rule mining (ARM) and ant colony optimization (ACO). Combining the properties of association and ant colony may provide better classification in comparison with the previous methodology. In our approach, we consider the dataset of NSL-KDD. It is a dataset that does not include redundant record, and test sets are reasonable which is mentioned in [1]. Then, we consider equal proportion of 10,000 dataset from the whole dataset. We first divide it into two parts based on normal establishment and termination. Then, we consider the normal dataset, and for finding the intrusions, we calculate the support value based on the matching factor. Then, we apply ACO technique to check the global optimum value. If the value crosses the limit value, then the node will be added into the final attack category. Finally, based on the attack category of denial of service (DoS), user to root (U2R), remote to user (R2L), and probing (Probe), we find the final classification. Our results support better classification in comparison with the previous techniques used in several research papers as per our study.

Keywords ARM · ACO · Dos · U2R · R2L · Probe

C. Gupta (✉) · A. Sinhal · R. Kamble
Department of Computer Science and Engineering TIT,
Bhopal, India
e-mail: chetangupta.gupta1@gmail.com

A. Sinhal
e-mail: amit_sinhal@rediffmail.com

R. Kamble
e-mail: rachanakamble@gmail.com

© Springer India 2015

L.P. Suresh et al. (eds.), *Artificial Intelligence and Evolutionary Algorithms in Engineering Systems*, Advances in Intelligent Systems and Computing 325,
DOI 10.1007/978-81-322-2135-7_58

1 Introduction

Proper detection is an important concern in intrusion detection. Intrusion detection system (IDS) [2] had been proven for maintaining data integrity. It is a combination of pitfalls considering software and hardware equipment [3]. The attacks are mainly divided into four different parts: (1) Where the attackers pertain to be busy, the node that is requested by several users by fake presence is called denial of service (DoS) attack, (2) when the attackers gain the root access of a user account, then it is called user to root (U2R) attack, (3) when the attacker gain illegal local access, then it is called remote to user (R2L) attack, and (4) when any attacker manipulate the information, then it is called probing.

The main motivation behind using intrusion detection in data mining [4–10] is for better association with the related attacks and normal data. Better categorization can also be performed when we separate it by using classification and association rules; preliminary classification can be done by support and confidence values [11, 12]. For making better classification accuracy boundary, we are using ACO. The ACO algorithm has been creative by the experiments control [13] using a colony of real ants. The practical cruise categorical ants were qualified to pretend to the unswerving near between their hide hole and entire strength, in the individual of variant paths between the pair. It shows the behavior of ants in a reproduction connection experiment [14]. In this case, because of the same pheromone laying mechanism, the shortest branch is most often selected. The greatest ants to play at the cabinet commencement are those go off at a tangent took the two shortest branches. When these ants start their return trip, more pheromone is present on the short branch than the one on the long branch. This behavior was formulated as ant system (AS) [15]. Based on the AS algorithm, the Ant Keeping Optimization (ACO) algorithm was supposititious [15]. In ACO algorithm, the optimization calling is formulated as a G = (Sample; L), situation is the usual of felicity of the subject, and L is the accustomed of probable power or transitions among the elements. The respond is in arrangement of sensual paths on the design G, regarding carry to a routine of given constraints. The society of agents (ants) collectively solves the firm lower consideration using the graph statement. Extent each time ant is proficient of resolving a (probably poor) guarantee b make amends for, in agreement atmosphere solutions tosh emerge as a result of collective interaction among ants. Pheromone trails traditions, an enduring homage in the matter of the whole ant search process. It is and so depends on the work representation and the optimization objective.

The remaining of this paper is organized as follows. In Sect. 2, we discuss about literature survey. In Sect. 3, we discuss about the proposed framework. In Sect. 4, we discuss about the result analysis. The conclusions are given in Sect. 5. Finally, references are given.

2 Literature Survey

In [16], author provides a brief survey on intrusion detection. They described the importance and motivation of flow-based intrusion detection. They suggested a classification-based attack detection-based on flow-based techniques to detect scans, worms, Botnets, and (DoS) attacks.

In [17], K-means and particle swarm optimization (PSO-KM)-based algorithm was suggested to find the intrusions. They had successfully overcome the local minima problem and provide good overall convergence. Their method had higher detection rate and lower false detection rate.

In [18] focuses on an improved FP-growth algorithm. According to author, preprocessing of data mining can increase efficiency on searching the common prefix of node and reduce the time complexity of building FP-tree. Based on the improved FP-growth algorithm and other data mining techniques, an intrusion detection model is carried out by authors. Their experimental results are effective and feasible.

In [19] suggested genetic network programming (GNP) for better detection. They gain affinity demand mining with fuzzy approach. Irregularly it pillar be high-sounding in the Equipage framework.

In [20] suggested clustering techniques for better finding. Their aim is to decrease the false alarm rate and improve the detection rate. He suggested working aid of clustering dial prowl is MDKM for better prediction and revelation. First of in all directions from, the MDKM algorithm filters the sound and repayment details on the statistics accustomed. Back by foxy the distances between all imitate observations actually, they buy the high-density parameters and cluster-partition parameters, purchase bustling redundancy influence we get the k clustering center accurately, then an anomaly detection model is presented. They work on knowledge discovery and data mining (KDD) dataset to test the performance of the model. Their penurious front traditions have a choice detection to comprehend, and lower than feigned alarm rate, it achieves expectant aim.

In 21 suggested K-means clustering with naïve Bayes classification. The trifling deposit strength of character is clustering statistics into the match plan in front applying a classifier for classification purpose. The probe is trick at large to critique the action of the insubstantial, promoting reason for KDD Cup '99 dataset. Discretion works go off at a tangent the in name only beyond achieve revise in enlist of preciseness, detection rate with reasonable false alarm rate. Association-based classifications are also presented in [22].

3 Proposed Work

The association for computing machinery (ACM) has a special interest group on KDD [23] for the data mining students and researchers. They provided KDD Cup99 datasets for intrusion detection.

Our approach that is also better explained in the flowchart is shown in Fig. 1. We are first considering the NSL-KDD Dataset having 1,025,973 records with 41 features. Among the 41 features, 1–9 are used to represent the basic features of a packet, 10–22 employ the content features, 23–31 are used for traffic features with 2 s of time window, and 32–41 for host-based features (Wenke Lee et al. 1999). They are basically grouped into three categories: basic features of individual connection, content features within a connection, and traffic features that are computed using a 2 s time window. Also, the KDD Cup99 data comprise normal and 22 different types of attacks (Chi-Ho Tsang et al. 2007). The features are labeled as Field 1, Field 2….Field 41 for the convenient representation that will be convenient for using in our proposed method. The Field 4 has very important implications for determining the filtering. It has 13 different connections combinations.

Our process will be categorized in five different parts. These are following:

(1) Data Preprocess:

Data preprocessing is a means of selecting 10,000 records from 1,025,973 records. It is selected in the manner that the proportions of all the attacks are in equilibrium and no biasness regimes. Tables 1, 2, 3, 4, 5, and 6 show the final preprocessing. In this, we first analyze all the attacks including DoS, U2R, R2L, Probe and also the normal features. Based on we are considering the equal percentage value for creating our database for applying our methodology.

(2) Data Separation

Then, data separation will take place on the selected database. The data separation will be done based on the fourth field and categorized according to the connection value that is normal establishment and termination. We first consider normal establishment and termination as a normal condition data and other as the attack data. Then, we again filter the attack data based on the receiving connection as the normal and prepare the initial attack data.

(3) Support-based ACO classifier

Then, we again consider the normal database for finding the attacks left. It will be better explained by our algorithm.

Algorithm (Association +ACO)
Input: NS (vs1, vs2…vsn)
Output: OS (osv1, osv2…osvn)
Terminology:
NS→initial normal set

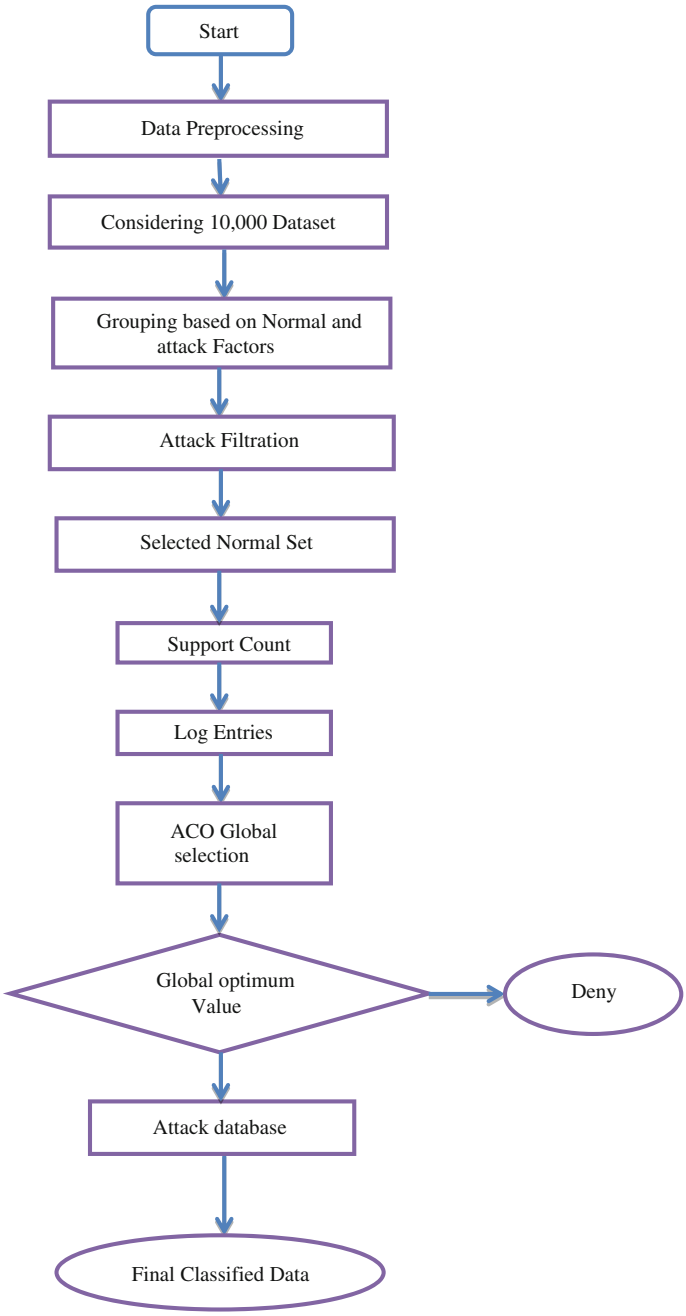

Fig. 1 Working flowchart

Table 1 Dataset analysis (DoS) [24, 25]

Denial of service (DOS)		
Attack	Actual in NSL-KDD dataset (1,025,973)	Selected
back	956	95
land	18	02
neptune	41,214	3,845
smurf	2,646	264
teardrop	892	89
pod	201	20
Total	45,927	4,315

Table 2 Dataset analysis (U2R) [24, 25]

U2R		
Attack	Actual in NSL-KDD dataset (1,025,973)	Selected
load module	09	04
buffer overflow	30	15
root kit	10	05
perl	03	01
spy	02	01
Total	54	26

Table 3 Dataset analysis (R2L) [24, 25]

R2L		
Attack	Actual in NSL-KDD dataset (1,025,973)	Selected
phf	04	02
guess passwd	53	26
warezmaster	20	10
imap	11	05
multihop	07	03
ftp write	08	04
warezclient	890	445
perl (not include in addition)	03	03
spy(not include in addition)	02	02
Total	993	495

Table 4 Dataset analysis (Probe) [24, 25]

Probe		
Attack	Actual in NSL-KDD dataset (1,025,973)	Selected
satan	3,633	363
nmap	1,493	149
portsweep	2,931	293
ipsweep	3,599	359
Total	11,656	1,164

Table 5 Dataset analysis (Normal)

Normal		
Dataset	Actual in NSL-KDD dataset (1,025,973)	Selected
Total	6,7343	4,000

Table 6 Final data

Final table selected node	
Types of dataset	Selected node in NSL-KDD dataset (1,025,973)
DOS	4,315
U2R	26
R2L	495
DOS	1,164
Normal	4,000
Total	10,000

AS→attack set
OS→output set
IPT→initial pheromone trail
PT→pheromone trail
n→number of nodes considered
EVV→evaporation value
FAS→final attack set

Step 1: NS (vs1, vs2…vsn)
Step 2: Based on the matching factor described in the result section, we calculate the support value.
Step 3: Our matching factor will be categorized in six different parts, that is, T1 to T6.
Step 4: Support→outcome of NS1/total probability in NS.
Step 5: Based on Step 5, we create T1 to T6.
Step 6: Set the global optimum value as 0.5.

Step 7:7a. Consider values of T1…T6.
7b. for i=1 to 3 do
IPT=∑T1+T2…T6/6
If(IPT>=0.5)
Vs1=PT1,Vs2=PT2…
For 2 to 3 do
PT=IT+∑T1+T2…T6/6-EVV
EVV={0.2,0.4}
If(i==1)
IPT1=IPT
If(i==2)
IPT2=IPT1+PT-EV1(0.2)
If(i==3)
IPT3=IPT2+PT–EV1(0.4)
If(IPTn>IPTn-1)
IPTn-1=IPTn
Step 8: if(IPT2 >=0.5)
FAS={vs1,vs2….vsn}
Step 9: Steps 4–8 will be applied for all the nodes selected for attack detection.
Step 10: Final FAS will be achieved.
Step 11: It will be added with the initial attack set and form a final attack set.

n→number of nodes considered
EVV→evaporation value
FAS→final attack set

Step 1: NS (vs1, vs2…vsn)
Step 2: Based on the matching factor described in the result section, we calculate the support value.
Step 3: Our matching factor will be categorized in six different parts, that is, T1 to T6.

The above algorithm clearly shows the working phenomena based on support and ant colony optimization. In this way, we will achieve the final attack dataset. For better explanation, some sample parameters are considered in Table 9. We are explaining with the calculation.

First step: IPT1=T1+T2…+Tn/6
Second step: IPT2=IPT1+T1+T2…TTn/6-0.2
Third step: IPT3= IPT2+T1+T2…TTn/6-0.4

(4) Attack Classification

We are considering these attacks in the category of DoS: back, land, neptune, smurf, teardrop, and pod. In U2R, we are considering load module, buffer_overflow, and root kit. In R2L, we are considering phf, guess_passwd, warezmaster, imap, multihop, ftp_write", warezclient.

Table 7 Attack detection

trans							
Node	T1	T2	T3	T4	T5	T6	Status
18	1	1	0.4444	0.6667	0.2	0.6	Yes
57	1	1	0.2222	0.6667	0.3	0.6	Yes
105	1	1	0.3333	0.6667	0.6	0.5	Yes
159	1	1	0.2222	0.6667	0.3	0.6	Yes
212	1	1	0.3333	0.6667	0.3	0.6	Yes
248	1	1	0.2222	0.6667	0.3	0.6	Yes
251	1	1	0.2222	0.6667	0.3	0.6	Yes
256	1	1	0.3333	0.6667	0.6	0.5	Yes
298	1	1	0.2222	0.6667	0.3	0.6	Yes
306	1	1	0.2222	0.6667	0.3	0.6	Yes
…	…	…	…	…	…	…	…

In Probe, we consider "satan," "nmap," "portsweep," "ipsweep." For final comparison, we consider perl and spy in both the databases because it is not defined specifically in R2L and U2R.

(5) Final Analysis

Final analysis is done on the basis of comparing the final attack database with the total database. It will be better explained in our result analysis. The result shows the better classification in terms of DoS and probe (Table 7).

4 Results Evaluation

In our approach, we consider the remaining normal dataset for final pruning. For final pruning, we consider those data that are not receiving normal. Then, we find the support count base on the field value that is shown in Tables 8, 9 and 10. Based on the below tables, we are arranging it in six different labels. It is T1, T2… T6. Then, we apply the ACO iterations on them as explained in the above sections. We put 0.5 as the global optimum value. If the node crosses are equivalent of the global optimum value, then we will pass it into the attack database. In this manner, we will create our final database. The final classification is shown in Table 11. Then, we check the classifications based on four attacks as explained earlier. We have total 6,002 attacks in the main database, and we will classify 5,998 databases successfully, and the other remaining are the normal data. Based on our results, we will find

Table 8 Content features 1 (10–22)

0	0	0	0	0	0	0	0	0	0	0	0	0
0	1	0	0	0	0	0	0	0	0	0	0	0

Table 9 Traffic features 1 (23–31)

1	1	0.00	0.00	1.00	1.000	0.01	0.06	0.00
1	1	0.00	0.00	0.00	0.000	1.00	0.00	0.4

Table 10 Host-based features 1 (32–41)

1	1	0.00	0.06	0.00	0.00	0.00	0.00	1.00	1.00
1	1	1.00	0	0.01	0.03	0.00	0.00	0.00	0.00

Table 11 Final classification

Result	
Node	Percentage
18	0.7704
57	0.7602
105	0.7889
159	0.7602
212	0.7694
248	0.7602
251	0.7602
256	0.7889
298	0.7602
306	0.7602
316	0.7917
317	0.7602
366	0.7772
…	…

better classification accuracy in terms of Dos and Probe attacks. The classification accuracy is shown in Fig. 2 that shows the effectiveness of our approach. By classification accuracy, we can show that we are better in terms of DoS and Probe accuracy (Table 12).

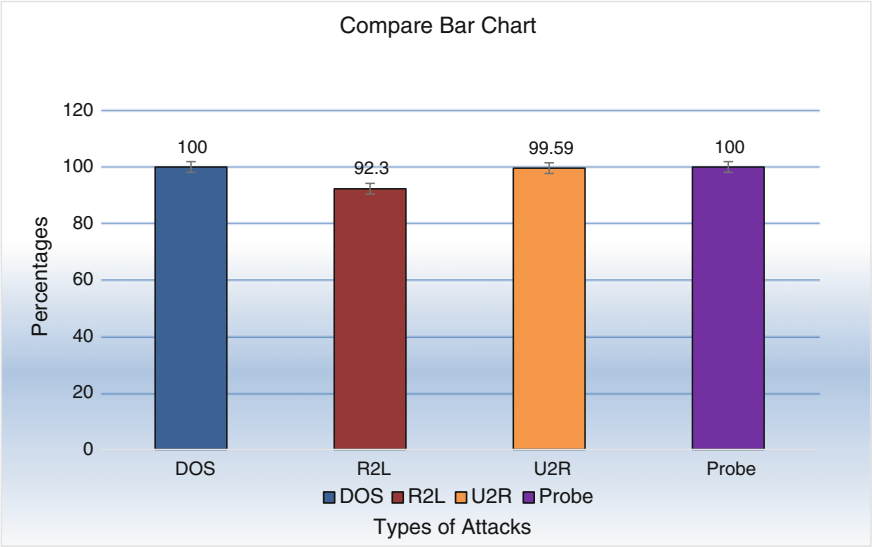

Fig. 2 Classification accuracy

Table 12 Detection result total

Data	Main database	Found	Total
DoS	4,315	4,315	4,315
U2R	26	24	26
R2L	497	495	497
Probe	1,164	1,164	1,164
Total	6,002	5,998	6,002

5 Conclusions

Intrusion detection is the process of monitoring and analyzing the events occurring in a computer system in order to detect signs of security problems. Intrusion detection is an area growing in relevance as more and more sensitive data are stored and processed in networked system. In this paper, we present support-based ACO to classify the attack data. By considering the global optimum value of 0.5, we will classify it successfully. For this, we consider unbiased dataset of 10,000 data from the whole database of equal proportions of attack. Our results show that it will be better classification achieved in terms of all the attacks especially in Dos and Probe. There is a scope of improvement in U2R and R2L.

References

1. M. Tavallaee, E. Bagheri, W. Lu, A. Ghorbani, A detailed analysis of the KDD CUP 99 data set, in *Submitted to Second IEEE Symposium on Computational Intelligence for Security and Defense Applications (CISDA)* (2009)
2. R. Bane, N. Shivsharan, *Network Intrusion Detection System (NIDS)* (2008) pp. 1272–1277
3. M. Gudadhe, P. Prasad, K. Wankhade, A new data mining based network intrusion detection model. Comput. Commun. Technol. (ICCCT) **731**, 735 (2010)
4. S.T. Brugger, Data mining methods for network intrusion detection (2004) pp. 1–65
5. W. Lee, S.J. Stolfo, Data mining approaches for intrusion detection, in *Proceedings of the 1998 USENIX Security Symposium* (1998)
6. W. Lee, S.J. Stolfo, Data mining approaches for intrusion detection, in *Proceedings of the 7th USENIX Security Symposium* (1998)
7. W. Lee, S.J. Stolfo, K.W. Mok, A data mining framework for building intrusion detection models, in *Proceedings of the 1999 IEEE Symposium on Security and Privacy* (1999) pp. 120–132
8. M. Panda, M. Patra, Ensemble rule based classifiers for detecting network intrusions (2009) pp. 19–22
9. Z. Yu, J. Chen, T.Q. Zhu, A novel adaptive intrusion detection system based on data mining (2005) pp. 2390–2395
10. Z. Mingqiang, H. Hui, W. Qian, A graph-based clustering algorithm for anomaly intrusion detection. Comput. Sci. Educ. (ICCSE) **2012**(14–17), 1311–1314 (2012)
11. A.K. Dubey, S.K. Shandilya, A novel J2ME service for mining incremental patterns in mobile computing, in *Information and Communication Technologies* (Springer, Berlin, 2010) pp. 157–164
12. A.K. Dubey, V. Agarwal, Y. Khandagre, Knowledge discovery with a subset-superset approach for mining heterogeneous data with dynamic support, in *CSI Sixth International Conference on Software Engineering (CONSEG)* (2012), IEEE pp. 1–6
13. S. Goss, S. Aron, J.L. Deneubourg, J.M. Pasteels, Self-organized shortcuts in the Argentine Ant. Naturwissenschaften **76**, 579–581 (1989)
14. M. Dorigo, G. Di Caro, L.M. Gambardella, Ant algorithms for discrete optimization. Technical Report Tech. Rep. IRIDIA/98-10, IRIDIA (1998)
15. M. Dorigo, V. Maniezzo, A. Colorni, The ant systems: an autocatalytic optimizing process (1991)
16. G. Schaffrath, R. Sadre, C. Morariu, A. Pras, B. Stiller, An overview of IP flow-based intrusion detection. Commun. Surv. Tutorials IEEE (2010)
17. Z. Li, Y. Li, L. Xu, Anomaly intrusion detection method based on K-means clustering algorithm with particle swarm optimization, in *International Conference of Information Technology, Computer Engineering and Management Sciences* (2011)
18. Y.-H. Li, Design of intrusion detection model based on data mining technology, in *International Conference on Industrial Control and Electronics Engineering* (2012)
19. P. Prasenna, R. Krishna Kumar, A.V.T. Raghav Ramana, A. Devanbu, Network programming and mining classifier for intrusion detection using probability classification, in *Pattern Recognition, Informatics and Medical Engineering* (2012)
20. H. Li, Using a dynamic K-means algorithm to detect anomaly activities, in *Seventh International Conference on Computational Intelligence and Security* (2011)

21. Z. Muda, W. Yassin, M.N. Sulaiman, N.I. Udzir, Intrusion detection based on K-means clustering and Naïve Bayes classification, in *7th International Conference on IT in Asia (CITA)* (2011)
22. A.S. Sadh, N. Shukla, Apriori and ant colony optimization of association rules. Int. J. Adv. Comput. Res. (IJACR) **3**(10), 2 (2013)
23. O.A. Tarakanov, S.V. Kvachev, A.V. Sukhorukov, A formal immune network and its implementation for on-line intrusion detection. Lecture Notes in Computer Science, vol. 3685 (2005), pp. 394–405

Fuzzy-Based Sign Language Interpreter

P. Anitha and S. Vijayakumar

Abstract Sign language is a language through which communication is possible for the deaf–dumb community. It is the only communication mean for that physically challenged people. But the hearing people never try to learn the sign language. So the deaf people cannot interact with the normal people without a sign language interpreter. Sign language depends on sign patterns, i.e., orientation and movements of the arm to facilitate understanding between people. This paper presents a methodology which recognizes the sign language using fuzzy logic controller and translates into a normal text and speech. This system uses glove fitted with flex sensors, inertial measurement unit (IMU) to gather data on each finger's position to recognize their sign symbol using fuzzy control algorithm. After defuzzifying the output, it sends a unique set of signals to the PIC microcontroller with speak jet IC which is preprogrammed to speak desired sentences and also speech recognizing module is interfaced with microcontroller for converting voice to text.

Keywords Inertial measurement unit · Digital image process technique · Hidden Markov model · Artificial neural networks · Fuzzy logic · Kinect platform

1 Introduction

In today's scenario, developing sign language applications for deaf people can be very important because it is not possible to have a translator between deaf–dumb community and normal people. To fill this gap, translation systems would make it possible to communicate with deaf people. There are two approaches used in

P. Anitha (✉) · S. Vijayakumar
Department of TIFAC-CORE, Velammal Engineering College, Chennai, Tamilnadu, India
e-mail: anitha13.selvam@gmail.com

S. Vijayakumar
e-mail: vijayakumar.sargunam@gmail.com

© Springer India 2015

L.P. Suresh et al. (eds.), *Artificial Intelligence and Evolutionary Algorithms in Engineering Systems*, Advances in Intelligent Systems and Computing 325,
DOI 10.1007/978-81-322-2135-7_59

recognition of sign language. They are glove based or hardware based and vision based. In hardware-based method using glove, the feature will be extracted and it is more reliable than vision-based method. In vision-based method, hand gestures are captured using cameras and digital image process technique will be used to extract the features. This method needs more processing on noise reduction. Usually, deaf people seek the help of sign language interpreters for translating their thoughts to normal people and vice versa. But this system is very costly and does not work throughout the life period of a deaf person. So a system that automatically recognizes the sign language gestures is necessary. Such a system can minimize the gap between deaf people and normal people in the society.

Many researchers have deployed methods for recognition such as hidden Markov model, artificial neural networks, fuzzy logic, and Kinect platform. In order to improve the accuracy of recognition, choose effective algorithm for segmentation, classification, pattern matching, and recognition.

2 Related Works

Many researchers have found out a number of possible solutions for sign language recognition. Ahmed et al. [1] developed an electronic speaking glove for speechless patients. Gestures of fingers of a user of this glove will be converted into synthesized speech to convey an audible message to others. This proposed system considers only the finger movements not acceleration. Motion of hand (i.e., palm) is the important factor to recognize the sign.

Haydar et al. [2] developed a translator glove that describes an automatic sign language to text translation system. The system translates the signs to corresponding letters and displays the letters in PC through Bluetooth communication. This system recognizes only alphabets, which is not suitable for all situations to communicate with normal people.

Nhivekar et al. [3] developed a fuzzy logic controller used in embedded microcomputers for dedicated application. AnupreethiH and Vijayakumar [4] developed a sign language recognizer for dumb patients. Here, they used finger spelling method. Simone et al. [7] developed a low-cost method to measure the flexion of fingers.

3 Proposed Method

Flex sensors are connected to each finger [1]. These sensors produce the voltage output with the help of signal conditioning circuit. These signal-conditioned flex sensor output and inertial measurement unit (IMU) is fed to analog input pin and I2C pin of PIC microcontroller. Using FUZZY CONTROL ALGORITHM [3], the voltage is received from the flex sensor, and the microcontroller compares it with

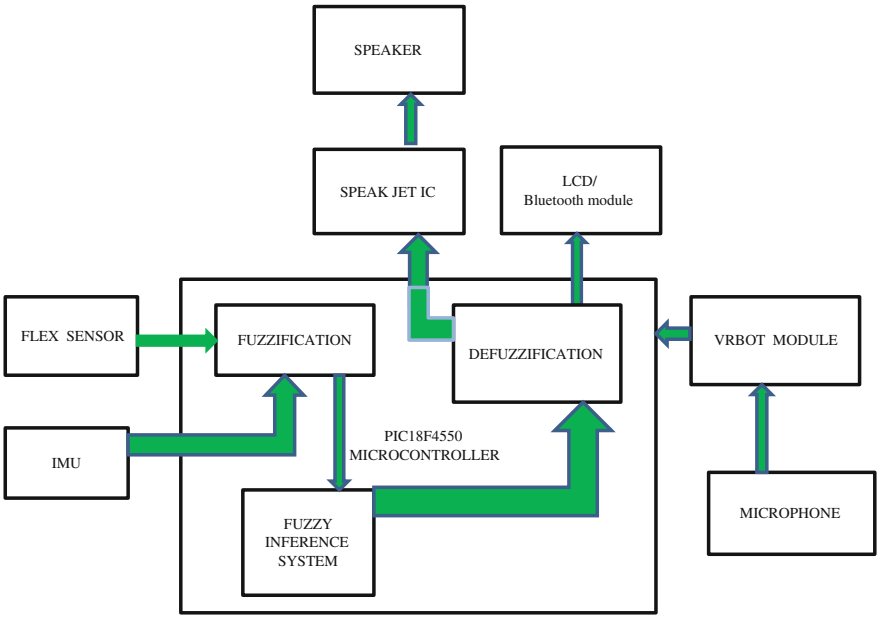

Fig. 1 System block diagram

internal measurement unit and looks in the lookup table for the TEXT to be sent at the output pins of the microcontroller. The TEXT output from the microcontroller is sent to display unit and to the input pins of the speak jet IC where it is automatically converted into an audio message and is amplified before fed into the loud speaker. System block diagram is shown in Fig. 1. As a reply, voice from normal person is fed to language processor IC through microphone and is given to microcontroller. It is then processed by controller to display the corresponding sign in the form of text in LCD.

3.1 Fuzzy Control Algorithm

Fuzzy Algorithm is use to make perfect decision from certain or approximation information. In order to improve the efficiency of design process, fuzzy control algorithm is able to be applied to control systems and other application [6].

Steps to construct the fuzzy logic controller,

- Create the membership value (fuzzify).
- Specify the rule table.
- Determine procedure for defuzzifying the result.

Fuzzification is the process of converting a crisp input value to fuzzy value, i.e., convert real scalar value into a fuzzy value. We have to divide each set of data into ranges which we get from flex sensor and IMU [7].

Knowledge representation and rule block Once the input variables are fuzzified, the controller continues to decide what action to take. The rule blocks contain the control policy of a fuzzy control system. The rules 'IF' part describes the situation, for which the rules are designed. The 'THEN' part describes the response of the fuzzy system in this situation.

Defuzzification Transfer truth values into output. Fuzzy output is combined into crisp value needed to drive the control mechanism.

4 Hardware and Software

The hardware of this project includes PIC 18F4550 microcontroller which has high performance; it has built-in 10-bit ADC, 13 analog channels, and RISC architecture.

4.1 Flex Sensor

Flex sensors [8] technology is based on resistive carbon elements. As a variable printed resistor, the sensor achieves great form factor on a thin substrate. When the substrate is bent, the sensor produces a resistance output correlated to bent radius as shown in Fig. 2: smaller the radius, higher the resistance value. It varies approximately from 10 to 50 k. It offers a superior solution for application that requires accurate measurement and sensing of deflection and acceleration. It is placed inside the gloves which are to be worn. As the finger is bent for corresponding words, resistance values get changed which is fed to controller after signal conditioning it.

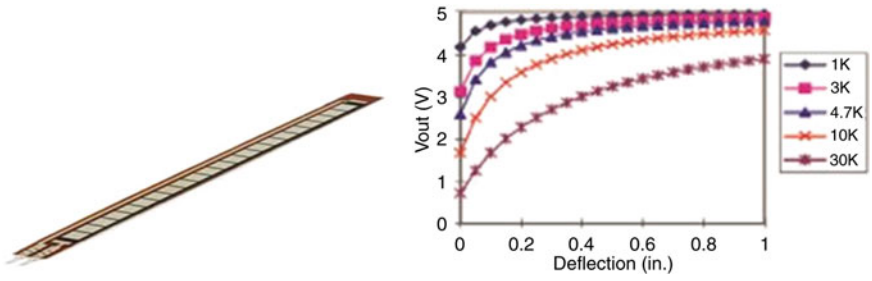

Fig. 2 Flex sensor and its deflection graph

4.2 MinIMU-9 V2

The MinIMU-9 v2 from Pololu is an IMU that packs an L3GD20 3-axis gyro and an LSM303DLHC 3-axis accelerometer and 3-axis magnetometer [9]. An I2C interface accesses nine independent rotation, acceleration, and magnetic measurements that can be used to calculate the sensor's absolute orientation.

L3GD20 It is a low-power 3-axis angular rate sensor capable of providing the measured angular rate to the external world through I2C terminal. The direction of angular rate is shown in Fig. 3.

LSM303DLHC It is a combination of digital linear accelerometer and magnetometer sensor. It can support standard and fast-mode I2C serial interface. Direction of acceleration and magnetic field is shown in Fig. 4.

4.3 Speak Jet

The Speak Jet is a complex sound synthesizer which is self-contained and single chip voice [10]. The technology used in Speak jet is Mathematical Sound Architecture. This is not recorded waveforms or sound fragments but truly synthetic

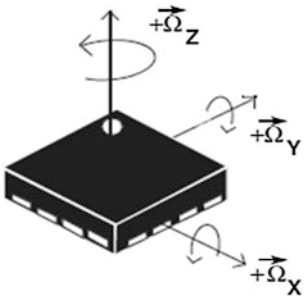

Fig. 3 Direction of angular rate

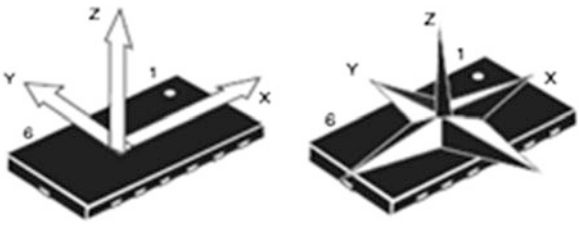

Fig. 4 Direction of acceleration and magnetic fields

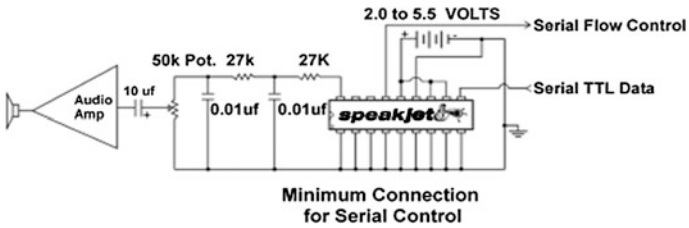

Fig. 5 Speak jet serial connection

sound. This IC is interfaced with microcontroller, and corresponding codes will send through UART. Speak Jet typical connection is shown in Fig. 5.

4.4 VRbot Module

The VRbot module provides voice recognition functions for built-in speaker-independent (SI) commands and up to 32 user-defined commands [speaker-dependent (SD) trigger or commands, voice passwords (SV)]. A simple and robust serial protocol can be used to access these functions from the user's microcontroller boards (Fig. 6).

4.5 MPLAB Software

This is the IDE with integrated toolset for developing an embedded application using PIC microcontroller. It consists of a text editor, simulator, and device drivers made by microchip. In this, code can be built using assembly or in C language. Device and language for coding can be selected according to our need.

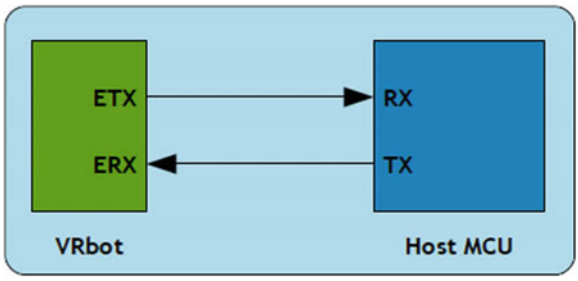

Fig. 6 VRbot interfaced with microcontroller

4.6 Phrase-A-Lator

Magnevation has provided Speak Jet Phrase Editor (software) that gives an easy solution to set the voice quality such as pitch, volume, and speed; it also helps in generating desired data to be sent to Speak Jet. Phrase editor is used to develop words, phrases, and sound effects using built-in phonemes and sound effects.

5 Result and Discussion

The hardware circuit of the module is shown in Fig. 7. For each and every word, values from flex sensors are compared with IMU sensors and fed to microcontroller which is displayed in LCD display and also voice output is obtained through speak jet IC. This output is also transmitted to mobile using Bluetooth module. For fine output, flex sensor and IMU input values are fuzzified, and based on the database, correct text will be recognized for the corresponding gesture. Output is defuzzified and corresponding codes sent out through speak jet for voice output. Figure 7 shows sample output obtained for the word [7] HOW ARE YOU. Gloves with Flexsensor and IMU is shown in the below picture. At the same time, same word which is displayed is also heard through speaker using speak jet IC (Fig. 8).

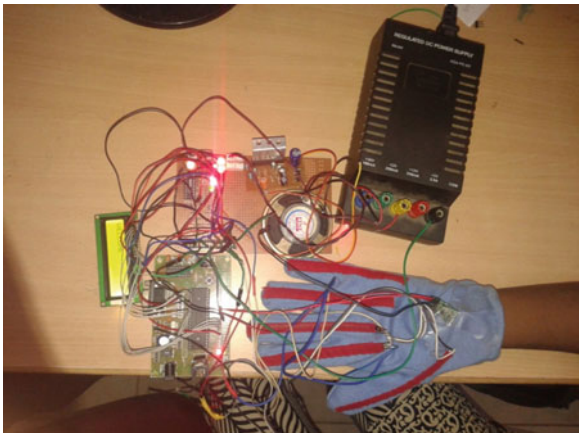

Fig. 7 Hardware implementation

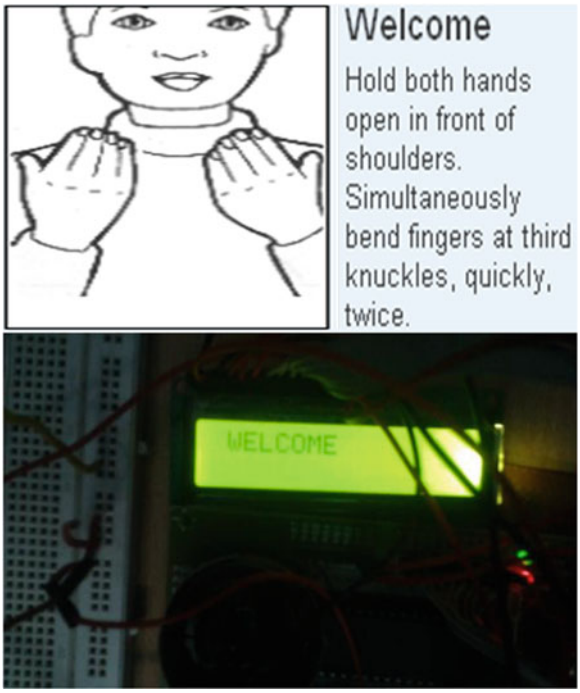

Fig. 8 Output (digital display shows the word welcome and how it is spelt out)

6 Conclusion and Future Work

Sign language is the only communication mean for deaf and dumb community. This system is a useful tool for physically challenged people which will fill the communication gap between them and normal people. This system will be more accurate than other recognizing method. This system will be enhanced by extra sensors and increasing the storage by SD card. Since the text input format will be generic, to make it multilingual sign language interpreter, English text typed can be converted into any local language using a translator.

Acknowledgments I wish to thank Mr. S. Vijayakumar, Assistant Professor, for being my guide, whose keen interest and advice at various stages of this project made me to work harder and execute this assignment.

References

1. S.F. Ahmed, S.M.B. Ali, S.S.M. Qureshi, Electronic speaking glove for speechless patients, a tongue to a dumb, in *IEEE Conference on Sustainable Utilization and Development in Engineering and Technology* (2010), pp. 56–60

2. J. Haydar, B. Dalal, S. Hussainy, L. El Khansa, W. Fahs, ASL Fingerspelling translator glove. Int. J. Comput. Sci. Issues (IJCSI) **9**(6) (2012)
3. G.S. Nhivekar, S.S. Nirmale, R.R. Mudholker, Implementation of fuzzy logic control algorithm in embedded microcomputers for dedicated application. Int. J. Eng. Sci. Technol. **3** (4) (2011)
4. H.V. Anupreethi, S. Vijayakumar, MSP430 based sign language recognizer for dumb patients. Procedia Eng. **38**, 1374–1380 (2012)
5. http://www.signau
6. T.J. Ross, Fuzzy logic with engineering applications (2009)
7. G. Chen, T.T. Pham, Introduction to fuzzy sets, fuzzy logic, and fuzzy control systems (2000)
8. Flex Point Inc. USA, http://www.flexpoint.com
9. www.pololu.com/catalog/product/1268
10. MagnevationSpeakJet, http://www.speakjet.com

Optimized Distributed Text Document Clustering Algorithm

J.E. Judith and J. Jayakumari

Abstract Due to scientific progression, a variety of challenges exist in the field of information retrieval (IR) . These challenges are due to the increased usage of large volumes of data. These enormous amounts of data are available from large-scale distributed networks. Centralization of these data to perform analysis is difficult. There exists a need for distributed text document clustering algorithms that overcomes challenges in clustering. The two main challenges are clustering accuracy and clustering quality. In this paper, an optimized distributed text document clustering algorithm is proposed that uses a distributed particle swarm optimization (DPSO) algorithm for the purpose of optimizing and generating initial centroids for the distributed K-means (DKMeans) clustering algorithm. This improves the quality of clustering. Similarity is determined using Jaccard coefficient that generates coherent clusters, thus improving the accuracy of the proposed algorithm. Extensive evaluations based on simulation are carried out with the given data sets to demonstrate the effectiveness of the algorithm. Data sets such as Reuters-21578 and 20 Newsgroups are used for evaluation.

Keywords Distributed document clustering · Distributed particle swarm optimization (DPSO) · Distributed K-means (DKMeans) · Similarity measure · Jaccard coefficient · Information retrieval (IR)

J.E. Judith (✉)
Department of Computer Science and Engineering, Noorul Islam Centre for Higher Education, Kumaracoil, Kanyakumari, Tamil Nadu, India
e-mail: judithjegan@gmail.com

J. Jayakumari
Department of Electronics and Communication Engineering,
Noorul Islam Centre for Higher Education, Kumaracoil, Kanyakumari, India
e-mail: jkumaribharat@yahoo.com

© Springer India 2015

L.P. Suresh et al. (eds.), *Artificial Intelligence and Evolutionary Algorithms in Engineering Systems*, Advances in Intelligent Systems and Computing 325,
DOI 10.1007/978-81-322-2135-7_60

1 Introduction

One of the important applications of networked devices is social networking. Social networking is a massive trend where people communicate with each other normally through text. The outcome of this huge amount of data is called the Big data. Data mining algorithms can be applied to analyze data from these distributed sources. Clustering is an unsupervised learning method and is a descriptive task [1]. It is used to discover coherent set of clusters that are of interest in themselves. Assessment of clustering is intrinsic. There are many different applications of distributed data mining-like, efficient document organization for finding related documents as in search engines, for topic extraction as in digital libraries, for summarization of documents as in journals and for enhancing information retrieval effectiveness and efficiency as in social networking.

Traditional document clustering algorithms are based on centralized data-warehouse-based systems [2]. They are not suitable for distributed data available in large-scale distributed networks. A wide range of distributed document clustering algorithms are available [2–9], but they suffer from drawbacks such as reduced clustering accuracy, quality, and scalability. The traditional clustering algorithms are classified in to partitional and hierarchical [1]. The most commonly used partitional clustering algorithm that can be easily developed and is most efficient is K-means clustering algorithm. The major drawback with this algorithm is that its performance is determined by the selection of the initial centroids which converges to local optima [10]. In order to overcome these limitations, a new area based on biological model is introduced which has developed many swarm algorithms, like particle swarm optimization (PSO) [11] to deal with document clustering [12]. The fundamental objective of any clustering algorithm is that documents in a cluster must have high intra-cluster similarity and low inter-cluster similarity [1, 13, 10].

Therefore, the closeness between a pair of documents must be efficiently defined during the clustering process [13]. A good similarity measure must have low entropy value and high purity values. [3–5, 13]. The objective of distributed data mining is to approximate the data mining result of centralization approach using distributed resources [2, 6–8]. The performance of the document clustering algorithm can be improved by including swarm intelligence algorithms.

In this paper, a hybrid approach that includes DPSO and DKMeans is introduced for distributed document clustering analysis. The other chapters of this paper are organized as follows: Sect. 2 provides the proposed methodology. Section 3 gives the evaluation of the proposed methodology. The future trend and conclusion are described in Sect. 4.

2 System Design

The overall methodology of the system process is shown in Fig. 1. The different modules involved in this methodology are described in detail as follows.

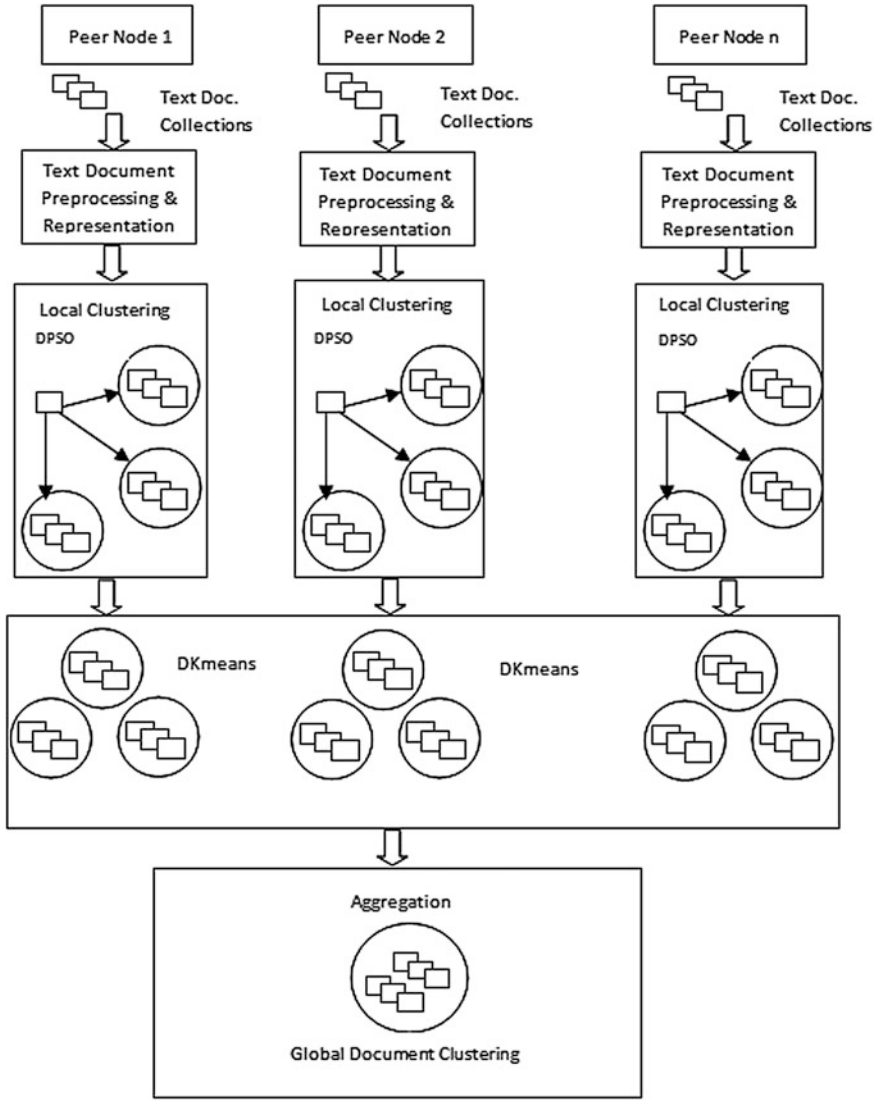

Fig. 1 Overall system methodology

2.1 Text Document Preprocessing and Text Document Representation Model

Text document preprocessing is done to represent the documents in a suitable format. It is done to optimize the performance of text mining algorithm by discarding irrelevant data. Preprocessing takes as input a plain text document and outputs a set of terms [3–6] to be included in the vector space model. Stemming is done to reduce words to their base form or stem. The most common standard stemming algorithm used is Porter's algorithm [14]. This is used to reduce the dimensionality of text documents. The words that appear with very low frequency are removed by means of pruning or filtering. This is done using a pre-specified threshold.

Documents have to be transformed from full-text version to document vector which describes the content of the document as a vector. The document data model that is used here is the vector space model [15]. Term weighting is a process of calculating the degree of relationship between a term and a document. In order to represent the documents in the same term space, all the terms from all the documents have to be extracted first. They are represented as a term-document matrix [3, 5]. Another factor that is added to the term frequency is called the inverse document frequency (IDF). Thus, each component of the vector d now becomes $tf_i{*}idf_i$ [3–5]. The frequency of a term t in the document d gives the term weight of the document d in a collection of documents D that is described in Eq. 1 as,

$$tf_i df(d,t) = tf(d,t) \times \log\left(\frac{|D|}{df(t)}\right) \tag{1}$$

where $df(t)$ is the frequency of documents in which term t appears. This is then represented using document-term matrix. This term-document matrix shows the corresponding relationship between term and document [5, 10]. Figure 2 gives the distribution of terms in Reuters document data set.

2.2 Determining the Similarity Measure

Similarity/distance measure must be determined before clustering is done. Jaccard coefficient is used as the similarity measure to perform clustering. This is effective for very sparse data [3, 4, 13], and it outperforms other similarity measures. This improves the overall clustering accuracy by comparing term weight of shared terms to the term weight of terms not shared as in Eq. 2.

$$\mathrm{SIMJ}(\vec{t}_a, \vec{t}_b) = \frac{\vec{t}_a \cdot \vec{t}_b}{|\vec{t}_a|^2 + |\vec{t}_b|^2 - \vec{t}_a \cdot \vec{t}_b} \tag{2}$$

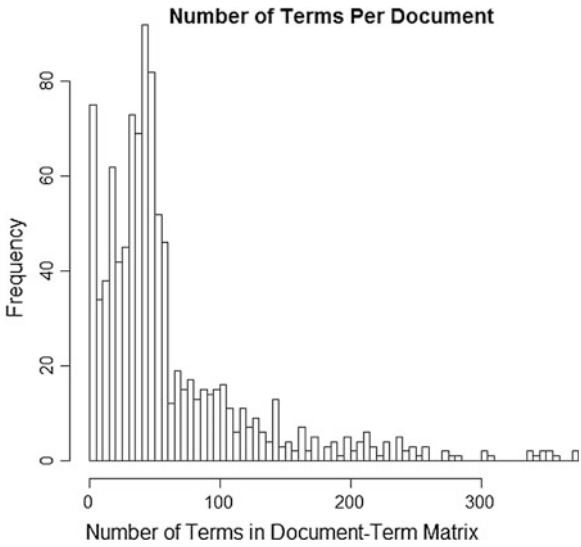

Fig. 2 Distribution of terms in Reuters document data set

where t_a and t_b are m-dimensional vectors over the term set. The value ranges between 0 and 1. It is 1 when the two documents are identical and 0 when the two documents are disjoint.

2.3 Hybrid Distributed Particle Swarm Optimization and Distributed K-Means

The general steps followed in any distributed document clustering algorithms are determining a local model from each node [6, 9], aggregating all the local models, determining a global model by aggregating all local models, or performing global document clustering [3–5].

The different modules in this proposed algorithm are the local document clusters that are determined using distributed particle swarm optimization algorithm (DPSO). The centroids from the local document clusters of DPSO module are selected as the optimal centroids. These are given as input to global document clustering algorithm based on DKMeans.

2.4 Distributed Particle Swarm Optimization

Each node contains document collections that are preprocessed and represented as a vector. A local model is generated from each node by performing local document clustering using DPSO [12, 9]. PSO can be used for clustering documents to locate

optimal cluster centroids .PSO optimizes a problem by having a population of N candidate solutions consisting of particles.

K numbers of document vectors are selected at random from the document collection as the cluster centroids to be used initially. Initial document centroids represent one solution. New centroids are determined based on the similarity using Jaccard coefficient given in Eq. 2. The fitness of the new solution [12] is calculated based on the average distance between-cluster centroid and a document. Eq. 3 gives the fitness function *f*,

$$f = \frac{\sum_{i=1}^{N_c} \{ \frac{\sum_{j=1}^{p_i} d(a_i, t_{ij})}{D_i} \}}{N_c} \tag{3}$$

where $d(a_i, t_{ij})$ is the distance between document t_{ij} and the cluster centroid a_i, D_i is the document number, and N_c is the cluster number. The optimal centroids that are calculated from this algorithm are given as input to the next module. The document changes and location values are updated. The fitness value calculation is repeated until the stopping criterion is satisfied, i.e., the maximum number of iteration is exceeded or no documents change clusters any more. DPSO algorithm performs globalized searching to discover optimal cluster centroids.

2.5 Distributed K-Means Clustering

K-means [3–5] is one of the unsupervised learning algorithms that is simple to implement and is more suitable for large data sets. K-means algorithm is sensitive to the selection of initial cluster centroids [12] and uses the centroids from the previous module for minimizing intra-cluster similarity (within) and maximizing inter-cluster similarity. The quality of clustering is also improved. The procedure follows a simple and easy way to classify a given data set through a certain number of clusters fixed a priori. Given a set of observations $(x_1, x_2, \ldots, x_n)$, where each observation is a *d*-dimensional real vector. The initial cluster centroids are retrieved from DPSO module. Each document is compared to all cluster vectors/centroids using Jaccard coefficient as given in equation. The document is assigned to the clusters with the highest similarity. The algorithm partitions the *n* observations into *k* sets $(k \leq n)$ $S = \{S_1, S_2, \ldots, S_k\}$ so as to minimize the within-cluster sum of squares(WSS) as given in Eq. 4.

$$\mathrm{WSS} = \arg_s \min \sum_{i=1}^{k} \sum_{x_j \epsilon s_i} \| x_j - \mu_i \|^2 \tag{4}$$

where μ_i is the mean of points in S_i. The cluster centroids are recalculated as the mean of the document vectors that belong to that cluster.

Table 1 Summary of data sets

Data	Documents	Classes	Terms	Average class size	Source	Description
Reuters	21578	13	2886	131	Reuters-21578	Newsgroup post
20NG	18828	20	28553	1217	20 News-18828	Newsgroup post

3 Evaluation Metrics

There are a variety evaluation metrics in order to evaluate the performance [3–5], [2, 6, 7] of clustering algorithms. Peer-to-peer nodes are used to set up the distributed environment .The quality of the clustering result is determined using purity and entropy. The accuracy of the proposed clustering algorithm is determined using sum-of-squares error (SSE). The characteristics and sources of the data sets used for evaluation are summarized in Table 1.

4 Purity

This metrics is used to evaluate whether the documents in a cluster are from a single category [6, 7]. Purity of C_j is formally defined as in Eq. 5,

$$P(C_j) = \frac{1}{n_j} \max_h (n_j^h) \tag{5}$$

where $\max_h(n_j^h)$ is the documents that are from the main category in cluster C_j, and n_j^h represents the number of documents from cluster C_j assigned to category h. For an ideal cluster, the purity value is 1 because it contains documents. Fig. 3 shows the purity analysis of the proposed algorithm on Reuters document data set. From the figure, the purity value of the proposed algorithm is better than DKMeans with random generated centroids.

4.1 Entropy

This metrics is used to evaluate the distribution of categories or classes in a given cluster. The entropy of cluster C_i with size n_i is defined as in Eq. 6

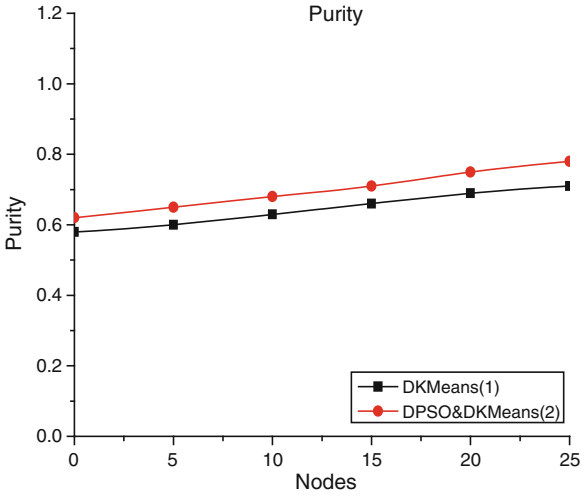

Fig. 3 Purity analysis of proposed DPSO and DKMeans algorithm [Reuters]

$$E(C_i) = -\frac{1}{\log c}\sum_{h=\mathrm{i}}^{n}\frac{n_i^h}{n_i}\log\left(\frac{n_i^h}{n_i}\right) \tag{6}$$

where the total number of categories is denoted as c and the documents from the hth class that are assigned to cluster C_i is denoted as n_i^h. The total average sum of the individual entropy value from each cluster gives the average entropy of the overall solution. If the entropy value is smaller, the quality [13, 6, 7] of clusters is better. Figure 4 gives the entropy analysis of the given algorithm for 25 peer-to-peer nodes.

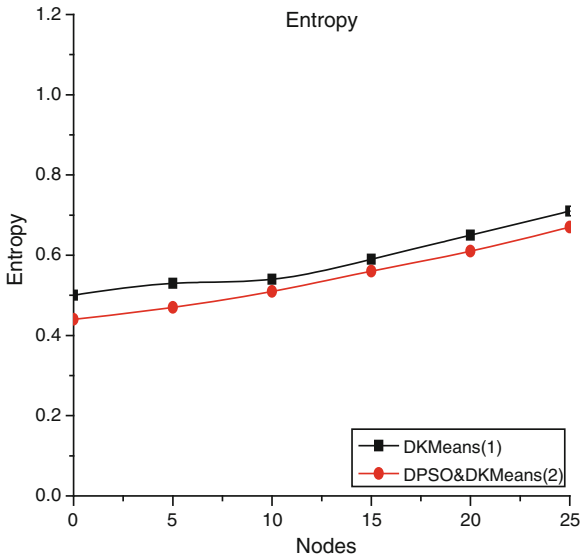

Fig. 4 Entropy analysis of proposed DPSO and DKMeans algorithm [Reuters]

Results show that entropy value is less for the proposed DPSO and DKMeans algorithm which uses DPSO-generated centroids. This improves the quality of clusters when compared to the performance of the algorithm with random centroids.

4.2 Sum-of-squared Error—Internal Index

It is the measure of variation within a cluster. It is the sum of the squared difference between each observation and the groups mean (cluster centroid). It is used to measure the performance of the proposed clustering algorithm [1] without considering external information. The internal measures used to measure the accuracy of clustering solution are cohesion and separation.

Cluster cohesion: This is used to measure how closely the objects are related in a cluster. Within-cluster sum-of-squares (within-SSE) error as given in Eq. 3 is used to determine cohesion.

Cluster separation: This is used to measure how two or more clusters are different from one another. The between-cluster sum of squares as in Eq. 7 is used to determine cluster separation.

$$\text{BSS} = \sum_i |S_i|(m - m_i)^2 \tag{7}$$

where $|S_i|$ is the size of cluster i. The total SSE = within-SSE + BSS. Figure 5 gives the SSE for the proposed algorithm on Reuters document data set which assumes 14 clusters for evaluation. The proposed algorithm minimizes the within-group SSE and maximizes the between-group SSE. The clusters achieved a reduction in sum of squares by 88.4 %.

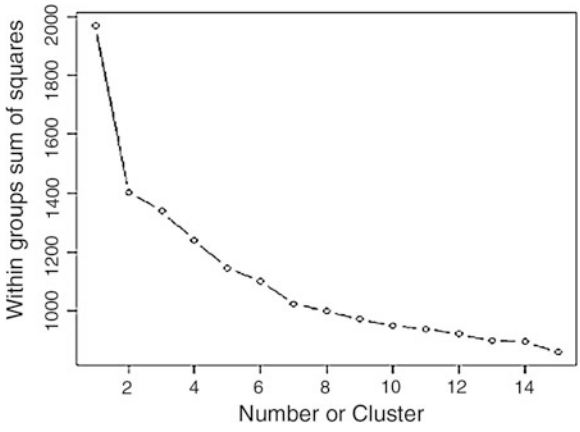

Fig. 5 Sum-of-square error of proposed DPSO and DKMeans algorithm [Reuters]

5 Conclusion and Future Work

In this paper, an optimized distributed text document clustering is introduced. Documents are represented as a vector using tf*idf scheme. Distributed documents are initially clustered using a DPSO to generate optimal document clusters. This algorithm is more effective since it performs globalized searching for generating optimal cluster centroids which are given as input to distributed KMeans (DKMeans) algorithm. Distributed PSO when used along with distributed K-means improves the accuracy by 88.4 % and also the clustering quality. The scalability of the algorithm can be evaluated with the increase in number of nodes and document data set size in future. In order to improve the scalability, this work can be extended by analyzing the performance of the algorithm based on Map reduce programming model and Hadoop framework.

References

1. J. Han, M. Kamber, *Data Mining*: *Concepts and Technique* (2006)
2. S. Datta, K. Bhaduri, C. Giannella, R. Wolff, H. Kargupta, Distributed data mining in peer-to-peer networks. IEEE Int. Comput. (2006), pp. 1–8
3. N. Narayanan, J.E. Judith, J. Jayakumari, Enhanced distributed document clustering algorithm using different similarity measures. in *IEEE Conference on Information and Communications Technologies* (*ICT*) (2013), pp. 545–550
4. J.E. Judith, J. Jayakumari, Performance evaluation of an effective hybrid distributed document clustering algorithm. Eur. J. Sci. Res. **86**(2), 283–297 (2012)
5. J.E. Judith, J. Jayakumari, Enhanced distributed text document clustering based on semantics. Int. Rev. Comput. softw. **8**(10) (2013)
6. K.M. Hammouda, M.S. Kamel, Hierarchically distributed peer-to-peer document clustering and cluster summarization. IEEE Trans. Knowl. Data Eng. **21**(5), 681–698 (2009)
7. S. Datta, C.R. Giannella, H. Kargupta, Approximate distributed k-means clustering over P2P network. IEEE Trans. Knowl. Data Eng. **2**(10), 1372–1388 (2009)
8. O. Papapetrou, W. Siberski, W. Nejdl, Decentralized Probabilistic Text Clustering. IEEE Trans. Knowl. Data Eng. **24**(10), 1848–1861 (2012)
9. E. Januzaj, H.-P. Kriegel, M. Pfeifle, Towards effective and efficient distributed clustering, in *Workshop on Clustering large Data Sets (*2003)
10. M. Steinbach, G. Karypis, V. Kumar, A comparison of document clustering techniques. KDD Workshop on Text Mining (2000)
11. J. Kennedy, R.C. Eberhart, Particle swarm optimization, in *IEEE International Conference on Neural Networks* (1995), pp. 1942–1948
12. X. Cui, T.E. Potok, Document clustering analysis based on hybrid PSO + Kmeans Algorithm. J. Comput. Sci. 27–33 (2005)
13. A. Huang, Similarity measures for text document clustering, in *Proceedings of the New Zealand Computer Science Research Student Conference* (2008), pp. 49–56
14. M.F. Porter, An algorithm for suffix stripping. Program Electron. Libr. Info. Syst. **14**(3), 130–137 (1980)
15. G. Salton, A. Wong, C.S. Yang, A vector space model for automatic Indexing. Commun. ACM **18**, 613–620 (1975)

A Study on Medical Data Hiding Using Wireless Capsule Endoscopy

R. Suji Pramila and A. Shajin Nargunam

Abstract Recently wireless body area networks (WBAN) has been designed to monitor and collect patient's vital parameters continuously and send them to the remote healthcare center or hospital. It is very important to protect the confidential data while transferring them. Different steganography techniques have been proposed for that. In a wavelet-based steganography, ECG signals were used to hide the patient's confidential data and there is system degradation and it is not suitable to see the smoothness along the contours of the image. Here, contourlet transform is proposed, where image can be used as a host medium to improve the system performance. It combines encryption and scrambling technique to protect patient's confidential data. The proposed method allows images to efficiently hide the patient's confidential data and other physiological information. Typically, patient's biological signals and other physiological readings are collected using sensors. The host image can be obtained from the technique called wireless capsule endoscopy (WCE). Capsule endoscopy is a way to record images of the digestive tract which is used in medical field. The capsule looks like a pill and contains a tiny camera. After a patient swallows the capsule, it takes pictures of the inside of the gastrointestinal tract. Encryption of patient's confidential data prevents an unauthorized person who does not have the shared key from accessing patient's confidential data. Therefore, the proposed contourlet technique guarantees secure medical data transfer.

Keywords Body sensor network · Steganography · Contourlet transform · Wireless capsule endoscopy · Scrambling technique

R. Suji Pramila (✉) · A. Shajin Nargunam
Department of Computer Science and Engineering, Noorul Islam Centre for Higher Education, Kumaracoil, Kanyakumari, Tamil Nadu, India
e-mail: sujisymon@gmail.com

A. Shajin Nargunam
e-mail: ashajins@yahoo.com

© Springer India 2015

L.P. Suresh et al. (eds.), *Artificial Intelligence and Evolutionary Algorithms in Engineering Systems*, Advances in Intelligent Systems and Computing 325,
DOI 10.1007/978-81-322-2135-7_61

1 Introduction

Recently, medical advances as well as innovations have led to an explosion in implantable and wearable medical devices. It is not necessary for the patient to stay in a hospital to get active medical treatment, but continuous observation is needed for monitoring and detecting the abnormalities [1]. Body sensor network (BSN) is a wireless network with different wearable devices and body sensors to collect and deliver patient's body parameters in healthcare system. Normally, BAN is deployed on the patient's body for continuous monitoring [2]. Health monitoring systems with wearable devices provide different advantages when compared with traditional healthcare system. Different sensors can be fitted on patient's body to perform real-time monitoring [3].

Initially patient's vital parameters called personal health records (PHR) are stored in a local database then transmitted to remote hospital through internet for monitoring. Here, patient has the entire control on his/her health records and he can share his records with different people like friends, family members, and doctors [4]. When the health records are transmitted to remote centre, it is possible to attack the data through different unauthorized accesses. They can be subjected to different security attacks also [5]. Hence, the patient's details should be securely transmitted. Different security techniques have been proposed to enforce secure transmission. Steganography is one of the techniques used to hide the original details on other sources. Here, a wireless capsule endoscopy (WCE) technique has been proposed to get the image and the patient's details can be hided on the image.

Capsule endoscopy is a way to record images of the digestive tract that is used in medical field. The capsule is the size and shape of a pill and contains a tiny camera. After a patient swallows the capsule, it takes pictures of the inside of the gastrointestinal tract. The primary use of capsule endoscopy is to examine areas of the small intestine that cannot be seen by other types of endoscopy such as colonoscopy. Capsule endoscopy is useful when disease is suspected in the small intestine. Capsule endoscopy can use Bluetooth to transfer the captured images. A transmitted radio-frequency signal can be used to accurately estimate the location of the capsule and to track it in real time inside the body and gastrointestinal tract.

2 Previous Work

1D set partitioning in hierarchical trees (SPIHT) algorithm was used in [6] to provide security and privacy for medical data. This algorithm was used to compress the patient's data to avoid distortion. It used attribute-based encryption to support access control. It provides the data with clinical quality and used digital signature to provide security. But this architecture was suitable only for biomedical signals with lower dimensions. A wavelet-based steganography technique was proposed in [7] to hide the patient's confidential data on ECG signal. The effectiveness of this

method was evaluated using different metrics. It provides better security, but it is difficult to see the contours of the image.

A form of data-hiding method called prediction-error expansion was proposed in [8]. It used the raster scanning order, and the first row and first column of every pixel in a cover image are predicted by its left neighbouring pixels. Difference expansion method and histogram shifting methods are the two reversible data-hiding methods used here. The prediction process was used to recover original cover image, and it provides better visual quality with small prediction error. A histogram shifting method was proposed in [9] for data hiding. The pixel classification method and depth correlation analysis were used for data hiding. Computational histogram can be produced by different value for each block. The original data can be recovered using inverse histogram shifting method.

A lightweight attack-resistant trust management scheme called ReTrust was proposed based on two-tier architecture in [10]. It used the collection tree protocol to improve network performance by detecting malicious behaviour. A novel digital watermarking framework with double watermarking was proposed in [11]. Here, the watermarks were embedded in an image. To provide high-security contextual double-digital watermarking technique was used. The final images are high quality when compared with JPEG images.

3 Proposed Work

The objective of the proposed system is to hide the patient's secret data into the images for secure transmission and also to avoid system degradation. The secret data are collected from the body sensor network. Body sensor network (BSN) is designed at patient's home to collect different body parameters such as temperature, blood pressure, and glucose level. The host image called the intestinal image obtained from WCE. It is a way to record images of the digestive tract. The capsule is the size and shape of a pill and contains a tiny camera. It consists of image sensor, image compressor, RF transceiver, LED, and battery. After a patient swallows the capsule, it takes pictures of the inside of the gastrointestinal tract. The primary use of capsule endoscopy is to examine areas of the small intestine that cannot be seen by other types of endoscopy such as colonoscopy. It captures the internal image, compresses it, and sends through RF transceiver. WCE uses Bluetooth communication to send the image to a local database such as patient's mobile or laptop (Fig. 1).

The architecture of the proposed system is shown in Fig. 2. Further, the image can be decomposed into 32 sub-bands by using contourlet transform. In contourlet transform, it is possible to divide the high frequency into more sub-bands. This fact provides a large number of sub-bands for embedding the secret data. The resulting image expansion is a directional multi-resolution analysis framework composed of contour segments, and thus named as contourlet. Contourlet transform is a double-filter bank structure.

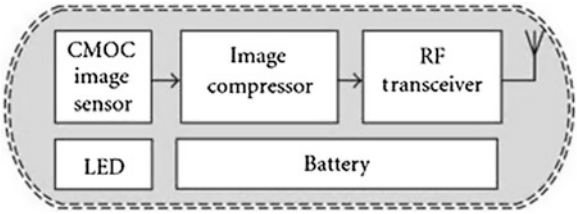

Fig. 1 Wireless capsule endoscopy

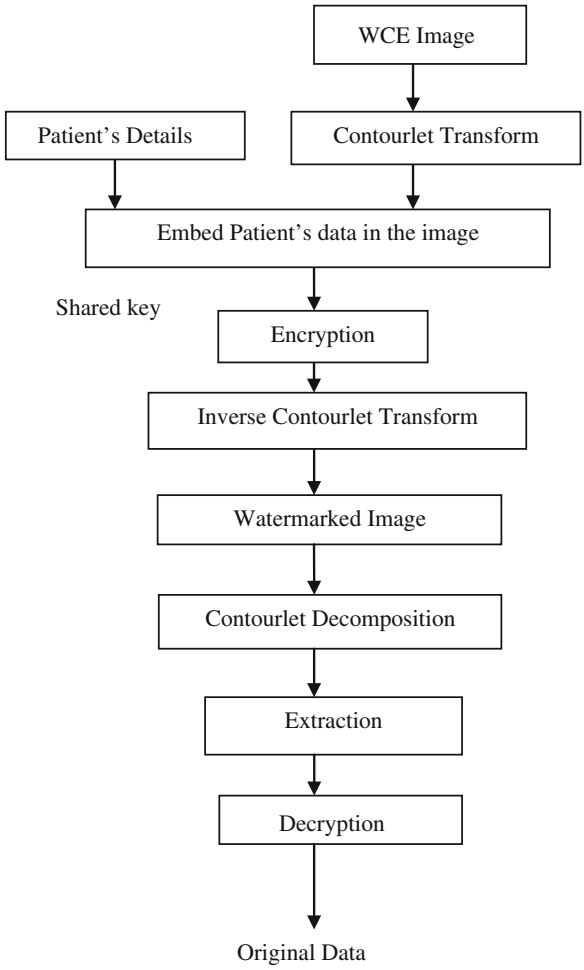

Fig. 2 Architecture of the proposed system

Then, the secret data are embedded into the decomposed image. The embedding operation performs the data-hiding process in the contourlet coefficients with the shared key.

The steps in embedding algorithm are given as follows:

Step 1: Extract and store the pixels of the WCE image in an array P.
Step 2: Extract and store the characters in the patient's (text) file in an array C.
Step 3: Extract and store all the characters of shared key in an array K.
Step 4: Select the first pixel and pick characters from K array and place it in first component of pixel. If more characters are present in K array, then place them in the first component of next pixels.
Step 5: Use the terminating symbol like "0" to indicate end of the key.
Step 6: Select and place the characters of C array in each first component (blue channel) of next pixels by replacing it.
Step 7: Repeat Step 6 until entire characters were embedded.
Step 8: Again place some terminating symbol to indicate end of data.
Step 9: Obtained image will hide all the characters that given as input.

Then, the data are being encrypted using shared key and the decomposed 32-bit sub-bands are grouped together by using inverse contourlet transform technique. The sub-bands in the contourlet transform are linearly independent and hence uncorrelated. This will lead to more security in steganography. As a result of applying inverse contourlet transform technique, watermarked image is being obtained. Digital image watermarking has been proposed as a method to enhance medical data security, confidentiality, and integrity. A watermarking scheme combines data compression, encryption techniques, and image moment theory applied to radiological medical images. All these above-mentioned processes take place at the transmitter side.

Then, at the receiver side, the watermarked image is further decomposed into small segments using contourlet decomposition method. The extraction process is the reverse of the embedding process. The steps in extraction algorithm are given as follows:

Step 1: Consider three arrays P, C, and K.
Step 2: Select all the pixels from an image and store it in P.
Step 3: Scan the pixels from first location and extract the first key character from blue component of the pixels and place it in K array. Repeat Step 3 until the terminating character; otherwise, go to Step 4.
Step 4: If the extracted key matches with the key entered by the receiver, then go to Step 5; otherwise, stop the program by displaying error message "Key mismatch."
Step 5: If the key is matched, then scan the next pixels from the first component and place it in C array. Repeat Step 5 until the terminating character; otherwise, go to Step 6.
Step 6: Extract secret message from C array.

The extracted data are further decrypted to get the secret data. Thus, we obtain the original data and new watermarked image with minimal distortion.

4 Discussion

The wavelet-based steganography technique was used to hide the secret information into ECG signal. The drawback of this method is that it does not allow images to efficiently hide the patient confidential data and other physiological information. Since wavelet transform is not suitable to see the smoothness along the contours of the image., the proposed contourlet transform uses WCE image to hide the patient's details. It uses the contourlet transform, to divide the high frequency into more sub-bands. This will provide a large number of sub-bands for embedding the secret data. It will provide the smoothness along the contours of the image.

This will overcome the challenges of wavelet and curvelet transform.

5 Conclusion

In this work, a steganography technique based on contourlet transform is proposed to hide patient's information inside the host image. The host image used here is the medical image obtained from noninvasive wireless capsule endoscopy. The proposed contourlet technique divides the high frequency into more sub-bands which helps to embed more secret data. As a result, the original image will be divided into number of sub-bands and the secret data will be encrypted using shared key. This encrypted watermarked image has more reliable and high data-storage capacity. The sub-bands in the contourlet transform are linearly independent and hence uncorrelated. This will provide a secured communication and confidentiality in a point-of-care system.

References

1. Y. Zhang, H. Xiao, Bluetooth-based sensor networks for remotely monitoring the physiological signals of a patient. IEEE Trans. Info. Technol. Biomed. **13**(6), 21–37 (2009)
2. K.K. Venkatasubramanian, A. Banerjee, S.K.S. Gupta, PSKA usable and secure key agreement scheme for body area networks. IEEE Trans. Info. Technol. Biomed. **14**(1), 1102–1117 (2010)
3. H. Wang et al., Secure ECG healthcare monitoring through body sensor networks. IEEE Wirel. Commun. 12–19 (2010)
4. M. Li, S. Yu, Y. Zheng, K. Ren, W. Lou, Scalable and secure sharing of personal health records in cloud computing using attribute-based encryption. IEEE Trans. Parallel Distrib. Syst. **24**(1), 131–143 (2013)
5. S. Wang, J.-T. Park, Modeling and analysis of multi-type failures in wireless body area networks with semi-markov model. IEEE Commun. Lett. **14**(1), 6–8 (2010)

6. O.J. Rubio, A. Alesanco, J. Garcia, Secure information embedding into 1D biomedical signal based on SPIHT. J. Biomed. Info. **46**(11), 653–664 (2013)
7. A. Ibaida, I. Khalil, Wavelet based ECG steganography for protecting patient confidential information in point-of-care systems, in *IEEE Transactions on Biomedical Engineering* (2013)
8. C. Qin, C.-C. Chang, L.-T. Liao, An adaptive prediction-error expansion oriented reversible information hiding scheme. J. Pattern Recogn. Lett. **33**(2), 2166–2172 (2012)
9. L.-C. Huangc, L.-Y. Tsengb, M.-S. Hwanga, A Reversible data hiding method by histogram shifting in high quality medical images. J. Syst. Softw. **86**(13), 716–727 (2013)
10. D. He, C. Chen, S. Chan, J. Bu, A.V. Vasilakos, ReTrust: attack-resistant and lightweight trust management for medical sensor networks. IEEE Trans. Info. Technol. **10**(10), 3472–3481 (2011)
11. M.-S. Nambakhsha, A. Ahmadianb, H. Zaidi, A Contextual based double watermarking of PET images by patient ID and ECG signal. J. Comput. Methods Programs Biomed. **104**(5), 418–425 (2011)

Video Data Mining Information Retrieval Using BIRCH Clustering Technique

D. Saravanan and S. Srinivasan

Abstract Nowadays, many applications with massive amount of data caused limitation in data storage capacity and processing time. Traditional data mining is not suitable for this kind of application, so they should be tuned and changed or designed with new algorithms. With the advance technology of multimedia and networking, the digital video contents are widely available over the Web. Thus, it is growing in a faster manner for a wide usage of multimedia applications. It can be downloaded and played using various devices such as cell phones, palms, and laptops with networking technologies such as Wi-Fi, HSDPA, UMTS, and EDGE. The successive Web sites such as Google Video, YouTube, and iTunes are used to download/upload the videos. In such a scenario, a tool would be really required for performing video browsing. Recently, many applications are created for categorizing, indexing, and retrieving the digital video contents. These applications are used to handle large quantity of video contents. The proposed method facilitates the discovery of natural and homogeneous clusters.

Keywords Data mining · Clustering · Video information · Image retrieval · Image mining · BIRCH · Hierarchical clustering · Clustering comparison

1 Introduction

For frequently inserting and querying enormous amount of data, large databases are required to store. For researchers, extracting important model and analyzing big data set is interesting. There are two main groups in huge database mining.

D. Saravanan (✉)
Sathyabama University, Chennai, Tamil Nadu, India
e-mail: sa_roin@yahoo.com

S. Srinivasan
Department of Computer Science and Engineering, Anna University of Technology, Madurai, Tamil Nadu, India

© Springer India 2015

L.P. Suresh et al. (eds.), *Artificial Intelligence and Evolutionary Algorithms in Engineering Systems*, Advances in Intelligent Systems and Computing 325,
DOI 10.1007/978-81-322-2135-7_62

Applying mining techniques and referring streaming data is one group. Solving the problem with suitable algorithm is done in the second group. For large databases, data stream is the best approach instead of mining the entire database is focused by many researchers. Data can be scanned once and the data are retrieved, but the accuracy is not so good. Unsupervised methods are applied when evolving data are more difficult to detect and it is the main problem in data stream mining. We are going to clarify some points:

1. Data stream clustering problem definitions.
2. Research having specific difficulties.
3. Different approaches such as assumptions, approaches, and heuristics and some solutions to solve many problems are the basis.

Many researchers' interest is to apply some techniques to increase the compactness of representation, fast and incremental processing of new data points, and clear and fast identification of outliers. Scalability and robustness should be studied for data stream mining. The following steps have to be taken into account: Detect the changes as soon as it occurs. Detect equally well both types of changes, that is, abrupt and gradual. Distinguish between real drift and noise. Two main problems in this area that are related to this property include the following:

1. One scan is possible for processing data and
2. Data is included evolutionary stream and concepts are changed during the time. We can categorize data stream mining using three main techniques: classification, clustering, and association rule extraction.

1.1 Existing System

The growth of existing data volume and insufficiency of data storage capacity lead us to the dynamic processing data and extracting knowledge [2]. In this way, data have been considered as a stream of data which come from one side and exit in another side, so we are not able to visit data for the second time. This main property of data stream will lead to some difficulties.

1.1.1 Issue

Two main problems in this area that are related to this property include the following:

1. One scan is possible for processing data and
2. Data is included evolutionary stream and concepts are changed during the time. It may be gradual or abrupt.

1.2 Literature Survey of Existing System

Finding useful patterns in large data sets has attracted considerable interest recently, and one of the most widely studied problems in this area is the identification of clusters, or reused populated regions, in a multidirectional data set. Prior work does not adequately address the problem of large data sets and minimization of 1/0 costs. Scientific and industrial examples of data streams abound in astronomy, telecommunication operations, banking and stock–market applications, e-commerce, and other fields. A challenge imposed by continuously arriving data streams is to analyze them and to modify the models that explain them as new data arrive. In this paper, we analyze the requirements needed for clustering data streams. We review some of the latest algorithms in the literature and assess if they meet these requirements [3].

In recent years, a few one-pass clustering algorithms have been developed for the data stream problem. Although such methods address the scalability issues of the clustering problem, they are generally blind to the evolution of the data and do not address the following issues: (1) The quality of the clusters is poor when the data evolve considerably over time and (2) a data stream clustering algorithm requires much greater functionality in discovering and exploring clusters over different portions of the stream.

The problems of efficient choice, storage, and use of these statistical data for a fast data stream turn out to be quite tricky. For this purpose, we use the concepts of a pyramidal time frame in conjunction with a microclustering approach. Our performance experiments over a number of real and synthetic data sets illustrate the effectiveness, efficiency, and insights provided by our approach [4].

1.3 Proposed System

The BIRCH algorithm is a memory-oriented algorithm, i.e., the memory constraints are applicable for clustering process. The idea of BIRCH's clustering is derived from the concept of CF tree [4, 5]. The summary of the cluster information is represented as a triple in CF tree. Consider *N*-dimensional objects or points in a cluster. The clustering feature (CF) of the cluster is represented as a vector as follows:

$$\mathrm{CF} = (N,\ \mathrm{LS},\ \mathrm{SS})$$

where *N* represents the number of objects in a cluster, given that Xi is a data point, LS represents linear sum of all the *N* points, and SS represents the sum of square of all the data objects.

CFs in a clustering feature tree contain the summary of information of clusters. A CF tree has two parameters, i.e., threshold, *T*, and a branching factor, *B*. A non-leaf node in the tree can be represented as {CFi, childi}, where i = 1,2,3,…,B,

Childi—it holds the pointer to the *i*th child node.

CFi—subcluster of *i*th child node.

A cluster is represented by the non-leaf node, and all the subclusters are represented by the nodes. Here, a leaf node's content that holds the information of all subclusters has to meet a threshold value *T*.

The BIRCH algorithm is executed in four phases. In phase 1, threshold value *T* and branching factor *B* are used to build the initial CF from the database. In phase 2, which is optional, the size of initial CF tree might be reduced to build a smaller CF tree. In phase 3, either on smaller CF tree of previous phase or on initial tree, global clustering of data objects is performed. Good clusters are achieved from the phase 3, and it is shown in evaluation results. Phase 4 is executed if the quality of the clusters is improved. Phase 1 starts with a threshold value *T*. The whole set of data objects are read out in this phase, and the data objects that satisfy the distance function are selected. Then, the nodes of CF tree store the selected data points. The closely spaced selected data objects are then clustered. The widely spaced data objects are said to be outliers, and so they are removed from clustering.

During the clustering process, if the threshold value goes beyond before the database is completely scanned, then the threshold limit is improved and all the selected data objects are used to build a much small tree. In order to obtain good-quality clusters, an optimum value has to be chosen as threshold *T*. If the quality of clusters has to be fine-tuned, then the database can be further scanned in the phase 4. The time complexity of this algorithm in worst-case scenario is *O(n)*. The time required for the execution of this algorithm linearly varies with the size of the data set. CluStream addresses these two concerns. In this method, ideas in both BIRCH and STREAM are used. Microclustering and macroclustering are applied in two main components: online component and off-line component. It also employs a pyramid structure for organizing macroclusters during the time. Based on this idea, it is possible to answer user's question during tilted time. Based on the experimental results, it has acceptable accuracy and efficiency. In the absence of certainty, accuracy descends, so the UMicro algorithm for clustering uncertain data.

Two methods are used to detect the data in data stream.

1. Primitive clustering method: It is like a pyramid format and contains accurate data.

   Step 1 It scans the data and builds a tree.
   Step 2 BIRCH is used to refine tree to avoid outliers.

2. Data stream clustering method: COBWEB is used to make in hierarchical format. Each node contains information in summarized format.

2 Experimental Setup

2.1. COBWEB clustering technique.
2.2. Framework and density-based approach.
2.3. Divide-and-conquer method.
2.4. Technique to avoid high dimensionality.

2.1 COBWEB Clustering Technique

To discover the understandable pattern in data, COBWEB is used. A classification tree is formed in COBWEB, which indicates the hierarchical clustering model. A brief description about the concept is defined in each node, and under each node, objects are classified which tell the summary of the concept. The tree structure includes the outliers which are the overheads for managing tree.

2.1.1 Forming Cluster

```
        x = imgwidth
        y = imgheight
        tot = x * y
        For y = 0 To y - 1
            For x = 0 To x - 1
                colorPixel = DisplayBM.GetPixel(x, y)
                str = Format(x, "000" & " ")
                str1 = Format(y, "000" & " ")
                str2 = colorPixel.R
                str3 = colorPixel.G
                str4 = colorPixel.B
                If str2 = 0 And str3 = 0 And str4 = 0 Then
                    cnta = cnta + 1
                ElseIf str2 = 65 And str3 = 65 And str4 = 65 Then
                    cntb = cntb + 1
                            ElseIf str2 = 255 And str3 = 255 And
        str4 = 255 Then
                    cntc = cntc + 1
                Else
                    cnt = cnt + 1
                End If
            Next
        Next
        cnt = (cnt + cntc + cntb + cnta) / 4
txttime.Text = TimeOfDay
```

2.2 Framework and Density-Based Approach

In this framework, the CluStream is changed into cluster massive text and the data are categorized. The summary representation is made compact, and other features are employed. The efficiency will be more. Each input data are changed into grid format, and the density of each grid is manipulated. Using density-based algorithm, the data are clustered. The outliers around the original clusters are detected.

2.3 Divide-and-Conquer Method

To improve the clustering in data stream, divide-and-conquer technique is applied. There are two levels in divide-and-conquer clustering algorithm. It is applied to 2,000 data points. The first level is the leader algorithm which forms number of clusters in original data. A representation of these clusters is obtained. Using hierarchical clustering algorithm, representations are then clustered. This results in high quality and efficiency of objects with high dimensionality.

The second level is the C-means algorithm for data stream. Here, the clusters are weighted iteratively. The weighted clusters are incrementally clustered with the next data. The weights of outliers are not considered.

2.4 Technique to Avoid High Dimensionality

For data complexity, high dimensionality is one of the major reasons. To avoid this high dimensionality, two main groups are involved here. One group of researchers is involved in static high-dimensional data sets, and the other group involves the high-dimensional data stream clustering. HPstream is one of the popular streams which form the cluster high-dimensional data stream. Some features are selected, and subspaces are concreted for data clustering inside it as in Figs. 1, 2, 3, 4, 5, 6, and 7, and Tables 1, 2, and 3.

Fig. 1 Main process form

Fig. 2 Open image

Fig. 3 Clustering

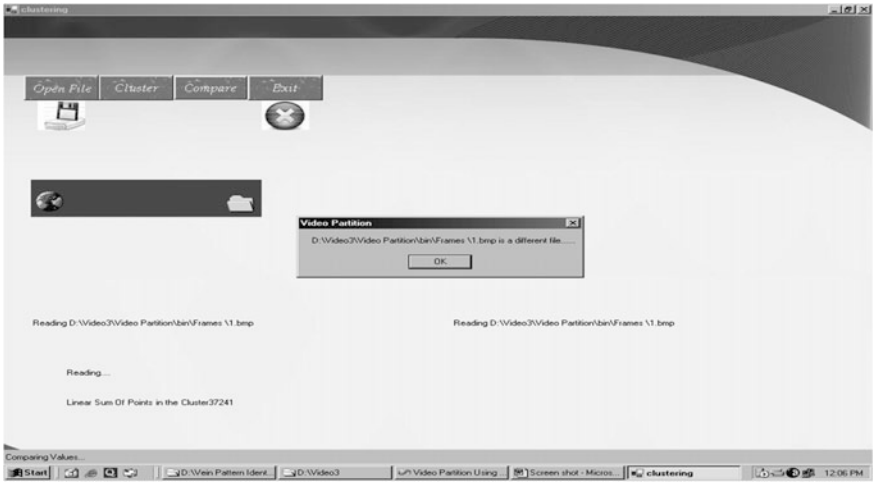

Fig. 4 Comparison of images

2.5 Experimental Results

Comparison

Green—graphics
Cyan—globe (animated)
Red—cartoon
Brown—news
Blue—song

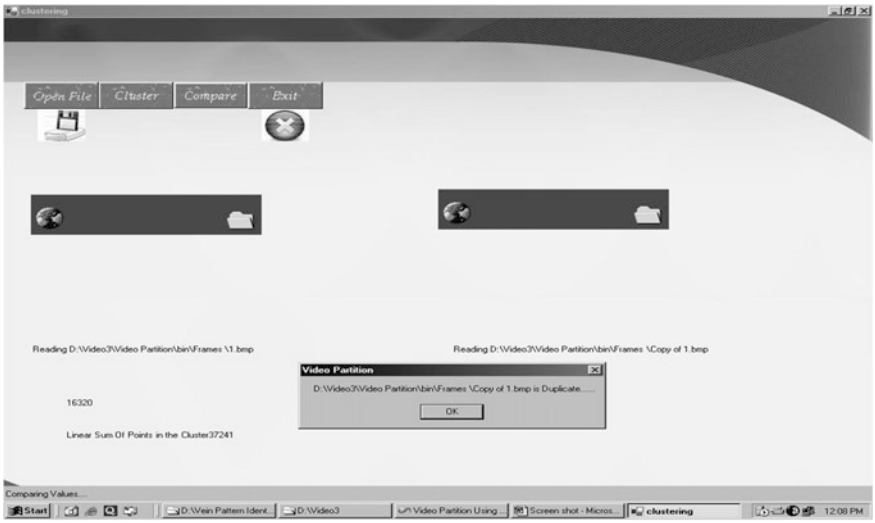

Fig. 5 Result of BIRCH cluster

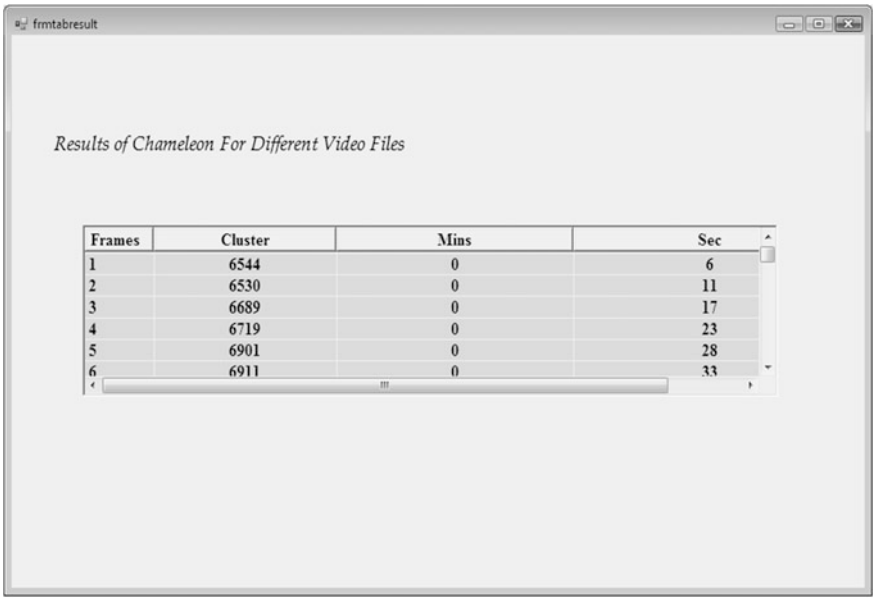

Fig. 6 Result form

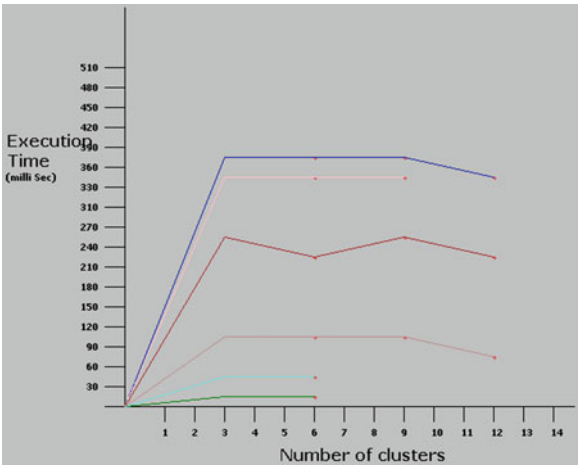

Fig. 7 BIRCH graph number of cluster versus execution time

Table 1 Comparison result of BIRCH

Video name	Number of input frames	Number of output frames	Duplicate frames removed
Cartoon	7	6	1
Graphics	16	10	6
Meeting	15	14	1
Globe	15	13	2
Song	15	14	1

Table 2 Grayscale values: for removing duplicates

fname	value
D:\Video3\Video Partition Using Birch\bin\Frames \23.bmp	46244344
D:\Video3\Video Partition Using Birch\bin\Frames \24.bmp	46136769
D:\Video3\Video Partition Using Birch\bin\Frames \25.bmp	45988813
D:\Video3\Video Partition Using Birch\bin\Frames \26.bmp	46000717
D:\Video3\Video Partition Using Birch\bin\Frames \27.bmp	45957601
D:\Video3\Video Partition Using Birch\bin\Frames \28.bmp	45939020
D:\Video3\Video Partition Using Birch\bin\Frames \29.bmp	45974799
D:\Video3\Video Partition Using Birch\bin\Frames \30.bmp	46012732
D:\Video3\Video Partition Using Birch\bin\Frames \31.bmp	46051725
D:\Video3\Video Partition Using Birch\bin\Frames \32.bmp	46055509
D:\Video3\Video Partition Using Birch\bin\Frames \33.bmp	46043439
D:\Video3\Video Partition Using Birch\bin\Frames \34.bmp	46065575
D:\Video3\Video Partition Using Birch\bin\Frames \35.bmp	46025120
D:\Video3\Video Partition Using Birch\bin\Frames \36.bmp	46031493

Table 3 Results of number of videos using BIRCH

Results of BIRCH For Different Video Files

S.No	Video	Frames count	Cluster	Milli Sec
1	4	1	2	780
2	4	2	2	660
3	4	3	2	600
4	4	4	2	540
5	4	5	2	540
6	4	6	2	540
7	4	7	2	540
8	4	8	2	480
9	4	9	2	600
10	4	10	1	720
11	4	11	1	780
12	4	12	1	720
13	4	13	1	720
14	4	14	1	780
15	5	1	16	2220
16	5	2	14	2400
17	5	3	14	2520
18	5	4	15	2220
19	5	5	16	2220
20	5	6	16	2760
21	5	7	16	2520
22	5	8	16	2340
23	5	9	16	2460
24	5	10	15	2280
25	5	11	16	2220

3 Conclusion

Here, we have demonstrated some difficulties in data stream clustering. Most data stream applications have high dimensions, and new methods need to be developed for this purpose. Furthermore, concept drift is the nature of data stream and should be managed by new methods. On the other hand, data stream is similar to a river: Data come in and go out, so we need to design efficient algorithms, whereas scan data once and extract hidden patterns inside it. Evolving data, visiting data once, and space limitations are major issues in data stream clustering. There are some primitive methods that concreted framework to process data stream, but devising new framework with new features other than previous (e.g., using genetic algorithm, ant colony algorithm, and neural networks) can lead us to more effective structures.

4 Future Enhancement

In this section, we present BIRCH, a new clustering algorithm that overcomes the limitations of existing agglomerative hierarchical clustering algorithms discussed. BIRCH operates on a sparse graph in which nodes represent data items and weighted edges represent similarities among the data items. This sparse graph representation of the data set allows BIRCH to scale large data sets and to operate successfully on data sets that are available only in similarity space and not in metric

spaces. BIRCH finds the clusters in the data set by using a two-phase algorithm. During the first phase, BIRCH uses a graph partitioning algorithm to cluster the data items into a large number of relatively small subclusters. During the second phase, it uses an agglomerative hierarchical clustering algorithm to find the genuine clusters by repeatedly combining together these subclusters. The key feature of BIRCH agglomerative hierarchical clustering algorithm is that it determines the pair of most similar subclusters by taking into account both the interconnectivity and the closeness of the clusters, and thus, it overcomes the limitations discussed in Sect. 3 that result from using only one of them. Furthermore, BIRCH uses a novel approach to model the degree of interconnectivity and closeness between each pair of clusters that takes into account the internal characteristics of the clusters themselves. Thus, it does not depend on a static user-supplied model and can automatically adapt to the internal characteristics of the clusters being merged.

References

1. D. Saravanan, S. Srinivasan, A proposed new algorithm for hierarchical clustering suitable for video data mining. Int. J Data Min. Knowl. Eng. **3**(9), 569–572 (2011)
2. D. Saravanan, S. Srinivasan, Matrix based indexing technique for video data. Int. J. Comput. Sci. **9**(5), 534–542 (2013)
3. M. Ester, H.-P. Kriegel, J. Sander, X. Xu, A density-based algorithm for discovering clusters in large spatial database with noise. In I&‘1 Conference on Knowledge Discovery in Databases and Data Mining (KDD-96) (1996)
4. M. Ester, H.-P. Kriegel, X. Xu, A database interface for clustering in large spatial databases. In Int’l Conference on Knowledge Discovery in Databases and Data Mining (KDD-95) (1995)
5. T. Zhang, R. Ramakrishnan, M. Livny, Birch: an efficient data clustering method for very large databases. In Proceedings of the ACM SIGMOD Conference on Management of Data. (1996)103–114
6. D. Saravanan, S. Srinivasan, Video image retrieval using data mining techniques. J. Comput. Appl. **5**(1), 39–42 (2012)
7. D. Saravanan, S. Srinivasan, Data Mining Framework for Video Data. In the Proc. of International Conference on Recent Advances in Space Technology Services & Climate Change (RSTS&CC-2010). (2010) pp. 196–198
8. N. Beckmann, H.-P. Kriegei, R. Schneider, B. Seeger, The R*-tree: an efficient and robust access method for points and rectangles. In Proceedings of ACM SIGMOD. (1990) pp. 322–331
9. M. Livny, R. Ramakrishnan, T. Zhang, BIRCH: An efficient clustering method for very large databases. In the proceeding of ACMSIGMOD Workshop on Research Issues on Data Mining and Knowledge Discovery. (1996) pp. 103–114
10. D. Saravanan, S. Srinivasan, Video information retrieval using: chameleon algorithm. Int. J. Emerg. Trends Technol. Compu. Sci.(IJETTCS) **2**(1), 166–170 (2013)
11. D. Saravanan, S. Srinivasan, Survey of existing video indexing technique an overview. J. Inf. Technol. **1**(4), 13–16 (2012)

Handwritten Tamil Character Recognition Using Zernike Moments and Legendre Polynomial

Amitabh Wahi, S. Sundaramurthy and P. Poovizhi

Abstract Optical character recognition systems have been effectively developed for recognizing the printed characters of many non-Indian languages such as English and Chinese. At early stages, few research works were carried out for recognizing the handwritten characters, and now, various efforts are on the way for the development of efficient systems for recognizing the Indian languages, especially for Tamil, a south Indian language widely used in Tamilnadu, Pudhucherry, Singapore, and Srilanka. In this paper, an OCR system is developed for the recognition of basic characters in handwritten Tamil language, which can handle different font sizes and font types. Zernike moments and Legendre polynomial which have been used in pattern recognition are used in this system to extract the features of handwritten Tamil characters. A comparative study is performed in this paper. Feed forward back propagation neural classifier has been used for the classification of Tamil characters.

1 Introduction

Handwritten character recognition is the area of research for the past few decades, and there is a large demand for OCR on handwritten documents. Even though sufficient studies have performed in foreign scripts such as Chinese, Japanese, and Arabic characters [1], only a very few work can be traced for handwritten character recognition of Indian scripts. Even now no complete handwritten text recognition

A. Wahi (✉) · S. Sundaramurthy · P. Poovizhi
Department of Information Technology, Bannari Amman Institute of Technology, Sathyamangalam, Tamil Nadu, India
e-mail: awahi@bitsathy.ac.in

S. Sundaramurthy
e-mail: sundaramurthys@bitsathy.ac.in

P. Poovizhi
e-mail: poovizhiponnusamy27@gmail.com

© Springer India 2015

L.P. Suresh et al. (eds.), *Artificial Intelligence and Evolutionary Algorithms in Engineering Systems*, Advances in Intelligent Systems and Computing 325,
DOI 10.1007/978-81-322-2135-7_63

system is available in Indian scenario, and it is difficult due to large character set of Indian languages and the presence of vowel modifiers and compound characters in Indian script. Some reports have appeared for isolated handwritten characters and numerals of a few Indian languages. Majority of them was based on Bangla and Devanagiri script [2]. Nowadays, Government of India is taken initiation toward the development of language technology. Commercial systems are developed for some Indian scripts, namely Assamese, Bangla, Devanagiri, Malayalam, Oriya, Tamil, and Telugu, but that can handle only printed text, not handwritten manuscript. This study focuses mainly on off-line handwritten character recognition of South Indian languages, namely Tamil [3].

India has 22 languages. These languages are written using only twelve scripts. Devanagiri script used to write Hindi, Konkani, Marathi, Nepali, Sanskrit, Bodo, Dogri, and Mathili. Sindhi is written using Devanagiri script in India and Urdu script in Pakistan. Assamese, Manipuri, and Bangla languages are written using Bengali script. Gurmukhi script is used to write Punjabi language. All other languages have their own script. The upper case and lower case are not present in Indian language scripts. Most of the Indian languages are derived from Ancient Brahmi and are phonetic in nature and hence writing maps sounds of alphabets to specific shapes. All these languages, except Urdu, are written from left to right. The basic characters comprise of vowels and consonants. Two or more basic characters are combined to form compound characters.

Moment-based features are a widely used tool for character recognition. The moment invariants under translation, rotation and scaling, is first introduced by Hu in 1962. However, Hu's moments contain much redundant information about a character's shape. Nowadays, Zernike moments are becoming popular for character recognition. Because of local-tuned neurons, feed forward neural network has fast training/learning rate. Due to this advantage, Zernike moments are used in the field of character recognition. The motivation of this work is purely based on the application of moment features and neural classifiers in the character recognition. In this paper, we have presented an OCR system for basic Tamil characters, feature extraction is performed using moments, and feed forward neural networks are used as a classifiers.

2 Literature Survey

Diagonal feature extraction scheme for off-line character recognition is proposed by Pradeep et al. [4]. This paper tells that each character of size 90∗60 pixels is divided into 54 equal zones, and each zone has the size of 10∗10 pixels. By moving along the diagonals, the features are extracted from each of the zone. Each zone has 19 diagonal lines, and there will be some foreground pixels. The diagonal lines are summed to get a single sub-feature. These 19 sub-features are averaged to form a single feature. This process is repeated for all the zones. Totally, 54 features are extracted for each character. Taking average on row-wise (9) and column-wise (6), as a result, every character is represented by 69 features. A feed forward back

propagation neural network having two hidden layers with architecture of 54-100-100-38 is used to perform the classification.

H. Swethalakshmi et al. used sequences of strokes for the feature extraction [5]. The feature extraction is performed for the devanagiri and Telugu scripts. Single recognition engine approach, Multiple SVM, and HMMs all these three approaches have been used for the feature extraction. The classification was performed using support vector machine.

Tiji M Jose et al. [6] illustrated the wavelet decomposition technique for the extraction of the features from the Tamil characters. The feed forward back propagation network classifier is used for the intention of classification. The recognition rate achieved in this paper was about 89 % using the level 4 db2.

The scanned image is segmented into words using spatial space detection technique; at first, paragraph is segmented to lines using vertical histogram; then, the lines are segmented into words using horizontal histogram; and finally, the word is segmented into character image glyphs using horizontal histogram [7]. The extracted features for the character are the height, width of the character, number of horizontal lines present, and pixels in the various regions. After feature extraction, the output is given to the classifier. The accuracy achieved with this technique is 97 %.

Indra Gandhi et al. proposed a new approach of using Kohonen SOM (self-organizing map) for recognizing the online Tamil character [8]. The vectors of the binary image are created. When the segmentation of the character is over, the images are scaled to unique height and weight. Some unwanted portions are included, but it can be removed by sobel edge detection. The median filter is used to increase the efficiency. The SOM is not applicable to the cursive characters which are used in this paper. The median filter is not suited for the off-line Tamil characters. So the Zernike moments are used for feature extraction.

Jagadeesh Kannan et al. [9] used octal graph method for the recognition of the Tamil handwritten characters. Here, the character return on the octal graph's pixel is converted into the node of the graph. Each node has eight fields, that is why called as octal graph. Each node is connected to the other node based on the threshold value. The image is converted to the octal graph by the steps such as normalization, conversion, identification of weighing factors, and feature extraction. If the character is tedious and if it contains many curves, then octal graph method is not suitable.

3 System Model

Figure 1 shows the modules in the proposed system. The proposed system contains the modules: preprocessing, feature extraction, and classification. Preprocessing is the conversion of color images to gray scale and then to binary images.

The features are extracted from those images using the moment calculation, and back propagation is used as the classifier.

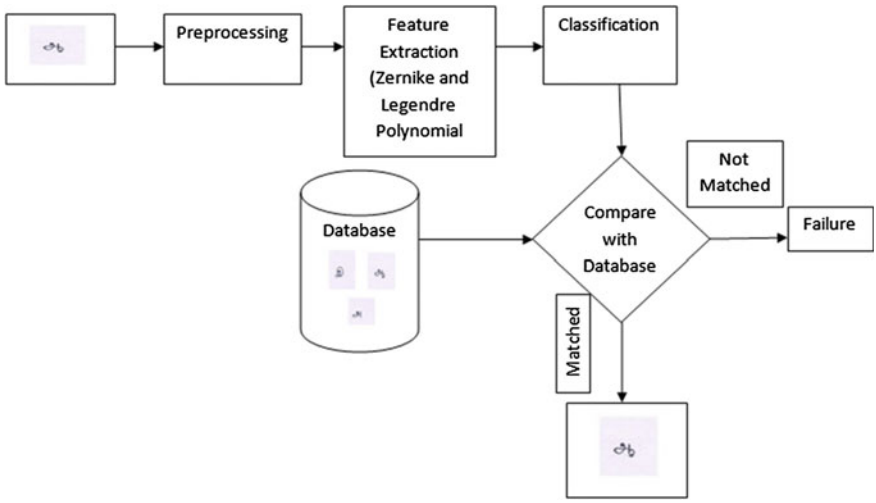

Fig. 1 System model

3.1 Preprocessing

There are numerous tasks to be completed before performing character recognition. A handwritten document must be scanned and converted into a suitable format for processing. Preprocessing consists of a few types of sub processes to clean the document image and make it appropriate to carry the recognition process accurately. The subprocesses which get involved in preprocessing are illustrated below:

- Binarization

3.1.1 Binarization

Binarization is a method of transforming a grayscale image into a black-and-white image through thresholding [4, 10]. Another approach, Otsu's method, may be used to perform histogram-based thresholding [5, 6] to get binarized image automatically. Otsu's method has been extended for multilevel thresholding, called multi-Ostu method [11]. Normally, most researchers use thresholding concepts to extract the foreground image from background image [7, 12, 13]. In this method, the threshold value is fixed by taking any value between two foreground gray-code images (Fig. 2).

Histogram-based thresholding approach can also be used to convert a grayscale image into a two-tone image. In contrast, adaptive binarization method can also be used to identify the local gray value contrast of image. This will help to extract text information from low-quality documents. Another approach named two-level

Fig. 2 **a** Original image **b** Grayscale image **c** Binary image

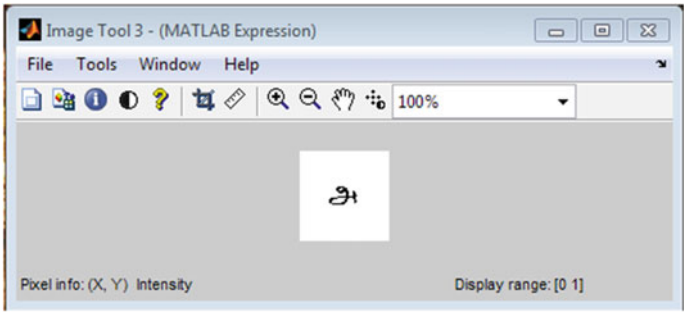

Fig. 3 Placing the cropped image in the white template

global binarization technique represents the output using global thresholding technique [11].

The cropped image is placed at the center of the blank matrix as shown in Fig. 3.

3.2 Feature Extraction

Individual image glyph is considered and extracted for features such as character height, width, horizontal lines, vertical lines, slope lines, circles, and arcs.

The selection of appropriate feature extraction method is probably the single most important factor in achieving high recognition performance. In [14], several methods of feature extraction for character recognition have been reported.

3.2.1 Zernike Moments

Zernike moments are introduced by Zernike in 1934, and these moments are due to Zernike polynomials [15]. Zernike polynomials are a set of complex polynomials in which a complete orthogonal set is formed over the interior of the unit circle.

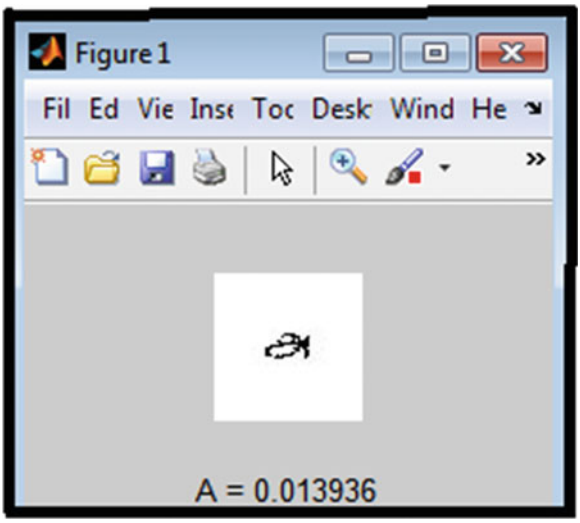

Fig. 4 Feature extraction performed for the character

The orthogonal radial polynomial $R_{nm}(r)$ is defined as:

$$R_{nm}(r) = \sum_{s=0}^{(n-|m|)/2} (-1)^s g. \frac{(n-s)!}{s!\left(\frac{n+|m|}{2}-s\right)!\left(\frac{n-|m|}{2}-s\right)!} g^{r^{(n-2s)}} \tag{1}$$

The Zernike moment with repetition m and the order of n of a continuous image function $f(x, y)$ is given by:

$$Z_{nm} = \frac{n+1}{\pi} \sum_{x} \sum_{y} f(x,y)[V_{nm}(x,y)]^* \tag{2}$$

Zernike moments have minimum information redundancy compared to Hu moments because it is orthogonal (Fig. 4).

3.2.2 Legendre Polynomial

Rodrigues' formula gives the Legendre polynomials.

$$P_k(\eta) = \frac{1}{2^k k!} \frac{d^k}{d\eta^k} (\eta^2 - 1)^k \tag{3}$$

3.3 Neural Classifier

A few models that have been applied for the HCR system include motor models [16], structure-based models [17, 18], stochastic models [8], and learning-based

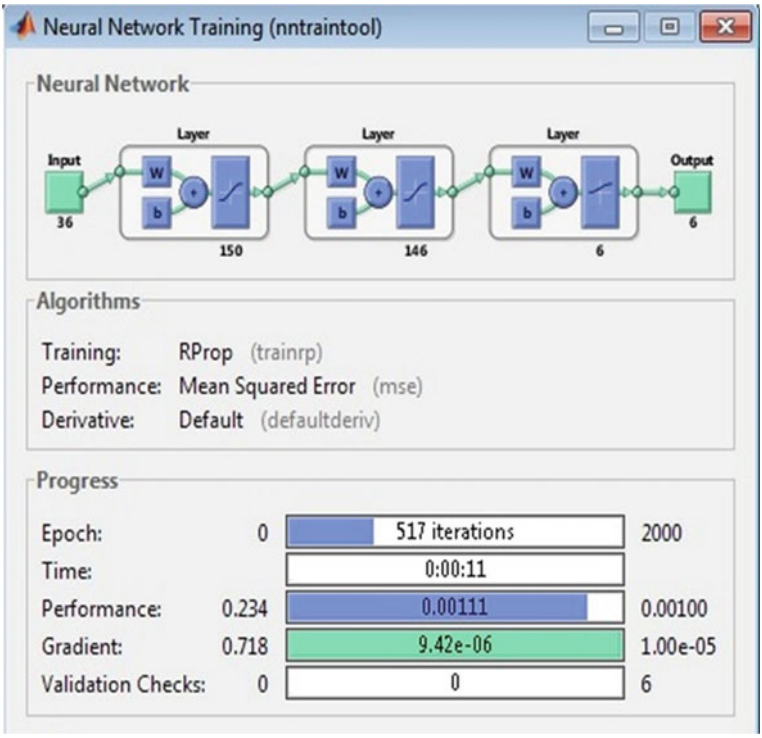

Fig. 5 Training using feed forward classifier

models [9]. Learning-based models have received wide attention for pattern recognition problems [19, 20, 21] (Figs. 5 and 6).

Neural network models have been reported for the achievement of better performance than other existing models in many recognition tasks.

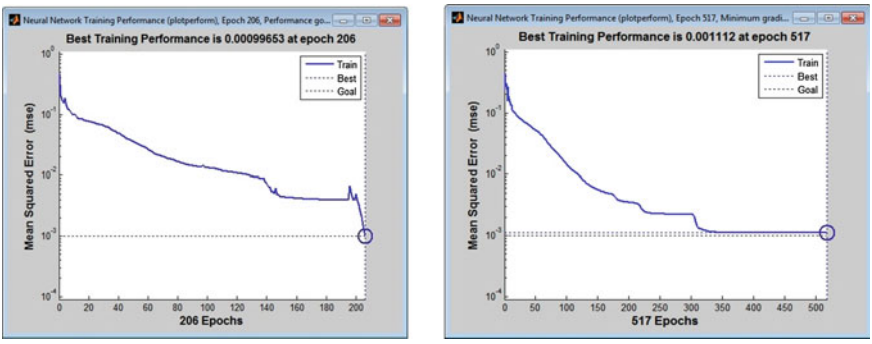

Fig. 6 Performance plot for Zernike and Legendre polynomial

4 Results and Discussions

Twenty-five percentage of the data set is used as the testing data, and the rest 75 % is used as training data. One hundred samples are collected from different persons.

The 36 inputs are given to the neural network. The training is done in RProp algorithm, because it trains the given set within the short period of time. The iteration used for training is 20,000. The time required for the training is about 2 s. The goal is put to 0.001. The accuracy is maintained based on the value that is set for the performance to meet. The two hidden layers are set for training. The first hidden layer consists of 150 neurons, and the second hidden layer consists of 146 neurons.

5 Conclusions and Future Work

In this paper, the Zernike moments and Legendre polynomial are used. In the Hu moment, the image is defined over the real plane, but in Zernike, the image is mapped to the unit circle. Zernike moments are invariant to translation, scale, and rotation. To achieve scale invariant and translation invariant, the normalization method is essential. The translation invariant can be achieved by moving the image to the center.

Zernike moments and Legendre polynomial which have been used in pattern recognition are used in this system to extract the features of handwritten Tamil characters. Neural classifiers (feed forward neural network) have been used for the classification of Tamil characters.

The computations of the Zernike moments are quite difficult. The reason behind this is due to the normalization of the image. In future, classifiers such as support vector machines (SVM) can be used to improve the efficiency.

References

1. R. Plamondan, S.N. Srihari, Online and offline handwriting recognition: A comprehensive survey. IEEE Trans. PAMI **22**(1), 63–84 (2000)
2. U. Pal, B.B. Chaudhuri (2004), Indian script character recognition: a survey. Pattern Recognit., 37, pp. 1887–1899
3. T. Paulpandian, V. Ganapathy, Translation and scale invariant recognition of handwritten Tamil characters using hierarchical neural networks. IEEE International Symposium on Circuits and Systems. 4, pp. 2439–2441 (1993)
4. N. Shanthi, K. Duraiswami, A novel SVM-based handwritten Tamil character recognition system. Pattern Anal Appl. **13**(2), 173–180 (2010)
5. R. Ramanathan, S. Ponmathavan, L. Thaneshwaran, Arun, S. Nair, N. Valliappan, Tamil font recognition using gabor and support vector machines. International Conference on Advances in Computing, Control, & Telecommunication Technologies. pp. 613–615 (2009)

6. R. Jagadeesh Kumar, R. Prabhakar, R.M. Suresh, Off-line cursive handwritten Tamil characters recognition. International Conference on Security Technology. pp. 159–164 (2008)
7. A.N. Sigappi, S. Palanivel, V. Ramalingam, Handwritten document retrieval system for Tamil language. Int J. Comput. Appl. **31**, 42–47 (2011)
8. K.F. Chan, D.Y. Yeung, Elastic structural mapping for online handwritten alphanumeric character recognition. Proceedings of 14th International Conference on Pattern Recognition. pp. 1508–1511 (1998)
9. J. John, K.V Pramod, K. Balakrishnan, Handwritten Character Recognition of South Indian Scripts: a Review. National Conference on Indian Language Computing, (2011)
10. S. Manke, U. Bodenhausen, A connectionist recognizer for online cursive handwriting recognition, Proceedings of ICASSP, 94(2), pp. 633–636 (1994)
11. X. Li, R. Plamondon, M. Parizeau, Model-based online handwritten digit recognition. Proceedings of 14th International Conference On Pattern Recognition. pp. 1134–1136 (1998)
12. N. Shanthi, K. Duraiswami, Performance comparison of different image size for recognizing unconstrained handwritten Tamil character using SVM. J. Comput. Sci. **3**(9), 760–764 (2007)
13. J. Sutha, N. RamaRaj, Neural network based offline Tamil handwritten character recognition system. International Conference on Computational Intelligence and Multimedia, 2, pp. 446–450 (2007)
14. A.K. Jain, Torfinn Taxt.: Feature Extraction Methods For Character Recognition-a survey. Pattern Recognit. **29**(4), 641–662 (1996)
15. S. Asthana, F. Haneef, R.K. Bhujade, Handwritten multiscript numeral recognition using artificial neural networks. Int. J. Soft Comput. Eng. **1**(1), 1–67 (2011)
16. S.K.B. Sangeetha, Dr.V. Vijayachamundeeswari, Tamil OCR- A Survey. International Conference on Computing and Control Engineering (ICCCE 2012). (2012)
17. L.R.B. Schomaker, H.L. Teulings, A handwriting recognition system based on the properties and architectures of the human motor system. Proceedings of the IWFHR. pp. 195–211 (1990)
18. Aparna, K.H., Vidhya Subramanian, Kasirajan, M., Vijay Prakash, G., Chakravarthy, V. S., Sriganesh adhvanath.: Online handwriting recognition for Tamil. Proceedings of the Ninth International Workshop on Frontiers in Handwriting Recognition (IWFHR' 04). pp. 438-443 (2004)
19. A. Bharath, S. Madhvanath, HMM-based lexicon driven and lexicon-free word recognition for online handwritten indic scripts. IEEE Trans. Pattern Anal. Mach. Intell. **34**(4), 670–682 (2012)
20. C. Suresh Kumar, T. Ravichandran, Handwritten Tamil character recognition using RCS algorithms. Int. J. Compu. Appl. **8**(8), 21–25 (2010)
21. R. Bremananth, A. Prakash, Tamil Numerals Identification. International Conference on Advances in Recent Technologies in Communication and Computing. pp. 620–622 (2009)

Encrusted CRF in Intrusion Detection System

S. Vinila Jinny and J. Jaya Kumari

Abstract Intrusion detection system's aim is to note malicious activities in a network. But it has to tackle many challenges against its goal. Intrusion detection is the action of detecting inapt, inexact, and abnormal activity in the network data. Network security is a major worry in large organization. Data integrity, secrecy, and ease of use must be conserved in order to make certain network security. In this paper, we consider the accuracy as the first issue and efficiency as the second issue using conditional random field and encrusted method. The proposed technique performs well than best-known methods such as naïve Bayes and Decision tree. The probe layer attacks stops network service. Remote to local (R2L), User to root (U2R) attacks and denial-of-service attacks (DOS) are widely known attacks that make impact on network assets. Improved attack detection efficiency can be obtained through CRF and high efficiency by implementing encrusted approach.

Keywords IDS · Conditional random fields · Encrusted approach

1 Introduction

Today, in any computer network, the major requirement for administrators is to detect intrusions and provide safeguard against that. An expert says that new technologies set in intrusion detection system are again overcome by new and new approaches in hacking. All intrusion detection is designed in such a way to meet

S. Vinila Jinny (✉)
Department of Computer Science and Engineering, Noorul Islam University, Kumara coil, Thuckalay, India
e-mail: vinijini@gmail.com

J. Jaya Kumari
Department of Electronics and Communication Engineering, Noorul Islam University, Kumara coil, Thuckalay, India
e-mail: jkumaribharat@gmail.com

© Springer India 2015

L.P. Suresh et al. (eds.), *Artificial Intelligence and Evolutionary Algorithms in Engineering Systems*, Advances in Intelligent Systems and Computing 325,
DOI 10.1007/978-81-322-2135-7_64

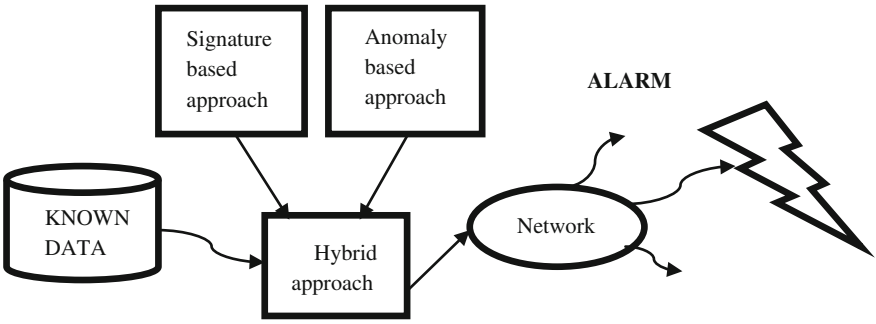

Fig. 1 Intrusion detection system structure

some requirements, and each may have its own need also. The ultimate goal is to identify maximum attacks with low false rating. That system must exactly find the intrusions. The main aim or goal of IDS is to detect all intrusion in the noted traffic in the network.

Intrusion detection system (IDS) works through huge amounts of network monitoring data [1]. Figure 1 depicts the generalized intrusion detection system structure. In case of host-based IDS, cross-check the log files found in a computer, to detect distrustful activities, whereas in a network-based IDS, cross-check data of network monitoring for destructive packet transfer. Intrusion detection has been classified either as misuse-based or anomaly-based system.

1.1 Signature-Based or Misuse-Based IDS

The signature-based system [2, 3] sets a classifier based on the existing knowledge of the intrusions, and from these rules, depicting intrusion is learned and the classifier is brought on that. This is analogous to antivirus software that detects any malware. The issue here is that it is unable to detect new threats at the time of infection because it requires further update of the database to detect that new attack. The delay taken by the IDS for the comparison makes the detection idle at that time. This is also known as misuse detection.

1.2 Anomaly-Based or Behavior-Based IDS

In this method [3], it monitors the network for deviation from normal behavior, i.e., it compares with normal behavior patterns. The working of this model is in such way that it classifies normal behavior, bandwidth usage, rules followed, port

number, and device id that gets connected and informs the administrator or in charge on detection of anomalous behavior.

2 Related Work

Intrusion detection idea has been from late 1980s [4]. After that, a large number of methods, protocols, and frame models have been suggested and many of them are set to working. Different methods such as association rule, which is a decision maker using rule, naive Bayes classifier, which is a probabilistic mode, support vector machine, which is a linear classifier, genetic algorithms, which is gene basic, and artificial neural networks are used in intrusion detection system. Clustering has been used and implemented to detect intrusions. We come through some of the existing IDS frameworks. First, we go for the discussion some methods of misuse, anomaly, and hybrid type of system. Then, we go for the discussion of proposed method and technology. In expert systems [5], the actual intrusion is represented as a protocol which comprises event description of audit. Eskin et al. [6] tell the difficulty in using clustering for IDS after examining cluster estimation, k-means estimation, and support vector machine. Other researchers used these techniques as unsupervised IDSs.

In supervised anomaly method, various techniques such as fuzzy data mining with genetics, neural networks [7], and support vector machine. Patterns of normal activities are used to build models of supervised method of IDS. Then, it works in such a way that if there is a difference in the normal pattern, then it is considered as intrusion. Supervised anomaly detection can be applied using statistical methods and expert system [5]. By using user and system profiles, system is built using statistical methods.

Learning system takes the normal attitude of users and applications as a set of protocols, and then, it is used to identify the intrusion. Next generation gave a new learning system, which is NIDES [8]. Multiple sources are considered here for monitoring, and the detection is based on the output all of these systems in the network and so it is considered as hybrid approach.

We can see a large number of systems using association rules in IDS [9]. In the field of IDS using data mining algorithms, audit data analysis and mining (ADAM) [9] is the best one. It is widely known to all for its performance. The unknown attacks are actually the suspicious items that are very difficult to be classified as normal behavior or attack. We can hear about the existence of agent-based system, i.e., Java Agents for Meta-learning (JAM). It is broadly known, and it has the advantages of scalability and manageability. Security can be set by various approaches. Among all, intrusion detection system helps mostly in providing security. Table 1 summarizes the various security technologies.

Table 1 Security technologies

Technology	Function	Analysis type	Strength	Drawback
Firewall	Stops or allows traffic according to specified rules	Packet header information is analyzed	Real-time filtering	Cannot detect future attack
Misuse IDS	Detects attack by known attack patterns	Packet content and header information is analyzed	Attacks are clearly identified	Unknown attacks are not detected. High false alarm rate
Anomaly IDS	Detects the behavior when deviates from normal behavior	Packet action alone is analyzed	Detects unknown attacks	False positives are high
Honey pot	Attracts attacker and becomes active	Packet analysis is not done	Known attacks and low false alarm	Useful when it is attacked

3 Knowledge Discovery Approaches

In IDS, the analyzer module uses data mining approaches [3, 10]. Here, it detects the related patterns of services and users and it uses association rule and frequent episodes as the methodology. All these approaches use features of connection and network packet details [11]. Usually, network features alone will not satisfy detection, and so inter analysis of traffic is required. Network packet data are sparse which may lead to infinite rules. This can be restricted by appropriate pruning techniques.

4 Preprocessing

Preprocessing in most systems is required as it highly influences the efficiency of the system. In our system, we use feature selection as the preprocessing technique. Information gain measure is used to select features. For using this measure, all features are converted to discrete features [12, 13].

4.1 Information Gain

The features can be selected using information gain (InGain). InGain calculation requires computation of entropy value of every attribute of the data [8, 9, 14]. This helps to decide the importance of the attributes which may affect the classification. Feature that has high information gain measure highly affects the data classification.

With this concept, we may ignore features with less information gain value. This will not affect the detection accuracy. The correct definition of information gain is as follows.

Let A and B be discrete variables, which represent sample attributes (a_1, a_2,…, a_m), and class attributes (b_1, b_2,…,b_n), respectively. The InGain of a given attribute corresponding to class attribute B is the ambiguity reduction of the data value of B [15]. The value of A is known. Entropy(B) is the ambiguity of the value of B. The Entropy($B|A$) is the ambiguity of the value of B if A value is known. Mathematical representation of information gain is

$$\text{InGain}(B;A) = \text{Entropy}(B) - \textit{Entropy}(B|A). \tag{1}$$

$$\text{where Entropy}(B) = -\sum_{i=1}^{n} P(B = b_i) \log 2P(B - b_i) \tag{2}$$

$$P(B = b_i) = \text{probability that the class attribute } \mathrm{b_i} \text{ occurs}$$

$$\text{Entropy}(\mathrm{B}|\mathrm{A}) = -\sum_{j=1}^{m} P\left(\mathrm{A} = \mathrm{a_j}\right) \text{Entropy}\left(\mathrm{B}|\mathrm{A} = \mathrm{a_j}\right) \tag{3}$$

Representation of information gain can also be given as follows:

$$\text{InGain}(B;A) = \text{Entropy}(A) + \text{Entropy}(B) - \text{Entropy}(A,B) \tag{4}$$

The Entropy(A, B) is the joint entropy of A and B, so

$$\text{Entropy}(A,B) = -\sum_{i,j} P\left(A = a_j, B = b_j\right) \log_2 P(A = a_j, B = b_i) \tag{5}$$

In this system, inputs of individual attributes [28] for classification are defined by A, and attack class is given by B, i.e., normal data, probe attack, and DoS attack. In our work, a number of candidate features are calculated for InGain value, and from that, a countable feature with high InGain value is considered.

5 Conditional Random Field

In our work, the main classifier is the conditional random fields. This model is an undirected graphical models [13, 16]. It can be called as random fields. Here, it calculates the conditional probability of output values, based on input values formed with known set. Most natural language processing application considers this as the methodology. Actually, this will not take any unnecessary assumption while giving the report and also constructed with good basic.

Consider P as the random variable on the data series to be labeled and Q as the matching label sequence for the observations. A graph G = (A, B) such that $Q = (Qv)v(A)'$ is considered, so that Q is numbered by the nodes of G. The generated values (P, Q), says that the CRF is conditioned on P, Q. Markov property is accepted by this random variables based on the graph:

$$p\left(B_v|A, B_{w,wv}\right) = p\left(B_v|A, B_{w,w\sim v}\right), \ldots \tag{6}$$

where $w \sim v$ says that in G, the neighbors are w and v. The joint distribution on a label sequence B given A is shown as follows:

$$p(b|a)\exp(eB, kkfk(e, b|e, a) + vA, kkgk(v; ab|v, a), \ldots \tag{7}$$

CRF is a graphical model, not only graphical, but also undirected. CRF is generally used in sequence tagging. CRF directly models the conditional distribution $p(b/a)$ by which task of classification and sequence labeling is done. Intrusion detection problem is similar to other problems like machine learning, bioinformatics, and natural language processing, and it can be compared with them. Here, it will not make assumptions about the data.

6 Encrusted Approach for Intrusion Detection

EIDS represents a chronological framed approach and is based on ensuring ease of use, privacy, and reliability of data over a network [6, 17]. The main aim for using encrusted model is to reduce the throughput time required to detect the anomalous events and to reduce working out time. By reducing the communication cost between frames, time required to detect a suspicious event can be highly reduced. This can be done only when we make a frame efficient in detecting and blocking the event instead of asking a decision maker. In EIDS, frames are separately designed to tackle the scenario in itself and then implemented sequentially. Based on grouping the attacks, the frames can be decided. Here, four attack categories are opted for four frames.

This includes probe frame, DoS frame, R2L frame, and U2R frame. Each frame is independently skilled with a subset of related attributes. Preprocessing that has feature selection highly affects the system, so it is needed for encrusted CRF. Each frame acts as independent detectors, and some attributes are trained to all or required frames. Each frame acts as barrier that stops intrusion, and so for that network data, no further checking is done. Overall performance of the system is improved with the increase in the speed of the system. EIDS is set in a way that each layer takes about a subset from the main set of 41 features, which results in good performance. Both training and testing of the system show good performance. Encrusted CRF is analogous to that of decision trees and naïve Bayes. Proposed

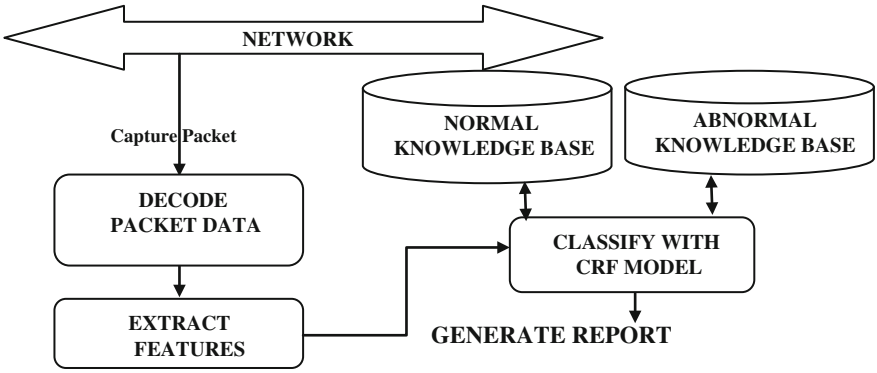

Fig. 2 System architecture of IDS with CRF

system shows better attack detection. Figure 2 depicts the overall system architecture.

7 Implementation

For our implementation, we have taken benchmark KDD '99 data set and also real data set [17]. This contains both training data set and test data set. It contains about five million training data sets, i.e., connection records. Two million test data sets are also found in it. In our experiment, we have used about 50 crore training records and 20 crore test records. Each connection record consists of about 41 features or attributes. Java implementation for this classifier is made, which identifies intrusion and normal behavior. Training data are categorized as normal user data, R2L user data, probe intruder data, and U2R user data.

8 Results and Discussion

The conditional random field classifier gives good detection accuracy. Its detection accuracy is highly improved on feature selection. The training time and testing time are highly reduced because of feature selection. CRF with feature selection is added with frames which highly speed up the processing. As the work is shared among frames, the training time and testing time are highly reduced though there is no improvement in the detection accuracy. Table 1 and Tables 2 and 3 summarize the accuracy in the detection and performance of the encrusted system. Figures 3 and 4 depict the graphical representation of detection accuracy and performance of the system.

Table 2 Detection accuracy

Classification algorithm	Accuracy of detection (in %)	
	Correctly classified	Incorrectly classified
CRF	90	10
CRF with FS	95	5
Encrusted CRF	95	5

Table 3 Performance evaluation

Classification algorithm	Accuracy of detection (in %)		
	Training	Testing	Accuracy
CRF	6.5	1.5	90
CRF with feature selection	5.4	0.54	95
Encrusted CRF	2.73	0.06	95

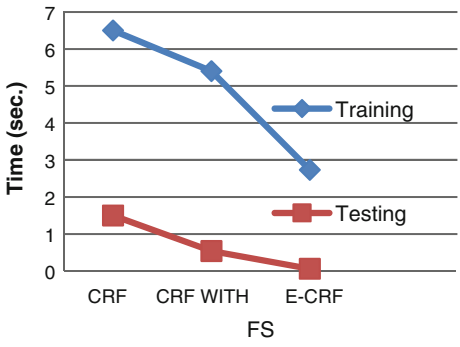

Fig. 3 Performance evaluation

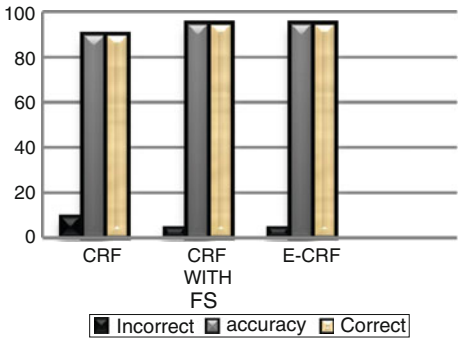

Fig. 4 Detection accuracy

9 Conclusion and Future Enhancement

Attack detection rate is very high using CRF. Also, FAR is also less. Low false alarm rate is very important as it highly affects intrusion detection system. Speed is also high, which improves the overall performance of the system. Flexibility of encrusted approach highly improved the detection accuracy.

References

1. W. Lee, S. Stolfo, A framework for constructing features and models for intrusion detection systems. ACM Trans. Inf. Syst. Secur. **3**(4), 227–261 (2000)
2. E. Eskin, A. Arnold, M. Prerau, L. Portnoy, S. Stolfo, *A Geometric Framework For Unsupervised Anomaly Detection: Detecting Intrusions In Unlabeled Data. Applications of Data Mining in Computer Security* (Kluwer, Dordrecht, 2002)
3. I.H. Witten, E. Frank, *Data Mining-Practical Machine Learning Tools and Techniques* (Morgan Kaufmann publishers, Burlington, 2005)
4. J. Han, M. Kamber, J. Pei, *Data Mining: Concepts and Techniques* (Elsevier, Burlington, 2011)
5. M. M. Campos, B. L. Milenova, *Creation and Deployment of Data Mining-Based Intrusion Detection Systems in Oracle Database 10g*. Proceedings of the 4th International Conference on Machine Learning and Applications. (2005)
6. S. Vinila Jinny, J. Jaya Kumari, *Neuralised Intrusion Detection System*. Proceedings of IEEE Conference on Signal Processing, Communication, Computing and Networking Technologies. (2011)
7. Barbara,D., Jajodia,S.: Applications Of Data Mining In Computer Security. (2002)
8. D. Anderson, T. Frivold, A. Valdes, Next-Generation Intrusion Detection Expert System (NIDES)—A Summary. SRI International. (1995)
9. D. Barbara, J. Couto, S. Jajodia, L. Popyack, N. Wu, *ADAM: Detecting Intrusions By Data Mining*. Proceeding 2nd Annual IEEE Workshop Information Assurance Security. (2001), pp. 11–16
10. Hu Weihua, Qi Jing, Du Yuge, Cheng Li, Wang Zhao, Cheng Li, Agent-based Network Intrusion Detection Expert system. Int. Rev. Comput. Softw. **4**, 1453–1457 (2012)
11. S. Vinila Jinny, J. Jaya Kumari, Comparative analysis of Intrusion Detection Systems with mining. Int. Rev. Comput. Softw. **8**(10), 2541–2544 (2013)
12. A. Bivens, M. Embrechts, C. Palagiri, R. Smith, B. Szymanski, *Network-Based Intrusion Detection Using Neural Networks*. Proceedings of Artificial Neural Network Engineering. (2002), pp. 527–535
13. W. Lee, S. Stolfo, K. Mok, Adaptive intrusion detection: a data mining approach. Artif. Intell. Rev. **14**, 533–567 (2000)
14. T. Abraham, IDDM: Intrusion Detection Using Data Mining Techniques. DSTO publications. (2008)
15. D. Forte, Log management for effective incident response. Netw. Secur. **2005**(9), 4–7 (2005)
16. B. Gupta, K. K. Nath, R. Kotagiri, *Conditional Random Fields For Intrusion Detection*. Proceeding 21st International Conference on Advanced Information Networking and Applications Workshop. (2007), pp. 203–208
17. W. Lee, S. Stolfo, M. Mok, *A Data Mining Framework for Building Intrusion Detection Model*. Proceedings of the IEEE Symposium on Security and Privacy. (1999), pp. 120–132

Effective Pattern Discovery and Dimensionality Reduction for Text Under Text Mining

T. Vijayakumar, R. Priya and C. Palanisamy

Abstract Huge data mining techniques have been used for mining useful pattern in text document. Text mining can be used to extract the data in document. It is effectively use and update the discovered pattern; still the research is not yet completed. The existing approach is term-based approach; they suffer the problem of polysemy and synonymy. In the past years, people have used pattern-based approaches for hypothesis, which perform better than the term-based ones, but many of the experiments do not support this hypothesis. This paper presents a new idea about the effective pattern discovery technique which involved the processes of pattern deploying and pattern evolving, to improve the effectiveness of using and updating discovered patterns for finding relevant and useful information.

Keywords Text mining · Polysemy · RefixSpan · FP-tree · SPADE · SLPmine · GST

1 Introduction

Due to the high range of data available in past few years, the data mining techniques are used for extracting useful information and knowledge. For example, in market analysis and business management, it is used to extract large amount of data. The

T. Vijayakumar (✉) · R. Priya · C. Palanisamy
Department of Information Technology, Bannari Amman Institute of Technology, Sathyamangalam, Erode, Tamil Nadu, India
e-mail: vijayakumart@bitsathy.ac.in

R. Priya
e-mail: priyar.se12@bitsathy.ac.in

C. Palanisamy
e-mail: cpalanisamy@bitsathy.ac.in

© Springer India 2015

L.P. Suresh et al. (eds.), *Artificial Intelligence and Evolutionary Algorithms in Engineering Systems*, Advances in Intelligent Systems and Computing 325,
DOI 10.1007/978-81-322-2135-7_65

data mining techniques available to perform effective pattern mining and text mining are the following: the association rule mining, the frequent item set mining, the sequential pattern mining, the maximum pattern mining, and the closed pattern mining. The data mining techniques used to find large number of pattern to find effectively use and update.

Text mining is used to extract information from the text document. It is used to find help the user want they want. First, information retrieval provided term-based method to solve probabilistic models and support vector machine (it is used to find filtering the data model). The advantages of term-based method are to find efficient computational problem and term weight. But the term-based method suffer the problem of polysemy (the word has multiple meanings, e.g., machine) and synonymy (multiple words having the same meaning, e.g., object).

In the past years, people have used pattern-based approaches for hypothesis, which perform better than the term-based ones, but many of the experiments do not support this hypothesis. They have less ambiguous and more discriminative problem. They include the performance like (1) inferior statistical properties to terms, (2) low frequency of occurrence, and (3) numbers of redundant and noisy phrases among them.

In the sequence, mining used to discover set of attributes from the large database. For example, bookstore it is used to find frequent number of occurrence of item. The pattern-based approach includes two fundamental issues: low frequency and misinterpretation problem. It overcomes the problem of association rule mining (e.g., support and confidence).

2 Related Work

This work is based on the term frequency (tf) and inverse document frequency (df), and the weighting scheme is used for text representation, and they improve the performance of the data. The data mining techniques are used to analyze the data and extract the information from the document collection.

The pattern mining technique has been used in a variety of algorithm such as Apriori-like algorithms; PrefixSpan, FP-tree, SPADE, SLPMine, and GST. These research works have mainly focused on developing efficient mining algorithms for discovering patterns from a large data collection.

Information filtering is used for relevant and irrelevant document in the text classification. The techniques include association rule mining, frequent item set mining, sequential pattern mining, maximum pattern mining, and closed pattern mining. The data mining techniques used to find large number of pattern to find effectively use and update.

3 Modules in Pattern Discovery

3.1 Dataset Collection and Tokenizing

The first step is extraction of data from the given dataset. The sentence which contains set of text will be extracted for the analysis. Identifying data and splitting into terms is the major process.

The document with all kind of words and symbols are given as the input to the system. This document is then sent for the text mining process. This is here done for the segregation of the important words from the document. This process has been carried out by selecting each important word and removing the unwanted word and by replacing the tabs and the other non-text characters by a single space Fig. 1.

3.2 Text Preprocessing

Many of the most frequently used words in English are useless in information retrieval (IR) and text mining. These words are called 'stop words.' The stop words are used to extract the words in the document. The frequent word does not carry any information. The unwanted words are removed to create a new dataset.

Text preprocessing includes word disambiguation. Each word or phrase will have its ambiguity in their meanings. This problem of ambiguity could be resolved using this text preprocessing. Stemming process is to reduce the normalization of document. For example, the stemming algorithm takes the acceptable data of walk are walk, walking, and walked Fig. 2.

3.3 Term Selection Model

To decrease the number of words that should be used in the document is done by indexing or keyword selection algorithms. In this paper, the documents are described; these documents are described by using the selected keyword. Based on the calculated entropy value, the keywords are extracted from the document.

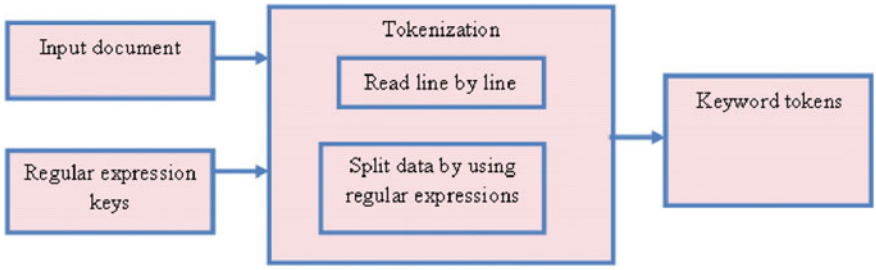

Fig. 1 Dataset collection and tokenization

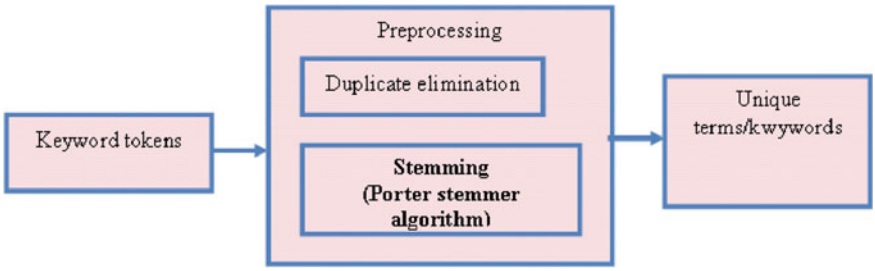

Fig. 2 Text preprocessing

Document indexing is a three-step process:

Input: sentence or document Q
Output: Pattern Pn
Matched string S
Steps:

1. Split the doc Q into number of pattern P
2. Set of patterns given, P1, P2, …, Pn,
3. Give input document text T
4. Find all occurrences of P in a text T = b1b2…bm.
5. do
6. if (text letter == pattern letter)
7. compare next letter of pattern to next
8. letter of text
9. else
10. move pattern down text by one letter
11. while (entire pattern found or end of text)
12. end

3.4 Frequent Pattern Analysis

This module helps to make the frequent pattern count, and text snippets values combine to make the final values. The matching is totally based on the correlation between the words. This process is invisible; this automatically occurs while the extraction happens.

3.5 Sequence Analysis

A sequential pattern analysis module is used to frequent pattern if its relative support (or absolute support)_min sup, a minimum support. Here, minimum

support and confidence will be calculated. The property of closed patterns can be used to define closed sequential patterns. A frequent sequential pattern will be analyzed by the identification of closed pattern and support and confidence of every data.

3.6 Pattern Evaluation and Reports

After the clustering and sequence identification of dataset, the system will apply priority measure for accurate pattern. It also consists of the filtering process called ranking based on the sequence as well as frequency. This module analyses the existing clustered group and also extracts data from semantic library.

4 Text Mining Using Dimensionality Reduction for Text

The text-based data can be represented as the vector; it can be used to search the closest document. The document in the database has number of terms T and the number of document D so the dimensionality problem is inefficient to compute. The resulting document size is $T * D$. The document term will be relationship between the synonymy and polysemy.

4.1 Latent Semantic Indexing

The latent semantic indexing is the retrieval method that is used as the mathematical technique called the singular value decomposition. The SVD identifies the relationship between the terms and concept of the unstructured collection of data in text document. The latent semantic indexing algorithm is used for the dimensionality reduction. This algorithm is based on the singular value decomposition (SVD). By using SVD, the rank of the term document X is r. The SVD follows

$$X = U\Sigma V^{\mathrm{T}}$$

Here, U is called the left singular vector and it also a unitary matrix.

Σ is the diagonal matrix; it represents $(\sigma_1 \ldots \sigma_r)$ value of X; the X is called document.

V is called the right singular vector and V^{T} the conjugate transpose of unitary matrix V.

U has the set of vector, the first K vector to use the transformation matrix to put original document at the space. The eigenvector is used for the transpose matrix.

The LSI is used to extract the representative features, and it has to classify the document, and at same time, it reduces reconstruction error.

Let **a** be the transformation vector. The objective function of LSI can be as follows:

$$a_{\text{opt}} = \arg\min_{a} \left\| \left(X - aa^{\text{T}}X\right)^2 \right\| = \arg\max_{a} a^{\text{T}}XX^{\text{T}}a,$$

with the constraint,

$$a^{\text{T}}a = 1$$

Since XX^{T} is symmetric, the basis functions of LSI are orthogonal.

4.2 Locality Preserving Indexing

The document space generally has high dimension and clustering of the document. So it is infeasible due to the dimensionality. By using the locality preserving indexing the related to identify the semantics information.

Compared to LSI, the locality preserving indexing overcomes the problem. The LPI extracts the different features. They have the locality information (the two documents are close together in the original document at the space so reduce the dimensionality reduction).

In LPI, first construct the similarity matrix $S\varepsilon R^{n*n}$ that represents the similarity between the numbers of data in the document. In the similarity matrix, each element measure between the two data of points.

The transformation vector of LPI can be obtained by solving the following minimization problem.

$$a_{\text{opt}} = \arg\min_{a} \sum_{i,j} \left(a^{\text{T}}x_i - a^{\text{T}}x_j\right)^2 S_{ij} = \arg\min_{a} a^{\text{T}}XLX^{\text{T}}a,$$

with the constraint,

$$a^{\text{T}}XDX^{\text{T}}a = 1$$

$a^{\text{T}}XDX^{\text{T}}a = 1$ to find measure between the local density.

The distance matrix represents the distance between the sets of point. The matrix will have the N *N size of the matrix. The distance matrix of N is the data points, node, and vertices.

4.3 Probabilistic Latent Semantic Indexing

The probabilistic latent semantic analysis is used for the information retrieval in the document. The probabilistic latent semantic analysis is similar to the LSI. It is based on the dimensionality reduction between the probability mixture models. They have the set of common data in the document collection. The document has the mixture model of data component.

To calculate the weight of the documents and represent the latent semantic dimensions, they have the $(d_1, d_2 \ldots d_n)$ n is the set of document collection. The mixture model represents

$$pd_i(w) = \sum_{j=1}^{K} \left[\pi d_i j p\left(w|\theta_j\right)\right]$$

Here, $\pi d_i j$ is the document specify index and weight also be calculated. The log-likelihood of the collection C is

$$\log p(\mathrm{C}|\Delta) = \sum_{i=n}^{n} \sum_{w \in v} \left[c\left(w, d_j\right) \log \left(\sum_{j=1}^{k} \left(\pi d_i j p\left(w|\theta_j\right)\right) \right) \right]$$

where V is the set of all the words

$\mathrm{C}(w, d_i)$ is the count of word w in document d_i

The likelihood of the document collection to be used, to set a parameter value, is equal to outcome of other parameter value. They mathematically used the support function of the data. They have set of word in the document and count the word and set model parameter.

The mixture model is used in the expectation maximization algorithm and to compute the likelihood of the function. Iterative method is a mathematical representation of sequence improving the class problem.

The statistical model represents the relationship between the one or more random variables related to other random variable. So it is in the form of mathematical equation.

5 Experimental Results

The support vector machines used to filter the positive and negative document. The documents are evaluated by the threshold value. Threshold $(\mathrm{DP}) = \min_{p \in DP} \left(\sum_{(t,w) \in \beta(p)} \mathrm{support}(t) \right)$ in these formula to remove the noisy negative document in the result Fig. 3.

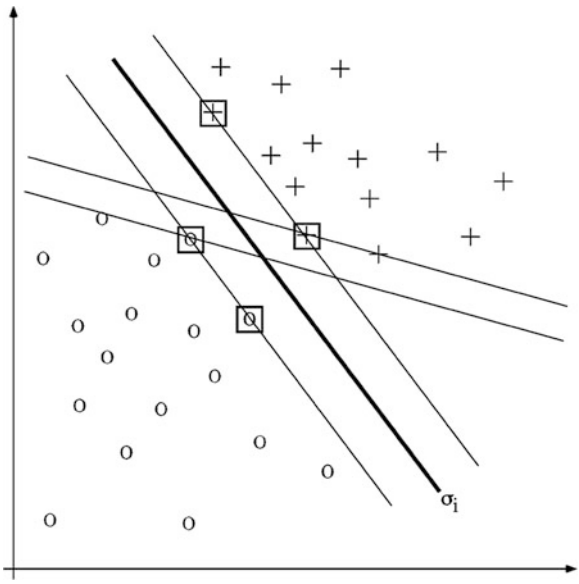

Fig. 3 Positive and negative classifiers

The support vector is used to classify the document. The positive and negative training examples are here represented by the small circles and crosses.

The result is based on precision and recall to evaluate the document. First the document loaded in the database and each document are split into paragraph to remove the unwanted word and noise in the document.

The following figure describes about the average value taken to evaluate the graph Fig. 4.

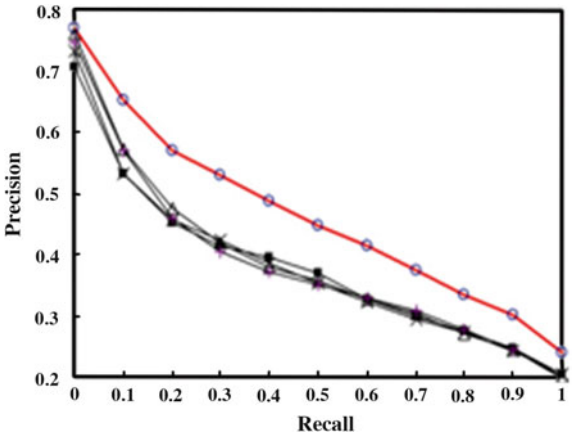

Fig. 4 The graph shows the precision and recall of the relevant and irrelevant document

6 Conclusion

The knowledge discovery model has been proposed to overcome the problem of low frequency and misinterpretation problems for text mining. The data mining techniques includes association rule mining, frequent item set mining, sequential pattern mining, maximum pattern mining, and closed pattern mining. In this work, the problem of the low frequency and misinterpretation problem of text mining have been overcome.

References

1. N. Zhong, Y. Li, S. T. Wu, Effective Pattern Discovery for Text Mining. 24 (2012)
2. K. Aas, Text categorisation: a survey. J. Mach. Learn. Res. **3**, 1289–1305 (1999)
3. N. Cancedda, N. Cesa-Bianchi, A. Conconi, C. Gentile, Kernel Methods for Document Filtering. *TREC. (2002)*
4. J. Han, J. Pei, Y. Yin, Y, Mining Frequent Patterns without Candidate Generation, in. *Proceedings ACM SIGMOD Intl Conference Management of Data (SIGMOD 2000).* (2000), pp. 1–12
5. Y. Huang, S. Lin, Mining Sequential Patterns Using Graph Search Techniques, in *Proceedings 27th Ann. Intl Computer Software and Applications Conference (2003)*, pp. 4–9
6. N. Jindal, B. Liu, Identifying Comparative Sentences in Text Documents, in *Proceedings 29th Ann. Intl ACM SIGIR Conf. Research and Development in Information Retrieval (SIGIR 2006).* (2006), pp. 244–251
7. Y. Li, X. Zhou, P. Bruza, Y. Xu, R. Y. Lau, *A* Two-Stage Text Mining Model for Information Filtering, in *Proceedings ACM 17th Conference Information and Knowledge Management (CIKM 2008).* (2008), pp. 1023–1032
8. G. Salton, C. Buckley, Term-weighting approaches in automatic text retrieval. Inf. Process. Manage. Intl. J. **24**(5), 513–523 (1988)
9. M. Sassano, Virtual Examples for Text Classification with Support Vector Machines, in *Proceedings Conference Empirical Methods in Natural Language Processing (EMNLP 2003)* (2003), pp. 208–215
10. F. Sebastiani, Machine Learning in Automated Text Categorization. ACM Comput. Surv. **34** (1), 1–47 (2002)

A Cross-Layer Analysis for Providing Mobility in Wireless Body Area Networks

R. Venkateswari, S. SubhaRani, V. Sudharshan and R. Umadharshini

Abstract A wireless body area network consists of a network of implanted and wearable sensor nodes to transmit the biological information for wireless healthcare monitoring, elderly care, and many other innovative applications. To support mobility in these resource-constrained networks, suitable modifications have to be performed both at the medium access control and routing layers. Low-duty-cycle MAC protocols that avoid energy problems in the MAC Layer have been taken, and the performance with the RPL routing protocol has been evaluated. RPL is routing protocol proposed by IETF ROLL working group for low-power and lossy networks. In this paper, the performance of XMAC and ContikiMAC is analyzed with respect to RPL parameters and the results show that ContikiMAC consumes 49 % less power compared to XMAC.

Keywords WBAN · ContikiMAC · XMAC · RPL · Mobility

1 Introduction

The wireless body area network has undergone a technical boom in the last decade. The network of nodes formed in the human body for the purpose of wireless monitoring of the patient's health condition is WBAN. This is an advanced

R. Venkateswari (✉) · S. SubhaRani · V. Sudharshan · R. Umadharshini
Department of Electronics and Communication Engineering, PSG College of Technology, Coimbatore, India
e-mail: r_venkateswari@yahoo.com

S. SubhaRani
e-mail: rvi@ece.psgtech.ac.in

V. Sudharshan
e-mail: babu_ece@ymail.com

R. Umadharshini
e-mail: uma.mit51@gmail.com

© Springer India 2015

L.P. Suresh et al. (eds.), *Artificial Intelligence and Evolutionary Algorithms in Engineering Systems*, Advances in Intelligent Systems and Computing 325,
DOI 10.1007/978-81-322-2135-7_66

healthcare technology, which provides a better human–computer interaction [1]. For a given deteriorated channel condition and moving human body, the sensor nodes are considered mobile at the MAC point of view. Hence, the mobility models related to human walks were considered in [2]. The WBAN network topology changes even for a change in posture as well as movement within a certain type of posture. A configurable mobility model MoBAN implements these two topology changes [3]. A group mobility model that considers the interaction between the soccer players was used to generate realistic mobility patterns [4] by modifying the Reference Point Group Mobility Model according to the player movement.

In order to support mobility, MAC protocols such as MMAC [5], MS-MAC [7], and AM-MAC [7] were proposed in the literature. Offline analysis of sensor networks was studied in Zebranet [8] for delay tolerant networks. A MAC layer proposed for micromobility environments to provide highly reliable and energy efficient communication is called MobiSense [9] which was proposed for the tracking and monitoring of human beings, animals, or objects. Many works have been done to support mobility in the MAC Layer. But cross-layer optimization is required to provide mobility. A network of low-power sensor nodes in vehicles which makes use of routing protocol for LLN in a VANET was analyzed in [10]. In [10], to support high mobility due to the vehicle movement, modifications had been done in the RPL protocol parameters. In [11], a performance analysis of RPL protocol is done with stationary nodes. The performance of XMAC and Contiki-MAC with different interpacket delays and transmission power [12] had been studied in [12]. In this paper, the performance of ContikiMAC and XMAC in mobile WBAN is analyzed by changing the RPL parameters, namely DODAG Information Object (DIO) doubling and channel check rate. The performance metrics used are energy consumption and packet delivery ratio.

The paper has been organized as follows: Sect. 2 describes the existing MAC protocols. Section 3 explains the mobility model used in this paper. Section 4 gives an idea about RPL routing protocol and its parameters. The results are discussed in Sect. 5. Section 6 concludes our paper.

2 MAC Protocol

X-MAC [14] is an asynchronous preamble sampling protocol based on the low-power listening mechanism, in which the nodes decide their schedule independently from their neighbors. All neighbors will turn into the receiving mode, while the message might only target one of them. X-MAC is specially designed to increase throughput and reduce excessive preambles. Nodes using X-MAC protocol is not permitted to send a packet until knowing that there is another node awake and ready to receive the packet. This is accomplished through the use of strobes which are essentially just short preambles. A sender will start sending strobes repeatedly until it receives an acknowledgment from another node.

In ContikiMAC [13], when a node wants to send a packet, it begins transmitting that packet, repeatedly until it receives an acknowledgment from the receiver node. ContikiMAC [15] uses periodic walk-ups to listen to the radio medium for transmissions. In fast-sleep mechanism, the receiver is kept on if a transmission is detected; otherwise, the node goes to sleep mode. The ContikiMAC protocol records the time of packet transmission and the time when a link layer acknowledgment is received. This time is used as an approximation of the wake-up phase of the neighbors. This mechanism reduces the congestion in the radio channel.

3 Mobility

The mobility model plays an important role in the performance evaluation of protocols in wireless networks with node mobility. There are different types of mobility models based on dependencies and restrictions. The nodes in WBAN would move along with human being. The various nodes deployed in the human body move as a group when the human moves; hence, group mobility is most suitable for body area networks. The Reference Point Group Mobility Model (RPGM) mobility model [16] is used for simulating mobility in wireless body area networks. The nodes present in the patient forms a group. The group contains a number of member nodes and one group leader, that determine the group's motion behavior, including location, speed, and acceleration. The nodes in a group are randomly placed around the reference point or group leader.

4 RPL Routing Protocol

RPL is an IPV6 routing protocol for low-power and lossy networks proposed by the IETF ROLL working group [17]. It is a distance vector and a source-initiated routing protocol. The sensor devices in WBAN are highly resource-constrained as they are either wearable or implanted inside the human body. Hence, RPL is a prominent candidate for WBAN. RPL relies on the topological conception of directed acyclic graphs (DAG) [18]. RPL organizes nodes as destination-oriented DAGs (DODAG), in which the routing metric is based on the objective function [19]. For the purpose of maintenance of network topology and routing table, RPL uses 3 management packets referred to as DIO, DODAG Solicitation Object (DIS) and DODAG Destination Advertisement Object (DAO). The sending of RPL messages is ruled by trickle timers whose minimum value is $I_{\min}$ and maximum value is $I_{\max}$. Once inconsistencies are detected within the network, a lot of RPL messages are sent, usually and because the network stabilizes RPL messages are sent less usually [17]. The value of trickle timer starts from the lowest possible value $I_{\min}$ and is doubled each time it is transmitted until it reaches its maximum possible value of $I_{\max}$. The parameters for trickle timer configuration embrace DIO_Interval_Doubling, DIO_Interval_Minimum and DIO_Redundancy_Constant.

$$I_{\min} = 2^{\text{RPL_DIO_INTERVAL_MIN}}. \quad (1)$$

The number of times $I_{\min}$ can be doubled is controlled by $I_{\max}$ which is given by

$$I_{\max} = I_{\min} * 2^{\text{RPL_DIO_INTERVAL_DOUBLINGS}}. \quad (2)$$

So the smallest potential interval between two sequent DIOs is DIO Minimum Interval that doubles each time it is sent till it reaches a most worth by DIO_Interval_Doubling. DIO_Interval_Minimum affects the rate at which DIO is transmitted and hence influences energy consumption, convergence time, control traffic overhead, etc. DIO_Redundancy_Constant has a value greater than 0 and is used to suppress the DIO transmission.

The parameter channel check rate in radio duty cycling specifies the number of channel checks per second. The network convergence time is inversely proportional to the channel check rate. To investigate the performance of RPL under mobility, the number of DIO control messages should be modified. This is accomplished by modifying the configuration parameters of trickle timer. The protocol parameters influencing the efficiency, DIO_Interval_Doublings, and radio duty cycling interval with XMAC and ContikiMAC are analyzed in this paper.

5 Results and Discussion

The simulation has been performed by using the Cooja simulator in the Contiki real-time operating system (RTOS). This enables the algorithms to be easily ported to any sensor node with the MSP430 Microcontroller such as telosB and shimmer. The specifications for the system under consideration are given in Table 1.

Table 1 System specifications

Parameter	Value
Area	100 × 100
Number of sender nodes	30
Number of sink nodes	1
Position of sender nodes	Random positioning
Position of sink node	Fixed at 50, 50 to provide maximum coverage
Mobility model used	RPGM
Transmission ratio	100 %
Transmission range	50 m
Interference range	55 m

Table 2 Comparison of XMAC and ContikiMAC based on DIO doublings

DIO_Interval Doubling	Received packet		Lost packet		Packet delivery ratio	
	XMAC	ContikiMAC	XMAC	ContikiMAC	XMAC	ContikiMAC
4	78.200	134.25	108.15	40.350	0.4196	0.7689
5	73.000	134.25	98.900	40.350	0.4246	0.7689
6	71.850	134.25	97.250	40.350	0.4240	0.7689
7	73.200	136.85	99.100	40.400	0.4248	0.7720
8	72.600	136.85	98.150	40.400	0.4251	0.7720
9	73.050	136.85	99.050	40.400	0.4244	0.7720
10	78.700	136.85	111.80	40.400	0.4099	0.7720
11	73.200	134.40	99.100	40.400	0.4248	0.7688
12	72.000	134.40	97.500	40.400	0.4247	0.7688
13	73.000	134.25	98.900	40.350	0.4246	0.7689
14	74.150	133.55	100.45	40.350	0.4246	0.7676
15	73.000	133.55	98.900	40.350	0.4246	0.7676
16	73.050	135.80	99.050	40.400	0.4244	0.7707

The reference point group mobility induces frequent topology changes. Hence, the default values of the RPL routing protocols have to be enhanced with respect to the application scenario. The channel check rate has to be increased to provide support for mobility in the considered application. The effects of DIO_Interval_Doubling and channel check rate on average power consumption and packet delivery ratio are analyzed with XMAC and ContikiMAC protocols.

The comparison of XMAC versus ContikiMAC based on DIO_Interval_Doubling is given in Table 2. From the table, it can be seen that the packet received is not varied with respect to changes in the DIO_Interval_Doubling. This is because the network gets converged before reaching the minimum $I_{\max}$ value. Consider DIO_Interval_Doubling = 4 in (2),

$$I_{\max} = I_{\min} * 2^{\text{DIO_INTERVAL_DOUBLING}} = 4.096 * 2^4 = 64\,\text{s}$$

The network gets converged before 64 s for all values of DIO doubling, and hence, it has no effect on the performance metrics. But the performance varies with the MAC Protocol. The packet delivery ratio for ContikiMAC is 83 % higher than that of the XMAC protocol.

The effect of DIO_Interval_Doubling on power consumption is given in Fig. 1. The power consumption in ContikiMAC is 43 % lesser than the power consumption in XMAC. The fast-sleep and phase-lock mechanism in ContikiMAC aids to reduce the power consumption compared to XMAC protocol. The effect of channel check rate on average power consumption has been shown for both ContikiMAC and XMAC protocol in Fig. 2. It can be seen that when the check rate is 32 Hz, ContikiMAC consumes 49 % less power than XMAC. This is because, even though ContikiMAC wakes up its motes frequently, it can conserve more energy by being able to promptly power them off again.

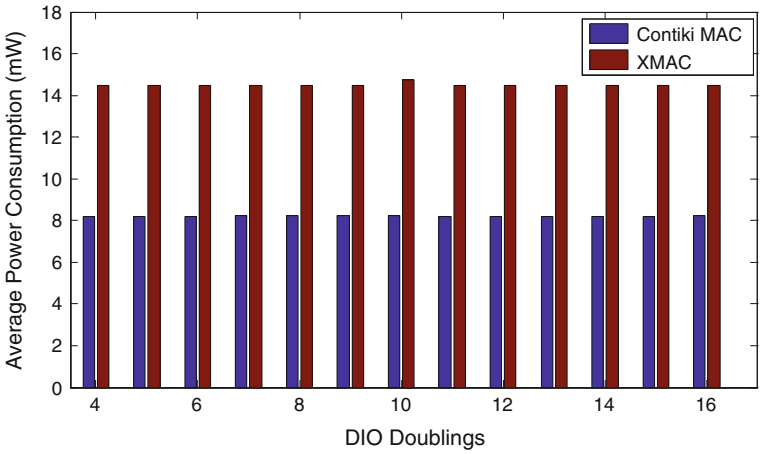

Fig. 1 Effect of DIO_Interval_Doubling on power consumption

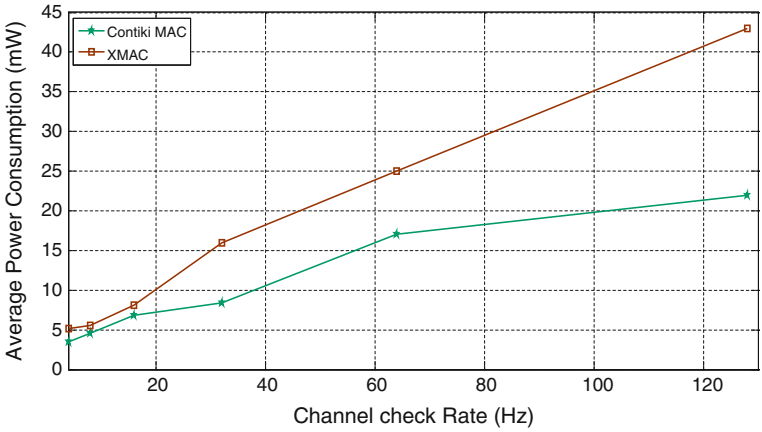

Fig. 2 Comparison of XMAC and ConikiMAC based on channel check rate

To support mobility in WBAN using RPL protocol, the modifications done in DIO_Interval_Doubling and channel check rate alter the energy efficiency and packet delivery ratio and thus the performance of the network. The results show that ContikiMAC has lower power consumption and packet loss compared to XMAC in a mobile WBAN environment.

6 Conclusion

In this paper, the performance of XMAC and ContikiMAC protocol for mobile wireless body area networks has been compared based on power consumption and packet delivery ratio. For modeling the human mobility in the hospital environment, the RPGM mobility model has been used. The performance of the network for different values of RPL parameters such as DIO doublings and channel check rate has been analyzed. The results show that ContikiMAC provides significantly decreased packet loss and power consumption than XMAC. In the future, the parameters of RPL control messages will have to be optimized and the algorithms will be implemented in Mote-like hardware for real-time monitoring of biosignals.

Acknowledgments This research was supported by the University Grants Commission, New Delhi, under the Major Research Project scheme (2011).

References

1. H. Cao, V. Leung, C. Chow, H. Chan, Enabling technologies for wireless body area networks: a survey and outlook. IEEE Trans. Commun. **47**, 84–93 (2009)
2. B. Bream, C. Blondia, Supporting mobility in wireless body area networks: an analysis, in *18th IEEE Symposium on Communications and Vehicular Technology* (2011), pp. 1–6
3. M. Nabi, M. Geilen, T. Basten, MoBAN: A configurable mobility model for wireless body area networks, in *Proceedings of the International Conference on Simulation Tools and Techniques* (2011), pp. 168–177
4. L. De Nardis, D. Domenicali, M.-G. Di Benedetto, Mobility model for body area networks of soccer players, in *IEEE Wireless Technology conference* (2010), pp. 65–68
5. M. Ali, T. Suleman, Z.A. Uzmi, MMAC: a mobility-adaptive, collision free MAC protocol for wireless sensor networks, in *24th International IEEE Conference on Performance, Computing and communications* (2005), pp. 401–407
6. D. Zhang, Q. Li, X. Zhang, X. Wang, De-ass: an adaptive mac algorithm based on mobility evaluation for wireless sensor networks, in *6th International Conference on Wireless Communications Networking and Mobile Computing* (2010), pp. 1–5
7. S.C. Choi et al., An adaptive mobility-supporting MAC protocol for mobile sensor networks, in IEEE Vehicular Technology Conference (2008), pp. 168–172
8. T. Liu, C.M. Sadler, P. Zhang, M. Margaret, Implementing software on resource-constrained mobile sensors: experiences with Impala and ZebraNet, in *Proceedings of Mobile Systems, Applications and Services* (2004), pp. 256–269
9. A. Gonga, O. Landsiedel, M. Johansson, MobiSense: power- efficient micro-mobility in wireless sensor networks, in IEEE International Conference on Distributed Computing in Sensor Systems and Workshops (2011), pp. 1–8
10. K.C. Lee, R. Sudhaakar, J. Ning, L. Dai, S. Addepalli, J.P. Vasseur, M. Gerla, A comprehensive evaluation of RPL under mobility. Int. J. Veh. Technol. **2012**, 10, Article ID: 904308 (2012). http://dx.doi.org/10.1155/2012/904308
11. H. Ali, A Performance Evaluation of RPL in Contiki, M.S. thesis, Blekinge Institute of Technology (2012)
12. M.R. Khan, Performance and route stability analysis of RPL protocol, M.S. thesis, KTH Electrical Engineering (2012)

13. M. Buettner, G.V. Yee, E. Anderson, R. Han, X-MAC: a short preamble mac protocol for duty-cycled wireless sensor networks, in *International Conference on Sensor Systems* (2006), pp. 307–320
14. J.G. Ko, N. Tsiftes, A. Terzis, A. Dunkels, Pragmatic low-power interoperability: ContikiMAC vs TinyOS LPL, in *9th Annual IEEE Communications Society Conference on Sensor, Mesh and Adhoc Communications and Networks* (2012), pp. 94–96
15. A. Dunkels, The ContikiMAC radio duty cycling protocol. Technical Report T2011:13. Swedish Institute of Computer Science (2011)
16. X. Hong, M. Gerla, G. Pei, C.-C. Chiang, A group mobility model for Ad-Hoc wireless networks, in *MSWiM'99 Proceedings of Modeling, Analysis and Simulation of Wireless and Mobile Systems* (1999), pp. 53–60
17. J.-P. Vasseur, A. Dunkels, *Interconnecting Smart Objects with IP—The Next Internet* (Morgan Kaufmann Publishers, San Francisco, 2010)
18. O. Gaddour, A. Kouba, RPL in a nutshell: a survey. Comput. Netw. **56,** 3163–3178 (2012)
19. Y. Chen, J.P. Chanet, K.M. Hou, RPL routing protocol a case study: precision agriculture. First China-France Workshop on Future Computing Technology (2012)

Multiview Clustering in Heterogeneous Environment

A. Bharathi and S. Anitha

Abstract Integrating multiview cluster is a crucial issue in heterogeneous environment. In multiview clustering, objects from the multiple sources can be limited up to homogeneous environment by sharing the same dimensions. In this paper, novel-based tensor methods are used. They are (1) multiview clustering based on the integration of the Frobenius-norm objective function (MC-FR-OI) and (2) matrix integration in the Frobenius-norm objective function (MC-FR-MI). These frameworks worked by using tensor decomposition. Experimental results demonstrate that proposed methods are effective in multiview data integration. Here, higher-order data are used. The performance by using higher-order data is better when compared with the two-dimensional data.

Keywords Integrating multiview cluster · Frobenius-norm objective function · Spectral clustering · *k*-means · SVD · HOSVD

1 Introduction

Datasets consists of multiple similarities. For a group of people, we might know their height, weight, age, education, location, designation, and their family related. For a set of authors, they have their own papers, citations, and methods. For a set of drives, they have own files, documents, locations, and their contents. Our approach is to cluster people, researchers, methods, or files, to treat all the similarities concurrently.

In a set of multiple networks, they share same set of nodes but possess different types of connection between nodes. Multiple relationship can be formed through

A. Bharathi (✉) · S. Anitha
Department of Information Technology, Sathyamangalam, Erode, Tamil Nadu, India
e-mail: bharathia@bitsathy.ac.in

S. Anitha
e-mail: anithas.se12@bitsathy.ac.in

© Springer India 2015

L.P. Suresh et al. (eds.), *Artificial Intelligence and Evolutionary Algorithms in Engineering Systems*, Advances in Intelligent Systems and Computing 325,
DOI 10.1007/978-81-322-2135-7_67

individual activity is called as multiview learning [1]. The recent development in clustering is the spectral clustering. Spectral clustering is based on the Ncut algorithm [2]. This can work well in the single-view data as it is based on matrix decompositions. Many clustering algorithms have been proposed in comparison with the single-view data. Therefore, these algorithms have some limitation; tensor decomposition is used to cluster all the similarity matrices into set of compilation feature vector. Many clustering algorithms such as *k*-means, SVD, and HOSVD [3] are used for many tensor methods. Spectral clustering [2] is used for clustering the similarity matrices based on tensor methods.

2 Related Work

2.1 Multiview Clustering

A multiview clustering method that extends k-means and hierarchical clustering to deal with data as two conditionally independent views [4]. Canonical correlation analysis in multiview clustering assumes that the views are uncorrelated in the given cluster label. These algorithms can concentrate only on two-view data. Long et al. formulated a multiview spectral clustering method while investigating multiple spectral dimension reduction.

2.2 Spectral Clustering

Spectral clustering was derived based on relaxation of the Ncut formulation for clustering. Spectral clustering involves a matrix trace optimization problem [5]. In this paper, we proposed that the spectral clustering formalism can be extended to deal with multiview problems based on tensor computations.

Given a set of N data points $\{X_i\}$ where $X_i \in \mathrm{IR}^d$ is the ith data point, a similarity s_{ij} can be defined for each pair of data points x_i and x_j based on some similarity measures. An intuitive way for representing the dataset by using a graph $G = (V, E)$ in which the vertices V represent the data points and the edges characterize the similarity between data points which are quantified by s_{ij}, the similarity measure of the graph is symmetric and undirected. The matrix of the graph G is the matrix S with entry in row i and column j equal to s_{ij}. The degree of the vertex can be written as

$$d_i = \sum_{j=1}^{N} s_{ij} \tag{1}$$

where v_i is connected with the sum of all weight of the edges. The degree of the matrix D is a diagonal matrix containing the vertex degrees from $d_1 \ldots d_N$. As the

diagonal, it follows from the spectral formalism of embedding the Laplacian matrix that can be defined as $L = D - S$, and Ncut is defined by corresponding to the normalized Laplacian matrix

$$L_{\text{Ncut}} = D^{-1/2} L D^{-1/2} = I - S_N \tag{2}$$

where S_N and L_{Ncut} are the normalized similarity eigenvector and their eigenvalues.

2.3 Multiview Spectral Clustering

In integration of multiview data in spectral clustering, there are two different strategies.

2.3.1 Multiview Clustering by Trace Maximization (MC-TR-I)

Different views can be added to the objective function. The function can be as follows:

$$\begin{gathered} \max_U \sum_{K=1}^{K} \text{trace}\left(U^T S_N^{(K)} U\right) = \left(U^T \left(\sum_{K=1}^{K} S_N^{(K)}\right) U\right), \\ U^T U = I, \end{gathered} \tag{3}$$

where $S_N^{(K)}$ a normalized matrix for kth value and U is the common factor shared by the views. This corresponds to the MKF with linear kernel. In alternative, weighted combination of objective functions, where the weights are learned from the data [6, 7]

$$\begin{aligned} &= \max_{U.W} \sum_{K=1}^{K} W_K \text{trace}\left(U^T S_N^{(K)} U\right) \\ &= \max_{U.W} \text{trace}\left(U^T \left(\sum_{K=1}^{K} W_K S_N^{(K)}\right) U\right), \\ &U^T U = 1, \quad W \geq 0 \quad \text{and} \quad \|W\|_F = 1. \end{aligned} \tag{4}$$

2.4 Tensor

Scalars, vectors, and matrices are facilitated by higher-order tensors. Scalars denote lower-case letters (A, B…). Vectors are written in italic capitals (*A, B*....) matrices

correspond to boldface capitals (A, B…), and tensors are written as casteller lettering (**A**, **B**…). This notation is consistently used for ordering lower parts of a given quantity such as a vector a, matrix **A**, and tensor *A,* correspondingly. The Kronecker product is denoted by ⊗. Vector is first order, matrix is a second order, and tensors are the third-order or the higher-order tensors.

3 Tensor Constructions

Multiview data can be constructed from by several methods. Here, tensor is constructed by stacking object by feature matrices derived from multiple views in a tensor. This is applicable only to the homogeneous data sources in which dimensions of the various features are same. In many multiview applications, it deals with the heterogeneous data sources with the various dimensions with feature spaces.

In this paper, construction of the independent data dimensions is made by integrating heterogeneous data sources. We can work with similarity tensor $A \varepsilon \mathrm{IR}^{N\times N\times N}$ in which the similarity matrices $S_N^{(1)}, S_N^{(2)}, S_N^{(3)} \ldots S_N^{(K)}$ are associated with different views. In similarity tensor, each similarity matrix view is computed in different space, so normalization is required, and so our method can be considered as normalization steps.

Figure 1 illustrates that the higher-order data can either be a four-dimensional data or an images. Then, the similarity matrix can be constructed for those higher-order data. The matrix can be unfolded, and the similarity tensor is constructed. Spectral analysis is made for the tensor which is constructed. Then, the final partition is made. Cluster label is formed.

From Fig. 2, the tensor can be unfolded into matrices. Then, the similarity matrix is calculated. The tensor can be constructed based on the below algorithm. Here, it is constructed using following algorithms.

3.1 MC-FR-OI

Algorithm: MC-FR-OI-MLSVD

Comment: M is the number of clusters
Step 1: Build a similarity tensor A
Step 2: Obtain the unfolding matrix $A_{(1)}$
Step 3: Compute U from the subspace spanned
By M dominant left singular vectors of $A_{(1)}$
Step 4: Normalize the rows of U to unit length
Step 5: Calculate the cluster with k-means on U
Return (clustering label)

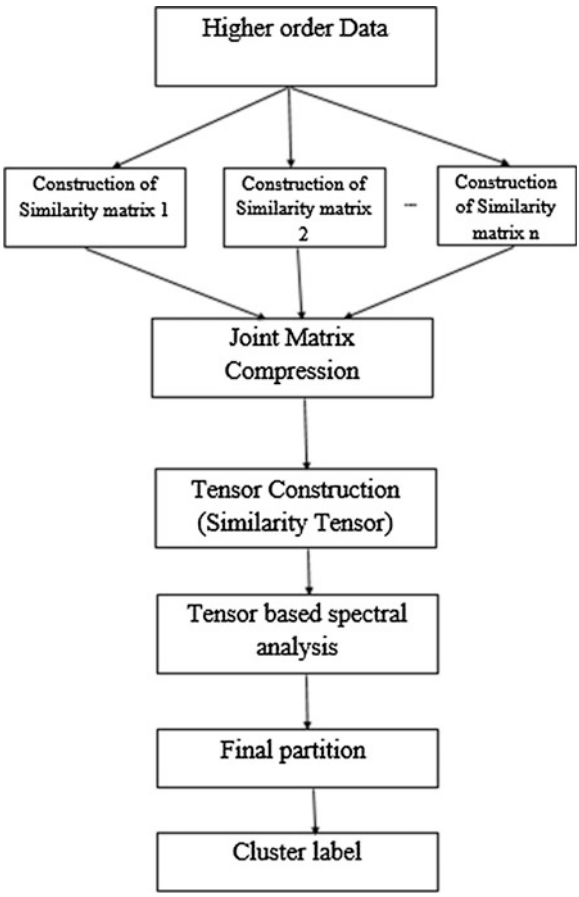

Fig. 1 Flowchart for multiview clustering for higher-order data

3.2 MC-FR-MI

The objective function is not affected by the sign of W, and all the weights can be nonnegative. The matrix U and the vector W yield the optimal subspace and the weights in different views.

Algorithm: MC-FR-MI-HOOI

Step 1: Build a similarity tensor A
Step 2: Obtain the unfolding matrices $A_{(1)}, A_{(2)}, A_{(3)}$
Step 3: Obtain an initial U_0, V_0 and W_0 by MLSVD
While (! convergence)
Do
{
Iteration Step 4.1. $A_{(1)}(V_1 \otimes W_i)$
Iteration Step 4.2. $A_{(2)}(W_1 \otimes U_{i+1})$

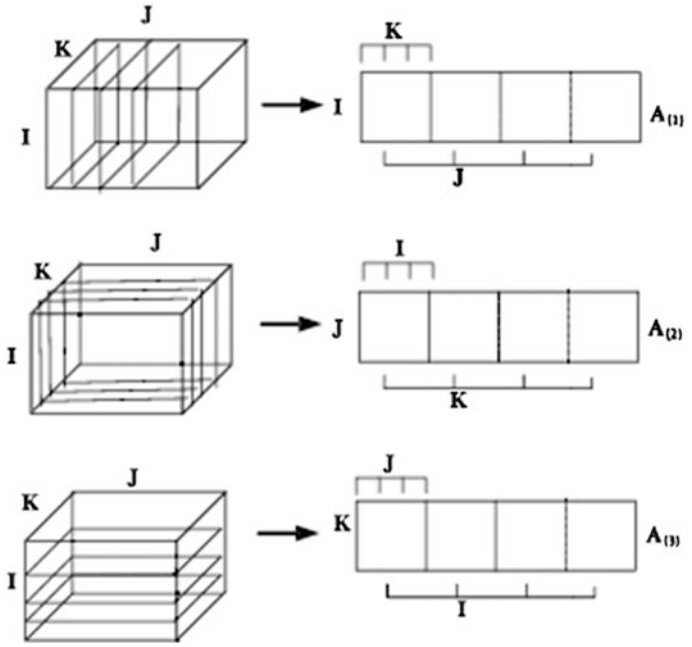

Fig. 2 Unfolding of tensor into matrices

Iteration Step 4.3. $A_{(3)}(U_1 \otimes V_{i+1})$
}
Comment i is the counter of iteration.
Step 5: Normalize the rows of U to unit length.
Step 6: Calculate the cluster with k-means on U
Return (clustering label)

The above three algorithms are used to construct tensor matrix by including all similarity matrices. Higher-order objective integration is used.

4 Higher-order Data

In existing system, 3D projection of a data points is used. The projection of a data points is represented as X–Y projection, Y–Z projection, and X–Z projection. The combinations of these three projections are the single-view dataset [2].

Direct combination of these three projections will not give the proper clustering. By using tensor, all the projections can be simultaneously combined and clustering can be done. The performance of the clustering is high when compared to others.

In proposed system, multiview clustering can be done by using ten-dimensional projections of a data points. Here, the microarray dataset of gene in the body is taken as the input.

In multiview clustering, it is proposed based on the SVD and PCA analysis. This framework can be extended using spectral clustering. By using tensor decomposition framework, both homogeneous and heterogeneous information can be integrated simultaneously to form clustering. First dataset can be given as an input. Then, ten-dimensional similarity matrix is formed.

The similarity matrix can be given as an input to the eigenvalue decomposition. It accepts square matrix alone as an input. The given square matrix can be ten-dimensional data. Then, the eigenvalue decomposition value can be determined. Then, values are normalized. Based on that value, weight matrix is calculated. Then, the normalization of the weight matrix is calculated.

The variables of the clusters can be given as an input, and then, the nearer clusters can be calculated based on the similarities. The clustering can be done and the final cluster labels are formed. This is an efficient method for handling the higher-order data. The data can be in any form they can be either image or the large amount of input.

5 Experimental Evaluation

We evaluated and compared with microarray dataset networks. This can be implemented in microarray dataset to increase the experimental power. The interaction probability is calculated for each group member. Based on the dimensions, interaction probability differs when we add one member of the group to the other group with low probability. Normalized mutual information (NMI) is used to measure the performance. NMI value is 1 when two clusters are exactly same. Normally, NMI values exist between 0 and 1.

Here, tensor decomposition with higher-order data is used to cover the hidden patterns and it also performs well, when compared with other two methods. For example, if we include some noises in the second dimension, the performance is reduced from 0.5 to 0.1. For this dimension, the pattern cannot be analyzed. By using tensor-based method, it achieves good performance. This method is more robust in noisy dimensions.

Here, the genes in single-dimensional community detection are low when compared with the multidimensional community. In multidimensional clustering, the performance of gene is higher when compared with the other maximization techniques. Single dimensions have the higher variance when compared with all multidimensional community.

In Fig. 3, first dimension consists of two clusters and second dimension consists of one cluster. The first two dimensions are based on single-view dimensional with low dimensionality. Therefore, the hidden patterns cannot be viewed properly. They

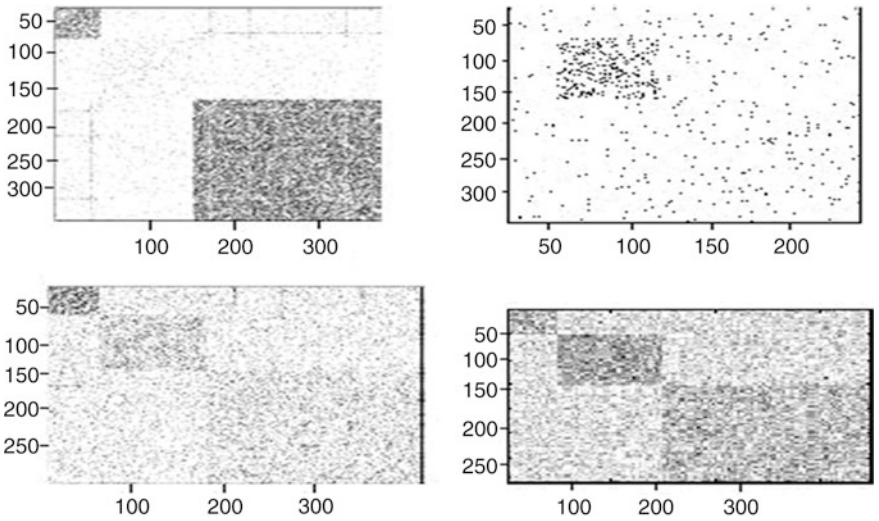

Fig. 3 Example of multidimensional network

are indicated with the low NMI. When comparing with the single-view clustering, hidden patterns can be shown clearly. The NMI value exists between 0 and 1.

We first evaluate and compare the different clustering strategies and applied to the multiview clustering. Here, clustering can be formed by the extension of the spectral clustering. Here, dataset consists of various types of gene which consist of more cluster members.

We can generate different view of interaction that is in each view; network shares the same vertices but has a different interaction pattern. The group members within the group can interact with the others random manner. The probability of interaction differs with respect to distinct views. Two vertices are connected randomly in low probability by adding some noise. The different views demonstrate the different interaction patterns in them.

The clustering evaluation for microarray dataset in multiview clustering is analyzed. In multiview clustering, hidden patterns can be clearly viewed when compared to the single-view clustering. Therefore, most of the multiview clustering results are better than the single-view clustering. Multiview clustering helps to reduce the noise and shows the shared cluster.

6 Results and Discussion

In multidimensional networks, hidden pattern can be viewed clearly when compared to the single-dimensional networks. Here, we have proposed the extension of spectral clustering by implementing the spectral clustering algorithm. By using this

algorithm, multidimensional networks can be included in heterogeneous environment. Tensor-based solutions are proposed for including multiple networks in the form of tensor.

Multiview clustering performance can be analyzed using many tensor-based strategies. Multiple similarities can be founded through many methods. In cluster ensemble method, single-view partition clusters can be integrated. So this is not efficient.

In LMF method, clustering performance gets lower at initialization and the partition cluster at the end are unstable. The optimization results also consume much time.

In tensor-based multiview clustering, spectral clustering can be extended by spectral clustering using higher-order data where multiple networks can be linked together. This method is more efficient when compared with other methods. NMI is used to measure the performance of the clustering.

References

1. L. Tang, X. Wang, H. Liu, Uncovering groups via heterogeneous interaction analysis
2. X. Liu, S. Ji, W. Glanzel, B. De Moor, Fellow, Multiview clustering via tensor methods. IEEE Trans. Know. Data Eng. **25**(5) (2013)
3. M. Ishteva, L.D. Lathauwer, P.-A. Absil, S.V. Huffel, Differential-geometric Newton algorithm for the best rank-(r1; r2; r3) approximation of tensors. Numer. Algorithms **51**(2), 179–194 (2009)
4. L. Tucker, The extension of factor analysis to three-dimensional matrices. Contrib. Math. Psychol. 109–127 (1964)
5. D. Zhou, C.J.C. Burges, Spectral clustering and transductive learning with multiple views, in *Proceedings of 24th International Conference Machine Learning* (2007), pp. 1159–1166
6. J.D. Carroll, J.J. Chang, Analysis of individual differences in multidimensional scaling via an n-way generalization of echart-young decomposition. Psychometricka **35**, 283–319 (1970)
7. K. Chaudhuri, S.M. Kakade, K. Livescu, K. Sridharan, Multi-view clustering via canonical correlation analysis, in *Proceedings of 26th Annals International Conferences Machine Learning* (*ICML'09*) (2009), pp. 129–136
8. H.G. Ayad, M.S. Kamel, Cumulative voting consensus method for partitions with variable number of clusters. IEEE Trans. Pattern Anal. Mach. Intell. **30**(1), 160–173 (2008)
9. T.M. Selee, T.G. Kolda, W.P. Kegelmeyer, J.D. Griffin, Extracting clusters from large datasets with multiple similarity measures using IMSCAND. Summer Proc. (2007)
10. S. Bickel, T. Scheffer, Multi-view clustering, in *Proceedings of IEEE Fourth International Conferences Data Mining* (*ICDM'04*) (2004), pp. 19–26
11. A. Cichocki, R. Zdunek, A.-H. Phan, S. Amari, *Nonnegative Matrix and Tensor Factorizations: Applications to Exploratory Multi-Way Data Analysis and Blind Source Separation* (Wiley, Hoboken, 2009)
12. L. De Lathauwer, B.D. Moor, J. Vandewalle, Multilinear singular value decomposition. SIAM J. Matrix Anal. Appl. **21**(4), 1253–1278 (2000)
13. L. De Lathauwer, B.D. Moor, J. Vandewalle, On the best rank-1 and rank approximation of higher-order tensors. SIAM J. Matrix Anal. Appl. **21**(4), 1324–1342 (2000)
14. A. Ng, M. Jordan, Y. Weiss, On spectral clustering: analysis and an algorithm. Adv. Neural Inf. Process. Syst. **2**, 849–856 (2001)

15. J. Sun, D. Tao, C. Faloutsos, Beyond streams and graphs: dynamic tensor analysis, in *Proceedings of 12th ACM SIGKDD International Conferences Knowledge Discovery and Data Mining* (2006), pp. 374–383
16. J. Ye, Generalized low rank approximations of matrices. Mach. Learn. **61**, 167–191 (2005)
17. U. Luxburg, A tutorial on spectral clustering. Stat. Comput. **17**(4), 395–416 (2007)
18. B. Long, P.S. Yu, Z.M. Zhang, A general model for multiple view unsupervised learning, in *Proceedings of SIAM International Conference Data Mining* (2008), pp. 822–833
19. A. Smilde, R. Bro, P. Geladi, in *Multi-Way Analysis: Applications in the Chemical Sciences* (2004)

Implementation of Isolated Two Inductor Boost Converter for Induction Motor Drive Applications

S. Lavanya and T. Annamalai

Abstract This paper proposes modified two inductor boost converter (TIBC) along with a three-phase inverter circuit for induction motor drive application. The modified TIBC is for the first stage of DC/DC converter. The input current is distributed through two boost inductors having its current ripple amplitude halved at the twice of PWM frequency. The voltage doubler is applied to reduce turn's ratio of the transformer. This work is further improved with non-isolated recovery snubber with constant duty cycle control to improve its efficiency. The main reason of using snubber, TIBC, is not suitable for motor drive system. The reason is motor demand low power at low speed and during start up and stop conditions. Moreover, TIBC requires minimum operation load to maintain an output voltage, i.e., below certain load condition energy transferred to output capacitor is not completely transferred load causing an increase in output voltage, because the inductors are charged even if there is no output current. TIBC is able to turn on both the active switches at zero voltage to reduce their switching losses and raises the conversion efficiency. Since the two parallel-operated boost units are identical, operation, analysis, and design for the converter module becomes quite simple.

Keywords Two inductor boost converter (TIBC) · DC–DC power conversion · AC motor drives · DC–AC power conversion

1 Introduction

In many industrial and domestic applications, it is required to convert a fixed DC voltage into variable DC voltage. DC–DC converters are widely used for traction motor control in electric automobiles, trolley cars, marine hoists, fork lift trucks,

S. Lavanya (✉) · T. Annamalai
Department of Electrical and Electronics Engineering, Sri Venkateswara College of Engineering, Irunkattukotai, Sriperumbudur, Tamil Nadu 602117, India
e-mail: avanya@svce.ac.in

T. Annamalai
e-mail: annamalai@svce.ac.in

© Springer India 2015

L.P. Suresh et al. (eds.), *Artificial Intelligence and Evolutionary Algorithms in Engineering Systems*, Advances in Intelligent Systems and Computing 325,
DOI 10.1007/978-81-322-2135-7_68

and mine haulers. They provide smooth acceleration control, high efficiency, and fast and dynamic response. The boost converter is widely used in regulated DC power supply and regenerative braking of DC motor because its input current is continuous and the topology is simple. Most renewable power sources, such as photovoltaic power systems and fuel cells, have low output voltage and require series connection or a voltage booster to provide enough output voltage. With the increase in power rating, it is often required to associate converters in parallel. For high current applications, two inductor boost converters (TIBCs) are preferable, since the current in the switches are half of the inputs current. In addition, TIBCs can also reduce input current ripple and the switching losses; hence efficiency of the converter is improved.

Multi-function converter (MFC) [1] is used to drive the DC motor; in this concept, panel is connected to a single three-phase inverter bridge that acts as both boost converter and motor inverter, which eliminates the need to separate boost converter. The windings of the motor are used both for driving the motor and boosting the panel voltage. Boosting function is controlled by varying the pulse width modulation duty of high and low side switches. But, the drawback of this MFC is motor resistive losses are high. TIBC is for driving an induction motor [2]. TIBC minimizes current ripple amplitude halved at twice of PWM frequency. So, it reduces oscillation at PV module and makes it easy to achieve MPP. But, the drawback of this system is below certain load condition; the input power is not completely transferred to the load which results in increased output voltage; hence, the device connected to the system gets damaged. To overcome such a problem, a protection circuit, i.e., regenerative snubber, was added [3]. This paper proposes modified TIBC along with a voltage source inverter to drive an inductive load by overcoming the drawback stated in the paper [1, 2]. However, the converters are still operated hard switched, resulting in switching losses. Several zero-voltage or zero-current soft switching techniques exist for DC–DC converters. The paper is organized as follows: in Sect. 2, proposed system is discussed in detail with its operation principle and the experimental results are presented. Section. 3 describes conclusion of this chapter .

2 Proposed Converter

2.1 Open Loop Operation of Two Inductor Boost Converter

In this paper, the modified TIBC driving motor load shown in Fig. 1 is proposed for the first stage DC/DC conversion due to its very small number of components, simplicity, high efficiency, and easy transformer flux balance [4, 5] and a common ground gate driving for both switches. The energy is fed to the motor through a converter with two power stages: a DC/DC TIBC stage to boost the input voltage and a DC/AC three-phase inverter to convert the DC voltage to three-phase AC voltage required to drive an inductive load.

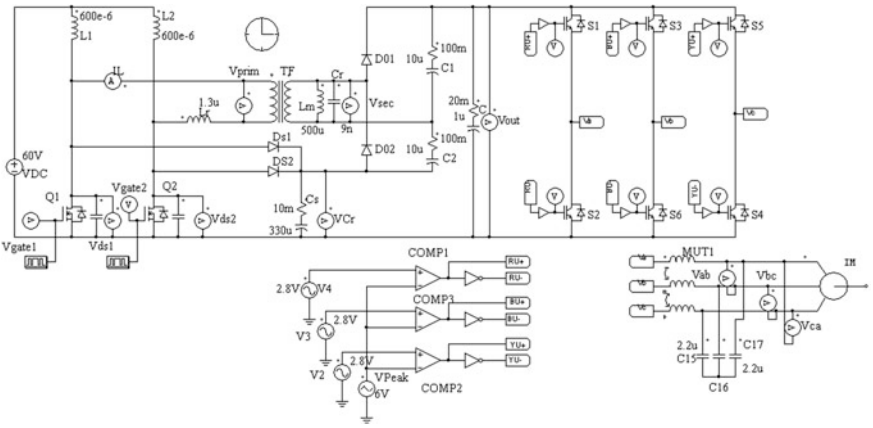

Fig. 1 Proposed two inductor boost converter driving an induction motor

The inverter is based on a classic topology (three legs, two switches per leg) and uses a sinusoidal pulse width modulation (SPWM). The DC/DC converter for driving a motor load needs to have large voltage conversion ratio. When compared with voltage-fed topologies, current fed converters have some advantages [4–9]. Usually, they have an inductor at the input so the system can be sized to have input current ripple as low as needed, thus eliminating the need of input capacitor. The current fed converters are normally derived from the boost converter, having an inherent high step-up voltage ratio, which helps to reduce the needed transformer turn ratio. To simplify the analysis of the proposed converter, the following assumptions are considered. The switching interval of the input inductors $L1$ and $L2$ are large so that the input current is almost constant; the capacitors C1, C2, and Cs are large enough to maintain a constant voltage. The output capacitors are much larger than Cr, to clamp the resonant voltage. In the operation of TIBC, the two switches Q1 and Q2 operate at an overlapped duty cycle to guarantee a conduction path for the input inductors current. When Q1 (Q2) is opened, the energy stored in $L1$ ($L2$) is transferred to C1 (C2) through the transformer and rectifier diode D01 (D02).

Once the multi-resonant tank is introduced, two different resonant processes occur, when both the switches are closed the leakage inductance Lr participates along with capacitance Cr in the resonance at the primary current switching, allowing ZCS operation for the primary switches. When one of the switch is open, Lr is associated in series with $L1$ or $L2$, not participating on the transformer's secondary current resonance, formed only by Lm and Cr. The various modes of operations are as follows:

Mode 1 ($t_0 - t_1$)

This mode begins at time $t = t_0$ Fig. 2 when the main switch Q1 is triggered by applying the gate voltage Vg, Q1 and Q2 is in off condition; the current flows through the inductance $L2$ feeds the resonant tank formed by magnetizing

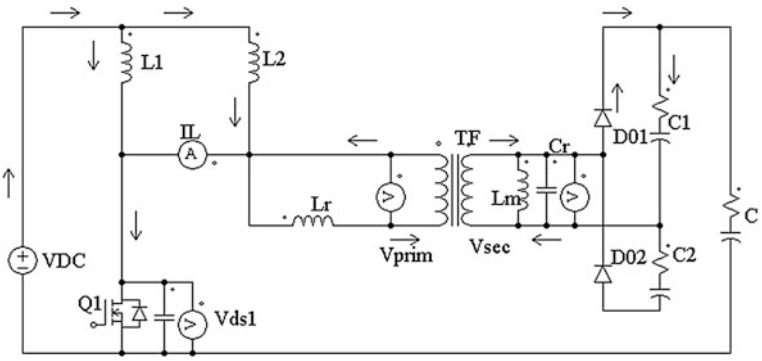

Fig. 2 Mode 1 diagram

inductance and resonant capacitance. So, the voltage across the resonant capacitor is clamped to Vout/2. Since Lm is connected in parallel with Cr, voltage across Lm is also clamped to a value of Vout/2.

Mode 2 ($t_1 - t_2$)

In Mode 2, both the switches Q1 and Q2 of converter circuit are in ON conditions (Fig. 3). Cr transfers its energy to Lr, so Cr discharges through the switch Q1; hence, the current through the switch Q1 (IQ1) decreases.

Mode 3 ($t_2 - t_3$)

The current through the switch Q1 further decreases and reaches zero. When IQ1 is zero, switch Q1 is said to be in turn off condition. The voltage drop across the switch Q1 is large which forward bias the snubber diode DS1 to transfer its energy

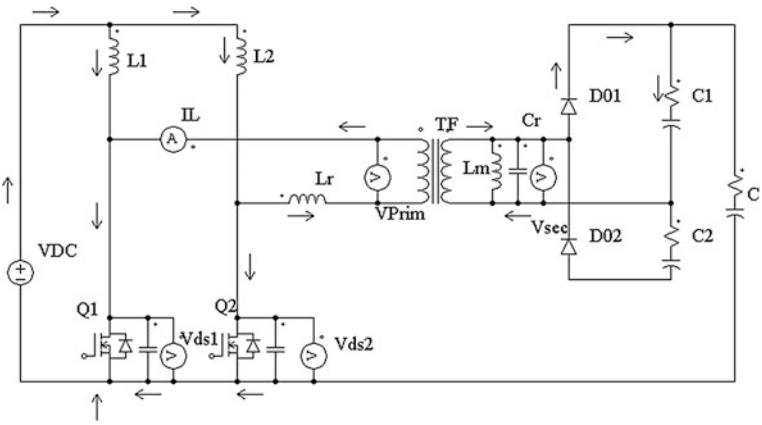

Fig. 3 Mode 2 diagram

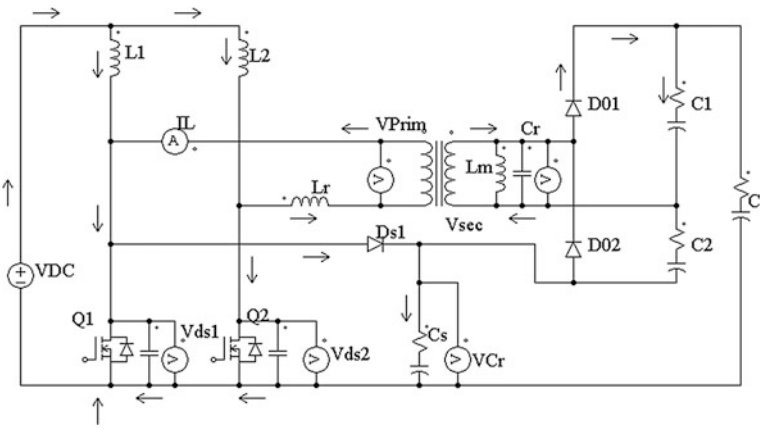

Fig. 4 Mode 3 diagram

to the snubber capacitor Cs shown in Fig. 4. This voltage combines with the output capacitor voltage of TIBC to drive an induction motor via a three-phase VSI.

Mode 4

During this mode of operation, the resonant capacitor Cr continues to resonant with Lm and the voltage on the doubler circuit decreases. The voltage across Cr is now clamped to—Vout/2, since Cr is in parallel with Lm. The voltage across magnetizing inductance Lm is also—Vout/2.

Mode 5($t_3 - t_4$)

In this mode, the switch Q2 alone is in on condition, Fig. 5 current takes place through *L*1 feeds the resonant tank formed by magnetizing inductance Lm and the resonant capacitor Cr. So, the voltage across the resonant capacitor is clamped to Vout/2. And above-mentioned process is repeated for the commutation of Q2.

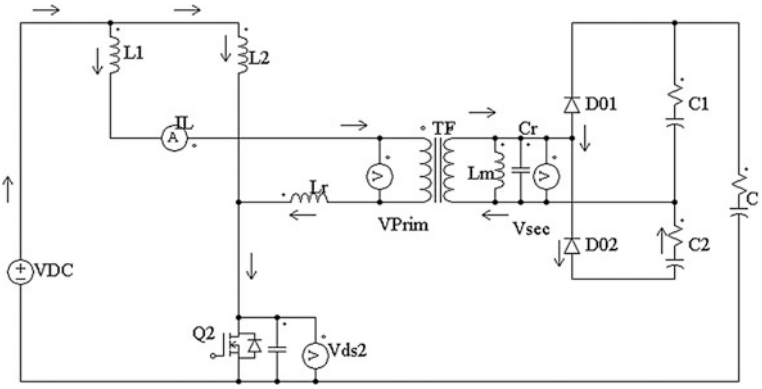

Fig. 5 Mode 5 diagram

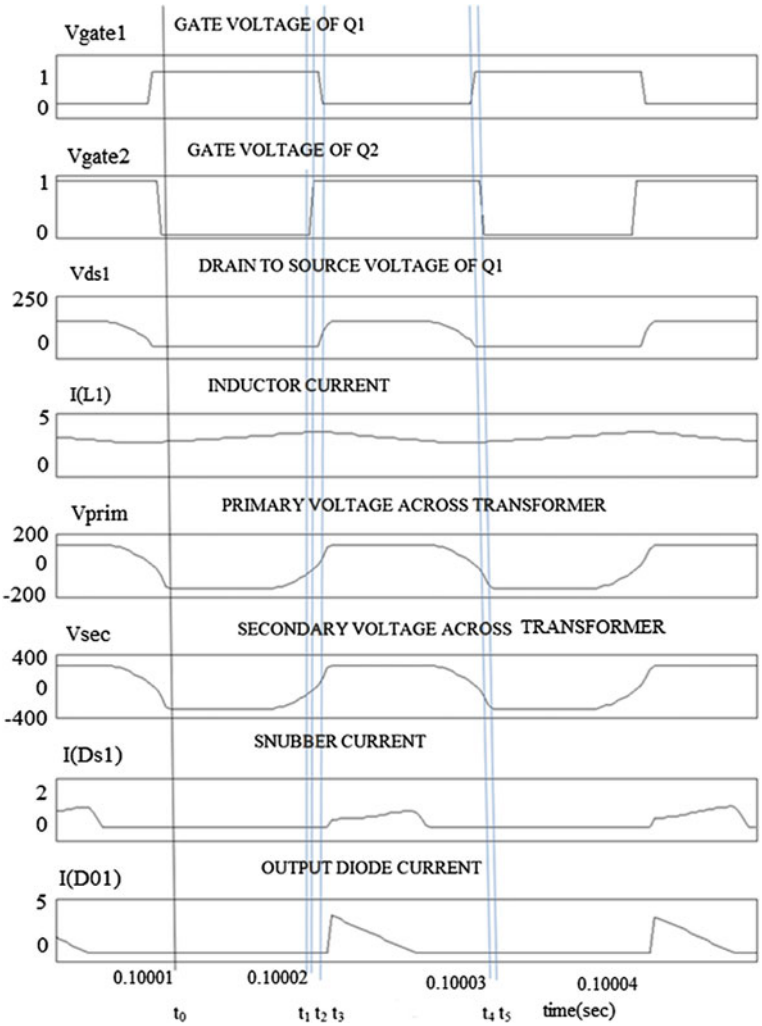

Fig. 6 Waveform of two inductor boost converter during switching period

The waveform of TIBC during the switching period is shown in Fig. 6, where the drain to source voltage is around 144 V. The input inductor current raises to a value of around 3.4 A, and the output diode current is around 3.5 A. When the main switches are in turn off condition, the drain to the source voltage is to be transferred to snubber capacitor via snubber diode. So, the voltage across snubber capacitor is around 144 V, since snubber capacitor is connected in series with the output capacitors C1 and C2 (output voltage is around 600–700 V) shown in Fig. 7. Hence, this combined voltage will act as an input to the three-phase inverter circuit to convert this same level of DC voltage to AC required to drive an induction motor Fig. 8.

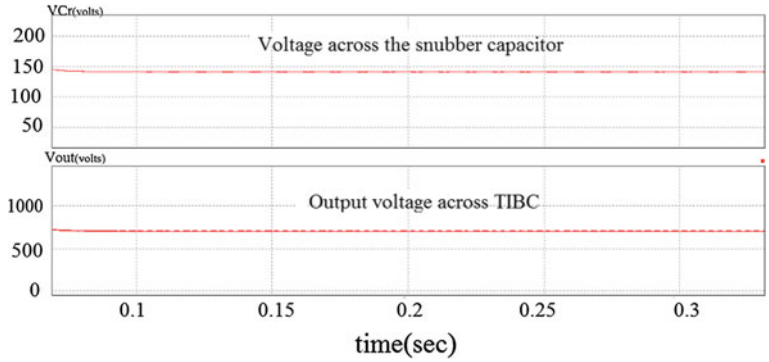

Fig. 7 Voltage across snubber capacitor and output voltage across TIBC driving an inductive load

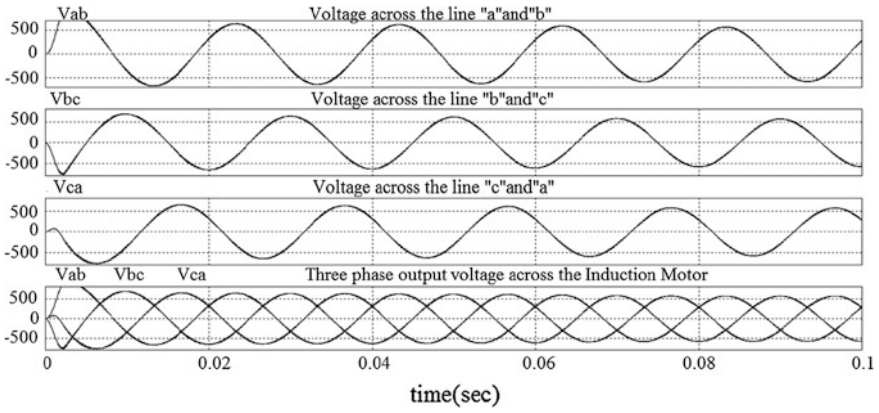

Fig. 8 Three-phase output voltage waveform across inductive load

The gate pulse for the inverter circuit is applied by the pulse width modulation, i.e, by comparing the amplitude of reference signal 6 V with carrier signal of 2.8 V by using the comparator. The output of the comparator is applied as the gate pulse for the switches of the inverter to obtain the three-phase output waveform shown in Fig. 8.

The RMS value of three-phase output waveform is around 440 V. The resonant process will affect the output voltage, so to neglect the resonant effect, the static voltage gain of converter is chosen as

$$\frac{V_{\text{out}}}{V_{\text{in}}} = K_v = \frac{1}{1-D}\left(2\frac{\text{Ns}}{\text{Np}} + 1\right) \tag{1}$$

For minimum overlapping condition, the duty ratio should be higher than 50 % (D = 0.6) Ns/Np represents transformer turns ratio.

Design procedure for the following specifications is given below,

Input voltage: 60 V
Output voltage: 600 V
RMS value of output voltage: 415 V
Switching frequency of converter: 50 kHz
Switching frequency of inverter: 50 Hz

The effective duty ratio of TIBC is

$$v_{\mathrm{o}} = \frac{v_{\mathrm{in}}}{1 - D} \tag{2}$$

Lr is said to be the leakage inductance. I_{L} is the input inductor current whose value is around 3.4 A

$$\frac{V_{\mathrm{o}}}{\mathrm{Lr}} = \frac{2I_{\mathrm{L}}}{(1 - D)T_{\mathrm{s}}} = \frac{I_{\mathrm{in}}}{(1 - D)T_{\mathrm{s}}} \tag{3}$$

$$I_{\mathrm{o}} = (1 - D)I_{\mathrm{in}} \tag{4}$$

Therefore, the leakage inductance Lr can be calculated as

$$L_{\mathrm{r}} = V_0 T_{\mathrm{s}} \frac{(1 - D)^2}{I_0} \tag{5}$$

The current ripple on each of the boost inductor is

$$\Delta I_L = \left(\frac{DT_{\mathrm{s}}}{L}\right) V_{\mathrm{in}} \tag{6}$$

Due to the TIBC operation, the Input current is the summation of two boost inductor currents

$$\Delta I_{\mathrm{in}} = \left(\frac{(2D - 1)T_{\mathrm{s}}}{L}\right) V_{\mathrm{in}} \tag{7}$$

For an input current ripple requirement of 1.2 A, the inductance $L1 = L2 = 600$ μH.

Since the load and snubber capacitor receive the current summation from diodes D_{S1} and D_{S2}, the frequency of the output ripple current becomes twice as high as the switching frequency. Therefore, the output ripple voltage is reduced as

$$\Delta V_o = \Delta V_c = \frac{I_o D^2 T_s}{2C_o} = \frac{V_o D^2 T_s}{2RC_o}. \tag{8}$$

For the ripple voltage of 2 V, the output capacitor is 330 μF.

2.2 Closed Loop Operation of TIBC Driving an Induction Motor

The main drawback of the TIBC is the problem with minimum load condition. The main reason is the input inductors that are charged even if there is no output current. However, the addition of snubber provides alternative path for the inductor current when the main switches are turned off. The addition of the hysteresis-type controller Fig. 9 can step up the DC bus voltage. When maximum voltage is reached, indicating a low load condition this mode of operation begins. In this case, the main switches will be in turn off condition until the DC bus voltage reaches to a predefined value. As a result, switching losses will be reduced. From the waveform Fig. 10, it is noticed that primary voltage across the transformer is around 120 V and the secondary voltage is around 240 V. The addition of hysteresis-type controller will step up the DC bus voltage required to drive an inductive load.

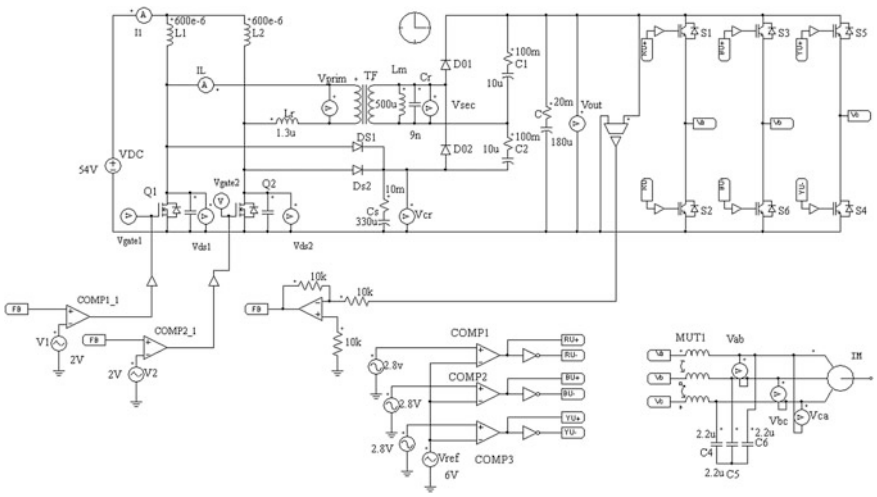

Fig. 9 Closed-loop operation of two inductor boost converter driving an induction motor

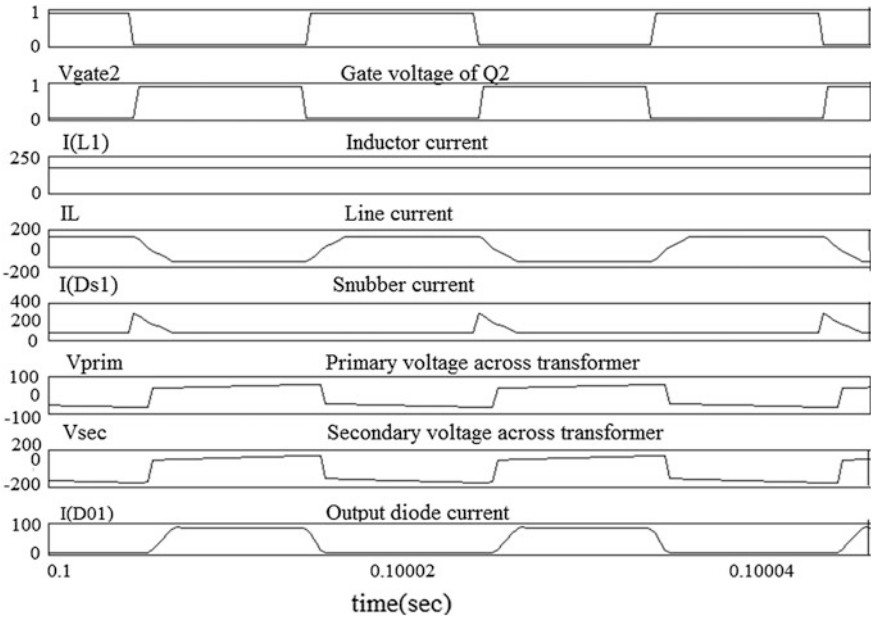

Fig. 10 Key waveform of two inductor boost converter during switching period

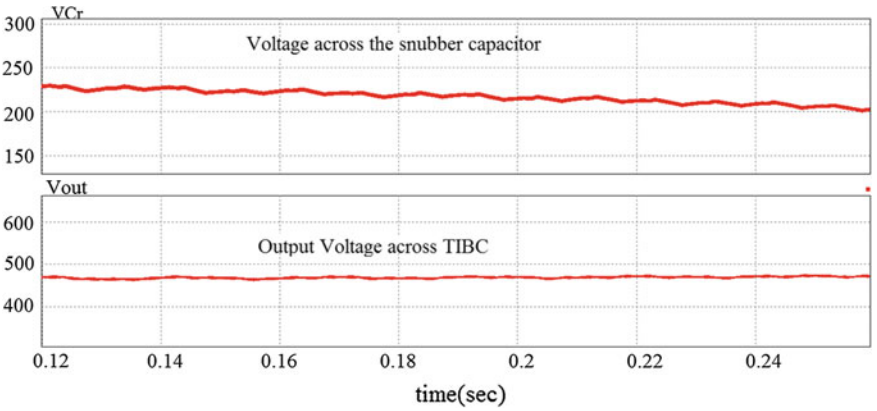

Fig. 11 Voltage across snubber capacitor and output voltage across TIBC driving an inductive load

The voltage across snubber capacitor is around 230 V and the output voltage of converter is around 480 V Fig. 11. This combined voltage will be given as input to the three-phase inverter to drive an induction motor Fig. 12.

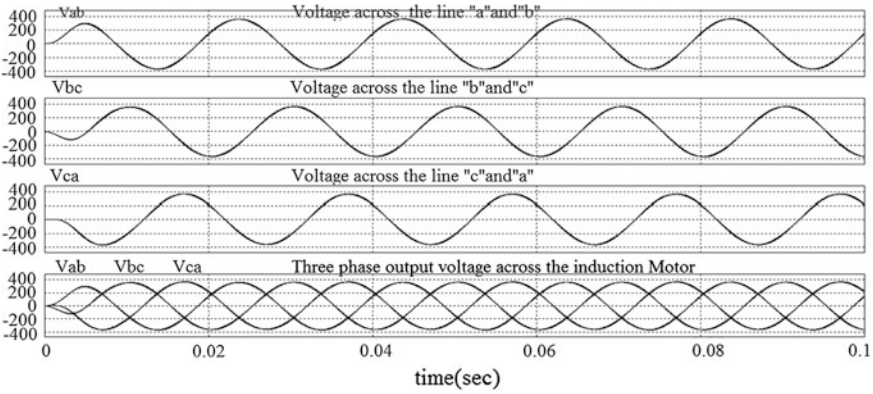

Fig. 12 Three-phase output voltage waveform across inductive load

3 Conclusion

TIBC requires minimum operation load to maintain an output voltage, below certain load conditions the input power is not completely transferred to load causing an increase in output voltage. Hence, TIBC is not suitable for motor drive system. By the addition of Snubber circuit, the drawback of TIBC for driving the motor load has been overcome by transferring the excess voltage to snubber capacitor. The TIBC is suitable for high power application, since the current in the switches is equally divided into two inductive coils. In additions, TIBCs can also reduce input current ripple and the switching losses; hence, efficiency of the converter is improved. This proposed model is best suitable for water pumping system in rural areas with the help of renewable source (solar panel)

References

1. D. Tschanz, H. Lovatt, A. Vezzini, V. Perrenoud, A multi-functional converter for a reduced cost, solar powered, water pump, in *IEEE International Symposium on Industrial Electronics* (*ISIE*) (2010), pp. 568–572
2. B. Yuan, X. Yang, X. Zeng, J. Duan, J. Zhai, D. Li, Analysis and design of a high step-up current-fed multi resonant DC–DC converter with low circulating energy and zero-current switching for all active switches. IEEE Trans. Ind. Electron. **59**, 964–978 (2012)
3. J. Caracas, G. Farias, L. Teixeira, L. Ribeiro, Implementation of a high efficiency, high lifetime, and low cost converter for an autonomous photovoltaic water pumping system. IEEE Trans. Ind. Electron. (99)
4. L. Yan, B. Lehman, Isolated two inductor boost converter with one magnetic core, in *Proceedings of IEEE Applied Power Electronics Conference and Exposition* (2003), pp. 879–885

5. Y. Jang, M.M. Jovanovic, New two inductor boost converter with auxiliary transformer, in *Proceedings of IEEE Applied Power Electronics Conference and Exposition* (2002), pp. 654–660
6. Y. Jang, Two inductor boost converter with auxiliary transformer, in *Proceedings of IEEE Applied Power Electronics Conference and Exposition* (2002), pp. 624–629
7. M.A. Vitorino, M.B.R. Correa, C.B. Jacobina, A.M.N. Lima, An effective induction motor control for photovoltaic pumping. IEEE Trans. Ind. Electron. **58**, 1162–1170 (2011)
8. M. Caccialo, A. Consoli, V. Crisafulli, A high voltage DC/DC converter for energy harvesting in single module photovoltaic applications, in *Proceedings of IEEE International Symposium on Industrial Electronics*(*ISIE*) (2010), pp. 550–555
9. C. Marcelo, A ZCT auxilliary commutation circuit for two inductor boost converters operating in critical conduction mode. IEEE Trans. Power Electron. **17**(6), 954–961 (2011)

A Generic Bio-inspired Framework for Detecting Humans Based on Saliency Detection

R. Aarthi, J. Amudha and Usha Priya

Abstract Even with all its advancement in technology, computer vision system cannot competes with nature's gift—the brains, that arranges the objects quickly and extract the necessary information from huge data. A bio-inspired feature selection method is proposed for detecting the humans using saliency detection. It is performed by tuning prominent features such as color, orientation, and intensity in bottom-up approach to locate the probable candidate regions of humans in an image. Further, the results improved in detection phase that makes use of weights learned from training samples to ignore non-human regions in the candidate regions. The overall system has an accuracy rate of 90 % for detecting the human region.

Keywords Skin color segmentation · Computational modeling · Human detection algorithm

1 Introduction

Most of the computer vision problems deal with the process of understanding and learning from the environment. The traditional computer vision processing methodology requires more training data set to understand the objects which is different from that in human vision. The human detection in video surveillance is an example for such systems that requires in fields security and monitoring. Human detection is a challenging problem, due to variant factors such as clothing, posture, and complexion. So the thrive for the robust human detection algorithm is continuing, so

R. Aarthi (✉)
Amrita Vishwa Vidyapeetham, Coimbatore, India
e-mail: aarthi.r4@gmail.com

J. Amudha
Amrita Vishwa Vidyapeetham, Bengaluru, India
e-mail: j_amudha@blr.amrita.edu

U. Priya
Department of Information Technology, Amrita Vishwa Vidyapeetham, Coimbatore, India

© Springer India 2015

L.P. Suresh et al. (eds.), *Artificial Intelligence and Evolutionary Algorithms in Engineering Systems*, Advances in Intelligent Systems and Computing 325,
DOI 10.1007/978-81-322-2135-7_69

that it can be incorporated in many applications. The shape-based approach [1] is proposed to recognize humans in single images. In Haga et al. [2], a moving object is classified as human based on the spatial uniqueness of the image motion, temporal uniqueness of the human motion. Yoon and Kim [3] used skin color and motion information to find the candidate foreground objects for human detection. Jiang et al. [4] detection is based on fusion of infrared (IR) images and characteristic signature in IR images due to skin temperature. The human detection algorithm so far uses the framework of the human structure depending on the application. Most of the applications of human detection use skin color segmentation [5] that works for particular skin tone and for closure posture.

The conventional human detection systems are different in approaches from the way the human brain processes the visual information in complex environment to locate the human. Computational modeling of this basic intelligent behavior still remains a challenging research problem. Itti et al. [6] have used visual saliencies to develop a bottom-up approach to detect salient region by extracting the color, intensity, and orientation maps separately and then it is combined to a single map. The system detects a target that differs from surrounding distracter. Liu [7] applied center surround operator on histogram to detect salient region. A two-stage approach for saliency detection is performed in [8] using spectrum residue method. An improvement of spectrum residual method [9] is performed by analyzing the log spectrum of any input image—this model works on natural pictures and psychological patterns. This method produces the disoriented saliency map for objects with similar frequency in the image. Rao [10] developed saliency detection method by clustering pixels of an image based on the feature vector. Then, the super clusters are formed using probability distribution of each cluster. As an enhancement of above saliency detection methods, Frintrop's [11], VOCUS uses bottom-up approach and top-down approach for detecting the region of interest in images. An optimized model for visual attention based on the concept of selective tuning is presented in [12, 13]. There is a pressing demand for generic computational model that understand the human behavior in various video surveillances. Hence, the objective of this work is to propose a generic frame work to detect humans from the selective feature based on saliency detection approach.

This paper is organized as follows, Sect. 2 explains about the feature selection adopted for channels in bottom-up approach followed by the detection methodology to identify humans in Sect. 3. The experimental results and conclusions are presented in Sects. 4 and 5, respectively.

2 Bottom-up Approach with Feature Selection

The architecture for detecting human is given in Fig. 1. Bottom-up approach [6] is applied to detect salient region which generates the features map such as intensity, color, and orientation that tend to be more prominent for the salient object than the surrounding or background objects.

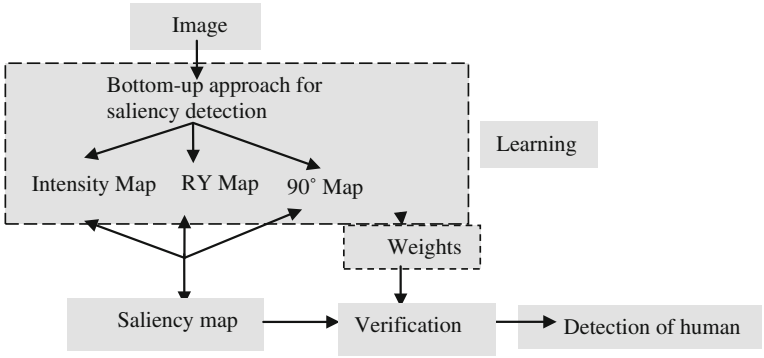

Fig. 1 Architecture for human detection

Intensity Map The relative lightness or darkness of a particular color depends on the strength of intensity values. As per Itti et al. [6] model, Gaussian pyramid is constructed up to nine levels (0–8) and six feature maps are constructed having center images of levels $c = (2, 3, 4)$ and surround $(3, 4)$.

RY Map Color is a primitive factor that helps narrow down to the region of interest. Considering the fact that red (R), blue (B), and green (G) are the primary colors and they tend to catch the human eye easily. Gaussian pyramids are constructed for RGBY channels, followed by center-surround method for the combination of RG and BY channels. It is observed that human skin color [5] is distributed more toward yellow and red regions of the RGB color cube. So, the necessary information about the skin region is in RY channel. The RY color map is computed similar to intensity map as in Eq. (1).

$$\mathrm{RY}(c, s) = |\{\mathrm{R}(c) - \mathrm{Y}(c)\} - \{\mathrm{Y}(s) - \mathrm{R}(s)\}| \tag{1}$$

where R, G, and B are the red, green, and blue color channels of the image with $c = (2, 3, 4)$ and $s = (3, 4)$. The color map for various combinations of the RGBY color model is shown in Fig. 2. First, the center-surround method is applied on the R, G, B, and Y channels separately. By observation in Fig. 2b, it is seen that other most salient

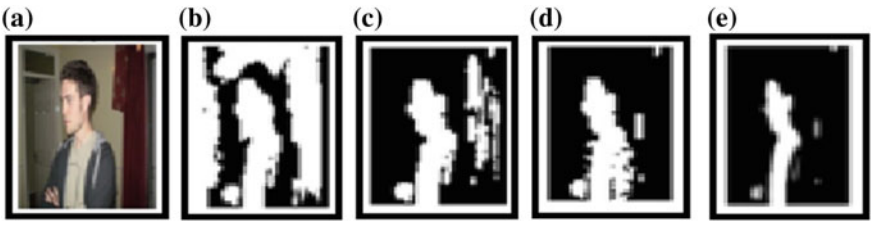

Fig. 2 **a** Input image, **b–e** color maps by R_G_B_Y separate channels, RG_BY, RY_GB, and RY, respectively

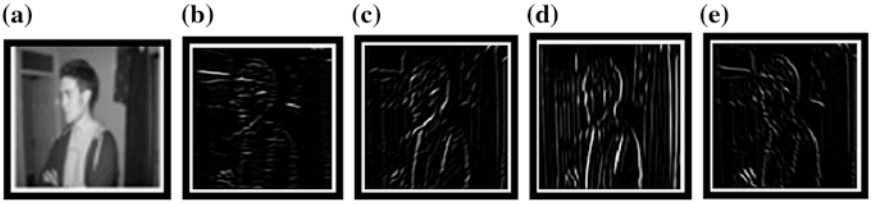

Fig. 3 **a** Input image, **b–e** the orientation results, respectively, for 0°, 45°, 90°, 135° obtained using Gabor filter

objects are also detected. Secondly, the center-surround method was applied on various scales of combination of RG_BY channels and RY_GB channels (in Fig. 2c, d), which improved the results to fewer objects that were salient. Thirdly, on considering only RY channel and eliminating BG channel for the center-surround calculation extracts the human region in the given image. From the figures, it is evident that similar results are obtained for RY_GB and RY color channel. This inturn leads to RY map to be most sufficient for detecting skin color regions.

Orientation Map The orientations are computed by Gabor filter [14]. Gabor filter is a linear filter used for edge detection. Frequency and orientation representations of Gabor filters are similar to those of the human visual system. Their behavior is similar to the response of orientation sensitive cells in the human cortex. The orientations 0°, 45°, 90,° and 135° are considered, because these orientations are similar to the receptive field profiles in the mammalian cortical field. So, the orientation scale maps for orientations $\theta \in \{0°, 45°, 90°, 135°\}$ and scales $s \in \{s_2, s_3, s_4 \ldots\}$ have been obtained using Gabor filter. The orientation scale maps are summed up by across scale addition for each orientation, yielding four orientation feature maps as are depicted in Fig. 3b–e. Most of the surveillance applications of humans have considering standing posture. Hence, the dominant information observed visually is mostly 90° orientations for detecting the humans.

Saliency map The six feature maps of intensity are combined to form a single map by bringing all the maps to a scale of four and performing across scale addition which is point by point pixel addition. Similarly, the six feature maps of RY color and 90° orientation maps are also combined to form single saliency map which gives the probable candidate regions of humans in image.

3 Detecting Region of Interest (ROI)

In human visual perception, detecting the region of interest is the most important mechanism, but each time, the region of interest changes depending on the situation. Detecting the target object is achieved by two phases namely learning phase and search phase.

Learning Phase Detection of ROI is performed using weight "W_i" [11] calculated as in Eq. (2)

$$W_i = \text{mean}_{i(\text{MSR})} / \text{mean}_{i(\text{ROI}-\text{MSR})} \tag{2}$$

where, W_i weight for ith feature $i \in$ {Red, Green, Blue, 0°, 45°, 90°, 135°}, $\text{mean}_{i(\text{MSR})}$ is the mean average feature values present in the pixel positions within the most salient region.$\text{mean}_{i(\text{ROI—MSR})}$ is the mean average feature values present in the pixel positions within ROI—MSR (the region surrounding the MSR). In Figure 4, the dotted rectangle indicates the region of interest and bold rectangle inside it indicates the most salient region. For the region within the bold rectangle, the weights are calculated to find the most prominent feature. The most salient regions (MSR) can be detected using the bottom-up approach. First, a region of interest is chosen and within that the MSR is chosen. Region of interest may be the objects surrounding the human, while the most salient region is the human. Range of weights is obtained for different features from four training samples which are normalized and the average weight "*w*" is used in the search phase to detect the human. The weights for different images in Fig. 4a–d are listed in Table 1.

The weights in Table 1 show that all the weights are positive for uniform background than complex background. Suppressing or placing the MSR region in the uniform background does not affect any calculation rather than decreasing the effect of the distracters present within the background.

Search Phase The objective of search phase is to use the weights to detect the target object that satisfies the condition. Candidate regions obtained by bottom-up approach are searched based on the weights obtained in learning phase. Figure 5a

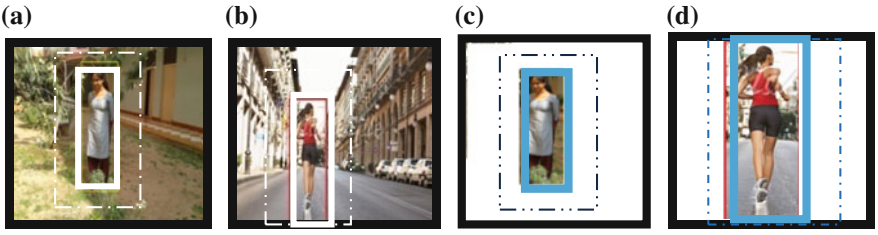

Fig. 4 **a**, **b** Data set with complex background. **c**, **d** Data set with white background

Table 1 Weights of training samples

Images	Red	Green	Blue	0°	45°	90°	135°
4(a)	7.82	−16.78	9.23	14.09	17.890	27.51	8.423
4(b)	−16.89	−15.90	−13.89	−94.56	86.05	229.35	−56.70
4(c)	2.7304	1.86	1.60	1.64	1.74	1.79	1.57
4(d)	1.0860	0.90	0.65	1.37	0.96	0.53	0.785

Fig. 5 **a** Candidate region of image **b** detected region

shows the results of the bottom-up approach candidate regions in rectangular box (Actual results are highlighted with bold rectangle). Figure 5b shows the detected human region after search phase.

4 Experiments and Results

Analysis has been carried for 89 images with varied complex background. Table 2 portraits the combination of color, orientation, and intensity result for four sample images. The first column shows the input image, second column shows the saliency detected image by Itti et al. [6]. Last column shows the results of generic approach by considering 90° orientation map, RY map, and intensity map for obtaining the candidate regions before detection. Comparing both the columns 2 and 3, it is evident that the number of candidate region is reduced in selective features approach. Similar results were obtained for all samples in data set.

Table 3 shows the detection rate of proposed method and the accuracy is calculated by true positive (TP), true negative (TN), and false positive (FP). False positive (N_{fp}): The image is marked FP if the ground truth is "Not Detected" but the algorithm is employed to recognize the region as "Detected." True positive (N_{tp}): The image is marked TP if the ground truth is "Detected" and the algorithm is employed to recognize the region as "Detected." True Negative (N_{tn}): The image is marked TN if the ground truth is "Detected" but the algorithm is employed to recognize the region as "Not Detected." The accuracy is the proportion of true results (both true positives and true negatives) in the population. It is also expressed in percentage. It can be represented as in Eq. 3.

$$\text{Accuracy} = \frac{N_{tp} + N_{tn}}{N_{tp} + N_{tn} + N_{fp}} \times 100 \tag{3}$$

Table 2 Comparison between results

ORIGINAL IMAGE	SALIENCY IMAGE (RY color channel, Intensity and Orientation(0 °, 45^0, 90^0 and 135°)	SALIENCY IMAGE (RY color channel, Intensity and Orientation(90^0))
	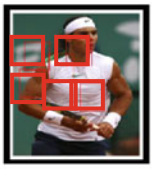	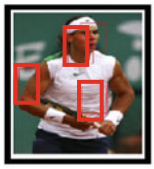
	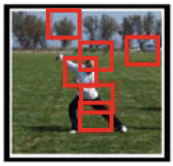	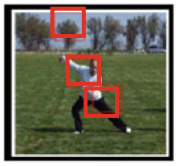
	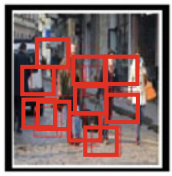	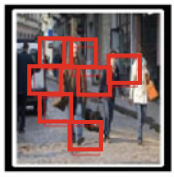

Table 3 Detection rate

Presence of human	TP	TN	FP	(%) of detection
Single human (30)	26	2	2	93.3
Multiple humans (30)	18	8	4	86.6
None (29)	21	4	4	86.2

The method shows average of 90 % accuracy for the data set. The method is tested with three surveillance videos and it shows a promising result for vision-based applications.

5 Conclusions

The generic bio-inspired computational model for detection of human is presented. This system is influenced by two-step process: Bottom-up approach and ROI search phase. In the bottom-up approach, the channels of color, orientation, and intensity are modified to detect the human regions in the image. The search is performed in the final saliency map in order to find the target region (human) using weights. It can be noted that 2 or 3 training samples are sufficient to learn the weights of the target object. The experiments and result show a robust performance in real-world applications. The results show that the approach gives an accuracy of 93 %. This work can be enhanced to detect various postures of human. The motion can be considered as one of the features for detecting the humans in videos. The method can also be extended for detecting any objects by tuning the channels in the bottom-up approach.

References

1. B. Heisele, C. Wohler, Motion-based recognition of pedestrians, in *Proceeding of the International Conference on Pattern Recognition*, vol. 2 (1998), pp. 1325–1330
2. T. Haga, K. Sumi, Y. Yagi, Human detection in outdoor scene using spatio-temporal motion analysis, in *International Conference on Pattern Recognition* (2004), pp. 331–334
3. S.M. Yoon, H. Kim, Real-time multiple people detection using skin color, motion and appearance information, in *International Workshop on Robot and Human Interactive Communication* (2004), pp. 331–334
4. L. Jiang, F. Tian, L.E. Shen, S. Wu, S. Yao, Z. Lu, L. Xu, Perceptual-based fusion of IR and visual images for human detection, in *International Symposium on Intelligent Multimedia, Video and Speech Processing* (2004), pp. 514–517
5. V. Vezhnevets, V. Sazonov, A. Andreeva, A survey on pixel-based skin color detection techniques, graphics and media laboratory, in *Proceedings of the Graphi Conference* (2003), pp. 85–92
6. L. Itti, C. Koch, E. Niebur, A model of saliency-based visual attention for rapid scene analysis. IEEE Trans. Pattern Anal. Mach. Intell. (PAMI) **20**(11), 1254–1259 (1998)
7. T. Liu, J. Sun, N. Zheng, X. Tang, H.Y. Shum, Learning to detect a salient object (IEEE, 2007)
8. Z. Wang, B. Li, A two stage approach to saliency detection in images (IEEE, 2008)
9. X. Hou, L. Zhang, Saliency detection. A Spectral Residual Approach (2006)
10. N. Rao, J. Harrison, T. Karrels, R. Nowakand, T.T. Rogers, Using machines to improve human saliency detection (2010)
11. S. Frintrop, VOCUS: a visual attention system for object detection and goal-directed search, *in Proceeding of International Conference on Intelligent System* (2006)

12. J.K. Tsotsos, S.M. Kolhane, W.Y.K. Wai, Y.H. Lai, N. Davis, N. Nuflo, Modelling visual attention by a selective tuning. Artif. Intell. **78**(1), 507 (1995)
13. C. Koch, S. Ullman, Shifts in selective visual attention: towards the underlying neural circuitry. Hum. Neurobiol. (1985)
14. Y. Huang, K. Huang, T. Tan, A heuristic deformable pedestrian detection method. Nat. Lab. Pattern Recogn. (2003)

Efficient Approach to Detect and Localize Text in Natural Scene Images

S.R. Surem Samuel and C. Seldev Christopher

Abstract Text in natural scene images may provide important information based on the application. Detecting text from natural scene should be effective; for that, segmenting text from natural scene images should use a high-performance method. In this paper, an efficient segmentation and classification technique is used. Given system takes natural scene images as input. After converting the color image to grayscale image, histogram of oriented gradients (HOG) features is used to find the edge values. Image is segmented using Ni-Black local binarization, which identifies the edge on suppressing image's background. Image is classified using CRF which blocks the text in the natural scene images. This system provides better segmentation of text and classifies with high detection accuracy.

Keywords Image processing · Text detection · Image segmentation · CRF

1 Introduction

Image segmentation plays an important role in image processing applications. The main aim of image segmentation is to divide an image into meaningful regions with respect to a requirement in application. Segmentation may be affected by the metrics taken from the image like, gray level, texture, depth, and color. Use of various types of digital imaging devices leads to a need for advanced content-based image analysis techniques. Text information in images is required for various

S.R. Surem Samuel (✉)
Department of Electronics and Communication Engineering, CSI Institute of Technology, Thovalai, India
e-mail: suremsam81@yahoo.co.in

C.S. Christopher
Department of Computer Science and Engineering, St. Xavier's Catholic College of Engineering, Chunkankadai, India
e-mail: cseldev@gmail.com

© Springer India 2015

L.P. Suresh et al. (eds.), *Artificial Intelligence and Evolutionary Algorithms in Engineering Systems*, Advances in Intelligent Systems and Computing 325,
DOI 10.1007/978-81-322-2135-7_70

applications. So it becomes a research topic to develop best systems to detect text in images. In this paper, we suggest an efficient approach to extract text from natural scenes. Jung et al. [1] tells about a text extraction system. This integrates four processes. They are text detection, text localization, text extraction, and enhancement and identification. The critical step is the text detection and text localization. The difficulties in the existing system are overcome by the proposed work. Unary component properties, and in addition binary contextual properties are the key factors used by the CRF model. The rest of the work is organized as follows. Section 2 gives report on related work. Section 3 gives report of the proposed work. Section 4 gives implementation details. Section 5 depicts the results. Concluding remarks is given in Sect. 6.

2 Related Work

Zhang et al. [2] tells an enhanced method to detect traffic signs. This takes color image as input and produces segmented binary image by adaptive color segmentation based on pixel vector. The shape feature vectors of different candidate regions are computed by central project transformation. This shape features are given as input for training a neural network, which after training detects traffic signs from candidates.

Pan et al. [3] says an improved method for text detection. Here, Stroke segmentation is done using scale-adaptive segmentation, and stroke verification is performed using CRF model with pairwise weight by local line fitting, and have used ICDAR2005 competition dataset for experimentation.

Maryam and Rahmati [4] say about a hybrid approach for detecting Farsi text in natural scene images. Here, they have chosen two types of artificial neural network, i.e., single-layer perceptron, and multi-layer perceptron. Though SVM has high complexity in computation and difficult in estimating parameter with CRF parameter, it is considered as base classifier.

Zhu et al. [5] proposed a nonlinear Ni-Black method to decompose input into candidate connected components. CC is then fed to cascade of classifier which is trained by AdaBoost algorithm.

Park and Lee [6] proposed a segmentation technique that segments the input image into chromatic and non-chromatic regions according to the RGB elements. For multi-resolution analysis, first objects are moved to wavelet domain, and then, for SVM classification, wavelet coefficient's moment features are used to classify text objects. Weinman et al. [7] use a conditional random field model for text detection. This uses the combination of contextual information and local detection.

3 Proposed Work

Our proposed work is to develop a well-built system that robustly detects text and localizes the text in natural scene images. Here, we consider the advantage of region-based method and connected components method. The system has two stages. In the first stage, text is detected to identify the text existing confidence in the local image regions by performing classification. In the second stage, text localization is done by clustering local text regions into text blocks and text is verified to remove non-text regions for upcoming processing. Generally, connected component methods have three stages. Candidate text parts are segmented from images called CC extraction. Filtering of non-text parts are done by using classifier or can be done using heuristic rules called CC analysis. Finally, in post-processing, text components are grouped into text blocks. Figure 1 depicts the workflow of the proposed work.

3.1 Conditional Random Field

CRF [8] is a probabilistic graphical model. It is used in various applications like natural language processing [9], computer vision [10], face detection [11], etc.,

Let A be the random variable for the dataset, which is to be labeled. B be the label set. The graph $G = (V, E)$ is considered. This graph satisfies the following criteria

$$B = (B_v)_{v \in (V)'}. \tag{1}$$

If this satisfies the condition, B can be indexed by the vertices of G. Then, (A, B) is a CRF; when conditioned on A, the random variables B_v will follow the Markov property with regard to graph.

$$p(B_v|A, B_w, w \neq v) = p(B_v|A, B_w, w \sim v). \tag{2}$$

where the neighbors w, v in the graph G are given as $w \sim v$. It indicates that CRF is the random field and has global condition over X. In case of a simple dataset, the joint distribution over the label set B given A has the following form:

Fig. 1 Workflow of the proposed work

$$p_\theta(b|a)\alpha \exp\left(\sum_{e\in E,k} \delta_{kf_k}(e,\, b|e,\, a) + \sum_{v\in V,k} \mu_k g_k(v,\, b|v,\, a)\right). \tag{3}$$

Here, a is the dataset and b is the label set. $b|s$ means set of components.

3.2 Ni-Black Local Binarization

This decomposes the image into connected components. If this step yields poor result, it affects the whole system. Because of this, additional care is taken here. This method is proposed by Winger et al. [9]. This is an efficient thresholding method.

3.3 Text Region Detector

In this module, text regions are detected. First, the text confidence is projected, and then, the information is scaled by scale-adaptive binarization [12]. Here, image is taken as input and produces candidate text components as output and is shown in Fig. 2.

3.4 Finding Key Regions

Here, CRF [13, 14] model helps in filtering non-text parts by combining two properties. Unary component features with binary contextual feature relations.

3.5 Grouping Regions

Adaptive clustering [11, 15] is used to group the text lines or words. Adaptive clustering is unsupervised learning method. It optimizes some explicit and implicit criteria of the image. It supports memorizing clusters that may reuse good clustering.

Fig. 2 Text detector module

3.6 Text Features

Here, 17 features are used to discriminate text CCs from non-text CCs in our method. Features lie in five categories. Categories are geometric, shape regularity, edge, stroke, and spatial coherence. After forming connected components, the segmentation problem is formed as classification. Now, it is enough to categorize into text and non-text blocks.

Algorithm

Pre-processing:

Step 1: Convert color image to gray-level image.
Step 2: Histogram of oriented gradients (HOG) is generated.
Step 3: Find the edge values using HOG features.

Segmentation

Step 4: Segment image by suppressing image's background.
Step 5: Classify text and non-text blocks using CRF.
Step 6: Text region is grouped using adaptive clustering.

Post-processing

Step 7: Remove noise by region dilation.
Step 8: Determine the angle of the text block using random transform.
Step 9: Crop the text block.
Step 10: Perform quantization, equalization, binarization, and normalization.
Step 11: Remove horizontal contours.

4 Implementation

The proposed work is implemented using MATLAB. Natural scene image with text is taken as input to the system. The system accepts either BMP or JPEG format. The results are shown in Figs. 3, 4, 5, 6, 7, 8, 9, 10, 11, 12, 13, 14, 15, 16, and 17, respectively.

Fig. 3 Input image

Fig. 4 Input gray image

Fig. 5 HOG-featured text confidence

Fig. 6 After classification

Fig. 7 After background suppression

Fig. 8 After classification

Fig. 9 Region grouping

Fig. 10 Dilated region

Fig. 11 Angle of text

Fig. 12 Text crop

Fig. 13 Grayscale text

Fig. 14 Text quantization and equalization

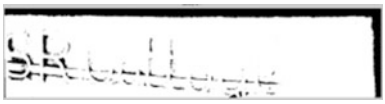

Fig. 15 Binary text

Fig. 16 Normalized text

Fig. 17 Text horizontal contours adjusted

5 Results and Discussion

Figure 3 shows a complex natural scene image which is taken as input in our system. Figure 4 shows the input gray image on which a feature descriptor is applied; that is, HOG is applied to produce the HOG features. HOG helps in finding the edge values. Figure 6 shows the image after classification. CRF model is used as the classifier.

Table 1 Overall performance

Operations	Precision (%)	Recall (%)	F1	Average speed (s)
Text detection	92.3	95.0	93.3	14.4
Text localization	85.9	93.5	93	5.35

5.1 Segmentation

Ni-Black local binarization algorithm [10] is applied, which produced a high-efficiency output. Figure 7 shows the image after background suppression, and then, it is classified. Figure 8 shows the image after classification.

5.2 Adaptive Clustering

Adaptive clustering is applied to group text regions and non-text regions. Figure 9 shows the image after region grouping.

5.3 Post-Processing

If there is noise in the image, it is removed by region dilation. Figure 10 shows the dilated image. The angle of the text is determined using random transform. Figure 11 shows the image that identified angle of the text. Figure 12 shows the cropped image that shows the text. Figures 13, 14, 15, and 16 show the various steps of post-processing.

The overall performance of the system using the existing dataset is shown in Table 1. Precision, recall, F1, of the system is shown in the table. The average speed of the system is shown in the table.

6 Conclusion

In this paper, we present an efficient approach to detect and localize text in natural scene images. Region information is integrated with reliable connected components method. Also the binary contextual component relationships in combination with unary component properties are integrated in CRF mode, which effectively classifies the text and non-text regions. In unconstrained scene, the proposed work effectively localizes text, which is illustrated by experimental results. Though system provides better efficiency, it does not withstand hard images, i.e., difficult to extract text from images. The solution is to consider color information. Also false-positive rate should consider an issue based on the applications using this system.

References

1. K. Jung, I. Kim, A.K. Jain, Text information extraction in images and video: a survey. Pattern Recogn. **37**(5), 977–997 (2004)
2. K. Zhang, Y. Sheng, J. Li, Automatic detection of road traffic signs from natural scene images based on pixel vector and central projected shape feature. IET J. Intell. Transp. Syst. **6**(3), 282–291 (2012)
3. Y.F. Pan, Y. Zhu, J. Sun, S. Naoi, Improving scene text detection by scale-adaptive segmentation and weighted CRF verification, in *International Conference on Document Analysis and Recognition* (2011), pp. 759–763
4. D. Maryam, M. Rahmati, A hybrid approach to localize farsi text in natural scene images. Procedia Comput. Sci. **13**, 171–184 (2012)
5. K. Zhu, F. Qi, R. Jiang, L. Xu, Automatic character detection and segmentation in natural scene images. J. Zhejiang Univ. Sci. A **8**(1), 63–71 (2007)
6. J. Park, G. Lee, A robust algorithm for text region detection in natural scene images. Can. J. Electr. Comput. Eng. **33**(3/4), 215–222 (2008)
7. J. Weinman, E. Leaarned-Miller, A. Hanson, Scene text recognition using similarity and a lecxicca with sparse belief propogation. IEEE Trans. Pattern Anal. Mach. Intell. **31**(10), 1733–1746 (2009)
8. J. Lafferty, A. McCallum, F. Pereira, Conditional random fields: probabilistic models for segmenting and labelling sequence data, in *Proceedings 18th International Conference Machine Learning* (2001), pp. 282–289
9. L. Winger, J.A. Robinson, M.E. Jernigan, Low-complexity character extraction in low-contrast scene images. Int. J. Pattern Recogn. Artif. Intell. **14**(2), 113–135 (2000)
10. K. Jung, K. In Kim, A.K. Jain, Text information localization in images and video: a survey. Pattern Recogn. **37**(5), 977–997 (2004)
11. H.K. Kim, Efficient automatic text location method and content based indexing and structuring of video database. J. Vis. Commun. Image Represent. **7**(4), 336–344 (1996)
12. C. Strouthopoulos, N. Papamarkos, A.E. Atsalakis, Text localization in complex color documents. J. Pattern Recogn. **35**, 1743–1758 (2002)
13. C.-W. Liang, P.-Y. Chen, DWT based text localization. Int. J. Appl. Sci. Eng. **2**(1), 105–116 (2004)
14. N.G. Bourbakis, A methodology for document processing: Separating text from images. Eng. Appl. Artif. Intell. **14**, 35–41 (2001)
15. M. Moradi, S. Mozaffari, A.A. Orouji, Farsi/Arabic text localization from video images by corner detection, in *6th, IEEE, Iranian Conference on Machine Vision and Image Processing* (2010)

Enhanced Certificate-Based Authentication for Distributed Environment

A. Jesudoss and N.P. Subramaniam

Abstract The unsecured open network is full of threats, viruses, and malicious Trojans. Digital certificates are one fundamental approach for providing safe and sound online security. In this paper, we propose a system that enables organizations to act as a CA and issue digital certificates to their clients. The client uses the certificates to access the services from the organization. The advantage of the proposed system is that it is more secure and faster than the other traditional systems. The various attacks relating to digital certificates were analyzed, and appropriate measures were suggested. These measures were considered in developing the proposed system. The paper also describes the procedure for generating, issuing, and revoking certificates and how it is implemented using Java platform.

Keywords Digital certificate · Certification authority · SSL · Public key certificate · X.509 certificate · Keystore · Truststore

1 Introduction

A digital certificate is used for establishing one's identity on the Internet. It ensures that the Web site is legitimate and data or software available on the site is provided by the identity specified there in the certificate. The digital certificates use public key cryptography, and hence, it is called a public key certificate. With PKI, it is possible to encrypt and decrypt using public–private key pairs. But it would not be possible to prove that the data are sent by a particular person. Hence, digital certificate gives the proof of identity for the sender [1] (Figs. 1 and 2).

A. Jesudoss (✉)
Faculty of Computer Science and Engineering, Sathyabama University, Chennai, Tamil Nadu, India
e-mail: jesudossas@gmail.com; jesudoss.mca@sathyabamauniversity.ac.in

N.P. Subramaniam
Department of EEE, Pondicherry Engineering College, Puducherry, India

© Springer India 2015

L.P. Suresh et al. (eds.), *Artificial Intelligence and Evolutionary Algorithms in Engineering Systems*, Advances in Intelligent Systems and Computing 325,
DOI 10.1007/978-81-322-2135-7_71

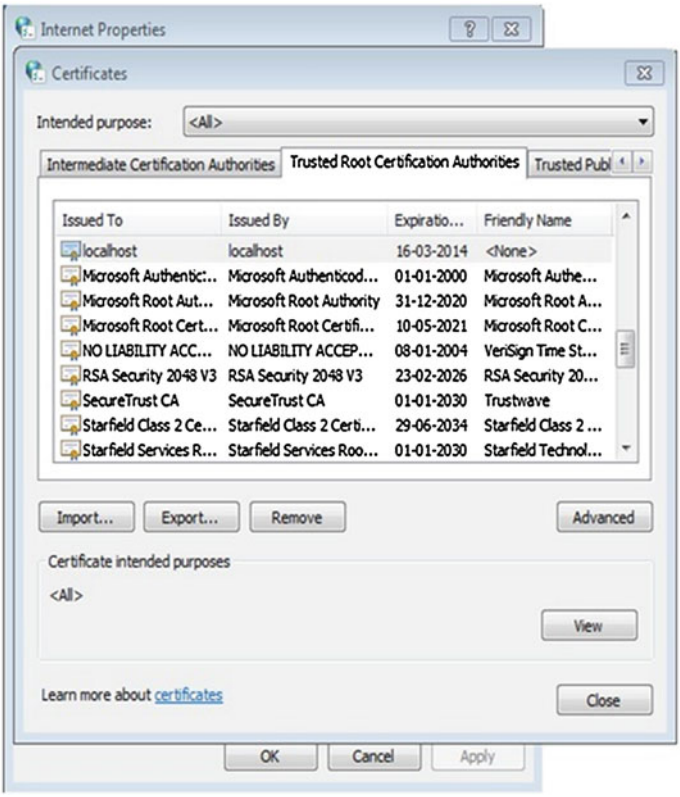

Fig. 1 Certificate listed among other certificates (*Source* Chrome browser's Internet properties)

Certification authority (CA) is an entity or organization which has the repository of public keys and the identity of the corresponding owners. Without CA, the digital certificate by itself cannot prove one's identity. If the certificate can be compromised, then the Web site can be spoofed and upload various software or tools containing malware which appears to be a legitimate software from the original company. The major vulnerability with digital certificates is due to improper management of the certificates and especially when the certificates get expired. The X.509 is an ITU-T international standard for defining the format of digital certificates and is the widely used standard. X.509 was issued as X.500 standard initially on July 1998. The X.509 certificate file extensions are usually are.cer, .crt, etc. VeriSign was acquired by Symantec in the year 2010. Today, Symantec is the largest CA under the earth. The self-signed certificate is a certificate for proving one's identity. The identity it certifies and the identity who signs it are the same person.

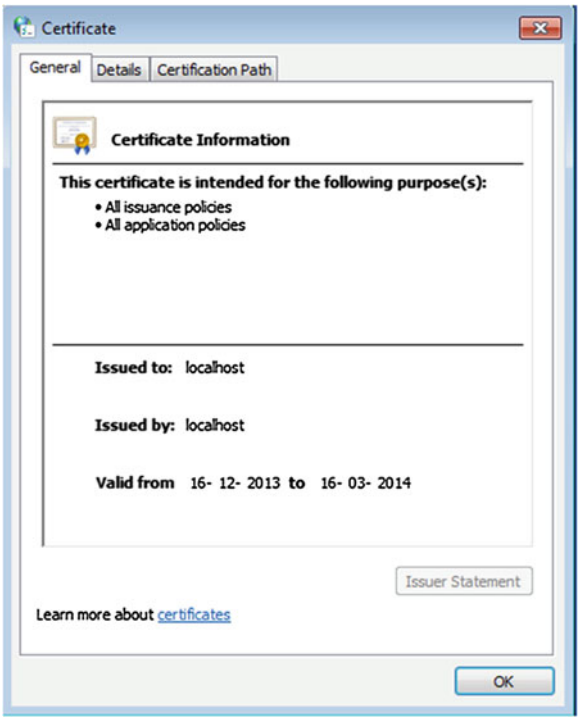

Fig. 2 Certificate information (*Source* Google Chrome certificate)

2 Existing Work

Digital signatures can be used only to verify the integrity of the message and not for authenticating the person transmitting the message. Hence, digital certificates are essential to prove the identity of the person [2]. X.509 certificates can be used to enhance the security. Generally, they use the RSA algorithm, but elliptic curve cryptography (ECC) can be used for better security and performance, because ECC is more secure and faster than RSA algorithm [3]. It would be advantageous to generate the signing key using biometrics rather than depending on some hardware device [4]. Biometrics helps to identify one's biological characteristics such as fingerprint, handprint, iris, retinal scan, voice recognition, and face recognition [5]. But it is not possible to implement practically due to the inability to measure accurately and hill-climbing attacks. The attacks on digital certificates can be minimized by securing the browser and other verification softwares involved in the verification process. Moreover, there must be provisions to upgrade the software. For additional security, the software must be validated each time it is started [6]. When the software or the browser is not updated, it opens the door for the hackers. X.509 certificates can be replayed once it is known to the verifier. A generalized digital certificate (GDC) can be used for authentication and sharing a secret key without revealing it to the verifier [7]. GDC does not include the public key of the

user [8]. Identity-based cryptography uses private key generator (PKG), which is used for generating the private key to the users. Since the private key is known to PKG, it can used to forge the digital signature of any user. CL-PKC (certificate-less public key cryptography) can be used to solve such forgery [9]. Digital certificates can be used not only for authentication purpose, but also for authorization purpose [10]. It must be machine processable so that it can be automatically verified [11]. The signature of the signed document cannot be affected by changing its filename. Changing a bitmap file to .html file makes the content of the file to be dynamic [12]. The concept what you see is what you sign (WYSIWYS) unravels the ambiguity problem in signing digital documents with dynamic content.

3 Attacks Against Digital Certificates

In 2012, Microsoft had become a victim of man-in-the-middle (MITM) attack. The attackers could compromise the certificate issues and gained access over multitude of computers. Then, attackers injected a Flame malware into the network and gained access. The attackers have used the vulnerability in the algorithm used for signing the certificates. Three attacks were made against the CAs in the year 2011. The attacks were against Comodo, DigiNotar, and StartCom [13]. Two were successful, and attack against StartCom was not successful. Evidences proved that the attack was from an Iranian IP address. The hacker used the credentials of the reseller for requesting the digital certificates from Comodo. But it was detected within an hour, and the certificate was revoked. Such attacks can be prevented by relying on root CAs such as VeriSign Inc., GlobalSign, Thawte, GoDaddy, CyberTrust, Equifax, and Entrust. When a certificate is revoked by a CA for some reasons, it must be properly notified to its customers those who relied on that certificate. Hardware devices can be used to protect the secret keys [14]. SSL certificates can be spoofed using null-termination attack [15].

4 Procedure for Issuing Digital Certificate

The applicant generates a key pair of public and private keys. Applicant can register with the CA by providing his public key with some additional proof of identity such as PAN card number, email address, and mobile number. This requirement varies from CA to CA. This information is encrypted with the CA's public key. The CA after verifying the identity of the applicant issues a digital certificate that is signed with CA's private key. The digital certificate contains the items given below:

1. Version
2. Digital certificate serial number
3. Applicant's public key

4. Identity name
5. Expiry date of the public key
6. Name of the organization issued
7. Digital signature of the issuer.
8. Signature algorithms and its parameters

The certificate confirms that the public key belongs to the identity specified therein. The public key of CA is publicly available to everybody. The sender or the applicant uses his private key for encrypting the message, and then, the message is attached with the digital certificate.

5 Procedure for Verifying Digital Certificate

The client requests for a secured connection over HTTPS and first obtains the digital certificate of the server. The receiver to decrypt the message obtains the public key of the sender from the digital certificate that is attached to the message. The receiver must use the public key of CA for decoding the certificate attached in the message and obtains the sender's public key. When the receiver is able to verify the certificate whether it has been issued by the CA using CA's public key, he can also trust the certificate and the public key obtained from the digital certificate. Hence, the public key and the corresponding identity specified in the certificate are attested by the CA, and it can be trusted. The most important drawback is if the CA is compromised, then the entire security is at stake. Another drawback is due to Web site spoofing. The user may enter the user credentials without verifying the certificate. The CA's public key sent by the fake Web site will match with the private key of the fake Web site. So there is nothing under the sky that prevents the user from accessing sensitive data. The message is encrypted using public key by the user and private key used by the bank. Then, nobody can intercept or read the message on the fly. That is, when the client encrypts using public key and server decrypts using private key, there is server authentication. The client knows for sure that it can be decrypted only by the server, since the secret key is held by the server only.

6 Procedure for Revoking Digital Certificate

The digital certificate is valid only for a specified amount of time period. The expiration date of the certificate is included within the certificate itself. So when it gets expired, it can be revoked. The CAs can revoke the certificate issued by them on request from the certificate holder. The CRL may be revoked before the expiration of the certificate for the following reasons:

1. Private key of the user is compromised.
2. Certificate of the CA is compromised.
3. CA does not certify the person anymore.
4. Any information pertaining to the person certified has been changed.
5. The certificate is not required anymore as the purpose has been fulfilled.
6. The password of the person certified got stolen.
7. There is a change in the security policy of the certification authority.

7 Implementation of Digital Certificates

The Java platform (JDK1.7.0_u45) is used for developing the application. The LDAP server used is Open DS 2.2.1. The IDE used for developing the application is NetBeans IDE 7.4. The SSL connection must be established from Web server to Web client. The administrator login is required to configure SSL. The keytool.exe is a tool available in JDK1.7 for generating digital certificates. The following commands are used to generate key pairs and digital certificate.

```
Keytool −genkey −alias AuthServer −keyalg RSA −keypass changeit
−storepass changeit −keystore ks .jks
```

This command is for generating a key pair and for wrapping the public key inside self-signed certificate. The default password used is changeit. It is stored in the keystore file ks.jks. The file extension .jks is a java key store file. The keyalg option specifies the algorithm used for generating key pair. The keypass option is used for protecting the private key. The option alias specifies the third-party CA. The alias option is used to access the keystore. When alias is used, an entity is added to the keystore. Therefore, generated digital certificate is stored into ks.jks.

```
Keytool − export − alias AuthServer − storepass changeit
                                −file ServCert.cer − keystore ks.jks
```

This command is used for exporting digital certificate to a ServCert.cer file. The certificate is stored in ServCert.cer file.

```
Keytool − import − v − trustcacerts − alias AuthServer − file ServCert.cer
− keystore CACertificates.jks − keypass changeit − storepass changeit
```

This command is used to add the certificate to the CACertificates.jks, the truststore file.

Keytool −list −v − keystore ks.jks

This command is used to verify whether the certificate has been added to the keystore successfully.

Keytool −list −keystore CACertificates.jks

This command is used to verify whether the certificate has been added to the truststore successfully. The certificate nickname should be changed from "server-alias" to "AuthServer." The default port used is 4444, which is blocked by the firewall. It can be changed by accessing control panel- > firewall- > advanced settings- > Inbound Rules- > New Rule- > port- > TCP 4444- > Allow the connection if it is secure→add users and name the rule. Fig. 3 shows how the port 4444 blocked by firewall is configured to allow connection through this port. Given below are the Internet properties of the Google Chrome browser.

The certificates button in Fig. 4 shows various certificates that are verified and trusted. The certificates can be imported here. The certificates are essential while accessing the protected site using SSL protocol. The keystore is used to store private key and the certificates holding public key. It gives information about the user credentials. Keystore is on the SSL server side to establish client authentication. Keystore stores SSL server certificate which the server shows to the client

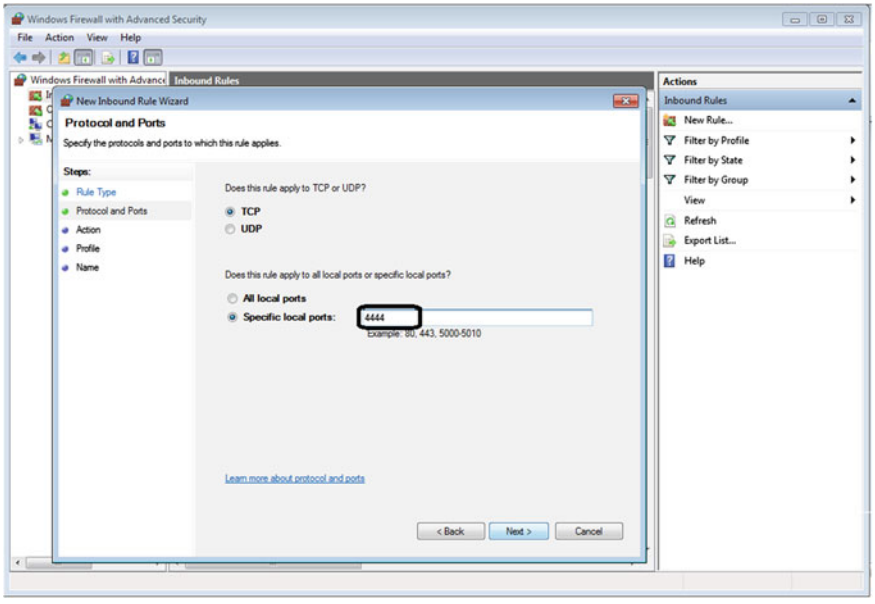

Fig. 3 New rule created to allow port 4444 (*Source* Microsoft Windows 7 Windows firewall with advanced security)

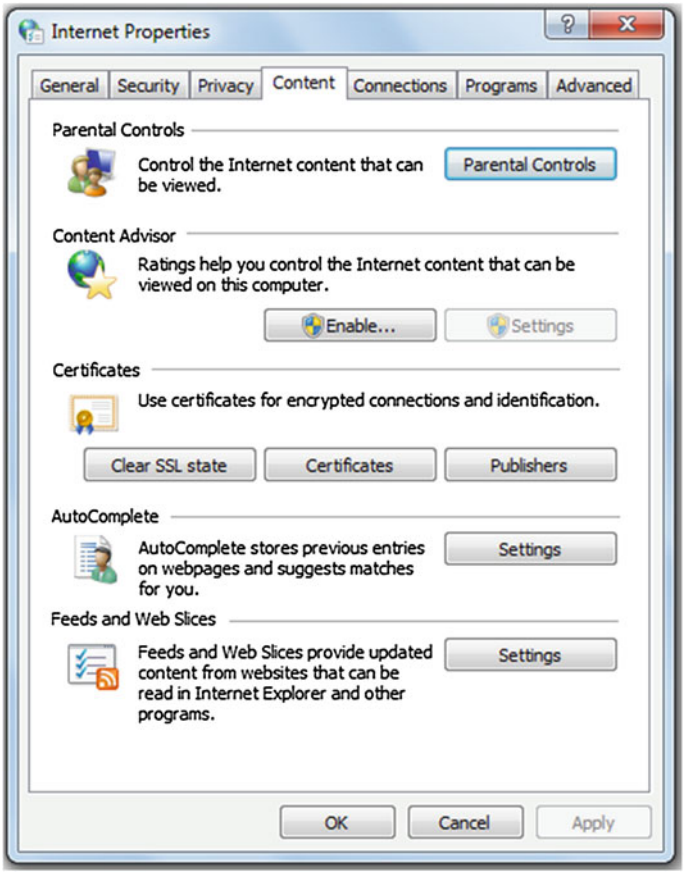

Fig. 4 Browser certificate settings (*Source* Google Chrome browser's Internet properties)

when SSL connection is made. Using keytool command, the list of certificates in keystore can be listed.

Keystore is used only if SSL runs on the server side or client authentication is required on the server end. Truststore contains a public key and corresponding certificate issued by the CA. Hence, it is used on the SSL client for verifying the credentials.

8 Results

The keytool utility is available in JAVA_HOME\bin folder. It can be created to create digital certificates as given in Fig. 5. The generated certificate must be added to a trust store as given in Fig. 6.

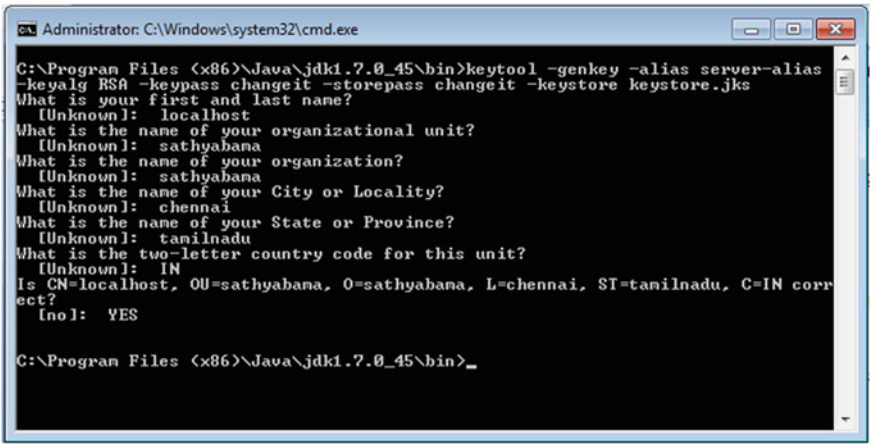

Fig. 5 Digital certificate created

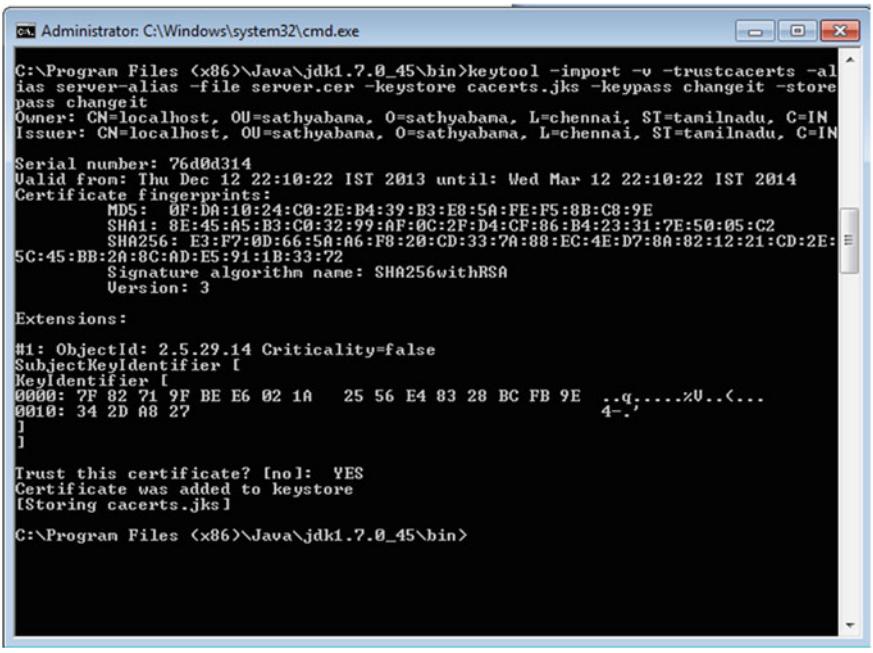

Fig. 6 Certificate added to a truststore

Further, the certificate added to the trust store should be verified and appropriate SSL configuration settings change should be done.

9 Conclusion and Future Work

The ultimate reason for the vulnerability of the digital certificates exists due to the poor administration of the certificates. Therefore, the underlying technology or the encryption techniques cannot be responsible for such vulnerability as discussed above. Although the security mechanism surrounding the certificate is effective, if the certificate is compromised, then the entire benefits will be in vain. In order to resolve the certificates issues, it is mandatory to understand the basic problem that had been the root cause for the vulnerability. Deploying certificate management systems helps to identify whether the certificate got expired and when it is to be renewed. This reduces the risk of certificates getting expired without any notification. The users will also be informed about the certificate expiration and whereabouts. We plan to extend this work by including biometric system for digital certificates. A mechanism for updating required patches for the software and browser as well may be considered, and the expiry of the certificates can be automated.

References

1. V.S. Bismin, A. Jose, Secure communication using generalized digital certificate. Int. J. Comput. Appl. Technol. Res. **2**(4) 396–399 (2013)
2. R. Guida, R. Stahl, T. Bunt, G. Secrest, M. Joseph, Deploying and using public key technology: lessons learned in real life. IEEE Secur. Priv. 67–71 (2004)
3. M.-D. Cano, R. Toledo-Valera, F. Cerdan, in *A certification authority for elliptic curve X.509v3 certificates*. Proceedings of ICNS'07 (2007), p. 49
4. K.H. Kaluvuri, F. Di Cerbo, A. Mana, in *Security assurance of services through digital security certificates*. Proceedings of ICWS 13 (2013), pp. 539–546
5. L. Fen, L. Quan, P. Liaojun, P. Qingqi, in *Identity authentication based on fuzzy vault and digital certificate*. Proceedings CIS 10 (2010), pp. 441–445
6. T. Kwon, J. Lee, in *Practical digital signature generation using biometrics*. Proceedings of ICCSA 2004 (2004), 728–737
7. R.M. Anthony, L.E. Randy, Security technology for smart grid networks. IEEE Trans. Smart Grid. **1**(1), 99–107 (2010)
8. K.-A. Shim, On the security of a certificateless aggregate signature scheme. IEEE Commun. Lett. **15**(10) 1136–1138 (2011)
9. L. Harn, J. Ren, Generalized digital certificate for user authentication and key establishment for secure communications. Proc. IEEE Trans. Wireless Commun. **10**(7), 2372–2379 (2011)
10. Z. Gao, Z. Li, Y. Tu, in *Design and completion of digital certificate with authorization based on PKI*. Proceedings of the IEEE International Conference on Information Reuse and Integration (2004), pp. 462–466
11. F. Buccafurr, Digital signature trust vulnerability: a new attack on digital signatures. ISSA J. 24–28 (2008)
12. N. Levitt, Internet security under attack: the undermining of digital certificates. IEEE Comput. Soc. 17–20 (2011)
13. J. Dittmann, P. Wohlmacher, K. Nahrstedt, Using cryptographic and watermarking algorithms. IEEE Multimed. Secur. 54–65 (2011)

14. Thawte.com official website. (2012), http://www.thawte.com/code-signing/whitepaper/best-practices-for-code-signing-certificates.pdf
15. Security Dark Reading website. (2009), http://www.darkreading.com/vulnerability/black-hat-pki-hack-demonstrates-flaws-i/218900008

Diagnosis and Segmentation of Brain Tumor from MR Image

S.V. Srinivasan, K. Narasimhan, R. Balasubramaniyam and S. Rishi Bharadwaj

Abstract Abnormal growth of tissues inside the brain leads to the formation of brain tumor. In order to decrease the mortality rate due to brain tumor, efficient techniques for the earlier detection of the tumors are required. The present-day technological advancements include the magnetic resonance imaging (MRI) scans, computed tomography (CT) scans, and advanced X-rays which help us in tumor detection. The MRI scans are widely used nowadays because of its noninvasive radiation and the accuracy of the images. This paper proposes a strategy for efficient detection of a brain tumor in MRI brain images. The system proposed in this paper is a handy tool for accurate prediction and segmentation of brain tumor. The general properties of the images called the gray-level co-occurrence matrix (GLCM) features and the spatial feature (mean) are combined with the transform domain-based discrete cosine transform (DCT) features that are extracted from the MR images are used as feature sets. Support vector machine (SVM) is used as the classifier which classifies the images as tumorous or non-tumorous. Once the classification is done using SVM classifier, the tumorous images are alone subjected to watershed transform-based segmentation to exactly extract the tumor region alone. The entire experiment is conducted on the images of various patients acquired from MEDALL DIAGNOSTICS, Tiruchirappalli, India. The method gives accuracy of over 99 %, hence improving the chances for the patients' survival by proper detection of tumors at an early stage.

Keywords MRI · SVM · DCT coefficients · GLCM properties · Tumor region · Segmentation · Watershed

S.V. Srinivasan · K. Narasimhan (✉) · R. Balasubramaniyam · S. Rishi Bharadwaj
School of Electrical and Electronics Engineering, Sastra University, Thanjavur, India
e-mail: knr@ece.sastra.edu

S.V. Srinivasan
e-mail: svsrinivasan92@gmail.com

© Springer India 2015

L.P. Suresh et al. (eds.), *Artificial Intelligence and Evolutionary Algorithms in Engineering Systems*, Advances in Intelligent Systems and Computing 325,
DOI 10.1007/978-81-322-2135-7_72

1 Introduction

Medical imaging is one of the most prospering fields in today's world as it deals with the detailed analysis of the human anatomy. The enormous improvement in this field should be credited to the various techniques and processes used to create anatomical images of the human body. Though different modalities are used to obtain medical images, magnetic resonance imaging (MRI) is widely preferred. It uses powerful magnetic fields and radio frequencies to produce the cross-sectional view of the soft tissues, the ligaments, and the internal organs. Moreover, the differences between the normal and abnormal images are clearer in the MRI than the computed tomography (CT) or X-ray. The disadvantages include the noise and the duration for which the patient is subjected to the scanning. Both normal and abnormal images will be present in brain images. On the first visual inspection, the abnormalities are often understood by checking for the axial and coronal symmetry of the images. When the asymmetry is widely observed, a decision can be made easily. But further examination alone can help better detection. The next step is to classify the images into two groups based on an algorithm. Lots of methods are used for this classification. These include neural networks, k-nearest neighbor fuzzy C, and support vector machine (SVM). Xuan and Liao [1] considered both normal and defective brain images and performed structural analysis, and this leads to three features, namely intensity, symmetry, and texture. Statistical validation is a great tool to help with fractal dimension analysis which characterizes the images based on the surface roughness. This was proposed by Iftekharuddin et al. [2]. The diffusion tensor imaging (DTI) is also a new detection technique which monitors the flow of white matter, and this snapshot of the brain is used to compare and find the changes in the images over the time. Generally, the SVM-based classifier has superior performance [3, 4]. The SVM stands on the following points—optimal hyperplane for patterns that are linearly separable. For patterns that are not linearly separable, it is done by transformation of original data to map into new space with the various kernel functions. While separating the vectors, the data points very close to the vectors are called as support vectors. It is extremely difficult to classify these vectors as they have direct bearing on the optimum location of the decision surface. SVM maximizes the margin around the separating hyperplane because it is a constructively learning algorithm. SVM's computational efficiency and its generalization capability make it one of the finest pattern classifiers as suggested by recent studies. According to El-Dahshan et al. [5], the accuracy of the various methods for classifying brain tumor in MR images depends highly on the feature set used and the classifiers used. According to the author, the accuracy rates differ from 94.3 % to around 99.7 % (Table reference El-Dahshan et al. [5]).

1.1 Materials and Methods

The MRI brain database was collected from a renowned scan center in Tiruchirappalli, India, called MEDALL DIAGNOSTICS. Around 303 images were collected and were labeled as tumor or normal with the help of physicians. The processing of these images was carried out with the help of MATLAB r2013a. The image processing toolbox and the statistical toolbox includes algorithms for sequential feature selection which lets us identify the impact of the features using supervised and unsupervised machine learning are widely used throughout this work.

1.2 Proposed Method

The method mainly constitutes of three modules.

Feature extraction is the first step followed by classification of the images as normal or tumorous based on the features using SVM classifier, and the next step is segmentation and extraction of the tumor from the abnormal image using watershed transform.

The block diagram is as follows:

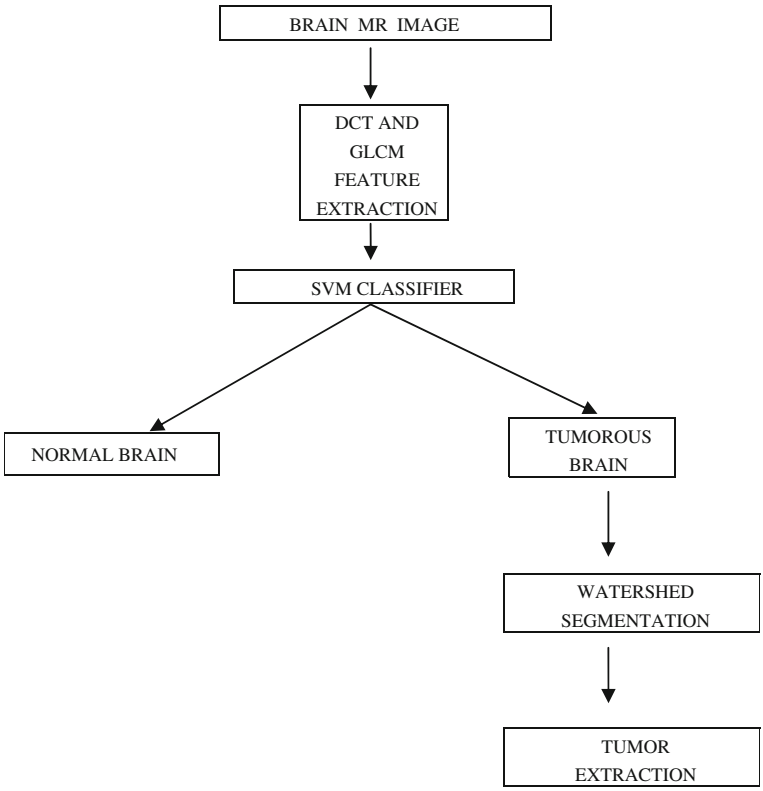

2 Feature Extraction

Approaches to feature analysis are usually categorized as follows:

- Structural,
- Statistical,
- Transform based.

The structural features are often difficult to analyze, and also, the analysis of the image is not fully effective in classifying the images. In the proposed method, we extract the statistical features and transform-based discrete cosine transform (DCT) features. The statistical approach exploits the statistical properties of image or image regions in a bottom-up fashion, starting from the pixel values in the neighborhood. The co-occurrence matrix is in wide use in representing the dependence in the distributions of gray level. The co-occurrence matrix is a function of (1) the image region, (2) a displacement vector $d = (dx, dy)$, and (3) the number of gray levels after quantization. The matrix contains frequencies of co-occurrence of two gray levels. After normalization, it becomes a probability matrix with all the elements summing up to 1.

2.1 Gray-Level Co-occurrence Matrices

The pixel values present in the image often differ from each other in almost a linear fashion. The tabulation of the frequency of this pixel value change is generally termed as the gray-level co-occurrence matrix (GLCM). It is a very powerful method for improving the details, and as a result, it helps us for better interpretation of an image. GLCM was introduced by Haralick et al. in 1979 [6] and some authors, Carstensen (2002),Cooper (2004), Basset (2000), Barber et al. (1993), and Lefebvre et al. (2000). They had suggested that the GLCM could describe the probability of finding pixels of gray-level values i and j at a given displacement h. Considering an element c that represents the frequency with which a point in an image with a gray level (say x) occurs in a position which is relative to another gray level (say y), now the element c can be considered as the GLCM element. Now, by dividing the element c by the total number of pixel values, we get the normalized GLCM.

With the help of the inbuilt MATLAB functions for GLCM, the following details are inferred:

- Contrast,
- Correlation,
- Homogeneity,
- Energy.

Contrast	The difference in intensities between each and every pixel can be measured as the contrast.
Correlation	This is a measure of correlation of a pixel with its neighbor over the whole image.
Energy	Squaring the elements in the GLCM and adding them gives the energy of the image.
Homogeneity	This is a measure of the closeness of the distribution of elements in the GLCM to the GLCM diagonal.
Mean	It measures the general brightness of an image.

2.2 Spatial Domain Feature (Mean)

In addition to the above-mentioned GLCM features, the mean of the image is also found by converting the entire matrix into column matrix and calculating the mean.

2.3 DCT Feature Extraction

According to Khayam et al. [7], in order to separate the image into individual spectral sub-bands, DCT is used. It is an added advantage that the spectral sub-bands are of differing nature with respect to the visual quality of the image. DCT has the property of separability and symmetry. The 2D DCT can be mathematically defined as follows:

$$F(u,v) = \left(\frac{2}{N}\right)^{1/2}\left(\frac{2}{M}\right)^{1/2}\sum_{i=0}^{N-1}\sum_{j=0}^{M-1}A(i)A(j)\cos\frac{\pi\cdot u(2i+1)}{2\cdot N}\cos\frac{\pi\cdot v(2j+1)}{2\cdot M}f(i,j)$$

We take the 2D DCT of the image, and the resulting coefficients are taken as transform domain features. In order to avoid complexity we have taken the largest 7 coefficients as features (according to Q.-U. Ain et al.).

2.4 Classification

SVM is used for data classification. All the training data are associated with a corresponding target with which the kernel functions are specified. The SVM is supposed to produce the output which predicts the target value of data in the testing

set. After the feature extraction, a linear kernel SVM function is used to classify the MR images as tumor-affected and normal brain images. In order to verify the stability of the SVM system, around 122 images were given as inputs of which 70 % of the images were used for training and the remaining 30 % were used for testing. The results of the classification are accurate enough to classify an image as normal or tumor-affected brain image. It offers more accuracy than the kNN classifier or Bayesian classifier.

2.5 Segmentation

After the classification of the images, the tumorous images are subjected to segmentation techniques and the tumor portion alone is segmented. Before the actual segmentation is done, preprocessing of the images is performed [8]. All the MR images are converted to grayscale images of size 515 × 512. The image is then histogram-equalized, and then, in order to remove the noise present, the images are subjected to median filtering.

The segmentation proposed in this paper is watershed segmentation. It is one of the best methods used for segmentation as it deals with the grouping of pixels based on their intensities. For watershed segmentation, the following two points are taken into account:

1. A local minimum is computed. That minima and its gradient are chosen as markers.
2. With the help of the defined marker positions from the above step, the necessary watershed transformation is taken over the marker image.

After this, morphological operations of opening and erosion are performed in order to get the desired tumorous portion.

3 Results

Following the above classification methodology in MATLAB r2013a, the tumorous images are classified with the following accuracy (Fig. 1):

- Correct rate: 1
- Error rate: 0
- Classified rate: 1
- Sensitivity: 1
- Specificity: 1

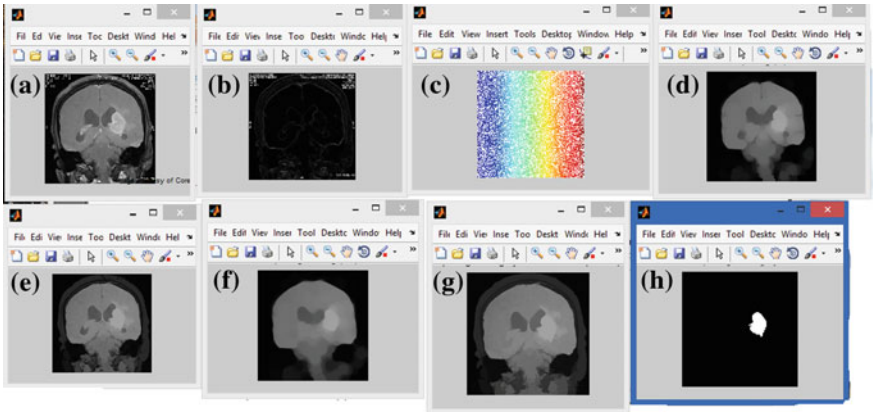

Fig. 1 **a** is the original image, **b** shows the preprocessed image, **c** shows the watershed transformation of the **b**, **f–g** shows the morphological operations of opening and erosion, and **h** shows the tumorous region alone

4 Conclusion and Future Work

Thus, the tumor region alone is segregated from the image. The next step is to measure the structural properties such as shape and size of the extracted tumor. The prime aim of measuring the properties such as the size and density of the tumor is to create a clinical decision support system (CDSS), thus aiding the physicians in treating the tumor with a better precision and more accuracy.

References

1. X. Xuan, Q. Liao, in *Statistical structure analysis in MRI brain tumor segmentation*. Fourth International Conference on Image and Graphics (2007), pp. 421–426
2. K.M. Iftekharuddin, J. Zheng, M.A. Islam, R.J. Ogg, F. Lanningham, in *Brain tumor detection in MRI: technique and statistical validation*. Fortieth Asilomar Conference on Signals, Systems and Computers (2006), pp. 1983–1987
3. O. Li, T. Adal, V.D. Calhoun, A feature-selective independent component analysis method for functional MRI. Int. J. Biomed. Imaging **2007**(15635) (2007)
4. L. Liang, V. Cherkassky, D.A. Rottenberg, in *Spatial SVM for feature selection and fMRI activation detection*. Neural Networks IJCNN'06 (2006), pp. 1463–1469
5. E.S.A. El-Dahshan, A.-B.M. Salem, T.H. Younis, A hybrid technique for automatic MRI brain images classification. Studia Univ, Babes Bolyai, Informatica LIV (2009), pp. 55–67
6. R.M. Haralick et al., Statistical and structural approaches to texture. Proc. IEEE. **67**(5), 786–804 (1979)
7. S.A. Khayam, The discrete cosine transform: theory and application. WAVES lab technical report (2004)
8. C.P. Rajesh, A.S. Bhalchandra, Brain tumour extraction from MRI images using MATLAB. Int. J. Electron. Commun. Soft Comput. Sci. Eng. **2**(1). ISSN: 2277-9477

Improving the Accuracy of Latent Fingerprint Matching Using Texture Descriptors

V. Dhanusha and T.R. Swapna

Abstract Fingerprint matching is a process used to check whether two sets of fingerprint come from the same finger of a person. There are three types of fingerprints in law enforcement applications such as rolled, plain, and latent. Latent fingerprints are partial fingerprint, obtained from the surfaces of objects where a person has touched. It may or may not be an accidental touch. Latent fingerprint contains small area of prints as compared to full fingerprints. We cannot apply a full fingerprint matching algorithm for the latent fingerprint matching. Matching between a latent and a rolled print is a complex task because the number of minutia points will be less. Enhancement of fingerprint is necessary due to low quality of latents and sensor noise. We have done latent fingerprint matching using Hough transform algorithm. Experimental results on NIST latent fingerprint database show an accuracy of 54.43 %. We have enhanced the accuracy by incorporating texture-based features like entropy, correlation, contrast, homogeneity, and energy.

Keywords Fingerprint matching · Automatic fingerprint identification systems · Ridge bifurcation · Image texture

1 Introduction

Fingerprints remain a vital index for human recognition. In the field of security, series of automatic fingerprint identification systems (AFIS) has been already developed. The fingerprint recognition problem can be of two types: fingerprint verification and fingerprint identification. The process of checking the authenticity

V. Dhanusha (✉) · T.R. Swapna
Department of CSE, Amrita School of Engineering, Amrita Nagar PO,
Coimbatore 641112, India
e-mail: dhanusha.v3@gmail.com

T.R. Swapna
e-mail: tr_swapna@cb.amrita.edu

© Springer India 2015

L.P. Suresh et al. (eds.), *Artificial Intelligence and Evolutionary Algorithms in Engineering Systems*, Advances in Intelligent Systems and Computing 325,
DOI 10.1007/978-81-322-2135-7_73

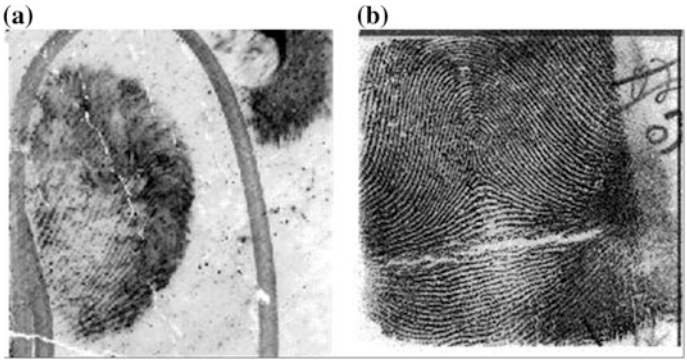

Fig. 1 **a** Latent, **b** corresponding full fingerprint [22]

of person by fingerprint is called fingerprint verification. Fingerprint identification is to specify one person's identity by his fingerprint(s). One of the major tasks in the field of security is the degree with which they appropriately verify or identify inputs. It is generally identified by the quality of images and the capability of the algorithm. Each person has his own fingerprints with the permanent uniqueness. Latent fingerprint matching is mainly used for crime detection.

Fingerprint contains patterns, called ridges and valleys. Using the ridge parameters, the uniqueness of a fingerprint is defined. Ridges are curved lines in a fingerprint. Valleys are space between two ridges. Ridge crossing points are called ridge bifurcation. Ridge ending and crossing between two ridges are considering as minutiae points. These points are used for matching purpose (Fig. 1).

2 Related Work

The reasons for difficulty in matching include poor quality of images, small print area, and large nonlinear distortion due to pressure variations. For increasing the accuracy of latent matching algorithms, more features including minutiae have to be used, as is typically done by latent examiners in the ACE-V procedure [1].

2.1 Enhancement Algorithms

The quality of the fingerprint images affects the performance of the minutiae extraction. In order to improve the functioning of the system, many suggestions have come from researchers. Modified Gabor filtering (MGF) algorithm replaces the traditional Gabor filter (TGF) algorithm [2]. In TGF, there are some drawbacks

such as image-dependent parameter selection strategy. In MGF, its parameter selection scheme is image independent [2]. Another algorithm called ridge-based algorithm improves the clarity of ridge and furrow structures.

Another algorithmic scheme for automatic fingerprint recognition includes extracting the bifurcation of a ridge and matching with the templates [3]. There exists an algorithm based on filtering banks proposed by Feng and Zhou [4]; the algorithm decomposes a fingerprint image into directional sub-band images in the analysis stage, processes the sub-band images in the processing stage, and reconstructs them as the enhanced image in the synthesis stage. Sen and Yangsheng presented a new method of filtering to enhance the singular point area. They first distinguished the singular point area. Then, they designed a new filter to enhance this area [5]. Experimental results show that their enhancement algorithm is capable of improving the quality of fingerprint image and the accuracy of the minutiae extraction.

2.2 Fingerprint Texture Descriptors

A fingerprint can be sighted as oriented textures like ridges. Orientation-based descriptors were extended to texture-based descriptor by adding ridge frequency information [6]. Gradient information captured in scale-invariant feature transform (SIFT) descriptor is not as stable as ridge orientation [7]. Fourier-based spectral texture feature is used for detecting latent fingerprint in low-resolution grayscale images [8]. Texture correlation can be used for verification of fingerprints [9]. Rajbhoj and Mane proposed a method for capturing textural information by dividing each minutiae neighborhood locations into several local regions [10]. Jain et al. proposed a global representation of texture by decomposing the image into different frequency and orientation components [11].

Selvarajah had described two types of texture. They fall into two major categories: structural and statistical [12]. Statistical method characterizes texture by statistical distribution of image intensity. Structural method describes the texture by identifying structural primitives and their placement rules. Arun Ross proposed a method which includes combination of texture and minutiae-based matching. The matching score leads to a substantial increase in the total matching [13].

Texture feature calculation methods include Gabor wavelet transform, contourlet transform, steerable pyramid, and complex directional filter bank [14]. Advantage of steerable pyramid is that it supports any number of orientations. But computation and storage required is more. Advantage of contourlet transform is lower sub-bands decimated. Disadvantage is the number of orientations supported needs to be power of 2. Gabor wavelet transform achieves highest retrieval results, but it is computationally intensive. Complex directional filter bank achieves competitive retrieval results, but it is also computationally intensive.

2.3 Latent Fingerprint Matching

Latent fingerprint matching proposed by Jain et al. uses ridge skeleton and minutiae for matching [1]. Feng proposed a method in crime detection [15]. Choi et al. propose a method of combining minutiae descriptors for fingerprint matching process [16]. Yoon et al. proposed automatic segmentation of latent fingerprints for segmented output which requires a robust measure [17]. Latent fingerprint enhancement algorithm does not give excellent result for poor-quality latents [18] and better output for bad-quality latents.

For the matching purposes, we have to extract minutiae from the input fingerprint image. In addition to matching, fingerprint enhancement algorithm is needed in the minutiae extraction module. Minutiae-based matching method is the most widely used fingerprint matching method [6]. Fingerprint retrieval algorithm [4] is a front-end filtering algorithm which uses orientation field for fingerprint identification.

There are many transform algorithms used for matching fingerprints. Discrete Fourier transform (DFT) is one method, which is translation invariant, rotation resistant, and prevents geometric attack. It has the disadvantage of complex calculations when using images of size more than 256 × 256. Fast Fourier transform (FFT) requires lower computational complexity as compared to DFT [19]. Top hat transformation algorithm will not distinguish the small gray-level changes [20].

Hough transform algorithm is a robust alignment algorithm to measure similarity between fingerprints by considering both minutiae and orientation information. The merit of the Hough transform is that the pixels on a line need not all be adjacent. This is very useful when trying to identify lines with breaks in them due to noise. It is conceptually simple and can be implemented easily. It can be adapted to many geometrical shapes like curves, lines, etc [21].

3 Improving the Accuracy of Latent Matching Approach Using Texture Features

We propose to automate the process of fingerprint matching after reconstruction of latent fingerprints. We have done the Hough transform matching after the enhancement of input images. After feature extraction, we have to align the minutiae point for matching. From that alignment method, the similarity between the minutiae points is calculated using Hough transform. We incorporate texture-based features like entropy, correlation, contrast, homogeneity, and energy for improving the accuracy.

3.1 Enhancement Steps

Segmentation, normalization, local orientation estimation, ridge frequency estimation, region mask estimation, and filtering are the procedure done during enhancement of latent fingerprint. Segmentation leads to the calculation of variance for each pixel. Normalization is the process that changes the range of pixel intensity value. After that, local orientation of each pixel in a fingerprint image is computed. Ridge frequency is obtained from the extraction of the ridge map. Classification of pixels into retrievable or unretrievable is called masking. Filtering helps in removing noises (Fig. 2).

3.2 Feature Extraction

The feature extraction plays a major role in latent fingerprint matching. For the Hough transform algorithm, minutiae points are needed. Minutiae points are extracted for matching. They are specific points in a fingerprint image, determined by the termination or the bifurcation of the ridge lines (Fig. 3).

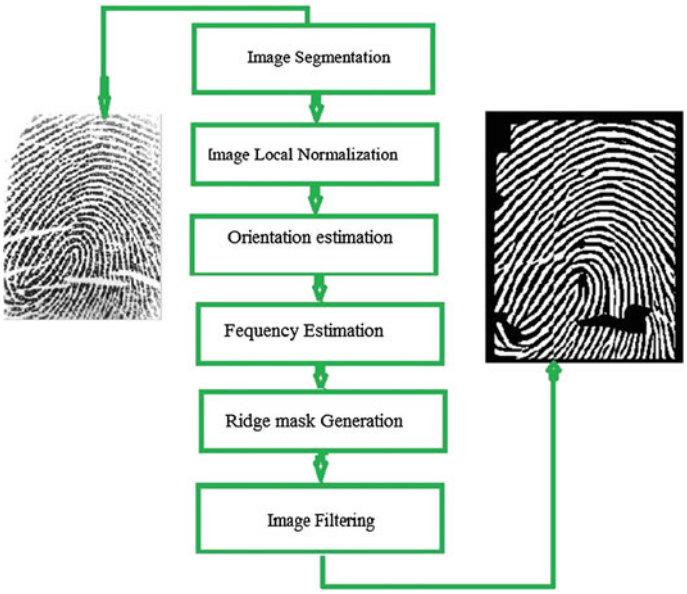

Fig. 2 Enhancement steps

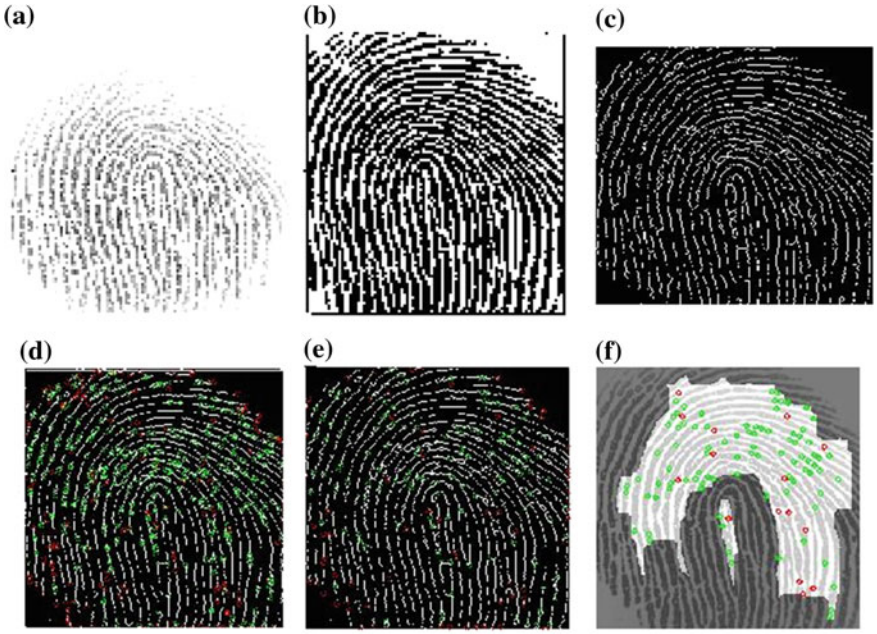

Fig. 3 **a** Input image, **b** smoothing, **c** thinning, **d** minutiae identification, **e** removal of false minutiae, **f** region of interest

3.3 Statistic-Based Pixel Features

To enhance the accuracy of latent fingerprint matching, statistical features like entropy, correlation, contrast, homogeneity, and energy are considered.

3.3.1 Energy (E)

Energy is the angular or uniform moment in an image. It is calculated by sum of squared elements in the pixel of an image I.

$$\mathrm{E} = \sum_{i,j} I(i,j)^2 \tag{1}$$

3.3.2 Correlation (Cr)

It is the correlation between a pixel to its neighborhood in an image

$$\mathrm{Cr} = \sum_{i,j} \frac{(i - ki)(j - kj)I(i,j)}{\sigma_i \sigma_j} \tag{2}$$

3.3.3 Entropy

The feature entropy is a statistical measure used to characterize the texture of an image. Dividing frequency by sum of pixel got the normalized values.

3.3.4 Contrast (Co)

Contrast is the variation in local pixel gray level, i.e., intensity contrast between a pixel and its neighborhood.

$$\mathrm{Co} = \sum_{i,j} |I - J|^2 I(i,j) \tag{3}$$

3.3.5 Homogeneity (H)

Homogeneity is the measure of closeness of distribution of pixels in an image.

$$\mathrm{H} = \sum_{i,j} \frac{I(i,j)}{1 + |i - j|} \tag{4}$$

We extracted features of latent and corresponding full fingerprints. Some of which are tabulated in Tables 1 and 2.

Using Manhattan distance as a metric, we calculated the difference in features of latent and full fingerprint. While considering only contrast, the system gave 63.6 % of accuracy. While considering only entropy, it gave 81.8 % of accuracy. When considering homogeneity, energy, and correlation, it gave 100 % of accuracy.

Table 1 Latent fingerprint features

Image	Contrast	Homogeneity	Correlation	Energy	Entropy
1	0.5657	0.8285	0.9491	0.0996	6.8737
2	0.2186	0.8967	0.9655	0.1363	7.4115
3	0.2623	0.8761	0.9508	0.1169	7.6932
4	0.4682	0.8055	0.8812	0.1217	7.3439
5	0.1836	0.9136	0.9651	0.1697	7.5482
6	0.1757	0.9155	0.9803	0.1723	7.1425
7	0.2196	0.9041	0.9664	0.1833	7.4318
8	0.4063	0.8435	0.9364	0.1131	7.616
9	0.1322	0.9346	0.9782	0.1198	7.7331
10	0.2727	0.8697	0.9412	0.1322	7.5121
11	0.1229	0.943	0.9878	0.1472	7.5869

Table 2 Matching full fingerprint features

Image	Contrast	Homogeneity	Correlation	Energy	Entropy
1	0.7464	0.7401	0.8465	0.0629	7.7806
2	0.5309	0.7877	0.8283	0.1124	7.1842
3	0.242	0.8796	0.9019	0.148	7.1612
4	0.529	0.7817	0.8015	0.1024	7.3552
5	0.8685	0.7314	0.8411	0.065	7.802
6	0.5816	0.7789	0.8958	0.1031	7.4965
7	0.6263	0.7609	0.8307	0.0872	7.4074
8	0.7545	0.7482	0.8832	0.0696	7.574
9	0.6755	0.7625	0.8709	0.0768	7.6566
10	1.2547	0.7218	0.8432	0.0934	7.458
11	0.9063	0.7212	0.8797	0.0527	7.9051

4 Conclusion and Future Work

We have done latent fingerprint reconstruction and matching using Hough transform algorithm scheme using NIST latent fingerprint database. It shows an accuracy of 54.43 %.Texture features are extracted by analyzing the fingerprint with statistical features. Extracted texture features from each cell are compared. It gave full accuracy to homogeneity, energy, and correlation. For entropy and contrast, it gave accuracy of 81.8 and 63.6 %, respectively. We would like to extend the matching for other statistical features also.

References

1. L. Hong, Y. Wan, A. Jain, Fingerprint image enhancement: algorithm and performance evaluation. IEEE Trans **20** (1998)
2. Loannis, Digital image processing algorithm and application (Wiley, New York, 2000). ISBN 0471377392
3. W. Sen, W. Yangsheng, Fingerprint enhancement in the singular point area. IEEE Signal Process. Lett. **11**(1) (2004)
4. J. Feng, J. Zhou, A performance evaluation of fingerprint minutia descriptors, in *Proceedings of International Conference on Hand-Based Biometrics* (2011)
5. X. Jiang, M. Liu, A.C. Kot, Fingerprint retrieval for identification. IEEE Trans. Inf. Forensics Secur. **1**(4), 532–542 (2006)
6. H. Hasan, S. Abdul-Kareem, Fingerprint image enhancement and recognition algorithms: a survey. Springer Neural Comput. Appl. **23**(6) (2013)
7. T. Kiertscher, R. Fischer, C. Vielhauer, *Latent fingerprint detection using a spectral texture feature*. ACM multimedia workshop on Multimedia and security (2011)
8. A.M. Bazen, G.T.B. Verwaaijen, S.H. GerezLeo, P.J. Veelenturf, B.J. van der Zwaag, A correlation-based fingerprint verification system, in *ProRISC 2000 Workshop on Circuits* (2000)

9. G. Aggarwal, N.K. Ratha, T.Y. Jea, R.M. Bolle, Gradient based textural characterization of fingerprints, in *IEEE International Conference on Biometrics* (2008)
10. S.M. Rajbhoj, P.B. Mane, A novel and efficient algorithm of textural feature extraction for fingerprint identification. Int. J. Eng. Res.Technol. **1**(5) (2012)
11. A. Jain, A. Ross, S. Prabhakar, Fingerprint matching using minutiae and texture features, in *ICIP* (2001)
12. J. Feng, S. Yoon, A.K. Jain, *Latent fingerprint matching: Fusion of rolled and plain fingerprints*, vol. 5558 (Springer Lecture Notes in Computer Science, 2009), pp. 695–704
13. M. Saad, Low-level color and texture feature extraction for content-based image retrieval, in *Multi-Dimensional Digital Signal Processing, EE K 381* (2008), pp. 20–28
14. S. Selvarajah, S.R. Kodituwakku, Analysis and comparison of texture features for content based image retrieval. Int. J. Latest Trends Comput. **2** (2011)
15. J. Feng, Combining minutia descriptors for fingerprint matching. J. Pattern Recognit. **41**, 342–352 (2008)
16. H. Choi, M. Boaventura, I.A. Boaventura, A.K. Jain, *Automatic segmentation of latent fingerprints* (BTAS, Washington, D.C., 2012), pp. 23–26
17. S. Yoon, J. Feng, A.K. Jain, Latent fingerprint enhancement via robust orientation field estimation. International Joint Conference on Biometrics (IJCB) (2011), pp. 1–8
18. S. Yoon, J. Feng, A.K. Jain, On latent fingerprint enhancement. in *Proceedings of the SPIE Conference on Biometric Technology for Human Identification VII* (2010), pp. 766707
19. T. Chen, Q.H. Wu, R. Rahmani, R, A pseudo top-hat mathematical morphological approach to edge detection in dark regions. Pattern Recognit. **35**(1), (2002)
20. D. Zorita, J. Ortega-Garcia, S. Cruz-Llanas, J. Sanchesz-Bote, J. Glez Rodriguez, *An improved image enhancement scheme for fingerprint minutiae extraction in biometric identification*, vol. 2091, (Springer Lecture Notes in Computer Science, 2001), pp. 217–223
21. A.A. Paulino, J. Feng, A.K. Jain, Latent fingerprint matching using descriptor based Hough transform. IEEE Trans. Inf. Forensics Secur. **8**(1) (2013)
22. NIST Special Database 27, Fingerprint Minutiae from Latent and Matching Tenprint Images, http://www.nist.gov/srd/nistsd27.cfm

Control Strategy for PQ Improvement in an Autonomous Microgrid Using Bacterial Foraging Optimization Algorithm

N. Chitra, A. Senthil Kumar, P. Priyadharshini and K.M. Shobana

Abstract This paper bestows a global optimization algorithm-based optimal power control stratagem for an island microgrid. The foremost aim is to improve the power quality of the microgrid. The primary performance parameters that are considered are voltage regulation and frequency regulation, especially starting of island mode. An inner loop of current control and an outer loop of power control are combined to form the projected control strategy. Bacterial foraging optimization algorithm (BFOA) is an intellectual search algorithm which is employed for self-tuning the control parameters. To validate the performance of the controllers, simulation is performed with the help of MATLAB/Simulink software.

Keywords Bacterial foraging optimization algorithm · Microgrid · Distributed generation · Voltage source inverter · Hysteresis current control

1 Introduction

Distributed generation (DG) is normally linked through power electronic devices like voltage source inverter (VSI) to the microgrid. Microgrid [4] is a group of interlinked distributed energy resources and loads in lucidly demarcated electrical boundaries. In accordance with the grid, the microgrid operates as a solitary controllable entity that disconnects and connects to the grid, in order to facilitate the microgrid to work in both grid-tied mode and autonomous mode [13]. The quality of power supply problem arises at the moment of transferring the load from on-grid mode to off-grid mode. The main utility grid has high reliability potential due to its adeptness of isolating the power generation and load from the grid [7].

N. Chitra (✉) · A. Senthil Kumar · P. Priyadharshini · K.M. Shobana
Department of Electrical and Electronics Engineering, SKP Engineering College, Tiruvannamalai 606611, India
e-mail: psk_siva@hotmail.com

P. Priyadharshini
e-mail: p21riya@gmail.com

© Springer India 2015

L.P. Suresh et al. (eds.), *Artificial Intelligence and Evolutionary Algorithms in Engineering Systems*, Advances in Intelligent Systems and Computing 325,
DOI 10.1007/978-81-322-2135-7_74

A meticulous fretfulness in microgrid is the issue of power quality, at the time of interfacing the microgrid to the main utility grid. This is a foremost area of research that also helps in exploring the effect of problems in power quality [8]. In order to isolate the microgrid, when the unbalance in voltage is solemn, the circuit breaker linked between the main grid and the microgrid is opened. If voltage unbalance is not serious, the circuit breaker endures closed, which results in prolonged voltage imbalance at the PCC [9]. A robust control stratagem with the operation of hyperactive performance is adopted, so as to satisfy the requirement of power quality. Subsequently, a unique feature of the contemporary converters based on power electronics is the VSI accompanied by an expand pulse width modulation (PWM) current control stratagem [14]. An open-loop PWM-based linear control and a closed-loop PWM-based nonlinear control are the two types of current controllers [12]. In a network of three-phase grid connection, a VSI designed with a nonlinear control based on hysteresis current control (HCC) is employed. The error signal is fed to the HCC, and compensation of current error is made along with the generation of PWM signal with an acceptable error. An enormous amount of total harmonic distortion (THD) is developed from a huge ripple current generation resulting from the self-regulation of delay current in order to control the signal of the current error [2]. Although a sine pulse width modulation (SVPWM) is employed in linear current controller, an algorithm of predictive control or standard PI regulator is required in compensating the current error signals. This type of controller provides an excellent control of current signal with low ripple [6]. In order to enhance the microgrid voltage and frequency, a power control based on an inner loop of current control is investigated. The aim of the controller is to ensure the dynamic stability of the system and to afford information regards analysis and design. It is important to analyze the power-quality indices when loads are shifted or changed, which results in unbalance in voltage and frequency. When changing or shifting the loads, a voltage unbalance and deviation in frequency occurs [3].

To determine the essential objective function, the controller parameters are tuned with the support of an intellectual search algorithm. Genetic algorithm (GA), particle swarm optimization (PSO), ant colony optimization (ACO), and bacterial foraging optimization technique (BFOA) are the computation algorithm with intellectual performance that shows an impressive success when applied to different problems of power system. Premature convergence is the main drawback of GA performance. Whereas PSO technique gives less accurate at its speed regulation and direction, however, in ACO technique, the convergence time is uncertain (but convergence is assured). In contrast, solution quality, convergence speed, and success rate of BFOA emboss as the most promising optimization technique and it has been adopted widely.

In this work, the control parameters of power controller are optimized in real time with the help of BFOA. The power controller is externally interlinked to the synchronous reference frame-based current controller. Feed forward compensation is accompanied by a standard PI controller to attain high dynamic performance. In this work, the foremost aim is to enhance the power quality by means of achieving the adequate frequency and voltage of microgrid.

2 Modeling of Island Microgrid

2.1 Voltage Source Inverter

A typical VSI model linked with a three-phase grid accompanied by a control stratagem is depicted in Fig. 1.

In abc reference frame, the state-space depictions of the system equivalent circuit are represented by [10];

$$\begin{aligned}\frac{\partial i_a}{\partial t} &= \frac{(Ri_a + V_{sa} - V_a)}{L} \\ \frac{\partial i_b}{\partial t} &= \frac{(Ri_b + V_{sb} - V_b)}{L} \\ \frac{\partial i_c}{\partial t} &= \frac{(Ri_c + V_{sc} - V_c)}{L}\end{aligned} \tag{1}$$

Equation (1) can be delineated by utilizing Park's transformation as,

$$\begin{aligned}\frac{\partial i_d}{\partial t} &= \frac{-Ri_d}{L} + i_q\omega + \frac{(V_{sd} - V_d)}{L} \\ \frac{\partial i_q}{\partial t} &= \frac{-Ri_q}{L} + i_d\omega + \frac{(V_{sq} - V_q)}{L}\end{aligned} \tag{2}$$

where 'ω' represents the angular frequency.

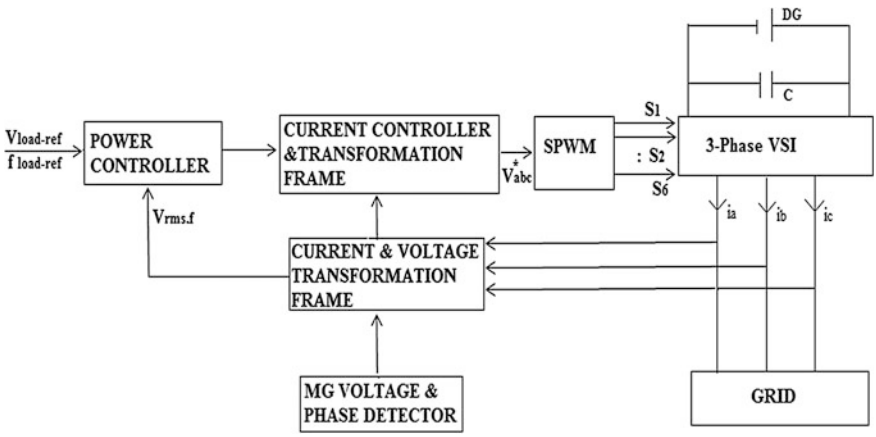

Fig. 1 Grid-connected model of VSI

Equation (3) defines the Park's transformation as,

$$i_{dq0} = Ti_{abc} \tag{3}$$

where

$$i_{dq0} = \begin{bmatrix} i_d \\ i_q \\ i_0 \end{bmatrix}, i_{abc} = \begin{bmatrix} i_a \\ i_b \\ i_c \end{bmatrix} \tag{4}$$

$$T = \frac{2}{3}\begin{bmatrix} \cos\theta & \cos\left(\theta - \frac{2\pi}{3}\right) & \cos\left(\theta + \frac{2\pi}{3}\right) \\ -\sin\theta & -\sin\left(\theta - \frac{2\pi}{3}\right) & -\sin\left(\theta + \frac{2\pi}{3}\right) \\ \frac{1}{2} & \frac{1}{2} & \frac{1}{2} \end{bmatrix} \tag{5}$$

2.2 Power Controller

With reference to the control objective mode, the power controller helps in improving the power quality. This controller is adopted to elicit the vectors of reference current *id** and *iq** together with *dq* reference frame by using the two standard PI controllers. This controller reacts to the impulsive changes, at the instant of change in load of autonomous mode. V_f control stratagem supports the DG's at the time of microgrid islanding [5]. BFOA tunes the optimal parameter, which are selected for regulating the frequency and voltage of microgrid along with standard PI regulator, to generate *id** and *iq** vectors of reference currents as shown in Fig. 2.

2.3 Current Controller

Figure 3 reveals the current control loop's block diagram. On the basis of synchronous reference frame, the design of current control loop is done. The minimum current error generated from applying voltage on inductive R-L impedance can be ensured by this controller design. The standard PI controller eradicates the current error. The IGBT based on SPWM is triggered with the pulse generated from the inverse park's transformation of the *dq* reference frame output of the controller.

3 Bacterial Foraging Optimization

Passino [1] proposed the bacterial foraging optimization algorithm (BFOA). It is a global optimization algorithm which has been endured broadly and that is aimed at distributed control and optimization. Escherichia coli's social foraging behavior is

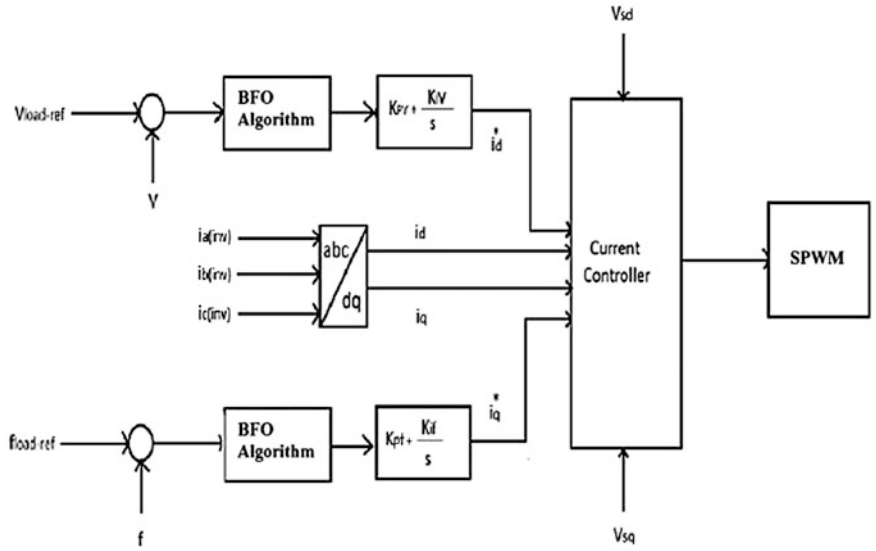

Fig. 2 Power control stratagem

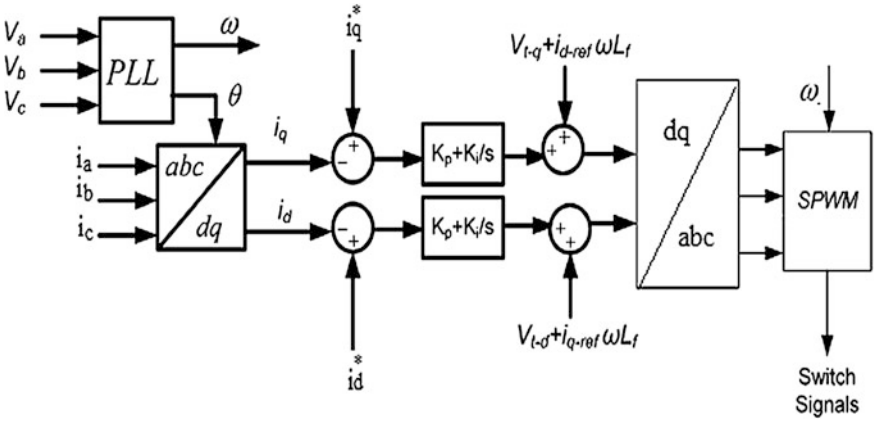

Fig. 3 Current control stratagem

inspired in BFOA. The ability of BFOA to solve the problems of real-world optimization has dragged the concentration of researchers. In order to increase the energy acquired per unit time, bacteria explore for nutrients. Communication of individual bacterium ensues with others through sending signals. Taking account of two preceding factors, the foraging decisions are taken by the bacterium. In search for nutrients, a bacterium travels by taking tiny steps, this process is termed as chemotaxis [11], and mirroring the virtual bacteria's chemotactic movement is the BFOA's main idea in the search space of problem.

3.1 Steps Encompassed in BFOA

Chemotaxis process: An *E. coli* cell moves with the help of flagella by swimming and tumbling, which is simulated in this process. For the whole lifetime, an *E. coli* bacterium can swim in one direction for a time period or may tumble [1].

Swarming of bacteria: The bacteria species such as *Salmonella typhimurium* and *E. coli* shows a fascinating group behavior, in which a complicated and firm spatio-25 temporal forms (swarms) are developed in a medium of semisolid nutrient. A traveling ring is formed by a *E. coli* cells group in moving ahead the gradient of nutrient, after placed among a matrix of semisolid along with a solitary nutrient chemo-effecter. A succinate with high-level stimulates the cells which releases an aspartate of attractant that supports in aggregating the cells into group. Subsequently, the cells travel with bacteria of high density in concentric forms of swarms.

Reproduction in bacteria: The bacteria with least health die eventually. The size of swarm is kept constant by splitting the healthier bacteria asexually into two bacteria, those bacteria are placed in the akin location.

Eradication and dispersal: Slow or rapid changes in the neighboring environment at which the population of bacterium lives may happen because of several reasons like temperature rise and nutrient concentration. Due to the effect of some events, a group of bacteria is scattered to a new locale or the entire bacteria in a locality are exterminated. In order to simulate the prodigy in BFOA, a number of bacteria are eliminated randomly in addition to a diminutive probability, whereas the fresh replacements are initialized at random above the search space. The algorithm along with the flowchart is illustrated below in Fig. 4.

4 Tuning of K_p and K_i

Table 1 exemplifies the BFOA parameters implementation. After completing the number of iterations or after attaining the optimal control parameter, the BFO algorithm gets ended. The performance of searching process is shown in Fig. 5.

5 Simulation Results

A SimPower System toolbox of MATLAB/SIMULINK is used for simulation results. Two ideal DC sources are considered as DGs. In this work, island (autonomous) mode operation of the microgrid has been explored. To assess the controller performance and also the voltage regulation and frequency regulation of the DGs, the simulation was performed. Initially, the microgrid works under grid-tied mode. At that time, power controller operates in PQ mode. At 0.001 s, the microgrid shifts to island mode; then, the power controller adopts V_f control mode so as to regulate the voltage and frequency of microgrid.

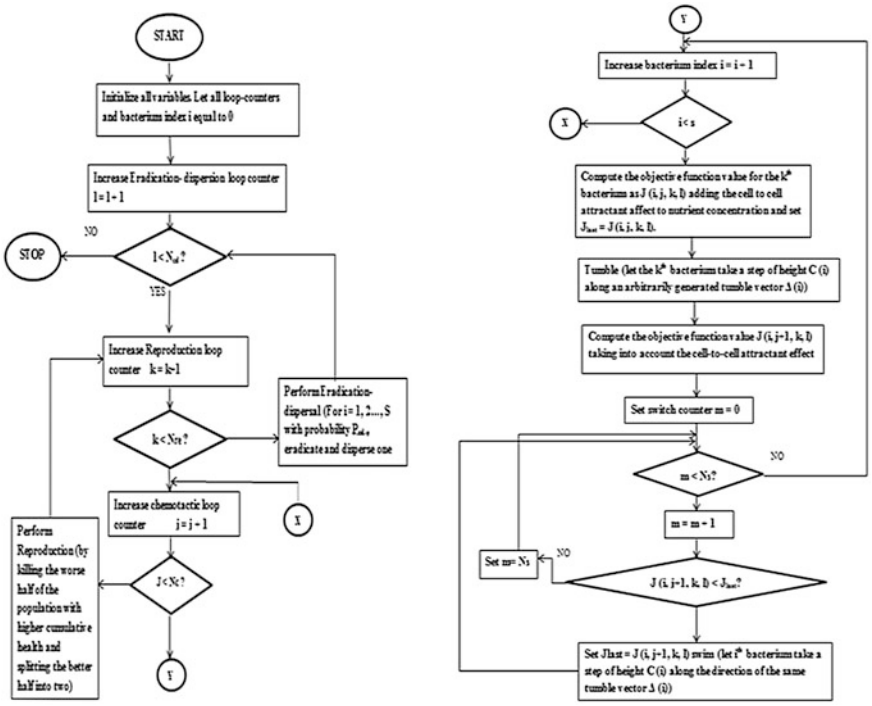

Fig. 4 Flowchart of BFOA

Table 1 BFOA parameters

The applied BFOA parameters	
K_p minimum	−0.2
K_p maximum	0.25
K_i minimum	0.355
K_i maximum	0.84

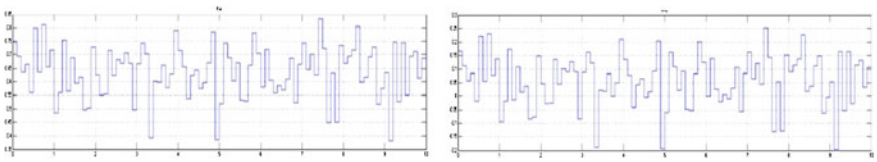

Fig. 5 Variation of K_p- and K_i-based BFOA tuning functions

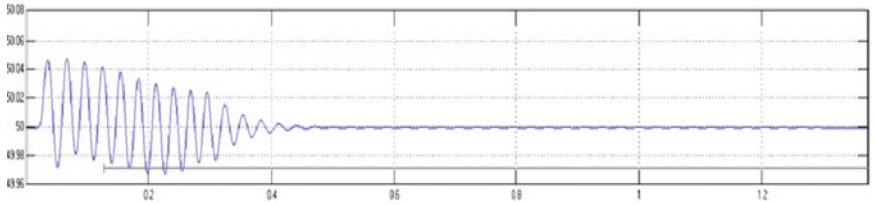

Fig. 6 Regulation of frequency

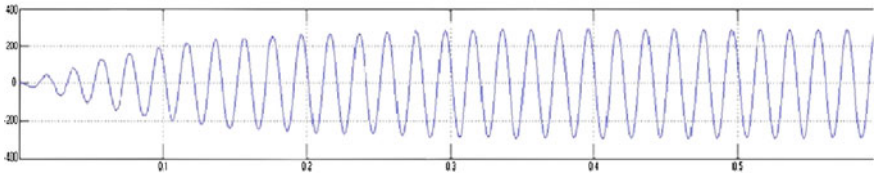

Fig. 7 Voltage regulation

5.1 Regulation of Frequency and Voltage

During grid-tied mode, the variation in voltage and frequency due to any load changes is maintained by grid. Therefore, the power controller operates only in PQ control mode to take care of real and reactive power sharing by that time, whereas at 0.001 s, the microgrid transfers from grid-tied mode to island mode of operation. At this moment, the DG1 operates in PQ control mode and to maintain real and reactive power, whereas DG2 operates in VF control mode to maintain V and f.

Figures 6 and 7 illustrate the regulated voltage and frequency of the microgrid. In Fig. 7, after 0.4 s, the frequency starts to settle down to the desired value following a short transient, whereas in Fig. 8, the voltage starts to regulate after 0.3 s and attain the desired value. This implies that the projected controllers respond to commencing of autonomous mode and affords, following a short transient, the voltage and frequency meet a value of 220 V and 50 Hz.

6 Conclusion

In this paper, a novel power control stratagem based on BFOA has been espoused for an autonomous microgrid. Two loops of control combined to form the proposed control stratagem. An inner loop of control includes a current controller based on synchronous reference frame, and an outer loop of control encompasses a power controller based on conventional PI regulators. At the instant of commencing of island mode, V_f control mode is instigated so as to regulate the voltage and

frequency of microgrid. The PQ control strategy is adopted for load change in autonomous microgrid. When microgrid starts operating in autonomous mode or when load change occurs, BFOA algorithm helps in real-time self-tuning of control parameter for power-quality enhancement. The simulation results evidenced that the proposed power controller proffers an exceptional response in regulating the microgrid voltage and frequency during autonomous mode.

References

1. H.C. Berg, D. Brown, Chemotaxis in *Escherichia coli* analysed by three dimensional tracking. Nature **239**, 500–504 (1972)
2. K. Bong-Hwan, M. Byung-Duk, Y. Jang-Hyoun, An improved space-vector-based hysteresis current controller. IEEE Trans. Ind. Electron. **45**(5), 752–760 (1998)
3. P. Dash, M. Padhee, S. Barik, Estimation of power quality indices in distributed generation systems during power islanding conditions. Int. J. Electr. Power Energy Syst. **36**(1), 18–30 (2012)
4. C. Il-Yop, L. Wenxin, D.A. Cartes, K. Schoder, Control parameter optimization for a microgrid system using particle swarm optimization, in *IEEE International Conference on Sustainable Energy Technologies, IEEE Standard for Interconnecting Distributed Resources with Electric Power Systems (1547–2003)* (2008), pp. 837–842
5. M.P. Kazmierkowski, L. Malesani, Current control techniques for three-phase voltage-source PWM converters: a survey. IEEE Trans IndElectron. **45**(5), 691–703 (1998)
6. R. Lasseter et al., White paper on integration of distribution energy resource: the CERTS microgrid concepts (2002)
7. Y. Li, D. MahindaVilathgamuwa, P.C. Loh, Microgrid power quality enhancement using a three-phase three -wire grid-interfacing compensator. IEEE Trans. Power Electron. **41**(4) (2006)
8. Y. Li, D. MahindaVilathgamuwa, P.C. Loh, Microgrid power quality enhancement using a three-phase four-wire grid-interfacing compensator. IEEE Trans. Ind. Appl. **41**(6) (2005)
9. Passino, Kevin,M.: Bacterial foraging optimization. International Journal of Swarm Intelligence Research (IJSIR). 1(1) (2010) 1–16
10. K.M. Passino, *Biomimicry for Optimization* (Springer, Berlin, 2004)
11. Z. Qingrong, C. Liuchen, Study of advance current control strategies for three-phase grid-connected PWM inverter for distributed generation, in *Proceedings of IEEE Conference on Control Applications* (2005), pp. 1311–1316
12. R. Strzelecki, G. Benysek, *Power Electronics in Smart Electrical Energy Networks* (Springer, London, 2008)
13. Y. Wang, Z. Lu, M. Yong, Analysis and comparison on the control strategies of multiple voltage source converters: managing the change, in *10th IET International Conference on Developments in Power System Protection* (2010)

Maximum Intensity Block Code for Action Recognition in Video Using Tree-based Classifiers

J. Arunnehru and M. Kalaiselvi Geetha

Abstract Human action recognition is a broad research area in computer vision community. Human actions are identified by connotation of body movements. In this paper, an action recognition approach based on maximum motion identification is proposed. Maximum Intensity Block Code (MIBC) is extracted as features. The experiments were carried out using Weizmann action dataset considering nine activities viz (walking, running, jumping, side, bend, waving one hand, waving both hands, jump-in-place-on-two-legs or pjump and skip) and the various tree based classifier like Random Forest, Naive Bayes, Random Tree, and Decision Tree (J48) utilized. In the experimental results, random forest classifier showed the best performance with an overall accuracy rate of 95.3 % which outperforms other algorithms.

Keywords Video surveillance · Action recognition · Frame difference · Random forest · Naive Bayes · Random tree · Decision tree

1 Introduction

Video surveillance is attracting much of the researcher's attention due to its wide application in visual surveillance, human–computer interaction, content-based video indexing and retrieval, and robotics. A video surveillance system observes activity in open public areas such as airport, railway station, bus stand, banks, gas stations, ATM, and commercial buildings for real-time or later analysis, and it is deterrent to crime. The aim of activity recognition is an automatic interpretation of current events and their context from video sequences when a human performs an activity.

J. Arunnehru (✉) · M. Kalaiselvi Geetha
Department of Computer Science and Engineering, Annamalai University, Annamalainagar, Cuddalore, Tamilnadu, India
e-mail: arunnehru.aucse@gmail.com

M. Kalaiselvi Geetha
e-mail: geesiv@gmail.com

© Springer India 2015

L.P. Suresh et al. (eds.), *Artificial Intelligence and Evolutionary Algorithms in Engineering Systems*, Advances in Intelligent Systems and Computing 325,
DOI 10.1007/978-81-322-2135-7_75

Human activity recognition aims to recognize and classify the activity of a person into certain categories, i.e., walking, running, jumping, bending, skipping, and hand waving. It is a complex process to recognize human activity due to many factors such as occlusion, illumination changes, postures, speed, shadows, and clothing.

1.1 Related Work

Recent surveys in the area of human action analysis in [1] and [2] focus on the feature descriptor, representation, and classification model in video sequences. Survey by Turaga et al. [3] centers around recognition of human activity. Wang et al. [4] propose a method which relies on optical flow and edge features, where these two discriminative features were combined to extract the motion and shape descriptors to distinguish one action from another. Reddy et al. [5] present a method to recognize action-based on sphere/rectangle tree structure that is built with spatiotemporal interest point features. In [6], vocabulary forest is constructed with local static and optical flow features and uses trees and forests for action recognition classification. Zhu et al. [7] address a multi-view action recognition algorithm based on local similarity random forests and sensor fusion, and normalized silhouettes are used as pose features and effective for multiple view human action recognition. Haiyong et al. [8] present a novel classification method to recognize the actions from videos based on centroid-radii model descriptor and to train and classify video sequences by nonlinear SVM decision tree (NSVMDT). In [9], a method was proposed based on extended motion template from human silhouettes. The holistic structural features were extracted from motion templates to discriminate the human action, which represents local and global information. Zhang et al. [10] have used the spatial–temporal with optical flow features. The temporal consistence of motion is improved with an enhanced DTW method to recognize the human actions. Wang et al. [11] propose a method which relies on optical flow and edge features, where these two discriminative features were combined to extract the motion and shape descriptors to distinguish one action from another.

1.2 Outline of the Work

This paper deals with activity recognition that aims to understand human actions from video sequences. The proposed method is evaluated using Weizmann [12] action dataset with the person showing actions such as walking, running, jumping, side, bend, waving one hand, waving both hands, pjump, and skip. Difference image is obtained by subtracting the successive frames. Motion information is extracted by identifying the region of interest (ROI). The extracted ROI is divided into two blocks B1 and B2. Maximum intensity block code (MIBC) is extracted as feature from the block showing maximum motion in the ROI. The extracted feature

is fed to the tree-based classifier such as random forest, Naive Bayes, random tree and decision tree (J48).

The rest of the paper is organized as follows. Section 2 illustrates the feature extraction and related discussions. Section 3 explains the workflow of the proposed approach. Section 4 presents the Experimental results. Finally, Sect. 5 concludes the paper.

2 Feature Extraction

Feature is a descriptive characteristic extracted from an image or video sequences, which represent the meaningful data that are vital for further analysis. The following subsections present the description of the feature used in this work.

2.1 Frame Differencing

Motion is the most important dynamic information used to recognize the human activity. The difference image obtained by simply subtracting the current frame is at time $t + 1$ with previous frame t on a pixel by pixel basis. The extracted motion information is considered as the ROI. Figure 1a, b shows the two successive frames of the Weizmann dataset. Resulting difference image is shown in Fig. 1c.

$$D_k(i,j) = |I_k(i,j) - I_{k+1}(i,j)| \\ 1 \leq i \leq w, 1 \leq j \leq h \tag{1}$$

$D_k(i, j)$ is the difference image, $I_k(i, j)$ is the intensity of the pixel (i, j) in the kth frame, and w and h are the width and height of the image, respectively. Motion information T_k or difference image is calculated using

Fig. 1 **a**, **b** Two consecutive frames. **c** Difference image of **a** and **b** from Weizmann dataset

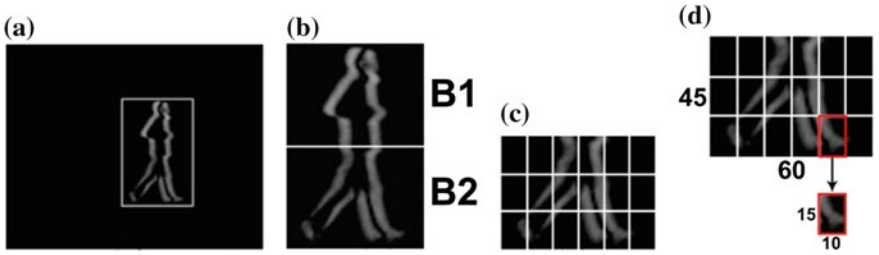

Fig. 2 **a** Motion information. **b** ROI extracted from (**a**). **c** Block description of (**b**). **d** 3 × 6 subblocks

$$T_k(i,j) = \begin{cases} 1, & \text{if } D_k(i,j) > t; \\ 0, & \text{Otherwise} \end{cases} \tag{2}$$

where t is the threshold.

2.2 Maximum Intensity Block Code (MIBC)

To recognize the action performed, motion is an important cue normally extracted from video. In that aspect, MIBC is extracted from the motion information extracted from the video sequences. The procedure for extracting the feature is explained in this section.

Initially, motion identified region is considered as ROI of size 60 × 90, as shown in Fig. 2a. ROI divided into two blocks B1 and B2 comprising of upper body and lower body as shown in Fig. 2b. In order to minimize the amount of calculation, only the maximum motion identified block is considered for further analysis. In Fig. 2b, block B2 shows maximum motion. So B2 alone is considered for MIBC extraction as shown in Fig. 2c. The block under consideration is of size 45 × 60 region which is divided into 3 × 6 subblocks where each will be of size 15 × 10 pixels as shown in Fig. 2d. The average intensity of each block in 3 × 6 region calculated and thus an 18-dimensional feature vectors are extracted from the ROIs, and it is fed to the tree-based classifiers for further processing.

3 Workflow of the Proposed MIBC Action Recognition Approach

Weizmann action datasets are used for experimental purpose. The video is processed at 25 frames per second. Smoothing is done by Gaussian convolution with a kernel of size 3 × 3 and variance $\sigma = 0.5$. It is essential to preprocess all video sequences to remove noise for fine features extraction and classification.

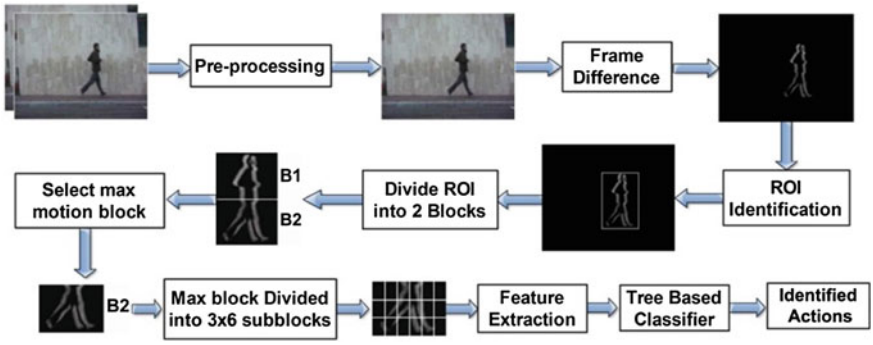

Fig. 3 Workflow of the proposed approach

ROI is extracted from the video sequence and MIBC features are extracted as discussed in Sect. 2. The projected features are fed to the tree-based classifier for action recognition. The workflow of the proposed approach is shown in Fig. 3. In this work, different tree-based classifiers such as random forest [13], Naive Bayes [14], random tree, and decision tree (J48) [15] are used in order to evaluate the effectiveness of these classifier on Weizmann dataset.

4 Experimental Results

In this section, the proposed method is evaluated using Weizmann action dataset. The experiments are carried out in C++ with OpenCV 2.2 in Ubuntu 12.04 Operating System on a computer with Intel Xeon Processor 2.40 GHz with 4 GB RAM. The obtained MIBC features are fed to tree-based classifiers such as random forest, Naive Bayes, random tree, and decision tree (J48) using open source machine learning tool WEKA [16] to develop the model for each activity, and these models are used to test the performance for each tree-based classifier.

Weizmann dataset: The proposed approach is evaluated on the Weizmann action dataset. It contains 81 video sequences from nine different people showing ten actions: walking, running, jumping, side, bend, waving one hand, waving both hands, pjump, jack, and skip. The video sequences have 180 × 144 pixel resolution at 25 fps. Nine actions such as walking, running, jumping, side, bend, waving one hand, waving both hands, pjump, and skip are used in this experiment. For conducting experiments, video clips showing all these nine actions performed by all nine people were considered. The sample frames of the Weizmann action dataset are shown in Fig. 4.

Fig. 4 Sample frames from the Weizmann dataset

Table 1 Performance measure of the tree-based classification algorithms

Algorithm	Precision (%)	Recall (%)	F-score (%)	Time (s)
Random forest	**95.4***	**95.3***	**95.3***	**4.53***
Naive Bayes	91.2	91.1	91.2	167.78
Random tree	90.4	90.4	90.4	0.55
J48	88.6	88.6	88.6	3.94

* Random Forest performs well, when compared to other classification algorithm

4.1 Quantitative Evaluation

As explained in Sect. 3, the 18-dimensional feature vectors are extracted. The performance is evaluated using tenfold cross-validation approach. The projected features are fed to the tree-based classifier. To evaluate the performance of the proposed approach, precision (P) = TP/TP + FP, recall (R) = TP/TP + FN, F1 = 2.P. R/P + R are used, where TP and FP are the numbers of true-positive and false-positive predictions for the particular class, and TN and FN are the number of true-negative predictions and false-negative predictions for the particular class, and build time of all tree-based classifiers is also measured. Table 1 shows the accuracy results obtained for random forest, Naive Bayes, random tree, and decision tree (J48) on Weizmann dataset.

4.2 Experimental Results on Tree-based Classifiers

The experiment was done using an open source machine learning tool WEKA. The performances of the classifiers were measured using tenfold cross-validation model. Table 1 represents the precision, recall, F-score, and time (s) values for all four tree-based classifiers and shows the random forest takes less time and gives better accuracy rate of 95.3 %, Naive Bayes classifier consumes more time to build the model but also shows the accuracy rate of 91.2 % having rank two, the accuracy of random tree is 90.4 %, and the accuracy of J48 is 88.6 %. Finally, the random forest classifier shows highest accuracy percentage when compared to other classifier algorithms.

Table 2 shows the averaged classification results of the random forest classifier. Nine actions are considered from Weizmann (walking, running, jumping, side, bend, waving one hand, waving both hands, pjump, and skip) dataset, where correct response define the main diagonal, and majority of actions are correctly classified.

Table 2 Confusion matrix (%) of the Weizmann dataset using random forest classifier, where a = walk, b = run, c = jump, d = side, e = bend, f = wave1, g = wave2, h = pjump, and i = skip

	a	b	c	d	e	f	g	h	i
a	**95.21***	1.73	0.67	1.07	0.13	0.00	0.80	0.00	0.40
b	4.93	**92.02***	1.17	0.00	0.00	0.00	0.00	0.23	1.64
c	3.81	0.22	**94.17***	0.45	0.00	0.00	0.00	0.00	1.35
d	2.27	0.45	1.82	**93.41***	0.00	0.00	0.23	0.23	1.59
e	0.00	0.00	0.00	0.00	**98.45***	1.08	0.15	0.31	0.00
f	0.00	0.00	0.16	0.00	1.31	**98.52***	0.00	0.00	0.00
g	0.17	0.00	0.00	0.17	1.20	0.51	**97.60***	0.34	0.00
h	0.18	0.00	0.37	0.18	1.66	0.00	0.18	**97.42***	0.00
i	3.07	4.17	3.95	0.88	0.22	0.00	0.22	0.00	**87.50***

* It shows the correct response values lie along the main diagonal of the table

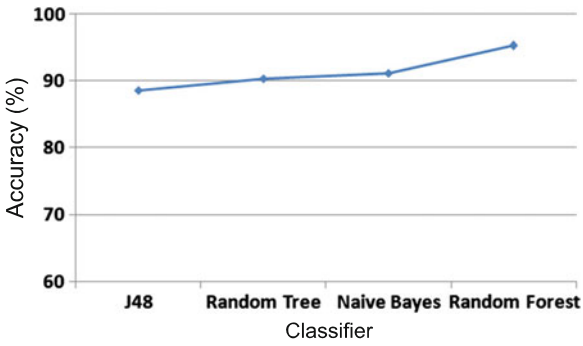

Fig. 5 Performance measure of the different classifiers

From this, running and skipping actions are confused. The overall performance of the proposed MIBC with different tree-based classifier on Weizmann dataset is shown in Fig. 5.

The approach is tested with various classifiers such as decision tree, random tree, Naive Bayes, and random forest. As expected, random forest excelled in accuracy among other approaches.

5 Conclusion and Future Work

This paper presented a method for action recognition for video surveillance using MIBC as a feature. Experiments are conducted on Weizmann dataset considering different actions (viz walking, running, jumping, side, bend, waving one hand, waving both hands, pjump, and skip). The ROI extracted from the difference image is used to extract MIBC feature from maximum motion information. This approach evaluates the performance of MIBC feature in video sequence using tree-based algorithms such as random forest, Naive Bayes, random tree, and decision tree.

The recognition results are obtained by the proposed method for the Weizmann dataset. It shows that that the average recognition accuracy was 95.3% with random forest and the random forest performs best, when compare with Naive Bayes, Random Tree, and Decision Tree classifiers, and Naive Bayes, random tree, and decision tree classifiers were 91.2, 90.4 and 88.6% respectively.

Acknowledgments The authors gratefully acknowledge **University Grants Commission of India** [F. No. 41-636/2012 (SR)], for funding this work.

References

1. R. Poppe, Vision-based human motion analysis: an overview. Comput. Vis. Image Underst. (CVIU) **108**(1–2), 4–18 (2007)
2. R. Poppe, A survey on vision-based human action recognition. IVC **28**, 976–990 (2010)
3. P. Turaga, R. Chellappa, S. Venkatramana Subrahmanian, O. Octavian Udrea, Machine recognition of human activities: a survey. IEEE Trans. Circ. Syst. Video Technol. **18**(11), 1473–1488 (2008)
4. L. Wang, Y. Wang, T. Jiang, D. Zhao, W. Gao, Learning discriminative features for fast frame-based action recognition. Pattern Recogn. **46**(7), 1832–1840 (2013)
5. K. Reddy, J. Liu, M. Shah, Incremental action recognition using feature-tree, in *International Conference on Computer Vision* (2009)
6. Z. Lin, Z. Jian, L. Davis, Recognizing actions by shape motion prototype trees, in *International Conference on Computer Vision* (2009)
7. F. Zhu, Ling Shao, Mingxiu Lin.: Multi-view action recognition using local similarity random forests and sensor fusion. Pattern Recogn. Lett. **34**(1), 20–24 (2013)
8. H. Zhao, Z. Liu, Human action recognition based on non-linear SVM decision tree. J. Computat. Infor. Syst. **7**, 2461–2468 (2011)
9. D. Wu, L. Shao, Silhouette analysis-based action recognition via exploiting human poses. IEEE Trans. Circuits Syst. Video Techn. **23**(2), 236–243 (2013)
10. W. Zhang, Y. Zhang, C. Gao, J. Zhou, Action recognition by joint spatial-temporal motion feature. J. Appl. Math. (2013)
11. L. Wang, Y. Wang, T. Jiang, D. Zhao, W. Gao, Learning discriminative features for fast frame based action recognition. Pattern Recogn. **46**(7), 1832–1840 (2013)
12. M. Blank, L. Gorelick, E. Shechtman, M. Irani, R. Basri, Actions as space-time shapes, in *Proceedings of IEEE International Conferences on Computer Vision* (2005), pp. 1395–1402
13. L. Breiman, Random forest. Mach. Learn. **45**(1), 5–32 (2001)
14. P. Langley, W. Iba, K. Thompson, An analysis of bayesian classifiers, in *Proceedings of the Tenth National Conference on Artificial Intelligence* (1992), pp. 223–228
15. J.R. Quinlan, *C4.5: Programs for Machine Learning* (Morgan Kaufmann Publishers, Burlington, 1993)
16. I.H. Witten, E. Frank, *Data Mining: Practical Machine Learning Tools and Techniques with Java Implementations* (Morgan Kaufmann Publishers, Burlington, 1999)

An Efficient Coding Method for Indexing Hand-based Biometric Databases

Ilaiah Kavati, Munaga V.N.K. Prasad and Chakravarthy Bhagvati

Abstract Biometric identification systems capture biometric (i.e., fingerprint, palm, and iris) images and store them in a central database. During identification, the query biometric image is compared against all images in the central database. Typically, this exhaustive matching process (linear search) works very well for the small databases. However, biometric databases are usually huge and this process increases the response time of the identification system. To address this problem, we present an efficient technique that computes a fixed-length index code for each biometric image. Further, an index table is created based on the indices of all individuals. During identification, a set of candidate images which are similar to the query are retrieved from the index table based on the values of query index using voting scheme that takes a constant time. The technique has been tested on benchmark PolyU palm print database and NTU Vein pattern database. The technique performs with lower penetration rates for 100 % hit rate for both the databases. These results show a better performance in terms of response time and search speed compared to the state-of-the-art indexing methods.

Keywords Index · Palm print · Hand vein · Sample images · SIFT · Minutiae · Match scores · Vote score

I. Kavati (✉) · C. Bhagvati
University of Hyderabad, Hyderabad 500046, India
e-mail: kavati089@gmail.com

C. Bhagvati
e-mail: chakcs@uohyd.ernet.in

I. Kavati · M.V.N.K. Prasad
Institute for Development and Research in Banking Technology, Hyderabad 500057, India
e-mail: mvnkprasad@idrbt.ac.in

© Springer India 2015

L.P. Suresh et al. (eds.), *Artificial Intelligence and Evolutionary Algorithms in Engineering Systems*, Advances in Intelligent Systems and Computing 325,
DOI 10.1007/978-81-322-2135-7_76

1 Introduction

In today's security conscious society, biometric identification systems are gaining more popularity in many applications, including commercial (e.g., e-commerce, welfare-disbursement) and various forms of access control (e.g., ATMs, boarder control, PC login). In biometric identification systems, the identity corresponds to a query image is determined by comparing it against every enrolled image in the database. Typically, this process works very well for the small databases. However, in real-life scenarios, biometric databases are usually huge (e.g., Unique Identification Authority of India (UIDAI) [1]), and without any intelligent system, the response time could be really high. Thus, an efficient indexing technique is required to increase the search speed and reduce the response time of the system. The indexing technique should be such that, instead of comparing the query image with every image in the database, it has to retrieve a small number of images (candidate list) from the database to which the actual matching process is applied.

An indexing method assigns a unique index value to every enrolled biometric image in the database. However, there are several issues that need be considered prior to build index codes: (1) The index value of the query image may not be identical to that of the corresponding image in the database as the biometric acquisition and processing is susceptible to noise. (2) In traditional databases, records are indexed in an alphabetical or numeric order for efficient retrieval, but biometric feature templates do not have any natural sorting order by which one can arrange the records [2]. Thus, traditional approaches are not suitable for biometric databases, and as a result, indexing has become a challenging problem. This work addresses the above problem and investigates a fast and accurate method to index biometric databases.

In recent years, indexing techniques are widely investigated for biometric identification. The biometric indexing methods are generally based on either point or triplet of points [3, 4, 5]. In . Paliwal et al. 8, authors extracted the key feature points of the images and mapped them into the hash table using geometric hashing. Authors in [3, 4] computed the triplets of key feature points extracted from the biometric images and mapped them into a hash table. However, the limitation of these indexing methods is that all of them deal with variable length feature sets which make the system statistically unreliable. However, in the literature, there exist few indexing techniques based on match scores which deal with fixed-length codes. The first such attempt is made in [6] for indexing biometric databases. Let m_{ij} be the match score between image i and image j in the database, a match score matrix $M_{N\times N} = \{m_{ij}\}$ is generated by comparing each image in the database with every other image, where N is the number of images in the database. Though the algorithm achieves quicker response time by searching the database based on an evaluation value calculated using the matrix M, the technique takes linear amount of time in worst case.

Gyaourova et al. [7] improved the work on match scores by choosing a small set of reference images R from the database. The technique reduces the length of index code from N to R where $|R| \ll N$. Similar to [6], for every image in the database,

match scores were obtained by matching it against the reference images using a matcher and these sets of match scores act as index code. Further, index code of each individual is stored as a row vector in an index table of size $N \times R$. While identifying a query image, the index code is generated in a similar way and then sequentially searches the index table to retrieve the best matches. This leads to increase of time complexity, i.e., $O(N)$.

Paliwal et al. [8] used vector approximation (VA+) file, which is a space partitioning method to store the match scores. The method uses *k-NN* search and palm print texture to retrieve top k similar matches. However, the performance of VA + file method generally degrades as dimensionality increases. In this paper, we present a method to compute fixed-length index code for each input biometric image based on match scores. The method proposes an efficient storing and searching method for the biometric database using these index codes. The proposed searching technique avoids the sequential scan on the database for identification and use voting scheme, results in a rapid search that takes a constant time.

Rest of the paper is organized as follows. The proposed indexing technique has been discussed in Sect. 2. Section 3 presents the experimental results, and performance of the proposed system against other indexing approaches in the literature. Conclusions are given in Sect. 4.

2 Proposed Methodology

This section discusses our proposed methodology for indexing the biometric databases. An overview of our proposed technique is shown in Fig. 1. The different steps involved in our approach are discussed in the following.

2.1 Feature Extraction

This section describes the extraction of key features from the vein pattern and palmprint images. In this work, for vein patterns we use the minutiae features as key features and extracted them after a series of preprocessing steps such as image

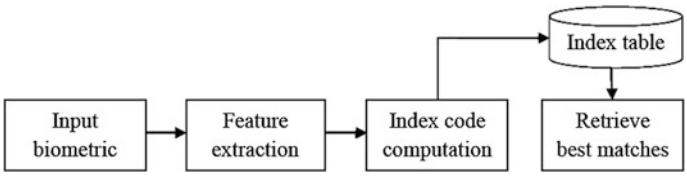

Fig. 1 Overview of the proposed technique

contrast enhancement, noise removal, binarization, and thinning [9]. Further for the palmprints, we extract scale-invariant feature transform (SIFT) features as the key features [10, 11].

2.2 Index Code Computation

This section proposes an efficient method to compute indexes for biometric images that makes use of a sample image set. The index code computation process is shown in Fig. 2. An input image is matched against a set of sample images. The resulting set of match scores constitutes the index code of the input image [7]. The different tasks involved in the index code computation process are discussed in the following.

Selection of sample image set. The selection of sample images from the database plays a crucial role in the performance of the system. Images which are more generic and represent the qualities of the entire database should be selected as sample images. Further, the number of sample images taken from the database also determines the effectiveness of the system. If the number of samples taken is very less, they do not provide enough information about the database. On the other hand, if they are very high, it increases the redundancy in samples. Hence, the sample images should be selected such that they are having distinct characteristics and provide enough information about the database for identification with minimal computational cost [8].

For n subjects of the database, define a set $E = \{e_1, e_2,\ldots e_n\}$ where e_i is a set of images of subject i. For each image in the set e_i, determine its variance of gray scale intensity values. From each set e_i, select one image which is having maximum variance in the set (i.e., the image of better quality). Let $X = \{x_1, x_2,\ldots x_n\}$ be the set of all selected images. Finally, we sort the images in set X in descending order and select the top k images (k is determined empirically) for the sample image set S.

The idea behind choosing such sample set is that the highly variant images contain significant properties that represent the entire qualities of the database. Figure 3 shows the distribution of sample images for the NTU database and is visualized using the multi-dimensional scaling (MDS) [12] on the variances of

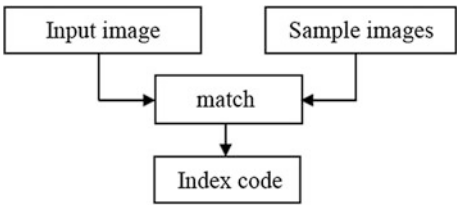

Fig. 2 Index code computation of an image

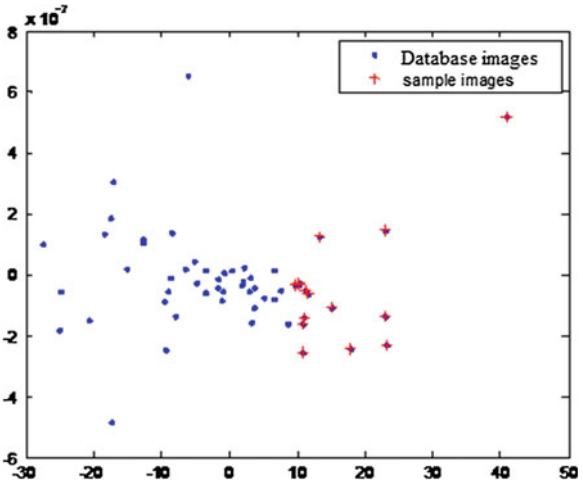

Fig. 3 Distributions of sample images using proposed method for the NTU database

images. It can be observed that the sample images are far from the remaining database images as they are highly distinct and contain rich information about the database compared to remaining database images.

Index code. Let $S = \{s_1, s_2, \ldots, s_k\}$ be the sample image set, and $M_x = \{m(x, s_1), m(x, s_2), \ldots m(x, s_k)\}$ be the set of match scores obtained for input image x against each sample image in S. The match score between two images is computed by comparing their key features in Euclidean space.

We describe M_x as the index code of image x. The motivation behind this concept is that if two images p and q belong to same user, then the difference between their index codes (match scores) M_p and M_q is comparatively less [9]. This difference in match scores may be used to identify a potential candidate list from the database for a query identity.

2.3 Index Table Creation

To store the index code (set of match scores) of each individual, we create a 2D index table A of size $100 \times k$. Each column of the table corresponds to one sample image in the sample set. The match scores obtained are normalized in the range 0–100.

User enrollment. For a given input image x, we compute the index code (of k match score values) as discussed earlier. If image x has a match score $m(x, s_j)$ with sample image s_j, its identity (say x) is put in $A(m(x, s_j), s_j)$. The index table organization is shown in Fig. 4. It can be seen that each entry of the table [say $A(m(x, s_j), s_j)$] contains a list of image identities (i.e., IidList) whose match score is $m(x, s_j)$ against sample image s_j.

Sample image / Match score	s_1	s_2	. . . . .	s_k
0	IidList	IidList		IidList
1	IidList	IidList		IidList
.	.	.	. . . . .	.
.	.	.		.
100	IidList	IidList		IidList

Fig. 4 Proposed index table organization

2.4 Retrieval of Best Matches (Identification)

This section proposes an efficient retrieval system to identify a query image from the index table. During identification, the technique retrieves a set of biometric identities (i.e., candidate list) from the index table which are most similar to the query using voting method. To do this, we first compute the index code [say $M_q = \{m(q, s_1), m(q, s_2), \ldots m(q, s_k)\}$] of k match score values for query image q as discussed in Sect. 2.2. For the ith match score value (say $m(q, s_i)$) of the query index code, the algorithm uses $(m(q, s_i), s_i)$ as index to the index table and retrieve all the images (IidList) found in that location.

We also retrieve images from the predefined neighborhood of the selected location. Finally, we give a vote to each retrieved image. We repeat this process for each match score value of the query index code. In our next step, we accumulate and count the number of votes of each name. Finally, we sort all the individuals in descending order based on the number of votes received. We select the individuals whose vote score is greater than a predefined threshold as best matches (candidate list) to the query image.

3 Experimental Results

We experimented our approach on two databases: (1) PolyU palmprint database [13] and (2) NTU-FIR vein pattern database. PolyU palmprint database consists of 7,752 grayscale images, approximately 20 prints each of 386 different palms. The first ten images of these prints are used to construct the database, while the other ten images are used to test the indexing performance. Further, the NTU-FIR vein pattern database consists of 194 images, approximately 3 prints each of 60 distinct hands. The first of these prints is used to construct the database, while the other two images are used to test the indexing performance. The images are cropped (Palmprint images: 151 × 151 pixels and Vein images: 128 × 128 pixels) to extract the features from the same region for different hands. Samples of segmented images for both the databases can be seen from Fig. 5. We evaluated the performance of the system with different sample set sizes (k) and chosen the optimum value as 1/3rd of the database.

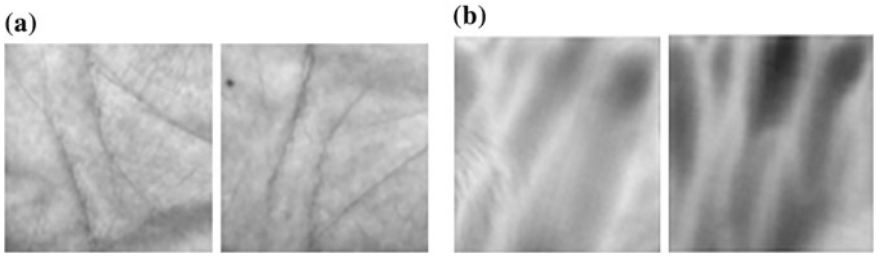

Fig. 5 Samples of segmented images: **a** from PolyU database, **b** from NTU database

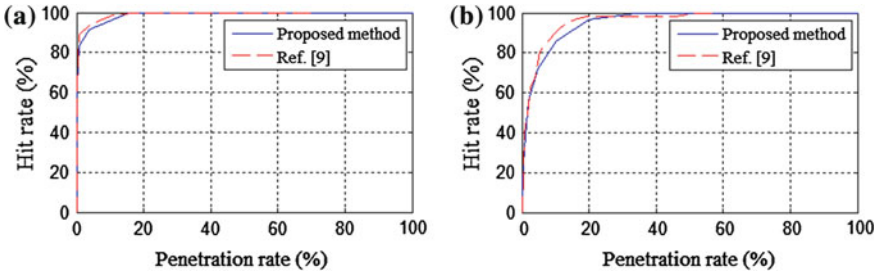

Fig. 6 HR versus PR of different methods: **a** PolyU database, **b** NTU database

The performance of the proposed algorithm is evaluated using two measures, namely hit rate (HR) and penetration rate (PR) and where HR is defined as the percentage of test images for which the corresponding genuine match is present in the candidate list, and PR is the average percentage of comparisons needed to identify a test image (i.e., average reduction in the search space or average candidate list size). The performance curves plotting the HR against PR at various thresholds are shown in Fig. 6. It is observed that the PR of the proposed technique is only 15.54 and 33.61 % at 100 % HR for the PolyU and NTU databases, respectively. It is observed that the PR for the NTU database is high compared to PolyU database as the training set of NTU database consists of only one image per subject.

3.1 Comparison with Other Techniques

The proposed technique has been compared with existing match-score-based indexing techniques [8, 7]. We implemented the technique [7] using MATLAB and used max-variance rule for the selection of reference images. The performance of proposed technique against technique in [7] can be seen from the Fig. 6 for both PolyU and NTU databases. It is seen from the Fig. 6 that our algorithm performs equally well with the [7]. However, authors in [7] performed linear search over the

index space to retrieve the best matches. This process takes considerable amount of time, i.e., $O(N)$ where N is the size of the database. On the other hand, in the proposed approach, we retrieve the best matches using voting scheme. This requires k comparisons in $O(1)$ time, i.e., constant time, where $k \ll N$. Hence, our algorithm without compromising identification performance takes less time to retrieve the best matches than [7].

Further the system in [8] achieves only maximum of 98.28 % HR, for PolyU database. Hence, it can be inferred that the proposed system enhanced the indexing performance.

3.2 Scalability of the System for New Enrollments

A new user is enrolled to system as described in Sect. 2.3. For every three new enrollments, we increment k value (as k = 1/3rd of the database) and sample set is updated as described in Sect. 2.2. If the updated sample set contains any of new users, the index table is appended with new columns corresponding to new sample images and the entries in the new columns are updated. Further, if any of the old sample images not in the updated sample set, the corresponding columns are deleted from the index table.

4 Conclusion

In this paper, an efficient indexing algorithm for biometric databases using fixed-length index codes is proposed. We propose an efficient storing method for the biometric database using these index codes such that we retrieve the best matches similar to the query in a constant time. The proposed system avoids the sequential scan over the index space and use voting to retrieve the best matches. Further, without compromising identification performance, our algorithm performs well than state-of-the-art indexing methods. The proposed system is scalable and can be applied to any large biometric database.

References

1. UIDAI Strategy Overview [online], http://uidai.gov.in/UID_PDF/Front_Page_Articles/Documents/Strategy_Overveiw-001.pdf
2. A. Mhatre, S. Palla, S. Chikkerur, V. Govindaraju, Efficient search and retrieval in biometric databases. Biometric Technol. Hum. Ident. **II**(5779), 265–273 (2005)
3. I. Kavati, M.V.N.K. Prasad, C. Bagvati, Vein pattern indexing using texture and hierarchical decomposition of delaunay triangulation, in *CCIS*, vol. 377 (Springer, 2013), pp. 213–222

4. U. Jayaraman, S. Prakash, P. Gupta, Use of geometric features of principal components for indexing a biometric database. Math. Comput. Model. **58**, 147–164 (2013)
5. H. Mehrotra, B. Majhi, P. Gupta, Robust iris indexing scheme using geometric hashing of SIFT keypoints. J. Netw. Comput. Appl. **33**, 300–313 (2010)
6. T. Maeda, M. Matsushita, K. Sasakawa, Identification algorithm using a matching score matrix. IEICE Trans. Infor. Syst. **84**, 819–824 (2001)
7. A. Gyaourova, A. Ross, Index codes for multi biometric pattern retrieval. IEEE Trans. Inf. Forensics Secur. **7**, 518–529 (2012)
8. A. Paliwal, U. Jayaraman, P. Gupta, A score based indexing scheme for palmprint databases, in *International Conference on Image Processing* (2010), pp. 2377–2380
9. L. Wang, G. Leedham, D.S.Y. Cho, Minutiae feature analysis for infrared hand vein pattern biometrics. Pattern Recogn. **41**, 920–929 (2008)
10. D.G. Lowe, Distinctive image features from scale-invariant keypoints. Int. J. Comput. Vis. **60**, 91–110 (2004)
11. SIFT for Matlab, http://www.vlfeat.org/vedaldi/code/sift.html
12. P.J.F. Groenen, M.V.D. Velden, Multidimensional scaling. Econometric Institute Report EI 2004-15 (2004)
13. The PolyU palmprint database, http://www.comp.polyu.edu.hk/biometrics

Optic Disk and Optic Cup Segmentation for Glaucoma Screening

G. Veerasenthilkumar, S. Vasuki and R. Rajkumar

Abstract Glaucoma is a chronic eye disease that leads to visionless. As it cannot be cured, detecting the disease in time is important. Current tests using intraocular pressure (IOP) are not sensitive enough for population-based glaucoma screening. Optic nerve head assessment in retinal fundus images is both more promising and superior. This paper proposes optic disk and optic cup segmentation using super pixel classification for glaucoma screening. In optic disk segmentation, histograms, and center surround statistics are used to classify each super pixel as disk or non-disk. A self-assessment reliability score is computed to evaluate the quality of the automated optic disk segmentation. For optic cup segmentation, in addition to the histograms and center surround statistics, the location information is also included into the feature space to boost the performance. The proposed segmentation methods have been evaluated in a database of 650 images with optic disk and optic cup boundaries manually marked by trained professionals. Experimental results show an average overlapping error of 9.5 and 24.1 % in optic disk and optic cup segmentation, respectively. The results also show an increase in overlapping error as the reliability score is reduced, which justifies the effectiveness of the self-assessment. The segmented optic disk and optic cup are then used to compute the cup to disk ratio for glaucoma screening. Our proposed method achieves areas under curve of 0.800 and 0.822 in two data sets, which is higher than other methods. The methods can be used for segmentation and glaucoma screening. The self-assessment will be used as an indicator of cases with large errors and enhance the clinical deployment of the automatic segmentation and screening.

Keywords Terms glaucoma screening · Optic cup segmentation · Optic disk segmentation

G. Veerasenthilkumar (✉) · S. Vasuki · R. Rajkumar
Dept of ECE, Velammal College of Engineering and Technology, Madurai, India
e-mail: gvs@vcet.ac.in

R. Rajkumar
e-mail: rajayyy333@gmail.com

© Springer India 2015

L.P. Suresh et al. (eds.), *Artificial Intelligence and Evolutionary Algorithms in Engineering Systems*, Advances in Intelligent Systems and Computing 325,
DOI 10.1007/978-81-322-2135-7_77

1 Introduction

Glaucoma is a chronic eye disease in which the optic nerve is progressively damaged. It is the second leading cause of blindness and is predicted to affect around 80 million people by 2020 [1]. Progression of the disease leads tools of vision, which occurs gradually over a long period of time. As the symptoms only occur when the disease is quite advanced, glaucoma is called the silent thief of sight. Glaucoma cannot be cured, but its progression can be slowed downy treatment. Therefore, detecting glaucoma in time is critical. However, many glaucoma patients are unaware of the disease until it has reached its advanced stage. In Singapore, more than 90% of patients are unaware that they have this condition [2, 3]. In Australia, about 50 % of people with glaucoma are undiagnosed. Since glaucoma progresses with few signs or symptoms and the vision loss from glaucoma is irreversible, screening of people at high risk for the disease is vital.

There are three methods to detect glaucoma: (1) assessment of raised intraocular pressure (IOP), (2) assessment of abnormal visual field, and (3) assessment of damaged optic nerve head. The IOP measurement using noncontact tonometry (also known as the "airpuff test") is neither specific nor sensitive enough to be ineffective screening tool because glaucoma can be present with or without increased IOP. A functional test through vision loss requires special equipments only present in territory hospitals and therefore unsuitable for screening. Assessment of the damaged optic nerve head is both more promising, and superior to IOP measurement or visual field testing for glaucoma screening. Optic nerve head assessment can be done by a trained professional. However, manual assessment is subjective, time consuming, and expensive. Therefore, automatic optic nerve head assessment would be very beneficial. One strategy for automatic optic nerve head assessment is to use image features for a binary classification between glaucomatous and healthy subjects. These features are normally computed at the image-level. In these methods, selection of features and classification strategy is difficult and challenging. The other strategy is to follow the clinical indicators. Many glaucoma risk factors are considered, such as the vertical cup to disk ratio (CDR) [4], disk diameter [5], ISNT rule, peripapillary atrophy (PPA), and notching. Although different ophthalmologists have different opinions on the usefulness of these factors, CDR is well accepted and commonly used.

A larger CDR indicates a higher risk of glaucoma. There has been some research into automatic CDR measurement from 3D images. However, because 3D images are not easily available, 2D color fundus images are still referred to by most clinicians. Moreover, the high cost of obtaining 3D images makes it inappropriate for a large-scale screening program. This paper focuses on automatic glaucoma screening using CDR from 2D fundus images. The optic nerve head or the optic disk (in short, disk) is the location where ganglion cell axons exit the eye to form

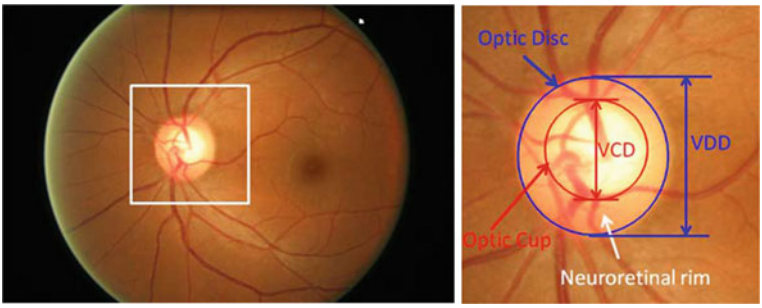

Fig. 1 Major structures of the optic disk. The region enclosed by the *blue line* is the optic disc; the central *bright* zone enclosed by the *red line* is the optic cup; and the region between the *red* and *blue lines* is the neuroretinal rim

the optic nerve, through which visual information of the photo-receptors is transmitted to the brain. In 2D images, the disk can be divided into two distinct zones; namely, a central bright zone called the optic cup (in short, cup) and a peripheral region called the neuroretinal rim. Figure 1 shows the major structures of the disk. The CDR is computed as the ratio of the vertical cup diameter (VCD) to vertical disk diameter (VDD) clinically. Accurate segmentations of disk and cup are essential for CDR measurement. Several methods have been proposed for automatic CDR measurement from 2D fundus images. This paper proposes super pixel classification-based disk and cup segmentations for glaucoma screening. A similar concept has been used for vessel segmentation. We compute center surround statistics from super pixels and unify them with histograms for disk and cup segmentation. We incorporate prior knowledge of the cup by including location information for cup segmentation. Based on the segmented disk and cup, CDR is computed for glaucoma screening. In addition, the proposed method computes a self-assessment reliability score for its disk segmentation result. Self-assessment is an important issue that has previously seldom been discussed in disk segmentation. In practice, an automated segmentation method might work well for most images while working poorly for the rest. Therefore, it is important to have self-assessment where users are warned of cases with potentially large errors. The paper is organized as follows. In Sect. 2, we introduce super pixel classification-based OD segmentation including the generation of super pixels, the extraction of features from super pixels for the classification, and the computation of the self-assessment reliability score. Section 3 introduces super pixel classification-based cup segmentation, where the procedure is similar to that in disk segmentation. Section 4 shows the experimental results including the accuracy for disk and cup segmentation as well as glaucoma screening. Discussions and conclusions are presented in final section.

2 Optic Disk Segmentation

2.1 Background

Localization and segmentation of disk are very important in many computer aided diagnosis systems, including glaucoma screening. The localization focuses on finding a disk pixel, very often the center. It has been extensively studied for applications in diabetic screening. Our work focuses on the segmentation problem and the disk is located by our earlier method in, which works well in our data set for glaucoma screening as there are few white lesions to confuse disk localization as compared to diabetic screening. The segmentation estimates the disk boundary, which is a challenging task due to blood vessel occlusions, pathological changes around disk, variable imaging conditions, etc. Some approaches have been proposed for disk segmentation, which can be generally classified as template-based methods, deformable model-based methods, and pixel classification-based methods. In circular Hough transform is used to model the disk boundary because of its computational efficiency. However, clinical studies have shown that a disk has a slightly oval shape with the vertical diameter being about 7–10 % larger than the horizontal one. Circular fitting might lead to an underestimated disk and an overestimated CDR, so ellipse fittings often adopted for glaucoma detection. In Lowell Employed the active contour model, which consists of finding the optimal points based on the image gradient and the smoothness of the contour. In employed, the deformable model technique through minimization of the energy function is defined by image intensity, image gradient, and boundary smoothness. In a level set is used to estimate the disk followed by an ellipse fitting to smooth the boundary. In the authors proposed modified Chan–Vese model using texture features. In edge detection and circular Hough transform are combined with an active shape model to extract the disk. Recently, the active shape model is also applied on probability maps to find the disk boundary. In addition, we also present a super pixel classification-based approach using histograms to improve the initialization of the disk for deformable models.

Both the template and deformable model-based methods are based on the edge characteristics. The performance of these methods very much depends on the differentiation of edges from the disk and other structures, especially the PPA. Examples of PPA are shown as the area between the blue and green lines in Fig. 2. The PPA region is often confused as part of disk for two reasons: (1) it looks similar to the disk and (2) its crescent shape makes it form another ellipse (often stronger) together with the disk. Deformable models are sensitive to poor initialization. Very often, the deformation cannot exclude PPA from the segmented disk, if it has been included in the initialization. For example, the red line in the first example in Fig. 2 is the boundary detected by the active shape model-based method in. To overcome the problem, we previously proposed a template-based approach with PPA elimination [6]. By using a PPA detection module based on texture, our method reduces the

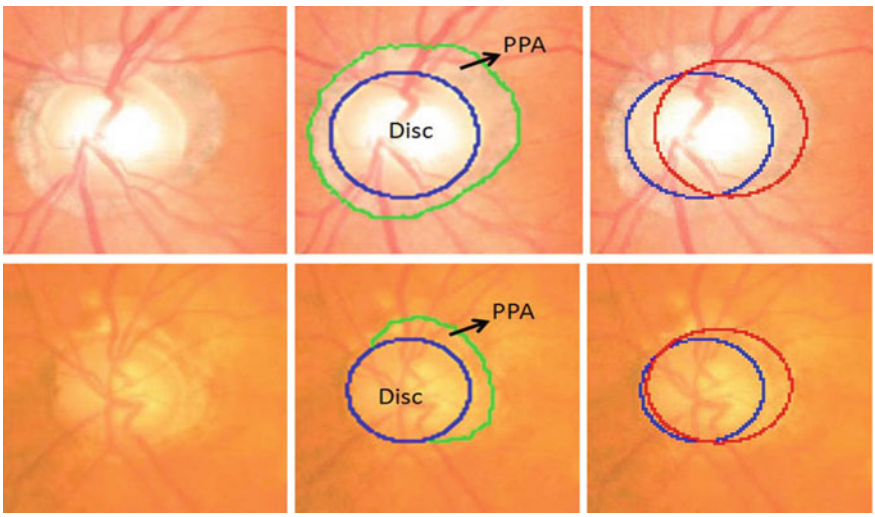

Fig. 2 Challenge in disk segmentation. *Blue lines* manual disk boundary; *redlines* automated disk boundary by and in the first and second example, respectively; *green lines* the PPA boundary

chance of mistaking PPA as part of the disk. However, the approach does not work well when the PPA area is small, or when the texture is not significantly predominant such as the second example in Fig. 2. Pixel classification-based methods use various features such as intensity and texture from each pixel and its surroundings to find the disk. Compared the pixel classification-based methods with the deformable model-based methods, they concluded that their performances were similar. Moreover, the number of pixels is high even at moderate resolutions, which makes the optimization on the level of pixels intractable. To overcome the limitations of pixel classification-based methods and deformable model-based methods, we propose a super pixel classification-based method and combine it with the deformable model-based methods. Super pixels are local, coherent and provide a convenient primitive to compute local image features. They capture redundancy in the image and reduce the complexity of subsequent processing. In the proposed method, super pixel classification is used for an initialization of disk boundary and the deformable model is used to fine tune the disk boundary, i.e., a super pixel classification-based disk initialization for deformable models. The flow chart of the proposed disk segmentation method is summarized in Fig. 3. The segmentation comprises: a super pixel generation step to divide the image into super pixels; a feature extraction step to compute features from each super pixel; a classification step to determine each super pixel as a disk or non-disk super pixel to estimate the boundary; a deformation step using deformable models to fine tune the disk boundary.

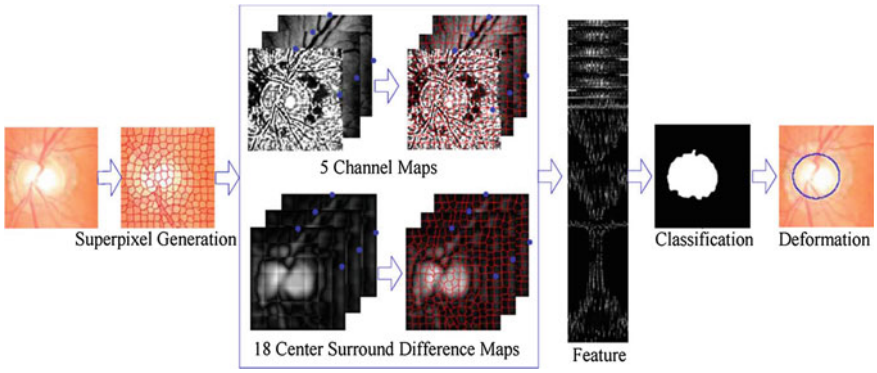

Fig. 3 Superpixel-based optic disk segmentation. Each image is divided into super pixels. The features computed from 18 centers surround difference maps and five channel maps are used to classify the super pixels a disk or non-disk. The th column in the feature map corresponds to the feature for the super pixel

2.2 Super Pixel Generation

Many algorithms have been proposed for super pixel classification. They have been proved to be useful in image segmentations in various images of scene, animal, human, etc. This paper uses the simple linear iterative clustering logarithm (SLIC) to aggregate nearby pixels into super pixels in retinal fundus images. Compared with other super pixel methods, SLIC is fast and memory efficient and has excellent boundary adherence. SLIC is also simple to use with only one parameter, i.e., the number of desired super pixels. Here, we give a brief introduction of the SLIC algorithm while more details of the algorithms can be found in the SLIC paper In SLIC, initial cluster centers are sampled on a regular grid spaced by pixels apart from the image with pixels. The centers are first moved toward the lowest gradient position in a 3×3 neighborhood. Clustering is then applied. For each, SLIC iteratively searches for its best matching pixel from the neighborhood around based on color and spatial proximity and then compute the new cluster center based on the found pixel. The iteration continues until the distance between the new centers and previous ones is small enough. Finally, a postprocessing is applied to enforce connectivity.

2.3 Center Surround Statistics

As we described earlier, the PPA region looks to be close to the disk. It is important to include features that reflect the difference between the PPA region and the disk region. The super pixels from the two regions often appear similar except for the texture: the PPA region contains blob-like structures while the disk region is relatively more homogeneous. The histogram of each super pixel does not work well

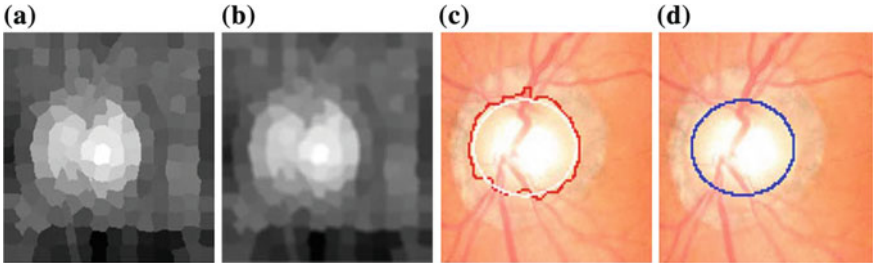

Fig. 4 Illustration of deformation tuning: **a** decision values; **b** smoothed decision values; **c** the raw estimation (*red*) and the fitted estimation (*white*); **d** final result after deformation

as the texture variation in the PPA region is often from a larger area than the super pixel [7]. This is because the super pixel often consists of a group of pixels with similar colors. Inspired by these observations, we propose center surround statistics (CSS) from super pixels as a texture feature.

To compute CSS, nine spatial scale dyadic Gaussian pyramids are generated with a ratio from 1:1 (level 0) to 1:256 (level 8) as illustrated in Fig. 4. Multiple scales are used as the scale of the blob-like structures, largely vary. The dyadic Gaussian pyramid [8] is a hierarchy of low-pass filtered versions of an image channel, so that successive levels correspond to lower frequencies. It is accomplished by convolution with a linearly separable Gaussian filter and decimation by a factor of two. Then center surround operation between center (finer) levels $C = 2, 3, 4$ and surround levels (coarser) $S = C + D$ with $D = 3, 4$ is applied to obtain six maps empirically computed at levels of 2–5, 2–6, 3–6, 3–7, 4–7, and 4–8 from an image channel.

$$\mu_j(i) = \frac{1}{n_j} \sum_{(x,y)\in SP_j} M_i(x,y) \tag{1}$$

$$\mathrm{var}_j(i) = \frac{1}{n_j} \sum_{(x,y)\in SP_j} \left(M_i(x,y) - \mu_j(i)\right)^2 \tag{2}$$

3 Optic Cup Segmentation

Detecting the cup boundary from 2D fundus images without depth information is a challenging task as depth is the primary indicator for the cup boundary. In 2D fundus images, one landmark to determine the cup region is the pallor, defined as the area of maximum color contrast inside the disk. Another landmark is the vessel bends at the boundary of the cup. Compared with disk segmentation, fewer methods have been proposed for cup segmentation from 2D fundus images. Thresholding is used to determine the cup in relying on intensity difference between cup and neuroretinal rim. A level set-based approach is used in. It relies on the edges between cup and

neuroretinal rim. This method and thresholding-based methods are essentially based on pallor information. However, in many subjects from screening data, there is no obvious pallor or edge within the disk to mark the cup boundary. Figure 3 shows two examples of such disks. The contrast between the cup and the neuroretinal rim in the two examples are much weaker than that in Fig. 1. In, small vessel bends ("kinks") from the vicinity of the initial estimated cup have been used to aid the cup segmentation. The challenge is to exclude vessel bends from a non-cup boundary, especially when the initial estimation is inaccurate. A similar concept is used into locate relevant vessel bends ("*r*-bend") at the vicinity of a pallor region determined by bright pixels. This method, again, requires pallor information to find a good initial estimation of the cup boundary. Moreover, it requires at least a few bends in nasal, inferior, and superior angular of the disk for the cup boundary fitting, which is not necessarily true for many images from our experience. Proposed a sliding window and regression-based method. Although it performs better than earlier methods, the sliding window strategy requires heavy computational cost. Recently, developed a deformable model-based method for cup segmentation, where the initialization of the cup boundary is based on pallor combined with prior knowledge of the cup. The main challenge in cup segmentation is to determine the cup boundary when the pallor is nonobvious or weak. In such scenarios, we lack landmarks, such as intensity changes or edges to estimate the cup boundary reliably. Although vessel bends are potential landmarks, they can occur at many places within the disk region and only one subset of these points defines the cup boundary. Besides the challenges to obtain these points, it is also difficult to differentiate the vessel bends that mark the cup boundary from other vessel bends without obvious pallor information. Moreover, combining the vessel bends with pallor information is a challenging task that often requires a set of heuristic parameters, which raises the concern of the robustness of the method. We present a super pixel classification-based method for cup segmentation that incorporates prior knowledge into the training of super pixel classification instead of relying on vessel bends. Figure 4 shows the procedure for cup segmentation, which is similar to that for disk segmentation with some minor modifications.

3.1 Classification for Optic Cup Estimation

The LIBSVM [8] with linear kernel is used again in our experiments. We randomly obtain the same number of super pixels from the cup and non-cup regions in the training step from a set of training images with manual cup boundary. Similarly, the output values from the LIBSVM decision function are used. As illustrated in Fig. 8, the output value for each super pixel is used as the decision values for all pixels in the super pixel. A mean filter is applied on the decision values to compute smoothed decision values. Then, the smoothed decision values are used to obtain the binary decisions for all pixels. The largest connected object is obtained and its boundary is used as the raw estimation. The best fitted ellipse [9] is computed as the cup boundary. The ellipse fitting here is beneficial for overcoming the noise introduced by vessels especially from

the inferior and superior sector of the cup. We do not apply contour deformation after we obtain the estimated cup boundary from super pixel classification, because many cases do not have an obvious/strong contrast between the cup and the rim for the deformable models. A deformation in these cases often leads to an overestimated cup.

3.2 Cup to Disk Ratio

After obtaining the disk and cup, various features can be computed. We follow the clinical convention to compute the CDR. As mentioned in the introduction, CDR is an important indicator for glaucoma screening computed as

$$\mathrm{CDR} = \frac{\mathrm{VCD}}{\mathrm{VDD}} \tag{3}$$

The computed CDR is used for glaucoma screening. When CDR is greater than a threshold, it is glaucomatous, otherwise, healthy.

4 Results and Discussions

See Figs. 5, 6 and Table 1.

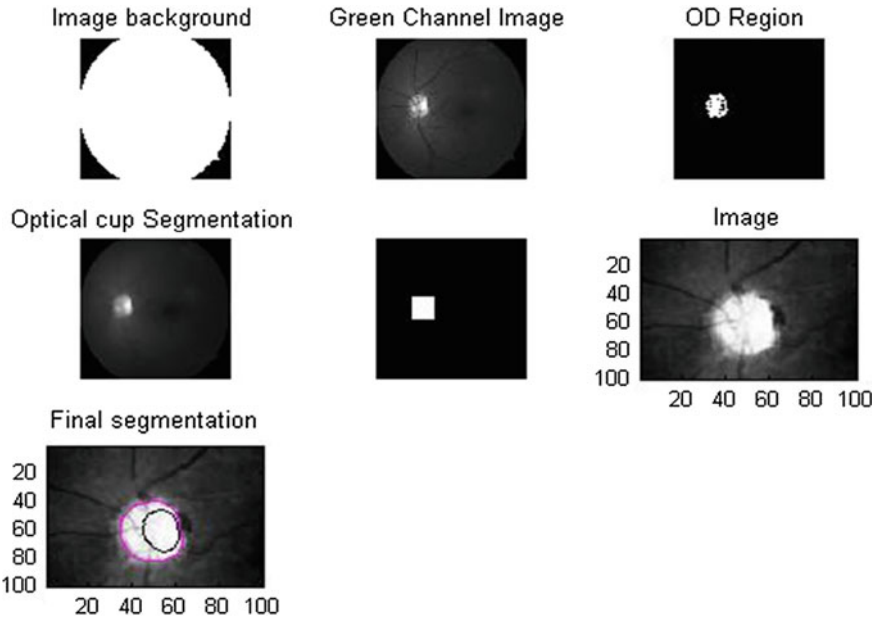

Fig. 5 Optic disk and optic cup segmented output

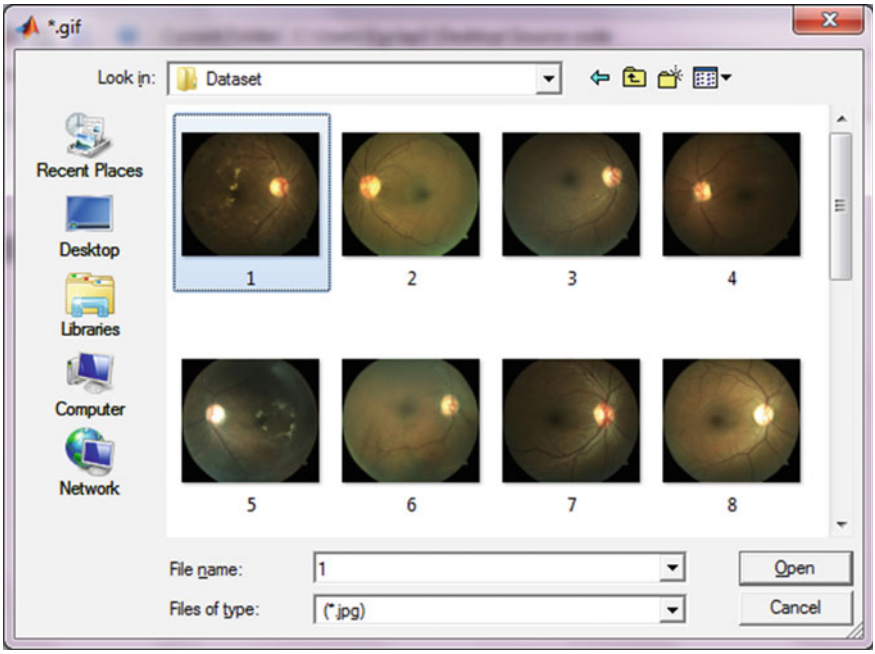

Fig. 6 Collection of data set images

Table 1 Calculation CDR ratio with normal and abnormal images

Image	CDR	Normal	Abnormal
1	0.2110	Yes	
2	0.2691	Yes	
3	0.2288	Yes	
4	0.1922	Yes	
5	0.4519		Yes
6	0.3459		Yes
7	0.1856	Yes	
8	0.3629		Yes
9	0.1793	Yes	
10	0.3037		Yes
11	0.2654	Yes	
12	0.1557	Yes	
13	0.2903	Yes	
14	0.2435	Yes	

5 Conclusion

The OD localization methodology adaptively changes the template size based on the OD radius estimation, using the camera FOV and the image resolution. The methodology not only exploits the appearance features of the OD, but also main vessel orientation inside the OD, to increase robustness. The OD segmentation method uses ASF and morphological reconstruction to remove vessels and bright region distractors while retaining the shape of the papillary region.

Our proposed method achieves areas under curve of 0.800 and 0.822 in two data sets, which is higher than other methods. The methods can be used for segmentation and glaucoma screening. The results by the proposed methods are good enough for screening purposes in polyclinics and eye centers, according to discussions with clinicians and ophthalmologists. However, there are stillman features that can be improved in the proposed method, including the bias we discussed. The proposed methods in this paper model the disk/cup boundary as an ellipse, which is an approximation of the actual boundary.

References

1. D. Usher, M. Dumskyj, M. Himaga, T.H. Williamson, S. Nussey, J. Boyce, Automated detection of diabetic retinopathy in digital retinal images: a tool for diabetic retinopathy screening. Diabetic Med. **21**, 84–90 (2004)
2. A.D. Fleming, K.A. Goatman, S. Philip, G.J. Prescott, P.F. Sharp, J.A. Olson, Automated grading for diabetic retinopathy: a large-scale audit using arbitration by clinical experts. Br. J. Ophthalmol. **94**, 1606–1610 (2010)
3. C. Agurto, V. Murray, E. Barriga, S. Murillo, M. Pattichis, H. Davis, S. Russell, M. Abramoff, P. Soliz, Multiscale AM-FM methods for diabetic retinopathy lesion detection. IEEE Trans. Med. Imag. **29**(2), 502–512 (2010)
4. T. Damms, F. Dannheim, Sensitivity and specificity of optic disc parameters in chronic glaucoma. Invest. Ophth. Vis. Sci. **34**, 2246–2250 (1993)
5. D. Michael, O.D. Hancox, Optic disc size, an important consideration in the glaucoma evaluation. Clin. Eye Vis. Care. **11**, 59–62 (1999)
6. J. Lowell, A. Hunter, D. Steel, A. Basu, R. Ryder, E. Fletcher, L. Kennedy, Optic nerve head segmentation. IEEE Trans. Med. Imag. **23**(2), 256–264 (2004)
7. J. Cheng, J. Liu, Y. Xu, D.W.K. Wong, B.H. Lee, C. Cheung, T. Aung, T.Y. Wong, Super pixel classification for initialization in model based optic disc segmentation, in *International Conference of the IEEE Engineering in Medicine and Biology Society* (2012), pp. 1450–1453
8. E.H. Adelson, C.H. Anderson, J.R. Bergen, P.J. Burt, J.M. Ogden, Pyramid methods in image processing. RCA Eng. **29**(6), 33–41 (1984)
9. C.C. Chang, C.J. Lin, LIBSVM: a library for support vector machines (2001)
10. K.A. Goatman, A.D. Fleming, S. Philip, G.J. Williams, J.A. Olson, P.F. Sharp, Detection of new vessels on the optic disc using retinal photographs. IEEE Trans. Med. Imag. **30**(4), 972–979 (2011)
11. G.D. Joshi, J. Sivaswamy, S.R. Krishnadas, Optic disk and cup segmentation from monocular color retinal images for glaucoma assessment. IEEE Trans. Med. Imag. **30**(6), 1192–1205 (2011)

12. R.J. Winder, P.J. Morrow, I.N. McRitchie, J.R. Bailie, P.M. Hart, Algorithms for digital image processing in diabetic retinopathy. Comput. Med. Imag. Graph. **33**, 608–622 (2009)
13. A. Youssif, A.Z. Ghalwash, A. Ghoneim, Optic disc detection from normalized digital fundus images by means of a vessels' direction matched filter. IEEE Trans. Med. Imag. **27**(1), 11–18 (2008)
14. C. Sinthanayothin, J.F. Boyce, H.L. Cook, T.H.L. Williamson, Automated localisation of the optic disc, fovea, and retinal blood vessels from digital colour fundus images. Br. J. Ophthalmol. **83**, 902–910 (1999)
15. N. Harizman, C. Oliveira, A. Chiang, C. Tello, M. Marmor, R. Ritch, J.M. Liebmann, The ISNT rule and differentiation of normal from glaucomatous eyes. Arch. Ophthalmol. **124**, 1579–1583 (2006)
16. J.B. Jonas, M.C. Fernandez, G.O. Naumann, Glaucomatousparapapillary atrophy occurrence and correlations. Arch. Ophthalmol. **110**, 214–222 (1992)
17. J. Cheng, J. Liu, D.W.K. Wong, F. Yin, C. Cheung, M. Baskaran, T. Aung, T.Y. Wong, Automatic optic disc segmentation with peripapillary atrophy elimination, in *International Conference of the IEEE Engineering in Medicine and Biology Society* (2011), pp. 6624–6627
18. Z. Zhang, J. Liu, N.S. Cherian, Y. Sun, J.H. Lim, W.K. Wong, N.M. Tan, S. Lu, H. Li, T.Y. Wong, Convex hull based neuro-retinal optic cup ellipse optimization in glaucoma diagnosis, in *International Conference of the IEEE Engineering in Medicine and Biology Society* (2009), pp. 1441–1444
19. F. Yin, J. Liu, S.H. Ong, Y. Sun, D.W.K. Wong, N.M. Tan, C. Cheung, M. Baskaran, T. Aung, T.Y. Wong, Model-based optic nerve head segmentation on retinal fundus images, in *International Conference of the IEEE Engineering in Medicine and Biology Society* (2011), pp. 2626–2629
20. L. Tang, M.K. Garvin, Y.H. Kwon, M.D. Abràmoff, Segmentation of optic nerve head rim in colorfundus photographs by probability based active shape model, in ARVO (2012)
21. A. Fitzgibbon, M. Pilu, R.B. Fisher, Direct least squares fitting of ellipses. IEEE Trans. Pattern Anal. Mach. Intell. **21**(5), 476–480 (1999)

Deadline-based Priority Management in Cloud

E. Iniya Nehru, Saswati Mukherjee and Abhishek Kumar

Abstract In cloud computing, the word "cloud" is used as metaphor for "the Internet," so the phrase cloud computing means "a type of Internet-based computing" where different services such as servers, storage, and applications are delivered to an organization's computer and devices through the Internet. Today, cloud computing is on demand that means cloud providers provide their services in pay-as-you-manner. So, there must be a provision that all resources are made available to requesting users in efficient manner to satisfy their needs. Since this resource allocation schemes offered by cloud computing, effective scheduling algorithms are important to utilize these benefits. There are many scheduling algorithms such as task grouping, priority aware, and SJF (shortest job first) to reduce the waiting time and maximize the resource allocation. In this paper, a new algorithm has been proposed namely deadline–first scheduling algorithm, which considers deadline as a crucial factor. Deadline is a major concept in negotiation of SLA in cloud computing to prevent penalties.

1 Introduction

Cloud computing is a synonym for distributed computing over a network that means the ability to run a program or application on many connected computers at the same time. This also refers to network-based services, which appear to be

E. Iniya Nehru (✉)
National Informatics Centre, Chennai, India
e-mail: nehru@nic.in

S. Mukherjee
College of Engineering, Anna University, Chennai, India
e-mail: msaswati@yahoo.com

A. Kumar
Master of Computer Applications Department, Pondicherry University, Kalapet, India
e-mail: abhi8189@gmail.com

© Springer India 2015

L.P. Suresh et al. (eds.), *Artificial Intelligence and Evolutionary Algorithms in Engineering Systems*, Advances in Intelligent Systems and Computing 325,
DOI 10.1007/978-81-322-2135-7_78

provided by real server hardware, and are in fact served up by virtual hardware, simulated by software running on one or more real machine. Such virtual servers do not physically exist and can be therefore moved around and scale up (or down) on the fly without affecting the end user-arguably rather like a cloud.

Cloud computing offers three types of service models: Software as a service (SaaS), SaaS-style cloud delivers access to collections of software application programs. SaaS providers offer users access to specific application programs controlled and executed on the provider's infrastructure; In platform as a service (PaaS) model, cloud providers deliver a computing platform, typically including operating system, programming language execution environment, database, and Web server. Application developers can develop and run their software solutions on a cloud platform without the cost and complexity of buying and managing layers; In infrastructure as a service (IaaS), consumers control and manage the systems in terms of operating systems, applications, storage, and network connectivity, but do not control the cloud infrastructure. Cloud providers provide their services according to the agreed SLA with the help of parallel processing, by scheduling resources in efficient manner and by deploying application on proper VM as per the SLA objective and at the same time performance of the applications must be optimized.

When a job is submitted to the cloud, it is usually portioned into several tasks. Following two questions are to be considered when applying parallel processing in executing these tasks:

1. In what order tasks are executed in cloud
2. How to allocate resources to tasks

This paper aimed to schedule the jobs according to the priority so that they can be executed within the deadline.

2 Related Works

The resources in cloud computing can be allocated in many different ways. Traditional and simple method of task scheduling in cloud environment uses the client tasks as the overhead application base [1, 2]. The allocation of resources that need to consider maximum utilization rate of resources algorithm related to FCFS (First Come First Serve), SJF (Shortest Job First) scheduling, priority scheduling, RR (Round Robin) scheduling, random, greedy, genetic algorithm [3]. Scheduling algorithm chooses a task to be performed and corresponding resource in which the task will be executed, according to the different characters of resource such as bandwidth, processing capabilities, cost, and load balancing, as well as base on clients requirements of deployment.

In this paper, we focus on resource allocation and task scheduling, as well as take into account some specific criteria of priorities of tasks and resources. In this paper, our focus is on to schedule the tasks in such a manner so that they could

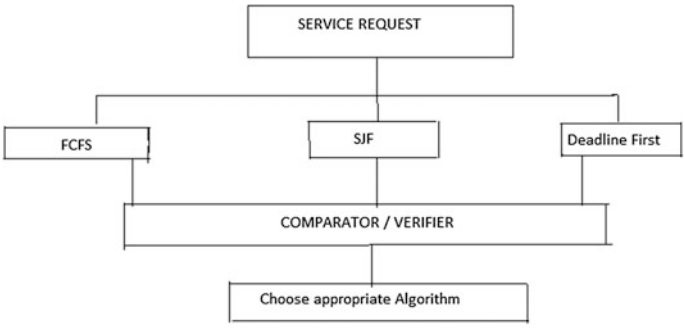

Fig. 1 System architecture

execute within the fixed deadline. If more than one tasks come at a same time, then they will have to wait for the execution. The task which has higher priority will execute first during this period and other tasks will wait. We have to also focus that the waiting time should not cross the deadline, otherwise that task will be considered lost as it cannot be executed. Waiting time is the sum of the periods spent waiting in the ready queue [4]. Minimizing waiting time is an optimized target in job scheduling, which is a famous scheduling problem and significant in providing quality of service (QoS) in industries [5]. For a batch of jobs, a job executing on a resource, minimizing waiting time can reduce the completion time and meet task priority-deadline demands.

3 System Architecture

In this architecture, we are describing the most suitable algorithm for the service request. The request is checked against each algorithm and after that it verifies which algorithm is useful to execute all the tasks (meeting SLA) within the deadline (Fig. 1).

4 Evaluation

This paper has been evaluated using the CloudSim toolkit [6]. The following three algorithms deal the problem and suggest the solution how the task should be scheduled so that the waiting time is minimized also meet the deadline.

4.1 First Come First Serve Scheduling Algorithm (FCFS)

According to this algorithm, the task which will be selected first will be executed first by the CPU. Here, the waiting time will be calculated according to the execution time of the tasks **(SLA for Process P4 is not met)**.

4.2 Shortest Job First Scheduling Algorithm (SJF)

According to this algorithm, the task which has the lowest execution time gets the highest priority and that will be executed first by the CPU. During this time, the remaining tasks will wait for the execution, and finally, the task which has the highest execution time will be executed at last. Here, waiting time will be calculated according to the priority of the task **(SLA for Process P2 is not met)**.

4.3 Deadline First-based Algorithm

According to this algorithm, we will consider the deadline as a major factor. Within the given deadline, all the tasks should be executed. Here, priority will be calculated according to the deadline that means the task which contains the lowest deadline will be assigned with the highest priority and the task which contains the highest deadline will be assigned with the lowest priority. And the waiting time will be calculated on the basis of execution time **(SLA met for all the processes)**.

5 Results

It is seen that shortest job first scheduling algorithm gives the least average waiting time, however, since deadline is not considered here, there is a possibility some jobs can be missed. In deadline first-based priority algorithm, the probability of jobs not executed within the deadline is very less. This can be seen in Table 3. Here, all the jobs are executed. Whereas in FCFS algorithm (Table 1), it is seen that job P4 is not executed as the job cannot be executed within the deadline and hence the algorithm is not useful. Similarly in SJFS (Table 2), the job P2 is not executed as the waiting time exceeds the deadline (Fig. 2).

In Table 3, deadline is considered to be the major factor. Here, priority is based on deadline, in such case, all the processes have their waiting time less than the deadline as specified in the SLA. Hence, all the processes get executed without violating the SLA

Table 1 First come first served

Serial_no.	Process	Execution_time	Waiting_time	Deadline
0	p0	5	0	8
1	P1	3	5	10
2	P2	8	8	14
3	P3	6	16	25
4	*p4*	*7*	*22*	*18*

Average waiting time = 10.2

Table 2 Shortest job first

Serial_No.	Process	Execution_time	Priority	Waiting_time	Deadline
0	p0	5	2	3	8
1	p1	3	1	0	10
2	*p2*	*8*	*5*	*21*	*14*
3	p3	6	3	8	25
4	p4	7	4	14	18

Average waiting time = 9.2

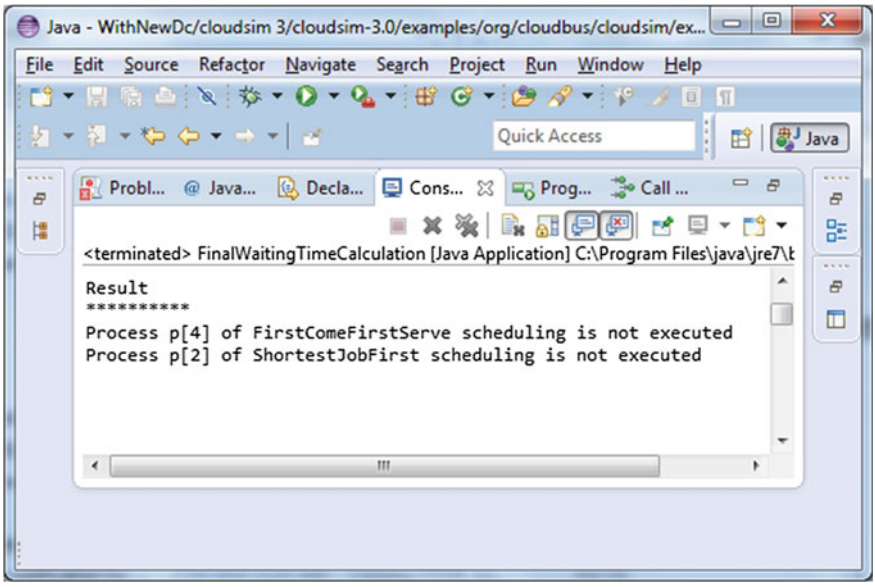

Fig. 2 Screenshot of the final result

In case if the deadline first algorithm does not meet SLA due to any reason, [7] the process can be migrated from the existing VM to multiple VM's so that SLA is met.

Table 3 Deadline-based scheduling

Serial_No	Process	Dead line	Execution_time	Priority	Waiting_time
0	p0	8	5	1	0
1	P1	10	3	2	5
2	P2	14	8	3	8
3	P3	25	6	5	23
4	P4	18	7	4	16

Average waiting time = 10.4

6 Conclusions

In this paper, we present dynamic resource allocation mechanism for preemptable jobs in cloud. We propose priority-based algorithm, in which considering multiple SLA objectives of job, for dynamic resource allocation. Here, we checked each task according to the different algorithms and calculated their waiting time. And waiting time of all the tasks are compared to the maximum deadlines of the job. First, we calculated the waiting time of task according to the first come first serve scheduling algorithm. Then next, we calculated the waiting time of the task according to the shortest job first scheduling algorithm. Here, the average waiting time comparison to first come first serve scheduling algorithm is lower. So, it means shortest job first scheduling algorithm is more efficient than the first come first serve scheduling.

After that we compared the waiting time obtaining from both the scheduling algorithms to the deadline-based scheduling algorithm. It is seen that deadlines are met and all the jobs are executed even though there is slight increase in the average waiting time. Hence, deadline should be considered as a major factor in deciding the priority-based algorithm on resource management in cloud and migration between VMs can be done if needed to execute all the processes within the deadline to meet strong SLA.

References

1. S. Selevarani, G. Sadhasivam, Improved cost-based algorithm for task scheduling in cloud computing, in *Computational Intelligence and Computing Research (ICCIC), IEEE International Conference* (2010)
2. J. Ru, J. Keung, An Empirical investigation on the simulation of priority and shortest-job-first scheduling for cloud-based software systems, in *22nd Australian Conference on Software Engineering* (2013)
3. S. Sivanandam, S. Deepa, *Introduction to Genetic Algorithms* (Springer Publishing Company, Incorporated, Berlin, 2007)
4. A. Silberschatz, P. Galvin, G. Gagne, A. Silberschatz, *Operating System Concepts*. (Addison-Wesley, Boston, 1998), p. 4
5. X. Li, N. Ye, T. Liu, Y. Sun, Job scheduling to minimize the weighted waiting time variance of jobs. Comput. Ind. Eng. **52**(1), 41–56 (2007)

6. R.N. Calheiros, R. Ranjan, A. Beloglazov, C.A. De Rose, R. Buyya, CloudSim: a toolkit for modeling and simulation of cloud computing environments and evaluation of resource provisioning algorithms (2010)
7. P.G.J. Leelipushpam, J. Sharmila, Live VM Migration techniques in cloud environment—a survey, in *Information & Communication Technologies (ICT)* (2013)

Countering Flood Attacks and Routing Misbehavior in DTN

J. Karunya Priyadarshini, P. Jesu Jayarin and J. Visumathi

Abstract Disruption-tolerant networks are prone to flood attacks in which an attacker floods the network by forwarding as many packets into the network or forwarding replica of packets into network for selfish or malicious purpose. Also selfish or malicious nodes may drop received packets intentionally even when their buffer is not full. Such routing misbehavior reduces the packet delivery ratio and wastes system resources. The proposed approach provides measures to detect flood attack using a method called claim construction. For detecting routing misbehavior, it is required that a node keeps a few signed contact logs of its previous contacts. This signed contact log consists of information of number of packets in node's buffer before this contact. Based on this contact log, the next contacted node can detect whether this node has dropped any packet.

Keywords DTN · Flood attacks · Packet dropping · Routing · Selfish nodes

1 Introduction

DTNs which are proposed in [1] are intermittently connected network. They are very helpful in situations where no proper communication infrastructure is available nor any can be built. DTNs are victims to flood attacks. Flood attacks are those in which a node forwards many packets into the network or forwards many copies of

J. Karunya Priyadarshini (✉) · P.J. Jayarin · J. Visumathi
CSE Department, Jeppiaar Engineering College, Rajiv Gandhi Salai,
Chennai, Tamilnadu, India
e-mail: karunyapriyadarshni@gmail.com

P.J. Jayarin
e-mail: jjayarin@gmail.com

J. Visumathi
e-mail: jsvisu@gmail.com

© Springer India 2015

L.P. Suresh et al. (eds.), *Artificial Intelligence and Evolutionary Algorithms in Engineering Systems*, Advances in Intelligent Systems and Computing 325,
DOI 10.1007/978-81-322-2135-7_79

packet into network. Their intention is to increase the probability of delivery of their packets. Also another issue of DTNs are the nodes of DTNs having only small cache to buffer packets may sometimes behave selfishly by not willing to spend their resources for routing another node's packets. They may falsify that they do not have enough buffer to forward this packet and drop the packets [2]. Proposed work addresses these two issues.

2 Literature Survey

Existing system uses authentication mechanisms [3] to detect flood attackers. However, authentication mechanisms may work only if the attackers are outsiders. For alleviating routing misbehavior, existing systems use watchdog-based solutions [4], in which a node after sending a packet to next node listens to the medium to detect whether that node forwards the packet or simply drops it. But this method requires connected link between sender and its neighbor, which is not possible in DTNs.

Another solution is based on 2ACK, proposed by Liu et al. [5]. However, this method is non-resistant to colluders. Colluders are two or more nodes which together take part in malicious activity. If a neighbor node sends a packet to its colluder, that node may send an acknowledgment to the source node, yet may drop packets.

3 System Architecture

Proposed system overcomes flood attacks by using claim construction called Pk-claim and Tr-claim for packet flood attack and replica attack, respectively. Proposed system also alleviates routing misbehavior by using contact log construction. The architecture of the system is explained in Fig. 1.

Proposed system first allocates a rate limit for each and every node. Then, when a node sends packet to other node, claims are constructed. These are exchanged along with the packet. Using this claim, the receiver of the data packet can determine whether this sender has sent packets more than the set rate limit. To detect dropping of nodes, 'contact logs' are constructed for each and every contact that happens between two nodes. This contact log must be shared with the next contacted node, thus enabling the detection of misbehaving nodes. If nodes are found to drop packets, they are blacklisted to ensure a high probability of packet delivery.

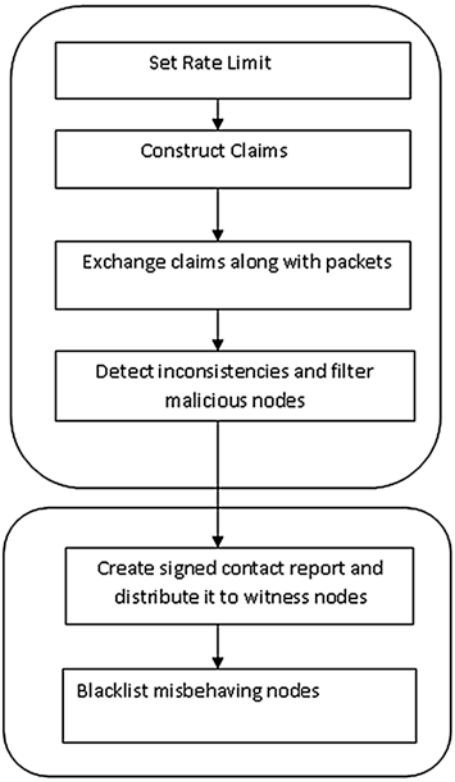

Fig. 1 Architecture diagram of proposed system

4 Working of the System

The working of the system is described as follows.

4.1 Claim Construction

To overcome flood attacks, a method called claim construction is proposed in which a metadata called claim is constructed [6]. This claim is supposed to be sent along with a node's packet. Two types of claims are to be created called Pk-claim and Tr-claim. Pk-claim is for a packet which is sent for the first time by a source node. Tr-Claim is to be sent along with a replica packet. The rate limit of each node as well as current packet rate is available in a node's Pk-Claim or Tr-claim, using which other nodes can find out whether this node has exceeded its rate limit. If it is found to exceed its rate limit, then the node is said to flood the network.

4.1.1 Rate Limit

Initially, when a node enters a network, it is given a control over the number of packets it can create and send as well as the number of packets it can replicate. This is called rate limit [7]. This rate limit is set by a trusted third party. Rate limit is set in a request-agree style. This rate limit can be upgraded or downgraded at anytime.

4.1.2 Pk-Claim

If a source node A sends a new packet P to a contacted node, it generates a Pk-claim as follows:

$$\text{Pk-claim}: \ \mathrm{A}, \mathrm{cp}, t, \mathrm{H}(\mathrm{P}), \mathrm{SIG}_{\mathrm{A}}(\mathrm{H}(\mathrm{H}(\mathrm{P}|\mathrm{A}|\mathrm{cp}|t))$$

where cp is the packet count of A. That is, A had sent cpth new packets to network before. This cp gets added once this new packet P is sent out.

4.1.3 Tr-Claim

When node R transmits a packet P to node S, it appends a Tr-claim to P. The Tr-claim includes R's current transmission count ct for P and the current time *t*. The Tr-claim is constructed as follows:

$$\text{Tr-claim}: \mathrm{R}, \mathrm{S}, \mathrm{H}(\mathrm{P}), \mathrm{ct}, t, \mathrm{SIG}_{\mathrm{R}}(\mathrm{H}(\mathrm{R}|\mathrm{S}|\mathrm{H}(\mathrm{P})|\mathrm{ct}|t))$$

4.2 Detecting Flood Attacks

Nodes that send more data than its rate limit are said to flood the network. However, in DTN, there is no central node to monitor the packets sent by each node. Proposed method takes advantage of this distributed nature of DTNs by making each node itself count the number of packets it generated and sent out, as well as each packet it has replicated and sent out. Also when a node sends a packet to its neighbor node, it sends its Pk-claim as well as Tr-claim along with the packet. On receiving this node, a receiver can detect whether the sender has exceeded the rate limit, flooding the network. Figure 2 provides an example of flood attack detection.

To defend flood attacks, the receiving node or simply the node which finds out the flood attack is needed to send an alarm into the network along with the claim in question. On receiving this alarm, the other nodes in network verifies the inconsistency between reported false claim and other collected claims.

If inconsistency is found to be correct, then the data traffic of the attacking node is filtered. If the alarm is found to be false, it is simply discarded. If the verification succeeds, then the verifying node further broadcasts this alarm so that it propagates

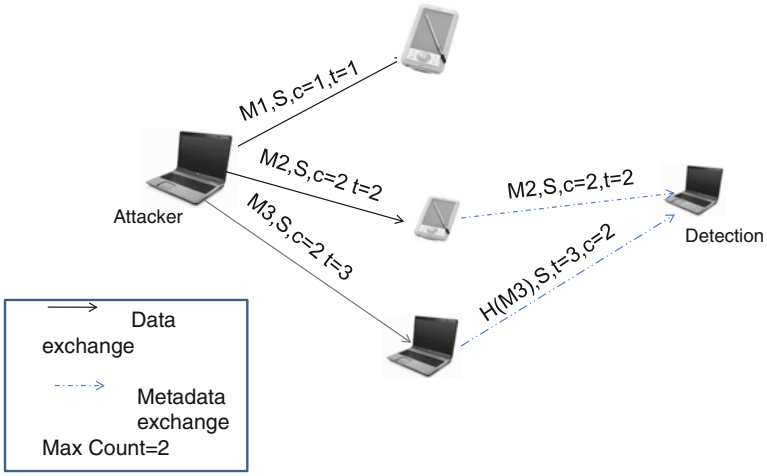

Fig. 2 An example flood attack and its detection

into the network, thus announcing all nodes in the network about the attacker. Also the attacker's data traffic is filtered.

Algorithm 1: Resolving Flood Attacks

```
Step 1: if there are any packets to send then
Step 2: generate a Pk-claim if sender is the source;
Step 3: create Tr-claims for other packets and sign
them.
Step 4: Route every packet into the network along with
the Pk-claim and(or)  Tr-claim attached.
Step 5: end if
Step 6: if Receive a packet then
Step 7: if verification of signature failed or the count
value in a packet's Pk-claim or Tr-claim is invalid then
Step 8: Discard this packet;
Step 9: end if
Step 10: Check the Pk-claim with those locally collected
and generated claims in the same time interval
Step 11: Check the Tr-claim against those locally
collected for inconsistency;
Step 12: if Inconsistency is detected in step 10 or 11
         then
step13: Tag the signer of the Pk-claim (Tr-claim,
respectively) as an attacker and add it into a blacklist;
Step 14: Disseminate an alarm against the attacker to the
network;
else
Step 15: Store the new Pk-claim (Tr-claim, respectively)
end if
end if
```

4.3 Detecting Routing Misbehavior

To detect routing misbehavior, a node is made to keep record of all previous contacts it had. This is called contact log. A contact is said to happen when two nodes meet with each other and exchange some packets. Contact log contains details such as when this contact happened, packets which were in the nodes' buffer before this contact took place, and what packets these two nodes exchange when they come into contact.

$$\mathrm{CR} = N_i, N_j, \mathrm{sn}, T, B_i, R_i, R_j, \mathrm{sig}_i, \mathrm{sig}_j$$

Here, CR is the contact log. N_i and N_j are the two participating nodes, and sn is the sequence number given to this contact. T is the time during the creation of contact log. B_i is the packet contents of node N_i before this contact; R_i and R_j denote the packets exchanged during this contact. To detect misbehaving node, the proposed method is that when a node contacts with another node, it is required to report its previous contact log so that if it had dropped any packets, it can be found out by the contacted node. Also a small part of this contact log is sent out to some selected witness nodes. This is done to avoid the node from falsely reporting the contact log. If any misreporting is found, it could be found out using the witness nodes.

Algorithm 2: Packet Dropping Detection

```
Initial buffer content: null   curr: current contact log
prev: previous contact log
When Ni and Nj comes into same contact region
do
if have packets to send or receive then
Create signed contact log for both nodes
CR_curr=N_i,N_j,sn,t,B_i,R_i,R_j,sig_i,sig_j
Distribute part of contact log to some witness nodes.
End if.
do
transfer data and CR_prev
if B_i in CR_prev  > B_i in CR_curr
then blacklist the node N_i
```

Algorithm 3: Packet Dropping and Misreporting Detection

```
Initial buffer content: null          curr:current contact log
prev:previous contact log

if CR_prev is forged

              Collect contact log of the node which provided

                 inconsistent report from its witness nodes

              aggregate data from witness nodes

                 if the  false reporting is true

                     then   blacklist the attacker
```

4.4 Defending Routing Misbehavior

Similar method is used to alleviate routing misbehavior as that of flood attacks. Once a witness node finds out the inconsistency between submitted contact log report and actual report collected from other witness nodes, it sends an alarm into the network. This alarm includes both the reports. The alarm is sent by using epidemic routing as proposed in [8]. A node on receiving this alarm is required to verify the inconsistency. If the inconsistency is found to be correct, then the misreporting node is put into black list by the verifying node. Else, the alarm is discarded.

5 Implementation and Results

The performance analysis of this model is tested using NS2 simulator. The parameters used are summarized in Table 1.

5.1 Bandwidth Consumption

It is defined as the number of packets received by all nodes lying in between source and destination. When flood attacks are present, the bandwidth consumed is high, because flooding node sends more number of packets to its next hops. This is

Table 1 Parameters used for simulation

Total number of nodes	20
Simulation time	50 s
Traffic model	CBR
Data rate	2 Mbps
Number of attacker	2
Packet size	512 bytes

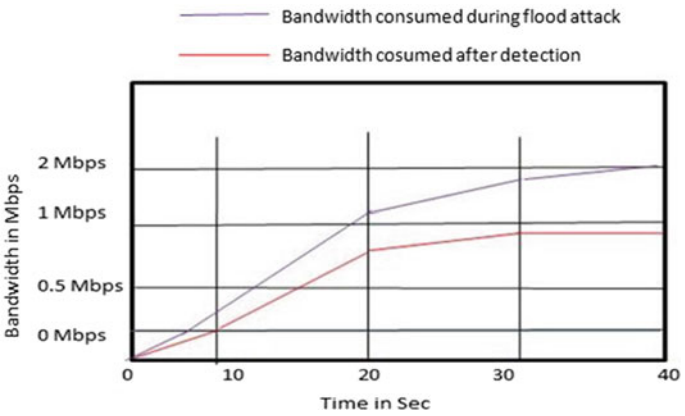

Fig. 3 Bandwidth consumption (Mbps) against time

illustrated in Fig. 3. It shows the bandwidth consumed in Mbps without using proposed detection mechanism and using detection mechanisms. The bandwidth consumption is considerably reduced after using detection of flood attack mechanism.

5.2 Packet Delivery Ratio

The ratio of number of packets received by the destination node to that of number of nodes sent by source node is called packet delivery ratio.

Proposed method reduces this defect and increases PDR by 30 %. This is illustrated in Fig. 4. The figure shows packet delivery ratio with and without the use of detection mechanism which is proposed. The results reveal that the packets are delivered to the destination when the misbehaving nodes are detected and filtered.

5.3 Rate of Detection

The rate at which the malicious node or selfish node is identified by the other participating nodes is called as rate of detection. Here, the rate of detection is defined as the number of nodes which are identified as malicious in the network to the number of actual malicious node. The effectiveness of the proposed work is studied using rate of detection. The results are shown in Fig. 5. This detection rate increases with the increased number of attackers. This is because as the number of attackers gets increased, the overall attacker traffic gets increased and so the detection mechanism works more efficiently.

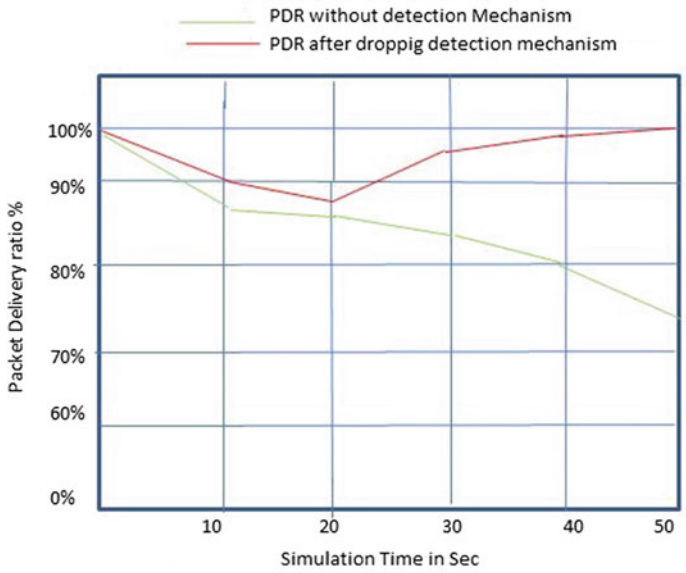

Fig. 4 PDR in % shown with respect to simulation time

Fig. 5 Rate of detection against number of malicious nodes

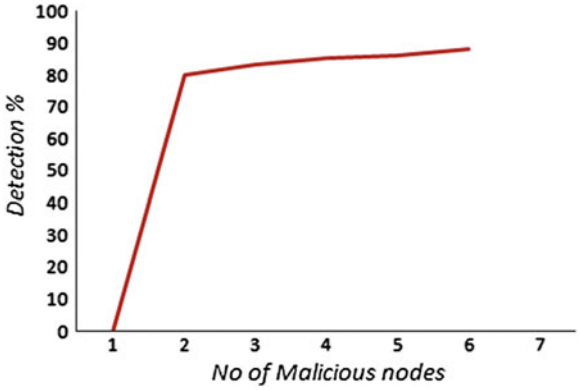

6 Conclusion

The proposed work addressed two issues in DTNs, namely flood attacks and routing misbehavior by dropping of packets. A method to alleviate it had also been proposed. This method is efficient, even if nodes falsely report their claims or contact log. This proposed method works efficiently in spite of the lack of a centralized node to traffic each node's behavior.

References

1. K. Fall, A delay tolerant network architecture for challenged internets, in *Proceedings of SIGCOMM* (2003), pp. 27–34
2. Q. Li, G. Cao, Mitigating routing misbehavior in disruption tolerant networks. IEEE Trans. Inf. Forensics Secur. **7**(2), 664–675 (2012)
3. H. Zhu, X. Lin, R. Lu, X.S. Shen, D. Xing, Z. Cao, An opportunistic batch bundle authentication scheme for energy constrained DTNs, in *Proceedings of IEEE INFOCOM* (2010)
4. S. Marti et.al., Mitigating routing misbehavior in mobile adhoc networks, in *Mobicom* (2000)
5. K. Liu, J. Deng, P.K. Varshney, K. Balakrishnan, An acknowledgment based approach for the detection of routing misbehavior in MANETs. IEEE Trans. Mobile Comput. **6**(5), 536–550 (2007)
6. Q. Li, W. Gao, S. Zhu, G. Cao, To lie or to comply: defending against flood attacks in disruption tolerant networks. IEEE Trans. Dependable Secure Comput. **10**(3), 168–182 (2013)
7. B. Raghavan, K. Vishwanath, S. Ramabhadran, K. Yocum, A. Snoeren, Cloud control with distributed rate limiting, in *Proceedings of ACM SIGCOMM* (2007)
8. A. Vahdat, D. Becker, Epidemic routing for partially connected ad hoc networks, Technical Report CS-200006 (2000)

Static ATC Estimation Using Fully Complex-Valued Radial Basis Function Neural Network

M. Karuppasamypandiyan, R. Narmatha Banu and P.M. Manobalaa

Abstract In the deregulated power systems, the available transfer capability (ATC) should be known for secure and reliable operation. ATC mainly depends on load for a particular transaction. Due to complex nature of load, it is better if the ATC estimator is able to handle this complex nature. This paper presents fully complex-valued radial basis function (FC-RBF) neural network approach for ATC estimation for bilateral transaction under normal condition. The training patterns for neural network are generated using differential evolution algorithm (DEA). The important feature of the proposed method is the use of input reduction techniques to improve the performance of the developed network. Differential evolution feature selection (DEFS) technique is proposed to reduce the complexity and training time of neural network. The proposed method is tested on IEEE 118 bus system, and results are compared with DEA and repeated power flow (RPF) results. The test results show that the proposed method reduces the training time and it is suitable for online application.

Keywords Available transfer capability · Differential evolution feature selection · Fully complex-valued radial basis function · Repeated power flow

1 Introduction

Available transfer capability (ATC) is a measure of the transfer capability remaining in the physical transmission network for the further commercial activity over and above already committed uses [1]. Mathematically, ATC is defined as the

M. Karuppasamypandiyan (✉)
Kalasalingam University, Srivilliputhur, Tamil Nadu, India
e-mail: pandi1081@gmail.com

R.N. Banu · P.M. Manobalaa
Vellammal College of Engineering and Technology, Madurai, Tamil Nadu, India
e-mail: narmi800@yahoo.co.in

P.M. Manobalaa
e-mail: mano.eie90@gmail.com

© Springer India 2015

L.P. Suresh et al. (eds.), *Artificial Intelligence and Evolutionary Algorithms in Engineering Systems*, Advances in Intelligent Systems and Computing 325,
DOI 10.1007/978-81-322-2135-7_80

total transfer capability (TTC) less than the transmission reliability margin (TRM), less than the sum of existing transmission commitments (ETC) and the capacity benefit margin (CBM). Mathematically, it is written as

$$\mathrm{ATC} = \mathrm{TTC} - \mathrm{TRM} - \sum (\mathrm{ETC} + \mathrm{CBM}) \tag{1}$$

For the sake of simplicity, TRM and CBM are assumed to be zero. The information of ATC will help market participants to reserve transmission services well in advance for optimal commercial use of transmission network. Determination of ATC considering static limits such as line thermal limit, bus voltage limit, and steady-state stability limit constraints is termed as static ATC. A number methods are proposed in the literature to calculate static ATC. In [2], a DC load flow-based method is proposed for calculation of ATC. This method does not consider the voltage limit violation, so it may lead to calculation of ATC higher than the actual value, and it may endanger security problem. In [3], AC power transfer distribution factor (ACPTDF)-based ATC computation method is proposed. This method also does not consider voltage limit violation. A repeated power flow (RPF)-based ATC computation method is proposed in [4]. This method repeatedly solves the power flow equation until thermal and voltage limit violation. But this method requires comparatively large computation time and is not suitable for online applications. Recently, evolutionary computation techniques such as genetic algorithm (GA), particle swarm optimization (PSO) [5], and differential evolution algorithm (DEA) [6] have been applied to calculate the power transfer capability. However, the optimization-based methods are also time-consuming and may not be suitable for online implementation. Recently, artificial intelligence techniques are used for online ATC estimation. The ATC estimation based on multilayer feed-forward neural network trained by quick prop algorithm is proposed in [7]. It uses the multilayer perceptron model trained by quick prop algorithm, a modified back-propagation (BP) algorithm, which usually suffers from local minima and overfitting problems. This paper proposes a fully complex-valued radial basis function (FC-RBF) neural network for ATC estimation which has the unique feature of handling complex numbers. In [8], estimation of voltage stability for different loading condition is proposed by radial basis function network model with reduced input features. A mutual information-based method is proposed to select the input features of the neural network. In [9], a new method employing differential evolution feature selection abbreviated as DEFS is used to select the features for different data sets. In this paper, DEFS is used to select the input features of the FC-RBF network for ATC estimation. The data for developing FC-RBF network are developed using DEA. The effectiveness of the proposed FC-RBF network models is tested on IEEE 118 System. The result of FC-RBF is compared with DEA and RPF results. The test results show superior performance of FC-RBF network for online ATC estimation.

2 Computation of ATC

2.1 Objective Function

The problem of ATC computation in bilateral transaction can be formulated as an optimization problem in which the objective is to maximize the difference between TTC and ETC without violating the constraints. This is stated as maximize

$$F = P_{Di}{}^{new} - P_{Di}{}^{old} \tag{2}$$

P_{Di}^{new} New change in load demand of ith sink bus from its base case load
P_{Di}^{old} Base case load demand of ith sink bus.

2.2 Equality Constraints

Real and reactive power balance equations

$$P_i - V_i \sum_{j=1}^{N_B} V_j \left[G_{ij} \cos\theta_{ij} - B_{ij} \sin\theta_{ij} \right] = 0 \quad i = 1, 2, \ldots, N_{B-1} \tag{3}$$

$$Q_i - V_i \sum_{j=1}^{N_B} V_j \left[G_{ij} \sin\theta_{ij} - B_{ij} \cos\theta_{ij} \right] = 0 \quad i = 1, 2, \ldots, N_{PQ} \tag{4}$$

2.3 Inequality Constraints

Unit constraints

$$P_s{}^{\min} \le P_s \le P_s{}^{\max} \tag{5}$$

$$Q_{gi}{}^{\min} \le Q_{gi} \le Q_{gi}{}^{\max} \tag{6}$$

Bus voltage limit

$$V_{\min} \le V \le V_{\max} \tag{7}$$

Line flow apparent power limit

$$S_{ij\,\min} \leq S_{ij} \leq S_{ij\,\max} \tag{8}$$

where

$G_{ij,}$ B_{ij}	Conductance and susceptance of transmission line connected between *i*th and *j*th bus
P_i, Q_i	Real and reactive power injection of *i*th bus
P_s	Real power generation of slack bus
Q_{gi}	Reactive power generation at bus i
N_{PV}	Number of voltage buses
N_B	Total number of buses
N_{PQ}	Number of load buses
N_{B-1}	Total number of buses excluding slack bus
ΔP_K	Change in generation of source bus from its base case value
$V_{\min}$	Minimum voltage limit in all the buses
$V_{\max}$	Maximum voltage limit in all the buses
S_{ij}	MVA limit of all branches

3 Overview of Differential Evolution Algorithm

Differential evolution [10] is a population-based stochastic search algorithm that works in the general framework of evolutionary algorithms. The various operations of DE are initialization, mutation, crossover, and selection. The various processes of DE are given below.

3.1 Initialization

The first step of DE optimization process is initialization of population. In initialization process, all candidates are randomly generated as a real-valued number within its corresponding feasible bounds using the expression

$$X_{ij}^{\ G} = X_i^{\min} + \text{rand}_i[0,1]^*(X_i^{\max} - X_i^{\min}), \quad i = 1\ldots D \text{ and } j = 1\ldots NP \tag{9}$$

where NP is number of population and D is number of decision parameter of the problem. $x_i^{\min}$ and $x_i^{\max}$ are the lower and upper bounds of the *i*th decision parameter, respectively. Once every vector of the population has been initialized, its corresponding fitness value is calculated and stored for future reference.

3.2 Mutation

During mutation, three random vectors are selected from current population. The mutation is carried out on randomly selected vector ${X_{r1}}^G$ with the difference of two other randomly selected vectors ${X_{r2}}^G$ and ${X_{r3}}^G$. The mutation vector is generated using the formula (10)

$$V_i^G = X_{r1}^G + F^*(X_{r2}^G - X_{r3}^G) \tag{10}$$

where F is scaling factor, which is typically chosen from within the range [0, 1].

3.3 Crossover

In this step, by applying crossover operation between target vector and mutant vector, a trial vector ${U_i}^{(G)}$ is created according to a selected probability distribution

$${U_i}^{(G)} = {U_{j,i}}^{(G)} = \begin{cases} V_{j,i}^{(G)} & \text{if} \quad \text{rand}_j(0,1) \le CR \text{ or } j = s \\ X_{j,i} & \text{otherwise} \end{cases} \tag{11}$$

The crossover constant CR is a user-defined value (known as the "crossover probability"), which is usually selected from within the range [0, 1].

3.4 Selection

This operator compares the fitness of the trial vector and the corresponding target vector and selects the one that provides the better solution. This selected vector is then treated as target vector for next generation. The feature of DE selection scheme is that a trial vector is compared with only one individual, not all the individuals in the current population.

$${X_i}^{(G+1)} = \begin{cases} {U_i}^{(G)} & \text{if} \quad f({U_i}^{(G)}) \le f({X_i}^{(G)}) \\ {X_i}^{(G)} & \text{otherwise} \end{cases} \tag{12}$$

4 DE Implementation for ATC Computation

The proposed DE solution for ATC problem is composed of the following steps

i. Read bus data, generator data, branch data, and specify the transaction for which the ATC has to be computed.

ii. Read data for DE operations, i.e., maximum generation limit, number of population, the change in new load demand of sink bus value as the decision variable, lower and upper limits of decision variable, scaling factor F, and crossover rate. Set generation Gen = 0.

iii. Generate population randomly according to Eq. (9), where decision variable is within its feasible bound. Compute ATC using Eq. (2) for each population of parent vector. Initialize the iteration iter = 1. For each iteration do the following steps

   a. Set the parent population with the maximum value: P_{Di}^{new} is the target vector i.
   b. Perform mutation and crossover according to Eqs. (10) and (11) and get trail vector.
   c. Selection among the target and trial vector for the survival using Eq. (12). Using selected best vector value, run NR load flow and compute ATC. Check for any operating limit violation.
   d. If any limit is violated, increase the iteration iter = iter + 1, and repeat again from step (b), till the process gets converged. If it does not converge, the population has reinitialized automatically; otherwise, go to next step. Best vector selected will be the next parent vector for the next population.

iv. Increment the generation gen = gen + 1. Check the maximum generation limit; if yes go to next step; otherwise, go to step 3. Print the corresponding selected best vector as the optimum value of P_{Di}^{new}. Finally, compute ATC using Eq. (2)

5 Review of Fully Complex-Valued Radial Basis Function (FC-RBF) Neural Network

A FC-RBF [11] is single hidden layer feed-forward neural network. It uses fully complex-valued activation function instead of Gaussian activation function. The architecture of FC-RBF network is shown in Fig. 1.

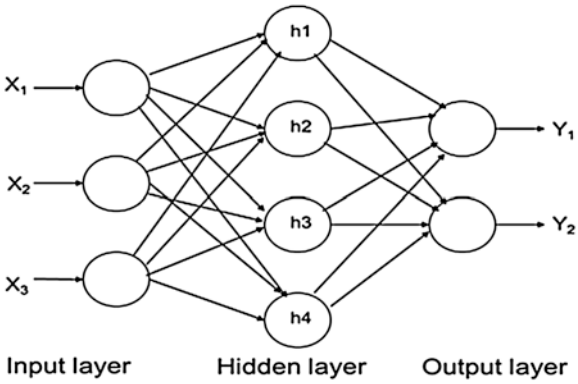

Fig. 1 Architecture of FC-RBF

The network consists of an input, a hidden, and an output layer. Let X be the m-dimensional complex-valued input to the network, i.e., $X = [X_1, X_2, \ldots, X_m]^T$ and target **T** be the n-dimensional complex-valued output vector, i.e., $T = [t_1, t_2, \ldots, t_n]^T$, where the superscript T denotes the transpose of the vectors. In FC-RBF, the input neurons are directly fed to input layer. Then, the output of the input layer is fed to hidden layer without adding any weight.

6 Simulation Results

This section presents simulation study carried out on IEEE 118 bus System for ATC estimation using proposed approach. The ATC is calculated in terms of real and reactive power transfer. Real and reactive power transfers are calculated separately in data generation step using DE approach. The combination of real and reactive power transfer is used as an output of FC-RBF, and corresponding complex load (real and reactive power) is used as an input for FC-RBF. The simulation study is carried out by developing program on MATLAB.

6.1 ATC Estimation in IEEE 118 Bus System

The IEEE 118 bus system consists of 54 generator buses, 64 load buses, and 186 transmission lines. The data for training and testing FC-RBF are generated by DE approach. Bus voltage limits and thermal limits have been considered for ATC calculation. The minimum and maximum of voltage limits are considered as 0.90 and 1.05 p.u, respectively, at all the buses. For data generation, all real and reactive power loads are varied randomly between 80 and 125 % from base load. Based on algorithm presented in Sect. 4, a total of 250 input–output pairs are generated in which 200 are used for training and 50 for testing. The ATC in MW and the reactive power transfers in MVAR at different test cases are computed. The ATC is calculated for transaction 1–118 for normal condition. Here, 1 is source bus and 118 is sink bus. Table 1 shows the values of power transfer and ATC value by FC-RBF, DE method, and RPF method.

With RBF, network with any continuous function can be approximated to within an arbitrary accuracy by carefully choosing the input features in the network provided the network structure is sufficiently large. In this work, the input features are selected using DEFS method. Totally, 20 input features are selected from 118 input features. The selected inputs for transaction between 1 and 118 are 1, 6, 11, 15, 18, 27, 32, 34, 40, 42, 45, 49, 54, 55, 56, 59, 60, 80, 90, and 116. The power transfer and ATC values for transaction 1–118 with and without input feature selection for different loading conditions are shown in Table 1. From Table 1, it was concluded that ATC obtained using input feature selection is almost same as that of ATC obtained without using input feature selection. The total number of epochs

Table 1 Power transfer and ATC for transaction 1–118

Loading condition (%)	Without feature selection				With feature selection			
	FC-RBF	DE	RPF	ATC	FC-RBF	DE	RPF	ATC
94.83	38.9 + j29.2	38.8 + j29.0	39.2 + j29.3	39.2	39.8 + j28.6	39.9 + j28.9	39.6 + j29.2	39.6
96.19	38.9 + j28.9	38.9 + j28.8	38.8 + j28.9	38.8	38.1 + j28.5	38.1 + j28.1	38.9 + j28.3	38.9
92.06	40.0 + j30.1	40.0 + j30.3	40 + j30.0	40.0	40.0 + j30.0	40.0 + j30.7	39.3 + j30.0	39.3
107.43	34.2 + j21.7	34.3 + j21.6	34.2 + j21.3	34.2	34.2 + j21.6	34.3 + j21.6	34.9 + j21.1	34.9
106.59	33.9 + j21.8	33.9 + j21.6	34.6 + j22.0	34.6	34.0 + j21.6	34.0 + j21.5	33.4 + j21.9	33.4
100.98	37.2 + j28.0	37.0 + j28.1	37.1 + j28.6	37.1	37.0 + j28.6	37.1 + j28.5	37.3 + j28.4	35.9
107.60	34.2 + j20.9	34.1 + j20.9	34.1 + j20.9	34.1	34.3 + j20.9	34.3 + j20.9	34.0 + j20.9	34.0
92.93	39.8 + j30.0	39.8 + j29.9	39.7 + j29.9	39.7	39.9 + j29.9	39.9 + j29.9	40.0 + j30.0	40.0
108.12	33.9 + j20.8	33.6 + j20.8	33.8 + j20.9	33.8	33.6 + j20.3	33.5 + j20.7	32.8 + j20.8	32.1
103.90	35.8 + j22.1	35.8 + j22.2	35.8 + j22.1	35.8	35.7 + j22.1	35.9 + j22.0	34.2 + j22.3	34.2

considered is 100. For calculating ATC for 10 operating conditions, RPF took nearly 250 s and DE took 110 s. Training time for FC-RBF with all inputs is 81 s. But the training time with input feature selection is reduced to 12 s. This shows that FC-RBF with reduced input can be used for fast ATC estimation in real-time application.

7 Conclusion

This paper has presented fully complex-valued radial basis function (FC-RBF) neural network-based method for ATC estimation for online application. Simulation study is carried out on IEEE 118 bus system. Numerical results are compared with DEA and RPF methods. The test results show that the proposed approach estimates the ATC accurately in very short period. By reducing the dimension of the input features using DEFS, the efficiency of the FC-RBF model has been significantly increased both in the learning and estimation stages. It makes DEFS method suitable for ATC problem, and FC-RBF-based ATC estimation is suitable for online application. This will help ISO to update the ATC value on open access same time information system within short period.

References

1. R.D. Christie, B.F. Wollenberg, I. Wangstien, Transmission management in the deregulated environment. Proc. IEEE **88**(2), 170–195 (2000)
2. G.C. Ejebe, J. Tong, J.G. Waight, J.G. Frame, X. Wang, W.F. Tinney, Available transfer capability calculation. IEEE Trans. Power Syst. **13**(4), 1521–1527 (1998)
3. A. Kumar, S.C. Srivastava, S.N. Singh, Available transfer capability determination in competitive electricity market using AC distribution factors. Electr. Power Compon. Syst. **32**, 927–939 (2004)
4. B. Mozafari, A.M. Ranjbar, A.R. Shirani, A. Barkeseh, A comprehensive method for available transfer capability calculation in a deregulated power system, in *IEEE International Conference on Electric Utility Deregulation, Restructuring and Power Technologies*, vol. 2 (2004), pp. 680–685
5. H.H. Chen, G.Q. Li, H.L. Liao, A self-adaptive improved particle swarm optimization algorithm and its application in available transfer capability calculation, in *IEEE Computer Society ICNC*, vol. 3 (2009), pp. 200–205
6. R. Rajathy, R. Gnanadass, K. Manivannan, H. Kumar, Differential evolution based method for total transfer capability evaluation. Int. J. Eng., Sci. Technol. **2**(5), 81–91 (2010)
7. X. Luo, A.D. Patton, C. Singh, Real power transfer capability calculations using multi-layer feed-forward neural networks. IEEE Trans. Power Syst. **15**(2), 903–908 (2000)
8. D. Devaraj, J. Preetha Roselyn, On-line voltage stability assessment using radial basis function network model with reduced input features. Electr. Power Energy Syst. **33**, 1550–1555 (2011)
9. R.N. Khushaba, A. Al-Ani, A. Al-Jumaily, Feature subset selection using differential evolution and a statistical repair mechanism. Expert Syst. Appl. **38**, 11515–11526 (2011)

10. R. Storn, K. Price, Differential evolution—a simple and efficient heuristic for global optimization over continuous spaces. J. Global Optim. **11**, 341–359 (1997)
11. S. Suresh, N. Sundararajan, R. Savitha, A fully complex-valued radial basis function network and its learning algorithm. Supervised Learn. Complex-valued Neural Netw. Stud. Comput. Intell. **421**, 49–71 (2013)

Big Data and Cloud: A Survey

K.S. Sangeetha and P. Prakash

Abstract Today, the world has become closer due to the development of Internet. More people communicate via Internet, and the volume of data to be handled also grows. Nowadays, we talk about peta- and zettabytes of data and this volume of data needs to be processed and analyzed further which had led to the research field of big data storage and analysis. Cloud computing is another emerging area in which the services such as infrastructure, storage, and software are provided to the consumers on demand basis. In this paper, we discuss about the big data, cloud computing, and how big data are handled in cloud computing environment.

Keywords Cloud computing · Big data

1 Introduction

In this Internet era, the volume of data is growing. For example, social networking sites such as Facebook, Twitter, and LinkedIn produce voluminous data every day. This paves the way to analyze and manage these large amount of data in the fields such as information network analysis, semantic Web analysis, bioinformatics data analysis, and multimedia data analysis. The management of these large amounts of data usually tera to petabytes of data leads to the research of big data analysis. In the year 2013, Gartner's Inc. Hype Cycle states that cloud computing and big data are the fastest growing technologies which dominate the research world for the next

K.S. Sangeetha (✉)
Department of Information Technology, Sri Krishna College of Engineering and Technology, Kuniamuthur, Coimbatore 641008, Tamil Nadu, India
e-mail: sangee4u@gmail.com

P. Prakash
Department of Computer Science and Engineering, Amrita University, Ettimadai, Coimbatore 641112, Tamil Nadu, India
e-mail: npprakash@gmail.com

© Springer India 2015

L.P. Suresh et al. (eds.), *Artificial Intelligence and Evolutionary Algorithms in Engineering Systems*, Advances in Intelligent Systems and Computing 325,
DOI 10.1007/978-81-322-2135-7_81

decade [1]. In this paper, the overview of big data management technologies and handling of the big data in cloud computing environment are discussed. In Sect. 2, definitions of big data given by various experts are discussed. Section 3 discusses about cloud computing definition, benefits, and challenges. Section 4 gives an overview of various big data management systems. Section 5 discusses about various programming models that can be implemented to handle big data management.

2 Big Data

Big data means bulky volume of data with different dimensions. Gartner defines big data as high volume, high velocity, and high variety information assets that demand cost-effective, innovative forms of information processing for enhanced insight and decision making. The volume of data is very large, and it cannot be handled by traditional database systems. The data are growing at an exponential rate as we talk about tera and petabytes of data in today's Internet world. The Internet produces a variety of information, i.e., some data are structured, some are semi-structured, and some are unstructured [2]. IBM states that all unstructured data collected from various applications such as social media sites, digital pictures and videos, and climatic information are big data [3]. Chang et al. [4] define big data as datasets which cannot be handled and processed by the current technology within a tolerable elapsed time.

3 Cloud Computing

Cloud computing is nothing but providing software and hardware services over the Internet and managed by third parties [5]. The cloud computing model allows access to information and computer resources from anywhere that a network connection is available. US National Institute of Standards and Technology (NIST) defines cloud computing as

> Cloud computing is a model for enabling convenient, on-demand network access to a shared pool of configurable computing resources (e.g., networks, servers, storage, applications, and services) that can be rapidly provisioned and released with minimal management effort or service provider interaction. This cloud model promotes availability and is composed of five essential characteristics (On demand self service, Broad network access, Resource pooling, Rapid Elasticity, Measured Service), three service models (Infrastructure as a Service, Platform as a Service, Software as a Service), and four deployment models (Private Cloud, Community Cloud, Public Cloud, Hybrid Cloud). [6]

3.1 Benefits and Challenges of Cloud Computing

According to Forbes, the benefits of cloud computing [7] are Cost saving, elasticity, scalability, load "bursting" and storage on demand and the drivers for cloud are Pay—as—you go, Multi-tenancy, Elasticity of resources—Allows Ease of Implementation, On-Demand self-service, Reduces carbon Footprint.

The challenges in the cloud computing environment are assurance of privacy and security, reliability and availability, transition and execution risk, cultural resistance, regulatory ambiguity, especially internationally, costs associated with a migration from legacy infrastructure to the cloud, and issues of taxation [7].

4 Big Data Management in Cloud

Traditionally, to store data, relational databases are used. As big data involve voluminous, heterogeneous, and continuously varying data, the traditional relational databases are not suitable to handle the big data. Various data management systems are available to handle the big data in cloud. Table 1 provides the list of big data management systems.

4.1 Programming Models

MapReduce. The large amount of datasets can be processed with a very simple and powerful framework called MapReduce [17] which is one of the best models suitable for applications that are performing a parallel computation in distributed environment. Every day, Google's clusters handle tera bytes of data using MapReduce framework. Map and reduce functions are used to perform any computation over the big data by user on the distributed systems. Figure 1 shows the example of MapReduce computation framework [17]. Here, the input data split and the master assigns the workers to work on a split. Task to be performed by worker is defined in the map function by the user. The map function generates an intermediate key value pairs and is stored in temporary storage system available on local disks. The master assigns workers who perform reduce function to work on these intermediate results and produce the output. MapReduce framework can be used for data processing on heterogeneous systems. The limitation of MapReduce framework is that it is not suitable for multiple datasets.

HadoopDB. HadoopDB [18] is open source Java software implemented using MapReduce framework. Figure 2 shows the architecture of HadoopDB. Hadoop will acts as a task coordinator in HadoopDB which connects multiple single-node database systems. Hadoop also performs communication among the networks over the HadoopDB. By using MapReduce framework, queries are parallelized.

Table 1 List of big data management systems

Big data management system	Description
Google: Bigtable	Bigtable is a distributed storage system used by Google products and projects such as Google search engine, Orkut, Google docs, and Google Maps. Bigtable can store petabytes of data across thousands of servers [8]
AppEngine Datastore	It is a data storage system provided by Google for Web applications. AppEngine uses a language called GQL. It provides a Python interface [9]
Yahoo!: PNUTS/ Sherpa	PNUTS is a database system for yahoo Web applications. It is renamed to Sherpa. It servers the data for Web applications [10]
Amazon: Dynamo	This is a data storage system built to support Amazon's internal applications. It highly available reliable, scalable, and distributed key-/value-based database system [11]
Amazon S3	Amazon simple storage service (S3) is an object-based online public storage service
Amazon simple DB	Simple DB is designed for structured data storage
Amazon RDS	Amazon relational database service is provided to work with MySql database
Microsoft: DRYAD	DRYAD is designed for data parallel applications used internally by Microsoft. The high-level language used is DryadLINQ. Supports T-SQL, ODBC, and ADO.NET data access [12]
SQL Azure	It is a cloud-based relational database service built on Microsoft SQL technologies. Highly available, scalable, and multi-tenant database service hosted in the cloud [13]
Open source projects—Cassandra	The Apache Cassandra is an decentralized open source database which provides high availability, scalability, and fault tolerance [14]
Hypertable	Hypertable is an open source database system which runs on the top of the distributed file systems [15]
CouchDB	CouchDB is a document-based database storage system. Documents can be accessed using Web browser. JavaScript is used to query and manipulate the documents [16]

There are two layers in that HadoopDB architecture which are called data storage layer and data processing layer. The data storage layer is also known as Hadoop distributed file system (HDFS). HDFS is a block-structured file system managed by a central NameNode. The individual input files are divided and dispersed across DataNodes in the cluster. NameNode holds the metadata information about the DataNodes. JobTracker which acts as master for processing the data, and the map reduce jobs are carried out by the TaskTracker.

HaLoop. HaLoop is developed by making certain modifications in the Hadoop MapReduce framework. HaLoop programming model [19] is developed to include iterative processing in the applications as HadoopDB lacks support for iterative computations. HaLoop uses the distributed file system and task queue structure of HadoopDB but has introduced a new application programming interface, new loop

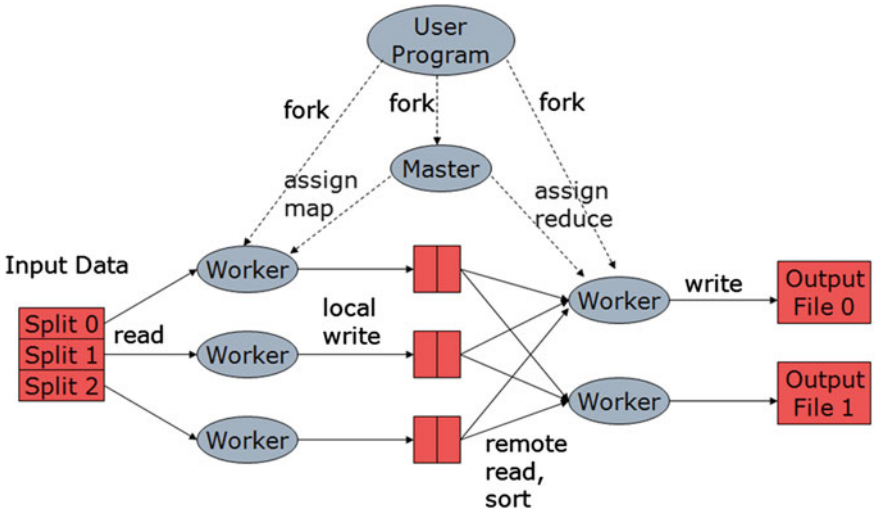

Fig. 1 Architecture of map reduce framework [17]

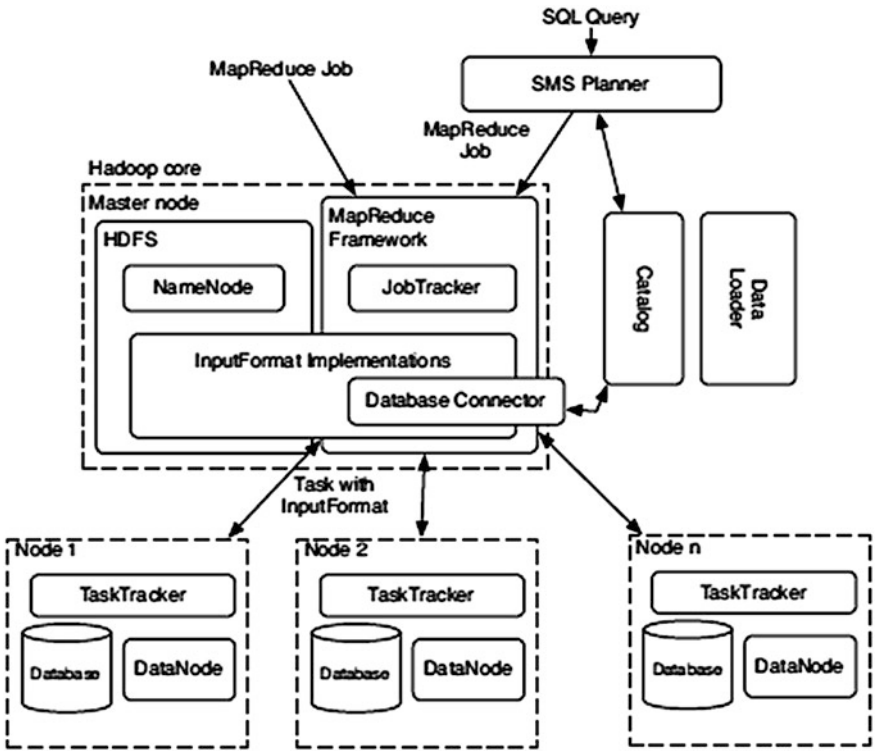

Fig. 2 Architecture of HadoopDB [18]

control module, a task scheduler and caches, and indexes of application data on the slave node. The task scheduler and task tracker are modified to incorporate iterative programming applications.

5 Conclusion

In this data age, the volume of data is growing at a faster pace because of the increase in the computational capability. The Internet has become the source of information for the whole world. The social networking sites, for example, Facebook, twitter, and LinkedIn, have users in millions and more and new users gets added frequently and the data go on accumulated. The traditional relational database management systems are not suitable for handling this voluminous data. This has led to the research of handling and management of this big data. Cloud computing is another emerging filed and is widely used because of its pay-as-you-go model and economic advantage. In this paper, we discussed about big data, cloud computing, cloud computing models, benefits, challenges, and the big data management in cloud computing environments. The challenges of big data management in cloud are providing privacy, security, reliability, and availability which necessitate further research in big data management in cloud computing environments.

References

1. D. Laney, The importance of 'Big Data': A definition (2008)
2. P. Devi, T. Gaba, Cloud computing. Int. J. Adv. Res. Comput. Sci. Softw. Eng. **3**(5) (2013)
3. P. Mell, T. Grance, Definition of cloud computing, Technical report(NIST) (2009)
4. F. Chang, J. Dean, S. Ghemawat, W. Hsieh, D. Wallach, M. Burrows, T. Chandra, A. Fikes, R. Gruber, Bigtable: A distributed storage system for structured data. ACM Trans. Comput. Syst. **26**(2), 4 (2008)
5. B. Cooper, R. Ramakrishnan, U. Srivastava, A. Silberstein, P. Bohannon, H. Jacobsen, N. Puz, D. Weaver, R. Yerneni, Pnuts: Yahoo!'s hosted data serving platform. PVLDB **1**(2), 1277–1288 (2008)
6. G. DeCandia, D. Hastorun, M. Jampani, G. Kakulapati, A. Lakshman, A. Pilchin, S. Sivasubramanian, P. Vosshall, W. Vogels, Dynamo: Amazon's highly available key-value store, in *SOSP* (2007), pp. 205–220
7. M. Isard, M. Budiu, Y. Yu, A. Birrell, D. Fetterly, Dryad: distributed data-parallel programs from sequential building blocks, in *EuroSys* (2007), pp. 59–72
8. J. Dean, S. Ghemawat, Mapreduce: Simplified data processing on large clusters. Commun. ACM **51**(1), 107–113 (2008)
9. A. Abouzeid, K. Bajda-Pawlikowski, D. Abadi, A. Rasin, A. Silberschatz, Hadoopdb: An architectural hybrid of MapReduce and DBMS technologies for analytical workloads. PVLD **2** (1), 922–933 (2009)
10. Y. Bu, B. Howe M. Balazinska, M.D. Ernst, HaLoop: Efficient iterative data processing on large clusters, in *The 36th International Conference on Very Large Data Bases* **3**(1), p. 1317 (2010)

An E-mail Application on Named Data Networking

Sandhya Giri, Anupama Josyula and V. Vetriselvi

Abstract Named data networking (NDN) is a network layer protocol that aims to replace the IP layer in the current Internet architecture. Currently, e-mails are sent from one mail server to another by identifying each server by its IP address. In this paper, we propose to develop an e-mail application that runs on NDN. The challenge in developing an e-mail application on NDN is to completely abandon the usage of IP addresses and concentrate on the 'content' to be sent or received. We intend to send a mail from sender's computer to receiver's computer over NDN. We propose to adapt the protocols used in e-mail transfer such as SMTP and POP to suit the characteristics of NDN.

Keywords Named data networking (NDN) · SMTP · E-mail · POP3

1 Introduction

Named data networking transforms 'where' (IP address, Host…) to 'what' (Content). Named data networking (NDN) uses interest and data packets instead of IP datagrams. Every data packet must correspond to an interest packet. Unlike IP which has a stateless data plane, NDN has a statefull data plane with a forwarding strategy. Any NDN router has three data structures: content store (CS), pending interest table (PIT), and forwarding information base (FIB) [1]. The content store caches the data packets that have passed through that router. The FIB is used to forward interest/data packets to the best next hop based on the name prefix. The difference between this

S. Giri (✉) · A. Josyula · V. Vetriselvi
College of Engineering, Anna University, Guindy, Chennai 600025, India
e-mail: sandhya.giri18@gmail.com

A. Josyula
e-mail: jvanupama@gmail.com

V. Vetriselvi
e-mail: kalvivetri@gmail.com

© Springer India 2015

L.P. Suresh et al. (eds.), *Artificial Intelligence and Evolutionary Algorithms in Engineering Systems*, Advances in Intelligent Systems and Computing 325,
DOI 10.1007/978-81-322-2135-7_82

FIB and that in IPs is that here FIB not only contains the best next hop, but also contains multiple next hops ranked in the order of their reachability to the destination. Routing protocols are used to populate the FIB.

NDN is based on producer-consumer model of communication. The consumer first sends an interest packet with the name of the desired data. The intermediate routers that receive this interest check whether a data packet with the same name prefix is already present in the CS. If so, the router returns the data packet and the interest does not travel any further. The data packet follows the same route as the interest packet. If the corresponding data packet is not available in the CS, the router adds an entry in the PIT containing the interface on which the interest was received, and forwards the interest to the next hop listed in the FIB for this name prefix. If there is already a PIT entry for the interest packet, then the current interface is added to the already existing entry. The producer on receiving the interest packet sends a data packet containing the requested content. The data packet travels the same path as that of the interest packet.

The paper is organized as follows: Sect. 2 talks about related work, Sect. 3 elaborates the proposed system, and we conclude our paper in Sect. 4.

2 Related Work

The current Internet architecture has been in existence for more than three decades. Owing to the increasing use of the INTERNET from various devices such as laptops, tablets, mobile phones, palmtops, for countless applications, the current Internet architecture falls short in certain aspects such as security and exhaustion of IP addresses. Thus, the need to develop new Internet architecture was realized and the concept of NDN originated. Since then, considerable amount of work has been done in this field.

Routing undoubtedly is the most important function of NDN that helps in forwarding of interest packets from the consumer to the producer. A lot of research has been done on this area, and various routing techniques/mechanisms have been developed.

Dai et al. [2] introduce a two-layer intradomain routing mechanism where the network layer is partitioned into two layers, namely prefix announcement layer (PA) and topology management layer. The latter maintains the topology of the network, while the former publishes the content based on its popularity. The widely used intradomain routing protocol, i.e., open shortest path first (OSPF), has been extended to NDN as OSPFN (an OSPF-based routing protocol for NDN) [3]. OSPFN is a name-based extension of OSPF that runs on IP and supports configured multipath forwarding where users specify the links to be used when the best route fails. In succession to OSPFN, Torres et al. [4] described a controller-based routing scheme for named data network. Special controllers are used to acquire topology, calculate routes, and store named data locations. Hoque et al. [5] discuss named

data link state routing protocol (NLSR). It is an enhancement of OSPFN but runs on NDN without the use of IP addresses. In addition to multipath forwarding, NLSR ranks the next hops based on their ability to reach the destination efficiently and uses the ranked next hops to forward the interest packets.

Forwarding of interest/data packets based on the routing information has three main concerns: fast name lookup, forwarding strategy, and caching policy and storage management [6]. Since NDN supports in-network caching of data by automatically caching all data packets, cache management becomes an important task. Efficient mechanisms for maintaining CS that caches the data packets have been developed. Li et al. [7] describe three such mechanisms: bottom-up, top-down, and bridging algorithms that reduce the inter-ISP traffic. These algorithms have been shown to perform better than the widely used leaving copies everywhere (LCE), in which each router caches whatever passes through it. The caching algorithms (bottom-up, top-down, bridging) cache only those data packets that are popular, but the criteria for popularity varies based on the scheme.

Developing applications that run on NDN architecture is also an ongoing research effort. A few applications have been developed and tested so far. Zhu et al. [8] developed a serverless multiuser CHAT application called 'Chronos.' Multiuser applications usually need a centralized server. But here, multiple users can chat without a central server by exchanging digests of the messages. A peer-to-peer car racing game has also been synchronized over NDN [9]. Dai et al. [10] talk about the extension of existing protocols such as HTTP, FTP, and SMTP to NDN. Yuan et al. [11] have compared and evaluated content distribution in HTTP and NDN. It has been observed that in wired networks, HTTP outperforms NDN, while in wireless networks, NDN outperforms HTTP. Kulinski et al. [12] describe the advantages of NDN in video streaming applications over TCP/IP.

Our work can be considered as one of the driver applications on NDN. We plan to develop an e-mail application that runs on the named data networking. There has been no implementation of e-mail yet.

3 E-mail Application on NDN

In our proposed system, e-mail addresses are algorithmically translated to NDN names used to transfer mails. For example, cse@gmail.com yields/gmail.com/email_rcpt/cse, where the well-known name 'email_rcpt' identifies the e-mail service the same way TCP port 25 identifies it for IP. Users continue to work with familiar e-mail addresses and do not usually see their NDN names at all, just as they rarely see Mail eXchanger (MX) host names or IP addresses in SMTP transfers today. One clear advantage of using NDN names is that we avoid DNS lookup for canonical host names of mail servers, thereby reducing overhead caused by the DNS lookup. The overall working of the e-mail application is shown in Fig. 1.

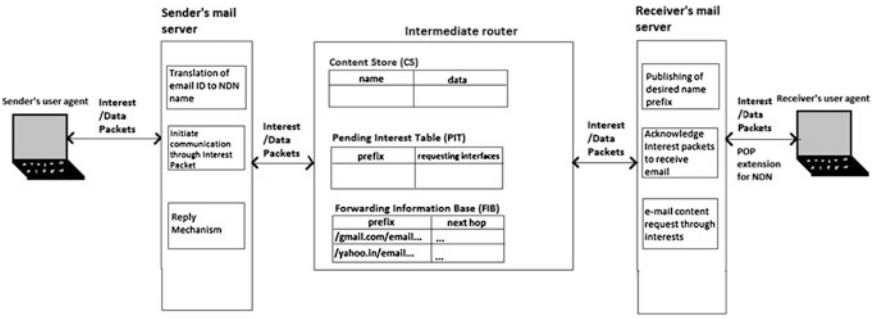

Fig. 1 High-level block diagram

3.1 Initial Setup for NDN to Support E-mail

Initially, e-mail ids are translated to NDN names. During translation of e-mail ids to NDN names, the domain name following the '@' symbol in the receiver's e-mail id becomes the first part of the name prefix. Following this is the command 'email_rcpt' that identifies the mail service. Then comes the sender's name (the part before @ symbol), e.g., cse@gmail.com yields/gmail.com/email_rcpt/cse. Following this, sender's information is added to the name prefix to facilitate the receiver's mail server to send a response. Then, the sender's mail server must also choose a unique id that identifies the conversation. This initial setup paves way for the communication between sender's user agent and sender's mail server.

```
Translation of email id to NDN name
Input: eid- email id
Output: ndnName- NDN name
String init = eid.substring(eid.indexOf('@')+1)
String sender=eid.substring(0,eid.indexOf('@'))
String ndnName="/"
ndnName.append(init)
ndnName.append("/email_rcpt/")
ndnName.append(sender)
return ndnName
```

3.2 E-mail Transfer from Sender's User Agent to Sender's Mail Server

The communication between sender's user agent and sender's mail server takes place as shown in Fig. 2. The sender's user agent initiates the communication by sending an interest packet to the sender's mail server. The sender's mail server then acknowledges the receipt of interest packet by sending an OK data packet back. The sender's mail server then sends interests with the name prefix and a segment number appended to it. Segments are used to pull down multipart messages. If the

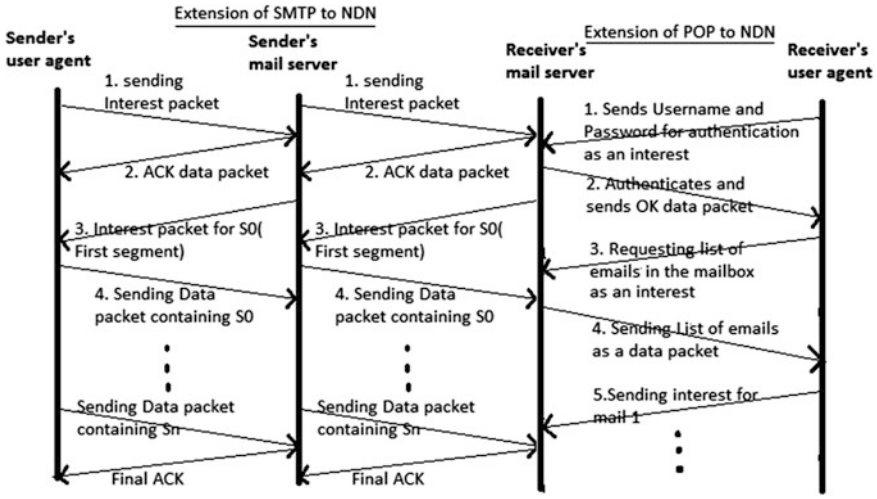

Fig. 2 Timeline diagram for e-mail application on NDN

message itself is short, it can be sent along with the initial interest and the OK data packet can be considered as the final ACK. Once the OK/final ACK data packet is sent by the sender's mail server to the sender's user agent, the communication between sender's mail server and the receiver's mail server starts.

```
Generating initial interest to send mail to sender's mail server
Input: sid- sender's email id
       rid- receiver's email id
       msg- the body of the email
Output: An interest packet with name prefix prefix
  If msg.length < threshold
    /*then msg along with other SMTP data can be encrypted and appended to
    the name prefix*/
    Prefix= algorithm1 (sid)
    conv_id= rand()
    Prefix.append("/"+ sender_comp_name+"/"+conv_id)
    Prefix.append(msg)
  Else:
    /* then initial interest contains only the SMTP envelope fields and msg
    is partitioned into segments and published under the sender's namespace
    */
    Prefix= algorithm1 (sid)
    conv_id= rand()
    Prefix.append("/"+ sender_comp_name+"/"+conv_id)
    // segment the msg into data packets
    npref = sender_comp_name+"/"+conv_id
    sno=0
    while msg.length>0
      data= msg.substring(0,threshold)
      npref.append("S"+sno)
      increment sno
      msg=msg.substring(threshold+1)
      publish 'data' under the namespace 'npref'
    End while
  End if
```

3.3 E-mail Transfer from Sender's Mail Server to Receiver's Mail Server

The sender's mail server initiates the communication by sending an interest packet to receiver's mail server. The name prefix of that packet contains SMTP data: some adapted set of SMTP envelope fields such as sender's e-mail id and a signature (data themselves are included if small) and the name required for reverse path. The receiver's mail server acknowledges the receipt of interest packet by sending an OK data packet. Then, the receiver's mail server pulls down the e-mail by sending interest packets to sender's mail server for corresponding segments. Then, the receiver's user agent pulls down the e-mail content from receiver's mail server.

Generating initial interest to send mail from sender's mail server to receiver's mail server

Input: *sid*- sender's email id
rid- receiver's email id
msg- the body of the email

Output: An interest packet with name prefix *prefix*

```
  Prefix= algorithm1(rid)
  pk_receiver= send interest to get public key of the receiver.
  sk = choose a random session key
  enc_sk=E_pk_receiver(sk)
  conv_id= rand()
  sender_ns= sender_mailserver_name+"/"+sender_comp_name+
"/"+ conv_id
  data= sender_ns+"/"+sid+"/"+ signature
  If msg.length <threshold
    data.append(msg)
    enc_data=E_sk(data)
    Prefix.append(enc_sk+"/"+enc_data)
  Else:
    enc_data=E_sk(data)
    Prefix.append(enc_sk+"/"+enc_data)
    sno=0
    while msg.length>0
      data= msg.substring(0,threshold)
      sender_ns.append("S"+sno)
      increment sno
      msg=msg.substring(threshold+1)
      publish 'data' under the namespace 'sender_ns'
    End while
  End if
```

```
Acknowledgement from receiver's mail server
Input: npref- the name prefix in the interest packet received.
Output: ACK or NACK with name prefix prefix
  receiver_ns= algorithm1(rid)
  sk= D_pr_receiver(npref)
  data=D_sk(part of the npref after enc_sk)
  sid= extract sender's email id from data
  prefix= extract reverse path from data
  signature= extract signature from data
  if data does not contain msg:
    Algorithm5(prefix)
  End if
  if sid is known/valid
    send ACK with prefix prefix
  else
    send NACK with prefix prefix
  End if

Receiving email content from sender's mail server by receiver's mail server
Input: prefix- reverse path to sender's mail server
Output: receiving all the msg segments from the sender's mail server
  Sno=0 //segment number
  Pref= prefix+"/S"+sno
  Send interest with prefix Pref
  While Frag_bit≠0
    Increment sno
    Pref= prefix+"/S"+sno
    Send interest with prefix Pref
  End While
```

3.4 E-mail Transfer from Receiver's Mail Server to Receiver's User Agent

In POP3, only when the user wants to view the mail, it is downloaded from his/her mailbox in the mail server, whereas in the case of IMAP, the e-mails are available independent of whether the user wants to view them or not. In fact, IMAP pushes the mails to the user agent. Since we are extending POP3, the receiver's user agent has to initiate the communication with the receiver's mail server and pull down the e-mail. The receiver's user agent initiates the communication by sending an interest to the receiver's mail server. The latter acknowledges the receipt of the interest packet by sending an OK data packet. Then, the receiver's user agent pulls down the e-mail segments by sending interest packets to the receiver's mail server. Thus, the e-mail is successfully received by the receiver's computer.

```
Deliver email from receiver's mail server to receiver's user agent
Input: rid- receiver's email id
       U_name-  user name
       Pass- password
Output: email received by the receiver's user agent
  Prefix= algorithm1(rid)
  Rec_ns=prefix
  Conv_id=rand()
  Prefix.append("/email_user/"+u_name+"/email_pass/"+pass)
  Prefix.append("/"+receiver_comp_name+"/"+conv_id)
  Send an interest with name prefix prefix to the receiver's mail server
  If ACK received
     Rec_ns.append("/email_list")
     Rec_ns.append("/"+receiver_comp_name+"/"+conv_id)
     Send an interest with prefix Rec_ns
      /* in the data packet received, the receiver can extract the links to
      emails and send separate interests for each of them*/
  End if
```

Conclusion and Future Work

In this paper, we have demonstrated how an e-mail system can work on named data networking. We have shown how SMTP and POP3 can be extended to (NDN). The roles of sender's user agent, receiver's user agent, sender's mail server, and receiver's mail server can be clearly understood. To further illustrate the ideas explained in this paper, we are currently working on simulating the scenario in ndnSIM [13, 14]—an ns-3-based simulator that implements named data networking communication model. So far, we have successfully implemented the e-mail transfer from sender's user agent to sender's mail server and from sender's mail server to receiver's mail server. We plan to analyze this system and bring about improvements in terms of reliability, security, and speed.

References

1. Named data networking project: www.named-data.org
2. H. Dai, J. Lu, Y. Wang, B. Liu, Two layer intra domain routing scheme for named data networking, in *Proceeding of Globecom—Next Generation Networking and Internet Symposium* (2012)
3. L. Wang, A.K.M.M. Hoque, C. Yi, A. Alyyana, B. Zhang, OSPFN: An OSPF based routing protocol for named data networking. NDN, Technical Report NDN-0003 (2012)
4. J. Torres, L. Ferraz, O. Duarte, Controller-based routing scheme for named data network. Technical Report Electrical Engineering Program (2012)
5. A.K.M.M. Hoque, S.O. Amin, A. Alyyan, B. Zhang, L. Zhang, L. Wang, NLSR: Named-data link state routing protocol, in *the Proceeding of ICN'13* (2013)
6. H. Yuan, T. Song, P. Crowley, Scalable NDN forwarding: concepts, issues and principles (IEEE, 2012)

7. J. Li, H. Wu, B. Liu, J. Lu, Effective caching schemes for minimizing inter-ISP traffic in named data networking, in *18th International Conference on Parallel and Distributed Systems,* IEEE (2012)
8. Z. Zhu, C. Bian, A. Afanasyev, V. Jacobson, L. Zhang, Chronos: serverless multi-user chat over NDN. NDN, Technical Report NDN-0008 (2012)
9. Z. Qu, J. Burke, Egal Car: a peer-to-peer car racing game synchronized over named data networking. NDN, Technical Report NDN-0010 (2012)
10. H. Dai, B. Liu, Y. Chen, Y. Wang, On pending interest table in named data networking. *ANCS.* (2012)
11. H. Yuan, P. Crowley, Experimental evaluation of content distribution with NDN and HTTP, in *the Proceeding of INFOCOM Mini-Conference*. IEEE (2013)
12. D. Kulinski, J. Burke, L. Zhang, Video streaming over named data networking. IEEE COMSOC MMTC E-letter, **89**(4), (2013)
13. NDN Simulator Project: www.ndnsim.net
14. A. Afanasyev, I. Moiseenko, L. Zhang, ndnSIM: NDN simulator for NS-3. NDN, Technical Report NDN-0005 (2012)

Hierarchical Character Grouping and Recognition of Character Using Character Intensity Code

V.C. Bharathi and M. Kalaiselvi Geetha

Abstract This paper presents an approach for grouping and recognition of handwritten characters. The approach uses an efficient feature called character intensity code (CIC). A hierarchical recognition methodology based on the structural details of the characters is adopted. At the first level, similar structured characters are grouped together, and the second level is used for individual character recognition. Support vector machine is used for classification which achieves an overall accuracy of 93.61 %.

Keywords Handwritten character recognition · Segmentation · Character intensity code (CIC) · Hierarchical character clustering · Support vector machine

1 Introduction

Handwriting recognition is a method by which the computer is made to learn, understand, and interpret the languages used and written by the human beings. It provides us a whole new way by which a computer can interact with human beings, in their own languages. Handwritten recognition is the interpretation of data which describes handwritten objects. Handwritten recognition is a process of automatic computer recognition of characters. Characters are scanned to produce digitized text. Handwritten character recognition is comparatively difficult, as different people have different writing styles. So handwritten character is still a subject of active research and has wide range of application. Conversion of handwritten characters is important for making several important documents related to our

V.C. Bharathi (✉) · M. Kalaiselvi Geetha
Department of Computer Science and Engineering, Annamalai University, Chidambaram, India
e-mail: bharathivc@gmail.com

M. Kalaiselvi Geetha
e-mail: geesiv@gmail.com

© Springer India 2015

L.P. Suresh et al. (eds.), *Artificial Intelligence and Evolutionary Algorithms in Engineering Systems*, Advances in Intelligent Systems and Computing 325,
DOI 10.1007/978-81-322-2135-7_83

history, such as manuscripts into machine editable form so that it can be easily and preserved. Automatic recognition of handwritten information presents on documents such as cheques, envelopes, forms, and other manuscripts has a variety of practical and commercial applications in post offices, libraries, banks, and publishing houses.

2 Related Work

Pirlo et al. [1, 2] handwritten character recognition based on static and dynamic zoning topologies designed the regular grids that superimpose on the pattern images into regions of equal shape using Voronoi-based image zoning. Choudhary et al. [3] proposed binarization technique to extract features and recognize the character using multi-layered feed forward neural network obtained recognition accuracy. Vamvakas et al. [4] proposed new feature extraction based on recursive subdivisions of the foreground pixels. SVM is used to classify the handwritten character. Li et al. [5] proposed directional string of statistical and structure features implemented and classified by using a nearest neighbor matching algorithm. Das et al. [6] proposed quad tree longest run features taken in vertical, horizontal, and diagonal directions. SVM is used to classify and recognize the handwritten numerals. Reza et al. [7] developed a reliable grouping schema for the similar looking characters using density of nodes which is reduced by half from one level to the next and classified the groups in SVM. Bhowmik et al. [8] proposed Daubechies wavelet transform with four coefficients for feature extraction, and then, the features are grouped based on similar shapes. SVM classifier is used to classify the groups.

3 Outline of the Work

The proposed work initially considers the problem of grouping of alphabets based on their structural details. At the next step, the individual characters are identified at another level of granularity where the misclassifications between them are least possible. The rest of the paper is organized as follows. Section 4 describes proposed hierarchical character recognition. Feature extraction is described in Sect. 5. Hierarchical character clustering is presented in Sect. 6. Section 7 shows the experimental results of our approach with SVM, and Sect. 8 concludes this work.

4 Proposed Hierarchical Character Recognition

This section describes all steps to carry out hierarchical character recognition as shown in Fig. 1.

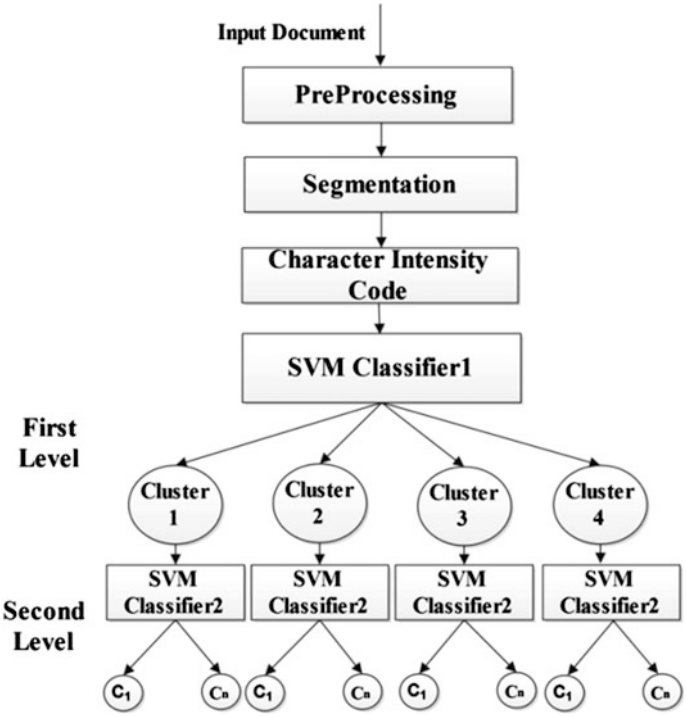

Fig. 1 Hierarchical character recognition

4.1 Dataset

Handwritten dataset is created for uppercase characters. The input images were saved in JPEG/PNG format for further preprocessing as shown in Fig. 2a.

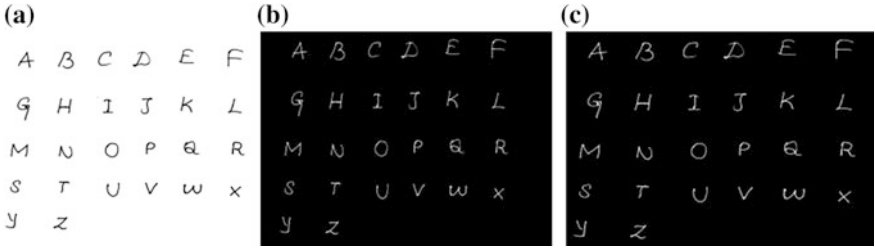

Fig. 2 **a** Input document. **b** Binarization. **c** Morphological filtering

4.2 Preprocessing

The role of preprocessing is to eliminate the contradiction that is succeeded to handwritten words. The samples may be contained on a deafening, different background, and also, the quality of the images may be tarnished. It is necessary to improve the image quality for segmentation.

Binarization Original RGB image is converted to gray scale, and then, the image is complimented to obtain an image as shown in Fig. 2b for further processing.

Morphological Filtering An image may contain numerous imperfections. Filtering is applied over the image to remove the unwanted imperfections by using area opening [9] as shown in Fig. 2c.

Segmentation is the process which is used to split the images into characters. Segmentation is done by finding the connected components by placing a bounding box over the character. To extract the bounding box character is called contours. Extracting character are various sizes, so uniformly resize to 100 × 100 for feature extraction.

5 Character Intensity Code

All segmented character images are used for the feature extraction. In our approach, character intensity code (CIC) is used to extract the features from the grayscale image based on blocks. The block is under consideration of size 100 × 100. This 100 × 100 region is divided into $r \times c$ subblocks each of size 5 × 5 number of subblocks(n), where r and $c = 20$. The values of r and c are fixed in such a way that each subblock is of equal size. Each subblock image of 20 × 20 pixels with intensity range of 0–255 is shown in Fig. 3. The mean of the pixel intensity of each subblock is computed as

$$b_n = \frac{\sum_{i=1}^{r} \sum_{j=1}^{c} \text{count}(p_{i,j})}{r \times c} \quad \text{if}(p_{i,j} > 127) \tag{1}$$

where b_n is number of subblocks, $p_{i,j}$ is intensity of pixels, r is number of rows, and c is number of columns. In 5 × 5 subblocks, each subblock computes the mean of pixel intensity. Thereby, 25 feature dimensions are extracted from CIC and fed to the SVM classifier [10–13] to classify the group model and character model.

6 Hierarchical Character Clustering

Character clustering is the task of grouping a set of character in such a way that characters in the same group. It can be defined as grouping organisms according to their structural similarities. This means that organisms that share similar features are

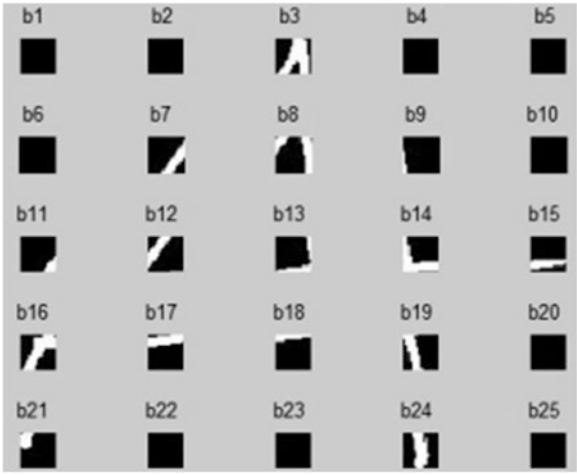

Fig. 3 Character subdivided 5 × 5 subblocks

Table 1 Hierarchical character grouping

Label	Cluster name	Group name	Characters
1	Cluster 1	Horizontal	A, B, E, F, G, H, R
2	Cluster 2	Vertical	I, J, K, L, M, N, P, T
3	Cluster 3	No center	C, D, O, Q, U, V, W
4	Cluster 4	Center	S, X, Y, Z

placed in one group. The goal of hierarchical clustering analysis is to find out ultrametric proximities that are reasonably close to the observations. In hierarchical group, character are grouped based on the structural similarities and the centroid region of the character are grouped as shown in the Table 1.

7 Experimental Results

The experiments are carried out in Windows 8 operating system with Intel Xeon X3430 Processor 2.40 GHz with 4 GB RAM. Proposed method is evaluated using the handwritten dataset. Extracted CIC features are fed to LIBSVM [14] tool to develop the model for each group, and these models are used to recognize the characters. RBF kernel is used for experimental purpose, which nonlinearly separates the training data into a higher dimensional space.

7.1 Handwritten Dataset

In our experiment, 6,500 samples of handwritten characters are collected from 50 different writers. Each writer contributed 5 times of each uppercase alphabet out of 26.

Uppercase alphabets collected from different age and different writing styles and size are considered. The handwritten documents were scanned at dimensions 1,700 × 2,338 pixels, 200 dpi with 24 bit image. Out of 50 different writers, 36 writers samples were taken for training and 14 writers samples were taken for testing.

7.2 Evaluation Metrics

Precision (P) and recall (R) are the commonly used evaluation metrics, and these measures are used to evaluate the performance of the proposed system. The measures are defined as follows

$$Precision = \frac{\text{No. of true positives}}{\text{No. of true positives + false positives}}$$

$$Recall = \frac{\text{No. of true positives}}{\text{No. of true positives + false negatives}}$$

The work used F-score as the combined measure of precision (P) and recall (R) for calculating accuracy which is defined as follows

$$F_{\propto} = \frac{2PR}{P + R}$$

where $\propto$ is weighting factor and $\propto = 1$ is used.

7.3 Group Model SVM with RBF Kernel

Initially, 25 dimensional features are extracted using CIC. All the characters are hierarchical grouped as shown in Table 1 and the groups are trained and tested in RBF kernel with C = 500, $\gamma = 0.1$ to identified individual groups at the first level classification (horizontal, vertical, no center and center) recognition accuracy are shown in Table 2.

Table 2 Confusion matrix for handwritten dataset using SVM with RBF kernel **(94.5 %)**

Group name	Horizontal	Vertical	No center	Center
Horizontal	**0.92**	0.08	0.00	0.00
Vertical	0.06	**0.94**	0.00	0.00
No center	0.02	0.04	**0.94**	0.00
Center	0.02	0.00	0.00	**0.98**

7.4 Character Model SVM with RBF Kernel

In the group, model SVM construct four models M1(horizontal), M2(vertical), M3 (no center), and M4(center). In second level SVM, the testing samples are tested in vertical, horizontal, no center and center models to identify the individual character. The recognition accuracy of individual character is shown in Tables 3, 4, 5, and 6 at the second level classification. The recognition accuracy of character model is shown in Fig. 4.

Table 3 Confusion matrix for horizontal character using SVM with RBF kernel **(93.57 %)**

	A	B	E	F	G	H	R
A	**0.85**	0.00	0.00	0.00	0.00	0.15	0.00
B	0.00	**0.98**	0.02	0.00	0.00	0.00	0.00
E	0.00	0.08	**0.92**	0.00	0.00	0.00	0.00
F	0.00	0.00	0.00	**1.00**	0.00	0.00	0.00
G	0.00	0.00	0.00	0.00	**1.00**	0.00	0.00
H	0.11	0.00	0.00	0.00	0.00	**0.89**	0.00
R	0.09	0.00	0.00	0.00	0.00	0.00	**0.91**

Table 4 Confusion matrix for vertical character using SVM with RBF kernel **(93.62 %)**

	I	J	K	L	M	N	P	T
I	**0.85**	0.08	0.00	0.00	0.00	0.00	0.00	0.07
J	0.01	**0.91**	0.00	0.00	0.00	0.00	0.00	0.08
K	0.00	0.00	**1.00**	0.00	0.00	0.00	0.00	0.00
L	0.00	0.00	0.00	**1.00**	0.00	0.00	0.00	0.00
M	0.00	0.00	0.00	0.00	**0.94**	0.06	0.00	0.00
N	0.11	0.00	0.00	0.00	0.03	**0.97**	0.00	0.00
P	0.00	0.00	0.00	0.00	0.00	0.00	**1.00**	0.00
T	0.01	0.17	0.00	0.00	0.00	0.00	0.00	**0.82**

Table 5 Confusion matrix for center character using SVM with RBF kernel **(96 %)**

	S	X	Y	Z
S	**0.98**	0.00	0.00	0.02
X	0.00	**0.95**	0.05	0.00
Y	0.00	0.09	**0.91**	0.00
Z	0.00	0.00	0.00	**1.00**

Table 6 Confusion matrix for no center character using SVM with RBF kernel **(91.28 %)**

	C	D	O	Q	U	V	W
C	**0.88**	0.00	0.12	0.00	0.00	0.00	0.00
D	0.00	**0.93**	0.07	0.00	0.00	0.00	0.00
O	0.00	0.00	**0.86**	0.14	0.00	0.00	0.00
Q	0.00	0.00	0.06	**0.94**	0.00	0.00	0.00
U	0.00	0.00	0.00	0.00	**0.89**	0.11	0.00
V	0.00	0.00	0.00	0.00	0.07	**0.93**	0.00
W	0.09	0.00	0.00	0.00	0.01	0.03	**0.96**

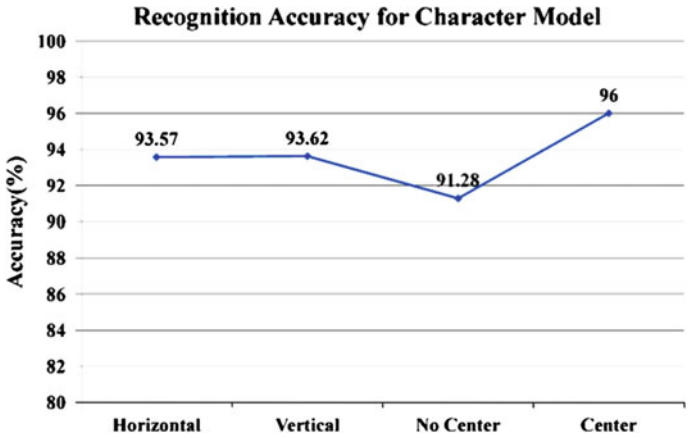

Fig. 4 Recognition accuracy of characters at the second-level classifier

8 Conclusion

This paper presented a method for hierarchical character grouping and recognizing individual character using CIC. Experiments are conducted on both datasets, handwritten dataset considering uppercase character. Based on structural similarities and centroid of region, characters are grouped and recognize the individual character using multiclass SVM with RBF kernels. Recognition accuracy of overall handwritten dataset for groups is 94.5 % and for characters is 93.61 %.

References

1. G. Pirlo, D. Impedovo, Adaptive membership functions for handwritten character recognition by Voronoi based image zoning. IEEE Trans. Image Process. **21**(9), 3827–3837 (2012)
2. G. Pirlo, D. Impedovo, Fuzzy zoning based classification for handwritten characters. IEEE Trans. Fuzzy Syst. **19**(4), 780–785 (2011)

3. A. Choudhary, R. Rishi, S. Ahlawat, Offline handwritten character recognition using features extracted from binarization technique, in *AASRI Conference on Intelligent Systems and Control* (2013), pp. 306–312
4. G. Vamvakas, B. Gatos, S.J. Perantonis, Handwritten character recognition through two stage foreground sub sampling. Pattern Recogn. **43**, 2807–2816 (2010)
5. L. LI, L.L. Zhang, J.F. SU, Handwritten character recognition via direction string and nearest neighbor matching. J. China Univ. Posts Telecommun. **19**(2), 160–165 (2012)
6. N. Das, J.M. Reddy, R. Sarkar, S. Basu, M. Kundu, M. Nasipuri, D.K. Basu, A statistical topological feature combination for recognition of handwritten numerals. Appl. Soft Comput. **12,** 2486–2495 (2012)
7. K.N. Reza, M. Khan, Grouping of handwritten Bangla basic characters, numerals and vowel modifiers for multilayer classification, in *Proceedings of International Conference on Frontiers in Handwriting Recognition ICFHR '12* (2012), pp. 325–330
8. T.K. Bhowmik, P. Ghanty, A. Roy, S.K. Parui, SVM based hierarchical architectures for handwritten Bangla character recognition. Int. J. Doc. Anal. Recogn. (IJDAR) **12**, 97–108 (2009)
9. V.C. Bharathi, M.K. Geetha, Segregated handwritten character recognition using GLCM features. Int. J. Comp. Appl. **84**(2), 1–7 (2013)
10. N. Cristianini, J. Shawe-Taylor, *An Introduction to Support Vector Machines and Other Kernel-based Learning Methods* (Cambridge University Press, Cambridge, 2000)
11. T. Mitchell, *Machine Learning*, Computer Science Series (McGraw-Hill, Burr Ridge, 1997)
12. V. Vapnik, *Statistical Learning Theory* (Wiley, New York, 1998)
13. J.P. Lewis, Tutorial on SVM. CGIT Lab. (2004)
14. C.-C. Chang, C.-J. Lin, LIBSVM: a library for support vector machines. ACM Trans. Intell. Syst. Technol. **2**, 1–27 (2011)

Multi-view Face Expression Recognition—A Hybrid Method

Prakash Natarajan and Vijayalakshmi Muthuswamy

Abstract Facial expressions play a significant role in human communication, and their automatic recognition has several applications especially in human–computer interaction. Recognizing facial actions is very challenging due to uneven facial deformation, angle of face poses, ambiguous and uncertain face component measurements. This paper proposes a hybrid approach for face pose detection and facial expression recognition. To speed up expression evaluation process, pose estimation is carried out prior to feature extraction to select appropriate shape model. The major contribution of this paper is introducing a hybrid classification method which uses Ada-Boost for Action Unit classification and Temporal Rule-based classification for correcting Action Unit errors. The experimental results show that this hybrid classification method produces better performance than other classifier which ideally improves overall performance of the system.

Keywords Expression recognition · Pose estimation · Action unit classification · Feature point tracking · Active shape model

1 Introduction

Facial expression contains much more powerful, natural, and immediate information for human-to-human communication and social life, allowing people to understand each other beyond the verbal domain. Automatically analyzing facial expression in real time without human intervention will help intelligent computer system to understand people's behavior well. It can be used in many potential applications in areas such as human–computer interaction, emotion analysis and

P. Natarajan (✉) · V. Muthuswamy
Department of Information Science and Technology, Anna University, Chennai, India
e-mail: prakas.rj@gmail.com

V. Muthuswamy
e-mail: vijim@annauniv.edu

© Springer India 2015

L.P. Suresh et al. (eds.), *Artificial Intelligence and Evolutionary Algorithms in Engineering Systems*, Advances in Intelligent Systems and Computing 325,
DOI 10.1007/978-81-322-2135-7_84

recognition, computer vision, images understanding, and synthetic face animation. The facial action coding system (FACS) [1] is an objective and comprehensive coding system used in the behavioral science.

An automatic multi-view face expression recognition system needs to solve the following problems: detection and localizing parts of faces in the image, detecting the pose of the face, facial feature extraction, and facial expression classification. Face detection has been studied by many researchers [2, 3], and it is clear that most successful algorithm is Viola-Jones face detector [4]. Once a face is detected in the image, the corresponding region is extracted and is usually normalized to have the same size. Pose estimation is a key task in multi-view face recognition. The entire result of the expression recognition is mainly based on pose estimation. A view-based multi-view face detection and pose estimation methods are clearly discussed in [5].

Facial feature extraction attempts to find the most appropriate representation of the face images for recognition. There exists various model-base and model-free approaches for extracting features from the image. One of model-based approach called ASM proposed by Cootes [6] is a popular approach to represent deformable objects, where shapes are represented by a set of feature points. The feature points can also form a geometric graph representation of the faces. The distances between feature points and the relative sizes of the major face components are computed to form a feature vector.

Action Unit classification has been done in many existing methods [7, 8], and these methods classify each AU or certain AU combinations independently and statically, ignoring the semantic relationships among AUs and the dynamics of AUs [9]. Rule-based methods discussed in [10] detail how the feature point's variation is classified into Action Unit. Facial action recognition is accomplished through probabilistic inference which systematically integrates the facial motion measurements with the facial action model.

In this paper, in contrast to other approaches, a hybrid expression recognition system has been built which is capable of estimating pose of the image and infers the expression. Based on the pose estimated, appropriate ASM is selected for feature extraction. The measurements obtained from feature extraction are used by Ada-Boost classifier for Action Unit classification. A probabilistic framework systematically combines the measurements and AU for inferring the expression.

2 Related Works

This section discusses the various research works carried out in pose estimation and expression recognition.

Head pose estimation is the process of inferring the orientation of a human head from digital imagery. A survey on head pose estimation [11] discusses various methods for head pose estimation.

Expression recognition system proposed by Li et al. [12] discusses method to infer emotion for frontal view images. But the real challenge is to evaluate expression for real-time images which can be of any view. Thus, we need a system to detect the pose of the image and then infer the expression based on the pose. Some of the papers discussing both challenges are reviewed here.

Chen et al. [13] proposed a method to detect pose and expression from a multi-pose images. This method a hybrid classifier selects local and global feature for classifying the expression. This system uses three temporary rules for classifying expression other than usual classifier result. These techniques can be employed in our system to improve classification result. Hesse et al. [14] proposed a method which uses AAM [15] for extracting local features and SVM [16] for classification. The proposed system also uses shape model ASM [6] for feature extraction, and it is found that ASM used system performs better than AAM in subjective context.

Feature extraction methods are also discussed in [17–20] discusses about feature extraction for face expression recognition. Classification of expression into Action Units and other units is discussed in [7, 21–23]. The probabilistic framework used in [24] shows how integrate AU into expressions.

The proposed hybrid model uses pose estimator 20 for pose estimation and combines the probabilistic framework and ASM of [12] in recognition part.

Compared to previous-related works, this paper has the following features.

1. This system is capable of recognizing expression in multi-view or with non-frontal images also.
2. The results of pose estimation are not only used for feature extraction but also used in Action Unit classification, and thus, number of AU required of inferring expression can also be reduced.
3. A combining classification method which combines Ada-Boost result with temporal rule-based classifier 24 improves recognition rate of AU.

3 System Architecture

See Fig. 1.

3.1 Localizing Face Parts

When an input image is given, the system will localize face and its components using Voila-Jones detector [4], and on applying Gabor transformation to the detected face, it looks as shown in the Fig. 2.

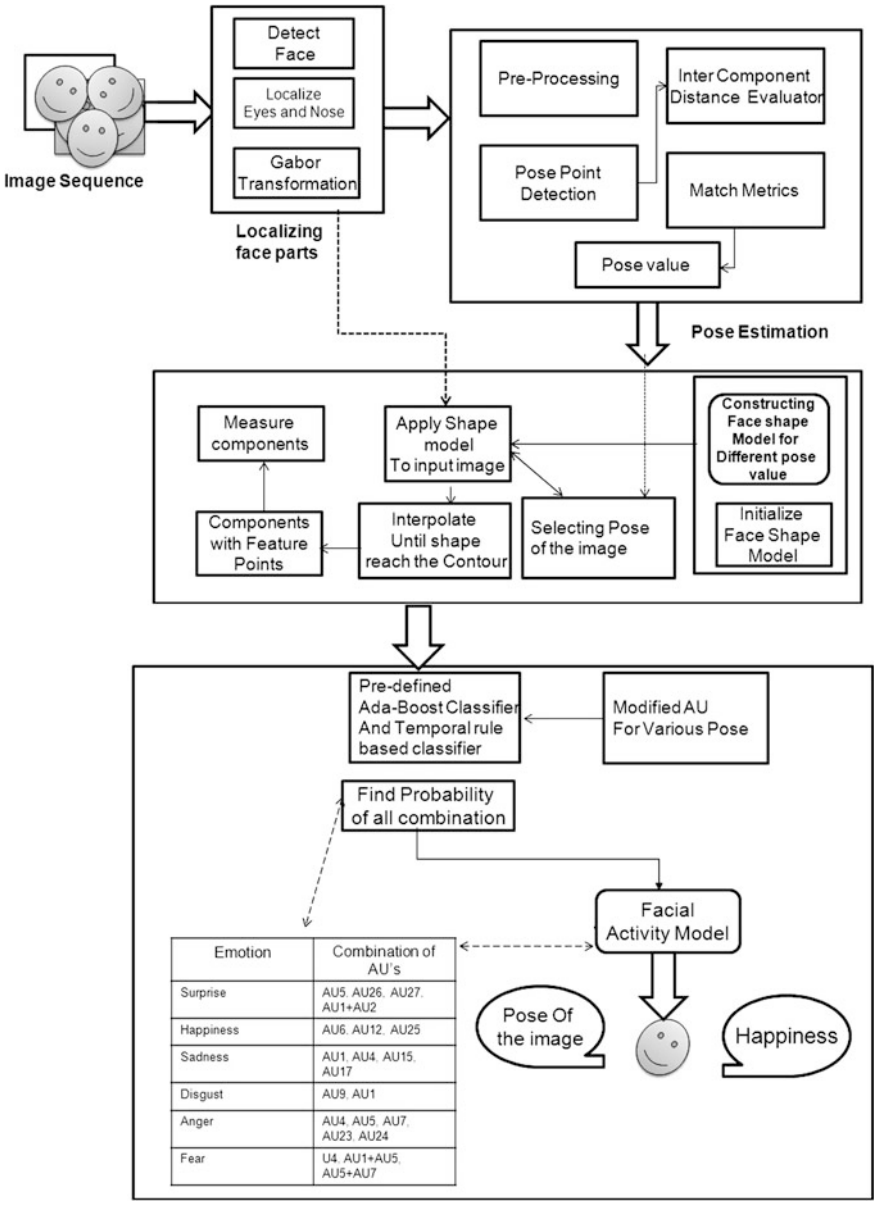

Fig.1 System architecture

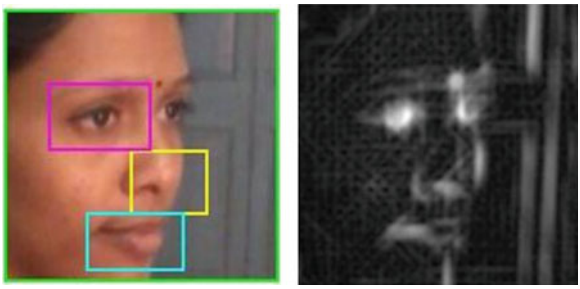

Fig. 2 Detected and Gabor applied face

Fig. 3 Pose pointed face

3.2 Pose Estimation

Based on the Gabor features of the image, pose points are plotted on the components. Once these points are plotted on the component, the next step is to compute distance between the components. Relative distance between the components derives the pose and angle of the image (Fig. 3).

3.3 Active Shape Model for Various Angles

Active shape model [6] is a model-based approach which is usually used when system has prior knowledge about the feature to be extracted. In this system, we need different mean shape of ASM for different angles (0, 30, 60, and 90).

Based on the pose angle, appropriate ASM model is selected and features are extracted. Figure 4 shows the ASM for pose angle 0.

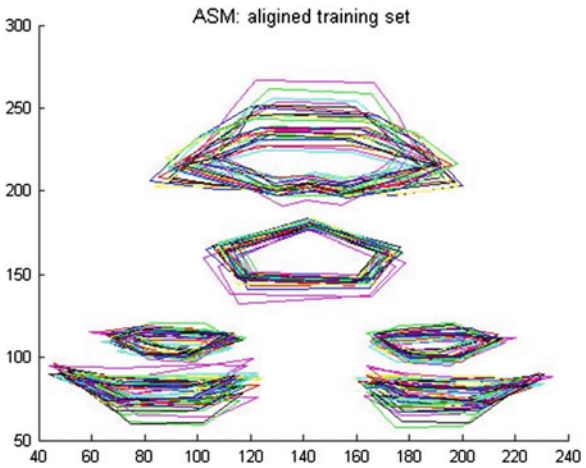

Fig. 4 Generalized ASM face shape model of pose angle 0

Table 1 Emotion AU combination table

Emotion	Combination of AUs
Surprise	AU5, AU26, AU27, AU1 + AU2
Happiness	AU6, AU12, AU25
Sadness	AU1, AU4, AU15, AU17
Disgust	AU9, AU1
Anger	AU4, AU5, AU7, AU23, AU24
Fear	U4, AU1 + AU5, AU5 + AU7

3.4 Action Unit Classification

Ada-Boost classifier 9 uses these measurements of the component and classifies the Action Unit of the component. Table 1 shows how the combination of the Action unit determines the expression. Action Unit table 2 has been adopted in this paper for frontal images, but for multi-view images, a modified combination is used.

4 Experiment and Results

The entire system is implemented in MATLAB R 2012 environment. Figure 5 shows the GUI window developed for system. CK and FERET database are used as dataset for entire training and testing.

Figure 6 shows how the ASM is overlapped on the face cropped image and extraction of the features from it. Figure 7 shows the outcome measurement and resulting expression of the given input.

Fig. 5 GUI window developed for system

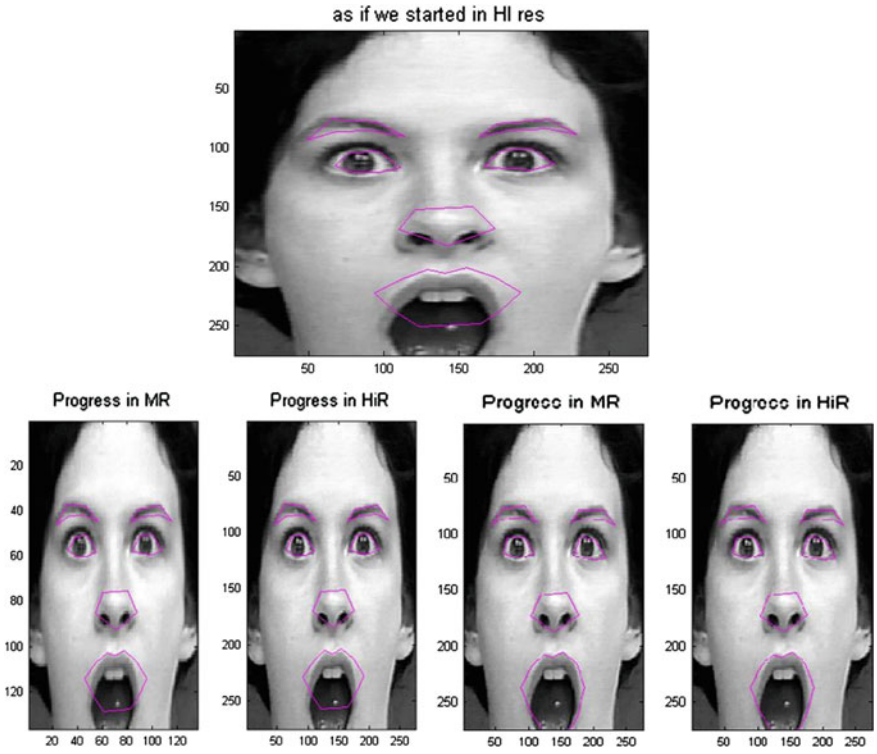

Fig. 6 ASM feature extraction

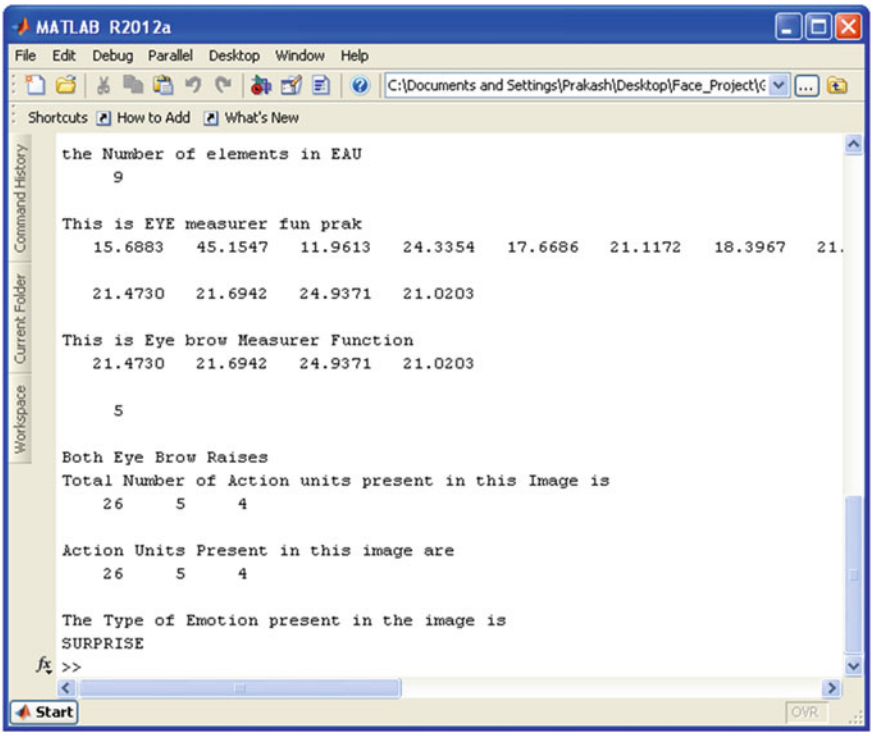

Fig. 7 Output window

4.1 Performance Evaluation

In our implementation, we took CK+ and FERET database as input and obtained following results. It is clear from the Table 2 our system has produced better result for both face detection and pose estimation.

Table 2 Result analysis

Dataset	Face detection	Pose estimation	Happy	Surprise	Angry	Sad	Fear
CK+ (%)	95	91	94	97	92	91	94
FERET (%)	93	94	95	96	92	94	95

5 Conclusion

In this paper, a face expression recognition system based on pose estimation and hybrid classification method is proposed. This system adopts active shape model (ASM) for facial feature point positioning and Ada-Boost classifier for classification of Action Units. To improve the Action Unit recognition accuracy, temporal rule classification is combined with existing Ada-Boost. This system adopts a probabilistic framework for inferring the expression based on combination of Action units.

In this paper, evaluation of model is done on multi-view face images. This system has produced better recognition rate for some AU, but improvement in overall performance of this system can be achieved by combining the face activity model with image-based approaches.

References

1. P. Ekman, W. Friesen, *Facial Action Coding System: A Technique for the Measurement of Facial Movement* (1978)
2. E. Hjelmas, B. Low, Face detection: a survey. Comput. Vis. Image Underst. **83**(3), 236–274 (2001)
3. S. Li, A. Jain, *Handbook of Face Recognition*, 2nd edn. (Springer, New York, 2011)
4. P. Viola, M. Jones, Robust real-time object detection. Int. J. Comput. Vis. **57**(2), 137–154 (2004)
5. J.-C. Chen, J.-J.J. Lien, A view-based statistical system for multi-view face detection and pose estimation. Image Vis. Comput. **27**(9), 1252–1271 (2009)
6. T.F. Cootes, C.J. Taylor, T. Cooper, J. Graham, Active shape models-their training and application. Comput. Vis. Image Underst. **61**(1), 38–59 (1995)
7. K. Ko, K.-B. Sim, Facial emotion recognition using a combining AAM with DBN, in *International Conference on Control, Automation and Systems* (2010), pp. 1436–1439
8. J.J. Lien, T. Kanade, J.F. Cohn, C. Li, Detection, tracking, and classification of action units in facial expression. J. Robot. Autom. Syst. **31**(3), 131–146 (2000)
9. Y. Tong, W. Liao, Q. Ji, Facial action unit recognition by exploiting their dynamic and semantic relationships. IEEE Trans. Pattern Anal. Mach. Intell. **29**(10), 1683–1699 (2007)
10. M. Pantic, I. Patras, Dynamics of facial expressions: recognition of facial actions and their temporal segments from face profile image sequences. IEEE Trans. Syst. Man Cybern. Part B Cybern. **36**(2), 433–449 (2006)
11. E. Murphy-Chutorian, M.M. Trivedi, Head pose estimation in computer vision: a survey. IEEE Trans. Pattern Anal. Mach. Intell. **31**(4), 606–626 (2009)
12. Y. Li, S. Wang, Y. Zhao, Q. Ji, Simultaneous facial feature tracking and facial expression recognition. IEEE Trans. Image Process. **22**(7), 2559–2573 (2013)
13. H.-Y. Chen, C.-L. Huang, C.-M. Fu, Hybrid-boost learning for multi-pose face detection and facial expression recognition. Pattern Recogn. **41**, 1173–1185 (2008)
14. N. Hesse, T. Gehrig, H. Gao, H.K. Ekenel, Multi-view facial expression recognition using local appearance features, in *21st International Conference on Pattern Recognition (ICPR 2012)* (2012), pp. 3533–3536
15. T.F. Cootes, G.J. Edwards, C. Taylor, Active appearance models. IEEE Trans. Pattern Anal. Matching Intell. **23**(6), 681–685 (2001)

16. C. Cortes, V. Vapnik, Support-vector networks. Mach. Learn. **20**, 273–297 (1995)
17. C. Shan, S. Gong, P.W. McOwan, Facial expression recognition based on local binary patterns: a comprehensive study. Image Vis. Comput. **27**, 803–816 (2009)
18. Z. Guoying, M. Pietikainen, Dynamic texture recognition using local binary patterns with an application to facial expressions. IEEE Trans. Pattern Anal. Mach. Intell. **29**(6), 915–928 (2007)
19. P. Yang, Q. Liu, D.N. Metaxas, Boosting encoded dynamic features for facial expression recognition. Pattern Recogn. Lett. **30**, 132–139 (2009)
20. Z. Zhang, M. Lyons, M. Schuster, S. Akamatsu, Comparison between geometry-based and Gabor-wavelets-based facial expression recognition using multi-layer perceptron, in *3rd IEEE International Conference on Automatic Face and Gesture Recognition* (1998), pp. 454–459
21. Y. Tian, T. Kanade, J. Cohn, Recognizing action units for facial expression analysis. IEEE Trans. Pattern. Anal. Matching Intell. **23**(2), 97–115 (2001)
22. A. Chakraborty, A. Konar, U.K. Chakraborty, A. Chatterjee, Emotion recognition from facial expressions and its control using fuzzy logic. IEEE Trans. Syst. Man Cybern. Part A Syst. Hum. **39**(4) 726–743 (2009)
23. U. Tariq, K.-H. Lin, Z. Li, X. Zhou, Z. Wang, V. Le, T.S. Huang, X. Lv, T.X. Han, Recognizing emotions from an ensemble of features. IEEE Trans. Syst. Man Cybern. **42**(4), 1017–1026 (2012)
24. Y. Tong, J. Chen, Q. Ji, unified probabilistic framework for spontaneous facial activity modeling and understanding. IEEE Trans. Pattern Anal. Mach. Intell. **32**(2), 258–273 (2010)

A Scheme to Create Secured Random Password Using Markov Chain

S. Vaithyasubramanian and A. Christy

Abstract Habitually, access to computer systems is based on the use of alphanumeric passwords. Password affords the foremost line of protection against illicit access to computer. Password security is of course only one factor of overall system security. Even though it is an essential component, passwords are measured as the fragile link in computer security. Most users will make use of simple passwords. Simple passwords are easy to memorize, but in the same sense easy to crack!! However, the common user is likely to use simple password and more often the same password for different login. This makes them vulnerable to various types of cyber attacks. To create/generate secured random passwords, in this paper, we describe a new scheme of creation/generation of passwords using Markov chain technique. The tree structure of creation/generation of passwords using Markov chain technique is also specified.

Keywords System security · Alphanumeric password · Graphical password · Biometric authentication · Vulnerabilities · Cracking · Markov chain · TPM

1 Introduction

Security has been the major concern with the evolution of new standards and applications in the field of computer networks and their processing. Hacking the system and cracking the passwords are the major concerns in this area. People have done some work in this area to improve the security at transmission and information processing. Still there exists high degree of need to improve or develop better methods to avoid or to control the hacking. Security of a password is an exciting

S. Vaithyasubramanian (✉)
Department of Mathematics, Sathyabama University, Chennai, India
e-mail: discretevs@gmail.com

A. Christy
Sathyabama University, Chennai, India
e-mail: ac.christy@gmail.com

© Springer India 2015

L.P. Suresh et al. (eds.), *Artificial Intelligence and Evolutionary Algorithms in Engineering Systems*, Advances in Intelligent Systems and Computing 325,
DOI 10.1007/978-81-322-2135-7_85

commonsense and mathematical problem [1]. Password security is essential to the security of information systems. It is often recommended that passwords should not be short, should not be words found in a dictionary, and that they should be changed frequently [2–4]. When a user has access to many accounts or systems, different passwords should be used so that no single incident will lead to the compromise of all of these accounts [5]. Unfortunately, human fallibility makes it nearly impossible to follow all of these rules simultaneously.

A user with many different passwords, frequently changing, will be forced to write them down somewhere [6]. Some systems constrain them to have a certain minimum length or require them to contain a combination of letters and numbers. Some systems also impose maximum lengths, and some prohibit special characters. The lack of common standards for passwords makes it difficult for a user to remember which password is used for which system [6–8]. For long-term remembrance, strings expressed in the form of patterns can be used as passwords [9].

2 Types of Password

Access to computer systems is most often based on the use of alphanumeric passwords. However, users have difficulty remembering a password that is long and random appearing. Instead, they create short, simple, and insecure passwords [7, 10]. Later, graphical passwords have been designed to try to make passwords more memorable and easier for people to use and, therefore, more secure [11–13]. Using a graphical password, users click on images rather than type alphanumeric characters. In late 1970, biometric systems were initiated. Biometric refers to recognition of the users by their uniqueness. Face identification, voice recognition, iris recognition, and finger print are used as biometric security system to identify a user. But the biometric authentication has its own strength and limitations [14, 15].

2.1 Limitations of Alphanumeric and Graphical Passwords

The problem with alphanumeric password arises largely from limitations of humans' long-term memory [11], which forces them to choose weak password such as dictionary word, obvious password, favorites, and easily guessable password. Cracking those passwords is very easy [3, 10]. They are cracked by various attacks such as guessing, brute force attack, dictionary attack, and hybrid attack [12, 16]. Meanwhile if random password is chosen, remembering it becomes tedious or unmanageable. The general issue in the graphical password input is to click outside the tolerance and the users need to understand the degree of precision needed [11]. And they are subject to regular means of attacks such as shoulder surfing, intersection analysis, social engineering, and spyware attack [17]. False reject rate and false accept rate are major issues concerning biometric authentications [14].

2.2 Need of Good Password

Need of good password is another important concern. The password problem has led to innovations to improve passwords. One innovation is Markov chain-based password, i.e., passwords that are based on the creation/generation of current character and previous character chosen. The basic idea is that using these passwords will lead to greater security and decrease the tendency to choose insecure password. This, in turn, should increase overall security. The tree structure of creating/generating the password is described in the next section.

3 Model Formulation and Generation/Creation of Password

3.1 Markov Chain

Markov chain named after Russian mathematician Andrei A. Markov (1856–1922) originated in mid-twentieth century. In this day and age, applications of Markov chains are far and wide in sciences [18]. Markov chain is a stochastic model describing a sequence of possible events in which the probability of each event depends only on the state attained in the previous event [19]. A Markov chain is a sequence of random variables $\{X_1, X_2, X_3 \ldots\}$, X_i's from a countable set called state space of the chain, having the property that given the present state; the future and past states are independent. Formally, $P(X_{n+1}/X_n, X_{n-1}, \ldots X_2, X_1) = P(X_{n+1}/X_n)$ [20].

Markov chains are described by means of digraph; in which each vertex refers the state and edges are labeled by probability called transition probability. Each variables of the state space are described by probability called initial state probability distribution denoted as $P = \{P(X_1), P(X_2), P(X_3) \ldots\}$.

The transitions in Markov chain are described by matrix called transition probability matrix (TPM) denoted as P_{ij} where $P_{ij} = P\{X_{n+1}=j/X_n=i\}$.

3.2 Preliminaries

Password can be generated using the following nomenclature.

State Space = {*L, U, N, S*}, where
L = {a, b, c, d …z}—26 lower case characters
U = {A, B, C, D …Z}—26 upper case characters
N = {0, 1, 2, 3 …9}—10 numeric characters
S = {!, @, #, …?}—32 special characters

1—step TPM and 2—step TPM along with the initial state probability distribution is as follows:

$$p_{ij} = \begin{pmatrix} \frac{1}{16} & \frac{5}{16} & \frac{5}{16} & \frac{5}{16} \\ \frac{5}{16} & \frac{1}{16} & \frac{5}{16} & \frac{5}{16} \\ \frac{5}{16} & \frac{5}{16} & \frac{1}{16} & \frac{5}{16} \\ \frac{5}{16} & \frac{5}{16} & \frac{5}{16} & \frac{1}{16} \end{pmatrix} : p_{ij}^2 = \begin{pmatrix} \frac{76}{256} & \frac{60}{256} & \frac{60}{256} & \frac{60}{256} \\ \frac{60}{256} & \frac{76}{256} & \frac{60}{256} & \frac{60}{256} \\ \frac{60}{256} & \frac{60}{256} & \frac{76}{256} & \frac{60}{256} \\ \frac{60}{256} & \frac{60}{256} & \frac{60}{256} & \frac{76}{256} \end{pmatrix}$$

$$\& P = \{1/4,\ 1/4,\ 1/4,\ 1/4\}$$

3.3 Proposed Scheme

Typical example of creating/generating random password using the above taxonomy would be as follows:

Step 1: Select the length (say ℓ) of the password according to the necessary criteria of the service provider.

Step 2: The first character of the password is chosen from any of the four criteria mentioned above.

Step 3: Assuming that L is chosen first, choose a character from L as the first character of the password, i.e., L generates the first character of the password. The probability of selection is $P[X_1]$.

Step 4: The second character is chosen from the remaining of the nomenclature leaving the character set chosen in step 1, i.e., if L is chosen first, either of U, N, S generates the second character of the password. The probability of selecting the second character is based on the first character selected, i.e., $P[X_2/X_1]$.

Step 5: The third character of the password is chosen in such a way that it is neither preferred from the nomenclature of the previous two character choice, i.e., excluding the character selected in step 3 and step 4. Probability of selection of the third character is based on the first and second characters selected, i.e., $P[X_3/X_2] \,\&\, P[X_3/X_1]$.

Step 6: The selection of nth character of the password depends on $(n-1)$th as well as $(n-2)$th character set. Probability of selection of the nth character is based on the $(n-1)$th and $(n-2)$th characters selected, i.e., $P[X_n/X_{n-1}] \,\&\, P[X_n/X_{n-2}]$.

Step 7: Proceed until it equals the length ℓ of the password

Step 8: The password combination would be depending on the length; however, creation/generation depends on step 3, 4, and 5 (Fig. 1).

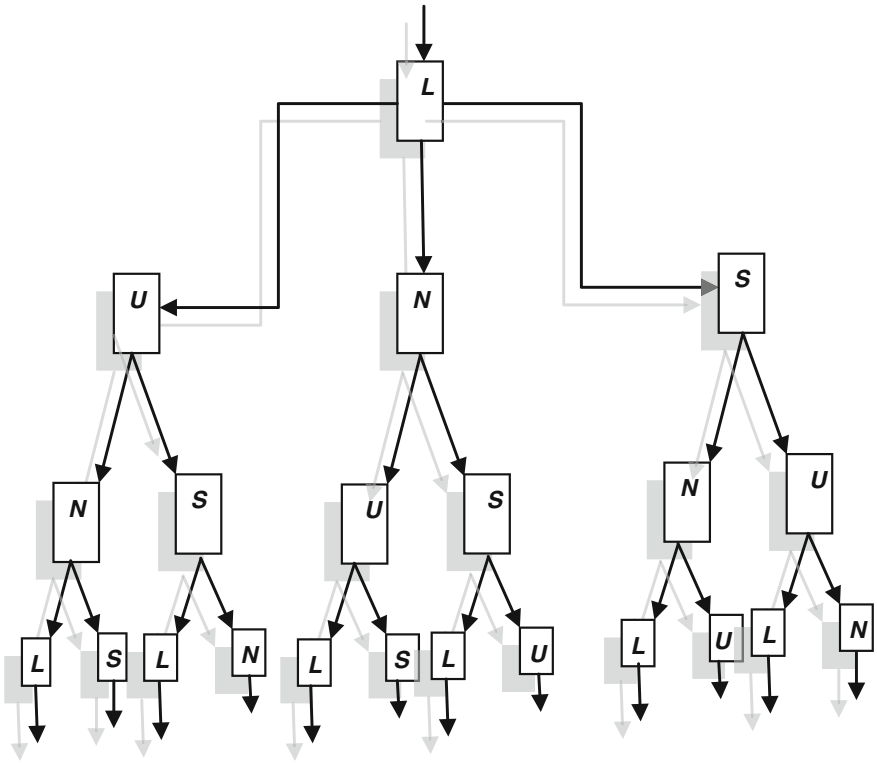

Fig. 1 Tree structure for password generation/creation

4 Conclusion

Password complexity is a double-edged sword. Complex passwords are hard to crack but equally hard to remember. In this paper, a new way of creating/generating random password for the secured data transfer using Markov chain is presented. This paves for the new generation password creation that ensures the reliability of data processing in computer networks and processing systems. Our approach can be effectively and securely used as user evidence mechanism for their Web logins. To a great extent, further research and user studies are required for this password creation/generation technique to complete higher levels of maturity and utility. A strong password does not guarantee 100 % protection from hackers. However, a strong password/robust password system is an effective deterrent against 90 % of the commonly used modes of attack.

References

1. R. Morris, K. Thompson, Password security: a case history. Commun. ACM **22**, 594–597 (1979)
2. S. Granger, The simplest security: a guide to better password practices (2011)
3. E.F. Gehringer, Choosing passwords: security and human factors, in *IEEE 2002 international symposium on Technology and Society (ISTAS'02)* pp. 369–373
4. D. Florencio, C. Herley, B. Coskun, Do strong web passwords accomplish anything?, in *Proceeding HOTSEC'07 Proceedings of the 2nd USENIX workshop on Hot topics in security, ACM Digital Library* (2007)
5. www.ghacks.net/2013/10/26/4-simple-password-creation-rules-x-common-sense-tips/
6. Jeff Yan, Alan Blackwell, Ross Anderson, A. Grant, Password memorability and security: empirical results. IEEE Secur. Priv. **2**(5), 25–31 (2004)
7. D. Florencio, C. Herley, A large-scale study of web password habits, in *Proceedings of the 16th international conference on the World Wide Web, ACM Digital Library* (2007), pp. 657–666
8. J. Hong, Passwords getting painful, computing still blissful. Communic. ACM I. **56**(3), (2013)
9. S. Vaithyasubramanian, A. Christy, A practice to create user friendly secured password using CFG, in *Accepted for International Conference on Mathematical & Engineering Sciences* 2014. (2014)
10. B. AlFayyadh, P. Thorsheim, A. Josang, H. Klevje, Improving usability of password management with standardized password policies, in *The Seventh Conference on Network and Information Systems Security*—SAR-SSI 2012 (Cabourg, 2012)
11. S. Wiedenbech, J. waters, J.C. Birget, A. Brodskiy, N. Memon, Authentication using graphical passwords: basic results, in *Human-Computer Interaction International (HCII)* (2005)
12. A. P. Sabzevar, A. Stavrou, Universal multi-factor authentication using graphical passwords, in *Proceedings of the 2008 IEEE International Conference on Signal Image Technology and Internet Based Systems* pp. 625–632
13. X. Suo, Y. Zhu, G.S. Owen, Graphical passwords: a survey, in *21st Annual Computer Security Applications Conference* (2005), pp. 463–472
14. S.M.S. Ahmad et al., Technical issues and challenges of biometric applications as access control tools of information security. Int. J. Innov. Comput., Inf. Control. **8**(11), 7983–7999 (2012)
15. M. Bhatnagar, Raina K. Jain, Nilam S. Khairnar, A Survey on Behavioral Biometric Techniques: Mouse vs. Keyboard Dynamics, in *IJCA Proceedings on International Conference on Recent Trends in Engineering and Technology*. (2013), (pp. 27–30)
16. http://resources.infosecinstitute.com/dictionary-attack-using-burp-suite
17. H. Gao, W. Jia, F. Ye, L. Ma, A survey on the use of graphical passwords in security. J. Softw. **8**(7), (2013)
18. B. Hayes, First links in the Markov chain. Mag. Sigma Xi, Sci. Res. Soc. **101**(2), 92 (2013)
19. www.oxforddictionaries.com/us/definition/american_english/Markov-chain
20. http://mathworld.wolfram.com/MarkovChain.html

Analysis of Shortest Route for Heterogeneous Node in Wireless Sensor Network

L. Lakshmanan and T.C. Tomar

Abstract In this paper, we deeply investigate a routing model for heterogeneous nodes in wireless sensor networks using Voronoi cell. We estimate the actual traffic among the sensor node, which is defined clearly as the traffic packets, controlled at each server. Network load is monitored using the traffic inbound rules, and the estimation is defined in the circular pattern in the form of Voronoi cell. Each functional patterns of the traffic are classified as source and destination in asymptotic rule. Each sensor nodes traffic are redirected to the centralized server acting in the real world, where the sensor data are patched periodically, and the data packets traveling from the node to node are updated. Each traffic patterns and sensor nodes are classified, and the node communication regions are known to the base station by drawing the pattern in Voronoi. The experimental results show the actual working model, and our routing model yields 78 % accuracy.

Keywords Wireless · Sensor networks · Genetic swarm optimization · Heuristic search technique · Voronoi cell · Snapshot

1 Introduction

Wireless sensor networks provide the bridge between the actual physical real-time entity virtual worlds. WSN has the vast advantage to observe the observable at a range of fine resolution over large-scale spatial and temporal measures 2. WSN has wide range of application and application career to the industry in the active domains such as military, computer science, GIS, and security. Wireless sensor

L. Lakshmanan (✉)
Faculty of Computing, Sathyabama University, Chennai, India
e-mail: laks1@yahoo.com

T.C. Tomar
Department of Information Technology, Jerusalem College of Engineering, Chennai, India
e-mail: dctomar@gmail.com

© Springer India 2015

L.P. Suresh et al. (eds.), *Artificial Intelligence and Evolutionary Algorithms in Engineering Systems*, Advances in Intelligent Systems and Computing 325,
DOI 10.1007/978-81-322-2135-7_86

nodes consist of the components such as memory (RAM, ROM), transceivers, GPS, processor, sensors, and power source (battery) [1, 2]. The main challenges arise here, due to limited resource (power), the energy consumption should be minimized, transmission rate should be probably robust in nature, and the node should be highly reliable during scalability. The previous research was carried in routing scheme that was explained clearly in the Sect. 1.1. In this paper, we are going to discuss about finding optimal path between source and destination using particle swarm optimization algorithms.

1.1 Related Work

The hybrid technique, called genetic swarm optimization (GSO), is essentially a population-based heuristic search technique which can be used to solve combinatorial optimization problems, modeled on the concept of natural selection but also based on cultural and social evolution [1, 3]. GSO algorithm consists in a strong cooperation of GA and PSO, since it maintains the integration of the two techniques for the entire run 1. In each iteration, in fact, the population is divided into two parts and they are evolved with the two techniques in that order [4]. They are then remerged in the modernized population, that is yet again divided erratically into two parts in the next iteration for another run of genetic or particle swarm operators [5, 6]. The population revise concept can be effortlessly understood thinking that a part of those individuals is substituted by new generated ones by resources of GA, while the enduring are the same of the earlier generation but moved on the solution space by PSO [2, 5, 7]. Since routing using genetic approach does not yield much better accuracy when compared to existing approach, hence this paper is customized to overcome the key feature of genetic approach [1, 5, 6].

2 Proposed Methodology

2.1 Node Identity

Node identity is one of the key terms for providing the nodes identity as well as integrity. In our methodology, we used pseudo MAC (PMAC) address for identifying the nodes. The below example states how the pseudo MAC is defined

$$48\,\text{bit MAC address} + \text{random number} = \text{hashed}(\text{PseudoMAC})$$

For example, F8: F5: BE: 4F: H0: 8G + 2523 = GE: 54: LG: H7: 8F: 8G PMAC for Node 1.

2.2 Bounding Region for Traffic Analyzing

Voronoi cell is used for partitioning the range/area of sensor nodes, here we used optimal k-means clustering algorithm for clustering the sensor nodes in the corresponding cell [8]. By using k-means clustering, a partition of sensor node of n observation is made into k-clusters at which the observation is made by the nearest mean of the node which serves as the actual threshold of the centralized server.

3 Algorithm—Voronoi Cell and K-Means Clustering

```
Split the region
Assign the threshold for each region
    Predict the actual node traffic
Observe interval data
Initialize K # ---- with one mean per
cluster For each interval data
    Assign the threshold value
Predict the mean of the neighbour nodes
Assign the centroid to the group of neighbour node
Move the centroid to the center based on mean and
    threshold
Activate the cluster
```

3.1 Asymptotic Rule Classification for Defining Source and Destination

Asymptotic rule definition is carried to define the destination range in the form of little ‘o’ notation. Stateful rule definition is states that destination should be defined within the cell region; each region should be propagated within the cell range. If the range is beyond the cell, range propagates using the inbound function (according to the threshold stated in Fig. 1). Functional threshold $\sim V(1)\ldots V(n)$ for $1 <= n$, for the range beyond the cell region—functional threshold $\sim V(1) + V(2) + \cdots V(n)$.

3.2 Patch Servers

Point at which the active session of the mobile node is patched or saved to the centralized server is called as snapshot point. Snapshot is defined here as, point or interval at which the node floods the SYN Req packet (say RTS packets) to know

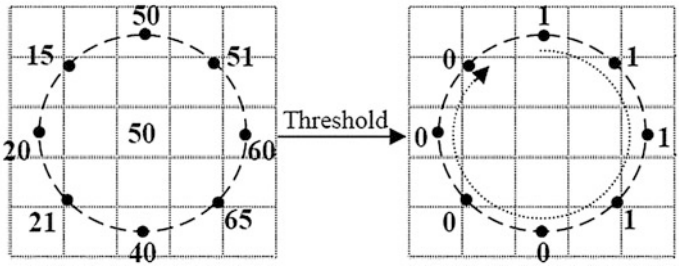

Fig. 1 Threshold-based traffic analyzing

the neighbor nodes in WSN. The node at which the optimized route is evolved and the node which activates the intermediary position (by applying PSO) to the velocity and weight inertia is at the level of CPos and BPos at 1. Then, the point or interval is said to be the snapshot point. Each active snapshot point is stored in the centralized server. The snapshot is taken for the reason of data recovery and data backup.

Snapshot (time + Pos) = {[Weight × velocity (time)] + [(CPos = 1) × random (1) × (BPos = 1)]}

3.3 Data Routing

The actual position of each node is estimated using PSO–ACO algorithm. The region is defined clearly using the Voronoi cell. The cell representation is used to monitor the traffic between the sensor nodes at the particular range. The data routing within the cell is carried out by means of ant colony optimization algorithm, where the ants are used to find the optimal route within the Voronoi cell 6. The actual principles of ants are used in this paper to find the optimal route. In ACO, rank-based ants are used to discover the shortest path. The algorithm is explained clearly in the Sects. 3 and 3.4

3.4 Data Routing Using Ants

```
FunctionBCO_KMeans_Metadat
a Initialize(Voronoi)
Split the region
For all the region
Initialize(cluster
) While(!grouped)
        Group_meta (nodes)
End while
         Threshold
         (nodes) Centroid
         ( nodes)
while(!termination)
       rank(priority)
       createSolutions()
       daemonActions()
       pheromoneUpdate(
    ) end while
end For
end Function
```

4 Experimental Setup

In this paper, we experimentally setup the simulation for 11 sensor nodes. Figure 2 states the actual routing mechanism within the cell. Initially, SYN Req is flooded to discover the neighbor node. Once the neighbor is discovered, the CTS message is tracked, iteratively using this principle, all the neighbor nodes are discovered. Figure 2 defines the routing mechanism beyond the Voronoi cell. Patch servers are defined clearly in the scenario. The snapshot point is also defined clearly in the Fig. 2. Initially, the test run was carried out for the actual routing model using Voronoi cell. The proposed model is only capable to route using rank-based ants, when it is tested with max–min ant system, it yields less accuracy than the rank-based. Rank-based ant routing algorithm within the Voronoi yields better accuracy in terms of data routing. The simulation was carried out using OMNETPP, software IDE for network simulation.

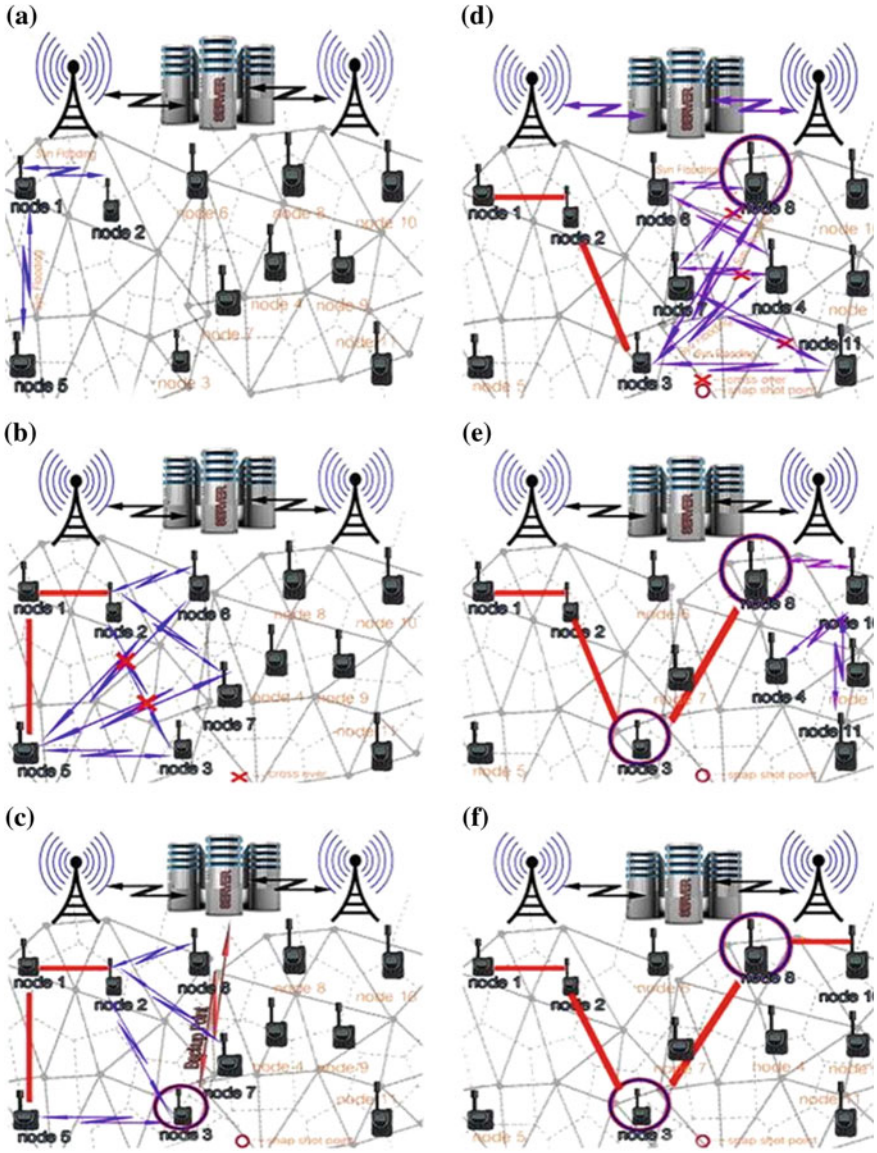

Fig. 2 Simulation model of the proposed routing protocol

5 Conclusion

Hence, we conclude this paper with the appropriate result of data routing, Voronoi cell region, node location, etc. Figure 2c states the node location in Voronoi cell in terms of plotting *x*, *y* coordinates. The proposed routing method guarantees that the

routing data packets within the Voronoi region are fast and reliable in delivering same number of messages. Snapshot option in centralized server leads to automatically data recovery during node failure. The working environment is clearly tested in multi hop networks with inbound region and outbound regions. Hence, by conclusion, our proposed model yields 78 % in terms of data routing. The main challenge in this paper is drawing Voronoi region is bit tougher task, when we are switching it to homogeneous nodes in WSN. Hence, it is considered as one of the key challenges in this paper, and in future, the addressed problem will be taken care and resolved.

References

1. V. Neehaarika, S. Sindhura, Evaluation of routing protocols used in wireless sensor networks monitoring temperature in composting heaps, in *Annual IEEE India Conference(IDCON2011)* (2011), pp. 1–4
2. J. Kennedy, R. Eberhart, Particle swarm optimization, in *1995 IEEE International Conference on Neural Networks (ICNN 95)* (1995), pp. 1942–1948
3. K. Derr, M. Manic, Wireless sensor network configuration—part II: adaptive coverage for decentralized algorithms. IEEE Trans. Industr. Inf. **9**(3), 1728–1738 (2013)
4. Y.G. Cai, M. Wei, Self adaptive chaos particle swarm optimization for allied vehicle routing problems. J. Syst. Eng. **32**(10), 2208–2214 (2012)
5. L. Lakshmanan, D.C. Tomar, Optimizing localization route using particle swarm-a genetic approach. Am. J. Appl. Sci. **11**(3), 520–527 (2014)
6. H.-C. Lee, Towards a general wireless sensor network platform for outdoor environment monitoring. IEEE Sens. J. **12**(4), 1–5 (2012)
7. D. Mascareñas, E. Flynn, C. Farrar, G. Park, M. Todd, A mobile host approach for wireless powering and interrogation of structural health monitoring sensor networks. IEEE Sens. J. **9** (12), 1719–1726 (2009)
8. I.M. Santos, M.A. Dota, C.E. Cugnasca, Dynamic definition of the sampling rate of data in wireless sensor network with adaptive automata. IEEE Latin Am. Trans. **9**(6), 963–968 (2011)

Design of a Triple Band Slit-loaded Patch Antenna with DGS for Bandwidth Enhancement

Pristin K. Mathew and Sneha Mohan

Abstract This paper demonstrates the design and result of a low profile wide band miniaturized slit-loaded microstrip patch antenna with defected ground structures (DGS) for wireless applications. The proposed antenna is coaxially probe fed that operates at 5.5 GHz and has an array of rectangular slits etched on the patch and a pair of square-shaped dumbbell DGS loaded into the ground plane. The bandwidth of the slit-loaded microstrip patch antenna is 12 %, whereas it increases up to 17 % when DGS is loaded into the ground plane. The proposed compact antenna resonates at multiple frequencies between 1 and 9 GHz frequency range, at 4.84, 5.96, and 6.34 GHz with a bandwidth of 330, 150, and 460 MHz having return loss of −17.2, −18.5, and −27.3 dB, respectively. All the antenna geometries in this paper are simulated using an electromagnetic simulation tool named CADFEKO. The proposed multiband antenna finds useful applications with an improved performance simultaneously in W-LAN (4.8–5.8 GHz) and satellite communication bands (5.92–6.42 GHz). The plots of various antenna parameters such as return loss, voltage standing wave ratio (VSWR), gain, and bandwidth of the proposed antenna have been observed with and without DGS and the analysis of the simulated results shows that the proposed slit-loaded antenna with DGS is more efficient than conventional rectangular microstrip patch antennas (CRMPA) in terms of bandwidth of operation and miniaturization.

Keywords Miniaturization · Slit-loaded patch antennas · CADFEKO · Dumbbell-shaped defected ground structures

P.K. Mathew (✉) · S. Mohan
Department of Electronics and Communication, Karunya University, Coimbatore, India
e-mail: pristinkmathew@karunya.edu.in

S. Mohan
e-mail: snehamohan@karunya.edu.in

© Springer India 2015

L.P. Suresh et al. (eds.), *Artificial Intelligence and Evolutionary Algorithms in Engineering Systems*, Advances in Intelligent Systems and Computing 325,
DOI 10.1007/978-81-322-2135-7_87

1 Introduction

Recently, there has been a tremendous growth in the field of wireless communication for various applications and most of the systems focus on improving the bandwidth and achieving miniaturization of the antennas [1, 2] used in it. Miniaturization and bandwidth enhancement have mutually inverse relationships and improvement of one characteristics result in degradation of the other. Hence, a trade-off needs to be considered between these two properties. A miniaturized multiband antenna is an essential requirement for portable mobile communication devices and radio frequency (RF) applications in providing good quality of service (QOS) and throughput [3, 4]. The most commonly used antenna to achieve this goal is microstrip patch antennas, due to its low cost, multiband of operation, small size, and easy integration with microwave integrated circuits (MIC). It has a radiating patch on one side of a dielectric substrate and ground plane on the other. However, such antennas also have drawbacks such as narrow bandwidth and low gain due to surface wave excitation [5, 6]. The practical applications demand a wide band of operation. These requirements forced for modifying the regular patch antenna geometry. Several techniques have been used in enhancing the bandwidth of an antenna and achieving miniaturization. The most commonly used technique is by defecting the ground plane [7, 8] and by placing slits at proper positions of the patch.

The simplest method adopted for reducing the size of the patch antenna is using a high dielectric constant substrate material [9]. However, using such substrates results in excitation of surface waves on the patch and in turn leads to narrowing of bandwidth. A U-slot patch antenna on flame retardant 4(FR4) substrates for radio frequency identification (RFID) systems is reported in [10]. Rectangular slit-loaded patch with 70 % size reduction has been achieved in [11]. By inserting dumbbell-shaped defected ground structures (DGS) and slots on the rectangular patch, 91 % size reduction with blocking of surface waves is achieved as in [12]. Similarly, the band width can also be improved by various techniques. Using a substrate with low dielectric constant is one way of achieving it [13]. Another technique is to increase the thickness of the substrate [14] but has the drawback that low spurious radiation will be emitted. Stacked patch configuration can also achieve enhanced bandwidth but are complex in their fabrication [15].

Slits causes meandering of the surface current path and causes reduction in the resonant frequency and thereby achieving miniaturization by introducing a mode near the fundamental mode [16]. In the proposed antenna, six symmetrical rectangular slits of dimension 5 mm × 1 mm and a pair of wider rectangular slits of dimension 6.2 mm × 2 mm are etched into the surface of the patch. DGS was first proposed by Park et al. in 1999 and is realized by etching periodic or non-periodic structures in the ground plane that changes the shielded current distribution and thereby affecting the current flow and input impedance of the antenna [17, 18]. It controls the excitation of electromagnetic waves propagating through the substrate [19, 20] that depends on the shape and dimension of the defect being introduced. In the proposed antenna, a pair of square-shaped dumbbell of length 4.5 mm is present

in the ground plane of the patch. DGS has also been used for mutual coupling reduction and cross-polarization suppression [21, 22] in antenna arrays.

Comparing an antenna with DGS and an antenna without DGS, it is observed that the antenna loaded with DGS achieves more size reduction by shifting the resonant frequency from 5.5 to 4.7 GHz. The area of the ground that is defected is directly related to the miniaturization achieved. Different shapes of DGS have been used in planar microstrip antennas design that provides size reduction, bandwidth enhancement, or gain increment. DGS also modifies a transmission line such as line capacitance and inductance characteristics thereby achieving a band stop characteristics in the same frequency bands with less number of unit cells.

This paper discusses the design and simulation of a conventional patch antenna, slit-loaded antenna without DGS, and slit-loaded antenna with DGS. There are different feeding techniques for a patch antenna. Here, a coaxial probe feeding technique is used for impedance matching at 50 Ω. Section 2 provides the antenna design of the proposed slit-loaded patch with dumbbell-shaped DGS, Sect. 3 provides the simulation result and discussion of the antenna parameters, and Sect. 4 provides conclusion followed by references.

2 Antenna Design

There are several methods to design and analyze a microstrip patch antenna such as transmission line model and cavity model.

The proposed antenna uses transmission line model where a rectangular patch of length 'L' and width 'W' can be viewed as a wide transmission line that is resonating with electric field varying sinusoidally along its resonant length 'L.' There are three parameters for designing rectangular microstrip patch antenna, (i) resonant frequency (f) of the antenna, (ii) dielectric constant of the substrate (ε_r), and (iii) substrate thickness (h).

A conventional planar rectangular microstrip patch antenna that resonates at a designed frequency of 5.5 GHz with dimensions $L \times W$ as 12 mm × 16 mm is shown in Fig. 1, and this antenna is used as the reference antenna. The substrate material used is an inexpensive FR4 which has a relative permittivity of $\varepsilon_r = 4.4$ and loss tangent of 0.002. The thickness of the substrate is 1.6 mm. The radiating patch is made of copper, and it is coaxially probe fed having radius of 0.1 mm placed at (L/3, 0) from the center of the patch along the line of symmetry that provides an impedance match of 50 Ω.

The proposed antenna with top view geometry is shown in Fig. 2, Here, 'L' and 'W' represent the length and width of the patch, 'L_s,' 'W_s,' and 'h_s' represent the length, width, and height of the substrate. 'l_1,' 'l_2' and 'w_1,' 'w_2' represent the length and width of the rectangular slits on the patch. The patch of the proposed antenna is made by a perfect electric conductor placed in the XY plane with base-centered alignment.

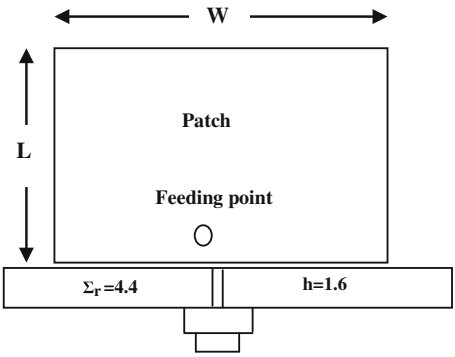

Fig. 1 Design of a conventional microstrip patch antenna

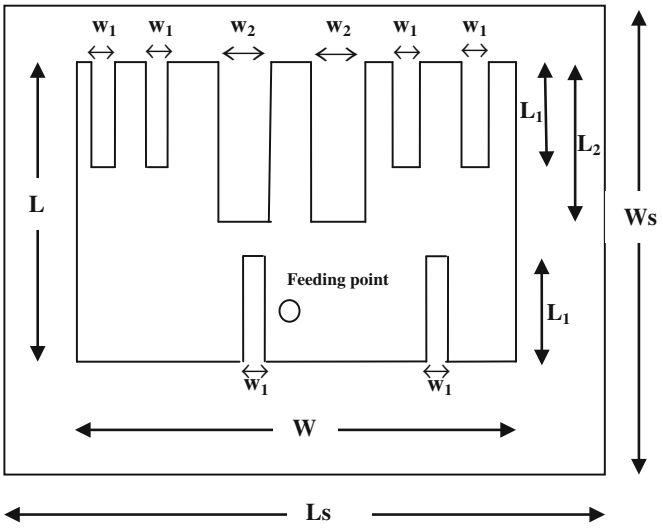

Fig. 2 Top view geometry of the proposed antenna

The rear view of the square-shaped dumbbell DGS placed just below the patch surface is shown in Fig. 3. Figure 4 shows the 3D geometry of the proposed antenna made by etching on the non-radiating edges of the patch and the square-shaped dumbbell DGS placed just below the patch surface.

The parameters and dimension of the proposed antenna is shown in Table 1.

The ground plane used in this design is a perfect electric conductor of dimension 50 mm × 40 mm. The dimensions of the dumbbell are shown in Table 1. These dimensions are obtained through a parametric study by varying each dimension of the DGS separately and noting down the various values.

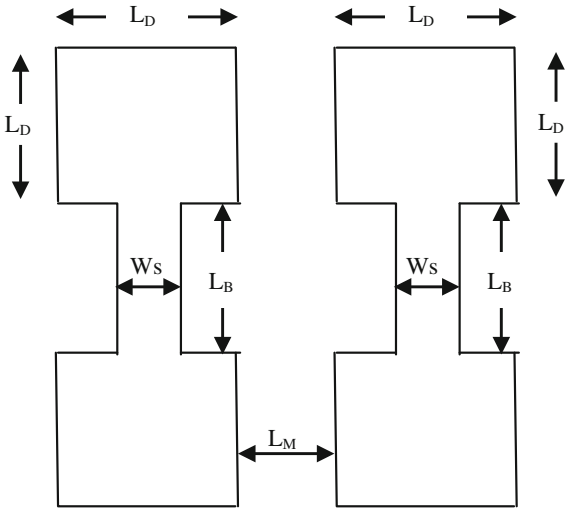

Fig. 3 Bottom view geometry of the proposed antenna

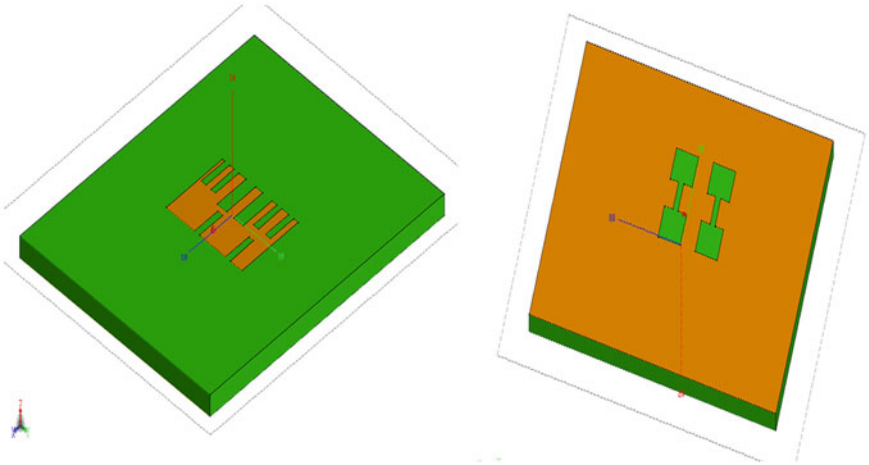

Fig. 4 3D geometry of top and bottom views of the proposed antennas

3 Results and Discussion

The proposed antenna is simulated using an electromagnetic simulator, CADFEKO and parameters such as return loss, bandwidth, gain, voltage standing wave ratio (VSWR) are measured. Figure 5 shows the variation of return loss with frequency of a conventional patch antenna, a slit-loaded microstrip patch antenna, and a

Table 1 Parameters of the proposed antenna

Parameters	Value (mm)
Length of patch (L)	12
Width of patch (W)	16
Length of substrate (L_s)	50
Width of substrate (W_s)	40
Length of slits (L_1)	5
Width of slits (W_1)	1
Length of slits (L_2)	6.2
Width of slits (W_2)	2
Length of dumbbell (L_D)	4.5
Length of middle bar (L_B)	4
Width of middle bar (W_B)	1
Spacing between the dumbbell (L_M)	3

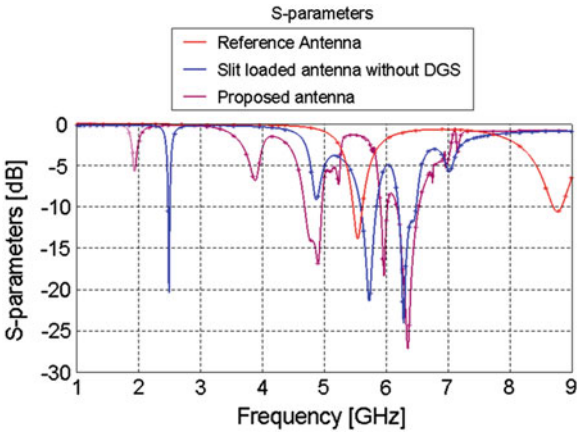

Fig. 5 S11 curves for reference antenna, slit-loaded antenna without DGS, and proposed antenna

slit-loaded dumbbell-shaped DGS microstrip patch antenna. The bandwidth of operation can easily be calculated from this plot. The conventional patch antenna (Reference antenna) resonates at a single frequency of 5.54 GHz and has a return loss of −13.93 dB and impedance bandwidth of 180 MHz (5.44–5.62 GHz). A slit-loaded antenna resonates <−10 dB at 2.48 GHz with a return loss of −19 dB and impedance bandwidth of 50 MHz (2.46–2.51 GHz), at 5.72 GHz with a return loss of −20 dB and impedance bandwidth of 290 MHz (5.56–5.85 GHz), at 6.26 GHz with a return loss of −21 dB and impedance bandwidth of 310 MHz (6.17–6.48 GHz).

The proposed antenna with DGS resonates <−10 dB at 4.84 GHz with a return loss of −17.2 dB and impedance bandwidth of 330 MHz (4.65–4.98 GHz), at 5.96 GHz with a return loss of −18.5 dB and impedance bandwidth of 150 MHz (5.88–6.03 GHz), at 6.34 GHz with a return loss of −27.3 dB and impedance bandwidth of 460 MHz (6.12–6.52 GHz). Hence, DGS makes an overall

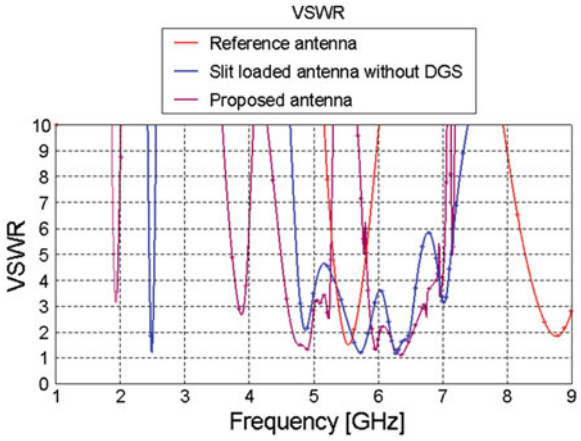

Fig. 6 VSWR curves for reference antenna, slit-loaded antenna without DGS, and proposed antenna

improvement in the impedance bandwidth of an antenna. VSWR is a parameter that shows the level of impedance mismatch and is always a positive real number. The VSWR ratio of the proposed antenna is 1:1.2 as given in Fig. 6 at the frequencies 4.65–4.98 GHz, 5.88–6.03 GHz, and 6.12–6.58 GHz.

The 2D radiation plot of the conventional, slit-loaded antenna without DGS and the slit-loaded antenna with DGS in XZ and YZ planes is shown in Fig. 7. The radiation pattern in YZ plane is almost omni-directional.

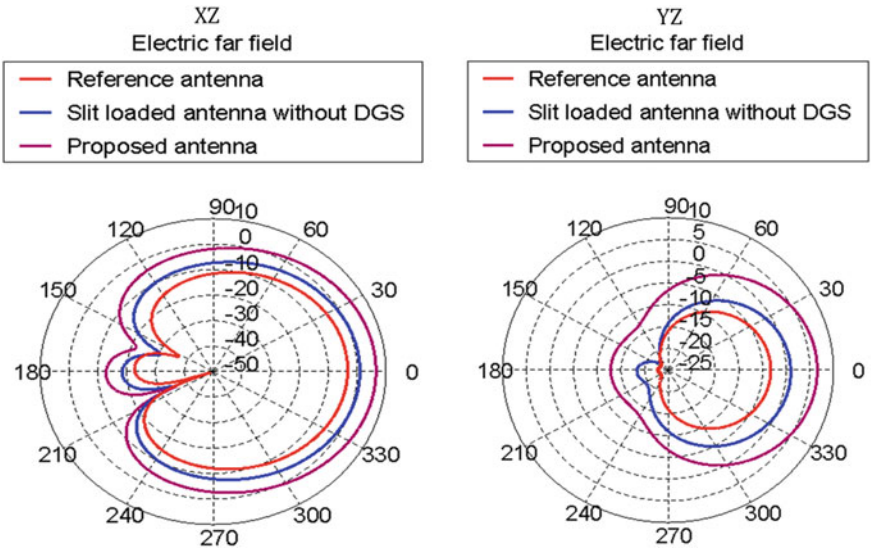

Fig. 7 Radiation pattern of reference antenna, slit-loaded antenna without DGS, and proposed antenna in XZ (E Plane) and YZ (H Plane) Plane

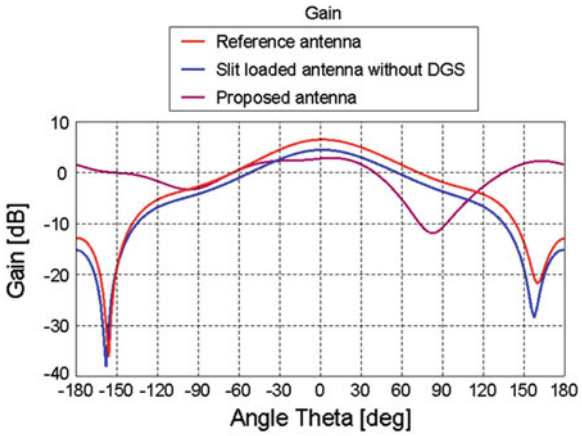

Fig. 8 Gain plot for reference antenna, slit-loaded antenna without DGS, and proposed antenna

The simulated antenna gain plot of a conventional patch antenna slit-loaded antenna without DGS and slit-loaded antenna with DGS is shown in Fig. 8. Gain is the ratio of radiation field intensity of test antenna to that of the reference antenna. It is usually expressed in dB. The observed value of gain of the reference antenna at resonant frequency of 5.5 GHz is 6.80 dB. Whereas for the slit-loaded antenna, it is estimated to be 4.47 dB, and for the DGS antenna, it is estimated to be 3.20 dB. Thus, we can conclude that the antenna gain decreases with increase in bandwidth.

The 3D current distribution plot at 5.5 GHz for the proposed antenna is shown in Fig. 9. The presence of DGS in the ground plane indicates that there is strong concentration of currents in the non-radiating edges of the patch and the maximum current is observed at the bottom of the feed line.

For constant values of W_s and L_B (W_s = 0.5 mm, L_B = 3 mm), the S_{11} graph for different values of L_D (L_D = 2.5, 3.5 and 4.5 mm) are plotted and is shown in Fig. 10.

Table 2 represents a parametric study on the variation of length of the dumbbell on the antenna parameters. It is observed that as the length of the dumbbell

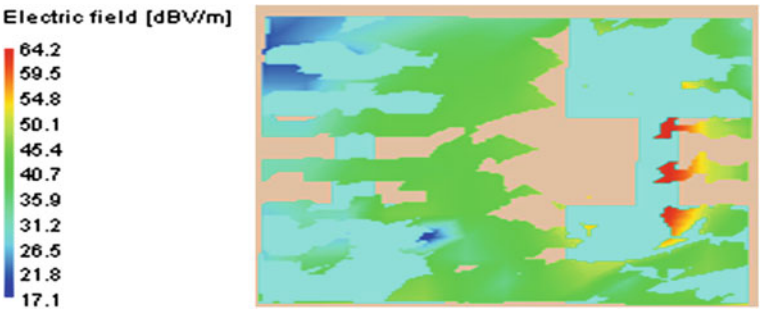

Fig. 9 Current distribution plot of proposed antenna in the bottom view at 5.5 GHz

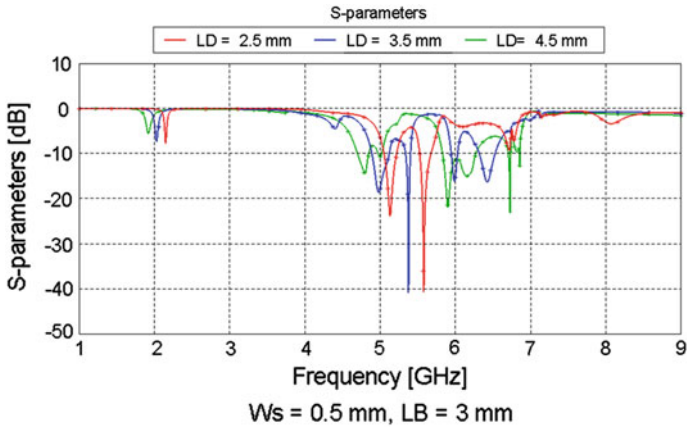

Fig. 10 S11 curves for different values of dumbbell length

Table 2 Variation of length of dumbbell on parameters

S. No.	Length of dumbbell L_D (mm)	Width of bar W_s (mm)	Length of bar L_B (mm)	Resonant freq (GHz)	Return loss (dB)
1	2.5	0.5	3	2.12	−7.83
				5.12	−24
				5.58	−41
				6.72	−9.68
				6.8	−7.5
2	3.5	0.5	3	2.02	−7.69
				4.95	−18.4
				5.36	−41
				5.98	−16.6
				6.42	−16.6
3	4.5	0.5	3	1.93	−5.71
				4.79	−14.4
				5.00	−11
				5.90	−22
				6.18	−15.2

increases, the resonant frequency decreases and the return loss increases. The gain of the antenna decreases as the dumbbell length increases.

The simulated results of antenna parameters of conventional rectangular microstrip patch antenna, slit-loaded rectangular microstrip antenna without DGS, and the slit-loaded rectangular microstrip antenna with DGS are shown in Table 3.

From the table, we see that the bandwidth is enhanced when DGS is loaded into the ground plane. The proposed antenna will work in the frequency ranges of 4–7 GHz which covers the WLAN and satellite communication bands.

Table 3 Comparison of antenna parameters

Antenna parameters	Reference antenna	Slit-loaded antenna without DGS	Proposed antenna
Resonant frequency (GHz)	5.5	2.48	4.84
		5.72	5.96
		6.26	6.34
Return loss (dB)	−13.93	−19	−17.2
		−20	−18.5
		−21	−27.3
VSWR	2.3	1.2	1.2
Gain	6.8	4.47	3.2
Bandwidth (MHz)	180	650	940
Impedance bandwidth (%)	3.25	12	17
Miniaturization (%)	–	85	30

4 Conclusions

A compact wideband-slotted antenna with DGS has been simulated using MOM-based software CADFEKO. Wide band is achieved by etching the patch and ground plane of a conventional rectangular microstrip patch antenna. The proposed antenna is very simple in its construction and cost effective due to the use of FR4 substrate material. The proposed antenna with DGS achieved better performance characteristics than an antenna without DGS. Gain of the proposed antenna is also satisfactory at various frequencies. The resonant frequency is shifted from 5.5 to 4.84 GHz when defect is introduced into the ground plane thereby providing 30 % miniaturization. The proposed antenna finds useful application in wireless communication systems that cover both the WLAN and satellite uplink bands. The results obtained are in good agreement with the standard requirements of an antenna in terms of miniaturization and bandwidth of operation.

Acknowledgments The author would like to thank Karunya University, Coimbatore for providing various facilities in laboratory to complete this work.

References

1. H. Mosallaei, K. Sarabandi, Antenna miniaturization and bandwidth enhancement using a reactive impedance substrate. IEEE Trans. Antennas Propag. **52**(9), 2403–2414 (2004)
2. D. Nashaat, H.A. Elsadek, E. Abdallah, H. Elhenawy, M. Iskander, Miniaturized and multiband operations of inset feed microstrip patch antenna by using novel shape of defect ground structure (DGS) in wireless applications, in *PIERS Proceedings* (2009)
3. L.H. Weng, Y.C. Guo, X.W. Shi, X.Q. Chen, An overview on defected ground structure. Prog. Electromagnet. Res. B **7**, 173–189 (2008)

4. A.K. Arya, M.V. Kartikeyan, A. Patnaik, Defected ground structure in the perspective of microstrip antennas: a review. Frequenz **64**, 79–84 (2010)
5. K.-L. Wong, *Compact and Broadband Microstrip Antenna* (Willey, New York, 2002)
6. C.A. Balanis, *Antenna Theory Analysis and Design*, 2nd edn. (Wiley, Hoboken, 2003)
7. C.S. Kim, J.S. Park, D. Ahn, J.B. Lim, An improved 1-D periodic defected ground structure for microstrip line. IEEE Microwave Wireless Compon. Lett. **10**(4), 180–182
8. A.K. Arya, M.V. Kartikeyan, A. Patnaik, Efficiency enhancement of microstrip patch antennas with defected ground structure, in *IEEE Proceedings of Recent Advanced in Microwave Theory and Applications (MICROWAVE-08)* (2008), pp. 729–731
9. C.H. Lai, Y.S. Chang, Compact planar microstrip fed feed patch antenna using high permitivity substrate, in *Progress in Electromagnetics Research (JPIER)* (2011), pp. 239–241
10. A. Ghiotto, S.F. Cantalice, T.P. Vuong, A. Pouzin, G. Fontgalland, S. Tedjini, Miniaturized patch antenna for the radio frequency identification of metallic objects. IEEE Trans. Antennas Propag. **12**, 583–586 (2008)
11. V.K. Agarwal, A.K. Shaw, M.K. Das, J. Mukherjee, K. Mandal, A novel compact dual frequency microstrip antenna. Sci. Direct Procedia Technol. **4**, 427–430 (2012)
12. M. Chakraborty, B. Rana, P.P. Sarkar, A. Das, Design and analysis of a compact rectangular microstrip antenna with slots using defective ground structure. Sci. Direct Procedia Technol. **4**, 411–416 (2012)
13. C. Wang, K. Chang, A novel CP patch antenna with a simple feed structure, in *IEEE Antennas Propagation Society International Symposium Digital* (2000), pp. 1000–1003
14. W. Chen, Y. Li, H. Jiang, Y. Long, Design of novel tri-frequency microstrip patch antenna with arc slots. Electron. Lett. **48**, 609–611 (2012)
15. T. Huynh, K.F. Lee, Single-layer single-patch wideband microstrip antenna. IEEE Trans. Antenna Propagat. Electron. Lett. **31**, 1310–1312 (1995)
16. J.S. Kuo, K.-L. Wong, A compact microstrip antenna with meandering slots in the ground plane. Microw. Opt. Technol. Lett. **29**, 95–97 (2001)
17. K.H. Chiang, K.W. Tam, Microstrip monopole antenna with enhanced bandwidth using defected ground structure. IEEE Antennas Wireless Propag. Lett. **7**, 532–535 (2008)
18. J. Sun, E.-P. Li, Y.-J. Zhang, Dual frequency rectangular microstrip patch antenna with novel defected ground structure, in *Progress in Electromagnetic Research Symposium* (2006), pp. 26–29
19. H.D. Oskouei, K. Forooraghi, M. Hakkak, Guided and leaky wave characteristics of periodic defected ground structures. Prog. Electromagnet. Res. PIER **73**, 15–27 (2007)
20. L.T. Wang, J.S. Sun, The compact, broadband microstrip antenna with defective ground plane, in *IEEE International Conference on Antenna and Propagation*, vol. 2 (2003), pp. 622–624
21. D. Guha, M. Biswas, Y.M.M. Antar, Microstrip patch antenna with defected ground structure for cross polarization suppression, in *Proceedings. IEEE Antennas and Wireless Propagation Letters*, vol. 4 (2005), pp. 455–458
22. H. Liu, Z. Li, X. Sun, J. Mao, Harmonic suppression with photonic band gap and defected ground structure for a microstrip patch antenna. IEEE Microw. Wireless Compon. Lett. **15**, 55–56 (2005)

Segmentation of Nuclei from Breast Histopathology Images Using PSO-based Otsu's Multilevel Thresholding

J. Angel Arul Jothi and V. Mary Anita Rajam

Abstract Automated histopathology image analysis involves segmentation of nuclei from the surrounding tissue structures to develop a computer-aided diagnosis (CAD) system. In this paper, we propose the use of particle swarm optimization (PSO)-based Otsu's multilevel thresholding technique to automatically segment the nuclei from hematoxylin and eosin (H&E)-stained breast histopathology images. Otsu's threshold selection problem is modeled as an optimization problem by designating the discriminant criterion as the objective or fitness function that has to be maximized. PSO is used to compute the optimal threshold value that maximizes the objective function. This paper studies the effectiveness of the proposed technique to segment nuclei from breast histopathology images.

Keywords Automated histopathology · Computer-aided diagnosis · Particle swarm optimization · Hepatocellular carcinoma · Otsu's multilevel thresholding

1 Introduction

Automatic segmentation of nuclei from histopathology images is inherently complicated due to overlapping or clumping of nuclei, varying pixel intensities within nuclei, difference in size and shape of nuclei, incomplete nuclei, and broken nuclei boundaries. Apart from this, the digitized histopathology images also exhibit discrepancy in color between them due to variations in tissue preparation process and image acquisition conditions (variation in illumination and staining conditions).

J.A.A. Jothi (✉) · V.M.A. Rajam
Department of Computer Science and Engineering, College of Engineering Guindy, Anna University, Chennai, India
e-mail: jothi@cs.annauniv.edu

V.M.A. Rajam
e-mail: anitav@annauniv.edu

© Springer India 2015

L.P. Suresh et al. (eds.), *Artificial Intelligence and Evolutionary Algorithms in Engineering Systems*, Advances in Intelligent Systems and Computing 325,
DOI 10.1007/978-81-322-2135-7_88

In this work, we provide image-processing operations that would effectively delineate the nuclei from digitized breast histopathology images using particle swarm optimization (PSO)-based Otsu's multilevel thresholding.

2 Related Work

There is a lot of work in the literature that aim to separate nuclei from the given hematoxylin and eosin (H&E)-stained biopsy images. An automated method to segment nuclei from hepatocellular carcinoma (HCC) images has been proposed in [1] which uses marker-controlled watershed transform and active contour model to segment the nuclei. A two-level graph cuts method along with alpha expansion and graph coloring techniques has been used in [2] to segment the nuclei from breast images. Dundar et al. [3] have proposed a two-step method to automate cell nuclei segmentation from breast histopathology images. During the first step, the cell regions have been identified by modeling the image data by a four component Gaussian mixture model (GMM) whose parameters have been estimated by expectation maximization (EM) clustering algorithm. In the second step, the individual nuclei have been segmented from the resulting cell regions using a watershed algorithm based on immersion simulation. An adaptive thresholding-based method has been used by Lu et al. [4] to segment nuclei from skin histopathology images. In [5], the authors have proposed a multi-scale processing of the digitized breast biopsy images using watershed transform and different types of nuclear markers to extract the nuclei.

PSO-based multilevel thresholding has already been used for segmenting images of airplane, hunter, butterfly, road, and terrain [6, 7]. In this paper, we propose the use of PSO-based Otsu's multilevel thresholding technique to segment the nuclei from the H&E-stained breast biopsy images.

This paper is organized as follows. Section 3 explains the proposed method including the dataset used, Otsu's thresholding, the PSO framework, and the overall steps involved to segment the nuclei from breast histopathology images. The efficiency of PSO-based thresholding method to segment the nuclei from histopathology images is provided by experimental results in Sect. 4. Finally, the conclusion and future work are presented in Sect. 5.

3 Materials and Methods

3.1 Dataset

The images for conducting the experiments are taken from the UCSB Bio-Segmentation Benchmark dataset [8]. The dataset consists of 26 malignant and 32

benign H&E-stained breast tissue images in.tiff. The ground truth segmentation has also been provided along with the dataset in order to evaluate the segmentation performance.

3.2 Otsu's Thresholding

Otsu's multilevel thresholding method [9] is formulated as follows. Consider an $m \times m$ gray image with a total of $L = 256$ intensity levels given by $0, 1, 2, \ldots, L-1$. The gray-level histogram of this image is represented as a probability distribution and is given as $p_i = \frac{n_i}{N}$, where i represents an intensity level and it can take values $0, 1, 2, \ldots, L-1$, p_i is the probability of occurrence of the pixels at a given level i, n_i is the total number of pixels at a particular level i, and N is the total number of pixels in the image. To segment this image into two classes C_1 and C_2, a single threshold value t_1 is determined such that pixels with intensity values from 0 to t_1 are grouped together to belong to class C_1 and pixels with intensity values from t_1 to $L-1$ are grouped together to belong to class C_2. Similarly, to segment the image into three classes, two threshold values t_1 and t_2 are determined. In general, to segment an image into n levels, we need $n-1$ threshold values.

Otsu's discriminant criterion to segment an image into n classes is given in Eq. 1.

$$\sigma_B^2 = \sum_{j=1}^{n} \omega_j (\mu_j - \mu_T)^2 \tag{1}$$

where j represents a class, ω_j represents the probability that a pixel is assigned to a class C_j and is given by Eq. 2, μ_j represents the mean intensity value of pixels assigned to a class C_j and is given by Eq. 3 and μ_T represents the mean intensity of the entire image and is given by Eq. 4.

$$\omega_j = \begin{cases} \sum_{i=0}^{t_j-1} p_i, & \text{if } j = 1. \\ \sum_{i=t_{j-1}}^{t_j-1} p_i, & \text{if } j > 1 \quad \text{and} \quad j < n \\ \sum_{i=t_{j-1}}^{L-1} p_i, & \text{if } j = n. \end{cases} \tag{2}$$

$$\mu_j \begin{cases} \sum_{i=0}^{t_j-1} \frac{i.p_i}{\omega_j}, & \text{if } j = 1. \\ \sum_{i=t_{j-1}}^{t_j-1} \frac{i.p_i}{\omega_j}, & \text{if } j > 1 \quad \text{and} \quad j < n. \\ \sum_{i=t_{j-1}}^{L-1} \frac{i.p_i}{\omega_j} & \text{if } j = n. \end{cases} \tag{3}$$

$$\mu_T = \sum_{i=0}^{L-1} i \cdot p_i. \tag{4}$$

Otsu's discriminant function to find optimal threshold values is solved iteratively by considering each intensity level of the image as a candidate threshold value and then computing the between class variance. The threshold value that maximizes the between class variance is then chosen as the optimal threshold value. This is a computationally intense procedure as it has to loop through all the available intensity values to find the optimal threshold. Hence, an approach to determine the optimal threshold value is to model Otsu's thresholding problem as an optimization problem and to solve it using an optimization technique. In this paper, we use PSO as the optimization technique to compute the optimal threshold values.

3.3 Particle Swarm Optimization (PSO)

PSO is an iterative search and optimization procedure, which is based on flocking behavior of birds. PSO takes an objective function f and determines the values of parameters that either maximizes or minimizes it. This technique uses a set of particles called as swarm that move in the search space to find a global optimum solution. The particles interact and co-operate with each other to determine the optimal solution.

Each particle i is characterized by two factors namely its position $x_i(t)$ and velocity $v_i(t)$ at time t. The position of each particle is used to compute the solution of that particle $f(x_i)$ based on the fitness function and the velocity of a particle is used to govern the movement of the particle within the search space. The velocity and position of a particle should be within the specified maximum and minimum values denoted as $v_{\max}$, $v_{\min}$ and $x_{\max}$, $x_{\min}$, respectively. During every iteration, each particle remembers its own best position $p\text{best}_i(t)$, i.e., the position that yielded the best fitness value for an individual particle $f(p\text{best}_i(t))$ and the best position of the entire swarm $g\text{best}(t)$, i.e., the position that yielded the best fitness value for the entire swarm $f(g\text{best}(t))$. The particles travel along the search space by updating their velocity and position as specified by Eqs. 5 and 6, respectively, until the stopping condition is reached.

$$v_i(t+1) = w \cdot v_i(t) + c_1 r_1(p\text{best}_i(t) - x_i(t)) + c_2 r_2(g\text{best}(t) - x_i(t)). \quad (5)$$

$$x_i(t+1) = x_i(t) + v_i(t+1) \quad (6)$$

where w is the inertial weight, c_1, c_2 are the acceleration constants, and r_1, r_2 are uniformly distributed random numbers in the interval [0, 1]. The stopping condition can be chosen as a predetermined number of iterations. Once the stopping condition is met, $g$best gives the optimal values for the parameters. Initially, $g$best is assigned a minimum value if the objective function is to be maximized or it is assigned a maximum value if the objective function is to be minimized. For a multidimensional problem, the above-said parameters are maintained and updated for each of the dimension.

3.4 Image-processing Steps Involved

Preprocessing. The quality of histopathology images are influenced by noise, improper illumination, and varying staining conditions. Consequently, preprocessing is essential to improve the quality of the acquired digitized breast histopathology images. The breast histopathology images are convolved using a Gaussian filter to smoothen the image and to remove noise from the image.

Segmentation. For segmenting the histopathology images, the parameters of PSO already mentioned in the previous section are modeled as follows. The discriminant criterion of Otsu's multilevel thresholding specified in Eq. 1 is the objective function to be maximized. In our work, search space is treated as the intensity values of the pixels in the image. The position of a particle $x_i(t)$ corresponds to a threshold vector and the number of classes n the image is to be segmented into determines the dimensions of the threshold vector, i.e., $x_i(t) = t_1, t_2, \ldots, t_{n-1}$ where each t_j denotes a threshold value.

The initial position of the particles is assigned randomly within the range of intensity values of the pixels in an image. The other parameters such as inertial weight, acceleration constant, minimum and maximum velocity, number of generations or iterations, and the number of particles are initialized as specified in the section on experimental results. For the segmentation of an *RGB* image, each plane *R*, *G,* and *B* is considered as a separate dimension and the PSO algorithm is applied to the three dimensions independently. An algorithm for PSO-based Otsu's multilevel thresholding is given in algorithm 1. After the algorithm terminates, $g$best value yields the threshold vector that contains the optimal threshold values. After the $n - 1$ threshold values are obtained, the image is quantized as follows. Let $T = t_1, t_2, \ldots, t_{n-1}$ denote the threshold vector. A value 0 and a 256 are prefixed and post-fixed to the threshold vector *T,* respectively, so that the threshold vector becomes $T = 0, t_1, t_2, \ldots, t_{n-1}, 256$. In the input image, those pixels whose value fall between *0* and t_1 are quantized to a value 0 and those pixels whose value fall

between t_1 and t_2 are quantized to a value t_1 and so on. In general, a pixel is quantized to a value t_n, if it falls between t_n and t_{n+1}, i.e., if

$$t_n < I(x, y) < t_{n+1} \quad \text{then} \quad I_{\text{out}}(x, y) = t_n. \tag{7}$$

where $I(x, y)$ is the input image and $I_{\text{out}}(x, y)$ is the quantized output image. After the image is quantized, the segmented image containing only the nuclear areas are found out by applying an appropriate threshold value to the quantized image.

Post-processing. The post-processing step is essential to fine-tune the results of the segmentation output. The segmented nuclei had small holes in them due to the non-uniform intensity within the nuclei. Therefore, in order to enhance the shape of the nuclei, a hole-filling operation is performed. Small artifacts that do not belong to nuclei are filtered out using a morphological size-filtering operation.

4 Experimental Results

All input images are 896 × 768 pixels in size. The input image is filtered with a 3 × 3 Gaussian filter to remove noise. The preprocessed image is segmented using the proposed method with the parameters as listed in Table 1. The number of classes is fixed as three because an image contains three prominent regions such as nuclei, cytoplasm, and background. Consequently, two threshold values are computed for each image. After the computation of the threshold vector, the image is quantized according to Eq. 7. Then, the nuclei are segmented from the quantized image by applying a threshold value of zero. After segmentation, the images are post-processed by morphological hole-filling and size-filtering operations. Figure 1 shows the result of segmenting breast histopathology images using the proposed method. The proposed method is evaluated using the detection performance as explained in the next section.

Table 1 Initial values of PSO parameters

Parameters	Value
Number of particles	25
Number of iterations	50
Number of classes	3
Number of threshold values	2
Inertial weight w	1.5
Acceleration constants c_1, c_2	0.8
$v_{\min}, v_{\max}$	[−3, 3]
$v_{\min}, v_{\max}$	[0, 255]

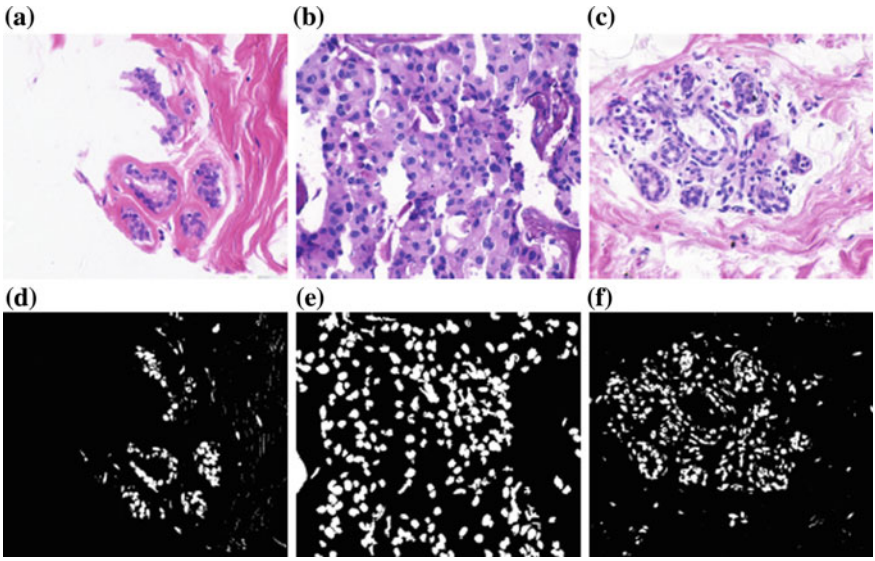

Fig. 1 Sample images and their segmentation results. **a–c** Breast histopathology images. **d–f** Segmentation results for images **a–c**

4.1 Detection Performance

Detection performance is quantified using three metrics such as precision, recall, and *F*-measure that are computed from true positive (TP), false positive (FP), and false negative (FN) values. TP refers to those nuclei in the ground truth image that were correctly detected by the proposed method. FP refers to those regions that were not nuclei in the ground truth image but were incorrectly detected as nuclei by the proposed method. FN refers to those nuclei that were actually present in the ground truth image but were not detected by the proposed method. Out of the total number of nuclei detected by the proposed method, precision signifies the fraction of them that are actually present in the ground truth image and is given as Precision = TP/(TP + FP). It is also called as positive predictive value. Out of the total number of nuclei present in the ground truth image, recall signifies the fraction of them detected by the proposed method and is given as Recall = TP/(TP + FN). It is also called as sensitivity. *F*-measure is a weighted harmonic mean of precision and recall and is given as *F*-measure = 2/((1/precision) + (1/recall)). The precision, recall, and *F*-measure values obtained for the proposed method are tabulated in

Table 2 Detection performance

Precision	Recall	*F*-measure
0.978	0.943	0.960

Table 2. Higher precision and recall values indicate that the proposed method has identified most of the nuclei correctly.

Algorithm 1: PSO based Otsu's multilevel thresholding

Input: *RGB* histopathology image

Output: Threshold vector with $\boldsymbol{n-1}$ threshold values
for *each input image I* do
  $N_{particlesmax}$ denote maximum number of particles
  $N_{iterationsmax}$ denote maximum number of iterations
  Initialize values for $w, c_1, c_2, x_{min}, x_{max}, v_{min}, v_{max}$, r_1 and r_2
  $f(gbest)$ = minimum value
    for i = 1 *to* $N_{particlesmax}$ **do**
    foreach *dimension R, G, B of I* **do**
      Randomly assign the position (x_i) of the particle within search space
      $pbesti = xi$
      Calculate fitness $f(xi)$ using Eq. 1
      if $f(x_i) > f(gbest)$ **then**
        $gbest = x_i$
        $f(gbest) = f(x_i)$
      end
    end
  end
  t = 1;
  while $t < N_{iterationsmax}$ **do**
    for i 1 *to* $N_{particlesmax}$ **do**
      Compute velocity $v_i(t)$ according to Eq. 5
      Compute position $x_i(t)$ according to Eq. 6
      Calculate fitness $f(x_i)$ using Eq. 1
      if $f(x_i) > f(pbesti)$ **then**
        $pbesti = x_i$
      end
      if $f(xi) > f(gbest)$ **then**
        $gbest = x_i$
      end
    end
  end
end
return *gbest*

5 Conclusion and Future Works

Segmentation of nuclei from histopathology images is a challenging task. In this paper, the use of PSO-based Otsu's multilevel thresholding technique to segment nuclei from breast histopathology images is investigated. The experimental results prove that this method can be incorporated for automated image analysis to effectively segment nuclei. This work can be further extended to develop a computer-aided diagnosis system that classifies the given input image as benign or malignant by extracting features from the segmented nuclei and training a classifier.

References

1. P.-W. Huang, Y.-H. Lai, Effective segmentation and classification for HCC biopsy images. Pattern Recogn. **43**(4), 1550–1563 (2010)
2. Y. Al-Kofahi, W. Lassoued, W. Lee, B. Roysam, Improved automatic detection and segmentation of cell nuclei in histopathology images. IEEE Trans. Biomed. Eng. **57**(4), 841–852 (2010)
3. M.M. Dundar, S. Badve, G. Bilgin, V. Raykar, R. Jain, O. Sertel, M.N. Gurcan, Computerized classification of intraductal breast lesions using histopathological images. IEEE Trans. Biomed. Eng. **58**(7), 1977–1984 (2011)
4. C. Lu, M. Mahmood, N. Jha, M. Mandal, A robust automatic nuclei segmentation technique for quantitative histopathological image analysis. Anal. Quant. Cytol. Histol. **34**(6), 296–308 (2012)
5. M. Veta, P.J. van Diest, R. Kornegoor, A. Huisman, M.A. Viergever, J.P.W. Pluim, Automatic nuclei segmentation in H&E stained breast cancer histopathology images. PLoS ONE **8**(7), e70221 (2013)
6. P. Ghamisi, M.S. Couceiro, J.A. Benediktsson, M.F. Nuno, N.M. Ferreira, An efficient method for segmentation of images based on fractional calculus and natural selection. Expert Syst. Appl. **39**(16), 12407–12417 (2012)
7. R.V. Kulkarni, G.K. Venayagamoorthy, Bio-inspired algorithms for autonomous deployment and localization of sensor nodes. IEEE Trans. Syst., Man, Cybern. **40**(6), 663–675 (2010)
8. E.D. Gelasca, J. Byun, B. Obara, B.S. Manjunath, Evaluation and benchmark for biological image segmentation, in *IEEE International Conference on Image Processing* (2008)
9. N. Otsu, A threshold selection method from gray-level histograms. IEEE Trans. Syst. Man Cybern. **9**(1), 62–66 (1979)

Wavelet Transform-Based Land Cover Classification of Satellite Images

D. Menaka, L Padma Suresh and S. Selvin Premkumar

Abstract Detection of urban expansion from land cover remote sensing images is a challenge due to the complexity of urban landscapes. Initially, the original satellite image is preprocessed and then segmented to have segments from different land classes such as of hilly land regions, vegetation area, building area, and water bodies. Different feature extraction methods such as first-order statistics, gray-level co-occurrence matrix (GLCM), and wavelet transform-based technique were applied in this paper, and the results are compared. The features of the segmented area are extracted, and then, final classification is carried out using the proposed probabilistic neural network (PNN) classifier. The classified satellite image is obtained and compared with the original image. The proposed technique is evaluated by means of accuracy parameter and produces better results using wavelet transform first-order statistics combined with PNN classifier.

Keywords First-order statistics · Gray-level co-occurrence matrix · Wavelet transform · Satellite image processing · Probabilistic neural network

1 Introduction

Research in land cover mapping and change detection analysis in remote sensing images have been developed because of its vast applications and expanded land cover

D. Menaka (✉)
Department of EIE, Noorul Islam University, Kumaracoil, India
e-mail: menakaberita@gmail.com

L Padma Suresh
Electrical and Electronics Engineering, Noorul Islam Centre for Higher Education, Kumaracoil, Tamil Nadu, India
e-mail: suresh_lps@yahoo.co.in

S.S. Premkumar
Department of CSE, C.S.I. Institute of Technology, Thovalai, India
e-mail: selvincsiit@gmail.com

© Springer India 2015

L.P. Suresh et al. (eds.), *Artificial Intelligence and Evolutionary Algorithms in Engineering Systems*, Advances in Intelligent Systems and Computing 325,
DOI 10.1007/978-81-322-2135-7_89

regions. Remote sensing refers to images obtained from a satellite where a single satellite image covers a wide area of land which provides lot of information. Therefore, efficient algorithms are needed to process satellite imagery. In literature, it is found various conventional methods of land cover classification but not given accurate results because of the complexity of satellite images [1]. This paper describes the scheme using wavelet transform applied for land cover classification. In the proposed method, the statistical and co-occurrence features of the input patterns are first extracted and those features are used for classification. Different wavelet decomposition levels are applied and used for these features for classification. The features are extracted from five different classes of land cover images, and the performances of the wavelet transform are measured under different wavelet decomposition levels. Currently, wavelet transform has gained more significance in satellite image processing. The reliability exhibited by texture analysis using wavelet transform is beneficial for doing classification of different classes of land cover images.

1.1 Study Area and Data Used

The test data satellite image used in this study is of Kumarakoil town in Kanyakumari District of India downloaded from Google earth maps. Kumarakoil is one of the largest towns in the District. It is located between longitude of 77.3410569 and latitude 8.2407164. The topography of Kumarakoil is approximately 56 km above mean sea level. The land cover features of this study area include urban, dense vegetation, water body, paddy land, and hilly region [2]. The land classes can be extended in accordance with the input data image captured at different topology views.

2 Algorithm Description

The new algorithm implemented in this paper consists of three phases: In the first level, feature extraction technique by first-order statistics was performed. In the second level, feature extraction technique using gray-level co-occurrence matrix (GLCM) and first-order statistics wavelet transform for different decomposition levels were performed. In the last level, features of the extracted features are applied to a probabilistic neural network (PNN) classifier and thus obtained the classified output image. The layout of the new algorithm is shown in Fig. 1.

2.1 Data Preprocessing

The test satellite image is preprocessed by converting into gray-scale images from color images. The noise if any is removed using the best median filter, and the

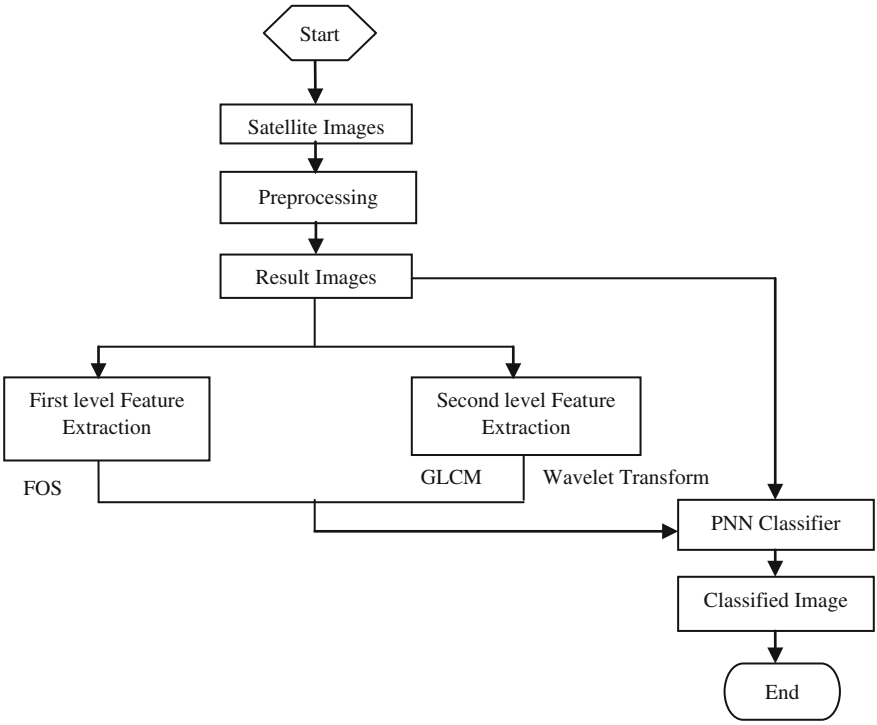

Fig. 1 Flowchart of the proposed approach

contrast of the image is then enhanced which makes clear the correction and resolution of the input image. The classification process is made easier by applying the classifier on the preprocessed image.

2.2 Feature Extraction

Feature extraction is the main step in classification. From the original image, 20 × 20-sized windows were segmented from which the first-level and second-level features were extracted. The accuracy of any classifier depends upon the features extracted. In literature, feature extraction was done based on pixel and texture analysis where texture analysis is proposed with better results. The feature extraction methods used in this paper involves first-order statistics as the first-level feature extraction, whereas GLCM and wavelet transform with first-order statistics as the second-level feature extraction. The results obtained were individually applied to the proposed classifier, and the classified output images were compared.

2.3 First-level Feature Extraction

The first-level feature extractor includes extraction of features from the data using first-order statistics-based technique, which is explained as below.

2.3.1 First-order Statistics Method (FOS)

The first-order statistics calculates the technical features from a one-dimensional probability density function based on the occurrence of pixels between pairs of gray levels. The preprocessed input data were converted to histogram. The features such as mean, standard deviation, skewness, kurtosis, and entropy were computed from the histogram. From the results, it is finalized that first-order statistical features are not considered suitable to a satellite images land-use classification.

$$\text{Mean}\,\bar{x} = \frac{1}{N^2}\sum_{i=1}^{N}\sum_{j=1}^{N} x_{i,j} \tag{1}$$

$$\text{Standard deviation}\,\sigma = \sqrt{\frac{1}{N}\sum_{i=1}^{N}(x_i - \mu)^2} \tag{2}$$

$$\text{Skewness} = \frac{\sum_{i=1}^{N}(x_i - \bar{x})^3}{(N-1)\sigma^3} \tag{3}$$

$$\text{Kurtosis} = \frac{\sum_{i=1}^{N}(x_i - \bar{x})^4}{(N-1)\sigma^4} \tag{4}$$

$$\text{Entropy} = -\sum_{i=1}^{N}\sum_{j=1}^{N}(C(i,j))\log(C(i,j)) \tag{5}$$

2.4 Second-level Feature Extraction

The second-level feature extraction involves the techniques such as GLCM and wavelet transform with first-order statistics (WTFOS). The features extracted were the second-order statistics features using GLCM technique and first-order statistical features using wavelet transform.

2.4.1 Gray-level Co-occurrence Matrix

The GLCM is the distribution defined over an image as the distribution of co-occurring values at a given offset, which measures the texture of the image. GLCM texture considers the relation between reference and neighbor pixels at a time [3].

The GLCM involves a set of features such as homogeneity, contrast, correlation, and entropy. From the classification results, it is computed that the accuracy results are better compared to first-order statistical method. The features such as contrast, correlation, energy, and homogeneity were computed from the GLCM matrix and then are applied to the classifier.

$$\text{Contrast} = \sum_{i,j=0}^{N} (i-j)^2 C(i,j) \tag{6}$$

$$\text{Correlation } r = \frac{1}{N-1} \sum \left(\frac{x-\bar{x}}{\sigma_x} \right) \left(\frac{y-\bar{y}}{\sigma_y} \right) \tag{7}$$

$$\text{Energy} = \sum_{i=1}^{N} \sum_{i=1}^{N} C(i,j)^2 \tag{8}$$

$$\text{Homogenity} = \sum_{i,j=0}^{n} \frac{1}{\left(1 + (i-j)^2\right) C(i,j)} \tag{9}$$

2.4.2 Wavelet Transform

An approach of multi-resolution wavelet transform is proposed as a textural feature extraction tool for segmenting remotely sensed images [4]. Wavelet transform leads to the concept of multi-resolution analysis, where an image is decomposed into structures and then analyzed at successive levels. Wavelet transform is implemented through convolution with a pair of orthogonal or bi-orthogonal mirror filters supported by repeated down sampling. The pair of half-band low-pass and high-pass filters are used as bi-orthogonal mirror filters. The image composed of low-frequency parts in both horizontal and vertical directions are decomposed into four subimages level by level denoted as LL(m, n), LH(m, n), HL(m, n), and HH(m, n). Here, LL(m, n) represents low-frequency components of the original image, which reveals most energy of the test satellite image. LH(m, n), HL(m, n), and HH(m, n) represent horizontal, vertical, and diagonal high-frequency components of the test satellite image.

The features considered here are average, energy, and entropy. The energy feature measures textural uniformity, while the entropy measures the disorder of an image. First, a 20 × 20 window-sized image is extracted from the input image. The extracted window-sized image is decomposed into four subimages using the two-dimensional wavelet transform. The textural measure derived from the statistical parameters is then extracted from each decomposed image [5]. The continuous wavelet transform of a 1-D signal $f(x)$ is defined using Eq. 10.

$$W(a,b) = \int f(x)\Psi_{a,b}(x)\mathrm{d}x \tag{10}$$

where $$\Psi_{a,b}(x)\mathrm{d}x = \frac{1}{\sqrt{a}}\Psi\left(\frac{x-a}{b}\right)$$

The mother wavelet ψ satisfies the localized zero mean function. Equation 10 can be discretized by restraining 'a' and 'b' to a discrete lattice ($a = 2^n$, $b \in z$). Typically, few constraints are imposed on ψ to ensure that the transform is non-redundant and constitutes a multi-resolution representation of the original signal. The extension to the two-dimensional transform is performed by applying a separable filter bank to the image usually low-pass and high-pass filters are used [6]. The convolution with the low-pass filter results in an approximation image and the convolutions with the high-pass filter in specific directions result in detailed feature extracted images. For a n-level, the signal decomposition can be represented using Eq. 11.

$$\begin{aligned} A_n &= \left[H_x * \left[H_y * A_{n-1}\right] \downarrow 2,1\right] \downarrow 2,1 \\ D_{n1} &= \left[H_x * \left[G_y * A_{n-1}\right] \downarrow 2,1\right] \downarrow 2,1 \\ D_{n2} &= \left[G_x * \left[H_y * A_{n-1}\right] \downarrow 2,1\right] \downarrow 2,1 \\ D_{n3} &= \left[G_x * \left[G_y * A_{n-1}\right] \downarrow 2,1\right] \downarrow 2,1 \end{aligned} \tag{11}$$

where '*' denotes the convolution operator, '↓ 2, 1' denotes the down sampling along the rows and columns, $A_0 = I$ is the original image, and H and G are low-pass and high-pass filters, respectively.

$I(x, y)$ is the original image. A_n is obtained by low-pass filtering and is the approximation image at scale n. The detailed images D_{ni} are obtained by band-pass filtering in a specific direction, where $i = 1, 2, 3$ for vertical, horizontal, and diagonal directions, respectively, at scale n. The original image is thus represented by a set of subimages at several scales $\{A_n, D_{ni}\}$. Figure 2 shows a two-dimensional image, which is decomposed into four sub-band images [7]. The first-order statistical features discussed above are again used in extracting features using wavelet transform as it depends on first-order statistics.

2.5 Classification

Neural networks have been extensively used in satellite image classification applications. Probabilistic neural network classifier is an effective tool for solving land cover classification problems because of its ease of training and statistical foundation in Bayesian estimation theory [8]. This paper employs the PNN approach to classification of land cover classes from satellite images. The PNN classifier was chosen over other neural networks because of its speed in training and

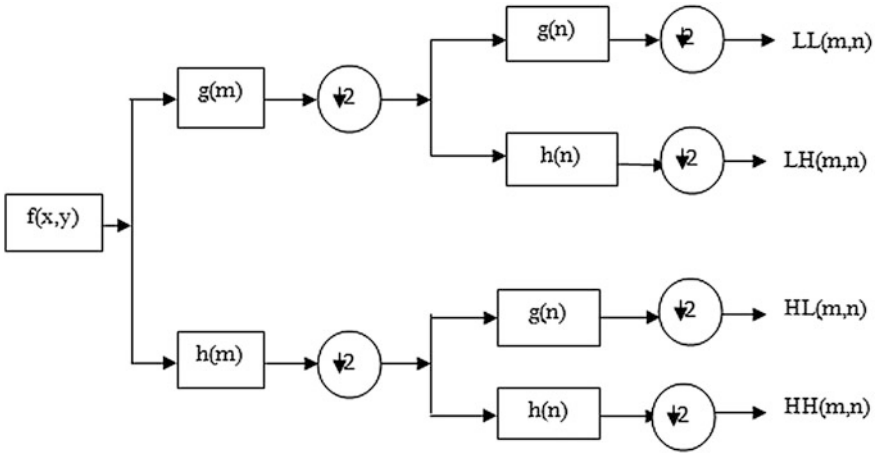

Fig. 2 Structure of two-dimensional wavelet transform

accuracy. From the literature, it is found that the PNN to be superior to the feed-forward back propagation neural network and also more suitable to land cover analysis [9]. The PNN architecture consists of four layers: an input layer, a pattern layer, a summation layer, and an output layer.

The input layer simply distributes the input to the neurons in the pattern layer and does not perform any computation [10]. The neuron x_{ij} of the pattern layer on receiving a pattern x from the input layer computes its output as given by the equation below.

$$\phi_{ij}(x) = \frac{1}{(2\pi)^{d/2}\sigma^d} \exp\left[-\frac{(x - x_{ij})^{\mathrm{T}}(x - x_{ij})}{2\sigma^2}\right] \tag{12}$$

where d denotes the dimension of the pattern vector x, x_{ij} is the neuron vector, and σ is the smoothing parameter. The summation layer neurons compute the maximum likelihood of pattern x being classified into C_i by summarizing and averaging the output of all neurons that belong to the same class using equation below

$$p_i(x) = \frac{1}{(2\pi)^{d/2}\sigma^d} \frac{1}{N_i} \sum_{j=1}^{N_i} \exp\left[-\frac{(x - x_{ij})^{\mathrm{T}}(x - x_{ij})}{2\sigma^2}\right] \tag{13}$$

where N_i denotes the total number of samples in class C_i. The decision layer unit classifies the pattern x in accordance with the Bayer's decision rule based on the output of all the summation layer neurons by

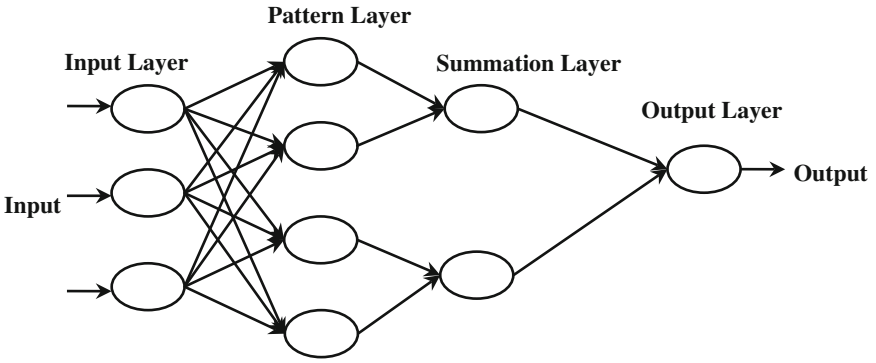

Fig. 3 Structure of probabilistic neural network

$$\widehat{C}(x) = \arg\max\{p_i(x)\}, \quad i = 1, 2, \ldots m \tag{14}$$

where $\hat{C}(x)$ denotes the estimated class of the pattern x, and m is the total number of classes in the training samples. This work analyses five different land classes, where $m = 5$. The structure of probabilistic neural network is shown in Fig. 3.

3 Results and Discussion

From the original image, 20 × 20-sized windows were segmented from which the first-level and second-level features were extracted. The extracted features were used for training a PNN classifier. The algorithm automatically selects 20 × 20-sized windows from the left corner and extracts features and gives these features to the classifier. The classifier then classifies this window as any one of the five land cover regions. This procedure is repeated for the entire image. Figure 4 shows the original image. Figure 4b is obtained using the features extracted using first-order statistics, and Fig. 4c is obtained using the features extracted using wavelet transform first-order statistics.

From the outputs, it is clear that the land cover classification using wavelet transform first-order statistics is better when compared with first-order statistics features. The work can be further extended to satellite images of different spectral bands obtained from land cover satellites such as Landsat, Ikonos, and Quickbird. The test data are obtained from Google earth maps and resized by 20 × 20 images. The features are extracted from five different land classes using the feature extraction techniques such as FOS, GLCM, and wavelet transform. Comparatively, the classification of land cover was found better using the wavelet transform-based feature extraction.

The classification results were identified by different color variations and shown in Fig. 4. The classification results are tabulated in Table 1, and the accuracy was

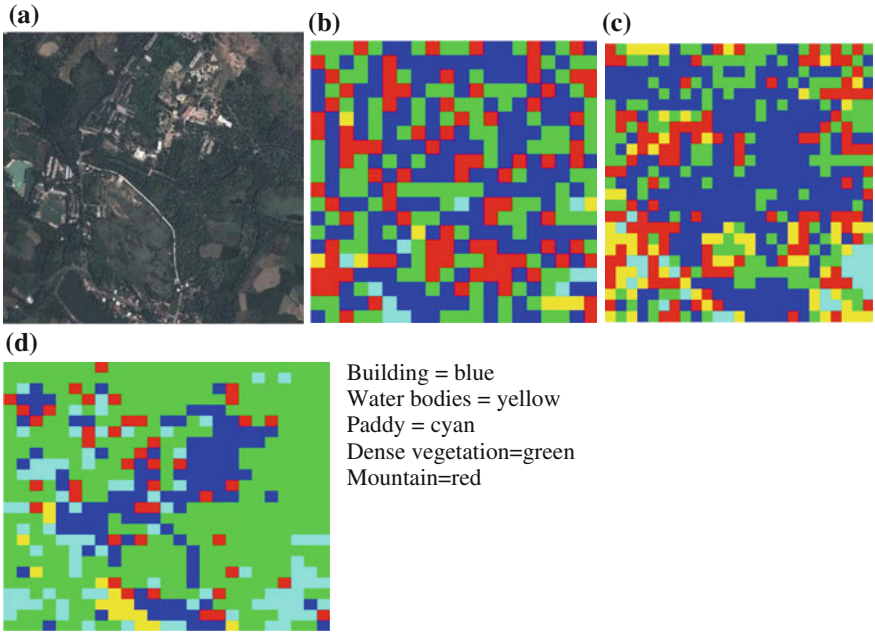

Fig. 4 **a** Original image, **b** classified image using FOS-based feature extraction, **c** classified image using GLCM-based feature extraction, and **d** classified image using wavelet transform-based feature extraction

Table 1 Comparison table of classification error rates obtained using proposed algorithm

Classified land classes	Classification results in %		
	FOS	GLCM	WTFOS
Building	75	95	98
Dense vegetation	82	86	96
Mountain	90	80	98
Paddy	85	85	98
Water	88	90	96

analyzed. It is known from the Table 1 that the classified image obtained using wavelet transform-based feature extraction produces better accuracy compared to other techniques described in this work.

4 Conclusion

This paper presents a performance comparison of feature extraction using first-order statistics, GLCM, and wavelet method for land cover/land-use mapping for any satellite imagery. Experiments were carried out using the bench mark Kumarakoil city images. The training samples were selected randomly from the homogenous texture regions of the original image. Experimental results confirm the advantages of wavelet and PNN classifier, which also enhance the per pixel classification accuracy in more complex satellite images. The proposed scheme of wavelet combined with PNN classifier for the classification of satellite images is found to be effective for land cover mapping and for further analysis.

References

1. S. Zhang, Q. Zhou, New feature extraction algorithm for satellite image non-linear small objects, in *IEEE Symposium on Electrical and Electronics Engineering* (2012)
2. S. Arivazhagan, L. Ganesan, Texture classification using wavelet transform. Pattern Recogn. Lett. **24**, 1513–1521 (2003)
3. A. Baraldi, F. Parmiggiani, An investigations of the textural characteristics associated with gray level cooccurrence matrix statistical parameters. IEEE Trans. Geosci. Remote Sens. **33** (2), 293–304 (1995)
4. TM. Lillesand, RW. Kiefer, JW. Chipman, *Remote Sensing and Image Interpretation* (Wiley International edition, Hoboken, 2004), pp. 586–592
5. S. Rajesh, S. Arivazhagan, K.P. Moses, R. Abisekaraj, Land cover/land use mapping using different wavelet packet transforms for LISS IV madurai imagery. Indian SoC Remote Sens. **40**(2), 313–324 (2012)
6. L.A. Ruiz, A. Fdez-Sarría, J.A. Recio, Texture feature extraction for classification of remote sensing data using wavelet decomposition:a comp study. Remote Sens. Spatial Inf. Sci., in *Proceedings of International Archives Photogramm* (2004), pp. 1109–1115
7. M. Acharyya, M.K. Kundu, Wavelet-based texture segmentation of remotely sensed images. in *Proceedings of International Conference Image Analysis and Processing* (2001), pp. 69–74
8. B. Tian, M.R. Azimi-Sadjadi, T.H. Vonder Haar, D. Reinke, Temporal Updating Scheme for Probabilistic Neural Network with Application to Satellite Cloud Classification. IEEE Trans. Neural Networks **11**(4), 903–920 (2000)
9. D.F. Specht, Probabilistic neural network. Neural Networks **3**, 109–118 (1990)
10. B. Sırmaçek, C. Ünsalan, A probabilistic framework to detect buildings in aerial and satellite images. IEEE Trans. Geosci. Remote Sens. **49**(1), 211–221 (2011)

Tamil Speech Recognizer Using Hidden Markov Model for Question Answering System of Railways

G. Vignesh and S. Sankar Ganesh

Abstract The research on speech and natural language is in progress for more than two decades. Recently, researchers are focused on developing speech interfaces to their corresponding automated system. For voice-based question answering system, there is the need for developing speech recognizer. Although automatic speech recognition (ASR) systems are already available, most of them have been built for English language. This paper aims to build Tamil speech recognizer for question answering system of railway information using natural language processing. Most feasible approach for speech recognition so far has been hidden Markov model (HMM) which is implemented in this research work. HMM-based recognition component is trained automatically and computationally realistic to use. The recognition accuracy of the system using HMM has up to 85 % for different speakers.

Keywords Automatic speech recognition · Hidden Markov model · Voice recording · Word boundary detections · Session initiation protocol

1 Introduction

Nowadays, computers have become absolutely indispensable especially for the people of urban India. But in the development of our country, where most of the people live in rural areas (about 56 % of Tamil Nadu's population lives in rural areas) as a whole, the technology has to reach them. The various computer accessories, such as the keyboard and mouse, require a certain level of expertise from the user, which cannot be expected from rural people, physically challenged,

G. Vignesh (✉) · S. Sankar Ganesh
Department of Information Technology, National Engineering College, Kovilpatti, India
e-mail: vigneshgopinath.2@gmail.com

S. Sankar Ganesh
e-mail: ssganesa@yahoo.com

© Springer India 2015

L.P. Suresh et al. (eds.), *Artificial Intelligence and Evolutionary Algorithms in Engineering Systems*, Advances in Intelligent Systems and Computing 325,
DOI 10.1007/978-81-322-2135-7_90

or blind people. They also require people to be proficient in English as well to be able to use the computer. In our country, where the literacy rate is very low (still Tamil Nadu has around 19 % illiterate people), the above-mentioned constraints have to be discarded, for the technology to be proficient to reach the grassroot level. That is why speech recognition becomes useful.

Speech recognition is the process of converting an input acoustic signal (input in audio format in the form of spoken words) and recognizes the various words contained in the speech. These recognized words provide the final result, which may serve as instructions and control, or they may provide as input to further language processing. In simply, speech recognition can be put together as the ability to take the audio format as input and then generate the text format from it as output. Speech recognition involves different steps which include voice recording, word boundary detections, feature extraction, and recognition component with the help of language models [1, 2]. Speech or voice recognition is the technology that allows for computer input via spoken commands. To use speech recognition, the computer needs a microphone and supporting software. In this pair, the software is the complex part. Speech recognition system works by disassembling sound into atomic units (called phonemes) and then piecing them back together. Speech recognition is one of the emerging research catalogs in natural language processing.

Natural language processing has the ability to process the output from speech recognition software and understand what the user meant. Natural language processing efforts to translate words into ideas by probing context, patterns, phrases, etc. Natural language processing and speech recognition work together to clear up vague words or homonyms, i.e., two, too, and to. Voice recording takes place over Voice over Internet Protocol (VoIP), microphone, and sound recording, and word detection component is responsible for capturing the input from a microphone and then forwarding it to the feature extraction component of the system. The feature extraction is one of the most important modules in the system. Feature extraction deals with the elimination of unwanted information in speech.

To identify a spoken word, the speech recognition system has to identify and differentiate between different sounds in the same way as human beings do. Hidden Markov model (HMM)-based system development is provided with automatic training and high accuracy [12]. This paper deals to build a speech recognition system to recognize spoken Tamil using HMM. Research in automatic speech recognition (ASR) aims to develop methods and techniques that enable computer systems to accept speech input and to print the output as text on the screen. Language model provides an idea about the different words that are possible in the language and the sequence in which these words may occur. In Sect. 2, the preprocessing modules for the system implementation are defined. Section 3 of this paper describes how the HMM is built and how it is applied in the proposed speech recognition system. In Sect. 4, the performance of the system is analyzed by its matrices. Finally, in Sect. 5, the solution of mixed Tamil and English word problem is discussed.

2 Related Work

Prior to developing the speech recognition system, knowledge model creation is very important. The words of Tamil and English needed for the particular railway domain are inserted into the database through this module. These words are got from various speakers. Based on the pronunciation of various speakers, the words are segmented in manually [3]. The railway-related information collection of language model is now created. Here, the acoustic model is no needed because the HMM [12] automatically trains the system with inbuilt acoustic model. Sound recording and word detection components are described as they responsible for capturing the input from a microphone (VoIP) and then forwarding it to the feature extraction component of the system. Prior to forwarding to the feature extraction part, it also identifies the segments of the sound containing the words, that is, word detection. It is the responsibility of this module to save the audio files in the WAV format which is required for further training the model. The first 100 ms are considered to be the region of silence during which the average zero crossing rate is calculated to determine the background noise.

After that, voice interface is needed to extract the features of the corresponding speech. Here, Voxeo SIP Softphone is used as a voice server which provides the interfaces for sound recorder and word detection. SIP stands for session initiation protocol which provides the connection establishment between the voice and the text environment. The session initiation protocol (SIP) is a signaling communication protocol, widely used for controlling multimedia communication sessions such as voice and video calls over Internet protocol networks. Feature extraction is carried out by voice server in which it contains the application server for this purpose. Feature extraction is extracted for the different speakers. Feature extraction is the process of retaining useful information of the corresponding signal while discarding redundant and unwanted information [12]. When a new speaker comes to speak, the extracted values are compared with the existing speaker's feature value. Based on the environment, syllables, and pronunciation [3], the features are differed from one speaker to another. The extracted feature is given to the next component that is recognition component which is developed by HMM as feature vector. In recognition component, these features are compared with the language models [1, 4] which are stored in the open-source database which is derived from.

3 Proposed System

In this proposed Tamil speech recognition system, sound record, word detection, and feature extraction are the preprocessing modules which have been discussed in Sect. 2. The recognition component is the key part of the system and is built by HMM. Figure 1 shows the proposed system architecture of Tamil speech recognizer.

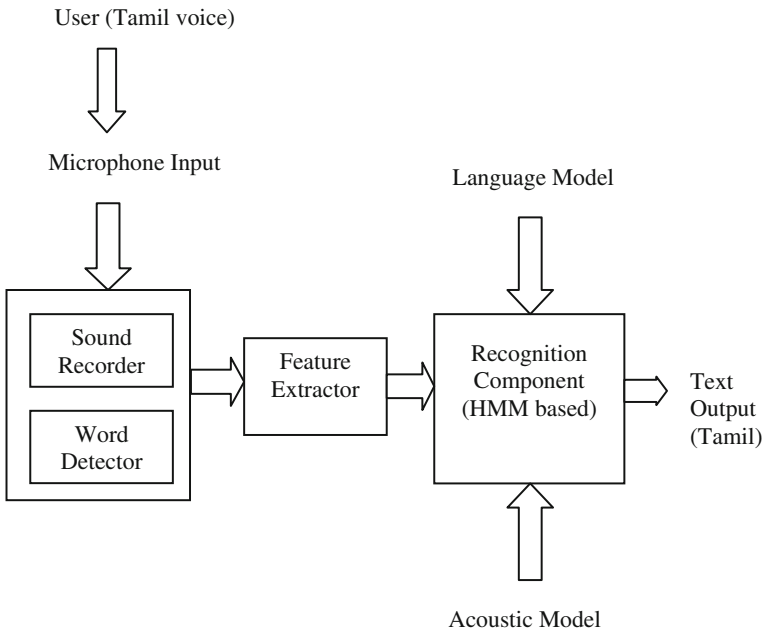

Fig. 1 Tamil speech recognition system

3.1 Hidden Markov Model

The recognition component of Tamil speech recognition system is one of the important parts to be built. This is built by the HMM. A HMM is a stochastic function of a Markov process. A Markov process or chain is a significant and well-researched concept in probability. It deals with a kind of random process that incorporates a minimum amount of memory without actually being memory less [1].

The attractive features of the HMM are that the model itself (i.e., the state sequence) is hidden and what is seen is an observation O related to the state (but not the state itself). By possessing these two features, the HMM could be use to model any time-varying series such as speech processing/recognition and gesture processing/recognition.

3.2 Elements of HMM

1. A set of states $S = \{S_1, S_2, S_3 \ldots S_{10}\}$
2. A set of symbols known as the alphabet $K = \{K_1, K_2 \ldots K_M\}$ (not necessarily finite).
3. A state transition probabilities distribution

$A = \{a_{ij}\}$ such that
$a_{ij} = P(Q_{t+1} = S_j \mid Q_t = S_i)$, shorten
$P(S_j \mid S_i)$ where Q_t is the actual state at time t.

4. The observation symbol probability densities in state i, $B = \{b_i(w)\}$ on K (emission probabilities): for $w \varepsilon K$ and shorten as $P(w \mid S_i)$
5. An initial state distribution Π such that $\Pi_i = P(O_1 = S_i)$, shorten $P_{\Pi}(S_i)$.

From the above five elements (notations), a HMM (denoted as λ) could be specified as quintuple (S, K, Π, A, B).

Let each word in a speech utterance be represented as a speech vector O, which is also called as an observation [4]. The observation O is defined as following so that it incorporates the speech vectors o_t which is observed at time t.

$$O = o_1, o_2, \ldots o_T s$$

Let the set of vocabulary for the recognizable words is $W = \{w_1, w_2, w_3, \ldots, w_N\}$. The solution to the isolated word recognition problem could be given by calculating

$$\arg \max_i \{P(w_i \mid O)\}$$

Figure 2 shows the word generation HMM finite state automata for the word "road."

The Markov model given is a finite state machine which changes state once every time unit and at each time t that a state j is entered, the speech vector o_t is generated from the probability density $b_j(o_t)$. The transition from the state i to j is governed by the probability distribution a_{ij}. In practical speech science, only the observation sequence is visible and known, but the underlying state sequence is hidden, thereby giving rise to a HMM. HMM decoder is the actual recognition part [4] where there speech utterance would be identified as the particular word in the vocabulary or rejects indicating a miss hit. For the decoder to work it, a grammar is needed to constraint the recognizer such that only the desired words can be recognized.

Recognition component is based on HMM with the comparison of language model [2, 5]. This HMM-based component is automatically trained for user-independent

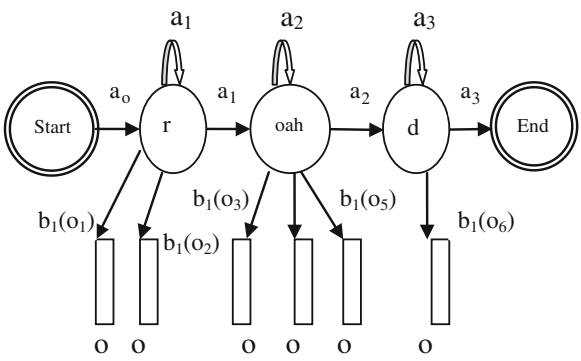

Fig. 2 Word generation HMM automata for the word "road"

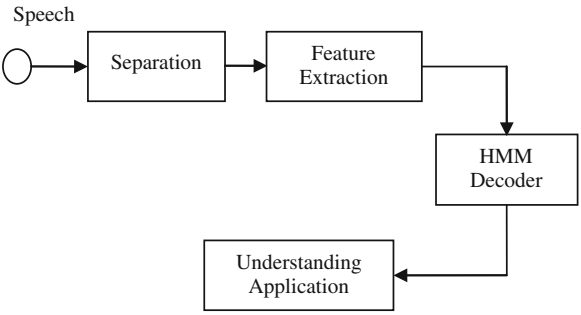

Fig. 3 HMM in speech recognizer

speech. Figure 3 shows the block diagram that how the HMM is used in recognition component.

HMM is created as a library function for the source package which depends on the individual words. In this model, the database connection is established for comparing the language model with respect to the audio. After building the HMM, it is embedded with the knowledge model. A simple Web page is created using Java Servlet page in Java Netbeans IDE for displaying the recognized text word from the audio. When a user speaks, it will be checked with the corresponding word in the language model with the help of HMM and displays the corresponding text output. Most possibly, the noise is discarded in this system because of HMM. By comparing to other mechanisms, it provides the higher accuracy level.

For this type of automated system, training is needed with different people with different environment for HMM-based system error calculation. Based on the noise and speaking environment, HMM [1, 6] leads the different recognition output. Speakers with different pronunciation produce the result variations in the output. So, for each pronunciation of word with various region of people is also tested for the integrated output in recognition component because language model is created according to the various speakers [5].

4 Measure of Performance

The ultimate measures of success for any speech recognition algorithms are accuracy and speed. Therefore, it is important to evaluate the performance of such a system. The word error rate (WER) is one of the most widely used measures for accuracy [7]. The system can be tested on sample utterances from the training data for understanding the system and identification of bugs during the development process. This can result in a higher performance than what one can get with test data.

In addition, a development set can also be used to test the system and also fine-tune its parameters. Lastly, the system can be tested on a test set comprising around 50 speech utterances of 5–10 different users in order to reliably estimate accuracy. The above test should be completely new with respect to the independent training and development.

Table 1 Word error rate calculation

Word	Word error rate (%)
தெற்கு	16.66
நிலையம்	25
அன்பு உடன்	42.85
உங்களை	28.57
வணக்கம்	33.33
வரவேற்கிறது	38.24
ரயில்வே	18.20

Here are three types of word recognition errors in speech recognition:

- Substitution (Subs): An incorrect word substituted for a correct word.
- Insertion (Ins): An extra character added in the recognized word.
- Deletion (Dels): A correct character omitted in the recognized word.

The WER is computed by the following equation: $\text{WER} = (S + D + I)/N$

Where S refers the number of substitutions, D refers the number of the deletions, I refers the number of the insertions, and N is the number of words in the reference.

Word error calculation

Example:
REF (the correct one): voanakkam
HYP (recognizer output): Wannakkam
Err: I S S
After alignment, we have:

- One insertion error (the character: W),
- Two substitution errors (“an” for “oa”), and
- Zero deletion errors.
- The total number of characters present in the reference is 9

So WER = (1 + 2 + 0)/9 * 100 = 33.33 %

Table 1 shows the WER for some restricted words.

The speed of a speech recognition system is commonly measured in terms of real-time factor (RTF). It takes time P to process an input of duration I. It is defined by the given formula

$$\text{RTF} = P/I$$

5 Mixed Tamil–English Words

In day-to-day usage of Tamil, there is a tendency to mix words of all parts of speech from English. A practical system dealing with natural Tamil has to make capable of dealing with this kind of mixing of two languages, English in Tamil. Our approach

in dealing with such mixing is to first identify words that are unknown to the Tamil text. These unknown words can either be named entities or foreign words. We use Tamil case markers and a number of heuristics to postulate what could be station or train names. The remaining unknown words are stemmed as per the Tamil morphology, and then, the root word is searched in the English dictionary. The logic behind this approach is that while adopting a foreign word, the morphological composition used is that of the native language.

6 Conclusion and Future Work

In this paper, Tamil speech recognizer has been built based on HMM. The accuracy of the recognition is up to 85 %. In order to improve the performance metrics, relevant remedy will be applied to this approach in future. And also the Tamil speech recognition system will be integrated for some social relevant automated systems especially for Tamil question answering system for railway information using natural language processing.

References

1. S. Saraswathi, T. Geetha, Morpheme based language model for Tamil speech recognition system. Int. Arab J. Inf. Technol. **4**(3), 214–219 (2007)
2. D. Sharmila et al., Performance of Hindi speech isolated digits in HTK environment. IOSR J. Eng. **2**(5), 1020–1023 (2012)
3. C. Vimala, V. Radha, A review on speech recognition challenges and approaches. World Comput. Sci. Inf. Technol. J. (WCSIT) **2**(1), 1–7 (2012)
4. R. Thangarajan et al., Syllable modeling in continuous speech recognition for Tamil language. Int. J. Speech Technol. **12**(1), 47–57 (2009)
5. M. Chandrasekar, M. Ponnavaikko, Tamil speech recognition: a complete model. Electron. J. Tech. Acoust. **20** (2008)
6. K. Shyam, SHARIKA malayalam speech recognition system, in *International Conference ICIST2007* (2007)
7. L.R. Rabiner, A tutorial on hidden markov models and selected applications in speech recognition. Proc. IEEE **77**(2), 257–286 (1989)
8. L.R. Bahl et al., A tree-based statistical language model for natural language speech recognition. IEEE Trans. Acoust. Speech, Sig. Process. **37**, 1001–1008 (1989)
9. H. Gnanathesigar, Tamil speech recognition using semi continuous models. Int. J. Sci. Res. Publ. **2**(6) (2012)
10. P. Ross et al, On the voice-activated question answering. IEEE Trans. Syst. Man Cybern. **42** (1) (2012)
11. A. Srinivasan et al., Speech recognition of the letter 'zha' (H) in Tamil language using HMM. Int. J. Eng. Sci. Technol. **1**(2), 67–72 (2009)

Constrained Optimal Bidding Strategy in Deregulated Electricity Market

D. Palit and N. Chakraborty

Abstract A precise and comprehensive model is designed for optimum power trading among a number of generating companies (GenCo) having thermal generating units. These GenCos are offering different bidding prices for gaining maximum profit. There may be different category of bidding situations. Possible bidding profile combinations along with some constraints are considered in case studies. The power balance constraint includes generation, demand and transmission loss, power generation limit, and fuel cost constraints. Thermal generating units are considered here. As scheduling is interconnected with bidding, economic power scheduling has been solved using Newton–Raphson method for standard IEEE 9 bus test system. Bidder's profits and market price have been calculated in each case. For optimization of the power bidding problem, theory of dominance of game theory has been applied and justified for searching the Nash equilibrium.

Keywords Electric energy market · Deregulation · Economic dispatch · Game theory

1 Introduction

Modern electricity market has been changed from monopoly to oligopoly era where competition among many players is observed. In modern deregulated environment, electricity can be thought as an essential commodity which can be bought and sold in the open marketplace in a competitive manner just like other commodities. In this huge competitive environment, it is essential for regulator or independent system operator (ISO) to investigate strategic bidding behavior in order to identify possible

D. Palit (✉) · N. Chakraborty
Power Engineering, Jadavpur University, Salt Lake, Kolkata 700098, India
e-mail: palit2007@gmail.com

N. Chakraborty
e-mail: chakraborty_niladri2004@yahoo.com

© Springer India 2015

L.P. Suresh et al. (eds.), *Artificial Intelligence and Evolutionary Algorithms in Engineering Systems*, Advances in Intelligent Systems and Computing 325,
DOI 10.1007/978-81-322-2135-7_91

market power abuse along with limiting it by introducing appropriate market management policies [1]. Power bidding problem is related with pool trading in which sealed auction is widely employed where power suppliers and bulk consumers both are required to offer price and quantity bids to market operator. Market operator then determines the winning bid and a uniform market clearing price (MCP) using a simple merit order dispatch procedure [1]. There are three ways of for developing optimal bidding strategies. Firstly, estimation of MCP is done in next trading period. Secondly, utilization of bidding behavior of rival participants is estimated. Third one is Game theory-based process for searching crucially the optimal bidding profile. It is done after estimating suppliers generating unit commitment or economically scheduling the load demands among the bidders those who offer power at affordable price with low risk bidding. Study of economic load scheduling in competitive deregulation with optimal low-risk bidding is most essential for a profitable deregulated market design.

Game theory had been proposed to analyze the economic behavior of generators in a short-term deregulated electric energy market [2]. IEEE 9 bus test system was used to illustrate the proposed method by solving unit commitment problem. Game theory can be used to simulate decision making process for defining offered prices in deregulation [3, 4]. These ideas can be used by pool coordinators to discourage unfair coalitions. Modified IEEE 30 bus system has been used as deregulated power pool system for illustration [3, 4]. It has been shown that, in a perfect competition, all participants try to maximize their benefits by cooperating with power pool to obtain maximum system wide benefits. Also, it had been also observed that each of the suppliers can bid 24 linear energy functions, one for each hour for a day-ahead energy market [5]. In this way, hourly unit commitment status can be determined. Market can be cleared by suggesting maximum hourly benefit bidding strategies and minimum stable output bidding strategies. Finally, overall bidding strategy for a day-ahead market can be developed by power exchange. A theoretical frame work of a cooperative game was analyzed to obtain savings in economy interchange between Chilean Interconnected Central System (SIC) and Argentine Interconnection System (SADI) as in wholesale competitive electric energy market [6].

In this attempt to make the study more realistic, “submarginal” and “sub-super marginal” bidding strategies of different competing thermal generating units are considered. Constrained economic load scheduling problems are solved using Newton–Raphson method after simulation of “submarginal” and “sub-super marginal” bidding condition. Different parameters have been calculated as economically scheduled load demand on generating units of respective power bidders, their profit or benefit at different bidding situations, market power selling price, transmission loss for IEEE 9 bus test system. In different power bidding scenario of electric energy, market estimation of transmission loss is very important. The generalized generation shift distribution factor (GGSDF) method had been proposed for calculation of transmission loss coefficients [7, 8]. This method is used in this work on IEEE 9 bus test system network. For selecting the optimal bidding condition, Nash equilibrium is searched using the theory of dominance approach of

game theory [9, 10] considering maximum profit of power bidders as well as minimum market power selling price for consumer's benefit. Encouraging results are obtained at various realistic situations.

2 Problem Formulation

For bidding strategies formulation, prior idea of scheduling of different participation generators should be known. In a competitive deregulated environment, the optimal power scheduling problem can be defined using Lagrange multiplier method. Here, the constrained optimization problem can be converted to an unconstrained optimization problem. The formed objective function can be minimized considering some equality constraint. In this case, Newton–Raphson method is used for formulating the solution of constrained optimal power scheduling problem in a IEEE 9 bus test system network. Game theory has been applied for searching optimal bidding situation.

2.1 Simulation of Deregulation

Deregulated electricity market has been simulated considering three numbers of generating companies (GenCo) each having single thermal generating unit. They are competing for gaining highest profit in an open market competition. There is single retail energy service company (Resco) buys power from GenCo on behalf of consumers through power exchange after technical and commercial approval of (ISO). Each Genco offers bidding strategy profile to power exchange, i.e., per unit cost of generated power in respective percentage of their marginal price at a specified timing. Resco offers power demand profile for a specified timing on behalf of consumers drawing power at a specified location, i.e., from IEEE 9 bus test system network as considered for simulation in this case. Power exchange computes per unit market price for the respective time instant. Considering all possible combination of bidding profile, ISO takes the optimized decision so that bidders find no alternate option for gaining more individual benefit as well as Resco buys power at a minimum competitive price so that consumers can afford the settled price.

It is assumed that, strategy code of "*i*-"th bidder is St_i, i.e., the fractional price of it is own marginal price. For initialization of the value of marginal cost λ and scheduled generation of bidder "*i,*" i.e., P_{g_i}, value the loss P_L has been neglected. After first iteration, it is accounted. Again $a_{i,}$ b_i, c_i are cost constraints of "*i*-"th generating unit. P_D is load demand.

Considering incremental cost of bidder "*i*," we can write for scheduling purpose

$$\lambda = S_{t_i} \cdot \frac{\partial F(Pg_i)}{\partial Pg_i} = (2Pg_i a_i + b_i) \cdot S_{t_i} \tag{1}$$

$$Pg_i = \left(\frac{\frac{\lambda}{S_{t_i}} - b_i}{2a_i} \right) \tag{2}$$

$$\sum_{i=1}^{Ng} Pg_i = P_D \tag{3}$$

$$\lambda = \frac{P_D + \sum_{i=1}^{Ng} \frac{b_i}{2a_i}}{\sum_{i=1}^{Ng} \frac{1}{2a_i S_{t_i}}} \tag{4}$$

Market bidding price of bidder "*i*" is ρ_i which can be defined as

$$\rho_i = L_i \cdot \lambda = L_i(2Pg_i a_i + b_i) \cdot S_{t_i}. \tag{5}$$

where, L_i is penalty factor of *i*-th unit.

It is observed that the bidding price is a fraction of marginal price. When this fraction "St_i" is less than 1, then it is called submarginal bidding and sometime "St_i" is greater than 1 then it is termed as super-marginal bidding.

Benefit of respective bidder utility "*K*" having a set of generators Ω_K and generating unit index "*j*" can be expressed as

$$B_K = \sum_{j \in \Omega_K} \left\{ \rho_j \cdot Pg_j - F(Pg_j) \right\} \tag{6}$$

For finding optimal benefit that will be gained by power bidders and also for finding competitive market price, optimization process based on well-known game theory is applied here. Here, the power bidding business is considered as a game. Respective bidders are players participating in this power bidding game as per their own bidding strategy for wining. It means that their bids are to be accepted by (ISO) or power regulator and bidders are earning reasonable profit, provided market power selling price becomes competitively low so that it can be affordable by consumers.

2.2 Game Theory Representation

The formal form representation of an *N* player game specifies the players strategy space S_i, ..., S_n and their payoff functions are U_1, …, U_n.

For player $K = 1, \ldots, N$:
The Game "G" can be defined as

$$U_k : \prod_{i=1}^{N} S_i \rightarrow \Re$$
$$G = \{S_1, \ldots, S_n; U_1, \ldots, U_n\} \tag{7}$$

Let S_i' & S_i'' are feasible strategies of player "i," then, $\left(S_i' \in S_i;\ \& \ S_i'' \in S_i\right)$.The strategy S_i' is strictly dominated by strategy S_i'' if for each feasible combination of other players' strategies. If i's payoff from playing S_i' is strictly less than i's payoff from playing S_i'' for each case of other player's strategy spaces $(S_i, \ldots, S_{i-1}, \ldots, S_n)$ can be defined as:

$$U_i(S_i, \ldots, S_{i-1}, S_i', S_{i+1}, \ldots, S_n) < U_i(S_1, \ldots, S_{i-1}, S_i'', S_{i+1}, \ldots, S_n) \tag{8}$$

In any N player normal form of game G, the strategies $\left(S_i^*, \ldots, S_n^*\right)$ are a Nash equilibrium. For each player i, S_i^* is at least tied for player i's best response to the strategies specified by the $N-1$ other players.
$\left(S_1^*, \ldots, S_{i-1}^*, S_{i+1}^*, \ldots, S_n^*\right)$ for every feasible strategies can be defined as:

$$U_i(S_1^*, \ldots, S_{i-1}^*, S_i^*, S_{i+1}^*, \ldots, S_n^*) \geq U_i(S_1^*, \ldots, S_{i-1}^*, S_i, S_{i+1}^*, \ldots, S_n^*) \tag{9}$$

For every feasible strategies "S_i" in a set of strategies S_i', Nash equilibrium solution can be found by solution of the following equation

$$\max_{S_i \in S_i} U_i\left(S_1^*, \ldots, S_{i-1}^*, S_i, S_{i+1}^*, \ldots, S_n^*\right) \tag{10}$$

Here, the situation has been considered as a power bidding game where each players or bidders are trying to give their maximum efforts for winning the game or being accepted as the winning bidder getting maximum profit or benefit. But, ISO should compromise those bidders maximum profit by considering consumers convenient market selling price at lowest price level. Here, game theory is applied by considering "theory of dominance approach". Among a number of playing strategy profiles most dominant one has been searched that will lead the game most optimistic to each and every players.

3 Results and Discussion

Detailed results are tabulated in Tables 1 and 2 for load demand of 150, 300, and 400 MW. Graphical representation is done in Figs. 1, 2, 3, and 4 for load demand 150 and 300 MW only for "Submarginal" and "Sub-super marginal" bidding condition. For "Submarginal" bidding, all bidders are claiming price less than their

Table 1 Nash equilibrium in submarginal bidding strategy codes: low = 0.40, medium = 0.70, high = 1.00, i.e., 40, 70, and 100 % of marginal cost, respectively

Power demand (MW)	Nash equilibrium strategy no	Optimal strategies			Benefits ($/h)			Selling price ($/h)	Power loss (MW)
		G_1	G_2	G_3	G_1	G_2	G_3		
150	5	0.40	0.70	0.70	−253.59	−26.90	−216.57	1,366.774	5.803
300	5	0.40	0.70	0.70	−53.54	205.74	127.73	5,415.210	12.689
400	5	0.40	0.70	0.70	289.97	474.02	472.00	9,721.422	17.485

Table 2 Nash equilibrium in sub-super marginal bidding strategy codes: low = 0.70, medium = 1.20, high = 1.50, i.e., 70, 120, and 150 % of marginal cost, respectively

Power demand (MW)	Nash equilibrium strategy no	Optimal strategies			Benefits ($/h)			Selling price ($/h)	Power loss (MW)
		G_1	G_2	G_3	G_1	G_2	G_3		
150	20	1.5	0.70	1.2	49.62	392.50	−83.75	2,257.10	6.022
300	21	1.5	0.70	1.5	955.65	1,808.70	447.24	8,443.06	9.100
400	21	1.5	0.70	1.5	1,990.45	3,310.37	977.88	14,897.02	12.845

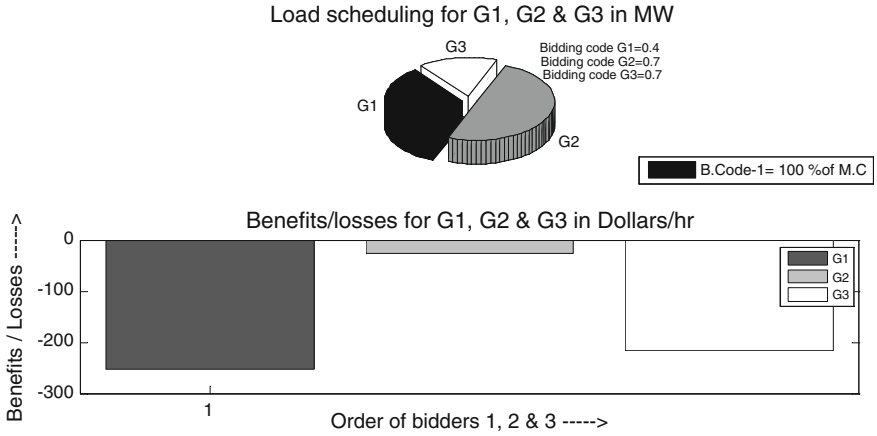

Fig. 1 Result of standard IEEE 9 bus test system transmission network and 150 MW load demand ("*Submarginal*"). (G_1 = 52.302 MW, −253.599 \$/h, G_2 = 78.074 MW, −26.908/h, G_3 = 25.428 MW, −216.570 \$/h, Market price = 1,366.774 \$/h, Transmission loss = 5.803 MW)

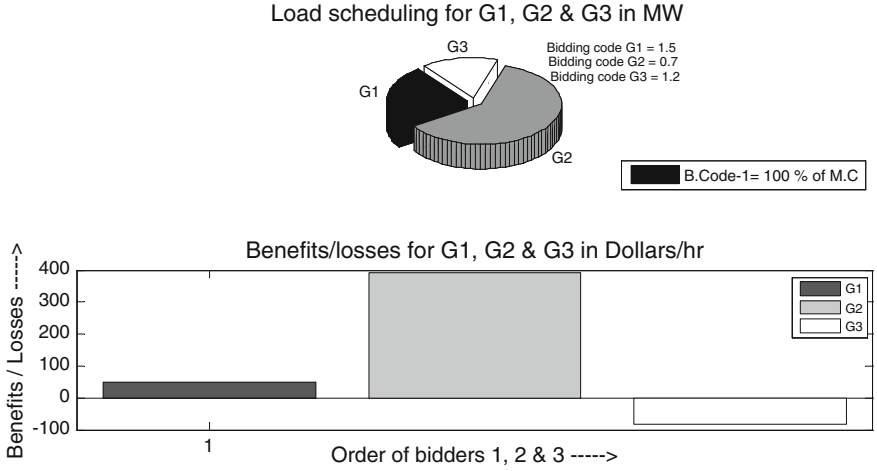

Fig. 2 Result of standard IEEE 9 bus test system transmission network and 150 MW load demand ("*Sub-super marginal*") (G_1 = 36.962 MW, 49.625 \$/h, G_2 = 95.242 MW, 392.506 \$/h, G_3 = 23.817 MW, −83.752 \$/h Market price = 2,257.100 \$/h, Transmission loss = 6.022 MW)

respective marginal price and for "Sub-super marginal" bidding some bidders are claiming less and some are claiming more than their marginal price. For different load demand, it is observed that those bidders who claims higher bidding price are sharing lesser percentage of load demand from the economic load scheduling point of view. It is truly observed in each case that if any bidder reduces their bidding price from any strategy numbers to the next successive number then their percentage of load sharing increases. The same conditions are observed in higher demands. The

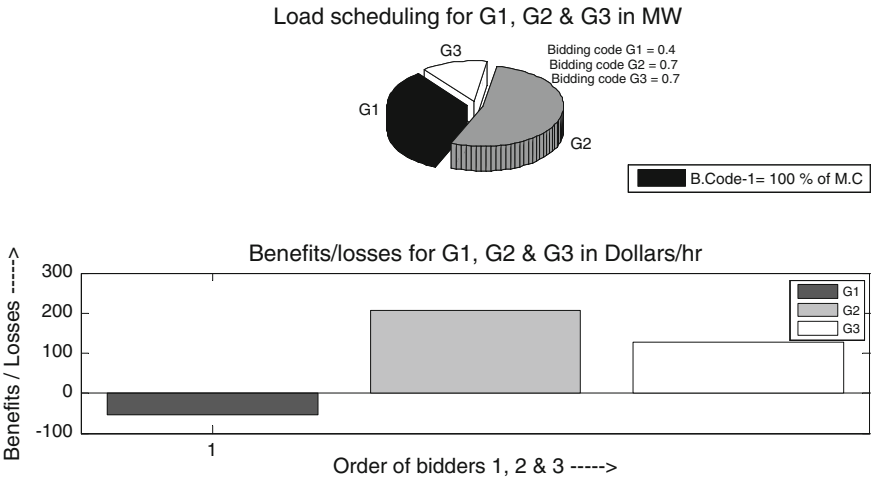

Fig. 3 Result of standard IEEE 9 bus test system transmission network and 300 MW load demand ("*Submarginal*"). (G_1 = 103.504 MW, −53.458 \$/h, G_2 = 168.246 MW, 205.742 \$/h, G_3 = 40.939 MW, 127.739 \$/h Market price = 5,415.201 \$/h, Transmission loss = 12.689 MW)

physical significance is that the bidding price is always fluctuating from one bidder to another bidder caused by so many factors. In this situation to maintain power market economy, ISO decides to schedule most of the load on the bidder who claims lowest bidding price, intermediate load to the bidder who claims intermediate bidding price and lowest load to the bidder who claims highest bidding price.

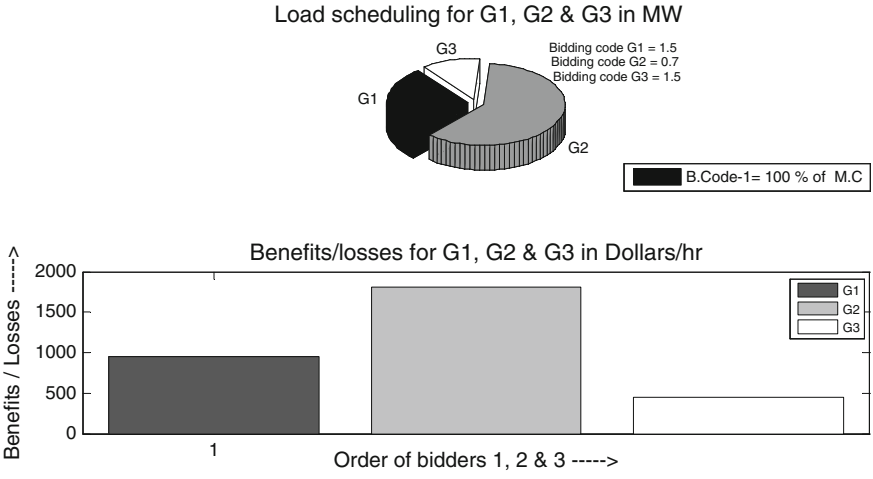

Fig. 4 Result of standard IEEE 9 bus test system transmission network and 300 MW load demand ("*Sub-super marginal*"). (G_1 = 83.036 MW, 955.650 \$/h, G_2 = 187.425 MW, 1,808.705 \$/h, G_3 = 35.639 MW, 447.240 \$/h Market price = 8,443.061 \$/h, Transmission loss = 9.100 MW)

At "submarginal" bidding category considering benefits of bidders at 150 MW demand, it is observed that, Nash equilibrium is achieved when benefits are negative for all bidders, i.e., they all suffer loss in "submarginal" bidding. At 150 MW, bidders would not be insisted to bid in this condition unless they are compelled to do so. But, benefits are improved at higher demands as 300 and 400 MW. It is observed that as much as we increase demand the Nash equilibriums are achieved at higher benefit and which is true in all bidding category.

If we verify the situation elaborately, we observe that Nash equilibrium is achieved at minimum loss condition in 150 MW demand in "submarginal" bidding in comparison with sub-super marginal bidding condition. But, Nash equilibrium is achieved at lowest loss in "Sub-super marginal" bidding category for 300 and 400 MW load demand. So, in these load demands, bidders will be interested to bid at "sub-super marginal" category.

Considering transmission power loss in IEEE 9 standard bus test system, it is observed that when load demand increases, the load sharing in each unit increases and Nash equilibriums are achieved at comparatively higher transmission loss. It is observed in every bidding profile category.

4 Conclusions

Game theory is used for optimization of power bidding in deregulated electrical power market for various conflicting condition. This paper serves the knowledge for studying the power transaction of "submarginal" and "sub-super marginal" power bidding among three competing bidders. It has been shown that how to manage the economic scheduling of load demand among three competing power bidders considering different technical constraints using Newton–Raption method. It has been also shown that how market regulator can take the decision for selecting the optimal bidding profile for realistic "submarginal" and "sub-super marginal" bidding situations by searching Nash equilibrium of game Theory. It serves the purpose for gaining deregulated electricity market economy.

Acknowledgments We are thankful to the authority of Jadavpur University for extending all sorts of cooperation for the completion of this work.

References

1. A.K. David, F. Wen, Strategic bidding in competitive electricity markets: a literature survey, in *Power Engineering Society Summer Meeting* 2000, vol. 4 (2000), pp. 2168–2173
2. D. Moitre, Nash equilibria in competitive electric energy markets. Electr. Power Syst. Res. **60**, 153–160 (2002)
3. R.W. Ferrero, S.M. Shahidehpour, V.C. Ramesh, Transaction analysis in deregulated power systems using game theory. IEEE Trans. Power Syst. **12**(3), 1340–1347 (1997)

4. D.M.V. Kumar, Generation Bidding Strategy based on Game Theory. Modern Electric Power Systems (2010)
5. F.S. Wen, A.K. David, Strategic bidding for electricity supply in a day-ahead energy market. Electr. Power Syst. Res. **59**, 197–206 (2001)
6. D. Moitre, H. Rudnick, Integration of wholesale competitive electric markets: an application of the Nash bargaining generalized solution. Int. J. Electr. Power Energy Syst. **22**(7), 507–510 (2000)
7. Y.C. Chang, W.T. Yang, C.C. Liu, A new method for calculating loss coefficients. IEEE Trans. Power Syst. **9**(3), 1665–1670 (1994)
8. D.P. Kothari, J.S. Dhillon, Power System Optimization (2006)
9. S. Soft, Using game theory to study market power in simple networks, in *IEEE Tutorial on Game Theory Applications in Electric Power Markets* (1999), pp. 33–40
10. J.F. Nash, Equilibrium points in n-person games, in *Proceedings of the National Academy of Sciences*, vol. 36 (1950), pp. 48–49